THE ELEVENTH INTERNATIONAL SYMPOSIUM ON DISTRIBUTED COMPUTING AND APPLICATIONS TO BUSINESS, ENGINEERING AND SCIENCE

DCABES 2012

PROCEEDINGS

Guilin, China

October 19~22, 2012

Editor in Chief Qingping Guo
Craig Douglas

IEEE CS Conference Publication Service

Published by:

CPS
Conference Publishing Services

Proceedings

11th International Symposium on
Distributed Computing and Applications to Business, Engineering & Science

DCABES 2012

Proceedings

11th International Symposium on
Distributed Computing and Applications to Business, Engineering & Science

DCABES 2012

19–22 October 2012
Guilin, China

Editors
Qingping Guo
Craig Douglas

CPS
Conference Publishing Services

IEEE Computer Society Order Number E4818
ISBN-13: 978-0-7695-4818-0
BMS Part # CFP1220K-CDR

Additional copies may be ordered from:

IEEE Computer Society
Customer Service Center
10662 Los Vaqueros Circle
P.O. Box 3014
Los Alamitos, CA 90720-1314
Tel: + 1 800 272 6657
Fax: + 1 714 821 4641
http://computer.org/cspress
csbooks@computer.org

IEEE Service Center
445 Hoes Lane
P.O. Box 1331
Piscataway, NJ 08855-1331
Tel: + 1 732 981 0060
Fax: + 1 732 981 9667
http://shop.ieee.org/store/
customer-service@ieee.org

IEEE Computer Society
Asia/Pacific Office
Watanabe Bldg., 1-4-2
Minami-Aoyama
Minato-ku, Tokyo 107-0062
JAPAN
Tel: + 81 3 3408 3118
Fax: + 81 3 3408 3553
tokyo.ofc@computer.org

Individual paper REPRINTS may be ordered at: <reprints@computer.org>

Editorial production by Lisa O'Conner

IEEE Computer Society
***Conference Publishing Services* (CPS)**
http://www.computer.org/cps

2012 11th International Symposium on Distributed Computing and Applications to Business, Engineering & Science

DCABES 2012

Table of Contents

Distributed / Parallel Applications

Computer Networks and System Architectures

Cloud/Grid Computing

E-business

Computational Modeling and Processes

Information Security

Intelligent Transportation

Image/Video Processing—Methodologies and Applications

Computation Theory and Algorithms

Other Relevant Topics

Preface

The DCABES is a community working in the area of Distributed Computing and Applications in Business, Engineering, and Sciences, and is responsible for organizing meetings and symposia related to the field. DCABES intends to bring together researchers and developers in the academic field and industry from around the world to share their research experience and to explore research collaboration in the areas of distributed parallel processing and applications.

The 11th International Symposium on Distributed Computing and Applications to Business, Engineering and Science (DCABES 2012) will be held on October 19~22, 2012 in a very famous world resorts, the Guilin, Guangxi, China.

All papers accepted by DCABES 2012 Proceedings have been peer reviewed and carefully modified. Since DCABES 2001, the first DCABES, each DCABES symposium has invited 4 to 5 world famous professors and experts in computer science and technology area to give keynote speeches for the conference. Ten years passed and dozens VIPs in distributed parallel processing have attended the DCABES conferences, among them there are Professor Jifeng He, a member of Academia Sinica, Professor Albert Y. Zomaya, the Editor-in-Chief of *IEEE Transactions on Computers* and Associate Editor-in-Chief of *IEEE Transactions on Parallel and Distributed Systems*, Professor C.-H. Lai, Editor-in-Chief of *JACT (Journal of Algorithms and Computational Technology*), Academia Sinica Professor Zhiwei Xu, Editor-in-Chief of *Journal of Computer Research and Development*, Professor Craig Douglas, distinguished professor in MGNET, et al.

The DCABES series began as a summer short course held at Hong Kong Polytechnic University in 2000 with the support of the British Computer Society - Hong Kong Chapter. The two co-chairs of DCABES, Professors GUO Qingping and LAI Choi-Hong, extended the short course into a series of conferences that continues today and grows yearly.

In recent years, more and more attentions have been put to the distributed parallel computing. We are confident that the distributed parallel computing will play an even greater role in the near future, since distributed computing resources, once properly cooperated together, will achieve a great computing power and get a high ratio of performance/price in parallel computing. In fact the grid computing, cloud computing and the multi-core processor are closely related to and evolved from the distributed parallel computing.

All papers contained in the Proceedings give us a glimpse of what future technology and applications are being studied in the distributed parallel computing area in the world. More papers concerning the distributed parallel algorithms and applications, the intelligent transportation as well as image processing have been selected and included in the DCABES 2012 Proceedings.

We would like to thank all members of the Scientific Committee, the Program Committee, the local organizing committee, and the external reviewers for selecting papers.

We are also grateful to Professor Xue-bin Chi (Computer Network Information Center of Chinese Academy of Sciences, the CNIC of CAS, China), Professor Choi-Hong Lai, (School of Computing and Mathematical Sciences, University of Greenwich), Professor Craig Douglas (University of Wyoming, Mathematics Dept.), and Professor Xinping Yan (Vice president of Wuhan University of Technology) for their contributions of keynote speeches at the conference.

We would also like to thank the WUT (Wuhan University of Technology, China), the NPCS (National Parallel Computing Society of China), Guangxi Teachers Education University, Guangxi Normal University, and the CAA (Computer Academic Association of Hubei Province & Wuhan Metropolis, China) for their support as local organizers of the conference.

Here thanks are extended to Miss Zhang Qinqin, Mr. Zhang Yuchao, and Mr. GUO Yucheng of Wuhan University of Technology for their hard working and contributions to the DCABES 2010 conference.

Enjoy your stay in Guilin, China. Hope to meet you again at the DCABES 2013.

Prof. Qingping Guo (Co-Chair of DCABES)
Wuhan University of Technology, China

Prof. Choi-Hong Lai (Co-Chair of DCABES)
University of Greenwich, UK

Prof. Craig Douglas (Program Chair of DCABES 2012)
University of Wyoming, USA

Committees

Conference Chair

Guo, Professor Q. P., *Wuhan University of Technology, China*

Conference Co-Chairs

Douglas, Professor Craig C., *University of Wyoming, USA*
Lai, Professor C.-H., *University of Greenwich, UK*

The Steering Committee

Guo, Professor Q.P. (Co-Chair), *Wuhan University of Technology, China*
Lai, Professor C.-H. (Co-Chair), *University of Greenwich, UK*
Douglas, Professor Craig C., *University of Wyoming, USA*
Tsui, Thomas, *Chinese University of Hong Kong, Hong Kong, China*
Xu, Professor W. *Jiangnan University, Wuxi, China*

Program Committee

Prof. Craig C. Douglas, (Chair) *Yale University, USA*
Prof. C.-H. Lai, (Co-Chair), *University of Greenwich, UK*
Prof. Q.P. Guo, (Co-Chair) *Wuhan University of Technology, Wuhan, China*
Prof. Frederic Magoules, *Ecole Centrale Paris, France*
Prof. Albert Y. Zomaya, Chair, *The University of Sydney, Australia*
Prof. Maurício Vieira Kritz, *National Laboratory for Scientific Computation, Petropolis - RJ, Brasil*
Prof. Peter Jimack, Pro Dean for Research, *University of Leeds, UK*
Prof. W.B. Xu, *Jiangnan University, Wuxi, China*
Prof. Xiao-Chuan Cai, *University of Colorado at Boulder, USA*
Prof. Jianwen CAO, *Institute of Software Chinese Academy of Sciences*, *Beijing, China*
Prof. Director, Chi XueBing, *Chinese Academy of Sciences, China*
Prof. Yakup Paker, *Queen Mary University of London,UK*
Dr. Turgay Altilar, *Istanbul Technical University, Istanbul, Turkey*
Dr. A/Prof., Souheil Khaddaj, *Kingston University, UK*
Dr. Andrew A. Chien, *University of California, San Diego, USA*
Dr. Pui-Tak Ho, *The University of Hong Kong, HK*
Prof. John W. T. Lee, *The Hong Kong Polytechnic University, HK*
Prof. Lishan Kang, *University of Geosciences, China*
Prof. David Keyes, *King Abdullah University of Science and Technology, USA*
Dr. Huang, Professor Tinglei, *Guilin University of Electronic Technology, China*
Dr. Chen, Professor Wei, *Wuhan University of Technology, Wuhan, China*

Dr. Xiao, Professor Xinping, *Wuhan University of Technology, China*
Prof. Wenjing Li, *Guangxi Normal University, Nanning, Guangxi, China*
Prof. Shesheng Zhang, *Wuhan University of Technology, China*
Dr. Ping Lin, Professor, *University of Dundee, UK*
Prof. Michael K. Ng, *The University of Hong Kong, HK*
Prof. SUN Jiachang, *Institute of Software, Academy of Science, China*
Dr. Alfred Loo, *Lingnan University, HK*
Dr. Man Leung Wong, *Lingnan University, HK*
Dr. Prof. Peter KACSUK, *Hungarian Academy of Sciences, HU*
Prof. Stefan Vandewalle, *Katholieke Universiteit Leuven, Belgium*
Dr. Robert Lovas, *Hungarian Academy of Sciences, Hungary*
Dr. Associate Professor Faouzi Alaya Cheikh, *Gjovik University College, Norway*
Dr. Prof. NIKOS Christakis, *University of Crete, Heraklion, Greece*
Prof. Haixin Lin, *Delft University of Technology, Netherlands*
Prof. Anne Trefethen, *University of Oxford, UK*
Prof. David Keyes, *Columbia University, USA*
Prof. Rassul Ayani, *Royal Institute of Technology (KTH), Sweden*
Prof. Zhihui Du, *Tsinghua University, China*
Prof. Meiqing Wang, *Fuzhou University, Fuzhou, China*
Prof. Yuhua Liu, *Central China Normal University, Wuhan, China*
Rongcong Xu, *Fuzhou University, Fuzhou, China*
Prof. Youwei Yuan, *Hangzhou Dianzi University, Hangzhou, China*
Prof. V. P. Kutepov, *Moscow Power Engineering Institute, ul., Russia*
Prof. Yi Pan, *Georgia State University, USA*
Prof. Alan Davies, *University of Hertfordshire, UK*
Prof. Peter Sloot, *University of Amsterdam, Netherlands*
Prof. Franck Cappello' CNRS, *Universite Paris-Sud, France,*
Prof. Simon Cox, *School of Engineering Sciences, UK*
Prof. Laurie Cuthbert, *Queen Mary University of London, UK*
Prof. Alex Shafarenko, *University of Hertfordshire, UK*
Prof. Liu Dan, *Henan Mechanic and Electric Engineering College, China*
Prof. Xiaojun Tong, *Harbin Institute of Technology at Wei Hai, China*
Dr. Liu, Professor Dan, *China Criminal Police University, China*
Dr. Ray Hyatt Jr, *Brown University, USA*
Dr. Lamine M. Aouad, *University College Dublin, Ireland*
Dr. Thi-Mai-Huong Nguyen, *Ecole Centrale Paris, France*
Dr. Haiwu He, *Hohai University, China*
Dr. Alan J. Davies, *University of Hertfordshire, UK*
Prof. Ziyue Tang, *Air Force Radar Institute, Wuhan, China*
Dr. Prof. Yalchin Efendiev, *Texas A&M University, USA*
Dr. Prof. Yuhui Shi, *Xi'an Jiaotong-Liverpool University, Suzhou, China*
Prof. Qifeng Yang, *Wuhan University of Technology, Wuhan, China*
Dr. Prof. Dongwoo Sheen, *Seoul National University, Seoul, Korea*
Professor Rule Hjelsvold, *Gjovik University College, Norway*
Dr. Morten Irgens, *Gjovik University College, Norway*

Dr. Prof. Mohamed Kamel, *University of Waterloo, Canada*
Dr. Prof. Dexin Zhan, *Wuhan University of Technology, Wuhan, China*
Dr. Prof. Liyi Zhang, *Wuhan University, Wuhan, China*
Dr. Pedro Leite da Silva Dias, *Petropolis, RJ, Brazil*
Professor Shengwu Xiong, *Wuhan University of Technology China*
Dr. Professor Xinming Tan, *Wuhan University of Technology China*
Dr. Professor Shu Gao, *Wuhan University of Technology, China*
Dr. Professor Hongxing Liu, *Wuhan University of Technology, China*
"Neal" Naixue Xiong, *Georgia State University*
Lecturer Yucheng Guo, *Wuhan University of Technology, China*

Scientific Committee (in alphabetical order)

Cai, Professor X.C. , *University of Colorado, Boulder, USA*
Cao, Professor J.W., *Research and Development Centre for Parallel Algorithms and Software, Beijing, China*
Chi, Professor X.B., *Academia Sinica, Beijing, China*
Douglas, Professor Craig C., *University of Wyoming Mathematics Department, Yale University Computer Science Department*
Guo, Professor Q.P., *Wuhan University of Technology, Wuhan, China*
He, Dr. H.W., *Hohai University, Nanjing, China*
Ho, Dr. P. T., *University of Hong Kong, Hong Kong, China*
Jesshope, Dr. Professor C., *University of Amsterdam, the Netherlands*
Kang, Professor L.S., *Wuhan University, China*
Keyes, Professor D.E., *Columbia University, USA*
Khaddaj, Dr. S.A., *Kingston University, UK*
Lai, Professor C.-H., *University of Greenwich, UK*
Lee, Dr. John., *Hong Kong Polytechnic, Hong Kong, China*
Lin, Dr. H.X., *Delft University of Technology, Delft, the Netherlands*
Lin, Professor Ping, *University of Dundee, Old Hawhill*
Ng, Professor Michael, *Baptist University of Hong Kong, China*
Loo, Dr. Alfred, *Hong Kong Lingnan University, Hong Kong, China*
Sloot, Professor P.M.A., *University of Amsterdam, Amsterdam the Netherlands*
Sun, Professor J., *Academia Sinica, Beijing, China*
Wang, Professor M.Q., *Fuzhou University, Fuzhou, China*
Xu, Professor W.B., *Southern Yangtze University, Wuxi, China*
Zou, Professor J., *The Chinese University of Hong Kong, China*

Local Organizing Committee

Guo, Professor Qingping (Chair), *Wuhan University of Technology, Wuhan, China*
Li, Prof. Wenjing (Co-Chair), *Guangxi Normal University, Nanning, Guangxi, China*
Dr. Chen, Professor Wei, *Wuhan University of Technology, Wuhan, China*
Dr. Xiao, Professor Xinping, *Wuhan University of Technology, China*
Dr. Zhang, Prof. Shesheng, *Wuhan University of Technology, China*
Dr. Zhong, Professor, L., *Wuhan University of Technology, Wuhan, China*
Kang, Professor L.S., *Wuhan University, Wuhan, China*
Lu, Professor J.G., *South Central China Nationality University*

Secretariat

Mr. Guo, Yucheng, *Wuhan University of Technology*
Miss Zhang,Qinqin, *Wuhan University of Technology*
Mr. Zhang, Yuchao, *Wuhan University of Technology*

Comparing the Laplace Transform and Parareal Algorithms

Craig C. Douglas and Li Deng Douglas
University of Wyoming
Laramie, WY, USA and
e-mail: cdougla6@uwyo.edu

Hyoseop Lee
Alcatel-Lucent Bell Labs - Seoul
Seoul, South Korea
e-mail: hyoseop.lee@gmail.com

Dongwoo Sheen
Seoul National University
Seoul, South Korea
e-mail: sheen@snu.ac.kr

***Abstract*—Both the Laplace Transform and the Parareal family of algorithms promise to provide completely parallel in time and space computational results. Given a random time dependent partial differential equation it is unclear which algorithm will run faster. We define the algorithms in question, including more specific details than usual. We define interesting parallel environments, some of which do not exist yet. Finally, we demonstrate some computational environments in which one of the algorithms can be expected to be faster than the other algorithm.**

Keywords-parallel computing, time-space parallelism, partial differential equations, PDE solvers

I. INTRODUCTION

We are interested in comparing two algorithms that allow for both time and space parallelism in solving either an ordinary differential equation,

$$u' = f(u), \tag{1}$$

or a parabolic equation,

$$\frac{du}{dt} = L(u) + f. \tag{2}$$

Classical methods for solving either (1) or (2) are based on simple time stepping over an ordered set with N_T time steps

$$\left\{t_1, t_2, \cdots, t_{N_T-1}, t_{N_T}\right\}. \tag{3}$$

Consider the computational complexity of one method for solving (1)-(3), namely using backward Euler for time stepping combined with a multigrid. For either two or three spatial dimensions with N_S total spatial points, the cost of solving the problems is one of the following two cases:

Serial	$O(N_T \cdot N_S)$
Parallel	$O(N_T \cdot \log^2(N_S))$.

The central question that this paper is interested in investigating is the following:

Can we robustly solve parts of the problem later in time before fully approximating the solution earlier in time using something similar to a traditional numerical algorithm for solving time dependent ordinary or parabolic differential equations?

Over a 60 year period, the answer was repeatedly proposed to be yes, but the general algorithmic technique in all cases was conclusively proven to be in error [1]. Then the Parareal algorithm [2] was published using a very different algorithmic technique.

The remainder of this paper is organized by algorithms and numerical experiments. In Section II, we define the Parareal algorithm and its interpretations. In Section III, we define the Laplace transform and its relevant properties. In Section IV, we compare the two algorithms in a simple way. In Section V, we draw some conclusions about which of the two algorithms to try first based on the number of computing cores in a parallel computer.

II. PARAREAL

Consider solving (1) starting from $u_1 = u(t_1)$. Use two time propagation operators of the form,

$$F(t_2, t_1, u_1), \tag{4}$$
$$G(t_2, t_1, u_1), \tag{5}$$

where F and G are the fine quality and coarse (or rough) operators for time stepping, respectively.

For example, both time propagation operators could be the same time stepping scheme, but on nested time meshes, i.e., F can be a standard time stepping operator (e.g., backward Euler or Crank-Nicolson) on (3), but G could be the same time stepping scheme except on every τ^{th} point in (3). If the time mesh spacing is Δt for F, then the time mesh spacing for G is $\Delta T = \tau \Delta t$.

Parareal starts with an initial guess U_n^0 at time points $t_1, t_2, \cdots, t_N$ and computes U_n^k by a series of correction iterations. Parareal is formally defined by

Loop over iterations
for $k = 0, 1, \rightleftharpoons$
  time steps
  for $n = 0, 1, \rightleftharpoons, N-1$

$$U_{n+1}^{k+1} = F(t_{n+1}, t_n, U_n^k) + G(t_{n+1}, t_n, U_n^{k+1}) - G(t_{n+1}, t_n, U_n^k)$$

The dominant part of the computation in Parareal is computing F at every time step each outer iteration.

978-0-7695-4818-0/12 $26.00 © 2012 IEEE
DOI 10.1109/DCABES.2012.106

However, this is embarrassingly parallel. Further, to implement Parareal to experiment with takes only five lines of Matlab.

The convergence required is the accuracy of the F time propagator at each time step t_n. We can see immediately that we are guaranteed this level of convergence after N steps since this is equivalent to just doing the original time stepping on (3). Recalling the central question of Section I, a reasonable question to ask is if this is all that Parareal can guarantee since if it really takes N steps, then all of the computations involving G are a waste of computational resources.

A typical theorem for Parareal is one proven in [2]:

Theorem 1: *For* $u' = -au$ and $u(0) = u_0$, *let* $F(t_{n+1}, t_n, U_n^k)$ *denote the exact solution at* t_{n+1} *and* $G(t_{n+1}, t_n, U_n^k)$ *be the backward Euler approximation with time step* ΔT. *Then*

$$\max_{1 \le n \le N} \left| u(t_n) - U_n^k \right| \le C_k \Delta T^{k+1}.$$

The proof can be found in [2].

Before interpreting the significance of Parareal, consider Multiple Shooting Methods [3], an older set of algorithms from an earlier era before parallel computers were common. For N intervals for solving (1) with $u(0) = u_0,\ t \in [0,1],$ define

$$U_{n+1}^{k+1} = u_n(t_{n+1}, U_n^k) + \frac{\partial u_n}{\partial U_n}(t_{n+1}, U_n^k)\left(U_n^{k+1} - U_n^k\right). \quad (6)$$

Then the following theorem can be proved. *Theorem 2*: *If in the multiple shooting method*,

$$u_n(t_{n+1}, U_n^k) \approx F(t_{n+1}, t_n, U_n^k), \quad (7)$$

$$\frac{\partial u_n}{\partial U_n}(t_{n+1}, U_n^k)\left(U_n^{k+1} - U_n^k\right) \approx \quad (8)$$

$$G(t_{n+1}, t_n, U_n^{k+1}) - G(t_{n+1}, t_n, U_n^k),$$

then the multiple shooting and Parareal methods coincide.

See [4] for the proof.

Parareal can be interpreted in three fundamentally different ways:

1. Just a solver for the F equations if Parareal iterates until convergence.
2. A new time integrator if the number of iterations is fixed in advance.
3. Different approximations to the Jacobian in (6)-(8) lead to different time-parallel algorithms.

Interpretations 2 and 3 are clearly of interest.

III. Laplace Transform

We solve (2) with $L(u) = -Au$ starting from $u(0) = u_0$. Given some $z \in \mathbb{C}$ and a function $u(\cdot, t)$, the Laplace transform in time is given by

$$\hat{u}(\cdot, z) \equiv L[u](z) = \int_0^\infty u(\cdot, t) e^{-zt}\, dt. \quad (9)$$

We are left solving (9) by any reasonable elliptic partial differential equation solver the transformed problem

$$\hat{u}(\cdot, z) = \left(zI + A\right)^{-1}\left(u_0(\cdot) + \hat{f}(\cdot, z)\right). \quad (10)$$

We assume for some $C_S \in \mathbb{R}^+$ the real parts of the singular points of $u_0(\cdot) + \hat{f}(\cdot, z) \le C_S$. Let the integral contour be a straight line parallel to the imaginary axis,

$$\Gamma \equiv \left\{ z \in \mathbb{C} \mid z(\omega) = \alpha + i\omega, \alpha \ge C_S, \omega \in \mathbb{R} \right\}. \quad (11)$$

The Laplace inversion formula is given by

$$u(\cdot, t) = \frac{1}{2\pi i} \int_\Gamma \hat{u}(\cdot, z) e^{zt}\, dz. \quad (12)$$

When $|z| \gg 0$ and $z \in \Gamma$ has negative real parts, the discretization error in evaluating the integrals in (12) for $u(\cdot, t)$ is significantly reduced for all $t > 0$. We deform Γ to the left half plane with all singularities to its left and a hyperbola contour

$$\Gamma = \left\{ \begin{array}{c} z \in \mathbb{C} \mid z(\omega) = \varsigma(\omega) + is\omega, \omega \in \mathbb{R}, \\ \varsigma(\omega) = \gamma - \sqrt{\omega^2 + v^2} \end{array} \right\}. \quad (13)$$

In essence, the hyperbola contour must be kept away from the spectrum of $-A$ and the singular points of $\hat{f}(z)$.

Define $\psi(\omega) = \tanh(\frac{\tau\omega}{2}) :\ (-\infty, \infty) \to (-1, 1)$. Then

$$u(t) = \frac{1}{2\pi i} \int_\Gamma e^{\left[z(\psi^{-1}(y))t\right]} \cdot \hat{u}\left(z(\psi^{-1}(y))\right) \cdot \left\{\varsigma'(\psi^{-1}(y)) + is\right\} \frac{d\psi^{-1}}{dy}(y) dy,$$

which can be discretized using something as simple as the trapezoidal rule. While it is not obvious mathematically, this last step leads to a roundoff problem that limits how parallel the Laplace transform method is. While it appears that there is no limit to the number of points $z \in \Gamma$ can be chosen, with each point z leading to an elliptic problem that can be solved in parallel, that is not the case, unfortunately.

IV. Numerical Experiment

Consider

$$u_t - \frac{u_{xx} + u_{yy}}{5\pi^2} = 0, \qquad (14)$$
$$u(x,y,0) = e\sin(2\pi x)\sin(\pi y)$$

with the exact solution

$$u(x,y,t) = e^{1-t}\sin(2\pi x)\sin(\pi y).$$

The Laplace transform (9) is given by

$$z\hat{u} - \frac{\hat{u}_{xx} + \hat{u}_{yy}}{5\pi^2} = e\sin(2\pi x)\sin(\pi y) \ in \ (0,1)^2,$$
$$u = 0 \ \partial(0,1)^2,$$

where

$$\Gamma = \left\{ \begin{array}{c} z \in \mathbb{C} \mid z(\omega) + is\omega, \ \mathrm{y} \in (-1,1), \\ \varsigma(\omega) = \gamma - \sqrt{\omega^2 + \upsilon^2}, \\ \omega(y) = \frac{2}{\tau}\tan^{-1} y = \frac{1}{\tau}\log\frac{1+y}{1-y} \end{array} \right\}.$$

Using [5,7], we get $\alpha \approx 1.1721$. Hence, for (11) and (13) we get,

$$\Lambda(\alpha) = \cosh^{-1}\left(\frac{2\alpha}{(4\alpha - \pi)\sin\alpha}\right),$$
$$\gamma = \frac{(4\alpha - \pi)\pi N_z}{\Lambda(\alpha)t},$$
$$\upsilon = \gamma\sin(\alpha), \ s = \gamma\cot(\alpha), \text{ and}$$
$$\tau = \frac{\log(2N_z - 1)}{\gamma\sin(\alpha)\sinh\left(\Lambda(\alpha)\frac{N_z - 1}{N_z}\right)},$$

which is quite complex, but simple to evaluate once α is known.

In our numerical experiments, in order to solve (10), we used $N_z = 32$ points on the hyperbola contour (13), a compact fourth order finite difference discretization on an $N_x \times N_x$ uniform mesh with $N_x = 160$, and MADPACK version 5 for the elliptic partial differential equation solver [6, 7]. In Fig. 1 we see the runtimes for each method. In Fig. 2 we see the speedups for each method. The Laplace transform method is the clear winner for this specific example based on runtimes.

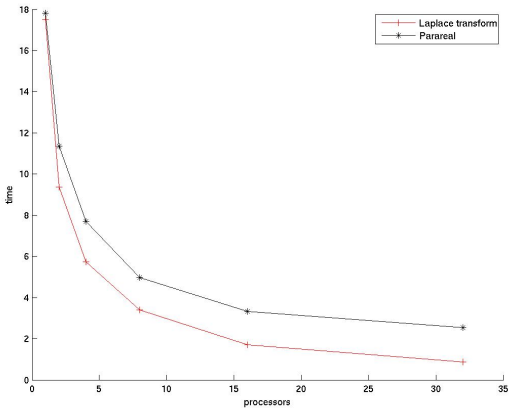

Figure 1. Wall clock time versus processors

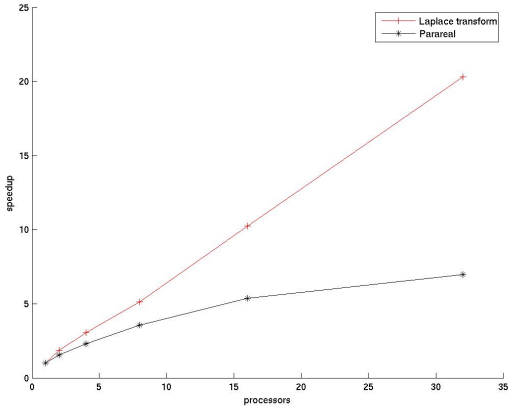

Figure 2. Speedup versus processors

V. CONCLUSIONS

There are at least two families of robust algorithms to create parallel in both time and space ordinary or parabolic differential equation solvers, namely Parareal and the Laplace transform.

For one processing core, neither is appropriate and both are guaranteed to run slower than standard serial solvers.

For a small number of processing cores, the Laplace transform approach will normally be the method of choice. Suppose that there are N_z chosen points on the contour hyperbola. For $P = C_{N_z} N_z$ processing cores, where $C_{N_z} \in \mathbb{N}$ is small, then the Laplace transform is the obvious choice, particularly if $C_{N_z} = 1$. This is because Parareal may use too many iterations, whereas we know we have N_z parallelism trivially with the Laplace transform (and possibly much more depending on the elliptic equation solver used).

For a (very) large number of processing cores, Parareal is the obvious method to try first. This is because a group of processors can be assigned to each time step in the time domain, where the size of the groups is determined by the parallel code used to advance the approximate solutions. Due to roundoff errors, there appears to be limits on how large N_z can be feasibly.

As to the principal question of the paper in Section I, there is no clear answer at this time.

ACKNOWLEDGMENT

This research was supported in part by the National Science Foundation grants CNS-1018072 and EPS-1135483, Air Force Office of Scientific Research FA9550-11-1-0341, National Research Foundation 2011-000344, the City of Seoul WR080951, and King Abdullah University of Science & Technology grant KUS-C1-016-04.

REFERENCES

[1] A. Deshpande, S. Malhotra, C. C. Douglas, and M. H. Schultz, "A rigorous analysis of time domain parallelism," Parallel Alg. Appl., vol. 6, 1995, pp. 53-62.

[2] J. L. Lions, Y. Maday, and G. Turinici, "A parareal in time discretization of PDEs," C. R. Acad. Sci. Paris Ser. I Math., vol. 332, 2001, pp. 661-668.

[3] H. B. Keller, Numerical Methods for Two-Point Boundary Value Problems, Waltham, MA: Blaisdell, 1968.

[4] M. J. Gander and S. Vandewalle, "Analysis of the parareal time-parallel time-integration method," SIAM J. Sci. Comput., vol. 29, 2007, pp. 556–578.

[5] J. A. C. Weideman and L. N. Trefethen, "Parabolic and hyperbolic contours for computing the Bromwich integral," Math. Comp., vol. 76, 2007, pp. 1341–1356.

[6] C. C. Douglas, "Madpack: a family of abstract multigrid or multilevel solvers," Comput. Appl. Math., vol. 14, 1995, pp. 3–20.

[7] C. C. Douglas, I. Kim, H. Lee, and D. Sheen, "Higher-order schemes for the Laplace transformation method for parabolic problems," Comput. Visual Sci., vol. 14, 2011, pp. 39–47.

Inducing Temporal Parallel Properties into Time Dependent Problems

N. Kokulan, C.-H. Lai
School of Computing and Mathematical Sciences
University of Greenwich
London, UK
e-mail: {N.Kokulan, C.H.Lai}@gre.ac.uk

***Abstract*—This paper provides an overview of the current status of methods that may be used to induce parallel properties into the temporal axis for time dependent problems described by differential equations. An extension to problems with two spatial dimensions is also included.**

Keywords-Temporal parallel methods; time dependent problems.

I. INTRODUCTION

Nonlinear time dependent problems appear in many modern applications, such as environmental science, image processing, thermal engineering, etc. Usually a time marching scheme may be employed along the temporal axis to allow explicit or implicit evaluation of the field quantity at a given time. These methods include Euler's method, Runge-Kutta methods, multi-step methods, etc. In addition there is usually a temporal step size restriction that one has to follow in order to ensure stability of an explicit scheme. Even though there is no temporal step size restriction for implicit schemes it is usually not possible to compute directly the field quantity at the final time in a time marching procedure. It is clear that any temporal integration method does not provide parallel properties within the algorithm. Transformation methods were introduced as one way to induce parallel properties into time dependent problems [1].

For some problems fine details of the field quantity at each temporal step are needed in order to provide accurate solutions at later time steps. For examples turbulence, solidification, etc. However in many other problems solution details are only required at only a few crucial steps and the steady state. In these cases effort in finding fine details of the solutions at many temporal steps is not computationally economic. In particular such effort becomes significant in the case of nonlinear problems where a linearisation process is needed. Suitable use of these crucial temporal steps would be able to introduce two temporal levels into the method so that finer details may be obtained in parallel.

The aim of this paper is to discuss computational properties of temporal integration methods and to provide an overview of current methods of inducing parallel properties into the temporal axis of nonlinear time dependent problems. Examples are included to demonstrate the concept. The technique is also generalised to handle problems with two spatial dimensions.

II. PROPERTIES OF TIME MARCHING SCHEMES

In this exposition the time-dependent problem denoted by

$$\frac{\partial u}{\partial t} = F(u, \mathbf{x}, t), \tag{1}$$

where F is a nonlinear functional dependent on u, the derivatives of u, the spatial coordinates $\mathbf{x} = (x, y)$ and the time, is used. It is also assumed that initial conditions are provided at time $t = 0$. A time marching scheme is a temporal integration method requiring a temporal step size δt suitably chosen to be used in the method. Let $t_k = k\delta t$, $k \geq 0$, and $u^{(k)} = u(\mathbf{x}, k\delta t)$.

A. Examples of Temporal Marching Schemes

An explicit scheme for Eq (1) is defined by

$$\frac{u^{(k+1)} - u^{(k)}}{\delta t} = F(u^{(k)}, \mathbf{x}, t_k), \tag{2}$$

and may be re-arranged as

$$u^{(k+1)} = u^{(k)} + \delta t F(u^{(k)}, \mathbf{x}, t_k). \tag{3}$$

Note that Eq (3) is a simple update formula for $u^{(k+1)} = u(\mathbf{x}, t_{k+1})$ which depends solely on the knowledge of F at $t = t_{k+1}$. The update formula has a stability criterion relating the temporal step size and the spatial discretisation imposing in many situations very small value of δt. On the other hand an implicit scheme may be written as

$$\frac{u^{(k+1)} - u^{(k)}}{\delta t} = F(u^{(k+1)}, \mathbf{x}, t_{k+1}), \tag{4}$$

and may be re-arranged as

$$u^{(k+1)} - \delta t F(u^{(k+1)}, \mathbf{x}, t_{k+1}) = u^{(k)}. \tag{5}$$

Note that Eq (5) provides an implicit formula for $u^{(k+1)} = u(\mathbf{x}, t_{k+1})$. Usually a linear system or a nonlinear system is required to be solved. The method does not have any stability criterion governing the temporal step size. However it should be noted that it is impossible to use an unreasonably large δt in Eq (5). In other words it is

978-0-7695-4818-0/12 $26.00 © 2012 IEEE
DOI 10.1109/DCABES.2012.50

impossible to compute the final step simply based on the initial data.

B. Some Parallel Temporal Methods

Almost all parallel temporal methods based on the temporal marching schemes require an iterative approach. This involves partitioning the temporal axis into a number of non-overlapped sections known as the time subdomains and the same time-dependent problem is considered in each of these time subdomains. A shooting method is applied so that the moving targets along the interface of the time subdomains form a nonlinear correlation through a functional equation to which an iterative solution is required. Several researchers have been using this approach. For examples Miranker and Kiniger proposed a family of parallel Runge-Kutta methods [2]; Lions, Maday and Turinici proposed the 'parareal' algorithm in time discretisation [3]. Gander and Vandewalle analysed the parareal algorithm and concluded that it is a version of multiple shooting methods [4], and provided a convergence analysis of the algorithm in [5].

Further enhancement of the about multiple shooting methods may be obtained by using a coarser temporal partitioning in conjunction with a finer temporal partitioning based on the concept of a defect correction principle.

Another popular way of introducing temporal parallel properties into time dependent problems is known as waveform relaxation methods. Gander and Vandewalle give a good review in [4]. The idea is based on a dynamic iterative concept or Picard-Lindelöf iteration which was originally applied to systems of algebraic equations. The iterative method was then extended to handle the system of ODE's resulted from a spatial discretisation of the time dependent problem.

Note that time lagged and overlapped computational efforts are possible if one attempts to update the approximate solutions based on the above parallel temporal integration schemes. The temporal data dependence, i.e. the intrinsic sequential computation and components remain there.

III. Inducing Parallel Properties by Transformation Methods

The idea of transformation has been around for a long time and is used to transform a given problem, depending on several independent variables, to another problem using certain parameters. The aim of such transformation is to produce a simplified equation dependent on the set of parameters only. Such tool was very useful in obtaining analytic solutions to many engineering problems. It was also very useful in studying the long term behavior of many time dependent problems. This section provides an overview of two transformation methods that are often used in obtaining analytic solutions of some nonlinear problems. Two examples are given below to demonstrate how a time dependent problem may be transformed into a parametric equation and the relationship to parallel and distributed algorithms. These parallel properties are induced into the problem itself through the use of transformation. This is the reason why such properties are known as induced parallel properties.

A. Similarity Transformation

For one spatial dimension time dependent problems the idea is to obtain a one-parameter family of transformation relating the independent variables. Substituting the transformation into the original problem leads to a parametric equation which does not involve the time axis.

Consider the linear time-dependent diffusion problem given by

$$\frac{\partial u}{\partial t} = \sigma \frac{\partial^2 u}{\partial x^2}, \quad 0 < x < L, \tag{6}$$

subject to $u(0,t) = u_0(t)$ and other suitable boundary condition at the other end. It is possible to choose the parameter linking the independent variables as $\eta = \frac{x}{\sqrt{\sigma t}}$ and $u(x,t) = u_0 f(\eta)$ lead to the transformed problem

$$\sigma \frac{d^2 f}{d\eta^2} + \frac{1}{2}\eta \frac{df}{d\eta} = 0, \tag{7}$$

subject to suitable boundary conditions transformed from the given ones.

Suppose one would like to compute $u(x,t_k)$, $k = 1,2,...,M$, by means of a finite difference method simultaneously on a spatial mesh with $\delta x = L/(N-1)$, where N is the number of mesh points used in the original problem. Using the parameter $\eta = \frac{x}{\sqrt{\sigma t}}$, one can easily see that $\delta\eta_k = \frac{\delta x}{\sqrt{\sigma t_k}}$ which is the mesh size used in the transformed problem when $t = t_k$. This suggests that the problem described in Eq (7) can be solved simultaneously using different meshes described by $\delta\eta_k$, $k = 1,2,...,M$.

Extension to nonlinear problem is straight forward. As an example consider a problem similar to Eq (6), i.e.

$$\frac{\partial u}{\partial t} = \sigma(u) \frac{\partial^2 u}{\partial x^2}, \quad 0 < x < L, \tag{8}$$

where σ is now a function of u. In order to apply the above technique Eq (8) needs to be linearised. Let $\bar{u}$ be an approximation of $\bar{u}$ of $u(x,t)$ at time t. $\bar{u}$ is updated in an inner iterative update process which involves the solution to the linearised problem $\frac{\partial u}{\partial t} = \sigma(\bar{u}) \frac{\partial^2 u}{\partial x^2}$ that can be solve in parallel by means of the algorithm described above.

B. Laplace Tranformation

Using the same example as in Eq (6) and taking the Laplace transform of $u(x,t)$ leads to

$$\int_0^\infty e^{-\lambda t}u(x,t)dt = U(x;\lambda), \tag{9}$$

such that the dependence on time is now converted to the dependence on the parameter $\lambda \in \left\{\lambda_p = \frac{p\ln 2}{T} : p = 1,2,...,m\right\}$. Here T is the final time of the simulation. This is a finite set of transformation parameters which is closely related to the inverse Laplace transform.

Applying the Laplace transform to Eq (6) leads to

$$\lambda_p U(x;\lambda_p) - u(x,0) = \sigma \frac{d^2U(x;\lambda_p)}{dx^2}, \tag{10}$$

subject to suitable boundary conditions derived from using the Laplace transform of the given boundary conditions. Note that the set of Laplace space solutions $\left\{U(x;\lambda_p) : p = 1,2,...m\right\}$ may be obtained simultaneously by solving Eq (10). The Laplace space solutions are needed to re-construct the solution in the original space. One such method is to apply an inverse Laplace transform using the weighted formula

$$u(x,T) \approx \frac{\ln 2}{T}\sum_{p=1}^{m} w_p U(x;\lambda_p), \tag{11}$$

where w_p can be obtained by means of Stehfast method [6].

The difference between similarity transform method and the Laplace transform method is the retrieval of the solution in the original problem, i.e. $u(x,T)$. The latter method requires additional computation whereas the former method is trivial. The parallelization of the former method should avoid very fine $\delta\eta_k$ whereas the latter method has the same mesh size in the spatial dimension for all of the parallel problems. On the other hand the former method also introduces a convection term into the transformed problem. This term needs careful treatment in terms of numerical computation in order to maintain accuracy. In the latter method no such convection term is introduced.

Extension to nonlinear problems such as the one in Eq (8) is the same where an inner iteration is needed by taking the same linearisation technique as shown in section 3.1.

IV. Using Laplace Transformation for 2-D Problems

Consider the nonlinear parabolic problem

$$\frac{\partial u}{\partial t} + \nabla\bullet\left(\sigma(u)\nabla u\right) = s(x,y,t) \quad \in \quad \Omega\times(0,T], \tag{12}$$

where $\Omega = \{(x,y) : 0 < x < L, 0 < y < L\}$ and subject to suitable boundary conditions on $\partial\Omega$ and initial conditions. Here σ is a given function of u, and s is a given function of x, y and t. For nonlinear problem the above linearisation technique is adopted. The temporal axis is divided into J parts such that $T_j = j\delta T$, $j = 0,1,...,J$. Let $\bar{u}$ be the approximation of $u(x,T_{j+1})$. The linearised problem of Eq (12) defined in the time interval $(T_j, T_{j+1}]$ is given by

$$\frac{\partial u}{\partial t} + \nabla\bullet\left(\sigma(\bar{u})\nabla u\right) = s(x,y,t) \quad \in \quad \Omega\times(T_j,T_{j+1}]. \tag{13}$$

Taking Laplace transform of Eq (13) leads to

$$\begin{aligned} &\lambda U(x,y;\lambda) - u(x,y,T_j) \\ &+\sigma(\bar{u})\nabla^2 U(x,y;\lambda) = S(x,y) \quad \in \quad \Omega \end{aligned} \tag{13}$$

where $S(x,y) = \int_0^\infty e^{-\lambda t}s(x,y,t)dt$.

V. Numerical Examples

Numerical experiments were performed by using an in-house parallel computer, consisting of two dual core each of 2.4 GHz AMD Opteron 2216 and six 4 quad core each of 2.2 GHz AMD Opteron 8354 connected with infiniband memory channel powered through Linux access, to demonstrate the performance of the numerical techniques. Only Laplace transformation method was tested as the other techniques are intrinsic parallel and do not involve any inversion.

A. Problem 1

$\sigma = 0.00038$, $\frac{\partial u(0,t)}{\partial x} = 1$, $u(1,t) = 100$, $u(x,0) = 1$, $T = 1000$, and $m = 8$. Parallel and sequential computing times are listed in Table I.

TABLE I. Problem 1 – Parallel and sequential computing times

Grid points	m = 6		m = 8	
	Sequential	Parallel	Sequential	Parallel
101	0.28	0.09	0.33	0.09
201	2.01	0.63	2.30	0.63
501	25.4	8.15	29.1	8.18
1001	168	54.8	192	54.8

Grid points	m = 10		m = 12	
	Sequential	Parallel	Sequential	Parallel
101	0.37	0.09	0.39	0.09
201	2.52	0.64	2.72	0.64
501	31.9	8.15	34.3	8.15
1001	210	54.8	225	54.8

Grid points	m = 14	
	Sequential	Parallel
101	0.43	0.10
201	2.82	0.64
501	36.3	8.17
1001	238	54.8

B. Problem 2

$\frac{\partial u}{\partial t} = \nabla \cdot (K \nabla u) + S$ where $K = u^2 + 2u + 50$ and S is chosen to have the analytic solution $u = (x^2 + y^2 + 100)e^t$ defined in a unit square with Dirichlet boundary condition. Here $T = 1$. Parallel and sequential computing times are listed below.

TABLE II. PROBLEM 2 – PARALLEL AND SEQUENTIAL COMPUTING

Grid points	m = 6		m = 8	
	Sequential	Parallel	Sequential	Parallel
21	9.08	1.62	1.19	1.64
51	335	58.6	442	58.7

Grid points	m = 10		m = 12	
	Sequential	Parallel	Sequential	Parallel
21	1.48	1.65	1.77	1.66
51	548	58.4	654	58.4

VI. CONCLUSION

An overview of parallel temporal method is given. Numerical examples of one- and two-dimensional nonlinear parabolic problems are used to demonstrate parallel computing times. Scalability of the parallel temporal methods is demonstrated.

ACKNOWLEDGMENT

The first author is sponsored by a University of Greenwich RAE award.

REFERENCES

[1] C.-H. Lai, "On Transformation Methods and the Induced Parallel Properties for the temporal Domain," in Substructuring Techniques and Domain Decomposition Methods, F. Magoulès, Ed, Stirling: Saxe-Coburg Publications, 2010, pp. 45--70.

[2] W.L. Miranker, W. Liniger, "Parallel methods for the numerical integration of ordinary differential equations," Math. Comp., vol. 91, pp. 303—320, 1967.

[3] J.L. Lions, Y. Maday, G. Turinici, "A parareal in time discretisation of PDE's," C.R. Acad. Sci. Paris, Serie I, vol. 332, pp. 661—668, 2001.

[4] M.J. Gander, S. Vandewalle, "Analysis of the parareal time-parallel time-integration method," SIAM J. Sci. Comput., vol. 29, pp. 558—578, 2007.

[5] M.J. Gander, E. Hairer, "Nonlinear convergence analysis for the parareal algorithm," in Lecture Notes in Computational Science 60, Springer, 2008, pp. 45--56.

[6] H. Stehfast, "Numerical inversion of Laplace transforms," Comm ACM, vol. 13, pp. 47—49, 1970.

The Architecture Design Of A Distributed Workflow System

Zheng Haibei
Computer School
Beijing Information and Science Technology University
Beijing, China
zseashell@163.com

Yin Xu
Computer School
Beijing Information and Science Technology University
Beijing, China
yinxu15@126.com

***Abstract*—To solve the problem existing in the traditional centralized workflow system—such as poor scalability and strong coupling between process management and business application, we present the architectural design of a distributed multi-engine workflow system based on web services. The separation of the process logic implementation and the application logic implementation improves the flexibility and scalability of workflow system.**

Keywords- workflow; distribution; multi-engine; web services

I. INTRODUCTION

Workflow has become widely applied to the enterprise information management system and traditionally we directly code the implementation of process management into business application system. Inevitably it has many disadvantages such as strong coupling, poor scalability and information isolation etc. However most modern enterprise application system demands the ability to cope with the distribution, heterogeneous or autonomy problem among different sub-systems, which makes it hard for the traditional centralized workflow system to meet the increasingly complex business process requirements. Under this circumstance, the research of distributed workflow system is becoming a hot issue in both academic realm and enterprise application. Also the development of web services make it technically feasible for us to present an architectural design of distributed workflow system based on web services.

II. WORKFLOW DISTRIBUTION THEORY

Workflow is a process that can be automatically executed according to specific rules. The tasks generated from different nodes in the process can be assigned to different person or organizations, the information and electronic sheet be transferred or shared among different nodes in the process [1]. The concept of workflow originates from the manufacture industry and office automation. It aims at improving working efficiency, lowering the cost of production and optimizing the management of enterprise by dividing the whole working process into different but well defined procedures.

The implementation of distributed workflow system can be classified into three different categories, as follows:

A. The distribution in the architecture of workflow system

The system architecture is divided into five parts according to the workflow reference model presented by WfMC(workflow management coalition). Specifically the five parts are process definition tools, client application, workflow management tools, workflow engine and other related application. And those different parts can interact with each other by the standard interfaces defined by WfMC.

B. The distribution in the process modeling of workflow system

When different companies need to cooperate to accomplish the whole implementation of one business process, for the concern of privacy and asset protection each company is responsible for its own part of process modeling and only provides a interface for further integration of those sub-models. To cope with this situation, firstly the whole process model is divided into different sub-models from top to bottom. Then all different parts will be integrated as the final process model.

C. The distribution in the execution of workflow engines

The workflow engine is the most important part in a workflow system which provides support for the functioning of the whole business process. And the efficiency of the workflow engine is crucial to the workflow system. The distribution of workflow engine is implemented by placing different workflow engines at different nodes to cooperate to finish the execution of one whole business process.

III. WEB SERVICES

Web services are web based applications that use open, XML-based standards and transportation protocols to exchange data with each other over network. A web service often provides an interface described in Web Services Description Language (known as WSDL) for other applications to invoke by using SOAP messages. Because of its platform independence, the technology of web services aims at solving the problem of integration and interaction between different applications.

A typical architecture of Web services contains three different parts, known as service provider, service requestor and service registry center. First the service provider deploys a web service and registers it in the web service registry center [2]. Then the service requestor can find the service by searching in the service registry center. Finally the requestor invokes the method of the service exposed by the provider to finish the whole process of the interaction. The architecture of web services is represented by figure1:

978-0-7695-4818-0/12 $26.00 © 2012 IEEE
DOI 10.1109/DCABES.2012.32

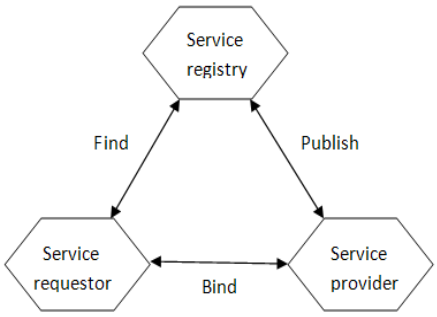

Figure 1. The Architecture of Web Services

SOAP is originally stood for Simple Object Access Protocol which acts as an unseen infrastructure in SOAP-based web services. SOAP is transport-neutral which means it doesn't rely on some specific transport protocol but HTTP is often the most common choice. A typical web services invocation is as follows :a client sends a SOAP message as a service request and the remote web service part will send back another SOAP message as the corresponding response. The back and forth of SOAP message between client and service allows the web services and client to be programmed in different languages which make the interoperability between different platform possible.

IV. THE ARCHITECTURE DESIGN OF THE DISTRIBUTED WORKFLOW SYSTEM

This workflow system aims at separating the process management from business application by using the technology of web services to implement the distribution in the execution and deployment of different workflow engines [3].

A. The Architecture Design

This distributed workflow system can generally be divide into three parts: client agent, the controller engine and domain engines which are distributed physically at different locations. The controller engine and domain engines are all deployed as web services described by web service description language and registered in the UDDI registry center. The client agent act as a proxy who will take over to interact with the service part of the system when the business application sends out a workflow related request. The client agent will bind to the web service of controller engine by finding the service endpoint in the UDDI registry center. And then the agent will send SOAP message which carries the request information from the business application to the controller engine[4]. Finally the controller engine will route the request to some specific domain engine for processing according to the request's domain attribute. After finishing the process related handling on the domain engine, the response will be sent back to the business application. When it comes to a situation that a sub-process or some activity of the process need to be executed on some other different physical nodes, more than one domain engines would be needed to collaborate with each other to accomplish the whole execution of this process and the controller engine would coordinate different domain engines to ensure the functioning of the whole process. One point to be mentioned is that some specific domain attribute should be assigned to every process template when we defined the process model at the beginning. This makes sure that those requests involving workflow related operation can be identified by the controller engines and then be routed correctly to the corresponding domain engine for processing according to its domain attribute.

- Client Agent: The client agent act as an intermediary, it will encapsulate all the requests sent from business application and then communicate with the service provider asking for handling of the process related request. In order to figure out who it will turn to for further handling when receiving the request, the client agent needs to find and bind to the web service of controller engine. The agent will serialize the encapsulated request into XML-format byte stream which is embedded into the SOAP body, then the SOAP message be sent to the controller engine service.
- Controller Engine: The controller engine act as a front controller which is responsible for receiving the process related request sent from the client agent and then dispatching the request to some specific domain engine. And when it comes to a situation that some of the different domain engines are needed to cooperate with each other to finish the whole execution of one process, the controller engine will coordinate those domain engines to ensure the data transfer among different domain engines. Along with the controller engine, a workflow database is needed to store the process templates and the domain attribute of those templates. So the controller engine can dispatch the process related request to the right domain engine for handling according to the domain attribute of the process instance. Also the execution information of process on all domain engines and the related data of the workflow instance are stored into the database, which makes it much more easy to monitor and manage the functioning of the whole process. A historical database is deployed to record the information of those process instance already accomplished. A work-item database is used to store the work-item generated at each node of the process.
- Domain Engine: Domain engine is responsible for instantiation and implementation of the process instance and activities of the process within its domain. when the domain engine receive the SOAP message dispatched from the controller engine, it will deserialize the XML-format byte stream in the SOAP body into a request object. After finishing the handling of the process related request, it will send back the result through the controller engine to the client. And a process instance database is deployed to store the necessary information of the process instance within its own domain. Besides a process template database is also needed to store a copy of

process template data of the workflow database on the controller engine part.

The whole procedure of how a business application sends out a process related request and then request dispatched by the controller engine and finally get handled by the domain engine is described by figure2:

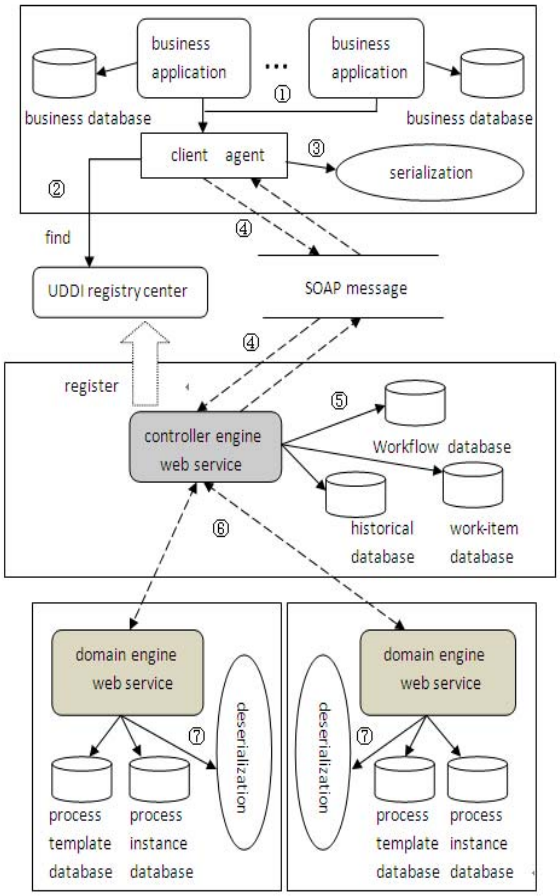

Figure 2. The Architecture Design of The Distributed Workflow System

①:The client agent receive a workflow related request for instantiation of a request message object which encapsulates request parameters and some other related information.

②:The client agent will manage to find the endpoint URL of the controller engine web service in the UDDI web service registry center.

③:Then the request object is transformed into XML-format byte stream by serialization operation.

④:The XML bytes will be embedded into a SOAP message body and then be sent to the controller engine service using a web services engine, axis2 for instance [5].

⑤:when the controller engine receive a process related request from the client agent, it will first search the workflow database to retrieve the corresponding process template and its domain attribute of the process instance or activity in order to decide the request should be sent to which domain engine for final handling.

⑥:As the domain engines are also deployed as web services, the communication between controller engine and domain engine is also via sending SOAP message by a web services engine, specifically axis2 in this system.

⑦:when the domain engine receives a SOAP message from controller engine, it will first get the XML bytes in the SOAP body and then deserialize them into request object. After handling of the java object model which represents the request message, the result will be sent back to the client.

B. The request and response message model structure design

The message structural design is present as a basic support for the communication across the client agent, the controller engine and the domain engines. The class diagram of the whole object model design is represented by figure3:

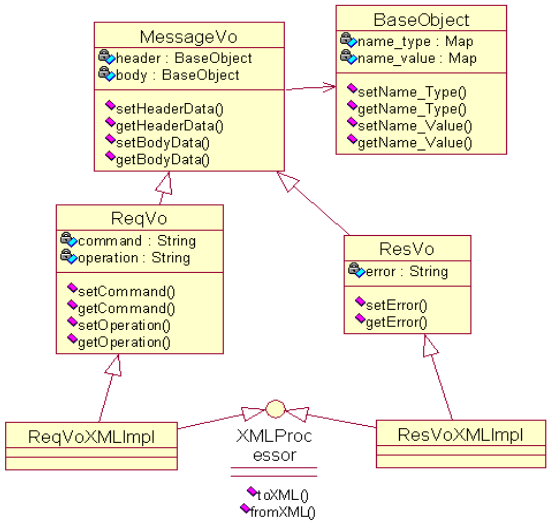

Figure 3. The Class Hierarchy Diagram of Message Object Model

If we want to get the integral information of a parameter, it should be described at least from three aspects: parameter name, parameter type and parameter value. As there is no three dimensional mapping model in java data structure, we present a solution by using two Map object to separately store the name and its type mapping information and the name and its value mapping information. BaseObject has two Map type member variables used to store the mapping of name-type and name-value of parameter. MessageVo is a base value object of the request and response message object. It consist of a header and a body whose type are both BaseObject, and the header encapsulate some common attribute of the message such as message ID ,etc; the body are used to store the process related parameter as a request message body, while the result of handling as a response body. The ReqVo which represents the request value object extends from MessageVo and adds two more key properties: command and operation property, the command property is actually a full name of a class which is

responsible for the request handling on the domain engine; the operation property is the truly operating method name of the class. By providing the handling class name and method name, the domain engine can decide to instantiate which class and invoke which method in the class according to those two properties to finally finish the handling work of the workflow related request. The ResVo which represents response value object add an error property to reflect if the request is correctly handled. As we need XML-format byte stream to assemble the SOAP message for different part of the system to communicate, an interface named XMLProcessor has two member methds: toXML()and fromXML() which are used to deal the problem of the transforming between java object model and XML-format byte stream. ReqVoXMLImpl and ResVoXMLImpl both implement the XMLProcessor interface, thus become the kind of request and response value object which support the serialization and deserialization operation.

The communication chain of request and response during the whole procedure is represented by figure4 and figure5 as follow:

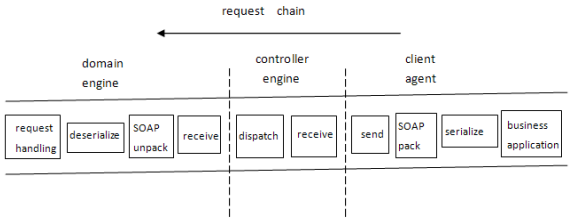

Figure 4. The Request Chain

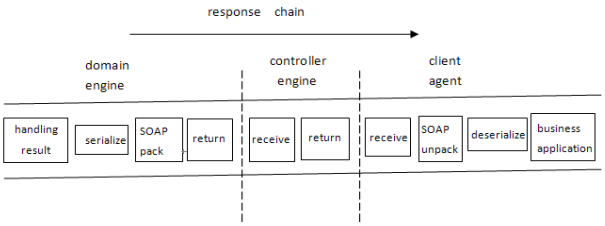

Figure 5. The Response Chain

V. ANALYSIS OF THE DESIN

A. *Advantages*

- the client agent provide a unified interface to deal with the multiple request from the business application ,which solve the tight coupling between the application layer and request handling layer.
- When it come to a situation that more than one domain engines are needed to cooperate to finish the execution of one process, the domain engines communicate with each other via the controller engine rather than with each other directly, which make it easier to maintain the consistency of the data in the distributed system.

B. *Problems Solution*

- It may occurs that some domain engine gets over-loaded caused by the frequent request with the same domain attribute asking the same domain engine for handling, which may result in the deterioration of the performance. As for this problem we can use some balancing strategy to balance the load on each domain engine.
- Frequent request for the engine web service may cause the problem of delay of the response. We can set cache on the client and make the server selectively write back some reusable workflow related information into the client in order to improve the performance of the whole system.

VI. CONCLUSIONS

The structure design of the distributed workflow system based on web services presents a relatively effective solution for the problem of the traditional centralized workflow system such as poor ability in supporting interoperation between different platforms. Also there are some design defects, for instance the data synchronization between the cache set on the client and the workflow engine still has much space to advance etc. Those problems unsolved in the system need to be worked on in the future in order to improve the overall performance of this workflow system.

ACKNOWLEDGMENT

Our research was supported by Science and Technology Funding Project of Beijing Education Committee KM201110772015 and Beijing talent education deepen and innovation project PHR200907220.

REFERENCES

[1] Yushun Fan. Fundamentals of Workflow Management Technology [M]. Tsinghua University Press, 2001. (In Chinese)

[2] Steve Graham. Use Java To Build Web Services [M]. Machinery Industrial Publishing Company, 118. 2003.

[3] Qiao Liang. The Design of A Multi-engine Workflow System Based on J2EE [M]. Ms D Thesis. Jilin University. 2003.

[4] Xiao bin, Qing Guangyuan. The Implementation of A Service Oriented Workflow System Based on Web Service [J]. Computer and Information Technology. 2009.

[5] Martin Kalin. Java Web Services Up and Running [M]. O'REILLY, 2009.

An Improved Multi-core Shared Cache Replacement Algorithm

Fang Juan
College of Computer Science
Beijing University of Technology
Beijing, China
e-mail: fangjuan@bjut.edu.cn

Li Chengyan
College of Computer Science
Beijing University of Technology
Beijing, China
e-mail: lisa890608@126.com

***Abstract*—Many multi-core processors employ a large last-level cache (LLC) shared among the multiple cores. Past research has demonstrated that traditional LRU and its approximation can lead to poor performance and unfairness when the multiple cores compete for the limited LLC capacity, and is susceptible to thrashing for memory-intensive workloads that have a working set greater than the available cache size. As the LLC grows in capacity, associativity, the performance gap between the LRU and the theoretical optimal replacement algorithms has widened. In this paper, we propose FLRU (Frequency based LRU) replacement algorithm, which is applied to multi-core shared L2 cache, and it takes the recent access information, partition and the frequency information into consideration. FLRU manages to filter the less reused blocks through dynamic insertion/promotion policy and victim selection strategy to ensure that some fraction of the working set is retained in the cache so that at least that fraction of the working set can contribute to cache hits and to avoid trashing; meanwhile we augment traditional cache partition with victim selection, insertion and promotion policies to manage shared L2 caches.**

Keywords-component; multi-core;replacement; shared cache

I. INTRODUCTION

Chip Multi-Processors (CMPs) have become a mainstream design choice for modern high-performance microprocessors with excellent performance. One of the key issues facing multi-processors is the higher and higher power consumption, which may in return leads to performance reduction. To lower the power consumption, many researchers have focused on the management of the on-chip shared last-level cache(LLC), which dominates in the processor's whole power consumption and proposed a variety of techniques to manage the LLC to provide better performance and fairness [1, 2, 3, 4, 5, 6, 7, 8, 9, 10, 11, 12]. Most of these schemes include the following three steps: information collection, policy selection, and enforcement. Information collection takes charge of collecting the memory reference behaviors; the policy selection decides the way to improve the performance, and the enforcement mechanism manages to implement it.

As we all know a cache miss will cause the processor to stall hundreds of cycles, and accesses to memory will lead to more power than accesses to cache. So paying attention to reduce the cache misses may make a contribution to improve the entire performance. The LRU replacement policy and its approximations have remained as the de-facto standard for replacement decisions in LLC. Recent studies have shown that in multi-processor system with a highly associative caches and a bigger capacity, the performance gap between the Least Recently Used (LRU) and the theoretical optimal replacement algorithm is large, (up to 197%) especially in the number of misses [13, 14]. One reason for this performance gap is that LRU replacement inserts a new block into the MRU position and gradually demotes its priority until it arrives at the LRU position, which means it can be evicted. However, in this condition a line that is no longer needed or only used twice has to occupy the cache until it becomes the LRU line in its set before it can be evicted. We call this unnecessary time dead time, which means, this block has become a dead block and never reused again. Apparently this dead time becomes longer with larger cache associativities. Another reason is that for memory-intensive workloads whose working set is greater than the available cache size, LRU behaves badly. That means the locality is not that obvious and large working set may leads to trashing. The other reason is that LRU replacement algorithm does not consider the access frequency and the core-to-core interference, which play an important role in multi-core processors accesses. For the above aspects, researchers propose corresponding solutions, including cache partition, insertion/promotion policy, access frequency based replacement algorithm and so on. This work gives a comprehensive consideration about multi-core interference, access frequency, insertion/promotion policy with the purpose of improve the performance and lower power consumption through lower cache miss rate.

The rest of our paper is organized as follows: section II describes the current situation of multi-core processors; section III gives the FLRU algorithm and section IV is the methodology and results of our experiments; we make a conclusion in section V.

II. BACKGROUND

Most main-stream CMPs use a large capacity and high association shared last level L2 cache to provide a fast access to resources. But compared to single-core processors, there exist many specific features. First, thread interferences are still a big problem and even more complicated, especially in CMPs: conflicting accesses to shared L2 cache will lead to a big performance reduction of concurrent executive threads; the real cache capacity of a thread will be influenced by

978-0-7695-4818-0/12 $26.00 © 2012 IEEE
DOI 10.1109/DCABES.2012.39

other threads, whose execution time will be uncertain. Second, for memory-intensive workloads whose working set is larger than the available cache size, trashing phenomenon may appear, which will lead to performance reduction. We observe that for some applications, there exist many cache lines that get brought into the cache and then are never used again or just reused few times before they are evicted. So we should try to retain some fraction of the working set in the cache so that at least that fraction of the working set can contribute to cache hits. Third, LRU doesn't take access frequency into consideration, which may contribute to performance enhancement. All these features motivate us to give a comprehensive consideration of multi-core processors with a new scheme instead of one sense only.

There have been numerous proposals to improve the performance of LRU. These works can be mainly classified into three parts: way granularity cache partitioning [1, 5, 6, 8, 11, 12] dynamic insertion/promotion policy [4, 20, 21, 22, 23, 25] and frequency based replacement policy [15, 16, 17, 18, 19, 24]. Cache partition mitigates inter-application cache contention by partitioning the cache based on how much the application is likely to benefit from the cache. Dynamic insertion/promotion policy improves cache performance through retaining some fraction of the working set in the cache so that at least that fraction of the working set can contribute to cache hits. Frequency based replacement policy takes access frequency into consideration when choosing a victim block, which plays am important role in cache access. While previously proposed work has also adopted counters for monitoring access frequency, they did not consider shared caches in CMPs which is the main factor of performance reduction. For cache partition has been a trend in multi-core, it is necessary to combine cache partition with other schemes.

In this paper, we mainly discuss how to combine the benefits of cache partitioning, cache insertion/promotion and frequency information together, and finally augment traditional cache partitioning with insertion/promotion and frequency based replacement policies. First, we partition cache ways into N parts, ensuring every core has its own belonging ways, and the replacement victim is chosen based on the partition and we allow cache way stealing among different cores. Next, we maintain M LRU ways as candidates to evict. When it comes to a victim selection, we choose a way in the M, according to the partition, cache stealing and the access frequency information. Finally, we propose an insertion/promotion policy to implement both dynamic insertion policy and dynamic promotion policy with a new method, regarding cache partition and the frequency information.

III. ALGORITHM

A. Cache Partition Policy

We adopt an average cache partition method in our paper, which partitions cache ways into N parts according to the number of cores, ensuring every core has its own belonging ways. The replacement victim is chosen based on the partition and we allow cache way stealing to a certain extent among cores. We maintain a table to record the stealing info. The main purpose of cache partition is that cache partition is an effective way to reduce cache confliction, so that we should take cache partition into consideration when modify cache replacement. We can adopt a more efficient partition method, and this is what to do next.

B. Insertion/Promotion Policy

We divide cache replacement into 3 steps: victim selection, block insertion and priority promotion. Victim selection provides the block to evict, block insertion decides the suitable insertion position, and priority promotion promotes the priority of the hit block based on the principle of locality. Fig. 1 illustrates an example cache set with sixteen lines, logically organized left-to-right from highest priority (A: keep in the cache) to lowest priority (P: to be evicted). For LRU replacement, the priority ordering is the access sequence (the least recently accessed line has the lowest priority for retention). When it comes to a miss, traditional victim selection will choose the LRU line to evict, inserting the new block into the MRU position (a). If hit, a non-MRU block will be promoted to the MRU position. It has been observed that there are cache lines that are accessed only once and then never accessed again [20, 25]. By installing these lines in the highest priority positions, LRU actually maximizes the blocks' occupation time of the cache without any performance profit. Paper [8] proposes a LRU Insertion Policy (LIP) which puts the new block into the LRU position (b). For non-reused lines, insertion of this particular line into the LRU position is actually much better as this minimizes the amount of time that the line spends in the cache. Paper [9] proposes a single incremental promotion policy (SIP), which moves the target block forward step by step as compared to traditional MRU promotion, LIP and SIP can both reduce the delay time of non-reused blocks but will have negative effects on those reused blocks. The two policies both choose the LRU block to evict.

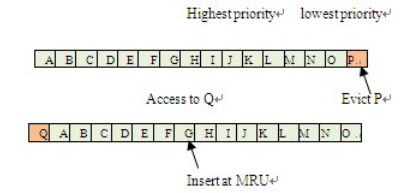

(a) Conventional LRU insertion policy

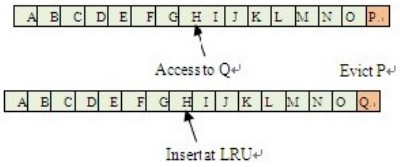

(b) LIP insertion policy

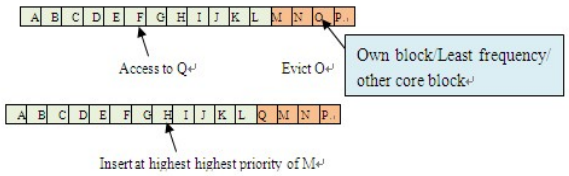

(c) FLRU insertion policy

Figure1. Different insertion policy

FLRU implements both Dynamic Insertion Policy and Dynamic Promotion Policy with a new method, regarding cache partition and the frequency information. We insert a new block in to the Mth (the number of candidates to evict) position instead of LRU and MRU (c), which will avoid dead block occupying too long time and reused block being evicted too fast. And when there's a cache hit, promote the block to the MRU position or M position according to the hit block characteristic. In our algorithm, we choose a victim block in three conditions based on the frequency, partition and stealing information, which will be elaborated in the following FLRU algorithm.

C. *Frequency Policy*

We use a counter to record the access frequency of every line and maintain M LRU ways as candidates to evict. When it comes to a victim selection, we choose a way in the M, according to the access frequency of the M candidates, the partition and the stealing information of concurrent core. The block with lowest frequency will be most probably but not definitely evicted, because we have to take partition information, cache stealing information into account. Table 1 shows the logical cache structure with counter. We add each cache line with a counter and it records the access frequency of the line. When there is a victim selection, take the counter into consideration instead of the LRU only. Partition information means the current core needs to select a victim within its own belongings. Cache stealing information is that a core may put its own blocks into other core's belonging ways when its belonging ways is full and the other's is available. Cache stealing provides a solution to the phenomenon that different cores have different access pattern. When there's a cache selection, we take all those information into consideration instead of LRU information only in order to make a best choice.

TABLE1. LOGICAL CACHE STRUCTURE WITH COUNTER

Tag	Data	LRU	Counter
1011	...	0001	11000110
1100	...	0111	11000011
0110	...	0010	11000010
0011	...	0001	11000001

D. *FLRU Algorithm*

Here assume N cores, L ways, and partition L into N parts, with every core owns L/N ways $\Pi = \{\pi_1, \pi_2 \ldots \pi_n\}$. Table s maintains the stealing information, core (i, j).core=1, means $core_j$ contains a block of $core_i$ and core (i, j).index[x] [y] =1, x is the corresponding set, y means the specific way. Select a victim within the M LRU lines（$w_1, w_2 \ldots w_m$）, here assume concurrent access core is i ,set number is x, and with a cache access, the algorithm is as follows:

1) Victim Selection

a) If there's a belonging block among the M LRU, that is w_i belongs to $core_i$, w_i is the victim, else

b) If $core_i$ contains block of other cores, that is core (j, i).core=1, and core (j, i).index[x] [y] =1, evict block y, and clear the corresponding record of core (j, i), else

c) Evict the lowest frequency block of M, and record the stealing info.

2) Insertion Promotion

a) Insert the block into the highest priority of the M

b) Update the access frequency of the hit block

3) Promotion Policy

a) When it comes to a cache hit,if the hie block is one of the M, promote block to the M position,else

b) promote block to the M position

c) Update the access frequency of the hit block

Traditional LRU inserts a new block into the MRU position, which extends the occupation time of dead blocks. DIP [9] inserts a new block into the LRU position which minimizes the time but may cause trashing phenomenon that the LRU block will be used again while it has already been evicted. Here our policy inserts a new block into the highest priority position of the M candidates, which avoids a long occupation and a soon eviction in the meantime. When selecting a victim line, we take frequency, LRU and partition information into consideration instead of only the LRU, this makes the replacement process more accurate , so as to get a lower miss rate. As our algorithm is used when there's a cache miss, there's no influence on the other access modules. Furthermore since the reference table is small; it can be located on chip. Experimental results show that the FLRU replacement algorithm low the miss rate and runtime greatly with an average of 22%, 28.12%.

IV. EXPERIMENTAL EVALUATION

A. *Experimental Environment*

We use a full-system experiment simulator SIMICS with a General Execution-driven Multiprocessor Simulator (GEMS) which provides a more detailed simulation. We use speccpu2000 suits as benchmarks, and choose 3 memory-intensive benchmarks gzip, vpr, bzip2 then get their IPC, MISSES, RUNTIME respectively. Our baseline CMP contains 4 cores, with independent data and instruction 8-way, 32KB L1 cache each, and shared 16-way, 2MB L2

cache; the block size is 64B. Table 2 gives the detailed simulator configuration.

TABLE2. SIMULATION CONFIGURATIONS

Processor Configuration	
Chip Num	1
Core per Chip	4
Frequency	2GHz
Micro Structure	Out of order,4 issue width, one cycle per instruction
Memory configuration	
L1 Cache	Private I-Cache and D-Cache I-cache：32KB，block size 64B，8-way, hit overhead 3 cycles D-cache：32KB，block size 64B，8-way ，hit overhead 3 cycles
L2 Cache	shared，2M B，16-way，block size 64B ，hit overhead 12 cycles
Memory	Access delay 400 cycles， 4GB

B. Experimental Result

We use average shared L2 cache partition with LRU replacement as the baseline, and evaluate the performance with 4 cores. Fig. 2 shows the runtime of the two schemes. We can see that the runtime has been shortened by 1.96%, 38.4%, and 44.4%, with an average of 28.12%. This is because our scheme makes a difference in core interference and makes a better use of different access pattern among different cores.

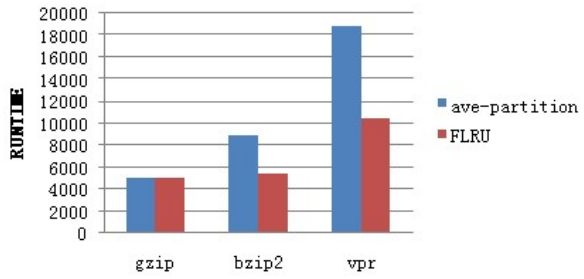

Figure2. Runtime of benchmarks

Fig. 3 illustrates the total misses of the two schemes. From the figure misses are reduced by 6.62%, 34.2% and 25.2%, with a comparatively increase of 22% averagely. With lower misses, the runtime can also be shortened, and this means our replacement algorithm has made a progress in miss rate compared to the LRU.

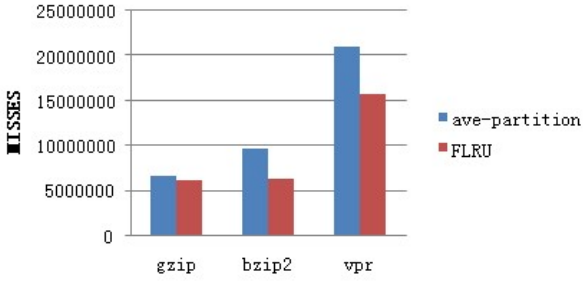

Figure3. L2 cache Misses

Fig. 4 is the total IPC of the two schemes. From the figure IPC has improved by 0.06%, 2.4% and 3.6% with an average of 2.02%. Apparently, with shorter runtime and lower miss rate, the IPC will be improved accordingly. This further proves our performance improvement.

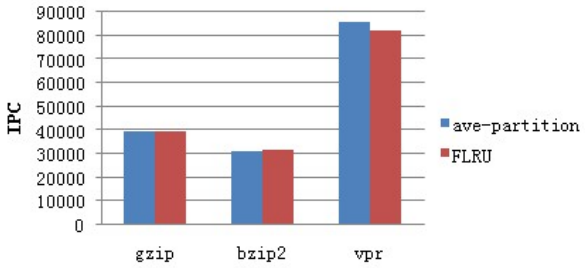

Figure4. IPC improvement

In general, our scheme has an obvious improvement in multi-core performance with low overhead, a 32KB counter, accounting for 1.5% of L2 cache, and a core-to-core stealing table of little capacity.

V. CONCLUSIONS

Many previous studies have proposed a variety of mechanisms to improve the performance of shared last-level cache by exploiting a variety of common memory access behaviors. In this work, we have introduced a technique that can combine the benefit of cache partition, adaptive insertion/promotion and inter-core capacity stealing together. By taking multi-core and their partition into consideration, FLRU arguments cache partition with insertion/promotion policy and frequency information, and our scheme delivers higher performance than previously proposed techniques.

With a good performance improvement, this work has a lot to extend to get a further success. First, we can adopt a more efficient partition mechanism. Second we plan to take way prediction into consideration, and combine way prediction, way partition and insertion/promotion policy together to get a much better result.

ACKNOWLEDGMENT

This work was supported by General program of science and technology development project of Beijing Municipal Education Commission (KM201210005022) and other

government sponsors. We thank the efforts of our reviewers for their helpful suggestions that have led to several important improvements of our work. We also thank all the teachers and students in our lab for helpful discussion.

REFERENCES

[1] D. Chandra, F. Guo, S. Kim, and Y. Solihin. Predicting Inter-Thread Cache Contenton on a Chip Multi-Processor Architecture. In Proc. of the 11th Int. Symp. on High Performance Computer Architecture, pages 340−351, SanFrancisco, CA, USA, Feb. 2005.

[2] J. Chang and G. Sohi. Cooperative Cache Partitioning for Chip Multiprocessors. In Proc. of the 21st Int. Conference on Supercomputing, pages 242−252, Seattle, WA, June 2007.

[3] L. R. Hsu, S. K. Reinhardt, R. R. Iyer, and S. Makineni.Communist, Utilitarian, and Capitalist Cache Policies on CMPs: Caches as a Shared Resource. In Proc. of the 15th Int. Conference on Parallel Architectures and Compilation Techniques, pages 13 − 22, Seattle, WA, USA, Sep. 2006.

[4] A. Jaleel, W. Hasenplaugh, M. Qureshi, J. Sebot, S. S. Jr., and J. Emer. Adaptive Insertion Policies for Managing Shared Caches. In Proc. of the 17th Int. Conference on Parallel Architectures and Compilation Techniques, 2007.

[5] S. Kim, D. Chandra, and Y. Solihin. Fair Cache Sharing and Partitioning in a Chip Multiprocessor Architecture. In Proc.of the 13th Int. Conference on Parallel Architectures and Compilation Techniques, pages 111 − 122, Antibes Juan-les-Pins, France, Sep. 2004.

[6] J. Lin, Q. Lu, X. Ding, Z. Zhang, and P. Sadayappan. Gaining Insights into Multicore Cache Partitioning: Bridging the Gap between Simulation and Real Systems. In Proc. of the 14th Int. Symp. on High Performance Computer Architecture,pages 367−378, Salt Lake City, UT, USA, Feb. 2008.

[7] M. K. Qureshi. Dynamic Spill-Accept for Scalable High-Performance Caching in CMPs. In Proc. of the 15th Int. Symp. On High Performance Computer Architecture, Raleigh, NC, USA, Feb. 2009.

[8] M. K. Qureshi and Y. N. Patt. Utility-Based Cache Partitioning: A Low-Overhead, High-Performance, Runtime Mechanism to Partition Shared Caches. In Proc. of the 39th Int. Symp. On Microarchitecture, pages 423−432, Orlando, FL, Dec. 2006.

[9] N. Rafique, W.-T. Lin, and M. Thottethodi. Architectural Support for Operating System-Driven CMP Cache Management. In Proc. of the 15th Int. Conference on Parallel Architectures and Compilation Techniques, pages 2−12, Seattle, WA, USA, Sep. 2006.

[10] S. Srikantaiah, M. Kandemir, and M. J. Irwin. Adaptive Set-Pinning: Managing Shared Caches in Chip Multiprocessors. In Proc. of the 13th Symp. On Architectural Support for Programming Languages and Operating Systems, Seattle, WA, USA, Mar. 2009.

[11] H. S. Stone, J. Tuerk, and J. L. Wolf. Optimal Paritioning of Cache Memory. Trans. on Computers, 41(9):1054−1068, Sep. 1992.

[12] G. E. Suh, L. Rudolph, and S. Devadas. Dynamic Partitioning of Shared Cache Memory. Jour. Of Supercomputing, 28(1):7−26, 2004.

[13] W.-F. Lin and S. K. Reinhardt. Predicting last-touch references under optimal replacement. University of Michigan Tech. Rep.CSE-TR-447-02, 2002.

[14] R. L. Mattson, J. Gecsei, D. Slutz, and I. Traiger. Evaluation Techniques for Storage Hierarchies. IBM Systems Journal, 9(2), 1970.

[15] John TRobinson, and Murthy V. Devarakonda,“Data Cache Management Using Frequency-Based Replacement,” In SIGMET-RICS, vol.18, p. 134-142, May 1990.

[16] Donghee Lee, Jongmoo Choi, Jong-Hun Kim, Noh, S.H., and Sang Lyul Min,”LRFU: A Spectrum of Policies that Subsumes the Least Recently Used and Least Frequently Used Policies,” IEEE Transactions on Computers,vol.50,pp.1352-1361,Dec 2001,doi: 10.1109/TC.2001.970573

[17] Jaafar Alghazo,Adil Akaaboune, and Nazeih Botros,”SF-LRU Cache Replacement Algorithm,” MTDT '04 Proceedings of the Records of the 2004 International Workshop on Memory Technology, Design and Testing,pp.19-24,2004

[18] Mazen Kharbutli, and Yan Solihin,”counter-based cache replacement algorithms,” IEEE International Conference on Computer Design,pp.61, Oct 2005,ios:10.1109/ICCD.2005.41

[19] Haakon Dybdahl, Per Stenström, and Lasse Natvig,”An LRU-based Replacement Algorithm Augmented with Frequency of Access inShared Chip-Multiprocessor Caches,” MEDEA '06 Proceedings of the 2006 workshop on MEmory performance,pp.45 – 52,2006.

[20] Moinuddin K. Qureshi,Aamer Jaleel,Yale N. Patt,Simon C. Steely, and Joel Emer,”Adaptive Insertion Policies for High Performance Caching,” ISCA '07 Proceedings of the 34th annual international symposium on Computer architecture,pp.381-391,May 2007.

[21] Yuejian Xie, and Gabriel H. Loh,”PIPP: Promotion/Insertion Pseudo-Partitioning of Multi-Core Shared Caches,” In Proc. of the 36th Intl. Symp. on Computer Architecture,June 2009

[22] Jonathan D. Kron , Brooks Prumo , Gabriel H. Loh Double-DIP: Augmenting DIP with Adaptive Promotion Policies to Manage Shared L2 Caches

[23] Xiufeng Sui,Junmin Wu,Guoliang Chen,Yixuan Tang, and Xiaodong Zhu,”Augmenting Cache Partitioning with Thread-Aware Insertion/Promotion Policies to Manage Shared Caches,” CF '10 Proceedings of the 7th ACM international conference on Computing frontiers”,pp. 79-80,2010.

[24] Aamer Jaleel,Kevin B. Theobald,Simon C. Steely, Jr. , and Joel Emer ,”High Performance Cache Replacement Using Re-Reference Interval Prediction (RRIP),” ISCA '10 Proceedings of the 37th annual international symposium on Computer architecture,pp.60-71,June 2010.

[25] Xi Zhang, Chongmin Li, Haixia Wang, and Dongsheng Wang, ”A Cache Replacement Policy Using Adaptive Insertion and Re-Reference Prediction , ”2010 22nd International Symposium on Computer Architecture and High Performance Computing,pp.95-102,Oct. 2010

An improvement to affine decomposition on distributed memory architecture

Ding rui
National Digital Switching System Engineering and Technological Research Center
Zhengzhou, China
dr2012earth@gmail.com

Zhao Rongcai, Liu Xiaoxian
National Digital Switching System Engineering and Technological Research Center
Zhengzhou, China
Xiaoxian0321@gmail.com

***Abstract*—Automatic decomposition is an optimization technique that distributes computation and data onto different processors. The consequence of decomposition directly affects the performance of parallel program. Since every computing node has its own memory in distributed memory parallel computers (DMPCs), false dependence does not hinder the parallelism. Affine decomposition is an effective method to represent and derive computation partition and data distribution, and its principle of adding dependence constraint is too strict to gain more parallelism. Some loop nests do not satisfy the affine condition, and are prohibited from parallelism by affine decomposition. However, if only the irregular access is caused by indirect array, loop and array reference can be partitioned at compile time. To tackle above problems of affine decomposition, an improved static decomposition algorithm of DMPCs proposed in this paper. The experimental results show that this algorithm can improve the performance of parallel programs.**

Keywords-affine decomposition; false dependence; indirect array; automatic parallelization;

I. INTRODUCTION

The growing complexity of the system architecture of modern high performance computers brings great difficulties for programmers coding parallel program. Automatic parallelization is a compiling technique, which automatic detects potential parallelism for serial program and transforms it to an equal parallel program. Automatic parallelization has significant impact on automatic generation of multi-level granularity and storage parallel program, and also assists programmer in designing parallel program.

Every computing node has its own memory on DMPCs. Explicit message passing is needed for inter-node data exchange. Because local memory access speed of the computing node is much faster than remote memory access, in automatic parallelization process, reasonable computation and data decomposition onto each processor is one of the key points in realizing parallel compiling under distributed memory environment.

Affine decomposition proposed by Anderson and Lam in [1] is an effective method to represent and derive computation partition and data distribution, and it's widely used in automatic parallelization research. It's very convenient for back-end to generate the target parallel code on account of affine decomposition considers data and computation at the same time. The architecture which is faced on by affine decomposition covers the distributed memory and shared memory. It also decided that it must enforce strict dependence constraint adding to limit the parallel of false dependence (anti and output), in order to ensure that the decomposition does not cause communication.

Many papers have been devoted to the research of automatic decomposition for DMPCs [1-9]. When coming cross anti and output dependences, the popular way to remove the dependence is to use some proposed methods, which include array data flow analysis, variable expansion, variable renaming and node splitting [10-12]. On shared memory parallel computers (SMPCs), memory is a unified addressing. After parallel execution, the results are written back to memory, without regard to the consistency of data distribution between the loops. So these methods have been proved very useful for affine decomposition to improve parallelization on SMPCs.

The situation is more complicated on DMPCs and the use of these technologies may lead to data redistribution. More importantly, the array privatization is naturally present on distributed memory architecture. False dependence does not hinder the parallelism and these technologies are not so necessary. But strict dependence constraint adding principle of affine decomposition still works, limit the parallelization of program.

Affine decomposition is for the domain of dense matrix code where the loop bounds and array subscripts are affine functions of the loop indices and symbolic constants. Although most of the practical applications satisfy this condition, still some do not, so as to be prohibited from parallelism by affine decomposition. Most previous research only can parallel irregular loop and array at run time or use feedback [14-16]. In fact, if only the irregular access is caused by indirect array, loop and array reference can be partitioned at compile time on DMPCs, and the parallel does not cause data competition.

Since the constraints added by affine decomposition are too strict on DMPCs, an improved static decomposition algorithm is proposed by this paper. Firstly, change the adding principle of dependence constraint of affine decomposition and release the restrictions on the false dependence. Secondly, if only the irregular of loop and array is caused by indirect array, partition the loop and distribute the array after marking necessary communication.

978-0-7695-4818-0/12 $26.00 © 2012 IEEE
DOI 10.1109/DCABES.2012.9

II. AFFINE DECOMPOSITION

Firstly, some necessary definitions and formulas of affine decomposition are given [1][2][13].

Definition 1: A loop nest of depth l defines an iteration space I. Each iteration of the loop nest is identified by its index vector $\vec{i} = (i_1, i_2, ..., i_l)$. An array of dimension m defines an array space A, and each element in the array is accessed by an index vector $\vec{a} = (a_1, a_2, ..., a_m)$. Similarly, an n-dimensional processor array defines a processor space P.

Definition 2: $b(\vec{i}) = B(\vec{i}) + \vec{\tau}$ is an affine expression derived from the loop bounds such that $\vec{i}$ is a valid loop index, if and only if $b(\vec{i}) \geq \vec{0}$. $f : I \to A, \vec{f}(\vec{i}) = F\vec{i} + \vec{k}$ is an affine array access functions, where F is a linear transformation and $\vec{k}$ is a constant vector. Furthermore, let $\vec{f}_{xj}^{t}$ be the t th array access function for array x in loop nest j.

Definition 3: Let $\vec{a} = (a_1, a_2, ..., a_m)$ be an index vector for an m-dimensional array. The data decomposition of the array onto n-dimensional processor space is an affine function $\vec{d} : A \to P, d(\vec{a}) = D\vec{a} + \vec{\delta}$, where D is an $n \times m$ linear transformation matrix and $\vec{\delta}$ is a constant vector.

Definition 4: Let $\vec{i} = (i_1, i_2, ..., i_l)$ be an index vector for a loop nest of depth l. The computation decomposition of the loop nest onto n-dimensional processor space is an affine function $\vec{c} : I \to P, c(\vec{i}) = C\vec{i} + \vec{\gamma}$, where C is an $n \times l$ linear transformation matrix and $\vec{\gamma}$ is a constant vector.

No communication is required if it is possible to define an computation decomposition for each loop nest j and an data decomposition for each array x such that the equation (1) holds for all array access functions k. The meaning of equation (1) is that loop iteration and array elements referenced by it are placed onto a single processor. The physical meaning of nullspace $N(C_j)$ of C_j and $N(D_x)$ of D_x is the spatial constraint that computing and data needs to be assigned to the same processor.

$$D_x(f_{xj}^{t}(\vec{i})) + \vec{\delta}_x = C_j(\vec{i}) + \vec{\gamma}_j \tag{1}$$

Equation (2) is a simplification equation of (1), and it abandons the displacement of data and computation decomposition to ensure that there is no expensive data reorganization communication between the dimensions of array. Equation (3) and (4) is derivate from (2), where $S_{xj}^{k} = range(F_{xj}^{k})$. In this way $N(C_j)$ and $N(D_x)$ can affect each other. In addition, $N(D_x)$ can propagate $N(C_j)$ to other loops along with the life region of x's definition, finally determine D_x and C of every loop. The derivation process of (3) and (4) can be found in [1][2].

$$D_x F_{xj}^{k} = C_j \tag{2}$$

$$N(D_x) \supseteq span\{\vec{s} \mid \vec{s} = F_{xj}^{k} \cdot \vec{t}, \vec{t} \in N(C_j)\} \tag{3}$$

$$N(C_j) \supseteq span\{\vec{t} \mid F_{xj}^{k} \cdot \vec{t} \in (N(D_x) \cap S_{xj}^{k}))\} \tag{4}$$

III. AFFINE DECOMPOSTION ON DMPCS

To guarantee no communication inside the loop, affine decomposition adds constraints according to equations (2), (5) and (6). But array distribution is widely implicated, so it is better relax some constraints to increase the distribution choice. And we can accomplish it based on characteristics of DMPCs.

$$c_j(\vec{i}_1) - c_j(\vec{i}_2) = \vec{0} \tag{5}$$

$$f_{xj}^{k1}(\vec{i}_1) - f_{xj}^{k2}(\vec{i}_2) = \vec{0} \tag{6}$$

A. Dependence constraints

The affine decomposition is designed for both distributed and shared memory architecture, so the restriction to the constraints of data dependence is very strictly. The equation (5) and (6) ensure the loop carried dependence can be satisfied, that means if two loop iteration accessed the same array element then they should partition into a same processor to avoid communication.

The parallelization of anti-dependence and output-dependence will bring data competition between threads on the shared memory. So it is forbidden by the affine decomposition. Although we can remove these memory-based or false dependences by using some methods, it may cause data redistribution on DMPCs. Moreover, the array privatization is naturally present on distributed memory architecture, and false dependence does not hinder the parallelism. So we just need to change the role of dependence constraint adding of affine decomposition, then can simply ignore the effects of false dependences to the parallelization without any loop transformation.

Definition 5: A data dependence set R of a program in distributed memory is represented as follow equation; in which ω_{vj}^{k} is true if and only if the kth array reference to array v in loop nest j is a write operation and r_{vj}^{k} is true if and only the kth array reference to array v in loop nest j is a read operation.

$$R = \{< f_{xj}^{k1}, f_{xj}^{k2} > | (\omega_{xj}^{k1} \wedge r_{xj}^{k2}) \wedge (\exists \vec{i}, \vec{i}' \in I \mid \vec{i} \prec \vec{i}') \wedge$$
$$(f_{xj}^{k1}(\vec{i}) - f_{xj}^{k2}(\vec{i}') = \vec{0}) \wedge (B_s(\vec{i}) \geq \vec{0}) \wedge (B_s(\vec{i}') \geq \vec{0})\}$$

The definition of R emphasizes f_{xj}^{k1} is a write operation and f_{xj}^{k2} is read, so anti-dependence and output-dependence can be excluded. If dependence $< f_{xj}^{k1}, f_{xj}^{k2} > \in R$, which means $\begin{cases} c_j(\vec{i}_1) - c_j(\vec{i}_2) = \vec{0}, (k1 \neq k2) \\ f_{xj}^{k1}(\vec{i}_1) - f_{xj}^{k2}(\vec{i}_2) = \vec{0}, (k1 = k2) \end{cases}$ is satisfied, then add it to the nullspace of computation decomposition as the constraints. Because $\forall \vec{t} \in N(F_{xj}^{k}), \vec{t} \in N(C_j)$, the adding principle of dependence constraints is:

$$\forall x, \textbf{if} < f_{xj}^{k1}, f_{xj}^{k2} > \in R_j \textbf{ then } add\ N(F_{xj}^{k})\ to\ N(C_j) \tag{7}$$

In figure 1, though $c_2\begin{pmatrix} i-1 \\ j \end{pmatrix} = c_2\begin{pmatrix} i \\ j \end{pmatrix}$ of Loop nest 1 is caused by the $< a[i-1][j], a[i][j] >$, we can just ignore this constraint for $< a[i-1][j], a[i][j] > \notin R$.

B. Indirect array

Affine decomposition requires that the array subscript is an affine function of the loop variable or constant. But in the practical application, there are plenty of array references like $p[colidx[j]]$, which does not satisfy affine conditions. And it is difficult to decide the data decomposition of p at compile time. So the affine decomposition adds the constraint of self-input and self-output dependence to restrict the distribution of this kind of array reference.

```
/*Loop Nest 1*/
for i = 1 to N do
   for j = 1 to N do
     a[i-1][j] = a[i][j] + b[i][j]

/*Loop Nest 2*/
for i = 1 to N do
   for j = 1 to N do
     a[i][j] = a[i-1][j] + p[colidx[j]]
```

Figure 1. Code used to illustrate constraints adding principle

The input-dependence is caused by multiple reading of the same memory unit, so there is no true dependence carried by loop j on loop nest 2. Though the partition of j leading to irregular distribution of p, it will cause no communication inside loop nest 2. If we can make sure that the input-dependence is only caused by indirect array, then we can release the limitations of its parallelization in affine decomposition.

Furthermore, in loop nest 2, the data referenced by p is upward exposed and its data distribution is irregular, so we have to solve the problem of data redistribution. Most previous research can only redistribute irregular array at run time or use feedback. Because the distribution of irregular array is hard to decide at compile time, so it is unlikely to determine the target processor of the data migration. We use two methods to deal with this problem.

1). Serial execution. The parallel program generated by our compiler is SPMD (Single Program Multiple Data), in which serial data executed on each processor redundantly. If p is not distributed before loop nest 2, then the data referenced by $p[colidx[j]]$ is in the local, and there is no need to redistribute p. 2) computation partition and array references. The irregular problem brought by indirect array is relatively simple. We can achieve the use data space of irregular array according to the iteration space of every processor (by the computation partition of iteration space) and access function of array. Take the redistribution code of $p[colidx[j]]$ as example, and illustrate it in figure 1. Pid is the process number and bk is the block size.

Self-output dependence is brought by $p[colidx[j]]$ when it is write-only array in loop. The execution of SPMD program is still following the execution sequence of the serial program on DMPCs. So no communication will be brought by the parallelization of output dependence. If the irregular access is only caused by indirect array, and no true dependence, then the distribution can be let go. For the data redistribution may be caused, efficient code can be generated at compile time same as self-input dependence.

```
for j = max(pid*bk, 1) to min(pid*bk+bk -1, N) do
        send_buf = p[colidx[j]]

        Mpi_Communicaiton_Primitive

for pid = 0 to np do
   for j = max(pid*bk, 1) to min(pid*bk+bk -1, N) do
        p[colidx[j]] = receive_buf[pid]
```

Figure 2. Code to redistribute irregular array

For both cases, we should record the irregular references and the loop they locate, and set their distribution to a special value when calculating the data distribution and computation partition to illustrate its irregular. Only the serial execution of definition can avoid the redistribution of irregular references. Considering 2.1 and 2.2, an improved static decomposition of affine decomposition is proposed in figure 3. Static decomposition is the foundation of the dynamic, and our improvement concentrate on the part of constraint adding. Only improvement part is show in detail. For calculation of decomposition matrix and offset, refer to [1][2].

algorithm Calc_Nullspaces(v, *Irregular_list*, Γ, Δ)
// v : node in the *CFG*;
  foreach array x in v **do**
    if $< f_{xv}^{k1}, f_{xv}^{k2} > \in R_j$ **then** *add* $N(F_{xv}^k)$ *to* $N(C_v)$; //(7)
    if ((f_{xv} is irregular) $\wedge$ (index i of f_{xv} is not indirection array)) **then**

$$\begin{cases} c_v(\vec{i}_1) - c_v(\vec{i}_2) = \vec{0}, \Rightarrow c_v(\vec{i}_1 - \vec{i}_2) = \vec{0}, \Rightarrow c_v(\overrightarrow{e_q}) = \vec{0}, \overrightarrow{e_q} \in N(C_v) \text{ //(5)} \\ f_{xv}^k(\vec{i}_1) - f_{xv}^k(\vec{i}_2) = \vec{0}, \Rightarrow f_{xv}^k(\vec{t}) = \vec{0}, \vec{t} \in N(F_{xv}^k), \vec{t} \in N(C_v) \quad \text{//(6)} \end{cases}$$

    else
      add $< x, v >$ to *Irregular_list*; // let go the indirection array
  end
  s_v = static subset of v
  G' = CFG of s_v;
  Propagate_Nullspaces(G', Γ, Δ); // *By using* (3) and (4)
  return (Γ, Δ)
end algorithm
algorithm Static_Decomp(*CFG*, *Irregular_list*, Γ, Δ)
// *Irregular_list* : list of irregular array;
// Γ, Δ : set of vector_space;
  $\Gamma = \Delta = \varnothing$;
  foreach v in *CFG* **do**
    <Γ, Δ>=Calc_Nullspaces(v, *Irregular_list*, Γ, Δ)
  end
  foreach *element* in *Irregular_list* **do**
    $< x, v > = Pop$(*Irregular_list*);
    set D_x of $v = \Omega$;
  end
  Calc_Matrices(*CFG*, Γ, Δ); //same as others
  calc offsets for *CFG*; //same as others
end algorithm

Figure 3. Improved static decomposition algorithm

IV. EXPERIMENT AND ANALYSIS

Experiment is performing on Sunway MPP, which consists of 16 computing nodes, and each node is configured with 4 processors clocked at 2.8GHz. The mpich2 version is 1.4.1. The program CG (Conjugate Gradient) and IS (Integer Sort) from NPB (NAS Parallel Benchmark) are chosen for

experiments. NPB is also known as NAS (Numerical Aerodynamic Simulation) Benchmark, which is developed by NASA (National Aeronautics and Space Administration), and widely used in the parallel computer performance testing and comparing.

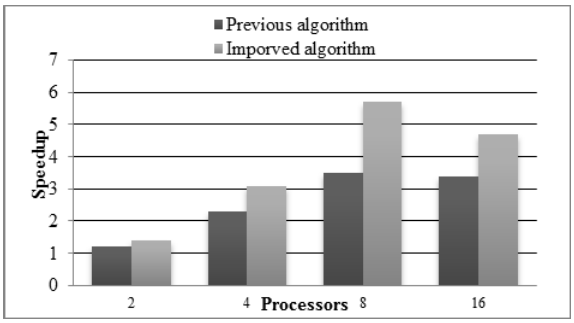

Figure 4. Speedup of IS

IS performs a large integer sorting by using bucket sort, and does not contain a floating-point operation. The kernel of IS contains loop carried anti-dependence and self-output dependence caused by indirect array. In CG, a conjugate gradient method is used to compute an approximation to the smallest eigenvalue of a large, sparse, symmetric positive definite matrix. The outer iteration of CG uses inverse power method, and the inner iteration uses conjugate gradient method, which contains self-input dependence caused by indirect array.

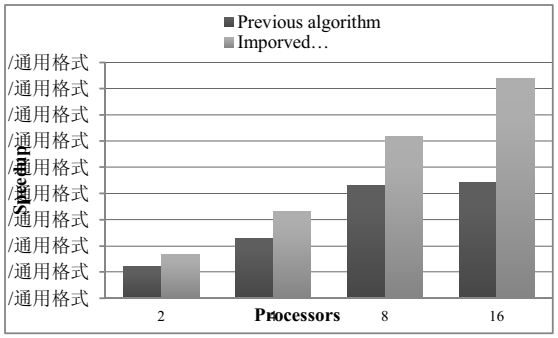

Figure 5. Speedup of CG

CLASS of two programs chosen for experiment is A. The critical loop of CG locates in the inner iteration, contains indirect array. After parallelization, a visible speedup is achieved. IS has relatively less computation and the speedup reach the turning point on 8 processes. This is similar to the MPI version developed by NASA. Experiment results show that affine decomposition improved by this paper can increase the number of the loop partitioned and can improve the performance of the parallel programs.

V. SUMMARY AND CONCLUSIONS

In the automatic parallelization for DMPCs, affine decomposition strictly limits the false dependence and indirect array. So we make some improvement in this paper and achieve good effects. During the process of research, we found that the affine decomposition ignores the factor of the data flow, and will make further improvements based on the define-use graph in the next step.

REFERENCES

[1] J.M. Anderson and M.S. Lam, “Global optimizations for parallelism and locality on scalable parallel machines,” In R. Cartwright, Proceedings of the PLDI’93, ACM New York, 1993, pp. 112–125.

[2] J.M. Anderson, “Automatic computation and data decomposition for multiprocessors,” California: Stanford University, 1997.

[3] P.Z. Lee and Z.M. Kedem, “Automatic data and computation decomposition on distributed memory parallel computers, ” ACM Transactions on Programming Languages and Systems, vol. 24, Jan. 2002, pp. 1-50, doi:10.1145/509705.509706

[4] K. Kennedy, U. Kremer, “Automatic data layout for distributed-memory machines ,” ACM Transactions on Programming Languages and Systems, vol.20, Jul. 1998, pp. 869-916, doi: 10.1145/291891.291901.

[5] L. Han, R.C. Zhao, J.M. Pang, “Dynamic decomposition algorithm merging control flow analysis,” In Arabniaed HR, ed. The 2007 International Conference on Parallel and Distributed Processing Techniques and Applications, Las Vegas Nevada: CSREA press, 2007, pp. 245-250.

[6] T.S. Chen, C.Y. Chang, “Skewed data partition and alignment techniques for compiling programs on distributed memory multicimputers,” The Journal of Supercomputing, vol. 21, 2002, pp. 192-211, doi: 10.1023/A:1013683521693

[7] J. Ramanujam, P. Sadayappan, “Compile-time techniques for data distribution in distributed memory machines,” IEEE Transactions on Parallel and Distributed Systems, vol. 2, Oct. 1991, pp. 472-482, doi: 10.1109/71.97903.

[8] J. Li and M. Chen, “The Data Alignment Phase in Compiling Programs for Distributed-Memory Machines,” J. Parallel and Distributed Computing, vol. 13, Oct. 1991, pp. 213-221, doi: 10.1016/0743-7315(91)90090-V.

[9] C.H. Huang and P. Sadayappan, “Communication-Free Hyperplane Partitioning of Nested Loops,” J. Parallel and Distributed Computing, vol. 19, Oct 1993, pp. 90-102, doi: 10.1006/jpdc.1993.1094.

[10] D.E. Maydan, S.P. Amarasinghe and M.S. Lam, “Array data-flow analysis and its use in array privatization”. In Proceedings of POPL '93, New York, ACM Press, 1993, pp. 1-15.

[11] P.Y. Calland, A. Darte, Y. Robert and F. Vivien, “On the removal of anti and output dependences,” International Journal of Parallel Programming, vol. 26, 1998, pp. 285-312, doi: 10.1023/A:1018790129478.

[12] D.A. Padua and M.J. Wolfe, “Advanced compiler optimizations for supercomputers, ” Communicaiton of the ACM - Special issue on parallelism, vol. 29, Dec. 1986 ,doi: 10.1145/7902.7904.

[13] A.W. Lim, M.S. Lam, “Maximizing parallelism and minimizing synchronization with affine partitions,” Parallel Computing, vol 24, May 1998, pp. 445-475, doi: 10.1016/S0167-8191(98)00021-0.

[14] G. Agrawal and J. Saltz, “Interprocedural compilation of irregular applilcations for distributed memory machines,” Supercomputing, 1995, Proceedings of the IEEE/ACM SC95 Conference, pp. 48.

[15] M.Y. Guo, Y. Pan, Z. Liu, “Symbolic communication set generation for irregular parallel applications,” The Journal of Supercomputing, vol. 25, 2003, pp. 199-214, doi: 10.1023/A:1024262610201

[16] C.J. Hu, J. li, G.L. Yao, Y.H. li, L. Ding, J.J. Li, “Communication set generation for a special case of irregular parallel applications,” Chinese journal of computers, vol. 21, 2008, pp. 120-126.

Parallel Construction of Approximate *k*NN Graph

Dilin Wang[1,2], Yanmei Zheng[1], Jianwen Cao[1]
1. Laboratory of Parallel Software and Computational Science of Software, Institute of Software Chinese Academy of Sciences, Beijing, 100190, China;
2. Graduate University of Chinese Academy of Sciences, Beijing, 100049, China.
Email: yanmei@iscas.ac.cn

Abstract: Building *k*-nearest neighbor (*k*NN) graphs is a necessary step in such areas as data mining and machine learning. So in this paper, we attempt to study the *k*NN furthermore, we first propose a parallel algorithm for approximate *k*NN graph construction and then apply the *k*NN graph to the application of clustering. Experiments show that our MPI/OpenMP mixed mode codes can make the construction of approximate *k*NN graph faster and make the parallelization and implementation easier. Finally, we compare the results of agglomerative clustering methods by using our parallel algorithm to illustrate the applicability of this method.

Keyword: Approximate kNN; MPI/OpenMP; Parallel algorithms; Clustering

I. INTRODUCTION

The computation of *k*-nearest neighbor graph is usually essential to solve problems arising from data mining [1], robot motion planning [2] and other research fields. As an example, research in data mining, *k*NN graph can be used for detecting outliers [3], and it can also be used for solving clustering problems [4, 5]. Given a set of points $X = \{x_1, \dots, x_n\}$ in $\mathbb{R}^d$ and a positive integer $k \le n-1$, the *k*NN graph is a graph with vertex set X and edge set E which is a subset of $X \times X$. Each vertex has exactly k edges according to a given distance function. Here, the distance of two points x_i and x_j is defined as their Euclidean distance $\| x_i - x_j \|$.

The contribution of our work is to develop a MPI/OpenMP [6, 7, 8] mixed modes parallel algorithm that efficiently computes the *k*NN graph in high accuracy. The traditional serial algorithm cannot work well for data ocean quickly, it is also essential to study the parallel algorithm of *k*NN. By utilizing a mixed mode programming model we could be able to take advantage of the following benefits: (a) load balance, (b) ease of parallelization and implementation, (c) high overlapping ratio between communication and computation, etc.

Our parallel algorithm can be extended in many ways, one possible extension is the computation based on *k*NN graph [9]. We can construct an approximate *k*NN graph with our parallel algorithm, instead of computing exactly *k*NN graph. Approximate *k*NN graph provides a trade-off between efficiency of computation and quality.

The rest of the paper is organized as follows. In section II we review the related work. Section III introduces a parallel method to construct an approximate *k*NN graph. We show several experiments and results obtained in section IV, then clustering application in section V. Finally, we conclude in section VI with a discussion on the parallel algorithm.

II. RELATED WORK

The naive approach to construct *k*NN graph uses $O(n^2)$ time. Motivated by challenging problems in many research fields, a large amount of work [10, 11, 12] has been devoted to the development of efficient algorithms for the construction of *k*NN graph. Jie Chen et al. [12] presented a serial method (algorithm GLUE in this paper) to build an approximate *k*NN graph.

Algorithm GLUE:
Sequential method to compute approximate *k*NN graph

```
1: function G = GLUE (X, k, a)
2:     if |X|< n_k then
3:         G ←BRUTEFORCE (X, k)
4:     else
5:         (X1, X2, X3) ← DIVIDE-GLUE (X, a)
6:         G1 ←GLUE (X1, k, a)
6:         G2 ←GLUE (X2, k, a)
7:         G3 ←GLUE (X3, k, a)
8:         kNN graph ← CONQUER(G1,G2,G3)
9:         REFINE（kNN graph）
10:    end if
11: end function
```

In the GLUE method, BRUTEFORCE method is used for constructing an exactly *k*NN graph. The method is called when the size of the set X is smaller than a threshold (n_k). DIVDE-GLUE method is based on a spectral bisection technique which employs a Lanczos procedure that divides the set of data points X into three subsets: X_1, X_2, X_3. The criterion of DIVID-GLUE is:

$$\begin{cases} X_1 \cup X_2 = \mathrm{X} \\ X_1 \cap X_2 = \emptyset \\ X_1 \cap X_3 \neq \emptyset \\ X_2 \cap X_3 \neq \emptyset \end{cases}$$

The parameter a controls the overlap size of the subsets in the divide step. In Figure 1, the data set X_3 contains $(100a)\%$ of the X data set. GLUE recursively call themselves on smaller subsets. The next step is to conquer the data points. When a point belongs to more than one subset, its *k*-nearest neighbors are selected from its neighbors in each subset. The step REFINE can effectively enhance the quality of the resulted *k*NN graph. For each point x_i, its k nearest neighbors are reselected from its neighbors and the neighbors of its neighbors.

978-0-7695-4818-0/12 $26.00 © 2012 IEEE
DOI 10.1109/DCABES.2012.87

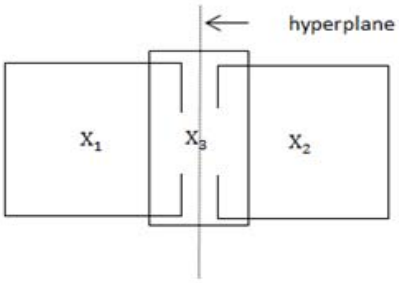

Figure 1. Divide X into subesets.

GLUE method builds kNN graph in $\Theta(dn^t)$ time for high dimensional data. Figure 2 illustrates the value of t where each plotted point in the figure corresponds to a specific a, where $a = (0.05,0.1,0.15,0.2,0.25,0.3)$. The exponent t and the parameter a have positive correlation (t is close to 1).

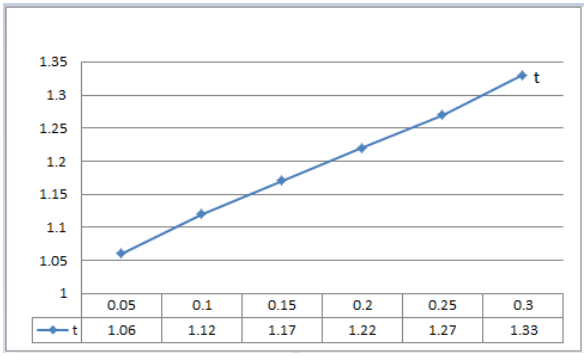

Figure 2. Complexity of GLUE method.

GLUE is a sub-quadratic time method, which performances well on high dimensional data. However, GLUE method is a serial algorithm that cannot achieve good performance on multi-core machines. Moreover, in order to obtain high quality of the resulted kNN graphs, a larger a is required, and this leads to lower efficiency.

III. Parallel Computation

Our parallel algorithm for the computation of the kNN graph based on sequential algorithms, such as those surveyed in section II. In this section we describe our algorithm details.

A. Model of Computation

First, an OpenMP parallelism strategy is to place a number of TASK directives around the computationally intense recursive steps, which has resulted in minimal code changes. Second, the array X is shared and each thread is responsible for computing a subset (X_1, X_2, X_3) when it is available. Meanwhile, with PARALLEL DO directives around the outer of iterative loop, parallel algorithm can reduce the running time.

B. Improving

In order to improve the quality of the final resulting graph, a procedure showed in Figure 3 is taken.

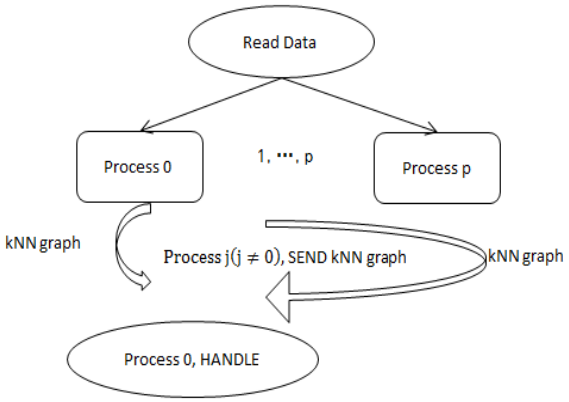

Figure 3. Refine approximate kNN graph.

Each processor computes the initial approximate kNN graph independently. Finally, process j ($j \neq 0$) (no-master process) sends the result to the master process, and then process 0 (master process) receives the resulted kNN graph from no-master processes in order to improve its own kNN graph. The improving step (HANDLE) is simple, formally, for each point x_i, we reselect its k nearest neighbors from the kNN graph resulted from master process and the graphs resulted from no-master processes. Therefore the time is $O(kn)$ for the improving step.

C. The algorithm

Parallel implementation of this algorithm majority happens in two phases. For the first phase, a parallel distribution recursive step is used in place of a standard recursive routine. Second, improving the quality of kNN graph resulted from master process. See algorithm GLUE and GLUE-P. They both fall in the same framework of divide and conquer. p_{id} is used to show the current procedure being restrict executed by the process that process index equals to id. $Thread_i$ means thread i from process id enter this part.

Algorithm GLUE-P
Parallel construction of approximate kNN graph

1: **function** G =GLUE-P (X, k, a)
2: p_{id} **if** |X|< n_k **then**
3: p_{id} G ←BRUTEFORCE(X, k)
4: p_{id} **else**
5: p_{id} (X_1, X_2, X_3)←DIVIDE-GLUE (X, a)
6: $p_{id} \leftarrow Thread_i$ G1←GLUE-P (X_1, k, a)
7: $p_{id} \leftarrow Thread_i$ G2←GLUE-P (X_2, k, a)
8: $p_{id} \leftarrow Thread_i$ G3←GLUE-P (X_3, k, a)
8: $p_{id} \leftarrow Thread_i$ kNN graph←CONQUER(G1,G2,G3)
9: **synchronize**
10: $p_{id} \leftarrow Thread_i$ REFINE(kNN graph)
11: p_{id} **end if**
12: $p_0 \leftarrow p_{id}$ SEND(kNN graph)
13: p_0 HANDLE(kNN graph)
14: **end function**

IV. Experiments and Results

Our experiments are designed here to evaluate first the running time of the parallel implementation compared with the sequential implementation, and then the qualities of the resulting graphs. All of the data, source code and results are available at: https://docs.google.com/open?id=0B9Snn49jOU7LWF9iWDBMNmtzMnM(named *k*NN_SOURCE_URL).

A. Hardware and software setup

The implementation of GLUE-P method is carried out in ANSI c/c++ using the MPICH implementation of MPI standard and OpenMP for communication, and the programs are compiled using mpic++. The experiments are performed under a Linux workstation (3.0.0-16-generic) with four i7-2600 3.4GHz CPUs and 4GB memory. In this paper, we set $k = 12$.

B. Running time

Figure 4 (a) (b) plots the running time versus the number of data points and the dimension d on randomly generated points. Figure 4 (c) (d) plots the running time ratio compared GLUE-P method with GLUE method, which (c) shows the running time ratio in (a) and (d) is related to (b). GLUE-P method uses 1 MPI process and 10 OpenMP threads, and the parameter $a = 0.2$. Generally, in (a) and (b), we can find the GLUE-P is more efficient than the GLUE. Figure 4 (c) illustrates the ratio is averaged at 55% when n is variable. Similarly, GLUE-P is faster than GLUE when d is variable. In (d), the ratio is slightly more than 50%.

C. Quality

In this experiment, we use real-life data set (named D1, available at *k*NN_SOURCE_URL) to test the quality of the resulted *k*NN graphs. D1 contains 1965 points and each point is a 560-dimensional vector. GLUE-P uses 5 MPI processes and 10 OpenMP threads. The accuracies of the resulted graphs are plotted in Figure 5. Each plotted point in the figure corresponds to the choice of $a = (0.05,0.1,0.15,0.2,0.25,0.3)$. The accuracy is defined as (graph G – the exact *k*NN graph, graph G' – the approximate graph)

$$\frac{|E(G') \cap E(G)|}{|E(G)|}$$

where $E(.)$ means the set of directed edges in the graph. Obviously, better quality brings higher accuracy. If the result is an exact *k*NN graph, the accuracy equals to 1.

The Figure 5 shows the following information: GLUE-P method is more accurate than GLUE method, especially when a is relatively smaller ($a \leq 0.15$), the accuracy enhanced significantly, and the former method can yield high quality graph even when a is small. In addition, the GLUE-P method is faster than the GLUE method for the same a. The result illustrates that the improving procedure (in section II-B) is effective, which makes our parallel algorithm to be more convinced than serial algorithm for the same a.

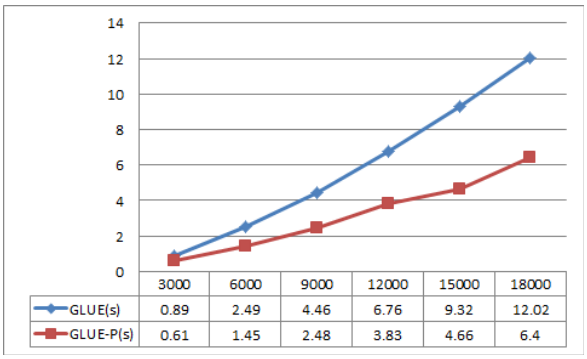

(a) $d = 500$, $a = 0.2$, n varying.

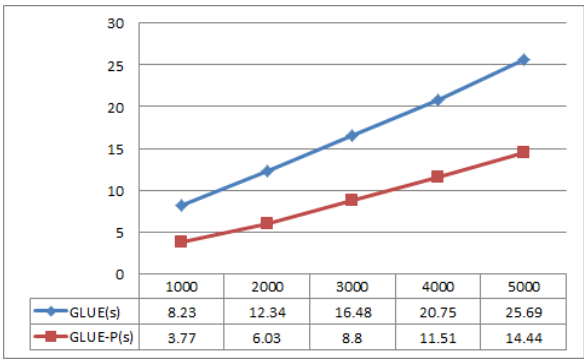

(b) $n = 10000$, $a = 0.2$, d varying.

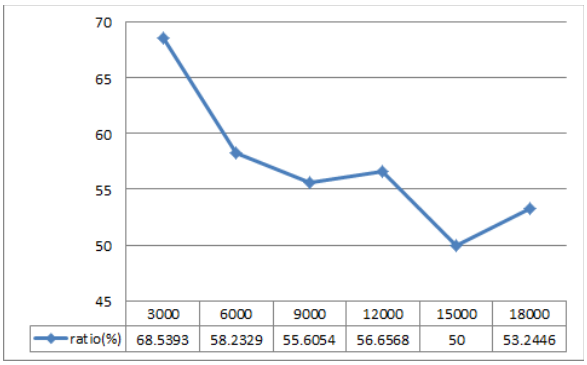

(c) Ratio of GLUE and GLUE-P in (a).

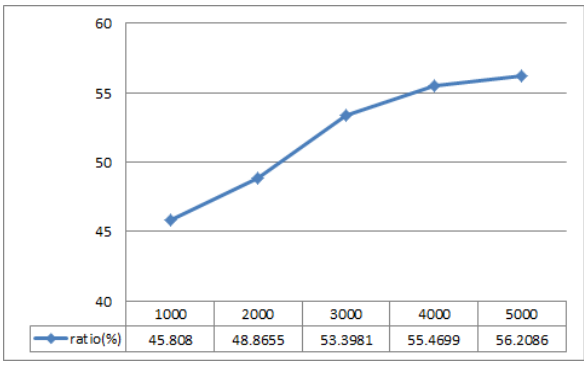

(d) Ratio of GLUE and GLUE-P in (b).

Figure 4. The running time for randomly generated data (a), (b).The ratio is the running time of GLUE-P to the running time of GLUE (c), (d).

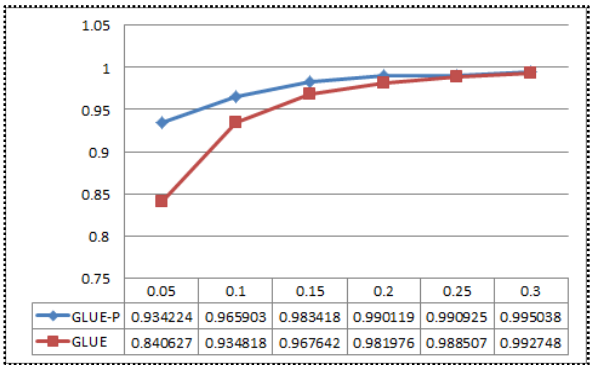

	0.05	0.1	0.15	0.2	0.25	0.3
GLUE-P	0.934224	0.965903	0.983418	0.990119	0.990925	0.995038
GLUE	0.840627	0.934818	0.967642	0.981976	0.988507	0.992748

Figure 5. Graph accuracy based on data set D1 computed by GLUE-P to GLUE, respectively. Each plotted points corresponds to a choice of *a*.

V. Applications

Clustering is a discovery process in data mining. It groups a set of data in a way so that the data in the same cluster are more similar (in some sense or another) to each other than to those in other clusters. Chameleon is a hierarchical clustering method that overcomes the limitations of existing clustering algorithms. In this section, we discuss a scenario where the approximate *k*NN graphs resulted from the proposed parallel algorithm can be an effective replacement for the exact *k*NN graph in the Chameleon algorithm. Figure 6 provides an overview of the overall approach used by Chameleon to find the clusters.

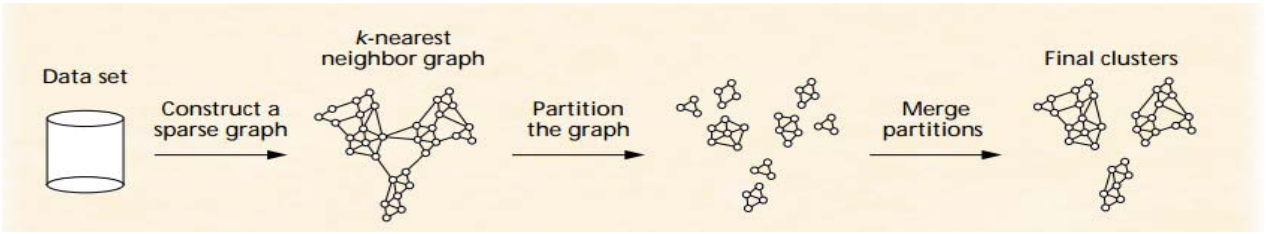

Figure 6. Chameleon. First, partition the graph by using k-nearest neighbor graph, followed by cluster merging using measures of relative closeness and relative interconnectivity. (Reprinted with permission from The Institute of Electrical and Electronics Engineers. Copyright 1999 IEEE).

We compare Chameleon's performance against that of GLUE and GLUE-P on two different data sets. These data sets contain from 1100(a) to 1600(b) points in two dimensions (see Figure 7). In (a), this set of 1100 points form two nearby connected diamonds in two dimensions, which is named D2; in (b), this set of 1600 points form a more complicated shape than D2, named D3 (available at kNN_SOURCE_URL). We create the data sets based on the related work from George Karypis et al [9].

We perform a serial of experiments on the data set D2 with 2 classes and 7 classes on D3. Figure 8 shows the clusters that Chameleon found for each of the two data sets. In particular, we used $k = 15$ and the *k*NN graph used in Chameleon constructed in different ways: (a) GLUE algorithm, set $a = 0.05$; (b) GLUE-P algorithm, set $a = 0.05$; (c) GLUE algorithm, set $a = 0.06$; (d) GLUE algorithm, set $a = 0.1$; (e) GLUE-P algorithm, set $a = 0.06$. For data set D2, both of the GLUE algorithm and parallel algorithm GLUE-P achieved good performance when a small a is set ($a = 0.05$). The results of 2 classes appear clearly as the areas of blue and red in the (a) and (b). However, in (c), the D3 clusters, result is not satisfactory when the parameter a is as small as 0.06, that c-shaped cluster does not belong to a same class. When $a = 0.1$, Chameleon correctly identifies the genuine clusters in D3, as shown in (d). Comparing (c) with (e), which both have the same parameter a, it can be seen that GLUE-P algorithm is more effective than GLUE algorithm in the same condition when applied in clustering application.

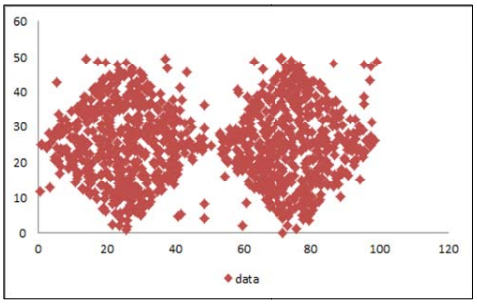

(a) D2-1100 points.

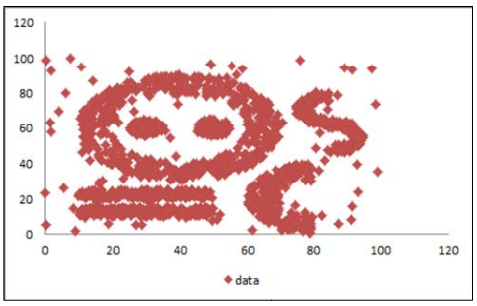

(b) D3-1600 points.

Figure 7. Two data sets used in our experiments.

VI. Conclusions

In this paper, we present an efficient parallel *k*NN construction algorithm which takes advantage of multiple processors. It is clear from experiments that the parallel algorithm is not only faster than the sequential algorithm but also achieved higher quality in the same condition. Finally the clustering application shows that the resulted approximate *k*NN graph can be safely used as alternatives to the exact *k*NN graph.

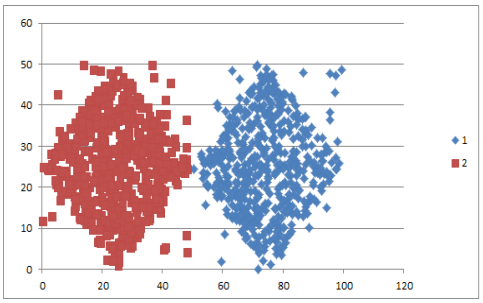

(a) GLUE, $a = 0.05$.

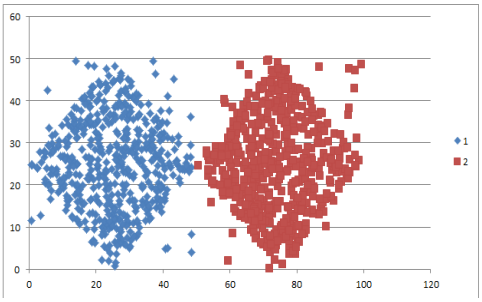

(b) GLUE-P, $a = 0.05$.

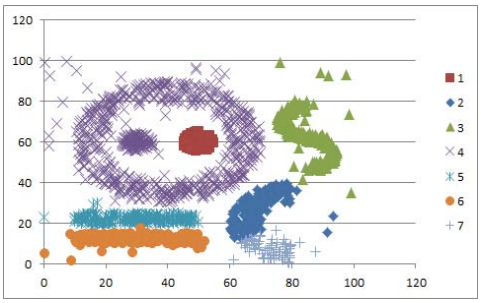

(c) GLUE, $a = 0.06$.

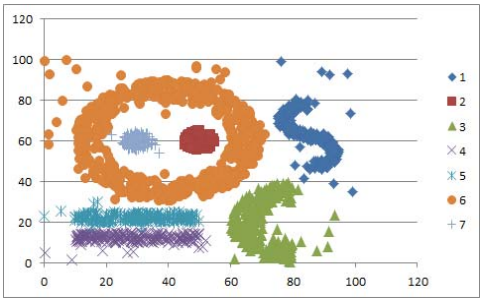

(d) GLUE, $a = 0.1$.

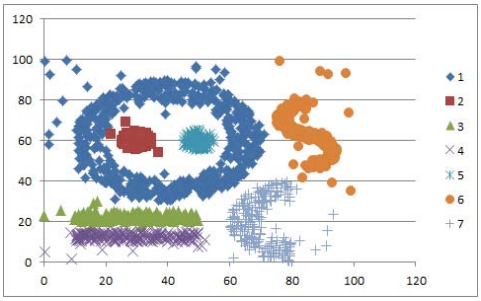

(e) GLUE-P, $a = 0.06$.

Figure 8. Chameleon algorithm using approximate *k*NN graphs on data set D2 and D3.

ACKNOWLEDGMENTS

The authors would like to thank Yu-Chiao Chao for helpful discussions and comments.

The project was supported by NSFC under the grant (61170325).

REFERENCES

[1] P. Tan, M. Steinbach and V. Kumar. Introduction to Data Mining. Addison Wesley, 2005.

[2] H. Choset, K. M. Lynch, S. Hutchinson, G. Kantor, W. Burgard, L. E. Kavraki and S. Thrun. Principles of Robot Motion: Theory, Algorithms, and Implementations. The MIT Press, 2005.

[3] Ville Hautamäki, Ismo Kärkkäinen and Pasi Fränti. Outlier Detection Using k-Nearest Neighbour Graph. Conference: International Conference on Pattern Recognition, 3: 430-433, 2004.

[4] P. Fränti, O. Virmajoki and V. Hautamäki. Graph-based agglomerative clustering. In Proceedings of the Third IEEE Int. Conf. on Data Mining, 525–528, 2003.

[5] P. Fränti, O. Virmajoki and V. Hautamäki. Fast agglomerative clustering using a k-nearest neighbor graph. IEEE Transactions on Pattern Analysis & Machine Intelligence, 28(11):1875–1881, 2006.

[6] Lorna Smith and Mark Bull. Development of mixed mode MPI / OpenMP applications. Scientific Programming, 9(2-3): 83-98, 2001.

[7] Eduard Ayguadé, Nawal Copty, Alejandro Duran, Jay Hoeflinger, Yuan Lin, Federico Massaioli et al. A Proposal for Task Parallelism in OpenMP. Conference: International Workshop on OpenMP, 1-12, 2007.

[8] G. Aparício, I. Blanquer and V. Hernández. A Parallel Implementation of the *K* Nearest Neighbours Classifier in Three Levels: Threads, MPI Processes and the Grid. Proceedings of the 7th international conference on High Performance Computing For Computational Science , 225-235, 2006.

[9] George Karypis, Eui-hong Han and Vipin Kumar. Chameleon: Hierarchical Clustering Using Dynamic Modeling. Computer , 32(8): 68-75, 1999.

[10] Erion Plaku and Lydia E. Kavraki. Distributed Computation of the knn Graph for Large High-Dimensional Point Sets. Journal of Parallel and Distributed Computing, 67(3): 346-359, 2007.

[11] M. Connor and P. Kumar. Parallel Construction of k-Nearest Neighbor Graphs for Point Clouds. Proceedings of the Eurographics / IEEE VGTC Workshop on Volume Graphics, Los Angeles, California, USA, 2008.

[12] Jie Chen, Haw-ren Fang and Yousef saad. Fast Approximate kNN Graph Construction for High Dimensional Data via Recursive Lanczos Bisection. The Journal of Machine Learning Research archive. 10: 1989-2012, 2009.

A parallel algorithm of non-linear high-order boundary condition problem for hydrodynamics

Zhang Haoyue Shesheng Zhang
Association of Mathematical Modeling, Wuhan University of Technology, Wuhan, 430070
sheshengz@qq.com

Liu Chao Chen Xing Wang Weicang
Association of Mathematical Modeling, Wuhan University of Technology, Wuhan, 430070
Contact: wangweiceng83@163.com

***Abstract*—A parallel algorithm of non-linear high order boundary condition problem is discussed, and super-cavitation hydrofoil with finite span near free surface is given. by using non-linear initial boundary two dimension condition and three dimension lifting line theories, the numeric results of a flat plate hydrofoil are better than that of Furuya.**

Keywords- boundary condition problem; hydrofoil, parallel algorithm

I. INTRODUCTION

Three dimension super-cavitation hydrofoils with free water surface is an interesting project in the field of ship building. Furuya[1] solved the nonlinear integral and algebraic equations of this problem. Fast and stable convergence results by starting the iteration with a readily chosen initial solution. Some representative numerical computations are made for practical hydrofoils having both generally shaped camber and leading-edge thickness distributions. A nonlinear exact solution to the problem of two-dimensional gravity-free incompressible potential flow around an arbitrarily shaped supercavitating hydrofoil near a free surface is obtained. He also considered supercavitating hydrofoils of large aspect ratio operating near a free surface are investigated, assuming an inviscid and irrotational flow with the effects of gravity and surface tension neglected. The flow near the foil, treated as two-dimensional, is solved by a nonlinear free-streamline theory, then a three-dimensional 'downwash' correction is made using Prandtl's lifting-line theory. The strength of the lifting-line vortex is determined by information from the two-dimensional solution through a matching procedure, in which the inverse of aspect ratio is used as a small parameter for asymptotic expansions. The analysis incorporates a free-surface reference level to determine the submergence depth of the foil. Ito[3] applied the lifting-line theory for a supercavitating hydrofoil in two-dimensional shear flow (where velocity varies in both spanwise and vertical directions) between two parallel planes is applied to partial cavitation.. Li[4] observe the patterns of supercavitating flows around a hydronautics foil by means of a high-speed video camera and the digital particle image velocimetry (DPIV). The results show that the cavitation structure depends on the interaction of the water-vapor mixture phase and the vapor phase. Ito[5] researched on unsteady inviscid incompressible and small disturbance flow, three-dimensional characteristics of supercavitating hydrofoil between parallel plane walls are analyzed. Antipov[6]solved the problem of reconstructing the free surface of a channel and the shapes of the cavities behind two hydrofoils placed in an ideal fluid In the framework of the Tulin model of supercavitating flow. Chen[7] propose an efficient semi-direct numerical procedure for the problem where the cavitation number in prescribed. The approach is based on a simple interpolation procedure which seems to be of universal use for two-dimensional supercavitating hydrofoils. The problem is still treated as a nonlinear one in the sense that both the cavity length and the cavity shape are parts of the solution. The results of numerical experiments show that the present approach is effective and economical in terms of computation, compared with approaches based on other theories and numerical methods...

II. TWO DIMENSION SUPERCAVITATING HYDROFOIL

In the filed fluid dynamics, the Navier-Stokes equation and continuity equation are:

$$\frac{\partial V}{\partial t} + (V * div)V = \mu \Delta V - \nabla(\frac{P}{\rho})$$
$$\nabla V = 0 \qquad (1)$$

Where V is the velocity at the point X in the solution domain Ω, and time t>0. We suppose fluid is inviscidity and irrotation. Above equation may reduced to

$$\Delta \psi = 0$$

Where ψ is stream function of two dimension. On the boundary S_w of free surface, the pressure is taken as zero, inside cavitation, the pressure is taken as p_c. On the surface S_o of hydrofoil, the velocity is zero in the normal direction. That is:

$$\begin{aligned} p &= 0 \quad X \in S_w \\ p &= p_c \quad X \in S_c \\ V_n &= 0 \quad X \in S_o \end{aligned} \qquad ()$$

Let

$$\xi = x \qquad \psi = \psi(x, y) \qquad (3)$$

978-0-7695-4818-0/12 $26.00 © 2012 IEEE
DOI 10.1109/DCABES.2012.81

It transfer physic plan Oxy to mapping plan Oξψ,see Fig.1. In the figure 1, CT and DA are cavitation boundary, EF is water surface, TL and LA are hydrofoil surface, FH is enter boundary, EG is exit boundary. On mapping plan CTLAD on the same horizontal line. Taking open cavitation model, we have super-cavitation hydrofoil variational principle

$$J(\Omega)=\iint_A udA+\frac{1}{g}\int_{CT+AD+EF}\frac{\partial^2\Omega^0}{\partial\xi^2}\Omega d\xi + \int_{TL+LA}\tan\beta\Omega d\xi+\int_{HF+EG}\frac{\Omega}{u}d\xi \tag{4}$$

Here Ω is lifting function, tan(β) is hydrofoil surface slop, superscript "0" is known function, the velocity u is also known function on enter boundary and exit boundary. A is numerical domain. We easy get formula as:

$$\frac{\partial\Omega}{\partial\xi}=\Pi=\frac{p}{\rho}+gy \qquad \frac{\partial\Omega}{\partial\psi}=-v \tag{5}$$
$$u^2=2(B-\frac{\partial\Omega}{\partial\xi})-(\frac{\partial\Omega}{\partial\psi})^2$$

By using method of integration by parts, we have

$$\int_a^b\frac{\partial^2\Omega^0}{\partial\xi^2}\Omega d\xi=\frac{\partial\Omega^0}{\partial\xi}\Omega\,|_a^b-\int_a^b\frac{\partial\Omega^0}{\partial\xi}\frac{\partial\Omega}{\partial\xi}d\xi \tag{6}$$

And obtain dimensionless variational principle as

$$J(\Omega)=\iint_A udA-F_r^2\int_{CT+AD+EF}\frac{\partial\Omega^0}{\partial\xi}\frac{\partial\Omega}{\partial\xi}d\xi+\int_{TL+LA}\tan\beta\Omega d\xi + \int_{HF+EG}\frac{\Omega}{u}d\xi+F_r^2\frac{\partial\Omega^0}{\partial\xi}\Omega\,|_{C,\ A,\ E}^{T,\ D,\ F} \tag{7}$$

In this case, the coming velocity is taken unit, and chord length is also unit, and F_r is defined as:

$$F_r=\frac{V_\infty}{\sqrt{gc}} \tag{8}$$

Where c is the length of hydrofoil chord.

III. PARALLEL CALCULATION

. The numerical domain A: -L<x, ξ<L, 0<ψ<H_0, here is the height of free surface measure from batten. The domain A is decomposed into M subdomain A_k: -L+ks-s<x, ξ<L+ks, 0<ψ<H_0. According to finite element theory, we divide subdomain into triangle grid. For every grid, the lifting function may be represented as

$$\Omega=a+bx+c\psi \tag{9}$$

It is a linear function, so derivation are:

$$\frac{\partial\Omega}{\partial\xi}=a \qquad \frac{\partial\Omega}{\partial\psi}=b \tag{10}$$

Let Ω_j is the value of lifting function at vertex of triangle grid, j=1,2,..,N, and let

$$\frac{\partial J(\Omega_j)}{\partial\Omega_j}=0 \tag{11}$$

Because velocity u is non-linear function of lifting function Ω, the above is also non-linear, and written as:

$$F_j(\Omega_{j1},..\Omega_{jNj})=0 \qquad j=1,2,...N \tag{12}$$

Where Nj is the number of neighbouring lifting function. It is easy shows Nj<6.

IV. L IFTING LINEAR THEORY

. Suppose hydrofoil length is l=2b, chord length is c, aspect ratio is λ, see Fig.2. We consider aspect ratio is large enough that we can consider it is a lifting line. On lifting line, the circulation is Γ(z), and can be expanded as

$$\Gamma=4bV_\infty\sum A_n\sin n\theta \qquad z=-b\cos\theta \tag{13}$$

The coefficient A_n may be solved by using two dimension result as:

$$C_{L2}(\beta-\Delta\beta)=4\lambda\sum A_n\sin(n\theta) \tag{14}$$

Where C_{L2} is the two dimension lifting coefficient, βis effective angle of attack, and Δβis angle of downwash, and has relation with downwash velocity V_y as:

$$\Delta\beta=\frac{V_y}{V_\infty} \tag{15}$$

The control points are

$$\theta_j=\frac{\pi}{n+1}j \qquad j=1,2,..,n \tag{16}$$

V. NUMERIC RESULTS

. After the two dimension lifting coefficient is calculated, we may obtain three dimension hydrofoil lifting and resistant coefficient as:

$$C_{L3}=\pi\lambda A_1 \qquad C_D=\pi\lambda\sum nA_n^2 \tag{17}$$

Example 1, take parameter F_r=6 H_0/c=1, aspect ratio λ=4, angle of attack β=15^0,20^0,25^0,The lifting and resistant coefficient varied with cavitation parameter σ is shows in Fig.3. In Fig.3, solid line is results calculated by using our theory, dashed line is calculated by using Furuya's theory, ▲○× are results of Furuya's experiment. Figure 3 shows that our results is close with Furuya's. experiment.

VI. CONCLUSION

We discuss time dependent initial boundary super-cavitation hydrofoil fluid dynamics, the two dimension

variational principle is given, and calculated by using parallel algorithm. The two dimension lifting coefficient is calculated with angle of attach. It is modified to three dimension by using lifting line theory.

ACKNOWLEDGMENT

The paper is financially supported by by China national natural science foundation (No.51139005)..

REFERENCES

[1] Furuya, O, Nonlinear calculation of arbitrarily shaped supercavitating hydrofoil near a free surface[J], Journal of Fluid Mechanics, v 68, n pt 1, p 21-40, Mar 11 1975.

[2] Furuya, O, Three dimensional theory on supercavitating hydrofoil near a free surface.[J], Journal of Fluid Mechanics, v 71, n pt 2, p 339-359, Sep 23 1975.

[3] Ito, J, et al, Lifting-line theory of a supercavitating hydrofoil in two-dimensional shear flow (application to partial cavitation)[J], JSME International Journal, Series B: Fluids and Thermal Engineering, v 45, n 2, p 287-292, May 2002

[4] Li Xianbin, el al, Experimental measurements on the characteristics of water-vapor mixture in supercavitating flows around a hydrofoil[J], Journal of Experiments in Fluid Mechanics, v 26, n 1, p 61-65+104, February 2012.

[5] Ito. J. et al,, Characteristic analysis of supercavitating three dimensional hydrofoil between parallel walls[J], Transactions of the Japan Society of Mechanical Engineers, Part B, v 72, n 2, p 361-367, February 2006

[6] Antipov, Y.A., Silvestrov, V.V., Method of Riemann surfaces in the study of supercavitating flow around two hydrofoils in a channel[J], Nonlinear Phenomena, v 235, n 1-2 SPEC. ISS., p 72-81, November 2007.

[7] Chen, Jiahn-Horng; Weng, Ying-Chieh, Semi-direct method for analysis of flow past a two-dimensional supercavitating hydrofoil[J], Physical Science and Engineering, v 23, n 5, p 591-598, 1999.

[8] Wu Xiuhen et al, the numeric model of super-cavitation hydrofoil near water botten[J], China ship building, 1984(1), 9-17.

.

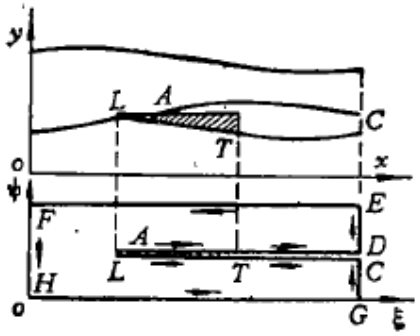

Figure 1. transfer physic plan Oxy to mapping plan Oξψ

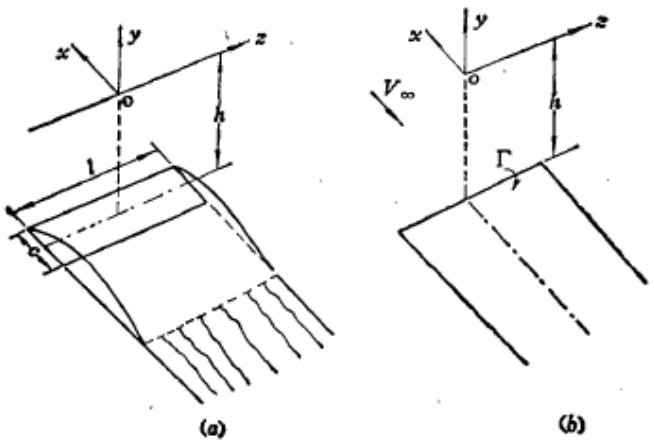

Figure 2. high aspect ratio of super-cavitation hydrofoil near free surface with bottom

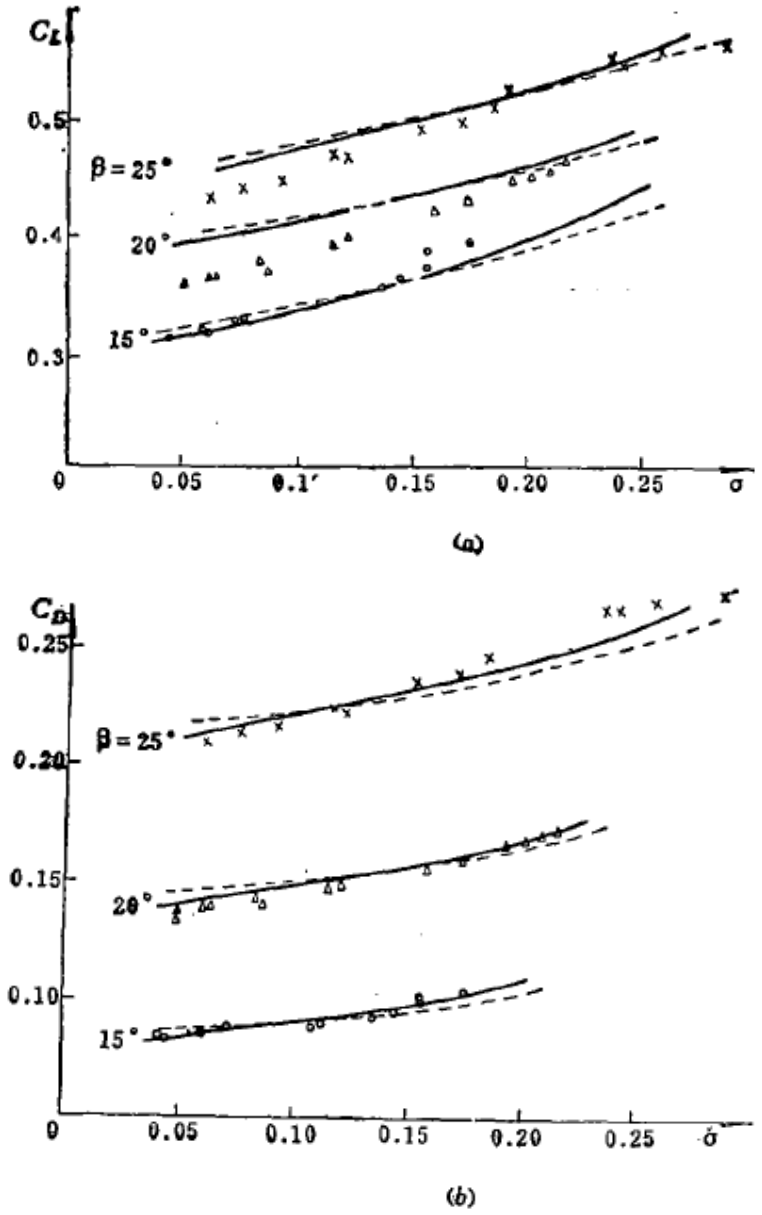

Figure 3. The lifting and resistant coefficient varied with cavitation parameter, solid line is our theory, dashed line is Furuya theory, ▲○× are Furuya experiment.

Optimization Of Parallel I/O For Cannon's algorithm Based On Lustre

Yunchun Li
Beijing Key laboratory of network technology
Computer Science Department
Beihang University
Beijing, China
lych@buaa.edu.cn

Hongda Li
Beijing Key laboratory of network technology
Computer Science Department
Beihang University
Beijing, China
hongda.li.cn@gmail.com

***Abstract*—Matrix multiplication is one of the most important operations in linear algebra, widely used in many fields of science and engineering. Cannon's algorithm is a classical distributed algorithm for matrix multiplication for two-dimensional meshes. Generally, MPI-IO is used for its I/O requirements. However it has been well documented that MPI-IO performs poorly in a Lustre file system environment. As the scale of matrix multiplication increased, this problem trends to be serious, becoming one key factor impacting performance of the program. In order to improve the performance of Collective I/O of Cannon's program, we proposed a new aggregation pattern (Stripe-continuous aggregation pattern), which fully considers the stripping mechanism and lock protocol of Lustre file system. The theoretical analysis and experimental results show that the pattern can make full use of the capacity of Lustre file system compared with the other patterns, and improve the I/O performance of the Cannon's program efficiently.**

Keywords- Cannon's algorithm; Parallel I/O; Lustre file system; MPI-IO; Collective I/O

I. INTRODUCTION

Matrix multiplication is one of the most common operations in linear algebra, widely used in many fields of science and engineering, such as signal processing, oil exploration and theoretical physics. And it is significant to improve the performance of matrix multiplication for scientific computing. Cannon's algorithm is a distributed algorithm for matrix multiplication for two-dimensional meshes first described in [1]. A new method is proposed to improve Dense Matrix Multiplication for many-core architecture in [2]. And solutions are putted forward for sparse matrix multiplication on the CUDA platform in [3]. Most of these researches focus on computing, but none of the I/O efficiency. However, with the size of matrix increasing, I/O efficiency often becomes the key factors to the performance of the program.

Usually, the Master-slave pattern is applied to I/O of Cannon's program. The master reads input matrices, and distributes to the slaves. After the completion of calculation, the sub-matrices are collected and wrote to file system by master. It makes I/O serialization, which might slow performance. Assumed that the write rate of disk is 70MB/s , it would take about 1000 seconds to serial write an 100000×100000 matrix of double-precision floating-point(74.5GB data in total), even more than the time consumed by calculation. Another way is that each process takes responsibility to read and write its own part of matrices through POSIX interfaces concurrently. However, shared-file I/O performs poorly in this way because these I/O requests are not well coordinated. To address this concern, MPI-IO [5] can be used, which is defined by the message passing interface (MPI) standard. It can combine multiple non-contiguous requests into large contiguous ones, which has demonstrated to be very successful, as modern file systems perform large contiguous requests more efficiently. However, the even aggregation pattern does not necessarily produce the best I/O performance on all file systems such as Lustre.

In this paper, we proposed a new aggregation pattern (Stripe-continuous aggregation pattern), which fully considers the stripping mechanism and lock protocol of Lustre file system [4]. And our experiments demonstrate that this pattern can gain greater I/O parallelism and improve the I/O perform of Cannon's program efficiently.

II. RELATED WORKS

To improve the parallel I/O performance, many scholars have proposed solutions of different forms. MPI standard defines a set of programming interfaces for parallel file access, commonly referred as MPI-IO [5]. There are two types of functions in MPI-IO: collective and independent. The collective functions require process synchronization which provides an MPI-IO implementation an opportunity to collaborate processes and rearrange the requests for better performance. Collective I/O can be performed at the disk level (disk directed I/O), at the server level (server-directed I/O) or at the client level (two-phase I/O). ROMIO [12] is a popular MPI-IO implementation developed at Argonne National Laboratory. It has been incorporated as part of several MPI implementations, including MPICH, SGI MPI, IBM MPI and NEC MPI. Since ROMIO is a portable, user-level library with no separate I/O servers, it performs collective I/O at the client level, including a data redistribution phase and an I/O phase. The two-phase strategy first calculates the aggregate access file region and then evenly partitioned it among the I/O aggregators into file domains. The I/O aggregators are a subset of the processes

978-0-7695-4818-0/12 $26.00 © 2012 IEEE
DOI 10.1109/DCABES.2012.61

that act as I/O proxies for the rest of the processes. In the data redistribution phase, all processes exchange data with the aggregators based on the calculated file domains. In the I/O phase, aggregators access the shared file within the assigned file domains. Two-phase I/O can combine multiple small non-contiguous requests into large contiguous ones. ROMIO can improve parallel I/O performance of Cannon's program greatly, but the even aggregation pattern used in ROMIO does not necessarily produce the best I/O performance on all file systems such as Lustre.

In [6], the Lustre file-join mechanism is used to implement the MPI-IO collective write operations. In this approach, the I/O processes write separate, independent files in parallel, and then merge these files using the Lustre file-join mechanism. They showed that this approach significantly improved the performance of the collective write operation, but that the reading of a previously joined file resulted in low I/O performance. After calculation by Cannon' algorithm, each process holds a sub-matrix of result. It is non-continuous between lines of sub-matrix in the file region.

In [8] and [9], a user-space client side cache and Active Buffering have been shown to improve the performance of parallel I/O. However, as there methods do not take internal mechanism of parallel file systems into consideration, they preform not well enough on object-based parallel file system such as Lustre.

In [7], it was shown that aligning the data to be written with the basic striping pattern improves performance. They also showed that it was important to align on lock boundaries. It performs well and is adopted by MPI-IO (ROMIO). One-to-one aggregation pattern is proposed in [11], which maps one I/O aggregator to one OST (Object Storage Target).This method can solve contention caused by the file domain of aggregator cross many OSTs. These will be addressed in more detail later in this article and compared with the method we proposed.

III. CANNON'S ALGORITHM

Use p processes for matrix multiplication $C = A \times B$, where p is square number. A, B, C are decomposed into $\sqrt{p} \times \sqrt{p}$ block matrices and mapped to p processes. Each element $C_{i,j}$ of C is calculated by the formula (1).

$$C_{i,j} = \sum_{k=1}^{\sqrt{p}} A_{i,k} \times B_{k,j}, \left(1 \le i \le \sqrt{p}, 1 \le j \le \sqrt{p}\right). \quad (1)$$

As shown in Figure 1, the processes are labeled from $P_{1,1}$ to $P_{\sqrt{p},\sqrt{p}}$ and initially assign sub-matrices $A_{i,j}$ and $B_{i,j}$ to process $P_{i,j}$. Cannon's algorithm [1] is descripted as follow:

1) Shift all sub-matrices $A_{i,j}$ to the left by $i-1$ steps and all sub-matrices $B_{i,j}$ to the up by $j-1$ steps;

2) Each process multiplies its local sub-matrices and then shifts all sub-matrices $A_{i,k}$ to the left by 1 step and all sub-matrices $B_{k,j}$ to the up by 1 step;

3) Repeat step two $\sqrt{p}-1$ times to calculate $C_{i,j}$。

After the calculation, each process holds a sub-matrix $C_{i,j}$ of C. This paper focuses on the output performance of Cannon's algorithm, namely the procedure of the matrix C stored to the parallel file system process because write operation likely become the bottleneck.

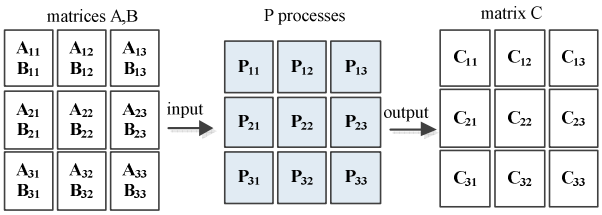

Figure 1. Matrices mapped to processes.

IV. LUSTRE ARCHITECTURE

As a large-scale global parallel file system, Lustre file system [4] plays a key role in High Performance Computing (HPC) system. It consists of three primary components: file system clients (that request I/O services), object storage servers (OSSs) (that provide I/O services), and meta-data servers that manage the name space of the file system. MDS has a single metadata target (MDT) that stores namespace metadata, such as filenames, directories, access permissions, and file layout. Each OSS can support multiple Object Storage Targets (OSTs) that handle the duties of object storage and management. The scalability of Lustre is derived from two primary sources. First, file meta-data operations are de-coupled from file I/O operations. The metadata is stored separately from the file data, and once a client has obtained the meta-data it communicates directly with the OSSs in subsequent I/O operations. This provides significant parallelism because multiple clients can interact with multiple storage servers in parallel. Second, the striping of files cross multiple OSTs, which provides parallel access to shared files by multiple clients. Lustre provides APIs allowing the application to set the stripe size (the maximum size of a stripe, typically 4 MB), the stripe count (the number of OSTs across which the file will be striped), the stripe offset (the index of the OST in which the first stripe will be stored). The striping information is set when the file is opened and cannot be modified once set. It can improve the I/O performance efficiently to configure proper striping parameters depend on the programs.

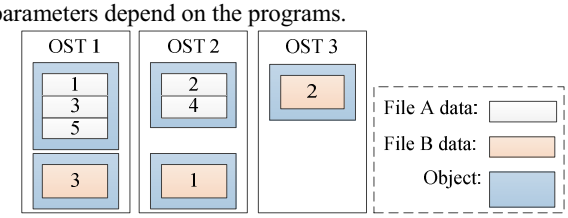

Figure 2. File striped with a stripe count of 2 and 3 with different stripe sizes [4].

All of Lustre's consistency guarantees are enforced by the lustre distributed lock manager (DLM). OSTs of Lustre adopt an extent-based locking protocol in which a lock manager tends to grant a request as the largest file region as possible. For example, the first requesting process to a file will be granted the lock for entire file. When the second write from a different process arrives, the first process will

relinquish part of the file to the requesting process. If the starting offset of the second request is bigger than the first request's ending offset, the relinquished region will start from the first request's ending offset toward the end of file. Otherwise, the relinquished region will contain a region from file offset 0 to the first request's staring offset. The advantage of this protocol is if a process's successive requests are within the already granted region, then no lock request is needed. By default, lock granularity of Lustre is a stripe size.

V. AGGREGATION PATTERN

A. ROMIO's pattern

ROMIO performs collective I/O at the client level, including a data redistribution phase and an I/O phase, referred as the Two-phase I/O.

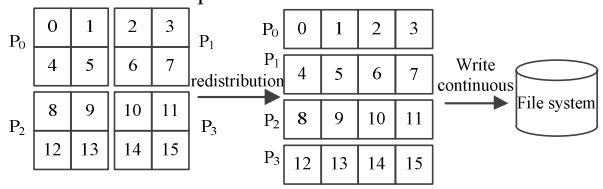

Figure 3. Store matrix C into a single file via ROMIO.

As shown in Figure 3, after the calculation of a 4 × 4 matrix multiplication using Cannon's algorithm, each process holds a piece of data of the result. For example, P_0 holds non-continuous data 0, 1, 4 and 5, and it has to request I/O twice to write data 0, 1 and data 4, 5 when using POSIX I/O interfaces. Therefore, it needs 8 times of I/O requests to write the entire matrix C into a single file. As all processes launch I/O requests concurrently without any collaboration, it preforms badly, especially when the size of matrix is larger. To address this problem, ROMIO's collective I/O is used to combine multiple non-contiguous requests into large contiguous ones as Figure 3 shows. After redistribution, every I/O aggregator gets a piece of continuous data. This method has demonstrated to be very successful, as modern file systems large contiguous requests more efficiently.

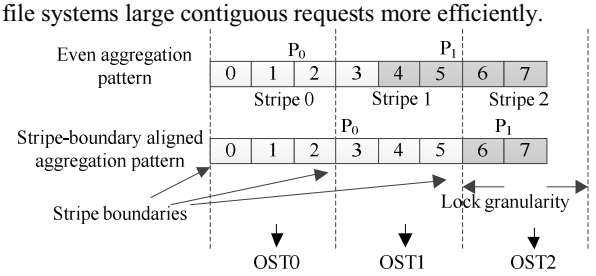

Figure 4. The even aggregation pattern and stripe-boundary aligned aggregation pattern.

Although it can reduce I/O requests and improves performance by merging small I/O requests, the even aggregation pattern of ROMIO might cause the problem that I/O accesses that are not aligned on stripe boundaries. Figure 4 helps to illustrate this problem. Assume it is going to write eight data via ROMIO and the stripe size is three data width. After data redistribution phase of ROMIO's two phase I/O, the two aggregators are writing four data to non-overlapping sections of the file; however because the requests are not aligned on stripe boundaries, both processes are accessing different regions of stripe 1. Because of Lustre's locking protocol, each process must acquire the lock associated with the stripe, which results in unnecessary lock contention. Thus the writes to stripe 1 must be serialized, resulting in suboptimal performance. To address this problem, an ADIO driver for Lustre has been added to ROMIO. This new Lustre driver insures that disk accesses are aligned on Lustre stripe boundaries, as shown in Figure 4.

B. One-to-one pattern

Stripe-boundary aligned method makes ROMIO solve the lock contention. However, the problem with performing large, contiguous writes still exists, which can cause significant contention at the network layer, and the OST level.

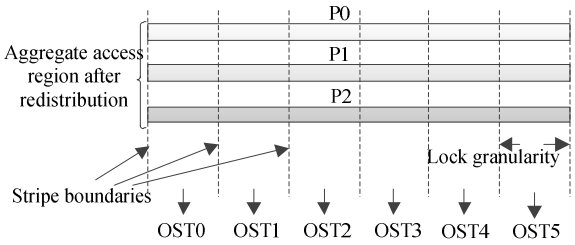

Figure 5. Each aggregator of ROMIO crosses many OSTs.

The point can be explained with a simple example, as shown in Figure 5. Assume a two-phase collective write operation with the following parameters: three processes, an 18 MB file, a stripe size of 1 MB, and a stripe count of six. After the three processes have completed data redistribution phase of the collective write operation, each process is ready to write a contiguous 6 MB block to disk. Thus process P0 will write stripes 0~ 5, process P1 will write stripes 6~11, and process P2 will write stripes 12~17. Two problems become apparent immediately. First, every process is communicating with every OSS. Second, every process must obtain six locks from different OSTs. Thus there is significant communication overhead and contention at each lock manager for locking services (but not for the locks themselves). As the file size, number of processes, and number of OSTs becomes large, it can be imagined that there is significant degradation in performance.

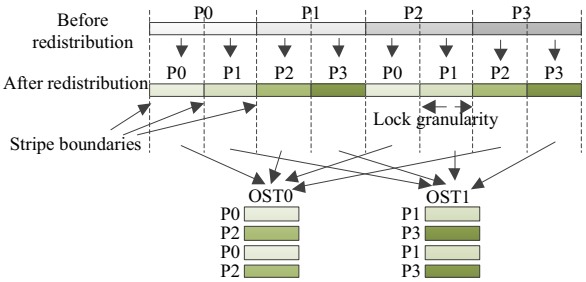

Figure 6. One-to-one aggregation pattern.

The simplest solution to resource contention when performing large, contiguous writes is to limit the number of OSTs across which a file is striped. In One-to-one aggregation pattern [11], the data is arranged such that each aggregator process communicates with exactly one OST.As Figure 6 shows, aggregate access region is decomposed into stripes, which are assigned to aggregators by turns.

C. *Stripe-contunuous pattern*

When the number of I/O aggregators is much larger than the number of I/O servers, the One-to-one method may cause higher lock acquisition cost as Lustre uses the extent-based locking protocol. In the example shown in Figure 6, there are four I/O aggregators and two OSTs. In the One-to-one method, although OST 0 only receives requests from processes P0 and P2, the file stripes accessed by the two processes are interleaved. In this case, if the extent-based locking protocol is used, lock requests to each of the interleaved stripes must be resolved by remote processes. Such lock acquisition pattern can be harmful to the performance.

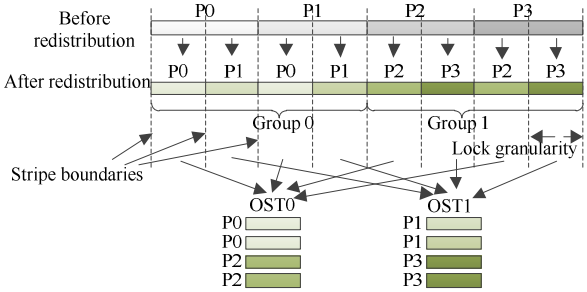

Figure 7. Stripe-continuous aggregation pattern.

To avoid the interleaved access, the stripe-contiguous aggregation pattern divides the I/O aggregators into groups, each of size equal to the number of OSTs. The aggregate access region of a collective I/O is then divided among the groups with the boundaries aligned to the file stripe size. Within each group, the One-to-one method is used. The group which a given process P_i belongs to can be calculated by formula (2), where $\lfloor x \rfloor$ means rounding x downwards to the nearest integer.

$$g = \left\lfloor \frac{i}{stripe\_count} \right\rfloor. \quad (2)$$

The grouping is made in the continuous, round-robin aggregator rank order. Within each group, an aggregator will only make requests to one OST. For example, in Figure 7, processes P_0, P_1 belong to group 0, and processes P_2, P_3 belong to group 1. From the view of OST, the data accessed by each process is stripe-continuous.

VI. EXPERIMENTS

The hardware environment of experiment is high performance clusters, which contain one control node and 64 computing nodes. Every node is equipped with two 2.4-GHz Intel quad-core processors (Intel Xeon E5530) and 24GB memory. These processers support Hyper-Threading Technology, and each of them can virtualize two logical processors. Thus, there are 1024 processors in total. The clusters are deployed two types of network: Infiniband and gigabit Ethernet, and Lustre1.8.5 is installed on Infiniband, including 16 OSSs, each of which hosted one OST. Every OSS provides a 60MB/s throughput, thus the peak aggregation throughput can reach about 960MB/s.

In our experiment, files are striped with the following parameters: a stripe size of 4 MB, a stripe count of 8 and a stripe offset of 0.In order to reduce the impact from programs of other users, their I/O requests is limited to OST 8~15 by configuring the striping parameters. In addition, several MPI implements are installed, including MPICH2-1.0.7, openmpi-1.4.1 and mvapich-1.2.0 supporting Infiniband. Each data point represents the mean value of 30 trials below.

A. *Aggregation patterns without redistribution*

In this set of experiments, we were interested in the impact of the data aggregation patterns on the throughput obtained when performing collective I/O operations in a large-scale Lustre file system. We varied three key parameters in these experiments: The implementation of the collective I/O operation, the number of processors that participated in the operation, and the file size. In particular, we varied the number of processors from 4 to 128, where each processor wrote 1.5 Gigabyte of data to disk. Thus the file size varied between 6 Gigabytes and 192 Gigabytes. This set of experiments assumed that the data was already assigned to the processors in the required distribution, so the data wrote by aggregator without redistribution.

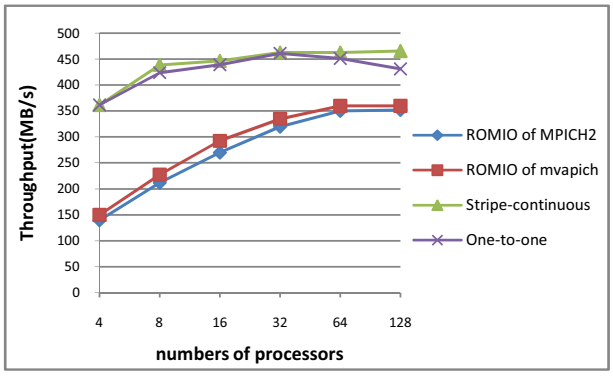

Figure 8. Aggregation patterns without redistribution.

The experimental result is shown in Figure 8.The stripe-continuous pattern and One-to-one pattern significantly outperformed the ROMIOs of MPICH2 and mvapich. As there is no need to redistribute data, the difference between the ROMIO of MPICH2 and the one of mvapich is not obvious. As the number of processors that participated in the operation increasing, the throughput of One-to-one pattern trends to decrease while the one of stripe-continuous pattern maintain smooth. When the number of processors reaches 128, the stripe-continuous pattern raises throughput by 29.3 percentages compared to the ROMIO of mvapich, and 8.12 percentages compared to the One-to-one pattern.

B. *Parallel I/O of Cannon's algorithm*

In this next set of experiments, we were interested in the impact of the data aggregation patterns on the throughput obtained when storing the result matrix C into a single file after computed by Cannon's algorithm. We varied three key parameters in these experiments: The implementation of the collective I/O operation, the size of input matrices that calculated by Cannon's algorithm. In particular, we varied the size of matrices (double-precision floating-point) from 5000×5000 to 100000×100000. We kept the number of processors that participated in the calculation 64, and 32 of them acted as I/O aggregator. After calculated by Cannon's algorithm, the data held by the processors is in a way that required it to be redistributed to reach the desired aggregation pattern. Thus, it contains the entire procedure of tow-phase I/O. In order to reduce the impact from the calculation, all processors made synchronization after the completion of the calculation.

The experimental result is shown in Figure 9. As the size of matrices increasing, the throughput of ROMIO of MPICH2 trends to decrease while the one of stripe-continuous pattern maintain smooth. When the size of input matrices reaches 100000×100000, the stripe-continuous pattern raises throughput by about 20 percentages compared to the ROMIO of MPICH2.

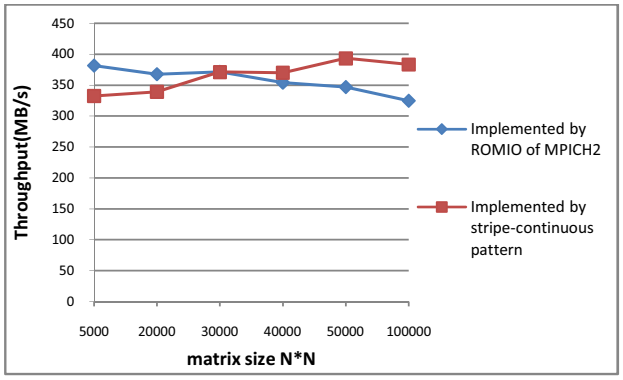

Figure 9. Parallel I/O of Cannon's algorithm.

VII. SUMMARY

This research was motivated by the poor I/O performance of Cannon's program, whose I/O is implemented by MPI-IO (ROMIO) in a Lustre environment. Part of the reasons is that the pattern of writing large, contiguous blocks of data to file system is not suitable for the striping mechanism and lock protocol of Lustre. With the full consideration of internal mechanism of Lustre, we proposed a new aggregation pattern (stripe-continuous aggregation pattern). And our experiments demonstrate that this pattern can gain greater I/O parallelism and improve the I/O perform of Cannon's program efficiently.

In the future, we plan to research the impact of inter-core communication on the data redistribution phase of two-phase I/O as CPUs of clusters mostly are multi-core architecture at present.

ACKNOWLEDGMENT

This work was supported by The National Natural Science Foundation of China (Key Program) under Grant No.61133004 and National High-Tech Research and Development Program of China (863 Program) under Grant No.2010AA012404.

REFERENCES

[1] Cannon L.E, "A Cellular Computer to Implement the Kalman Filter Algorithm", Ph.D. Thesis, Montana State University, Bozeman, MT, USA , 1969.

[2] E. Garcia, I. E. Venetis, R. Khan, and G. Gao, "Optimized Dense Matrix Multiplication on a Many-Core Architecture", In Proceedings of the Sixteenth International Conference on Parallel Computing (Euro-Par 2010), Part II, vol.6272 of Lecture Notes in Computer Science, pp.316–327, Ischia, Italy, 2010.

[3] N. Bell and M. Garland. "Efficient Sparse Matrix-Vector Multiplication on CUDA", NVIDIA Technical Report NVR-2008-004, NVIDIA Corporation, December 2008.

[4] Peter J Braam, "The Lustre Storage Architecture", Cluster File Systems Inc, 2002.

[5] Message Passing Interface Forum, "MPI-2: Extensions to the Message Passing Interface", http://www.mpi-forum.org/docs/docs.html, Jul. 1997.

[6] Yu, W., Vetter, J., Canon, R.S. and Jiang, S., "Exploiting Lustre File Joining for Effective Collective I/O", In the Proceedings of the Seventh IEEE International Symposium on Cluster Computing and the Grid (CCGrid '07), 2007.

[7] Liao, W.-k., Ching, A., Coloma, K., Choudhary, A. and Ward, L., "An Implementation and Evaluation of Client-Side File Caching for MPI-IO", In the Proceedings of the International Parallel and Distried Processing Symposium (IPDPS '07), 2007.

[8] Kenin Coloma, Alok Choudhary, Wei-keng Liao, Lee Ward and S.T., "DACche: Direct Access Cache System for Parallel I/O", In Proceedings of the International Supercomputer Conference, June 2005.

[9] Lee, J., Ma, X., Ross, R., Thakur, R. and Winslett, M., "RFS:Efficient and Flexible Remote File Access for MPI-IO", In the Proceedings of the IEEE International Conference on Cluster Computing, 2004.

[10] Logan, J. and Dickens, P., "Using Object Based Files for High Performance Parallel I/O", In the Proceedings of the To Appear: IEEE International Workshop on Intelligent Data Acquisition and Advanced Computing Systems: Technology and Applications. Dortmund, Germany, 2007.

[11] Phillip M. Dickens and Jeremy Logan, "Towards a high performance implementation of MPI-IO on the Lustre file system", In Proceedings of GADA'08: Grid computing, high-performance and Distributed Applications. Monterrey, Mexico, November 2008.

[12] Rajeev Thakur, William Gropp, Ewing Lusk, "Data Sieving and Collective I/O in ROMIO", Proceedings of the The 7th Symposium on the Frontiers of Massively Parallel Computation, p.182, February 21-25, 1999 .

[13] Zhao T Z, Verdi M, Dong S B, et al, "Evaluation of a performance model of Lustre file system", The Fifth Annual ChinaGrid Conference. Guangzhou: IEEE Computer Society, p.191-196, 2010.

Research on Data parallel and Scheduling Mechanism based on Petri nets

Jing Zhao
School of Computer Science and Technology
Nanjing Normal University
Nanjing, China
njnu_zj@163.com

Xuejun Liu
Virtual Geographic Environment Key Laboratory of the Ministry of Education
Nanjing, China
liuxuejun@njnu.edu.cn

Wanfeng Dou
Nanjing Normal University
Nanjing, China
douwf_fly@163.com

Kun Yang
School of Computer Science and Technology
Nanjing Normal University
Nanjing, China
757389791@qq.com

***Abstract*—** There are two method frequently used for parallelization: data parallel and task parallel. According to the characteristics of analysis of digital terrain, data parallel is more applied, so Petri nets is introduced in this paper to describe the parallel relationships within data patitions based on granularity model. As for different storage environment, corresponding scheduling algorithms are proposed for load balance.

Keywords- PDTA, Petri nets, data parallel, dependent relation.

I. INTRODUCTION

In recent years, along with the emerging parallel computing architecture such as distributed cluster, grid and pervasive computing, which characterizes the parallel computing with high speed, low input, etc, the parallel computing is becoming the mainstream technology of scientific computing.

Digital Terrain Analysis (DTA) is digital information processing technology based on Digital Elevation Model (DEM) which is used to compute all the kind of attributes of terrain and extract the features of terrain[1]. Parallel analysis of digital terrain (PDTA) is the combination of parallel computing and geography, and its development is closely related with the daily innovation of parallel computing technologies. The connotation of DTA is becoming deeper and deeper, with its application wider and wider, which makes parallelization of various terrain analysis algorithms possible.

II. RELATED RESEARCH

The researches on PDTA were started abroad early, while were lack of systematic theory at home, despite of tremendous development of PDTA recently. At present, for the characteristics of DEM data, most scholars realized parallelization of PDTA algorithms by data parallel strategies, the typical researches of which are as follow: Mower[2] compared the performance of different parallel strategies for different data on parallel machines. Gong[3] segmented the data by river watershed to realize parallel computing on high performance computers. Ortega[4] brought up parallel strategy by row-splitting based on CUDA. Zhao[5] acquired high parallel efficiency by segmenting the ordering raster data into small block. Mills[6] parallelized the serial visible algorithms using adjacent view. Kinder[7] proposed reverse area-area parallel algorithm of visibility based on M/S structure. Germain[8] brought up parallel visibility algorithm based on row-scanning under the SPMD structure.

To take full advantage of parallel computing platform composed by multi-core processors, some scholars parallelize serial algorithms making use of Directed Acyclic Graph (DAG)[10-11] to describe the dependent relationships within tasks. Guo[9] proposed algorithms which are used to transform serial structures into parallel one, while Zhang[10] suggested parallel scheduling algorithm based on DAG analysis and Du[11] optimized the construction of DAG regarding the best parallel degree. DAG can show a good description of tasks-flow, however, for PDTA it is not enough. Problems like resource competition, load balance and so on, are needed to regard to avoid faults such as deadlock, even system crash, etc. Petri nets are better in concurrent systems[12], because it not only uses transitions to express tasks of PDTA, but also describes data entity delivered between tasks by places with tokens. Petri nets can express relationships within data and tasks when compared with DAG, so this paper introduces Petri nets to construct parallel dependent relationships.

III. BRIEF INTRDUCTION OF PETRI NETS

Petri nets originated from "Kommunikation mit Automaten"[13] by Carl Adam Petri (Germany) in 1962, and it is also called Net Theory, which is a branch of theoretical computer science including auto machine model and formal language theory.

Petri nets use intuitionistic graphics to show the resources flow and collision relations in system, so it’s

978-0-7695-4818-0/12 $26.00 © 2012 IEEE
DOI 10.1109/DCABES.2012.117

applied widely in many fields. At present, Petri nets model is mainly used in the modeling and simulation of discrete-time system and workflow, description and validation of network protocol and valuation of network performance, knowledge representation in the AI, and reasoning of software system, etc. Petri nets theory have been developing and improving in more than 40 years, with the longitudinal development from the basic conditions/events nets to position change nets and to senior nets. Its crosswise developments are from the nets without parameters to time Petri nets and random Petri nets, from the atom transition to predicate and subnet transition, and the fuzzy Petri nets with knowledge representation, etc[15].

IV. ORIENTED-PDTA CONSTRUCTION OF PETRI NETS AND CORRESPONDING SCHEDULING ALGORITHMS

PDTA is dually characterized by data and tasks intensive, within which are complex interdependent relations. In order to analyze data and tasks by quantification, granularity model was brought up and detailed in another thesis of our project. Granularity can be classified into atom and poly ones by dividable angle, data, task and structure ones by represent object. Atom granularity is the basic unit in parallel computing, while the poly granularity composed of atom ones can be instantiated into an independent system operates like atom one, moreover, it can be further divided into lower granularities which are instantiated into corresponding system operates.

In this thesis, the construction of Petri nets based on data parallel is discussed in detail, in which data and tasks are expressed by granularity so as to quantify. In regard of data parallelization, we classify some situation from the partitionablity of input data.

A. Atom data granularity – Atom task granularity Model (ADG-ATG model)

When the input is atom data granularity which is not dividable from data angle, it can not be parallel in data. At the same time, atom task granularity which is also undividable cannot be operated in parallel. As in Figure 1, the transition represents atom task granularity or a couple of atom task granularity with flow relation. Task granularity with flow relation refers to such tasks between which have input or output delivery, so there is no possibility to parallel in task. ADG-ATG model is the basic model in parallel computing, which belongs to situations when poly data or tasks granularity are partitioned into lower ones.

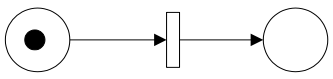

Figure 1 Petri nets of ADG-ATG model

B. Poly data granularity – Atom task granularity Model (PDG-ATG model)

When the input is ploy data granularity which is dividable, we can realize parallel computing by data-splitting. As to the atom task granularity, there is no partitionablity by itself, but several such task granularities composed into task flow with in or out parameters delivery. The same task flow is operated on different data granularity divided from poly granularity.

At present, in parallel computing, the data is accessed in two kinds of environment: shared memory and distributed memory . Shared memory is such model based on overall storage space from which processors or threads read and write data. The advantage of shared memory is that it is easy to realize for programmer, while the disadvantage is reading and writing bottleneck caused when the system has too many computing points. Distributed memory is accessed in form of part index, which avoid the shortcomings of shared storage, but it also brings in frequent data communication which adds time cost. Above all, different pattern of storage needs different data parallel strategies.

1) Shared Memory

When the scale of cluster is small, shared memory can reduce the communication of data so as to improve the efficiency of parallel computing. The poly data granularity stored in sever is segmented and distributed by method which proposed in another thesis of ours. Using shared memory would bring in bottlenecks when several threads reading from or writing into the memory at the same time and "dirty data", so reading and writing of parallel computing is needed to control. In hence, the task flow is segmented into three steps instanced as atom task granularity: data-reading, computing and data-writing.

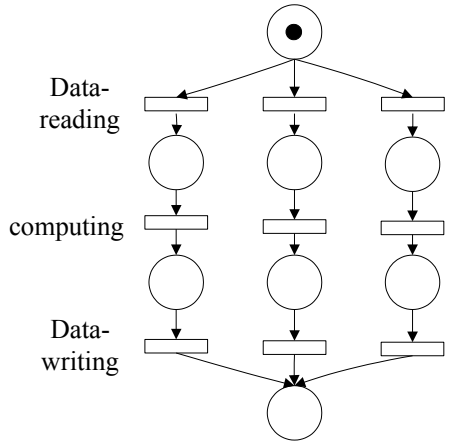

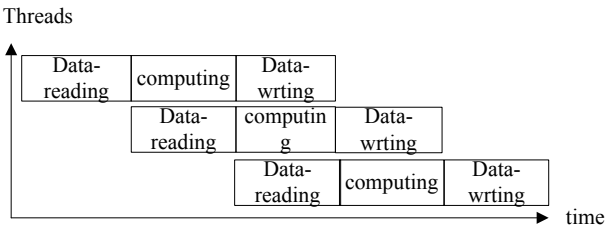

Figure 2 Petri nets of PDG-ATG model in shared storage

Figure 3 the flow pipeline scheduling

As in Figure 2, the relations within data-reading,

computing and data-writing are flow relationship, in which the computing step must execute after data-reading, and data-writing should be after computing. Because the disk only has one head for reading or writing, operates can just execute in serial. When the data-reading of first pipeline is completed, the computing of it and the reading of second pipeline can be carried out in parallel to achieve higher performance, because there is no dependency relation between them. In conclusion, PDG-ATG model in shared storage can be realized in parallel by flow pipeline technology, such as in Figure 3.

In this algorithm, the main thread is responsible for the control of pipeline processing. When the first slave thread completes reading data, it sends a signal to the main thread, which informs the next pipeline to begin reading data. At the same time, the slave thread of the first pipeline from begins the computing step. When the slave thread of the second pipeline sends a signal, the slave thread of the third pipeline starts reading data. The whole process is such and so on.

The pseudo-code of flow pipeline processing algorithm of PDG-ATG model in shared storage is shown as follows.

```
Main thread
void Share_MDSP(int kernel, double DEM[row][col]){
    cell=DG.row;
    while (tag=true) {
        for(i=1; i<=kernel; i++){
          creat Tread[i];
          tag=false;
          break;}
          }
```

```
Slave thread[i]
    read DEM[i~i+cell-1][col];
    read the redundant rows and cols;
    tag=true;
    compute;
    write DEM[i~i+cell-1][col];
    i--;
```

2) Distributed Memory

When the cluster system is in large scale, several nodes request for the reading and writing to shared memory at the same time, which will be challenges to the ability of system's I/O. It's needed to adopt necessary synchronization strategies to ensure the consistency of the data in shared memory which brings in resources consumption and a waste of time. Moreover, the shared memory scalability will become the bottleneck of system's performance, which can not meet the further storage needs of mass DEM data. But the distributed memory can well solve the above problems.

Messages are communicated between nodes in distributed memory to coordinate each processor, and the main node is used to record the position information of each block by directory structure. The scalability of distributed memory is good, while communication is the key of its performance. In regard of PDG-ATG model, different node executes the same task flow, so it is important to determine data granularities to ditribute. As the precision of digital terrain analysis is impacted by boundary point, so we need redundancy for data. Data granularity with neighbor relation should be deployed in the adjacent nodes to reduce the communication distance. In distributed memory, it's needed a thread for algorithm to distribute data and complete merging of data, as shown in Figure 4.

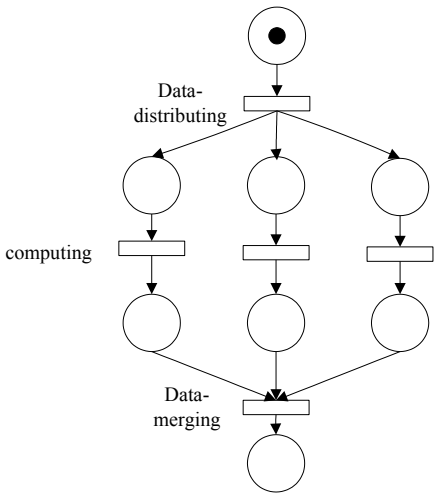

Figure 4 Petri nets of PDG-ATG model in distributed memory

The pseudo-code of pipeline processing algorithm of PDG-ATG model in distributed storage is as follows.

```
Main thread
compute the size of data Poly-Granularity;
G_Row <— the value of the row of data Poly-Granularity;
G_Row <— the value of the col of data Poly-Granularity;
creat N threads;  send G_Row and G_Row to all slave threads;
receive search message from thread[n];
search the neiboghor_data of thread[n];
send neiboghor_data[1~(G_Row -L_Row)][1~(G_Col - L_Col)] to thread[n];
Send neiboghor_result_data[1~(G_Ro-L_Row)][1~(G_Col -L_Col)] to neighor of thread[n];
```

```
Slave thread[n]
    receive G_Row and G_Row;
    L_Row <— the value of the row of local data;
    L_Col <— the value of the col of local data;
    if (G_Row <= L_Row^ G_Col <= L_Col )
        digital terrain analysis;
    else
        send search message to main thread;
        receive neiboghor_data [1~G_Row-L_Row][1~G_Col-L_Col] to thread[n];
        digital terrain analysis;
    write local memory;
    send neiboghor_result_data [1~G_Row-L_Row][1~G_Col-L_Col] to main thread;
```

In this algorithm, the main thread is the responsible for distributing and receiving messages from the slave threads. The slave threads execute computing according to the local data. If the local data is cannot meet the computing needs assigned by the main thread, the slave thread sends request to main thread to get data from adjacent node .

V. CONCLUSIONS

Firstly, the basic concepts of the Petri nets are introduced in this paper. Secondly, construction of Petri nets is discussed in detail based on granularity model, and the corresponding scheduling strategies are given in view of the different storage mechanism. Parallel computing can be realized through the data parallel and task parallel. In order to face parallel computing platform such as clusters with multi-core, task parallel mechanism based on Petri nets should be studied deeply. The atom data granularity–poly task granularity model and poly data granularity–poly task granularity model will be discussed further to analyze the possibility of parallelization for terrain computing algorithms.

ACKNOWLEDGEMENT

This paper is supported by the National Natural Science Foundation of China (Key Project No. 41171298), National High Technology Research and Development Program of China (863 Program, NO.2011 AA120304) and the Foundation of Graduate Innovation Training Plan of Jiangsu Province(NO.CXZZ12_0393).

REFERENCE

[1] Zhou Qiming, Liu Xuejun. Digital Terrain Analysis [M]. Beijing: Science Press, 2006. (in Chinese)

[2] Mower James E. Data-parallel procedures for drainage basin analysis [J]. Computer & Geosciences, 1994, 20(9):1365-1378.

[3] Gong Jianya, Xie Jibo. Extraction of drainage networks from large terrain datasets using high throughout computing [J]. Computers & Geosciences, 2009, 35(2): 337-346.

[4] Ortega L Rueda A. Parallel drainage network computation on CUDA[J]. Compute & Geosciences, 2010, 36(2):171-178.

[5] Zhao Xiang hiu, Miao Qing, Fu Zhong liang,etc. Research and realization in parallel algorithm of confluence analysis based on CUDA. Application research of computers,2010, 27(7): 2447-2451.

[6] Mills Kim, Fox Geoffrey, Heimbach Roy. Implemention an intervisibility analysis model on a parallel computing system [J]. Computers & Geosciences,1992, 18(8): 1047-1054.

[7] Kidner D B, Railings P J, Ware J.A. Parallel processing for terrain analysis in GIS: visibility as a case study [J]. Geoinformation, 1997, 1(2) :183-207.

[8] Germain D, Laurendeau D, Vézina G. Visibility analysis on a massively data-parallel Computer. Concurrency: Practice and Experience, 1996, 8(6): 475～487.

[9] Guo Long, Chen Hongzhong, Ye Qing. Develop Direct Acyclic Graph (DAG) corresponding to serial program [J]. Computer Engineering and Applications, 2007, 43(1): 41-44. (in Chinese)

[10] Zhang Aiqing, Mo Zeyao. A New Scheduling Algorithm for Digraph-Based Parallel Computing [J]. Chinese Journal of Computers, 2009, 32(11): 2178-2186. (in Chinese)

[11] Wang Shuang, Li Xinke. Grid task scheduling algorithm based on LBT [J]. Journal of Hefei University of Technology, 2010, 33(1): 64-67. (in Chinese)

[12] Pet Du Jiancheng, Huang Hao, Chen Daoxu, Xie Li. Optimum Degree of Parallelism-based Task Dependence Graph Scheduling Scheme [J]. Journal of Software, 1999, 10(10): 1038-1046. (in Chinese)

[13] Yuan Chong yi. Theory and application of Petri nets. Electronic Industry Press: 2005.(in Chinese)

[14] C.A.Petri. Kommunikation mit Automaten. PhD thesis, Institut fur Instumentelle Mathematik, Bonn, Germany 1962. In German.

[15] Feng Ding. Research on the use of colored timed Petri net and stochastic Petri net[D]. He fei:He fei university of technology, 2009.(in Chinese)

Adapting Matrix-Vector-Multiply Wavefront Reconstruction to SMP

Haotian Zhang, Mei Li, Luchun Zhou
The Key Laboratory on Adaptive Optics
Institute of Optics and Electronics, CAS
Chengdu, China
E-mail: zhanggaotai@gmail.com

***Abstract*—In adaptive optics systems, the process time of wavefront controller is a critical parameter. For a fixed frame rate, decreasing the process time results in higher control bandwidth. Among the process steps of a wavefront controller, wavefront reconstruction is a time consuming task. In this paper, we parallelized wavefront reconstruction algorithm on a cutting edge shared-memory eight-core DSP to reduce process time. The conducted experiment shows that even using the most computation and memory intensive matrix-vector-multiply (MVM) reconstruction algorithm, performance requirements can be met with reconstruction latency around 130us in a 913 actuators AO system. With parallelization of the reconstruction algorithm, it's possible to apply high frame rate in the system and easy to scale up to larger systems with more actuators.**

Keywords- Adaptive Optics; Wavefront reconstruction; DSP; Parallel processing

I. INTRODUCTION

Large ground-based telescopes are often equipped with adaptive optics (AO) systems to obtain better imaging. The concept of AO was brought forward by H.W. Babcock in 1953. A typical AO system consists of Wave Front Sensor (WFS), Wave Front Controller (WFC) and several deformable mirrors (DM). Wavefront errors caused by atmospheric turbulence are sampled by WFS and sent as input to WFC. Control signals are then generated by the WFC through several steps and sent to DMs' actuators for real-time compensation [1]. As the atmosphere between the target and telescope changes fast, high sample rate is needed to close-loop the system. At a fixed frame rate, shorter WFC process delay provides higher control bandwidth. Wavefront reconstruction is one of the most time consuming task in WFC. Its computational complexity is proportional to the square of number of actuators to be controlled. To achieve the goal of shorter processing time, distributed parallel solutions are deployed on different hardware platforms like FPGA [2, 3] and GPU [4]. We parallelize wavefront reconstruction to reduce process delay on an 8-core symmetric multi-processor (SMP). An experiment is used to demonstrate that, with a configuration of 968 sub-apertures WFS and 913 actuators DM, the most computation and memory intensive Matrix-Vector-Multiply (MVM) wavefront reconstruction method takes less than 130 us to complete. In part II, we briefly introduce the MVM algorithm. Part III is detail design for parallelization. Experiment is explained in part IV.

II. MVM WAVEFRONT RECONSTRUCTION ALGORITHM

MVM is a classic wavefront reconstruction algorithm that has been used for a long time. The former implementation of the Keck observatory [5] and the new SPARTA [6] both deploy this method. MVM takes the slope vector g from previous step as input and calculates the DMs' control signal v. The calculation is a simple matrix operation as (1). The reconstruction matrix R can be calculated or measured offline and is fixed during real-time operation. Usually, the number of sub-apertures represented by n is close to that of actuators represented by m. So the computational complexity of MVM is O(n*n). In modern AO systems, the WFS usually consists of more than 1000 sub-apertures making the computational burden heavy for MVM.

$$v = Rg = \begin{pmatrix} r_{1,1} & \cdots & r_{1,2n} \\ \vdots & \ddots & \vdots \\ r_{m,1} & \cdots & r_{m,2n} \end{pmatrix} * \begin{pmatrix} g_1 \\ g_2 \\ \cdots \\ g_{2n} \end{pmatrix} \quad (1)$$

There are three typical parallelization schemes for MVM, column-wise, row-wise and hybrid [7]. Row wise MVM starts calculation after receiving full frame's slope data. Column wise and hybrid MVM start calculation after receiving partial slope data and do MVM operation on part N slope data of a total frame while the step before reconstruction in WFC produces part N+1 slope data, forming a pipeline to reduce reconstruction delay. Row wise and hybrid MVM are used and compared in this paper. As Fig. 1 shows, the reconstruction matrix is divided into several smaller matrixes and calculated on multiple threads at the same time, the results is then combined.

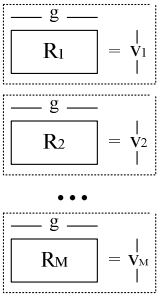

(a)

978-0-7695-4818-0/12 $26.00 © 2012 IEEE
DOI 10.1109/DCABES.2012.43

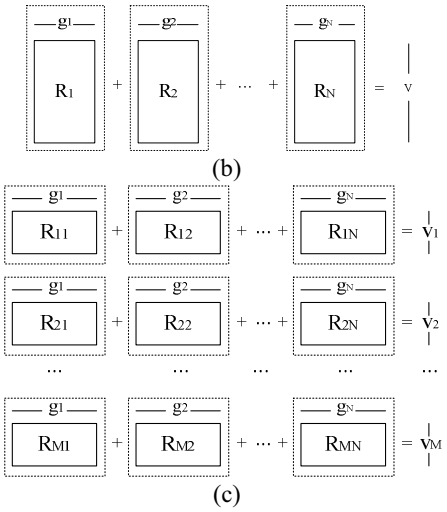

Figure 1. Parallelization schemes for MVM: (a) row wise (b) column wise (c) hybrid. M and N stands for number of partition row and column wise.

III. PARALLELIZATION OF MVM

The digital signal processor (DSP) we choose is TI's latest 8-core, high speed TMS320C6678. Each chip consists of eight C66x cores able to operate at 1.25 GHz and a 4 MB shared memory. In the later tests, we run the chip at a frequency of 1.25 GHz. TI provides users with a tool called IPC to communicate between different cores and fully utilize the power of multicore.

A. Row wise

When using the row wise MVM scheme, the multiplication task is divided into the same number of parts as the cores and assigned to a thread on each core. The division is equal among each thread so all threads finish calculation at approximately the same time resulting in minimum processing time. Master/Slave model is used for task scheduling and synchronization [8]. A master core is responsible for synchronization of all the slave cores. As in Fig. 2, when all slope data arrive, the master core sends start event to all the slave cores, after receiving start event, a slave core starts to calculate its own task and sends a finish event to the master core when calculation is done. After the master core has received finish event from all the slave cores, the processing of a frame is done.

IPC provides two modules that can implement the event mechanism, MessageQ and Notify. MessageQ is the common messaging API for most applications providing the ability to send variable length of data to other cores. But in our scenario, the extra overhead of MessageQ can't be neglected. The measured overhead of MessageQ on an 8-core configuration is around 90 us while the simpler Notify has a shorter overhead of 32 us. To achieve shorter reconstruction delay, we use Notify for frame synchronization. The reconstruction matrix and slope vector are stored at a fixed address during one run. Before the run starts, the master core sends address and size of matrix and vector to slave cores using MessageQ. For each frame, the procedure shown in Fig. 2 is triggered once using Notify as the event mechanism. The results are written to a fixed address to avoid extra messaging. To ensure cache coherency, functions Cache_inv and Cache_wb can be called.

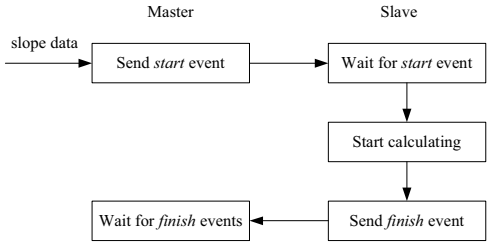

Figure 2. Master/Slave parallel processing model

B. Hybrid

The only difference between row wise and hybrid is that the hybrid does calculation when slope data are being generated while row wise won't start until all slope data have been generated. The comparison is shown in Fig. 3. In hybrid scheme, slope data of one frame is divided into N parts. The delay is only the processing time of the last part of a frame's slope data but not the whole frame. To make sure no pipeline stall happens, the MVM processing time of part i must not exceed the slope generation time of part i+1(i is from 1 to N-1); the MVM processing time of the last part N must not exceed the slope generation time of the first part. After acquiring time parameters of slope generation and MVM, a partition of the slope data is carefully chosen.

IV. PERFROMANCE TEST

We use a configuration of 968 sub-apertures and 913 actuators to test reconstruction performance. The input slope data's type is fixed 16 bit integer. The experiment is conducted on a TMDXEVM6678L evaluation board provided by TI. A total number of 1000 frames are used to get average results and jitter.

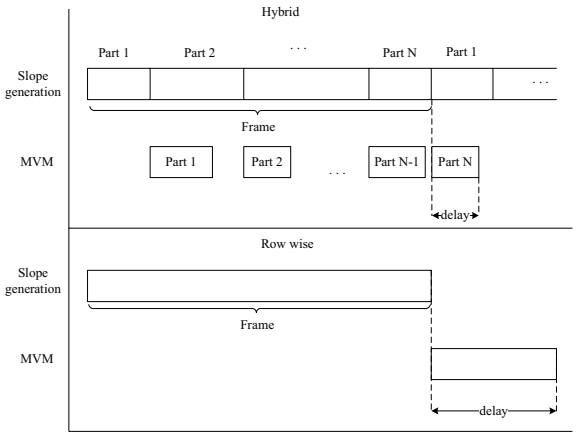

Figure 3. Comparison of hybrid and row wise

TABLE I. TIME PERFORMANCE OF ROW WISE

Average delay	Synchronization overhead	Pure computation time	Peak to Peak (jitter)
129.7 us	32.9 us	96.8 us	7.6 us

TABLE II. TIME PERFORMANCE OF HYBRID

Average delay	Peak to Peak
57.2 us	6.4 us

A. *Row wise*

The reconstruction matrix is divided into 8 parts evenly row wise and assigned to 8 cores of DSP. Test results are shown in table 1. The pure computation time can also be calculated. After optimization, a single C66x core can perform 2 MAC per cycle, a result seems a little low for the high performance DSP. Due to the memory intensive nature of MVM algorithm, memory bandwidth becomes the bottleneck of overall performance. The estimated processing time can be calculated as (2), which is close to the measured time, 96.8 us.

$$\frac{2\times 968\times 913(\mathrm{MAC})}{2(\mathrm{MAC/cycle})\times 8(\mathrm{core})\times 1.25(\mathrm{GHz})} = 88.4(us) \quad (2)$$

B. *Hybrid*

By applying partition both row and column wise, the last part of slope vector g contains only 340 sub-apertures. The test results are shown in table 2.

Using hybrid scheme, the delay time is reduced significantly compared to that of row wise (from 130 us to 57 us).

V. CONCLUSIONS

By parallelizing MVM, the reconstruction requirements of a 968 sub-apertures, 913 actuators system can be met with a single DSP chip. For larger systems or higher frame rate requirements, scaling up can be as easy as interconnecting multiple chips to provide more processing power.

REFERENCES

[1] Wenhan Jiang, Technology of Adaptive Optics, Advances in Chinese science and technology, No. 6, pp. 94-121, 1998.

[2] Wenjia Zheng, Chunhong Wang, Wenhan Jiang, Mei Li and Duanwu Tang, Wavefront reconstruction used for adaptive optics system on a linear and bidirectional systolic array, Infrared and Laser Engineering, Vol. 36, pp. 936-940, 2007.

[3] Luchun Zhou, Chunhong Wang, Mei Li and Wenhan Jiang, Real-time wavefront reconstruction based on a control flow systolic array, Opto-Electronic Engineering, Vol. 35, pp. 39-42, 2008.

[4] Tuan N. Truong, Antonin H. Bouchez et al., Real-time wavefront control for the PALM-3000 high order adaptive optics system, Proc. of SPIE, Vol. 7015, 70153I, 2008.

[5] Marcos A. van Dam, David Le Mignant and Bruce A. Macintosh, Performance of the Keck Observatory adaptive-optics system, Applied Optics Vol. 43 No. 29, 5458-5467(2004).

[6] E. Fedrigo and R. Donaldson, SPARTA roadmap and future challenges, Proc. SPIE 7736, 77364O (2010).

[7] Rodolphe Conan and Jean-Pierre Veran, Advances in real-time control algorithms, Proc. SPIE 7736, 773613(2010).

[8] David Bell and Greg Wood, Multicore programming guide, Texas Instruments, (2009).

Hybrid Deterministic/Monte Carlo Neutronics using GPU Accelerators

Jeff Willert *, C. T. Kelley*, D. A. Knoll †, Han Dong ‡, Mahesh Ravishankar §,
Paul Sathre ¶, Michael Sullivan ‖, William Taitano **
*Department of Mathematics, North Carolina State University, Raleigh, NC 27695-8205
Email: jawiller@ncsu.edu, tim_kelley@ncsu.edu
† Theoretical Division, MS B216, Los Alamos National Laboratory, Los Alamos, NM 87545
Email: nol@lanl.gov
‡ Computer Science and Electrical Engineering Department
University of Maryland Baltimore County, Baltimore, Maryland 21250 Email: han6@umbc.edu
§ Department of Computer Science and Engineering
Ohio State University, Columbus Ohio 43210 Email: ravishan@cse.ohio-state.edu
¶ Department of Computer Science, Virginia Tech University
Blacksburg, VA 24060, Email: sath6220@cs.vt.edu
‖ School of Electrical and Computer Engineering, University of Texas at Austin, 1 University Station
Mailcode C0803, Austin, TX 78712 Email: mbsullivan@utexas.edu
‖ Chemical and Nuclear Engineering Department, 1 University of New Mexico
Albuquerque, New Mexico 87131 University of New Mexico, Email: taitae25@unm.edu

***Abstract*—In this paper we discuss a GPU implementation of a hybrid deterministic/Monte Carlo method for the solution of the neutron transport equation. The key feature is using GPUs to perform a Monte Carlo transport sweep as part of the evaluation of the nonlinear residual and Jacobian-vector product. We describe the algorithm and present some preliminary numerical results which illustrate the effectiveness of the GPU Monte Carlo sweeps.**

***Keywords*-Neutron Transport, Jacobian-Free Newton-Krylov, GPU, Monte Carlo**

I. Introduction

In a recent paper [1] we considered a Jacobian-Free-Newton-Krylov (JFNK) solver for the Nonliner Diffusion Acceleration (NDA) formulation of the neutron transport equation using a hybrid deterministic/Monte Carlo approach for evaluation of the nonlinear residual. In certain reactor calculations it may be highly preferable to solve the neutron transport equation using Monte Carlo methods [2]. Monte Carlo methods allow for a continuous treatment of space, angle and energy, removing discretization errors. Monte Carlo methods allow for us to simulate the exact physics using known probability distributions and continuous cross-section data. Furthermore, Monte Carlo methods allow us to treat complex geometries exactly. In addition, recent advances in computing allow us to exploit the massively parallel nature of the Monte Carlo simulation. In this paper we show how the Monte Carlo (MC) computations can be efficiently implemented on a GPU.

A. The Neutron Transport Equation

We consider the steady-state, mono-energetic, neutron transport equation in one space dimension with anisotropic scattering in a homogeneous medium [2]–[4]

$$\mu\frac{\partial\psi}{\partial x}(x,\mu) \quad +\Sigma_t\psi(x,\mu) = \frac{\Sigma_s}{2}\int_{-1}^{1}\psi(x,\mu')\,d\mu' + q(x)/2, \tag{1}$$

for $0 < x < \tau$ and $\mu \in [-1,0)\cup(0,1]$. We impose boundary conditions

$$\psi(0,\mu) = \psi_l(\mu), \mu > 0; \psi(\tau,\mu) = \psi_r(\mu), \mu < 0. \tag{2}$$

In (1)

- ψ is intensity of radiation or angular flux at point x at angle $\cos^{-1}(\mu)$
- $\tau < \infty$,
- $\Sigma_s \in C([0,\tau])$ is the scattering cross section at x,
- $\Sigma_t \in C([0,\tau])$ is the total cross section at x,
- ψ_l and ψ_r are incoming fluxes at the boundaries, and
- $q \in C([0,\tau])$ is the fixed source

The quantity of interest is the scalar flux

$$\phi(x) = \int_{-1}^{1}\psi(x,\mu')\,d\mu'. \tag{3}$$

One way to solve for ϕ is a linear fixed point approach called source iteration. Here one updates an approximation ϕ_c to ϕ by solving the one parameter family of ordinary differential equations

$$\mu\frac{\partial\psi_c}{\partial x}(x,\mu) + \Sigma_t\psi_c(x,\mu) = S(x) \equiv \frac{\Sigma_s}{2}\phi_c(x) + q(x)/2 \tag{4}$$

by integrating forwards with initial data ψ_l for $\mu > 0$ and integrating backwards with final data ψ_r for $\mu < 0$. One

978-0-7695-4818-0/12 $26.00 © 2012 IEEE
DOI 10.1109/DCABES.2012.37

obtains a solution ψ_c and new approximation to the flux is

$$\phi_+(x) = \int_{-1}^{1} \psi_c(x,\mu')\, d\mu'.$$

The fixed point formulation is $\phi_c = \phi_+$. One can express this as a compact fixed point problem

$$\phi - K\phi = g$$

and solve it with, say, a Krylov iterative method [5] rather than simple successive substitution. The Krylov approach performs much better, as do multilevel methods [6], [7].

Another approach is to reformulate the equation as a nonlinear problem for the flux [8]–[13]. We will describe the method in terms of *nonlinear diffusion acceleration* (NDA) [8], [9]. In this method one converts the fixed point problem for ϕ into a "low-order" nonlinear diffusion equation. The low-order equation is coupled to the "high-order" transport equation to make enforce consistency.

Evaluation of the nonlinear residual, given a low-order flux ϕ^{LO}, begins with solving (4) with $\phi = \phi^{LO}$ subject to the original boundary conditions (2). From ψ compute the high-order flux ϕ^{HO} and current J^{HO} from

$$\phi^{HO}(x) = \int_{-1}^{1} \psi(x,\mu')\, d\mu'.$$

and

$$J^{HO}(x) = \int_{-1}^{1} \mu'\psi(x,\mu')\, d\mu'.$$

Define

$$\hat{D} = \frac{J^{HO} + \frac{1}{3\Sigma_t}\frac{d\phi^{HO}}{dx}}{\phi^{HO}}.$$

We have solved the problem if ϕ^{LO} is the solution of the diffusion equation

$$\begin{aligned} F(\phi) &= \tfrac{d}{dx}\left[\tfrac{-1}{3\Sigma_t}\tfrac{d\phi}{dx}\right] + (1-c)\,\phi \\ &\quad + \tfrac{d}{dx}\left[\hat{D}(\phi^{HO}, J^{HO})\phi\right] \\ &= 0, \end{aligned} \tag{5}$$

with appropriate boundary conditions.

The numerical results in [1] and in § III of this paper use the standard second-order finite difference discretization of (5). The fully deterministic approach from [1], [8] used a diamond-difference S^N [2] discretization for (4). We will not go into details of the discetizations in this paper.

We will briefly discuss solvers here and refer the reader to [5], [14], [15] for the details on Newton-Krylov nonlinear solvers. Recall that Newton's method for a nonlinear equation $F(\phi) = 0$ updates a current approximate solution ϕ_c to a new one ϕ_+ by adding the Newton step

$$\phi_+ = \phi_c + s$$

where s is the solution of

$$F'(\phi)s = -F(\phi) \tag{6}$$

and F' is the Jacobian (finite dimensions) or the Fréchet derivative (infinite dimension). In a Jacobian-Free Newton-Krylov solver, one solves (6), the linear equation for the Newton step, with a preconditioned Krylov method.

In [1] we describe a preconditioned JFNK approach for solving (5). In that paper, solving (4) was the dominant cost of the computation. The Jacobian-vector product one needs in the GMRES iteration for the Newton step may be done with a forward difference

$$F'(\phi)v \approx \frac{F(\phi + hv) - F(\phi)}{h}$$

with an appropriate choice of difference increment h [5] or, as we did in [1] an analytic Jacobian-vector product, assuming that product can be evaluated in an efficient way. For the algorithm considered here, evaluation of an analytic Jacobian-vector product $F'(\phi)v$ is a simple application of the chain rule and the solution of (4) with $\Sigma_s v/2$ as the right side. Our approach solves (4) and recovers fluxes and currents with a MC computation. In this way both the nonlinear residual and Jacobian-vector product can be done with MC.

B. Monte-Carlo

In recent years it has become increasingly popular to approximate the solution the neutron transport equation using stochastic methods. In order to make these stochastic calculations more efficient, we would like to create hybrid algorithms that utilize accelerators such as NDA [1], [8] or Quasi-Diffusion [8], [13], which were originally developed for deterministic methods. We will use MC simulation to approximate the scalar flux, current and Eddington tensor.

MC simulations use random number generation to sample probability distributions that describe likelihoods for physical events. By simply considering the physical process we're trying to model we can write a MC algorithm that will approximate these desired physical quantities.

For every neutron in the system which we are modeling, we must track its location and direction. If we isolate a single neutron, we can describe its "particle history" in very simple terms:

1) The particle is "born" at some location in the medium. The probability of being born in any given location is dependent on the fixed source, the scattering source, and, in general, the fission source. We'll only concern ourselves with the fixed and scattering sources in this application.
2) The particle travels in some straight-line direction away from its starting location until it undergoes an interaction ("collision") within the medium or it leaves the medium. It is important to note that neutrons interact only with the medium, not other neutrons. This makes each particle history independent of one another.

3) At the point of a collision, one of two things may occur. The neutron may be absorbed by the medium and this concludes the particle history. Also, the neutron may scatter off the material at the location of interaction. In this case, the particle will assume a new direction and continue along its particle history. If the particle scatters, we return to Step (2) and continue.

Once all of the particle histories have been observed, we can tally the physical quantities in which we are interested. We consider both *face tallies* and *track-length tallies*. With *face tallies*, a particle contributes to the overall tally each time it cross the face of a cell. In this case, when a particle crosses a face, we add a small contribution based on its relative weight factor to the tally. In a particle does not cross any cell faces, the particle does not contribute to the tally statistics.

With *track-length tallies*, every particle will offer some contribution to the over tallies. In this case, a particle gives a contribution to the overall tally in every cell which it travels. In this case, the contribution to a given cell is based on the distance the particle traveled within that cell times the particle's relative weight factor. Track-length tallies are generally preferable because they give a more "continuous" tally and each particle gives us some information that helps shape the overall physical quantities.

Within every algorithm for solving the neutron transport equation, we must compute one or more transport sweeps, that is solve (4) for ψ_c and then compute fluxes and currents.

This same idea can be used to build a MC transport sweep (i.e. compute the action of a transport sweep using a MC simulation). Just as we do for the deterministic case, we build a fixed source term for (4) and ask the MC simulation to solve a scattering-free problem. This amounts to simulating particle flights in which all particles are absorbed at the point of their first interaction (collision within the medium).

In this case, our MC algorithm simplifies dramatically. We have removed the need to loop through the simulation process within each particle history and all logic has been removed from the particle simulation process. The new, simplified algorithm for simulating a single particle history results:

1) Determine a starting location for the particle and a starting weight based on the source term $S(x)$.
2) Use random number generation to compute a direction for the particle to travel.
3) Use random number generation to compute a distance for the particle to travel.

After the particle travels the pre-determined distance, it undergoes a collision within the medium and is absorbed. This concludes the particle history, and there is no need to test whether or not the particle has been absorbed or whether or not the particle has left the medium (however, this will need to be handled during the tallying phase). All logic has been eliminated from the simulation. It is important to note that tallying has been greatly simplified as well. Instead of being forced to tally fluxes, currents and Eddington tensors between every interaction, we must only tallying along one flight per particle.

II. Hybrid NDA with GPUs

The final part of the algorithm is the use of GPUs to perform the Monte-Carlo transport sweep with NDA, *i. e.* accumulate fluxes and currents from (4). If we consider the MC transport sweep, we realize that there is a significant potential for parallelism. Since each particle history is independent within the MC transport sweep routine, we can simulate each of these particles in parallel. It is important to remember that particles only interact with the medium, not each other. GPUs allow us to take advantage of massive thread-level parallelism in accelerating this process.

Furthermore, if we consider the mathematics required to simulate a particle history, the operations required are simple. We generate three to four random numbers and perform additions, multiplications and some division. These simple operations are well-suited for a GPU implementation of the algorithm. GPUs excel when they're asked to perform a large volume of simple, parallel computations in which memory storage is low. In addition, by removing all (or most) of the logical checks within the algorithm, we've made the routine more GPU-friendly.

Given the choice of N particle histories per function evaluation and N_x spatial cells for binning the scalar flux, current and Eddington tensor, our storage cost is $O(4N + 3N_x)$. It is important to recall that $N \gg N_x$. This can be broken down into storage for the simulation phase and the tallying phase. During the simulation phase, we must store a particle weight, starting location, ending location and direction for each particle (four vectors of length N). During the tallying phase, we reduce the data from the simulation into a scalar flux, current and Eddington tensor (three vectors of length N_x or $N_x + 1$). Since N can be quite large, we may simulate only a subset (or batch) of particles before performing a partial tally. If we choose to use b batches, our storage cost may be reduced to $O(\frac{4N}{b} + 3N_x)$.

We have also investigated using the GPUs for particle simulation only, and letting the CPU execute the tallying phase. In this case, storage becomes less of a concern. Here, as particle histories are generated, the data is periodically sent from the GPU to the CPU for tallying. Using this method, we incur a communication expense, but it allows us to better use our resources if CPU(s) are available. One further option is to perform a partial tally on the GPU and send these partial tallies to the CPU where they are collected and a final tally is computed. This option has the advantage that the storage requirements are still low for the GPU, yet communication costs have been reduced. In this case, we

are only required to send three vectors of length N_x from the GPU to the CPU.

A. Algorithmic Description

The formal description of the algorithm is below. We express the use of MC in both the evaluation of the nonlinear residual F and the Jacobian-vector product J by making the number of particles N_{MC} and explicit argument. Hence $F(\phi, N_{MC})$ will denote the approximation of $F(\phi)$ with N_{MC} particles and $J(\phi, d, N_{MC})$ will be the Jacobian vector product $F'(\phi)d$ using MC with N_{MC} particles.

Newton-GMRES-MC

Evaluate $R_{MC} = F(\phi, N_{MC})$; $\tau \leftarrow \tau_r \|R_{MC}\| + \tau_a$.
while $\|R_{MC}\| > \tau$ **do**
  Use GMRES with a limit of I_{max} iterations to find d such that $\|J(\phi, d, N_{MC}) + R_{MC}\| \leq \eta \|R_{MC}\|$
  if the GMRES iteration fails **then**
    $N_{MC} \leftarrow 100 * N_{MC}$
    Evaluate $R_{MC} = F(\phi, N_{MC})$
  else
    $\lambda = 1$
    Evaluate $R_{Trial} = F(\phi + \lambda d, N_{MC})$
    while $\|R_{Trial}\| > (1 - \alpha\lambda)\|R_{MC}\|$ and $\lambda \geq \lambda_{min}$ **do**
      $\lambda \leftarrow \lambda/2$
      Evaluate $R_{Trial} = F(\phi + \lambda d, N_{MC})$
    end while
    if $\lambda \geq \lambda_{min}$ **then**
      $\phi \leftarrow \phi + \lambda d$
      $R_{MC} = R_{Trial}$
    else
      $N_{MC} \leftarrow 100 * N_{MC}$
      Evaluate $R_{MC} = F(\phi, N_{MC})$
    end if
  end if
end while

III. Computational Results

In this section we report timings for a transport sweep. The hardware configuration was an Nvidia Tesla c2075 GPU and an Intel(R) Core(TM) i5-2400 CPU with 8GB RAM.

In Table I we tabulate the number of particles, the average time for a transport sweep, and the ratios of the timings from one suite of particles to the next. The table shows that the timings scale very well with the number of particles.

Table I
Transport Sweep Timings

Particles (Millions)	Time (ms)	Ratio
0.03	0.7	
0.10	1.3	2.0
1.00	8.8	6.6
10.00	85.8	9.8
20.00	167.4	2.0

IV. Conclusion

In this paper we describe a Jacobian-free Newton-Krylov solver for the NDA formulation of the neutron transport equation. The novel feature in this paper is the use of a GPU to solve the low-order problem. We discuss the algorithm, the GPU implementation of the MC transport sweep, and present computational results.

Acknowledgment

This work was been partially supported by the Consortium for Advanced Simulation of Light Water Reactors (www.casl.gov), an Energy Innovation Hub (http://www.energy.gov/hubs) for Modeling and Simulation of Nuclear Reactors under U.S. Department of Energy Contract No. DE-AC05-00OR22725 and Los Alamos National Laboratory contract No. 172092-1.

References

[1] J. Willert, C. T. Kelley, D. A. Knoll, and H. K. Park, "Hybrid deterministic/monte carlo neutronics," 2012, submitted for Publication.

[2] E. E. Lewis and W. F. Miller, *Computational Methods of Neutron Transport*. Grange Park, IL: Americal Nuclear Society, 1993.

[3] S. Chandrasekhar, *Radiative Transfer*. New York: Dover, 1960.

[4] I. W. Busbridge, *The Mathematics of Radiative Transfer*, ser. Cambridge Tracts. Cambridge: Cambridge Univ. Press, 1960, no. 50.

[5] C. T. Kelley, *Iterative Methods for Linear and Nonlinear Equations*, ser. Frontiers in Applied Mathematics. Philadelphia: SIAM, 1995, no. 16.

[6] ——, "Multilevel source iteration accelerators for the linear transport equation in slab geometry," *Trans. Th. Stat. Phys.*, vol. 24, pp. 679–708, 1995.

[7] ——, "A fast multilevel algorithm for integral equations," *SIAM J. Numer. Anal.*, vol. 32, pp. 501–513, 1995.

[8] D. A. Knoll, H. Park, and K. Smith, "Application of the Jacobian-free Newton-Krylov method to nonlinear acceleration of transport source iteration in slab geometry," *Nuclear Science and Engineering*, vol. 167, pp. 122–132, 2011.

[9] ——, "A new look at nonlinear acceleration," *Nuclear Science and Engineering*, vol. 99, pp. 332–334, 2008.

[10] D. Y. Anistratov, "Nonlinear quasidiffusion acceleration methods with independent discretization," *Nuclear Science and Engineering*, vol. 95, pp. 553–555, 2006.

[11] W. A. Wieseiquist and D. Y. Anistratov, "The quasidiffusion method for transport problems in 2d cartesian geometry on grids composed of arbitrary quadrilaterals," *Nuclear Science and Engineering*, vol. 97, pp. 475–478, 2007.

[12] M. M. Miften and E. W. Larsen, "The quasi-diffusion method for solving transport problems in planar and spherical geometries," *Transport Theory Statist. Phys.*, vol. 22, pp. 165–186, 1993.

[13] V. Y. Gol'din, "A quasi-diffusion method for solving the kinetic equation," *USSR Comp. Math. and Math. Phys*, vol. 4, pp. 136–149, 1967, original published in Russian in Zh. Vych. Mat. I Mat. Fiz. 4,1078(1964).

[14] C. T. Kelley, *Solving Nonlinear Equations with Newton's Method*, ser. Fundamentals of Algorithms. Philadelphia: SIAM, 2003, no. 1.

[15] D. A. Knoll and D. E. Keyes, "Jacobian-free newton krylov methods: A survey of approaches and appliciations," *J. Comp. Phys.*, vol. 193, pp. 357–397, 2004.

GPU Acceleration of Saliency Detection Algorithm

Zhenhai Xiong, WanQing Chi, Kai Lu, Xiaoping Wang, Gen Li

School of Computer Science

National University of Defense Science and Technology

Changsha, 410073, China

E-mail:zhenhai0913@126.com

***Abstract*—Saliency detection is an important step in image processing on computer, which has been widely used in network graphics, fingerprint recognition and other fields. The method of saliency detection based on structural similarity theory uses the structural similarity to abstract high-level human visual system, measuring the saliency of images through a new Center-Surround operator. It overcomes the mosaic phenomenon of Itti algorithm caused by near interpolation. However, the computational overhead is very large as each pixel needs to be processed. In this paper, we adopt GPU to accelerate this algorithm, which speeds up over 90X compared with original method running on CPU. To the best of our knowledge, the approach we proposed that using GPU to accelerate the saliency detection algorithm is the first one in the field of image processing.**

***Keywords*—Saliency detection, Center-Surround operator, image processing, structural similarity, GPU**

I. INTRODUCTION

The salient target detection of images is one of the most challenging problems in computer vision. So far, there have been many saliency detection algorithms. These algorithms explain the saliency of an image from different field or different perspective, and they all have achieved fair results in their own scenarios.

Itti algorithm (e.g. [1]) based on the feature integration theory and detected the saliency of multiple visual features and integration. Le Wang (e.g. [2]) automatic extracted the salient goal in a single image by the segmentation of the salient object and learning of the auto-context model iteratively. Ma, Zhang (e.g. [3]) proposed a contrast-based method and Achanta (e.g. [4], [5]) simplified it: computing the average density and the color values between different pixels. In addition, the structural similarity theory (e.g. [6], [7], [8]) proposed by Zhou, Wang is used to visually saliency detection. The 3×3 matrix surrounding the computing pixel is the basic unit of calculation.

These algorithms are all limited by large computation and long execution time. There is a common method to improve the computing speed.

In recent years, GPU has been widely used in various fields (e.g. [9], [10]), especially in computer graphics. It is good at dealing with a series of complex calculations because of its highly parallel structure compared to CPU processor.

GPUs are parallel processors that consist of a number of *streaming multi-processors*(SM), which are made of a number of processing cores running in lockstep. They support the execution of computational *kernels* – blocks of threads executed together on each of the available SMs. Massive parallelism is achieved as a large number of threads is interleaved onto a smaller number of processing cores. Using GPU to acceleration work can make full use of hardware performance and improve application performance obviously.

When an image is processed on CPU, we deal with each pixel in order. Several characteristics make it a great advantage when running on GPU:

1. All of process data are read from the same image. Although adjacent pixels' surrounding areas have some overlapped part, these overlapped data is read-only, their reading order does not affect the correctness;
2. There is no data dependency between the pixels. We can deal with all pixels out of order which means they are very suitable for parallel;
3. As we mentioned above, adjacent pixels' surrounding areas have some overlapped part. Using GPU for acceleration can greatly reduce the number of memory access which in turn accelerated the algorithm.

Our experiments show that using GPU for acceleration of saliency detection algorithm is entirely feasible. Take the structural similarity theory-based algorithm (e.g. [11]) for example, performance improved is considerable, the speedup can reach 40X or even nearly 100X.

II. BACKGROUND

A. *The Structural Similarity Theory*

The structural similarity (SSIM) index is a method for measuring the similarity between two images and it is designed to improve traditional methods like *peak signal-to-noise ratio* (PSNR) and *mean squared error* (MSE), which have been proved to be inconsistent with human eye perception. The difference to other techniques mentioned previously such as MSE or PSNR, is that these approaches estimate perceived errors, on the other hand SSIM considers image degradation as perceived change in structural information. Structural information is the idea that the pixels have strong interdependencies especially when they are spatially close. These dependencies carry important information about the structure of the objects in the visual scene.

In this paper, we take the global saliency detection algorithm as an example, shown in Figure 1. The 3X3 matrix in the central region of the image is calculated, marked with black. Part of the pixels in the upper left corner is black, marking that these pixels are repeatable read by multiple areas. When the calculation scope is determined, the saliency of the pixel is calculated after all pixels finished traversing.

978-0-7695-4818-0/12 $26.00 © 2012 IEEE
DOI 10.1109/DCABES.2012.8

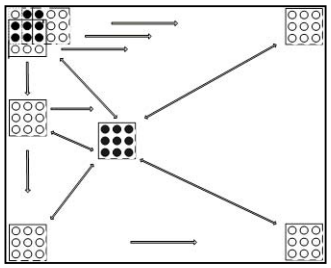

Figure 1: The Saliency detection algorithm based on global structural similarity

In order to calculate the saliency of a pixel in the image, the 3X3 matrix surrounding the pixel is regarded as a basic computing unit of this pixel which has some characteristics: *average values* and *variance*. The covariance between two different matrices is also an important feature. The specific formula is shown in equation (1).

$$\mathrm{SSIM} = \frac{(2u_x u_y + C_1)(2\sigma_{xy} + C_2)}{(u_x^2 u_y^2 + C_1)(\sigma_x^2 \sigma_y^2 + C_2)} \qquad (1)$$

Taking the human visual characteristics and psychological feelings into account, there will be a factor L multiplied by their results when comparing the structure similarity between two matrices. The value of L, C_1 and C_2 are calculated according to the equation, as in [11]. We can get the saliency of a pixel through several steps if the calculation scope has been determined:

Step1: get a 3X3 matrix surrounding the pixel and compute the average values and variance;

Step2: if there is a matrix in background areas is not traversed, go to Step3 or Step4;

Step3: get the 3X3 matrix and compute the average values, variance;

Step4: compute the covariance and factor L between central matrix and surrounding matrix;

Step5: compute the structural similarity between two matrices;

Step6: add the result of structural similarity to the saliency value, go to Step2;

Step7: weight the sum of saliency value as the final result;

The saliency map is obtained through traversing all pixels of the image.

B. *OpenCL Memory Model*

OpenCL (Open Computing Language) is a framework for writing programs that execute across heterogeneous platforms consisting of CPUs, GPUs, and other processors. This framework includes a language for writing kernels (functions that execute on OpenCL devices), plus APIs that are used to define and then control the platforms. It provides parallel computing using task-based and data-based parallelism, which greatly improves speed and responsiveness for a wide spectrum of applications. In addition, OpenCL is an open standard maintained by Khronos Group. It has been adopted by Intel, Advanced Micro Devices, Nvidia, and ARM Holdings.

OpenCL made your code more readable and provided strong expansibility. However, OpenCL needs programmers write their memory management code, the programmer needs to have a more in-depth understanding of the OpenCL memory model, as we see from Figure2.

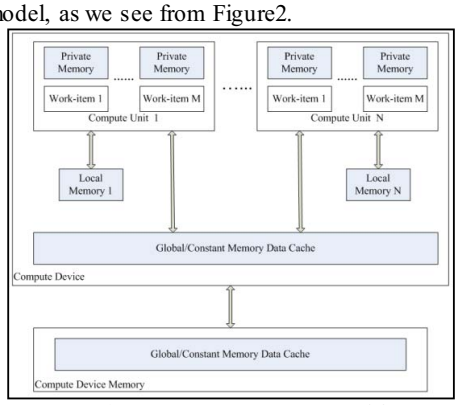

Figure 2: OpenCL Memory Model

OpenCL memory model (e.g. [12]) is similar with the computer's memory hierarchy: It either has a large capacity or high-speed access. It is worth our attention:

1. Private memory can only be accessed by the corresponding work-item;
2. Local memory can be accessed by all work-items that belong to the corresponding workgroup;
3. All work-items can access the global memory.

If we can take full advantage of this point that the work-items from the same workgroup are able to access the corresponding local memory, there would be a significant reduction in the number of memory access. Reasonable use of the access speed gap between the local memory, private memory and global memory can also improve the average access speed.

III. DESIGN

A. *A Simple Scheme*

First of all, we do not consider the impact of memory, all data were stored in the global memory to take full advantage of the parallelism of the GPU to accelerate, and then we optimize the scheme step-by-step. The key idea of the Kernel part is as is as shown in pseudo code 1:

```
__kernel void im_ker(__global char* A, __global char* B ){
  get the workitem's id of X dimension and Y dimension:x,y.
  get the computing boundary:L
  read the computing pixel's data of 3*3 matrix from A
  computing the matrix's mean value and variance:ux,σx
  float ssim = 0, K=0.0;          //saliency and weigh coefficient
  for(int X=x-L/2;X<x+L/2;X++)
      for(int Y=y-L/2;Y<y+L/2;Y++){
            conputing the coefficient between (X,Y) and (x,y):k
            read a matrix surrounding the pixel (X,Y)
            computing the matrix's mean value and variance:uy,σy
            computing the two matrixs' covariance:σxy
            computing the salient degree:temp
            ssim += temp;
            K += k;}
  ssim = ssim/K;
  write back the result to B }
```

Pseudo code 1: the simple scheme's key idea

B. *Algorithm Adjustment*

The experimental results show that the speedup obtained by the above method did not meet our expectations. The loop portion of the algorithm limits the speed. Actually, when calculated the saliency of multiple adjacent pixels, these pixels' surrounding areas have some overlapped part. The part of the overlapping data has also been double-counting of ten times or even dozens of times and the execution time could be greatly shortened if this part of data was processed only once. However, the covariance between the matrix and surrounding matrix is closely related to the data, this part of calculation can't be avoided.

Noted that by the Cauchy inequality:

$$\sigma_{xy} = \frac{1}{n-1}\sum_{i=1}^{n}(x_i - ux) * (y_i - uy) <= \frac{1}{n-1}\sqrt[2]{\sum_{i=1}^{n}(x_i - ux)^2 * \sum_{i=1}^{n}(y_i - uy)^2} = \frac{n}{n-1}\sigma_x * \sigma_y \approx \sigma_x * \sigma_y \quad (2)$$

The maximum value of the covariance between the two matrices is approximately equal to the product of the variances.

Formula (1) becomes (3) through replacing the covariance:

$$SSIM = \frac{(2u_x u_y + C_1)(2\sigma_x * \sigma_y + C_2)}{(u_x^2 u_y^2 + C_1)(\sigma_x^2 \sigma_y^2 + C_2)} \quad (3)$$

After that, the part of overlapping data is processed first, compute the mean value and variance and they are read as intermediate results when compute the saliency. We did a lot of inspection work about this formula, Section 4 will show more detail about it.

C. *Algorithm Optimization*

Despite that the algorithm was adjusted in previous section, and reduced a large amount of repeat calculation, the algorithm did not achieve the best and there is still much room for improvement.

As we said in section 3.1, the thread has to read a large amount of data before calculate the saliency. It is assumed that the areas each pixel takes has the same boundary of L * L while s^2 is the size of workgroup. The reduced ratio of the number of memory accesses could achieve K after we took full advantage of the local memory. And K is calculated according to:

$$K = \frac{(s*s)*(L*L)}{(L+s)(L+s)} \quad (4)$$

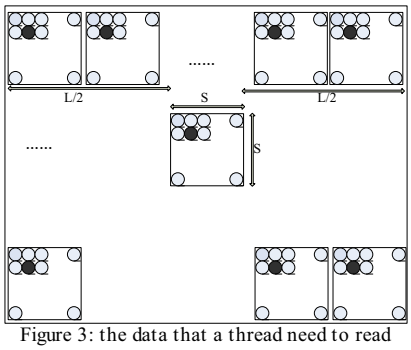

Figure 3: the data that a thread need to read

In addition, the access speed of the local memory is much faster than the global memory. Take L>>s into account that the acceleration is very impressive. Assume that L is multiple of 2s, then all the required data can be divided into $(L+s)^2/s^2$ blocks, each block has the same size with the workgroup. The thread processes the pixel (x, y) is responsible for copying data from the global memory to local memory if the data has the same offset in each of the workgroups. Figure3 show an example that which part of data a thread need to read. All threads execute in parallel in a workgroup, you can get all the required data after all threads finished. Theoretically, the number of memory access can reduce to $1/K$ of the original. We can get more information from the following pseudo-code:

```
__kernel void im_ker(__global float* I1, __global float * I2,.....
                     __local float* II1, __local float* II2,..... ){
.....
read the mean value and variance of the pixel (x,y) from I1,I2....
/* ******* transfer data from global memory to local memory ******* */
for(int i=x-L/2; i< x+L/2; i += s)
    for(int j=y-L/2; j<y+L/2; j += s){
            II1[ j*(L+s) + i ] = I1[ j*width+i ];
        II2[ j*(L+s) + i ] = I2[ j*width+i ];
        ……}
barrier(CLK_LOCAL_MEM_FENCE );
computing the salient degree
write back the result to output map }
```

Pseudo code 2: optimization algorithm

IV. EVALUATION

In order to obtain the speedup after adjustment the algorithm, we did some tests on several sizes of images. The GPU in experiments is ATI Mobility Radeon HD 5650. The specific data are shown in Table1 and Table2. As shown in Table1, the results are very obvious for CPU, and the speedup has achieved 3X to 4X, while Table 2 seems to be a little confused.

Table1 Running-time (CPU) (ms)

Im_size\Method	CPU_ICO	CPU_bef	CPU_aft
256*256	540	8170	2860
256*512	930	17550	5740
512*512	1770	296330	78710
512*768	2630	454810	118450
768*768	3620	1922920	476550

In theory, the running time should be shorter after adjusting the algorithm as shown in the first few rows of Table 2. On the contrary, it takes more time when the image is a little larger. There are several reasons can explain this phenomenon:

At first, the size of the local memory is limited. We can obtain some information of the local memory through calling some APIs and the memory size is 32K. It is a very limited and it is very useful for us to take full advantage of local memory;

Secondly, it requires a lot of parallelism when read data while the computer units can't provide. Actually, the exper-mental GPU model has only 5 compute units, for an image

size of 768*1024, the number of workgroup it divided is as large as three thousand. And the larger the image, more workgroup it divides.

Last, the fence operation blocked the threads as it needs to wait for all data is ready.

Table2 Running-time (GPU) (ms)

Im_size\Method	GPU_ICO	GPU_bef	GPU_aft
256*256	180.06	94.46	89.44
256*512	303.99	155.87	140.09
512*512	423.11	1019.28	836.51
512*768	581.89	1521.28	1241.9
768*768	736.30	5037.07	8572.33
768*1024	1011.33	6720.88	11482.88

We can do some simple arithmetic operations on these data got from the two tables. Before we adjusted the algorithm, the speedup ranged from 40X to 200X. Generally speaking, the larger the image is, the more speedup we get. After that, the speedup was a little lower which ranges from 15X to 60X. A reasonable explanation is that the base value becomes much smaller. And there still are several limitations existed as we analysis above. All in all, this result is acceptable.

By the way, we found that it affects little to the results of the salient objectives if we adjust the formula, but there is a little bit flawed when extracting the contour of the target.

V. CONCLUSIONS

We proposed that using GPU to accelerate saliency detection algorithm and did several test on the algorithm based on the structural similarity theory. We made some adjustments to the algorithm, got a good performance boost. We took full advantage of the characteristics of the local memory in OpenCL, obtained a good speedup. We confirmed the feasibility of this approach in the image field. We believe that other algorithms can also achieve good performance boost.

However, several problems limit the performance and we would focus on these issues. First of all, the areas we choose as background of a pixel is a little larger that the GPU can't provide enough threads to support the parallelism. This problem will only appear in this algorithm. We will optimize the algorithm further. Secondly, the size of the local memory is limited. We are wondering whether we can accelerate the algorithm through dividing the image or using multi-GPU. And finally, as future work, we would like to confirm that this approach we proposed that using GPU to accelerate saliency detection algorithm is also applicable to other algorithms.

ACKNOWLEDGMENT

This work is partially supported by National Science Foundation (NSF) China 61003075, 61103193, and 61170261. This work was supported in part by the National High-tech R&D Program of China (863 Program) under Grants 2012AA01A301.

REFERENCES

[1] Itti L, Koch C and Niebur E. "A model of saliency-based visual attention for rapid scene analysis". In IEEE Trans. On Pattern Analysis and Machine Intelligence, 1998, 20(11):1254-1259

[2] Le Wang, Jianru Xue, Nanning Zheng. "Automatic Salient Object Extraction with Contextual Cue", In IEEE International Conference on Computer Vision, 2011, p.105-112

[3] Y F Ma, H J Zhang. "Contrast-based image attention analysis by using fuzzy growing". In ACM Int'l Conf. on Multimedia, 2003

[4] R. Achanta, S. Hemami, F. Estrada and S. Susstrunk. Frequency "Frequency-tuned salient region detection", In CVPR, 2009

[5] R. Achanta and S. Susstrunk. "Saliency detection using maximum symmetric surround", In Proc. of Int'l Conf. on Image Processing (ICIP), 2010

[6] Zhou Wang, A C Bovik. "A universal image quality index", IEEE Signal Processing Letters, 2002, 9(3):81-84

[7] Zhou Wang, A C Bovik, H R Sheikh, E P Simoncelli. "Image quality assessment: from error visibility to structural similarity", IEEE Transactions on Image processing, 2004, 13(4):600-612

[8] Wikipedia -- Structural_similarity. [Online]. Available:http://en.wikipedia.org/wiki/Structural_similarity, 2010-8-2

[9] Joshua E. Cates, Aaron E. Lefohn, Ross T. Whitaker: "GIST: an interactive, GPU-based level set segmentation tool for 3D medical images", Medical Image Analysis 8(3): 217-231 (2004)

[10] Stefan Schenke, Burkhard C. Wunsche, Joachim Denzler. "GPU-Based Volume Segmentation", Image and Vision Computing New Zealand - IVCNZ , 2005

[11] Chongfei Li, Zhiguo Qu, Kai Lu, Yinghui Gao. "Visual salient region detection method based on structural similarity", Computer engineering &science.

[12] OpenCL. [Online]. Available: http://developer.amd.com/zones/openclzone/pages/default.aspx

Parallelized Force-Directed Edge Bundling on the GPU

Delu Zhu
Computer Network Information Center, Chinese Academy of Sciences
Graduate University of Chinese Academy of Sciences
Beijing, 100190, China
jasmine@cnic.cn

Kaichao Wu, Danhuai Guo
Computer Network Information Center, Chinese Academy of Sciences
Beijing, 100190, China
kaichao@cnic.cn,
guodanhuai@cnic.cn

Yuanmin Chen
China Internet Network Information Center
DNSLAB
Beijing, 100190, China
chenyuanmin@cnnic.cn

***Abstract*—How to draw large scale spatial interaction data clearly and quickly is a challenge in high performance data visualization research and application field. Force-Directed Edge Bundling (FDEB) helps display graph clearly with significant clutter reduction, but with high time complexity. This paper presents a parallelized FDEB on the GPU (GPU-FDEB), which reforms FDEB and achieves a balanced partitioning of data and calculation to suit computation on the GPU. GPU-FDEB addresses the problem of high time complexity and accelerates FDEB by an order of magnitude.**

Keywords-GPU; parallel; FDEB; visualization; CUDA

I. INTRODUCTION

Graphs are widely used to model relationships among data such as connections between people, traffic between locations and migration between counties. An intuitive way to visualize graphs is using node-link diagram, however, when graphs comprised of a large number of nodes and edges are visualized as node-link diagrams, visual clutter quickly becomes a problem (see Fig. 8a) [1]. Many methods have been proposed to reduce visual complexity [6-10]. These methods can be classified into two major categories: adjust node positions and improve edge layout [2].

Hierarchical Edge Bundling (HEB), Geometry-Based Edge Bundling (GBEB) and Force-directed Edge Bundling (FDEB) proposed in [1, 2, 3] reduce visual compatibility by adjusting edges (merging similar edges into bundles). HEB is limited to visualize graphs with a hierarchical structure [3]. GBEB is suitable for general graphs, but need to generate a control mesh to guide the edge clustering process [2]. While FDEB is suitable for general graphs and don't require a hierarchy or a control mesh [1]. FDEB is a self-organizing edge-bundling approach in which edges are modeled as flexible springs that can attract each other and be grouped into bundles [1].

FDEB can reduce visual complexity with a significant clutter reduction, but the computational complexity of FDEB is $O(N \cdot M^2 \cdot K)$, with N = iterations, M = edges, and K = subdivision points per edge [1]. When the number of edges comes to 15000, the runtime of FDEB will exceed 6 minutes. The high computational cost of large graphs is the major drawback of FDEB. We may consider parallelize FDEB using multi-core platforms or clusters to achieve real-time response. However, it's not only difficult to design multi-core or do deployment in a clustered environment but also costly [17]. While GPU has hundreds of cores and low cost. Furthermore, CUDA (Compute Unified Device Architecture) makes GPGPU (General-Purpose computing on GPU) easier and more available to end users [4, 11, 12, 16].

We present a parallelized FDEB on the GPU (GPU-FDEB) according to some criterion such as maximize the independence between threads and maximize the computational intensity to achieve a maximum speedup.

The remainder of this paper is organized as follows. In Section 2 we give an overview of FDEB. Section 3 presents the algorithm of parallelized FDEB. Section 4 describes the implementation of our algorithm on the GPU and the accelerate technique in detail. In Section 5 we present experimental results and analysis. Finally, Section 6 presents conclusions and directions for future work.

II. FORCE-DIRECTED EDGE BUNDLING

Take population migration graph for example (see Fig. 8a), in which nodes depict migration locations and edges depict population migrated between locations. In this node-link diagram comprised of a large number of edges, visual clutter is such a serious problem that we can't detect any visible high-level migration patterns. FDEB can achieve significant clutter reduction in visualizing large graphs (see Fig. 8b).

In FDEB, edges are subdivided into segments. The positions of end-points of all edges remain fixed and the position of each subdivision point is changing by the combined force of spring force and electrostatic force while bundling [1].

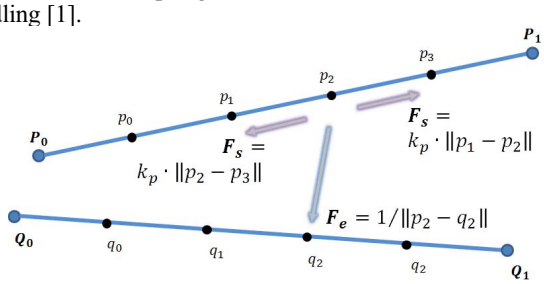

Figure 1. F_s and F_e on point P_2.

Take Fig. 1 for example, there are two spring forces (F_s for short) exerted on subdivision point p_2 by p_1, p_3 and one electrostatic force (F_e for short) exerted on p_2 by q_2. F_s is used

978-0-7695-4818-0/12 $26.00 © 2012 IEEE
DOI 10.1109/DCABES.2012.16

between each pair of consecutive subdivision points on the same edge, and F_e is used between each pair of corresponding subdivision points of a pair of interacting edges [1].

In the process of bundling, each subdivision point of edges makes a step in the direction of the combined force exerted on it during each iterative step, which will iterate many times until the edges are bundled sufficiently [1].

Furthermore, to control the amount of interaction between edges, FDEB introduce the concept of edge compatibility [1]. A pair of edges P and Q is considered as interactive if edge compatibility $C_e(P, Q)$ between P and Q is above a certain threshold, which reduces the amount of bundling desirably and the computation largely [1].

In [1] the combined force F_{pi} exerted on subdivision point pi on edge P is defined as:

$$F_{p_i} = k_p \cdot (\|p_{i-1} - p_i\| + \|p_i - p_{i+1}\|) + \sum_{Q \in E} \frac{C_e(P,Q)}{\|p_i - q_i\|},$$

With

k_p: spring constant for each segment of edge P,

E: set of all interacting edges except edge P.

III. GPU-FDEB ALGORITHM

The crucial way to improve the efficiency of GPU-FDEB is to properly distribute tasks between CPU and GPU [4, 11, 12, 15]. FDEB uses an iterative refinement scheme to calculate the bundling [1]. The calculation of spring force, electrostatic force and the moving of subdivision points are coupled together at each iteration step, which is not suitable for GPU computing, so we reform the calculation of each iteration step into 3 independent steps: calculate spring force, calculate electrostatic force, and update the positions of subdivision points.

Fig. 2 displays the flow chart of GPU-FDEB, in which the blue blocks (1, 3.1, 4) are executed on the CPU, while the green blocks (2, 3.2, 3.3.1, 3.3.2, 3.3.3) which are of high computational cost are executed on the GPU.

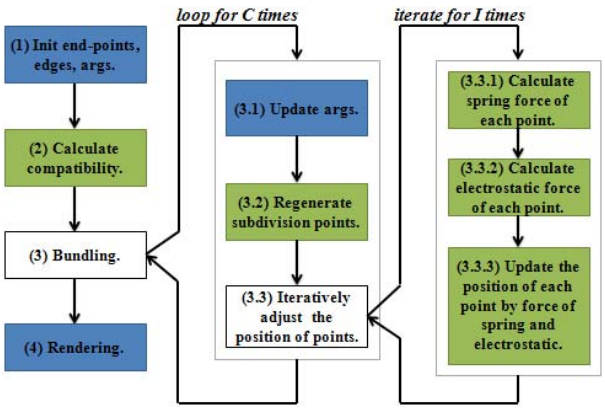

Figure 2. The algorithm flow of GPU-FDEB.

The algorithm is described in details as follows:

(1) Initialize:

(1.1) Input nodes and edges.

(1.2) Initialize the parameters such as the number of iteration steps I, the number of subdivision points P, the step size S.

(1.3) Allocate device memory, transfer edges from CPU to GPU.

(2) Calculate edge compatibility for each combination of edges on the GPU: Thread (i, j) is responsible to calculate edge compatibility between edge i and edge j.

(3) Bundling:

For cycle: =1 to C do

Begin

(3.1) Update parameters: P is increased by a fixed rate, I and S are decreased by a fixed rate.

(3.2) Regenerate subdivision points:

(3.2.1) Thread (i, j) is responsible to calculate the length of segment j on edge i.

(3.2.2) Thread (i, 0) is responsible to generate P subdivision points on edge i.

(3.3) Iteratively adjust the positions of subdivision points:

For iterator: =1 to I do

Begin

(3.3.1) Calculate spring force: Thread (i, j) is responsible to calculate two neighboring F_s exerted on subdivision point j on edge i.

(3.3.2) Calculate electrostatic force: Thread (i, j) is responsible to calculate the sum of F_e exerted on subdivision point j on edge i by corresponding subdivision points on edges interacted with edge i.

(3.3.3) Update the position: Thread (i, j) is responsible to move the subdivision point j on edge i to a distance of S in the direction of the combined force exerted on it.

End.

End.

(4) Rendering.

IV. GPU IMPLEMENTATION

A. Data storage

The layout of data in memory has great influences on the efficiency of GPU-FDEB [12, 15]. In GPU-FDEB, the graph is represented as a matrix where all the points on each edge are placed in each row (see Fig. 3), and the matrix is stored in FORTRAN order in memory, i.e., all the 1st points of each edge are stored in sequence, so are the 2nd points and the 3rd points, etc. Furthermore, the coordinate X and Y of all the points are separately stored in two matrixes.

We choose this data layout for two reasons. First, the number of subdivision points P is not fixed but increased with increasing cycles. If we store the matrix by row, we have to modify each row every time we add new subdivision points. Second, since the major calculation of GPU-FDEB is

processed column by column, there is no dependency between columns, thus storing points by column can maximize memory access locality. e.g., we can load the whole column into cache and manipulate the elements there instead of accessing the elements one by one from memory.

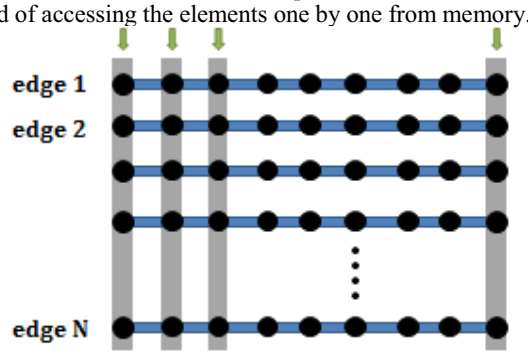

Figure 3. The points are stored by column.

Besides, to hide memory access latency, we expand the column dimension into multiples of 16, thus the starting address of each column is times of 64 (16×4) bytes, which meets the requirement of memory coalescing, i.e., 16 simultaneous memory accesses can be coalesced into a single memory transaction.

B. *Calculate edge compatibility*

This kernel is responsible to calculate compatibility between every two edges. The input is the end-points and lengths of N edges, and the output is an N×N compatibility matrix (N is the number of edges after expanded, times of 16). Considering that compatibility matrix is symmetric, we only need to calculate the lower triangular matrix.

Since row dimension of compatibility matrix is N (times of 16) and we store compatibility matrix by row, thus it is memory coalesced to write the lower triangular matrix back into global memory after the calculation of edge compatibility.

C. *Regenerate subdivision points*

This kernel is responsible to regenerate subdivision points for each edge. The input is the data matrix comprised of end-points and subdivision points of N edges, and the output is the regenerated subdivision points of N edges. The layout of data matrix in Fig. 3 is specified as Fig. 4 shows. The 2nd end- points of N edges are stored in the 1st column, the 1st end-points of N edges are stored in the 2nd column and the regenerated subdivision points are stored in the rest columns.

We do this for two reasons. First, the number of subdivision points will increase with increasing cycles, it's reasonable to store the constant end-points in the first two columns while leave the variable subdivision points behind. Second, it maximizes memory access locality to store the 1st end-points close to the 1st subdivision points.

From step (3.2) of GPU-FDEB algorithm, to calculate the positions of regenerated subdivision points on each edge, we need to calculate and sum the length of each segment on each edge (the red segments showed in Fig. 4) to get the length of each edge, then get the positions of the points which divide edges equally. It can be seen that calculating the length of each segment is independent with each other and so is regenerating subdivision points on each edge. A large parallelism is achieved in this kernel.

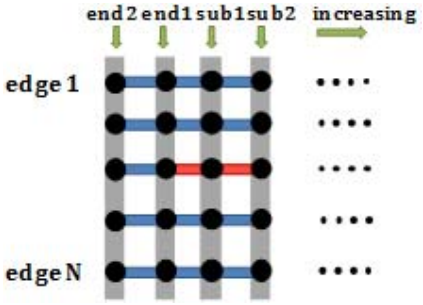

Figure 4. Generate subdivision points.

D. *Calculate electrostatic force*

This kernel is responsible to calculate the total electrostatic force exerted on each subdivision point, which is the most time-consuming part in FDEB. The input is the data matrix comprised of end-points and subdivision points, the weights of N edges and the compatibility matrix, while the output is a matrix of the total electrostatic force exerted on each subdivision point. Given the concept of electrostatic force defined in FDEB (see Section 2), the total electrostatic force exerted on subdivision point j in Fig. 5 is the sum of the electrostatic force exerted on j by each point in the same column as j.

Since there is no dependency among columns in this kernel, all the columns can be processed in parallel. To calculate the total electrostatic force exerted on each subdivision point in each column, we need to calculate the electrostatic force F_e for every two points in this column, i.e. we need to calculate an N×N F_e matrix. The F_e is interactive which means that the F_e matrix is symmetric, so we only need to calculate the lower triangular matrix (the green part in Fig. 6) which reduces the calculation largely.

To obtain the total electrostatic force exerted on each subdivision point, we need to calculate the sum of each row in the F_e matrix. However, we only calculated the lower triangular matrix, it's impossible to sum each row directly. Considering that the F_e matrix is symmetric, the uncalculated upper triangular matrix can be obtained from the calculated lower triangular matrix. As Fig. 7 shows, the sum of blue part in the left matrix equals the blue part in the right matrix.

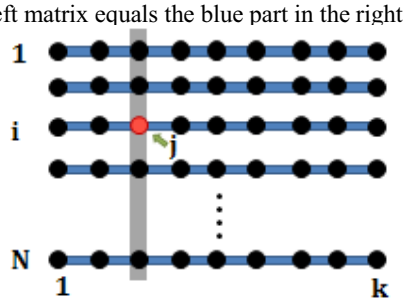

Figure 5. Calculate the electrostatic force.

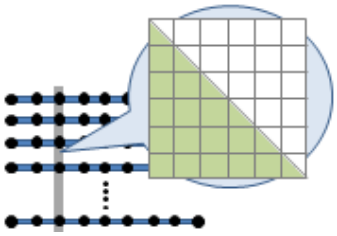

Figure 6. Each column corresponds to a F_e matrix.

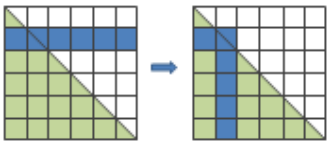

Figure 7. Map the uncalculated part to calculated.

V. EXPERIMENTAL RESULTS

We have carried on detailed experiments on our GPU-FDEB algorithm. The experiment platform is showed in Table 1.

TABLE I. EXPERIMENT PLATFORM

	Model	Cores	Frequency	Cache	Memory
CPU	Intel Xeon X5650	6×2	2.67GHz	12M	10G
GPU	Nvidia Quadro 5000	352×1	1.03GHz	655K	2.56G
Runtime	RHEL 6, CUDA Driver Version 4.0				

The experimental data are obtained from population migration between counties of US (3219 node, 375374 edges). The maximum number of edges can be processed on our GPU is between 15000 and 16000, which is limited by the size of GPU memory. So we select a subgraph comprised of 15000 edges and 372 nodes as our test graph and process it with FDEB and GPU-FDEB respectively. Fig. 8a shows the original graph. Fig. 8b and Fig. 8c shows the bundled graph processed by FDEB and GPU-FDEB respectively. Fig. 8a and Fig. 8b show that FDEB has reduced visual clutter largely and reveal high-level migration patterns. Fig. 8b and Fig. 8c show that GPU-FDEB gets almost the same bundled graph as FDEB.

To measure the efficiency of GPU-FDEB, we record the time taken by FDEB and GPU-FDEB to calculate the bundled graph respectively as the number of edges changes. All the time accepted in Fig. 9 is an average of ten successive times.

In Fig. 9, we can see that the time consumed by FDEB increases rapidly as the number of edges increases, while slowly for GPU-FDEB. In terms of time-consumption, the advantage of GPU-FDEB is more obvious with the number of edges increasing. When it comes to 4000 edges, the time consumed by FDEB is more than 19 seconds, while less than 3 seconds by GPU-FDEB. When it comes to 15000 edges, FDEB takes more than 6 minutes while GPU-FDEB only need 36 seconds.

Fig. 10 shows the variation of speedup (the ratio of time consumed in FDEB to GPU-FDEB) as the number of edges increases. The speedup is increasing gradually as the number of edges increases until it comes to 2000 edges, followed by a gradual decrease until it comes to 5000 edges, and then has an ascent trend in the end. The drop of speedup around 5000 edges indicates that there's a decrease in GPU performance.

Overall, our GPU-FDEB algorithm is reliable and effective.

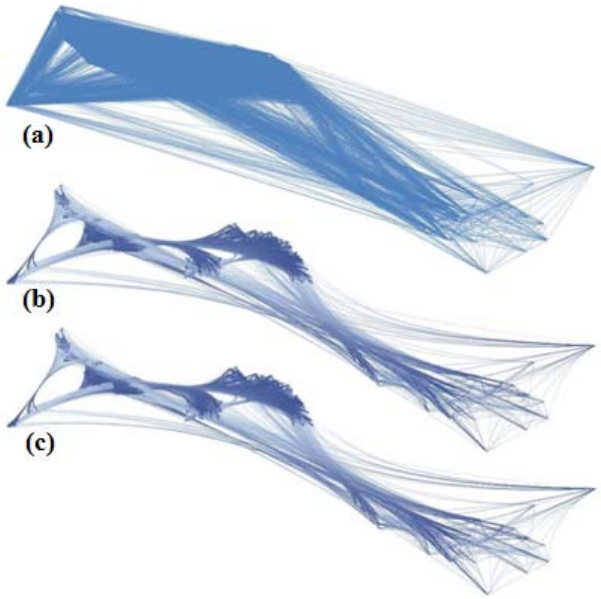

Figure 8. Population migration graph (a)origin(b)FDEB(c)GPU-FDEB.

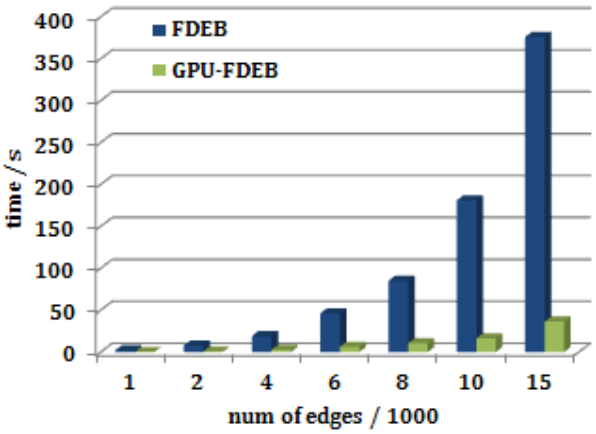

Figure 9. Time consumption.

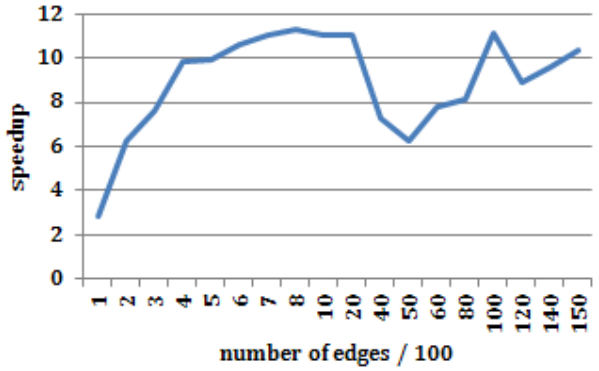

Figure 10. Speedup over FDEB.

VI. CONCLUSION AND FUTERWORK

This paper has presented a parallelized FDEB implemented on the GPU. Furthermore, we have optimized the layout of data in memory to maximize memory access locality. Most memory accesses have been coalesced to reduce memory access latency. Compared with FDEB implemented in C, GPU-FDEB achieves a speedup of 11 at most on the platform showed in table 1.

The GPU-FDEB implemented in this paper only support single GPU, thus the quantity of data can be processed is limited by hardware resource (e.g., the number of SM and the size of GPU memory). A straightforward way to address this is to use multi-GPU system or GPU cluster, which we would implement in our next work. Furthermore, it is possible to split edges of general graph into blocks according to edge compatibility, which could be used in multi-GPU system or GPU cluster.

ACKNOWLEDGMENT

This work is supported by National Development and Reform Commission of China in project “Scientific Research Information Infrastructure Construction and Typical Demonstrations Based on CNGI”, Chinese Academy of Sciences #CNIC_ZR_201201, and DNSLAB of China Internet Network Information Center #DNSLAB-2012-D-U.

REFERENCES

[1] D. Holten and J. J. van Wijk, “Force-directed edge bundling for graph visualization,” Computer Graphics Forum, vol. 28, pp. 983-990, 2009.

[2] W. Cui, H. Zhou, H. Qu, P. C. Wong, and X. Li, “Geometry-based edge clustering for graph visualization,” IEEE Transactions on Visualization and Computer Graphics, vol. 14, pp. 1277-1284, 2008.

[3] D. Holten, “Hierarchical Edge Bundles: Visualization of Adjacency Relations in Hierarchical Data,” IEEE Transactions on Visualization and Computer Graphics, vol. 12, pp. 741–748, 2006.

[4] J. Sanders and E. Kandrot, CUDA by Example: An Introduction to General-Purpose GPU Programming. Addison-Wesley, 2010.

[5] A. Grama, A. Gupta, G. Karypis, and V. Kumar, Introduction to Parallel Computing, Addison Wesley, 2nd ed, 2003.

[6] G. Ellis and A. Dix, “A taxonomy of clutter reduction for information visualisation,” IEEE Transactions on Visualization and Computer Graphics, vol. 13, pp. 1216-1223, 2007.

[7] F. van Ham and J. J. van Wijk, “Interactive visualization of small world graphs,” IEEE Symposium on Information Visualization, pp. 199-206, 2004.

[8] A. Noack, “An energy model for visual graph clustering. In Proceed. of Symposium on Graph Drawingg,” pp. 425-436, 2003.

[9] N. Wong, M. Carpendale, and S. Greenberg, “Edgelens: An interactive method for managing edge congestion in graphs,” IEEE Symposium on Information Visualization, pp. 51-58, 2003.

[10] H. Qu, H. Zhou, and Y. Wu, “Controllable and progressive edge clustering for large networks,” In Proceed. of Symposium on Graph Drawing, pp. 399-404, 2006.

[11] J. D. Owens, M. Houston, D. Luebke, S. Green, J. E. Stone, and J. C. Phillips, “GPU Computing,” Proc. Proceedings of IEEE, 2008,pp. 879-899, doi:10.1109/JPROC.2008.917757.

[12] NVIDIA, nVidia CUDA Programming Guide 3.0, NVidia, 2010.

[13] NVIDIA, The CUDA Compiler Driver NVCC, NVidia, 2008.

[14] NVIDIA, CUDA-GDB: The NVIDIA CUDA Debugger User Manual 2.1, 2008.

[15] M. Garland, “Parallel computing with CUDA,” Proc. IEEE International Symposium on Parallel & Distributed Processing (IPDPS), 2010,pp. 1, doi:10.1109/IPDRS.2010.5470378.

[16] J. Nickolls and W. J. Dally, “The GPU Computing Era,” Proc. Micro, IEEE, vol. 30, 2010,pp. 56-69, doi:10.1109/MM.2010.41.

[17] Quinn and J. Michael, Parallel Programming in C with MPI and OpenMP, McGraw-Hill Science, 2004.

[18] Y. Frishman and A. Tal, “Multi-level graph layout on the GPU,” IEEE Transactions on Visualization and Computer Graphics, vol. 13, pp. 1310-1319, 2007.

Optimized GPU Sorting Algorithms on Special Input Distributions

Quan Yang [1], Zhihui Du[1*] and Sen Zhang[2]

[1] *Tsinghua National Laboratory for Information Science and Technology*

[1] *Department of Computer Science and Technology, Tsinghua University, 100084, Beijing, China*

[2] *Department of Mathematics, Computer Science and Statistics, State University of New York, NY 13820, U.S.A.*

***Abstract*—**We present a high performance graphics processing unit (GPU) sorting algorithm ISSD (Improved Sorting considering Special Distributions) implemented with the Compute Unified Device Architecture (CUDA). The ISSD focuses on two aspects to improve parallel sorting performance. One is how to decompose the sorting tasks into independent and balanced subtasks which can then be easily distributed to thousands of threads to realize the concept of "parallel sorting" as well as to efficiently explore the power of GPU. The other one is how to take advantage of special data distributions to further optimize the algorithms and improve their performance. The algorithm is redesigned based on our previous general data distribution version and optimized both on general implementation methods and special input distributions. Experimental results show that for the general data distribution inputs, the ISSD outperforms the existing parallel sorting algorithms by about 10% in performance due to its practical optimization in implementation; and for three special data distribution inputs, the ISSD outperforms the existing algorithms by more than 40% due to its special optimization based on the data distributions. Therefore, the algorithm is viable and efficient when dealing with specific data distributions.

Keywords—GPU, parallel sorting algorithm, special data distribution

I. INTRODUCTION

In this paper, we describe our design of a set of efficient parallel sorting algorithms, ISSD (Improved Sorting considering Special Distributions), which are adapted from our previous algorithm for general distributions on NVIDIA many-core GPUs [1] using the CUDA architecture [2, 3]. The idea of ISSD is that we can make optimization by considering some special data distributions to further improve the performance of parallel sorting.

For most parallel sorting algorithms, only some main data distributions - Uniform distribution, Gaussian distribution, Zero distribution, Bucket distribution, Staggered distribution and so on - are put into consideration; while other kinds of data distributions have not been properly treated. As a result, the existing algorithms' performances begin to deteriorate when they come to the input datasets that are governed by special data distributions. To remedy this defect, we propose a parallel algorithm that can fit the specific distributions of the data and can be applied to special uses that are related to these data distributions thus improve the efficiency of the sorting process. The experimental results show that our ISSD algorithm outperforms several other existing algorithms even including the comparison-based Merge Sort, which is widely recognized as one of the most efficient sorting methods. Actually, when running on NVIDIA GPU, even our previous algorithm is faster than any other previously proposed parallel sorting algorithms on GPUs. We further demonstrate that because of the optimization targeting at the special data distributions, our ISSD algorithm can outperform our previous version, which is designed for general purposes.

The remainder of the paper is organized as follows. Section 2 presents related work on parallel sorting algorithms. Section 3 recaptures our previous work handling data with general distributions. Section 4 discusses an optimized algorithm tailored to the input data with special distribution. Section 5 presents our experimental results and Section 6 concludes the paper.

II. BACKGROUND AND RELATED WORK

A. Parallel Sorting Algorithms

One of the dominant trends of high performance sorting algorithm research is to explore the inherent parallelism of the basic sorting operations. Generally speaking, parallel sorting algorithms can be classified into the following 3 categories [4]:

1) **Merge-based sorting algorithms.** This method first sort the subsequences divided from the input data, and then merge the sorted ones to a complete ordered one. According to the different principles of mergence, this kind of algorithm includes bitonic merge, odd-even merge, thrust merge, etc.
2) **Splitter-based sorting algorithms.** The first phase of this method is to partition the input data into several disjoint buckets using the partition keys, or the splitters, generated and sorted in a special way, such as the parallel sorting by regular sampling (PSRS). The second phase is to concatenate the buckets to get the sorted sequence. This includes sample sort, bucket sort, etc.
3) **Other parallel algorithms.** This includes quick sorting algorithm, etc, which are the parallelization of the traditional versions and have basic characteristics of divide and conquer strategy.

B. GPU Programming with CUDA architecture

The CUDA architecture comprises a parallel computing platform and programming model invented by NVIDIA. It aims at improving the efficiency of parallel algorithm implementation and facilitating programmers in harnessing the power of the modern NVIDIA GPU that consist of hundreds of scalar processing elements per chip [1]. Specifically, CUDA provides developers a platform that is realized through a C programming language extension and a set of powerful APIs, so that the developers can work on GPU without being bothered by the underlying hardware details. In CUDA, there is a hierarchy comprised of threads, blocks, and grids. It works in a single instruction, multiple threads (SIMT) manner. Through warp, which means a dozen of threads, the threads are mapped to streaming processors (SMs). In addition, the memory are classified into several types, which are register, local memory, share memory, global memory, constant memory, etc. The designation and optimization are to solve the problem on how to organize the hierarchy and how to schedule the memory access to achieve a better performance.

978-0-7695-4818-0/12 $26.00 © 2012 IEEE
DOI 10.1109/DCABES.2012.57

C. Parallel Sorting Algorithms Based On GPU

At the beginning of the development of parallel sorting algorithms, there existed a constraint execution environment using the graphics API and the pixel shader programs it provides. The most successful GPU sorting routines have been based on bitonic sort [5]. Govindaraju et al [6] proposed GPUSORT system which is considered one of the best graph-based algorithms. But it suffers from a time complexity $O(n\log^2 n)$, which is typical in bitonic methods. Greß and Zachmann [7] used an adaptive data structure for merging the sequential data to achieve a linear time result. This GPU-ABiSort system has improved the complexity to $O(n\log n)$ and results in better performance.

A CUDA-based hybrid algorithm was introduced by Erik Sintorn [8], who combined bucket sort with merge sort. Its limitation is that it can be efficient only in sorting floats since it uses a float4 for internal merge sort to achieve high performance. Quichsort was implemented in CUDA by Cederman [9], but its performance is sensitive to the data distribution owing to the load balance problem. Nadathur Satish, et al. then proposed the Thrust Merge which is a combination of odd-even merge and two-way merge to overcome the load balance problems mentioned above. An even faster GPU radix sort was presented by Satishet et al. [10] for integer sorting. A randomized sample sort method for GPUs significantly outperforms Thrust Merge Sort in [11], although it still suffers from the load balance problem.

III. Our Previous Algorithm for General Distributions

Our previous algorithm implementation on GPU is based on the sample sort. It makes efforts in balancing the costs between the splitter generation and the subsets sorting process. In this algorithm, a novel strategy is applied to select the splitters. It combines the merits of both deterministic sample and random sample. According to the experiment, the loads in the blocks are much more balanced than that using the traditional PSRS method. In particular, the procedures are as follows.

Step 1: Randomly choose (s-1)*k*M samples from the input data, where M is the maximum size of array that can be processed in the share memory of one SM. In the following steps, s and k will be explained.

Step 2: Split the set of samples into k subsets, and sort them respectively using k blocks.

Step 3: Select s-1 equidistance samples from each subset, then merge these (s-1)*k samples to form a sorted array.

Step 4: Pick s-1 equidistance data from the sorted array, i.e., choose a number every k data, and then add the largest number into it, so we get s splitters.

Once we get the sorted array of splitters, use it to cut the sorted data in the subsets into s parts $P_{i1},P_{i2},...,P_{ij},...,P_{is}$, where $i\in[1,k], j\in[1,s]$. Then put the numbers that have the same j to one bucket. So we get s buckets now $B_1,B_2,...B_s$. This step guarantees that the numbers in B_j are no greater than anyone in B_{j+1}. Next assign each bucket to SMs and sort the buckets in parallel using the parallel quick sort. Finally, concatenate the data in the buckets to get the sorted array. This strategy makes a great trade-off between splitters generation and the sorting process of the subsets and performs better than using the PSRS of DSPS alone, thus increase the efficiency of the sorting process.

Compared with the above mentioned algorithms, we mainly made two optimizations. First, we increased the block number from 8 to 256 in step 2, thus the sorting task can be divided to 256 subtasks, instead of 8 used in the previous algorithms. As a result, there are more blocks to sort the subsets simultaneously, contributing to a more paralleled implementation. Secondly, we made an improvement on the subsets sorting process. We found that the odd-even sort algorithm performs better than parallel quick sort does, when there are not too much elements to be sorted, for example, when the number of element is less than 512. So we adopted the odd-even algorithm to sort the buckets $B_1,B_2,...B_s$ in step 4 during these circumstances, while used quick sort algorithm in the other situations. The experimental results show that after the optimization, the algorithm performs better than the previous version. To be specific, the sorting time has been reduced by 10% for the data with general distributions.

IV. Optimization Based on the Data Distribution

There is substantial potential to optimize the algorithm according to different distributions of the data sets, so we make corresponding analysis of the data distribution and their features. Based on the analysis and our previous sorting algorithm implementation, we make optimizations of the algorithm. Experimental results show that the optimization contributes a lot to the speed-up of the algorithm. To achieve the high performance of the algorithm on GPU and CPU, we assigned different tasks to host and device according to their characteristics so that we can take the advantages of CPU and GPU respectively.

A. Narrowly distributed data set

1) Definition of narrowly distributed data set

Narrowly distributed data set is defined as a massive set of data which has a very limited range of values. It implies that there is a relatively small set of keys (a key is a unique value.) and each key is highly duplicated. For example, in a narrowly distributed data set, there are only m different values. If we n is the size of the input dataset, then m is much smaller than n according to the definition.

2) Optimization of the algorithm for narrowly distributed data set

To sort this kind of data set, we can find all the unique values: $x_0, x_1 \cdots x_{m-1}$, and then we can reconstruct an ordered array. The methods are as follows:

Step1: Find all the values in the array. First, we select a small amount of data from the entire data set S as a sample S'. The size of S' is much smaller than that of S. Sort the elements in S' and then record different types of the values $x_0, x_1 \cdots x_{m-1}$ in a new array X which has the size m. Here, we assume that S' has covers all the possible values in S since the narrowly distributed feature of S. Then we can reconstruct an array as the result based on the work above.

Step2: Calculate the number of elements that has the same value. We create an array R to record the numbers of keys that have the same value. Then visit all the elements in S. For each element, $y_i, 0 \le i < n$, we apply a binary searching to find the corresponding value $x_j, 0 \le j < m$ in array X and increase the corresponding record r_j by one.

To implement the optimization, we store the search list of the binary search in the shared memory of each block, which greatly

reduces the time cost to access the search list. We have used a method called double-buffering when updating the record in array R. We get record r_j" in each thread of a block and record r_j' in each block. Only when r_j" has been calculated can we calculate r_j' and r_j. This way frequent atomic access of global memory can be avoided, which brings a great improvement to the performance efficiency.

Step3: Reconstruct an ordered array. Now, we get all the keys from the original data set S saved in R and the corresponding count for each key in S saved in X, it is straightforward for us to reconstruct a sorted array, which is also the sorted form of S. This work can be done by GPU. But if we assign this work to CPU, we can avoid the time cost of data transition from device to host. So in order to improve the efficiency, we choose to send X and R to the host, then use CPU to complete the reconstruction to obtain the sorted result of the input narrowly distributed dataset S.

3) Discussion

Because the optimization lies in the premise that the input data is narrowly distributed, there exist some limitations concerning the size of the input data and the number of key values appearing in the data. To be specific, the time spent on the operation like binary searching increases with the growth of the number of the elements' values, which leads to dramatic decrease of the efficiency. But for a limited input data size, especially when the data size is under 512, the time overhead can decrease 40% compared with the previous algorithms. When the data size exceeds 512, the advantage of the optimization begins to fade. Another limitation is that in step 1, we assume that the selected array S' has covered all the possible values in array S. This is because input data is narrowly distributed. But when the input data cannot satisfy this premise, the performance cannot achieve the merits as it is supposed to. Besides, because of the sequence of the shared memory of the threads in GPU, it is hard to store the search tree if the data has a large scale of possible keys. Thus the method is limited to the database which is narrowly distributed, especially for the case in which the number of the data values is under 512.

B. Mainly sorted data set

1) Definition of the data set.

Mainly sorted data set is defined as an almost sorted data set which has a small proportion of the set is off the sequence, called the exceptional points (or outliers, especially when the exceptional points take a proportion under 0.5%.

2) Optimization of the algorithm for mainly sorted data set

To sort this kind of data set, we simply screen the exceptional points and sort them. Then merge the sorted exceptional points into the original ordered sequence. The steps are as follows:

Step1: Find all the exceptional points. Traverse the whole data set S to find all the exceptional points $x_i, i = 0,1,2,\cdots n$, and then put them into another array S'. Meanwhile, mark x_i as the invalid position, or null. So these invalid points will not be considered when calculating the length of S.

Step2: Sort the exceptional points array S'. Sort the new array S' to get an ordered one S". The sorting time is much less than that of sorting S because the length of S' is much shorter than that of the data set S.

Step3: Merge the two ordered arrays. Merge the array S and S" to get the final output.

To avoid the visiting consummation caused by moving data to interpolate S" into S, we adopt an improved merge method as follows:

Step1: Read a subsequence $x_i, x_{i+1}, \cdots x_{i+m}, i \geq 0, i+m<n$ of the ordered array S". Then use the subsequence to split S into subsets $T_i, T_{i+1} \ldots T_{i+m-1}$, $x_i \leq \min(T_i) \leq \max(T_{i+m-1}) \leq x_{i+m}$.

Step2: Transfer the subset $T_i, T_{i+1}, \cdots T_{i+m-1}$ to CPU, and then merge the subsequence $x_i, x_{i+1}, \cdots x_{i+m}$ with the subset $T_i, T_{i+1}, \cdots T_{i+m-1}$ to get the sorted sequence.

Step3: Repeat the steps above until the sorting work has completed. This method does not need to move a great deal of data in the interpolation process. In addition, the time of searching for the subset $T_i, T_{i+1}, \cdots T_{i+m-1}$ can be overlapped with the time of transferring the previous subset, thus decreasing the time overhead.

3) Discussion

Since the optimization is targeted mainly at sorted data, the improved sort algorithm can accelerate the previous algorithm dramatically. When the exception points take a proportion of 0.5%, the time overhead decreases 30%. Also the experiment indicates performance gets better as the proportion decreases.

Whereas, the limitation of this method is that if the exceptional points take a relatively large proportion of the input data, it will create a lot of difficulties to the merge sort in step 3. On one hand, in the improved merge sort, if the size of the subsequence $x_i, x_{i+1}, \cdots x_{i+m}$ is a constant, then the merge sort will be repeated too many times, resulting in a decline of the performance. On the other hand, if the merge sort runs a constant time, then the size of the subsequence $x_i, x_{i+1}, \cdots x_{i+m}$ will get quite large, resulting in numerous subsets $T_i, T_{i+1}, \cdots T_{i+m-1}$ divided by the subsequence, resulting in a decrease of the transfer efficiency. Thus, this method is applicable when the exceptional points are few and meets the prerequisites of mainly sorted data set.

C. Stair data set

1) Definition of this data set.

Stair data set includes ascending stair data set and descending stair data set. Ascending stair data set is defined as a data set which can be divided into n sequential sections $S_1, S_2 \cdots S_n$, and meet the condition that $Max(S_i) < Min(S_{i+1}), \forall i \in [0, n)$. Each section S_i is called a step of the stair data set. The number of data in each step is $l_1, l_2 \ldots l_n$. This kind of data indicates that every data in step S_i is larger than those in step S_{i-1}, and is smaller than those in step S_{i+1}.

2) Optimization of the algorithm for stair data set

We consider each step as a bucket when the lengths of the steps are proper and close to each other. Thus we can sort each step independently to save the time of bucket separation algorithm. Based on the feature of the data set, we can get the sequential data after sorting the data in each step. The procedures are as follows:

Step1: Change the input data into a stair data set. When the number of steps is more than n, take the equidistance n-1

points $P_1 \cdots P_{n-1}$, which separate the data set evenly, so we get n subsets $S'_0, S'_1 \cdots S'_{n-1}$. Then traverse the subsets to get the minimums of each subset $\min(S'_0), \min(S'_1) \cdots \min(S'_{n-1})$. Find the $x_i \in S'_i, i \in [0, n-2]$ in the n-1 subsets $S'_0, S'_1 \cdots S'_{n-2}$, in which x_i is the first data that meets the condition that $x_i \geq Min(S'_{i+1})$ .Thus the sequence $x_0, x_1 \ldots x_{n-2}$ divides the data set into n subsets $S_0, S_1 \cdots S_{n-1}$, which is a stair data set by definition.

Step2: Use quick sort to make each step ordered, where each step can be considered as a data bucket. The result will be an ascending sequence if the stair data set is an ascending one. But a further process is needed when the stair data set is a descending one.

Step3: Swap the inverted sequence. For the inverted sequence, it is necessary to swap the elements in the data set. The time overhead is unavoidable if we put the data in a new array in the inverted sequence. Thus we propose an optimization to transfer the result to the CPU in a reverted sequence. The new method save the time spent on swapping the elements and overcome the problem of generating great time overhead.

3) Discussion.

Although the optimization is aimed at stair data set, there are some limitations to the data set, which has a significant influence on the performance of the algorithm. First, the lengths of the steps in the stair data set should not vary in a large range, or it will cause the load balance problem. As we mentioned above, each data step is a bucket and is sorted in one block. If the sizes of the buckets vary, the load of the block will not be balanced and this will deteriorate the parallelization and the performance of the optimized algorithm. Thus the method can be applied to the cases when the number of steps has little changes and the lengths of the step are almost the same, or close to each other.

V. EXPERIMENTAL RESULTS

A. Hardware Environment

Table 1. GPU Memory bandwidth measurement results

Test Cases	Bandwidth
Device to Host	3038.5MB/s
Host to Device	3285.5MB/s
Device to Device	106481.5MB/s

Our experimental system consists of two GPU 260GTX co-processors, 16GB DDR3 main memory and an Intel Quad Core i5-750 CPU. Each GPU connects the main memory through exclusive PCIe 16X data bus, providing 4GB/s bandwidth with full duplex. Experiments have shown that data transmissions between GPU and main memory will not be affected to an appreciable degree. Also, time consumed by data transmission between GPU and main memory can be almost overlapped with GPU computation. Table 1 shows the bandwidth measurement results. GTX 260 with CUDA consists of 16 SMs, with each having 8 processors executing the same instruction but using different data. In CUDA, each SM supports up to 768 threads, owns 16KB of share memory and has 8192 available registers. Threads are logically divided into blocks which are assigned to a specific SM. Depending on the number of registers and the local memory the block of threads requires, there could be multiple blocks assigned to a SM. GPU Data is stored in a 512MB global memory. Each block can use share memory as cache. Hardware can combine several read or write operations into a big one, so it is necessary to keep threads visiting memory consecutively.

B. Data sets in test

1) We used a commonly accepted set of distribution motivated and described in [12] to assess the performance of different algorithms. The data sets are defined as follows. In both Uniform and Gaussian distribution, the elements in this data set are in a range from 0 to (2^{31}-1). Zero means zero entropy input, created by setting every value to a constant such as zero. Bucket Sorted means an input that is sorted in p buckets, obtained by setting the first n/p^2 elements at each processor to be random numbers between 0 and $2^{31}/(p-1)$, the second n/p^2 elements at each processor to be random numbers. Staggered [S] is created as follows: if the processor index i is less than or equal to $(p/2-1)$, then we set all n/p elements at that processor to be random numbers between $2^{31}(2i+1)/p$ and $2^{31}(2i+2)/(p-1)$. Otherwise, we set all n/p elements to be random numbers between $2^{31}(2i-p)/p$ and $2^{31}(2i-p+1)/(p-1)$.

2) Then we use the mainly sorted data set, stair data set and narrowly distributed data set, which have been described in section 4 to test the performance of our ISSD algorithm.

C. Performance Evaluation

In this part, we first compare ISSD algorithm with GPU Sample Sort, GPU QuickSort and Thrust Merge Sort based on different data sets of unsigned integers. Six different types of data sets include Uniform, Sorted, Zero, Bucket, Gaussian, and Staggered [11]. Fig. 1 shows the effects of different array sizes on the performances of the algorithms.

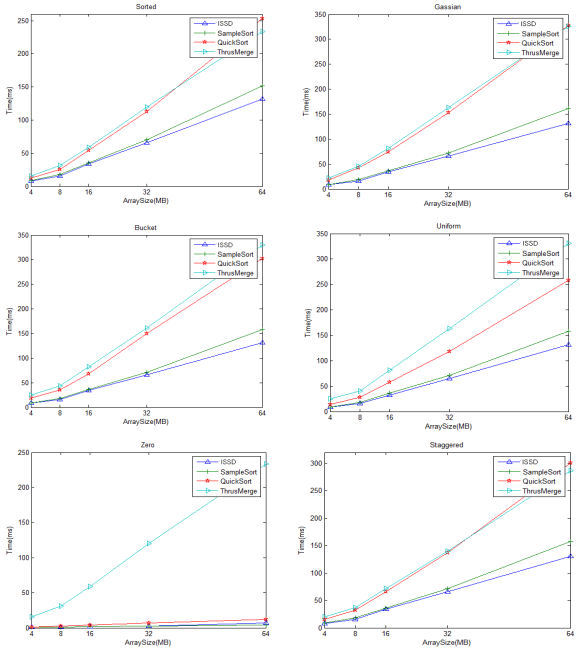

Figure 1. Performance comparison between ISSD and other existing sort algorithms on the six general data distributions

From the figure, we can tell that ISSD algorithm outperforms the others because it can achieve good load balance at relatively small cost. For Uniform, Sorted, Bucket, Gaussian, and Staggered data, our algorithm reduces the time overhead to

50%~60% of that in the QuickSort and Thrust Merge Sort, and outperforms GPU Sample Sort by about 20%. This is an interesting comparison, because both belong to the splitter-based sorting algorithm.

The performance evaluation of ISSD algorithm based on the three data sets of special distribution described in Section IV is shown in Fig. 2. These results clearly indicate that the performance of algorithm has been improved in comparison with the other algorithms to varying degrees. We also notice that the parameters of the data set have a visible influence on the performance of ISSD algorithm. The effect of our optimization is significant, as they are specially designed to take advantage of specific data distributions of different types of data. The scalability of improved algorithms is also clear.

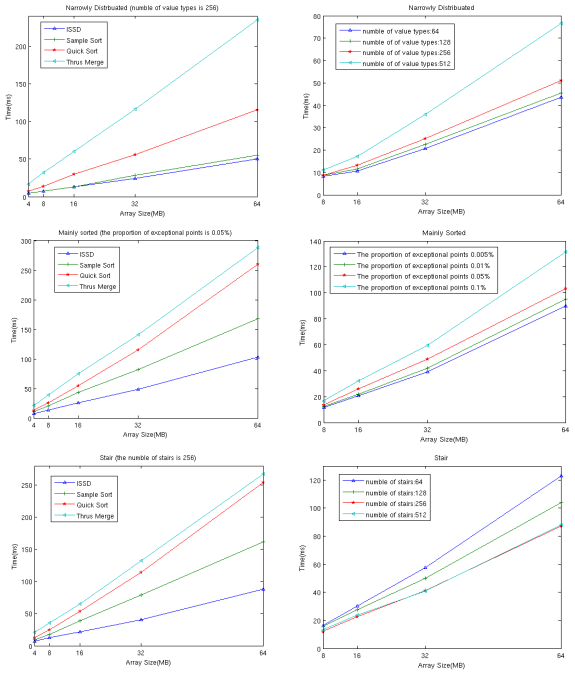

Figure2. Performance comparison between the ISSD algorithm and other algorithms and ISSD self-contrast on the three special data distributions

The first graph on the left hand shows that for the narrowly distributed data set, our ISSD algorithm does accelerate the process to a great extent. When there exist 256 data values, ISSD can be 5 times faster than the Thrust Merge Sort, 3 times faster than parallel quick sort, and slightly faster than the Sample Sort. On those right hand charts, the result indicates the ISSD's performance improves as the number of values decreases. When the number of values drops from 512 to 64, the speedup of the ISSD algorithm increases, which is a dramatic improvement compared with the other algorithms. Also we can learn from the graph that when the number of key values is smaller than 128, the performance has little change. This implies that the ISSD algorithm is highly efficient for the narrowly distributed data whose value is under 128.

From the second row of the graph we can learn that for the mainly sorted data set, the ISSD algorithm outperforms the Thrust Merge, Quick Sort and Sample Sort by 2.7, 2.2 and 1.7 times, respectively under the circumstance that the proportion of the exceptional points is 0.05%. Also, the second column of this row indicates when the proportion of outliers continues to drop, the speedup of ISSD algorithm increases slowly. This is because the number of exceptional points is relatively tiny compared to the whole data set, and then its change will not result in much difference in the performance of the optimized algorithm.

For stair data set, ISSD algorithm only takes 80ms to sort 64MB data when the stair number is 256, and it takes almost 270ms if we use Thrust Merge Sort. Also, ISSD lessens about two thirds of the time overhead taken by the Quick Sort algorithm, and half of the time overhead in the Sample Sort. This is a remarkable improvement in the parallel sorting concerning the stair data set.

In addition, the last graph shows that the performance gets better when the number of stairs increases, because the more stairs the data has, the more blocks we use to sort each stair data, or a data bucket. Besides, the data size in one stair gets smaller when the stair number increases. With more block dealing with less work, the ISSD algorithm performs better than before. Furthermore, the time overhead is determined by the whole data size when the stair number is larger than 256, which indicates that the sorting algorithm is no longer sensitive to the stair data size once the number of stairs has passed a large enough value.

VI. CONCLUSIONS

We have presented the ISSD algorithm and the optimization work based on the data distributions, including the narrowly distributed data set, the mainly sorted data set, and the stair data set. The experimental results show that the methods outperform previous algorithms. In the future, we will try to extend our algorithms to some other conditions which have different data distributions or have special applications in both academic and industrial fields based on the use of GPU.

ACKNOWLEDGMENT

This research is supported in part by National Natural Science Foundation of China ((No. 61073008, 60773148 and No.60503039), Beijing Natural Science Foundation (No. 4082016).

REFERENCES

[1] E. Lindholm, J. Nickolls, S. Oberman, and J. Montrym. NVIDIA Tesla: A unified graphs and computing architecture. IEEE Micro, 28(2):39–55, Mar/Apr 2008.

[2] J. Nickolls, I. Buck, M. Garland, and K. Skadron. Scalable parallel programming with CUDA. ACM Queue, 6(2):40–53, Mar/Apr 2008.

[3] NVIDIA Corporation. NVIDIA CUDA Programming Guide, Nov. 2007. Version 1.1.

[4] E. Solomonik and L. KaleHighly. Scalable Parallel Sorting. In IEEE International Parallel &Distributed Processing Symposium (IPDPS), Apr/ 2010

[5] P. Kipfer and R. Westermann. Improved GPU sorting. In M. Pharr and R. Fernando, editors, GPU Gems 2: Programming Techniques for High-Performance Graphs and General-Purpose Computation, Chapter 46. Addison Wesley Professional, Apr/2005.

[6] N. K. Govindaraju, J. Gray, R. Kumar, and D. Manocha. GPUTeraSort: High performance graphs coprocessor sorting for large database management. In Proceedings of the ACM SIGMOD conference, pages 325–336, Apr./2006.

[7] A. Greß and G. Zachmann. GPU-ABiSort: Optimal parallel sorting on stream architectures. In Proc. 20th International Parallel and Distributed Processing Symposium, pages 4554, Apr./2006.

[8] E. Sintorn and U. Assarsson. Fast Parallel GPU-Sorting Using a Hybrid Algorithm, Journal of Parallel and Distributed Computing, pages 1381-1388, 2007.

[9] D. Cederman and P. Tsigas. A Practical Quicksort Algorithm for Graphs Processors, Technical Report, Department of Computer Science and Engineering, Chalmers Gotborg University, Gothenburg, Sweden, pp. 246- 258, 2008

[10] N. Satish, M. Harris, and M. Garland. Designing efficient sorting algorithms for many-core GPUs. In IEEE International Parallel and Distributed Processing Symposium, 2009.

[11] N. Leischner, V. Osipov, and P. Sanders. GPU sample sort. In IEEE International Parallel and Distributed Processing Symposium, 2010.

[12] D. R. Helman, D. A. Bader, and J. J´aJ´a. A randomized parallel sorting algorithm with an experimental study. Journal of Parallel and Distributed Computing, 52(1):1–23, 1998.

A CUDA Pseudo-spectral Solver for Two-dimensional Navier-Stokes Equation*

Kaiyuan LOU, Zhaohua YIN
Institute of mechanics, Chinese Academy of Sciences, Beijing, China, 100190
Email: zhaohua.yin@imech.ac.cn Tel: 010-82544100

ABSTRACT

In this paper, the two dimension incompressible Navier-Stokes equations with pseudo-spectral method are solved using the related subroutines in FFTW and CUFFT. Compared with the codes on CPU, the performance of the codes on GPU is much better, especially when the resolution increases. For the resolution of 2048 × 2048, the acceleration reaches 14.45 times. We also try to combine MPI (Message Passing Interface) and CUDA (Compute Unified Device Architecture) in our solver. Due to the inevitable frequent data transfers between Host and Device, the speedup is not so ideal compared with that of the single node, and 1.82 times acceleration is obtained in double precision for the resolution of 4096 × 4096.

Keywords: CUDA, spectral method, N-S equation.

1. INTRODUCTION

In recent years, the Graphics Processor Unit (GPU) has tremendously developed. Though the purpose of these advances is to calculate the complex visual effects in computer games, it has been found that the same technology can be applied in scientific computing. In 2006, NVIDIA developed a Compute Unified Device Architecture (CUDA) on the extended set of C language. CUDA is a very convenient architecture because programmers do not need to master the graphical knowledge. Hence, CUDA provides a low entry level for the learning of many-core programming, so the general-purpose scientific computing on the GPU develops rapidly.

Legyel first used GPU in scientific computing about the robot first [1], and it was then applied in various areas including fluid dynamics. In the past few years many researchers have studied how to use GPU to optimize the CFD (Computational Fluid Dynamics) codes, and found GPU can really improve the code's performance for one or two grades compared with that on CPU (Central Processing Unit). For example, Antoniou found that finite difference method WENO obtained 53 times acceleration for single-precision float when CUDA was adopted. Cohen and Molemaker found similar performance improvements in the solution of three-dimensional incompressible Navier-Stokes (N-S) equations (double precision) [2]. Dong Tingxing *et al*. simulated two-dimensional RAE2822 wing flow around in the scale of 1024 × 128, and obtained 2.33 times acceleration [3]. When calculating two-dimensional diffusion equation in the size of 1024 × 1024, Dong Tingxing et al achieved a 34 times speedup [4].

According to the above information, CUDA is successfully applied in solving N-S equation with finite difference method, but few studies about spectral method have been done. For a comparable error on the uniform mesh, spectral method requires a much finer mesh than finite difference or finite element methods. Unlike finite difference methods, most computation of spectral method is in DFT (Discrete Fourier Transform). FFTW is the widely adopted open-source DFT package in CPU, while CUFFT is mostly used on GPU [5]. In this paper, we use both FFTW and CUFFT to solve two-dimension incompressible N-S equations and focus on the performance improvement when replacing FFTW with CUFFT.

Sometimes, due to memory limitations, a large-scale problem cannot be computed in a single GPU, so we also use the multi-node parallel computing with MPI (Message Passing Interface). Some tests in combination of MPI and CUDA are also performed.

2. GOVERNING EQUATIONS & NUMERICAL METHODS

2.1. Governing Equations

Two dimension incompressible N-S equations:

$$\begin{cases} \nabla \cdot \vec{\mathbf{v}} = 0, \\ \dfrac{\partial \vec{\mathbf{v}}}{\partial t} + \vec{\mathbf{v}} \cdot \nabla \vec{\mathbf{v}} = -\dfrac{1}{\rho}\nabla p + \nu \nabla^2 \vec{\mathbf{v}} + \vec{\mathbf{f}}. \end{cases} \quad (1)$$

Here, $\vec{\mathbf{v}} = (u, v)$ is the velocity, $\vec{\mathbf{f}}$ the external force, ρ the density, p the pressure, and ν the kinetic viscosity coefficient. There is no external force in our problem, so $\vec{\mathbf{f}} = 0$.

The computing domain is $(x, y) \in [0, 2\pi] \times [0, 2\pi]$, and the periodic boundary conditions are adopted. The initial condition is $\vec{\mathbf{v}}(\mathbf{x}, 0) = \vec{\mathbf{v}}_0(\mathbf{x})$.

2.2. Numerical Method

Spectral method is applied to discrete space. p, $\vec{\mathbf{v}}$ is mapped from physical space to Fourier space as the following:

$$\begin{cases} \vec{\mathbf{v}}(\mathbf{x}, t) = \sum_{\mathbf{k}} \hat{\mathbf{V}}_{\mathbf{k}} e^{i\mathbf{k}\cdot\mathbf{x}}, \\ p(\mathbf{x}, t) = \sum_{\mathbf{k}} \hat{p}_{\mathbf{k}} e^{i\mathbf{k}\cdot\mathbf{x}}, \end{cases} \quad (2)$$

where $\mathbf{x} = (x, y)$ is the position in physical space, and $\mathbf{k} = (k_1, k_2)$ represents different wave numbers.

Applying the Fourier-Galerkin method to the N-S equations Eq. (1) and with the approximation Eq. (2), we get a set of differential equations for determining the Fourier coefficients $\hat{\mathbf{V}}_{\mathbf{k}}$ and $\hat{p}_{\mathbf{k}}$:

$$dt\hat{\mathbf{V}}_{\mathbf{k}} + \nu k^2 \hat{\mathbf{V}}_{\mathbf{k}} = -\hat{\mathbf{A}}_{\mathbf{k}} + \frac{\mathbf{k} \cdot \hat{\mathbf{A}}_{\mathbf{k}}}{k^2}\mathbf{k}. \quad (3)$$

* This project is supported by the NSF of China (Contract No. G11172308).

978-0-7695-4818-0/12 $26.00 © 2012 IEEE
DOI 10.1109/DCABES.2012.93

When $k^2 = 0$, no matter what the value of $\hat{\mathbf{V}}_0$ is, the original equation is automatically satisfied. We set $\hat{p}_0 = 0$ at that time, which means value of pressure is zero.

$$d t\hat{\mathbf{V}}_{\mathbf{k}} = -\nu k^2\hat{\mathbf{V}}_{\mathbf{k}} - \hat{\mathbf{A}}_{\mathbf{k}} + \frac{\mathbf{k}\cdot\hat{\mathbf{A}}_{\mathbf{k}}}{k^2}\mathbf{k}\,. \tag{4}$$

In Eq. (4), $-\nu k^2\hat{\mathbf{V}}_{\mathbf{k}}$ is linear term (viscous term) and $-\hat{\mathbf{A}}_{\mathbf{k}} + \frac{\mathbf{k}\cdot\hat{\mathbf{A}}_{\mathbf{k}}}{k^2}\mathbf{k}$ nonlinear term (convection term).

To carry out the time integration, the third order Runge-Kutta method is adopted.

$$\frac{\partial \mathbf{v}}{\partial t} = L(\mathbf{v}) + N(\mathbf{v})\,. \tag{5}$$

Here, $L(\mathbf{v})$ is the linear term $-\nu k^2\hat{\mathbf{V}}_{\mathbf{k}}$ and $N(\mathbf{v})$ the nonlinear term $-\hat{\mathbf{A}}_{\mathbf{k}} + \frac{\mathbf{k}\cdot\hat{\mathbf{A}}_{\mathbf{k}}}{k^2}\mathbf{k}$.

We define $\mathbf{v}_n$ as the speed at time t and $\mathbf{v}_{n+1}$ the speed at time $t + \Delta t$. The following equations show how the calculation of $\mathbf{v}_{n+1}$ from $\mathbf{v}_n$ is conducted in three steps [6]:

$$\begin{aligned}
&\mathbf{v}' = \mathbf{v}_n + \Delta t[L(\alpha_1\mathbf{v}_n + \beta_1\mathbf{v}') + \gamma_1 N(\mathbf{v}_n)],\\
&\mathbf{v}'' = \mathbf{v}' + \Delta t[L(\alpha_2\mathbf{v}' + \beta_2\mathbf{v}'') + \gamma_2 N(\mathbf{v}') + \zeta_1 N(\mathbf{v}_n)],\\
&\mathbf{v}_{n+1} = \mathbf{v}'' + \Delta t[L(\alpha_3\mathbf{v}'' + \beta_3\mathbf{v}_{n+1}) + \gamma_3 N(\mathbf{v}'') + \zeta_2 N(\mathbf{v}')],
\end{aligned} \tag{6}$$

where

$$\begin{aligned}
&\gamma_1 = 8/15, \gamma_2 = 5/12, \gamma_3 = 3/4,\\
&\zeta_1 = -17/60, \zeta_2 = -5/12,\\
&\alpha_1 = 29/96, \alpha_2 = -3/40, \alpha_3 = 1/6,\\
&\beta_1 = 37/160, \beta_2 = 5/24, \beta_3 = 1/6.
\end{aligned}$$

The linear term $L(\mathbf{v})$ can be easily computed in Fourier space, but the calculation of the nonlinear term $N(\mathbf{v})$ is a bit involved. So the nonlinear term is obtained by being transferred back and from the physical space with FFTs; in the meantime, the de-aliasing procedure has to be adopted to remove the aliasing errors. There are two kinds of de-aliasing techniques available: padding-truncation and phase-shifts. In this paper, we use phase-shifts, which reserves more high wave numbers information than that for padding-truncation. In summary, the calculation process is shown in Figure. 1:

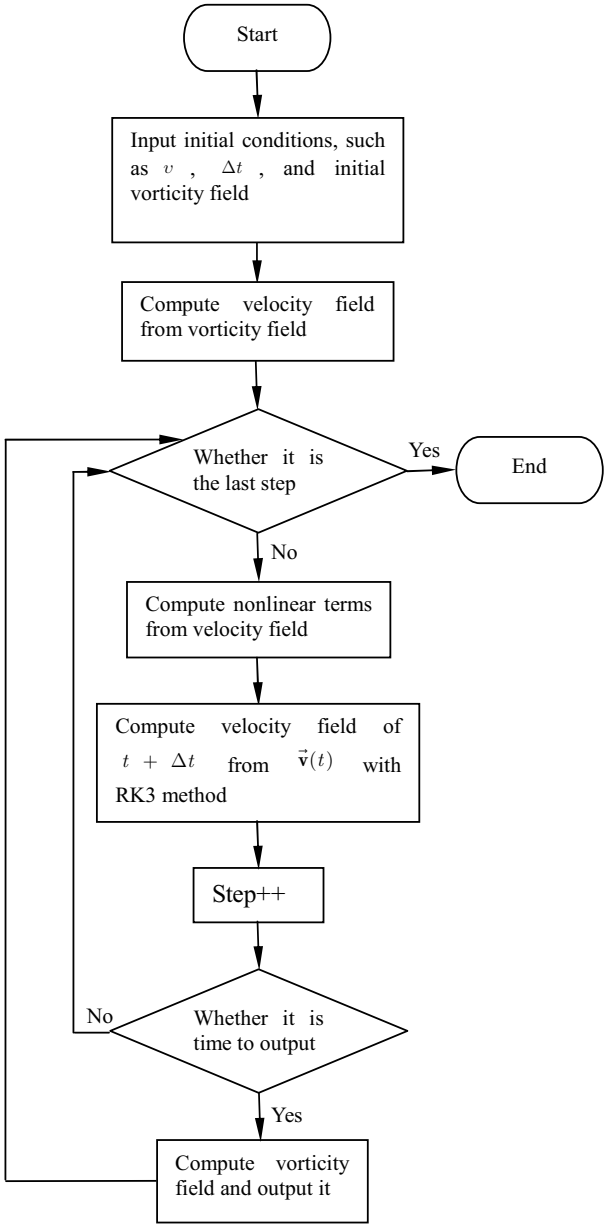

Figure 1. Computing process

3. INTRODUCTION TO GPU COMPUTING

3.1. The Structure of CUDA

The CUDA code is divided into two parts: one part is on the CPU, known as the Host section, and another part in the GPU, which is called the Device portion. Host part completes a call to the GPU through Kernel function. As a highly parallel programming model, CUDA divides the tasks in the Kernel into the threads. The structure of the threads is indicated in Figure 2. Threads are organized by blocks, and each block is the same in size. A kernel function can be performed by multiple blocks, and each block is organized as a one-dimensional or two-dimensional grid [7]. This model guides the programmer to partition the problem into coarse sub-problems which can be solved independently in parallel by blocks of threads, and each sub-problem into finer pieces that can be solved cooperatively in parallel by all threads within the block. Indeed, each block of threads can be scheduled on any of the available processor cores, in any order. That is, blocks can be executed in parallel if there are available units; otherwise, they will be executed sequentially [7].

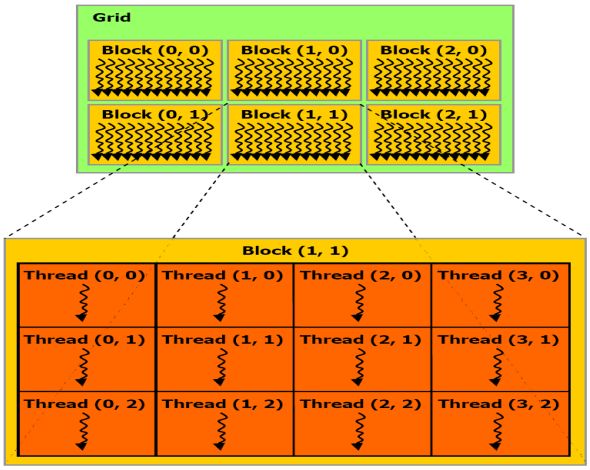

Figure 2. Structure of threads in CUDA

3.2. The Advantage of GPU over CPU in Computing

There exist differences between the CPU and GPU in scientific computing capability, and the reason is that GPU is designed for compute-intensive, highly parallel computing. Thus, the design of GPU adopts more transistors in data processing rather than in the data cache or flow control. Many lines parallel collaboration is GPU internal design, and each computing pipeline is equal to a computing unit in CPU internal core (core) which can compute a set of data independently. Therefore, GPU can be considered as hundreds of simple CPU doing data calculations at the same time, or we can say that a GPU is a small MPI parallel cluster. The floating-point computing capability of GPU is much higher than that of the CPU in the same level. Of course, the development of computing ability is accompanied by some sacrifice. The GPU does not have the flow control unit, so it is only suitable for the program of order processing with a large amount of data.

In CUDA, the thread structure is like matrix, so it is suitable for grid computing. The equations in this paper need to disperse the computational region into grids. This is naturally in line with the CUDA thread structure. In CFD, similar computation is often required again and again. The amount of computation is great but logical judgment is few. So CFD is suitable for GPU to perform its great computing capability.

4. OPTIMAZATION STRATEGIES

4.1. Reduce the Time in Host and Device Communication

PCI-E bandwidth is relatively small, only the 8GB / s, and lags far behind the bandwidth of the GPU (the GPU adopted in this article uses is C1060, and its memory bandwidth is 102GB / s). Data transmission between CPU and GPU will inevitablely cause bottleneck. So the best strategy is to minimize the amount of data transferred between the CPU and GPU. Therefore, unnecessary transmission should be avoided. In order to achieve the purpose of reducing transmission quantity, we reduce the times of transmissions. We put all process into GPU, and the exchange of data between the GPU and CPU only occurs in data I/O.

In a test of a 2048 × 2048 simulation, when data exchange 3 times at each time step, each 1000 steps takes about 20 minutes, while only 16 minutes is needed without these exchanges.

No direct communication between the GPU exists in a multi-node computing. There is no good way to avoid the exchange between CPU and GPU. In the low resolution case, data exchange has become the most time-consuming part in the whole program.

4.2. Shared Memory

The latency accessing to shared memory is 1 to 2 clock cycles (in the situation with non-Bank Conflict), much smaller than to the global memory (about 500 clock cycles). According to the information provided by the NVIDIA SDK, the program of matrix transpose speeds up 10 times compared with the case in which shared memory is not used. NVIDIA offers an idea to avoid bank conflict by padding an empty row. In this program, the little teaser is also applied in other sub program. Because the data in shared memory is visible to the threads in the same block, we use shared memory to avoid every thread getting its data from global memory one by one in the program of matrix adding.

4.3. Memory Coalescing

In C language, memory storage is arranged by line. 16 continuous threads' visit to continuous data period in global memory can be combined into a storage affair. In our program, besides FFT, memory operation to matrix fits this condition naturally.

Warp is organized by the SM automatically in a continuous way. For example, if there are 128 threads in a block, they will be divided into four warps: 0-31 threads will be warp 1, 32-63 warp 2, 64-95 warp 3, and 96-127 warp 4. So the best amount of threads per block is a multiple of 32. Otherwise, it will cause a warp less than 32 threads to use the same resources as a warp full of 32 threads. In this paper, each block contains 16 × 16 = 256 threads in a single node case. In multi-node computing, we just call CUFFT functions, and the left computation is on CPU, so we needn't take it into consideration.

4.4. Others

Some constants are calculated in the CPU, and then copied them to GPU for repeated calls.

When we have to operate with a small number of threads, we use “if threadID<N” to avoid multiple threads running at the same time which takes more time or even produce incorrect results.

Because synchronization in our program is relatively few, it is difficult to have a big performance improvement at this point.

5. RESULTS AND COMPARISON

5.1. Computing Environment

Our programs run at tesla.sccas.cn, a server of Supercomputing Center of Chinese Academy of Science. Its environment is shown as the following.

Single node: CPU Intel Xeon E5410, 2GHz CPU Clock Speed, 2×6MB second-level cache; GPU tesla C1060×2; memory 8GB; hard disk SATA 500GB.

Compiler: FFTW program uses “g++” to compile and CUFFT program employs “nvcc”.

Multi-node uses 4 nodes with the same configuration as above.

5.2. Result in Single Node

Two codes are programmed with CUFFT and FFTW. We test our codes with different resolution (128 × 128, 512 × 512, 2048 × 2048). The performance is shown in Table 1. To confirm whether our result is right, three different times are chosen to output. After comparison of each resolution, the results of FFTW and CUFFT are found the same (Figure 3, Figure 4).

In 128 × 128 resolution, we calculate 6000 steps. At last, the streamlines both become two vortexes. It is a stable situation. The result of CUFFT(float) is the same, so we won't show the picture here to save space.

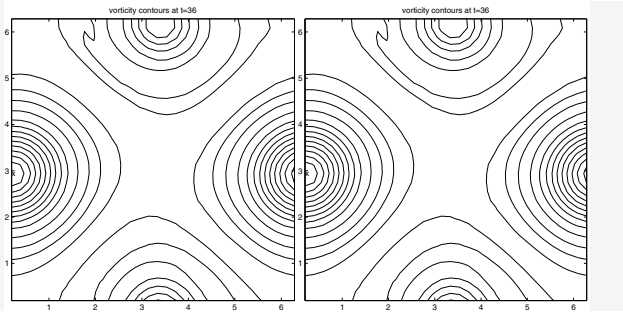

Figure 3. 128×128 result at t=36 CUFFT(double)(left), FFTW(right)

We also calculate 10000 steps in 512 × 512 resolution. At last, they both reach the stable situation (two vortexes).

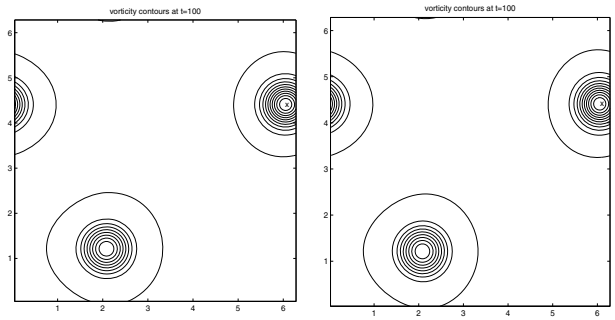

Figure 4. 512×512 result at t=100 CUFFT(double)(left), FFTW(right)

In 2048 × 2048 resolution, the results are also the same. We calculate 170000 steps, but do not reach the two vortexes' stable situation at last. However, we can see the tendency to stable situation. When calculated 100000 steps, the streamlines become several vortexes and small vortexes roll into big vortex. At last, there are two big skew vortexes in the streamline chart, which are not like the regular ones above.

Table 1. Till 1000 steps, time required by different methods

resolution	FFTW(s)	CUFFT(double)(s)	CUFFT(float)(s)
128×128	35.3	11.7	3.7
512×512	695	56	21
2048×2048	14431	999	424

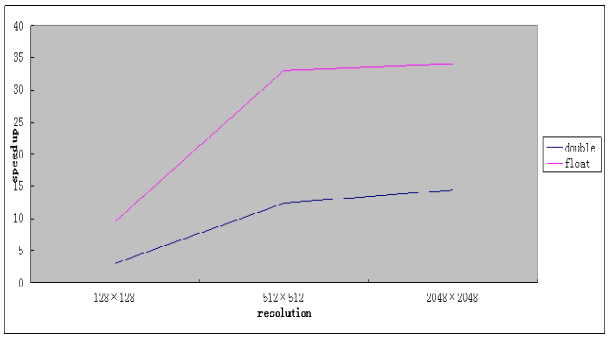

Figure 5. Speed up with CUFFT in different resolution

In 128 × 128, 512 × 512, and 2048 × 2048 cases, the corresponding CUFFT speedups are 3.03, 12.41, and 14.45.

From Figure 5, we can see CUDA's acceleration is more and more obvious with the increase of the resolution.

5.3. Performance of CUFFT and FFTW

We test the performance of CUFFT and FFTW which don't contain the communicating time. We use arrays of different sizes to test our codes. Every array performs FFT and IFFT, and then we count the time. The function clock() is adopted for timing in FFTW and the function cudaevent in CUFFT.

Table 2. Time required by different resolutions

Array size	FFTW(ms)	CUFFT(double)(ms)	speedup
128×128	1	0.3026	3.30
512×512	20	1.189	16.82
2048×2048	370	18.099	20.44

Table 2 shows that as the size increases, the advantage of CUFFT is more obvious. It meets the conclusion we get in 5.1. In addition, it is worth mentioning that the speedup radio of both the N-S equation and pure FFT becomes smaller as the size increases. As the size grows, the communication time grows too, but we never take any measures to speed up the communication.

Table3. The different performance of CUFFT in single and double precisions

Array size	CUFFT(float)(ms)	CUFFT(double)(ms)	double/float
128×128	0.1505	0.3026	2.01
512×512	0.308	1.189	3.86
2048×2048	2.968	18.099	6.10

By comparison, we can find that single precision data has an advantage over that of double precision in GPU computing. In addition, the advantage gets bigger with the increase of the resolution. However, with the increase of data amount, besides computing ability, the bandwidth will become a limit to the calculating speed [8].

5.4. Result in Multi-Node

As the case in a single node, we use CUFFT and FFTW programming to solve the N-S equations at 4 nodes. At last FFTW and CUFFT achieve the same results under different resolutions.

In the following, the time of 100 steps' calculation at 4 nodes is shown for different methods. In the case of 2048 × 2048

resolution, CUFFT needs 374s and FFTW needs 493s; the speedup is 1.32 times. When resolution is 4096 × 4096, 1063s is required for CUFFT and 1936s for FFTW; the speedup increases to 1.82 times.

By the above comparison, we find that as the resolution increases, GPU shows a greater advantage. When calculating the case of 4096 × 4096, MPI is used to collaborate on multiple nodes. So the data transfer between Host and Device is inevitable in every step in our code. Because of a lot of time consumed in coping data, acceleration is not so obvious as which in single node. Even so, there is noticeable advantage when using GPU to compute a large amount of data. With the larger resolution, CUFFT will have better acceleration. However, limited by communication problems, acceleration will not be as obvious as that in the single node.

6. DISCUSSION AND CONCLUSION

We use CUDA to accelerate our CFD code, and there is obvious improvement after we replace the FFTW subroutines with those of CUFFT.

In the case of a single node, the performance improvement of CUDA can be found in every resolution. In addition, with higher resolution, the accelerating effect is more obvious. When the resolution is 2048×2048, the speedup is 14.45 times. This allows us to use a higher resolution to observe the changes of the vorticity field in a fixed calculating time, and more subtle fluid structures can be observed.

TeslaC1060 is about 3 times more expensive than Intel XeonE5410. When the calculated amount is small, the economic benefit of using GPU is not very obvious, and it is not very economical to use GPU. When the resolution of our simulation increases, it is much cheaper to use GPU.

The tests in Section 5.2 show that CUDA has better performance in the single-precision calculation than in double precision, but the gap between single and double precisions does not reach the eight times speedup in theory. On the GPU of the next generation (C2050), the gap between single and double precision becomes only two-times speedup in theory. If our double-precision program is carried out on tesla C2050, better acceleration may be achieved.

Direct communication between the GPU is not supported in CUDA2.0 in multi-node. When using MPI to increase the resolution, communications must occur between Hosts. The communication between GPU and CPU is inevitable; a lot of time has to be wasted in coping data, so the advantages of GPU computing will be hidden. Maybe for a problem in which transfers between nodes are not required so frequently, the performance of GPU will be better.

7. REFERENCES

[1] Lengyel J, Reichert M, Donald B, Greenberg D, "Real-time robot motion planning using rasterizing computer graphics hardware", ACM SIGGRAPH Computer Graphics, Vol.24,Issue.4, Aug 1990, pp.327~335.

[2] Cohan J, Molemaker M, "A fast double precision CFD code using CUDA", Parallel CFD, 2009, pp.414~427.

[3] Dong Tingxing, Li Xinliang, Li Sen, Chi Xuebin， "Acceleration of Computational Fluid Dynamics Codes on GPU", Computer Systems & Application，Vol.20, No.1, 2011, pp.104~109.

[4] Dong Tingxing, Wang Long, Chi Xuebin, "the GPU acceleration of a two-dimensional diffusion equation", Computer Engineering and Science，Vol.31, No.11, 2009, pp.121~127.

[5] Http: // www.nvidia.cn/object/cuda_home_cn.Html.

[6] Claudio Canuto, M. Yousuff Hussaini, Alfio Quarteroni, Thomas A. Zang, Spectral Methods in Fluid Dynamics, New York: Springer-Verlag Inc. Pub., 1998.

[7] NVIDIA CUDA Programming Guide. http://www.nvidia.cn/object/cuda_develop_cn.html.

[8] J. Appleyard, D. Drikakis, "Higher-order CFD and interface tracking methods on highly-Parallel MPI and GPU system", Computer & Fluids, Vol.46, Issue.1, July 2011, pp101~105.

A Parallel Packet Processing Runtime System On Multi-Core Network Processors

Yunchun Li, Lianqiang Shan, Xinxin Qiao
Beijing Key laboratory of network technology, Computer Science Department
BeiHang University Beijing, China
lych@buaa.edu.cn, slian1126@gmail.com, qiaoxinxin1126@gmail.com

***Abstract*—More and more network devices and chips commonly apply multi-core architectures to meet increasingly performance demands. But the lack of efficient program level parallelism and workload allocation in the packet processing system greatly limits the utilization of multi-core architectures. In this paper, we propose a parallel packet processing runtime system and explore an affinity-based packet scheduler with the goal of raising load balancing and decreasing cache miss. We can use the system that handles the allocation of processing tasks to simplify the implementation of new applications. The experiment results show task distributor and scheduler can achieve a better compromise between load balancing and cache affinity in the parallel packet processing system.**

Keywords-multi-core; load banlance; parallel packet process

I. INTRODUCTION

With recent development in network technologies, speed of network is becoming more faster. Especially a lot of streaming media and P2P application appear, data on network are exponentially growing. It requires higher network packet processing capabilities.

Additionally, more and more intelligence is requested to the network. The traditional network equipment based on general processor cannot meet the needs of the development of the network, ASICs (Application Specific Integrated Circuit) guarantee extremely high packet rates, but they cannot be reprogrammed and the time needed to develop a new chip is increasingly high. Network Processors' architecture is particularly targeted to network packet processing and have a new form of programmability and short developing time [1]. Meanwhile, multi-core technology and parallel computing technology which can speed packet processing up are used in network processors. Therefore, multi-core network processors become the trend of network equipment for they have high performance and programmability.

Multi-core architectures can boost packet processing by executing concurrent processes/threads on different cores, but a key question is how to allocate a suitable workload to each processing core. Then efficient core utilization and parallel processing mechanism in a multi-core architecture remains a challenge. The lack of efficient program level parallelism in legacy network applications greatly limits the utilization of multi-core architectures. They often perform no better than single core systems. And communication among processors restricts system scalability [2].

In this paper, we propose a packet processing runtime system, including a task allocator with the goal of load balancing and minimal cache misses, explore connection level parallelism and an affinity-based scheduler in the system. We assign packets belong to the same connection to the same thread which is dispatched to a dedicated core on a multi-core processor at the same time. To examine the performance, we present the definition of load balancing degree, and implement parallel DPI (Deep Packet Inspection) based on the system to carry out some experiments. We treat cache miss, load balancing degree and speedup rate as performance indicators. Though the comparing the results from our scheduling method and two other common methods, point out our scheduling method can achieve a better compromise between load balancing and cache affinity and higher performance .

The reset of the paper is organized as followed: In section II, we analyze current network application and packet processing model. In section III, we introduce the architecture of packet processing model. In section IV, we propose an affinity-based packet scheduling algorithm. In section V, some experiments are carried out, and we analyze the performance. In section VI, we conclude the paper and point out our future research directions.

II. RELATED WORKS

In the network applications, they have higher performance requirements for program, such as network data transmission, analysis, and so on. The main treatment in the application is in the form of flow. It has a large quantity of data, a single data flow direction, and high real-time demand. There is good parallelism in data processing itself, but it is difficult to do further optimization in the traditional serial structure [3]. While in the multi-core architecture, some terms should draw lots of attention, packet distribution, load balancing and scheduling [4, 10].

A. Parallelism in network applicatons

Often, the parallelism in program mainly includes instruction level parallelism and task level parallelism. And for most network application, more parallelism lies in processing packet.

978-0-7695-4818-0/12 $26.00 © 2012 IEEE
DOI 10.1109/DCABES.2012.59

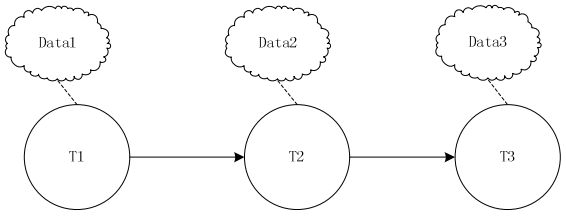

Figure 1. Packet processing.

As Fig. 1 shows above, T1 is processing data1 when T2 is dealing with data2. It indicates a characteristic in network application, SPMD (Single Program Multiple Data), namely the data parallel. The key point of data parallel is to grasp parallel scheduling mechanism. In the process we should consider how to make effective use of data parallel to improve scheduling performance.

B. Packet scheduling mechanism

Packet is the main data that network equipment need to deal with. Therefore partition of task granularity is the key in parallel processing. For now scheduling in packet processing can be divided into two types [5]: packet based scheduling, flow based scheduling.

Packet based scheduling: in packet based scheduling, packets are assigned to cores on a packet-by-packet basis. Such as Round-robin, it is an example of a simple packet based scheduling mechanism. More complex algorithms assign packets to the least loaded core. Packet based scheduling does a good job of balancing the load across cores. However, packet reordering can occur and impact network performance. In addition, packet based scheduling in shared memory systems can be cache inefficient resulting in reduced performance.

Flow based scheduling: flow based scheduling maintains a table of active flows where each flow is associated with a resource. Packets are mapped to flows and scheduled on the resource associated with their flow. New flows are assigned to the least loaded resource. Since all packets on the same flow are assigned to the same resource, per flow packet order is maintained. Also, it is cache efficient for the same reason. But it has poor performance in load balancing.

The ideal packet scheduler has following features [2-5]:

- Load balancing: packet is evenly assigned among all cores.
- Cache affinity: packets are scheduled on cores that have their associated data structures already in cache.
- Low scheduling overhead: the cost of scheduling packets is very small in comparison to the work performed on the packet.
- Flow ordering: packets on the same flow at egress are in their arrival order.

To achieve better performance, many researchers summarize two methods. IBMResearch [6] use indirect hash mapping method to assign flow and introduce time stamp, flow redistribution and message spray mechanism to obtain load balancing between cores. Kencl [7] propose IP packet scheduling mechanism based on extension HRW. The biggest characteristic is no need to keep scheduling state information. When the load is not balanced, it will adjust each core hash weight dynamically to change load mapping target. But they do not consider packets ordering. In the paper [8], they divide flow into high speed flow and low speed flow to avoid flow re-mapping. Regulate less high speed flow when the load is not balanced. Pappu [9] put forward local scheduling and local perception prediction scheduling to maintain flow consistency and avoid cache failure, but this mechanism does not account for load balancing and packet ordering. In [5], they evaluate the performance of three packet scheduling algorithms, the results show that packet scheduling based on cache affinity is more important than trying to balance packets.

III. ARCHITECTURE OF SYSTEM

We adopt macroscopic multi-layer model in packet processing system and propose multi-queue parallel model for runtime system to maximize the performance of multi-core architecture.

A. macroscopic multi-layer model

According to different demand for hardware, tasks that the network equipment process can be divided into two types, basic message forwarding and complex message content detection. Basic message forwarding need high IO throughput, and complex message context detection need more CPU and memory. In such cases separation design technology is used in network equipment. Control plane is responsible for specific network processing tasks, such as DPI, while work on data plane is packet forwarding and simple pre-process. As shown in Fig. 2, it includes control plane and data plane. Our runtime system is working on OS. New network application is implemented using runtime system. It includes task scheduler, thread pool, and packet input modules. Task scheduler treats a coming packet processing as a task, and allocates it to the thread pool binding to cores as shown in Fig. 3.

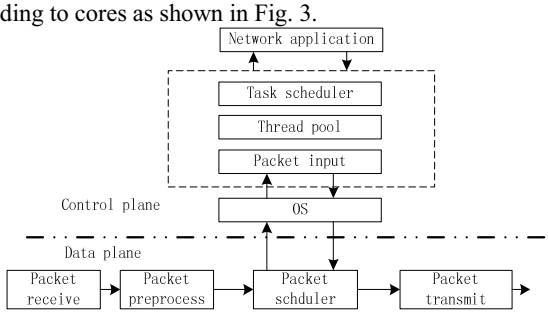

Figure 2. Two-layer model.

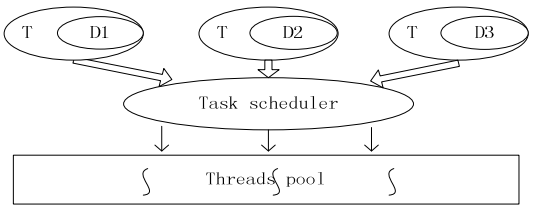

Figure 3. Runtime system model.

Data plane send packets which need complex processed to control plane. We can develop various network applications based on task manger on OS which runs on control plane.

B. Multi-queue parallel model

We create multi-threads on cores and map every thread to each core. As shown is Fig. 4, for high performance, every thread which is set affinity to core has its local queue and operates local data. This is due to that processes created in an SMP system are placed on a given CPU's runqueue. In the general case, it is impossible to predict the life of a process. Therefore, the initial allocation of processes to CPUs is very likely to be suboptimal. To maintain a balanced workload across CPUs, OS checks to see whether an adjustment balancing of tasks is necessary. When a thread blocking for I/O is signaled, it will be awakened on the core where the migration occurred. Affinity threads ensure that application processing of a flow's packets is likely to be executed on the same cores as its packets processing and reduce cache miss.

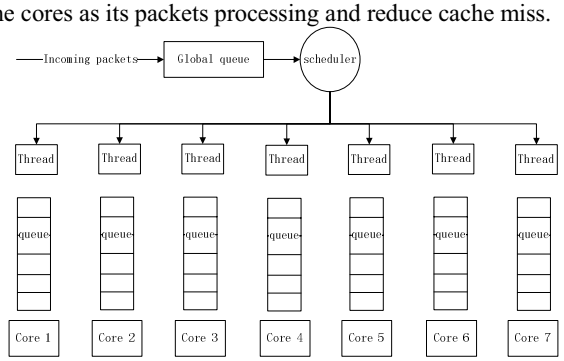

Figure 4. Multi-queue parallel model.

When multiple threads are created, each thread deals with packets in local queue, the thread will always run on the same core. Packets from same flow will be sent to same queue by scheduler as much as possible. It will reduce additional cache overhead by copying packets of the same flow to different cores. For better load balancing and cache affinity, we adjust scheduling mechanism to solve the multithreading scheduling problem.

IV. TASK SCHEDULING

Task scheduling is key part in the runtime system. Scheduling strategy will be proposed based on multi-queue parallel model given in section III. We treat each packet processing as a task. Task scheduling can be handled as packet scheduling. As we set up affinity threads to cores, better packet scheduling mechanism should reach the best compromise between load balancing and cache affinity. Our packet scheduling algorithm belongs to flow based scheduling, and combines the flexibility of packet based scheduling.

A flow table (FT) is used to keep active flow information. Every entry in the FT includes flow identifier, time stamp, core number. When a packet is received, packet scheduler parses the source IP address, source port, destination IP address, and destination port of the packet. The 4-tuple is be used to identify a flow. If there is one same 4-tuple flow information in flow table, the packet will be sent to the core which this flow entry (FE) is mapped to and time stamp is refreshed in the FE. If the packet does not belong to any flow in the FT, this indicates that it is a new flow's packet. Then a new FE will be created. The number of Core that has the shortest queue length is best choice for this flow. The queue length is defined and calculated as follows:

Queue length: we calculate the length of queue using method of moving average in statistics. The method based on the index of the weighting moving average is often used in network field, for example, the calculation of round-trip-delay in TCP prototype. The queue length is calculated as follows:

$$\text{queue\_len} = \text{current\_queue\_len} \times (1 - \omega) + \text{real\_queue\_len} \times \omega$$

$queue\_len$: average length after arrival of packet;

$current\_queue\_len$: average length before arrival of packet;

$real\_queue\_len$: current queue length;

ω: weight of queue;

The selection of suitable ω impact the queue length, if ω is too big, the burst flow will make forwarding plane jitter. Conversely, the impact of flow change on queue length would be small, it cannot correctly reflect the current load conditions.

When the FE is created, packets belonging to this flow will be sent to same core.

At the same time, to avoid more and more memory for FT and achieve load balancing, we get T as a threshold which is the longest time used in a packet processing. If the difference between current time and time stamp in the FE is greater than T when a packet is about to scheduled, the core number in this FE should be refreshed as above.

We propose load balancing degree to test scheduling strategy. The definition of load balance degree as follows:

$p_i(t)$ is packets that are processed by processor node p_i(i=1,2,…,m), $|p_i(t)|$ is packet number of $p_i(t)$, $|\text{Len}_i(t)|$ is byte number of $p_i(t)$, and $p(t) = \bigcup_{i=1}^{m} p_i(t)$, $\text{Len}(t) = \bigcup_{i=1}^{m} \text{Len}_i(t)$, then the autocovariance of $|\text{Len}_i(t)|$ can be calculate as follows:

$$\text{CV}[|\text{Len}_i(t)|] = \frac{\text{D}(|\text{Len}_i(t)|)}{\left(\text{E}(|\text{Len}_i(t)|)\right)^2} = \frac{\text{E}(|\text{Len}_i(t)|^2) - \left(\text{E}(|\text{Len}_i(t)|)\right)^2}{\left(\text{E}(|\text{Len}_i(t)|)\right)^2}. \quad (1)$$

According to formula (1), reduce into interval [0, 1], we will get the load balancing degree，$\text{bLBM}(t)$:

$$bLBM(t) = \frac{CV[|Len_i(t)|]}{CV[|Len_i(t)|]+1} = 1 - \frac{\left(E(|Len_i(t)|)\right)^2}{E(|Len_i(t)|^2)}. \quad (2)$$

Because the mathematical expectation of $|Len_i(t)|$ and $|Len_i(t)|^2$ can be expressed in their observations in time interval $(t-\Delta t, t)$

$$E(|Len_i(t)|) = \frac{\sum_{i=1}^{m}|Len_i(t)|}{m}. \quad (3)$$

$$E(|Len_i(t)|^2) = \frac{\sum_{i=1}^{m}|Len_i(t)|^2}{m}. \quad (4)$$

Therefore, formula (2) can be expressed as follows:

$$bLBM(t) = 1 - \frac{(\sum_{i=1}^{m}|Len_i(t)|)^2}{m\sum_{i=1}^{m}|Len_i(t)|^2}. \quad (5)$$

According to Cauchy inequality, $0 \ll bLBM(t) \ll 1$, the better balance load is, $bLBM(t)$ is more closer to 0.

$bLBM(t)$ figures up balancedness of load distribution in bytes, embodies microscopic equilibrium degree. In processing system based on the content of the packets, it can get better performance. If use $p_i(t)$ as the measure of load balancing instead of $Len_i(t)$, we can get load balancing degree based on packet.

$$pLBM(t) = 1 - \frac{(\sum_{i=1}^{m}|p_i(t)|)^2}{m\sum_{i=1}^{m}|p_i(t)|^2}. \quad (6)$$

The difference between two formulas is different granularity that they count. $pLBM(t)$ use the number of packets as statistical standards, while $bLBM(t)$ use the number of bytes. If each packet has same length, then two calculation results are same. In the application based on packets, good macro balanced degree can get good processing performance.

V. EXPERIMENTAL RESULTS

A. Experimental platform

We choose Cavium Octeon 5860 [11] as our test platform. It has 16 MIPS cores, each core's frequency is 750MHz, and each core has 32KB instruction cache and 16KB data cache. 16 cores share a 2MB L2 cache. We implement DPI using regular expression as packet processing application and evaluate scheduler by comparing with Round-robin, simple connection based scheduling.

B. Experimental results

We compare the cache performance in terms of L2 data cache miss by using profile tools. Because cache topology becomes increasingly important in modern multi-core chips, the efficient exploration of the cache hierarchy can significantly improve system performance. In Fig. 5, we compare cache performance between affinity threads and non-affinity threads. As Fig. 5 shows, with the increase of core, cache performance all become worse. While affinity threads do better than common threads, because there is no migration and the scheduler deals with load balancing instead of OS scheduler.

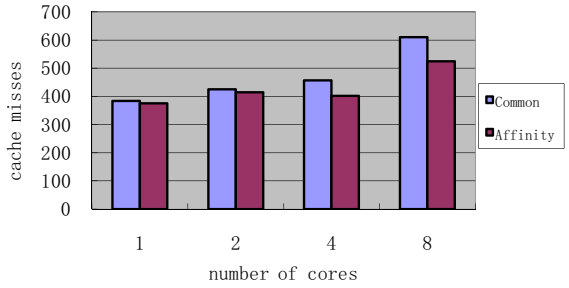

Figure 5. Cache miss.

We calculate bytes load balancing degree of three scheduling mechanisms as we discussed in section III. As it shows in Fig. 6, Round-robin has best load balancing degree because of polling distribution. But it needs other mechanism to keep packet order and cache affinity. About flow based scheduling, our algorithm has better performance in load balancing than common flow based scheduling, because flow re-mapping can adjust load in scheduler.

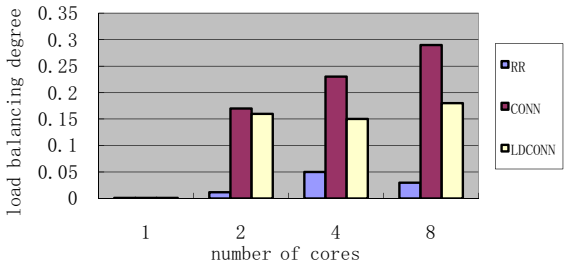

Figure 6. Load balaning degree.

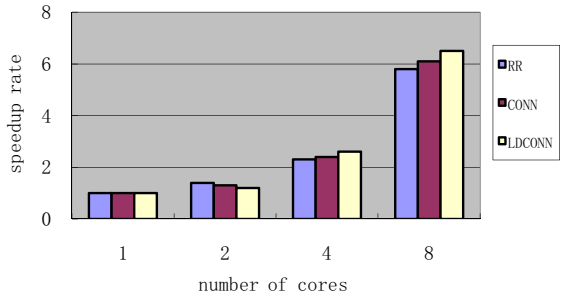

Figure 7. Speedup rate.

According to analysis above, our scheduling algorithm achieves a better compromise between load balancing and cache affinity. As it shows in Fig. 7, in circumstances of

different cores, our scheduling algorithm has better speedup rate than others.

VI. SUMMARY

In this paper, we propose a packet processing runtime system, and explore connection level parallelism and an affinity-based scheduler with the goal of load balancing and minimal cache misses in the system. We introduce our packet scheduling algorithm that belongs to flow based scheduling, and combines the flexibility of packet based scheduling, and apply some definitions to examine the scheduler's performance. Then we carry out some experiments. The results show that it can achieve a better compromise between load balancing and cache affinity.

In the future, we plan to research memory management in the parallel packet processing system. It is another factor affecting performance in multi-core system. Especially, it need to malloc and free memory frequently in packet processing system.

ACKNOWLEDGMENT

This work was supported by The National Natural Science Foundation of China (Key Program) under Grant No.61133004 and National High-Tech Research and Development Program of China (863 Program) under Grant No.2010AA012404.

REFERENCES

[1] Shimonishi H, Murase T. "A network processor architecture for flexible QoS control in very high-speed line interfaces"[C], IEEE Workshop on High Performance Switching and Routing, 2001.

[2] Danhua Guo, Guangdeng Liao. "A Scalable Multithreaded L7-filter Design for Multi-Core Servers", ANCS'08, November 6–7, 2008, California, USA.

[3] Jayanth G, Mendel R. "Stream Programming on General−purpose Processors"[C]. Proc. of the 38th Annual Int Symp on Microarchitecture, 2005.

[4] Weiguang Shi, M. H. MacGregor. "load Balancing for Parallel Forwarding". IEEE/ACM TRANSACTIONS ON NETWORKING, VOL. 13, NO. 4, 2005.

[5] Terry Nelms, Mustaque Ahamad. "Packet Scheduling for Deep Packet Inspection on Multi-Core Architectures", ANCS'10.

[6] G. Dittmann, A. Herkersdof. "Network Proeessor load balancing for high-speed links". In SPECTS 2006.

[7] L. Kencl, J. LeBoudee. "Adaptive load sharing for network Proeessors". IEEE INFOCOM 2002

[8] W. Shi, M. H. MacGregor. An Adaptive Load Balancer for MultiProeessor Routers. SIMULATION, March 2006, vol. 82, No. 3, pp. 173-192.

[9] P. Pappu, T. Wolf. "Seheduling Proeessing Resourees in Programmable Routers". IEEE INFOCOM 2002.

[10] Qiang Wu, Tilman Wolf. "On Runtime Management in Multi-Core Packet Processing", ANCS'08, November 6-7, 2008.

[11] http://www.caviumnetworks.com/.

A Novel Online Measure of Cache Utility Efficiency in Chip Multiprocessor

Huang Zhibin[1,2], Zhu MingFa[1,2], Xiao Limin[1,2], Ruan Li[1,2], Ding Yi[1,2]

[1]State Key Laboratory of Software Development Environment, Beijing 100191, China

[2]School of Computer Science and Engineering, Beihang University, Beijing 100191, China

{Huangzhibin, dingyi}@cse.buaa.edu.cn,{zhumf,xiaolm,ruanli}@buaa.edu.cn

***Abstract*—The cache partition mechanism is introduced to solve the problem of contention and pollution of caches in Chip Multiprocessor. One of the key questions is to analyze online the utility characteristics and efficiency of cache requests originating from different sources. Cache request is differentiated by hardware thread context id. Based on the working set model, within a certain sampling time frame, a number of specific cache lines are preserved by modifying the cache address mapping mechanism and its number is the same as that of the hardware threads of the processor, performing statistics on the frequency of Stack Distance under LRU respectively. Based on the characteristic of the frequency distribution of Stack Distance, We propose a metric, L*D, to measure online the recognition of the cache utility efficiency of the working set and providing information for the decision-making of cache allocation and management. Experiments performed in multiple Benchmarks in Spec Cpu2000 show that the online monitoring mechanism and quantitative metric discussed in this article have achieved fine-grained online monitoring of the efficiency of cache utility based on the working set. Not only do they allow the online recognition of cache space utility characteristic, but they do also enable the identification of any changes in the efficiency of cache utility, achieving an accuracy of over 75%.**

Keywords- CMP; cache; Working Set; Cache Partitioning; Shared last level cache; Online;

I. INTRODUCTION

Due to the influence of the imbalanced increase between off-chip memory bandwidth and the number of cores, the average LLC cache capacity per core decrease so that there is intense demand to improve LLC cache space efficiency [1] and shared LLC is commonly used in commercial multi-core. Cache pollution and contention have become a significant opening question [2,3,4,5,6]. Cache partitioning [2,4,5,9] is proposed to alleviate this problem. One of the key issues in cache partitioning is how to measure the cache utility characteristic and utility efficiency in order to optimize cache allocation between cores. Cache utility characteristic (denoted by MissRate(t)|C) refer to the change of feature in the MissRate of the working set at different times when its cache allocation is constant; cache utility efficiency (denoted by ΔMissRate(ΔC)) refers to the change of feature in the MissRate of the working set when its cache allocation is increased or decreased.

Researches on cache utility characteristic have focused mainly on locality, including spatial locality and temporal locality. MissRate is calculated through the frequency of Stack Distance [11] and hence cache utility characteristic is obtained. Kobayashi et al.[12] proposed the ratio of frequency in MRU to that in LRU as a metric to measure locality and cache utility characteristic.

Miss Rate Curves (MRC) is proposed to express the cache utility characteristic. The x-coordinate of MRC is the size of cache allocated to the working set; the y-coordinate is MissRate per Instruction (or per thousand Instructions). Through identifying the characteristic of MRC, cache utility efficiency is obtained. Mattson [11] has proposed Stack Distance, which is based on the concept of critical capacity, and calculated the MissRate through the frequency of different critical capacity so that MRC is plotted.

Our research find that stack distance and distribution of the frequency, as similar to the idea of Kobayashi et al.[12], could be utilized to quantify Cache Utility Efficiency, avoiding the calculation of MissRate.

When the association of set is relatively large (greater than 8), the behavior of set-associative cache is similar to that of full-associative cache [2,15]. We propose a novel online measure of cache utility efficiency, establishing a dedicated cache line group for every core to simulate full-associative cache managed by LRU, performing a statistic on its frequency of stack distance online to calculate the newly proposed metric of cache utility characteristic, L*D.

Our main contributions in this paper are as following:

(1) Based on the working set model, we propose a novel online measure of cache utility efficiency through specifying a dedicated cache line group for every core to simulate a full-associative cache managed by LRU which traces the utility characteristic and efficiency of the working set running on that core.

(2) We propose a novel metric for cache utility efficiency, L*D, based on the Stack Distance and the distribution of its frequency.

II. MOTIVATION

Different workload has different cache Utility Efficiency so that cache space efficiency is different. In order to enhance the cache space efficiency in LLC, the change in cache utility efficiency is monitored and analyzed and then different strategies are adopted to optimize cache allocation. Qureshi et al.[4] classified the workload into three classes based on MRC: (1) High Utility Workload;(2) Low utility Workload;(3) Saturating Utility Workload. Chang et al.[5] further classified the High Utility Workload into two subtypes: Sensitive Thread and Thrashing Thread. The classification proposed by Qureshi et al.[4] is based upon

978-0-7695-4818-0/12 $26.00 © 2012 IEEE
DOI 10.1109/DCABES.2012.67

U_a^b, that is, when the size of cache allocation has increased from a to b, the change of miss number could be used to determine online the status of the utility efficiency of the applications. However, not only is the change of miss number related to space allocation, but it is also closely dependent on the number of requests from the workload. The trace and analysis of cache access in Qureshi et al[4] is based on Auxiliary Tag Directory(ATD) requiring a significant amount of storage overhead.

Based on experimental observations, it is discovered that, within a specific sampling period:

(1) Utility characteristic exhibits different patterns at different times: as Fig.1, during the 2000th to 2500th sampling period intervals, Twolf has detected a small change in the MissRate, however, during the 2800th to 3000th intervals, the MissRate changes drastically. Gzip has detected drastic changes in the MissRate during the 200th to 300th intervals and the MissRate changes stably during the 300th to 400th intervals. However, Mcf has experienced a relatively stable change in MissRate during most sampling intervals, only detecting more drastic changes during the 250th to 300th intervals.

(2) Utility efficiency varies as the allocated cache space changes. Fig.1 shows that when the number of occupied lines is increased from 2 to 4, utility efficiency is increased by 20% whereas when it is increased from 6 to 8, only an increase within 5% is observed. On the other hand, gzip and mcf have experienced a small boost in utility efficiency when the number of occupied lines is increased from 2 to 4 but when already allocated with 4 lines further adding lines to it, little change to utility efficiency is observed.

(3) When the allocated cache space remains constant,

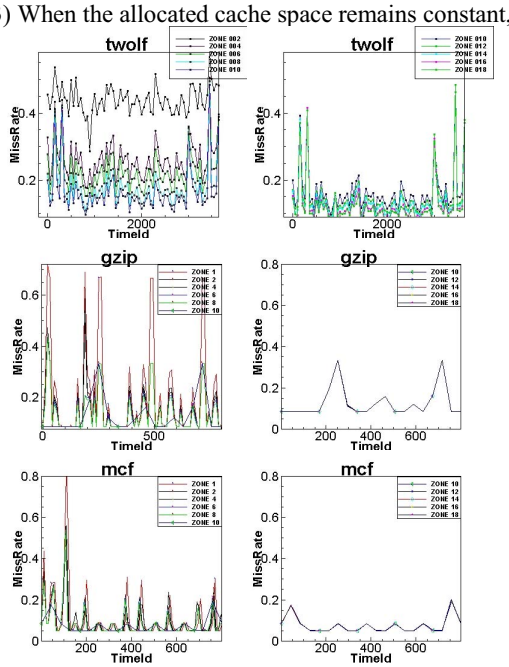

Figure 1: Miss Rate in twolf, gzip and mcf when the size of dedicated cache line group varies from 2 to 18 based on LRU. Time Id is sample id.

utility efficiency varies significantly at different times. Fig.1 shows that Twolf at TimeId 100, 2500 and 3000 experiences low utility efficiency. However, when the allocated lines are increased from 2 to 4, there is 20% increase in utility efficiency. Gzip and mcf have experienced very low utility efficiency at most TimeId, increased sharply only at a few TimeId.

(4) Within a certain time interval, ΔT, the range of access address is limited so that a relatively small number of lines can be used to capture requests to obtain their locality. Fig.1 illustrates that dedicated lines managed by LRU are used to capture individually requests from twolf, gzip and mcf. When the size of lines varies from 2 to18, the change in MissRate varies differently across three benchmarks. For example, twolf is relatively sensitive to cache size. When mcf occupies more than 1 way, the pattern of MRC is similar. Gzip is sensitive to cache size at the beginning but when occupies more than 4 ways MissRate tends to be close to each other. However, when the three benchmarks occupy more than 8 ways, sampling statistic shows that the MissRate is close indicating that within a certain time period, ΔT, only a small number of lines are needed to capture requests, accurately reflecting changes in cache utility characteristic and utility efficiency of the working set.

We can conclude based on the above observations: (1) Utility efficiency differs at different stages of execution of the same workload. Therefore, an online measure of utility efficiency is required to optimize cache allocation. (2) Utility efficiency is closely related to the capacity of allocated space for the workload.(3)A relatively small number (>8) of dedicated lines can be used to obtain utility characteristic and efficiency of the working set. Therefore, we modify the mapping of access address to cache to preserve some lines and to allocate these dedicate lines to every core respectively. These dedicated lines simulate a full-associative cache managed by LRU, so that we can trace all accesses to that core and obtain its utility characteristic and efficiency of the working set running on it.

III. ONLINE MEASURE OF CACHE UTILITY'S EFFICIENCY

A. *A Quantitive Metric for Utility Efficiency*

According to stack property of LRU, every position within the stack is assigned to a counter, supposed C is the size of line group, $Count_{LRU_i}(1 <= i < C)$ stands for the counter in LRU_i, and another counter $Count_{total}$ is established to sum all accesses to that set (LRU0 refers to the top position of the stack, marked as MRU; LRU(c-1) refers to the bottom position of the stack, marked as LRU). In order to quantify utility characteristic and efficiency, the ratios of these counters and their distribution are used instead of their values. In LRU, the most recently used cache line is placed into MRU when hit or firstly loaded into. Further, if next access has not hit MRU, then MRU line moves down toward the bottom of the stack. Therefore, a certain counter

$Count_{LRU_i}(1 <= i < C)$ increases when the line has been reused. As a result, the distribution of these counters reflects the access pattern of the lines. We define the following three metrics:

$$L = \frac{Count_{MRU}}{Count_{total}} \qquad D = \frac{\sum_{i=\frac{C}{2}}^{C-1} Count_{LRU_i}}{Count_{MRU}}$$

$$L*D = \frac{\sum_{i=\frac{C}{2}}^{C-1} Count_{LRU_i}}{Count_{total}}$$

L represents the extent of locality (higher value of L indicates a high locality and vice versa) and D the degree of dispersion (higher D indicates higher dispersion and vice versa).

Nevertheless, the separate use of L or D does not provide an adequate basis of a meaningful utility efficiency evaluation. For example, in Fig.2, at point A, L reaches its minimum, indicating a lowered locality and increasing cache size may enhance target hitting rate. However only a small enhancement in target hitting rate is observed and the added cache space has low utility efficiency. But at point B, L reaches its maximum, indicating increased locality and increased cache space should have lower efficiency. Quite the contrary, in Fig.2, high utility efficiency is observed. Therefore it is obvious that the separate use of L cannot adequately evaluate utility efficiency.

Similarly, point C and D have also reached the extremes, having high dispersion degree and theoretically, increasing cache space should significantly enhance hit rate. However, such a conjecture is not observed in Fig.2, but a low utility efficiency is observed. Point D displays a minimum with low dispersion and increasing cache space should have little impact on enhancing hit rate. However, Fig.2 displays an enhancement in target hit rate at point D which is the highest among adjacent TimeId. Therefore, it is also obvious that the solo presence of D is not adequate to evaluate utility efficiency.

Finally, when L and D are combined to form the metric L*D, it provides an accurate foundation to truly reflect changes in utility efficiency.

When L*D exceeds a certain threshold value, increasing cache space can drastically increase target hitting rate and the cache space utility efficiency is high; when L*D is below the threshold value, the utility efficiency of increasing cache space is low. The selection of the threshold value is crucial and this paper has proposed taking the arithmetic mean of L*D at the current and previous TimeId.

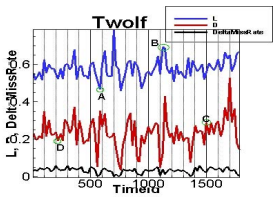

Figure 2: Sampling by Twolf at different TimeId, L, D and DeltaMissRate(the change in Miss Rate).

B. Identify The Source of Cache Access

In CMP or SMT, the hardware thread context ID is used to identify the working set that are currently running on it, namely, working set id. The ID is then inserted into the message structure of the cache request so that every cache request can be identified with the specific working set that it belongs to.

There are two classes of the source of cache access in LLC: (1) requests triggered by lower level cache due to its miss (for example, L1-I or L1-D).(2) requests triggered by consistency engines. For class one, it is easy to inherit the working set ID. For class two, the working set id which triggers consistency request is inserted.

C. Online Measurement of Cache Request

A dedicated line group is allocated for every concurrent working set to measure online all cache access from that working set. The dedicated line group can be preserved by modifying the mapping from the request address to LLC. The size of the dedicated line group is equal to the association of the set. The number of the dedicated line groups equals the maximum number of concurrent working sets which is (the number of cores) * (the number of hardware thread contexts per core). This method possesses excellent scalability due to the fact that only a limited number of sets are required to be added to support more hardware thread contexts.

The dedicated line group simulates a full-associative cache which is managed by LRU and it can then be used to measure the cache request utility characteristic and efficiency of the corresponding working set. When a request arrives to the dedicated line group and hits, the status of LRU is updated; otherwise, select a victim from the dedicated line group and load data from LLC into the dedicated line group. The processing of the dedicated line group occurs after the access is finished in LLC. It is not in the crucial path of access and has no influence on the hit time of LLC.

Supposed the size of the dedicated line group is C and add C counters to sum the frequency of Stack Distance from 0 to C-1 in the dedicated line group and another counter to sum all requests to that, denoted by $Count_{total}$.

By selecting a certain sampling period, ΔT, and performing a statistic on the (C+1) counters, the metric L*D can be calculated at the end of every sampling period. Two additional counters are created: one for L*D of the previous sampling period, denoted by $Count_{PreLD}$; the other for the threshold value, Δ, denoted by $Count_{\Delta}$. When each sampling period is over, L*D could be calculated by the (C+1) counters and $Count_{\Delta}$ is calculated based on $Count_{PreLD}$. Then the current L*D value is used to update $Count_{PreLD}$ and by comparing L*D to $Count_{\Delta}$, a

conclusion could be established. For example,(1) if L*D>= $Count_{\Delta}$ then increasing cache space results in high utility efficiency; (2) if L*D< $Count_{\Delta}$, increasing cache space results in low utility efficiency.

In this paper, ΔT =1000000 sampling periods and $Count_{\Delta}$ of the threshold value, Δ, is initially set to 0. The initial value of $Count_{PreLD}$ is also 0.

When the above procedures are done, all stack distance frequency counters were set back to 0 but the content of the dedicated set is retained. The purposes are: (1) avoiding code miss; (2) inheriting the reuse status and characteristics. When should hardware thread switching or migration occur, all data are configured with the initial settings.

D. An Analysis of the Main Factors

The most influential factor in measuring online cache utility is the time interval, ΔT . Too long of ΔT will result in a large number of request series and the size of line group used for measuring is constant. Therefore, when the miss number is too large, there is a negative interference to accurately determining locality characteristics. The solution is to determine the length of ΔT based on $Count_{total}$. When the total number of requests exceeds a certain value, a new sampling period is initiated.

The second influential factor is the selection of dedicated line group. According to experimental results, the number of lines within the dedicated group needs to exceed 8 in order to achieve an effective result. Moreover, the current LLC set's association greatly exceeds 8. Therefore, the use of one set is sufficient to collect all cache requests from the corresponding core, accurately reflecting cache utility efficiency of the working set.

The third factor is the sampling time interval. The change in spatial locality is most accurately assessed in two adjacent time intervals however the associated overhead is maximized although the sampling process does not interfere with normal cache access. Therefore, it is feasible to sample with a specific sampling period.

IV. SIMULATION

By using full-system simulation based on Virtutech Simics[14]. Here a 16-core CMP is used as the baseline. The default system configuration is given in Table 1.

The experiment has modified the g-cache module of Simics. The main modifications are: (1)The sources of cache requests are differentiated by ini_type of struct generic_transaction_t. (2)The dedicated line groups are achieved by modifying the mapping from the request address to LLC. (3) Required Counters and Registers are added to store the frequency of Stack Distance and values related to L*D. (4) Histogram is added.

The benchmarks are as following in Table 2:

The sampling period ΔT =1000000 intervals. A test result file is generated for every 1000 sampling intervals.

Table 1.System Configuration Parameters

Processor.	16-core, single-issue, in-order
L1 cache	split I/D, each 32KB, 8-way, 64B line, 3-cycle latency, write-back
L2 cache	unified, 12MB, 8-way, 64B line, 11-cycle per bank access latency
Coherence	MESI

Table 2: benchmark

Benchmark	Instructions	Requests
164.gzip	1Billion	35M
181.mcf	1Billion	43M
300.twolf	1Billion	67M

A. Results and Analysis

The experiment has utilized dedicated cache line groups to investigate the MissRate, the change in MissRate, the L*D metric and the threshold value of L*D at different times with various cache space sizes through periodic online collection of cache requests.

Table 3: The Precision of Using L*D and U_a^b

	164.gzip		181.mcf		300.twolf	
	L*D	U_a^b	L*D	U_a^b	L*D	U_a^b
C(2->4)	0.99	0.99	0.99	0.99	0.99	0.99
C(4->6)	0.98	0.99	0.99	0.99	0.76	0.82
C(6->8)	0.99	0.89	0.98	0.94	0.80	0.69
C(8->10)	0.98	0.84	0.98	0.92	0.82	0.79
C(10->12)	0.88	0.87	0.93	0.98	0.80	0.76
C(12->14)	0.92	0.89	0.91	0.91	0.83	0.85
C(14->16)	0.96	0.85	0.97	0.92	0.86	0.30
C(16->18)	0.84	0.99	0.92	0.90	0.80	0.89
C(18->20)	0.82	0.99	0.91	0.89	0.79	0.66
C(20->22)	0.81	0.99	0.99	0.99	0.81	0.65

The result shows that L*D accurately quantifies utility efficiency most of the time. By re-analyzing all valid data collected, a statistic is performed on the relations between the two groups: MissRate increase vs. decrease and L*D vs. the threshold value. A "+" is assigned to MissRate decreases; "-" to MissRate increases; "+" when L*D is greater than the threshold value and "-" when L*D is less than or equal to the threshold value. When the two groups share the same sign, then L*D is considered to be accurately reflecting utility efficiency. Refer to Table 3 U_a^b proposed by Qureshi et al.[4] used to determine utility efficiency is also calculated. It is obvious from Table 3 that when the cache size varies, experimental data have shown that the accuracy of L*D in indicating utility efficiency is over 75% whereas the accuracy of U_a^b is lower than 31% in the worst case.

V. RELATED WORK

Miss Rate Curve is calculated by the Stack Distance as firstly proposed by Mattson [11]. There are two main categories of methods to obtain MRC according to the property of stacks: the offline method and the online method.

The main offline methods are: tracing the request and then analyzing request files offline. For example, some

profile tools (e.g. ATOM [15], Pin [16] and JIFL [17]) deploy this method. Though easy and direct to implement, the overhead associated with online usage is significantly high. In order to reduce overhead, sometimes tracing is achieved by an intermittent method such as DynamoRIO; nevertheless, the overhead is still above 13%.

There are two subtypes of online methods, one based on hardware and the other on software. Hardware Methods include Qureshi et al.[4] that calculate MRC based on stack distances. The tracing of cache requests is achieved by Auxiliary Tag Directory (ATD) in order to reduce storage overhead. Qureshi et al.[4] proposed three methods, UMON-LOCAL , UMON-Global and UMON-DSS. Software Methods include: RapidMRC proposed by David et al.[18] that uses commercial Processor Monitoring Unit (PMU) to extract required information and processes them to obtain MRC online; another method proposed by Zhao et al.[13] uses a memory introspection framework to obtain MRC online but induces high overhead. Another way to obtain MRC is by analytic models [7, 10].

Besides expressing utility characteristic and efficiency by MRC, other researchers have proposed investigating directly utility characteristic by the distribution of Stack Distance frequency based upon LRU. The proposition of this paper is based on a similar concept. Kobayashi et al.[12] proposes a metric to express locality based on the frequency distribution of MRU and LRU. However, the emphasis is placed upon assessing the locality but not the evaluation of utility efficiency.

VI. CONCLUSIONS

In this paper, we purpose a metrics, L*D, measuring the online recognition of the utility efficiency of the working set and providing information for the decision-making of cache allocation and management. Experiments performed in multiple Benchmarks in Spec Cpu2000 show that the online monitoring mechanism and quantitative indices discussed in this article have achieved fine-grained online monitoring of the efficiency of cache utility based on the working set model, achieving an accuracy of over 75%.

ACKNOWLEDGMENT

We thank Zhang Han for her helpful discussions, and the anonymous reviewers for their comments. This work was supported by the fund of the State Key Laboratory of Software Development Environment under Grant No. SKLSDE-2012ZX-07 and NSFC 60973008 and supported by the Hi-tech Research and Development Program of China (863 Program) under Grant No.2011AA01A205 and supported by Beijing Natural Science Foundation (4122042).

REFERENCES

[1] David Wentzlaff, Nathan Beckmann, Jason Miller,and Anant Agarwal.”Core Count vs Cache Size for Manycore Architectures in the Cloud”. MIT-CSAIL-TR-2010-008,February 11, 2010.

[2] G. E. Suh et al. Dynamic partitioning of shared cache memory. Journal of Supercomputing, 28(1), 2004.

[3] Dhruba Chandra, et al. Predicting Inter-Thread CACHE Contention on a Chip MultiProcessor Architecture, HPCA-11 2005.

[4] M. Qureshi and Y. Patt, “Utility-based cache partitioning: A low-overhead, high-performance, runtime mechanism to partition shared caches,” MICRO-2006, pp. 423–432.

[5] J. Chang and G. S. Sohi, “Cooperative cache partitioning for chip multiprocessors,” in International Conference on Supercomputing (ICS), 2007, pp. 242–252.

[6] A. Sandberg, D. Ekl ov, and E. Hagersten. Reducing Cache Pollution Through Detection and Elimination of Non-Temporal Memory Accesses. In Proc. ACM/IEEE Conf. Supercomputing (SC). 2010.

[7] F. Guo and Y. Solihin. An analytical model for cache replacement policy performance. In Int’l Conf. on the Measurement & Modeling of Computer Systems (SIGMETRICS), pages 228–239, 2006.

[8] K. J. Nesbit, M. Moreto, F. J. Cazorla, A. Ramirez, M. Valero, and J. E. Smith. Multicore Resource Management. IEEE Micro, 38(3), June 2008.

[9] J. Lin, Q. Lu, X. Ding, Z. Zhang, X. Zhang, and P. Sadayappan, “Gaining insights into multicore cache partitioning: Bridging the gap between simulation and real systems,” HPCA-2008, pp. 367–378.

[10] X. Shen, J. Shaw, B. Meeker, and C. Ding. Locality approximation using time. POPL-2007, pages 55–61, 2007.

[11] R. L. Mattson, J. Gecsei, D. R. Slutz, and I. L. Traiger. Evaluation techniques for storage hierarchies. IBM Systems Journal, 9(2), 1970.

[12] Kobayashi, H., Kotera, I., Takizawa, H.: Locality analysis to control dynamically way-adaptable caches. SIGARCH Comput. Archit. News 33(3) (2005) 25–32

[13] Q. Zhao, R. Rabbah, S. Amarasinghe, L. Rudolph, and W.-F. Wong. Ubiquitous memory introspection. In Int’l Symp. on Code Generation & Optimization (CGO), pages 299–311, 2007c.

[14] P. S. Magnusson, M. Christensson, J. Eskilson, D. Forsgren, G. Hallberg, J. Hogberg, F. Larsson, A. Moestedt, and B.Werner. Simics: A full system simulation platform. IEEE Computer, 35(2):50–58, Feb. 2002.

[15] E. Berg, E. Hagersten. StatCache: a probabilistic approach to efficient and accurate data locality analysis, in the International Symposium on Performance Analysis of Systems and Software, 2004.

[16] C.-K. Luk, R. Cohn, R. Muth, H. Patil, A. Klauser, G. Lowney, S. Wallace, V. J. Reddi, and K. Hazelwood. Pin: building customized program analysis tools with dynamic instrumentation. PLDI-2005, pages 190–200, 2005.

[17] M. Olszewski, K. Mierle, A. Czajkowski, and A. Demke Brown. JIT instrumentation: a novel approach to dynamically instrument operating systems. EuroSys-2007, pages 3–16, 2007.

[18] R. Azimi, D. Tam, L. Soares, M. Stumm, "Enhancing Operating System Support for Multicore Processors by Using Hardware Performance Monitoring", Special Issue on the Interaction Among the OS, Compilers, and Multicore Processors, Vol. 43, No. 2, Apr 2009, pp. 55-65.

Research on parallel computing algorithm of the second harmonic generation coefficients of nonlinear optical crystals based on MPI

Rong Liu[1], Yongfan Zhang[2,*], Meiqing Wang[1,*]
[1]College of Mathematics and Computer Science, Fuzhou University
[2]College of Chemistry and Chemical Engineering, Fuzhou University
Fuzhou, Fujian, 35000
liu_r@fzu.edu.cn, zhangyf@fzu.edu.cn, mqwang@fzu.edu.cn

Abstract: The second harmonic generation (SHG) coefficients of nonlinear optical crystals play an important role in measuring the nonlinear optical properties of materials, but it is time-consuming to get the SHG coefficients by the theoretical calculation. In this paper, we proposed two sorts of parallel computing schemes for the SHG coefficients based on Message Passing Interface (MPI). If the amount of nodes is small, we will choose the the master slave model and statically allocated tasks; on the other hand, we will select the work pool mode for large amount of nodes, which can prevent the main node to suffer bottlenecks and get a sufficient load balancing. The experimental results show that with the master slave model, the efficiency reaches to 98% when using 4 nodes and declines with the nodes becoming large; while the work pool mode reaches the stable efficiency of 85% in the parallel computing with more than 24 processors.

Key words: Second Harmonic Generation Coefficient; Parallel Computing; Message Passing Interface (MPI)

I. INTRODUCTION

Nonlinear optical (NLO) crystals have been receiving extensive investigations because of their wide applications in laser frequency conversion, telecommunication, and message storage etc. To get insight into the nonlinear optical properties, the understanding of the relationship between electronic structures and second harmonic generation (SHG) effects of compounds from micro perspective based on the theoretical simulation is very important. Generally, an essential requirement for a good NLO crystal is that it must exhibit large SHG coefficient[1]. So if the SHG coefficients of a NLO crystal can be determined by theoretical methods, it is possible to predict the performances of the corresponding material before experimental synthesis, which is a crucial step for designing new NLO crystals.

The analytic expressions for the nonlinear response functions employed in the present work are based on the length-gauge formalism developed by Sipe and Aversa[2,3], and have been rearranged by Rashkeev, Lambrecht and Segall to exhibit the Kleinman symmetries [4], which is suitable for parallelization. With the experimental development of synthesizing NLO crystals, the systems faced by theoretical investigations become more and more complicated, especially when both the types of elements and the number of atoms in the unit cell are grown larger. Accordingly, the calculations of SHG coefficients are time consuming and often need a few days for those complex systems using the method proposed by [4]. Therefore it is very important to maximize computational efficiency.

In this paper, we propose parallel computing schemes for the calculations of SHG coefficients based on Message Passing Interface (MPI). It can be expected that the calculating time for SHG coefficients could be reduced significantly by parallel computing technique.

* Corresponding author. This work was supported by National Natural Science Foundation of China (grant No. 11071270 and No. 90922022).

II. SHG COEFFICIENTS

The SHG coefficients χ^{abc} of NLO crystals compose a three-rank tensor, each of which is the function of frequency ω:

$$\chi^{abc}(-2\omega,\omega,\omega)=\chi_e^{abc}(-2\omega,\omega,\omega)+\chi_i^{abc}(-2\omega,\omega,\omega) \quad (2\text{-}1)$$

where χ_e^{abc} is the contribution of the purely interband transitions, and $\chi_i^{abc}(-2\omega,\omega,\omega)$ reflects the contribution of the mixed interband and intraband processes. Here a, b, and c are Cartesian indices. At zero-frequency limit, χ_e^{abc} and $\chi_i^{abc}(-2\omega,\omega,\omega)$ can be expressed as following:

$$\chi_e^{abc}=\frac{1}{V}\sum_{nml,k}\frac{r_{nm}^a\{r_{ml}^b r_{\ln}^c\}}{\omega_{nm}\omega_{ml}\omega_{\ln}}[\omega_n f_{ml}+\omega_m f_{\ln}+\omega_l f_{nm}] \quad (2\text{-}2)$$

$$\chi_i^{abc}=\frac{i}{4V}\sum_{nm,k}\frac{f_{nm}}{\omega_{mn}^2}[r_{nm}^a(r_{mn;c}^b+r_{mn;b}^c)+r_{nm}^b(r_{mn;c}^a+r_{mn;a}^c)+r_{nm}^c(r_{mn;b}^a+r_{mn;a}^b)] \quad (2\text{-}3)$$

where k is the number of the k-points in the Brillouin zone, determined by the size and shape of the crystal, $\omega_n,\omega_m,\omega_l$ are the energies of bands, m,n,l range from the begin of valence bands to the end of conduction bands respectively. And f_n,f_m,f_l are the Fermi distribution functions corresponding to these bands. $\omega_{nm}=\omega_n-\omega_m$ are the

978-0-7695-4818-0/12 $26.00 © 2012 IEEE
DOI 10.1109/DCABES.2012.7

energy difference between energy bands n and m $f_{nm} = f_n - f_m$ is the difference of the Fermi distribution functions. The definitions of $\omega_{ml}, \omega_{\ln}$ and $f_{ml}, f_{\ln}$ are similar. V is the unit cell volume.

With E being the energy level of the band, r is the position operator, which is derived from transition matrix element p by the following relationship,

$$r_{nm}^{i} = \frac{-ip_{nm}^{i}}{E_n - E_m} \tag{2-4}$$

and $r_{mn;a}^{b}$ is so-called generalized derivative of the coordinate operator in k space, and expressed as,

$$r_{mn;a}^{b} = \frac{r_{nm}^{a}\Delta_{mn}^{b} + r_{nm}^{b}\Delta_{mn}^{a}}{\omega_{nm}} + \frac{i}{\omega_{nm}}\sum_{l}(\omega_{lm}r_{nl}^{a}r_{lm}^{b} - \omega_{nl}r_{nl}^{b}r_{lm}^{a}) \tag{2-5}$$

where $\Delta_{mn}^{a} = (p_{nn}^{a} - p_{mm}^{a})/m$ is the electron velocity difference between bands m and n.

When the frequency of incoming light changes, χ_e^{abc} and χ_i^{abc} can be expressed as：

$$\chi_e^{abc}(-2\omega,\omega,\omega) = \frac{1}{V}\sum_{nml,k}\frac{r_{nm}\{r_{ml}^{a}r_{\ln}^{b}\}}{(\omega_{\ln}-\omega_{ml})}[\frac{2f_{nm}^{c}}{\omega_{mn}-2\omega} + \frac{f_{\ln}}{\omega_{\ln}-\omega} + \frac{f_{ml}}{\omega_{ml}-\omega}] \tag{2-6}$$

$$\chi_i^{abc}(-2\omega,\omega,\omega) = \frac{i}{2V}\sum_{nm,k}f_{nm}[\frac{2}{\omega_{mn}(\omega_{mn}-2\omega)}r_{nm}^{a}(r_{nm;c}^{b}+r_{mn;b}^{c}) + \frac{1}{\omega_{mn}(\omega_{mn}-\omega)}(r_{nm;c}^{a}r_{mn}^{b}+r_{nm;b}^{a}r_{mn}^{c}) - \frac{1}{2\omega_{mn}(\omega_{mn}-\omega)}(r_{nm;a}^{b}r_{mn}^{c}+r_{nm;a}^{c}r_{mn}^{b}) + \frac{1}{\omega_{mn}^{2}}(\frac{1}{\omega_{mn}-\omega} - \frac{4}{\omega_{mn}-2\omega})r_{nm}^{a}(r_{mn}^{b}\Delta_{mn}^{c} + r_{mn}^{c}\Delta_{mn}^{b})] \tag{2-7}$$

III. THE SEQUENTIAL ALGORITHM FOR CALCULATION OF SHG COEFFICIENT

Since under the dynamic frequency and zero-frequency conditions, the calculations of SHG coefficients share the same parallel computing model, we only take zero-frequency condition for example.

1. Initialization: prepare the volume of primitive cell V, band gap value EG0, band range, energy eigenvalue read from EIGENVAL file, the number of k point(nk), amount of energy bands(nband), ω_m.

2. Computing the Fermi values and scissors values, then correcting the calculated band gap values through relevant measured results.

3. Read the transition matrix elements (obtained by the Vienna ab initio simulation package) and adjust via introducing scissors operator to move all the bands to fit band gap values from the experimental result.

4. Calculate SHG coefficients based on (2-2) to (2-7).

IV. PARALLELIZATION

The parameters r, ω, f from formulas (2-2) to (2-7) are related to the amount of k(nk). To parallelize the calculation, let

$$\chi_e^{abc,k} = \sum_{nml}\frac{r_{nm}^{a}\{r_{ml}^{b}r_{\ln}^{c}\}}{\omega_{nm}\omega_{ml}\omega_{\ln}}[\omega_n f_{ml} + \omega_m f_{\ln} + \omega_l f_{nm}] \quad \text{k=1,…,nk} \tag{3-1}$$

$$\chi_i^{abc,k} = \sum_{nm}\frac{f_{nm}}{\omega_{mn}^{2}}[r_{nm}^{a}(r_{mn;c}^{b}+r_{mn;b}^{c}) + r_{nm}^{b}(r_{mn;c}^{a}+r_{mn;a}^{c}) + r_{nm}^{c}(r_{mn;b}^{a}+r_{mn;a}^{b})] \tag{3-2}$$

then the equations (2-2), (2-3) can be simplified as

$$\chi_e^{abc} = \frac{1}{V}\sum_{k}\chi_e^{abc,k} \tag{3-3}$$

$$\chi_i^{abc} = \frac{i}{4V}\sum_{k}\chi_i^{abc,k} \tag{3-4}$$

A. data decomposition

The output values $\chi_e^{abc,k}$ based on formulas (3-1), (3-2) could be calculated independently by the transition matrix function. Consider the data files are so huge that we assume every transition matrix as 3 × nband × nband, then we decompose the calculating part as nk tasks, each of them burden the computing of $\chi_e^{abc,k}$ and $\chi_i^{abc,k}$.

B. parallel computing simulation

In this paper the work pool model and the master slave model are used. Assumed that there are n processors $p_0, p_1, \cdots p_{n-1}$.If the number of processors is small, the master slave model is used; otherwise the work pool model is used.

No.1 strategy: the master slave model

In this strategy a processor is chosen as the master and the other processors as slaves.

The master calculates relevant basic data, broadcasts them to all slaves, and reads transition matrix elements for distributing all of them to processors. None of message exchanges between slaves.

The following steps are processed in the Master processor:

1) Calculate relevant basic data, and broadcast the amount of k-points (nk), the amount of energy band (nband), band range and ω_m, f.
2) Read circularly a k data and its position *i*, where $i = k(\text{mod n})$.
3) If *i*=0, then compute $\chi_e^{abc,k}$, $\chi_i^{abc,k}$, $\chi_e^{abc} = \chi_e^{abc} + \chi_e^{abc,k}$ and $\chi_i^{abc} = \chi_i^{abc} + \chi_i^{abc,k}$.
4) If i≠0, send the data to a processor p_i.
5) Back to step 2) until final.
6) Receive calculating results from processors and sum them up.
7) .End.

The following steps are processed in the slave processors:

1) Calculate relevant basic data, and broadcast the amount of k-points (nk), the amount of energy band (nband), band range and ω_m, f.
2) Receive allocated tasks.

3) Calculate $\chi_e^{abc,k}$, $\chi_i^{abc,k}$, $\chi_e^{abc} = \chi_e^{abc} + \chi_e^{abc,k}$ and $\chi_i^{abc} = \chi_i^{abc} + \chi_i^{abc,k}$.
4) Back to step 2) until final. Each processor gets s task, where s is about to nk/n.
5) Send results χ_e^{abc} and χ_i^{abc} to master processor.

No.2 strategy: the work pool model

In this strategy the work pool model is used which distributes tasks according to the computing ability of the processors. One processor is chosen to run the main process which should calculate relevant basic data and broadcast to all slaves, read transition matrix elements and send them to any free processor. After the task is complete, the slave processor will send a signal to the main processor, and wait for next task, till the end signal sent by the main processor. Similar to the master slave model, none of message exchanges between slaves.

.The processing steps in the main processor:

1) Calculate relevant basic data, and broadcast the amount of k-points (nk), the amount of energy band (nband), band range and ω_m , f .
2) Read circularly a k data.
3) Receive free signal from slave processors.
4) Send data to free slave processors.
5) Back to step 2 till final.
6) Send the end signal to all processors.
7) Receive calculating results from processors and sum them up.
8) End.

The processing steps in the slave processors:

1) Calculate relevant basic data, and broadcast the amount of k-points (nk), the amount of energy band (nband), band range and ω_m , f .
2) Wait the end signal from the main processor.
3) Judge the task will be end or not.
4) Calculate $\chi_e^{abc,k}$, $\chi_i^{abc,k}$, $\chi_e^{abc} = \chi_e^{abc} + \chi_e^{abc,k}$ and $\chi_i^{abc} = \chi_i^{abc} + \chi_i^{abc,k}$
5) Sent free signal.
6) Back to step 2.
7) Send χ_e^{abc} and χ_i^{abc} .

V. PARALLEL ALGORITHM IMPLEMENTATION AND ALGORITHM PERFORMANCE ANALYSIS

MPI（Message Passing Interface）is the leading model used in HPC at present[5]. MPI aims at high performance, scalability and portability. MPI define the standard message communication library, which could use C or FORTRAN to develop transportability message communication programs. MPI standard define a settle of grammar of kernel library routine, which plays important role in writing message communication programs. MPICH is a freely available, complete implementation of the MPI specification, designed to be both portable and efficient. MPICH came into being quickly because it could build on stable code from existing systems[8]. Our work use mvapich2[9] (MPI over InfiniBand, 10GigE/iWARP and RoCE) and Intel Fortran Compiler， under Linux operating system to implement the calculating of SHG coefficients. Mvapich2 is an MPI-2 implementation (conforming to MPI 2.2 standard) which includes all MPI-1 features. It is based on MPICH2 and MVICH.

The experiments were performed on the hardware environment of the hardware under 4 HP ProLiant BL280c CTO blade servers, each of them configured with two 6-core 5600 series processors. 2 HP BL280c G6 E5645 CPU, 12GB PC3-10600R-9 Kit RAM，12MB L3 cache, InfiniBand. The programming tool in the experiments is FORTRAN, the operating and combining system is Linux+mvapich2+ifc.

The SGH system for calculation: $AgGaSe_2$ crystal doped by In atom, the unit cell contains 16 atoms (4Ag、1Ga、3In and 8Se), the volume of unit cell is 453 $Å^3$.

Number of electrons: 104
Number of k-points : 592
Number of energy bands : 400
Range of valence bands : 1 to 52
Range of conduction bands : 53 to 300
The file size of transition matrix is about 4.3GB.

The running time of the sequential program is about 8402s，and the running times of the parallel program by using two strategies with different number of processors are listed in Table 1. In the table, P is the number of processors and S is the parallel speed-up defined as $S = TC / TB$ where TC is the sequential running time and TB the parallel running time. E is the parallel efficient defined as $E = S / P$.

Amount of processors P	No.1 strategy			No.2 strategy		
	Running time	Parallel speed-up rate S	Parallel efficient E	Running time	Parallel speed-up rate S	Parallel efficient E
4	2133	3.94	0.98	2507	3.35	0.84
8	1129	7.44	0.93	1166	7.2	0.9
12	806	10.42	0.87	844	9.95	0.83
24	427	19.67	0.82	411	20.44	0.85
36	288	29.17	0.81	275	30.55	0.85
48	266	31.59	0.66	207	40.59	0.85

TABLE 1 Parallel speed-ups and efficiency for different number of processors by using two strategies

Figure 1, 2 and 3 shows the comparison of two strategies and different number of processors in execution times, speed-up and efficiency.

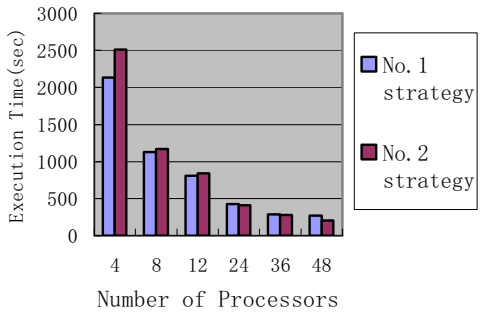

Figure 1. Execution time versus number of processors

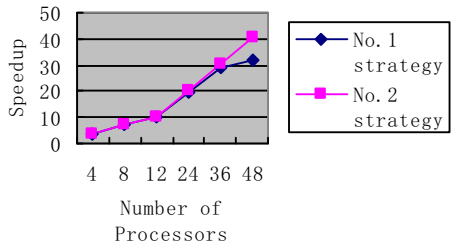

Figure 2. Speedup versus number of processors

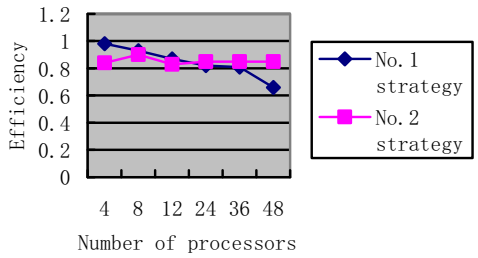

Figure 3.Efficiency versus number of processors

From Figure 1 and Figure 2, it can be found that when $p \leq 24$, No.1 strategy takes less time, and the speed-up ratio is higher. When p=4, the parallel efficiency reach the top, about 0.98, and 1 is ideal value as we know. Two sets of strategies' speed-up ratio almost increase linearly, if the number of processors is further increased, No.2 strategy performs better.

When p=48, the efficiency of No.1 strategy sharply declined. The primary reason is that the main processor takes part in calculating, which amount of computing is far more than relevant amount of data. The main processor becomes bottleneck while the processors have a huge amount, the first strategy is useless at this time. On the other hand, the parallel efficient of second strategy balance in 85% when the processors became 24. For the main processor is free for calculating, tasks are distributed by dynamic allocation, no message exchange among them. At this time, the expanse of work pool visiting only a little fraction but offer a big computing amount, that is why the more amount of process, the linear increasing of speed-up ratio with stable efficient .

VI. CONCLUSION

The calculation of SHG coefficients is one of an important factor in studying nonlinear optional crystallizing properties. Our paper implemented the computing SHG coefficients under gathering servers, aimed at the amount of task in every processor, and provided two parallel strategies to solve. When the amount of processors is small, we adopted master slave model and allocated tasks statically; otherwise we chose the work pool model, which dynamically allocate to slave processors, avoid the main one becomes bottleneck. The result shows that the parallel algorithms get good efficiency. No.1 strategy has a higher speed-up ratio and No.2 strategy has stable parallel efficiency. The parallelization of the SHG coefficients calculating sharply reduces the computing time, which also provide some technique supports in the field of designing nonlinear optional materials.

REFERENCE

[1] Zhang K C, Wang X M. Science of nonlinear optical crystal material(Second Edition). Beijing, Science Press, 2005.

[2] Sipe J E,Ghahramani Ed. Nonlinear optical response of semiconductors in the independent-particle approximation. Phys. Rev. B, 1993, 48, 11705.

[3] Aversa C, Sipe J E. Nonlinear optical susceptibilities of semiconductors: Results with a length-gauge analysis. Phys. Rev. B, 1995, 52, 14636-14645.

[4] Rashkeev S N, Lambrecht W R L,Segall B. Efficient ab initio method for the calculation of frequency-dependent second-order optical response in semiconductors. Phys. Rev. B, 1998, 57, 3905-3919.

[5] Mehnaz Hafeez,Sajjad Asgahr, Usman A. Malik, Adeel-ur-Rehman, and Naveed Riaz, Survey of MPI Implementations, International Conference on Digital Information and Communication Technology and its Applications (DICTAP 2011), Dijon - France

[6] Ananth Grama, George Karypis, Vipin Kumar, Anshul Gupta. Introduction to Parallel Computing(Second Edition). Addison Wesley, 2003

[7] DU Zhihui. High performance programming-design of MPI parallel code[M]. Beijing,Tsinghua University Press, 2001.

[8] William Gropp, Ewing Lusk, Nathan Doss, Anthony Skjellum. A high-performance,portable implementation of the MPI message passing interface standard.Parallel Computing 22 (1996) 789-828

[9] MVAPICH2, http://mvapich.cse.ohio-state.edu/overview/mvapich2/

A FAULT TOLERANCE SCHEDULING ALGORITHM FOR PARALLEL TERRAIN ANALYSIS

Xiaodong Song[1], Wanfeng Dou[2], Guoan Tang[1], Kun Yang[2], Kejian Qian[1]
[1]Key Laboratory of Virtual Geographic Environment of Ministry of Education, Nanjing Normal University, Nanjing, China
[2]School of Computer Science and Technology, Nanjing Normal University, Nanjing, China
Email: xiaodongfly@yahoo.com.cn, douwanfeng@njnu.edu.cn

***Abstract*—In recent years, due to the increasing calculation demands for the massive spatial data analysis, the parallel computing based on high-performance computers has become an inevitable trend of Digital Terrain Analysis (DTA in short). A key problem is to design fault-tolerant software to enhance the stability and robustness of scientific application. This paper presents an approach of failure recovery solution in distributed parallel computing environment. This approach to schedule the failing task is built by dividing all the failing data into several partitions according the calculating scale of failure. By means of the Fault-Tolerant Granularity Model, the scheduling algorithm can assign the failing task dynamically. Finally, two experiments focusing data size and failure size are discussed.**

Keywords- DEM; Digital Terrain Analysis; Parallel Computing; Fault Tolerance

I. INTRODUCTION

The rapid development of digital photogrammetry and remote sensing technologies has made it possible to obtain a large amount of digital elevation models (DEMs) data, generated by various methods [1]. With increased precision and accuracy, DEMs have gone from 1,000 meter resolutions 5-10 years ago to 1-5 meter resolutions today in many areas. As a result of the increased precision and file sizes, many land surface parameters, such as slope, profile curvature and hydrologic land-surface parameters for lower resolutions and smaller DEMs become prohibitively time consuming when being applied to high-resolution and large-scale data.

Recently, cluster computing has become an attractive computing schema for solving a lot of computation-intensive and data-intensive applications because clusters can provide the aggregate computing and memory capacities effectively and economically. However, many of the high performance Geo-computations take much time to finish their computation on distributed processors. At the same time, the reliability of the system becomes a foremost key while the stability of cluster with tens of thousands of processors is threatened constantly by a larger number of hardware and software failures, such as network, memory, processors and operating systems. High reliability of scientific computation urges manufacturer to increase the Mean Time Between Failure (MTBF) of massive systems with over 100 thousand processors, BlueGene/L produced by IBM [2], for example, to tens of minutes even higher. The validity of these scientific and commercial applications will be influenced and too unreliable to be useful by any failure which may take places anytime. Therefore, the fault-tolerance has become a necessary component of the reliable computations.

Many researchers have paid close attention to the check-pointing technique of message passing applications, and there are many projects proposing checkpoint/restart facilities for a parallel application based on MPI, such as LAM/MPI [3, 4], MPICH-V/V2/V3 [5], and Open MPI [6]. MPI application developers need not to handle the failures themselves with these projects. Hence, the system-level check-pointing technique in parallel and distributed computing environment has been applied extensively. Most of these implementations of check-pointing are based on globally coordinated check-points which are stored into a shared storage, because it can keep the synchronization among processors easily. The main demerit of these methods is that the overhead of writing data into stable storage is time-consuming. Furthermore, the characteristic of parallel digital terrain analysis is computation-intensive and data-intensive. When processing large DEMs, the transfer of data between hard disk and memory, rather than the CPU time, becomes the performance bottleneck. However, achieving reliable operation has become increasingly difficult with the growing number of processors and data scale under cluster computing environment. It is important for the fault tolerant solution to be diskless, so as to obtain higher reliability and availability.

In order to improve these system-level fault tolerant mechanisms, many researchers have been studied diskless checkpointing techniques. Diskless checkpointing approach was proposed to avoid the excessive overhead associated with stable storage operation [7]. The various diskless checkpointing techniques can be broadly classified into three categories: neighbor-based, parity-based, and Reed-Solomon code-based [8]. Plank et al. explored the performance gains of storing checkpoints in the memories of remote processors [9]. To solve our fault tolerance problems on huge distributed systems, Engelmann adopted diskless checkpointing of FFTs to super-scale architectures [2]. In the design of Fault-tolerant FFT, a peer-to-peer diskless checkpointing algorithm was used which replicates process state at the memory of neighbor processes based on the consideration of local stable storage and the limited bandwidth to remote stable storage. However, the overall reliability of the system may decrease with the number of processors increasing. Many researches have proposed improved solution to reduce the overhead of diskless checkpointing [10, 11]. Dealing with high performance Geo-

978-0-7695-4818-0/12 $26.00 © 2012 IEEE
DOI 10.1109/DCABES.2012.47

computation of huge spatial data, these methods have two main problems, which could be improved: narrow limitation in some specific cases and common architecture for multiple processor failures.

In this paper, we provide a low-cost fault tolerance scheme on this problem, especially tailored to the needs of scientific computation with large dataset. The solution is based on the checkpoint data of dynamic fault-tolerant granularity model. In this approach, log checkpoint is incorporated into a system to prevent failures and local calculation results are not saved on checkpoint data. A global data management mechanism is established and responsible for the parallel computing task on each processor.

II. PRELIMINARY

A. Assumptions

There are two kinds of fault-tolerant technology, hardware redundancy and software fault tolerance. It is widely agreed that the overhead of hardware redundancy is the dominant cost, while large numbers of computing resources are wasted and the software error cannot be properly settled in real-time multi-tasking system.

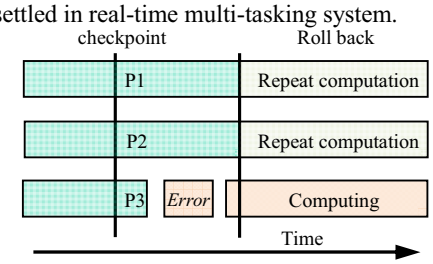

Figure 1. A case study of Transient Faults' recovery in system-level software fault-tolerance

Software fault-tolerance could be primarily divided into two aspects, one as the system-level fault tolerance and the other one as application-level fault tolerance. All the execution content of computation, including space address of threads, information of the register and the communication states, will be periodically stored in a reliable storage in the system-level fault tolerance scheme, as shown in Fig.1. Furthermore, all the processes will roll back to the latest checkpoint if any process fails with enormously resources waste. Application-level fault tolerance technology allows users to specify the setting of checkpoint and save less information. This method is not versatile because users should always have a deep understanding of program execution. Therefore, reducing the cost to improve fault tolerance could be considered on the basic requirement of new fault-tolerant technology, in order to ensure the computational performance as much as possible to improve system reliability and to reduce the complexity of the system architecture to meet the needs of the practical application.

It also should be pointed out that the availability of spatial data of Geo-Computation depends on the availability of necessary I/O operations even if check-pointing data do not store computing results repeatedly. The probability of I/O failures should be taken into account when evaluating the availability of parallel tasks. In general, computing on processors is much more reliable than software. However, the software reliability and hardware availability are nearly of the same magnitude for the reason of I/O operations' failure. The algorithm presented in this paper considers hardware failures and is focused on task scheduling of the reduplicative computing granularity after error detection. Some common causes for hardware failures are also considered by the achievement of a redundant architecture [3]. At the same time, several hypotheses are considered as follows, reliable network and stably CPU computing.

B. Computational Model and Definitions

To formalize the idea, assume we have a dataset including n data blocks $D=\{d_1, d_2, \ldots, d_n\}$, where d_i is the partition data on each compute node i for $1 \le i \le n$. There is also a collection of log checkpoint $L=\{l_1,l_2,\ldots,l_n\}$, where l_i is the log file of each processor i for $1 \le i \le n$.

Definition 1. Minimum fault tolerant granularity:

$$FG_m = k \times 4kB, \tag{1}$$

FGm is the primary scheduling unit of fault tolerant computing. We select the *kB* as the computing units for the quantification of spatial data, where k is the quantization coefficient.

Definition 2. Composite fault tolerant granularity:

$$FG = 4^h \times FG_m, \tag{2}$$

Where h is a positive integer in the range [0, H], H is the depth of the quad tree of DEM. On the basis of the Minimum fault tolerant granularity, the Composite fault tolerant granularity is defined as a compound processing unit for less I/O operation, so as to increase the efficiency of computer processing.

Definition 3. Precedence Relationship:

$$D_i \rightarrow D_{i+1}, \tag{3}$$

if data block D_i is finished before D_{i+1}. In our fault tolerant algorithm, the anterior data block is deemed as correct computing results. These precedence relations will be saved in a global log file, meanwhile some dependent relations may exist between adjacent data.

Definition 4. Recovery state:

$$S = (s_1, s_2, \ldots, s_n), \tag{4}$$

Where s_i is the state records on each compute node i for $1 \le i \le n$.

Two states of the s_i can be used, first execution and non-first execution which is the fault tolerant computing. At the same time, if any precedent task is finished, these tasks would not be calculated again.

Definition 5. In-processing block, d_p, if d_i is being calculated for $d_p \subset D=\{d_1, d_2, \ldots, d_n\}$.

Definition 6. Fault-Tolerant Granularity Model: {*FG*, *S*, *Nerr*}, where *Nerr* is the number of failed nodes. After several definitions, we can obtain a Fault-Tolerant Granularity Model (FTGM in short) which schedules any failed task by the evaluation of *FG*, *S* and *Nerr*.

$$FG = \frac{Nerr \times D}{n - Nerr}, \tag{5}$$

Where *D* is the data volume of a computing node.

III. The Fault-Tolerant Granularity Model based Scheduling Algorithm–FTGM-SA

The algorithm stores all the Executes states and data directories of each thread based on diskless checkpointing. If the program is executed on *n* processors, then there are two managerial processors called the Master processor with responsibility for the backup of log files [12]. Architecture of algorithm is shown in Fig. 2, master2 is a redundancy of master1. All the precedence relations and file directories of the processed data block, and the recovery states of each processor are periodically stored in these two computing nodes. If any processor fails, then its state will be modified to the non-first execution and the unfinished data will be divided into *n*-1 partitions and distributed to the remaining processors.

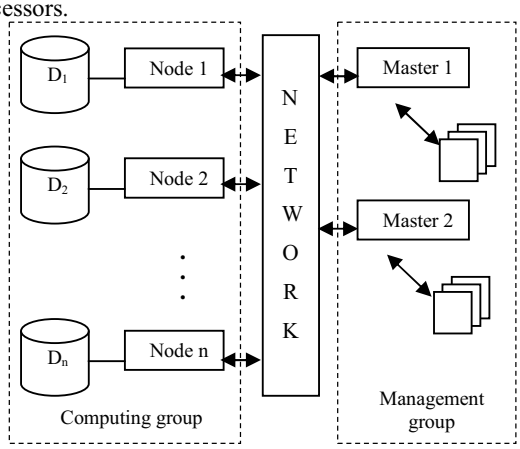

Figure 2. Basic diagram of algorithm

The master1 is responsible for the failure detection and failure recovery of all the computing nodes. Similar to other fault-tolerant algorithm, the checkpoint data will be saved regularly on another processor under the passive copy mode. The main purpose is to avoid the failure of master1 and thus give rise to the case of request missing. The following steps illustrate how the algorithm can be executed so that traditional fault tolerant strategy eliminates (or at least reduces) plenty of rollback and data redistribution costs.

The master node is responsible for the data distribution of slave processors. Each slave processor will receive a file directory of Net File System (NFS) after the data distribution from master node. This computing task is based on the *FG* and all the computing data is essentially equal. Consequently, a load balancing is achieved and the difference of computing time of each processor will not be too wide. As often introduced in the literatures, fault detection is the first step of fault tolerance and hence we should design fault detection algorithms. After the initialization, master node will periodically send an inquiring to each thread and will receive an acknowledgement accordingly. So, this confirmation message can be used as a condition to judge whether the processor fails or not. The fault recovery has six steps, as illustrated in Fig.3:

Step1: Master node records numbers and file directory of failure nodes;

Step2: All the Recovery state of the global table $S=(s_1,s_2, \ldots, s_n)$ *will be modified;*

Step3: Update all the precedence relation of each data block;

Step4: Reading spatial data from NFS, normal slave nodes receive a new computing task and the data volume is calculated by Eq. (5);

Step5: All the updated information will be recorded in the log file on the Master1 node and backed up on the Master2.

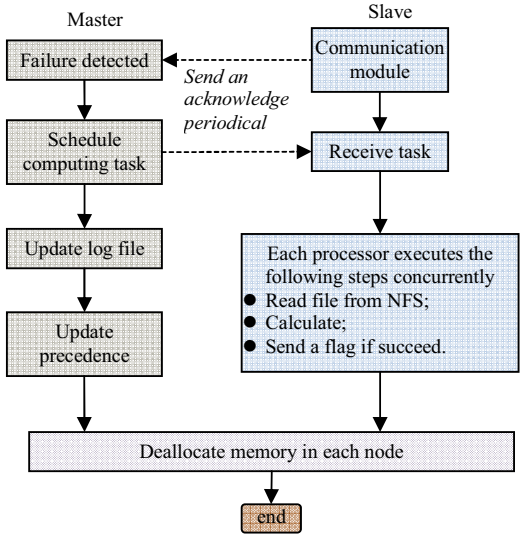

Figure 3. Flowchart for fault recovery

IV. Experimental Results

The parallel algorithm proposed in this paper has been implemented in C++ using MPI library and tested on a small cluster. A cluster computing environment was created for distributed data organization and parallelized data analysis. Our cluster is constituted by 18 homogeneous computers with the same configuration (CPU, memory, hard disk and operating system) and is connected through an Ethernet network with Gigabit speed (1000 Mbit/s). Two of the 18 PCs were selected as master servers to take charge of sending calculation tasks, receiving and merging results, generating output files and scheduling the progress of them. Three sizes of the data on Loess Plateau in Shaanxi province

are chosen as study area: small (0.5GB), medium (2GB) and large (6.5GB) with 5m resolution.

In order to assess the robustness of our algorithm, we have designed the following test. We set up a failure recovery module based on surface roughness algorithm [13]. For the contrast of other algorithms, we established the rollback-recovery algorithm (RRA in short) [14] and the interval of checkpoints is set to 10s. The two experiments are described in this section, which have different requirements with respect to different data and different failures have to be recovered by each process.

A. Performance of the two algorithms of different failures

Fig.4 gives an overhead of failure recovery of the two algorithms with a 2GB DEM data of different failures. This figure also shows the difference of recovery cost between RRA and FTGM-SA algorithms. In the PB-scheme, each failure will be calculated at corresponding computing node so that the recovery times are the same due to the same amount of computation and the homogeneous processors. It takes cluster about the same amount of time to deal with different-size failure, whereas only part computing nodes are used and most nodes of cluster are idle causing a massive waste.

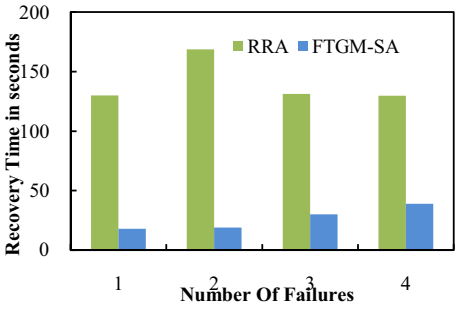

Figure 4. Overhead of failures recovery of 2G DEM of different algorithms

As the graph shows, the recovery time of FTGM-SA basically shows upward trend with the increase number of failures and yet is less than RRA. Now, in case a failure occurs, before starting the computing procedure, the master processes have to partition the computing task and equally spread the recovery load to each processor by means of targeted file directory in the NFS database. All the nodes in the cluster will be worked because each node executes same computation received from master nodes. Consequently, the more failures occur in the cluster, the longer computing time of this algorithm will be cost.

B. Overhead Comparisons of Different Data

In this section, we tested the overhead in percentage terms of three different data size. This percentage is calculated by the

$$Per = \frac{Rec}{Com}, \tag{6}$$

where *Rec* is the recovery time, *Com* is the computing time of this task. The overhead of RRA of different dataset is various and show a trend of decreasing in Fig. 5. This is because the parallel DTA is mainly used upon the spatial data which is huge with large scale and high resolution. Hence, the increased I/O operation cost the rollback procedure much time. The proportion of I/O will be declined for the increase computation of large dataset so that the trend of overhead percentage of RRA is declining. In contrast, the overhead of FTGM-SA keeps a low percentage for the sake of load-balanced recovery solution. The overhead of I/O is divided equally to each node. As presented in Fig.5, we achieve an overhead as low as 6.5%, when checkpoint the medium data size.

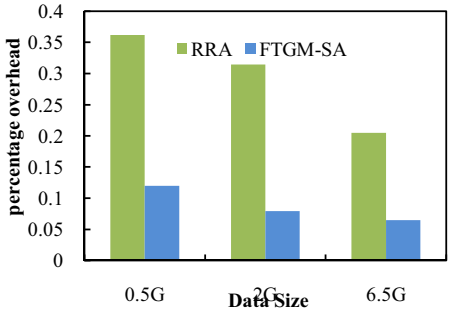

Figure 5. Failure overheads in percentage

V. COMPARISON OF RELATED WORK

This paper describes a versatile architecture to support fault tolerance of system-level and the primary contributions of this work are two-fold. Compared with other fault tolerant solutions of parallel computing in literature [15, 16], the contributions of this approach as follows:

- *Load balancing*

Compared with the fault-tolerant systems proposed in [15], this work proves that the fault tolerance of parallel computing is based on a load balancing mechanism in a computational cluster without adding any additional hardware. In this approach, the suggested algorithm allows analysis to evaluate the expected performance and reliability of complex fault-tolerant hardware-software system consisting of nonidentical hardware components. It considers both reliability of software versions and availability of hardware units without the failure recovery based on load balance. In our paper, an optimal schedule of fail tasks is taken into account, which will be executed absolutely on some other processors in traditional scheme. Spatial data of fail tasks can be divided into small parts which will be recalculated by all normal processors.

- *Fault-Tolerant Granularity Model*

Secondly, it develops an analytical model, based on precedence relation and recovery state, to secure the data dependent relations of the proposed scheduling algorithm, which can also be easily used to protecting the data relation in any other non-centralized system. The data dependent relations are always ignored, because the data access from one node to another node has to experience the queuing delay and network latency in cluster environment. To

maintain the quantized calculation of failure recovery on each slave node, the scheduling algorithm dynamically sends the calculation task to each slave node based on the Composite fault tolerant granularity. Simultaneously, all the operational information will be recorded in the log file on both master node and redundant node.

VI. CONCLUSION AND FUTURE WORK

In this paper, a new Diskless checkpointing algorithm has been proposed to support High performance Geo-Computation based on log file which stores all the file directory and execution states. We have demonstrated its effectiveness on an important and real application of great technological significance.

Future work will be focused on the mechanism of failure recovery of parallel task including a Task dependencies based on Fault-Tolerant Granularity Model, failure detection control and failure recovery mechanism while multiple failure arose simultaneously. We also hope to investigate the tradeoff when considering fault-tolerant parallel file system.

ACKNOWLEDGEMENT

This work has been supported by the National Natural Science Foundation of China (No. 41171298, No. 41071244), National High Technology Research and Development Program of China (863 Program, No. 2011AA120303) and the Foundation of Graduate Innovation Training Plan of Jiangsu Province (NO. CXZZ12_0393).

REFERENCES

[1] U. Wegmüller, M. Santoro, C. Werner, T. Strozzi, A. Wiesmann, and W. Lengert, "DEM generation using ERS-ENVISAT interferometry," Journal of Applied Geophysics. 2009, 69(1), pp. 51-58.

[2] C. Engelmann and A. Geist, "A Diskless Checkpointing Algorithm for Super-Scale Architectures Applied to the Fast Fourier Transform,"

Proceedings of the 1st International Workshop on Challenges of Large Applications in Distributed Environments, 21 June 2003, pp. 47-52.

[3] S. Sankaran, J. M. Squyres, B. Barrett, A. Lumsdaine, J. Duell, P. Hargrove, and E. Roman, "The LAM/MPI Checkpoint/Restart Framework: System-Initiated Checkpointing," International Journal of High Performance Computing Applications, 19(4), pp. 479-493, 2005.

[4] G. Burns, R. Daoud, and J.Vaigl, "LAM:An open cluster environment for MPI," In Proceedings of Supercomputing Symposium, In Proceedings of Supercomputing Symposium (1994), 1994, pp. 379-386.

[5] A. Bouteiller, P. Lemarinier, G. Krawezik, and F. Cappello, "Coordinated checkpoint versus message log for fault tolerant MPI," in: Proceedings of Cluster 2003, Hong Kong, December 2003, pp. 242-250.

[6] A. Bouteiller, G. Bosilca, and J. Dongarra, "Redesigning the message logging model for high performance," in: ISC 2008, International Supercomputing Conference, Dresden,Germany, 2010, 22(16), pp. 2196-2211.

[7] J. S. Plank and K. Li, "Faster Checkpointing with N+1 Parity," Proc. IEEE Symp. Fault-Tolernnt Computing (FTCS '94), June 1994, pp. 288-297.

[8] G. M. Chiu and J. F. Chiu, "A New Diskless Checkpointing Approach for Multiple Processor Failures," IEEE Transactions on Dependable and Secure Computing, pp. 481-493,2011.

[9] J. S. Plank, Y. Kim, and J. Dongarra, "Algorithm-based diskless checkpointing for fault tolerant matrix operations," in:25th International Symposium on Fault-Tolerant Computing, Pasadena, CA, June 1995, pp. 351-360.

[10] D. Hakkarinen and Z. Chen, "Multi-Level Diskless Checkpointing," IEEE Transactions on Computers, 2012, in press.

[11] L. A. B. Gomez, M. Naoya, C. Franck, and M. Satoshi, "Distributed Diskless Checkpoint for Large Scale Systems," 10th IEEE/ACM International Conference on Cluster, Cloud and Grid Computing (CCGrid), May 2010, pp. 63-72.

[12] E. N. Elnozahy, L. Alvisi, Y. Wang, and D. Johnson, "A survey of rollback-recovery protocols in message-passing systems," ACM Computing Surveys, 34(3), pp. 375-408, 2002.

[13] T. Hengl and H. I. Reuter, "Geomorphometry-Concepts, Software Applications. Developments in Soil Science amsterdam," Elsevier, 2009.

[14] R.Koo and S. Toueg, "Checkpointing and Rollback-Recovery for Distributed Systems," Seventh Symposium on Reliable Distributed Systems, Oct. 1988, pp. 13-21.

[15] G. Levitin, M. Xie, and T. Zhang, "Reliability of fault-tolerant systems with parallel task processing," European Journal of Operational Research, 177(1), pp. 420-430, 2007.

[16] A. Benoit, M. Hakem, and Y. Robert, "Contention awareness and fault-tolerant scheduling for precedence constrained tasks in heterogeneous systems," Parallel Computing, 35(2), pp. 83-108, 2009.

Research on Hydrological Information Organization Based on Virtualization

Ping Ai, Peng Feng
Hohai University
Nanjing, China
E-mail: aip@hhu.edu.cn
E-mail:hydroinformatics@qq.com

Ping Mu
Guangdong Research Institute of Water Resources and Hydropower
Guangzhou, China
E-mail: mpdream2012@163.com

Abstract—**How to organize and utilize the self-governing, multi-sourced and heterogeneous hydrological information is an urgent problem in Chinese water resources informatization. To solve this problem, the paper proposes the architecture of hydrological information organization. The architecture introduces the mechanism of dynamic configuration based on description and virtualization to satisfy the dynamic requirements of water information applications. Based on the architecture, an example integrating heterogeneous data is given. Virtualization and dynamic configuration can also be applied to organize other forms of resources. Therefore, hydrologic information organization can offer inspiration and reference for the further study of cloud computing to be applied in Chinese water resources informatization.**

Keywords-hydrological information; virtualization; organization architecture; cloude computing; water resources informatization

I. INTRODUCTION[1]

With the development of information technology, we have witnessed the explosion of hydrological information in China at last few decades. Institutions at different levels and sectors have developed many information systems related to water resources to meet their own requirements. However, due to the variety of acquisition methods and heterogeneity of management, hydrological information can hardly be exploited comprehensively. Lacking of an overall organizational consideration, the distributed hydrological information cannot be uniformly used, as in [1]. Thus it is imperative to organize the hydrological information, which is the foundation of various decision-supporting systems and services.

Under such conditions, the hydrological information organization architecture manages to satisfy the dynamic and uncertain requirements. The data sources, which are heterogeneous, distributed and multi-sourced, remain to be self-governed. A dynamic configuration mechanism is also introduced to support the dynamitic register of data sources, on which requirements are usually uncertain. At last, the architecture is practical and simple to reduce the complexity of the decision-supporting services.

1 corresponding author: Ping Mu, E-mail: mpdream2012@163.com

II. CONCEPT OF INFORMATION ORGANIZATION

A. The Process of Information Organization

Information organization is generally regarded as a process that converts information from disordered state into ordered and user-friendly state. Water information is the numerical description of the water related activities, and hydrological information, which may be structured, unstructured or semi-structured, is the numerical description of hydrological cycle. The purpose of hydrological information organization is to describe hydrological cycle in an integrated and user-friendly way.

Information organization is a process that transforms the disordered original information into ordered refined and integrated information. In this process, there are two types of operation, as is in Figure 1.

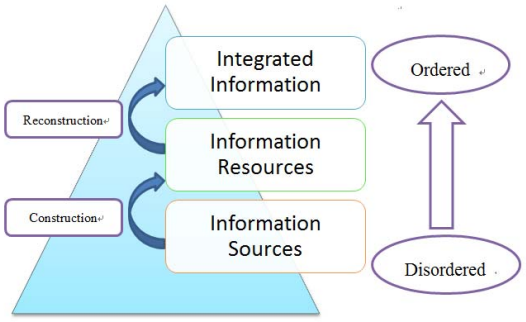

Fig.1 Process of Information Organization

In the construction operation, original information sources are processed into information resources, which are easy to be described, analyzed and restored. Various sources are transformed and organized into structured, unstructured or semi-structured forms, i.e. resources, such as files, databases. Besides, descriptions of the information called meta-information are also to be made. In the reconstruction operation, information resources are reorganized in a more focused, integrated and systematic way. Requirements at such level are usually theme-oriented and made by decision-

978-0-7695-4818-0/12 $26.00 © 2012 IEEE
DOI 10.1109/DCABES.2012.75

supporting systems. Information resources generated in construction could no longer satisfy these requirements. Therefore, according to the dynamically changed requirements, resources should be reorganized by meta-information. Construction and reconstruction can be operated circularly in order to generate resources at different integration level.

In the process of information organization, two issues are significant, how to organize the distributed sources and how to organize the heterogeneous sources.

B. The Mechanism of Dynamic Configration

To deal with the distributed sources and dynamic requirements, information organization should include a dynamic configuration mechanism.

Software development based on components is the trend. Not only the software packages, but also the information or data can be treated as resources in the development of information systems. To register resources dynamically, configuration mechanism based on description is a practical method. Meta-information provides the description of resources. Information organization employs these descriptions to choose which sources are supposed to be registered into systems, and which sources are temporarily not useful and need to be removed. Mechanism of dynamic configuration is shown in Figure 2.

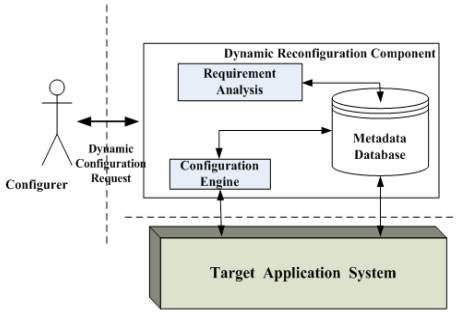

Fig.2 Mechanism of Dynamic Configuration

In dynamic configuration, reflection mechanism is the key technology, which is the foundation of evolution. Reflection enables the information sources to register and execute according to the desired goals.

The concept of reflection refers to ability that the software could recognize, examine and modify its own state or behavior at runtime. Reflection usually use virtual machine supported by programing languages like Java. Reflection allows inspection of classes, interfaces, fields and methods at runtime without knowing the names of the interfaces, fields, methods at compile time. It also allows instantiation of new objects and invocation of methods

The reflection system is divided into base level and meta-level, as shown in Figure 3. The base level generally describes specific problems, while the meta-level is the abstract of base level and the internal system. There can be more than one meta-level in a reflection system. The set of base level and meta-level is called reflection tower. The mutual relation between two levels is conducted by two actions called reification and reflection. The reification refers to process that describe the behavior and internal state of base level, and generate the meta-information. The reflection refers to the process that observes and adjusts the internal system and the structural behavior of the relevant part in base level by the meta-information.

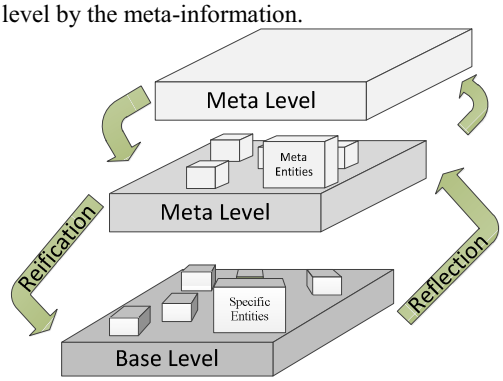

Figure 3 Reflection Tower in Reflection Mechanism

C. Virtulization

Acknowledging the fact that various data have their own mode of organization, management and operation in corresponding information system, hydrologic information organization should provide an unified, overall, integrated and comprehensive view of information resources. The concept of "virtualization" is necessary to be adopted to accomplish these tasks.

"Virtualization technology" has started since the 1960's. The word "virtualization" comes from optics for the first time and is used to describe an object in mirror, as in [2]. Virtualization in information technology can be expressed as "the logic expression of information resources, regardless of physical constraints". The organization of virtual information resources is their logic expression, supporting users to exploit them as if they are single-sourced and real. In the paper, virtualization technology is introduced to organize the self-governing, heterogeneous and multi-sourced information into a unified virtual demonstration.

As mentioned above, hydrological information in China is self-governing, heterogeneous and multi-sourced, and is under the management of institutions at different levels and sectors. To unify all the information into a certain standard cannot be achieved in a short period. Hydrologic information organization based on virtualization is a practical method to satisfy the need of decision-supporting application for the time being.

III. HYDROLOGICAL INFORMATION ORGANIZATION

A. The Architecture of Hydrological Information Organization

According to the thought of dynamic configuration and virtualization discussed above, the architecture of virtual

hydrological information organization is therefore designed as is shown in Figure 4.

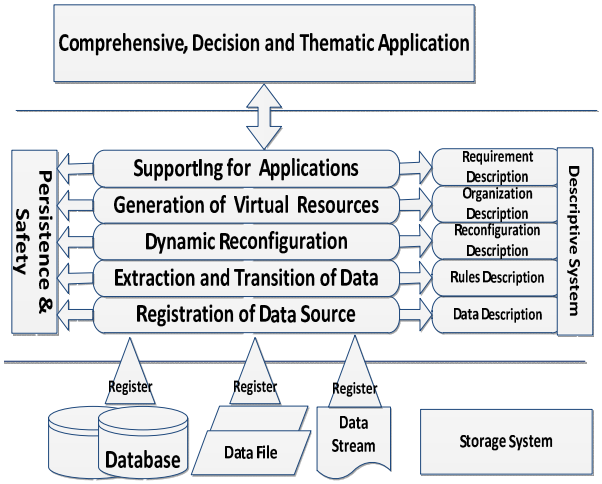

Fig.4 Architecture of Hydrological Information Organization

The architecture consists of three subsystems and five layers. The subsystems are storage system, description system, persistence and safety control system. And the layers are registration, extraction and transformation, dynamic configuration, virtual resources generation, development supporting.

Storage system consists of various types of self-governing hydrological information resources. These independent data resources remain their existing structure or running pattern. It provides description of data to the registering mechanism. According to the description of data, users accomplish the storage of data resources data online.

Description system consists of data description, rule description, configuration description, organization description and requirement description. Each description fulfills the corresponding level of processing in the virtual information organization. Data description is used in data source register and provides basic information for operating heterogeneous data by the self-explanation of sources. Rule description corresponds to data extraction and conversion process. Data extraction and transformation process constructs and applies appropriate rules according to users' requirement, in order to shield heterogeneous data for users. Configuration description corresponds to dynamic configuration, by which data from different sources are configured. Description of organization corresponds to the generation of virtual information resource, which is collection of isomorphic specific information resources. Description of requirement is in fact the service and application interface constructed for the users. The layers above, from the bottom to the top, gradually accomplish the process of virtual hydrological information organization.

The system of persistence and safety control of resources provides supporting environment for virtual organization. It mainly solves the permissions for the access to various resources and maintains the persistence of virtual resources, ensuring the relatively stability and usability of virtual resources.

The three subsystems and five layers ensure the original pattern of information resources, and convert web resources into comprehensive hydrological information logic set. According to the architecture, we can design the corresponding supporting system, which can promote the share of hydrological information resources. Especially, it can satisfy the comprehensive analysis of various hydrological information, and generation virtual database after extraction and configuration. Furthermore, it can help the data mining and knowledge discovery applications in the virtual resources set.

B. An Example of Hydrological Information Organization

Figure 5 is the Framework of Unified Organization Platform for Hydrological Information. The platform is based on the architecture of virtual hydrological information organization, with the application of reflection. Figure 6 is an example of conversion of multi-sourced information in the unified organizing platform system of hydrology information.

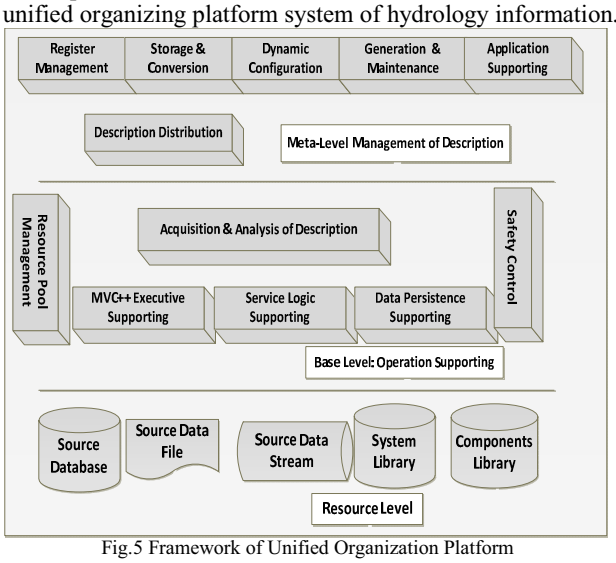

Fig.5 Framework of Unified Organization Platform

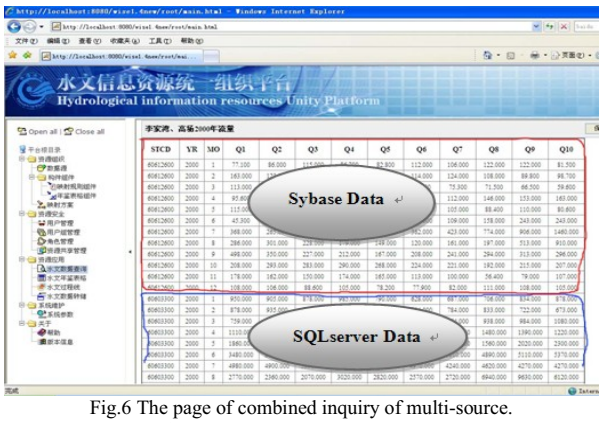

Fig.6 The page of combined inquiry of multi-source. Data in different database management systems are combined into single one.

C. *Application in Water Information Cloud Computing*

Hydrologic information organization can offer inspiration and reference for the further study of cloud computing to be applied in Chinese water resources informatization. As mentioned above, dynamic configuration mechanism can register desired resources according to the dynamic requirements. Virtualization can shield the heterogeneous resources and provide a uniformed presentation or service interface for users. In fact, dynamic configuration and virtualization are two important topics in cloud computing.

In terms of water information processing, Chinese public sectors and hydrologists have witness the change from hydrologic archives to hydrologic data. With the emphasis on the water resource conservation, comprehensive and decision-supporting applications and services are on great demand. The existing resources, mainly databases, are distributed, multi-sourced, heterogeneous and under different administration. Minister of Water Resources of China is initiating the construction of National Water Information Data Center, in hoping to lay a solid foundation of further water resources informatization.

With the popularization of concept such as cloud computing, internet of things and service-oriented architecture, SOA, it can be anticipated that water information systems will adopt the form of web services, sharing cloud platform, data center, and resources pools. The next stage of water resources informatization will probably be the time of mega projects that support the decision makers to get an overall and comprehensive understanding of the situation of water resources. These projects organize, configure, and utilize distributed and heterogeneous resources dynamically, in other words, at runtime. Water information like water level of remote dams or rainfall in areas thousands miles away must be immediately acquired, transmitted and processed. To accomplish tasks given above, technologies in further water resources informatization are shown in Figure 7.

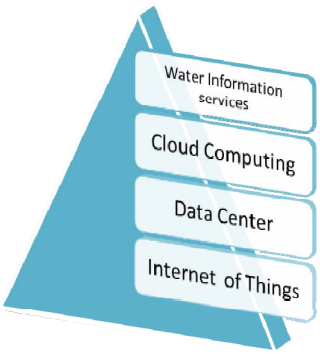

Fig.7 Technologies in further water resources informatization

Hydrological information organization mainly deals with the databases. Database is one of the resource forms. Program package (component), model, description and even infrastructure can be treated as resources, too. Dynamic configuration mechanism and virtualization, which can function well in coping with data, can also be applied in other forms of resources.

Based on the architecture of hydrologic information organization, architecture of water cloud computing in China can be put forward as shown in Figure 8.

The architecture consists of three parts, resource pool, water cloud platform and water application and services. Resource pools collect and organize various resources. Proper description should be taken into account. Description files are the medium that enables the cloud system function well. The construction of resource pools is in fact the construction operation in hydrologic information organization. Water cloud platform is the core part. Resource organization mechanism chooses desired resources to register into the platform, under the control of dynamic configuration. The process can be regarded as the reconstruction operation. Safety control and web services are of strategic importance in cloud computing, however, they are beyond the discussion of this paper.

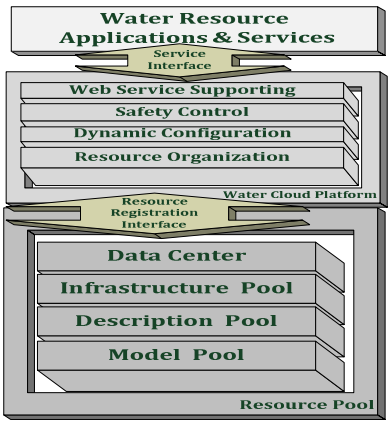

Fig.8 Architecture of Water Cloud Computing

Water cloud computing is still an academic discussion in China. Hydrologic information organization provides a trial practice to the discussion. The dynamic configuration based on description and virtualization mechanism is key technologies in the construction of cloud computing. As described above, architecture of water cloud computing takes the mode of software as a service, SaaS. Web service, as mentioned above, is still issues to be promoted and examined in Chinese water resources domain. It calls for the cooperation of hydrologists and IT industry.

IV. CONCLUSION

To support the comprehensively utilization of water resources, the paper put forward architecture of hydrological information organization. It applies the mechanism of dynamic configuration and the technology of virtualization to fulfill the operation of construction and reconstruction in the organization process. With respect to the current administrative regime and management mode of water information, the architecture organizes the distributed and

heterogeneous hydrologic information and manages to provide a unified virtual presentation of the databases. An example based on the architecture, Unified Organization Platform, performs well in integrating the self-governing and heterogeneous databases.

In hydrologic information organization, mechanism of dynamic configuration and virtualization play significant roles. Recognizing that program packages (component), model, description and even infrastructure can be treated as resources, dynamic configuration based on description could as well be applied to organize these forms of resources. Therefore, framework of water cloud computing is then clear, even though cloud computing is still under academic research in China. Water cloud platform dynamically register desired resources from resource pools with the help of description (metadata). Water applications and services call the services through interface.

Hydrologic information organization proposed by this paper is practical and convenient in supporting the comprehensive and theme-oriented applications. Dynamic configuration based on description and virtualization can provide a useful reference for cloud computing applied in Chinese water resource domain.

ACKNOWLEDGMENT

This research was supported by the Major Research Plan Training Project of the National Natural Science Foundation of China under Grant No. 90924027； the Key Project of the National Natural Science Foundation of China under Grant No. 41030636.

REFERENCES

[1] AI Ping, CHEN Yali, CHENG Haiyun, SHI Fangbin. Implementation of Software Platform of Unified Organization for Hydrological Information Resources[J]. Water Resources Informatization, 2010(12), 05:1-4. (In Chinese)

[2] SUN Yu-zhong. The revival of virtualization [J].Communications of CCF,2008,4(4):1-3. (In Chinese)

[3] Jianfeng Li. The Organization and Applied Research of Multi-source Hydrological Information[D].Nan jing:Hohai Univisity,2010,06.

[4] Ping Ai, Ping Mu, Ya-Li Chen. A Definition of the Water Information[A]. Proceedings - 2011 10th International Symposium on Distributed Computing and Applications to Business, Engineering and Science, DCABES 2011[C], p 364-367, 2011.

[5] Ping Mu. The Research on the Characteristic and Organization Pattern of Information Based on Hydrological Cycle Process[D].Nan jing:Hohai Univisity,2010,06. (In Chinese)

[6] CHEN Ya-li , MA Qin , CHEN Chun-hua. Research on Virtualization Organization of Self-governing and Heterogeneous Multi-source Hydrological Information Resources [J]. JOURNAL OF CHINA HYDROLOGY, 2010（5）:12-15. (In Chinese).

[7] Ping Ai. Introduction to Water Information Engineering [M].Wuhan: Changjiang Press, 2010

[8] CHEN Yali AI Ping YAO Chengxia, Dynamic Reconfiguration Mechanism and Its Application in Water Information System, Water Resources Informatization, 2010（3） : 13-27, 40. (In Chinese)

[9] Wand, M., Friedman D.P. The mystery of the tower revealed: a non-reflective description of the reflection tower[A]. In P.Maes editors, Meta-Level architectures and reflection[C], pp.111-134. North-Holland, 1988.

[10] P. H. Gum. System/370 Extended Architecture: Facilities for Virtual Machines [J].IBM Journal of Research and Development,Nov. 1983,27(6): 530-544.

[11] Thais Batista, Ackbar Joolia, Geoff Coulson. Managing Dynamic reconfiguration of Component based Systems[J]. Lecture Notes in computer Science, 2005,3527:1-17

Study of Location and Navigation Services in Complex Indoor Scenes Based on the Android Mobile Computing Platform

Yucheng Guo
Wuhan University of Technology
Wuhan, China
e-mail: ycheng.g@gmail.com

Lei Cao
Wuhan University of Technology
Wuhan, China
e-mail:349185395@qq.com

***Abstract*—The emerging mobile platform has provided convenient facilities for indoor navigation software development. The paper has focuses on design and realization of a navigation system based on the Android mobile computing platform for complex indoor scenes, which takes the two-dimensional code for positioning and generates a route with color block sequence by A*algorithm, realizing non-GPS indoor positioning and navigation. The system has innovated upon the method of indoor navigation.**

Keywords- Android; indoor positioning and navigation; non GPS navigation; two-dimensional code.

I. MOTIVATION

In a modern society, there are more and more large-scale buildings as well as more and more complicated types of indoor environment, such as shopping malls, large multistory car parks, train stations, subway stations, airports, etc. It is an important and significant problem that how to determine a position in a complex indoor environment and reach the destinations quickly and safely. The outdoor GPS navigation has become mainstream and matured in recent years. However, because of the building wall materials, building structures and other factors, GPS signals can't penetrate thick walls. Therefore, the existing navigation system can't achieve precise positioning and navigation in that the satellite signals can't be correctly received inside large buildings, underground construction, skyscrapers and some other complex indoor environments [1].

In order to solve the technology block point of mobile phone indoor navigation, this paper has proposed a navigation system based on Android mobile computing platform for indoor environment. The system can guide user in a right route to realize indoor positioning and non-GPS navigation by the two-dimensional code. The navigation route is generated by A* algorithm [2], and the directions in crossroads are labeled with different color block. These solutions and applications are able to successfully solve the problem that the current existing navigation technology can't achieve effective navigation with inaccurate positioning. In a word, the system has great practical value.

II. TWO-DIMENSION CODE OF MOBILE PHONE

The two-dimensional code [3, 4] records the symbol information by some black and white graphics, which follow certain rules in planar (two-dimensional direction) map with some particular geometric shapes. The "0", "1" bit stream formed internal logic basis is used for the code compilation. And it uses a plurality of geometric shape corresponding to the binary code to represent text-numerical information, it can be read automatically and processed via the image input device or a photoelectric scanning device [5]. At present, the common usages of two-dimensional code are as follows:

- It can be used for image bitmap array to store lots of data because of the large capacity.
- Using the encryption and printed form it can be used for saving confidential documents or can be used as anti-fake mark.
- The two-dimension code can be stored in the form of electronic images, so it can be made for electronic certificates, such as electronic coupons, electronic movie tickets, electronic boarding passes, electronic voucher, electronic sign and so on.
- With the characteristics of convenient recording and fast recognition, it can be used for identification, mainly including business cards or conference registration.

Two-dimension code can be also used for product traceability, logistics tracking and so on. In general, according to its advantage of localization function, the two-dimensional code is widely used in electronic commerce and logistics transportation and other fields. In some sense, the key factor in electronic commerce is regarded as commodity positioning, and logistics transportation as goods location. The advantages of Two-dimension Code can be used in the area of location service; that is to say, the indoor positioning and navigation are realized through locating landmark facility in the building. In following sections the architecture, fundamental principles and implementation of the Two-dimension-code based indoor positioning and navigation system have been described in details.

III. THE ARCHITECTURE OF NON-GPS INDOOR POSITIONING AND NAVIGATION SYSTEM

For solving above problems, considering that the indoor area has been basically covered by the network signal of Wi-Fi/2G/3G, a local network scheme for indoor position navigation is proposed in this section. In this scheme the two-dimensional code is adopted and the famous A* algorithm plays a very important role.

978-0-7695-4818-0/12 $26.00 © 2012 IEEE
DOI 10.1109/DCABES.2012.111

The two-dimensional code is very mature, which contains plenty of information, and it has been widely used in electronic commerce, logistics and other industries. However it is not used in the complex indoor scene positioning and navigation yet. With the help of a local network signal, the two-dimensional code's positioning can be more precise than base station positioning and satellite positioning.

The A* is an algorithm that is widely used in path finding and graph traversal, plotting an efficiently traversable path between points (or nodes). Noted for its performance and accuracy, it enjoys widespread use.

For displaying the navigation path vividly a multi-color scheme is adopted in the system. The different path directions in an intersection are distinguished by multiple color blocks, then the system can guide the user to find destination according to the generated color sequence blocks. This method avoids inaccurate indoor positioning in existing technology. Using of the color or the pattern to guide the direction, which is consistent with human's habits, has an intuitive and vivid effect. It simplifies the navigation method and does not lose operability. This method is a useful innovation in the navigation mode.

Generally speaking the proposed system has five basic characteristics:

1) All the locations in a Complex Indoor Scene have their own unique two-dimension code on the scene map;

2) The two-dimension code of predetermined landmark locations is posted on the wall acompaning with predetermined color block;

3) All the outlets of an intersection are marked with distinguished color blocks;

4) The A* algorithm is used for pathpositionning between current location and destination.

5) The local severs and networks are used to implement the indoor non-GPS navigation.

The system main modules and frameworks have been illustrated in figure 1.

The system is composed of three main parts: server, mobile platform and database. The system's basic framework is shown in Figure 1, the orange part expresses the server, the green part expresses the mobile platform, and the purple part expresses the database.

IV. NAVIGATION PATH DISPLAIED WITH COLOR BLOCK SEQUENCE

At present, the accuracy of indoor localization with GPS or other methods is low, so this system uses the two-dimensional code for accurate indoor positioning to avoid GPS weak signal and noise interference. The key points of the proposed navigation method are:

1) Determine the current position and the target position firstly;

2) Then calculate the navigation path and display it with a sequence of the color blocks. According to its guidance, the user goes forward, and reaches the destination.

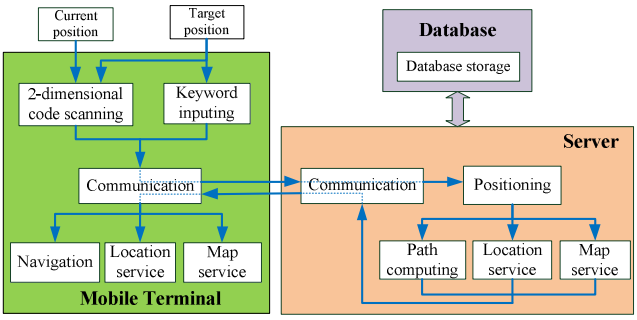

Figure 1. The basis diagram of the system

An example of the color allocation at the intersection landmark is shown in Figure2. In order to let color weakness or colorblind use the system normally, the block colors in landmarks don't appear in red and green, or using different shapes of color blocks represents different turnning directions. After a navigation operation, the path symbol on the indoor map is generated as shown in Figure3. In this figure the red line represents the user's path from current position to target position. The path pattern consists of relevant landmark color blocks on the path, which is generated by the navigation system, as shown in Figure 4. From the view we can know that the user depends on this sequence of the color block to navigate, and one intersection correspond to one color that is chosen to be right direction.

In order to facilitate the user to navigate intuitively and efficiently, the sequence diagram with colors in Figure 4 can be improved. The path, which is formed by the landmark blocks with different colors and distinguished shapes, is displayed in the navigation window of the mobile terminal. The color blocks of mobile phone navigation window and landmark color blocks deployed in the indoor environment should be one-to-one correspondence. Utilizing intelligent features in Android mobile phone, the navigation path in this system can be shown with a cartoon style. That is to say, an current landmark or intersection chosen color is highlighted in the middle of displayed color block sequence (DCBS), while going to the next intersection, sliding the DCBS, the next intersection's color block is moved to and highlighted in the middle of the DCBS. In other words, the color sub-block in the middle of the DCBS can be continuously replaced with the intersections passed by the user. The highlighted biggest color block represents the correct direction of the current intersection. After passing an intersection, the displayed path pattern is updated by sliding the navigation DCBS. The user will choose the forward direction in next intersection according to the prominent color in the DCBS.

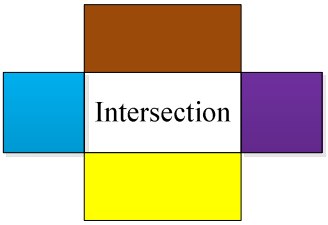

Figure 2. The color blocks of the landmark

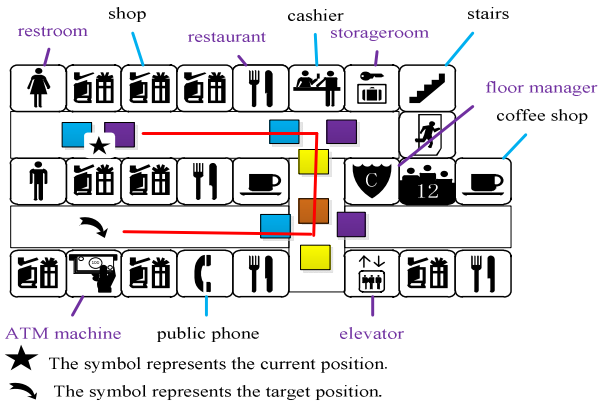

Figure 3. The application of the color blocks in the lines

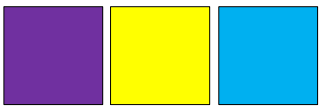

Figure 4. The path with the color blocks

V. PRE-ARRANGEMENT OF THE INDOOR ENVIRONMENT

A preliminary work for implementing the indoor navigation system for a complex scene involves following jobs:

1) Design corresponding two-dimensional code;

2) Determine appropriate landmarks;

3) Decorate intersections and chosen landmarks with corresponding colors;

4) Paste the two-dimensional code label on the wall of chosen landmarks accompanied with relevant color block.

The design of appropriate two-dimensional code can be done through the early-collected image information. The two-dimensional code labels need to be posted in the conspicuous place of the landmark stores, while the merchant's landmark two-dimensional code is also existed in the merchant's brochure. The marks of the color blocks are only highlighted in the intersection, and the kinds of the color and the number of the outlets are one-to-one matching. The successful design and decoration of the scene makes the navigation system working correctly, locating accurately and navigating quickly.

VI. CONCLUSION

This paper has proposed a brand new non-GPS navigation system framework for indoor complex scenes. The creative ideas are: it adopts the two-dimension code and A* path positioning algorithm techniques, and smartly uses the color-block-sequence to display the navigation path for the indoor non-GPS navigation system design. The system has being implemented on the Android mobile computing platform, but it also can be implemented on other OS of mobile terminals. This navigation system can be widely applied to the complex scenes of large-scale indoor environments, and provide users with good location services.

REFERENCES

[1] Anon. High precision indoor navigation mobile phone. Digital Communication Word,2010,pp.82-82.

[2] Patrick Lester .A* Pathfinding for Beginners. http://www.gamedev.net/page/resources/_/technical/artificial-intelligence/a-pathfinding-for-beginners-r2003. Artificial Intelligence, Oct 09,2003

[3] Kang Fu. The development of mobile phone on location service[J]. China Internet,2009(9),pp.46-47. (in Chinese)

[4] Zhou Zhe. On the Application of Two-dimensional Bar Code in Book Borrowing and Lending Management System [J]. Journal of Changzhou Institute of Technology, 2010,23(2/3),pp.53-59. (in Chinese)

[5] Zhou Di.On the application of two-dimensional code[J]. Journal of Shandong Institute of Light Industry (Natural Science Edition),May2011,pp.62-64.

ControlLogix–based Large Bulk Grain Silos Control System Design

Xing Guo[1], Haiying Wang[2], Guoxian Wang[1]
[1]School of Logistics Engineering
Wuhan University of Technology
Wuhan, Hubei Province, China
[2]Bulk Division Company
Qinhuangdao Port Group Co., Ltd.
Qinhuangdao Hebei Province, China
Email: guoxing1967@sohu.com

***Abstract* - A large number of devices are involved in bulk grain silos system and the control flows are particularly complicated. To cope with the complexity, a structured system program design approach is proposed in this study while the ControlLogix system is adopted as the operating platform. Meantime, an intelligent flow path selection method by means of a flow table is used to select the control flow. The readability of the programming codes is greatly improved and the complication of sequence control for large-scale equipment is simplified. A range of functions are realized by help of the configuration software iFIX, including flow select, start, stop and suspend, as well as display of the running status of the devices and real-time alarming, etc.**

Keywords - bulk grain silos; control system; ControlLogix; process flow

I. INTRODUCTION

The bulk grain silos system is an important loading and unloading technology in modern ports. In recent years, the bulk grain silos system has been greatly improved with the development of China economy. A large number of devices are involved, and the dependent relations among these devices are complicated, which further make it particularly complicated to control the loading and unloading operations. If traditional programming approach is used, the inherent complex logic relationships are confusing, and the programs developed are difficult to understand while the developers themselves are also liable to make mistakes. The structural programming approach used in this study primarily aims at characterizing the software implementation with well modularity and hierarchy organization so that the readability of the programs developed is enhanced greatly. Flow path selection, which is the key part of such a control system, is another concern of the current study. It is known that only when the control flow path is properly selected out, can the corresponding devices run well according to the process requirements. Traditional rule-guided flow selection method is only suitable for the system, which only includes a few process flows, which further only includes a few control devices [1, 2, 3]. For systems with complex flows involved, the flow table-based intelligent selection method presented in this paper has unique advantages over the traditional ways.

The devices used in the control flows are indexed and documented in a table which makes it easy to identify the corresponding flows that each device belongs to, and thus it is easy to design the complete control programs in a coherent and consistent way. The sequential control of this type of large-scale process systems is thus significantly simplified. In the current implementation, the flow monitoring software for the master server is programmed with IFIX configuration software tool. IFIX provides a design environment suitable for integration and collaboration among plant-level or company-level systems. It is of good openness, safety and scalability, which does not only meet the control and management requirements to run a complex system, but also makes it possible to greatly improve the universality and reliability of the system [4].

II. THE NETWORK STRUCTURE OF THE CONTROL SYSTEM

The bulk grain silos control system presented in this paper uses the ControlLogix system made by Rockwell Automation Company as the operating platform. The 1756-L55 series processor with plentiful powerful functions is used to control all I/O operations of the system. The controllogix platform allows multiple networks and I/Os being unified together and the networking ways of the current system include EtherNet, ControlNet DH+ and universal remote I/O communication [5, 6].

The network architecture of the control system is shown in Figure 1. The upper monitoring and management part of the system includes one server computer, four CGP (Computer-vision Graphics Processor) computers and one report sheet management computer, which constitute a small-scale local area network. They exchange data with the ControlLogix system through a switch. The ControlLogix system is composed of the persistent processor frame and the expanded remote I/O frame. The report sheet management computer works as the production management layer of the system, and four CGP computers work as production monitoring layer of the system. The PLC (Programmable Logic Controller) I/O modules are connected with the field electrical control cabinets through relay isolations and directly control the field devices.

978-0-7695-4818-0/12 $26.00 © 2012 IEEE
DOI 10.1109/DCABES.2012.82

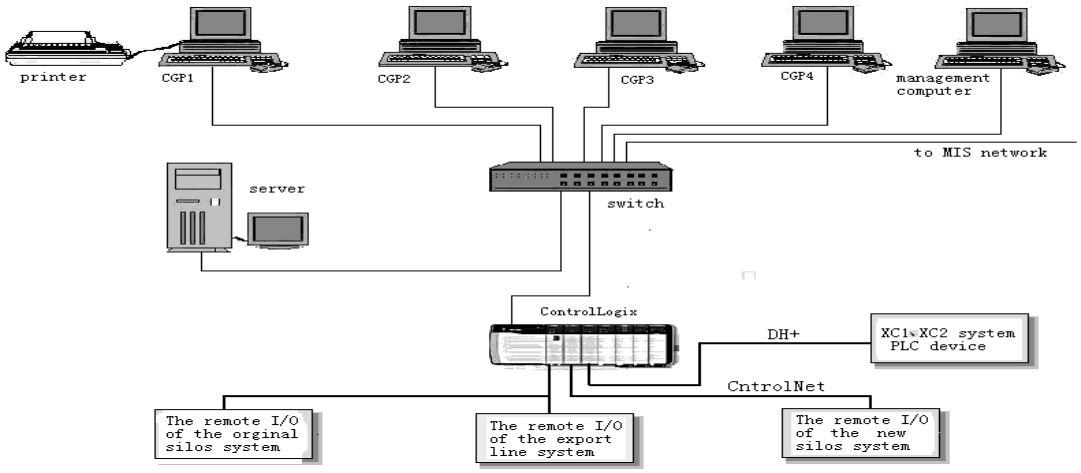

Figure 1. The Network Structure of the Control System

III. STRUCTURED PROGRAM DESIGN APPROACH

For the systems with complex process flows, the traditional empirical programming approach is error-prone and tends to make the programs designed difficult to understand. On the other hand, the structured programming approach primarily aims at characterizing the software implementation with well modularity and hierarchy organization. It emphasizes on an overall analysis of the process features and the functionality of the system before the program design is elaborated. All the program design tasks are carried out in a top-down way and the details are materialized progressively thus the readability of the program is enhanced greatly. Within the bulk grain silos system, all the controlled operations are treated as a node of a process flow, or the grain transportation path. According to the process handling requirements, the flow control function is composed of several sub-functions, i.e., flow select, start, run, stop and suspend due to unexpected faults. The start, run and stop actions for each device should be allotted to a specific process flow and are restricted by the interlock relations with its upstream and downstream parallels: the devices should sequentially start along the direction opposite to the grain flow direction and sequentially stop along the grain flow direction. For a running flow, if one device has to be stopped because of a fault, all the upstream devices included in the same flow must be stopped simultaneously, while all the downstream devices can continue run in order to avoid the grain congestion, which may result in grain leakage or equipment damage. Once the faults are identified and removed, one can press the “restore" button, and the devices involved in the flow are sequentially restarted along the direction opposite to the material flow direction. According to these process features, the three-layer control architecture is adopted, i.e., device control layer, automatic interlock control layer and flow control layer respectively, as shown in Figure 2.

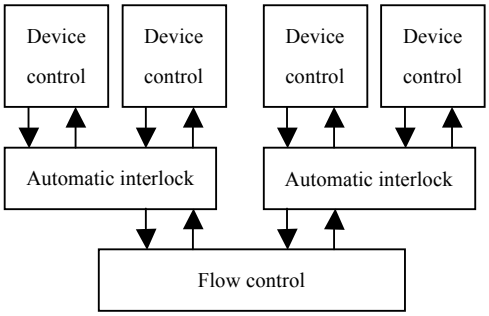

Figure 2. The Three-layer control architecture

IV. CONTROL FLOW SELECTION

Flow path selection is the key part of the flow control. Only when the flow is selected out, can the corresponding devices properly run according to the process requirements. As many as 486 process flow paths are contained in the current bulk grain silo system. An intelligent flow selection method by the help of a flow table is used in the system design. It proves to be especially suitable for the system in which there are a large number of devices and process flows while the dependent relationships among the devices are complicated.

About 80 large-scale devices, such as belt conveyors, en masse conveyors and bucket elevators, are sequentially arranged in the order following the grain flow direction and all the 486 process flows are compiled into the flow table as shown in Table 1. The flow table is stored in Controllogix processor in the way of a two-dimension array. The corresponding position of the table is set as "1" if the device belongs to a certain flow, and "0" if does not.

With the flow-table-based intelligent selection method, an appropriate flow path is selected from the flow table according to the predefined starting and the ending device included within the required flow path. After the Controllogix processor received the flow selection order, the starting and the ending device as well as the key device

involved in the candidate flow are indicated and saved as an index. The flows contained in the flow table are then sequentially scanned while comparisons are simultaneously made by the help of the index. The flow that has been scanned can be determined as an candidate flow according to the comparison results only when: (1) it contains the starting device, the ending device and the key device, (2) the starting device works upstream relative to the ending device, and (3) the status corresponding to the indexed device is "0". Once a flow that satisfies the above requirements is found, it is tentatively reserved while the scanning process continues till to the last flow path within the flow table. If another flow that also satisfies the requirements is found, the program is then informed that the flow to be selected is not unique and the flow selection process stops while the signal is sent to the man-machine interface to remind the operator that the current flow selection operation fails and another new flow selection process should be initiated.

If the selected flow path is unique, the states of all the devices, the gate valves as well as the dust collector involved in the selected flow are checked to make the last decision by the processor.

TABLE I. Flow Table

Flow Number	Device				
	DEV1	DEV2	…	DEV66	…
1	1	1	…	1	…
2	1	1	…	1	…
3	1	1	…	0	…
4	1	1	…	0	…
5	0	0	…	0	…
…	…	…	…	…	…
486	0	0	…	1	…

At most four flows are allowed to run at the same time according to the bulk grain silos processing requirements. Each effective device that is selected to be contained in a certain flow is reserved and marked. The devices that are marked and attached to a specific flow shall be sequentially started according to the running status of the downstream parallels and sequentially stopped according to the running status of the upstream parallels. Any devices that are selected and marked to be attached to a specific flow or are running within a specific flow is prohibited to be selected by other flows.

V. FLOW MONITORING SYSTEM DESIGN

A. Hardware Components of Monitoring System

The monitoring system is composed of four graphical workstation computers, as shown in Figure 1. Three of them are used for flow selection and operation, while the other is used as a platform for dynamic data display. All the graphical workstations are linked with the master server via Ethernet. All the information from PLC is collected together by RSLinx software residing in the master server, and then transmitted to each graphical workstation through the TCP / IP protocol of the Windows 2000-based network.

B. Data Acquisition

The master monitoring software is coded with help of the configuration software tool iFIX. The iFIX is a large-scale configuration software tool developed by Intellution Corporation with features of supporting multi-tasks and multi-platforms with well timeliness and openness. The iFIX obtains the field data through the OPC (OLE for Process Control) module, which is a client / server module with a common interfaces and allows iFIX communicating with standard objects, functions and entities [7, 8]. Through the OPC module, the iFIX application sends the field data to the specified address of Drive Image Table (DIT) from the PLCs with an allotted IP address. The Scanning Alarm Control (SAC) reads the data from the DIT. After the data are handled, they are then sent to the Process DataBase (PDB). The internal query function of the Database tool reads the data from the PDB and transmits them to the general applications that require the data. The data can also be written to PLC to realize the control function along the reversed direction.

C. Graphical Display Function

The graphical display function is one of the most important functions of the iFIX, and supplies a visualized window for users to handle the process information [9]. Users visit the information contained in PDB, DDE application program or ODBC database through the graphical application programs, which transfer it visualized flow information displayed on the screen.

The drafting tool provided by the iFIX is used to simulate the working processes involved in the overall system within the Workspace environment, and the running status of the devices under control are displayed in an animation way.

The flow execution is displayed through three layers of frames that can be conveniently zoomed. The first layer frame relates to the general layout of the process flows in the system. The second layer frame relates to monitoring the specific process flow being selected. The third layer frame relates to monitoring the status of the chief and secondary devices involved in a specific process flow.

The first layer frame is activated after the iFIX software is launched. All the effective devices included within the bulk grain silos system are displayed in the frame on the screen, as shown in Figure 3. The functions of each device are:

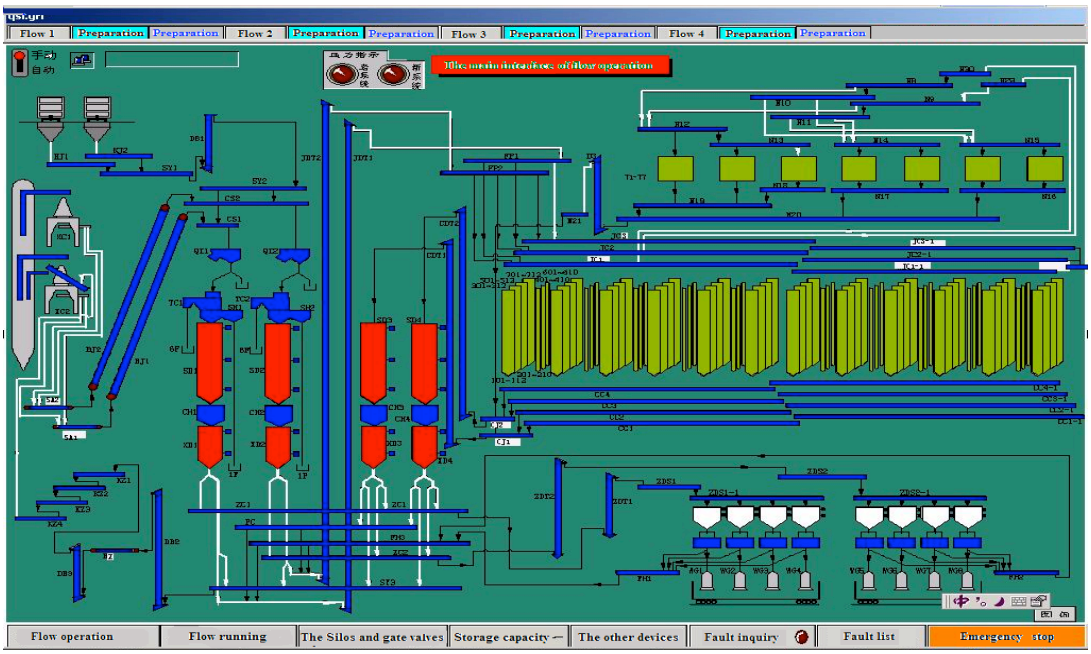

Figure 3. Snapshot of the main user interface

1) The buttons on top bar of upper part of the frame show the flow status: Four flows can run simultaneously in the system and each flow has two alternatives reserved for use in need. If the button to activate the flow is clicked, dialogues for flow operations will be automatically popped up which show the name of the starting and ending device involved, the corresponding warehouse ID, related parameters to be checked and set, and the name of the reserved devices with corresponding warehouse ID.

2) The central part of the frame shows the details of the running flow.

3) The buttons on bottom bar of lower part of the frame show the main menus: Once a menu is clicked, the corresponding window will be launched.

D. Main Functions of Flow Monitoring System

1) Execution control function: By clicking the buttons contained in the operation interface of the monitoring software installed in the central control room, a range of flow operations can be executed, such as flow select, flow start/stop, flow cancel, flow stop emergently, and flow restore.

2) Rendering function: The device running status, the flow operation mode and the process flow path can all be intuitively displayed on the monitoring screen.

3) Alarming and state inquiry function: The status of the devices can be checked out through the field signal query function. In the course of process execution, once a device is broke down, an alarming signal is sent out to the interface and stored within the persistent database for future analysis.

4) Report sheet generation function: The monitoring software can automatically handle the device running status information and the production information. The related data can be sorted, compiled and stored, and can further be used to automatically generate report sheets.

VI. CONCLUSIONS

This study shows that the Controllogix system is a high performance control platform. Its modularized structure satisfies different application environment requirements while its strong data handling ability secures smooth running for various large-scale process systems. For the systems with complex process flows, the structured program design approach proposed in the paper makes coding the control programs greatly simplified and the programs developed have good readability. The intelligent flow path selection method based on the flow table has a lot of advantages and especially suitable for the system with a large number of devices and complex dependent relationships among them.

REFERENCES

[1] J. Yan and X.B. Chen, “Application of ControlLogix Technology and RsviewSE in Grain Distribution Control in Port”, Grain Distribution Technology，no. 2，2007，pp. 60-64. (in Chinese)

[2] Qinghui Liu, “Application of ControlLogix System in Bulk Grain Silos Control System in Jinzhou Port” Grain Distribution Technology，no. 1，2010，pp. 28-30. (in Chinese)

[3] G.G. Sun, “Application of PLC in Bulk Groins Distribution Monitoring System in Port,” Port Operation, no. 3, 2008, pp. 34-35.

[4] W. Hou, “Design and Implementation of Jinzhou port bulk grain silos monitoring system” (D), Dalian: Dalian Maritime University, 2011. (in Chinese)”

[5] A-B Company , System User Manual ControlLogixTM. Rockwell Automation, 2000.

[6] A-B Company, Rslinx for Rockwell Automation Networks and Devices. Rockwell Automation ,1999.

[7] C.Y. Yang and D.X. Huang , “Research and Application of Advanced Control Software Platform based iFIX,” Intelligent Control and Automation, (WCICA2006), IEEE Press , Jun. 2006, pp. 7896-7899,dio:10.1109/WCICA.2006.1713508.

[8] K.X. Wui and Y.Q. Zheng, “The Analysis and Design of Steel Plant Electrostatic Precipitator Control System based on IFIX, ” Proc. IEEE Measuring Technology and Mechatronic Automation, (MTMA2009), IEEE Press, Apr. 2009, pp. 898-900, dio:10.1109/ICMTMA. 2009.34.

[9] A. Yui and Z.H. Xie, “Research and Application based on PLC in Electrical Drainage Station’s Computer Monitoring System, ” Proc. IEEE Mechatronic Automation and Control Engineering, (MACE2011), IEEE Press, Jul. 2011, pp. 5985-5987, dio:10.1109/MACE. 2011.5988398.

Application of Map Display on handheld devicesUsing Flex

Li Zhen
Institute of Cartography and GIS
CASM
Beijing, China
Lizhen7962143@163.com

Guo Peipei
Institute of Cartography and GIS
CASM
Beijing, China
Guopeipei925@163.com

Yuan Xuewang
Institute of Cartography and GIS
CASM
Beijing, China
Yuanxue1988@126.com

***Abstract*—This article summarizes the architecture and the characteristic of Flex technology as well as its advantage in handheld devices design, proposed the system framework of the handheld terminal based on Flex. Combined with the NewMap Server, using the RIA SDK and Flash AIR technolygy, map display on handheld devices is realized. Project experience justifies that appliction software based on Flex used in handheld terminals has an advantage of cross-platform.**

Keywords-Flex; NewMap; Handheldterminal; API; Cross-platform

I. INTRODUCTION

With the popularity of handheld devices, nowadays handheld devices tend to be various and have complicated scheduler OS.Therefore, platform-crossed map display system has become the public focus of some programmers. Considering WebGIS development experience, a methodology based on NewMap Server using Flex technology is proposed in this article for map display on handheld devices.

II. SUMMARIZATION

A. Disadvantage of map display in conventional handhelds

Mobile telephones account for the vast majority of handhelds, map display on mobile phone originates from map display on PDA. Designers usually place the whole map system or fat client-side in the PDA or mobile phone. Along with the design are a few flaws: (1) less mount of data . (2) bad real-time performance. (3) lack of map related oprations and functions. (4) being time-consumming because of low hardware configuration . (5) short woking time due to low battery storage. With the fast pace of developement in electronic technology and embedded technology, more and more handhelds with various operation systems appear in recent years, and have a great impact on peolple's life. Most map display systems could solve some of the problems described above,but the approval is only for one handheld device OS. With frequent upgrade of handhelds, the work for developer is burdensome and repeating because they have to solve the same problems for various handheld OSs.

B. The Adobe Flex platform

The application is designed based on Flex. Flex is a platform independent environment for developing rich internet applications which are Flash AIR runtime. Actionscript3.0、MXML and classes library are included in Flex developement. Actionscript3.0 is compatible for object-oriented script of ECMAScript. MXML is a model descriptive language based on XML , and used for visual edition. Flex class library consists of Flex components, manager and behaviors and so on. Adding new component models or classes is easy for developers.Application is based on asynchronous C-S communication model providing support for fast client-side interaction.Only the changed data is transferred, which shortens response time and makes user experience smooth.In the meantime, burden of server is lightened.

Figure 1. server structure of map display.

III. DESIGN CONCEPT

A. Service Mechanism

The design introduced in this article is based on NewMap Server Flex API. NewMap is a large service software developed by the Institute of Cartography and Geographic Information System of CASM. As shown in Fig.2,the GISWeb Services software is designed based on SOA architecture and accords with the OGC standards.It uses C/S system structure and offers RIA SDK. OGC is a main drivers of GIS network setvices.It defines a series of interfaces for data service,such as WMS (Web Map service) WFS (Web Feature Service) WCS (Web Coverage Service). Functional services provide service through the interface with data processing functions.NewMap Server is a large comprehensive WebGIS application

978-0-7695-4818-0/12 $26.00 © 2012 IEEE
DOI 10.1109/DCABES.2012.30

platform,providingframwork for creating GIS application and service.Map display application get service data released by NewMap Server, use map functions and GIS inquires and analytical functions provided by REST interface conveniently, Specific services relate to: map service (MapServer), network analysis service (NetWorkServer), geo-Code service (GeocodeServer).All the functional process modules are released as Web Service, include input 、 output parameter 、 burst mode, support POST,GET methods in HTTP and SOAP transport protocol.So,client-side can select the most appropriate interface mechanism to its will.Flex provides three data communication modes:HTTP service, Web service and Flash Remoting.Experiment in this article uses HTTP, invoking map services to complete map rendering and map location in client-side, invoking geo-code services to complete location search in client-side, invoking network analysis services to complete path planning.

Figure 2. NewMapFrameWork

B. *Implementation of Client-side*

Development of applications in handheld terminal using Flex is different from Web programming in data store and management strategy.The former has to take the screen size and resolution power into consideration.It also balances the management power and battery consumption.The functional structure of map display application designed in this experiment is shown in Fig. 3.

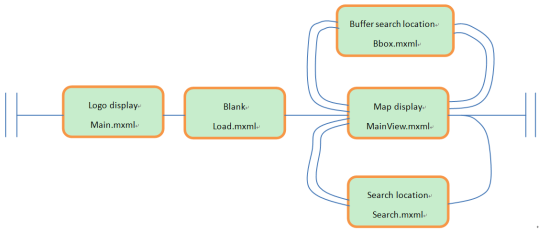

Figure 3. function structure of map display application.

In the Fig. 3, two vertical lines denote the start and the end of the programme, while the pane denotes a view.By observing the Fig. 3, we consider it as a railway.The train runs along the track only.Vertical lines on the left means start, likewise means end when on the right.It tries its best to take the single track other than the double track,because taking the double track meaning unloading cargo.Run the program, at first, a title picture comes into view, then directly the main view, which is used to display map and related functional operations.After the search location is input into the main view, it is sent to the server to be analysed.The client-side receives the result data sent from the server,and display it in the search view.Select the result needed ,the location is shown in the map on the main view.Meanwhile, functional operation buttons appear,somesecondary operations can follow by.Secondary operations include: former result display, next result display, returned results list, search circumjacently, start position setting, destination position setting.Meanwhile location button is available in main view.If GPS is on,user's location displays ,followingwith some related operation buttons and some secondary interactive operations,such as search circumjacently, start position setting, destination position setting.In the Fig. 3,there are three double tracks denoting location data transportation.No location data, no operations along the double tracks.The blank view in the figure is kept in the OS view stack to make sure that in Android system, double presses on the return button not one press result in the exit of the program.This has a benefit of low battery consumption and memoryusage.However, in the iOS, the system kill process automatically,so there's no need for return operation.

1) *Reuse of Component Library*

Not all the existing Spark componentsare endowed with touchable appearance by Adobe Company, namely it is far from the point where developers can do whatever they want to with the existing available components.With this problem in hand, tip box components and their skin classes are designed in this experiment. Tip boxes are used in main view,search view and surrounding search view, and modified according to different situations.In main view, logical judgement is designed for tip box components to make sure that , in Android system, double presses will trigger exit program command.All the tip boxes share a skin class with rounded edge and shadow effects, making it more friendly to usethe application.

2) *Interface and Map Display*

Screen resolution is an inevitable issue for handheld application developments.Even on the same operating system, different screen resolution may lead to programrewrite.To solve this problem, Flash AIR can adapt to screens with different resolutions,but still can not adapt to screens with different dpi.Components are displayed in proportion to its size. Fill the button with a fixed sizepicture, and the button remains unchanged at different DPI resolutions.

3) *Service Data Parsing*

The search view and surrounding search view receive data sent back from the server in the form of XML.Parse the data sent back form NewMapServer.Combine location information and position name into an object, put it into the result array, then the parsed array is displayed in buttonlist.SetdestructionPolicy attribute of search view and surrounding search view, use FlashAIR permanent conservation technology to avoid the view being deleted.When user decide to return result list in main view, it is successful returned and displayed.

4) *Permanent Conservation*

Appliction in handheld device is often interrupted by other applications such as text messages,income or outcome calls.Permanent conservation helps application get back to previous state.This can be used in two situations.Firstly, among application executions,namely when the application exits or restarts.Secondly,among application views.However, without any encoding or protection,the data can be stored or analysed locally. To solve this problem, custom permanentconservation mechanism is designed in this experiment.After using the data or when the application exits or user presses the clear button,the permanent conserved data is deleted.Seondaryinteractive operations in main view involve start position setting and destination position setting.In most cases, start position setting and destination position setting can not be finished in the same view.This need at least two operations back to main view.It makes no differences whether start position or destination position is set first because the start position or destination position is stored in some fixed place for read or delete.

5) Implementation Code

Components Class library encapsulation.Some of the related components are written based on spark.components.SkinnablePopUpContainer andspark.components.supportClasses.Skin.SkinnablePopUp Container can be written as a view. Key code in skin:<s:Rect left="0" right="0" top="1" bottom="0" id="background"topRightRadiusX="15"topLeftRadiusX="15"bottomLeftRadiusX="15"bottomRightRadiusX="15"><s:filters><s:DropShadowFilter color="0x000000" blurX="20" /></s:filters></s:Rect>. Set the SkinnablePopUpContainer used here with rounded conners and shadow.

Data analysis.Mainly uses Nrequest interface of NewMap Server Flex API.key code of callback functions to receive data:temp.Name=tempName;temp.Loc=tempLoc; temp.x=tempX; temp.y=tempY; Result.push(temp);ResultList.dataProvider=newArrayCollection(Result); After this, data is organized in the form of array, and shown in list component.

Custom data persistence.Key code in data persistence:varstream:FileStream=new FileStream();stream.open(slon,FileMode.WRITE);stream.writeUTFBytes(data[PointNum].x);stream.close();stream.open(slat,FileMode.WRITE);stream.writeUTFBytes(data[PointNum].y);stream.close(); key code in reading persistent data: stream.open(slon,FileMode.READ);spx=stream.readUTFBytes(stream.bytesAvailable);stream.close();stream.open(slat,FileMode.READ);spy=stream.readUTFBytes(stream.bytesAvailable);stream.close(); key code in delete persistent data: slon.deleteFile();slat.deleteFile();.

IV. EXPERIMENTAND RESULTS ANALYSIS

The experiment environment is SamSung GT-P7500, Android 3.1, connectible WCDMA network or WLAN net work, GPS module, iPad 2,iOS 5.0.1.

Location search and map rendering:

Figure 4. server structure of map display.

Figure 5. display results and map rendering

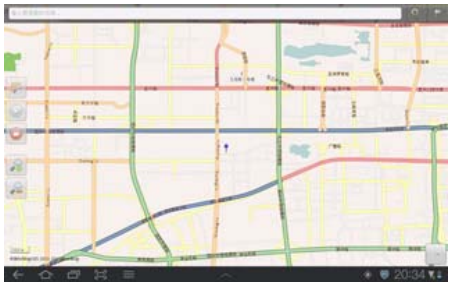

Figure 6. display location

Pathplanning:

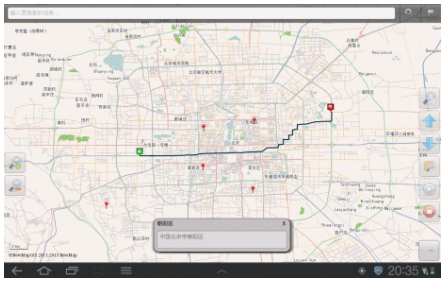

Figure 7. Pathdisplay

The map display system realized in this experiment supports different handheld device OSs, provides friendly interface and operations.However, it does badly when it involves multi-finger intetactiveexperiences.Thus, map amplification is realized by double click alternatively.

V. CONCLUSION

Friendlly handheld device application is developed using Flex technology, realizing complicated control logic.Combined with Web Service data, loosely coupled architecture is achieved, which sproves that it is a effective way to develop handheld application combining RIA with Web Services.

REFERENCES

[1] Zhang Chuancai, “On The Collectivity Design Scheme ofPDATour ElectronicMap System,” Journal of Anyang Institute of Technology,NO 6, pp. 36-39,december 2005.

[2] Chen Lin,WangHua, “Solution of electronic map based on Flash technique and application in WebGIS,” Computer Engineering and Design,Vol.28,No.19, pp. 4796-4799,Oct. 2007.

[3] Sun Yu, Li Guoqing and Huang Zhenchun, “Research on Implementation of OGCWeb Processing Service,” Computer Science,Vol.36,No.8, pp. 86-88,Aug. 2009;.

[4] Zhang Kangshou,Feng Bing,SunYangang and WANG Futao, “Development ofWebGIS System Based on RIA and Web Services,” Geospatial Information,vol. 7, NO 2,pp. 109-111,April, 2009..

Intelligent Decision-Making Service Framework Based on QoS Model in the Internet of Things

Qi Zhang
School of Computer Science and Technology
Wuhan University of Technology
Peace avenue 1040, Wuhan, Hubei Province, China
e-mail: zhangqi_whut@163.com

DeWei Peng
School of Computer Science and Technology
Wuhan University of Technology
Peace avenue 1040, Wuhan, Hubei Province, China
e-mail: pengdewei@gmail.com

***Abstract*—The Internet of Things (IOT) has recently become popular to emphasize the vision of a global infrastructure of networked physical objects. The service framework based on IOT global infrastructure can provide full context resources and transform everyday objects into smart objects that automatically understand and react to their environment. However, the framework is still lacking because of unclear structural standards in IOT. In this paper, we construct an intelligent decision-making service framework based on the general IOT global structure and explicitly define its components' function and which IOT layer it belongs to. As to key problem of the framework—how to make intelligent decision depended on the context, we propose a QoS model according to improved Analytical Hierarchy Process (AHP). We use hierarchical clustering algorithm, fuzzy comprehensive evaluation, scale-extending method, entropy weight method, etc. to overcome AHP's inherent defects such as subjectivity. In the end, we perform a simulation to verify our study results, which reflects that the service decision-making controller in our framework can promptly evaluate available services and select the best service for users with the model.**

Keywords-IOT;smart objects;service framework;QoS model; improved AHP

I. INTRODUCTION

The Internet of Things (IOT) is a vision in which the Internet extends into our everyday lives through a wireless network of uniquely identifiable objects [1]. And it is partly inspired by the success of Radio Frequency Identification (RFID) technology, which is now widely used to track objects, people, and animals [2-4].

The incredible amount of information captured by a trillion RFID tags has a tremendous impact on our lives. However, some issues remain such as how to build service infrastructure in order to support effective RFID service provision in the Internet of Things Computing (IOTComp) environment[5]. Its key challenge is to identify automatically whether the provided service is loadable for the mobile RFID reader with limited resource and whether the provided service can meet the users' needs.

IOT service infrastructure, also called IOT service framework, is expected to promptly evaluate the quality of services (QoS) and provide satisfying services for the users depending on the RFID context [6].The context represents the knowledge of IOTComp environment, which includes users' preference, device capability and current network status, etc. and can be used to provide intelligent service decision-making. The first contribution of this paper is to build an intelligent decision-making service framework based on IOT global structure. Another contribution is to propose a context-oriented QoS model by extending the Analytical Hierarchy Process (AHP) and address the critical problem in IOT service framework.

The rest of the paper is organized as follows. Section II is devoted to discussing related work, and provides a summary of various QoS modeling techniques in IOT. Section III is devoted to building an intelligent decision-making framework based on IOT. Section IV addresses the problem of constructing QoS model. In Section V, we perform a simulation to validate the result of our model. Then we state some conclusions and future working directions in the last section.

II. RELATED WORK

QoS model in IOT can analyze IOPComp context and provide methods to compute the value of QoS which acts as a metric for optimal service decision-making. Most previous studies focus on the RFID network protocols, middleware, RFID devices reliability, safety, and cost, etc.[7,8], while the research on QoS model for IOT global infrastructure is much less.

Reference [9] first proposed a QoS model of grey decision-making from the view of IOT global infrastructure and built an adaptive service framework. In [10], a quality evaluation technique of RFID middleware according to ISO/IEC 9126 standard and EPC global middleware quality factors was built by simple AHP. It really provided an idea of simplifying complicated evaluation factors in IOT. In [6], the author constructed another AHP QoS model based on IOT global infrastructure. Moreover, in most QoS models, many factors such as device performance, resource state, etc. were considered but users' feedback like user preferences was often ignored.

A good QoS model, on the one hand, should aim at IOT global infrastructure and don't rely on internal protocols. On the other hand, it must fully take users' feedback into consideration.

978-0-7695-4818-0/12 $26.00 © 2012 IEEE
DOI 10.1109/DCABES.2012.26

III. INTELLIGENT DECISION-MAKING SERVICE FRAMEWORK IN IOT

There are different types of low-level RFID context which includes any information used to mark the characteristics of things in IOT. In service evaluation, the premise of intelligent decision-making is to transform these low-level contexts into meaningful, high-level information by classifying them and then to apply them. In this paper, context resources are divided into three categories: device performance context, resource state context, user feedback. This classification also constitutes three types of QoS evaluation indicator such as device performance indicator, resource state indicator, user feedback indicator.

Due to the computing complexity and mobility of IOT applications, more and more user requests need to be completed by the cooperation of more than one device. Therefore the service framework based on IOT global infrastructure is very important. It can use kinds of context to make an optimal service selection from all the usable services regardless of user's and thing's location.

We abstract an intelligent decision-making service framework from general IOT structure [11], it is shown in Fig.1.

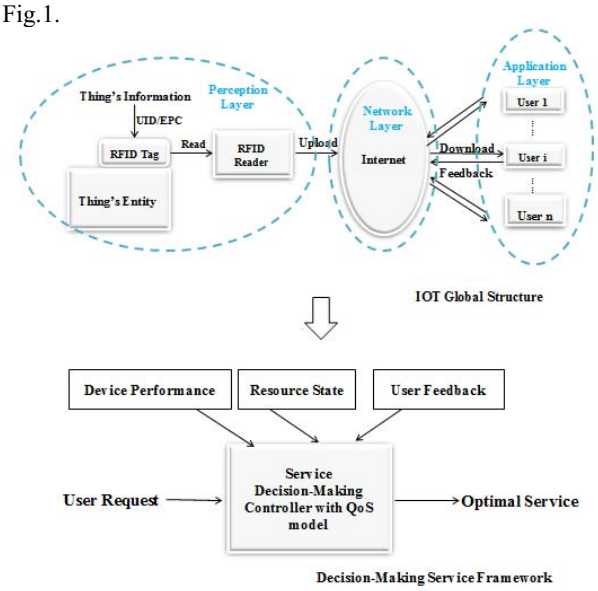

Figure.1 Abstraction process of decision-making service framework

The above decision-making service framework can be also defined as

$$
\begin{aligned}
&F(I,C,V,O)\\
&I=\{req_1,req_2,req_3\ldots req_k\}\\
&C=\{device-context,resource-context,feedback-context\}\\
&V=\{QoS_1,QoS_2,QoS_3\ldots QoS_m\}\\
&O=service_i,i\in\{1,2,3\ldots m\}
\end{aligned}
\tag{1}
$$

Where F represents service framework, it has four components of I , C , V , O . I includes the k users' requests from IOT application layer and is the input section of service framework. C means service framework's three types of RFID context in which device- and resource-context are all from IOT perception layer but feedback-context is from IOT application layer. V is the set of m services' QoS value, which is computed by service decision-making controller of IOT network layer. The final O is the selected optimal service which will output to application layer.

IV. THE QOS MODEL BASED ON IMPROVED AHP

In section III, we build the service framework based on IOT infrastructure. In this section, we will be devoted to studying the framework's key problem. That is namely the construction of QoS model in service decision-making controller, which provides calculation method of QoS and is particularly important for intelligent service decision-making.

AHP is a common method of evaluation and decision-making. Introducing it into QoS evaluation in the IOTComp environment simplifies the complicated IOTComp and can construct a QoS model based on IOT global infrastructure. However, the problem about AHP's strong subjectivity is still not resolved. In this paper, we further improve AHP and make it overcome subjectivity defects by the hierarchical clustering algorithm and fuzzy comprehensive evaluation method [12]. Our model's evaluation flow can be seen in Fig. 2.

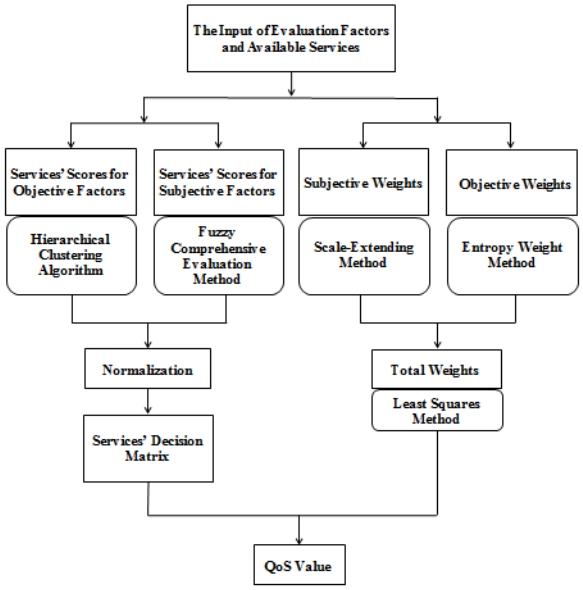

Figure.2 QoS model's evaluation flow chart

A. THE INPUT OF EVALUATION FACTORS AND AVAILABLE SERVICES

Evaluation indicators are equivalent to different types of RFID context, which are also divided into three types of device performance, resource state, user feedback. Every indicator has its several factors. In our service framework, evaluation factors and available services are generally input

by service provider. Here, we consider n factors and m available services.

B. AVAILABLE SERVICES' SCORES FOR DIFFERENT FACTORS

According to types of indicators, we can know three kinds of evaluation factors. Among them, factors of device performance indicator and resource state indicator belong to objective factors and factors of user feedback indicator belong to the subjective factors. To facilitate description, we take n_d, n_r, n_u as the factors'number of device performance indicator, resource state indicator, user feedback indicator.

1) Service's scores of objective factors: The hierarchical clustering algorithm[13] first need provision classification levels, and then decide the clustering standard of service, finally cluster according to algorithm. We assume has $1\sim t$ levels and use the historical context resources as clustering standard, thus main steps of the algorithm are

---

Begin

Initialize $t, t' \leftarrow m, L_i \leftarrow \{service_i\}, i = 1,2,3 \ldots m$

Do $t' \leftarrow t'-1$

$D(L_i, L_j) = Min\sqrt[\varphi]{(\sum_{u=1}^{n_d+n_r} \left| f_{iu} - f_{ju} \right|)^{\varphi}}$,clustering L_i and L_j

Until $t = t'$

Return t service clusters

End

Where m is the number of available services, t' is the current number of service clusters, u is the number of objective factors which includes n_d factors of device performance indicator and n_r factors of resource state indicator, φ is an optional parameters (we take $\varphi = 2$). In the algorithm, we compute $D(L_i, L_j)$ with historical factors' value in context resource to find the minimum D and then merge L_i, L_j to a cluster.

Through the algorithm, we will eventually get t service clusters' respective level and determine service's scores of objective factors:

$$A_{obj} = \begin{bmatrix} a_{11} & a_{12} & \cdots & a_{1(n_d+n_r)} \\ a_{21} & a_{22} & \cdots & a_{2(n_d+n_r)} \\ \vdots & \vdots & \vdots & \vdots \\ a_{m1} & a_{m2} & \cdots & a_{m(n_d+n_r)} \end{bmatrix} \quad (2)$$

2) Service's scores of subjective factors: In this paper, fuzzy comprehensive evaluation method is introduced to get service's scores of subjective factors. The steps are as follows:

- Consider n_u evaluation factors, the set U includes them and is credited as $U = \{f_1, f_2, f_3 \ldots f_{n_u}\}$.
- Determine the appropriate evaluation level and every level's score. When there are l levels, evaluation set $E = \{e_1, e_2, e_3 \ldots e_l\}$.
- Define the evaluation matrix

$$R = \begin{bmatrix} r_{11} & r_{12} & \cdots & r_{1l} \\ r_{21} & r_{22} & \cdots & r_{2l} \\ \vdots & \vdots & \vdots & \vdots \\ r_{n_u 1} & r_{n_u 2} & \cdots & r_{n_u l} \end{bmatrix} \quad (3)$$

  where r_{ij} represents the membership degree to evaluation level score e_j of evaluation factors f_i.
- Then the u service's scores of subjective factors are $a_{uv} = ER'$, where $v \in \{1,2 \ldots n_u\}$. Repeat the above steps for each service and we will get

$$A_{subj} = \begin{bmatrix} a_{1(n_d+n_r+1)} & a_{1(n_d+n_r+2)} & \cdots & a_{1n} \\ a_{2(n_d+n_r+1)} & a_{2(n_d+n_r+2)} & \cdots & a_{2n} \\ \vdots & \vdots & \vdots & \vdots \\ a_{m(n_d+n_r+1)} & a_{m(n_d+n_r+2)} & \cdots & a_{mn} \end{bmatrix} \quad (4)$$

In our paper, we adopt 5 evaluation levels, so let $l = 5$ and $E = \{0.2, 0.4, 0.6, 0.75, 0.9\}$. Besides, we derive membership degree equation with statistical voting results of user feedback, thereby obtaining the evaluation matrix R. The membership degree equation is

$$r_{ij} = \frac{N_{ij}}{\sum_j N_{ij}} \quad (5)$$

where N_{ij} is the number of votes with which the users think factor i belong to the evaluation level j.

From *1)* and *2)*, we compute services' scores for all evaluation factors and normalize them, thus obtaining the final service decision matrix

$$A = \begin{bmatrix} A_{obj} & A_{subj} \end{bmatrix} = \begin{bmatrix} a_{11} & a_{12} & \cdots & a_{1n} \\ a_{21} & a_{22} & \cdots & a_{2n} \\ \vdots & \vdots & \vdots & \vdots \\ a_{m1} & a_{m2} & \cdots & a_{mn} \end{bmatrix} \quad (6)$$

C. CALCULATE WEIGHTS

1) The Subjective Weights: We adopt scale-extending method to obtain the weights.

Firstly, we obtain factors' order of importance based on feedback: $p_1 \geq p_2 \geq p_3 \cdots \geq p_n$;

Secondly, according to the order we establish a scale matrix

$$C=\begin{bmatrix} 1 & c_1 & c_1c_2 & \cdots & c_1c_2\cdots c_{n-1} \\ 1/c_1 & 1 & c_2 & \cdots & c_2c_3\cdots c_{n-1} \\ 1/c_1c_2 & 1/c_2 & 1 & \cdots & c_3c_4\cdots c_{n-1} \\ \vdots & \vdots & \vdots & \vdots & \vdots \\ 1/c_1c_2\cdots c_{n-1} & 1/c_2c_3\cdots c_{n-1} & 1/c_3c_4\cdots c_{n-1} & \cdots & 1 \end{bmatrix} \quad (7)$$

Where the scale value

$$c_i = \frac{p_i}{p_{i+1}} \in \{1.2, 1.4, 1.6, 1.8, 1/1.2, 1/1.4, 1/1.6, 1/1.8\}.$$

Therefore, subjective weights are

$$w_j^1 = \frac{\sqrt[n]{\sum_{k=1}^{n} c_{jk}}}{\sum_{k=1}^{n}\sqrt[n]{\sum_{l=1}^{n} c_{kl}}}, j = 1,2\cdots n \quad (8)$$

2) The Objective Weights: We use entropy weight method to caculate the weights[4].

In accordance with decision matrix A and information theory, the entropy H_j of the factor j is

$$h_{ij} = \frac{a_{ij}}{\sum_{i=1}^{m} a_{ij}}$$
$$H_j = -(\ln m)^{-1}\sum_{i=1}^{m} h_{ij}\ln h_{ij} \quad (9)$$

when $h_{ij} = 0$, the $h_{ij}\ln h_{ij}$ is set to 0. Then we can get the objective weights

$$w_j^2 = \frac{1-H_j}{n-\sum_{k=1}^{n} H_k}, j = 1,2\cdots n \quad (10)$$

Finally, by least squares method we calculate the total weight vector $W = \{w_1, w_2, w_3 \cdots w_n\}$ with (8) and (10):

$$\sum_{j=1}^{n} w_j = 1$$
$$Min\{\sum_{i=1}^{m}\sum_{j=1}^{n}\left[((w_j - w_j^1)a_{ij})^2 + ((w_j - w_j^2)a_{ij})^2\right]\} \quad (11)$$

D. COMPUTE THE QOS VALUE

Each service's QoS can be computed as

$$QoS_i = \sum_{j=1}^{n} w_j a_{ij}, i = 1,2\cdots m \quad (12)$$

Obviously, the higher QoS value is , the better.

V. APPLICATION SIMULATION

To verify the QoS model, we perform a simulation. The users' request faces IOTCommunication, which has four available services. They are

- Objective-to-Internet-Human (OIH),
- Human-to-Internet-Objective(HIO),
- Objective-to- Internet-Objective (OTO),
- Objective-to-IOT Objective (OIOTO)[7].

We provide all the evaluation factors, which are shown in Table.1.

Table.1 Evaluation factors in the simulation

Factor Types	Factor Description		
Objective Factors	Device Performance	D_R	reliability
		D_S	memory storage
		D_T	fault tolerance
	Resource State	R_C	CPU cost
		R_E	battery energy
		R_B	bandwidth usage
Subjective Factors	User Feedback	U_F	user friendly

- Using the hierarchical clustering algorithm and fuzzy comprehensive evaluation method to establish the decision matrix, then normalize it.

$$A = \begin{bmatrix} 0 & 0 & 1 & 0 & 1 & 0 & 1 \\ 0.25 & 0.25 & 0.25 & 1 & 0.875 & 0.625 & 1 \\ 1 & 0.33 & 1 & 0.33 & 0.33 & 1 & 0.33 \\ 0.33 & 1 & 0 & 0 & 0 & 0.33 & 1 \end{bmatrix}$$

- Through scale-extending method and entropy method, we get the subjective and objective weights, then deriving the total weights.

  W={0.2988,0.1026,0.0901,0.1234,0.0295,0.1607,0.1949}

- From the above results, the final QoS values are

$$QoS=\begin{bmatrix}0.3146\\0.5674\\0.6982\\0.2542\end{bmatrix}\begin{matrix}OIH\\HIO\\OIO\\OIOTO\end{matrix}$$

From these QoS values, we can know the optimal service based on the assumed RFID context is OIO and the rank of their QoS is OIO > HIO > OIH >OIOTO. With the model's evaluation results, service decision-making controller in service framework evaluates instantly all the usable services and provides the best service for users.

VI. CONCLUSIONS

In this paper, we abstract an intelligent decision-making service framework based on the IOT global infrastructure, at the same time analyzing its several components' functions and layers. Then, for the key problem of framework, we propose a context-oriented QoS model. It's based on the improved AHP which overcomes inherent subjectivity by introducing hierarchical clustering and fuzzy comprehensive evaluation. Moreover, the model aimed at IOT global infrastructure, don't rely on internal protocols and take users' feedback into consideration fully.

As future work, we plan to design new IOT service framework because the structure standard of IOT is not clear at present and is still improving. We will correct and optimize our study according to the latest scientific research.

ACKNOWLEDGMENT

The work in this paper was supported by the national college students' innovative training projects (No. 20121049710008) of the Wuhan University of Technology in 2012 and the Fundamental Research Funds for the Central Universities.

REFERENCES

[1] E. Welbourne, L. Battle, G. Cole, K. Gould, K. Rector and S. Raymer, et al, "Building the internet of things using RFID: the RFID ecosystem experience," IEEE Internet Computing, 2009, vol. 13, pp. 48-55.

[2] G. Kortuem, F. Kawsar, D. Fitton, and V. Sundramoorthy, "Smart objects as building blocks for the internet of things," IEEE Internet Computing, 2010, vol. 14, pp. 44-51.

[3] G. Broll, E. Rukzio, M. Paolucci, M. Wagner, A. Schmidt and H. Hussmann, "PERCI: pervasive service interaction with the internet of things," IEEE Internet Computing,2009, vop. 6, pp.74–81.

[4] L. Atzori, A. Iera, G. Morabito, "The Internet of Things: A survey," Computer Networks, 2010, vol.54,pp.2787–2805.

[5] G.Pujolle,"An Autonomic-oriented Architecture for the Internet of Things,"IEEE John Vincent Atanasoff 2006 International Symposium on Modern Computing (JVA'06) ,2006,pp.163-168.

[6] Fan Shaoshuai, Shi Wenxiao, Wang Nan and Liu Yan, "MODM-based Evaluation Model of Service Quality in the Internet of Things," Procedia Environmental Sciences ,2011,vol.11,pp. 63 – 69.

[7] G. Ferrari, F. Cappelletti and R. Raheli, "Simple Performance Analysis of Multiple Access RFID Networks Based on the Binary Tree Protocol," International Journal of Sensor Networks, 2008, vol.4, pp.194-208.

[8] C. Ko, S. Roy, J. R. Smith, H. W. Lee and C. H. Cho, "RFID MAC Performance Evaluation Based on ISO/IEC 18000-6 Type C," IEEE Communications Letters,Vol.12,No.6,June 2008.

[9] Jianhua Liu, Weiqin Tong, "Adaptive Service Framework Based on Grey Decision-Making in the Internet of Things," 2010 6th International Conference **on** Wireless Communications, Networking and Mobile Computing, WiCOM ,2010.

[10] G. Oh, D. Y. Kim, S. I. Kim, Sung and Y. Rhew, "A quality evaluation technique of RFID middleware in ubiquitous computing," 2006 International Conference on Hybrid Information Technology, 2006, vol. 2, pp.730-735.

[11] Yinghui Huang, Guanyu Li, "Descriptive Models for Internet of Things," International Conference on Intelligent Control and Information Processing, 2010.

[12] Biqing Huang, Ting Wang, Xiao Xue, "Extended QoS model driven logistics services selection approach," J T sing hua Univ (Sci & Tech),2011, Vol.51, pp.19-24.

[13] R. Duda, P. Hart, D. Stork, Pattern Classification, New York: Wiley, 2001.

Identification of CTG Based on BP Neural Network Optimized by PSO

Zhou Hongbiao, Ying Genwang

Faculty of Electronic and Electrical Engineering
Huaiyin Institute of Tech., Huaiyin 223003, China
E-mail: hyitzhb@163.com, 15189544918@163.com

***Abstract*—Aiming at the normal, atypical and abnormal cardiotocography (CTG), the BP neural network (BPNN) classification model was created. The particle swarm optimization (PSO) technique was used to optimize the initial weights and threshold value of the neural network based on the inherent local minimum problem of BPNN and the good global convergence and global search ability of PSO. The CTG set of the UCI was used to test the algorithm. The simulative results indicated that the recognition accuracy of the normal, atypical and abnormal CTG reached 98.35%、95.48% and 98.46% based on PSO-BP, more than GA-BP and traditional BP. The model has good ability both in learning and generalization and the algorithm can also effectively be used in other signal processing fields.**

Keywords-cardiotocography; identification; BP neural network; particle swarm optimization

I. INTRODUCTION

Intrapartum cardiotocography (CTG) is a procedure of graphically recording fetal heart activity and uterine contraction. It is a frequently used technique of fetal monitoring to evaluate the well being of the fetus during pregnancy and in labor, which makes an influence on obstetricians' clinic decisions. The terms of new classification system for CTG is normal, atypical and abnormal. The clinical method to analyze the cardiotocography is artificial analysis, its accuracy and consistency is not good. Computerized analyses can mitigate the intra-observer and inter-observer variability of visual CTG recording explanation; decrease the examination time, and the need of additional tests for fetal health. Therefor, researchers develop computerized-aided analysis systems for CTG on PC[1].

Chen Yu Chen of National Taiwan University developed a LabVIEW pattern analysis software based on FHR and uterine contraction (UC), which utilized median filter and peak/valley detection method and has great potential for home-care use[2]. PA Warrick of McGill University trained support vector machine classifiers with feature sets from an model which signal pair as an input–output system using a system identification approach to estimate their dynamic relation in terms of an impulse response function[3][4].H.Cao of University of Virginia adapted cross-correlation analysis to quantify the timing and extent of heart rate changes during uterine contraction[5].

Neural networks have been widely applied to pattern recognition, function approximation, feature extraction, fault diagnosis and system control. The Back Propagation network not only has strong mathematical theory, but also can approximate any arbitrary function[6]. But BP network has many disadvantages. In order to improve the local search ability of BP algorithm, many researchers utilize the PSO algorithm to train the neural network. A good training algorithm combining PSO with BP is proposed in this paper and in the hybrid algorithm PSO is used to optimize the initial parameters of the BP neural network. The experiment results show that the method in this paper plays effectively over conventional BP algorithm[7].

This paper is organized into 4 sections. In section 1, there is a brief description of importance of the CTG analysis, the advantages and disadvantages of neural network in identification. In section 2, BP neural network based particle swarm optimization algorithm is introduced. In section 3, there are experimental results analyses. In the final section the conclusions are given.

II. DESCRIPTION OF BP AND PSO

A. BP neural network

BP neural network is a multi-layer feed forward neural network, its transfer function in the hidden layer is Sigmoid function, and it can achieve arbitrary nonlinear mapping from input to output. The learning process of BP neural network is composed of the signal being spread and the error back-propagation. When the signals were spread, the samples were imported from the input layer through hidden layer by dealing to the output layer. If the actual output did not meet the desired output, turned to the phase of error back propagation[7]. BP neural network

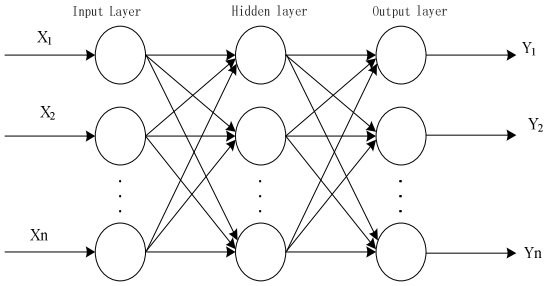

structure is shown as figure 1.

Figure 1. The BPNN structure

The main steps of BP algorithm can be summarized as follows[8]:

*Step*1: Network initialization. It is assumed that three layers in the BP network, ω_{ij} is the network weight for the input and hidden layers, ω_{jk} is for hidden and output layers. The a_j is the j_{th} bias value of the hidden layer, b_k is the k_{th} bias value of the output layer.

978-0-7695-4818-0/12 $26.00 © 2012 IEEE
DOI 10.1109/DCABES.2012.97

*Step*2: According to the transfer function calculate the output value of the hidden layer

$$H_j = f(\sum_{i=1}^{n} \omega_{ij} x_i - a_j) \quad j = 1,2,...,l \tag{1}$$

Where $f(a) = 1/(1+e^{-a})$ is nonlinear function, l is the total number of hidden layer units.

*Step*3: Calculate the actual output value of the output layer

$$O_k = \sum_{j=1}^{l} H_j \omega_{jk} - b_k \qquad k = 1,2,...,m \tag{2}$$

*Step*4: Computing network error

$$e_k = Y_k - O_k \qquad k = 1,2,...,m \tag{3}$$

*Step*5: Network error and the maximum allowable error, if met, the end. Otherwise, according to the following equation adjust the network weights and threshold, and turn to the step 2.

$$\omega_{ij} = \omega_{ij} + \eta H_j (1 - H_j) x(i) \sum_{k=1}^{m} \omega_{jk} e_k$$

$$i = 1,2,...,n; \; j = 1,2,...,l \tag{4}$$

$$\omega_{jk} = \omega_{jk} + \eta H_j e_k \quad k = 1,2,...,m \tag{5}$$

$$a_j = a_j + \eta H_j (1 - H_j) \sum_{k=1}^{m} \omega_{jk} e_k$$

$$j = 1,2,...,l \tag{6}$$

$$b_k = b_k + e_k \qquad k = 1,2,...,m \tag{7}$$

Where the η is speed of learning.

B. PSO algorithm

PSO is an evolutionary computation technique developed by Dr. Eberhart and Dr. Kennedy in 1995,inspired by social behavior of bird flocking or human activities [9].The birds using simple rules to delineate their flight direction and flight speed.Each bird is trying to stop in the flock to ensure that no collision will happen.If a bird flies away from the flock to the habitat,other birds around it will also fly to the same direction.If a habitat is founded,these birds will tell more birds about the position of the habitat,and finally the entire flock will fall on the habitat.Therefore,similar techniques can be used to find the optimal solution to a specific problem.

Supposing the dimension for a searching space is D ,the total number of particles is n ,the position of the ith particle is expressed as $X_i = (x_{i1}, x_{i2}, ..., x_{iD})^T$; the velocity of the ith particle is expressed as $V_i = (V_{i1}, V_{i2}, ..., V_{iD})^T$;the best position of the ith particle is denoted as $P_i = (P_{i1}, P_{i2}, ..., P_{iD})^T$;the best position of the whole swarm is denoted as $P_g = (P_{g1}, P_{g2}, ..., P_{gD})^T$. According to the following formulas, they update their velocity and location:

$$V_{id}^{k+1} = \omega V_{id}^{k} + c_1 r_1 (P_{id}^{k} - X_{id}^{k}) + c_2 r_2 (P_{gd}^{k} - X_{id}^{k}) \tag{8}$$

$$X_{id}^{k+1} = X_{id}^{k} + V_{id}^{k+1} \tag{9}$$

Where c_1 and c_2 are two positive acceleration constants between 0 and 2, r_1 and r_2 are two random numbers in the range [0, 1]. The constants c_1 and c_2 represent the weighting of the stochastic acceleration terms that pull each particle toward P_i and P_g position. V_{id} is the rate of the velocity change for particle in order to reduce the possibility to leave the search space in the process of evolution. In addition, the position and velocity of the particle is limited to the range $[-X_{\max}, X_{\max}]$ and $[-V_{\max}, V_{\max}]$[10].

C. PSO-BP MODEL STRUCTURE

The basic principle which BP neural network is trained by PSO is optimize the initial parameters of the network to improve network speed training by introducing particle swarm algorithm[10].The procedure for this PSO-BP algorithm can be summarized as follows:

*Step*1: Establish BP neural network and initialize the positions and velocities of a group of particles randomly.

*Step*2: Compute every particle's fitness value and *present* is set as the positions of the current particles while P_g is set as the best position of the initialized particles.If current fitness value is smaller than the *present* fitness value,the current particle replaces the *present* particle.

*Step*3: The best particle of the current particles is stored. The positions and velocities of all the particles are updated according to (8) and (9), then a group of new particles are generated.

*Step*4: Evaluate each new particle's fitness value, and the worst particle is replaced by the stored best particle. If the *ith* particle's new position is better than P_i , P_i is set as the new position of the ith particle. If the best position of all new particles is better than P_g ,then P_g is updated.

*Step*5: Judge the stopping criteria, if the maximal iterative times are met, stop the iteration, and the positions of particles represented by P_g are the optimal best solution. Otherwise, the process is repeated from step2.

*Step*6: Taking the weights and threshold value which optimized by PSO as the initial parameters, the BP network makes autonomous learning.

III. THE SIMULATION RESULT AND ANALYSIS

A. Experiment data

In order to test the performance of the algorithm given above,the classification problem of UCI database-cardiotocography (CTG) database which is perhaps the best known database to be found in the pattern recognition literatures. In the database three kinds of CTG are recorded,including normal,atypical

and abnormal CTG.21 attribute information like LB, AC, Fm and UC are contained in every instance, totally 2126 instances,1655 in normal class,295 in atypical class,176 in abnormal class. BP neural network structure is designed as follows:Input layer has 21 nerves, middle layer has 25 nerves,and output layer has 3 nerve. Therefore,21×25×3 BP neural network is adopted in the experiment.The attribute of three CTG classification are defined as 100、010 and 001 in 3-D space.

The activation functions used in BP neural network like sigmoid, purelin and tansig are continuous and able to difference.The boundary of the activation function is[0,1].So the sample data must be preprocessed.In this paper the preprocessing formula is as follows:

$$F_i = (x_i - x_{i\min}) / (x_{i\max} - x_{i\min}) \qquad (10)$$

Where F_i is the standardized value of x_i ; $x_{i\min}$ is the pre-determined minimum value of the i index; $x_{i\max}$ is the pre-determined maximum value of the i index.

B. Experiment results

In this study, particle number is 50. We choose $c_1 = c_2 = 2$, $X_{\max} = 10$, $V_{\max} = 0.5$, the inertia weigh ω linearly decreased with increasing iterative times, and ω ranges from 0.9 to 0.4. In experiments, the maximum training times of network is setted by 200 iteration.The parameters of the BP algorithm are defined.In the training phase,1926 of three classes is randomly selected as training samples,while the left 200 is used as test samples. From the experiment simulation we obtain Figure 2.

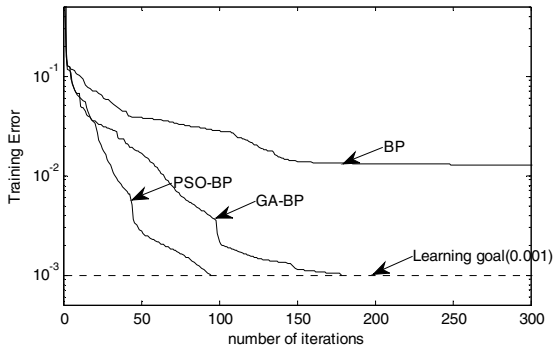

Figure 2. training curve for PSO-BP

From figure 2,we can learn that BP neural network which is optimized by PSO has better convergence rate and higher learning precision.Meanwhile PSO-BP neural network can obtain better simulation results compared with BP and GA-BP algorithm. From the CTG experiment simulation we obtain classification error of BP、GA-BP and PSO-BP showed as Figure 3 to Figure 5.

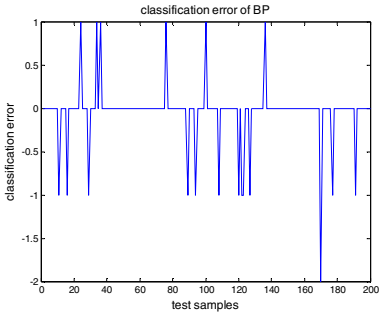

Figure 3. classification error of BP

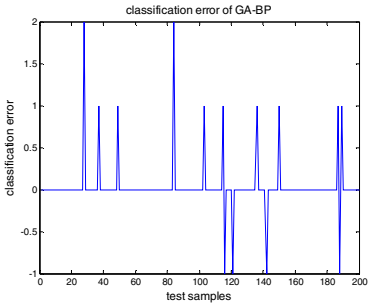

Figure 4. classification error of GA-BP

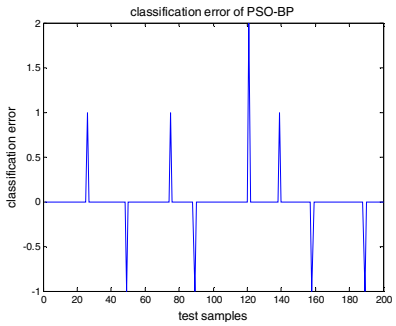

Figure 5. classification error of PSO-BP

The simulation results indicates the hybrid training algorithm by combining the PSO and BP algorithm has greater improvement of feasibility and validity than BP and GA-BP.Comparison of three classification methods is shown in Table 1.

Tab.1 Analysis of the results

Class	Accuracy/%		
	Normal	Atypical	Abnormal
BP	97.32	71.97	95.45
GA-BP	98.24	82.67	95.65
PSO-BP	98.35	95.48	98.46

IV. CONCLUSION

In this paper, the particle swarm optimization is used to optimize the parameters of BP neural network. The hybrid algorithm takes full advantages of the better

performance of global optimized search of PSO and the local optimized search of BP neural networks. The experiment results of CTG classification show that the PSO is powerful in BP neural network learning. The experiment underlines the validity of the optimized BP neural network based on PSO algorithm. Comparing with the GA-BP and original BP neural network, the recognition accuracy of PSO-BP is obviously improved than that of original neural network and GA-BP. Accordingly, this method has great application foreground in the classification of CTG.

REFERENCES

[1] Palomaki O,Luukkaala T, Luoto R,et al.Intrapartum cardiotocography-the dilemma of interpretational variation[J]. Journal of Perinatal Medicine, 2006, 34(4):298-302.

[2] Chen Yu Chen, Ju Cheng Chen, Chun Yu,et al.A Comparative Study of a New Cardiotocography Analysis Program[J].31st Annual International Conference of the IEEE EMBS,September 2-6,2009,pp.2567-2570.

[3] PA Warrick, RE Kearney, D Precup, et al. System-Identification Noise Suppression for Intra-Partum Cardiotocography to Discriminate Normal and Hypoxic Fetuses[J]. Computers in Cardiology,2006,33:937−940.

[4] Philip A.Warrick, Emily F.Hamilton, Doina Precup,et al.Classification of Normal and Hypoxic Fetuses From Systems Modeling of Intrapartum Cardiotocography[J].IEEE TRANSACTIONS ON BIOMEDICAL ENGINEERING, 2010, 57(4): 771-779.

[5] H.Cao,D.E.Lake,C.A.Chisholm,etal.Toward quantitative monitoring of human cardiotocography during labor. Proceedings of the 25th Annual lntemational Conference of the IEEE EMBS,September 17-21,2003,pp.236-239.

[6] Wang MY,Chen J,Shen XL and Yu GL,Early warning model of enterprise operating ability using BP neural network[J], Information Technology For Manufacturing Systems. 2010,pp.948-953.

[7] Liu Ming, Liang Yan-chun. The Application of GA-BP Algorithm to Intelligent Diagnosis of Coronary Heart Disease [C] . CMCE 2010, pp. 367-370.

[8] Tao Jiang, Yufang Zhang, Yinhui Liu. A study of application of an improved algorithm in BP Network[J].Computer Science, 2006,(3):164-166.

[9] Jie Hu,Xiangjin Zeng.A Hybrid PSO-BP Algorithm and Its Application[C].ICNC 2010,pp.2520-2523.

[10] Zhang JingRu, Jun Zhang. A hybrid particle swarm optimization-back-propagation algorithm for feed forward neural network training[J]. Applied Mathematics and Computation 2007,185: 1026-1037.

The Impact of Online Games on the Network Teaching Interaction Design

Wang Daping, Wang Lin,Zhang Junhua,Meng Hong,Guo Xin

Beijing City University
Beijing,P.R.China
{wangningmei5288, wanglin,zjh,menghong,guoxin}@bcu.edu.cn

***Abstract*—The importance and emphasis on interactive teaching is to implement the modern educational thought, but also to achieve quality education. Especially in online teaching, the strengths and weaknesses of the interaction is an important guarantee for the quality of teaching. This article describes the history and development of the game theory, summarizes three features of online games in the view of learning, social and entertainment, and puts forward situated cognition theory combining online game with network teaching. Lastly it indicates how the online games influence on the network teaching interaction design.**

Keywords- online teaching; teaching interaction; online games

I. INTRODUCTION

Currently, there are two teaching problems occurred in the network teaching: one is collaborative learning or activities and the other is the issue of instructional interaction network. The latter has become a bottleneck in the development of online teaching as online teaching interaction design education has become a major driving force in the current network. Computer games become increasingly popular, according to data provided by the Ministry of Culture, in 2001, only the scale of the global online gaming market reached 16.5 billion U.S. dollars. It attracted gamers beyond the imagination as the 30% of the Internet users is online gamer. The profit earned by online game is amazing, but it is a sharp double-edged sword. Most of the people hold a negative attitude toward the game, but the game has played an important role in the development of human civilization as well as the growth of human individuals. Moreover, people have gradually come to discover and study the educational value of the game. So the game-learning is put forward, whose aim is to put people into the first place, to respect for education and humanity, and to pay the main emphasis on culture and creativity of learners.

This article attempts to explore the learning network teaching interaction design in the view of game-learning, and learn from its advantages as reference to the network teaching interaction design.

II. GAME- LEARNING

Game- learning is to select the appropriate development tools, evaluation methods, teaching strategies taken from game in the process of instructional design. It is worthwhile to not that learning is not a simple game with learning, either the use of digital tools for learning. However, it is to make full use of the game education in teaching where students learn in more pleasant environment. It focuses on people-oriented, human nature education, and the main body of students and creativity.

A. The development of the game

The game is ubiquitous in the animal kingdom, and happened even earlier than the existence of mankind. The game accounts for a large proportion of the human social life, and the percent has increased with the development of society. In primitive societies, the game was basically a simulation of real-life situations, or trained skills in games. Entering into the class society, mankind created the wars which are the background of many sports games. All the games are accompanied by social development of modern science and technology, along with the evolution and development of the social life. In some degree, it has reflected the characteristics of each era. In the digital and the Internet 21st century, our game is also reflected the characteristics of the times. Online game is the most typical, which has become widely accepted by integration of the entertainment, sports, simulation and interaction.

B. The theory on the game

Theories on the game is as follows:

1) Instinct

Schiller believes that human life is subject to the double bondage of moral and material where one will lose ideals and freedom. So people create the game, a freedom world, by use of the remaining spirit, which results in a human instinct.

2) Residual energy

Residual energy is proposed by British philosopher Herbert Spencer, which further to add the Schiller's instinct. The theory is there is still remaining energy after completing the main tasks of keeping human life and bearing. the game is an outlet to remaining energy. There is on utilitarian purpose in the game itself while its goal is a game process.

3) Practice

Herbert Groos , German biologist, revised the theories of British philosopher Herbert Spencer 's residual energy and Schiller's instinct. The theory is that the game is neither without a purpose nor the actual activities. Game is a preparation for the future life, such as girls feed dolls to act as a mother while the boys play war games to simulate the battle.

4) Piaget's games

978-0-7695-4818-0/12 $26.00 © 2012 IEEE
DOI 10.1109/DCABES.2012.74

Game theory is derived from Piaget's cognitive development theory, which is an important faction of the current research on children's play. According to Piaget's theory, wisdom comes from the balance between assimilation and responsive. He thinks the game is out of balance between assimilation and conformance. Why do children play it? He believes the game provides children a solid understanding of their structure and access to new opportunities for the development of their emotions. Stages of cognitive development determine their different games. He divided game into three categories: practice of the game, symbolic play and the rules of racing game, respectively corresponding to the perception of exercise stages, the first stage and the concrete operational stage during the cognitive development.

C. Characteristics of the game

Huizinga, a Dutch scholar, summed up the game characteristics as follows:

- voluntary act;
- a certain distance to the normal life;
- time and space constraints;
- not an important event, but very attractive to those who participated;
- rule-bound;
- to promote the formation of organization among private players.

III. ONLINE GAME INTERACTING WITH NETWORK TEACHING ——SITUATED COGNITION THEORY

A. The overview of the situated cognition theory

Situated cognition theory has become a research focus in contemporary western learning theory. It has become another important research direction after stimulus – response learning theory based on animal behavior and information processing learning theory. Since the late 80s, the situated cognition theory can provide meaningful learning and promote the transformation of knowledge to real life situations, in which learner obtain not only a lot of factual knowledge, but the genuine cultural practice. The results show that the knowledge gained in certain situations is more useful than the so-called general knowledge.

B. Overview of network teaching interaction

Currently, the definition of instructional interaction are as followers:

Definition I: Learning interaction happens between a teaching system and the learners, including the exchange of relevant information, real-time, dynamic, mutual giving - the extraction process"(Merrill, Li & Jones, 1990);

Definition II: learning interaction is a two-way communication that two or more interactive individuals complete learning tasks or the establish social relations during the learning. (Gilbert & Moore, 1998);

Definition III: Daniel and Marquis define interaction from the difference between the interaction and the independent. They proposed the distance learning includes independent learning activities and exchanges with others (Daniel & Marquis, 1979), while the first activity is referred to as independent activity, and the latter category interaction.

The first two definitions are proposed in the traditional teaching environment, and the definition III failed to clearly define the content of teaching interaction. Interactive online teaching aims to develop learner knowledge acquisition and capacity-building in the network environment. There is mutual exchange between the learner and the learning environment, including the learner and learning materials, the exchanges and interactions between learning support organization (such as counseling teachers, counselors, administrators, institutional settings, etc.) (Chen Qing, 1999). Learners are the core of network teaching interaction, whose roles are to change the behavior of the learner and to promote the behavior of the learner closer to teaching objectives.

C. Characteristics of network instructional interaction

Compared with traditional classroom, features of online teaching: interaction are as follows:

1) Learners are equal in the network teaching interaction

Equality of educational opportunity is one of the principles of higher education activities. Multimedia computers and Internet-based network communication technology create the ideal teaching environment for the realization of this principle. It is a profound impact of advanced electronic communication technology and computer networks to people's learning and life, where it is possible to exclude the inequality generated from the identity and individual background.

2) The roles of student and teacher change in the online teaching interaction

the teacher in the network teaching has become a mentor to students in independent study; an assistant to build students' own cognitive structure; and a navigator to access learning resources rather than the monopoly. On the other hand, learners are autonomous in the network learning, where learners can facilitate the learning time, learning speed, learning content, communication objects in personalized control. However, due to the unpredictable learner's interactions and interactive content, there are higher requirements for interactive teaching guide the design.

3) Time and spatial separation of teaching interaction

In the network learning, the time and spatial separation exist between teachers and learners. In such case, interaction happens in different locations, and the communications in view of time are asynchronous and synchronous. Moreover, with the development of network technology, it can achieve synchronization in two dimensional or multidimensional. Related technologies include network video phone, Internet real-time lectures and real-time network meetings. In this interaction, those who share a common task are in the joint activities, where the students may not adequately think but the exchange is very timely. And it has an important role in the formation of positive learning environment and social environment.

IV. THE INSPIRATION AND INFLUENCE OF ONLINE GAMES ON THE NETWORK TEACHING INTERACTION DESIGN

A. To stimulate learning motivation

Motivation is to create and maintain the activities of individuals, and to guide the activity towards a target to meet the individual needs. As in the network teaching communication between learners and others are not face to face, learners is always facing a computer in the learning process, and there is no social atmosphere compared to traditional classroom teaching. As the lack of emotional aroused in this particular teaching methods is not conducive to a positive learn, the key to the success of online teaching is to take a variety of ways to trigger interest in the learning, stimulate motivation, and reinforce learning initiative. Only if a person takes an interest in things or activities with the motive of activity, one will persist in overcoming difficulties.

Network teaching can stimulate learning motivation in these following ways:

1) To provide learning incentives

problem creation has proved to be an effective way in stimulating learning motivation and waking up cognitive drive. More problem-based learning activities should be engaged in the network teaching to create a discordant between content and learning psychology. Therefore, it causes learners cognitive interest so that the students actively thinking about the problem in order to achieve Solution.

2) To give learners successful experience

Learners in the learning process continue to be some of the successful experience, which has been one of the most important means in stimulating learning motivation in the modern psychological research. Once learners can experience success, they are enhance self-efficacy (self-efficacy) with confidence in learning activities, so that students continue to be achieved in some specific goals, and they are learning every step in the growth and progress. So learners are offered the opportunity to experience the joy of success, and make them aware of their ability.

3) To create a real situation

owing to the attractive role-playing in online games, the learner's role in certain situations can greatly improve the learner's active participation. Cognitive theory emphasizes that the study is conducted in an environment similar to the situation with the real situation, while it is difficult to achieve in the traditional teaching model. However, virtual reality technology does achieve this. For example, students can experience a virtual driving to avoid the possible risk, but also to eliminate unnecessary waste in the real driving. The multimedia information on the learner's multi-sensory stimulation can increase the interest in the learning content to help learners to obtain and maintain knowledge.

4) To enhance the clarity of learning objectives

Learning goal is found to simulate the incentive for external motivation. Only with clear learning objectives, learners have a learning orientation, and can have passion for active learning. Learning objectives should be presented in a clear way, and the objective should be specific and realistic. Practical experience and psychological studies have proven that too difficult or too easy objectives lead to lose confidence. Therefore, before designing specific objectives, it is required to study the learners' learning state, such as the possessed knowledge and learning styles. Also goals must be so challenging that students can actively learn.

B. To promote the interaction between learners and teaching resources

Learning in a networked environment is neither teachers in traditional schools, nor the help and supervision between students, nor the intangible impact on campus. As it mainly relies on the learners themselves to complete, there will have higher requirements for the design of teaching resources compared with traditional face to face teaching. A teaching resource designed to promote the learner's independent learning can meet the individual needs of learners.

Contemporary online teaching has been changed the traditional three centers (namely, teacher-centered, textbook-centered, classroom-centered) to a modern three centers (namely, learner-centered, resource center, community or social activities center). This requires the design of online teaching resources from the perspective of the learner design. When teaching resources designed note that learners have different learning styles, learners' cognitive learning styles are also different in different.

Now, the controllability of the game is the key to attract the players in the online games. The game offers a variety of roles, different backgrounds, and many tools by which gamers might start over owing to failure. Players have great control authority in operations which they allow to fully play in accordance with the rules of the game. In recent years, learner-centered teaching design has been firmly established. The network self-organization and the open nature have applied to the interactive design. It should be able to control in the learning process of Web-based self-learning, including autonomous control and process control learner (or teacher control).

In online teaching, as an individual independent study the learner are varied in the level of knowledge, learning motivation, and cognitive styles. Their learning process is completely personalized, for example, there are individual differences in the learning path and learning strategies. The following two aspects have shown the personalization: the use of student model as a tool to describe the individual differences; optional additional teaching programs to accommodate individual differences of learners.

In online teaching interaction, feedback for learners is required to not only be timely, but also the message rather than a judge, so that learners can be left to reflect. And learners should enable know the current learning process, the distance away from the learning objectives, and the learning objective. In the process of learning learners are provided with heuristics which the support task should be created to help learners, where learners are provided a scaffolding, and gradually removed the scaffolding erected until the learner can be fully independent learning.

V. THE TECHNOLOGY OF GAME LEARNING NETWORK TEACHING SYSTEM

A. The front technology of systems development

HTML markup language, JAVA and scripting languages

Hyper Text Markup Language (HTML) is the simplest interactive content development tool. Webpage generated with the HTML is transferred into HTTP protocol to play on the WWW, which is a platform-independent, good portability, multimedia support, and comprehensive openness and good scalability. An important feature of Java is platform independent, but multi-threaded programming. Programs in Java can be transplanted from one platform to another platform without modification. But HTML itself is limited in dynamic features. A variety of collaboration tools can automatically generate HTML, and can realize integration of the multimedia data (maps, text, sound, image),

such as FrontPage, Dreamweaver, etc., which all support the multimedia formats of mov, avi, jpg, gif and so on.

B. Back-end technology of systems development

In online teaching, it needs to manage large amounts of data such as students personal information, various types of teaching resources, exam, exam results, online learning activities, discussion board. These data are not only large but also fast updated with the conduct of online teaching, so database management are used to update the data. It can be said that the database service is the basis of online teaching background.

Database management systems support for dynamic data types and dynamic protocol, including Access, SQL Server, Oracle, Active Server Pages (ASP), DHTM programming technology, Java Applet, JavaScript, ActiveX VBScript, ActiveX Data Object (ADO) and so on. They dynamically adapt to the changing environment, satisfy the requirements of teaching and learning. Database connection technology is Interface program between the server and web, through which the HTML files are associated with the database. It is the bridge between the learners to access the database. According to the application programming interface, the learners allow to read database files. Current database connection technologies are CGI programming, Microsoft ODBC, DAO, RDO, ADO and other technology solutions.

VI. CONCLUSION

It has become a hot field in distance education by the use of information technology for interactive distance education. And there are many case studies in the literature. However, it is a very complex issue with regard to how to promote student interaction to enhance distance learning. Therefore, it is difficult to directly instruct the teaching design owing to the lack of the relative research and theory of the general characteristics. This article explores the design of the network teaching interaction in the new perspective of the game learning, promotes interaction by full use of the characteristics of online games, where students act self-learning in a more relaxed atmosphere.

REFERENCES

[1] Zhou Yuxia, Li Fangle,Xie Yongxiang,"Transfer of Learning in an Educational Game",Distance Education in China,No.4,Apr.2011,pp.79-83.

[2] Liu Ling, He Jin ,Wu Xiaoning ,"Design and Implementation of Role Playing Games Learning Community Based on Situated Cognition Theory", Distance Education in China,No.8,Aug.2010,pp.57-61.

[3] Zhong Hongrui,Zhou Zhuohui," Impacts of Game-based Learning on Learning Motivation: An Action Research", Modern Educational Technology ,vol.22, No.3,2012,pp.91-94.

[4] Wang Bin,Wu Zhongjie,"Considering of Learning Foreign Language through Edutainment—Based on RPG Game", Modern Educational Technology, vol.22, No.1,2012,pp.77-79.

[5] Zhang Qi,Chen Lin,"The Survey and Outlook of EducationalGaming Research in China",Open Education Research,vol 15,No.5,Oct.2009,pp.107-110.

[6] Guo Xiu," On learning Motivation of Students," Educational Theory and Practice, vol. 6,2004,pp.58.

[7] Zhang Jianwei, Sun Yanqing,"On Distance Learning Efficacy and related Factors," Beijing Normal University, vol.4,2003,pp.73.

[8] Pang Guimei,"On the Game and Its Educational Value",Tianjin Academy of Educational Science, vol.6,2002 ,pp.11-13.

[9] David H. Jonathan as editor, Tainian Zhen, Youqun Ren as translators,"the Theoretical Basis of Learning Environment", Shanghai, East China Normal University Press,2002,pp.5-30.

Design and Implementation of Address Filtering in Network Handoff Based on IPv6

Feng Guochang, Chen Siguo, Mou Heming, Shi Xianwei, Wei Da
College of Computer Science and Technology
Jilin University
Changchun, 130012, China
weida@jlu.edu.cn

***Abstract*—In order to guarantee the security of the communication between the in-vehicle IPv6 subnet and internet, a scheme is putted forward based on the address filtering in the network handoff. This scheme considers the address filtering in the network handoff, when the mobile node came into a different network, it only needs to filter its own IPv6 address without the need to re-access authentication. Tests show that the scheme can not only guarantee the security of the network handoff but also meet the time demand of the system.**

Keywords-IPv6, network handoff, address filtering, in-vehicle gateway

I. INTRODUCTION

With the rapid development of vehicular communication technologies and the IPv6 network, the ECU (Electronic Control Units) can communicate with network servers. As in the current, the CDMA network of China does not support IPv6, so the in-vehicle ECU, which have Ipv6 address and use the CDMA network for communication, can not be accessed by network servers. In a mobile environment, mobile nodes need to move between different access points. Wireless network is open and vulnerable to various attacks, which has brought great challenges to the wireless mobile network security. Therefore, in the mobile IP network, we are not only to consider the wireless transmission channel to support the mobile IP but also the network security.

Mobile terminal switching between different regions in the homogeneous network is called horizontal handoff [1]. Compared with horizontal handoff, vertical handoff is in the heterogeneous network, and the vertical handoff process can be divided into three parts: network discovery, switch determine and switch execution [2]. For seamless switching, there are already some researches on switching mechanism to improve the performance, such as Policy-based approach [3], neural network-based approach [4]. These methods are not suitable for limited computing power of the in-vehicle gateway.

II. ANALYSIS OF EXISTING TECHNOLOGIES

The Mobile IP principle has the HA (Home Agent) and the FA (Foreign Agent).The HA is located in the home network, and the FA is in the foreign network. In Mobile IP, the host which communicates with the MN (Mobile Node) is defined as CN (Correspondent Node). If the MN is in the home network, It will use the normal IP protocol to communicate with the network servers; when the MN is in the foreign network, the MN will apply for a CoA (Care of Address) from the FA, and then the CoA is forwarded to the HA to register, The packets are sent to the HA by the CN at first, and then the HA will encapsulate packets and send to the FA through the tunnel .After the packets reach the FA, the FA will re-opened the packets and send the original data packets to the MN.

In the Mobile IP protocol, the MN needs to move among different Access points, and communicate with the CN through its FA and home network. So the security and reliability of the foreign network affect the security of the communication. At present time, there are mainly two techniques to solve the problem of data communication security in wireless networks.

- VPN (virtual private network). It uses the internet or other public internet infrastructure to create and provide a private network for users, and has the same security and functional security as the Private network.
- Authentication Mechanism. It adds a trusted user list to the access points in the wireless network. Only existing in the list of network devices can join a wireless local area network, otherwise it will be rejected to connect.

But the mobile environment requires highly real-time protection, and the MN in the different access point handoff will consume a certain amount of time. It is not possible to access authentication in each handoff.

Reference [5] and [6] has realized the switch in heterogeneous network without the security mechanisms. In this paper, we propose the security mechanisms in the mobile handoff, and there is no clear impact on real-time demand for mobile network.

III. SYSTEM ARCHITECTURE

System architecture shown in Figure 1.The tunnel proxy server can as HA, the in-vehicle gateway can as the MN, where the MN is an intermediate point connecting with the Internet. As the WLAN coverage area is limited and it is not able to meet some of long time limit application. And the CDMA network access fee is higher then the WLAN internet's. Considering the rate of network traffic and the use of cost, we provide two internet modes on the in-vehicle gateway: CDMA and WLAN. Within WLAN coverage, you

978-0-7695-4818-0/12 $26.00 © 2012 IEEE
DOI 10.1109/DCABES.2012.46

can communicate by WLAN, otherwise, the CDMA network. When the car starts, the CDMA network is the default way to communicate with the network servers. If the car comes into the WLAN coverage area, the network way will automatically switch.

Each ECU of the car has a separate IPv6 address. So in fact each car is an IPv6 subnet, and each ECU of the car can be accessed by network servers. As in the current time, the CDMA does not support the IPv6 protocol, we establish an IPv6 over IPv4 tunnel [7] between the in-vehicle gateway and proxy server.

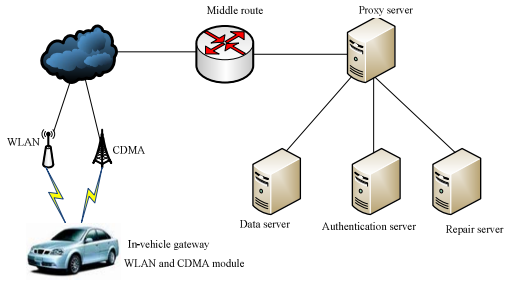

Figure 1. System Architecture

IV. IMPLEMENT OF THE IP FILTER IN HANDOFF

In our implementation, the in-vehicle gateway has a fixed IPv6 address, the ECU of car also has the fixed IPv6 address. At the in-vehicle getaway start-up, it sends packets to the FA to register IP information. The registration packet contains the IPv6 address and the current IPv4 address of the in-vehicle gateway, as well as the IPv6 address of the ECU. So we need to build two lists on the proxy server as shown in Figure 2.

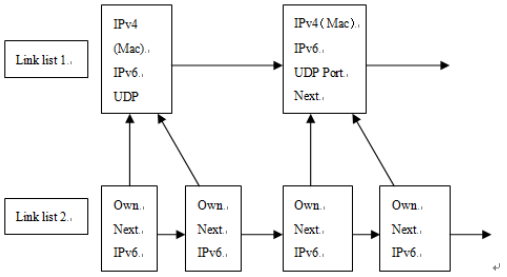

Figure 2. The Structure of The Link List

In the link list 1, the node saves the vehicle gateway address of Ipv4 and IPv6, as well as the encapsulated information, such as the MAC, the UDP port. In the link list 2, the node saves the IPv6 address of the ECU, there is an own pointer to point to which in-vehicle gateway it belongs.

The client on the vehicle sends the authentication message to the authentication server. After the message has been packaged by the in-vehicle gateway, it will be sent to the protocol conversion proxy server. For the authentication packets, the proxy server will not filter or release. Once the authentication server receives the message that the client sends for authentication, it will send an authentication feedback upon the requested information. There are two copies of the feedback, one sends to the vehicle terminal, and the other sends to the proxy server which is contains of the reliable IP address and the services permission level.

In the proxy server, we need to run a Linux kernel, which used the hook function NF_Ipv6_PRE_ROUTE of the Netfilter framework to receive the authentication information that the authentication server sends, and stored the authentication information to the link list for IP filter.

At the mobile terminal communication with the internet, we default that the CDMA is the first start. For the first time to communicate with the network, it needs to access authentication and store the authentication information to the proxy server. In normal communication, the packet put through the proxy server all needs to IP filter. So only the certified mobile node can communicate with the network. When the mobile terminal finds a new access point and its signal strength is greater than the threshold, the mobile terminal sends a DHCP request to obtain a new address. Then the vehicle gateway sends the new address to proxy server for binding update. After that, it can communicate with the network by the new address. In the process, it does not need to access authentication, but still filter the IP of the packet to the network. The overall process is shown in Figure 3.

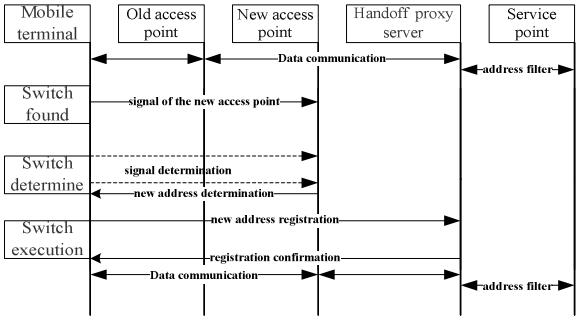

Figure 3. The Process of IP Address Filtering in Handoff

The network handoff IP filter process can be divided into two parts: the discovery and switch of the channel and the tunnel proxy IP filtering.

A. the discovery and switch of the channel.

- Switch found. In our implementation, we default that the wireless network equipment of the in-vehicle gateway is in the CDMA network coverage. At the first, we start the CDMA devices to communicate with the network, and then determine the MN entering or exiting the WLAN coverage is available by detecting the WLAN network signal, and then contrast the intensity of the network signal and the threshold we set to determine whether to switch.
- Switch to determine. Suppose you are using the CDMA network, and found the signal strength is greater than the threshold we set. Then we will switch to the WLAN from the CDMA, otherwise, switch to the CDMA from the WLAN.

- Switch execution. For example, we switch to the WLAN from the CDMA. At first the in-vehicle terminal sends a DHCP request to the wireless access point. When it obtains the IPv4 address, it writes the IPv4 address to the file. And then the file will be transferred to the virtual network device in the in-vehicle gateway. The virtual network device modules in the in-vehicle gateway contrasts the IPv4 address in the file to the source IPv4 address of the last sent message. If not, it will send the update packet which contains the current IPv4 address and IPv6 address information to the tunnel proxy server.

B. the tunnel proxy IP filtering.

In the proxy server, it needs to determine the type of the received IPv6 packets. For the registration packets, we need to establish the relevant information based on the contents of the packet in the link list 1 and the link list 2. For the update packet, we need traverse the link list 1 at first to find the same IPv6 address of the node, and then update the IPv4 address. For the normal communication packet, we need to filter the IP address to ensure the security of the node that has the communication privileges communicates to the network.

The address filtering is to filter IP packets flowing through the proxy server and intercept the packet that did not authorize. Specific process is shown in Figure 4. If the packet of destination address is not the authentication server, we need to filter the source address of the packet according to the filtering address link list to determine whether the packet is released. First of all we need to judge whether the source address of the packet is in the list. If it exists, to determine the service permissions level: 0(authorized), 1(repairable), 2(unauthorized). If the privilege level is zero, release the packet; if the privilege level is one, then to determine whether the destination address is the repair server, if it is, the packet release, otherwise the packet is discarded.

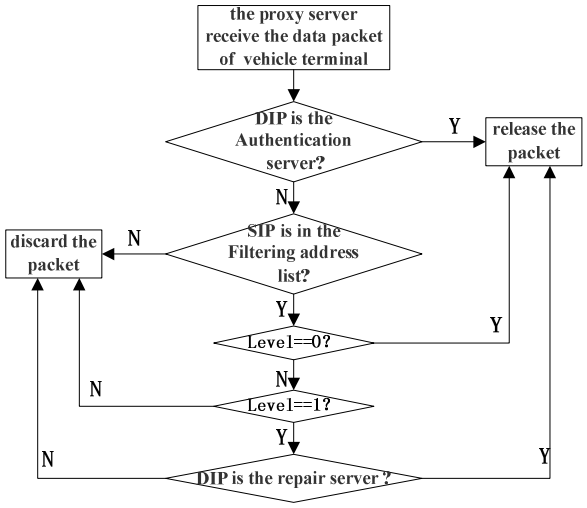

Figure 4. the Process of the IP Address Filtering

V. EXPERIMENTAL ANALYSIS

The test environment is as following: our test car is a Jetta, the AP is the ASUA WL-520GC, the predetermined signal threshold is 30dB. The proxy server is a PC (personal computer), its operating system is Linux with the kernel version of 2.4.20. The configuration of the vehicle gateway is as following:(1) The CPU is S3C2410 with 32-bit RISC microprocessor; (2)10M/100M adaptive Ethernet interface; (3)64Mbytes SDRAM and 16Mbytes FLASH; (4)Ralink RT 73 series Wireless LAN; (5) FD-810CDMA modules. The operating system of vehicle terminal is the ARM-Linux with the kernel version of 2.4.18-rmk7.

The CDMA covers all test area. When the car is driving to the coverage of AP, and the signal strength is greater than 30dB, it will switch from CDMA to WLAN, when the signal is less than 30dB, it will switch from WLAN to CDMA. Each time the car can switch twice through the coverage of AP. Five laps as a group, we tested for the packet loss and the handoff delay under different speed. The results are shown in table 1.

TABLE I. RESULT OF TEST

Speed(km*h-1)	10	20	30	40	50
C-W latency(ms)	140	142	146	150	178
Pocket loss rate(loss packet per group)	0	0	0	1	1
W-C latency(ms)	1120	1148	1250	1762	1843
Pocket loss rate (loss packet per group)	1	0	0	1	2

In the test, the car speed can not be fully maintained, so we use the average speed as the reference value. It can be seen from Table 1 as the speed increasing, the handoff latency and packet loss rate have increased. And the handoff latency and packet loss rate can be acceptable for the most of the automotive applications.

For the safety test, we use the uncertified vehicle terminal to send the connection request to the network server. Tested result is that the uncertified vehicle terminal can not connect with the network.

VI. CONCLUSIONS AND PROSPECTS

This article has realized the IP filter in network handoff, it can make the node of vehicle which has the IPv6 address to access the network security. With only filtering the IPv6 address in the proxy server side, it makes that the mobile terminal do not need to re-certificate after the network handoff. The tests show that, through the IP filtering, the handoff latency and packet loss rate are still meeting the majority of automotive applications, and ensure the credibility of the mobile terminal. In the following work, we will continue to explore the better handoff strategies and algorithms to reduce the handoff latency and improve network performance.

REFERENCES

[1] Liu Min, Li Zhong cheng, Xu Gang , etal. Performance evaluation models and metrics for vertical handoff algorithms in heterogeneous wireless network [J]. Journal of System Simulation, 2007, 19(2): 277-281.

[2] Stevens Navarro E, Wong V W S. Comparison between vertical handoff decision algorithms for heterogeneous wireless networks[C] Proceedings o f the 63rd IEEE Vehicular Techno log y Conference, Melbourne, Australia, 2006.

[3] Fang Zhu, McNair J. Optimizations for vertical handoff decision algorithms [C] IEEE Wireless Communications and Networking Conference, Atlanta, USA, 2004.

[4] Pahlavan K, Krishnamur thy P, Hatami A. Handoff in hybrid mobile data networks [J] . IEEE Personal Communications, 2000, 7(2) : 34-47.

[5] Qu Liang dong, Liu Yan heng, Wei Da, etal. Realization o f communication between in-vehicle information and internet based on in-vehicle gateway [J] .Chinese Journal of Scientific Instrument, 2008, 29(11): 2330-2334.

[6] QU Liang-dong, LIU Yan-heng,WEI Da. System of vertical handoff for heterogeneous wireless network based on VPN on in-vehicle gateway[J]. Chinese Journal of Scientific Instrument, 2010, 40(05). Pp.1292-1297.

[7] Tushar M.Raste, D.B.Kulkarni. Design and implementation scheme for deploying IPv4 over IPv6 tunnel [J] .Journal of Network and Computer Application, 2008, 31, pp.66-72.

MPI-Based Heterogeneous Cluster Construction Technology

Yucheng Guo, Dongxu Hu, Peng Wu
Department of Computer Science
School of Computer Science and Technology
Wuhan University of Technology Wuhan, Hubei
Ycheng.g@gmail.com; hdxlgd@163.com; ejoywx@163.com

***Abstract*—Nowadays, the applications of MPI-based clusters are used widely, such as the damage prediction of nuclear explosion and gene decryption. However, the usages of MPI-based heterogeneous cluster are nearly reported in contrast to the MPI-based homogeneous clusters due to the immature technology. This paper focuses on building a MPI based heterogeneous cluster with the MPICH2, which is released last year and has not supported the heterogeneous cluster yet. Beside, we give the reasons and test results in the paper to illustrate the benefits of using the MPI-based heterogeneous cluster without virtualization.**

Keywords:MPI;cluster;heterogeneous cluster;virtualization

I. INTRODUCTION

A computer cluster is composed of fully functional computers. The nodes of a cluster are connected by high-speed link (twisted pair or optical fiber). The nodes can work coordinately; the internal architecture of the cluster is opaque to the user. Due to the good availability, high extension, and considerable performance-to-price ratio, the cluster technology has attracted attentions of HPC (High Performance Computing) and HPS (High Performance Service) in applications, especially in industry applications, and academia researches. The HPC is concerning with specialized computing hardware, thousands of computers operated in parallel, and distributed storages or processes "in the cloud" to solve problems which are too complex for single computer or network to address alone. There are two kinds of clusters for the HPC, homogeneous or heterogeneous. Clusters may be built with homogeneous or heterogeneous architectures. In most cases, the homogeneous cluster is preferred because it is easier to agglomerate, ascribing to their identical hardware architectures, OS and so forth. Notwithstanding the homogeneous clusters have many advantages, it is difficult to keep the cluster homogeneous as nodes break which need to be replaced, or you want to upgrade the nodes in your cluster. The heterogeneous clusters are more considerable compared with homogeneous clusters.

Currently, MPI (Message Passing Interface) is a standardized and portable message-passing system framework to function on a wide variety of parallel computers. The MPI standard defines the syntax and semantics of a core of library routines useful to a wide range of users writing portable message-passing programs with common programming languages. Several well-tested and efficient implementations of MPI, such as MPICH2 etc., have been issued. These fostered the development of a parallel software industry, and encouraged development of portable and scalable large-scale parallel applications for HPC programming [1, 2]. Since it is easy to acquire the state of resources and processes in MPI, for solving the heterogeneity issues in cluster implementation, the MPI becomes a natural choice on heterogeneous platform [3]. However, popular implementations of MPI most likely support homogenous clusters rather than heterogeneous one. The recent issued version of MPICH2 also does not support the heterogeneous clusters [4]. This paper proposes an approach to build heterogeneous clusters based on the MPI mechanism, and, taking the MPICH2 for instance, explores the detailed techniques. Finally the paper has done some performance comparisons between the virtual machine (VM) and physical machine (PM) cluster implementations with the test data obtained from the heterogeneous cluster.

II. THE ISSUES OF CONSTRUCTING THE HETEROGENEOUS CLUSTER BY VIRTUALIZATION TECHNOLOGY

A. *The Definition of Heterogeneous Clusters*

Generally speaking, the differences among ISA (instruction set architecture), API, low-level implementation of language features, and memory interface hierarchy all belong to the category of heterogeneous cluster.

The definition of heterogeneous clusters can be divided into four types: (1) Processor heterogeneity; the processors of the connected computers may have various architectures (SMP, MMP, GPU, NUMA), various CPU cores or instruction sets. (2) Runtime environment heterogeneity; different Operating Systems, scheduling systems, authentication realms, etc. may locally administrate multiple resources across the computing platform. (3) Network heterogeneity; there are diverse communication protocols, communication lines with different performances among mixed networks. (4) Key component libraries heterogeneity of the cluster platform; such as different version of MPI in each nodes of the heterogeneous cluster.

B. *How to Convert Homogeneous to Heterogeneous*

Usually, there are two ways to convert the homogeneous to heterogeneous. One way is replacing the heterogeneous

978-0-7695-4818-0/12 $26.00 © 2012 IEEE
DOI 10.1109/DCABES.2012.116

nodes in the cluster so that each node has the same CPU cores, OS and so on; however, these replacements are time-consuming and creating extra resources redundant. The other is resorting to virtualization, it takes advantage of virtual machine in order to convert heterogeneous to homogeneous, and hence the redeployment of software will be simplified. The applications of virtualization technology allow the users to run several VM (virtual machine) at one physical machine (PM); the Operating System of each VM can be different.

C. *The Mainstream Virtualization Technologies and Softwares*

Hitherto, Xen and VMware are the most popular virtualization products in the market; both of them offer enterprise-ready virtualization. The architecture of VMware ESX Server is based on Direct Computing (executing the ring3 level virtual machine codes in the hardware directly) and Binary Decoding (dynamic compilation for ring0 level codes) [5]. Basically, ESX makes sure that different versions of OS, which based on the X86 architectures, can run on virtual machine without modification. In terms of the architecture of Xen, it takes advantage para-virtualization, which modifies the virtual client Guest OS kernel and run with VMM (Virtual Machine Monitor) cooperatively to achieve high performance [6]. Xen is a native, or bare-metal hypervisor; it runs in a more privileged CPU state than any other software on the machine.

D. *The drawback of Virtualization Technologies and Softwares*

The ESX is too expensive, Xen is free, but it cannot deploy in Windows yet. In the test of VMware Infrastructure 3 Suite, the VMware ESX Server gives rise to the deterioration of performance, about 10% to 20%, as for Xen3.0, the ratio of deterioration was nearly 3% [7]. No matter VMware or Xen, both of them cannot neglect the Buckets Effect, it means that in the virtual machine, each virtual OS executes the instructions, transferring the signal to the hardware, but there only one real hardware exists, if too many virtual machines run on the same system, the I/O operation, the resources of CPU, even the volume of RAM all become the bottle neck. What's more, the emulation drains much of host system's resources. The emulator has to intercept most of the instructions used for guest-kernel-to-application communications and has to simulate a complete set of virtual hardware devices; this emulation implies several layers imposing a natural lower bound for extra network latency, which cannot be undercut. Last but not the least, both VMware and Xen requires a huge amount of memory, the total amount of memory that is allocated will be a bit bloated, these are the problems the user cannot ignore, which will lead to the deterioration of system performance eventually.

III. HETEROGENEOUS ENVIRONMENT BASED ON DIFFERENT MPI-SUPPORTED VERSIONS AND CURRENT PROBLEMS

The virtualization technologies bring out the deterioration of clusters' performance; hence some researchers have been trying to construct the heterogeneous clusters directly based on MPI. However, most of their researches focused on the heterogeneity of hardware, few about the heterogeneity of software.

As heterogeneous computing provides an opportunity to maximize available computing resources, there has been a fair amount of works done on inter-process communications in MPI applications. Many current MPI implementations support the operation of applications within such an environment. For example, HeteroMPI aims at solving the heterogeneous computing, extending the standard MPI, providing relevant MPI interfaces in order to support heterogeneity. It allows the application programmer to describe a performance model of the implemented algorithm in generic form in order to deal with the network heterogeneity, but it cannot handle the case of different Operating Systems. MPICH-VMI2 uses high performance protocol in the internal cluster, each node in the cluster communicates with each other with TCP/IP protocol, however, it does not support the simultaneous use of multiple network interfaces on a single node. MP-MPICH stands for Multi-Platform MPICH, it is a modification and extension to the MPICH distribution, but the MP-MPICH project is finished and the software is no longer being maintained, so that few users would like to choose MP-MPICH without technology support, besides, it only complies with the MPI-1 standard. LAM/MPI supports the heterogeneity of processor architecture, it can deal with the conversion of sequence of bytes, but if the length of data or format is different, in this case, LAM/MPI can do nothing about it. As for PVMPI, it is a powerful combination of the proven and widely ported Parallel Virtual Machine (PVM) system and MPI. PVMPI is transparent to MPI applications thus allowing intercommunication via all the MPI point-to-point calls [8]. Indeed, there are two major disadvantages in PVMPI; firstly the user has to change his source codes and secondly he may only use point-to-point communication after having created an inter-communicator between the different machines. Again, the user has to add some non-standard calls to the code; and only point-to-point communication is possible.

Although the application prospect of heterogeneous cluster based on MPI is appealing, it doesn't get widely used, especially in the case of different Operating System. Most of heterogeneous MPI cluster aims at dealing with processors heterogeneity, such as the Cone Bean Tomograph [9], the team built the cluster with 6 computers, the OS in the nodes is Solaris with different processor architectures (Sun 4/330, Sun 4/470, Sun 4/490, SPARC 2), and the cluster is based on MPI. Some researchers develop some kind of portable libraries to deal with parallel MPI application in

heterogeneous environment, such as MPIXternal, which tries to circumvent the obvious semantic gap within the current MPI standard that allows an application programmer to develop heterogeneity-aware application without the need of relying on non-portable optimization features provided by MPI implementation [10]. Last but not the least, some researchers succeed in a new MPI implementation (LMPI stands for Lightweight MPI) for heterogeneous embedded system [11].

All in all, most of the researchers attempt to take advantage of MPI in order to construct the heterogeneous cluster, aiming at dealing with the heterogeneity of hardware, but not the heterogeneity of software. Hence in this paper, we mainly discuss MPI-based heterogeneous cluster construction technique on software layer.

IV. THE KEY TECHNIQUE OF CONSTRUCTING MPI BASED HETEROGENEOUS CLUSTERS WITH DIFFERENT OS

In this section we try to construct a MPI based heterogeneous cluster, on each node of which different operating systems are running. For simplicity we take two nodes as example and use the recent released MPICH2 as the MPI platform.

A. MPICH2

MPICH2 is a high-performance and widely portable implementation of the Message Passing Interface (MPI) standard [12]. The reasons that based on MPICH2 we build the heterogeneous clusters are as follows:

1) It provides a MPI implementation, which efficiently supports different computation and communication platforms including commodity clusters (desktop system, shared-memory system, multicore architectures), high-speed networks and proprietary high-end computing system (Blue Gene, Cray).

2) It is enable cutting-edge reseach in MPI through easy-to-extend modular framework for other derived implementation.

B. The Generic Deployment

We take the steps as follows:

At first, we should choose some nodes in order to build the hardware environments of the cluster. Secondly, the installation of different versions of Operating System (such as Windows, Unix or Linux) is essential. Then we install the same version of MPICH2 and ping each node in the cluster so that we can confirm the connectivity.

We take the tests in the cluster, which contains two nodes.

In node 1, we install ubuntu10.10 and set the host name as “tlibx”, the IP is 192.168.128.128, the user name “tlib” and password;

Then we install C/C++ development environment, input the command “sudo apt-get install build-essential” and “sudo apt-get install gdb”;

Later, we install SSH service, execute “sudo apt-get install openssh-server”, and then implement the password-free SSH connection,

A set of commands is shown as below:

```
shell$ssh-keygen -t dsa
shell$cd ~/.ssh
shell$cp id_dsa.pub authorsized_keys
shell$cd ../
shell$ssh tlibx
```

At last step it should make sure that the MPICH2 is compiled and installed. The developers of MPICH2 provide a vital hybrid process management called “SMPD”, which can be used in Unix, Linux, and Windows. The process manager of Unix and Linux is called “HYDRA” by default, but HYDRA doesn’t support MS Windows, that’s the key point we choose SMPD both in the test (we should use the same version of MPICH2, password). Extract the pack of mpich2-1.4 to the directory of “/home/tlib/mpich2”. Having accepted to choose the same process manager (HYDRA), we should choose the same communication channel of MPICH2 on both Windows and Linux. There are two kinds of channels: Nemesis or Sock as shown in Fig.1. The Nemesis channel is a new low-latency channel that uses shared memory for intra-node communication and various network for inter-node communication; the Sock Channel is based on TCP sockets.

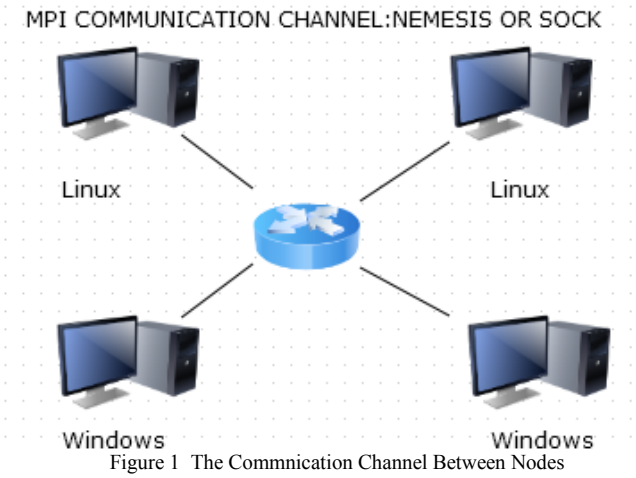

Figure 1 The Commnication Channel Between Nodes

Then input the commands:

```
Shell$ cd mpich2;
       mkdir build;
       cd build;
       ./configure –with-pm=smpd –with-device=ch3:
sock –disable-f77 –disable-fc –disable –cxx;
       make all;
       sudo make install;
       smpd –s
```

Run the demo of CPI in the development kit of MPICH2 so that we can get the information whether mpich2 deployed in node 1 is successful or not (omit extension name “.exe” on Windows as the exact executable name in Linux).

Input the commands:

```
shell$ mpicc –o icpi icpi.c –Os –s
shell$ mpiexec –n 2 ./icpi
```

In node 2, the following steps are taken.

Install Windows XP SP3 at first, and set the host name as "NLIB", the ip address is 192.168.128.133, the user name "tlib" and password (warning: you shouldn't use the account of "Administrator", or else you cannot build the heterogeneous cluster between different Operating Systems as expected).

The default path of MPICH2 installation is "C:\Program Files\MPICH2", it is advised that do not modify the default path.

The default password of MPICH2 is behappy, which should be modified as the same as node 1.

Find the "wmpiregister.exe" under the installation path of MPICH2, and then register the user name and password of "mlib".

Adjust the path of "mpiexec.exe", copying the "mpiexec.exe" in the installation path to the system directory " C:\Windows\system32".

You can judge that whether the installation of MPICH2 in node 2 is successful or not by running the demo in the directory of example, contained in the installation path of MPICH2.

V. THE PERFORMANCE COMPARISON TEST

At very beginning, we built the test environment as follows:

1) The hardware of the heterogeneous cluster are shown as below; the CPU, RAM and the volume of disk are Intel Core 2 T5450, 384MB DDR2, 5.0G in node 1, while in node 2 are nearly the same as node1 except the RAM volume, it is 256MB.

2) The Operating System of node 1 is Ubuntu10.10 (32-bits, desktop version), the node 2 is Windows XP SP3. Both of the MPICH2 versions are mpich2-1.4.1.

Based on this heterogeneous cluster, we draw up two testing schema: run the test case twice in node 1(Linux) and node 2 (Windows) to validate the feasibility of our method. The codes are shown below:

```
#include <stdio.h>
#include <mpi.h>

int main(int argc,char *argv[])
{
        int    mpi_rank,mpi_pid,nameLen=128;
        char   mpi_name[128] ;

        MPI_Init(&argc,&argv);
        MPI_Comm_rank(MPI_COMM_WORLD,&mpi_r
                        ank);
        MPI_Get_processor_name(mpi_name,&nameLen);
        mpi_pid=getpid();
        printf("[%d] I am %s and my pid
        is %d.\n",mpi_rank,mpi_name,mpi_pid);
        if(mpi_rank==0)
        {
                MPI_Send(&mpi_pid,1,MPI_INT,1,0x123
        4,MPI_COMM_WORLD );
        }
        else if(mpi_rank==1)
        {
                MPI_Recv(&mpi_pid,1,MPI_INT,0,0x123
        4,MPI_COMM_WORLD,MPI_STATUS_IGNOR
        E);
        }
        printf("[%d] I am %s and my pid
        is %d.\n",mpi_rank,mpi_name,mpi_pid);fflush(stdo
        ut);
        MPI_Finalize();
        return 0;
}
```

In node 1, the running command is "mpiexec –n 2 –machinefile mf –chanel sock –path "/home/tlib;c:\mpi" ./X".

In node 2, the running command is "mpiexec –n 2 –machinefile mf –chanel sock –path "c:\mp;/home/tlib" ./X".

Running the commands in each node per time, the results will be shown in the terminal as follows:

[1] I am tlibx and my pid is 2318.
[2] I am tlibx and my pid is 2111.
[3] I am NLIB and my pid is 1272.
[4] I am NLIB and my pid is 1274.

The result of test may be slightly different in PID due to the process scheduler of OS.

In order to validate the efficiency without virtualization, we ran a another test case (CPI, it stands for the ratio of circumference), which was provided by the demo of MPICH2.The test environment was based on the server, the configuration of the node was: Intel Xeon 5500, DDR3 16GB, 2 CPUs with 8 cores in total (the technology of Hyper Thread is supported). The test results are shown in Table 1 and Fig.2 (Fig.2 is the histogram of Table 1).

We ran 3 groups of tests in total. In each group, we ran the demo of CPI in the VM and PM (Physical Machine), the field of "process" in Fig.2 means the numbers of MPI processes which were started by "MPIEXEC". For instance, in the row of "Group1" and the column of "Process 4", we started 4 MPI processes in 4 VMs (each VM got one MPI process, all of the VMs were running in the same server) at the beginning, it took approximately 2.32 seconds, after that we started 4 MPI processes in the PM without VMs, the outcome was nearly 2.18 second.

The Fig.2 shows that it take less time in PM than in the VM, the performance is ameliorated without virtualization. The performance in VMs goes down as the increment of number of VMs, especially when the total number of VMs is far more than the CPU cores in the server.

TABLE I. THE TEST RESULT

	Process 1		Process 2		Process 3		Process 4	
	VM	PM	VM	PM	VM	PM	VM	PM
Group1	8.92	8.29	4.41	4.14	3.17	2.76	2.32	2.18
Group2	8.89	8.29	4.40	4.14	3.24	2.76	2.27	2.17
Group3	8.90	8.29	4.42	4.14	2.98	2.76	2.30	2.17
Average	8.90	8.29	4.41	4.14	3.13	2.76	2.30	2.18

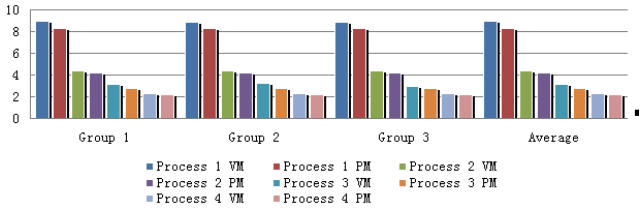

Figure 2 The Comparison of Performance Between VM And PM

VI. CONCLUSION

This paper proposes an approach for constructing MPI based heterogeneous cluster directly and discusses the reasons of giving up the virtualization approach, aiming at trying to resort to an effective way to convert homogeneous to heterogeneous. We focus on building an MPI-based heterogeneous cluster with the MPICH2, which is released last year and has not supported the heterogeneous cluster yet. The proposed approach is smart and without drastic modification to the source code. Several comparison tests have shown the proposed method of constructing the heterogeneous cluster directly is feasible and efficient, and the hybrid Operating System cluster runs better without virtualization.

REFERENCES

[1] http://www.mpi-forum.org/

[2] Barry W.Parallel Programming.2nd version,pp,50-51,2005

[3] Massetto FI,Sato LM,Li Kuan-Ching.SCI,Journal of Supercomputing,vol 1,pp,87-116,2012

[4] http://www.mcs.anl.gov/research/projects/mpich2/about/index.php?s=about

[5] VMware,Inc.VMware Infrastructure Architecture Overview.pp,8-9,2006

[6] http://searchservervirtualization.techtarget.com/definition/server-virtualization,Jul 2009

[7] http://www.searchvirtual.com.cn/showcontent_25455.htm,April 2008

[8] Graham E.Fagg,Jack J.Dongarra,Al Geist.“Heterogeneous MPI application interoperation and process management under PVMPI,”Lecture Notes in Computer Science,vol,1332,pp,91-98,1997.

[9] David A.Reimann,“Cone beam tomography using MPI on heterogeneous workstation clusters,” IEEE, pp,142-148,Jul 1996.

[10] Clauss C.“MPI Xternal A library for a portable adjustment of parallel MPI applications to heterogeneous environments,”IEEE,pp,1-8,May 2009.

[11] Agbaria A.“LMPI MPI for heterogeneous embedded distributed systems,”IEEE,Parallel and Distributed Systems,vol 1,Dec 2006

[12] http://www.mcs.anl.gov/research/projects/mpich2/.2012

A Routing Algorithm of Multiple Objective GA Based on Pareto Optimality

DONG Tongli, CHEN Niansheng, LI Zhi, FANG Xiaoping, GUO Yu
College of Computer Science and Technology
Hubei Normal University
Huangshi, Hubei, 435002, China
E-mail: hschenns@163.com

***Abstract*—Wireless Multimedia Sensor Networks (WMSNs) is a novel information acquiring and processing technology which is more competent than traditional sensor networks in transferring and processing of huge amount of multimedia information data, such as audio, video, images and so on. It plays critical role in application in civil, military and commercial fields. In this paper, a Non-control sorting method is used to construct the Pareto optimal routing path set and the multiple attribute decision making method is adopted to search for the best routing path from the Pareto optimal routing path set. The simulation experiment result shows that our method can increase the probability of finding the optimal routing path, the TOPSIS method which is based on the Multiple Attribute Decision Making method obtains the best routing path from the Pareto Optimal routing set.**

Keywords- WMSNs; QoS; Multi-objective optimization； GA

I. INTRODUCTION

Wireless multimedia sensor networks(WMSNs) is a special kind of wireless sensor networks(WSNs) which has attracted the interest of many researchers and became a hot spot in network field[1-2]. WMSNs is competent in transferring huge amount of multimedia data, such as real-time image, audio, video and so on. As for the WMSNs, it is necessary to provide a perfect route to guarantee the relative service for transmission[3], but the QoS parameter is sensitive, which is a very important feature of WMSNs. So, QoS routing technology is the most critical technology in the research of WMSNs application. In QoS routing technology, the feasible paths should be calculated within multi-constraint conditions and then the best route path will be selected by further optimizing them. Ref.[4-5] proposed a single objective optimization genetic algorithm which added weight coefficient to the QoS attributes(such as bandwidth, delay, jitter and so on) to construct the evaluation function, but there are problems that are difficult to determine the weight coefficients and the multiple objects cannot be optimized at the same time. Ref.[6] proposed a multiple objective genetic algorithm based on Pareto optimality to obtain a set of Pareto Optimal routing path, but it didn't find the best routing path. In this paper we use a non-control sorting method to construct the Pareto optimal routing set and adopt the multiple attribute decision making method to search for the best optimization routing path from the routing path set. The simulation experiment result shows that our method can increase the probability of finding the optimal routing path, and the TOPSIS method which is based on Multiple Attribute Decision Making method can obtain the best routing path from the Pareto Optimal routing set.

II. QOS ROUTING DESCRIPTION AND THE NETWORK OPTIMIZATION MODEL

Definition 1: Pareto optimal path: Given a weighted undirected graph $G = (V, E)$ in WMSNs, each route P from source node to destination node has two or more objective functions $F_1, F_2, \ldots, F_k (k \geq 2)$ which need to be optimized, and route P is a best optimization non-dominated route in the Pareto Optimal routing path set; suppose P and P^* satisfy the QoS constraint conditions, only when there is not another route P^* , for $\forall F_i, i = 1,2,\ldots,k$, satisfy $F_i(P) \geq_p F_i(P^*), i = 1,2,\ldots,k$, and there is at least one objective function $F_i, i = 1,2,\ldots,k, \mathrm{F_i}(P) >_p \mathrm{F_i}(P^*)$.

Definition 2: Multi-objective network optimization model: Multi-objective network optimization based on Multi-objective optimization can obtain a set of Pareto Optimal routing path by optimizing multi-objective function at the same time. The bandwidth, delay, jitter are the critical parameters which influence the service quality of WMSNs mostly, and the three objective functions of these parameters conflict with each other. The multi-objective model based on these three parameters is defined as follows:

$$\begin{cases} \min & y = \mathrm{F}(\mathrm{P}) = (F_{B(P)}, F_{D(P)}, F_{J(P)})^T \\ s.t & B(P) \leq -B_{\min} \\ & D(P) \leq D_{\max} \\ & L(P) \leq L_{\max} \\ & J(P) \leq J_{\max} \end{cases} \quad (1)$$

Here, y is the cost function which needs to be optimized, $D(P)$ 、 $B(P)$ 、 $L(P)$ 、 $J(P)$ represent the delay, available bandwidth, packet loss rate and delay jitter of a path P respectively, while $D_{\max}, J_{\max}, B_{\min}, L_{\max}$ present the relative maximum value of them. $F_{B(P)}$、 $F_{D(P)}$、 $F_{J(P)}$ represent the function of bandwidth, delay and delay jitter respectively, and these three functions need to be optimized.

978-0-7695-4818-0/12 $26.00 © 2012 IEEE
DOI 10.1109/DCABES.2012.72

III. THE MULTI-OBJECTIVE OPTIMIZATION ALGORITHM BASED ON PARETO

The critical problem of Multi-objective optimization is that the multiple functions are conflicting with each other. In the process of optimizing, the improvement of a function's performance may lead to a setback of another optimization function's performance, thus it is very difficult to make all the optimization functions achieve the best values at the same time. So it is a better alternate to obtain a set of Pareto optimal routing path by optimizing the multiple objectives. When calculating the best routing path from them according to the actual needs of network applications, this is the best multi-objective optimal satisfactory routing path. In this study, we use the non-control sorting method to get a set of Pareto optimal routing path, and then use the multi-attribute decision-making method to obtain the best path from them with the Multiple QoS constrains.

A. Multi-objective QoS routing genetic algorithm based on Pareto

(1)Encoding

For a given WMSNs and a routing request, in order to find a path P, the sensor node can be encoded by a series of numbers. A possible path can be encoded as chromosome $Chrom = \{v_1, v_2, \ldots, v_n \mid v_i \in V\}$, $v_1, v_2, \ldots, v_n, v_i$ representing the sensor nodes. For example, a path from the source node 170 to the destination node 113 can be represented as $\{170,25,34,78,2,113\}$.

(2)Crossover

The crossover operation generates new individuals, but some of them may be unfeasible solutions. So the new individuals must be as feasible solution as possible to accelerate the evolution process. We adopt the single-point crossover operation method which can be seen in Ref. [5]. In this method, a number of chromosomes are chosen randomly from the father individuals. First, two father individuals are compared to find the same gens (the numbers of sensor nodes), and then one of them is selected randomly as the cross point; then the gene string from the cross point will be exchanged. The advantage in this way is that the new individual is still a feasible solution after exchange, so the calculation of infeasible solutions can be largely reduced.

(3)Mutation

Mutation operation can produce new individuals by changing a part of gene randomly, and it can improve the diversity of population to prevent the excessive convergence. Unfeasible solutions may also appear in the mutation process like the crossover operation process. In order to avoid that, we adopt the mutation method describing in Ref. [5], the operation process is described as following:

Step 1: choose one individual randomly.

Step 2: generate a mutation position randomly from the node set and encode it as *V*.

Step 3: Set *V* as a new source node, use the random walking method to find a route to original destination node, and connect the new route and the original route to be a new path.

The advantage of this mutation way is that it can reduce the calculation of unfeasible solution as it does not produce unfeasible route in the calculating process

(4) Algorithm Flow

Step 1: Generate the initial population *P*.

Step 2: Calculate the bandwidth, delay and delay jitter of each routing path in the initial population *P*, and then construct the QoS decision matrix.

Step 3: use the non-control sorting sort method to sort the QoS decision matrix and put solution into set *Q*.

Step 4: if *t*<=gen, then execute the operations as follows, otherwise end and go to step 5:

①select individuals from all the *M* individuals by binary tournament selection method to construct the father population *T*;

②execute the genetic operation (crossover and mutation) on population *T* and obtain the next population *S*;

③Merge the non-control routing path set *Q* and *S* to obtain population P'. $P' = Q \cup S$

④use non-control sorting method to sort population P'

⑤t=t+1; go back to Step 4.

Step 5: use multi-attribute decision-making to get optimal satisfactory solution from the above generated Pareto optimality solution sets.

By step 1 to step 4, we can obtain the Pareto optimal routing paths set. After that, we will use multi-attribute decision-making method to get the most satisfactory routing path.

B. Get the most satisfactory Pareto solution

Every node in WMSNs has the attributes of bandwidth, delay, jitter, energy and so on. The multiple attribute decision making method just makes use of the relative attributes to evaluate the individuals comprehensively.

Definition 3: Attribute the value of a path *P*: A route $P = \{e_1, e_2, \ldots, e_n \mid i = 1,2,\ldots,n\}$ presents a path which is composed of n edges. For each edge e_i, ($\forall e_i, i = 1,2,\ldots,n$), it has three attributes (B, D, J) (representing the bandwidth, delay, jitter respectively), then for a route *P*, the attributes value can be defined as $B = \min(e_i)$, $D = sum(e_i)$, $J = \max\{e_i\} - \min\{e_i\}$.

For example, for a route $P = \{e_1, e_2, e_3\}$, the node set is (170, 15, 20, 113), each edge (e_i) has three attributes (B, D, J) as shown in Fig.1. The three attribute values for this path are: (min{20,15,20}, sum{150, 100,120}, max{2,2,1}-min{2,2,1}), that is (15,370,1).

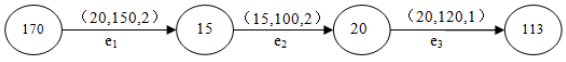

Fig.1.the path *P* consist of three attributions

Suppose that A is one of the feasible scheme set of path P which meets the QoS constraints, usually, there are more than one feasible scheme sets for a path, the corresponding attribute values for each feasible scheme are defined as definition 3.

Definition 4: multiple attribute decision making matrix for QoS routing: $A = \{A \mid A = P_1, P_2, \ldots, P_m\}$ $(m \geq 2)$, a routing path has n attributes $X_1, X_2, \ldots, X_n$, and x_{ij} represents the value of attribute j in routing path i, then the decision matrix is defined as following:

$$M = \begin{matrix} P_1 \\ P_2 \\ \vdots \\ P_m \end{matrix} \begin{bmatrix} X_{11} & X_{12} & \cdots & X_{1n} \\ X_{21} & X_{22} & \cdots & X_{2n} \\ \vdots & \vdots & \vdots & \vdots \\ X_{m1} & X_{m2} & \cdots & X_{mn} \end{bmatrix}$$

, the matrix $M = (x_{ij})_{m \times n}$ is the multiple attributes decision matrix for QoS routing problem.

TOPSIS(Technique for Order Preference by Similarity to Ideal Solution) is called close-to-ideal solution sort method. Its basic idea is: for the original data matrix, after its normalization, confirm the best solution(the positive idea solution)and the worse solution (the negative idea solution), then comparing each evaluated scheme with the best solution and the worse solution, find out how far the scheme is from the best solution and from that of the worst, use the result as a criteria to evaluate the evaluated objects. According to the TOPSIS method in Ref. [7-10], the flow of calculating the Pareto optimal satisfactory solution is described as following:

Step 1: construct the decision-making matrix M which includes the three attributes (bandwidth, delay and delay jitter).

Step 2: standardize the bandwidth by formula (2), delay and delay jitter by formula (3).

The efficient data: $$r_{ij} = \frac{X_{ij} - X_{j\min}}{X_{j\max} - X_{j\min}} \quad (2)$$

The cost data: $$r_{ij} = \frac{X_{j\max} - X_{ij}}{X_{j\max} - X_{j\min}} \quad (3)$$

Step 3: calculate the weight by entropy method, and construct the decision-making matrix $M' = (R_{ij})_{m \times n}$ by formula (4)

$$M' = \begin{matrix} P_1 \\ P_2 \\ \cdots \\ P_m \end{matrix} \begin{bmatrix} W_1 r_{11} & W_1 r_{12} & \cdots & W_1 r_{1n} \\ W_2 r_{21} & W_2 X_{22} & \cdots & W_2 X_{2n} \\ \cdots & \cdots & \cdots & \cdots \\ W_m r_{m1} & W_m r_{m2} & \cdots & W_m r_{mn} \end{bmatrix} \quad (4)$$

Step 4: determine the ideal solution x^+ and negative solution x^- for each attribute according to formula (5) and formula (6).

$$x_j^+ = \begin{cases} \max\{R_{ij}\}, & j \text{ is efficient data} \\ \min\{R_{ij}\}, & j \text{ is cost data} \end{cases} \quad (5)$$

$$x_j^- = \begin{cases} \max\{R_{ij}\}, & j \text{ is cost data} \\ \min\{R_{ij}\}, & j \text{ is efficient data} \end{cases} \quad (6)$$

Step 5: calculate the distances of each path to the ideal positive solution x^+ and the negative solution x^- by formula (7) and formula (8).

$$D_i^+ = \sqrt{\sum_j^n (R_{ij} - x_j^+)^2}, \quad i = 1,2,\ldots,m \quad (7)$$

$$D_i^- = \sqrt{\sum_j^n (R_{ij} - x_j^-)^2}, \quad i = 1,2,\ldots,m \quad (8)$$

Step 6: calculate evaluation index for each route by formula (9).

$$C_i = \frac{D_i^-}{D_i^+ + D_i^-}, \quad i = 1,2,\ldots,m \quad (9)$$

Step 7: sort the comprehensive evaluation index. The largest value is the required Pareto optimal solution.

IV. SIMULATION EXPERIMENT

We used the same Random graph model as Waxman's research [11] to generate simulated network topology. In plane [a, b], nodes are randomly placed by position distribution. A topology of 191 nodes is generated. As is shown in Fig.2, the communication distance between each two nodes is 20, and the number of edges between each node is at least 2. Suppose the Qos constraint for parameters: $D_{\max} = 200$、$J_{\max} = 2$、$B_{\min} = 2$

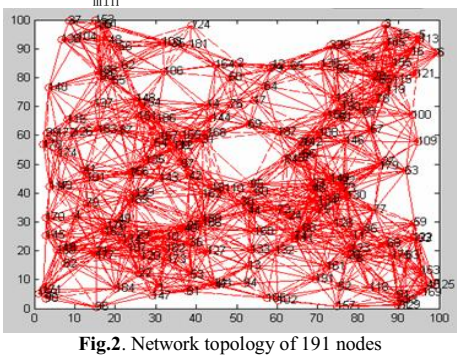

Fig.2. Network topology of 191 nodes

A. Experiment content

The program of the multi-objective population optimal genetic algorithm is run for 100 times. One of the optimal routing paths obtained is shown in fig.3. The 100 best fitness values of variations by the100 times running are shown in

fig.5. The changes of the best fitness value and the average fitness value with the changes of the evolutionary algebra are shown in fig.6. The Pareto optimal solution set of bandwidth, delay and jitter for one time running of multi-objective population optimal genetic algorithm is shown in fig.7. For easier comparing, fig.8 shows the changes of the 100 best fitness values on 100 times' running of the genetic algorithm

For the above Pareto optimal solution set, the Pareto optimal route obtained by the TOPSIS method is shown in fig 3.

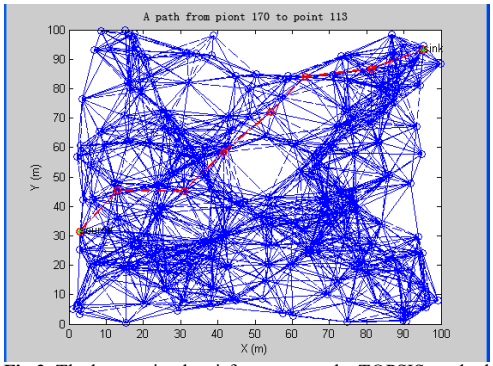

Fig.3. The best optimal satisfactory route by TOPSIS method

B. Analysis of simulation result

By comparing fig.5 and fig.8, it can be seen that the running times to obtain the best fitness value of 0.1429 through the Pareto based multi-objective genetic algorithm is more than the times by traditional genetic algorithm, it illustrates that the probability of finding the optimal solution is increased. From fig.7, we can see that the set of optimal routing paths obtained by Pareto based multi-objective genetic algorithm contains 183 paths, all of the 183 paths meet the QoS constraint condition. So the TOPSIS method is used to find the best Pareto optimal satisfactory routing path from the 183 paths. From fig.4,the final best routing path is: 170→101→143→31→17→65→34→113.

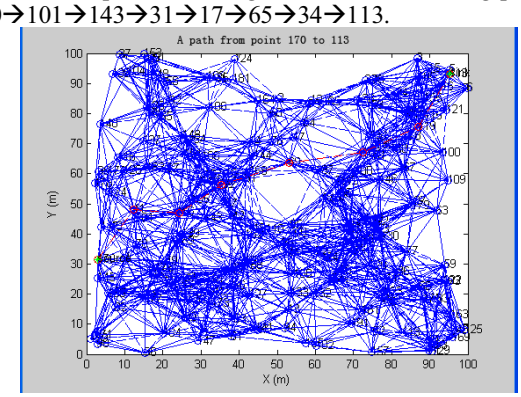

Fig.4. an optimal routing path obtained by multi-objective optimal population algorithm

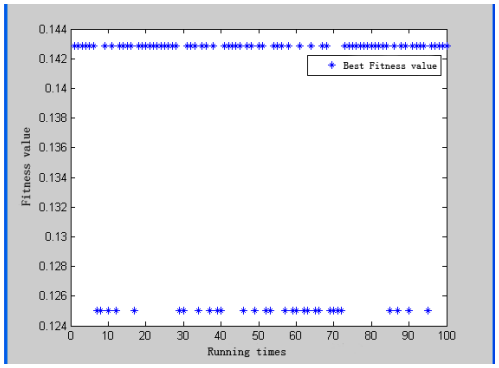

Fig.5. the changes of fitness value by multi-objective optimal population genetic algorithm

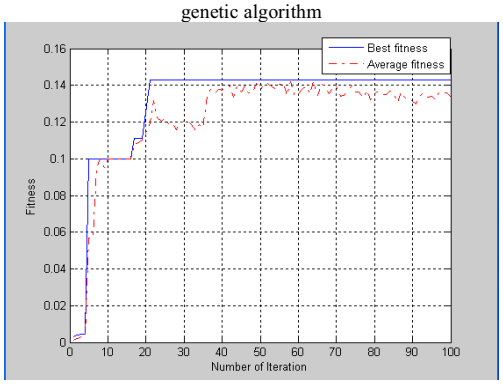

Fig.6. the changes of the best fitness value and the average fitness value according to the number of iteration

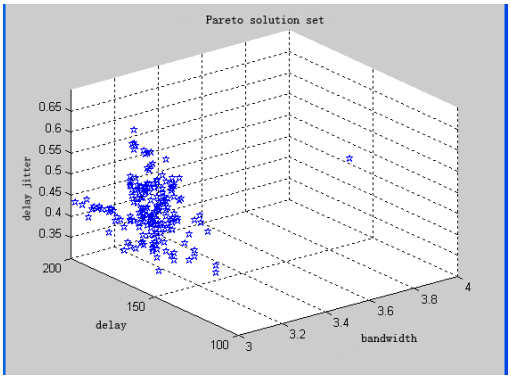

Fig.7. the Pareto optimality set of bandwidth, delay and jitter

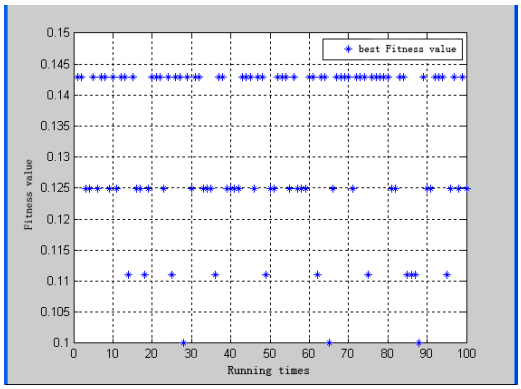

Fig.8. changes of the best fitness value on 100 times running

V. CONCLUSION

In this paper we use multi-objective optimization method and the non-control sorting technology to construct the Pareto optimal routing path set, and then use the TOPSIS method to evaluate the optimal routing path set to find the best Qos routing path for wireless multimedia sensor networks. Simulation experiment shows that our method can increase the probability of finding the most optimal routing path comparing to traditional genetic algorithm. However, there is still room for improvement of the method in constructing the Pareto solution set, and this deserves further consideration.

ACKNOWLEDGMENT

The work was supported by the supporting plan for scientific and technological innovation team of excellent young and middle-aged staff in higher learning institutes in Hubei Province in P.R. China (Grant No:T200806) and The young researchers supporting project of Hubei Province Department of Education in P.R,China(Grant NO: Q20082203).

REFERENCES

[1] Akyildiz IF, Melodia T, Chowdhury KR.A survey on wireless multimedia sensor networks[J].Computer Networks, 2007,51(4): 921-960.

[2] Bulent Tavli, Kemal Bicakci et.A survey of visual sensor network platforms[J].Multimedia Tools and Applications,2011, DOI:10.1007/s11042-011-0840-z .

[3] Ehsan, S., Hamdaui, B. A Survey on Energy-Efficient Routing Techniques with QoS Assurances for Wireless Multimedia Sensor Networks[J]. IEEE Communications Surveys and Tutorials 99, 2011,1–14.

[4] CHEN Niansheng,Li Layuan. A QoS Multicast Routing Algorithm Based on GA and TS Hybrid Strategy[A]. ISICA 2005 Proceedings[C]. Wuhan:China University of Geosciences of Press,2005:153-158.

[5] Ke Zong Wu. Research on QoS Routing Algorithm for Wireless Multimedia Sensor Networks [Ph.D. Thesis]. Wuhan: Wuhan University of Technology,2009,9:12. (in Chinese)

[6] Hamidreza Eskandari,Christopher D. Geiger.A fast Pareto genetic algorithm approach for solving expensive multiobjective optimization problems[J].Journal of Heuristics,2008,14(3):203-241.

[7] ZHAO Qin na,YAO Shang li, FAN Li-jun. Evaluation of Environment-friendly City Construction Based on Entropy Weight TOPSIS Method[J]. Journal of Hefei University of Technology,2012,26(1):26-33. (in Chinese)

[8] Lihua Zhong. A Game Method for Multiple Attribute Decision Making without Weight information[A]. IEEE ICIA2009 Proceedings[C]. Piscataway, NJ: IEEE, 2009:1302-1307.

[9] Xin chang Wang ,Xin ying Xiao. On Weights Determination in Ideal Point Multiattribute Decision-Making Model[J]. Information Systems Development, 2011, 6, 475-481.

[10] Houxing Tang.Multiple-Attribute Decision Making with Complete-Imperfect Substitution between Attributes[A].The IEEE ICICTA Proceedings[C]. Piscataway, NJ: IEEE, 2011:1078 -1081.

[11] Waxman BM.Routing of multipoint Connections [J].IEEE Journal on Selected Areas in Commuciations,1988,6(9):1617-1622.

Research on Routing Protocol Based on Dynamic Mask Address

Zhang Jian, Feng Shiyan, Lü Hui, Meng Lei

(School of Computer ,Wu Han University, Wu Han, Hubei 430072)

***Abstract*—AODV and Cluster-Tree are usually used as route protocol in ZigBee network. In AODV, the broadcast mechanism makes energy run fast. Cluster-Tree protocol gets a long route path, which leads to high delay. This paper has done detailed research on these two protocols, and proposes a new address allocation scheme in order to make addresses carry with the topology information. In the process of route discovery, request packets will be send with the directivity. That will cut down packet delay and energy consumption in the systemic level.**

Keywords-ZigBee; dynamic mask; NS2; energy consumption

I. INTRODUCTION

ZigBee is a group of technical standards of network, security and application software which are developed on the basis of wireless standard IEEE802.15.14. ZigBee architecture is composed of Physical layer, Data link layer, Network layer, Application convergence subl ayer and High-level application specification[1].

At present research on how to design high performance ZigBee network in different environments and how to achieve reliable interconnection between the ZigBee network becomes the major project and hot point.These can be classified to the routing problem of Network layer. An effective routing algorithm can effectively decrease network delay and save node energy consumption.

II. ZIGBEE NETWORK CONFIGURATION

For the network configuration, ZigBee network nodes are divided into three types： ZigBee routing node,ZigBee coordination node,ZigBee terminal node。

ZigBee routing node can only work as the full functional device(FFD) node. It's main task includes data storage and forwarding ,route discovery and maintenance .ZigBee routing nodes can also play the role of a normal coordinator node.

ZigBee coordination node must also be FFD. It can also serve as a convergence node in the wireless sensor network. Usually there is only one coordination node in a ZigBee network. It is responsible for the launching of new network, the setting of network parameter, the management of nodes and the storage of network node' information. It may also play the role of routing node.

ZigBee terminal node is the reduced function device (RFD) or FFD. Other nodes cannot join the network through a terminal node. A node connects to the ZigBee network only through the coordination node or the routing nodes.

Three network topologies are defined in ZigBee protocol standards. They are Star topology, Tree topology and Mesh topology. Star network and tree network can actually be seen as a subset of the mesh, so this paper only focuses on the mesh network.

III. ZIGBEE ADDRESS ALLOCATION MECHANISM

If a node in network allows a new node to join in the network by it, they construct a parent-child relationship. Parent node distributes a unique 16-bit short address. Assume the number of child nodes accepted by a parent node is C_m, he maximum depth of the network is L_m, the largest number of routers of child nodes is R_m, then the parent node can calculate the offset $C_{skip}(d)$ for child nodes address through formula 1(The depth of the parent node is d).

$$C_{skip}(d)=\begin{cases}1+C_m(L_m-d-1), & R_m=1\\ \dfrac{1+C_m-R_m-C_mR_m^{L_m-d-1}}{1-R_m}\end{cases} \quad \text{(Formula 1)}$$

For different joining child nodes, the calculation method of the addresses is also different. If node A is a reduced function device(RFD)node, which joins in the network through A_p, A_p uses the formula 2 to allocate a network address for A.

$$A=A_p+C_{skip}(d)R_m+n,\quad 1\le n\le C_m-R_m \quad \text{(Formula 2)}$$

If a child node is the FFD node with routing ability, the parent node A_p uses formula 3 to allocate a network address for A.

$$A=A_p+1+C_{skip}(d)(n-1) \quad \text{(Formula 3)}$$

IV. ZIGBEE NETWORK ROUTING ALGORITHM

A. Cluster-Tree Routing Algorithm

In Cluster-Tree routing algorithm[5], nodes calculate next hop node address according to the network address of the destination node. Assume that the address of a ZigBee node is A and its depth is d. When it receives a data frame with destination address D, node A will first judge that if destination node is its offspring node through formula 4.

$$A<D<A+C_{skip}(d-1) \quad \text{(Formula 4)}$$

If the calculated destination node is the offspring node of the receiving node,a message will be sent to its child node N. It could be judged by formula 5 that the message is transmitted to end child nodes or routing child node.

$$N=\begin{cases}D, & D>A+R_mC_{skip}(d)\\ A+1+[\dfrac{D-(A+1)}{C_{skip}(d)}]C_{skip}(d), & \text{others}\end{cases} \quad \text{(Formula 5)}$$

978-0-7695-4818-0/12 $26.00 © 2012 IEEE
DOI 10.1109/DCABES.2012.88

If the destination node is not the offspring node of the receiving node, a message will be sent to the parent node of the receiving node along tree structure, and the parent node do similar judgment or forwarding.

B. AODV Routing Algorithm

AODV algorithm is based on vector routing algorithm, which mainly includes three kinds of message format[2].They are routing request (RREQ), routing response (RREP), routing error (RRER). Specific steps of the algorithm as follows：

If it wants to find a path to destination node，a source node will first search its own routing table. If no records ,the source node will broadcast a RREQ to all its neighbor nodes. A RREQ includes source node, destination node, request sequence number, hop from the source node and so forth. After receiving this RREQ, neighbor nodes compare request sequence number and destination address to judge whether they have received the same request. If they has done, the message is directly discarded. If not, the hop is added by 1 first and then a table is created to record the reverse path to source node through the RREQ information .If containing the routing path to destination path, neighbor node could directly return a RREP to the source node. Otherwise, neighbor nodes continue to broadcast RREQ to their neighbor nodes until destination node received. Destination node would send a RREP to its upstream node and establish a reverse routing. As getting request path from reverse routing，all of the intermediate node will establish reverse routing, until source node receives RREP. Intermediate nodes will broadcast information to the neighbor node when its location has changed or lose efficacy. Then neighbor nodes will send a RREP to the upstream node. The RREP will be transmitted to the source node. The routing request process will be re-launched by the source node according to the actual situation.

Above two routing algorithm don't associated routing with the node address. In the Cluster-Tree protocol, addressing path is so long that the end-to-end delay is quite high. In AODV protocol, broadcasting mechanism leads to node energy consumption faster. This paper proposes an address allocation solution based on dynamic mask address, which enables the network address to reflect topology information. Forwarding routing request packet will be more directed and thus reduce network delay and power consumption in the system level.

V. ROUTING BASED ON DYNAMIC MASK ADDRESS ALLOCATION

A. The Allocation of the network address

In ZigBee network, the address is allocated by tree structure. Coordinator is located in the root node .Generally its depth is 0 and its initial address is 0x0000. A joining node sends request to its parent node who works as the coordinator or FFD nodes. An address will be allocated after the approval of the parent node[6].In the dynamic mask address allocation, the parent node will still continue to monitor for a while after it received a request from child nodes, and record these nodes. After the parent node gets the number y of joining nodes, mask length n of child nodes could be confirmed as following:

$$n = \lceil \log_2 y \rceil \quad (n<16)$$

Then, the parent node allocates network address of child node according to its own mask and address. And address length still takes short address of 16bit.

Assume mask length of parent node is k bit（k<16，if parent node is a coordinator, then k=0）.The mask of the parent node is:

$$\underbrace{1 \cdots 1}_{k \text{ bits}}\ \underbrace{0 \cdots 0}_{16-k \text{ bits}}$$

Assume the network address of parent node is:

$$\underbrace{f_{k-1}\ f_{k-2} \cdots f_0}_{k \text{ bits}}\ \underbrace{0 \cdots 0}_{16-k \text{ bits}}$$

Assume the mask length of child nodes calculated by the parent node is n, then mask of child nodes is:

$$\underbrace{1 \cdots 1}_{k \text{ bits}}\ \underbrace{1 \cdots 1}_{n \text{ bits}}\ \underbrace{0 \cdots 0}_{16-k-n \text{ bits}}$$

Thus 2n-1 subnets could be divided (excluding total 0). If each subnet is allocated to one child node, the network address of child nodes is:

$$\underbrace{f_{k-1}\ f_{k-2} \cdots f_0}_{k \text{ bits}}\ \underbrace{S_{n-1}\ S_{n-2} \cdots S_0}_{n \text{ bits}}\ \underbrace{0 \cdots 0}_{16-k-n \text{ bits}}$$

The middle n bits sn-1,sn-2,……,s0 is set to different values for different child nodes.

B. Judgment About Address Correlation

It can be seen from the process of network address allocation that the former k bits of the child nodes' address are the same as the parent's . So the address of the child node has a strong correlation with his parent node and brother nodes, while the correlation with the other nodes will be weak. So the greater the correlation, the stronger is the reachability. Routing discovery mechanism based on dynamic mask address allocation takes the advantage of this correlation. Sending node will select a neighbor node who has the strongest correlation with the destination node as the next hop .

Address correlation calculation is to determine the next hop. Node D will search all the neighbor nodes D_{nab} from the neighbor table and calculate correlation with destination node D_{des}. Mask M is used to judge address correlation. Correlation between two nodes is calculated as following:

$$\text{RelationShip} = (D_{nab} \,\&\, M) \,\&\, (D_{des} \,\&\, M)$$

The value of RelationShip is based on the number of consecutive 1 from the highest bit . The bigger the number of consecutive 1, the closer is the relationship between two nodes.

C. Route Discovery and Establishment

The process based on dynamic mask address mainly includes the following six steps:

(1)The source node initializes route request table and routing table. First perform the correlation computation.One node or some neighbor nodes that have the strongest correlation are selected as the next hop node. Then establish the routing table according to the calculated next hop address and set the route record status to discovery. Fill in the routing table with destination address and the next hop. A route request packet (RREQ) can be produced and a route discovery table can be established after the direction of the routing request is ensured[8].

(2)The source node sends a route request message:the path cost of the routing request message is set to 0, and other parameters is set according to the relevant status.

(3)The receiving node compares the routing request number and the destination node address with the message in the routing discovery table of this node. If there is a same record, this node discards this repeated information. Otherwise go to step (4).

(4)Compare the network address of the destination node with its own network address and the addresses in the neighbor table and the routing table. If there is the same destination address,the message is forwarded to the destination address and the node responses route reply message(RREP), which is transmitted back to source node according to reverse routing formed in routing process. Otherwise, turn to (5).

(5)Fill in relevant content and create new record in route discovery table. The source node network address and route request number can be extracted directly from the message, and sending node address can be extracted in the same way. The prior cost is determined by the message path cost, and the current time is added to the timeout. With the extracted source node as the destination node address field in routing discovery table and sending node address filled in node address field of previous hop, the reverse routing is established by route discovery table. Turn to (6).

(6)Repeat the above steps. If the current time is found to be greater than the timeout period set in step (1),the process of route discovery is terminated. If the destination address is found in step (4) , search the route discovery table and return routing reply packet to the previous node. The previous node responses in the same way until the reply packet arrives the source node. So far, the process of routing discovery is finished.

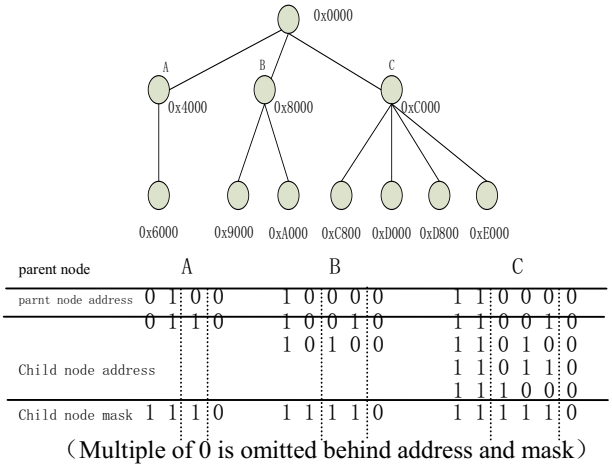

Figure 1. Address allocation process instance diagram

Figure 1 is an example of dynamic mask address allocation. Coordinator with the address 0x0000 listens to the access request of 3 nodes A, B and C.So the mask length is calculated to be 2 bits according to the address allocation rule and 3 child nodes are respectively assigned the address 0x4000,0x8000, 0xC000. Node B with the address 0x8000 has two child nodes, but mask cannot be allocated only one bit because mask set to all zeros cannot be used. Thus node B should add two bits on the basis of its own mask length so that the network addresses of two child nodes are respectively 0x9000 and 0xA000. The child nodes of Node A and Node C can get their network addresses similarly.

Figure 2 is an example of the route step. Now assume finding a path from 0x9000 to 0xD000. First, the source node with the address 0x9000 searches its own neighbor table and finds two nodes 0x8000 and 0xA000. Then the source node carries on the correlation calculation between the destination node 0xD000 and its two neighbor nodes (Due to the different length of mask, only the first two bits need to be used when calculated for the address 0x8000, while the first four bits need to be used when calculated for the address 0xA000). The source node send the request message to two neighbor nodes because the correlation is the same. After receiving the route request, the node 0xA000 finds out its neighbor node includes one node with the address 0x8000 besides the source node. So it only forwards the request message to the node 0x8000. But the node 0x8000 has received the same message so that the message will be discarded. The node 0x8000 has five neighbor nodes including the node 0x9000 and 0xA000 who have send the request message to it. After making correlation calculation for other three nodes 0x0000, 0x4000 and 0xC000, the node 0x8000 finds out the node 0xC000 has the closer correlation with the destination node. So the request message is forwarded to the node 0xC000. At last, the request message will be sent directly to the destination node because it has already existed in the neighbor table of the node 0xC000. Thus, a reverse routing is found. The node 0xD000 establishes the forwarding route according to the reverse path.

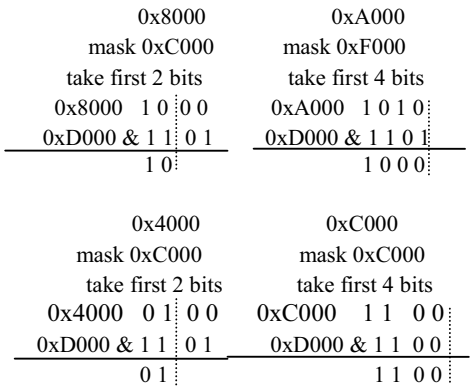

Figure 2. Correlation Calculation of Dynamic mask

VI. ROUTING PROTOCOL SIMULATION EXPERIMENT

This paper chooses the NS2 as the network simulation platform.Based on the provided IEEE802.15.4 MAC layer and PHY layer, it simulates the AODV, the Cluster-Tree and the new protocol proposed in this paper. Specific simulation parameters can be seen in Table 1.

TABLE I. Simulation Parameters

Network Size	50 × 50
Number of Nodes	21
Node Initial Energy	1J
Business source Type	CBR
Rate	2.0
Size of Packets	512B
Cluster-Tree parameters	Cm=4，Rm=4，Lm=3

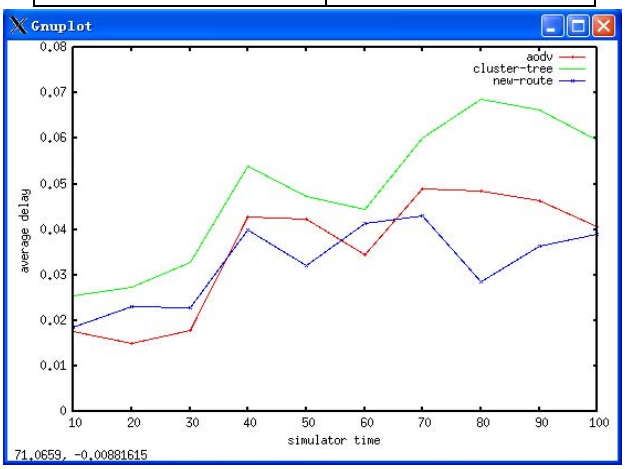

Figure 3. the contrast figure of each protocol on end- to-end delay simulation

Figure 3 is the end-to-end delay simulation diagram of each protocol. It can be seen clearly that the average time delay of Cluster-Tree routing algorithm is higher than that of AODV and New-Route. Because a node transmits the request message to its parent node when the message cannot be directly forwarded to the destination node in the Cluster-Tree algorithm. This will lead to the greater probability that the path is not the shortest and the time delay is increased. On the whole the time delay of New-Route and AODV algorithm is similar. In AODV, the time delay is suddenly increased in 30 to 40 seconds. Because there are a lot of routing request and response packet to cope with. New-Route algorithm tends to more stable and it finds the shortest path in the tree topology. Compared with the AODV, it does not take advantage in the path length, but in the process of setting up route it effectively reduces the scope of broadcast, so that the data packets would be much less than AODV.

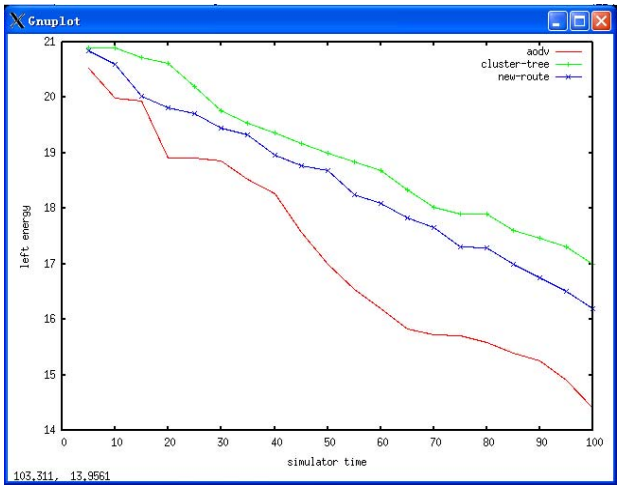

Figure 4. the contrast figure of each protocol on surplus energy simulation

Figure 4 shows the surplus energy simulation diagram of each protocol in network. The differences among the three curves are significant. At 100s, the surplus energy of AODV, New-Route and Cluster-Tree is respectively 14.2532 joules, 16.205766 joules and 17.1253 joules. It fully demonstrates the choice of routing algorithm has the great influence on the wireless network. The trend of the curve also can get the reasonable explanation. In the process of establishing route in AODV algorithm, each node constantly broadcasts routing request packet, sends response packet to the prior node and maintains the routing table. This process expend large amount of energy of nodes. Cluster-Tree algorithm neither needs to establish a route, nor has a routing table. The energy is mainly consumed in calculating next node and the energy consumption is the lowest. New-Route algorithm is located between AODV and Cluster-Tree. It has to maintain its own routing table , but the scope of broadcast is reduced.

VII. CONCLUSION

This paper focuses on the research of the network layer, proposes an improved networking and routing scheme and

completes the simulation on NS2 platform. This method has improved the performance at some aspects compared to the commonly used AODV and Cluster-Tree algorithm. But each protocol has its own applicability. The idea presented in this paper has its own shortcomings compared to some existed protocols at some performance indicators.

The performance of ZigBee network depends largely on the distribution of network nodes. It is difficult to have a pervasive network environment due to the broad application scope of the ZigBee network. So the problem of how to put the theory algorithm to use in practice is also worthy of research.

REFERENCES

[1] Shouwei Gao, Canyang Wu. ZigBee Technology Practice.Beijing : Beijing University of Aeronautics and Astronautics Press, 2009.6

[2] Dilip Kumar Ahirwar, Prashant Verma and Jitendra Daksh. Enhanced AODV Routing Protocol for Wireless Sensor Network Based on ZigBee. Department of Electronics and Telecommunication, SVNiT, Sagar, India,2012

[3] ting Jiang , Chenglin Zhao. ZigBee technology and its application.Beijing: Beijing University of Posts and Telecommunications Press, 2006.50-60

[4] Shuanghua Huang.ZigBee Research and Implementation on Wireless sensor network.Electronic Measurement Technology,2007,30(2):59-64

[5] Zhian Lü.ZigBee Network Principle and Application Development. Beijing : Beijing University of Aeronautics and Astronautics Press, 2008.10-12

[6] jing sun,Zhongxiao Wang,hongwang,Research on Routing Protocols Based on ZigBee Network.Shenyang Normal University,2008

[7] Tachong Kin, Daeyoung Kim, Noseong Park, Seong-enu Yoo. Tomas Sanchez Lopez Shortcut Tree Routing in ZigBee Netorks.IEEE,2007

[8] Kwang Koog Lee,g Hoon Kim.Cluster Label-based ZigBee Routing Protocol with High Scalability,Second International Conference on Systems and Networks Communications,2007

Wireless Interconnects Enabled On-Chip Multicast Communication

Baoliang Li, Jia Lu, Jiahui Sun, Lei He, Wenhua Dou
School of Computer Science
National University of Defense Technology
Changsha, Hunan 410073
Email: libaoliang@nudt.edu.cn

***Abstract*—The ability of multicasting is necessary and useful for Chip Multiprocessors (CMPs) to benefit and implement cache coherence protocols, parallel algorithms, etc. Whereas the design and implementation of high-efficient multicasting in traditional wired Network-on-Chip (NoC) is an arduous task. With the aid of wireless interconnects, not only the bandwidth and latency of NoC can be improved dramatically, but also the inherent broadcast properties of wireless signals can be adopted for multicasting. In this paper, we propose a mesh-like multicast enhancing mechanism based on wireless interconnects. Equipped with 9 wireless transceivers in a traditional 9×9 mesh NoC, this approach realizes a high efficiency, low latency group interconnection. Simulation results show the promising performance boosting of the wireless interconnection.**

***Keywords*—Wireless Interconnects; Multicast Communication; Networks-on-Chip**

I. Introduction

Nowadays, many-core has become a promising approach for improving the computing performance of a single chip. However, while entering many-core era, there are still some new challenges preventing us improving the performance of Chip Multiprocessors (CMPs), e.g. the communication bottleneck. And the Network-on-Chip (NoC) [1] has been proposed to meet this huge requirement.

The ability of high efficiency multicasting is a so important aspect that the architects should consider seriously while designing NoC architecture. First, multicasting is necessary for the cache coherence protocol (e.g. snooping protocol [2], directory protocol [3], token protocol [4], etc.) in a shared memory multiprocessor to distribute the state transition and cache invalidation information. Second, multicasting is very useful for parallel algorithms (e.g. matrix multiplication, search and graph theory, etc.) to realize group communication [5]. Finally, unicast and broadcast can also be considered as special cases of multicast. So, high-efficiency multicast is a key factor for the performance of application running on CMPs.

Implementing multicast in traditional wired NoC is an arduous task, although researchers have devoted much efforts on it. The existing proposals can be classified into two catalogs according the forking position. The simpler one is replicating the multicast packets at source node (either in hardware or software), and all these packets will be treated as unicast thereafter and sent to different nodes in the multicast set. Although simplified the design of routers, it leads to high latency and low throughput. A more sophisticated multicasting scheme replicates the packets inside routers, e.g. path-based multicast [6] and tree-based multicast [7]. Tree-based multicasting scheme leads to lower latency compared with path-based schemes because the paths in multicast tree are always the shortest paths, although more control logic should be added into routers. Recently, in order to guarantee the Quality-of-Service (QoS) of multicasting, a connection-oriented multicasting scheme [8] has been proposed too. The multicast process of this scheme is decomposed into three steps: path-setup, data-transmission and path-tear. Obviously, the latency of this scheme is very high because of these additional stages.

Novel interconnection technologies, such as photonics [9], millimeter-wave/RF [10] and wireless interconnects can also be used to realize multicasting. But there're mainly three drawbacks on realizing multicast by means of photonic or millimeter-wave. First, the optical/RF devices such as modulator, detector and waveguide, multiplexer usually very huge (tens or hundreds of μm), which leads to serious on-chip area overhead. Second, waveguides will occupy large amount of on chip area, and burden the floorplanning complexity. Thirdly, the heterogeneous integration of photonic or RF interconnects is very difficult. The breakthrough of on-chip wireless interconnects provide us great opportunity to realize a high-bandwidth, low-power and single-hop global multicast.

On-chip wireless interconnects was first used in the clock distribution network to reduce clock skew [11]. And nowadays, researchers have proposed several on-chip wireless communication paradigms: Ultra-WideBand (UWB) [12], optical free-space interconnects [13], capacitor coupling [14], inductive coupling [15] and Carbon NanoTubes (CNTs) [16]. Among all these new technologies, UWB is the easiest way of integrating into the traditional CMOS manufacturing process, and the intrinsic broadcast property of wireless signals makes the on chip broadcast much easier compared with the traditional wired, photonics and millimeter-wave approaches, and all the wireless receivers within the transmission range of the wireless transmitter will receive the multicast messages nearly at the same time. What's more, with the aid of wireless interconnects, on chip planning and routing can be alleviated significantly, too.

In this paper, we propose a mesh-like wireless enhanced on-chip interconnection architecture. By applying the high-

978-0-7695-4818-0/12 $26.00 © 2012 IEEE
DOI 10.1109/DCABES.2012.23

bandwidth, low-power and low latency wireless interconnects, this architecture realizes the long-range, large bulk of data transmission and high-efficient multicasting. We take mesh as a basis topology based on the observation that mesh has many promising properties among all these popular topologies: shorter wires, ease of floorplaning and structure regularity.

The rest of this paper is organized as follows. Section II introduces the architecture of the wireless enhanced multicast NoC, including the topology, packet format, deadlock avoidance and flow control mechanism. Section III evaluates the proposed wireless architecture. Our conclusion and future work are then provided in Section VI.

II. Wireless Enabled Multicast Architecture

While designing and implementing a NoC with multicast, the architects must keep the following requirements in mind:

- Global ordering of multicast: all the IP cores receive the multicast packets in the same order, which is very useful and necessary for cache coherence protocol.
- Low latency: packets should be delivered to their destinations as soon as possible to meet the rigorous timing requirement of on-chip communication.
- Low overhead: multicast hardware should be as simple as possible to reduce hardware complexity and power consuming.
- Dynamical update of multicast set: the multicast set should be updated dynamically, to meet the various requirements of different applications.
- Separation of multicast and unicast traffic: Multicast traffic only forms a small portion of total traffic, and it should not interfere with the unicast traffic significantly.

In this section, we will introduce a novel wireless enabled multicast NoC architecture to meet these requirements listed above.

A. Topology of Wireless Enabled Multicast NoC

The wireless enabled multicast NoC architecture is based on a 9×9 mesh topology, which can be viewed as a hierarchy wired/wireless hybrid architecture: the basic building block is a 3×3 mesh, and a secondary hierarchy are constructed with 9 basic building blocks to form a block-level 3×3 mesh, as shown in Fig. 1. That's to say, all the 81 tiles in this NoC are grouped into 9 subnets, and each subnet contains 9 tiles: 1 wireless tile and 8 wired tiles around the wireless tile. A wired tile consists of a processor core, Cache, Cache controller and Network Interface (NI). The central wireless tile is composed of a processor core, cache and cache controller, a special NI and a wireless transceiver which takes responsibility for delivering the multicast packets for the wired tiles. And the ID of all these 9 tiles equipped with wireless transceivers is 10, 13, 16, 37, 40, 43, 64, 67 and 70, respectively. Each wireless tile has a transmitting queue and a receiving queue, the transmitting queue buffers the packets that will be sent to the tiles that located in other subnets, and the receiving queue buffers the packets that sent by the No. 40 tile's wireless transmitter.

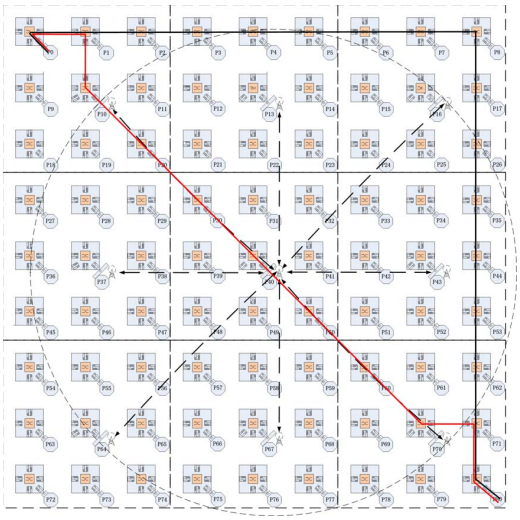

Fig. 1. Wireless Enabled Multicast NoC

Tiles in this architecture are connected through the traditional wormhole routers, and the communication between any two tiles can be realized by either wired or wireless interconnects. A sophisticated way is that delivering local unicast packet in wired interconnects as the traditional NoC does, and transmitting the global unicast and multicast packets in wireless interconnects. When a global unicast or multicast packet is generated, it's first be encapsulated with a mask field and some usual header fields, then sent to the nearest wireless tile as a 'unicast' packet via the traditional wired routine.

NI in wireless tile is specially designed to support the multicast operation. On receiving a multicast packet from wormhole router, NI should check the mask field to ensure that whether there're some bits is set to '1', if so, send a copy of packet to the central wireless tile to broadcast it through the wireless channel. On receiving a multicast packet from the wireless receiver, it should check the mask field to ensure whether delivering a copy of this packet to the local subnet. NI in the No. 40 wireless tiles should also send a copy of multicast packet received from the wireless receiver to the wireless transmitting queue. In contrast with the traditional wired channel, the packet in wireless channel will be transmitted at packet granularity. That's to say, sending the whole packet at a time to utilize the high bandwidth of wireless channel and simplify the control logic. On sending a packet to the central tile, the wireless tile can infer that the packet has been sent to all the destination tiles correctly. When the packet is received and buffered in the receiving queue, it should be forwarded to the processor tile as soon as possible.

B. Packet Format of Wireless Wireless Enabled Multicast NoC

Message generated in the application layer can be divided into serval segments, each segment will be encapsulated into a single packet, and there's a SQ field in the packet header to identify the sequence of these segments. In order to identify

the destinations of multicast packet, an 81 bits mask field is required in the packet header: mask[i]=1 means that tile i is in the multicast set of this packet. The packet format in this hybrid architecture is shown as Fig 2. In the wormhole router, these packets will be divided into serval flits, and each flit has two common field (flit type, virtual channel ID) to identify the flit type and VC ID.

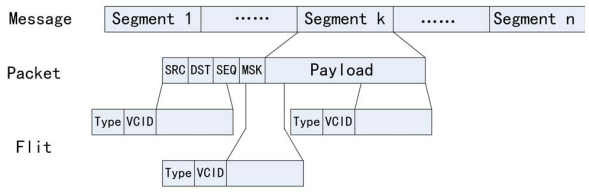

Fig. 2. Packet Format of Wireless Multicast NoC

C. Deadlock Avoidance and Flow Control

Congestion, caused by multicast packet replication in traditional wired NoC is much more complicated than the unicast counterpart, and the introduction of wireless interconnects make thing even worse. So the architects must take the flow control into consideration while designing wireless enabled multicast NoC. The flow control of wired part in this architecture is the same as traditional credit-based flow control. In this subsection, we will describe the flow control mechanism used in this hybrid architecture that involves wireless tiles.

If the buffer in central tile is overflowed, then all the other 8 wireless tiles should stop sending packet to it, but they can still receive packets from the central tiles. If one or more borderline wireless tiles's receiving buffer are full, the they must inform the central tile of their overflow, on receiving overflow information of borderline wireless tile, the central wireless tile stop sending multicast packets but it's still able to accept the multicast packets that were sent by borderline tiles.

D. Wireless Channel Arbitration

Borderline and central wireless transmitters work at different frequency to avoid collision. And we can tune the transmission power of each wireless transmitter to make the wireless transmission range cover the whole chip area. We can view the wireless channel as a kind of virtual bus, in which all the multicast packets are ordered while transmitting across the chip. The central wireless tile (No. 40) acts as a "baton" to arbitrate the usage of wireless channel, and the global multicast order of packets that come from different tiles are kept by the arbitration of accessing the wireless channel. Whenever the channel is idle, the arbiters allocate the channel to the next requesting tile according to the round-robin policy. And all the other 8 wireless tiles can transmit data only when the central tile granted to. Multicast packets in the central tile equipped with identical and omnidirectional UWB will be sent to all these borderline wireless tiles at the same time, and removed from the central tile's buffer immediately. In contrast with traditional wired multicasting schemes, only when the packet has been transferred successfully to all the destination tiles, can the packet could be removed from buffer. That's why the wireless multicast scheme in this architecture could reduce the multicast time significantly.

III. Performance Evaluation

In this paper, we propose a on chip wireless interconnection architecture, which is capable of long-range transmission in a short latency. In order to compared with the traditional wired scheme, we carried out the simulation on HNoCs NoC Simulator [17] which is developed upon OMNeT++ simulation platform. Suppose tile 0 will communicate with tile 80 and the NoC adopts Dimension-Order-Routing (DOR). The transmission path of wired and wireless interconnects is shown in Fig.1. Simulation results is shown in Fig.3, which gives us a intuitive hint on the attractive performance improvement of wireless global interconnects. A fact that must be mentioned is that, in the traditional CMPs, a large percent of traffic is local because of the locality property of program, so the aggregate traffic might be very low, which further implies that, the proposed wireless architecture is capable of high-efficient on-chip long-range transmission.

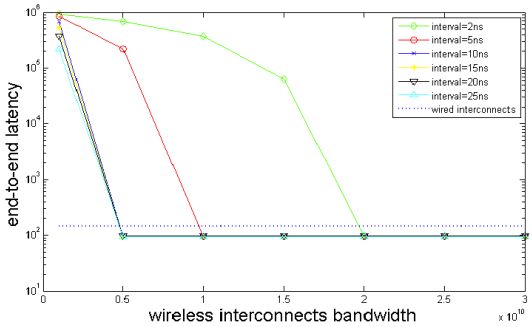

Fig. 3. end-to-end latency of wired vs. wireless NoC

In order to evaluate the multicast performance of on-chip wireless interconnects, we need to introduce the concept of multicast duration, which is defined as the time interval from being generated to the latest node receive it. As mentioned before, the wireless NoC need fewer hops to reach the destination node compared with the wired counterpart. Therefore, the multicast duration might be smaller than the wired ones, too. We configure the HNoCs with the following parameters to validate our predication.

As mentioned in previous sections, there have been many multicast proposals for NoC in the literatures. Different proposals have different performance and features, and we can not compare with all of them. Therefore, in this paper, we adopt a simplified and generalized way (as shown in Alg. 1), the intrinsic idea is that we simplify the multicast process to get a lower bound of all these multicast proposals. After processed by the multicast pruning algorithm Alg. 1, multicast becomes unicast. Obviously, compared with the original multicast scheme, the

TABLE I
CONFIGURATION PARAMETERS

parameters	value
buffer depth (in flits) Per VC	8
packet size	3flits
network link	32bit/1cycle latency
number of VC	4
NoC Topology	9x9 Mesh
mean rate of multicast	100ns
simulation cycles	500000
routing algorithm	DOR
wireless bandwidth	100Gbps, 200Gbps, 300Gbps

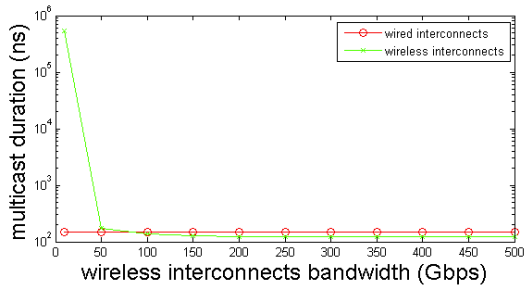

Fig. 4. multicast duration of wired vs. wireless interconnects

simplified one has a lower end to end latency. If the wireless scheme outperforms the simplified multicast scheme, then it outperforms all of these multicast proposals appeared in the literatures. Simulation results is shown in Fig.4.

Algorithm 1 multicast tree pruning algorithm

Require:

Multicast set Ω of all tiles that sending multicast packets

Ensure:

Pruned multicast set

1: **for** all node i sending multicast packets **do**
2: **if** node k's manhattan distance is the longest in Ω_i **then**
3: $\Omega_i := \{k\}$
4: **end if**
5: **end for**

IV. Conclusion

Applying wireless interconnects to NoC could increase the accessability, bandwidth utility and eliminate the long latency and crosstalk introduced by the global wired interconnects. The Wireless NoC proposed in this paper adopts a distributed arbitration strategy to ensure the global order, which is very attractive in implementing the on chip snooping-based cache coherence protocol.

The transmission power of UWB transceiver will grow at an exponential rate while increasing transmission range, therefore, one drawback of our proposal is that the power consuming is a little high. As a future work, we plan to design a multi-level wireless multicast NoC to shorten the per-hop transmission range, so as to reduce the transmitting power and increase the power-bandwidth gain.

Acknowledgment

The authors would thank the reviewers for their suggestions and comments. This research is supported by National Natural Science Foundation of China (Grant No. 61103010, 61103190, 60803100), National Basic Research Program of China (Grant No. 2012CB933500) and High Technology Research and Development Program of China (Grant No. 2012AA011001, 2012AA011902).

References

[1] W. J. Dally and B. Towles. Route packets, not wires: On-chip interconnection networks. In *Proceedings of the 38th Design Automation Conference*, pages 684–689, Jun. 2001.

[2] James Goodman. Using cache memories to reduce processor-memory traffic. In *In Proceedings of the International Symposium on Computer Architecture*, 1983.

[3] Alberto Ros, Manuel E. Acacio, and Jose M. Garcia. A direct coherence protocol for many-core chip multiprocessors. *IEEE Trans. Parallel Distrib. Syst.*, 21:1779–1792, December 2010.

[4] Milo M. K. Martin, Mark D. Hill, and David A. Wood. Token coherence: A new framework for shared-memory multiprocessors. *IEEE Micro*, 23:108–116, November 2003.

[5] Faizal Samman, Thomas Hollstein, and Manfred Glesner. New theory for deadlock-free multicast routing in wormhole-switched virtual-channelless networks-on-chip. *IEEE Trans. Parallel Distrib. Syst.*, 22(4):544–557, April 2011.

[6] X. Lin, P.K. McKinley, and L.M. Ni. Deadlock-free multicast wormhole routing in 2-d mesh multicomputers. *Parallel and Distributed Systems, IEEE Transactions on*, 5(8):793–804, 1994.

[7] MP Malumbres and J. Duato. An efficient implementation of tree-based multicast routing for distributed shared-memory multiprocessors. *Journal of systems architecture*, 46(11):1019–1032, 2000.

[8] Z. Lu, B. Yin, and A. Jantsch. Connection-oriented multicasting in wormhole-switched networks on chip. In *Emerging VLSI Technologies and Architectures, 2006. IEEE Computer Society Annual Symposium on*, pages 6–pp. IEEE, 2006.

[9] J. Chan, G. Hendry, A. Biberman, and K. Bergman. Tools and methodologies for designing energy-efficient photonic networks-on-chip for highperformance chip multiprocessors. In *Circuits and Systems (ISCAS), Proceedings of 2010 IEEE International Symposium on*, pages 3605–3608. IEEE, 2010.

[10] M.F. Chang, J. Cong, A. Kaplan, M. Naik, G. Reinman, E. Socher, and S.W. Tam. Cmp network-on-chip overlaid with multi-band rf-interconnect. In *High Performance Computer Architecture, 2008. HPCA 2008. IEEE 14th International Symposium on*, pages 191–202. Ieee, 2008.

[11] B.A. Floyd et al. The projected power consumption of a wireless clock distribution system and comparison to conventional distribution systems. In *Interconnect Technology, 1999. IEEE International Conference*, pages 248–250. IEEE, 1999.

[12] Dan Zhao and Yi Wang. Sd-mac: Design and synthesis of a hardware-efficient collision-free qos-aware mac protocol for wireless network-on-chip. *IEEE Trans. Comput.*, 57:1230–1245, September 2008.

[13] J. Xue, A. Garg, B. Ciftcioglu, J. Hu, S. Wang, I. Savidis, M. Jain, R. Berman, P. Liu, M. Huang, et al. An intra-chip free-space optical interconnect. In *ACM SIGARCH Computer Architecture News*, volume 38, pages 94–105. ACM, 2010.

[14] K. Kanda, D.D. Antono, K. Ishida, H. Kawaguchi, T. Kuroda, and T. Sakurai. 1.27 gb/s/pin 3mw/pin wireless superconnect (wsc) interface scheme. In *Solid-State Circuits Conference, 2003. Digest of Technical Papers. ISSCC. 2003 IEEE International*, pages 186–487. IEEE, 2003.

[15] N. Miura, D. Mizoguchi, T. Sakurai, and T. Kuroda. Analysis and design of inductive coupling and transceiver circuit for inductive inter-chip wireless superconnect. *Solid-State Circuits, IEEE Journal of*, 40(4):829–837, 2005.

[16] R.H. Baughman, A.A. Zakhidov, and W.A. De Heer. Carbon nanotubes–the route toward applications. *Science*, 297(5582):787–792, 2002.

[17] Eitan Zahavi and Yaniv Ben Izhak. The technion matrics project. http://webee.technion.ac.il/matrics/software.html.

An Intelligent Traffic Grooming Scheme for IP over WDM optical Internet

Qingjun Wang, Xingwei Wang, Wuwen Lai, Min Huang
College of Information Science and Technology
Northeastern University
Shenyang, P.R. China
wangxw@mail.neu.edu.cn

***Abstract*—In this paper, an intelligent static traffic grooming scheme based on predatory search algorithm (PSA) and gaming is proposed in IP over WDM (Wavelength Division Multiplexing) optical Internet. Based on the layered graph, the proposed scheme tries to maximize the comprehensive user traffic request delay satisfaction degree and minimize the network relative cost, and then the optimal traffic grooming scheme is found through the transition between the local and the global search realized by adjusting the restriction level of search area. It is simulated over actual network topologies. Simulation results show that it is both feasible and effective with better performance than certain existing traffic grooming scheme.**

Keywords-static traffic grooming; predatory search; gaming

I. INTRODUCTION

In the IP over WDM (Wavelength Division Multiplexing) optical Internet, the required bandwidth of each traffic request is always much lower than a wavelength capacity, if it were assigned a whole wavelength, huge amount of bandwidth would be wasted. Traffic grooming is thus necessary to combine many low-bandwidth requests into high-bandwidth wavelength channel to improve bandwidth utilization.

The research on traffic grooming focused on ring network in early stage, and now mesh network, aiming at reducing network cost directly or indirectly, for example, minimizing the amount of the used optical add-drop multiplexers (OADMs) and optical transceivers. In Ref [1], several optimized algorithms solving the grooming, routing and wavelength assignment (GRWA) problem in ring network were proposed to minimize the number of the used wavelengths and OADMs. In Ref [2], the network flow method was used to solve the traffic grooming problem in WDM mesh networks. In Ref [3], a QoS dynamic traffic grooming scheme in optical Internet was proposed to minimize the network cost. In Ref [4], the idea of orthogonal design evolution was proposed to solve the static traffic grooming problem in WDM mesh networks. In Ref [5], in order to minimize the amount of OADMs, the integral linear programming was used to solve the traffic grooming problem. A general auxiliary graph model was devised in Ref [6] to solve the traffic grooming problem in WDM mesh networks. In Ref [7], in order to minimize the optical equipment costs and the number of the used wavelengths, the approximate algorithms were proposed to solve the traffic grooming problem in WDM mesh networks. However, the delay constraint, especially the flexible delay constraint of traffic request was considered inadequately in most studies, and the network cost was not considered in depth. In this paper, in order to maximize the comprehensive user traffic request delay satisfaction degree and minimize the network relative cost, by using the layered graph, an intelligent static traffic grooming scheme based on the predatory search algorithm (PSA) [8] and game theory [9] is proposed for IP over WDM optical Internet. It is simulated and evaluated, and the results have shown that it is both feasible and effective.

II. MODEL DESCRIPTION

A. Network Model

IP over WDM optical network can be denoted as a graph $G(V,E)$, where V is node set, E is edge set. $\forall v_i \in V$ ($i=1,...,|V|$), N_{t_i} and N_{r_i} are the number of transmitters and receivers, R_{t_i} and R_{r_i} are the number of the unused transmitters and receivers, C_{t_i} and C_{r_i} represent the transmitter cost and receiver cost. C_{c_i} and D_{c_i} represent the wavelength conversion cost and delay of v_i, and if v_i cannot do wavelength conversion, C_{c_i} and D_{c_i} are set to 0. C_{g_i} and D_{g_i} represent the traffic grooming cost and delay of v_i, and if v_i cannot do traffic grooming, C_{g_i} and D_{g_i} are set to 0. $\forall e_{ij} \in E$, W is the number of wavelength provided by e_{ij}, C_{ij} and dl_{ij} represent the transmission cost and delay of e_{ij}.

B. Mathematical Model

$R=[r_{sd}]_{|V|\times|V|}$ is the traffic request matrix, where $r_{sd} =< bw_{sd}, [dl_{sd}, dh_{sd}] >$ is the traffic request from v_s to v_d, bw_{sd} is the bandwidth constraint and $[dl_{sd}, dh_{sd}]$ is the delay constraint interval to reflect certain flexibility.

The notations of P_{sd}^{ij}, AD_{sd}^{i}, DP_{sd}^{i} and WC_{sd}^{i} are introduced . If r_{sd} traverses e_{ij}, P_{sd}^{ij} is set to be 1, otherwise 0; if r_{sd} is locally added at v_i, AD_{sd}^{i} is set to be 1, otherwise 0; if r_{sd} is locally dropped at v_i, DP_{sd}^{i} is set to be 1, otherwise 0; if r_{sd} traverses v_i and the wavelength conversion occurred, WC_{sd}^{i} is set to be 1, otherwise 0.

The network delay DL_{sd}^{G}, processing delay DP_{sd}^{G} and transmission delay DT_{sd}^{G} of r_{sd} under the grooming scheme G are defined as follows:

$$DL_{sd}^{G} = DP_{sd}^{G} + DT_{sd}^{G} \quad (1)$$

978-0-7695-4818-0/12 $26.00 © 2012 IEEE
DOI 10.1109/DCABES.2012.92

$$DP_{sd}^{G}=\sum_{i=1}^{|V|}D_{g_i}\times\left(AD_{sd}^{i}+DP_{sd}^{i}\right)+\sum_{i=1}^{|V|}D_{c_i}\times WC_{sd}^{i} \quad (2)$$

$$DT_{sd}^{G}=\sum_{i=1}^{|V|}\sum_{j=1}^{|V|}dl_{ij}\times P_{sd}^{ij} \quad (3)$$

The user satisfaction degree ST_{sd}^{G} to DL_{sd}^{G} under G is defined as follows:

$$ST_{sd}^{G}=\begin{cases}1 & DL_{sd}^{G}\le dl_{sd}\\ \dfrac{dh_{sd}-DL_{sd}^{G}}{dh_{sd}-dl_{sd}} & dl_{sd}<DL_{sd}^{G}<dh_{sd}\\ \varepsilon & DL_{sd}^{G}=dh_{sd}\\ 0 & DL_{sd}^{G}>dh_{sd}\end{cases} \quad (4)$$

Here, ε is a positive pure decimal far less than 1.

The traffic request relative importance matrix is denoted as $[I_{sd}]_{|V|\times|V|}$, where I_{sd} is the relative importance of r_{sd} in R, $0\le I_{sd}\le 1$, $\sum_{s=1}^{|V|}\sum_{d=1}^{|V|}I_{sd}=1$.

The comprehensive satisfaction degree ST_{R}^{G} to delay under G for R is defined as follows:

$$ST_{R}^{G}=\sum_{s=1}^{|V|}\sum_{d=1}^{|V|}I_{sd}\times ST_{sd}^{G} \quad (5)$$

The network cost NC_{R}^{G}, processing cost PC_{R}^{G} and transmission cost TC_{R}^{G} of R under G are defined as follows:

$$NC_{R}^{G}=PC_{R}^{G}+TC_{R}^{G} \quad (6)$$

$$PC_{R}^{G}=\sum_{s=1}^{|V|}\sum_{d=1}^{|V|}\sum_{i=1}^{|V|}C_{g_i}\times\left(AD_{sd}^{i}+DP_{sd}^{i}\right)+\sum_{s=1}^{|V|}\sum_{d=1}^{|V|}\sum_{i=1}^{|V|}C_{c_i}\times WC_{sd}^{i} \quad (7)$$

$$TC_{R}^{G}=\sum_{s=1}^{|V|}\sum_{d=1}^{|V|}\sum_{i=1}^{|V|}\sum_{j=1}^{|V|}\left(C_{ij}\times P_{sd}^{ij}\right)+\sum_{i=1}^{|V|}\left(\left(N_{t_i}-R_{t_i}\right)\times C_{t_i}+\left(N_{r_i}-R_{r_i}\right)\times C_{r_i}\right) \quad (8)$$

The network full-load cost NC can be calculated as follows:

$$NC=\sum_{i=1}^{|V|}\sum_{j=1}^{|V|}C_{ij}+\sum_{i=1}^{|V|}\left(C_{gi}+N_{t_i}\times C_{t_i}+N_{r_i}\times C_{r_i}+C_{ci}\right) \quad (9)$$

Then, the network relative cost NRC_{R}^{G} of R under G can be defined as follows:

$$NRC_{R}^{G}=\frac{NC_{R}^{G}}{NC} \quad (10)$$

C. Gaming Analysis

The set of gaming participants is denoted as $S_p=\{1,2\}$, where 1 and 2 represent the network provider and the user. Under G, $S_N=\{s_{11},s_{12}\}$ and $S_U=\{s_{21},s_{22}\}$ is the strategy set of the network provider and that of the user. Here, s_{11} and s_{21} represent that the network provider or the user accepts G, while s_{12} and s_{22} represent that the network provider or the user refuses G. The utility matrixes of the network provider and the user are defined as follows:

$$U_{N}^{G}=\begin{bmatrix}a_{11} & a_{12}\\ a_{21} & a_{22}\end{bmatrix}=\begin{bmatrix}\dfrac{ST_{R}^{G}}{E_0}-1 & -\dfrac{1}{NRC_{R}^{G}}\\ -\delta_1\times\dfrac{ST_{R}^{G}}{E_0}-1 & 0\end{bmatrix} \quad (11)$$

$$U_{U}^{G}=\begin{bmatrix}b_{11} & b_{12}\\ b_{21} & b_{22}\end{bmatrix}=\begin{bmatrix}ST_{R}^{G} & -\delta_2\times ST_{R}^{G}\\ -ST_{R}^{G} & 0\end{bmatrix} \quad (12)$$

Here, a_{11}, a_{12}, b_{11} and b_{12} are the network provider utility and the user utility respectively when the network provider employs s_{11} and the user employs s_{21} and s_{22}; a_{21}, a_{22}, b_{21} and b_{22} are the network provider utility and the user utility respectively when the network provider employs s_{12} and the user employs s_{21} and s_{22}; E_0 is the lower bound of ST_{R}^{G} which is set according to experience; δ_1 and δ_2 are penalty factors, representing the negative impact when the network provider refuses G while the user accepts G and that when the network provider accepts G while the user refuses G, $\delta_1,\delta_2>1$. If the following is satisfied, the Nash equilibrium [9] is achieved.

$$\begin{cases}a_{i^*j^*}\ge a_{i^*j}\\ b_{i^*j^*}\ge b_{ij^*}\end{cases} \quad (13)$$

Here, $i,j,i^*,j^*=1,2$. Apparently, the bigger the ST_{R}^{G} and the smaller the NRC_{R}^{G}, the better the network provider utility and the user utility can be achieved.

III. GROOMING SCHEME DESCRIPTION

The objective of the proposed grooming scheme in this paper is to maximize the comprehensive user traffic request delay satisfaction degree and minimize the network relative cost simultaneously with both the user request delay and bandwidth constraints satisfied.

A. Layered Graph Construction

At first, the layered graph $G'(V',E')$ is constructed according to $G(V,E)$ to ensure that nodes and edges are not considered separately when grooming is performed [6]. The procedure of constructing layered graph is described as follows:

Step1: Input $G(V,E)$.

Step2: Generate the vertexes in $G'(V',E')$: $\forall v_i\in V$, insert $(W+2)\times 2$ vertexes into $G'(V',E')$, that is $v_i^{1,0},\cdots,v_i^{W+2,0}$ and $v_i^{1,1},\cdots,v_i^{W+2,1}$.

Step3: Generate the edges in $G'(V',E')$.

Step3.1: Generate the edges in $G'(V',E')$ according to the vertexes in $G(V,E)$.

Step3.1.1: $\forall v_i \in V$, add the wavelength bypass edge we_{il} on each wavelength layer of $G'(V',E')$, and the edge weight is set to be 0.

Step 3.1.2: $\forall v_i \in V$, add the grooming edge ge_i on access layer of $G'(V',E')$, and the edge weight is set to be D_{g_i}.

Step 3.1.3: $\forall v_i \in V$, if there is an available transmitter for wavelength λ^l, add the transmitter edge te_{il} into $G'(V',E')$, and the edge weight is set to be 0.

Step 3.1.4: $\forall v_i \in V$, if there is an available receiver for wavelength λ^l, add the receiver edge re_{il} into $G'(V',E')$, and the edge weight is set to be 0.

Step 3.1.5: $\forall v_i \in V$, if the wavelength λ^l can be converted to the wavelength λ^w, add the converter edge ce_{ilw} into $G'(V',E')$, and the edge weight is set to be D_{c_i}, $1 \le l, w \le W$.

Step 3.2: Generate the edges in $G'(V',E')$ according to the edges in $G(V,E)$. If there is e_{ij} from v_i to v_j and the wavelength λ^l is available, add the wavelength edge le_{ijl} into $G'(V',E')$, and the edge weight is set to be dl_{ij}.

Step 4: $G'(V',E')$ construction is over.

B. Grooming procedure

When animals seek preys, they search along a certain direction at a fast pace at first until they find preys or food evidences around them; then, they will slow their speed down and intensify their search in the neighboring area in a clear attempt to find more preys. After searching a period of time without finding any prey, they will give up the intensified area-restricted search and continue to search in the whole area.

By simulating the predatory search strategies of animals, a new bio-inspired computing method named predatory search algorithm (PSA) [8] is proposed. When this algorithm searches for the optimum, it at first seeks in the whole solution space until the current optimal solution is found. Then, it intensifies the search in the nearby space (neighborhood) around the current optimal solution. After searching a period of time without further solution improvement, it gives up the 'area-restricted' search and turns to the original extensive search. This cycle continues until the optimal (or satisfied suboptimal) solution is found. The particular way is to find the adjacent solution of the current optimal solution by defining neighborhood and to use the restriction to represent the size of the current optimal solution's neighborhood. In order to expand the search area in current optimal solution's neighborhood gradually, PSA defines a list of n restriction levels: *Restriction*(0), … , *Restriction*(i), … , *Restriction*(n-1). *Restriction*(i) represents the restriction value under the level i. The bigger the restriction level is, the greater size of the search area is. The initial restriction level is set to be 0. Under certain restriction level, if the algorithm searches the current optimal solution's neighborhood certain times and does not find a better solution, the restriction level increases by 1, and then continues searching. When the restriction level is increased to the preset threshold, it means that the algorithm has searched the optimum sufficient times in the restricted area and has not found any better solution; then, the algorithm gives up the intensified area-restricted search and sets the restriction level to a higher one, which means jumping out of the restriction of the current space and turn to search in the wider space. When the current optimal solution is improved during the searching, each restriction level value is recomputed, and then repeats the above procedure. The transition between the local and global search is realized by adjusting the restriction level of the searching space, and thus the algorithm can avoid getting into the local optimal solution.

Based on PSA and gaming, a static traffic grooming scheme is proposed to find optimal grooming solution.

1) Solution expression and generation: A solution $x=[a_{sd}]_{|V|\times|V|}$ corresponds to a grooming scheme G. $\forall r_{sd} \in R$, the *Dijkstra kth* shortest path algorithm [10] is run on $G'(V',E')$ to find the paths of whch bandwidth is not lower than bw_{sd} and delay is not higher than dh_{sd}, and then the feasible path set $P_{sd}=\{P_{sd1},...,P_{sdi},...,P_{sdk}\}$ is constructed. Here, sdi is the sequence number of the path P_{sdi} in P_{sd}, $i=1,...,k$. A path is selected randomly from P_{sd}, and then assign its sequence number to a_{sd} which corresponds to r_{sd}, thus x is constructed.

2) Definition of neighborhood: For x, a node pair consisted of s and $d(s \ne d)$ is selected randomly, then choose a sequence number of path from P_{sd} randomly which is not equal to the current value of a_{sd} and replace a_{sd}. Thus an adjacent solution of the current solution is found. Using the same method, many adjacent solutions are generated, and the current solution's neighborhood is constructed.

3) Determination of the target value: The target value function of x is defined as follows:

$$f(x)=\frac{1}{\Omega\cdot\left(\alpha\cdot\frac{1}{NRC_R^G}+\beta\cdot ST_R^G\right)} \tag{14}$$

Here, Ω is the gaming weight, and if the Nash equilibrium between the network provider and the user is attained, its value is set to be larger than 1, otherwise it is set to be 1. α and β are adjustment coefficients which is used to reflect whether the network provider or the user is preferred. If α and β are equal, that means it is fair to both sides. Obviously, the smaller the NRC_R^G and the bigger the ST_R^G, then the smaller the $f(x)$ and the better the G corresponding to x.

4) Calculation of restriction: When the current optimal solution is improved, it is needed to recalculate restrictions and reset the restriction level to be 0. Suppose the number of restriction levels is n. The procedure of the restriction computation is defined as follows:

Step1: Search the current optimal solution's neighborhood for $n-1$ times, and the $n-1$ adjacent solutions of the current optimal solution are obtained.

Step2: Sort the target values of the above $n-1$ adjacent solutions and the current optimal solution by the ascending order.

Step3: Assign the sorted n target values to $Restriction(0), \cdots, Restriction(n-1)$ sequentially.

Step4: Choose $Restriction(0), \cdots, Restriction(n-\lfloor n/t \rfloor)$ as the local search restriction, and $Restriction(n-\lfloor n/t \rfloor), \cdots, Restriction(n-1)$ as the global search restriction. Here, t is determined according to n.

5) Grooming procedure description: It is described as follows:

Step1: Generate an initial solution x, and initialize the current optimal solution $x_{best} = x$, restriction $level = 0$, cycle $counter = 0$. Set the neighborhood search times m and the maximum cycle times CM under each restriction, and calculate restriction value.

Step2: If $level < n$, then search the neighborhood of x for m times and select the solution with the minimum target value $x_{\min}$, go to step 3, otherwise go to step 7.

Step3: If $f(x_{\min}) \le Restriction(level)$, then $x = x_{\min}$, go to step 4, otherwise go to step 5.

Step4: If $f(x) < f(x_{best})$, then $x_{best} = x$, $level = 0$, $counter = 0$, re-compute restriction, go to step 2, otherwise go to step 5.

Step5: $counter = counter + 1$, if $counter < CM$, go to step 2; otherwise, $level = level + 1$, $counter = 0$, go to step 6.

Step6: If $level = \lfloor n/t \rfloor$, then $level = n - \lfloor n/t \rfloor$, go to step 2.

Step7: Output x_{best} as the optimal grooming scheme.

IV. SIMULATION AND PERFORMNCE EVALUATION

The proposed scheme has been simulated based on VC++6.0. The simulation software has the following functions: topology management, traffic grooming request generation, grooming solution computation, performance evaluation and result analysis. Its main functions are listed in table I. In order to test its feasibility and effectiveness, the proposed scheme (S1) in this paper and the heuristic grooming scheme (S2) in [6] are simulated over CERNET, CERNET2 and NSFNET. Table II shows the comparison of ST_R^G and NRC_R^G between S1 and S2 under different traffic grooming request ratios (TGR). Obviously, S1 is better than S2.

V. CONCLUSION

In order to maximize the comprehensive user traffic request delay satisfaction degree and minimize the network relative cost, a traffic grooming scheme based on PSA and gaming is proposed in this paper. Simulation studies show that the proposed scheme has good performance. The future research will focus on developing its prototype implementation to verify and increase its practicability.

TABLE I. MAIN FUNCTIONS

Name	Function
ConvertTpToLg(…)	Generate the layered graph based on the physical topology.
void SearchNeib(…)	Search the neighborhood.
void Restriction(…)	Compute restrictions.
void SortSolution(…)	Sort out the solutions.
int FindCurOPT(…)	Find the current optimal solution.
int Nash(…)	Find the Nash equilibrium.
void UMatrix(…)	Compute the user utility matrix.
void NMatrix(…)	Compute the network provider utility matrix.
float TargetVal(…)	Computer the target value of a solution.

TABLE II. PERFORMANCE COMPARISON

TGR	CERNET (S1:S2)		CERNET2 (S1:S2)		NSFNET (S1:S2)	
	ST_R^G	NRC_R^G	ST_R^G	NRC_R^G	ST_R^G	NRC_R^G
20%	1.010	0.806	1.006	0.709	1.010	0.768
40%	1.015	0.938	1.001	0.685	1.040	0.945
60%	1.011	0.936	1.022	0.935	0.994	0.894
80%	1.032	1.093	1.014	1.071	1.049	0.916
100%	1.030	0.943	1.016	0.960	1.071	0.917

ACKNOWLEDGMENT

This work is supported by the National Natural Science Foundation of China under Grant No. 61070162, No. 71071028 and No. 70931001; the Specialized Research Fund for the Doctoral Program of Higher Education under Grant No. 20100042110025 and No. 20110042110024; the Fundamental Research Funds for the Central Universities under Grant No. N110204003.

REFERENCES

[1] Xijun Zhang and Chunming Qiao, "An effective and comprehensive approach for traffic grooming and wavelength assignment in SONET/WDM rings," IEEE/ACM Transactions on Networking, vol. 8(5), 2000, pp. 608-617.

[2] Shi Xiao, Gaoxi Xiao and Leung Y, "A network flow approach for static and dynamic traffic grooming in WDM networks," Computer Network, vol. 50(17), 2006, pp. 3400-3415.

[3] Xingwei Wang, Chengcheng Tong and Min Huang, "A QoS Dynamic Traffic Grooming Scheme," Journal of Northeasten University: Natural Science, vol. 30(6) ,2009, pp. 802-804.

[4] Xingwei Wang, Chengcheng Tong and Min Huang, "Delay and Bandwidth Constrained Intelligent Static Traffic Grooming Scheme," Journal of Northeasten University: Natural Science, vol. 30(9), 2009, pp. 1253-1256.

[5] Junghee Han, "A traffic grooming problem considering hub location for synchronous optical network-wavelength division multiplexing networks," Journal of Computers&Industrial Engineering, vol. 59(1), 2010, pp. 1-8.

[6] Hongyue Zhu, Hui Zang, Keyao Zhu and Mukherjee, B, “A novel generic graph model for traffic grooming in heterogeneous WDM mesh networks,” IEEE/ACM Transactions on Networking, vol. 11(2), 2003, pp. 285-299.

[7] Spyridon A and Lisa Z, “Approximation algorithms for grooming in optical network design,” Theoretical Computer Science, vol. 29(412), 2011, pp. 3738-3751.

[8] Linhares A, “Preying on optima: A predatory search strategy for combinatorial problems,” Proc of IEEE International Conference on Systems, 1998, pp. 2974-2978.

[9] Varian Hal, Microeconomics, 3rd. Beijing: Economic Science Press, 1997.

[10] Kleinberg Jon and Tardos Eva, Algorithm Design. Beijing: Tsinghua University Press, 2006.

Research and simulation of node localization in WSN based on Quantum particle swarm optimization

Litao Gong
School of IOT Engineering
Jiangnan University
Wuxi, China
glitao@126.com

Jun Sun, Wenbo Xu
School of IOT Engineering
Jiangnan University
Wuxi, China
sunjun_wx@hotmail.com

Jian Xu
Chongqing Medical and
Pharmaceutical College
Chongqing, China

***Abstract*—there're so many kinds of localization algorithms with a big localization error. And how to reduce this error is really a very important problem. This paper studies four distributed localization algorithms in WSN, and introduces a pretty popular optimization algorithm named quantum particle swarm optimization algorithm into it. In the end, this paper does some simulations with matlab. And it proves that the QPSO algorithm works well in node localization algorithm.**

Keywords- Wireless network; Distributed; Node localization; QPSO

I. INTRODUCTION

In recent years, the advancement of microelectronics, computing and wireless communication technology promotes the development of the multi-sensor with lower consumption. So the information collection, data processing and wireless communication or other functions can be gathered in the same small volume. Because of the uncontrollable deployment of the nodes, a large majority of the nodes' localizations is unknown so that we cannot get the correct information we need. Neither deploying the nodes artificially nor equipping all nodes with GPS receiver is feasible for the restrictions caused by cost, power and scalability issues. We cannot use a number of nodes to do a lot communication and computing works since the sensor network is very sensitive for power. When those nodes power off, the sensor network appears a hole.

Consequently, we should use distributed algorithms as much as possible to lengthen the using time of the sensor network. The main evaluation criteria for node localization algorithms are: localization precision, scale, anchor node density, node density, fault-tolerant and adaptive, power consumption and cost. The significance of localization algorithm simulation lies in that we can get the performance data of the algorithm as close as possible to the realistic environment, which is useful in finding the algorithm's disadvantage and application environment.

QPSO algorithm is an improved PSO algorithm developed by Jun Sun etc. It improves PSO's global convergence from a quantum mechanics perspective which turns out to have a good performance.

This paper focuses on the research of some representative distributed localization algorithm. And we will do some simulation to see how the algorithm affected by the environmental parameters, for example, the GPS ranging error, anchor node density and node transmitting radius etc. At last, we develop the Dv-Hop algorithm for the simulation combined with the QPSO algorithm.

II. DISTRIBUTED LOCALIZATION ALGORITHM

Distributed localization algorithm can be divided into two modules normally: module of measuring the distances between unknown node and anchor nodes, and module of computing the localization of the unknown node. The unknown nodes firstly measure the distances to the anchor nodes by method of range-based or range-free, and secondly find the location by those distances. Distributed localization algorithm needs no centralized computing, the node can figure out its location itself with limited communication to its neighbors.

III. MEASURE THE DISTANCES BETWEEN UNKNOWN NODE AND ANCHOR NODES

A. Dv-Hop algorithm

DV-hop is a range-free algorithm for node localization, which can get the topology information by calculating the hops among nodes. The algorithm can be divided into two stages. Firstly, every node passes its position information to all the neighbor nodes by broadcast which includes the node's identification, coordinate (x_i, y_i) and hops, called h_i, which initialized with 0. Every other node that acquires this message records it into a list and broadcast it again with h_i plus one.

At the first stage, when a node acquire a message, the h_i should be compared with the earlier one, if the earlier one is less than the later one, the h_i should be placed by the latter. If it not, the later message should be ignored without any handling.

After that, all the anchor nodes known the others' information, furthermore, every sensor node get information of all anchor nodes. So the anchor node can figure out the average distance C_i of a hop between anchor node i and anchor node j(j is every other anchor node but i) using the formula (1)

978-0-7695-4818-0/12 $26.00 © 2012 IEEE
DOI 10.1109/DCABES.2012.58

$$C_i = \frac{\sum_{j \neq i}^{n} \sqrt{(x_i - x)^2 + (y_i - y)^2}}{\sum_{j \neq i}^{n} h_j} \quad (1)$$

At the second stage, every anchor node broadcast the average distance it computed, as well as the anchor node's self-identification. The nodes that get this message add it to the schedule and then send it to all the neighbors. After this, every node knows the C_i computed by the anchor nodes, so it can figure out the average C_i : n is the number of the anchor nodes. As a result, every node gets the average distance of a hop among all the anchor nodes with which we can get the distance between it and every anchor node.

B. APIT algorithm

APIT algorithm is a zone-about locating strategy, and it can be easily used with little cost. This algorithm chooses three unknown nodes from its neighbors by random, then find that whether the node is in the triangle that the three nodes formed or not. If it does, mark this triangle. Do this until there's no three nodes never composed before. Figure out the centroid of the polygon formed by the intersection of all the triangles marked before.

C. Amorphous algorithm

The basic ideas of Amorphous algorithm is to multiply the hop-count of two nodes and average distance of two nodes in the whole net as the direct distance of them, which is similar to DV-Hop algorithm.

D. Bounding Box algorithm

The multilateral measurement localization algorithm based on least square method is the most popular algorithm in localization, and it applied in many localization algorithms. The shortcoming is that it needs lot floating point arithmetic. To solve this problem, Semic from University of California at Berkeley presents a simpler algorithm named Bounding box, whose main ideas is to draw a bounding box using the anchor node location and distance, and then figure out the intersection of the boundary box. The center of the intersection is the estimate position. The point of this algorithm is simplifying the solution of two equations to one equation, thus avoiding the complex least square method and greatly reduces the computational overhead.

IV. COMPUTING THE LOCATION OF THE UNKNOWN NODE

There are some algorithms can be used in the module of computing the node's location, such as, three edge measuring algorithm, polygonal line algorithm, Min-Max algorithm and particle swarm optimization algorithm we mentioned before.

A. three edge measuring algorithm

Three edge measuring algorithm is the simplest method in localization. When the unknown node gets the distance to the anchors, it can be considered that the unknown node is in the circle's edge whose center is the anchor nodes and the radius is the distance. After we get three anchors we can get a set of equations (2)

$$\begin{cases} (x_1 - x)^2 + (y_1 - y)^2 = d_1^2 \\ (x_2 - x)^2 + (y_2 - y)^2 = d_2^2 \\ (x_3 - x)^2 + (y_3 - y)^2 = d_3^2 \end{cases} \quad (2)$$

The value of (x, y) is the node's position we get.

B. Multilateral algorithms

Multilateral algorithm originates from three edge measuring algorithm whose has more than three nodes so that we can get a set of equations just like above

$$\begin{cases} (x_1 - x)^2 + (y_1 - y)^2 = d_1^2 \\ (x_2 - x)^2 + (y_2 - y)^2 = d_2^2 \\ . \\ . \\ . \\ (x_n - x)^2 + (y_n - y)^2 = d_n^2 \end{cases} \quad (3)$$

Equation (3) can be linearized as

$$A = -2\begin{bmatrix} (x_1 - x_n) & (y_1 - y_n) \\ (x_2 - x_n) & (y_2 - y_n) \\ . & . \\ . & . \\ . & . \\ (x_{n-1} - x_n) & (y_{n-1} - y_n) \end{bmatrix} \quad (4)$$

$$b = \begin{bmatrix} r_1^2 - r_n^2 - x_1^2 + x_n^2 - y_1^2 + y_n^2 \\ r_2^2 - r_n^2 - x_2^2 + x_n^2 - y_2^2 + y_n^2 \\ . \\ . \\ . \\ r_{n-1}^2 - r_n^2 - x_{n-1}^2 + x_n^2 - y_{n-1}^2 + y_n^2 \end{bmatrix} \quad (5)$$

Due to the ranging error, reasonable linear model should be: $Ax + N = b$ .Among them, N on behalf of a $k-1$ dimensional random error vector. By the principle of least square method, the value of X should make the model error as small as possible, namely minimizing $Q(x) = \|N\|^2 = \|b - Ax\|^2$. Find the node's least square estimate value: $\$x = (A^T A)^{-1} A^T b$.

C. *Particle swarm optimization algorithm and Quantum particle swarm optimization algorithm*

PSO models social behavior of a flock of birds. It consists of a swarm of s candidate solutions called particles, which explore an n-dimensional hyperspace in search of the global solution (n represents the number of optimal parameters to be determined). The difference between PSO and QPSO lies in the different way of evolution, that is different ways of updating the particle's position.

In the PSO algorithm, the particles must be on a limited search range to ensure the particle swarm's aggregation, thereby making the algorithm convergent to the global minimum or local optima. However, in the QPSO algorithm, particle could appears everywhere in the feasible search space with a certain probability, which could have a better fitness value than the current pbest. QPSO algorithm is easily to be realized and it has less parameters. It also has a good stability and convergence. This paper mainly discusses the QPSO algorithm.

V. SIMULATION OF LOCALIZATION ALGORITHM

This simulation is realized by Matlab.

A. *the anchor node ratio changes*

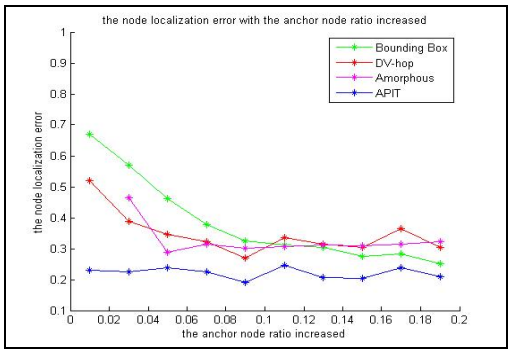

Figure 1. localizaition error affected when node ratio changed

Figure 1 shows that when the emission radius is 25, the anchor node ratio increased by 2% from 1% to 19%. The localization error is going down with the anchor node ratio increased, and it changes little when the anchor node ratio arrive 10%.

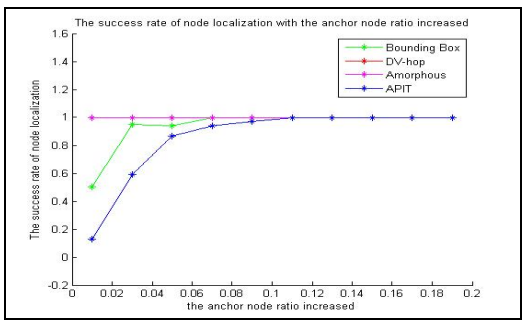

Figure 2. ratio of successful unknown node with node ratio changed

Figure 2 shows the ratio of unknown nodes which is localized successfully about the four algorithms. We can see that the success node ratio is going up while the anchor node ratio increasing. And when the anchor node ratio arrives 10%, all the unknown nodes can be localized. However, Dv-Hop algorithm and Amorphous algorithm has the same line for their global localization strategy.

B. *the emission radius changes*

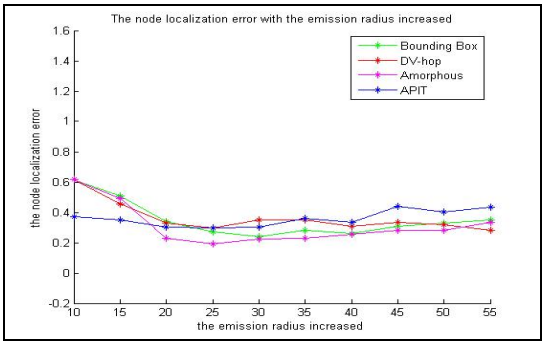

Figure 3. localizaition error affected when the emission radius changes

Figure 3 shows that when the anchor node ratio is 10%, how the four algorithms' performance effected by the changing emission radius which increased by 5 from 10 to 55. We can see that the emission radius has little influence to the localization error.

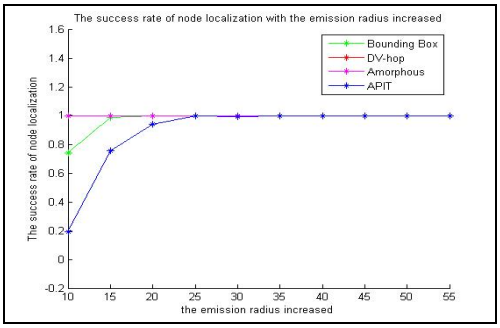

Figure 4. ratio of successful unknown node with emission radius changes

Figure 4 shows a different result that the unknown nodes ratio which located successfully is going up with the emission radius' increasing until it reaches 25.

C. *the GPS ranging error changes*

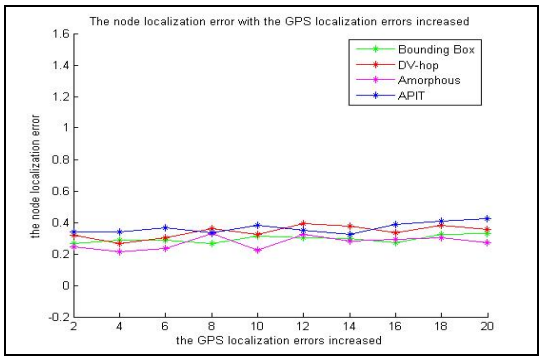

Figure 5. localizaition error affected when GPS ranging error changes

Figure 5 shows the performance of the four algorithms when the anchor node ratio arrives 10%, and the emission radius reaches 25, with the GPS error increases by 2 from 2 to 20. We can conclude that the GPS ranging error has little effect on the localization error.

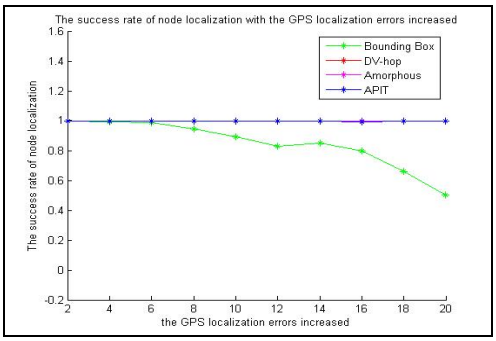

Figure 6. ratio of successful unknow node with GPS error changed

Figure 6 shows the performance of the four algorithms at this situation, with the GPS error increases by 2 from 2 to 20. From all the figures above, we can conclude that when the anchor node ratio arrives 10%, and the emission radius reaches 25, the GPS ranging error can be ignored except Bounding Box algorithm.

VI. SIMULATION OF DV-HOP ALGORITHM BASED ON QPSO

The second part of this simulation focuses on the new Dv-Hop algorithm which is developed by QPSO at its last stage compared with paper 10 since paper 10 has already combined the Dv-Hop algorithm with PSO.

Conclusion can be made from the first part that when the Dv-Hop algorithm applied in a certain situation, namely, the monitoring section is 100-by-100, there are 600 nodes deployed randomly, the anchor node ratio arrives 10% and the emission radius is 25, the Dv-Hop algorithm can get a lower localization error between 30% and 40%. And our simulation environment is just like that.

A. The development of Dv-Hop

This simulation figures out the distances between the unknown nodes and the anchor nodes at the first step in Dv-Hop algorithm, and then use QPSO algorithm instead of LSE to estimate the value of the position.

B. The fitness function

The fitness function is designed like formula (7):

$$f(x_j)=\sum_{i=1}^{n}\left|\left\|P_i-x_j\right\|-D(j,i)\right| \tag{7}$$

P_i means the anchor node's position, x_j means the unknown node's position, and $D(j,i)$ means the distance between the unknown node j and the anchor node i. That is the value of errors of the unknown node to all of the anchor node, which should be as small as possible.

C. The figures

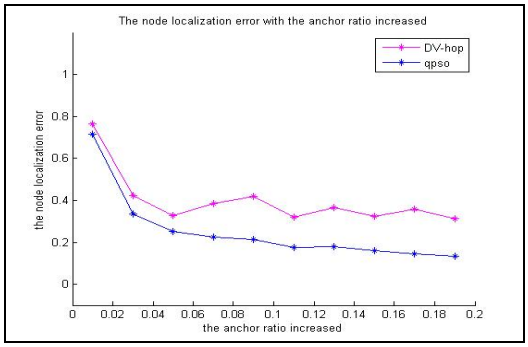

Figure 7. localizaition error affected of the developed algorithm

Figure 7 shows that the localization error is close to 20% with the new algorithm developed by QPSO, while the localization error of the original algorithm is from 30% to 40% as discussed before. That result is better than paper 10's 30% localization error as well. Conclusion can be made that in this situation, QPSO algorithm works better than PSO algorithm or the original Dv-Hop algorithm.

The experience also tells that both Dv-Hop algorithm and the new Dv-Hop could locate all the unknown nodes, and the new algorithm doesn't worse the Dv-Hop algorithm.

CONCLUSION

With the experience, we can see that the QPSO algorithm works well in node localization algorithm, and more attention should be paied here, and we will do more research in this for the more efficient node localization algorithm.

ACKNOWLEDGMENT

The authors would like to thank Mr Xu and Mr Sun for their helpful comments which could significantly improve the quality of the paper. This paper belongs to a National Natural Science Foundation and the foundation number is:

61170119. And it also belongs to a Jiang Su provience Natural Science Foundation whose number is BK2010143.

REFERENCES

[1] Sun Jun. Quantum behaved Particle Swarm Optimization: Theory and Application.M.Beijing China: Tsinghua University press, 2011:31-50.

[2] J. Sun, W. Fang, X. J. Wu, Z. P. Xie, W. B. Xu. Quantum-behaved particle swarm optimization: analysis of the individual particle's behavior and parameter selection[J]. Evolutionary Computation(MIT Press). Uncorrected Proof

[3] J. Sun, B. Feng, W. B. Xu. Particle swarm optimization with particles having quantum behavior[C]. Congress on Evolutionary Computation, Portland, Oregon, USA, 2004, 325-331.

[4] W. Fang, J. Sun, Y. R. Ding, X. J. Wu, W. Xu. A review of quantum-behaved particle swarm optimization[J]. IETE Technical Review, 2010, 27(4): 336-348.

[5] Guowei Shen. Performance Comparison of TOA and TDOA Based Location Estimation Algorithms in LOS Environment. PROCEEDINGS OF THE 5th WORKSHOP ON POSITIONING, NAVIGATION AND COMMUNICATION 2008.

[6] Xing Mingyan. Application of particle swarm optimization to positioning for wireless sensor networks. J. Computer Engineering and Applications,2009,45(32):72-74.

[7] Raghavendra V. Kulkarni. Particle Swarm Optimization in Wireless-Sensor Networks: A Brief Survey.J. IEEE TRANSACTIONS ON SYSTEMS, MAN, AND CYBERNETICS—PART C: APPLICATIONS AND REVIEWS, VOL. 41, NO. 2, MARCH 2011:262-267.

[8] Duan Weijun. Research and Development of Localization Systems and Algorithms for Wireless Sensor Networks.J. Information and Control:100220411 (2006) 0220239207.

[9] Yuan Hao. Wireless Sensor Network Path Optimization Based on Particle Swarm Algorithm.J. Computer Engineering:1000—3428(2010)04—0091.

[10] DRAGO¸S NICULESCU. DV Based Positioning in Ad Hoc Networks.J. Telecommunication Systems, 2003,22:1–4, 267–280.

[11] Tian He, Range-Free Localization Schemes for Large Scale Sensor Networks.J. Computer Communication Networks, ACM 1-58113-753-2/03/0009.

[12] Zhang Changshan. Research on node self-localization algorithm for wireless sensor networks.J. Transducer and Microsystem Technologies,2011 TN929.5:43-49.

[13] Chen Xingzhou. Improvement of node localization in w ireless sensor network based on particle swarm optim ization.J. Journal o f ComputerApp lications,2010, TP393. 17:1736-1739.

Tracking Algorithm of WSN Based on Improved Particle Filter

Guodong Zhang[1], Yanrui Ding[1], Jian Xu[2], Wenbo Xu[1]
[1]School of IOT Engineering, Jiangnan University;
[2] Chongqing Medical and Pharmaceutical College.
Wuxi , China
gordon2001@sina.com, yr_ding@jiangnan.edu.cn, xwb@jiangnan.edu.cn

***Abstract*—In this paper, in order to achieve single target tracking in the wireless network, the original particle filter algorithm has been improved. I introduce the essence of the APIT algorithm about how to infer the particle position. Firstly, we determine the measured target position range. Secondly, we remove parts of the sample sets which have the great error. Thus, we can optimize the allocation of weights and improve the reliability of the weight so as to improve tracking accuracy and reduce the error effectively.**

Keyword: WSN; wireless sensor networks; particle filter; APPT; target tracking;

I. INTRODUCTION

Wireless Sensor Network（WSN） has become the most popular research direction in recent years，which relates to wireless sensing technology 、 electronic information、computer network、automatic control、 embedded technology, and so on. Generally, the nodes of wireless sensor network are cheap, small and have communication ability, so they are widely used in the tracking of moving target. According to the actual requirement of localization and tracking in the wireless sensor network，we can effectively reduce the noise interference by using proper filtering method. In the practical application，common filtering algorithm are α-β Filter、Grid—Based Filter、Kalman Filter、and Particle Filter, and so on. The calculated amount of α-β filter is very simple，and tracking result is good. However, it only can be used in the model which target is in uniform velocity and uniform acceleration. Grid-Based Filter is a very suitable filter in the case of limited discrete space. However, it requires that the target apace is consisted of limited and discrete spaces. Kalman Filter is often used in linear system estimation as a standard method because of its small calculated amount and accurate result. However, the error is obvious in linear approximating the nonlinear function, and noise ordinarily requires in the Gauss distribution. Particle Filter has simple principle which speculates the probability of something happening easily through using multiple sampling, so it can be easily applied in non-linear, non-Gaussian stochastic systems, especially in tracking system.

II. ORIGINAL PARTICLE FILTER ALGORITHM

A. *The theory of Particle Filter*

The idea of Particle Filter (PF) used for various forms of state-space model comes from Monte Carlo. What's more, it uses the frequency of an event to show the probability of this event, which adopts the particle set to record the probability of the event. In the beginning of the filtering process, we sample x. Then, apply a large number of sampling distribution to express the P(x).Firstly, according to x(t) and its probability distribution, we generate a large number of sample and we can call these sample collections particles. This sampling distribution in the state space actually can be seen as the probability distribution of x(t). Secondly, according to the state transition equation and the control amount, we can infer the probability distribution of the next particle x（t+1) which can be predicted by the probability distribution of each particle. We can deal with any form of probability in the filtering process rather than Kalman Filter which only can be used in deal with Gaussian distribution, because of this thinking method.

Specifically, Particle Filter searches a group of state space in transmission of the random samples to approximate probability density function, and uses sample mean instead of integral operations to get state minimum variance estimation. By the way, we named the sample "particle". When the sample number N approach ∞, it can approximate any form of probability density distribution.

B. *Algorithm of original Particle Filter*

Step1. Initialization, K=1, for i = 1，2，…，N, it is the first time for measured target to enter the region of randomly distributed nodes. Sample N particles obeys $x_0^{(i)} \sim p(x_0)$， get an N-point set of particles $\{x_0^i\}$,the initial probability density distribution $p(x_0)$, initial weights $w_0^i = 1/N$.

Step2. Important sample, for i=1，…，N，extract N particles from many particles obeying distribution $\hat{x}_k^{(i)} \sim q(x_k|x_{k-1}^i)$.

Step3: Update the weights, for i =1，2,…,N,

978-0-7695-4818-0/12 $26.00 © 2012 IEEE
DOI 10.1109/DCABES.2012.24

$$w_k^{(t)} = w_{k-1}^{(t)} \frac{p(y_k|\hat{x}_k^i)p(\hat{x}_k^i|\hat{x}_{k-1}^i)}{p(\hat{x}_k^i|\hat{x}_{k-1}^i, y_{1:k})}$$

Step4: normalize to get probability of acceptance. For i=1，2，…，N,

$$\overline{w}_k^{(i)} = \frac{w_k^{(i)}}{\sum_{i=1}^{N} w_k^{(i)}}$$

Step5: Resample N new particles according to

$$pr(x_{k|k}^{(i)} - x_{k|k-1}^{(i)}) = \overline{w}_k^{(j)}$$

Step6: State estimation.

$$\hat{x}_k = \sum_{i=1}^{N} \overline{w}_k^{(i)} \times x_k^{(i)}$$

Step7: k=k+1, go to step2 or end the algorithm.

C. *Problem about Particle Filter*

As Particle Filter Mainly approximates the probability distribution of the true distribution, and adopts the way of Non-parametric, it avoids a problem that random quantity must satisfy the Gaussian distribution when it solves the problem of nonlinear filtering. What's more, Particle Filter can express a wider range of distribution than the Gaussian model, and have more powerful modeling capabilities for nonlinear characteristics of the variable parameters. However, particle degradation is an inevitable phenomenon in the PF. Although the resample can weaken the particle degradation, but degradation still exists. What is worse, it may cause samples to be poor. This paper introduces the essence of APIT algorithm, and the particle filter algorithm has been optimized.

III. IMPROVED PARTICLE FILTER ALGORITHM

Suppose there are three arbitrary nodes A, B and C, which have known location and do not exist in a straight line. Thus the three nodes can form a triangle ABC. We can easily detect the strength of the signal between the measured target and the three nodes of the triangle ABC in order to determine the distance between the node and the measured target. According to the APIT algorithm, we can believe the measured target is outside the triangle, when the measured target is close to or away from the three triangle nodes at the same time, otherwise, the measured target is within the triangle. In figure 1 (1), measured target T is away from the points A, B, and C at the same time, so we can determine the measured target T is within the triangle. In figure 1 (2), measured target T is away from the points B, but close to the point A and C at the same time, so we can determine the measured target T is outside the triangle . Taking this approach, we can calculate the direction of movement range of the measured target.

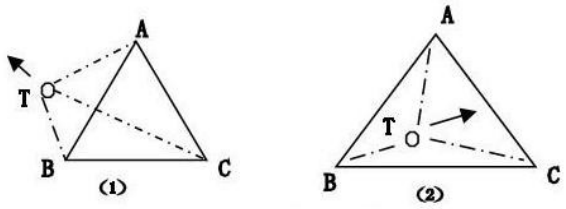

Figure1 the judgment of the measured target position

In the WSN communication process, the signal strength that the wireless signal node especially anchor node received may be subject to the impact of noise, and this causes the prediction error increasing and makes a series of predicted values becoming inaccurate. So the APPF algorithm adopts the method described above to improve Particle Filter which predicts a series of prediction values what is the movement direction of the forecast target rather than specific location. Improved particle filter algorithm APPF description as follows：

Step1. Initialization, K=1, for i = 1，2，…，N, it is the first time for measured target to enter the region of randomly distributed nodes. Sample N particles obeys $x_0^{(i)} \sim p(x_0)$， get an N-point set of particles $\{x_0^i\}$,the initial probability density distribution $p(x_0)$, initial weights $w_0^i = 1/N$.

Step2. Important sample, for i=1，…，N，extract N particles from many particles obeying distribution

$$\hat{x}_k^{(i)} \sim q(x_k|x_{k-1}^i) \quad .$$

Step3. According to the triangle determining method above in this article, we use the location and direction of movement of the particle and signal strength with a triangle of three nodes in (k-1)-time to speculate whether the position of the particle is within the triangle in (k-1)-time. If part of the sample particles is not inside the triangle, remove this part of particles. Then assign weights value according to the following formula.

Step4. Update the weights, for i =1，2,…,N,

$$w_k^{(t)} = w_{k-1}^{(t)} \frac{p(y_k|\hat{x}_k^i)p(\hat{x}_k^i|\hat{x}_{k-1}^i)}{p(\hat{x}_k^i|\hat{x}_{k-1}^i, y_{1:k})}$$

Step5. Normalize to get probability of acceptance. For i=1，2，…，N,

$$\overline{w}_k^{(i)} = \frac{w_k^{(i)}}{\sum_{i=1}^{N} w_k^{(i)}}$$

Step6. Resample N new particles according to

$$pr(x_{k|k}^{(i)} - x_{k|k-1}^{(i)}) = \overline{w}_k^{(j)}$$

Step7. State estimation.

$$\hat{x}_k = \sum_{i=1}^{N} \overline{w}_k^{(i)} \times x_k^{(i)}$$

Step8. k=k+1, go to step2 or end the algorithm.

IV. SIMULATION

MATLAB version 7.0 is used as software platform for simulation. We distribute 200 wireless sensor nodes known location in the region of 100m × 100m, and set node communication radius as 12m. What is more, we track single goal in the two-dimensional plane, and the target sampling period is 1second. We assume that the target initial position is at (10.0, 10.0), initial velocity is (10, 10) and Acceleration is (1.0, 1.0). We consider each simulation times is100, the effective number of particles N =150, and the total number of particles = 500. Target motion equation of state as follows:

$$x_{k+1=}\lambda x_k + \gamma w_k$$

$$\lambda = \begin{bmatrix} 1 & T & 0 & 0 \\ 0 & 1 & 0 & 0 \\ 0 & 0 & 1 & T \\ 0 & 0 & 0 & 1 \end{bmatrix}, \gamma = \begin{bmatrix} T^2/2 & 0 \\ T & 0 \\ 0 & T^2/2 \\ 0 & T \end{bmatrix}.$$

Where λ is state transition matrix, γ is noise processing formula.

In addition, the observation formula is $\sqrt{(x - x_i) + (y - y_i)} + v(k)$, where v is measurement noise.

Table 1 The computing time of two algorithms

Filter(s)	Time(seconds)
Original PF	4.26
Improved PF	5.71

Table 1 plots the improved Particle Filter must cost a little more time than the original Particle Filter in computing. However, we need more accurate tracking in a great number of situations despite taking more time.

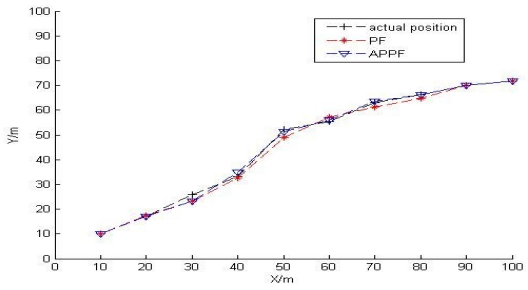

Figure 2 target tracking trajectory

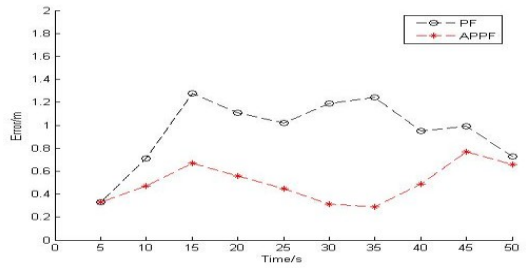

Figure 3 the average error

Relative to the actual position, we can get the target track position errors plotted in Figure 2 and the average error plotted in Figure 3 by comparing general particle filter algorithm with improved particle filtering algorithm. Figure 2 plots that, relatively speaking, tracking trajectory of the improved particle filter algorithm named APPF is closer to the real trace than the original particle filter algorithm PF. Figure 3 plots the average error of the two filter methods in the 100 simulation trials. The overall average error of the original particle filter is about 0.95m. However, the overall average error of APPF is about 0.50m, so the overall error reduces by 47% than the original particle filter.

V. CONCLUSION

In this paper, the original particle filter algorithm has been improved as the way of filter particles has been optimized and the reliability of the replaced weights has been increased. This paper shows that the tracking error of the method reduces 47% than the original particle filter according to the simulation results. Tracking technology in this algorithm is applied in wireless sensor networks, and it is significant for the tracking technology of wireless sensor networks.

REFERENCES

[1] Ronghui Zhan, Ling Wang, Jianwei Wan and Kang Zhong, "Passive target tracking using marginalized particle filter," Sun System Engineering and Electronics, pp.503 - 508, 2007.

[2] Li, H.-W., Wang, J., Su, and H.-T. "Improved particle filter based on differential evolution," Electronics Letters, pp1078 - 1079, 2011.

[3] Bolic, M., Djuric, P.M. and Sangjin Hong. "Resampling algorithms and architectures for distributed particle filters," Signal Processing, IEEE Transactions, pp. 2442 - 2450, 2005.

[4] Yang Qiaohe, Yan Jun, Shi Huichang, Xing Jianjun, Li Yuzhen, Kong Wei and Ding Yaping, "An effectual algorithm for particles number reducing in WSN particle filtering tracking process," Wireless Mobile and Computing (CCWMC 2009), IET International Communication Conference, pp. 70-73, 2009.

[5] Wei Gao, Hai Zhao, Chunhe Song and Jiuqiang Xu, "A New Distributed Particle Filtering for WSN Target Tracking," 2009 International Conference on Signal Processing Systems, 2009.

[6] Sheng Wang, Xue Wang, Yong Wang and Xinyao Sun, "Distributed lightweight target tracking for wireless sensor networks," Mobile Adhoc and Sensor Systems, 2009. MASS '09. IEEE 6th International Conference, pp.870 - 875, 2009.

[7] Ahmed, N., Rutten, M., Bessell, T., Kanhere, S.S., Gordon, N. and Jha, S, "Detection and Tracking Using Particle-Filter-Based Wireless Sensor Networks", Mobile Computing, IEEE Transactions, pp.1332 - 1345, 2010.

[8] Yan Zhou, Jianxun Li and Dongli Wang, "Posterior CramÉr–Rao Lower Bounds for Target Tracking in Sensor Networks With Quantized Range-Only Measurements," Signal Processing Letters, IEEE, 2009.

[9] Movaghati, S. and Ardakani,M, "Particle-Based Message Passing Algorithm for Inference Problems in Wireless Sensor Networks," Sensors Journal, IEEE, pp.745 - 754, 2011.

[10] Xue Wang, Liang Ding and Daowei Bi, "Reputation- Enabled Self-Modification for Target Sensing in Wireless Sensor

Networks," Instrumentation and Measurement, IEEE Transactions, pp.171- 179, 2010.

[11] Bo Jiang and Ravindran, B, "Completely Distributed Particle Filters for Target Tracking in Sensor Networks," Parallel & Distributed Processing Symposium (IPDPS), 2011 IEEE International, pp.334 - 344, 2011.

[12] Kirsch, C. and Röhrig, C, "Position tracking using sensor fusion of a wireless network and a laser range finder," Positioning Navigation and Communication (WPNC), 2010 7th Workshop, pp. 193 - 199, 2010.

[13] W. Fang, J. Sun, Y. R. Ding, X. J. Wu and W. Xu, "A review of quantum-behaved particle swarm optimization,"[J].IETE Technical Review, 2010, 27(4): 336-348.

[14] J. Sun, B. Feng and W. B. Xu, "Particle swarm optimization with particles having quantum behavior," [C].Congress on Evolutionary Computation, Portland, Oregon, USA, 2004, 325-331.

A New Reputation Mechanism Based on Referral's Credibility for P2P Networks

Yulian Zhang
School of Information Science and Engineering
Yanshan University
Qinhuangdao, China
E-mail: 13930316909@163.com

Lihua Wang
School of Information Science and Engineering
Yanshan University
Qinhuangdao, China
E-mail: wanglh729@163.com

Abstract— *Due to the open nature of peer-to-peer (P2P) networks, distributed systems usually employ reputation systems (RSs) to help peers identify trustworthy resource providers and steer away from the malicious peers who may release harmful files or resources in their benefits. In this paper, we propose a new reputation mechanism based on referral's credibility for P2P networks called RBRC. More specifically, we incorporate the trust relationship between the service requestor and the referral to model the target user's reputation. Besides, our method takes into consideration many critical factors, including the rating time, transaction value, transaction times, incentive factors and the referral's credibility. In this way, it would be too expensive for the malicious users to launch a malicious attack in terms of both money and time cost. Experimental results show that our method can effectively strengthen the robustness of reputation systems in combating malicious attacks.*

Keywords-component; E-commerce; Reputation System;P2P ; Credibility

I. INTRODUCTION

In a P2P network, peers can freely join and leave the network and they can interact with other peers without knowing who they real are and building up non-face-to-face connections. Due to the openness and anonymity, P2P networks are very vulnerable to malicious attacks, for example providing incorrect or false information given from unreliable peers. Reputation system is hence introduced to help peers identify trustworthy resource providers and steer away from the malicious ones [1-3].

Generally, a P2P reputation system consists of peers that may play the roles of trustor, trustee and referral simultaneously [4]. Trustor is the role of the active peer who wants to make a safe decision regarding whether to participate in a transaction with some target peer - the trustee, because it could be harmful for the trustor to access a service provided by the trustee, e.g. downloading a file, with virus from an untrustworthy peer could harm the trustor's computer. Therefore, trustors usually turn to other peers for more information about the trustee. A peer is regarded as a referral when he/she provides the trustor with information (a.k.a. recommendation) about the trust value of the trustee. Referral's credibility refers to the confidence that a trustor can place on a referral regarding his useful recommendations. An effective reputation system is expected to assess the referral's credibility accurately in order to assist user's decision making.

The calculation of a trust value needs two parts: direct trust value and reputation value. And the major contributions of this paper are two folds. First, the rating time, the improved transaction value, transaction times, incentive factors are incorporated to the calculation of a peer's direct trust value. By combining these factors, we can evaluate the direct trust value more accurately. Second, the reputation value is the aggregated recommendation information that the trustor collects from the referral. The referral's credibility is used to weigh the recommendations. We incorporate the trust relationship between the trustor and referral to improve the assessment of referral's credibility.

The reminder of this paper is organized as follows. Section 2 reviews several existing works on P2P networks and Section 3 describes their methods to model referral's credibility. Section 4 delineates the proposed model in details. The simulation and experimental results are represented in Second 5. Finally, we conclude our work and outline the future work in Section 6.

II. RELATED WORK

There has been a number of reputation mechanisms based on credibility theory proposed in the literature. TrustBuilder [5] is a reputation mechanism for B2B e-commerce based on the source credibility theory [6]. In order to calculate the user's credibility, users have to assign explicit ratings to other users. Q-rater [7] is proposed by Cho et al., which uses raters' ratings to estimate their underlying credibility. It is also based on the source credibility theory, and employs several concepts from collaborative filtering. Tian et al. propose the R^2Trust [8], which incorporates both reputation and risk to evaluate peer' trust values. They do not consider the price of transaction. The malicious users can accumulate their reputation by making various low-priced transactions and then deceive in a high-price trade. In [9], Ruohomaa et al. compare 11 reputation systems within taxonomy of the credibility aspects. The survey reviews a variety of excellent mechanisms and methods for credibility. In Sorcery [10], each peer establishes its own friend-relationship social network. Peers utilize the overlapped rating histories between their friends and the content providers to judge whether the content provider is a colluder. Srivatsa et al. [11]

978-0-7695-4818-0/12 $26.00 © 2012 IEEE
DOI 10.1109/DCABES.2012.60

propose a personalized credibility measurement in which similar raters' feedbacks are given a higher weight than others. It can be used to defend against potential collusive peers who give good ratings within the group and bad rating outside the group.

All previous methods rarely take the relationship between trustor and referral into consideration to calculate peers' credibility. However, the social relationship is important and has a critical impact on the evaluation of other's credibility. It is reported that peers tend to buy products/service from socially-close friends, and rate socially-close peers with high ratings [12]. Researchers have shown that recommendations from friends have a higher success rate than those from systems [13-14]. Based on Q-rater [6], we propose a new reputation metric which offers a comprehensive approach by including the rating time, transaction value, transaction times, incentive factors and the referral's credibility. Since malicious attacks cannot be completely eradicated, our mechanism makes these attacks too expensive and time-consuming to be launched. The experimental results show the effectiveness of our mechanism in comparison with other reputation mechanisms.

III. REFERRAL CREDIBILITY

In this section, we will investigate how to calculate the referral's credibility. Suppose there are three peers: trusor *i*, trustee *j* and referral *m*. We introduce two new notions: social network and transaction network.

Each peer has a "social network" (SN) and a "transaction network" (TN). The "social network" of peer *i* is a network that comprises of i's acquaintances in reality or online (e.g. relatives and friends). The "transaction network" records *i*'s business contact. Every time after peer *i* completes a transaction with a new partner, (s) he adds this partner into his/her transaction network.

If a referral belongs to the trustor's SN, then his/her credibility is 1 in the view of the trustor. That is to say, the information he/she recommend is completely reliable, his/her direct transaction records are equivalent to the trustor's. In this way, we increase the trustor's direct transaction records.

Let Cr_m denotes the credibility of peer *m* in peer *i*'s view. It is used to describe the extent to which a peer can trust the recommendations from referrals. We define credibility value as follows:

If $m \in SN_i$, $Cr_m = 1$

else

$$Cr_m = \begin{cases} 1 - \dfrac{\sum_{k=1}^{n_{mi}} | R_{mi}^{t_k} - \overline{R}_{mi} |}{n_{mi}}, m \in TN_i \\ 1 - \dfrac{\sum_{k=1}^{n_{mj}} | R_{mj}^{t_k} - \overline{R}_{mj} |}{n_{mj}}, \text{others} \end{cases} \quad (1)$$

Where,

$R_{mi}^{t_k}$ is the *k*-th rating peer *m* reports toward peer *i*; $R_{mj}^{t_k}$ is the *k*-th rating peer *m* reports toward peer *j*; $\overline{R}_{mi}$ denotes the average rating peer *m* reports toward peer *i*; $\overline{R}_{mj}$ is the average rating peer *m* reports toward peer *i*; n_{mi} is the number of transactions between peers *i* and *m*; n_{mj} is the number of transactions between peers *j* and *m.*

Collusive peers usually give high ratings to peers in the same group while low ratings to the peers outside the group. There is a significant difference between the peers in a collusive group and the peers outside the group. Cr_m is able to help identify collusive peers.

IV. THE PROPOSED TRUST AND REPUTATION MODEL

The transaction process as follows:

Step1. Trustor *i* sends transaction request to the other peers in the e-commerce system;

Step2. The peer who can provide the service sends a response message to peer *i*;

Step3. *i* chooses one provider from response peers, It is denoted by *j*. If there are direct transactions between *j* and *i* or members of *i*' SN , *i* get *j*' direct trust value according to his/her and his/her SN' historical transactions, else sends request to the other peers(they are expressed by *m*) for *j*' reputation information, and then uses it to get *j*' reputation value;

Step4. According the direct trust value and reputation value, *i* get the trust value for *j*, and then decide whether transact with peer *j* or not. If the trust value is higher than the threshold τ, then transaction with *j*, do step5, else do step3 repeatedly.

Step5. After the transaction, peer *i* gives a rating to peer *j* and update the direct trust value of peer *j* based on the trading results.

A. Calculation of Trust Value

The calculation of trust value is composed of two parts' information: direct trust value and reputation value. Let T_{ij} denote the trust value from peer *i* to peer *j*. It can be defined as follows:

$$\begin{cases} T_{ij} = \alpha DT_{ij} + (1-\alpha) RE_{ij}, & N \neq 0 \\ 0.5, & N = 0 \end{cases} \quad (2)$$

Where,

DT_{ij} represents the direct trust value from peer *i* to peer *j*; RE_{ij} is the reputation value of peer *j*; *N* is the direct transaction numbers; α are confidence factors and $0 \leqslant \alpha \leqslant 1$. Confidence factor describes how confident trustor *i* is regarding its direct trust value on trustee *j*.

B. Direct TrustUnits

Direct trust value DT_{ij} is computed directly from peer *i*'s historical ratings with peer *j*. If *j* has a number of direct interactions with *i*, we define DT_{ij} as follows:

$$DT_{ij} = r \cdot \left(\frac{\sum_{k=1}^{N_{ij}} \varphi(t_k) \cdot M_{ij}^{t_k} \cdot R_{ij}^{t_k}}{\sum_{k=1}^{N_{ij}} \varphi(t_k) \cdot M_{ij}^{t_k}} \right) - e^{-\frac{1}{N_f}} + e^{-(1+\frac{1}{N_s})} \quad (3)$$

Where,

$R_{ij}^{t_k}$ is the *k*-th transaction rating peer *i* reports toward peer *j*, $0 \le R_{ij}^{t_k} \le 1$; N_{ij} is the total transaction number between *i* and *j*; $\varphi(t_k)$ is Decay function; $M_{ij}^{t_k}$ is value factor; $e^{-\frac{1}{N_f}}$ is penalty factor while $e^{-(1+\frac{1}{N_s})}$ is incentive factor; *r* is correction coefficient.

Two distinct positive feedback values should not be treated the same if there is a significant difference in the price of the trade. If all feedback is treated equally without adjusting, a peer can easily accumulate a high reputation value by making multiple trades with low-priced commodities. To alleviate this problem, we introduce the value factor $M_{ij}^{t_k}$, which is obtained as follows:

$$M_{ij}^{t_k} = \begin{cases} \dfrac{m_{ij}^{t_k}}{\overline{m_i}}, k > 1 \\ 1 \quad ,k = 1 \end{cases} \quad (4)$$

Where,

$m_{ij}^{t_k}$ is the *k*-th transaction value peer *i* reports toward peer *j*.

Time is an important factor too, so we import Decay function $\varphi(t_k)$, which is a time discount function, giving higher weight to values closer to current time t. It is represented as $\varphi(t_k) = e^{-\lambda(t-t_k)}$, where $0 \le k \le N_{ij}$, λ is the rate of decay; its value is determined by the user.

Peers may achieve a high reputation through a few high-priced transactions, and then begin to deceive. To avoid this situation, we introduce correction coefficient, its definition is $r = \dfrac{1}{1 + e^{-\frac{N_{ij}}{2}}}$.

The last two parts are incentive factors, N_f, N_s denote the failure and successful transaction number. In order to prevent malicious peers improving his reputation value from the oscillation behavior. Therefore, the degree of punishment must be greater than the reward, i.e. when $N_f = N_s \ge 1$,

$e^{-\frac{1}{N_f}} > e^{-(1+\frac{1}{N_s})}$

The following is the process of the proof.

Let $N_f = N_s = n \ge 1$,

since $e^{-(1+\frac{1}{N_s})} = e^{-(1+\frac{1}{n})} = e^{-1} \cdot e^{-\frac{1}{n}}$, and $e^{-1} < 1$,

hence $e^{-(1+\frac{1}{N_s})} < e^{-\frac{1}{n}} = e^{-\frac{1}{N_f}}$.

When there are oscillation behaviors, the peer' total direct trust value will be decreased in the future, so our model can prevent the malicious behavior to some extent.

C. Reputaion Evaluation

The reputation value is the aggregated recommendation information that *i* collect from referrals (represented as *m*).

In the paper, a referral' credibility is used to weigh his/her recommendation from other peers. Then all the recommendations are aggregated to calculate the reputation of the trustee. From the view of peer *i*, the reputation value RE_{ij} of peer *j* is illustrated as follows:

$$RE_{ij} = \sum_{m \in N} \left(Cr_{im} \times DT_{mj} \right) / \sum_{m \in N} Cr_{im} \quad (5)$$

Where,

N is the set of referrals; DT_{mj} represents the direct trust value of referral *m* reports toward peer *j*; Cr_{im} is referral *m*'s credibility in the view of trustor *i*. Its definition is described in Section 3.

It can be observed from Eq. (5) that the higher the credibility a recommender has, the more weight his/her recommendation carries.

V. PERFORMANCE EVALUATION

A. Simulation Environment

The simulation is based on the latest version of the Peersim simulator (Peersim-1.0.4), which is an open source, Java based, P2P simulation framework developed for large-scale and dynamic environment.

In this paper, we focused only on the reputation calculation for sellers (i.e. trustees).

We assume that there are 1000 peers in the network, among which, there are 100–500 malicious peers in our opinion.

New peers have no historical transactions, so we cannot get their trust value from the direct trust value and reputation value. Therefore we consider their initial trust value is 0.5.

Other parameters in the experiments are in Table 1.

TABLE I. THE PARAMETER IN THE EXPERIMENT

Parameter	*Value*	*Description*
α	0.7	Confidence factor
λ	1	Decay factor
τ	0.5	The threshold of trust value

B. Experimental Results

We have conducted two groups of simulation experiments, each simulation we compare the successful transaction rate (STR) of our model with R^2Trust and EigenRep. STR is the ratio of the number of successful transactions over overall transaction numbers.

In the first group, we test the STR of the three models under collusive, which is shown in Fig.1. Collusive peers assign high ratings to peers in the collusive group, and provide denigrated ratings to those non-collusive peers when selected as referrals. The number of malicious peers was increased in steps of 10%.

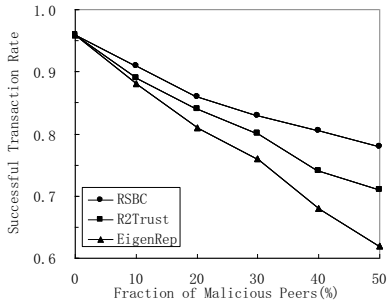

Figure 1. STRs under collusive.

In the second group, we examine the STR of the three models under oscillation behaviors, which is shown in Fig.1. This type of malicious peers may behave properly in a period of time, after they build up a high reputation, and then begin to deceive [4].

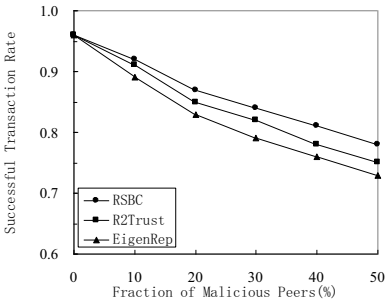

Figure 2. STRs under traitors.

As it is seen in Figure 1 and 2, with the number of malicious peers increasing, STRs of all the three models decrease and EigenRep and R^2Trust drop more quickly than our model. They don't consider the relationship between the trustor and the referral. Furthermore, EigenRep cannot punish these malicious peers and it, therefore the successful transaction rates fall heavily. R^2Trust don't take the price value into consideration.

VI. Conclusion and Future Work

The main contribution of this paper is that we have developed a framework called RBRC for reputation management denoted to P2P networks. The proposed model incorporates various types of information to evaluate the direct trust and the reputation, and then aggregates them by assigning different weighs to them. To calculate trustee's direct trust, transaction ratings are weighted by taking into account the time, value and number of the transaction. And incentive factors are considered as also. To calculate trustee's reputation, we make use of the relationship between the trustor and the referral to assess the referral's credibility. Experiments were conducted to evaluate the effectiveness of our method. The results show that our method can perform well even if over 50 percent of peers are malicious. In the future, we will investigate: 1) how to determine more appropriate thresholds for trust value， decay factor and confidence factor. 2) how to incorporate other factors to further improve the measure of the referral's credibility.

Acknowledgment

This research is funded by the Natural Science Foundation of Hebei Province P. R. China under Grant No. F2011203219. The authors also gratefully acknowledge the helpful comments and suggestions of the reviewers, which have improved the presentation.

References

[1] S D Kamvar, M T Scholosser, H G Molina. "The EigenTrust Algorithm for Reputation Management in P2P Networks", in Proceedings of the 12th International World Wide Web Conference, New York, USA, 2003, pp. 640-651. doi:10.1145/775152.775242.

[2] A Josang, R Ismail, C Boyd. "A Survey of Trust and Reputation Systems for Online Service Provision", Decision Support Systems, 2007, pp. 618-644. doi:10.1016/j.dss.2005.05.019.

[3] M. Wang, F. Tao, Y. Zhang, G. Li, "An adaptive and robust reputation mechanism for P2P network", in Proceedings of the IEEE International Conference on Communications, Cape Town, South Africa, 2010. doi: 10.1109/ICC.2010.5502541.

[4] E Koutrouli, A Tsalgatidou, "Taxonomy of attacks and defense mechanisms in P2P reputation systems—Lessons for reputation system designers", Computer Science Review, 2012. doi:10.1016/j. cosrev.2012.01.002.

[5] M A Ekstrom , H C Bjornsson, C I Nass, "A reputation mechanism for business-to-business electronic commerce that accounts for rater credibility", Journal of Organizational Computing and Electronic Commerce, 2005, pp.1–18. doi:10.1207/s15327744joce1501_1.

[6] D I Hawkins, J R Best, A K Coney, Consumer Behavior: Building Marketing Strategy, 9th edition, McGraw Hill-Irwin, Boston, USA, 2004.

[7] J Cho, K Kwon, Y Park, "Q-rater: A collaborative reputation system based on source Credibility theory". Expert Systems with Applications, 2009, pp. 3751–3760.doi:10.1016/j.eswa.2008.02.034.

[8] C Tian, B Yang, "R^2Trust, a reputation and risk based trust management framework for large-scale, fully decentralized overlay networks", Future Generation Computer Systems, 2011, pp.1135-1141. doi:10.1016/j.future.2011.03.006.

[9] S Ruohomaa, L Kutvonen, E Koutrouli, "Reputation Management Survey", the second International Conference on Availability, Reliability and Security, 2007, pp. 103-111.doi:10.1109/ARES.2007.123.

[10] M. Srivatsa, L. Xiong, L. Liu, "Trustguard: Countering vulnerabilities in reputation management for decentralized overlay networks", in Proceeding. of WWW, 2005.doi: 10.1145/1060745.1060808.

[11] E. Zhai, R. Chen, Z. Cai, L. Zhang, E. K. Lua, H. Sun, S. Qing, L. Tang, and Z. Chen, Sorcery: "Could we make P2P content sharing systems robust to deceivers?" In Proceeding of P2P, 2009.doi: 10.1109/P2P.2009.5284532

[12] Z Li, H Shen, K Sapra, "Leveraging Social Networks to Combat Collusion in Reputation Systems for Peer-to-Peer Networks", in proceeding of IEEE International Parallel & Distributed Processing Symposium, 2011, 532-543.doi:10.1109/IPDPS.2011.58.

[13] R Sinha, K Swearingen. "Comparing recommendations made by online systems and friends", Available from http://onemvweb.com/s-ources//sources/comparing_recommendations, 2011.

[14] F K Liu, H J Lee. "Use of social network information to enhance collaborative filtering performance", Expert Systems with Applications, 2010, pp.4772-4778.doi: 10.1016/j.eswa.2009.12.061.

Path Planning Based on Hybrid Adaptive Ant Colony Algorithm for AUV

Peng Wang,
College of Marine
Northwestern Polytechnical University
Xi'an, P.R. China
E-mail: wangpeng305@nwpu.edu.cn

Peng Meng,Tengfei Ning
College of Marine
Northwestern Polytechnical University
Xi'an, P.R. China
E-mail:mp1220@163.com

***Abstract*—Ant Colony Algorithm is one of the important methods in dealing with the NP-hard problem. In order to overcome the deficiencies of the algorithm effectively such as slow convergence, easy to fall into local optimal solution, a hybrid adaptive ant colony algorithm was proposed and it has been used in the AUV path planning problem. We established a mathematical model for it and made a practical engineering example for simulation and analysis of the correlative parameters to the influence on the algorithm. Finally we get the optimal path and the best preferences of parameters. The experimental results show that the proposed method in this paper is effective, realistic, easy and versatile.**

Keywords—path planning; hybrid adaptive ant colony algorithm; NP-hard problem

I. INTRODUCTION

Autonomous Underwater Vehicle (AUV) is an underwater unmanned vehicle which is intelligent, autonomous navigation, processing module assembled on the bases of its assignment and actualizing multifunctional integration [1]. It plays a very tremendous role in executing the mission of underwater as detecting the environment of ocean, underwater observation, hydrology measurement and landform plotting of the benthal. With the broaden of ocean district utilizing and the emergence of far voyage AUV, the amount of cruise points which need to reconnoiter by AUV has increased more, meanwhile, the region of cruise points is distributed more widely. Therefore, during the path planning for AUV, it is very important to make scientific programming for the reconnoiter order about legions of cruise points prompt and efficient. It requests that AUV must visit all of the cruise points, moreover minimize the summation cost the voyage.

The cruise path planning of AUV belongs to NP hard problem. At present the main methods to solve these problems are classic algorithm and intelligent optimization algorithm. The classical algorithm solves the accurate solution through the dynamic programming problem [2], but the time complexity and space complexity is higher, the consumption of system resources is bigger, feasibility is poorer, such as exhaustively method [3], et al; although intelligent optimization method can solve the problem, there are some defects like slow convergence speed, easy to fall into the local optimal and computing time is too long, etc. This article in view of the AUV path planning problem, adopted the Hybrid Adaptive Ant Colony Algorithm, established the AUV path planning model and solved the path planning problem which has 31 cruise points. This algorithm overcomes the defect of ant colony algorithm, and gets the ideal results.

II. HYBRID ADAPTIVE ANT COLONY ALGORITHM

In this section, we introduced the traditional Ant Colony Algorithm including its basic principle. On the other hand, explained a new algorithm named Hybrid Adaptive Ant Colony Algorithm.

A. Ant Colony Algorithm[4]

Ant colony algorithm is a kind of intelligent optimization algorithm, the bionics home has found that ants transfer information between individuals through a material called pheromone, ants can sense this substance, and so as to guide the direction. Therefore, when a large number of ants take action collective, the more through a path of ants, the greater probability the newcomers choose the path, and finally ant colony can find the shortest path between food source and the nest.

B. Hybrid Adaptive Ant Colony Algorithm

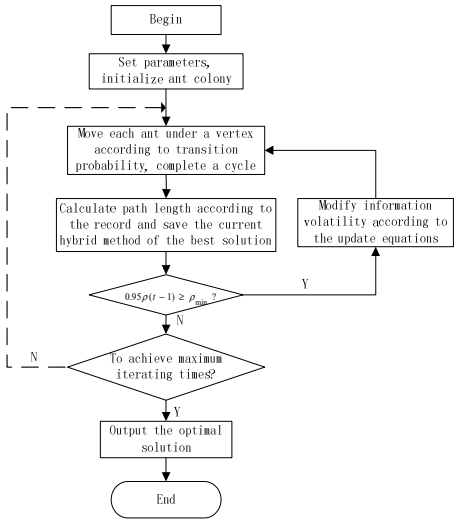

Figure 1. Hint of Hybrid Adaptive Ant Colony Algorithm

The specific progress of hybrid adaptive ant colony algorithm is as figure 2 shows. For reforming the defects and insufficiency of traditional ant colony algorithm maximum ,

978-0-7695-4818-0/12 $26.00 © 2012 IEEE
DOI 10.1109/DCABES.2012.64

improving ant colony algorithm for the global searching ability and speeding up the searching speed, the traditional ant colony algorithm was improved, introducing the hybrid adaptive ant colony algorithm.

When the next ant finds a path, comparing every path which has stored before, when exiting crossing paths, the hybrid methods are as explained as Chen[5]. When problems in large scale, if the element information volatile coefficient is too large as ρ, it will affect the global search ability, or will reduce the convergent speed if smaller, so puts forward a pheromone volatile coefficients changing adaptively. The initial value of ρ is that $\rho(t_0)=1$, when the optimal value has no significant improvement during the N times, making the following changes for ρ.

$$\rho(t)=\begin{cases}0.95\rho(t-1) & \text{if } 0.95\rho(t-1)>=\rho_{\min}\\ \rho_{\min} & \text{else}\end{cases} \quad (1)$$

Where ρ_{min} means the minimum value of pheromone volatile coefficient, in this paper, taking that $\rho_{min}=0.01$.

III. Mathematical Modeling for AUV Cruise Path Planning

The AUV cruise path planning is a dynamic, multi-objective and constraint nonlinear programming problem, the mathematical model can be expressed as:

$$\min f = f(x,y,n)$$
$$s.t.\begin{cases}x \to \min\\ y \to \min\\ n \in N_+\end{cases} \quad (2)$$

Where $f(x,y)$ means the total cost of the AUV cruising; x means the energy needed for the AUV cruising; y means the amount of time spending during the AUV cruising; n shows the number of cruise point.

Suppose m represents the number of AUV every time, d_{ij} means the distance between the cruise points i and j, $\tau_{ij}(t)$ denotes the information on the edge of $e(i,j)$ when t second. So P_{ij}^{k} which means the transition probability from cruise point i to j by AUV-k(denotes the first k AUV, k=1,2,…,m) at t second could denotes as follows:

$$p_{ij}^{k}(t)=\begin{cases}\dfrac{\tau_{ij}^{\alpha}(t)\eta_{ij}^{\beta}(t)}{\sum_{j\in allowed_k}\tau_{is}^{\alpha}(t)\eta_{is}^{\beta}(t)}, & j\in allowed_k\\ 0, & otherwise\end{cases} \quad (3)$$

Where $allowed_k$ means the cruise points which can be allowed by the AUV-k next; α denotes the information heuristic factor which represents the extent of pheromone during route choice; β denotes the expect type stimulating factor which represents the relative importance of visibility; n_{ij} denotes the visibility of edge $e(i,j)$, taking $n_{ij}=1/d_{ij}$ generally[6] .

After n times, the AUV-k completes a cycle, each path of information make changes according to the following formulas:

$$\tau_{ij}(t+n)=\rho\cdot\tau_{ij}(t)+\Delta\tau_{ij} \quad (4)$$

$$\Delta\tau_{ij}=\sum_{k=1}^{m}\Delta\tau_{ij}^{k} \quad (5)$$

In equation (4) and (5), τ_{ij} denotes the information of edge $e(i,j)$ in this cycle by the AUV-k; $\Delta\tau_{ij}^{k}$ denotes the amount of information on incremental during this cycle.

IV. Simulation Examples Analysis

According to the AUV cruise path planning model, adopting the hybrid adaptive ant colony algorithm, to make a simulation experimental analysis about AUV path planning which has 31 cruise points.

A. The Impact Analysis about AUV Quantity

The figure.2 indicates that when m is smaller, the search ability of algorithm drops, it may reduce the number of choice to the best way for AUV, cause waste of the optimization result searched before and appear the optimal path of value in violent shake; when m was too big, the computational complexity is increased, the efficiency of searching for the optimal solution reduces significantly, and there exist in much randomness in the original route choice, the original optimal value is selected too quickly, easy to fall into local optimum.

B. The Analysis about Information Heuristic Factors

The figure.3 indicates that if the value of α is too small, the algorithm convergence speed will be reduced; if too great, the probability to choose a cruise path which has got before will be bigger, but it will reduce the efficiency of searching the optimal solution and make the searching fall into the local optimum value early.

C. Analysis the Influence of Expectation Stimulating Factor

The figure.4 shows that if β is smaller, there has violent shake in the early searching, the efficiency drops; when β is bigger, the more possible for AUV to choose the cruise point which is near itself, but the possibility to searching for the optimal solution is lower.

When m, α, β take different values respectively, the optimal cruise order as shown in figure5, length of the shortest cruise path is shown in figure 6.

The length of shortest cruise path getting by the hybrid adaptive ant colony algorithm which has 31 cruise points is 15719, the average length is 18321, the optimal path length has shortened 14% comparing with the average path length.

V. Conclusion

AUV cruise path planning is NP hard problem, although traditional ant colony algorithm can solve the problem, there are some defects such as slow convergence speed, easy to fall into the local optimal and computing time too long. This paper has proposed hybrid adaptive ant colony algorithm, improved traditional ant colony algorithm through the path hybridization and pheromone volatile coefficients changing adaptively. Established the mathematical model of AUV cruise path planning, given the detailed steps of the hybrid adaptive ant colony algorithm to solve the problem, made

the simulation test about the AUV path planning problem which has 31 cruise points, get the optimal path and analysis the algorithm parameters on the effect of optimization ability particularly. The research results not only provide effective new methods for AUV path planning problems, but also afford reference for the promotion and application of hybrid adaptive ant colony algorithm.

VI. ACKNOWLEDGMENTS

This project was funded by the National Nature Science Foundation of China (NSFC) (Project code: 50909082) and the Hoverer Star Foundation of Northwestern Polytechnical University (Project code: 11GH0317)

VII. REFERENCES

[1] Xu Demin, Song Baowei. The development and pivotal technology. Higher Education Press, Beijing, 2004.

[2] Ding Guoxing, Liu Fei, et al. Improved produce-storage problem algorithm based on dynamic programming, Journal of Chongqing University of Posts and Telecommunications (Nature Science). Vol. 18(3): 413-415, 2006.

[3] Dahmouni, H. Girard, A. Ouzineb, M. Sanso, B. The Impact of Jitter on Traffic Flow Optimization in Communication Networks. IEEE Transaction on Network and Service Management. Vol. 99, pp. 1-14, 2010

[4] D. Alves, J. van Ast, Zhe. Cong, B. De Schutter, "Ant Colony Optimization for Traffic Dispersion Routing". Jounal of Annual Conference on Intelligent Transportation System Madeira Island, Portugal. Vol. 13, pp. 683-688, 2010

[5] Chen Lichao, Liu Jia. An Ant Colony Algorithm with Crossover Operators for the Shortest Path Problem in Dynamic Networks. Computer Engineering & Science. Vol. 29(5), 2007.

[6] Mao, Yuxing. Extraction of affine invariant features for shape recognition based on ant colony optimization. Journal of Systems Engineering and Electronics. Vol. 22(6):1003-1009, 2011.

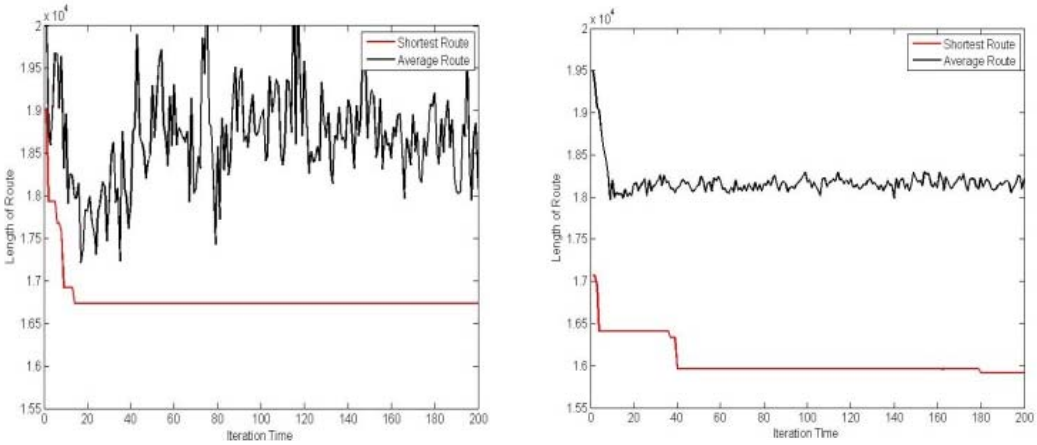

(a) m=5 (b)m=100

Figure 2. Length of Cruise Path When the Amount of AUV Get Different Values

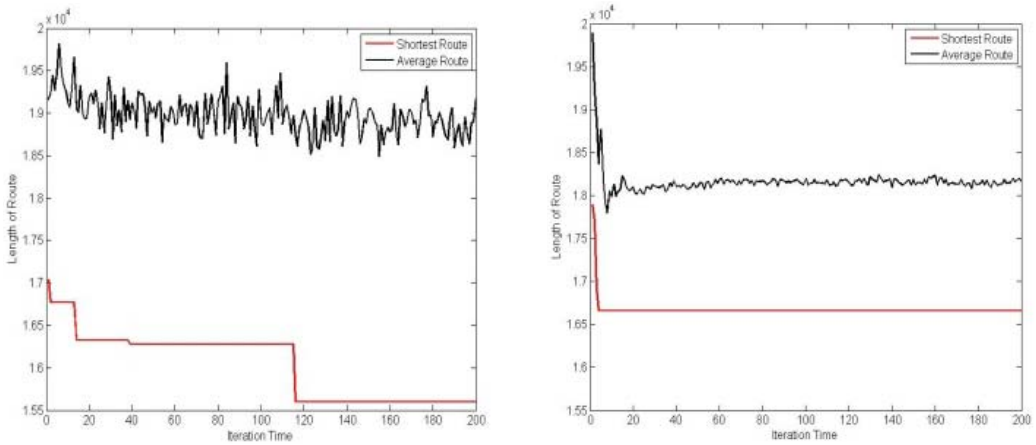

(a) α=0.1 (b) α=5

Figure 3. Length of Cruise Path When the Factor of Elicitation Get Different Values

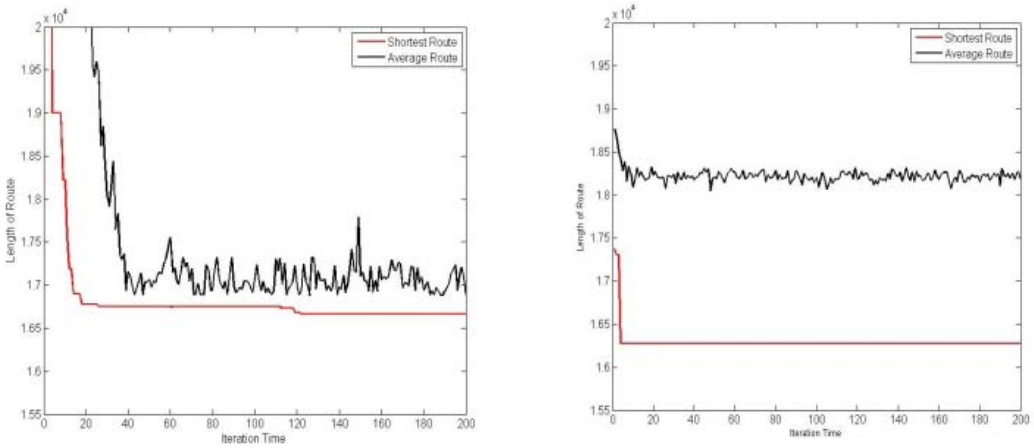

(a) β=0.5 (b) β=50

Figure 4. Length of Cruise Path When the Factor of Expectation Get Different Values

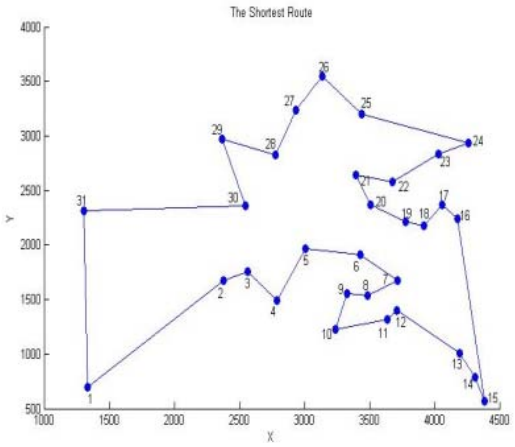

Figure 5. The Shortest Cruise Route for AUV

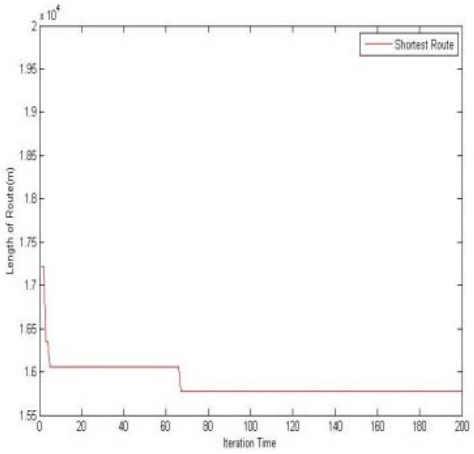

Figure 6. Length of Cruise Path for AUV

The Research of audio and video public network platform based on CDN and P2P

Chun Liu[1], Yucheng Guo[1], Yunchuan Luo[2], Weidong Jiang[2] , Xiaofeng Hu[2],Xiao Wu[2], Xiangye Meng[2], Yanping Chen[2], Jinliang Zhang[2], Yanjie Jiao[2], Zaoyang Chen[2], Ping Liu[2]

[1.] *The school of Computer science and technology, Wuhan University of Technology, Wuhan, China*
Email:liuchun_0206@163.com, ycheng.g@gmail.com

[2.] National Cultural Information Resources Management Center of China
Email:{luoyc,jwd,huxf,wux,mengxy,chenyp,zhangjl,jiaoyj,chenzy}@ndcnc.gov.cn

***Abstract*—the paper first analyzes the basic theory of the CDN (Content Delivery Network) audio and video system and the P2P (peer to peer) audio and video system, and presents its own limitations of each kind of the architecture. Then a hybrid model has been proposed, which integrates CDN and P2P to build the audio and video public network platform. The paper describes the architecture of the hybrid model, its work processes and characters in detail. The model takes full advantage of the two kinds of technologies, reducing the construction cost of the CDN as well as promoting the effective supervision of the P2P, so it gives us a brand new view of building the audio and video public network platform.**

Keywords: CDN, P2P, streaming media

I. INTRODUCTION

The public network platform for Internet culture, audio and video distribution is a symbol of national cultural soft power. It is the channel works of building digital resources given to millions of households, and the powerful weapon against the vulgar violent content out of the Internet

Currently, there are 475,000 distribution nodes in our Sharing Project nationwide, whereas these nodes are disconnected to each other through the network to serve the cultural life of the masses. This project supported by the Ministry of Culture, analyses the present problem of service resource consumption in single CDN network and the difficulty of monitoring resources in single P2P network. It studies the combination of CDN and P2P technology, the realization of audio and video communication networks by combining a core layer of CDN technology, and the edge layer of distribution of P2P technology. And furthermore the construction of this model is applied to the national culture of audio and video distribution of public network platform, to maximize the social benefits of cultural information resources.

II. THE CDN AUDIO AND VIDEO SYSTEMS AND THE P2P AUDIO AND VIDEO SYSTEMS

A. The Model of CDN audio and video systems

CDN (Content Delivery Network) is a distributed content distribution network in data network. The essential idea of CDN is that the audio and video files provided by the content provider are cached into the cache of the proxy server in the Internet "edge". The clients obtain the contents of the audio and video files they want from the local cache of the proxy server; thereby it can reduce the network traffic of backbone, and promote the performance of the user's access [1].

The CDN architecture of the network model consists of three parts, the central server, the edge server and the client, as shown in Figure 1.

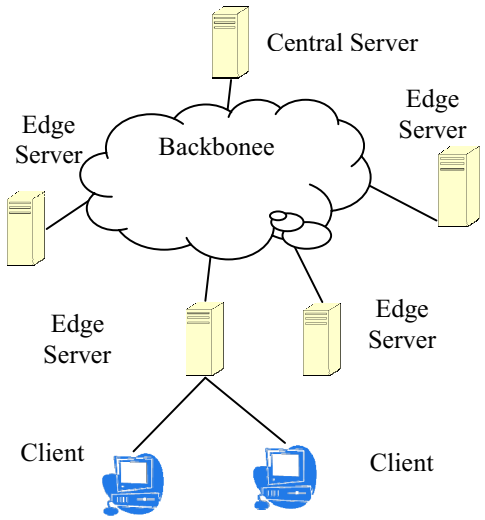

Figure 1. The CDN Network Model

From Figure 1, the central server plays two roles: providing audio and video file resources and scheduling user requests, so the central server can also be divided into two parts: central resources server and central schedule server.[2]

And In this architecture, the central server and edge server compose one distributed network which is regarded as a whole to the clients. The whole network is transparent to the client, to which the clients just put forward its request without indicating which server.

It is also not difficult to find the edge server to act in two roles: from the central server' point of view, the edge server is a terminal which requests resources from the central server, while from the client's point of view; the edge server is a server which provides resources to the clients. Through some strategy, central server pre-distributes the audio and video content to the edge of the

978-0-7695-4818-0/12 $26.00 © 2012 IEEE
DOI 10.1109/DCABES.2012.112

edge server via the backbone network. When the clients access the desired audio and video content, the central server acted as a scheduling server guides the client to the nearest edge server according to the balance of the global load, so clients can conveniently access the desired audio and video documents. Assume that the edge server does not have contents which the user wants, and then the edge server will send request to the central server to obtain the user needed content. According to the Baledo's law, the most clients can find what they need at the edge node. So the CDN model can effectively solve the problem of server crash caused by the large concurrent flow access to the central server.

B. The Model of P2P audio and video systems

P2P (Peer to Peer) is a kind of network model different from the C/S mode. The essential idea is to take full advantage of the free resources of computers distributed in different locations in the Internet, and to provide the Internet clients various services via distributed computing model.

The P2P architecture of the network model consists of all kinds of terminals, which are all called peers, as shown in Figure 2:

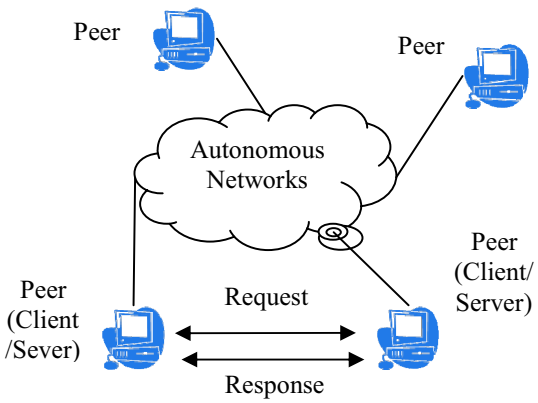

Figure 2. The P2P Network Model

In the Figure 2, it can be found that in the P2P network, each node plays two roles: server and client, which provides services for other nodes, and accesses to the services from other nodes at the same time in the shared resources system. This network model with self-organizing behavior can improve resource utilization, reduce costs, speed up document distribution, and reduce the dependence on the server.

From above we can find that the CDN model is able to effectively monitor the distribution of content and flow, but the expansion and maintenance costs are higher, while the P2P model network costs low, but it cannot provide effective supervision on the data content and flow, which is difficult to control the content that is transferred in the Internet. So it will be an efficient and practical solution of combing the two techniques, and applying it to the audio and video public network platform.

III. THE RESEARCH OF AUDIO AND VIDEO PUBLIC NETWORK PLATFORM SYSTEM MODEL COMBINED WITH THE CDN AND P2P

The design of public network platform for audio and video system combines two technologies, which are CDN and P2P. The CDN is used for reliable web and audio and video file content distribution, while the P2P for contents exchange with low cost. Combing the P2P's scalability and the CDN's controllability and manageability, builds a management integration platform, which can carry ultra-large-scale content distribution delivery applications. It will be the best solution for the development of audio and video public network platform.

A. CDN and P2P integration system architecture

CDN and P2P integration system architecture also consists of three parts: the central server, the edge server and the client. All of the edge server nodes form a P2P network, and all of the client nodes, which are closed to some edge server node, also form a P2P network. The CDN and P2P integration of audio and video public network platform system model is shown in Figure 3.

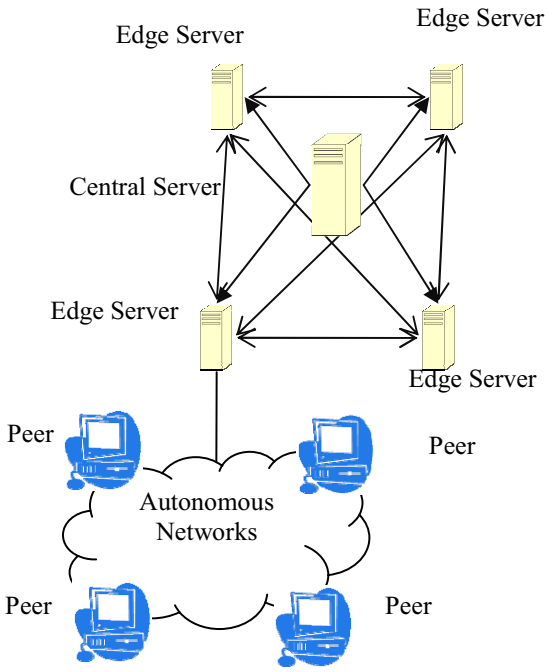

Figure 3. The CDN+P2P Network Model

In Figure 3, Central Server is responsible to distribute audio and video data slices to each Edge Server, as well as the central dispatch management and automatic load balancing.

When the client requests the P2P service to the system, the Central Server can dispatch the client to the autonomous system of the appropriate Edge Server according to the geographical relationship, and return the suitable Edge Server lists and Peer nodes back to the P2P clients.

Later the client builds the connection with the suitable Edge Server or Peer nodes for accessing data.

During the process, the Edge Server is responsible to receive data from Central Server or other Edge Servers in the autonomous system. When the new client accesses P2P channels, the Edge Server needs to provide rapid buffering capacity. And when there is lack of some data slices, which the clients want, the Edge Server needs to provide the slice compensation by requesting the data slice to the Central Server.

B. client request and response process

In order to give a better description of the operating principle of this model, the following shows the process of one client requests the resources and the response of the system.

(1) When the client first logs in the system, it sends all registration requests to the Central Server. The Central Server returns a Peer ID back to the client, which is certified as a unique node identifier of the client in the system.

(2) Then when the client orders some program from a channel, it first sent requests to the Central Server to join the channel. The Central Server returns the nearest Edge Server IP and Port and node IP and Port which is available to join back to the client through some dispatch policy.

(3) After the client is connected with the Edge Server, if the Edge Server cached resources can meet with the customer needs, the first fast buffer allows clients to watch the screen as soon as possible, meanwhile the connection Peer is returned back to the client. After a successful connection, the client request data stream from the Edge Server. Otherwise, if the Edge Server cached resources can't meet with the customer needs, it need to download the content from the Central Server or some other proxy servers and cache. Only after caching the demanded data, the client can see the audio and video content they want.

C. Characteristics of the model

(1) The integration of P2P and CDN improves the shortcomings in the streaming media services through the two kind of technologies mutual complementary. Introducing the CDN management mechanism and service capabilities into the P2P network to form the reliable content core of CDN, and the service edge architecture of P2P enhances the CDN service capabilities without increasing the CDN cost, and effectively avoids the shortcomings of P2P applications.

(2) Make full use of existing CDN, with little or no Modification on the existing CDN in order to protect operators' existing investments.

(3) The model provides the P2P fragmentation functions in the CDN edge node, which can provide streaming media services to P2PCDN users and original CDN users. In the backbone network, traditional streaming media is transported, without an increase in the backbone network traffic.The model slices the data in the CDN edge nodes, without increasing the fragmentation function for each client, and reducing the number of slice and the burden of the client.

IV. CONCLUSION

CDN and P2P integration, to build public network platform for audio and video, can better use the advantages of the two models, namely, to reduce the construction cost of the CDN network at the same time to monitor the data content and network traffic effectively. This network model is successfully used in audio and video public network platform in the build process, and achieved good results.

However, due to all the user dispatch by a central server to complete, when the number of users is very large, the central server will be the bottleneck of the system, which is problem that will be the direction of future improvement in this system.

V. ACKNOWLEDGMENT

This paper is sponsored by the audio and video communication technologies research project of the Chinese Ministry of Culture .

VI. REFERENCE

[1]. Lu Zhihui ,Wu Jie, Chen Lijiang,Huang, Sijia Huang, Yi.A novel CDN-P2P-hybrid architecture based VoD scheme.Lecture Notes in Computer Science (including subseries Lecture Notes in Artificial Intelligence and Lecture Notes in Bioinformatics), v 6488 LNCS, p 578-586, 2010, Web Information Systems Engineering, WISE 2010 - 11th International Conference, Proceedings

[2]. YANG Ge,LIAO Jian-xin,ZHU Xiao-min,FAN Xiu-mei. Survey of Key Technologies of the Distribution System for Streaming Media. ACTA ELECTRONICA SINICA. Vol. 37 No. 1Jan. 2009 (in chinese)

[3]. Lu, Zhihui , Wang, Ye, Yang, Yang Richard.An analysis and comparison of CDN-P2P hybrid content delivery system and model. Journal of Communications, v 7, n 3, p 232-245, 2012

[4]. Seyyedi, S.M.Y. Hybrid CDN-P2P architectures for live video streaming: Comparative study of connected and unconnected meshes.2011 International Symposium on Computer Networks and Distributed Systems, CNDS 2011, p 175-180, 2011, 2011 International Symposium on Computer Networks and Distributed Systems, CNDS 2011

[5]. Xu, Dongyan. Analysis of a CDN-P2P hybrid architecture for cost-effective streaming media distribution. Multimedia Systems, v 11, n 4, p 383-399, April 2006

[6]. J. Apostolopoulos, T. Wong, S. Wee, and D. Tan, On Multiple Description Streaming with Content Delivery Networks. Proceedings of IEEE INFOCOM2002, June 2002

[7]. Xinyan Zhang, Jiangchuan Liu, Bo Li,CoolStreaming/DONet: A Data-DrivenOverlay Network for Ef cient Live MediaStreaming. INFOCOM 2005, 13-17 March2005

[8]. T. Do, K. A. Hua, and M. Tantaoui,P2VoD: providing fault tolerant videoon-demand streaming in peer-to-peerenvironment. Proceedings of ICC' 04, Jun2004

[9]. X. Hei, C. Liang, J. Liang, Y. Liu,and K. W. Ross, Insights into PPLive:A measurement study of a large-scale P2PIPTV system. WWW 2006, May 2006

[10]. X. Liao, H. Jin, Y. Liu, L. M. Ni andD. Deng, AnySee: Peer-to-Peer LiveStreaming, INFOCOM ' 06, Apr 2006Dongyan Xu, Sunil Suresh Kulkarni,Catherine Rosenberg, Heung-KeungChai. Analysis of a CDN P2P hybridarchitecture for cost-effective streamingmedia distribution. Multimedia Systems,Volume 11, Number 4, 17 March 2006

A Mixed Localization Algorithm Based On RSSI And APIT With Fitness Analysis And Optimization

Bo Chen
School of IOT Engineering
Jiangnan University
Wuxi, China
chenb1221@sina.com

Jun Sun Wen Bo Xu
School of IOT Engineering
Jiangnan University
Wuxi, China
sunjun_wx@hotmail.com

Jian Xu
Chongqing Medical and
Pharmaceutical College
Chong Qing, China

Abstract*—As a new information acquisition and processing technology, wireless sensor networks can achieve tasks with complex large-scale monitoring and tracking in wide range of applications ,but the localization for node itself is the basis of most applications .APIT is a major localization algorithm of ranged free algorithms ,but the algorithm has the problems of big localization errors and low coverage rate ,it also has high dependence on the number of anchor nodes . In order to overcome these disadvantages ,this paper propose a mixed localization algorithm based on RSSI and APIT with fitness analysis and optimization ,According to the experiment and simulation ,the new algorithm has smaller localization errors ,higher coverage rate ,and improves the overall stability of nodes' localization.

Keywords-wireless sensor networks; localization; approximate point-in triangulation test(APIT);received signal strength indicator(RSSI);fitness

INTRODUCTION

With the deep research and many applications in the field of IOT(internet of things),The Information Awareness system that composed with the layer of information collection and the layer of information transmission becomes as a major field in IOT applications ,and wireless sensor network plays a key role in promoting this industry . The wireless sensor network is a multi-hop self-organizing network system .Getting the location information of sensor nodes is an important part of the sensor network applications .If there is no location information, the data obtained by network would be meaningless .So the research in the field of localization technology of wireless sensor network has been one of the hot topics [1-2].

The existing WSN(wireless sensor network) localization algorithms can be divided into two categories according to the localization mechanism :Range-based and Range-free[3-4].Range-based localization algorithm calculates the unknown node's position by measuring the absolute distance or orientation between adjacent nodes and using the actual distance between the nodes[5] .At the present stage ,there are many common rang-based localization algorithms: RSSI(received signal strength indicator),TOA(time of arrival),TDOA((time difference of arrival) and AOA (angle of arrival) .The range-based localization mechanism is merit in localization accuracy ,but it does not apply to low-power and low-cost applications .Range-free localization algorithm is based only on network connectivity information ,It does not depend on the distance and angle information .The common range-free algorithms have Centroid, convex programming, the DV-hop, Amorphous, MDS-MAP and APIT(approximate point-in triangulation test). The Range-free localization mechanism has advantages in cost, power consumption [6], and it is lower in hardware requirements, so it gets much more attentions.

Approximate point inside the triangle test is a range-free localization algorithm, it has low network costs and its implementation is easy .However, in a randomly distributed network, this algorithm has big localization errors and low coverage, therefore it is of great significance for improving APIT. In order to overcome these disadvantages this paper proposed a mixed localization algorithm based on RSSI and APIT with fitness analysis and optimization. According to the experiments, the new algorithm has smaller localization errors, higher coverage, and it improves the overall stability of nodes' localization.

I. RELATED LOCALIZATION TECHNOLOGIES

A. *RSSI Ranging Quantify Model* [7]

$$P_0 = 10*\lg\left(G_t * G_r * \lambda^2 \Big/ (4*\pi)^2 * (d_0)^2 * L\right) \quad (1)$$

In the above formula d_0 is reference distance of near-Earth, P_0 is path loss which is d_0 away from earth, G_t is transmitting antenna gain, G_r is receive antenna gain ,L is the system loss factor without relations to transmission(not less than 1).

$$P_{ij} = P_0 - 10*\eta*\lg\left(d_{ij}/d_0\right) + X_n \quad (2)$$

In the above formula P_{ij} is the power between the accept node j and launch node i, d_{ij} is the distance between node i and node j, η is the path loss exponent, X_n is the random variables with normal distribution caused by obstructions.

978-0-7695-4818-0/12 $26.00 © 2012 IEEE
DOI 10.1109/DCABES.2012.45

B. Trilateration

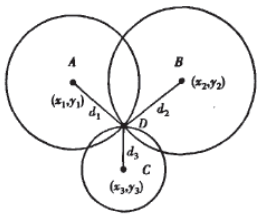

Figure 1 Trilateration

Trilateration[8],as shown in figure 1,A,B,C are known points ,and their coordinates are (x1, y1),(x2, y2) ,(x3, y3).The distances between three each point and the point D are d1,d2,d3,Assume that the point D whose coordinates is (x ,y),according to the distance formula between two points ,that:

$$\sqrt{(x-x_1)^2+(y-y_1)^2}=d_1 \quad (3)$$

$$\sqrt{(x-x_2)^2+(y-y_2)^2}=d_2 \quad (4)$$

$$\sqrt{(x-x_3)^2+(y-y_3)^2}=d_3 \quad (5)$$

According to the formula (3), (4), (5) we can obtain the coordinates of point D by solving the linear equations .The coordinates of point D is:

$$\begin{bmatrix} x \\ y \end{bmatrix}=\begin{bmatrix} 2(x_1-x_3) & 2(y_1-y_3) \\ 2(x_2-x_3) & 2(y_2-y_3) \end{bmatrix}^{-1} \begin{bmatrix} x_1^2-x_3^2+y_1^2-y_3^2+d_3^2-d_1^2 \\ x_2^2-x_3^2+y_2^2-y_3^2+d_3^2-d_2^2 \end{bmatrix}$$

C. Localization By Two Nodes

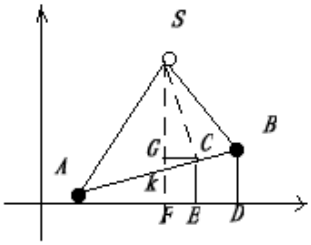

Figure 2 Localization By Two Nodes

When the neighbor anchor nodes' number of unknown node is equal to 2,as shown in the figure 2.Assume that A,B are the anchor nodes ,S is an unknown node, the coordinate of anchor node A is (Xa ,Ya), the coordinate of anchor node B is (Xb ,Yb), the coordinate of unknown node S is (Xs ,Ys).According to RSSI ranging ,we can obtain the distances between A,B and S denoted as d1,d2.As A ,B are anchor nodes ,their coordinate information are known ,we can get the distance between A and B denoted by d3. In the triangle ABS, draw two lines ,SC and SF ,which are vertical towards line AB and axis X ,through point S ,draw two lines ,BD and CE ,which are vertical towards axis X ,through point B and C ,and then draw a line CG ,which is vertical towards line SF ,through point C denote ∠ SAB=α, ∠ BAD=β.By the law of cosines $\cos\alpha=\frac{d_1^2+d_3^2-d_2^2}{2*d_1*d_3}$,we can obtain

$AC=t=d_1*\cos\alpha=\frac{d_1^2+d_3^2-d_2^2}{2*d_3}$, $SC=h=\sqrt{d_1^2-t^2}$,we also can calculate the sine and cosine of the angle β by the coordinate of point B. We can see from the triangle similarity theorem, ∠GSC=β， GC=FE and AF=AE-EF=AC*cosβ-SC*sinβ=t*cos-h*sinβ, finally we can calculate the coordinate of unknown node S:

$$x_s=x_a+t*\cos\beta-h*\sin\beta$$

$$y_s=y_a+t*\sin\beta+h*\sin\beta$$

D. APIT Algorithm [9]

The basic idea of the APIT localization algorithm: each unknown node monitor the information of nearby anchor nodes ,assume that the number of nearby anchor nodes is n ,each three anchor nodes out of the n anchor nodes form a triangle ,there are C_n^3 kinds of different combinations .Individually test whether the unknown node is located inside the triangle ,and finally find the centroid of the coincidence region of the all triangles who contain the unknown node ,then the location of the centroid can be regarded as the estimated location of the unknown node.

II. IMPROVED LOCALIZATION ALGORITHM

In APIT algorithm, the anchor node density has great impact in algorithm performance, as we know; localization accuracy and localization coverage will be great improved as the anchor node density increases. For this feature, in this paper we get the RSSI localization algorithm to assist localization, the accuracy and coverage will be improved by the new anchor nodes which are located by RSSI localization algorithm .However, the located nodes will perform better in the role of anchor nodes to assist localization only when the position information of located nodes is much closer to the actual . In order to overcome these disadvantages, this paper joins the analysis of fitness of the node's position in [10-12].

A. Fitness Fuction

Assume that an unknown node P has M neighbor anchor nodes in the two-dimensional space ,then we can obtain the distance of each one anchor node to the unknown node P by RSSI ranging ,denote as d_i ,i=1,2,…,m ,and then the coordinates of the unknown node (x ,y) satisfy the formula ,as follows:

$$\begin{cases} \sqrt{(x-x_1)^2+(y-y_1)^2}=d_1 \\ \sqrt{(x-x_2)^2+(y-y_2)^2}=d_2 \\ \cdots\cdots\cdots\cdots\cdots \\ \cdots\cdots\cdots\cdots\cdots \\ \cdots\cdots\cdots\cdots\cdots \\ \sqrt{(x-x_m)^2+(y-y_m)^2}=d_m \end{cases} \quad (6)$$

However because of the ranging error and environmental factors ,there is a certain error in measuring distance ,so the formula (6) cannot be fully established .Assume that f_i (i=1,2,…,m) is the ranging error values between the unknown nodes and anchor nodes ,then it satisfy the formula as follows:

$$f_i=\sqrt{(x-x_i)^2+(y-y_i)^2}-d_i \quad (7)$$

As we know that the localization results will be more accurate when the measuring error value f_i is smaller in the localization of WSN [13-15], so the fitness function can be defined as follows:

$$f_{itness}=\sum_{i=1}^{m}\sqrt{(x-x_i)^2+(y-y_i)^2}-d_i \quad (8)$$

B. Implementation Steps Of FRSSPIT Algorithm

Based on the idea that the nodes which are located at first time can be used for localization of other nodes to improve the coverage and using RSSI algorithm can improve localization accuracy [16-18], this paper puts forward an improved algorithm, detail steps as follows:

- Deploying anchor_n anchor nodes and node_n unknown nodes randomly ,and obtaining the id information and position information of these anchor nodes,
- Each unknown nodes records the information of anchor nodes which it can receive from, get the number of its neighbor anchor nodes ,denoted as neighbor_n ,and then calculate the distance from this node to each neighbor anchor by RSSI ranging ,denote as d,
- Localization for the unknown nodes whose number of neighbor anchor nodes is more than 3, The specific method is as follows :choose 3 anchor nodes to combine from all neighbor anchor nodes randomly, use the trilateration method for localization ,there will be kinds of combinations ,analyze the result (x ,y) of localization to each combination ,take the result (x ,y) into the formula (8),obtain the fitness by calculating ,and then find the combination where the result of fitness is the minimum ,record its localization result ,denoted as (x_{ir}, y_{ir}) ,
- Regarding the located nodes as new anchor nodes, assuming that the number of new anchor nodes is new_anchor_n ,then the total number of anchor nodes is the old ones plus the new ones ,we denote the total number as AN ,to all node_n nodes ,we use the AN anchor nodes for localization by APIT algorithm ,denote the localization results as (x_{ia}, y_{ia}) ,
- For the same unknown nodes ,we calculate the average value of the result in (3) and the result in (4),and regard the average value as the finally localization result,
- For the remaining unknown nodes ,we pay attention to their numbers of neighbor anchor nodes ,if the number is equal to 2,we locate by the method of two nodes localization ,if the number is equal to 1 or 0 ,we treat them cannot be located ,the end.

III. ALOGRITHM SIMULATION AND RESULTS ANALYSIS

A. Simulation Environment

This paper chooses MATLAB for simulation test. Assume that sensor nodes are distributed in a 100m * 100m square area ,all 100 nodes are deployed randomly ,a certain percentage of them are anchor nodes, the coordinates information of anchor nodes are known .We take the circular communication as the means of communication .In RSSI ranging model, the values of transmitting antenna gain ,receive antenna gain and system loss factor are all evaluate to 1, the value of earth nearby is 20,the value of path loss is 2.We mainly take observation and comparison from localization accuracy and localization coverage, All dates are taken from 100 times experiments.

- Localization Accuracy: the first evaluation of the localization technology is the localization accuracy ,it is generally expressed by using the ratio of the error(Error) value with the node radio range(R), Accuracy=(Error/R)×100%
- Node Localization Coverage: the ratio of the total number of the nodes who have been located (including the original anchor nodes) with the number of total nodes in the region.

B. Experimental Results Analysis

Figure 3 show that localization accuracy of different anchor node proportion where they have the same node communication radius, here we choose 30 meters as the communication radius.

In this paper ,I will compare three algorithms ,one is the new improved algorithm named frsspit ,one is the mixed algorithm based on RSSI and APIT without fitness analysis and optimization named rsspit ,and another is the original APIT algorithm named apit .As figure 3 shows ,we can see that the localization accuracy of rsspit algorithm and frsspit algorithm have been greatly improved compared to the original apit algorithm. With the increase in the proportion of the anchor nodes ,we will find that the localization accuracy of frsspit algorithm is taller than the localization accuracy of rsspit by 3-4 percentage points ,and after the anchor node proportion reach 50%,the localization accuracy of all three algorithms become closer and closer.

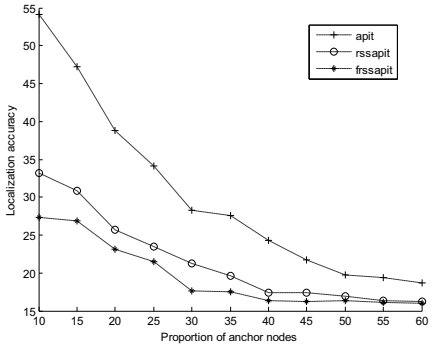

Figure 3 localization accuracy compared

Figure 4 shows that localization coverage of different anchor node proportion which have the same node communication radius ,here we choose 30 meters as the communication radius .As figure 4 shows ,in the same conditions ,we will find that the localization coverage of mixed algorithm based on RSSI and APIT is better than the original APIT algorithm ,and the new one with fitness analysis and optimization is a little larger than the rsspit algorithm ,when the anchor node proportion reach 55%,the localization coverage reach the consensus.

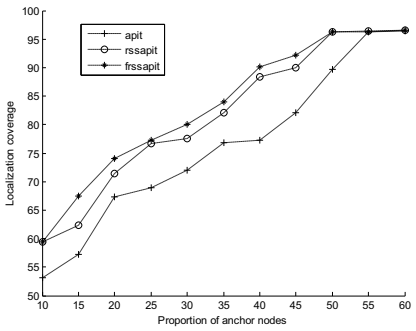

Figure 4 localization coverage compared in different proportion of anchor node

Figure 5 shows that localization coverage of different node communication radius where they have the same anchor node proportion ,here we choose 30% as the node communication radius .From the experiments we can find that the localization coverage of rsspit algorithm is a litter taller than the original apit algorithm when the node communication radius is small ,so is the frsspit algorithm ,as the communication increases ,the localization coverage of frsspit algorithm has greatly improved ,it is taller than the old one and rsspit algorithm, especially when the communication radius is between 20 meters and 35 meters. When the node communication radius reach 40 meters, the localization coverage of each three algorithms reach the same.

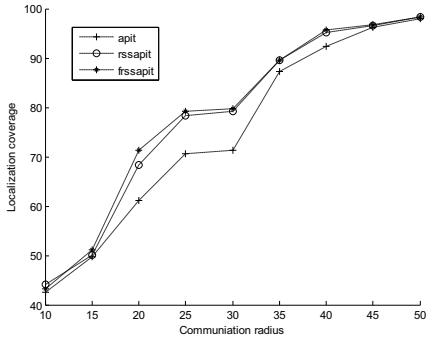

Figure 5 localization coverage compared in different communication radius

IV. CONCLUSION

This paper uses RSSI algorithm to assist for localization based on APIT algorithm ,and then joins the fitness analysis in the mixed algorithm .The experiment proved that the localization accuracy and localization coverage of this improved algorithm have been greatly improved ,however ,the spending of calculate is also increased when joining the fitness analysis and cycle localization .How to reduce the computational spending and use it in the actual situation while the algorithm performance is not poor is the direction of the key research.

REFERENCES

[1] FY Ren, HL Huang, C Lin.Wirness Sensor Network [J].Journalof Software,2003,14(7):1148-1157.

[2] Bulusu N,Estrin D,Heidemann J.GPS- less low-cost outdoor localization for very small devices[J].IEEE Personal Communications,2000,7(5):28-34.

[3] Oliveira,Horacio A.B.F.Boukerche,Azzedine,Nakamura,Eduardo F.,Loureiro,Antonio A.F..Localization in time and space for wireless sensor networks:An efficient and lightweight algorithm[J].Performance Evaluation, 2009 66(3-5),209-222.

[4] Rappaport T S. Wireless Communications: Princples and Practice[M].Prentice-Hall PTR,2001.

[5] Lewis Girod,Vladimir Bychkovskiy,Jeremy Elson,and Deborah Estrin.Locating Tiny Sensors in Time and space[C]//A Case Study.Proceedings of the 2002 IEEE International Conference on Computer Design:VLSI in Computers and Processors(ICCD02).

[6] FB Wang , L Shi , FY Ren . Self-Localization systems and algorithms for wireless sensor networks . Journal of Software , 2005, 16(5) : 857-868.

[7] Z Fang, Z Zhao, P Guo, YG Zhang. Analysis of Distance Measurement Based 0n RSSI [J]. CHINESE JOURNAL OF SENSORS AND ACTUATORS,2007,20(11):2526-2530.

[8] Daiya, V.; Ebenezer, J.; Murty, S.A.V.S. Experomental analysis of RSSI for distance and position estimation[C]. Recent Trends in Information Technology (ICRTIT). 2011 International Conference on Digital Object Identifier:10.1109/ICRTIT.2011.5972367 Publication Year: 2011 , Page(s): 1093 - 1098 .

[9] Y Zhou, SX Xia. An Improved APIT Node Self-Localization Algorithm in WSN Based on Triangle- Center Scan [J].Journal of Computer Research and Development,2009,46(4):566-574.

[10] W Fang, J Sun, WB Xu. DiVersity controlled particle swarm optimization algorithm[J].Control and Decision.

[11] T He, C Huang, B Blum, et al . Range - free localization schemes for large scale sensor networks [J]. MOBICOM,2003.

[12] XF Feng, ML Cao, C Sun. Mixed Localization Algorithm for Wireless Sensor Networks Based on APIT Algorithm [J]. MICROELECTRONICS and COMPUTER,2009,29(6):58-61.

[13] JJ Yao, Y Han. Research on Target Localization Based on Particle Swarm and Newton Iterated Algorithm [J].Application Research of Computers,2010,27(5):1700-1701.1713.

[14] J. Sun, W. Fang, X. J. Wu, Z. P. Xie, W. B. Xu. Quantum-behaved particle swarm optimization: analysis of the individual particle's behavior and parameter selection[J]. Evolutionary Computation(MIT Press). Uncorrected Proof

[15] W. Fang, J. Sun, Y. R. Ding, X. J. Wu, W. Xu. A review of quantum-behaved particle swarm optimization[J]. IETE Technical Review, 2010, 27(4): 336-348.

[16] MY Xing, LY Li. Application of Particle Swarm Optimization to Positioning for Wireless Sensor Networks [J] . Computer Engineering and Applications, 2009, 45(32) : 72-74.

[17] B Han, CB Xu, H Yuan. An Improved APIT positioning algorithm in wireless sensor network[J].Computer Engineering and Applications, 2008 ; 44(4) : 122—124.

[18] XF Feng, XF Cui, HB Qi. A Modified Localization Algorithm of APIT Based on Mobile Anchor Node for Wireless Sensor Network [J]. CHINESE JOURNAL OF SENSORS AND ACTUATORS,2011,24(2):269-274.

A Coverage Control Algorithm Based on Probability Model for Three-Dimensional Wireless Sensor Networks

Junqing Zhang, Ruchuan Wang, Yisheng Qian, Qianyi Wang

College of Computer, Nanjing University of Posts and Telecommunications, Nanjing
Jiangsu High Technology Research Key Laboratory for Wireless Sensor Networks
Key Lab of Broadband Wireless Communication and Sensor Network Technology
Ministry of Education , China
hhp@njupt.edu.cn

***Abstract*—The main study of traditional probability coverage problem in wireless sensor networks (WSNs) is aiming at two-dimensional space, however, most practical applications of wireless sensor network is placed in a three-dimensional sensor networks. Therefore, probability model is introduced for three-dimensional WSNs. This paper presents a method that using Voronoi divide to control the Scheduling of the probability model nodes in the target area. Also, a coverage control algorithm based on probability model (PMCCA) is proposed. We verify the effectiveness and the practice of PMCCA algorithm by comparing PMCCA algorithm to another algorithm in simulation experiment.**

Keywords-wireless sensor networks; three-dimensional coverage; probability model; Voronoi divide

I. INTRODUCTION

The sensory ability of WSNs to physical world is embodied in coverage which is often used to describe the monitoring standard of Quality of Service (QoS)[1,2]. However, due to the limited allocation energy of sensor nodes, how to prolong the service life of network on the premise that ensure the quality of network coverage, has become a most important aspects of the research in wireless sensor network application[3].

Probability coverage algorithm adopted the uncertain sensor detection model, that is, the detecting precision of sensors changes with the law of induced signal attenuation, considering the distance between targets and sensors and environmental factors, several sensor nodes work collaboratively to detect the targets at a certain probability. At present, many references adopted this detection probability model to discuss wireless sensor network covering problems. The author of reference [4] proposed a coverage configuration algorithm based on the detection probability model, which is only for the evaluation of point coverage probability. The author of reference [5] proposed a coverage maintain protocol which is based on the detection probability model, in the premise of keeping network coverage, make the amount of sensor network nodes which are worked as small as possible. But this protocol restricts the scale of the network for using central control algorithm to configure the network. In addition, most current references don't quote the probability model to three-dimensional wireless sensor networks. However, most practical applications of wireless sensor network is placed in a three-dimensional sensor networks, which can more accurately simulate in a real three-dimensional place[6,7]. In reference [6] Bai proposed and designed a series connected coverage model in low connected and covered three-dimensional wireless sensor networks, but still with high computational complexity. In reference [7] Nazrul Alam did some research of truncation octagonal deployment strategy, which is used to monitor the coverage situation of networks, however it under the restriction of truncation octagonal.

Based on the above problems, this paper extends the traditional two-dimensional probability coverage model and applied it into three-dimensional scene; hen probability model is introduced for three-dimensional WSNs. Further more, it presents a method that using Voronoi divide to control the Scheduling of the probability model nodes in the target area. Also, a coverage control algorithm based on probability model (PMCCA) is proposed. PMCCA algorithm adopts probability perception model, and uses properties of Voronoi to simplify the allocation algorithm, and divide the network to do accomplish the covering configuration.

This paper is organized as follows: section II gives the problem description and related definition. Section III describes the probability model of sensors and defines the related parameters. Section IV describes in detail the coverage control algorithm based on probability model (PMCCA). Section V verifies the validity of the algorithm via simulation experiments and makes contrast. At the end of this paper, we come to a conclusion and introduce the next step for the research plan.

II. DESCRIPTION OF THE PROBLEM AND RELATED DEFINITIONS

A. Description of the problem

The coverage of three-dimensional wireless sensor networks constituted by nodes of probability model can be described as follows: a large number of nodes randomly distribute in a given three dimensional target area and a certain coverage rate of the area is given. How to scheduling these nodes in the given three-dimensional area so that coverage rate in target area approaches given expectation in condition which the number of nodes is as small as possible.

978-0-7695-4818-0/12 $26.00 © 2012 IEEE
DOI 10.1109/DCABES.2012.52

B. Related assumptions and definitions

Before the research of this paper, we give the consumptions as follows.

- Every node in the sensor networks adopts the same probability model, namely, all the nodes have the same perception radius R_s and the communi cation radius R_c, which R_s is not smaller than R_c, in order to ensure the connectivity of the network configuration.
- Node energy is sufficient to support the node scheduling process.
- Every node can get the information of its location and sensing direction and the direction is steerable.

Assume in the three-dimensional bounded cube target area A, the location of random deployed sensor nodes are all meet the form of uniform distribution model, and any two sensor nodes is not in the same location. The relevant definitions are as follows:

Definition 1. Distance:

Node Ni is in (x_i,y_i,z_i) and target N_j is in (x_j,y_j,z_j), then the distance between target N_j and node N_i is defined as $D(N_i,N_j)$:

$$D(N_i,N_j) = \sqrt{(x_i-x_j)^2+(y_i-y_j)^2+(z_i-z_j)^2} \quad (1)$$

Definition 2. Euclidean distance:

Euclidean distance d_{ip} of node N_i to point P is defined as:

$$d_{ip} = \sqrt{(x_i-x_p)^2+(y_i-y_p)^2+(z_i-z_p)^2} \quad (2)$$

III. ANALYSIS OF THE SENSOR NODES WITH PROBABILITY MODEL

A. Probability detection model

Assume that N sensor nodes distributed in the three dimensional monitoring area randomly，node N_i located at (x_i, y_i, z_i), i = 1,2, ..., N. Then the observed target t located at (x_t, y_t, z_t) can be detected by node N_i with the probability P_{it}[8]:

$$P_{it} = \begin{cases} \dfrac{1}{(1+\alpha d_{it})^{\beta}} & d_{it} \le R_s \\ 0 & d_{it} > R_s \end{cases}, \quad i=1,2,\ldots,N \quad (3)$$

Where P_{it} represents the coverage probability of any point t which location is (x_t,y_t,z_t) in node N_i's sensing area; d_{it} represents the geometric distance between node N_i and point t, which satisfies the formula $d_{it} = \sqrt{(x_i-x_t)^2+(y_i-y_t)^2+(z_i-z_t)^2}$.α and β are related to the physical characteristics of the sensor type parameter. The coverage probability of any point P_{it} [0, 1], and when the point p and node N_i are in the same location, that is d_{ip} = 0, the coverage probability of p is 1. Usually β values between the number of [1, 4], and α is an adjustable parameter[8].

In the wireless sensor networks, node density is usually high; therefore, the events in the monitoring area will be detected by more than one sensor nodes. If a node exists neighbor nodes, the overlap of the sensing area between the node itself and the neighbor nodes will lead to the point t fall in the overlap region, thence the coverage probability of the point t will be influenced by the neighbor nodes. Assume that node N_i has *K-1* neighbor nodes, that is, node $N_1, N_2, \ldots, N_k$, the sensing area of node N_i and its neighbor nodes are $R(N_i)$, $R(N_1)$, $R(N_2)$, ..., $R(N_k)$, then the overlap region of these nodes is $M = R(N_i)\cap R(N_1)\cap R(N_2)\cap\ldots\cap R(N_k)$. At this point, the detection probability of observing the target t at (x_t,y_t,z_t) can be expressed as

$$P_t = 1-\prod_{i=1}^{K}(1-P_{it}) \quad (4)$$

Substituting equation (4), obtained that

$$P_t = 1-\prod_{i=1}^{K}\left(1-\frac{1}{(1+\alpha d_{it})^{\beta}}\right) \quad (5)$$

According to equation (5), when some sensor nodes detect the same events, the system detection probability P_t will be higher than the probability P_{it} of detection by any single node.

B. Definition of related parameters

Definition 3. γ-coverage probability:

If there is a collection of nodes, which locations are (x_i,y_i,z_i) , $i=1,2,\ldots,N$, if the value of system detection probability P_t of target point t (x_t,y_t,z_t) in the region is not less than γ, then we can claim that the point $t(x_t,y_t,z_t)$ meet γ-probability coverage. If and only if all the points in this region meet the probability of γ-cover can we claim that the region meet the probability of fully γ-cover.

Definition 4. K-probability covering distance:

In order to facilitate the research, we do the following approximate processing, assume that for each $i=1,2,\ldots,K$, has $d_{it}=r_k$, at this point, make

$$P_t = 1-\prod_{i=1}^{K}\left(1-\frac{1}{(1+\alpha d_{it})^{\beta}}\right) = \gamma \quad (6)$$

Where γ is the probability of system detection threshold at the target point.

K-probability covering distance can be calculated by formula (6) :

$$r_k = \frac{1}{\alpha}\left[1-\left[\frac{1}{1-(1-\gamma)^{\frac{1}{K}}}\right]^{\frac{1}{\beta}}\right] \quad (7)$$

Definition 5. Maximum perception distance R_s:

When node N_i works independently, if $d_{it}\ge R_s$, then the detection probability P_{it} of target by node N_i is negligible relative to the system detection probability, that is, when the the d_{it} reaches the perception distance of node N_i,

P_{it} = 0. We said the distance which meets the above conditions is maximum perception distance R_s.

IV. A COVERAGE CONTROL ALGORITHM BASE ON PROBABILITY MODEL

Before you begin to format your paper, first write and save the content as a separate text file. Keep your text and graphic files separate until after the text has been formatted and styled. Do not use hard tabs, and limit use of hard returns to only one return at the end of a paragraph. Do not add any kind of pagination anywhere in the paper. Do not number text heads-the template will do that for you.

Finally, complete content and organizational editing before formatting. Please take note of the following items when proofreading spelling and grammar:

A. Three-dimensional voronoi divide

Let $s = \{p_1, p_2, ..., p_n\}$ be a set of points in a two-dimensional Euclidean plane. These points are called sites. A Voronoi diagram decomposes the space into regions around each site, such that all points in the region around p_i are closer to p_i than any other point in *S*.

The Voronoi region $V(p_i)$ for each pi is expressed as:

$$V(p_i) = \{x : | p_i - x | \leq | p_j - x |, \forall j \neq i\} \quad (8)$$

$V(p_i)$ consists of all points that are closer to p_i than any other site. The set of all sites form the Voronoi Diagram *V (S)*.

The follow example, extracted from [9], illustrates a simple Voronoi diagram. Consider two points p_1 and p_2. Let $B(p_1,p_2) = B_{12}$ be the perpendicular bisector of the segment $\overline{p_1 p_2}$. Then every point x on B_{12} is equidistant fromp1and p_2. This can be seen by drawing the triangle (p_1,p_2,x) as depicted in Fig. 1. By Euclid's side-angle-side theorem, $|p1x| = |p2x|$.

To sum up, given input points presented in Fig. 2a, the corresponding Voronoi diagram is depicted in Fig. 2b.

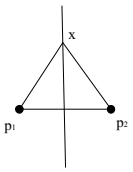

Figure 1. Two points |p1x| = |p2x|

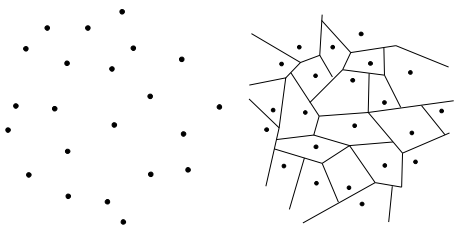

(a)Input points (b) Voronoi diagram

Figure 2. A set of points and its

In this paper, traditional two-dimensional Voronoi diagram will be extended to applications which are in three-dimensional wireless sensor networks. It is defined as follows:

Definition 6. The Voronoi area $V(N_i)$ of node N_i:

Assume that there is a sensor node collection $V=\{N_1, N_2, ..., N_n\}$ in the three dimensional space, then all the point (x, y, z) in the voronoi area of $V(N_i)$ meet the formula $\sqrt{(x - x_i)^2 + (y - y_i)^2 + (z - z_i)^2} \leq \sqrt{(x - x_k)^2 + (y - y_k)^2 + (z - z_k)^2}$, where (x_k, y_k, z_k) is the location of another node. That is to say, the distance from every sensor node in this $V(N_i)$ to node N_i is near than to any other node in the given scene.

Definition 7. Three dimensional sensor network Voronoi division:

Assume that *N* sensor nodes are randomly distributed in the observation area, by definition 1,we can divide a wireless sensor network observation region A into *N* bordering convex polyhedron $V(N_1)$, $V(N_2)$, ..., $V(N_n)$. Each convex polyhedron contains a sensor node N_i, with the mark of $V(N_i)$. The division of this definition is three-dimensional sensor network Voronoi division.

B. Node scheduling

1) Working state of sensor node

- Active state: The sensor nodes are in working condition and can perceive events within the target area.
- Hibernation state: The sensor nodes turn off the unnecessary features in order to save energy.
- Judgment state: The sensor nodes according to the ju dgment algorithm to determine whether this node can comply with the conditions into hibernation. If it meets the conditions, the node goes to sleep. Otherwise, it is still active.

2) Judgment algorithm

In the three-dimensional sensor network observation region, assume that any one sensor node N_j exists several adjacent nodes which are active. If N_j is closed, $V(N_1)$, ..., $V(N_i)$, ..., $V(N_N)$ (where $i= 1,2, ..., N$) all satisfy the definition of full γ-probability coverage proposed in section III, then the node N_j can go into hibernation, otherwise, if either $V(N_i)$ (where $i = 1,2,..., N$) does not meet the definition of fully γ-probability coverage, then the node N_j need to remain active in order to ensure the network coverage not less than γ when close part of the nodes in the network.

3) Node scheduling algorithm

Node scheduling works sub-round, rotating the node state at a certain period. In the beginning of each working cycle, firstly, the sensor nodes initialize the state information, including close the node-aware module, update location information of the node itself and its adjacent, according to the Voronoi partition method to calculate the vertex location of the convex polygon which contains the node. Then, this node executes the judgment algorithm to determine whether turn into

hibernation cycle. During each round of algorithm execution we can find the weakest point P in $V(N_i)$, as long as the system detection probability of this point P we just found meets the probability of fully γ-cover, we can claim that all the area of $V(N_i)$ meet fully γ-cover. Assume that there are K active sensor nodes N_1, N_2, ..., N_K and the target P, where the Euclidean distance between node N_i and target P is d_{ip}, d_{ip} can be calculated by formula (2).

If

$$\sum_{i=1}^{K} d_{ip} \le K \bullet r_k \tag{9}$$

then the target P meet the γ-probability coverage, where r_K is the K-probability coverage distance according to Definition 4 in section III.

The pseudo-code of the scheduling process is as follows:

//Initialization, N probability model nodes which are in working state are deployed in the three-dimensional sensor networks.

a) j←0;

b) Set the relevant parameters N、α、β、γ;

c) Set the maximum number of cycles Tmax;

while(j<Tmax) do

{

d) Read the coordinates od the location of node Ni;

e) Calculate $\sum_{i=1}^{K} d_{ip}$ *according to formula (2);*

f) Calculate the maximum $\sum_{i=1}^{K} d_{ip}$ *;*

g) Determine whether set this node into hibernation according to the judgment algorithm proposed in section IV;

h) If node in step g) goes to sleep, then continue to do the following steps; otherwise, jump to the end of the process;

i) j←j+1； N←N-1;}

j) K←N，the derived value of K is the number of the actual active sensor nodes in the network after the execution of PMCCA algorithm during this period;

k) End.

V. SIMULATION AND ANALYSIS

This paper uses Visual C++6.0 to develop a simulation software by ourselves which is appropriate for the study of wireless sensor network deployment and coverage, and utilize the software to make a large number of simulation experiments to verify the effectiveness of the algorithm of PMCCA.

A. Settings of the experimental parameters

Values of specific parameters are shown in Table I.

TABLE I. EXPERIMENT PARAMETERS

Parameter	Target region A	Distribution mode	Number of Node N
Value	30*30*30m3	Random distribution	300,500,1000,2000
Parameter	Sensory type parameter α	Sensory type parameter β	Threshold of detection probability γ
Value	adjustable	[1,4]	0.9

B. Analysis of Algorithm parameters on the effect of K

In order to discuss PMCCA algorithm parameters on the effect of K, which is the final value of node number, we conduct many groups of experiments for different parameters. Within the process, we make R_s=5m，R_c=15m.

According to the analysis of experimental data, we can draw the conclusion that the sensor parameters α, β have a great influence on the number of active node K. Along with the increase of α, β, signal decays seriously, hence the network needs more extra active sensor nodes to maintain the desired coverage.

C. Comparative Analysis of Algorithms

In this section, a series of simulation experiments are conducted to illustrate the effect on the performance of PMCCA algorithm from the two key parameters. They are node scale N and sensory radius R_s. Reference [5] proposed a protocol to maintain the coverage based on probability detection model (CPP), reference [6] put forward a connectivity and coverage algorithm for low connectivity and full coverage wireless sensor networks (FCKC). We compare these two algorithms to PMCCA algorithm proposed in this paper and analyze their performances.

Curve changes from Fig. 5(a) and 6(a) show that when fixing perception radius R_s of sensor nodes, along with the increase of the number of nodes, the network coverage increases. In the premise of putting into a certain number of nodes in the network, adopting PMCCA algorithm proposed in this paper can lead to a higher coverage rate compared with CPP algorithm and FCKC algorithm. For example, making the number of nodes N is 150, the network coverage rate controlled by PMCCA algorithm is 5 percentages more than the CPP algorithm and 3 percentages more than FCKC algorithm. This proves the efficiency of the proposed algorithm.

Curve changes from Fig. 5(b) and 6(b) show a similar conclusion, when fixing number of sensor nodes N, as the radius of sensor nodes R_s increases, the network coverage rate presents an upward trend. At the same time, the comparison of curves shows the use of PMCCA algorithm proposed has a higher coverage rate than CPP algorithm and FCKC algorithm. For example, making perception radius of nodes R_s is 2m circumstances, adopting PMCCA algorithm proposed in this paper can lead to a higher coverage rate compared with CPP algorithm and FCKC algorithm. For example, making the number of nodes is150, the network coverage rate controlled by PMCCA algorithm is 10 percentages more than the CPP algorithm and 6 percentages more than FCKC algorithm. This is also confirmed the efficiency of PMCCA algorithm.

Comparison with CPP algorithm and FCKC algorithm confirmed that PMCCA algorithm proposed in this paper has a better result for the control of the wireless sensor network, and further can lead the network to obtain a higher coverage rate using a certain number of wireless sensor nodes.

VI. CONCLUSION

Aiming at that the main study of traditional probability coverage problem in wireless sensor networks (WSNs) is usually in two-dimensional space, probability model is introduced for three-dimensional WSNs and design a coverage control algorithm based on probability model (PMCCA) in this paper. PMCCA can solve the following problem: given a three-dimensional target area A and a desired coverage rate, sufficient number of probability model nodes randomly distributed in the target area, and by scheduling these nodes to achieve expected coverage rate and to ensure to minimize the number of nodes used in the network. The simulation results show that our method can effectively scheduling the nodes of the target area, making the network to achieve the desired coverage rate. The algorithm proposed successfully apply the probability coverage model to coverage control of three-dimensional sensor networks, however in this paper we did not consider the energy consumption of sensor node scheduling and heterogeneous of sensor nodes, which will serve as our next research work.

ACKNOWLEDGMENT

The subject is sponsored by the National Natural Science Foundation of P. R. China (No.60973139, 61003039, 61170065, 61171053), Scientific and Technological Support Project (Industry) of Jiangsu Province (No.BE2010197, BE2010198), Natural Science Key Fund for Colleges and Universities in Jiangsu Province (11KJA520001), the Natural Science Foundation for Higher Education Institutions of Jiangsu Province (10KJB520013, 10KJB520014), Academical Scientific Research Industrialization Promoting Project (JH2010-14), Fund of Jiangsu Provincial Key Laboratory for Computer Information Processing Technology (KJS1022), Postdoctoral Foundation (1101011B), Science and Technology Innovation Fund for Higher Education Institutions of Jiangsu Province (CXZZ11-0409), the Six Kinds of Top Talent of Jiangsu Province (2008118), Doctoral Fund of Ministry of Education of China (20103223120007, 20113223110002), and the Project Funded by the Priority Academic Program Development of Jiangsu Higher Education Institutions (yx002001).

REFERENCES

[1] Meguerdichian S, Koushanfar F, et al. Coverage problems in wireless ad-hoc sensor networks[A]. INFOCOM'01[C]. New York: IEEE Press, 2001. 1380−1387.

[2] Rong-Guei Tsai, Hao-Li Wang. A Coverage-Aware QoS Control in Wireless Sensor Networks[J]. Communications and Mobile Computing (CMC), 2010, 3: 192-196.

[3] CARDEI M, WU J. Energy-efficient coverage problems in wireless adhoc sensor networks[J]. Journal of Computer Communications on Sensor Networks, 2005, 29(4): 413-420.

[4] ZHANG D X, XU M, CHEN Y W. Probabilistic coverage configuration for wireless sensor networks[A]. Wireless Communications, Networking and Mobile Computing, 2006 (WiCOM 2006)[C]. 2006.1-4.

[5] SHEU J P, LIN H F. Probabilistic coverage preserving protocol with energy efficiency in wireless sensor networks[A]. Wireless Communications and Networking Conference, 2007 (WCNC 2007)[C]. 2007.2631-2636.

[6] X. Bai, C. Zhang, D. Xuan and W. Jia, ''Full-Coverage and k-Connectivity (k=14, 6) Three Dimensional Networks,'' in Proc. of IEEE Annual Conf. on Computer Communications (IEEE INFOCOM), 2009, pp.145-154.

[7] S. M. Nazrul Alam and Zygmunt J. Haas, ''Coverage and connectivity in three-dimensional networks,'' in Proc. of the 12th Annual inter. Conf. on Mobile computing and networking, Los Angeles, CA, USA, Sep. 2006, pp. 346-357.

[8] Jun Lu , Suda T. Coverage-aware self-scheduling in sensor networks[A] . Proceedings of IEEE CCW 2003[C] . California : IEEE , 2003. 117-123.

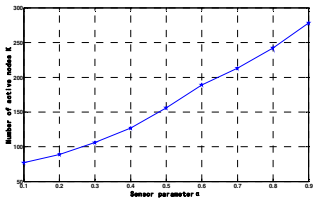

Figure 3. Effect of α on number of active nodes K

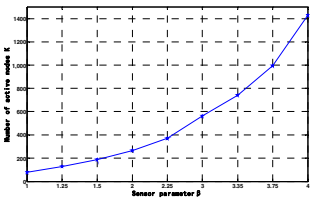

Figure 4. Effect of β on number of active nodes K

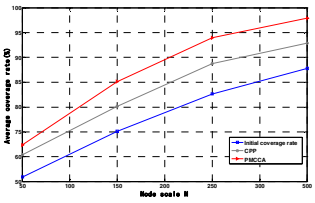

Figure 5(a). Effect of N on the coverage rate

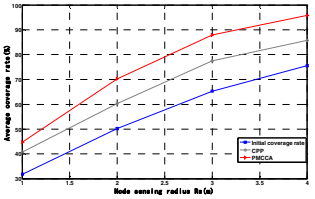

Figure 5(b). Effect of R_s on the coverage rate

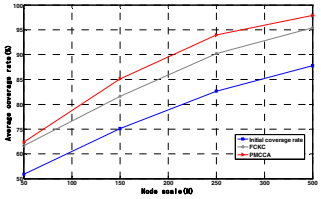

Figure 6(a). Effect of N on the coverage rate

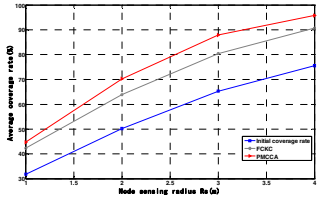

Figure 6(b). Effect of $R_s$on the coverage rate

An Optimized Mobility Management Architecture based on Identifier/Locator Split

Wei Han, Baosheng Wang, Xiaomei Chen, Zhihong Liu
College of Computer
National University of Defense Technology
Changsha, China
hanweistudent@gmail.com

***Abstract*—With the widespread of wireless network, the original TCP/IP has shown some drawbacks in supporting the mobility of network due to the semantic overloading of IP address. Therefore, the identifier/locator split method is put forward to improve the mobility support of network radically by decoupling IP into locator and identifier. In this paper, we propose an optimized mobility management architecture based on identifier/locator split, which introduces transitive routers into the network to avoid the participation of border router during the handover process. Besides, we implement the functions of caching and forwarding on the access router so as to eliminate the packet loss caused by handover. Finally, we evaluate our method and compare it with some typical mobility management models. Result shows that the handover latency is remarkably improved theoretically.**

Keywords-identifier/locator split; mobility management; seamless handover; Internet Architecture;

I. INTRODUCTION

The revolutionary development of the wireless network has made mobile terminals an increasingly popular part of people's daily life, and the demand on better performance of Internet is growing with each passing day. Due to the spite of the terminal's mobility, the IP address represents both network host's location for routing and its endpoint identifier. When the host is moving, its identifier is invariable while the location used for routing is changing, which leads to the semantic overloading of IP address. If we keep IP unchanged, the core route tables will be affected seriously when there are thousands of mobile terminals moving in the network, and if the IP address changes with the location, all communications on the mobile terminal will be suspended due to the early binding of TCP/IP. Mobile IP [1] tries to avoid the effect on the route tables but it suffers from the triangular routing problem. Mobile IPv6 [2] uses the care of address for routing relying on its huge address space but it requires considerable changes on end host and complex management.

IRTF put forward "identifier/locator split" [3-4] in order to tackle the semantic overloading of the IP address which separates IP address into two parts: the identifier is used to identify the host which is globally unique and the locator used for routing which may change during the movement of the node. The introduction of the identifier/locator split is conducive to the stability and convergence of core route tables on the one hand, on the other hand the security of network can be improved greatly due to the uniqueness of identifier.

However, the identifier/locator split also brings about a series of new problems and the most critical one is the mapping between identifier and location [5]. The host uses the identifier to communicate and the identifier needs to be mapped to location which is used for routing. The typical models for mapping are Push and Pull [6]. Pull model caches all the query result locally to minimize the size of storage but it results in the increase of the query latency. Push model copies a complete global database at each border network to decrease the query latency but the maintenance of database is time-consuming. The scale of the mapping database will be extremely large due to the global unique character of identifier which causes the inefficiency of searching. MILSA [8] proposes a hierarchical naming principal which is conducive to the aggregation of the identifier. Besides, there are some other problems need to be resolved such as the authentication of the accessed host, mobility support of the network, and the realization of the identifier/locator split in protocol stack.

Aiming at improving the handover efficiency based on identifier/locator split, we present an optimized mobility management architecture by introducing the transitive router into the subnet's border. When host is crossing subnet, the transitive router instead of the border router will forward the packets to the destined subnet so that the handover latency is decreased. Besides, we implement the functions of caching and forwarding on the access router so as to eliminate the packet loss caused by handover. Finally, we give an evaluation of this architecture and compare it with the traditional schemes. The result shows that the handover latency is remarkably improved theoretically.

The rest of the paper is organized as follows. Section II gives a description of the architecture. Details on mobility and handover management scheme are discussed in Section III. The handover efficiency is analyzed and compared in Section IV. The conclusion follows in Section V.

II. SYSTEM ARCHITECTURE

In this architecture, we introduce a kind of router called TR (Transitive Router) into the network. TR plays the role of buffer between subnets and decouples the traditional cross-subnet handover process into two steps. It is mainly used on the border of subnet and responsible for traffic forwarding between subnets during the handover process. By choosing one subnet to register mobile terminal's information

978-0-7695-4818-0/12 $26.00 © 2012 IEEE
DOI 10.1109/DCABES.2012.38

according to certain principle and express forwarding between subnets, the handover latency during the cross-subnet process is remarkably decreased.

The optimized architecture is shown in Fig. 1. The mapping service adopts a hierarchical architecture and is made up of two levels. BMS (Bottom-level Mapping Server) is responsible for the query from certain zone (we will explain later) and maintains the local mapping database. TMS (Top-level Mapping Server) is responsible for global mapping database. When BMS is updated, certain policy is adopted to synchronize with TMS. As we mainly focus on the mobility management of the optimized architecture, the detail of searching will not be discussed.

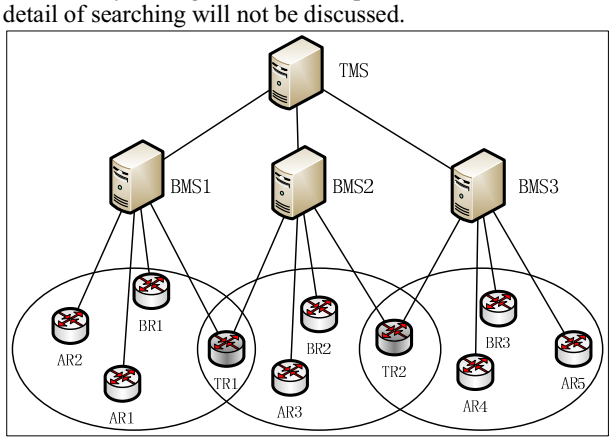

Figure 1. System architecture.

Each circle represents one zone which is both a physically connected network and a logically mapping domain. Each zone has a BMS running as the local mapping server and a BR (Border Router) as a bridge for communication between the inside and the outside. There are many ARs (Access Router) in each zone. AR works as a gateway and has many functions including allocating address for host, querying BMS for address based on the identifier, encapsulation and decapsulation, address rewriting and forwarding packet to another AR. AR needs to cache all the mapping items of the local ARs' addresses which are used for express forwarding.

Any two adjacent zones have an overlay and the router in this area is TR. TR is only deployed in the overlay between adjacent zones so it may belong to several zones. It is equipped with all functions that AR has and in addition they can choose one zone it belongs to register the accessed host's information. TR is deployed on the border of the zone and simultaneously surrounds the zone so that hosts would access TR when crossing zones.

The architecture adopts network based identifier/locator split. Routing is transparent to host and the host uses identifier to communicate. The host's identifier is globally unique and the address is hierarchical which helps the aggregation of routing tables.

III. MOBILITY MANAGEMENT SCHEME

There are mainly two scenarios in the communication process including the static and the dynamic. The static refers to the possible interactions when MN (Mobile Node) comes to a standstill which includes: registration, communication with CN (Communicate Node: node communicating with MN) and unregistration. The dynamic refers to that when MN is moving which includes: the handover between ARs, handover from AR to TR, TR to AR and TR to TR.

A. Static Scenario

When MN is not moving, there are three possible scenarios related to MN that may emerge on the network: MN registers at AR or TR, MN communicates with CN, MN unregisters at AR or TR. In the static scenario, the interactions are similar to that in traditional schemes except the registration on TR.

1) MN Registers: The registration process can be seen from Fig. 2. Once detected the periodical advertisement from AR1, MN will send the register packet to be authenticated. AR1 will allocate address for MN and return a packet in response. After that, AR1 will send packets to BR1 and BMS1 to register MN's information. Receiving the packet from AR1, BMS1 will check local database. If there is no mapping item about MN, the information will be added to the database and sent to TMS at the same time. If there is, the item will be modified locally according to the received information. When BR1 receives the packet from AR1, the item will be cached locally. When a packet with destination to MN is received, BR1 will check the destination identifier, rewrite the destination address and then forward the packet to MN. The scenario that MN registers at TR is different from that at AR in that TR will randomly select one zone among the zones it belongs to after allocating address for MN and then register MN's information in that zone.

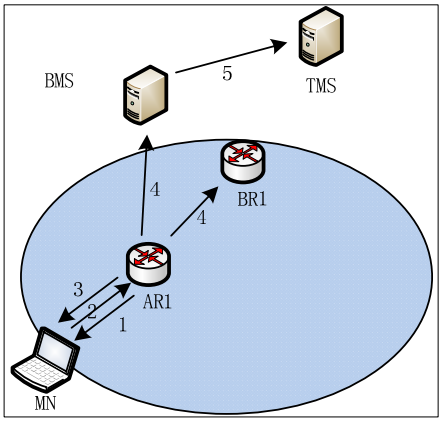

Figure 2. Registration process.

2) Communication Between MN and CN: When there's packet sent to AR1 from MN, AR1 will check the destination identifier. And if there's no corresponding mapping information, AR1 will query BMS1 or TMS. After receiving the packet in response, AR1 will cache the item, add address layer to the packet and then forward it. When there's packet sent from CN to MN, AR1 will check the

destination identifier, remove address layer and then forward it to MN. If MN just left, AR1 will cache the packet for a certain time and then delete the packet when there's no notification message received.

3) MN Unregisters: If MN actively sends an logout message, AR1 will delete all the related information and notify BMS and BR. When MN occasionally loses connection, same action will be taken when timeout.

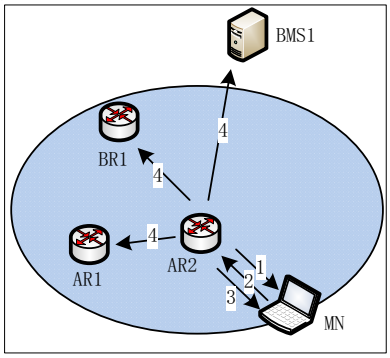

Figure 3. Handover between ARs.

B. Dynamic Scenario

When MN is moving, the handover process can be divided into four classes depending on access router's role: handover from AR to AR, handover from AR to TR, handover from TR to AR and handover from TR to TR.

1) AR to AR: When MN moves in the same zone, it can be seen from Fig. 4 that MN disconnected from AR1 and connects to AR2. The handover process here is the same as that in traditional architecture. During registration process, MN will send the identifier of AR1 it cached to AR2. AR2 looks up AR1's address from local cache and then notify AR1 that MN has connected to AR2. At the same time AR2 will send the new identifier-to-locator mapping item to BR1 and BMS1. BMS1 checks local database and modify MN's address to the latest. Receiving the notification, AR1 will forward all the packets it cached and all the information related to MN's communication to AR2. The whole handover process is completed here.

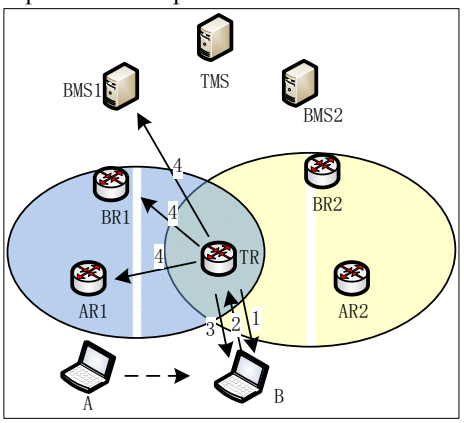

Figure 4. Handover from AR to TR.

2) AR to TR: Fig. 4 shows the procedure that MN moves from A to B. When MN registers to TR, TR will allocate IP address for MN and notify AR1 to forward the packet. After that, TR registers the information at BR1 and BMS1 according to the location of AR1's identifier. Then BR1 and BMS1 will modify corresponding item.This is a preparation step for the network handover. MN moves to register at TR which means that it is possible for MN to cross zone. Note that MN has not crossed zones at this time yet.

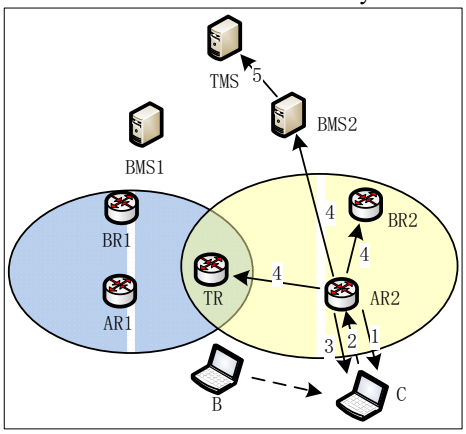

Figure 5. Handover from TR to AR.

3) TR to AR: Fig. 5 shows that MN moves from B to C. After authenticating MN, AR2 notifies TR to forward the packet with the destination MN to AR2 immediately because AR2 caches all the addresses of native ARs and TR is local too. Then AR2 registers MN's information at BR2 and BMS2 and notifies AR of CN to update MN's address. Detecting that it is the first time for MN to register in this zone, BMS2 will update TMS simultaneously. TR keeps forwarding the packet until the time exceeds threshold and then notify BMS1 and BR1 to delete related information. The cross-zone handover process happens in this scenario. We can see that the message flow is nearly the same as that when MN moves inside the zone except the update in TMS and AR of CN. In traditional scheme, BR2 need to query TMS for BR1's address and then notify BR1 to forward the packet with destination MN to BR2. Therefore the handover latency is increased.

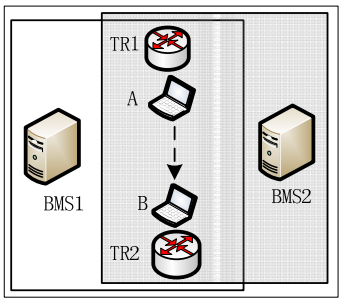

Figure 6. Handover between TRs.

4) TR to TR: Considering the deployment of TR, there may be a scenario that MN moves on the border of zones

which may causes it to disconnect from one TR and then connect to another which is shown in Fig. 6. Here, we adopt the same policy that TR selects the zone according to MN's previously accessed TR's location. The process after that is the same as we mentioned before.

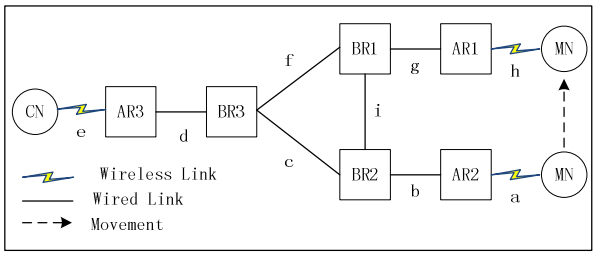

Figure 7. Analysis model for evaluation

IV. EVALUATION AND COMPARISON

In order to evaluate the performance of the optimized architecture, we adopt the model and evaluation method in [9]. Details are not included in this paper. The evaluation model is shown in Fig. 7.

A. Model Parameters and Assumptions

1) Assumptions are made regarding the evaluation model as follow.

a) The data packet arrival interval tp is independently istributed as exponential with parameter 1/λ.

b) The two sequential movement interval tm is independently distributed as exponential with parameter 1/μ.

c) The time cost at each node to process the message is equal.

d) The time cost by transferring data or control packet is proportional to the transmission distance.

e) The time period of the AR advertisement is TAR and the average delay of movement detection, denoted by ω is set to a uniformly distribution random between 0 and TAR.

2) Related parameters and their descriptions are shown in Table I: Here, we only list parmaeters that are related to the analysis of our scheme. There are some other parameters in later part, of which the descriptions can be found in [9].

TABLE I. PARAMETERS AND DESCRIPTIONS

Parameters	Descriptions
λ	Mean value of the data packet's arrival rate
μ	The average speed of mobile node
γ	The mean number of the data packets received by a mobile node during one movement which is equal to λ/μ
ν	Average cost of processing control packets or data packets
τ	Average cost of fetching a mapping result from MS or mapping update in the mapping system
ω	The average delay of movement detection
ρ	The proportionality between average cost of transferring control packet and the transmission distance
φ	The proportionality between average cost of transferring data packet and the transmission distance
θ	The mean cost of allocating a new address for MN

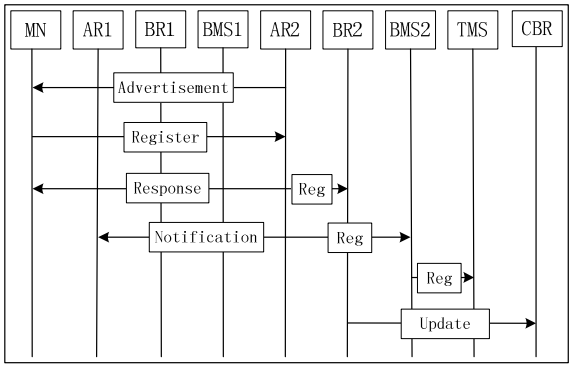

Figure 8. Message flow of handover under optimized architecture

B. Handover Latency

The L3 handover latency is mainly made up of the movement detection latency and location update latency. The movement detection latency is $T_{AR}/2$ and the location update latency is made up of several parts. Fig. 8 shows the message flow during the location update process.

BR and BMS in the same zone can be deployed together so that the update from AR to BR and BMS can be put together which helps to decrease the transmission latency. So BMS is not presented in Fig. 7 which means that BMS is deployed together with BR. It can be inferred that the handover latency based on the optimized architecture is:

$$T_{optmized} = \frac{T_{AR}}{2} + \rho h + \rho g + \rho f + \rho d + 8v \qquad (1)$$

C. Comparison

We compare the optimized architecture with three schemes which include: traditional scheme without optimization, LISP-MIP [10] and ISMS [11].

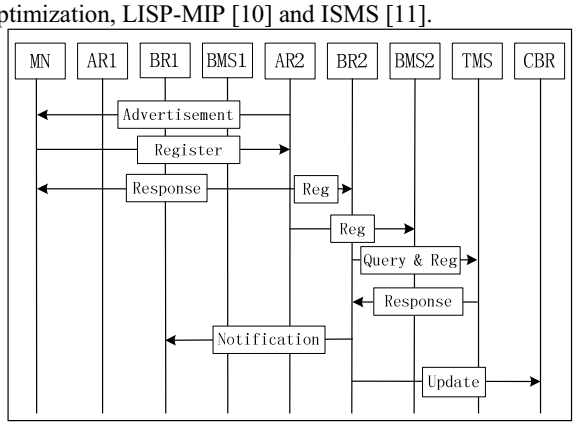

Figure 9. Message flow of handover without optimization

Fig. 9 shows the traditional message flow of the handover process. There exists latency which comes from BR2's query to TMS to search BR1's address. And after that BR2 needs to notify BR1 to forward the traffic flow destined to MN to BR1. During the query process, BR2 also registers

MN's new location which accelerates the handover process. So the handover latency without optimization is:

$$T_{traditional} = \frac{T_{AR}}{2} + \rho h + \rho g + \tau + \rho i + \rho f + 9v \qquad (2)$$

Handover latency of LISP-MIP is:

$$T_{LISP\text{-}MIP} = \frac{T_{AR}}{2} + t_{soli\_delay} + RetransTimer + 70\rho + \tau + \theta + 8v \qquad (3)$$

Handover latency of ISMS is:

$$T_{ISMS} = \frac{\lambda + \rho e + \rho d + \rho c}{2} + \rho h + \rho g + \rho c + 9v \qquad (4)$$

Similar as paper [9], the value of distance cost in the same zone(a = b = d = e = h = g) is 10ms, and distance cost between different zones(c = f = i) is 50ms. The values of ν, τ, TAR, θ is 10ms, 40ms, 50ms, 20ms respectively. And t_{soli_delay} and RetransTimer is 500ms and 1s respectively. Furthermore, the values of ρ and φ is 1 and 2 repectivly.

It can be seen from Fig. 10 that the handover latency of the proposed scheme is the smaller than the traditional one due to the removing of the query and notification latency. With the increase of λ, the performance of ISMS is degrading. LISP-MIP has the lowest handover efficiency.

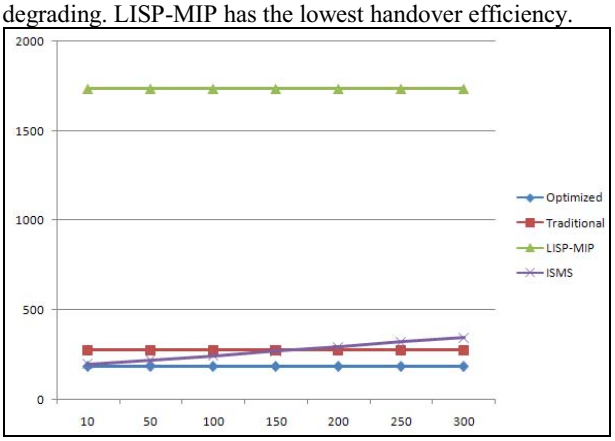

Figure 10. Handover latency comparison

Note that what we compare is the whole process of handover. As we know that the critical part of handover which can affect the experience of user lies in the forwarding time of BR1. If forwarding is early enough, packets from CN can be forwarded to MN directly so that user won't feel the handover latency. The forwarding of the proposed scheme is much earlier than that of the traditional one which has latency of query and notification. In traditional scheme, the forwarding is realized on BR and caching is realized on BR too. During the cross-zone handover process, packet which is already sent to AR from BR1 can be lost before BR2 notifies BR1 to forward. In the optimized scheme, the function is realized on the AR so there is no packet loss.

V. CONCLUSION

In this paper we present an optimized mobility management architecture by deploying TR on the border of zone and the handover latency is remarkably decreased. The introduction of TR splits MN's macro movement into micro movement. The macro movement is removed so MN can move universally at the price of micro movement's handover latency. Forwarding and caching is implemented on AR which helps to improve the QoS of network. Finally, we give an evaluation of the optimized architecture and compare it with several traditional models. The result shows that the proposed scheme can effectively reduce the handover latency.

ACKNOWLEDGMENT

This work is supported by Program for Changjiang Scholars and Innovative Research Team in University (No.IRT1012), "Network technology" Aid program for Science and Technology Innovative Research Team in Higher Educational Institutions of Hunan Province and Hunan Provincial Natural Science Foundation of China(11JJ7003).

REFERENCES

[1] C. Perkins, Ed., "IP Mobility Support for IPv4," RFC 3344, Aug. 2002.

[2] D. Johnson, C. Perkins, and J. Arkko, "Mobility Support in IPv6," RFC 3775, Jun. 2004.

[3] D. Meyer, L. Zhang and K. Fall, "Report from the IAB Workshop on Routing and Addressing," RFC 4984, Sep. 2007.

[4] B. Quoitin, L. Iannone, C. de Launois and O. Bonaventure, "Evaluating the benefits of the identifier/locator separation," in Proceedings of ACM SIGCOMM 2007 Workshops, Kyoto, Japan, August 2007, pp. 35-40.

[5] R. Tui, J. S. Su, and W. Peng, "Survey of Naming and Addressing Architecture Based on Identifier/locator Split," Journal of Computer Research and Development, vol. 46, Nov. 2009, pp. 1777- 1786.

[6] J. Scudder, "Routing/Addressing Problem Solution Space," https://www.arin.net/participate/meetings/reports/ARIN_XX/PDF/w-ednesday/SolutionSpace_Scudder.pdf

[7] D. Meyer, "The locator identity separation protocol," The Internet Protocol Journal, vol. 11, No.1, 2008, pp: 23-36.

[8] J. L. Pan, S . Paul, R. Jain, M. Bowman, "MILSA: A Mobility and Multihoming Supporting Identifier Locator Split Architecture for Next Generation Internet," IEEE GLOBECOM 2008, New Orleans, LA, Dec. 2008, http://www.cse.wustl.edu/~jain/papers/milsa.htm.

[9] J. Hou, Y. P. Liu, Z. H. Gong, "Performance Analysis of a Seamless Mobility Support Scheme in the Identifier/locator Separation Network," CSEEE 2011, CCIS, vol. 158, part 3, 2011, pp. 159–165, doi: 10.1007/978-3-642-22694-6_22.

[10] D. Farinacci, V. Fuller, et al, "Internet Draft: Locator/ID Separation Protocol (LISP)," draft-farinacci-LISP-03, Aug. 13, 2007.

[11] P. Dong, H. K. Zhang, H. B. Luo, et al, "A network-based mobility management scheme for future Internet". Computers and Electrical Engineering, vol 36, Issue 2, Mar. 2010, pp: 291~302.

The Research on SLP Optimization Technique towards DSP

Weiyi Suo, Rongcai Zhao, Yuan Yao, Peng Liu
National Digital Switching System Engineering & Technological R&D Center
Zhengzhou, Henan 450002, China
Email: weiyisuo@126.com

ABSTRACT

According to the application of Superword Level Paralleism （SLP） auto-vectorization compiling system in Digital Signal Processing (DSP), due to the specialized functions of DSP frame, such as the specific addressing model, a wide variety of registers, irregular data branch, the obstacle of dependence relation to vectorization non-aligned data or other reasons, which resulted in the compiler can not support SIMD auto-vectorization with the feature of DSP. In order to solve this problem, the SLP auto-vectorization method was studied towards DSP frame. Based on the specialized functions of DSP frame, the instruction analysis and optimization algorithm in SLP auto-vectorization were improved, so as to transform more high-efficiency source program. The experimental results show that the optimization method of this paper has a tremendous role on improving DSP performances and reducing power consumption.

Keywords: SIMD, DSP, Auto-vectorization, Redundancy optimization, Instruction analysis

I. INTRODUCTION

With the rapid development of multimedia industry, the digital signal, the graph manipulation and other multimedia applications have become the most important work load of general microprocessor. However, these multimedia applications mostly have the features, such as small data width, high data concurrency and neat calculation. In recent years, in order to preferably support multimedia, digital signal processing (DSP) and compute-intensive applications, many communication processors adopt the special instructions to improve the processing ability for the applications, such as, the SSE of Intel, the 3DNOW! of AMD, the AltiVec of PowerPC and other expanding instruction sets[1], and the TI C64x, StarCore, TigerSharc and other instructions[2][3][4] that are adopted by the digital signal processor (DSP).

In order to adapt to the needs of media processing, importing of SIMD instruction is a common feature in the hardware design of modern DSP. This is a big challenge for the compiler, it will directly influence on the performances of the system. Therefore, the auto-vectorization problem of SIMD instruction needs to be solved. But for the current research, the compiler is not adequate for supporting SIMD auto-vectorization with the feature of DSP. In this paper, the development platform is the processor that can be configured and expanded by Xtensa, according to the 160 bit high-performance VLIW DSP with the Open64 compiler, its auto-vectorization's design and implementation, performance and power consumption optimization were studied deeply. The Superword Level Parallelism（SLP） optimization strategy was put forward towards DSP, so it can preferably match the DSP special functions and play the best effect.

A. The architecture of Xtensa

The research and development of Xtensa configurable processor began in 1999, but it yet had provided the Diamond series of standard processor core until 2006, whose main field was from low-power dissipation MCU to CPU, and from low-power dissipation voice frequency DSP to high-performance general DSP.

Xtensa is the 32 bit fixed-point DSP microprocessor chip, which adopts the advanced eight outflow long instruction word structure, there are 80 core instructions with powerful interface function, 250MHz basic frequency and 2000MIPS fixed point operation performance. Application target is wireless base station, ADSL, image and multimedia information processing and other high-performance digital signal processing.

B. The introduction of auto-vectorization method

This paper adopted the Superword Level Parallelism (SLP) algorithm, which was put forward by samuel Larsen[5] et al. It can carry the vectorization for programs in scientific computation, the proposition of this algorithm is inspired by the idea of long instruction word (VLIW). Although the superword parallel vectorization method appeared late, its ability is strong, rather than the traditional vectorization, the SLP algorithm can not only excavate the parallelism of statement in basic block, but also transform the parallelism of loop and iterative statement to the parallelism of statement in basic block through loop unrolling. The parallelism of SLP algorithm development can reach the instruction level, but the performance improvement of the superword parallel vectorization method depends on the vector instructions selection strategy, and the operation of instruction level of statement in basic block increases the complexity of the instructions selection strategy.

There are 4 statements in a basic block, due to the superword parallelism exists between statements, the SIMD instruction is combined and formed, as shown in Figure 1.

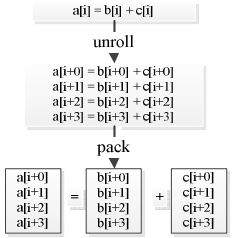

Figure 1. SLP vectorization method

II. THE RELATED WORK

In recent years, according to the power consumption problems of embedded processor (such as DSP), a series of optimization methods were put forward in order to

978-0-7695-4818-0/12 $26.00 © 2012 IEEE
DOI 10.1109/DCABES.2012.22

reduce the execution time of compiling programs and improve the efficiency. The special functions of DSP include a wide variety of registers, irregular data branch, separation program and data internal storage, generation address unit, special addressing model, such as cycle and bit flipping addressing, and instruction level parallelism[13], vector instructions combination[10]. Mostly DSP have the complex instruction set computing of lower reaction time, such as Data reconstruction instructions[11][12], Allow fixed-point algorithm, Saturation arithmetic and Piece together algorithm.

The literatures[9] described the problems that the SLP vectorization method in iteration met when it dealt with some cycles, such as protocol. Meanwhile, they put forward new ideas on how combined with the advantages in iteration and between iteration, and discussed the redundancy deleting and other conventional optimizations. Combining with the SLP algorithm, a series of optimization methods were put forward in this paper, it could be carried more efficient vectorization for the programs.

III. THE SPECIAL INSTRUCTION ANALYSIS OF DSP

A. Address update instruction and instructions combination

There are special addressing ways in DSP, such as Circular addressing and Bit-Reversed Addressing, it can carry out signal and graphics processing with high efficiency. The two addressing ways are illustrated as follows:

(1) Circular addressing: It executes for the model with N and accesses in the memory region N. The pointer increases linearly in the limits of the two buffers. As shown in Figure 2, the beginning address of the circulation buffer with the length of 4 words is 0x0F04 (The positioning of buffer is 0x0F04, 0x0F08, 0x0F0C and 0x0F10).

Figure 2. The circular buffer with the length of 4 words

(2) Bit-Reversed Addressing: It mainly makes use of FFT algorithm, the feature of this addressing way is inverting the address that has been operated. It is supposed that there is a 5 bit address, after the Bit-Reversed Addressing, bit-0 and bit-4 exchanged, at the same time, bit-1 and bit-3 exchanged, yet bit-2 was invariant. Circular addressing and Bit-Reversed Addressing need to assign the beginning position and the buffer length of instructions. It needs to calculate the next address in the register when it saves data to register.

Instruction combination can be called the original language recognition, after generating the vector code, it identifies the original language operation of vector that can merge according to its operation type and DU/UD relationship. The main idea of this algorithm is that a vector first instruction S1 that it meets every time, the instruction S2 that can be merged is sought according to DU, when the 3 conditions are satisfied, the two statements will be merged to form new statement, and the old definition using relationship and statements before merging will be deleted.

1) The operation of S2 can merge with S1.
2) S2 and S1 are in a same basic block.
3) S2 is the only statement with using the results of S1.

B. Supporting the fixed-point algorithm

The main reason of supporting the fixed-point algorithm is to ensure the number precision, and the cheap DSP cost is considered. Fixed-point plural was added in data type, according to adding compiling indication before source program, the fixed-point plural was identified, the imaginary part is in front of the fixed-point, the real part is behind the fixed-point. As follows, FCPX represents the plural type, the numbers in brackets respectively are variable name, variable imaginary part, variable real part that will be declared. As Example 1 shows,

Example 1：#pragma FCPX(a, 12, 4), FCPX(b, 12, 4), FCPX(k, 12, 4)

```
unsigned int i;
unsigned int n;
for (i=0; i<n; i++){
    b[i] = k * a[i];}
```

At the same time, under the precondition of without using floating point arithmetic, it carried out the following strategies to ensure the accuracy of the numbers:

(1) Registers expansion

In order to prevent the extra bit overflow in fixed-point complex operation, the extension techniques of registers were added in the DSP processors, the original 128 bit of 8x16 was extended to the 160 bit of 8x20, actually the original 16 bit could store one number was extended to 20 bit. This can avoid the overflow by extra bit.

The specific supporting for dense multiply-add operation in the DSP processors, when the fixed-point plural multiplication was carried, the multiplication instructions of two length simultaneously were supported: the 160 bit of MUL_8x20, the 320 bit of MUL_8x40. The former does not need to keep precision, the latter is called the accumulator register, it is generally suitable for dealing with multiple product and reduced operation, the accumulator register is wider than the other registers, it needs to keep the precision of intermediate results.

(2) Saturated operation, shift and restructuring instruction

The DSP adds the saturation arithmetic, sum shift and other restructuring instructions on instruction set and hardware. As mentioned in the above, the accumulator register need to save 8X40 to the register of 8X20 by the saturation arithmetic. The method is that the vr register is assigned for the designated right shift digits firstly; Then every 40 bit element in 320 bit register of 8x40 obtained new 20 bit element through the right shift vr register; At last, the saturation arithmetic was carried out, and the result was saved in destination register.

Because of the performance of non-aligned memory is relatively poor, the current many researches all make

an attempt to replace the memory instruction of non-aligned vectorization by adding some shift restructuring instructions on aligned memory. This paper puts forward a vector restructuring method of system to cross the non-aligned array index[6][7][8]. The vectorization can automatically generate data reconstruction instructions according to the data in register become aligned. Such as the packaging for load: L1 = a[4*i+1], L2 = a[4*i+2] …, L8 = a[4*i+4], they can generate the corresponding aligned vector code v1=vload (&(a[4*i])) and v2=vload (&(a[4*i+4])), but the corresponding elements of register v1 are a[4*i], a[4*i+1], a[4*i+2] and a[4*i+3], the corresponding elements of register v2 are a[4*i+4], a[4*i+5], a[4*i+6] and a[4*i+7], the specific restructuring way is shown as Figure 3.

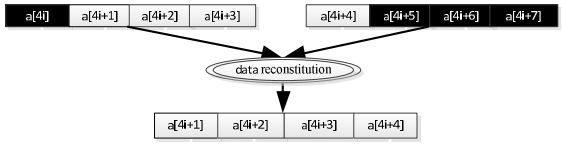

Figure 3. The non-aligned data reconstitution

IV. THE OPTIMIZATION STRATEGY OF AUTO-VECTORIZATION

A. The deleting of redundancy load/store statement

Due to the SLP algorithm is generated on the basis of the vector excavation of basic block and the vectorization code, under the frame of DSP, the redundant vector assignment will be created for the particularity of instructions, nested loop or crossing basic block vectorization. Only the load/store in same basic block will be analyzed, the read-write of the same location data will be found and optimized. The algorithm flow chart is shown as Figure 4, the algorithm steps as follows.

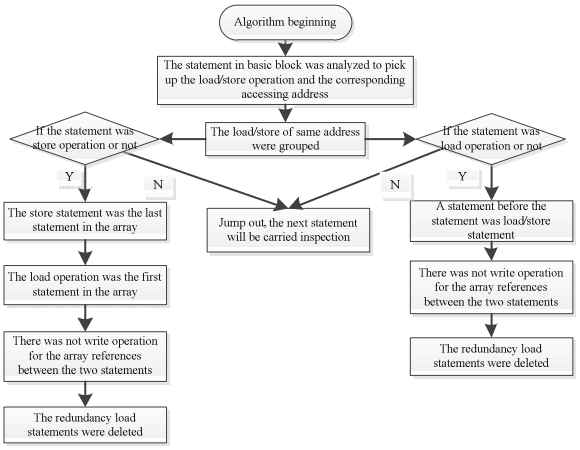

Figure 4. The algorithm flow chart of deleting redundancy load/store statement

Step 1: The statement in basic block is analyzed to pick up the load/store operation and take out the the corresponding accessing address.

Step 2: The load/store of same operation are grouped.

Step 3: For the statement in same group, if the statement is load operation.

(1) The former statement is load/store operation.

(2) There is not write operation for the array references between the two statements.

(3) The redundancy load statements are deleted.

Step 4: For the statement in same group, if the statement is store operation.

(1) The store statement is the last statement in the array.

(2) The load operation is the first statement in the array.

(3) There is not write operation for the array references between the two statements.

(4) The redundancy load statements are deleted.

B. The exterior submission of circulation invariant code

In the process of taking vectorization for loop, loop Invariant is generated by the intermediate representation in the process of transformation, yet the dead code or redundancy expression all are optimized off in the medium of compiler, however, the code generation stage of the back-end does not take the optimization of the compiler medium. And it only exists the external extraction optimization of variable in Open64 for scalar statements, thus it needs to add the loop invariant external extraction for vector statements in compiler back-end in order to improve the execution efficiency of vectorization code.

If each execution all invokes some constants assemblies into vector in loop, then it gets the vectorization code. It assumes V = vload（1, 2, 1, 2）, it can cause biggish performance loss, in fact, the statement used the ones are all constant, which is unrelated with the loop. Therefore, it can be picked outside the loop, then the execution times of statement are reduced and the system efficiency can be improved. How to identify circulation invariant is the next work, the algorithm flow chart is shown as Figure 5, the algorithm steps as follows:

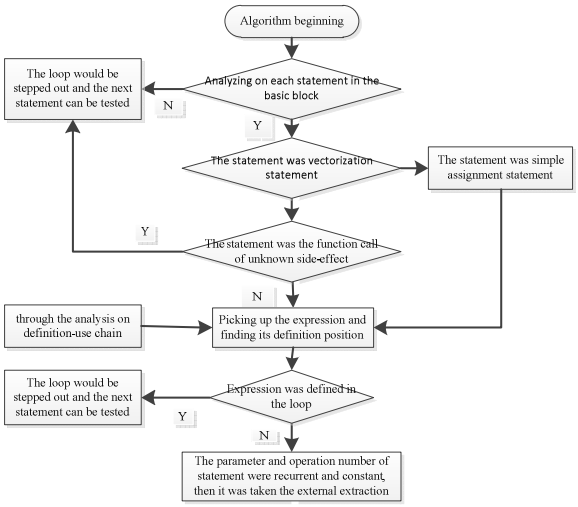

Figure 5. The algorithm flow chart of circulation invariant code's exterior submission

Step 1: Whether the statement is vectorization statement or not.

Step 2: Because of the object of SLP vectorization is basic block, there is no complex function calls in it, then to judge the statement is not the function call of unknown side-effect. If the statement is simple assignment statement or function call, the next step will be carried.

Step 3: The expression of each vectorization statement is analyzed through definition-use relationship,

then whether the definition of expression is in current loop or not will be judged.

Step 4: If the definition is out the loop, it will be taken the external extraction.

The stipulations vectorization program in Example 2 is carried the external extraction of loop invariant, it is shown as Figure 6.

Example 2：for(i=1 ; i< n ; i++){

sum += a[i]；}

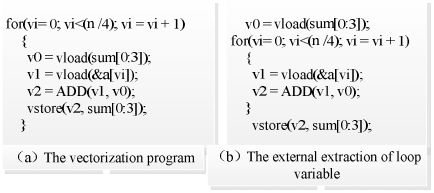

Figure 6. The demonstration of circulation invariant's exterior submission

The above vectorization program was tested, it is found that there is a big gap between the vectorization program diagram 6(b) and 6(c), the speed-up ratio of vectorization program 6(b) and 6(c) is respectively 0.93 and 2.97. Obviously, the reason why the the external extraction of loop invariant has higher speed-up ratio is the loop interior has load operation. It can take repetitive operation in the process of vectorization program carrying calculation, so the unnecessary spending was created, and the performance was effected.

C. The optimization of non-aligned memory access

If the array references alignment information is confirmed in some calculations, the loop multi-versioning optimization is used. When the situation with symbol appears in the unknown array first address of this reference point, the unknown array certain one-dimensional expansion or the linear subscript of certain one-dimensional expansion, it will use loop multi-versioning to confirm the alignment information, which is a improvement for vectorization performance through the method of loop transformation, the algorithm steps as Figure 7.

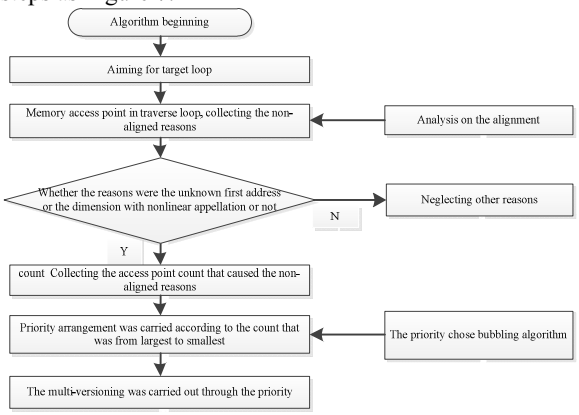

Figure 7. The optimization algorithm of circulation versions

The main idea of loop multi-versioning is adding a branch statement before vectorization to distinguish which treatment will be adopted in a same situation, the array reference aligned treatment or the array reference non-aligned treatment, as Example 3 shown. The results after loop multi-versioning transformation is shown as Example 4, S1 is the aligned array loading instructions after vectorization, S2 is the non-aligned array loading instructions after vectorization. But this is only the judgment between alignment and non-alignment, if there are m array references in loop, each array reference needs n alignment types, then it needs to carry n^m judgments. More branch statements can create performance dropping, therefore multi-versioning generally is used in the situation of less number of array references in loop.

Example 3：for(i=0 ; i< n ; i++)

a[i] = b[i] + c[i]；

Example 4：for(i=0 ; i< n ; i++){

if（a%32 == 0）

S1: a[i] = b[i] + c[i]；

else

S2: a[i] = b[i] + c[i]；}

V. EXPERIMENT RESULTS

In this paper, the DSP auto-vectorization compiling system was realized on the basis of the frame of open source compiler Open64 [14], the compile environment is Linux Operating System, the version is Redhat Enterprise 5. The CPU basic frequency of experimental platform is 2.0GHz, internal storage is 2GB, L1 data cache is 32KB, L2 cache is 256KB, Basic page is 8KB, the width of vector register is 160 bit, it can processing 4 fixed point plural type data, 8 short plastic data and 4 plastic data in the meantime.

As Figure 8 shows, the x-coordinate respectively represents a: Vectorization speed-up ratio, b: Address update instruction and instruction combination, c: The deleting of redundancy load statements, d: The external extraction of loop invariant, e: The optimization of non-aligned accessing memory.

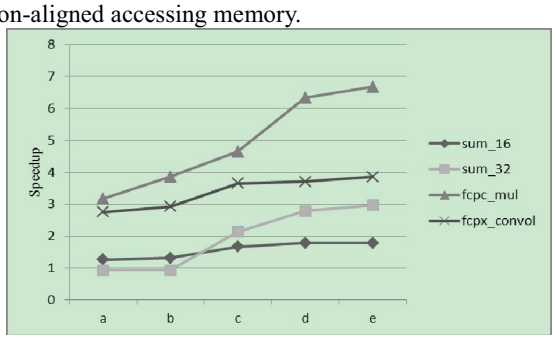

Figure 8. The speed-up ratio ascension of auto-vectorization optimization strategy

The speed-up ratios of each optimization stage were obtained by test cases, it can be seen from the experimental results:

(1) The deleting of redundancy load statements can get a excellent performance improvement for plastic statute adding.

(2) The external extraction of loop invariant can get a excellent optimization effectiveness for mostly ones. If it is used in concert with public subexpression optimization, it can take external extraction of subexpression outside

loop, so the execution times of statement can be reduced and the system efficiency can be improved effectively.

(3) The optimization of non-aligned accessing memory that the optimization algorithm finally carried can not improve the optimization efficiency effectively.

(4) The optimization results of vectorization aiming for nested loop are not obvious, its main reason is that there are dependence ring or statute operation in inner loop.

As shown in Table 1, it briefly described test cases that used in experiment, these cases were all obtained through the improvement of the examples of gcc-vect test concentration. Two of them involves in short plastic and plastic statute adding: one is A: sum_16, the other is B: sum_32; The two common using plural type multiplication are C: fcpc_mul and D: fcpx_pow; The one reflects the loop unrolling's plural type multiplication E: fcpx_unroll; The other is the common using plural type's convolution computation F: fcpx_convol; These programs has wide representative including some characteristics of vectorization, such as various computing ways, various data types and statutes, and the special processing type according to plural type.

The table respectively listed the test cases that passed serial programs, the vectorization programs before no optimization and the test results after optimization, the test results are the cycle count running on corresponding programs. With the reduction of cycle after optimization, it is illustrated that the above optimization measures are apparent for vectorization effect. Especially the plastic statute adding sum_32 has promoted to 219% than the previous vectorization performance.

TABLE 1.The test set

Test case	Serial program	Vectorization to program	After optimized	Optimized to enhance	Vectorization speedup	After optimized speedup
A	464	368	261	40%	1.26	1.78
B	2246	2410	755	219%	0.93	2.97
C	2870	772	430	80%	3.71	6.67
D	5653	2640	1676	58%	2.14	3.37
E	7196	2581	1958	32%	2.79	3.68
F	7196	2603	1867	39%	2.76	3.85

The test cases of these programs were carried testing according to the vectorization program before no optimization and the target system after optimization, then the speed-up ratio of the vectorization results with respect to source program was obtained under two situations, the test results is shown as Figure 9.

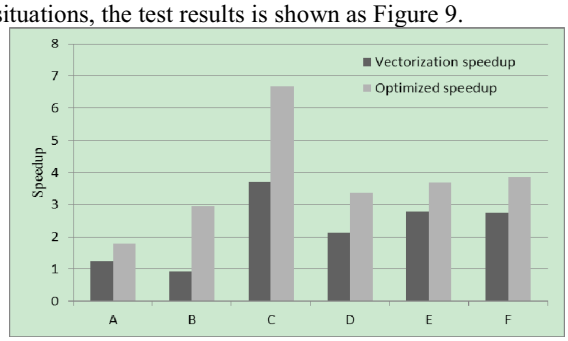

Figure 9. The speed-up ratio before and after optimization

VI. CONCLUSION

In this paper, according to the auto-vectorization performance of DSP frame, on the basis of DSP's special function and general optimization algorithm, some aspects that effected the vectorization performance were obtained: The replacement of address update instructions, The hardware cycle of zero cost, supporting fixed-point algorithm, the deletion of redundancy statement, the optimization of public subexpression, the instruction combination, the external extraction of loop invariant, the optimization of non-aligned accessing memory and the improvement for SLP algorithm. At last, the vectorization method after optimization was tested on the basis of test set, the experimental results show that the combination between this optimization method and the SLP algorithm can promote the execution efficiency of vectorization programs.

REFERENCES

[1] Franchetti F，Kral S，Lorenz J，et al．Efficiem utilization of SIMD extensions．Proceedings of the IEEE，2005，93(2)：409425．

[2] TMS320C6000 CPU and Instruction Set Reference Guide (Rev.F)．Texas Instruments Inc．，2000．

[3] SC140 DSP Core Reference Manual．Freescale Semiconductor，Inc．2004．

[4] Fridman J，Greenfield Z．The TigerSHARC DSP Architecture．IEEE Micro，2000,20(1)：66-76．

[5] Samuel Larson and Saman Amarasinghe，“Exploiting superword level parallelism with multimedia instruction sets”，PLDL 35(5)：145-156.2000.

[6] Alexandre E. Eichenberger, Peng Wu, Kevin O'Brien. Vectorization for SIMD architectures with alignment constrains. PLDI 2004.

[7] D. Nuzman, I. Rosen, A. Zaks. Auto-Vectorization of Interleaved Data for SIMD. In PLDI’06 , June 2006, pages 132-143.

[8] Dan E.Tamir ,Natan T.Shaked ,Wilhelmus J.Geerts ,and Shlomi Dolev. Combinatorial Optimization Using Electro-Optical Vector by Matrix Multiplication Architecture. OSC 2009，LNCS 5882，pp. 130-143. 2009.

[9] Ira Rosen, Dorit Nuzman, Ayal Zaks. Loop-Aware SLP in GCC[C]. In Proceedings of the GCC Developers’Summit. July, 2007, Ottawa, Canada, pages 131-142.

[10] Guillermo Paya-Vaya，Javier Martfn-Langerwerf，Florian Giesemann，et al. Instruction Merging to Increase Parallelism in VLIW Architectures. 5-7 Oct. 2009; 143 – 146. System-on-Chip, 2009. SOC 2009.

[11] Gang Ren，Peng Wu，David Padua. Optimizing Data Permutations for SIMD Devices. to appear in Proc.of the ACM SIGPLAN Conference on Programming Language Design and Implementation (PLDI)，June 2006.

[12] Libo Huang，Li Shen，Zhiying Wang. Permutation optimization for SIMD devices. May 30 2010-June 2 2010. 3849 - 3852．Circuits and Systems (ISCAS)，Proceedings of 2010 IEEE.

[13] Subrato K. De，Anshuman Dasgupta，Sundeep Kushwaha，et al. Development of an Efficient DSP Compiler Based on Open64. Open64 Workshop at CGO 2008.

[14] Open64，http://open64.sourceforge.net.

Improved IDCA Algorithm for TD-SCDMA Intensive Traffic Flow Scenes

Xu-Qing Chai
Network Center
Henan Normal University
Xinxiang, Henan, China
Email: cxq@htu.cn

Yu-cheng Guo
Dept of Computer Science
Wuhan University of Technology
Wuhan, Hubei, China
Email: 15972111920@139.com

【*Abstract*】 **With the continuous development of TD-SCDMA(Time Division - Synchronous Code Division Multiple Access) network, has begun a high-traffic areas; intensive traffic flow scenes, network configuration, with high frequency multiplexing, interference problems are more prominent; there will be residential uplink interference serious, KPI(Key Performance Indicator)have worsened and volatile, poor perceived by the user; how to reduce interference and optimize the KPI targets to enhance the user perception is particularly important, currently, in the interference suppression algorithms, IDCA(Intelligence Dynamic Channel Allocation) algorithm is a more sophisticated algorithms, but in the intensive traffic flow scenes, the IDCA algorithm for interference suppression aspects of the effect is less pronounced. This paper presents a sorting method, before the IDCA algorithm for carrier sorting, based on frequency multiplexing degrees and comprehensive consideration of user level. The method, optimizes the carrier sorting method of IDCA algorithm, avoids the occurrence of the same frequency at the same time gap as much as possible, and reduces interference within the system. Therefore, it is suitable for the intensive traffic flow scenes..**

【*Keywords*】 **TDSCDMA; Intensive Traffic Flow Scenes; Strong Interference; IDCA**

I. HIGH TRAFFIC SCENE UNDER THE STRONG INTERFERENCE CHARACTERISTICS

A. Network characteristics

The communities under intensive traffic flow scenes are often distributed in a commercial core area, office buildings, the campus users such as the relatively concentrated area, the area in the networking and network configuration has the following characteristics:

1) The large network configuration in a cell

Single cell carrier configuration at least at 9 carrier frequencies above, up to 12carrier; this configuration will cause a frequency reuse degree high, area exists between the same frequency carrier frequency;

2) The low spacing deviation in a cell

In order to improve the capacity of the network and absorb more users as far as possible in intensive traffic flow scenes, that user mobility and business sustainability, and on-site environmental reasons, these ways will cause the presence of multiple community covering an area, or switching with no apparent, more inter-cell overlapping coverage area, etc..

B. Users and business characteristics

Generally, through certain preferential benefit by market sector to absorb a large number of network users, and many users in more concentrated area or unit, so that the formation of these intensive traffic flow scenes, relative to other less TD users regions, intensive traffic flow scenes and users in the business of obvious characteristics as follows:

1) Focus on users

In the region more users to focus on one or a few within the community, and there is evidence of tidal effects, in a certain period of time the user focus, the traffic is high, but after class or work, users dispersed, sharp decline in the volume of business;

2) Focus on business

In a certain period of time users may have centralized business, such as a class or rest time, sudden produce business, led to the small interference dramatically decreasing, call quality decline;

3) Business types

In the business within the hot zone, type in the business also will be different, for example, in school, in the self-study time will focus on generating data service, data service flow is larger, but in the business center, voice service quantity is larger, the different business types on the network effect is also different.

C. Network performance characteristics

In a intensive traffic flow scenes, because of reasons from the user and networking, the area of interference is enhanced, KPI indicators of deterioration, on the user side is reflected in the decline in the quality of user calls, Internet access latency, appeared off and dropped, the users' perception of variation.

1) KPI index characteristics

In intensive traffic flow scenes, the uplink interference enhancement leads to cell inscribed pass rate to drop, drop rate and dropping rate increased, handover success rate decreased, the user call quality variation, the Internet has a lower rate, long delay problem.

2) Network utilization

The scene, more users, big business, will lead to community network average occupancy rate is higher, and the highest area can reach about 70%, which may also lead to deterioration of the KPI index [4].

978-0-7695-4818-0/12 $26.00 © 2012 IEEE
DOI 10.1109/DCABES.2012.114

II. ANALYSIS OF INTERFERENCE SOURCE UNDER INTENSIVE TRAFFIC FLOW SCENES

Currently, the mode of TD-SCDMA system is multi carrier frequency network, i.e. within a cell can configure multiple carrier, different area can be configured in the same frequency point. If the adjacent residential users in the same frequency point to accept service, it will cause inter-cell co-channel interference. Same frequency interference and can be divided into two different situations, have different effects on the network quality.

A. Main carrier frequency multiplexing interference

The main carrier co-frequency reuse scene occurs mainly in the district more outdoor macro station, a plurality of cells may be accomplished on a regional coverage, while outdoor frequency limited, will result in the area of the main carrier frequency point can not be completely separated, forming the same frequency interference. The main carrier with frequency multiplexing interference causes the user of difficulties, paging failure, handover failure problems such as to drop words.

B. Business channel co-frequency reuses interference

In the case, a number of areas are large configurations, so it must be co-frequency reuse in the inevitable business channel, and certain frequency reuse degree to be high, resulting in a traffic channel of a plurality of users to business in the course of the same frequency at the same time gap situation more.

Business channel co-frequency reuse will lead to poor quality of user speech, internet rate low, poor user experience, problems such as to drop words. The frequency planning of identified cases, along with the network load increases, the adjacent interval user with the same frequency as the collision probability will increase, as the entire network interference uplift and network KPI parameters deteriorated.

III. INTERFERENCE PROCESSING STRATEGY IN THE INTENSIVE TRAFFIC FLOW SCENES

The same frequency interference in the system, there are many ways, such as N frequency technology, frequency optimization, optimization and other means, but for intensive traffic flow scenes of conventional optimization methods may fail to produce efficient results, we need a concrete analysis of concrete problems, according to the strong interference regional topographic features, architectural features, community coverage characteristics, business behavior characteristic analysis, engineering optimization is to eliminate the interference of basic measures, the most effective measures, can fundamentally eliminate the interference, but due to certain scenes to limit, engineering optimization. The IDCA algorithm is actually a kind of interference from strategy; interference in the existing circumstances, the user access resource allocation, users will be divided into smaller interference carrier frequency time slots, to avoid interference with larger carrier frequency or time slot.

A. Engineering optimization

In order to reduce the same frequency interference in the frequency reuse, engineering optimization is a very important means to solve; Using engineering methods are frequency optimization and optimal coverage, from the source control of interference.

1) Frequency optimization

According to frequency reuse bring the interference problem, can be divided into the following kinds of situation and take corresponding measures. Local existence more serious interference in the same frequency, the frequency reuse, because TD available frequency point less, multiple carrier scene area under the same frequency problems inevitably exist between. As the main carrier of TS0（Time Slot 0）has been transmitting power timeslot, must confirm the verification of adjacent cell main carrier is the same frequency phenomenon even direct calling, this typically leads to local area network performance deterioration. At this point you can use manual verification peripheral frequency adjustments, or the use of frequency planning tool in the local area for frequency planning adjustment.[1]Special circumstances can borrow indoor frequency point to lower the local co-channel interference problems.

2) Coverage optimization

By covering the optimization, the reasonable control of cell coverage and direction, eliminate the area covered, is the solution of frequency reuse the same frequency interference of the important and effective means. Finding the coverage problem is an important means for the discovery of covering problem. [2]

Firstly, through a variety of road measurement tools such as mobile phone testing, frequency sweep meter etc to find all kinds of covering the root cause of the problem, (the area covered, the orientation is not reasonable, dorsal valve etc.). Coverage problems lead to the disturbance of solving methods are various, the ideal solutions is to adjust the height of the antenna, the antenna azimuth and inclination angle, many problems can be solved through the adjustment of the antenna; individual cases (such as the adjustment of the antenna can be adjusted by the property restrictions) cell PCCPCH（Primary Common Control Physical Channel）power to try (not generally recommended the way); some coverage by the means of problem cannot be solved completely, need to take engineering means such as a base station relocation were completely resolved.

B. IDCA algorithm

1) IDCA algorithm background

The traditional CDCA (Control Dynamic Channel Allocation) algorithms only consider the plot information, without considering the interference of neighborhood on the community impact, especially the down side [7]. If the adjacent area of the same frequency downlink transmit

power is higher, in two cells of the user, the downlink interference will increase apparently, necessary in considering the small power, increase the adjacent district power considerations. In general, a district may have multiple adjacent areas, from the geographical distribution; Different area adjacent to the area of influence is different. The first lap of the adjacent area affected, second ring adjacent regions relative impact on small lot. In the algorithm design process, only considering the impact is the biggest those strong and adjacent areas [5].

Currently, in addition to the OM (Operation and Maintenance) configuration, the upstream slot priority adjustment method, only Time slot priority ordering strategy based on the number of remaining RU (Resource Unit). There is not direct relationship with between how much of Remaining RU and the size of the uplink interference; and also no direct relationship with the user's QOS (Quality of Service) and Network performance. Therefore, it is needed to increase the timeslot Sort method based Interference [3].

So from the perspective of interference suppression, upstream increase / carrier adjustment algorithm based on the upstream of the slot of the ISCP(Interference Signal Code Power) can prevent users from access to upstream the ISCP large slot / carrier, enables users to access interfere with the smaller slot / carrier reduce the interference between users.

2) The description of iDCA algorithm functions

The basic principle of iDCA is integrating the loads / interference in this area and adjacent area, assessing the comprehensive interference of the different time slot area in the area, through information from lots of community, the, each district has formed its own optimal resource [6]; when the user has the resource changes, preferentially in the smaller interference frequency point and time slot on channel resource allocation, avoid the adjacent cell interference, or reduce the adjacent area interference probability. When the interference cannot differentiate resource priority, use the remaining RU allocation of resources. When the remaining RU cannot distinguish between resources, such as load, using the OM configuration mode, play advantage of frequency optimization.

IV. BASED ON THE FREQUENCY REUSE OF CARRIER PRE-SORT

In real networks, we found that it is not that the adjacent cell of a carrier / time slot has users, which will interfere with the district of the same carrier / time slot. At this point, during the carrier / slot sort, the IDCA algorithm will plot the carrier / time slot at the higher priority, at this point, if there has the weaker user access in the district, which will make the carrier / slot uplink interference enhanced, and affects the district's powerful neighbor of the same carrier / time slot at the same time.

A. Based on the frequency reuse of carrier pre-sort

Before based on the uplink ISCP sort in the IDCA, the cell carrier with its powerful neighbor the carrier frequency reuse of calculation is set to the highest priority of the lowest carrier frequency reuse, the carrier subject to the possibility of interference with adjacent areas the lowest. IDCA algorithm for sorting in the carrier, the first frequency reuse expense lowest carrier set aside to calculate the uplink ISCP of the other carrier, the carrier uplink the ISCP lower than would be the business impact threshold, then the user access to the carrier, so that will reduce the interference of the district adjacent areas

Table 1, Table 2 shows a district there are three powerful neighbor areas, respectively, have three frequencies. Frequency 10104 reuse lowest, highest priority.in pre-sorting, 10104 frequency points will be set aside. in IDCA algorithm, First calculate the frequency 10112, 10096 upstream ISCP value.

TABLE I. ADJACENT AREAS AND FREQUENCY LIST

CELLID	Primary Frequency	Second Frequency	Third Frequency
HomeCellID	10104	10112	10096
NeighborID1	10096	10088	10120
NeighborID2	10112	10120	10080
NeighborID3	10088	10080	10112

TABLE II. FREQUENCY REUSE AND PRIORITY LIST

Frequency	Frequency Reuse	Priority
10104	1	1
10096	2	2
10112	3	3

B. User' access selection of the carrier / slot

There will be Produce the same frequency at the same time gap interfere with the strongest scenes in system, When a user at the edge of the cell to initiate business in the user level is weak, the access stage due to open loop power control, in order to ensure the success rate of the access terminal uplink transmit power will be higher, resulting in the district a carrier frequency / time slot uplink the ISCP higher, will cause the adjacent areas to the same carrier / timeslot uplink ISCP uplift, cause interference to adjacent areas.

Initial access, first, through the RNC (Radio Network Controller)to judge when the user access level, if the good reception level, the IDCA algorithm in the same cell, the carrier of other lower priority calculation uplink ISCP value selected to interfere with the lower carrier access, reserved for the lowest carrier to carrier complex in degrees; If the user level is low, the user access to complex degrees minimum carrier / time slot, so that even if the strong interference of carrier / time slot caused by user, this district will be the impact on adjacent areas to a minimum [8].

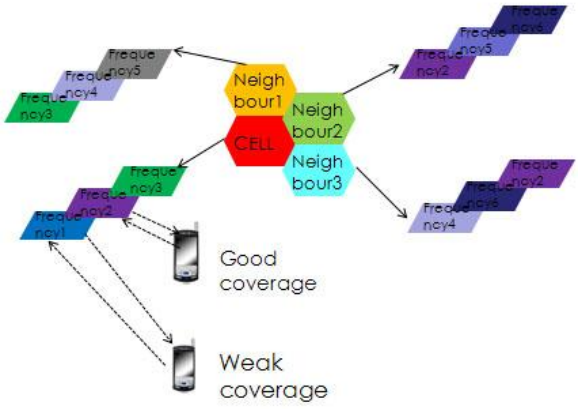

Figure 1. User access diagram

As shown in Figure 1, under the scene of weak coverage, priority access frequency reuse of low frequency, to reduce the interference to adjacent areas; under the scene of good coverage, the access frequency reuse slightly higher and the ISCP lower frequency points.

V. SUMMARY

You can find interference in TDCDMA system network everywhere. But when interference is enhanced to a certain degree, the network brings great negative impact, directly affect the network quality and user perception; IDCA algorithm is an effective algorithm of interference escape, but in more scenes of the user, the algorithm is less effective; By the carrier algorithm which is based on frequency multiplexing degrees, can effectively separate the resources of the occupied between the strong interference of the cell edge users and cover a good user, reducing interference within the system to avoid interference to further uplift, enhance network quality and user perception.

Reference

[1] Books: Sun Shewen, and Fu Haiming, TDSCDMA wireless network testing and optimization,
The people post and Telecommunications Press 2011-7-1

[2] Books: Peng Mugen, TDSCDMA mobile communication system is enhanced and the evolution ,
Mechanical Industry Press 2008-01-01

[3] Books: Peng Mugen, TD-SCDMA mobile communication systems (Third Edition),
Mechanical Industry Press 2009-07-01

[4] Books: Sun Shewen, and Fu Haiming, TDSCDMA wireless network testing and optimization ,
The people Post and Telecommunications Press 2011-7-1

[5] Books: Zhang Chuanfu, TD-SCDMA communication network planning and design
The people Post and Telecommunications Press 2009-01-01

[6] Books: DuanHongguang, Bimin, and Luo Yijing, TDSCDMA third generation mobile communication system protocol system and signaling flow,
People of Posts and Telecommunications 2007-03-01

[7] Thesis: Luo Zhinian, and Zhang Wenjun,TDSCDMA system base station interference analysis ,
Information Security and Confidentiality of Communications, 2010(05)

[8] Thesis: GuoJing, Thinning TDSCDMA wireless network optimization problem, Communication World , 2011(10)

The analysis and application of OSPF protocol in school domain network

Sun Qiuyun Yang Rui
Department of Management and Information
Shandong Transport Vocational College
Weifang, Shandong, P.R.China
shenknight@yahoo.com.cn

***Abstract*—This paper describes OSPF's work principles, calculation steps and application situations; mainly the application of OSPF in school domain network and relevant parameters setting. As an important internal gateway protocol, OSPF has an important effect on the network performance. The author makes a network planning by using OSPF to a university which is adapted to the multimedia teaching, network office and routine. In this paper the author expounds on the ideas and practical experience from this planning. The university has three scattered campuses, many students and teachers. Thus the flow of the network is complicated. For solving this problem, some parameters have been set in this planning, such as "cost" and "metric". The cost values decide the data, the metric values control routing priority. After analyzing the system operating data, the network has a good stability and effect.**

Keywords- OSPF protocol; working principle; network plann-ing; application; parameters setting

I. INTRODUCTION

Along with the development of routing technology and the needs of network, RIP (namely the Routing Information Protocol) can not adapt to the large-scale heterogeneous network interconnection. OSPF (namely Open Shortest Path First) has become one of the most widely used Routing technologies in the current network [1].OSPF has been well-known in the information industry for many years. At first, OSPF supports various size of the network. Then the rate of routing change convergence is fast, if the topology of the network changes, OSPF sends message updates immediately making the change synchronization in autonomous system. And OSPF supports area division, allows autonomous system divided into several regions to management easily, the exchange information between each other area sent further abstraction, thereby reducing bandwidth of the network. For its advantages, this paper applies it to design school domain network for a university.

II. WORK PRINCIPLES AND CALCULATION STEPS

OSPF is a kind of typical link-state routing protocol, which is normally used for the same routing domain [1]. The routers collect the connection status information of each router in its network, and then generate link-state database. According to the database, OSPF can understand the whole topological conditions of the network. Its routers independently calculate the routing to reach any destination by the algorithm-Shortest Path First. OSPF supports a hierarchical routing way, and takes the network divided into a main part (called the backbone area) and a group of independent each other parts (called area). The backbone area saves the link information of each other exchange in the whole network. Each area includes the network belongs to this regional and the corresponding routers, as an independent network; OSPF routers in this area only keep the link-state of the area. So each router link-state database can keep the size reasonable, and make time of computing routing, quantity of message not too large.

The calculation for routing basically has the following three main steps:

- Describe the network topology structure around the router, and produce LSA (namely Link-State Advertisement).
- Make owned LSA spreading in autonomous system, at the same time collect all of the other routers LSA generated.
- According to all LSA collected calculate routing.

III. APPLICATION SITUATIONS

As mentioned above, OSPF takes the large network divided into a group of small networks (called area), the division is not random, should choose regional boundary reasonably to make the quantity of information exchange between different area to small as far as possible. But in practical application the division of area often is not according to communication mode but according to geographic factor or other factors [2][3]. Usually OSPF can be used in the following situations: the number of routers of the network is more than 10 sets; the network is medium or large; the topology of the network is mesh, and it is connected between any two routers. When using OSPF, the routing changes can be fast convergence, and the routing itself costs low as far as possible [4]. At the same time the CPU processing power and memory size is high as far as possible.

IV. APPLICATION IN SCHOOL DOMAIN NETWORK

A. Basic Situation

To adapt to the current multimedia teaching work, the university ready to construct a school domain network based on OSPF. The network mainly has four types of online business areas: multimedia teaching area, network office

978-0-7695-4818-0/12 $26.00 © 2012 IEEE
DOI 10.1109/DCABES.2012.96

area, student living area and staff living area. Geographically, the school has A, B and C three campuses. A campus and B campus are apart from about 17 kilometers, A campus and C campus are apart from about 20 kilometers, B campus and C campus are apart from about 10 kilometers. In other words, these campuses are scattered. So OSPF is suitable for it.

B. Network Division And Link

As indicated above, the geographical factor determines the network division. At the same time, considering the A campus having more users, these users are divided into two areas: working area and living area. The working area is composed of teaching area and office area, and the living area is composed of students living area and staffs living area . Therefore, all of the users are divided into four areas. There is a CISCO 3560-24ps as the core switch in each area. The network video flow is very big in multimedia teaching area. So there is another CISCO 3560-24ps in the network center as the interactive video server switch. The network structure is shown in figure 1. This switch respectively interconnects with four core switches, internet port between it and each of them is GE-Channel by binding two gigabit fiber interfaces. So the internet bandwidth is 4.4Gbps between every two CISCO 3560-24ps switches. The four core switches down-link to CISCO 2950-24 switches according to the number of users, up-link CISCO 3560-24ps switches in the main chain. The backup line interconnects to backbone equipments of other areas.

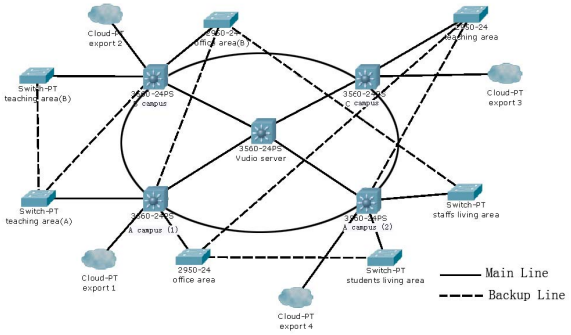

Figure 1. Network Topology

C. Data Configuration

According to the actual network scale, all of the routing equipments in the whole network are allocated in the same area0. And direct routing and static routing are distributed by using the command 'redistribute connected metric and redistribute static metric', with the result that all network segments can visit each other and it makes network monitor and user management convenient. OSPF uses the measure of cost to calculate the purpose path, in other words, the minimum cost is the shortest path. So link bandwidth, link delay and economy decide the configuration of the OSPF router. It can't be denied that the smaller of the link's cost, in all likelihood the link was chosen as a routing. When a router has several paths to a certain purpose network, routing protocol must judge out the best one and put it in the routing table. That is to say, routing protocol must calculate a number for every path. The number is metric; usually the value is no unit. The smaller the metric, this path is preferred. It is not the same to calculate the metric in the different routing protocols, so the best distance may be different.

V. PARAMETER SET

According to actual condition, the values of cost and metric were configured to control data flow.

A. Cost Set

The configuration of the cost value can control the flow of data [5]. To switch automatically between main road and backup line, the interface is configured with ip ospf cost 200 in the backup line. When main road is disrupting, the data can flow to backup line immediately. The interface between VIDEO SERVER6509 and one of the four core switches is configured with ip ospf cost 300 for controlling interactive video flow alone between them. The swap data among the four core switches exchanges along the elliptic loop in the figure2.

B. Metric Set

The configuration of the metric value can control the routing priority. In figure 1, four core switches connect an internet export respectively which does NAT address translation by firewall. Thus there is a static routing which the metric value is 0 pointing to the export firewall of these switches export firewall. Through the different of X(X is digital, configured in configuration-information originate metric X of the OSPF routing), Internet exports can remove these routings which the metric value is 0. The imports can compare the metric value on the other backbone equipment, and choose a new routing which the metric value is 0 again. Thus the network can fulfill the switching and backup of these exports.

VI. CONCLUSIONS

OSPF is an important internal gateway protocol, has a good application in the domain network. The whole network has a good stability, guarantees effectively the multimedia teaching and office automation, and brings convenience with network to students and staffs. The ideas and practical experience from designing the network help to further make use of OSPF principle and data configuration.

REFERENCES

[1] W H Zhou, L J Ding and P T Xie, "An Interior Gateway Protocol for Internet—OSPF," Computer Engineering, Vol. 26, Feb. 2000, pp: 13-15. (in Chinese)

[2] D WANG, "Application of OSPF Routing Protocol in Multi-area," Journal of Chongqing University of Science and Technology (Natural Sciences Edition), Vol. 12, Apr. 2010, pp: 172-174. (in Chinese)

[3] Y Cheng and J P Xu, “Multipath Routing Research Based on OSPF,” Information And Electronic Engineering, Vol. 5, Aug. 2007, PP: 301-303. (in Chinese)

[4] X N Huang, Y F Zeng and Y X Tan, “Discussion on technology of OSPF routing optimization,” Experimental Technology and Management, Vol. 29, Feb. 2012, PP: 104-108. (in Chinese)

[5] W D QIU and S H WANG, “OSPF in Campus Network Application,” Journal of Guangxi University (Natural Sciences Edition), Vol. 31, June. 2006, pp: 300-303. (in Chinese)

Cloud Computing: Service Provisioning and User Requirements

S. Khaddaj
School of Computing and Information System,
Kingston University,
Kingston upon Thames, KT1 2EE, UK
s.khaddaj@kingston.ac.uk,

***Abstract*—The Cloud Computing utility model has raised a number of challenges particularly in relation to service provisioning and user requirements. In such a service driven environment it is very important that resource provisioning can be optimized and users and applications have some level of assurance that their requirements can be satisfied. However, in order to guarantee a certain level of Quality of Service (QoS) Service Level Agreements (SLA) which specify contracts between providers and users are commonly used. This paper aims to investigate the QoS issues and SLA management within Cloud Computing and to present a framework for QoS assurance.**

Keywords- Cloud Computing, Quality of Service, Service Level Agreement.

I. INTRODUCTION

In the last few years Cloud Computing has been promoted as the most promising trend in the information technology sector [1], [2], [3]. The global economic crisis has raised the need for a cheap and flexible business model in information and communication technology. This has boosted the development of Cloud Computing, which gives the users the ability to access the applications as services from anywhere in the world.

The universal acceptance of this technology depends on the ability to provide desired Quality of Service (QoS) on dynamically assembled resources. Quality of Service is the ability of an application to have some level of assurance that users' requirements can be satisfied. It can be seen in the form of Service Level Agreement (SLA) between clients and suppliers to provide a service at a specified cost and within a guaranteed time frame. Moreover, with the unprecedented explosion in the growth in demand and usage of internet services, the need for efficient information delivery and management services with load balancing capabilities has become even more urgent. Cloud Computing is well positioned to support this new service-oriented paradigm.

We start with a brief discussion of user requirements, services and quality of service (QoS). Then, service level agreements and their management are presented with particular emphasis on the distributed nature of the Cloud. This is followed by proposing an approach for QoS and SLA management, together with some suggestions of how to deal with the different SLA processes. Finally, we conclude with some suggestions for future work.

II. USER REQUIREMENTS

The attempt to offer a real cloud based utility computing depends very much on meeting user requirements both functional and non-functional requirements. While functional requirements establish what the service does, non-functional requirements are concerned with how well this is achieved. Quality of service (QoS) is mainly associated with non-functional service properties.

A. Quality of Service

Cloud Computing is clearly motivated by business demand. Quality of Service is hence an inherent feature of Clouds. For example, Amazon S3 provides data storage service with tightly defined quality of service on availability, durability and persistence of data. However, a well-defined quality of service is not only limited to performance, availability, but also to other aspects such as security and reliability. Since Clouds offer storage and computing power through web-enabled interface, their QoS is strongly related to QoS of network, QoS of data, QoS of web services and QoS of computing resources.

Delivering QoS on the Internet is a critical and significant challenge because of its dynamic and unpredictable nature. Applications with very different characteristics and requirements compete for scarce resources. Changes in traffic patterns, denial-of-service attacks and the effects of infrastructure failures, low performance of Web protocols, and security issues over the Web create a need for Internet QoS standards. Unresolved QoS issues cause critical transactional applications to suffer from unacceptable levels of performance degradation. The major requirements for supporting QoS Cloud are typical software quality factors [7], [8], [9], which are also relevant for Web services, as follows:

Availability: Availability is the quality aspect of whether the service is present or ready for immediate use. Availability represents the probability that a service is available. Larger values represent that the service is always ready to use while smaller values indicate unpredictability of whether the service will be available at a particular time. Also associated with availability is time-to-repair (TTR). TTR represents the time it takes to repair a service that has failed. Ideally smaller values of TTR are desirable.

Accessibility: Accessibility is the quality aspect of a service that represents the degree it is capable of serving a service request. It may be expressed as a probability measure denoting the success rate or chance of a successful service

978-0-7695-4818-0/12 $26.00 © 2012 IEEE
DOI 10.1109/DCABES.2012.76

instantiation at a point in time. There could be situations when a service is available but not accessible. High accessibility of services can be achieved by building highly scalable systems. Scalability refers to the ability to consistently serve the requests despite variations in the volume of requests.

Integrity: Integrity is the quality aspect of how service maintains the correctness of the interaction in respect to the source. Proper execution of service transactions will provide the correctness of interaction. A transaction refers to a sequence of activities to be treated as a single unit of work. All the activities have to be completed to make the transaction successful. When a transaction does not complete, all the changes made are rolled back.

Performance: Performance is the quality aspect of service, which is measured in terms of throughput and latency. Higher throughput and lower latency values represent good performance of a service. Throughput represents the number of service requests served at a given time period. Latency is the round-trip time between sending a request and receiving the response.

Reliability: Reliability is the quality aspect of a service that represents the degree of being capable of maintaining the service and service quality. The number of failures per month or year represents a measure of reliability of a service. In another sense, reliability refers to the assured and ordered delivery for messages being sent and received by service requestors and service providers.

Security: Security is the quality aspect of the service of providing confidentiality and non-repudiation by authenticating the parties involved, encrypting messages, and providing access control. Security has added importance because service invocation occurs over the public Internet. The service provider can have different approaches and levels of providing security depending on the service requestor.

B. Applying Analytic Hierarchy Process (AHP) in QoS negotiation

In most of the cases, user requirements reflect multiple objectives, and users usually cannot express exactly what they want. The question is "Can the systems offer the best solution for them?" In practice, AHP is an excellent tool to solve this type of problem. AHP is a type of additive weighting method. It has been widely reviewed and applied in the literature, and its use is supported by several commercially available, user-friendly software packages. Decision makers often find it difficult to accurately determine cardinal importance weights for a set of attributes simultaneously. As the number of attributes increases, better results are obtained when the problem is converted to one of making a series of pairwise comparisons.

AHP formalizes the conversion of the attribute weighting problem into the more tractable problem of making a series of pairwise comparisons among competing attributes. AHP summarizes the results of pairwise comparisons in a "matrix of pairwise comparisons." For each pair of attributes, the decision-maker specifies a judgment about "how much more important one attribute is than the other." Each pairwise comparison requires the decision maker to provide an answer to the question: "Attribute A is how much more important than attribute B, relative to the overall objective ".

User requirements after the AHP are converted into weighted matrix W, which shows the importance of each QoS aspect of services. This matrix is then multiplied by the matrix of QoS values of services S. The matching mechanism compares values between matrix WxS and the matrix of QoS values of resources R. The processes are shown in Figure 1.

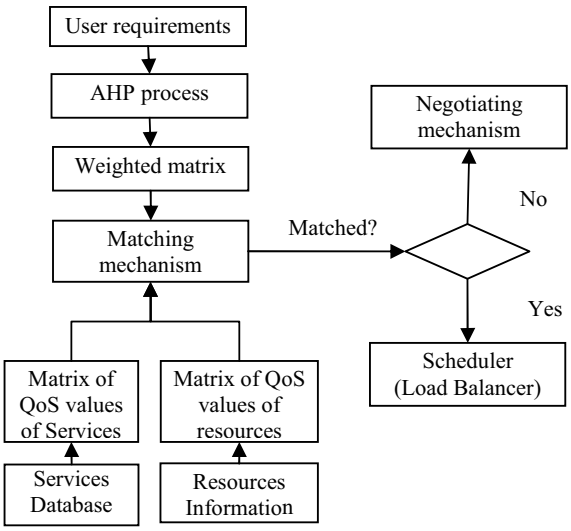

Figure 1 Matching mechanism

III. SLA MANAGEMENT

Fundamentally, SLA is a contract between suppliers and clients. In the domain of information system, the operation and management of SLA requires data integrity [11]. In fact a Service Level Agreement (SLA) is a representation of all those features that a user should expect to receive by a service. By features here we refer not only to the functionality delivered by the service, but also to the quality that the user experiences. As a matter of fact, SLAs are typically associated with Quality of Service (QoS), but in a formal representation it is reasonably expected to find the service description as well.

A. Service Level Agreement Standardization

The Web Services Agreement Specification (WS-Agreement) is one standard SLA form established by the Open Grid Forum. WS-Agreement is a Web Services protocol for establishing an agreement between two parties, using an extensible XML language for specifying the content of an agreement, and agreement templates used to discover appropriate agreement parties. The specification consists of three parts, first is the schema for specifying an agreement,

secondly is the schema for specifying an agreement template, and finally a set of operations for managing an agreements life-cycle.

B. Service Level Types

Most of major commercial cloud vendors provide best effort QoS provisioning and provide only the most basic guarantees on the availability and performance of resources, primary motivation to research further and publicize the benefits of QoS in Cloud Computing. The services are transparently scalable and are based on a pay per use model. In this model, the service guarantees cannot be obtained from the systems. A typical example of this type is the web services.

Another less popular model is guarantee based [6]. The basis function of QoS management of this type is to provide resources to one or a group of applications of services to satisfy at least application minimum requirements. It matches applications to the available resources by solving the conflict between requirements of user or application and capacity of resources. In the case when user requirements are not satisfied, the systems try to re-negotiate the QoS constraints instead of ignoring them.

At this point it is important to point out that there have been a number of works carried out in the domain of SLA enforcement for distributed systems. An example is the Grid Service Broker which is a project developed as part of the GridBus Programme [12]. It arbitrates collaboration between distributed participants as the broker identifies data sources for a given scenarios, e.g. an analysis or report. Suitable computational resources are discovered for specific job requirements. The broker provides a dynamic parametric programming model for writing grid applications [12]. GridBus targets a higher degree of details about available resources (machine level), jobs and files which inherently makes it less scalable in large environments.

Another example is the Maui scheduler for network clusters which enforces SLA driven scheduling schemas [13]. It functions as a SLA engine for managing and allocations of resources to processes, whilst optimizing the resources consumption. The Maui achieves optimization in influencing processes, nodes, composite objects, QoS (CTQs), and policies.

Policy based scheduling of grid-enabled resource allocation was also presented in [14]. The main difference with this approach is that the authors do not consider a centralised point of reference to SLA Enforcement. Policy based scheduling controls the request assignment to resources by adjusting resource priorities. Secondly, it efficiently manages resources in allocating usage quotas to target users. Thirdly it provisions for reservation based grid resource allocation.

As explained earlier, SLA is a formal agreement made between two or more parties: the service provider and the service recipient. The SLA defines the basis of understanding between the two parties for delivery a service to an agreed level of quality. Services use different collaborations between system resources and when analysing the collaborations or resource interactions, we observe that SLA issues can arise at multiple levels: 1) SLA enforcement where providers may agree to enforce the SLA under which resources are made available to consumers and 2) SLA management, where consumers may want to access and interpret SLA statements published by providers, in order to monitor their agreements and guide their activities. Both providers and consumers want to verify that SLA protocols are applied correctly. In the context of the study, there is a need to focus on the element of SLA enforcements, therefore we use the approach suggested in [9], [10] in an attempt to resolve the problems inherent in enforcing the conflicting quality models of robust SLA enforcement for example data integrity against performance. However, the management of SLA requires many processes as shown in figure 2.

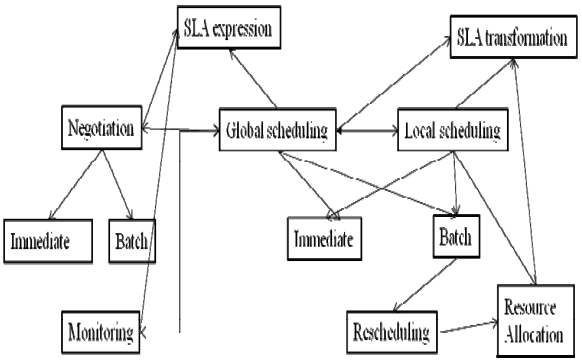

Figure 2 SLA management processes

IV. MULTILEVEL QUALITY OF SERVICE MANAGEMENT IN THE CLOUD

A. Service Provisioining in Cloud Computing

In Cloud Computing, services are accessible to user through internet based interfaces. From functional point of view, services can be categorized into system services and application services [1]. Systems services allow user to control actions on resources and systems such as file system services, monitoring system services, and communication service. Application services are built for direct use or for the compositions of new user applications.

The three common Cloud Computing service layers are 1) Infrastructure as a Service, 2) Platform as a Service, and 3) Software as a Service, as shown in Figure 3. In the first type, service providers leverage virtualization technology to provide scalable virtual resources as user demand their pool of resources which is fundamentally based on Grid Computing infrastructure. The systems of this type are Amazon Elastic Compute Cloud (EC2) and Microsoft Live Mesh. In the second type, consumers are provided with a platform where the system runs on. Salesforce.com, Microsoft Azure Services Platform and Google application Engine are typical services of this type. Microsoft Office Live and Google Docs are example of services of last type where the services are alternative of locally run applications.

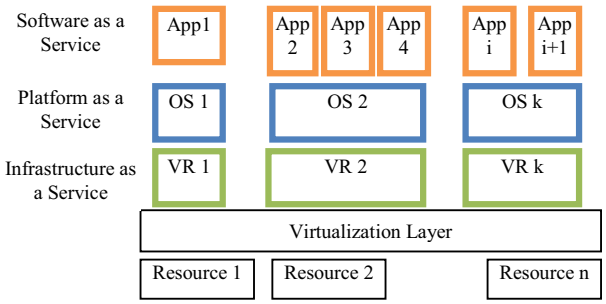

Figure 3 Cloud Services Layers

B. *Architecture*

As mentioned earlier in Cloud Computing, there are three layers of services. The services from upper layers were built on the services in lower layers which then become resources services for upper layers. Therefore, to measure user requirements of resources, it is necessary to predefine the QoS mapping which maps requirements from user to service, user to resources and services to resource, as shown in Figure 4. The two first mappings are fulfilled by user and the last one is defined by provider through their experiences.

The QoS mapping from service to resource defines the minimum capacities or resources which are able to run the services. Examples are minimum CPU and memory needs, reliability, type of traffic, etc. The QoS mapping from user requirements can be user's budget, resource prices or specified type of resources. To achieve this we propose a a generic model which is flexible and scalable. There are two main parts, resource broker and service broker. The lower part gives the resource broker permission to access directly the raw resources such as CPU, storage, bandwidth through the local management system. The upper part is to construct a broker located on the top of the cloud system, i.e. a service broker.

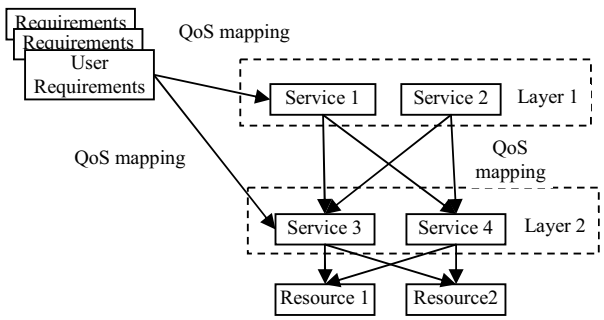

Figure 4 Requirement mappings

Let us consider the following scenario: "I have £2000. I would like to use 100 times the service A with 500MB of data to do an experiment. The deadline is one month." The high level broker will express the request into small requirement of each of the basic services and their relations. The service (A, QoS_A) is decomposed into basic service (A_1, QoS_1)... (A_k, QoS_k). Then the broker sends the request to the sites. Each site checks its status by using its broker, and then send back the offer to the broker. The broker chooses the site which is best suited, for example with the lowest price, for the user request. The broker of the chosen site splits into low level the services (A_1, QoS_1)... (A_k, QoS_k) and delivers the services to the resources which can guaranty the QoS of services.

Users input their expectations of services or resources that run the services. These expectations are then transformed to quality attribute requirements under the requirement evaluator. The QoS negotiator transfers the resource requirements to QoS matcher that matches to the resources meeting the requirements. In case that all resources are below user requirements, the QoS matcher offers the best possible QoS parameters to user expectation. The QoS negotiator then re-negotiates the QoS parameters (Figure 5). Raw information of capacities of resources is tracked by Resource Monitor and then processed by QoS Evaluators. The refined information is used as a reference for QoS matcher. The other references come from Services Repository, which contains services and QoS mapping of services such as resources consumption of services, resource requirements. When the SLAs are established, they are stored in SLA manager and the corresponding services are activated in the resources.

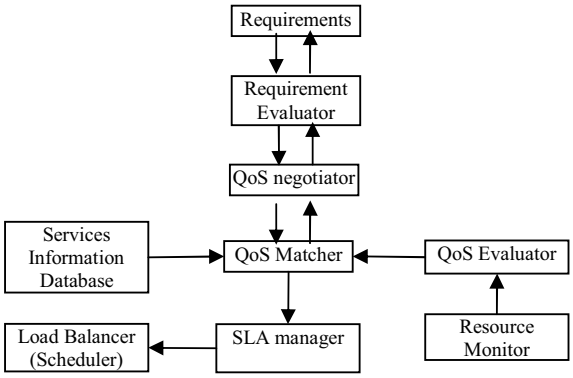

Figure 5 Architecture of QoS manager

C. *Matching and Scheduling*

In cloud virtualization technologies the concept of resources is extended from physical resources to virtual resource services. As a result, there has been a dramatic increase in the number of QoS parameters that have to be considered in order to meet the ever increasing users' requirements. Consequently, the dimension of parameters in the optimization problem of scheduling or load balancing will have a great impact on the scheduling time. The efficiency of the scheduling algorithms or strategies deeply depends on the status of the whole system, i.e the incoming tasks and the available resources. However, the majority of

scheduling strategies have been designed to meet specific requirements therefore, they perform well in some specific situations.

Recognizing these characteristics, an intelligent framework which acts on the scheduler of a multi-objectives broker is required. The broker allocates resources by enforcing quality of service i.e. it is not only system centric but also user centric. Therefore, it will autonomously harmonize the resource owner profit and user requirements.

In scheduling, the environment is just the composition of the resources and the tasks. Incoming tasks are usually stored in waiting queues which can be either unsorted or sorted by some policy. One common criterion is to sort the tasks by their priority. The priority of the task depends on the adopted system. It can be measured by the QoS metrics such as the price or the deadline etc. The resource list contains the information regarding the QoS of all resources in the system. Therefore, the scheduler contains two matrices, one for tasks the other for resources. The scheduling problem is actually the question how to match the two matrices such that the system gets the maximum profit (figure 6).

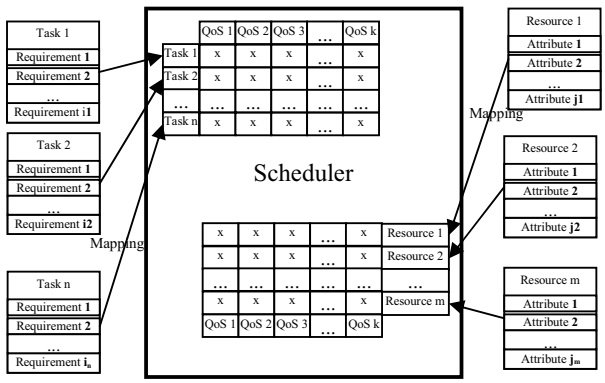

Figure 6 A matching mechanism in scheduler

V. CONCLUSION AND FUTURE WORK

In this paper quality of services issues and SLA management were considered for the Cloud Computing paradigm. The main contribution of this paper is to propose an approach for distributed resources management in the Cloud that is based on quality of service and SLA. This system can autonomously recognize the changes in a dynamic environment and make decisions regarding scheduling that is based on user requirements and available resources and services. However, the implementation and evaluation of the framework will be considered in future work.

REFERENCES

[1] Buyya R., Yeo C.S., Venugopal S., Broberg J., Brandic I., *Cloud computing and emerging IT platforms: Vision, hype, and reality for delivering computing as the 5th utility* (2009) Future Generation Computer Systems, 25 (6), pp. 599-616.

[2] Christof Weinhardt, Arun Anandasivam, Benjamin Blau, Nikolay Borissov, Thomas Mein, Wibke Michalk and Jochen Stößer, *Cloud Computing – A Classification, Business Models, and Research Directions***,** (2009) Business & Information Systems Engineering 1(5) pp. 391-399.

[3] T. Rings, G. Caryer, J. Gallop, J. Grabowski, T. Kovacikova, S. Schulz, I. Stokes-Rees. *Grid and Cloud Computing: Opportunities for Integration with the Next Generation Network***.** Number 3, s.l. : J Grid Computing, 2009, Vols. Volume 7, . ISSN 1570-7873 (Print) 1572-9814 (Online).

[4] J. Al-Ali, A. Hafid, F. Rana, W. Walker. *QoS adaptation in service oriented grids***.** s.l. : In Proceedings of the 1st International Workshop on Middleware for Grid Computing (MGC2003) at ACM/IFIP/USENIX Middleware 2003, Rio de, 2003

[5] D. A. Menascé, H. Ruan, H. Gomaa. , *QoS management in service-oriented architectures***.** 7-8, Amsterdam, The Netherlands : Elsevier Science Publishers, 2007, Vol. 64. ISSN:0166-5316 .

[6] Christophe Diot, Aruna Seneviratne, *Quality of Service in Heterogeneous Distributed Systems***,** Proc of the 30th International Conference on System Sciences (HICSS) Volume 5: Advanced Technology Track, 1997.

[7] G. Horgan, S. Khaddaj, "*Use of an adaptable quality model approach in a production support environment*", Journal of Systems and Software, 82(4), pp. 730-738, 2009.

[8] S. Khaddaj, *"Quality of Service Issues in Distributed Component Based Environments"* in 'Journal of Algorithms and Computational Technology', Multi-Science Publishing Co Ltd, *2010*.

[9] S. Khaddaj, G. Horgan, *"The Evaluation of Software Quality Factors in Very Large Information Systems"* in 'Electronic Journal of Information Systems Evaluation', pp. 43-48, *2004*.

[10] G. Horgan, S. Khaddaj, P. Forte, Chapter *"An Essential Views Model for Software Quality"* in 'Project Control for Software Quality', Edited by R. Kusters, A. Cowderoy, F.Heemstra, E. van Veenendaa, Shaker Publishing, *1999*.

[11] Debusmann M, Keller A, "*SLA-driven Management of Distributed Systems using the Common Information Model*", University of Applied Sciences, Kurt-Schumacher-Ring 18, IBM Research Division, 2003.

[12] Buyya R, GridBus: "A Economy-based Grid Resource Broker", University of Melbourne, 2004.

[13] Cluster Resources, "*Maui Scheduler Administrator Guide*", version 3.2, Cluster Resources Press, Cluster Resources Inc., 2005.

[14] In I J, Avery P, Cavanaugh R, Ranka S, "*Policy Based Scheduling for Simple Quality of Service in Grid Computing*", in the International Parallel & Distributed Processing Symposium (IPDPS), Santa Fe, New Mexico, April 2004.

A New Software Architecture for Ultra-large-scale Rendering Cloud

Zhou Weini, Lu Yongquan, Gao Pengdong, Qiu Chu, Qi Quan
High Performance Computing Center, Communication University of China, Beijing 100024, China
zwnrxk@163.com , pd_gao@cuc.edu.cn

***Abstract*- A kind of new five-level software architecture is presented in this paper, which is designed elaborately for ultra-large-scale rendering cloud. This software architecture consists of five levels, infrastructure layer, rendering service layer, rendering application layer, service management and access interface. Based on the proposed software architecture, we have developed a new type of rendering management software called Golden Farm Cluster Rendering Platform. And comprehensive tests have been carried on the super computer, TianHe 1A. Experimental results show that Golden Farm can effectively manage the rendering jobs on ultra-large-scale high performance cluster with up to 2000 computing nodes and also obtain good performance. In addition, the platform has created an important record, rendering a 3D model by using 24000 CPU cores in parallel.**

Keywords-animation rendering; five-level architecture; rendering cloud; Golden Farm; cluster rendering management platform

I. INTRODUCTION

Rendering is the process of generating an image from a model by the means of computer programs. A model would contain geometry, viewpoint, texture, lighting, and shading information as a description of the virtual scene. The data contained in the scene file are then passed to a rendering program to be processed and converted to a digital image or raster graphics image file [1].

Rendering is widely used in 3D animation production, advertising design, video games, simulators, architectural design and other fields. It plays an important role in the visual effect of the animation or video works. A high quality rendering can show materials texture, lighting effects and even shadows, and make images more vivid and lifelike.

Nowadays, with the rapid development of video technology, animation enterprise, which is driven by digital TV and high definition television, has higher demand on rendering. What's more, due to the complex scenes, a large number of source files and special effects, rendering costs quit a long time. Rendering management is also very complex. Due to these, the efficiency of rendering work is gravely affected. Rendering management becomes the bottleneck of the large-scale animation and video production. On the other hand, as high-performance computer develops, the exiting rendering management software now can't meet the demand for ultra-large-scale rendering better. It leads to a waste of the computing resources. Therefore, it becomes great significant to build an ultra-large-scale animation rendering service cloud. This service cloud would integrate large-scale high performance computing cluster with a variety of renderers and rendering plug-ins.

There is currently a lot of research in the area of rendering management software [2]. Up to now, the dominant products on the market for rendering management are Alfred from Pixar, Muster from Virtual Vertex and Enfuzion from Axceleon Inc. Alfred can manage and monitor the rendering nodes in real-time. Furthermore, the advantages of smaller-scale cluster rendering are that it can be given full played and idle rendering nodes can be avoided [3]. Muster is based on Client/Server model. It is an application program that has been designed to manage the complex multi-platform cluster rendering system. Rendering management on hundreds of computers can be provided by Muster. It has good stability and flexibility [3, 4]. Enfuzion, which has the support of unlimited platform, can segment a high resolution frame into several images for rendering. In addition, it supports image browser and thumbnail browser to view the status of rendering.

However, with the continuous expansion of the scale of rendering and higher demand for rendering efficiency, all kinds of existing job scheduling and management software can hardly meet the requirement of efficient rendering. Most of the current rendering management software use master-slave mode and centralized scheduling schemes, which leads to the management node bottleneck [5, 6]. In addition, many rendering management software use a centralized storage system to store scene files, texture, material as well as the rendering results. In this case, it seems hardly to fulfill a large number of simultaneous I/O request during rendering. To address those issues, a type of new five-level software architecture is presented in this paper. Based on this software architecture, we have developed Golden Farm Cluster Rendering Platform and tested it on the "TianHe 1A" super computer. The results of the test show that Golden Farm can manage ultra-large-scale rendering effectively, and improve rendering efficiency greatly.

The rest of this paper is organized as follows. In the next section, we present the new software architecture for ultra-large-scale rendering cloud. In section 3, Golden Farm Cluster Rendering Platform is introduced in detail, which is developed elaborately based on our software architecture. And then we will display some experimental results, which are obtained from TianHe 1A super computer. At last, the conclusions will be made in section 4.

978-0-7695-4818-0/12 $26.00 © 2012 IEEE
DOI 10.1109/DCABES.2012.10

II. SOFTWARE ARCHITECTURE FOR ULTRA-LARGE-SCALE RENDERING CLOUD

The rendering service cloud for animation and special effects is a software cloud based on high-performance computing. Its purpose is to solve the problem of job scheduling and management on ultra-large-scale clusters. A kind of new software architecture is proposed in this paper. It integrates the large-scale high-performance cluster with a variety of different renderers and rendering plug-ins. This software architecture makes it possible to manage large-scale rendering and improves the efficiency of rendering. As shown in Fig. 1, this software architecture consist of five levels, infrastructure layer, rendering service layer, rendering application layer, service management and access interface.

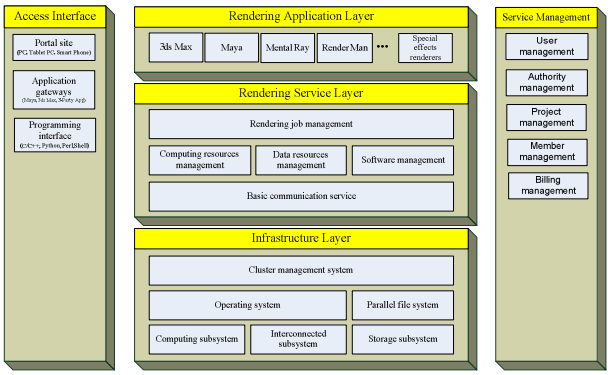

Figure 1. Software Architecture for Ultra-large-scale Rendering

1) *Infrastructure layer*

Infrastructure layer provides all kinds of necessary hardware and related system software for rendering service cloud platform. The main hardware equipment includes the following three parts: computing subsystem, interconnected subsystem and storage subsystem. Computing subsystem is the computing core of the rendering service cloud platform. Its main function is to perform calculation. Interconnected subsystem provides a connecting path between management node, login node, computing nodes and storage nodes. It helps to fulfill system management, real-time monitor and high speed exchange of information between computing nodes. Storage subsystem uses parallel file system in this software architecture. It provides rendering service cloud with a centralized data storage system. During rendering, the rendering jobs read various scene files, texture files, material files and others simultaneously. And then it generates a large number of image sequences. The parallel file system not only meets the requirement of the storage capacity, but also satisfies a large number of almost simultaneous data I/O during rendering. It is possible to overcome the I/O bottleneck of the rendering cloud by using the parallel storage system.

2) *Rendering service layer*

Rendering service layer provides a variety of basic service subsystem, including basic communication service, computing resources management, data resources management, software management and rendering job management. Basic communication service subsystem shields the heterogeneity of various resources and the complex correlation between equipments. It makes the messaging environment become convenient and transparent. Due to this, the rendering platform can not only make full use of local high-performance computing resources, but also make the most of other distributed computing resources. Computing resources management is mainly concentrated on managing computing resources used for rendering. When a rendering job is submitted, the corresponding computing resources are allocated to this job from the resource pool. And then these computing resources will be organized into a tree structure instead of master-slave mode. So the computing nodes can be effectively managed based on the tree topology. In this way, a solution to the bottleneck of management node is provided. Data resource management is used for managing all kinds of data, such as scenes, textures, materials as well as the data generated in rendering. By means of dynamically constructing a distributed cache system between the computing nodes of high-performance cluster, a safe and reliable service of data access is provided. Software management is responsible for managing various kinds of renderers, rendering plug-ins and some renderers for complex video special effects. Job management is the core component of the rendering service cloud which can schedule and manage rendering job efficiently.

3) *Rendering application layer*

To fully ensure that diverse rendering jobs can be carried out smoothly, rendering application layer provides various kinds of rendering software, engines and plug-ins, such as 3ds Max, Maya, Mental Ray, RenderMan, etc. For some complex video special effects, users can custom rendering engines by parallel computing technology.

4) *Service management*

Service management provides some background support services and the access rights management of these basic services. It not only ensures that the rendering platform is safe and reliable, but also provides strong support for each level of the rendering platform. This level includes the following functions: User management, Authority management, Project management, Member management and Billing management, etc.

5) *Access interface*

Access interface contains the following three parts: portal site, application gateways and programming interface. Portal site offers a variety of public information. On the other hand, it provides a unified entrance for users to access all kinds of rendering services. Application gateways map the rendering services of the platform to a web service so as to reduce the integration difficulty of business system and the rendering platform. In order to do some further development, programming interface supports C/C++, Python, Perl and Shell.

The software architecture described above makes it possible to overcome the problem of ultra-large-scale rendering management. It can improve the efficiency and

quality of large-scale rendering to some extent. On the premise of ensuring the security, reliability, availability of the rendering cloud platform, this software architecture have fully solved the bottleneck of the single management scheduling node and improved I/O performance. It is obvious that the utilization of hardware and software can be improved greatly.

III. GOLDEN FARM CLUSTER RENDERING PLATFORM

Based on the five-level software architecture mentioned above, we have successfully developed a new rendering platform, Golden Farm Cluster Rendering Platform. Usually, with more and more rendering nodes, the time of rendering could be reduced further. However, the master-slave mode and the centralized scheduling schemes makes the management node become the bottleneck and the rendering efficiency may decline when the rendering nodes is up to some scale [7]. Thus, Golden Farm adopts the hierarchical organization of computing nodes instead of the mode of single management scheduling node. In this case, it can dynamically set sub-management node and build compute node tree. This mode can effectively solve the bottlenecks of the single management scheduling node in large-scale animation rendering. All the resources will be released into the resource pool for other jobs after the current rendering job is completed. Therefore, the utilization of computing resources is improved greatly. Meanwhile, Golden Farm abandons the centralized storage mode used in the traditional rendering management platform. It utilizes a new storage mode based on distributed caching, which can dynamically construct a distributed cache system between the computing nodes of cluster. In this way, a high-performance data caching for the rendering operations is provided. Before rendering, all kinds of files, such as scene files, texture files and material files, etc, will be dispatched from the centralized storage system to the caching system. In this case, it will not need to read the rendering data from the centralized storage system any more, and the rendering outputs can be written into the local cache directly. After all the rendering operations are completed, data will be collected into the centralized storage automatically. This mode can greatly reduce the overhead of I/O.

Different from some existing rendering management software, Golden Farm Cluster Rendering Platform provided more functions for users, including rendering job management, service cloud system management, computing resources hierarchical management, intelligent data management, user membership management, online transactions and so on[3,8]. Based on this platform, the whole rendering business process, including signing a contract, creating rendering projects, submitting rendering jobs, job management and project settlement, can be completed on the same platform. Among these functions mentioned above, rendering job management is one of the most important functions of the platform. As Fig. 2 shows, the platform provides a friendly GUI to help users manage the rendering jobs. Through the GUI, all kinds of details of the rendering jobs can be viewed, including job ID, job name, job owner, job status, the number of running frames, the number of remaining frames, etc. Users can also do a lot of operations, such as, create a new job, search jobs, copy jobs, delete jobs, stop a running job, re-run a job, preview rendering results and so on.

Figure 2. Rendering Job Management

Golden Farm Cluster Rendering Platform provides the function to preview the rendering results by the means of thumbnail. Users can choose one frame to preview its rendering result, and also can choose a rendering job to preview the rendering results of the whole job. From Fig. 3 we can see the rendering results of all frames of the job we choose. Besides the rendering results, the rendering status of one frame, and the number of frames that have completed or being rendered can be viewed conveniently.

Figure 3. Preview of The Rendering Results

In order to illustrate the high performance of Golden Farm Cluster Rendering Platform, we have conducted some comprehensive tests on the famous “TianHe 1A” super computer. The following Table.1 is a contrast of the time-consuming of rendering 2000 frames respectively on 800, 1200, 1600 and 2000 computing nodes.

Table 1. Contrast of Rendering Time

Number of Rendering Nodes	Number of Frames	Rendering time (min:sec)
800	2000	25:36
1200	2000	25:23
1600	2000	25:46
2000	2000	22:25

Up to now, it is impossible for most existing rendering scheduling and management software to handle ultra-large-scale compute clusters with 600 or more computing nodes.

However, as the illustrated experiment results, Golden Farm has been specialized designed for ultra-large-scale rendering management. It can effectively conduct rendering management on high-performance computer with up to 2000 computing nodes. And it has created an important record, rendering a 3D model by using 24000 CPU cores in parallel.

IV. CONCLUSION

In this paper, we have introduced a new type of software architecture for ultra-large-scale rendering cloud. After the test and analysis described above, it is evident that this software architecture provides a highly reliable system software platform for ultra-large-scale rendering cloud. Golden Farm Cluster Rendering Platform combines the application of rendering and high performance computing cluster. It is an effective solution for ultra-large-scale rendering. It also has high availability, reliability and scalability and can give full play to the advantage of high performance computers.

ACKNOWLEDGMENT

The authors acknowledge the financial supports by the major national S&T program (E0305/1112/JC03), the 111 Project (B 08042) and Program Project of CUC (XNG1138) as well as Beijing Municipal Special Fund for Cultural and Creative Industries (2009).

REFERENCES

[1] http://en.wikipedia.org/wiki/Rendering_%28computer_graphics%29

[2] Chunming Gao, Limin Zhang, Shiying Li. “Research of energy saving control in 3D animation rendering cluster”. Computer Engineering and Applications, 2009, 45(5): 67-70.

[3] Minli Dai. “The Reseach and Development of Function Extension for Render Farm based on Muster”[D]. Hubei:Central China Normal University. 2007.

[4] Guoxin Tan, Zhanlei Deng, Jing Zhang, Rong Li. “Research on Muster-Based 3Dmax Network Rendering”.2007.

[5] Changda Chen. “Research on Job Management of Cluster Rendering System based on Hadoop”[D].Guangdong: Guangdong University of Technology. 2010.

[6] Qiuming Luo, Hongyuan Sun. “Building Technologies and Framework Design of Render for Cluster Management Software”, June 2008, 34(11): 249-251.

[7] Huajun Jing, Bin Gong. “The Design and Implementation of Render Farm Manager Based on OpenPBS”. In: Proceedings of 2008 IEEE 9th International Conference on Computer-Aided Industrial Design & Conceptual Design Vol.2, 2008, pp.1056-1059.

[8] Chaojian Fang, Yujiao Zhao, Zhengjun Wang. “Research and Design of a Service Management System for Deadline Render Farm”. 2009 International Conference on Environmental Science and Information Application Technology, 2009, pp.542-545.

SOA and Cloud Service Provisioning Framework

E Oppong, S. Khaddaj

School of Computing, Information Systems and Mathematics,
Kingston University, Kingston upon Thames, KT1 2EE, UK
{e.oppong, s.khaddaj}@kingston.ac.uk

Abstract – Internet technology and advances in IT in general has made another paradigm of distributed computing sort after strategy for IT organisations. From client-server computing, Grid computing and now cloud computing, distributed computing architecture made it possible for multiple uses of IT infrastructure and application with managed allocation policies to utilise shared resources and applications. Service oriented computing (SOC) implementing service oriented architecture (SOA) underlines computing as a service by leveraging internet technology such as webservice. Cloud computing is promoted as the type of distributing computing that will provide anything from basic computing need to high end delivery of IT services. Hence in this paper we consider two areas of distributed computing architecture, cloud and SOA by discussing the principles and how this fits into our framework to optimised provisioning of SOA over Cloud.

Keywords- Service Oriented Architecture, Cloud Computing.

1. INTRODUCTION

The dynamism of distributed computing has changed with cloud computing been promoted by industry players as a computing paradigm to deliver computing resources as services on demand over the internet. Buyya et al, [2] emphasise the use of technologies such as virtualisation over the internet as differentiating cloud over other distributed computing architectures. The services have different composition for specific solution based on users specific requirements, these requirements are mostly Quality of Service (QoS) that are expected to be met by the providers. Organisation are faced with implementing their own cloud (private cloud) or sourcing from a provider of cloud services (public cloud), or part source and part controlled (Hybrid) to reduce cost.

Cloud offer services like everyday utility to users without the need to know about the location of the service, this presents a challenge to meet user requirement by allocating resource without wastage in datacentres. With SOA architecture, businesses are able to deliver IT solutions as business services making SOA a compliment to the implementation of cloud [4]. SOA share similar technologies and protocols such as WSDL [12] in distributed computing allowing organisation to deliver services to its users. With the appropriate implementation SOA could deliver cloud service in ways that will improve the running of cloud facilities.

In this paper we consider Cloud and SOA in an attempt to introduce a framework for mapping software services over Cloud. The remainder of the paper is organised as follow. Sections 2 and 3 looks at cloud and SOA with section 4 showing our proposed mapping framework and discusses some of its components before leading on to section 5 which shows early experiment using cloud simulator CloudSim. Section 6 concludes with our future direction to develop the framework.

2. CLOUD COMPUTING

Cloud computing is a concept that is built firmly on distributed computing architecture of Grid computing. Cloud facilities consist of a single computer or a cluster of computers as data-centres connected together to provide on-demand services. High availability of resources is key to the delivery of cloud computing, data centres are situated in different geographical locations with many serving as backup in the unlikely event of failure at a data centre. Redundancy of data centres ensures providers are capable to deliver services and maintaining Service Level Agreement (SLA). The services here are Infrastructure as a Service (IaaS), Software as a Service (SaaS) and Platform as a Service (PaaS) (figure 1).

With these kinds of services, computing solutions can be modeled to meet a set of user needs as a combination of all services or one aspect of the service. Amazon, Google, Microsoft, IBM, Oracle and other organisation provide cloud services as follow.

Infrastructure as a Service (IaaS)

Computing resources such as storage [5] network and other essential hardware needed are provided on a rented basis to consumer for use to deploy and run application including operating systems. The

978-0-7695-4818-0/12 $26.00 © 2012 IEEE
DOI 10.1109/DCABES.2012.104

main emphasis is the use of resources which are controled and managed by the provider whilst the consumer takes control of deployed software and hardware that are licenced to be used.

Platform as a Service (PaaS)
PaaS offers consumers the environment to develop and run software application over the internet [4] with tools to develop, test and run software application and services. Google App Engine[1] is an example of PaaS which allows consumers to develop application running on Google's cloud infrastructure. The platform environment is mainly for application development, this saves the consumers time and money to purchase and maintain the necessary infrastructure for application development.

Software as a Service
This type of services has similarities with client-server architectures in mainframe computing where the clients only requires a thin client to run and use software that are distributed on a back-end computing infrastructure through web-based interface.

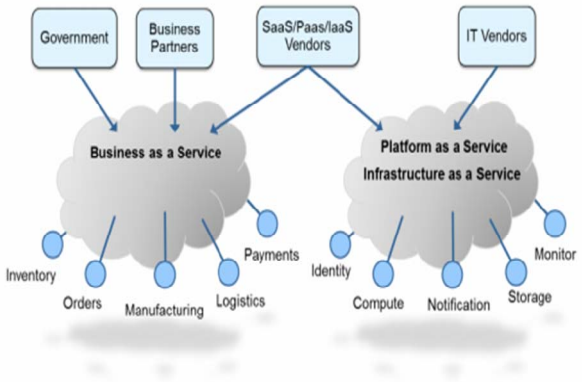

Fig 1: The Cloud and cloud services[2]

3. SERVICE ORIENTED ARCHITECTURE (SOA)

IT organisation uses SOA to model operation that represents a business model of its functions. SOA effectiveness is based on webservice, implementation of various operations as services (messages) delivering operational functionality to support an application when needed. As cloud becomes part of an organisations IT fabric, SOA makes the utilisation of cloud beneficial to the organisation, building on key SOA concepts such as availability, performance, reliability and interoperability. Proper implementation of SOA can enhance an organisation IT stronghold or poorly adopted can show vulnerability with the IT strategy been implemented. Where SOA is implemented poorly testing becomes disjointed making it complex and impossible to track and trace and measure the success of SOA. Implementing SOA based on the flexibility and the underlining principles makes the organisation's IT strategy truly fit-for-purpose and can be measured and tested to ensure greater integration of SOA when tested against SOA principles [6].Organisations will potentially miss-out on SOA if proper testing is not carried out which are QoS related, performance, interoperability, functional and suitability.

4. MAPPING SOA TO CLOUD FRAMEWORK

The framework consists of an intelligent resource allocation and management broker - Resource Manager (RM) that analyse resources using both QoS requirement provision of resources to map service and historical data of resource allocation used to determine the best possible match. There are many forms of identifying the resources; however, the best possible approach to be used will be a FIFO service of allocation.

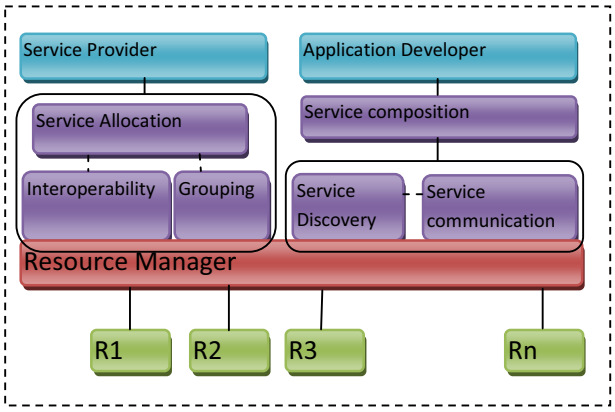

Fig 2: Service Discovery and Allocation

1 https://developers.google.com/appengine/docs/whatisgoogleappengine

2 Dr S. Khaddaj, Service Oriented Cloud Computing

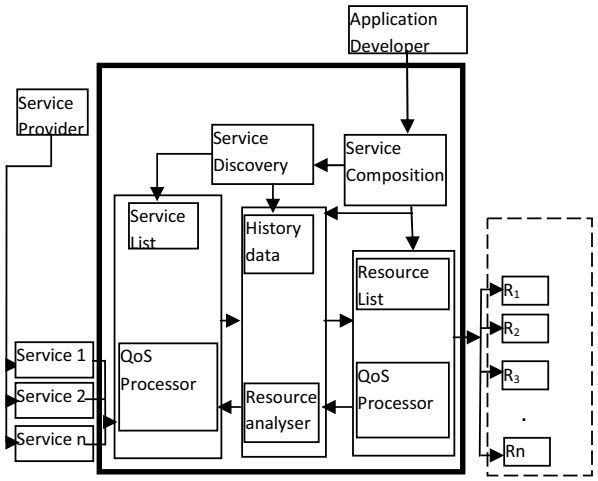

Fig 3: Detailed view of Framework

The architecture combines discovery and allocation based on the QoS provisions of the resources, the RM simply takes request for service allocation, discovers the services and matches the services to the resources.

The structure of the architecture consists of the service provider and the application developer at the top level, the allocation of services is categorised into different areas using QoS factors under the allocation of service from the service provider. The interaction between the application developers looking to discover services for resources is through the resource manager using the QoS provision of the resources to match to that of the services.

3.1 Service Composition:

The service composition collates service request message attributes which is evaluated to measure the capabilities of the resources based on the QoS attributes. The information gathering processes of the composition also enable the accurate computation of the resources and the performance which is recorded in the history repository for categorisation and use.

3.2 Service Allocation:

A service ASIH can give predictive information about the resource that will best suit the execution. For a new service the allocation will require the matching of ASIH attributes relating to the attributes from the resources. On the other hand, a service that has been allocated in a previous process will have information about the resources, attributes relating to the performance, the type of resources and the duration of the process. With this information, the allocation matching can be based on a pre-determined data from history or a new constructed execution, and also creating new allocation data using previous knowledge. The previous allocation might not necessary have all that is required and can be used to create a new one.

3.3 Service Matching

On the first instance a service matching to a resource will be based on the rule of classification of the type of the service weight, fine, course and fat service linking to a specified set of host that is, associating the fat service to the hosts with more capability to execute the service. Service match and allocation history is stored in a repository in the resource manager, the follow up of such service will be allocated based on the information stored for processing similar requests. This process reduces the time taken for identifying suitable services and resources. The information stored is not the actual service or host but mapping strategy for the type of service.

3.4 Authentication of service and Resource

The pool of services and resources are updated to ensure they are accurate and are kept in the history data and resource and service list. New resources and services that are added are authenticated by an Authenticating Agent (AA), the AA authenticates the provider agent based on the criteria for the provision as the framework request. The AA request the information for authentication from the provider, the information is tested against the required criteria which is stored in the framework repository. Only when the information satisfied the criteria before the resource and service is kept on the list.

When a provider provides updated information, the update would enforce regression testing to maintain the authenticity of the information kept on record.

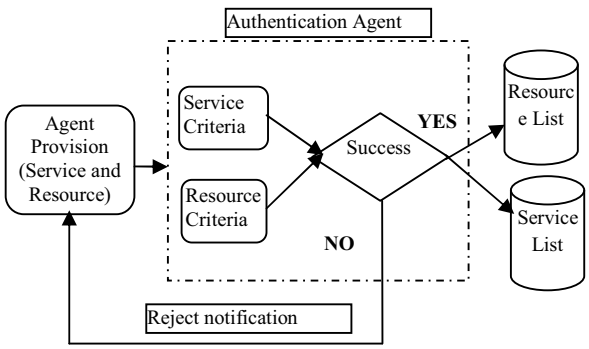

Fig 4: Authentication and service allocation

3.5 Resource Analyser - Service categorisation

The allocation will be monitored and re-adjusted if for example service A is allocated to resource R1 but R1 is in the pool to be allocated for service type C (fine-grain), when a request from C type is received, A will be re-allocated to the next appropriated resources (not necessarily the dedicated host for type A service) that will complete the execution with less execution time delay.

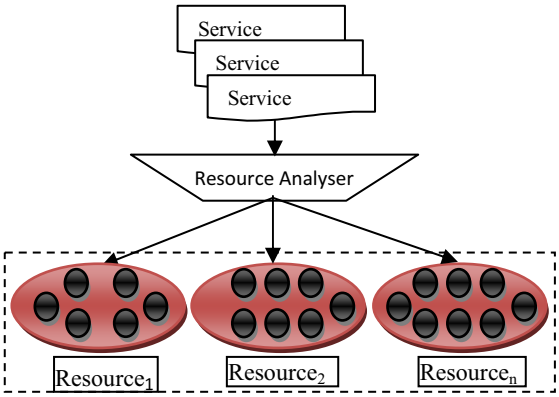

Fig 5: service categorisation

3.6 Service and Resource Mapping

The list of services and resources are maintained to enhance the allocation and mapping of services to resources. The services list offers quick approach to map services to resources using the previous mapping strategy. This approach maintains the needs to records the performance in terms of failure of execution and the level of success of previous rsources and services.

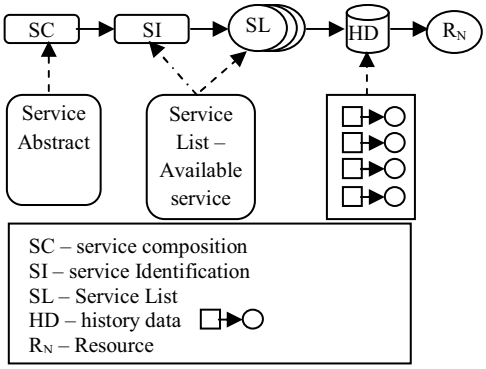

Fig 6: Resource Mapping

5. Experiment and Evaluation

We carried out an experiment to simulate the behaviour in terms of resource usage (CPU and RAM) in cloud computing environment. Our experiment was carried out using cloud simulator CloudSim. Cloudsim is a cloud simulation toolkit for creating various cloud computing situations on a single computer with single simulating single or multiple datacentres. Cloudsim support virtualisation of resources which makes it capable to simulate application level scenarios compared to other simulating toolkits like SimGrid and GridSim [3].

Our initial experiment is focused on the utilisation of resources in the cloud environment. We setup a simulated experiment using cloudsim with one datacentre with 10 host machines. Figure 7 and 8 shows the CPU usage RAM usage with 32 virtual machines (VM), figure 9 and 10 showing results with 64 VM's created and allocated to the 10 hosts. Rejections and allocation of service to the VM were unaccounted at this stage. Every VM represents a user application which is composed of individual services following service allocation, categorisation and composition as discussed in the previous sections, but the main aim as mentioned above is to test resource utilisations.

Experiment 1, Host= 10, VM =32

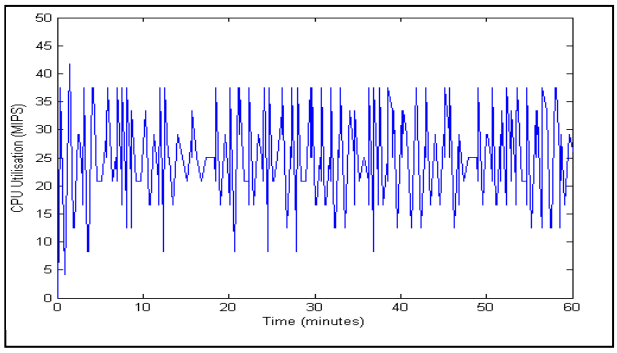

Fig 7: CPU Utilisation

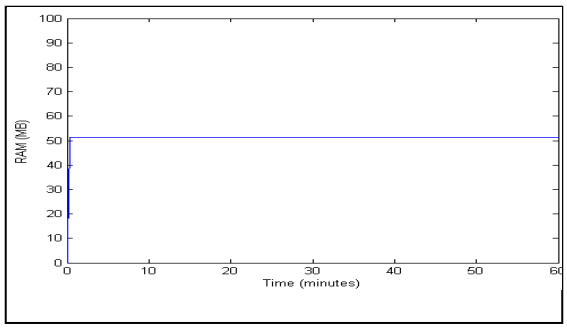

Fig 8: RAM Usage

Comparing the two results RAM usage maintained a level of consistency to show there is little waste in RAM space, this can be attributed to the configuration of the simulation.

Experiment 2, Host= 10, VM =64

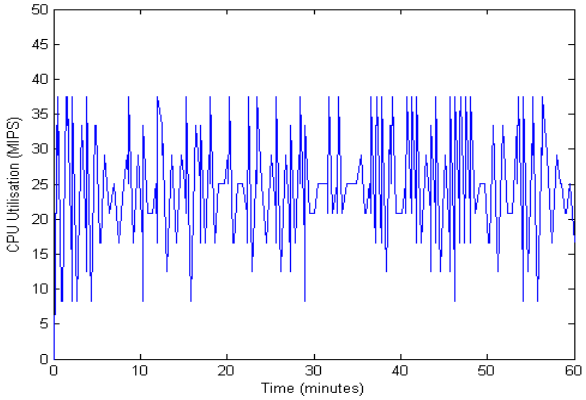

Fig 9: CPU Utilisation

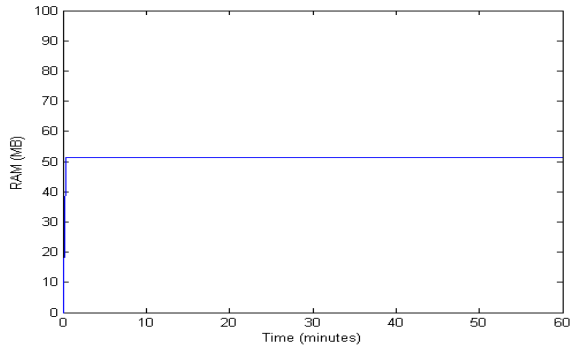

Fig 10: RAM Usage

With the demand of processing and execution time in the number of host, there is wastage of resource and processing time, example if a 2 hosts has 2400MIPS and a request of 3 VM's with 1000MIPS, the likely event is two VM's will be executed on one host and the third rejected or sent to the second host. This leaves a waste of 400MIPS on the first host.

6. CONCLUSION

Cloud computing fits in well with current IT eco-system providing organisations with boundless capability. Cloud computing share similar challenges with other distributing computing paradigm like grid and P2P for effective and optimised use of resources. In this paper we undertook the task of looking into how SOA can be mapped into cloud computing with a proposed framework to be developed in the future. SOA provides a good architecture for scalable, business oriented implementation that align business process with an organisations IT strategy. Services as a representation of business process can be delivered in a form that cuts down on cost and limit vulnerability to the organisation. Cloud is everywhere, meaning IT strategy implementing cloud computing will offer boundless access to services, the challenge is to optimise resources allocation and provide a solution that delivers based on users specific request.

With the results of the initial experiment, we intent to further introduce our approach to resource utilisation and allocation based on quality of service. Cloudsim offers us a platform to test our framework idea, the initial experiments give us the information about resource allocation and behaviour in cloud environment. The challenge ahead is to provide the algorithm and the implementation mechanism to test the framework in a controlled environment like cloudsim.

7. REFERENCE

1. Schwarz, J, H.: Service Oriented Architectures and Grid computing – A New Generation of Applications for Grid Enabled Data Centers and Public Utility Computing. Sun Microsystems. 2005
2. Buyya et al, : Cloud computing and emerging IT platforms: Vision, hype, and reality for delivering computing as the 5th utility. 2008
3. Rodrigo N. Calheiros et al: CloudSim: A Novel Framework for Modelling and Simulation of Cloud Computing Infrastructure and Service 2009
4. Cloud Computing and SOA http://www.mitre.org/work/tech_papers/tech_papers_09/09_0743/09_0743.pdf
5. Amazon Simple Storage Service (Amazon S3) http://aws.amazon.com/s3/
6. Rizwan Mallal : Pillars of SOA Testing
7. http://www.crosschecknet.com/soa_testing_pillars.php (Last visited 29/06/2012)
8. Josuttis, N M.: SOA in Practice: The Art of Distributed System Design. O'Reilly. 2007
9. Schmid, M. Kroeger, R.: QoS-Management in Service Oriented Architecture. In LNCS: Distributed Applications and Interoperable Systems (44-57) – (2008)
10. S. Khaddaj: Service Oriented Cloud Computing ISEEC 2012
11. Rob High: What's SOA got to do with cloud computing?:http://www-01.ibm.com/software/solutions/soa/newsletter/november11/whats_soa_got_to_with_cloud.html (last visited - 206/06/2012)
12. https://developers.google.com/appengine/docs/whatisgoogleappengine

High Efficiency Algorithm of Correctness of Web Service Composition Under Environment Constraint Based on IPN

Yinghua Feng
Department of Basic Courses
Huainan Union University
Huainan, China
e-mail: 278894811@qq.com

Lu Liu
Anhui University of Science and Technology
Huainan, China
e-mail: 604580255@qq.com

***Abstract*—The correctness of the composite Web service under the environment constraint needs new model and analyze methods. First, Web services domain and Web environment domain models based on interface Petri net are proposed. Then, an efficient determining algorithm about soundness of composite Web service is presented for the sake of analyzing the soundness of the composite Web service under the environment constraint. Finally, the algorithm is programmed and its validity is testified through the concrete example.**

Keywords—Interface Petri Net; Environment Constraint; Web Service Composition; Soundness; Efficient Algorithm

I. INTRODUCTION

The traditional Web services composition research usually only pays attention to the relationship among service components, and ignores the constraints between service components and the environment. But in fact the environment plays an important role in the soundness of Web services composition.

For example, the video streaming media Web service is composited by many Web service components, if it wants to work correctly, it must rely on the high bandwidth environment. So the soundness analysis of Web service composition under environment constraint becomes more important and necessary. In practical application, the correctness of composite Web service is not only constrained by other Web services, but also constrained by the Web environment. Because the Web environment has special features, it is difficult to model and analyze by traditional methods and the research on the correctness of composite Web service under environment constraint demands new modeling tools and analysis methods.

The literatures [1, 2] analyzed the influence on the mobile network service discovery by electromagnetism and bandwidth environment and proposed the perspective that the environment influences the correctness of services, but it lacked rigorous formalized model. In literature [3], the authors established the formalized model of the service composition through the service tree theory, etc. and presented a decision method about the soundness of the composition. However, the environment constrain factor was ignored.

Interface Petri nets model can model and formalized mathematical analyzes Web services and Web environment. Modeling process is realized through mapping the physical model to the interface Petri nets model, and dynamic behavior analysis of the model is realized through working the interface Petri nets. Interface Petri nets combines the structure analysis and behavioral analysis functions. Therefore Interface Petri nets have advantages on solving the problem.

But with the expansion of the modeling scale, and nets size and complexity are increase as exponential, the nets "explosion" problem appears. The "explosion" problem increases the difficulty of determining soundness by looking for reachable sequences in the running nets. In order to reduce the time and space complexity of the algorithm and improve the efficiency of the algorithm, the algorithm proposed in this paper will try to avoid massive nets operation.

II. PRELIMINARIES

At present, Web service composition doesn't have a unified and strict definition in academic and business. Generally, Web service composition is thought that it is such a process that some single by Internet and other network form. Usually, Web environment includes three parts: user environment, computing environment and physical environment. Web service environment does not provide true services, but the Web environment influences Web service composition, operation and correctness. This influence is called environment constraint.

Definition 1: Web service domain

A Web service domain (SD) is a 4-tuple $SD=(S_I,S_o,S_C,C_I)$, where S_I is a service input, So is a service output, Sc is a service component and C_I is a communication interface.

Definition 2: Web environment domain

978-0-7695-4818-0/12 $26.00 © 2012 IEEE
DOI 10.1109/DCABES.2012.11

A Web environment domain(ED) is a 4-tuple $ED = (E_I, E_o, E_C, C_I)$, where E_I is an environment input, Eo is a environment output, Ec is a environment component and C_I is a communication interface.

Definition 3[4, 5]: Petri Net

Petri net is a very important modeling tool for concurrent system modeling and dynamic behavior analysis which was first proposed by German C.A.Petri doctor in 1962. Petri net can not only describe the system structure, but also analyze the system dynamic properties.

A Petri Net is a $3\text{-tuple} N = (S, T; F)$, where

(1) $S \cup T \neq \phi$

(2) $S \cap T = \phi$

(3) $F \subseteq ((S \times T) \cup (T \times S))$

(4) $dom(F) \cup cod(F) = S \cup T$

$dom(F) = \{x \in S \cup T \mid \exists y \in S \cup T : (x, y) \in F\}$

$cod(F) = \{x \in S \cup T \mid \exists y \in S \cup T : (y, x) \in F\}$

Definition 4: IPN

Web services composition is an open system. Web service composition and Web service components will communicate, Web service composition and the environment will also communicate. The interface is the physical and logical realization of the component communication.

An Open Petri Net is a $7\text{-tuple}\ IPN = (S, T; F)$ [6], where:

(1) $P \cup I \cup O, T, F)$ is a Petri net;

(2) P is a set of internal places;

(3) T is a set of transitions;

(4) F is a set of flow relations;

(5) I is a set of input places, and $^{\bullet}I = \phi$;

(6) O is a set of output places, and $^{\bullet}O = \phi$;

(7) i is the initial marking;

(8). f is the final marking, and f is a deadlock.

We call the set $I \cup O$ is the interface places of the IPN. Two IPNs M and N are disjoint, if $\mathrm{P_N, P_M, I_N, I_M O_M O_M, T_N, T_M}$ are pairwise disjoint.

Definition 5: Models Mapping

Let $SD = (S_I, S_o, S_C, C_I)$ be a Web service domain, $ED = (E_I, E_o, E_C, C_I)$ be a Web environment domain and $M = (P, I, O, T, F, i, f)$ be an open Petri Net. If $S_I \subseteq \mathrm{i}$, $S_o \subseteq f$, $S_C \subseteq \mathrm{P}$ and $C_I \subseteq I \cup O$, SD should be mapped to an IPN and if $E_I \subseteq \mathrm{i}$, $E_o \subseteq f$, $E_C \subseteq \mathrm{P}$ and $E_I \subseteq I \cup O$, ED should be mapped to an IPN.

Through interface places, Web environment communicates with Web service, thus an interrelated whole is formed structurally and behaviorally. Because of the communication, Web environment inevitably constrains Web service behavior which is reflected by the correctness of composition.

Definition 6[7]: $\mathrm{A} \oplus \mathrm{B}$

Let A and B be two IPNs, their composition is an IPN $\mathrm{A} \oplus \mathrm{B} = (\mathrm{P, I, O, T, F, i, f})$ defined by:

(1). $P = P_A \cup P_B \cup (I_A \cap O_B) \cup (I_B \cap O_A)$

(2). $I = (I_A \setminus O_B) \cup (I_B \setminus O_A)$

(3). $O = (O_A \setminus I_B) \cup (O_B \setminus I_A)$

(4). $T = T_A \cup T_B$

(5). $F = F_A \cup F_B$

(6). $i = i_A \cup i_B$

(7). $f = f_A \cup f_B$

Two IPNs A and B are composable if and only if $(P_A \cup P_A \cup O_A \cup T_A) \cap (P_B \cup P_B \cup O_B \cup T_B) = (I_A \cap O_B) \cup (O_A \cap I_B)$

.

Definition 7[8]: Soundness of INP

Let N be an interface Petri net. The skeleton of N is defined as the Petri net $S(N) = (P_N, T_N, F)$ with $F = F_N \cap ((P_N \times T_N) \cup (T_N \times P_N))$ .We use $R(N)$ as a shorthand notation for $R(S(N), i_N)$. N is called sound if for any marking $\mathrm{m} \in R(N)$ we have $S(N) : \mathrm{m} \xrightarrow{*} f_N$.

In many cases, multiple Web service domains share a Web environment domain. As shown in Figure 1, we have three components A, B, and C. The composition of A with B is sound, as well as the composition of B with C. However, the composition of the three is not sound.

Definition 7[8]: $\Omega_{A,B}$.

A and B are two composable IPNs, $\Omega_{A,B}$ holds if and only if :

$\forall\ m \in R(A \oplus B), \sigma \in (T_A)^*$

$: (A : m \mid P_A \xrightarrow{\sigma} f)$

$\Rightarrow (\exists \tilde{\sigma} \in (T_A \cup T_B)^* :$

$(A \oplus B : m \xrightarrow{\tilde{\sigma}} f_A + f_B) \wedge \tilde{\sigma} \mid T_A = \sigma$

A and B are two composable IPNs, if A satisfies soundness and $\Omega_{A,B}$ holds, $\mathrm{A} \oplus \mathrm{B}$ satisfies soundness. Let A, B, C are three pairwise composable IPNs such that A and C have disjiont interface places, A, B, C pairwise composable, if $\mathrm{A} \oplus \mathrm{B}$ satisfies soundness, and $\Omega_{B,C}$ holds, $\mathrm{A} \oplus \mathrm{B} \oplus \mathrm{C}$ also satisfies soundness.

III. HIGH EFFICIENCY ALGORITHM OF CORRECTNESS OF WEB SERVICE COMPOSITION UNDER ENVIRONMENT CONSTRAINT BASED ON IPN

According to the definitions of Web service domain, Web environment domain and interface Petri nets, they are similar on the structure and function. They all include input terminal, output terminal, interface terminal and the internal components which have the logical connection among them. Therefore, we can map the components of Web service domain and Web environment domain to the corresponding components of open Petri nets. Through the one-to-one mapping we can model Web service domain and Web environment domain by open Petri nets.

The premise of the Web environment constraint is that Web environment and Web service can compose, so we must determine whether Web environment and Web service can compose firstly. A and B are two IPNs, if (PA ∪ IA ∪ OA ∪ TA) ∩ (PB ∪ IB ∪ OB ∪ TB) = (IA ∩ OB) ∪ (OA ∩ IB) holds; Then A and B can compose[6].

In the actual application, Web service domain/Web environment composition has large number and scale, so the interface Petri net model also become very complex and massive. It is almost impossible to run the interface Petri net with a large scale. Hence this paper proposes a new high efficiency determining algorithm about soundness of Web service composition under environment constraint.

Algorithm 1: soundness decision algorithm for arbitrary Web environment domain/Web service domain composition

Input: D1,……Dn are Web environment domains/Web service domains

Output: decision outcome

(1). By definition 5, put D1,……Dn map into IPN: $A1,\ldots\ldots An$, then execute step (2).

(2). By definition 6,if $(P_i \cup P_i \cup O_i \cup T_i) \cap (P_{i(c)} \cup P_{i(c)} \cup O_{i(c)} \cup T_{i(c)}) = (I_i \cap O_i) \cup (O_{i(c)} \cap I_{i(c)})$ holds, $A1,\ldots\ldots An$ are composable, then execute step (3). Otherwise algorithm terminates and returns the result that they do not satisfy soundness.

(3). $A1,\ldots\ldots An$ is a domain tree with the parent A1, if and only if let $c:\{2,\ldots\ldots n\} \to \{1,\ldots\ldots n-1\}$ be such that:

$\forall i \in \{2, \ldots \ldots n\} : c(i) < i$

$\forall 1 \le i < j \le n : i = c(j) \Rightarrow I_{Ai} \cap O_{Aj} \neq \theta \vee O_{Ai} \cap I_{Aj} \neq \theta$

$\forall 1 \le i < j \le n : i = c(j) \Rightarrow$

$I_{Ai} \cap O_{Aj} \neq \theta \vee O_{Ai} \cap I_{Aj} \neq \theta$

, then execute step (4).

(4). If $A1,\ldots\ldots An$ is a domain tree with the parent A1, A1 is sound and $\Omega_{Ai,Ac(i)}$ holds , $A1 \oplus \ldots\ldots \oplus An$ is also sound, then execute step (5). Otherwise algorithm terminates and returns the result that they do not satisfy soundness.

(5). Algorithm terminates and returns the result that composition of $A1,\ldots\ldots An$ satisfies soundness.

IV. EXAMPLE ANALYSIS

To realize the automatic analysis, the paper uses C# to program the algorithm by Microsoft Visual Studio 2008 platform. Because the map from Web environment domain/Web service domain into the IPN involves semantic, logic analysis and other factors, we use artificial way to edit the Web environment domain/Web service domain model according to the XML standard, in order to realize the map from the physical model to the IPN model. After software imports an XML file, Visual IPN models can automatically be generated. Then we determine the soundness of the IPN according to the above algorithm, finally the analysis operation results and conclusions are given.

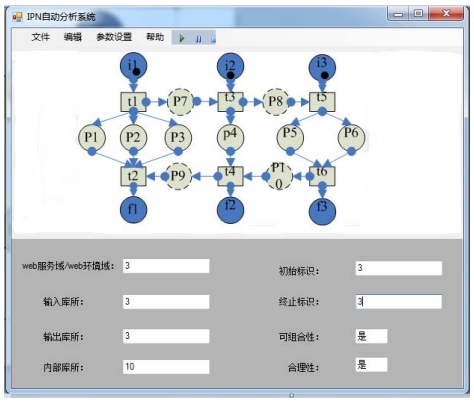

Figure 1. Soundness automatic analysis system based on IPN

In the IPN model, the operation times of transition t is usually used to estimate the time complexity, and every time the transition t runs is recorded as a unit running time. The marking state of the place is usually used to estimate the space complexity, and the number of the place in a reachable sequence is recorded as a space consumption unit.

Through the experimental simulation, we compare the algorithm in the paper and the traditional algorithm. The specific process is as follows:

The services generated randomly are used as test cases which follow OWL-S.

Test environment:

CPU: Intel core I3 2.4 GHz;

RAM:4GB;

OS : Windows7.

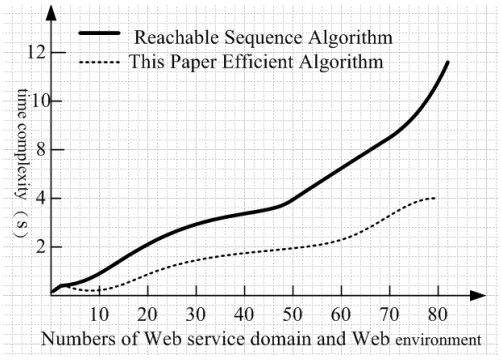

Figure 2. The two algorithm time performance comparison

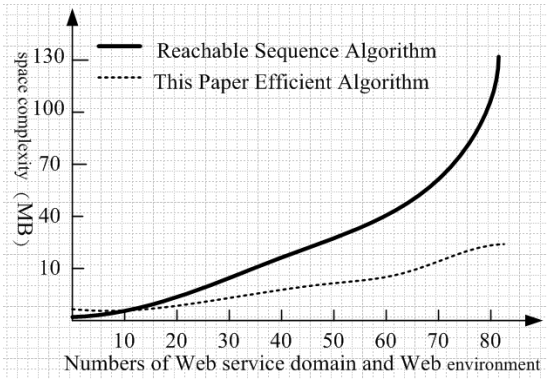

Figure 3. The two algorithm space performance comparison

Through the analysis, the time and the space complexity of the algorithm in the paper are similar to the linear growth, and the time and the space complexity of the traditional algorithm are similar to increase exponentially. Therefore the algorithm presented in the paper has advantages on reducing the time space complexity and solving the nets "explosion" problem.

V. CONCLUSION

Modeling and analyzing Web service composition under the environment constraint based on interface Petri net is an effective method. Through experiment we can find that the presented determining algorithm about soundness of composite Web service under the environment constraint is correct and effective. This algorithm performance in time complexity and space complexity is better than the method of finding reachable sequences in running nets. The future research emphasis is on transplanting this decision algorithm to commercial Web protocols and languages.

REFERENCES

[1] Ahlem Ben Hassine, A.Joshi.Finin, K.M.van Hee and W.M.P.vander Aalst. A Constraint-Based Approach to Horizontal Web Service Composition Munich: springer, 2006:130–143.

[2] O.Ratsimor, V.Korolev, A.Joshi.Finin, Ahlem Ben Hassine and N. Lohmann. Agents2Go:An Infrastructure for Location-Dependent Service Discovery in the Mobile Electronic Commerce Environment.New York: ACM Mobile Commerce Workshop, 2007: 163-165.

[3] W.M.P.vander Aalst, K.M.van Hee and TM. Weske. Service Trees. Eindhoven: echnische Universiteit Eindhoven, 2009:324-327.

[4] Wu Zhe-hui. Petri net theroy. BeiJing : China Machine Press, 2006:19-23.

[5] Yuan Chong-yi. Petri net principle and application. BeiJing : Electronic Industry Press, 2005:12-14.

[6] N.Lohmann, O.Ratsimor, V.Korolev, A.Joshi.Finin, Ahlem Ben Hassine and K.M.van Hee. From Public Views to Private Views: Correctness-by-Design for Services. Munich: springer, 2007:139–153.

[7] Kees M.van Hee, Ahlem Ben Hassine, A.Joshi.Finin, K.M.van Hee and W.M.P.vander Aalst. Compositional Service Trees. Munich: springer, 2009:287-289.

[8] K.M.van Hee, W.M.P.vander Aalst, K.M.van Hee and M. Weske. A framework for linking and pricing nocurenopay services. Munich: Springer, 2009:176-179.

[9] M. Beisiegel, N.Lohmann, O.Ratsimor, V.Korolev, A.Joshi Finin and Ahlem Ben Hassine. An SOA-Based Architecture Framework[J]. International Journal of Business Process Integration and Management, 2007, 12:91-91.

[10] P. Massuthe, W.M.P.vander Aalst, K.M.van Hee and M. Weske. Compositional service trees. Eindhoven: Technische Universiteit Eindhoven, 2009:23-25.

[11] W.M.P. vander Aalst, K.M.van Hee, M. Beisiegel, N.Lohmann, O.Ratsimor, V.Korolev and A.Joshi.Finin. From Public Correctness of Services. New York: Computer Science, 2008:193-195.

[12] W.M.P. vander Aalst, M.Beisiegel, N.Lohmann, O.Ratsimor, V.Korolev, A.Joshi.Finin and Ahlem Ben Hassine. Multi-party Contracts: Agreeing and Implementing Interorganizational Processes. The Computer Journal, 2009, 8:223-231.

[13] F. Casati, H. Kuno, V. Machiraju, W.M.P. vander Aalst and M.Beisiegel. Web Services Concepts, Archi-tectures and Applications. Munich: Springer, 2007:342-345.

[14] G.Decker, N.Lohmann, O.Ratsimor and M. Weske. Local enforceability in interaction petri nets. New York: Computer Science, 2007:195.

[15] Xin Gao.Constraint-aware Correctness Analyzing of Composite Web Service Based on Open Petri Net. New York: dcabes2011, 2011:195.

[16] W. Vogler, O.Ratsimor, V.Korolev, A.Joshi.Finin, Ahlem Ben Hassine and N. Lohmann. Asynchronous communication of petri nets and the renement of transitions. Munich: springer, 2008:605-616.

[17] N. Lohmann, P.Massuthe, C. Stahl, and D.Weinberg. Analyzing Interacting BPEL Processes. New York: Computer Science, 2006:17-32.

[18] N. Lohmann, P. Massuthe, and K. Wolf. Operating Guidelines for Finite-State Services. New York: Computer Science, 2007:321-341.

Quality Measurement for Cloud Based E-Commerce Applications

Jay Kiruthika
Kingston University
jay.kiruthika@gmail.com

Dr.Gerard Horgan
I. T. Consultant,
gmhorgan@hotmail.com

Dr.Souheil Khaddaj
Kingston University
s.khaddaj@kingston.ac.uk

***Abstract*— Cloud based e-Commerce applications are favored over traditional systems due to their capacity to reduce costs in various aspects like use of resources, low operating costs, eliminate capital costs, low maintenance and service costs. Its core functionality of optimizing performance and its automatic system recovery is crucial in web applications. Using a cloud platform for web applications increases productivity and decreases the replication of business documents saving businesses money in the current economic climate. A stable system is needed to achieve this and quality measurement is crucial to establish baselines to help predict resources for the future of the business. The proposed quality measurement model is one such designed for Cloud based e-Commerce applications. It aims to create a repository or an error-Knowledge Management System(e-KMS) for known online defects with capacity to add in future defects as they occur when using the applications. By mapping these defects directly to quality factors affected, accurate quality measurement can be achieved.**

Keywords-Software Quality; Quality measurement; Software Quality Management; Software Defects; Cloud Computing.

I. INTRODUCTION

Cloud based web applications differ from business to business depending upon their quality criteria. Current businesses use a business specific model to measure quality. In this paper a generic model is proposed which can be used for all cloud based web applications. As all web applications including the cloud based ones log in user requests as it executes in web logs, it can be used to calculate the frequency of a particular error occurrence. The web logs store defects from user perspective as well as system perspective. The System Event logs, Application logs, Security logs log the defects mostly from system perspective. As the cloud based web applications are geographically distributed the weblogs can be used as fingerprint to map quality. Cloud service providers store individual weblogs for separate applications. Using these web logs an e-KMS can be developed using the known defects as a common repository and the failed requests or defects can be classified according to its criticality of impact on the business. Gerald Weinberg defines quality in Quality Software Management: Systems Thinking, as "Quality is value to some person" [1]. This definition stresses that quality is inherently subjective – industries view of software quality varies depending on their goals and management policies.

A good software quality management model is driven by essential views of stake holders, project managers, business managers, financial managers, operational managers, applications managers and the end users. Businesses tend to measure quality and align its business goals by using Key performance indicators for measuring and monitoring revenues, gross margins, return on investment, productivity, customer satisfaction etc. [4].

II. KEY QUALITY FACTORS

The cloud based web applications normally rely on key quality factors like performance, availability for quality measurement. They are given priority from a cloud service provider's point of view to user's requirement. For example in air traffic control management system maintainability, correctness and reliability are given priority over performance as they need to be stable. The businesses tend to focus on the quality criteria and factors needed for applications which are referred to as Key Quality Factors (KQF) [6] [7] and these need not be the same for all the software it develops. This proposed generic model takes in the most of the quality factors and based on the criteria, essential views and tradeoffs can be done depending on Service Level Agreements (SLAs) [8] [9] to measure quality. The quality factors in this proposed model are defined using ISO 9126 [5] as listed below:

Performance
5 – Performed well and used required resources
4 - Performed satisfactory and used required resources
3 - Performed satisfactory and used resources slightly more than acceptable
2 - Performed poorly and used vast resources
1 - Did not perform and used all resources

Maintainability
5 - Easy to maintain
4 - Mostly easy to maintain
3 - Maintainable on few certain conditions
2 - Difficult to maintain
1 - Cannot be maintained

Security
5 - Not accessible to unauthorized users
4- Accessed by unauthorized users in certain areas but no damage to system
3- Accessed by unauthorized users in certain areas and damages are short term
2 – Accessed by unauthorized users damage is long term
1 – Accessed by anyone, no restrictions

Cost/Benefit
5 - Benefits far exceed Cost
4 - Benefits exceed Cost comfortably
3 - Benefits match Cost
2 - Low Benefits, Cost Exceed
1 - Higher Cost than Benefits

978-0-7695-4818-0/12 $26.00 © 2012 IEEE
DOI 10.1109/DCABES.2012.62

Timeliness
5 - System is delivered way ahead of delivery date
4 - System is delivered ahead the delivery date
3 - System is delivered on the delivery date
2 - System is delivered late after the delivery date
1 - System is undelivered

Correctness
5 – System meets and supports all its functional objectives
4 - System meets and supports most of its functional objectives
3 - System meets and supports some and missed few
2 - System missed 90% functional objectives and only few are achieved
1 - System did not meet any functional objectives

Reliability
5 - System executes and produces same results whenever executed
4 – System executes and produces mostly the same results whenever and wherever executed
3 – System executes and produces often the same results whenever and wherever executed
2 - System executes and produces rarely the same results whenever and wherever executed
1 - System executes and produces nothing when executed

Usability
5 - Easy to use by experienced and inexperienced users
4 - Easy to use by experienced but inexperienced users need training
3 - Often easy to use by experienced with some training and inexperienced users need extensive training
2 - used by experienced and inexperienced users with extensive training
1 - Very difficult/Cannot be used by experienced and inexperienced users and can be used only by a select staff

Availability/Consistency
5 - System required/expected to function in a period of time – Very satisfactory
4 - System required/expected to function in a period of time – Expected level
3 - System required/expected to function in a period of time – Below expected level but not to a very damaging level, down time manageable
2 - System required/expected to function in a period of time – Below expected level damaging level, more downtime
1 - System required/expected to function in a period of time – Not functioning at all

Scalability
5 - Ability/Capacity of a system to perform a given task under increased load -- Very Satisfactory
4 - Ability/Capacity of a system to perform a given task under increased load – Expected level
3 - Ability/Capacity of a system to perform a given task under increased load – Below expected level, slightly damaging
2 - Ability/Capacity of a system to perform a given task under increased load – Below expected level, hugely damaging
1 - Ability/Capacity of a system to perform a given task under increased load – Ceased functioning

III. CONSTRUCTION OF E-KMS FOR HTML AND USER ERRORS

Usually when a web page responds to a request, the underlying html responds with a three digit integer result which may be informational, successful responses, re-directional responses or error page [2] depending upon the situation. The following Table 1 lists few of the web responses and possible reasons with a detailed description. The table also classifies the web responses connected to Key Quality Factors (KQFs) and its impact which are given a value subjective 1-postive, 2-Neutral and 3-Negative depending upon the response.

Normally HTML numbered response can be classed as:

- 1xx - Informational responses - request received and continuing process
- 2xx - Successful responses - Requests successfully received, understood and accepted.
- 3xx – Re-directional responses - Further action must be taken in order to complete the request
- 4xx - Client Error responses - The request contains bad syntax or cannot be fulfilled
- 5xx – Server Error responses - The server failed to fulfill an apparently valid request

Table 1. Html Repository

Web Response / Error Number	Reason	KQFs affected directly/indirectly affected	Impact Negative –3 Positive – 1 Neutral - 2	Description of web responses/ messages
100	Continue	Performance Usability Maintainability	1	The client may continue with its request. This interim response is used to inform the client that the initial part of the request has been received and has not yet been rejected by the server.
400	Bad Request	Performance Usability Maintainability	3	Usually means the syntax used in the URL is incorrect (e.g., uppercase letter should be lowercase letter; wrong punctuation marks).
401 Etc..	Unauthorized	Security Usability Interoperability Maintainability Correctness	3	Server is looking for some encryption key from the client and is not getting it. Also, wrong password may have been entered.

The defects start from HTML code 400. The various key quality factors affected by few of the error codes are also listed in the table and the reasons of the occurrence of the

error are also listed. This repository is used as a foundation to develop the quality model to measure the quality of the software. This repository can be tuned to specific business by including user defined errors or specific application error which might show up in the weblogs. For example database connection error can come under HTML code 500. By sifting through the logs and isolating the reasons which might be logged as part of the application a separate repository can be created to include application errors which can then be included in the quality measurement for an accurate value. Figure 1 below shows the illustration of the processes involved in creating the e-KMS. The impact/severity scale based on the business is given a subjective value according to Likert [3] scale of 1 to 5 and listed in table 2 below. To summarize the proposed e-KMS system has

- Application defects with KQF scoring
- User defects with KQF scoring
- HTML defects with KQF scoring

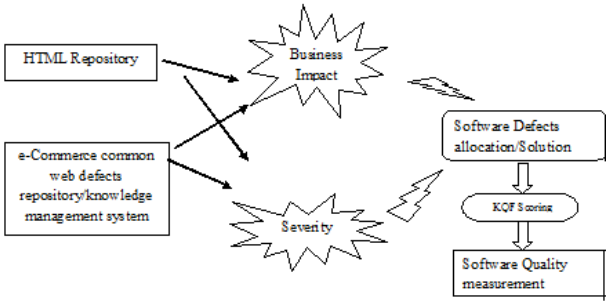

Figure 1. Proposed Repository to measure software quality for cloud based e-Commerce applications using defects

Table 2. Critical Level and their values based on Likert scaling system

Impact Level/Severity on business	Value
Very High/Critical or Red Alert	1
High	2
Medium	3
Low	4
Very Low	5

Most of the common defects can be mapped to solutions and form a repository with added information of what can be done to deal with them which can then be handed over to trained professionals, thereby reducing the burden on the resources, man power and IT development.

In an online cloud based e-business, most of the defects occurring in the software can be logged. This serves as a treasure trove for predicting uptime, downtime, meantime between failure for the business. This information is very crucial for reliability engineering. If key quality factor reliability can be measured using the logs, the rest of the key quality factors can be measured to a certain degree from the same logs provided a subjective value is given to the KQFs based on the essential view. A generic model can then be created using the logs as the repository.

IV. CALCULATING THRESHOLD USING DEFECT FREQUENCY

Defects and predicting them has always been a complex process. Linear equations [10], fuzzy logic, binomial distribution are some of the techniques used in quality models for predicting them.

The "defect potentials" are the total numbers of defects found in five sources in a software lifecycle and can be found in:

- Requirements
- Design
- Source code
- User documents
- Bad fixes or bugs in defect repairs

Frequency of a defect plays an important role in recalculating the critical level of a defect's impact has on quality. It can be defined as the number of times it occurred in a specified interval of time.

There is a need to normalize the frequency of defects to calculate the quality as they are needed to recalculate the KQF scoring from the original e-KMS used as a repository. For example a harmless "file not found" 400 error might be a crucial ebook file which the client has paid for it. If the frequency of the error goes beyond a satisfactory or a baselined value its priority has to be moved up as its criticality has gone up a notch. On the other hand the file not found on the client's perspective might be an order file download which has all the details of the clients ordered including credit card and vital crucial private encrypted data. Even if the frequency of this error occurence is below the threshold its criticality is high because of the nature of the defect, it not only affects the clients business but the credibility of the software itself [3] will be questioned. These issues need to be addressed while designing the e-KMS and while prioritising the defects to be handled in the queue.

As part of case study, weblogs from a cloud based e-Commerce online business whose products include ebooks, music, films, stationary etc., were examined and the frequency of html defects are extracted and stored. The weblogs which had logged few of the user defects occurring in a 12 week period were also extracted and stored in the Table 3 below.

Table 3. Frequency of HTML defects from Logs

Html error	W1	W2	W3	W4	W5…	W12
400	6305	4493	3663	3124	3586	4436
401	4675	3497	3242	2672	3246	3562
402	4946	3675	3172	2634	2936	3475
403	15667	5079	6208	7445	6647	5141
404	53359	37688	43801	70576	39792	62715
405	4273	2890	2876	2587	3050	2747
N.w	8	7	32	137	200	46
St td	9	3	58	758	3	16

The frequency of HTML defects from weblogs are extracted for the period of 12 weeks lists error codes from 400 to 500 and includes few application error specific to the software which are the Network error, ASP files missing, HTML files missing, PDF files missing, syntax error or bad search terms which comes under user errors, syntax errors. Their defect threshold/midpoint is calculated for each of the codes using the compounded averages which are then mapped to specific quality criteria.

Table 4. Re-evaluated KQF values using the defects frequency

Html error	W1	W2	W3	W4	W5…	W12
400	5	4	3	2	3	4
401	5	3	3	2	3	3
402	5	4	3	2	3	3
403	RedA	2	3	4	3	2
404	4	3	3	4	3	5
405	5	3	3	3	4	3
N.w	1	1	1	3	4	1
St. td	1	1	2	RedA	1	1

The re-evaluated KQF values listed in Table 4 lists the red-alerts where the frequency has exceeded the baselines or the threshold limits set by the businesses. This threshold limit can be reduced or increased depending on the sensitivity and nature of the software. Using these values graphs can be plotted to see the quality measurement for individual KQFs. Figure 2 is one such example for KQF performance and availability over 12 weeks.

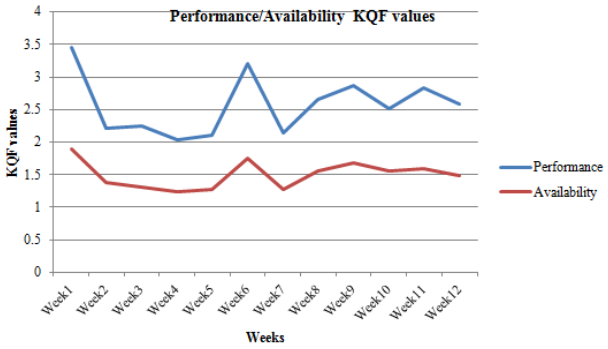

Figure 2. KQF values for Performance and Availability for 12 weeks

In the graph around week6 a new change in the existing software was introduced resulting in teething problems and few red alerts. This was resolved quickly in the week and as shown in week 7 it went down. The KQF value calculated changed due to

- Changes in the software
- Changes in the hardware
- Part of expansion to the future technologies
- Fixing Defects

New set of baselines will emerge resulting in the new values for the quality. Care should be taken during these stages to re-evaluate the essential views as users' views or the operation manager's views always change depending upon the platform and usability of the software. Change management is pivotal in businesses' quality management and defects management. Since cost/benefit is involved in every step of the way, crucial care is taken when implementing them as one misstep will cost the business.

V. CONCLUSIONS AND FUTURE WORK

Software metrics for quality is never a straightforward or a done deal. As new technology emerges the metrics to measure it will also differ due to its complexity. Particularly in a cloud based e-Commerce business there are issues such as the physical location, time difference, software platform, hardware platform to be taken into account when developing such models. Due to the diversity of hardware platforms like virtualization, the system defects tend to become hard to measure unlike the standardised individualised platforms. The proposed model generalizes and automates the measurement of quality for online cloud based businesses and can be adopted easily. For example, businesses like cloud based e-travel agent system, on-line product purchase stores or an online cloud-based music store can easily incorporate this model into the existing ones to measure quality. This model can be enhanced and tuned to measure key quality factors for individual business and can be deployed for large scale systems. There is future work to be done by calculating the percentage weight of more than one key quality factors affecting a defect. By reading the pattern of defects and scoring through the system logs, quality measurement from system perspective can be calculated and added into the overall quality measurement which can also be automated.

REFERENCES

[1] Gerald Weinberg, Quality Software Management: Systems Thinking, - Dorset House, 1991 - 978-0932633224

[2] Berkun, Scott, "Issue #10: The Web Shouldn't Be a Comedy of Errors," UIWeb.com, July 2000, www.uiweb.com/issues/issue10.htm

[3] Trochim, William M. "Likert Scaling". Research Methods Knowledge Base, 2nd Edition. October 20, 2006. Retrieved April 30, 2009.

[4] David Parmenter, Key Performance Indicators: Developing, Implementing, and Using Winning KPIs - Wiley; 2 edition, 2010 978-0470545157.

[5] ISO/IEC 9126-1:2001 Software Engineering — Product quality — Part 1: Quality model.

[6] Kiruthika J., Khaddaj S. and Horgan G, "Software Quality Factors and Defects Issues", Proc. International Conference on Semantic e-Business and Enterprise Computing, London., 2011.

[7] Khaddaj S. and Horgan G., A proposed adaptable quality model for software quality assurance. Journal of computer sciences, 1(4):82-487-2005.

[8] Khaddaj S. and Horgan, G. The evaluation of software quality factors in very large information systems. Electronic Journal of Information Systems Evaluation, 7(1), pp. 43-48, 2004.

[9] Horgan G. and Khaddaj S., Use of an adaptable quality model approach in a production support environment. Journal of Systems and Software, 82(4), pp. 730-738, 2009.

[10] Xiuxiang Zhao, Ying Liu, and Shi Yong, "Predicting Software Defects using Multiple Criteria Linear Programming", Proceedings of the International Symposium on Intelligent Information Systems and Applications (IISA'09), pp. 583-585, 2009.

Boosting Electronic Business Applications by Digitally Enabling SMBs with Cloud Computing Model

Shufeng Gao
College of Computer Science & Technology
Beijing Institute of Technology Zhuhai
Zhuhai, China
e-mail: gsfdl@163.com

Ai Xu
International Business Faculty
Beijing Normal University Zhuhai
Zhuhai, China
e-mail: gdxuai@163.com

Abstract--Cloud computing, as a brand new and powerful computing model, is achieving increased popularity. Its emergence will provide extraordinary opportunities for firms, especially Small and Medium Businesses (SMBs), to innovate and develop their electronic business. The paper starts with the discussion of the difficulties and challenges faced by SMBs during their development of electronic business. Then after mainly summarizing the definition and characteristics of cloud computing, the paper focuses on the benefits SMBs gained from cloud computing model to develop their electronic business applications and the new management challenges introduced through adoption of this new model.

Keywords- Electronic business; small and medium businesses (SMBs); cloud computing; cloud applications

I. INTRODUCTION

Nowadays, more and more people begin to talk about cloud computing and some are getting rather excited about it. Cloud computing is a general term for anything that involves delivering hosted services over the Internet, which is the development of distributed computing, parallel processing and grid computing. Cloud computing is a way of using computers where the computer resources such as software and hardware are provided as a service over the Internet and are dynamically scalable and often virtual (i.e. not necessarily in one known place). What this means to users is that the information they use is stored on computers somewhere else (other than their local PC) and can be accessed where, when and how they want it. The emergence of cloud computing will provide a brand new and powerful commercial computing model for firms to develop their electronic business, especially for Small and Medium Businesses (SMBs). There are extraordinary opportunities for SMBs to innovate and execute much more efficiently than ever before based on cloud computing platform, which will be an effective solution to the difficulties and challenges faced by SMBs during their development of electronic business in recent years.

II. CURRENT SITUATIONS OF ELECTRONIC BUSINESS FOR SMBS

A. E-business and its value for SMBs

Electronic business commonly referred to as "eBusiness" or "e-business", or an internet business, may be defined as the application of information and communication technologies (ICT) in support of all the activities of business. Commerce constitutes the exchange of products and services between businesses, groups and individuals and can be seen as one of the essential activities of any business. Electronic commerce focuses on the use of ICT to enable the external activities and relationships of the business with individuals, groups and other businesses [1]. Electronic business methods enable companies to link their internal and external data processing systems more efficiently and flexibly, to work more closely with suppliers and partners, and to better satisfy the needs and expectations of their customers. Therefore electronic business has become a vital choice firms should make in order to survive and prosper on the fierce competitive market.

The Internet is rapidly becoming the infrastructure of choice for electronic business because of its low-cost connectivity and universal standards, which are driving more and more SMBs to turn to e-business. The Internet can help SMBs create and capture profit in new ways by adding extra value to existing products and services or by providing the foundation for new products and services. Some Internet business models have emerged, all of which add value in one way or another. For example, selling goods directly to consumers online without using physical storefronts represents a new business model. Using the Internet and Web multimedia capabilities, SMBs are able to provide detailed product information quickly and inexpensively and detailed information specific to each customer to very large numbers of people simultaneously. SMBs can also extend digital technology to a wider range of activities and broaden their circle of trading partners. Take procurement for an example. Procurement involves not only purchasing goods and materials but also sourcing, negotiating with suppliers, paying for goods, and making delivery arrangements. SMBs can now use the Internet to locate the most low-cost supplier, search online catalogs of supplier products, negotiate with

978-0-7695-4818-0/12 $26.00 © 2012 IEEE
DOI 10.1109/DCABES.2012.18

suppliers, place orders, make payments, and arrange transportation. They can use the Web to work with any other business that is linked to the Internet. E-procurement over the Internet provides new opportunities for lowering costs and improving service. Internet and other information technologies have also strengthened traditional business models by helping SMBs reduce supply chain costs, increase production efficiency, and tighten relationships with customers. No company can afford to ignore the Internet and Internet technology, even if it does not do business online. Because of the use of information technologies and information systems, SMBs can also acquire some of the muscle and reach of larger companies. They can perform coordinating activities, such as processing bids or keeping track of inventory, and many manufacturing tasks with very few managers, clerks, or production workers. So e-business model makes SMBs operate much better than before and increases their competitiveness.

B. *Difficulties and challenges confronting SMBs in e-business environment*

Although many SMBs have benefited a lot from the application of Internet technology and new business models, there still are many difficulties and challenges, which has become an obstacle for SMBs to develop e-business and need to be paid more attention to.

*1) Lack of technical expertise for e-business applications:*Most of small and medium-sized businesses do not have enough technical staffs, or have their own information systems staffs but lack the required technical expertise. Most of the staffs in SMBs may be unfamiliar with the hardware, system software, application software, or database management system proposed for the e-business applications. Therefore, it is highly likely that the e-business applications will experience technical problems or take more time to complete because of the need to master new skills.

*2) Insufficient financial support for IT infrastructure:*To set up an e-business environment, SMBs need an information technology infrastructure, which means enough financial support. With the rising number of customers and business transactions, data flow increases correspondingly, which brings more requirements for hardware, software and other physical devices. However, SMBs often lack of fund and hard to obtain bank loans. Therefore, it is very difficult for SMBs to have sufficient financial support for maintaining e-business applications.

*3) More security risks and concerns:*E-Business systems naturally have greater security risks than traditional business systems, therefore it is important for e-business systems to be fully protected against these risks. Customers, suppliers, employees, and numerous other people use any particular e-business system daily and expect their confidential information to stay secure. Hackers are one of the great threats to the security of e-businesses. Some common security concerns for e-Businesses include keeping business and customer information private and confidential, authenticity of data, and data integrity. It is obviously much harder for SMBs to deal with such security issues because of the shortage of technical expertise, fund and necessary administration function. So security issues are really puzzles for SMBs while they choose to adopt e-business strategy.

III. CLOUD COMPUTING AND ITS CHARACTERISTICS

A. *The definition of cloud computing*

Cloud computing is the delivery of computing as a service rather than a product, whereby shared resources, software, and information are provided to computers and other devices as a metered service over a network (typically the Internet). It is a delivery model for IT services based on Internet protocols, and it typically involves provisioning of dynamically scalable and often virtualized resources [2][3]. It is a byproduct and consequence of the ease-of-access to remote computing sites provided by the Internet [4].

Cloud computing users don't generally own the physical infrastructure on which the applications run and store the data. Users access and use these web-based tools or applications through a web browser, desktop and mobile apps as if the programs were installed locally on their own computers. Indeed, users rent usage from a third-party provider and then use the system as they need it, much as people use gas or electricity. The more resources they use (such as more users having access to an application or using more disk space for storing data), the more they pay.

B. *Characteristics of cloud computing*

Cloud computing exhibits the following key characteristics:

*1) Professional processing and maintenance level:*Cloud computing concentrates a lot of computing resources in a public resource pool, where users can share computing resources through rented way and all the recourses are stored in the server cluster. The computing and processing ability can be extremely powerful due to the high-performance server and distributed computing method. The maintenance level can be increased too with the help of professional specialists and sufficient technical expertise.

*2) Declined cost:*Cost can be reduced and in a public cloud delivery model capital expenditure is converted to operational expenditure [5]. This is purported to lower barriers to entry, as infrastructure is typically provided by a third-party and does not need to be purchased for one-time or infrequent intensive computing tasks. Pricing on a utility computing basis is fine-grained with usage-based options and fewer IT skills are required for implementation (in-house) [6]. Meanwhile, the cloud computing service providers can benefits from economies of scale, because the same knowledge, skill, and capacity can be shared with many different customers. There often many subscribers in

the same cloud computing platform, which enables a large pool of user can share the resources and costs. Cloud computing service providers can also reduce their operation costs from many aspects, for example, centralization of infrastructure in locations with lower costs (such as real estate, electricity, etc.), peak-load capacity increases (users need not engineer for highest possible load-levels), utilization and efficiency improvements for systems that are often only 20% utilized.

*3) High reliability, flexibility and scalability:*Distributed data center can store large number of user information in different database server respectively, while users don't need to know where it is. The reliability is improved because multiple redundant sites are used, which makes well-designed cloud computing suitable for business continuity and disaster recovery [7].

Application software and hardware devices are isolated in cloud computing environment, which greatly reduces their interdependency. Meanwhile, the machine maintenance engineers can not see specific application running in the equipment and software users can only see the virtual devices. This method improves flexibility and makes dynamic distribution for resources possible.

The cloud computing platforms are allocated on hardware devices and software with different functions according to SPI architecture, and use middleware technology, so the scalability is high. Increasing or decreasing resources will not affect the normal operation of the system, so that it can meet stage demand and dynamic demand.

*4) Improved security:*In cloud computing environment, security could be improved due to centralization of data, increased security-focused resources, etc., but concerns can persist about loss of control over certain sensitive data, and the lack of security for stored kernels [8]. Security is often as good as or better than other traditional systems, in part because providers are able to devote resources to solving security issues that many customers cannot afford [9]. However, the complexity of security is greatly increased when data is distributed over a wider area or greater number of devices and in multi-tenant systems that are being shared by unrelated users. In addition, user access to security audit logs may be difficult or impossible. Private cloud installations are in part motivated by users' desire to retain control over the infrastructure and avoid losing control of information security.

Based on the above characteristics, cloud computing has become an important infrastructure which can be applied in many industries. Connecting cloud computing model with electronic business can effectively promote the development of electronic business.

IV. BENEFITS SMBs GAINED FROM CLOUD COMPUTING FOR E-BUSINESS

During the development of e-business, digitally enabling SMBs with cloud computing can bring a lot of benefits:

A. Increasing e-business application performance

The cloud computing service providers usually have more expertise in technology, management, and business process reengineering, who can help SMBs implement e-business applications rapidly and effectively. With the powerful processing ability of cloud computing providers, SMBs can exchange purchase and sale transactions directly with customers and suppliers, eliminating inefficient middlemen, streamline its processes to make communication and coordination more efficient, gain more valuable information to support high-quality decision-making, all of which cannot be afforded in the traditional systems. Therefore, the overall performance of SMBs can be increased. Furthermore, without the issues of server upgrades, hardware fixes, etc, SMBs can focus more on business need and thus improve their operational performance.

B. Reducing initial expenditure and operating costs

Outsourcing the e-business application systems to cloud computing providers has become popular because some organizations perceive it as a cost-effective measure that eliminates the need for maintaining their own computer centre and information systems staff. Cloud technology is paid for over time saving up front capital expenditure. This shows that SMBs does not need to spend lots of cash to get started the e-business applications and just pay for only what it uses rather than to build its own computer centre, which would be underutilized when there is no peak load. Meanwhile, fewer IT skills are required for implementation compared with the in-house IT strategy, which can save labour cost in some extent [10]. SMBs can dramatically reduce its operating cost too due to accomplish transactions more efficiently, work more closely with suppliers and partners, and better satisfy the needs and expectations of their customers, especially need not to maintain their e-business applications by themselves. This is surely vital for SMBs because the budget is often very limited.

C. Improving flexibility and mobility

Cloud computing can offer SMBs more flexibility, such as scalability and methods of access, than traditional computing methods. SMBs can store more data than on its private computer systems and increase it at will. Furthermore, employees of SMBs can access systems using a web browser regardless of their location or what device they are using (e.g., PC, mobile phone). As infrastructure is off-site (typically provided by a third-party) and accessed via the Internet, users can connect from anywhere. As for SMBs, they often have plant, warehouses and office at different places to save operating costs. If using cloud computing technology, employees of SMBs can access and accomplish their transactions everywhere, rather than having to remain at their desks within the company. SMBs can even hire some

people to work at other places (e.g. at home) to do business, which can reduce the increasing requirements of the workplace, especially in the same location.

D. Improving security protection

Security is of paramount importance in organizations where information systems make extensive use of networks, especially the Internet, because the Internet was designed to be open to everyone. In cloud computing model, security is often as good as or better than other traditional systems, in part because providers are able to devote resources to solving security issues that many customers cannot afford. Therefore, some security and privacy issued SMBs are concerning about can be protected better than before due to the technical means taken by the cloud computing service providers.

V. NEW MANAGEMENT CHALLENGES AND SOLUTIONS

Although digitally enabling with cloud computing model can help SMBs achieve new levels of competitiveness and efficiency, it does pose challenges for managers.

A. Organizational change challenges

E-business and e-commerce often require new organizational designs and management processes to take advantage of Internet technology. While deciding to adopt cloud computing model and to outsource the service to a third-party provider, SMBs may need to redesign entire business processes rather than trying to graft new technology on existing business practices. SMBs must consider a different organizational structure, changes in organizational culture, a different support structure for information systems, different procedures for managing employees and networked processing functions, and, perhaps, a different business strategy. Traditional boundaries between departments and divisions, and firms and distributors may be impediments to collaboration and relationship building. Therefore, SMBs should put in place a change management plan to implement cloud computing-based electronic business effectively.

B. Security and privacy

As cloud computing becomes more and more popular, concerns are being voiced about the security issues introduced through adoption of this new model. The effectiveness and efficiency of traditional protection mechanisms are being reconsidered as the characteristics of this innovative deployment model differ widely from those of traditional architectures. Although cloud computing service providers prioritize building and maintaining strong management of secure services, many security issues still exist, such as sensitive data access, data segregation, privacy, bug exploitation, recovery, accountability, malicious insiders, management console security, account control, and multi-tenancy issues, etc.

The cloud model has also been criticized by privacy advocates for the greater ease in which the companies hosting the cloud services control, thus, can monitor at will, lawfully or unlawfully, the communication and data stored between the user and the host company.

Because of adopting cloud computing model, security and privacy issues become more complex for SMBs, because the data and applications are stored in a third-party. SMBs do not physically possess the storage of their data, so responsibility of data storage and control in the hands of the provider. How can SMBs be 100% sure the data is safe? Therefore, SMBs should emphasize safeguarding security and privacy. SMB should be both more open and more closed at the same time, which means that SMBs need to be open to outsiders such as customers, suppliers, and trading partners, yet these systems also must be closed to hackers and other intruders and protective of customers. SMBs need a new security culture to do better and also need to reexamine corporate privacy policies to make sure they are properly respecting the privacy of customers and Web site visitors.

C. Loss of control

Not all organizations benefit from outsourcing its e-business applications to a third-party provider. The disadvantages of outsourcing can create serious problems for organizations if they are not well understood and managed. Many firms underestimate costs for identifying and evaluating vendors of cloud computing services, for transitioning to a new vendor, and for monitoring vendors to make sure they are fulfilling their contractual obligations. These hidden costs can easily undercut anticipated benefits from the adopting of cloud computing model. It should be noticed that when SMBs allocates the responsibility for developing and operating its information systems to another organization, it can lose control over its information systems function. If lacking the expertise to negotiate a sound contract, SMBs will be dependent on the vendor, which could result in high costs or loss of control. So SMBs should be well aware of the disadvantages and challenges of cloud computing model and try to avoid the loss of control.

VI. CONCLUSIONS

Internet technology has provided SMBs with powerful new tools to innovate and to execute much more efficiently. With the emergence of cloud computing solution, SMBs have new opportunities to quickly move to nearly all-paperless sales transactions, find new customers via online networks, increase the amount of product it sells to its existing clients, improve the relationship with suppliers and customers, reduce operational and management costs, etc. This can be accomplished without a lot of additional IT or business-process spending for SMBs if using cloud-based collaborative business commerce solutions. It can be seen that cloud computing solution is a good choice for SMBs to boost their e-business applications. Of course, SMBs should pay more attention to the new challenges posed by cloud computing model and try to solve them. Only by doing so, can SMBs promote the further development of their electronic business.

REFERENCES

[1] P. Beynon-Davies, E-Business. Basingstoke: Palgrave Macmillan, 2004, pp.480.

[2] John Doe, "Gartner Says Cloud Computing Will Be As Influential As E-business," http://www.gartner.com /it/page.jsp?id=707508, 2008.

[3] E. Knorr, G.Gruman, "What cloud computing really means," http://www.infoworld.com/d/cloud-computing/what-cloud-computing -really-means-031, 2008.

[4] John Doe, "Cloud Computing: Clash of the clouds.," http://www.economist.com/node/14637206?story_id=14637206, 2009.

[5] K. Subramanian, "Recession Is Good For Cloud Computing– Microsoft Agrees," http://www.cloudave.com/link/ recession-is-good-for-cloud-computing-microsoft-agrees, 2009.

[6] F.Gens, "Defining 'Cloud Services' and 'Cloud Computing'," http://blogs.idc.com/ie/?p=190, 2008.

[7] R King, "Cloud Computing: Small Companies Take Flight," http://www.businessweek.com/technology/content/ aug2008/tc2008 083_619516.htm, 2008

[8] J.Hughes, "Encrypted Storage and Key Management for the cloud.," http://www.cryptoclarity.com/CryptoClarityLLC/Welcome/Entries/ 2009/7/23_Encrypted_Storage_and_Key_Management_for_the_clou d.html, 2009.

[9] E. Mills, "Cloud computing security forecast: Clear skies,' http://news.cnet.com/8301-1009_3-10150569-83.html, 2009.

[10] S.L. Zhang, "The Application of Cloud Computing Technology in the Field of E-commerce," Value Engineering, No. 30, Oct. 2011, pp. 137-138

Study on Resources Scheduling Based on ACO Algorithm and PSO Algorithm in Cloud Computing

Xiaotang Wen[1], Minghe Huang[1], Jianhua Shi[1]
[1]School of Software
[1]Jiangxi Normal University
[1]Jiangxi, China
xiaotangwen2010@163.com, huangmh0093@sina.com, 0793shijianhua@163.com

***Abstract*—It improves the algorithm because of the shortcoming that the ACO algorithm is easy to fall into local optimal solution in the cloud computing resource scheduling. The improved algorithm makes particle optimization inosculated into ant colony algorithm, which first finds out several groups of solutions using ACO algorithm according to the updated pheromone, and then gets more effective solutions using PSO algorithm to do crossover operation and mutation operation so as to avoid the algorithm prematurely into the local optimal solution.**

Keywords-ACO algorithm; PSO algorithm; Cloud Computing; Resources Scheduling

I. INTRODUCTION

Allocation of computing resources is an important component of cloud computing technology, its efficiency directly affects the performance of the entire cloud computing environment. Currently, Domestic and foreign researchers study resource scheduling based on the ant colony algorithm(ACO) in cloud computing environment, which overcomes the shortcomings of huge size of the node and lower allocation of resources for a single node, ensuring user's jobs can be completed on time. But it still exist that the algorithm is easy to fall into local optimal solution, making inefficient resource scheduling. For this problem, it will improve algorithm by combining ACO with particle swarm optimization algorithm(PSO) to improve the efficiency of resource scheduling in cloud computing environments.

II. ALGORITHMS DESCRIPTION

2.1 ACO Description

Ant colony algorithm, also known as ant algorithm, is a bionic optimization algorithm which used to find an optimal path in a directed graph. The ants will leave a pheromone on the way of foraging, they communicate with others using pheromone to find a shorter path. The amount of pheromone on each path will reflect probability the other ants choose the path. Ants of a place is more, the strength of pheromone is greater. Ultimately, all ants will choose the shortest path. Ant colony algorithm is well suited for resources scheduling in cloud computing because of its concurrency and expandability.

- pheromone definition and update
  Inspired by Ref [1], we measure a node's pheromone by virtual machine's hardware resources. m is the number of CPU, p(MPIS) is processing capability, r is memory capacity, h is external memory capacity, b is bandwidth, which used to measure nodes' pheromone. This sets threshold with parameter according to Formula [1], if it exceeds the threshold, then it should calculate with threshold.
  $m_{max}=m_0$, $p_{max}=p_0$, $r_{max}=r_0$, $h_{max}=h_0$, $b_{max}=b_0$ (1)
- Initialize the hardware pheromone of the node :
  CPU's pheromone:

$$\tau_{ij}(0)=\frac{m*p}{m_0*p_0}\times 100\% \quad (2)$$

  Memory's pheromone:

$$\tau_{ij}(0)=\frac{r}{r_0}\times 100\% \quad (3)$$

  External memory's pheromone:

$$\tau_{ij}(0)=\frac{h}{h_0}\times 100\% \quad (4)$$

  Bandwidth's pheromone:

$$\tau_{ij}(0)=\frac{b}{b_0}\times 100\% \quad (5)$$

  Node i's pheromone is weighted sum of each pheromone above, that is

$$\tau_{ij}(0)=a\tau_{if}(0)+b\tau_{ir}(0)+c\tau_{ih}(0)+d\tau_{ib}(0)$$
$$a+b+c+d=1 \quad (6)$$

978-0-7695-4818-0/12 $26.00 © 2012 IEEE
DOI 10.1109/DCABES.2012.63

When a new task is assigned to the compute nodes, the CPU utilization ratio will increase and the pheromone decrease. Stipulate that when the new tasks are assigned to the compute nodes, the pheromone is updated by Formula (7).

$$\tau_i(t_1) = \tau_i(t) - \lambda\tau_i(t) \quad , \quad 0 < \lambda < 1 \tag{7}$$

$\tau(t)$ represents the pheromone concentrations of the compute nodes at time t, $\tau(t_1)$ represents the pheromone concentration that new tasks reach node i at time t_1, is regulatory factor.

$$p_{ij} = \frac{\tau_j^{\alpha} / A_j^{\beta}}{\sum_{m \notin N_s} \left(\tau_m^{\alpha} / A_m^{\beta}\right)}, \qquad j \notin N_s \tag{8}$$

$A_j = ET_j^{n_d}\left(J_d(t)\right)$, p_{ij} represents the probability that ants select next node j in node i. τ_j represents the pheromone concentration that node i observed node j. N_s represents node set of ants path. m is neighbor of node i. α, β are regulatory factor., which denote importance of τ_j and A_j.[1]

2.2 Description of PSO Algorithm

Initialize a group of random particles in a space, the particle position represents possible solution, each particle advances to a certain speed, particle swarm gradually approaches to the optimal location after repeated advances which are also called iteration, thus the optimal solution will be got. In each iteration, the particles update themselves according to two extreme values: one is the optimal solution finding by a single particle, namely the individual extremum; the other is the optimal solution finding by whole particle swarm, that is, namely the global extremum.

Particles update their velocity and position according to the two extreme values above and the following two formulas.

$$V = \omega * v + c_1 * rand() * (pBest - X) + c_2 * rand() * (gBest - X) \tag{9}$$

$$X = X + V \tag{10}$$

Among them, V=[v1,v2,⋯,v d] is the velocity of the particle, X=[x1, x2, ⋯, x d] is the current position of the particle, d is the dimension of solution space. pBest is the individual extremum, gBest is the global extremum, rand( ) is random number between 0 and 1. c_1, c_2 are called learning factors, which are used to adjust the particle update step, ω is a weighted factor.

The particle swarm gradually closes to the optimal solution location through continuous learning and updating, finally, the gBest which is the global optimal solution will be got using the algorithm.[2]

III. IMPROVED RESOURCES SCHEDULING ALGORITHM IN CLOUD COMPUTING

Ant colony algorithm uses of pheromones to transmit information, and particle swarm optimization algorithm uses own information, individual extremum information and global extremum information to guide the particles to select next iteration position. Ant colony algorithm combines positive feedback principle organically with some kind of heuristic algorithm, but it is prone to premature convergence and falling into local optimal solution. Hybrid algorithm, the idea is to let the ants also have the characteristics of the "particles". First of all, ants are in accordance with the ant colony algorithm to complete a traverse, and then they adjust solutions according to the local optimal solutions and global optimal solutions. Adjustment is as follows: to resource scheduling, its current position is behalf of the basic path node set. If it uses particle swarm algorithm to solve the problem, the speed is hard to express, so here the idea of genetic algorithm is adopted. $\omega * v$ can be seen as the mutation operation of genetic algorithm, and $c_1 * (pBest - X) + c_2 * (gBest - X)$ in formula (9) can be seen as the crossover operation of genetic algorithm, which lets the current solution do crossover operator with the individual extremum and the global extreum so as to produce a new location.

In this paper, the crossover strategy as follows: select a cross- region randomly in the second string, old_2 is added to the old_1 corresponding position, delete the nodes in old_1 appeared in the old_2 cross- region. Variation strategy: select the node of j_1 visits from the nodes of 1-n visit, exchange the j_1 visit node and the j_1+1 visit node in node set N_0, and the rest keep unchanged. At this time, the path set node is N_1.

A node may have to run multiple tasks at the same time in the cloud computing. But, it will improve performance of entire cloud that tasks are assigned to the most efficient node. Therefore, a task expected execution time model is established to predict execution time of the new tasks on the node, the formula as follows:

$$ET_j^{n_d}\left(J_d(t_2)\right) = \frac{n_d}{n_v} \times \left(\rho\, ET_j^{n_v}\left(J_v(t_0)\right) + (1-\rho)\, RT_j^{n_v}\left(J_v(t_1)\right)\right) \tag{11}$$

$ET_j^{n_d}\left(J_d(t_2)\right)$ indicates that the new task J_d estimated the expected execution time on the j node at time t_2, n_d indicates the load of the node j at time t_2, here the number of task running on node j indicates the load size. $ET_j^{n_v}\left(J_v(t_0)\right)$ indicates the expected execution time of

the previous completed task J_v at time t_0. $RT_j^{n_v}\left(J_v(t_1)\right)$ indicates the actual execution time of the previous task completed at time t_1. n_v indicates the load of previous task.[1]

The tasks become less and less on a node, so the expected completion time of the tasks is also less and less. Therefore, the expected execution time should be modified at intervals according to the following formula:

$$ET_e^{n_d}\left(J_d(t+1)\right) = (1-\rho_1)\times ET_e^{n_d}\left(J_d(t)\right), \quad 0 < \rho_1 < 1 \tag{12}$$

The algorithm steps of resources scheduling based on ACO algorithm and PSO algorithm in cloud computing are as follows:

- Step1: Initialize nc=0(nc is iterations), use ACO algorithm to complete the first traverse (form m path node set);
- Step2:Calculate the fitness value based on the current path node set(the expected execution time), set the current fitness value to individual extremum called ptbest, and set the current path nodes set to individual extreme nodes set called pcbest, then find out the global extremum called gtbest and the global extreme nodes set called gcbest;
- Step3:Put m ants randomly on n nodes, put initial staring node of each ant in the current path node set, to each ant k, move to the next node j according to the probability p_{ij}, put node j in the current path node set, compute task expected execution time based on formula(11).
- Step4: Operate as follows for each ant, the path node set of ant j termed $N_0(j)$ is crossed by gcbest which gets $N_1'(j)$, and $N_1'(j)$ is crossed by pcbest which gets $N_1''(j)$, $N_1''(j)$ variants with a specified probability which gets $N_1(j)$. accept the new value if the new objective function gets better, otherwise refuse and $N_1(j)$ remains $N_0(j)$, then, rediscover individual extremum ptbest and extremal node set pcbest for each ant, find out global extremum gtbest and global extremal node set gcbest;
- Step5: Calculate task expected execution time for each ant node set, record the current best solution;
- Step6: Update the pheromone concentration according to formula(7), modify the node task expected execution time according to formula(12);
- Step7: nc=nc+1;
- Step8: If nc<a predetermined number of iterations, go to step3;
- Step9: Output the optimal solution, allocate the tasks in the nodes which included in the optimal solution node set.

IV. THE EXPERIMENT

This paper does simulation using matlab7.0 to verify the improved algorithm. In order to verify the superiority of the improved algorithm, we are using ACO algorithm and PSO algorithm for task scheduling in this experiment. The expected execution time of task is shown in figure1. Experimental parameter settings: number of ants m=10, maximum number of iterations nc_{max}=500, α=1.5, β=2, ρ=0.9.

Overall, the tasks execute slowly because of a little pheromone when the ACO algorithm is put into use, but as the pheromone increasing later, and the positive feedback enhancing, the time increase rate becomes smaller. It is clear that the execution time for improved algorithm is shorter than the former, so it has higher efficiency.

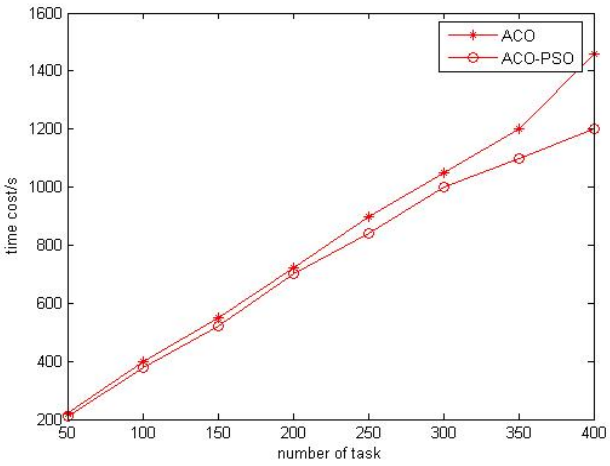

Figure 1.

V. CONCLUSION

This paper considered the series of characteristics of cloud computing, made particle optimization inosculated into ant colony algorithm and introduced crossover strategies and mutation strategies in genetic algorithm to overcome the defect that the algorithm is easy to fall into local optimal solution in the cloud computing resource scheduling. Experiment shows that the improved algorithm not only accelerated the convergence speed, but also avoided falling into local optimum solution, and achieved the purpose that the user tasks were efficiently provided appropriate resources in cloud computing, which improved the resource utilization ratio.

REFERENCES

[1] Y. Liu, X. H. Wang, C. M. Xing and S. Wang, "Resources scheduling strategy based on ant colony optimization algorithms in cloud computing," Computer Technology and Development, vol. 21(9), pp. 19-23, 2011.

[2] S. Gao, X. Z. Jiang, K. Tang and J. Y. Yang, "Hybrid Algorithm Combining Ant Colony Optimization Algorithm with Pariticle Swarm Optimization," Proceedings of the 25th Chinese Control Conference, pp. 1428-1432, 2006.

[3] Z. H. Zhang and X. J. Zhang, "A Load Balancing Mechanism Based on Ant Colony and Complex Network Theory in Open Cloud Computing Federation," 2010 2nd International Conference on Industrial Mechatronics and Automation, pp. 240-243, 2010.

[4] H. W. Tian, F. Xie and J. M. Ni, “Resource Allocation Algorithm Based on Particle Swarm Algorithm in Cloud Computing Environment,” Computer Technology and Development, vol. 21(12),pp. 22-25, 2011.

[5] Y. G. Wang and R. L. H, “Study on Cloud Computing Task Schedule Strategy Based on MACO Algorithm,” Computer Measurement and Control, vol. 19(5), pp. 1203-1204, 2011.

[6] S. H. Liu, Y. Zhang and H. Y. Wu, “Multi-robot task allocation based on swarm intelligence,” Journal of Northeast Normal University (Natural Science Edition), vol. 41(4), pp. 69-72, 2009.

Managing the Data Replicas Efficiently in Time-zoned Multilayer Chord

Mei Wang[1], Chang Kong[2], Wentao Dong[2], Qiuming Luo[2,3]
[1]School of Computer Engineering, Shenzhen Polytechnic
[2]College of Computer Science and Software Engineering
[3] National High Performance Computing Center
Shenzhen University, China
wmiss64@hotmail.com, clarkong89@gmail.com, hebdwt@163.com, lqm@szu.edu.cn

***Abstract*—**Replica is better than erasure coding when managing the redundancy of a storage system under high churn. It needs extra network communication to keep the target redundancy. By classifying the hosts into different categories of availability and placing the data replicas carefully may reduce the maintenance overhead. Considering a globe scale P2P system, the time-zoned multilayer Chord divides the hosts into 24 categories according to the time zone where they located. All the hosts are belongs to a Main Chord which consisted of all the hosts and one Local Chord which consisted of the hosts located in the same time zone. Because of the daily behavior of the people in same time zone are nearly similar, which means their computers are more likely to be available in the daytime and less likely to be available in the nighttime. So, for a certain time, there is nearly half of the hosts get higher availability than the other hosts. As the hosts in the same time zone are considered, their availability evaluated by the system is shifting periodically in a 24 hours cycle. By give a carefully placement of the data replicas on this two layered Chord, the less communication is needed to maintain the same target availability. The experiments show that dividing hosts by location of time zone might reduce the overhead of redundancy management.

Keywords: Data Replicas; Multilayer Chord; Time-zoned Churn Pattern; Peer-to-peer;DHT;

I. INTRODUCTION

Availability is a storage system property that is highly desired. In a peer-to-peer environment, hosts may only be transiently available. When connected, the data stored on a host contributes to the overall degree of redundancy and increases the data's availability; when disconnected, the degree of redundancy decrease which cause the data availability decrease accordingly. There are a wide range of mechanisms available for producing redundant representations of data. Each mechanism has unique trade-offs [1]. Both of pure replication and erasure coding need extra network communication to maintain the degree of redundancy. But it is clear that replica is more efficient than erasure coding when managing the redundancy of a storage system under high churn [10][11]. How much redundancy is required to deliver a specified level of availability is depend on the mean host availability [1]. Some researches investigate the diverse of host availability and provide a data placement which put the data replicas onto the hosts with the same or near availability. That placement can avoid wasting the capacity of high available hosts and overestimating the target redundancy. The less redundancy needs the less overhead of network communication. But how to classify the hosts into different categories of availability is still need to be study. The time-zoned multilayer Chord seems to be an efficient method to divide the hosts into different categories according to their availability roughly.

The rest of the paper is organized as follows. Section 2 describes the concept of time-zoned multilayer Chord, which is critical idea that proposed by this paper firstly. Then two data replicas placements methods are provided in section 3. The first one is rather simple. The second one is a litter more complicate than the former one and get a better performance. Some experiment results are shown in section 4. A conclusion is draw and some enhancements in the future works are discussed in section 5.

II. THE TIME-ZONED MULTILAYER CHORD

The hosts in time-zoned multilayer Chord belong to two Chords which are named the Main Chord and the Local Chord. The Main Chord is consisted of all the hosts. The Local Chord is consisted of the hosts located in a same time zone. There are 24 Local Chord2 which corresponding to the 24 time zones in our planet.

Each host has one unique ID as the ordinary Chord ring [3]. One host uses the same ID to join the Main Chord and the Local Chord.

There are five hosts in Figure 1. All these five hosts are in the Main Chord. There are 24 Local Chords numbered 0 to 24, which corresponding to West-12, West-11, …, West-1, East-1, …, East-11 and East-12 time zones. Three hosts are in Local Chord 0 which numbered N0-1, N0-2 and N0-3, which corresponding to West-12 time zone. Two hosts are in Local Chord 1 which numbered N1-1 and N1-2, which corresponding to West-1 time zone. One host is located in East-12 time zone and it joins the 23-th Chord ring. Every host is belongs to the Main Chord and one of the Local Chord. The level of time-zoned multilayer Chord is 2, although there are 25 Chords in this system.

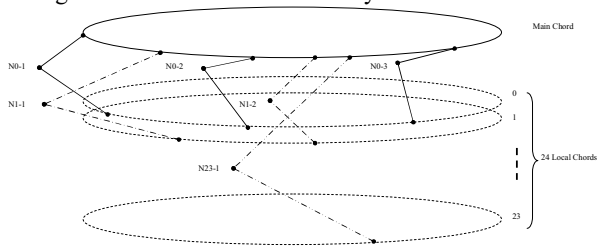

978-0-7695-4818-0/12 $26.00 © 2012 IEEE
DOI 10.1109/DCABES.2012.27

Figure 1 A time-zoned multilayer Chord.

To maintain the neighbor relationship, this two-layer Chord need more network communication than one layer Chord. As the number of hosts in Local Chord is nearly one twenty-fourth of that of the Main Chord. The overhead to maintain an extra Chord can be neglected as one host is concerned. The overall overhead of this system is nearly the same of the Main Chord.

The other Chord-based multilayer systems use an inter-layer Chord as a router or gateway between these Chords. The Main Chord acts as the router or gateway in our system.

Our previous research shows that the hosts in the same time zone are more likely to behave similarly which imply that their availability are shifting according to their behavior pattern statistically [8]. That means the hosts have a higher availability during the daytime and lower availability during the nighttime according to the local clock. This makes it a very efficient way to classify the hosts into categories according to their availability roughly.

III. THE DATA PLACEMENT AND REPLICATING

We put the data block into the Main Chord the as [1]. So we find a data block with $ID=id_x$ by seeking the host with *id=successor* (id_x). The replicating process is somewhat different from CFS or Total Recall. The traditional DHash-based system replicating process put the replicas at the k servers immediately after the data block's successor on the Chord ring.

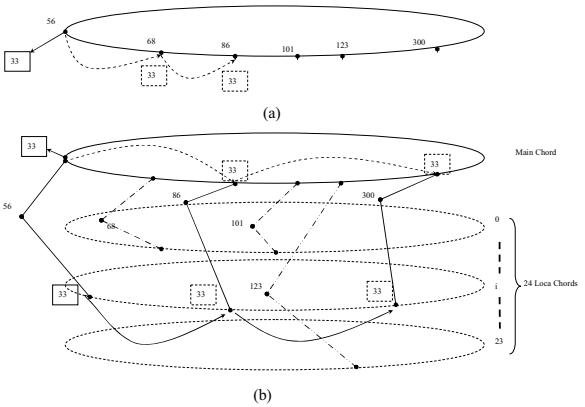

Figure 2. Data replication in time-zoned multilayer Chord.

Figure 2-(a) shows the replica placement in a DHash-based system. The data block with *id=33* is put at node *56*, if *successor (33)=56*. If the redundant level is three, the two replicas are put at the two hosts with *id=68* and *id=86*, which is immediately after host 56. While in our time-zoned multilayer Chord, the replicas are place at the hosts whose number is 86 and 300, which are immediately after the host *56* in the Local Chord. The data and its replicas are not contiguous in the Main Chord. There are node 68 between node 56 and node 86, and there are node 102 and node 123 between node 86 and node 300. The new placement is shown as Figure 2-(b).

That placement is very simple and renders a performance near the same as one Chord only, as the data communication overhead is concerned. Although this scheme of placement is conform to the rule that the replicas are place in the hosts whose availabilities are at the same level and avoid wasting the high available hosts' capacity, but the data movement need is much more than the traditional one, when the host that holds the first replicas is disconnected.

The repair procedure is the same as DHash. When replicas level is decrease to a threshold of minimal, the system initiates a repair procedure which copy the data block within its Local Chord to increase the replica number.

An enhancement of that placement is figured out by considering the diverse of availability. As we know that the Local Chord who is in its local daytime has higher availability than those in its local nighttime. As a traditional DHash-based system, one data block with $id=id_x$ is "put" into the system, we seek the hosts with *id=successor (idx)* to hold that data block. Now, we define an active window which includes the Local Chords whose local time is daytime.

The "*find_successor()*" function if [2] used to accomplish "put" procedure is modified by adding codes to handle the successor's Local Chord numbers. To distinguish with the former *find_successor()*, we give this new function a name "*find_successor_active()*". The pseudo code of *find_successor()* is shown as following Figure 3.

```
//ask node n to find the successor of id in the active Local
//Chords
n.find_successor (id)
{    if(id ∈(n, successor])
        return successor;
     else
        return successor.find.successor(id);
}
```

Figure 3 *find_successor()*'s pseudo code.

The modified function *find_successor_active()*'s pseudo code is shown as Figure 4. It will call *find_successor()* to seek the ordinary successor.

```
n.find_successor_active(id)
{    if(id ∈(n, successor])
       while(1)
        { if ( successor.timezone_num
                ∈active_win (current_time) )
            return successor;
          else successor++;
        }
     else
        { successor = successor.find_successor(id);
          if(id ∈(n, successor])
            while(1)
            { if ( successor.timezone_num
                    ∈active_win (current_time) )
                return successor;
```

```
                else successor++;
                }
            }
}
```

Figure 4 *find_successor_active()*'s pseudo code.

The function *find_successor_active()*' is a little different from the function *find_successor ()*. When the successor of *id* is obtained, it is not return directly. It used active_win() to verify whether the successor is within the active windows. The active window is shifting with current time. For example, Local Chord 21 can be considered as active when the time is GMT 1:00, because the local time of Local Chord 21 is about 9am. The active window might be set between Local Chord 21 to Local Chord 31 (31 mod 24=7). If it is not located in the active window, we try the immediate successor until a host is obtained who is located in active window.

The resource locating mechanism is changed. We cannot get the data block with $id=id_x$ by asking host with $id=successor\ (id_x)$. It should ask the host with $id=successor\_active\ (id_x)$. The repairing procedure is changed, too. If the host which holds the extra replicas is disconnected, another replica is made in the same Local Chord. But, when the host which holds the first data replica block is disconnected, all the replicas should be made if the new $successor(id_x)$ is located in another Local Chord. That will cause a lot of network communication, which will tradeoff our gain of reducing the bandwidth consume due to put the data replicas into a high available Local Chord.

IV. EXPERIMENT RESULTS

In order to verify the performance of new proposed data placement, some simulation is taken.

The churn event list used in simulation is generated following the GCP (Global Churn Pattern) model which proposed in [8]. The GCP is based on the underlying models as [4][6][7]. As mention above, the hosts in same time zone behave alike. To put it simple, the hosts' begin time of sessions of same time zone for particular applications are following a normal (or Gaussian) distribution. To make it more accurate, we might use two weighted Gaussians to distinguish the session begin in the morning and afternoon. Equation (1) is rewritten into equation (6).

$$f_z(x) = w_1 \frac{1}{\sqrt{2\pi}\sigma} e^{\frac{(x-tp_1)^2}{2\sigma_1^2}} + w_2 \frac{1}{\sqrt{2\pi}\sigma} e^{\frac{(x-tp_2)^2}{2\sigma_2^2}}, \quad where\ z=(0,1,...,23)\ ,\ w1+w2=1. \qquad (1)$$

For example, it is reasonable to set $w_1=w_2=0.5$, $tp_1=10:30$ am, tp_2=3:30 pm and $\sigma_1=\sigma_1=1\ hour$, which stands for 1/2 users begin their session in the morning and 1/2 users in the afternoon.

The session length is produced as follow. Median session times observed in deployed networks range from as long as an hour to as short as few minutes. It is pointed out by [5] that session lengths are fit by weibull or log-normal distributions, but not by exponential or Pareto. The users are classified into three groups in [9], according to their "up" time. We could use exponential one for simplicity.

As we use GCP to produce the churn events, the hosts' distribution among the 24 time zones is very important. The default uneven distribution of potential peers across the world is used. By convoluting the behavior function and the distribution, a global churn event sequence can be obtained. There are 900 hosts and 24 data blocks with redundant lever equal to 3 in the simulation. The expectation of session lengths is 1400 seconds.

The first simulation is to compare the network overhead to maintain the desire redundant level. As Figure 5-(a) shows, the simple placement of data replicas is nearly identical for Chord and time-zoned multilayer Chord, where the vertical axis represents the total replicas copying times of the whole system. Figure 5-(b) shows some more details. It seems that time-zoned multilayer Chord got a little better performance.

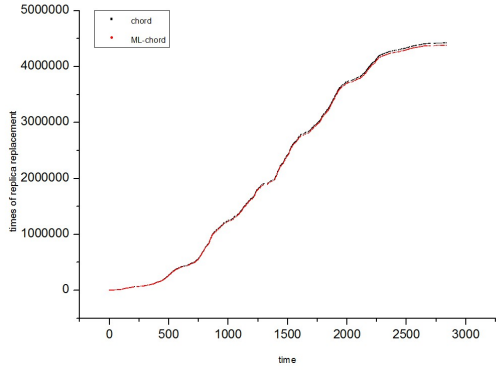

(a)

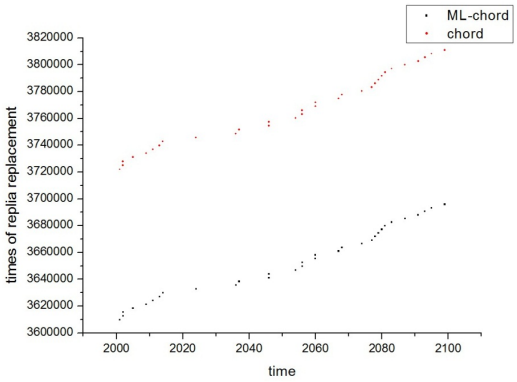

(b)

Figure 5. The data copy times of Chord and time-zoned multilayer Chord with simple data placement.

The simple placement based on time-zoned multilayer Chord reduced the replicas repairing by putting replicas of same data block in the same Local Chord. This takes the advantage of classifying the hosts into different categories of availability by simple dividing by their location of time zone. There is no extra effort to make that classification. This gain is reduced by copying more replicas when the hosts which hold the first replicas leave the network.

Then we investigate the second placement scheme. It gives an inspiring result. We defined three types of active windows, including the window of 9 to 22 o'clock (local time), 8 to 11 o'clock (local time) and 9 to 12 o'clock (local time). Figure 6 shows that the data copy times of time-zoned multilayer Chord with active window placement is much less than those of Chord and time-zoned multilayer Chord with simple data placement. The different active window makes different total copy times. The red curve has the best performance, which define an active window of 9 to 12 o'clock.

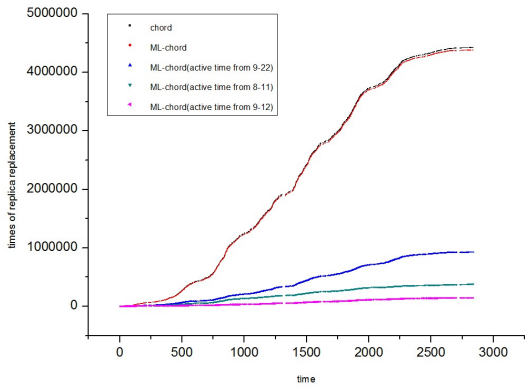

Figure 6. The data copy times of Chord, time-zoned multilayer Chord with simple data placement and time-zoned multilayer Chord with active window placement.

V. CONCLUSIONS AND FUTURE WORK

This paper proposes a new scheme for replicas management on a time-zoned multilayer Chord. The first advantage is the classification of hosts according to their availability by simply divides them into 24 groups of different time zones. That will decrease the network overhead of replicas repairing by avoiding the waste of the capacities of high available hosts. Defining the active window helps to decrease the network overhead further. The active window will shift with current time. And the placement with active window tends to make replicas on the Local Chord of daytime, which means a higher availability than those of nighttime.

Although the experiment result seems to be inspiring, the simulation should be refined by using the real churn event sequence which obtained by log files. The second refinement should be made to take the communication overhead between different Chord layers into account explicitly. And the method to get an optimized active window should be figured out.

ACKNOWLEDGMENT

This work was supported by the project (NO. 2011A090100037) funded by Guangdong Province and Chinese Academy of Sciences, and the project funded by State Key Laboratory of Computer Architecture, ICT,CAS.

REFERENCES

[1] R. Bhagwan, K. Tati, Y. C. Cheng, S. Savage, and G. M. Voelker, "Total recall: System support for automated availability management" in *Proceedings of Symposium on Networked Systems Design and Implementation (NSDI)*, March 2004. pp.337–350. doi=10.1.1.10.9775

[2] Frank Dabek, M. Frans Kaashoek, David Karger, Robert Morris, Ion Stoica, "Wide-area cooperative storage with CFS",SIGOPS Oper. Syst. Rev. In USITS'03: Proceedings of the 4th conference on USENIX Symposium on Internet Technologies and Systems, Vol. 35, No. 5. (2001), pp. 202-215.

[3] I. Stoica, R. Morris, D. Liben-Nowell, D. R. Karger, M. F. Kaashoek, F. Dabek, H. Balakrishnan, "Chord: a scalable peer-to-peer lookup protocol for internet applications", IEEE/ACM Transactions on Networking, Vol. 11, No. 1. (February 2003), pp. 17-32.

[4] S. Rhea, D. Geels, T. Roscoe, and J. Kubiatowicz, "Handling Churn in a DHT," In Proceedings of the 2004,USENIX Annual Technical Conference (USENIX'04), Boston, MA, USA, Jun. 2004, pp.127–140.

[5] Chun, B., Dabek, F., Haeberlen, A., Sit, E., Weatherspoon, H., Kaashoek, M. F., Kubiatowicz, J., and Morris, R. 2006. "Efficient replica Maintenance for distributed storage systems". In Proceedings of the 3rd Conference on Networked Systems Design & Implementation - Volume 3 (San Jose, CA, May 08 - 10, 2006). pp. 45-58

[6] Daniel Stutzbach, Reza Rejaie, "Understanding churn in peer-to-peer networks," Internet Measurement Conference 2006, pp.189–202.

[7] J. Chu, K. Labonte, and B. N. Levine, "Availability and locality measurements of peer-to-peer file systems," in Proc. of ITCom: Scalability and Traffic Control in IP Networks, 2002. [Online]. Available: http://eprints.kfupm.edu.sa/27741/

[8] Qiuming Luo,Yun Li,Wentao Dong and XiaoHui Lin, "A Churn Model Based on the Global Geographical Distribution of Nodes", 2010 Ninth International Symposium on Distributed Computing and Applications to Business, Engineering and Science,Hong Kong, China, August 10- 12, [Online] Available: http://doi.ieeecomputersociety.org/10.1109/ DCABES.2010.55

[9] Octavio Herrera, Taieb Znati, "Modeling Churn in P2P Networks", Simulation Symposium, Annual, 40th Annual Simulation Symposium (ANSS'07), 2007 , pp. 33-40. [Online] Available: http://doi.ieeecomputersociety.org/10.1109/ANSS.2007.28

[10] Weatherspoon H, Kubiatowicz J. "Erasure coding vs. replication : A quantitative comparison". Proc. of the IPTPS, 2002,2.

[11] Lin W, Chiu D, Lee Y. Erasure code replication revisited. In : Proc. of the 4th Int'l Conf. on Peer-to-Peer Computing. 2004. pp.90-97.

Research and Application of Improved Apriori Algorithm to Electronic Commerce

Shuo Yang
College of Computer Science and Technology
Dalian Jiaotong University
Dalian, China
yangshuodelove@163.com

***Abstract*—In order to analyze the shopping habits of consumers and more accurately mine the characteristics of consumption, we hereby have proposed and proved Theorem 1-3 to improve the classical Apriori algorithm, resulting in the reduction of database access. We improved the efficiency in the frequent-itemsets-based establishment of strong association rule. With this new design we fulfilled the timely recommendation of related products to customers, reflecting the principle of personalized service in e-shopping.**

Keywords-electronic commerce; association rule; apriori algorithm; frequent itemset

I. INTRODUCTION

As a new application of the Internet, e-commerce has entered all areas of traditional business activities, influencing and changing various aspects of social life both directly and indirectly. There is no doubt that the emergence of electronic commerce promotes productive force, and at the same time brings a revolution in business, management and the ways people live[1]. Fig. 1 shows the basic model of e-commerce.

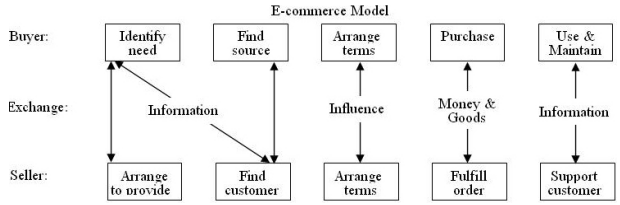

Figure 1. E-commerce Model

Generally speaking, seasonal alteration would influence sales. Selling goods in selling seasons would be scarce, therefore sellers and producers need to figure out the real-time information about the purchasing of goods to ensure the delivery rate of the hot commodities. When the off-season arrives, the sales of certain commodities will decline, thus sellers and producers would be well advised to grasp consumers' interest by mining strong association rules in order to optimize the promotion of products and increase sales. In the system of modern market economy, with the collection and storage of large amounts of data, businessmen are increasingly interested in mining association rules from their databases. From a large number of records of daily transaction, people would find interesting relationships that can help to optimize and allocate resources rationally and assist decision-making of business, such as cheap analysis, cross-shopping[2] and classified design.

The analysis of shopping basket is a typical example of association rule mining[3]. The general process is to analyze customers' purchasing habits via digging into the associations between different goods in customers' shopping baskets. By understanding consumption preference, retailers could develop efficient marketing strategies. For example, in a single experience shopping in a large supermarket, if we calculated the possibility of customers buying computers and office software (or what types of office software), the supermarket agents could optimize the layout of shelves and guide consumption on the basis of the parameter. If the parameter is greater than the minimum value fixed by dealers in advance, then computers and office software should be laid closely to each other, which may stimulate customers to purchase the two kinds of commodities at the same time.

Through the above analysis, we can see that the anticipation of purchase activities has practical application. In the research, we obtained association rules through data mining, valuable information and storage. Then, according to the preference, we can speculate their future purchase activities[4]. However, traditional Apriori algorithm of association rule requires a full scan in databases to find each collection of frequent itemset "L_k". When utilizing frequent itemsets to generate strong association rules, the algorithm needs to judge each frequent itemsets, which increases the complexity and reduces efficiency. The proposed algorithm in the research is based on the traditional Apriori algorithm but fulfills reduction in the frequency of traversal in the databases and optimization in the methodology of L_k generation, and in strong association rule construction the new algorithm uses relative theorems to shrink the number of frequency itemsets. This requires analysis from a large number of historical data of sales to identify the degree of associations among a number of commodities, extracting association rules that are applied to recommendation systems[5] in visual form to meet customers' personalized demands[6].

II. ASSOCIATION RULE

A. Data Mining

Simply speaking, data mining extracts useful and potential rules hidden in a massive, incomplete, noisy, fuzzy and random database[7]. In general situations, data mining is regarded as a fundamental step in the process of discovery of database knowledge, interacting with users or

978-0-7695-4818-0/12 $26.00 © 2012 IEEE
DOI 10.1109/DCABES.2012.51

knowledge bases by transmiting interesting models to the users or storing new knowledge in knowledge bases[3]. Based on the perspective, a typical data mining system has the following main components, shown in Fig. 2.

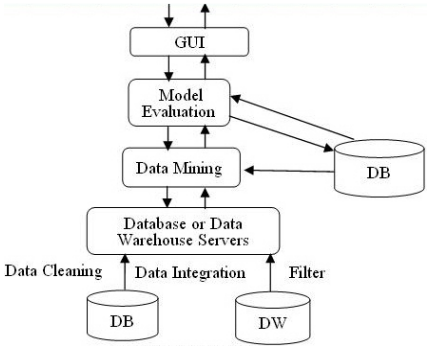

Figure 2. Data Mining System

B. The Definition of Association Rule and the Processes of Mining

Essentially, Association rule mining seeks valuable associations between different attributes in data sets. It is an important branch of data mining. Let $I=\{i_1, i_2, \ldots, i_m\}$ be a collection of items, D be a collection of transactions in a database. Each transaction T is a collection of different items, therefore $T \subseteq I$. Presumed A to be a set of items, a transaction T would contain A if and only if $A \subseteq T$. Association rule is an implication like the form "A→B" where $A \subset I$, $B \subset I$ and $A \cap B = \varnothing$. Established rules like "A→B" have parameters like "support degree" and "confidence level". Specifically, support(A→B)=P(A ∪ B); confidence(A→B)=P(B|A). Besieds, association rules meeting the minimum support degree(min_support) and the minimum confidence level (min_confidence)[8] are the strong association rules which will be used as knowledge to output.

The process of association rule mining is divided into two steps:

- Generate all frequent itemsets: the frequency of itemsets counted from each transaction in databases should not be less than min_ support.
- Produce strong association rules by the frequent itemsets obtained: the rules must meet the min_support and the min_confidence.

For convenience, we introduce the following concepts:

"Itemset" represents the collection of items. "K-Itemset" signifies a collection that contains K items. For example, {Computer, Office_Sofeware} is a 2-Itemset. "Support count" means the frequency of an itemset. It is equal to the number of transactions that contain the itemset. "Frequent Itemset" shows the itemset that meets the minimum support degree, usually denoted by l_k.

C. Improved Apriori Algorithm

1) Apriori Algorithm

The classical algorithm of association rule was firstly proposed by Agrawal et al., called Apriori. It is an iterative method of layer by layer search, applying K-Itemset to search for (K+1)-Itemset. Firstly, the algorithm identifies the collection of Frequent 1-Itemset, denoted by L_1. Collection of Frequent 2-Itemset "L_2" is computed from L_1. We use the same method to acquire L_k ($K \geqq 2$) until it cannot find L_{k-1}. Actually, the process contains two steps-connection and pruning. In order to improve the efficiency of obtaining frequent itemsets in each loop, Apriori algorithm introduces "Apriori characteristic" which means that non-empty subset of a collection of frequent itemsets must be frequent. Using the Apriori characteristic, non-frequent itemsets in the set of candidate itemsets "C_k" will be pruned. Fig. 3 shows the main steps of the Apriori algorithm.

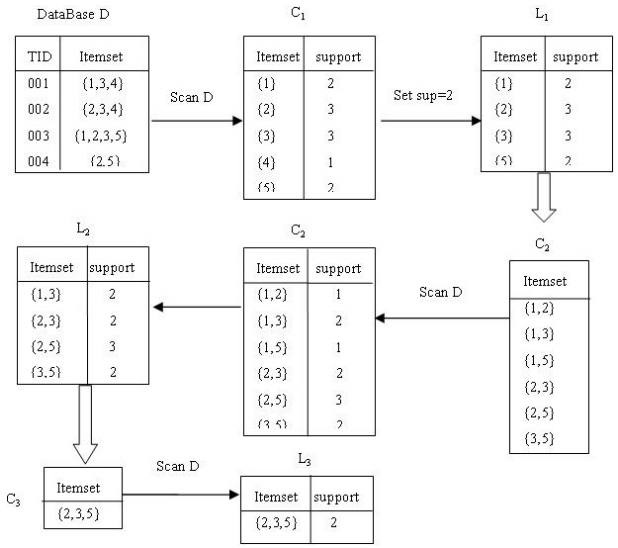

Figure 3. Main Steps of the Apriori Algorithm

2) Improvement of Apriori Algorithm

Through the analysis of the traditional Apriori algorithm, we know that it needs a full scan in databases to find each L_k ($K \geqq 1$), thus reducing its efficiency. In order to reduce the frequency of traversal of the databases, the research proposes an improved algorithm of L_k generation, which is realized via JSP dynamic web technology[10]. Based on the above viewpoints, the key point of optimization of L_k creation is to reduce the frequency of database access; therefore we put forward the following improvements.

In order to describe the remaining content suitably, we further introduce the following symbols: C[k] is a set of candidate itemsets in which each itemset's length is k; L[k] is a collection of frequent itemsets in which each itemset's length is k as well; T[k] is a subset of databases and it corresponds to C[k], also called reference database. To calculate each itemset's support degree in C[k], T[k] replaces DB as a search domain; Function "count(t)" represents the number of elements in a transaction in DB; Function Apriori_Gen(L[k]) is used to produce C[k+1] by L[k]; Function Subset(C[k+1], t) is used to get a subet based on transaction "t", and each itemset in the subet contains (k+1) items.

The pseudo code of the improved Apriori algorithm is given as follows:

(1) T[1] = D;

(2) L[1] = {Find_Frequent_1_Itemsets(T[1])};

(3) for(k =1; L[k]! =Φ; k++)
(4) begin
(5) C[k+1] =Apriori_Gen(L[k]);
(6) Foreach t∈T[k]
(7) begin
(8) sum =count(t);
(9) if(sum < k+1) T[k+1] = T[k]−t;
(10) end
(11) Foreach t∈T[k+1]
(12) begin
(13) Ct=Subset(C[k+1], t);
(14) Foreach candidate c∈C[k+1]
(15) if(c∈Ct) then
(16) c. support ++;
(17) end
(18) L[k+1] = {c∈C[k+1] | c.support >= min_support}
(19) end
(20) L = $\cup_k L_k$;
(21) Return Generate_Rules(L);

Multiple stages are involved in the improved algorithm. The first stage is to scan the database and to copy it to T[1], and then construct the collection of Frequent 1-Itemset "L_1", shown in step (1) and (2); the second stage is to generate C[k+1] by L[k], as in the step (5); thirdly, prune T[k] for originating T[k+1], illustrated in the step (6) - (10); forthly, using T[k+1] insteads the database to calculate the support degree of each candidate itemset in C[k+1], illuminated in step (11) - (18); fifthly, if L[k+1] is an empty set, exit the loop and combine all L_k by L = $\cup_k L_k$, otherwise rewind to the step (3); the loop continues; sixthly, according to the L acquired in the fifth stage, we use function "Generate_Rules(L)" to optimize the process of getting strong association rules, shown in step (21) (described in section 2.3.2.3 in detail).

The basic principle of the first improved part in the new algorithm is: If the number of elements contained in a transaction "t" in DB is less than k+1, then t is invalid when counting support degree of each itemset in C[k+1]. The improved Apriori algorithm introduces a variation "T[k]", which makes the calculation do not need to re-visit the DB. When k=1, T[1]=D; When k⩾2, the method to produce T[k] is shown in the step (5)-(10) in the above algorithm. The following two theorems is to prove that T[k] is reasonable to instead DB.

Theorem 1: The subset of the collection of frequent itemsets "L[k]" is frequent, including k itemsets of L[k-1] at least.

Proof: The function "Apriori_Gen(L[k-1])" generating C[k] is defined as follows:

(1) For any two itemsets "a, b" in L[k−1], the algorithm performs the computation of a × b. The specific procedure is: a={i_1, i_2, …, i_{k-2}, i_{k-1}}, b={j_1, j_2,…, j_{k-2}, j_{k-1}}, if i_1=j_1, i_2=j_2,…, i_{k-2} = j_{k-2}, i_{k-1}<j_{k-1}, then C[k]=a × b={i_1, i_2,…, i_{k-2}, i_{k-1}, j_{k-1}}.

(2) Foreach c∈C[k]
If Subset(C[k−1], c)∉ L[k−1] then
C[k] = C[k]−c

Due to the above definition and the fact that L[k] is produced by C[k], the (k−1)-dimensional subset of C[k] is involved in L[k−1] and therefore frequent. The subset has at least k(C_k^{k-1} =k) itemsets.

Theorem 2: Let t represent any transaction in a database. Function count(t) signifies the number of elements in t, then t∈T[k], if and only if count(t)≥k.

Proof: Firstly, from Theorem 1, it is known that k items constitute an itemset of L[k], so if count(t)≥k, then it can be used to count the support degree of candidate itemsets, therefore t ∈ T[k]. Furthermore, we use reductio ad absurdum to prove if t∈T[k], then count(t)≥k. Assume that "count(t)<k" which means the number of elements in t is less than k, thus t does not contain any itemset in C[k]. When computing the "support count" of c(c∈C[k]), t is invalid. In other words, computing the "support count" do not need to scan t, therefore t∉ T[k] which contradicts the proposition, thus if t∈T[k], then count(t)≥k. QED. (quod erat demonstrandum)

From theorem 1 and 2, we can use T[k] to count the "support count" of c(c ∈ C[k]) and the the number of itemsets in T[k] is apparently less than that of in DB; therefore utilizing T[k] to substitute DB would reduce the frequency of DB access.

a) Calculation of Support Degree

One of important factors to judge interest degree of a rule is to measure its potential usefulness. we usually use "support degree" to evaluate it. Support degree of an association rule is a percentage describing the qualified tuples' shares in all tuples. The expression using predicate logic is as follows: Let D be the object domain, A⊂D, B ⊂ D and A ∩ B=Φ. Unary predicate Support(X) signifies the support degree of X. Num(Y) denotes the number of tuples that contain Y. Then

$$\text{Support}(A \rightarrow B) = \text{Num}(A \cup B) \div \text{Num}(D) \quad (1)$$

"Num(A ∪ B)" is called "support count" which usually substitutes support degree to measure the usefulness of a rule.

b) Calculation of Confidence Level

Each association rule like "A→B" should have parameters to evaluate its effectiveness, one of which is the degree of confidence. The expression using predicate logic is as follows: Let D be the object domain, A⊂D, B⊂D, and A ∩ B=Φ. Predicate Confidence(X) indicates the confidence degree of X. Num(Y) denotes the number of tuples that contain Y. Then

$$\text{Confidence}(A \rightarrow B) = \text{Num}(A \cup B) \div \text{Num}(A) \quad (2)$$

c) Construction of Strong Association Rule

After preparing all frequent itemsets, they could generate strong association rules. The following equation is another way to calculate confidence degree:

$$\text{Confidence}(A \rightarrow B) = P(B|A) = \text{Support\_Count}(A \cup B) \div \text{Support\_Count}(A) \quad (3)$$

In (3), Support_Count(A ∪ B) is the number of transactions that contain itemset "A ∪ B"; Support_Count(A) is the number of transactions that contain itemset "A". According to (3), strong association rules are created as follows:

- For each frequent itemset "a", the first step is to produce all non-empty subset of it.
- For any non-empty subset "b" of "a", if suport_count(a)÷support_count(b)≥min_confidence, then the algorithm outputs a rule "b→(a−b)"

where min_confidence represents minimum confidence level.

In fact, the function "Generate_Rules(L)" further optimize the process according to Theorem 3.

Theorem 3: Let L be the collection of frequent itemsets, l be an itemset of L. For any subset a, $b \in l$, if support_count(a) < support_count(b) and $a \not\Rightarrow l\text{-}a$, then $b \not\Rightarrow l\text{-}b$.

Proof:

confidence($a \Rightarrow l-a$) = supprot_count(l) ÷ supprot_count(a)

confidence($b \Rightarrow l-b$) = supprot_count(l) ÷ supprot_count(b)

supprot_count(a) < supprot_count(b) and $a \not\Rightarrow l\text{-}a$

confidence($b \Rightarrow l\text{-}b$) < confidence($a \Rightarrow l\text{-}a$)

and confidence($a \Rightarrow l\text{-}a$) < min_ confidence

$b \not\Rightarrow l\text{-}b$ Q.E.D

Theorem 3 shows that the second advantage of the improved Apriori algorithm is that we could further implement the operation of pruning to reduce the frequency of traversal of the frequent itemsets in L. In fact, we can pre-sort frequent itemsets in L according to their support degrees. If the confidence level of a frequent itemset is lower than the minimum degree of confidence, then other frequent itemsets whose support degree is higher than that of it will not produce strong association rules.

III. A CASE REPORT

In order to apply the improved Apriori algorithm to electronic commerce, we develop a shopping site that achieves shopping online recommendation system. The front module of the website is used for commodity display, sales and recommendation, while the back module of it is designed for management of commodities and mining association rules. When customers enter the shopping site, the system will predict their future purchasing activities according to the goods already in their shopping baskets and recommend related products in order to stimulate consumption and gain more profit.

The development tool of the website is Macromedia Dreamweaver 8; the database management tool is Microsoft SQL Server 2000 and the WEB Server is Tomcat 6.0.

The mechanism of goods recommendation is the core part of the website. Its logical process is described as follows:

- In the admin interface, users input a minimum support count and a minimum confidence level according to the sales of all kinds of goods, shown in Fig. 4.
- Based on the minimum support count, the improved Apriori algorithm results in a collection of frequent itemsets "L".
- On the basis of minimum confidence level, we obtain a set of strong association rules which are stored in the database table "tb_Association" shown in Table 1.
- According to the goods already purchased by customers, the system queries the table "tb_Association" and recommends other relative goods to the customers, shown in Fig. 5.

Minimum Support Count 6 Minimum Confidence Degree 55 % Begin Mining

ID of Commodity	Name of Commodity	Support Count
14	White Wine	8
20	Pork	7
32	Home Theater	7
21	Lotion	6
23	Thermal Underwear	6

Figure 4. Sales List

The form of recommendation is shown in Fig. 5:

Products Already Purchased	Products Recommended	Support Count
White Wine	Pork	6
Lotion	Thermal Underwear	6

Figure 5. Recommendation of Commodity

From Fig. 6, it could be learned that frequent itemsets that cannot generate strong association rules are pruned according to Theorem 3, which improves the efficiency of the algorithm.

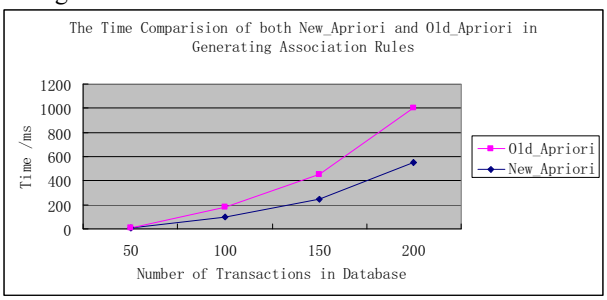

Figure 6. Comparision of Efficiency

IV. CONCLUSION

In the research, data mining is applied to e-commerce shopping areas, with an improved Apriori algorithm proposed. We establish the mechanism of recommendation of commodities and raise the method of calculating the support count and confidence level. From the application of the case, users could quickly build association rules by the improved Apriori algorithm and recommend appropriate products to customers in a timely approach.

The rules digged out are stored separately in a data table "tb_Association" shown in Table 1. Each time when customers settle accounts, system will scan what the customers has already purchased and query this table to recommend other products to them.

The structure of the data table "tb_Association" is as follows:

TABLE I. STRUCTURE OF TB_ASSOCIATION

Characteristic	Data Type	Length	Key	Description
ID	bigint	8	Yes	ID
GoodsName	varchar	200	No	The name of goods
Min_support	int	4	No	Minimum of support count
Min_confidendce	float	8	No	Minimum of confidence level
Num	Int	4	No	The categories of goods in this rule

REFERENCES

[1] Xiaotao Huang, Wang Fen, Ye Tao, Yanxiong Zheng. The Introduction of E-commerce. Tsinghua University Press, 2005: 1-29.

[2] Ron Kohavi, Foster Provost. Applications of Data Mining to Electronic Commerce. Data Mining and Knowledge Discovery, 5: 5-10, 2001.

[3] HAN Jiawei,KAMBER M. Data mining concepts & techniques(Version 1). Beijing: China Machine Press, 2001: 149-183.

[4] Zhongzhuang Wang, Lundan Deng, Wenbing Shi. Research on the Application of the Data Mining Technique to the E-Commerce Recommendation System. Microelectronics and Computer, 30(1): 197, 2007.

[5] Zhengguo Ding, Chen Jing. Individuation Recommendation System Based on Association Rule. Computer Integrated Manufacturing Systems, 9(10): 892, 2003.

[6] Xiong Feng, Qi Luo. Research on Personalized Recommendation Algorithm in E-Supermarket System. APWeb/WAIM 2007 Ws, LNCS 4537: 340–347, 2007.

[7] Yuanyuan Zhao, He Jiang, Baoyou Sun, Xiangjun Dong. Improved Apriori Algorithm Based on Weighted Mining Association Rules. DCABES 2008 Proceedings Volume 1. 2008: 433-436.

[8] Runsheng Shi, Zhao Qing. Improved Algorithm for Mining Association Rules and its Achievement. Journal of Tongji University, 30(2): 223, 2002.

[9] You Wen, Shuisheng Ye. E-Commerce Recommendation System and Collaborative Filtering Recommendation. Computer Technology and Development, 16(9): 70-72, 2006.

[10] Guohui Wang, Wenli Li, Yang Liang. A Comprehensive Manual of the Development of JSP Database Systems. People's Posts and Telecom Press, 2006: 1-30.

A Sampling Method for Mining User's Preference

Jianfeng Zhang, Weihong Han, Yan Jia
College of Computer
National University of Defense Technology
Changsha , Hunan, P.R.China
jfzhang@nudt.edu.cn

Peng Zou
Academy of Equipment Command and Technology
Beijing, P.R.China

***Abstract*—Recent years, society relies heavily on the network infrastructure and information system. Protecting these assets from frequently network attacks needs to deploy some distributed security systems. However the amount of data produced by many distributed security tools can be overwhelming. So it's very difficult and limited to get the most risky alert through manual process based on the huge network alerts with many attributes. The common method used to rank the alerts is scoring function, the higher the score, the more risky of the alert. Our motivation is that many times, user can not precisely specify the weights for the scoring function as their preference in order to get the preferable Ranking.**

In this paper, we propose a sampling method to mining user's preference. Based on this preference, the most risky alerts can be easily ranked for emergency response. An extensive performance study using both synthetic and real datasets is reported to verify its effectiveness and efficiency.

***Keywords*-Network Security Evaluation; Preference; Top K; Ranking; Sampling;**

I. Introduction

In recent years, with the development of human society, the network has been integrated into all aspects of people's lives. Along with the convenience, network also brings many security problems, the global Internet attacks occur frequently, and make a highly severely impact on the global network. At the same time, in our county a variety of network security incidents have become inevitable, such as network economic crimes, large-scale network attacks, network stolen and so on. All these have became a constraint to our economic development, especially became the key factors that threaten social stability and national security.

Fortunately, most companies and organizations have been aware of urgency of protecting their information system, which have become more important assets for them to develop their business fast. Especially to some security department of the country, the administrators and cyber security researchers have focused on the large scale network security evaluation.

Over the last few years, a considerable amount of research effort on developing approaches and methods to effectively evaluate the network security. The notion of assessing computer network security is proposed by Tim Bass [1]. In this paper, a multi-sensor distributed intrusion detection system is considered to assess computer network security through data fusion and data mining. Meanwhile, Chen Xiuzhen et al.[2] develop a quantitative hierarchical threat evaluation model to evaluate security threat status of a computer network system, the computational method in this model is based on the structure of the network and it focus on the threat situation. The threat indexes of services, hosts and local networks are calculated by weighting the importance of services and hosts.

In our previous work, we also build a novel network security index system to evaluate the network security objectively and comprehensively. This model is also a hierarchical model, and how to specify the weights for each factor is very important to the final evaluation.

Table I
A SET OF SOME ALERTS

Alert ID	Asset	Threat	Occurrence
1	0.3	0.7	0.9
2	0.8	0.6	0.3
3	0.5	0.8	0.8
4	0.6	0.2	0.5
5	0.2	0.4	0.2

The network security alerts often have many attributes, such as asset, priority, reliability, risk, type et al. The common method used to rank the alerts is scoring function, the higher the score, the more risky of the alert. Among various problem description, the simplest but very common case assumes that a monotonic scoring function is provided. Usually, the scoring function is specified as a weighted sum of scores. In this situation, the weight vector $\overrightarrow{\omega} = \{\omega_1, \omega_2, \cdots, \omega_d\}$ is specified as users' preference. Each ω_i represent the importance of the attribute A_i. Table I shows five alerts with three attributes. When a user sets $\overrightarrow{\omega}$ to be $(0.4, 0.5, 0.1)$, the alerts are ranked as a sequence (3, 2, 1, 4, 5), and the 3rd alert is considered to be most risky to this user. So specifying the precise weight vector for the scoring function to rank the network security alerts according to different application scenarios is very important. However, many times users are very confused to make sure the specific weight setting as their preference. Although many existing

978-0-7695-4818-0/12 $26.00 © 2012 IEEE
DOI 10.1109/DCABES.2012.14

Table II
THE SUMMARY OF FREQUENTLY USED NOTIONS

Notion	Meaning
D	A multidimensional data set
d	The dimensionality of D
D'	K skyband data set
p, q, r	Objects in D
$\prec$	A preference relationship
$\|S\|$	the number of objects in S

studies have working on how to get user's preference [3][4], effectively mining user preference is still a challenging problem.

The remainder of this paper is organized as follows. In Section II, we present a formal problem definition. In Section III we propose our sampling method to mining user's preference. An extensive empirical evaluation using both synthetic data sets and real data sets is reported in Section IV. Finally, our work of this paper is summarized in Section V.

II. PROBLEM DEFINITION

In this section we formally define the problem. Table II summarizes the notations that used throughout the paper.

Problem statement. In many applications, users are preferable to the objects with the small value, but in network security field, the security mangers want to know the most risky attacks which corresponding with the high value. An object with high value can be easily convert to with a lower value using a linear function. So in this paper, we still consider that an alert with small value is more risky. We assume that users can not precisely specify the weight vector for the scoring function as their preference to get the top k alerts. But actually they can easily choose the more risky alert from a small set with two or three alerts.

We have a dataset D of n objects. Each object is described by d attributes. We use $p.A_i$ to refer to the value of an attribute A_i for an object p. For ease of discussed, we assume that all of these numerical attributes are normalized to range form 0 to 1, and a smaller value indicates more risky alerts. As such we say p domain q if $p.A_i < q.A_i$ for at least one value of i and $p.A_i \leq q.A_i$ for $1 \leq i \leq d$. Given a set of objects, the skyline consists of all the objects that are not dominated by others. Then the skyband is generated by the notion of skyline in [5]. Specifically, the k-skyband of a data set includes all of the objects that are not dominated by fewer than k objects. Especially when k equals 1, the 1-skyband is the skyline. So in this paper the dataset we actually use is the K-skyband of the real dataset. We also have a linear scoring function which is defined as defined as weight for sum function. Users will specify their preference by providing a weight vector $\overrightarrow{\omega} = \{\omega_1, ..., \omega_d\}, 0 \leq \omega_i \leq 1$ and $\sum_{i=1}^{d} \omega_i = 1$. Then the score of an object can be calculate by $\sum_{i=1}^{d} \omega_i \times p.A_i$.

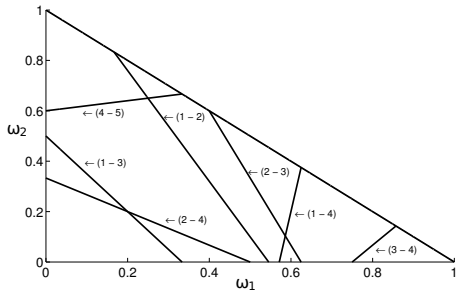

Figure 1. Possible Ordering

Now the problem of this paper is formally defined as follows.

Suppose we have the weight space in d-dimensional space formed from $\{\omega_1, ...\omega_d\}$, and every point in this space corresponds to a particular setting of the weights (represent as some user's preference). Based on these preferences, we can get a lot of different rankings in the whole weight space.

Let k be the sequence number of interactive comparison with user, C_k be the representative R objects that submitted to the user, c_k be the user's preferable object that in C_k, and O_k be the remaining orderings that after $k-1$ interactive comparison. Let

$$O_{k+1} = Interact(C_k, c_k, O_k) \tag{1}$$

be the ordering set that satisfied the condition $c_k \prec C_K - \{c_k\}$. Then we define a sequence as follows,

$$\Re = (C_i, c_i, O_i)_{i=1}^{k},\ k = 1, 2, \cdots, k. \tag{2}$$

Based on this sequence, the goal of our method is to find a minimized k that makes $|O_k| \leq 1$, then we can elicit the user's preference by this only ordering.

Let us give an example. Figure 1 shows all possible 11 orderings of alerts in Table I. Each line generated by two objects (p, q) divides the weight space into two part. If the weight vector $\overrightarrow{\omega}$ places in one part means that p is ranked before q, and in the other part q must be ranked before p. Suppose a user consider alert 1 is more risky than alert 2, then we can confirm that this user's preference must be placed in the area below line (1,2). After k times interactive comparison, we may decrease the weight space in a very small area. Then it's very easy to give an optimal weight setting according the knowledge that learned from this user.

III. SAMPLING METHODS TO MINING USER'S PREFERENCE

In this section, we use a sampling method to mining user's preference.

A. Basic idea

Let us start the discussion with the basic solution. Suppose we have a dimensional weight space. Firstly, we can use a uniform sampling method to get a list of weight vectors as $S = \{\overrightarrow{\omega}_1, \ldots, \overrightarrow{\omega}_s\}$, and use a k-skyband algorithm to get the dataset . Secondly, based on these weight vectors, we can use the scoring function to evaluate each object, and rank these objects by the ascending order. Thirdly after getting a lot of rankings, we can compare the difference among these rankings, and give a comparable oracle to ask user to choose his/her preferable object. This step is repeated until the unique ranking is left. Then we can get the user's preference according this ranking.

This naive sampling method mentioned above uses uniform sampling technique [6] to sample the whole weight space. Recall that the weight space is a d-dimensional space formed from $\omega_1, ..., \omega_d$, and each $0 \leq \omega_i \leq 1$. If the sampling accuracy is set as ϵ (i.e.$\epsilon = 0.01$) degrees, then the size of sampling is about $s = (1/\epsilon)^d$. This size is increasing exponentially with the larger dimensions.

To improving the sampling cost, we propose two sampling methods, Top-Down Sampling Generation and Constraint Uniform Generation.

B. Top-Down Sampling Method

In this section, we propose a top-down sampling method to sampling the weight space. We use a set to maintain the weight space, and initialize the set as only one element that describes the whole weight space. The element used to describe the weight space is formulated as $\Phi(\upsilon, \rho)$, where υ is the center point of the space in d dimensional Euclidean space , and ρ is defined as the maximizing distance from the central point υ to the surface of the space. This algorithm is shown in Algorithm 1.

Firstly, we divide the weight space at high level. Each sub-space can be described as $\Phi(\upsilon, \rho)$, that υ is the center point of the subspace in d dimensional Euclidean space , and ρ is defined as the maximizing distance from the central point υ to the surface of the subspace. In symbols, $\Phi(\upsilon, \rho) = \{\sum_{i=1}^{d}(\omega_i - \upsilon_i)^2 <= \rho^2\}$. Then we select the convex vertices of the whole space which can be expressed by means of a set of linear constraints $\Gamma = \{\sum_{i=1}^{d-1} \omega_i = 1, \omega_i >= 0\}$ to be the initialized points, and set the ρ to be 0.5 for all points (All the initialized Φ are stored in Ω).

Secondly, Checking the satisfaction of the each subspace $\Phi \in \Omega$. if Φ is out of the convex that constrained by Γ, then removing this subspace from the Ω. Otherwise, splitting this subspace to some small subspaces and adding them to Ω. Then , using the υ as the weight vector represents Φ to computer the ordering of the candidate.

Thirdly, According to some selection policy, a small candidate set $\{p, q\}$ will be returned to ask user to choose his/her preferable object.

Finally, based on the user's choice we add the preference ($p \prec q$ or $q \prec p$) in Γ. If $p \prec q$, we add $(\overrightarrow{p} - \overrightarrow{q})\overrightarrow{\omega} < 0$ to Γ. Otherwise $(\overrightarrow{q} - \overrightarrow{p})\overrightarrow{\omega} < 0$ is added to Γ. Then we'll go back to second step to check the satisfaction. This algorithm is terminated when the ρ of every Φ meets the sampling accuracy.

Algorithm 1: TopDownSamplingMethod

Input: K-skyband dataset $D^{'}$,Dimension d, Sampling reduction coefficient δ Sampling accuracy ε
Output: The weight space set Ω
Initialize Ω with some subspaces Φ;
Initialize constraints Γ with some basic knowledge;
while $\rho > \varepsilon$ **do**
  for *each* $\Phi in \Omega$ **do**
    Using Γ to check the satisfaction of Φ;
    if *satisfied* **then**
      According δ, Split all the $\Phi_i \in \Omega$;
      Set $\rho \longleftarrow \rho * \delta$;
    else
      Removing Φ from Ω;
  Computer the orderings that represented by each Φ;
  Select an optimal objects pair p, q;
  Answer the user to choose his/her preferred object between p and q;
  Adding constraint $p \prec q$ or $q \prec p$ in Γ according user's selection;
return Ω;

C. Constraint Uniform Sampling Method

In this section, we propose a constraint uniform sampling method to generate the sampling weight vectors. This algorithm is shown in Algorithm 2.

Firstly, we set the sampling size , and initialize the weight space as a set of constraints as follows.

$$\begin{cases} \omega_1 + \cdots \omega_{\mathrm{d}} = 1 \\ 0 \leq \omega_i \leq 1 \end{cases}$$

Secondly, we use the uniform sampling method to generate s weight vectors from the weight space that be constrained by the inequalities. Then using the scoring function to computer the ranking of the candidate with each weight vector in S.

Thirdly, According to some selection policy, a small candidate set will be return to let user choose his/her preferable object.

Finally. Based on user's choice, updating the constraints and getting the new constraint weight space to repeat the second step until the termination conditions are satisfied.

While repeating the procession, more and more inequalities are inserted into the constraints and divide the weight

space more and more small. As the sampling size is fixed, the sampling accuracy is becoming higher.

In this method, we want to uniform generate sampling point from a convex hull that constrain by some inequalities. So we define one of our terminal condition is that all the sampling weight vectors rank the same orderings, and another terminal condition is that the volume of convex hull is very small. However, computing the volume of convex hull in high dimensions is also very expensive. So we define a probability to guarantee this.

Suppose the volume of the convex hull is Vol, we unform sampling a point in d-dimensional space that locate in this convex hull has a probability $Vol/1^d = Vol$. If the probability of a uniform sampling point locates not in the convex hull is greater than Pr, then the algorithm is terminated. As shown in follows, Pr is a system parameter and we calculate an approximate Vol based on the sampling points. (i.e. if we sample 100 weight vectors in d-dimensions, only 5 locate in the convex, the $Vol = 0.05$)

$$(1 - Vol)^s \geq Pr \tag{3}$$

Algorithm 2: ConstraintSamplingMethod

Input: Dataset D,Dimension d, Sampling size s, Pr
Output: The weight space set Ω
Initialize constraints Γ with some basic knowledge;
Initialize $\Omega = \emptyset$;
Generate s weight vectors through s' unform sampling;
Initialize $Vol = s/s'$;
while $(1 - Vol)^s < Pr$ **do**
  Add the s weight vectors into Ω;
  Computer the orderings using every $s \in \Omega$;
  Select an optimal objects pair p, q;
  Answer the user to choose his/her preferred object between p and q;
  Add constraint $p \prec q$ or $q \prec p$ in Γ according user's selection;
  Remove all $s \in \Omega$;
  Generate s weight vectors through s' unform sampling;
  $Vol = s/s'$;
return Ω;

Take Figure 1 for example. As $\omega_d = 1 - \sum_{i=1}^{d-1}$ in every $\overrightarrow{\omega}$, we use the two dimensions plane to discuss the 3-dimensional weight space. First, we can constrain the original weight space by a set of constraints as $\{\omega_1 \geq 0, \omega_2 \geq 0, \omega_1 + \omega_2 \leq 1\}$. Based on some selection policy, alert 1 and alert 2 are returned to ask the user to choose. When user choose alert 1 as the more risky alert. then an inequality $(0.7-0.8)\omega_1 + (0.7-0.6)\omega_2 + (0.9-0.3)(1-\omega_1-\omega_2) < 0$ is insert into the constraint set to get the new weight space (i.e. the original space is divided by the line 1-2 and only the right of the space is reserved).

D. Finding Optimal Solution

No matter what sampling method we use, we can get a lot of different ranking of objects based on generated weight vectors. Each ranking can represent a small weight space, so the aim of our solution is to finding some well process that makes the weight space fast convergence rates. This is also means that we can minimize the count of interacting with users.

As discussed before, the interactive search is considered as a sequence $\Re = (C_i, c_i, O_i)_{i=1}^k,\ k = 1, 2, \cdots, k$. It's easily found that the $\Re_{i+1}$ depends on $\Re_i$, and finding the most optimal global solution that makes k minimized is very computational. So we use a greedy algorithm that try the best to decrease the possible orderings sharply in every interactive comparison. So every step we need to return some optimal objects to ask user to choose. To select the better object pairs, we define an evaluation function as follows.

$$eval\,(C_R) = \sum_{j=1}^{R} (|O_j| - \alpha * |O_i|) \tag{4}$$

where $|O_j|$ be the number of remaining orderings from O_i that satisfied $c_j \prec C_i - \{c_j\}$ and α be parameter to describe user's expectant remaining orderings. Based on this evaluated function, the C_R with minimized value will be returned to user. Based on this candidate, no matter which object is chosen by user as his/her preferable objects, the remaining orderings is reduced sharply.

IV. Experiments

In this Section we experimentally evaluate the effectiveness and the efficiency of our method described in this paper. Firstly, the efficiency of the methods in this paper is measured on synthetic data sets. Then the real NBA data (It's more intuitive than the alerts datasets) set is used to further illustrates the effectiveness of proposed methods. All the experiments are implemented by Java and compiled by JDK 1.7, and we run all the experiments on Ubuntu Linux Operating system with Intel Core-2 Duo Processor and 2GB memory.

A. Synthetic data

For synthetic data set, we use the classical method [7] to generate the anti-correlated distribution datasets. In this section, we mainly focus to the performance of our algorithm. We show the sampling size, running time and interactive count of our algorithm under different parameters. We compare three sampling methods. Uniform Sampling (US), Top-Down Sampling (TDS) and Constraint Uniform Sampling (CUS). We test the proposed algorithms with the data size ranged from 100 to 100K and the dimension from 2 to 5. By default, we set the sampling accuracy to be 0.001 and

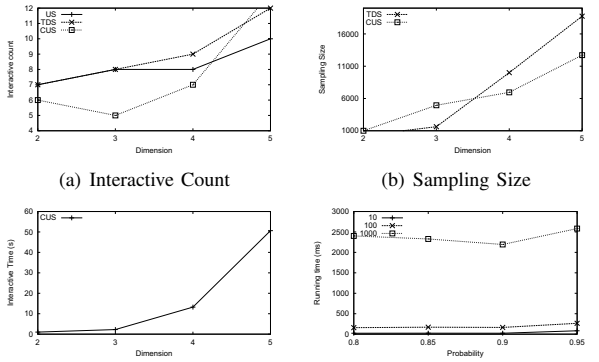

(a) Interactive Count (b) Sampling Size

(c) Running Time For CUS (d) Running Time with Varying Pr

Figure 2. Performance evaluation

the probability in algorithm CUS to be 0.9. The interactive count is shown in Figure 2(a), we can see all this count can be acceptable by users. From Figure 2(b), we can see the sampling size is increased almost linearly in CUS. Because the sampling size in US algorithm is exponentially increased, we don't show it in this figure. In Figure 2(c), we only show the interactive time for algorithm CUS on every steps. Because the other two algorithms with higher dimension are expensive. So we extend to test the parameter Pr of CUS. As shown in Figure 2(d), we set the probability from 0.8 to 0.95. and the number 10, 100, and 1000 are the size of sampling that used to represent the constraint weight space. we can see that the running time scales well with the number of dimension.

B. Real data

we use the NBA data set [8] to evaluate the efficiency of our methods. The NBA data set contains 16916 game statistics of all NBA players from 1973-2009. Each record represent a player by regular season (year), player name, GP, PTS, REB, AST, STL, BLK, A/T, PF, FGA, FGM, FTA, FTM, TPA and TPM. To testing the efficiency of our algorithm, we present several interesting cases.

The first case is to finding the top k center players in NBA history. Therefore, we issue a center player on three attributes PTS, REB and BLK. After using the 10-skyband algorithm, we get 92 candidates. When we use the Top-Down Sampling method to mining my preference. Then after 10 interactive comparison , The algorithm return my preference as the weight vector (0.02,0.2,0.78). the Top 5 players with this preference are Mark Eaton(1984), Elmore Smith(1973), Hakeem Olajuwon(1989)Rasheed Wallace(2003) and David Robinson(1991).

The second case is to find the top k forward players with the high ability to get scores. we evaluate the players on four attributes PTS, FGP, FTP and TPP. First we get 59810 skyband candidates, then we use Constraint Uniform Sampling Algorithm to elicit my preference. and set the sampling size to be 1000 and Pr to be 0.9. Then after 12 steps the weight vector (0.4,0.15,0.2,0.25) is returned as my preference. Under this preference, Top 1 and 2 players are Mike Conley in 2008 season and 2007 season, Kobe Bryant (2005)Michael Jordan (1989,1986) are the next three best players.

V. Conclusion

In this paper, we have studied the problem of mining user's preference. Our target is to use the minimized interactive comparison to find a user's preference. The sampling methods used in this paper can do well in lower dimensions, but in high dimensions (s.t. $d > 5$)is still hard problem. As a future work, we try to apply coordinate geometry methods in solving problems.

Acknowledgment

This paper is supported by the National 863 Program of China (2010AA012505, 2011AA010702, 2012AA01A401 and 2012AA01A402), National Natural Science Foundation of China (60933005), National Science Technology Support Program of China (2012BAH38B04) and National 242 Information Security Program of China (2011A010). We gratefully acknowledge the efforts of all team members in our project. Finally we would like to thank the reviewers for their insightful comments which significantly improved this paper.

References

[1] Tim Bass. Intrusion detection systems and multisensor data fusion. *Commun. ACM*, 43(4):99–105, 2000.

[2] C. Xiuzhen, Z. Qinghua, G. Xiaohong, and L. Chenguang. Study on evaluation for security situation of networked systems. *JOURNAL-XIAN JIAOTONG UNIVERSITY*, 38(4):404–408, 2004.

[3] Feng Zhao, Gautam Das, Kian-Lee Tan, and Anthony K. H. Tung. Call to order: a hierarchical browsing approach to eliciting users' preference. In Ahmed K. Elmagarmid and Divyakant Agrawal, editors, *SIGMOD Conference*, pages 27–38. ACM, 2010.

[4] Bin Jiang, Jian Pei, Xuemin Lin, David W. Cheung, Jiawei Han, and Jiawei Han. Mining preferences from superior and inferior examples. In *KDD*, pages 390–398, 2008.

[5] Dimitris Papadias, Yufei Tao, Greg Fu, and Bernhard Seeger. Progressive skyline computation in database systems. *ACM Trans. Database Syst.*, 30:41–82, March 2005.

[6] M.H. Kalos and P.A. Whitlock. *Monte carlo methods*. Wiley-VCH, 2009.

[7] Stephan Börzsönyi, Donald Kossmann, and Konrad Stocker. The skyline operator. In *ICDE*, pages 421–430, 2001.

[8] Databasebasketball_2009_v1.zip. http://www.databasebasketball.com/stats_download.htm.

Effect of Magnitude Differences in the Raw Data on Price Forecasting Using RBF Neural Network

Yonghua Yin
Faculty of Computer Engineering
Huaiyin Institute of Technology
Huaian, China
1165790450@qq.com

Quanyin Zhu*
Faculty of Computer Engineering
Huaiyin Institute of Technology
Huaian, China
hyitzqy@126.com

***Abstract*—In order to improve the stability on price forecasting with the RBF neural network, the researching and improvements on the raw data processing method for price forecasting using neural network are discussed in this paper. The magnitudes of the raw data are normalized to a relatively small magnitude, in other words, reducing the magnitude of the raw data to reduce the fluctuation range of the neural network training data. According to this idea, the different experiments are implemented with RBF neural network, which is using weekly price of 10 different agricultural products by enhancing and reducing the magnitude of the raw data. Comparing the experimental results with the actual data of three different experimental approaches, the experiment with the data reduced gets the best forecast results. And the forecasting average accuracy obtains 96.8 percent. Using the proposed improvements method not only improves the stability of the price forecasting by RBF neural network, but also being able to meet the needs of practical application.**

Keywords- RBF neural network; price forecast; stability; raw data; data processing

I. INTRODUCTION

In recent years, in order to improve the stability on price forecasting with the RBF neural network, at home and abroad have made a lot of improved methods: an improved BP neural network model based on projection pursuit optimization[1]; traditional BP algorithm and the additional momentum method, the adaptive learning rate method, a combination of both three kinds of additives into the algorithm[2]; a new bacterial colony Radial Basis Function Neural Network (RBFNN) algorithm[3]; futures prices by using neural networks with feature selection[4];a new Hybrid neural-evolutionary model[5];a new combined time series and neural network model[6]. It can be seen, existing improvements at home and abroad, both the improvements on the neural network model and the raw data processing method are researched. Two different improvement ideas to improve the effect of price forecasting using neural network both has the obvious effect. In the past study of price forecast using neural network, most of them use the data of the same order of magnitude for price, such as gold, electricity prices, international futures etc. The data used in this paper is the dozens of different agricultural products' 59 weeks of weekly average price and there is a difference in the magnitude of the data. It can be obtained with the analysis of experimental results which are gotten with the data normalized an order of magnitude that orders of magnitude difference have a great impact on the price forecasting using the RBF neural network in the environment of this experiment. In this paper, a method of improving the raw data processing method is put forward on the basis of the experiments to improve the stability on price forecasting with the RBF neural network. Reducing the magnitude of the raw data and using RBF neural network for price forecasting. The experimental results show improved forecast results are very satisfactory.

II. RBF NEURAL NETWORK MODEL

Radial Basis Function (RBF) neural network is based on function approximation theory as the basic structure of a class of forward network. It is a three-layer forward network. The first layer of the input layer is composed by the source node. The second layer is the hidden layer, the number of hidden units is depends. The RBF is the hidden unit transfer function and it is a nonlinear function of the center of radial symmetry and attenuation. The third layer is the output layer, it responds to the role of the input mode. Since the input to output mapping is nonlinear and the hidden layer space to the output layer space mapping is linear, it can greatly accelerate the learning speed and avoid local minima problems. RBF neural network topology is shown in Fig.1.

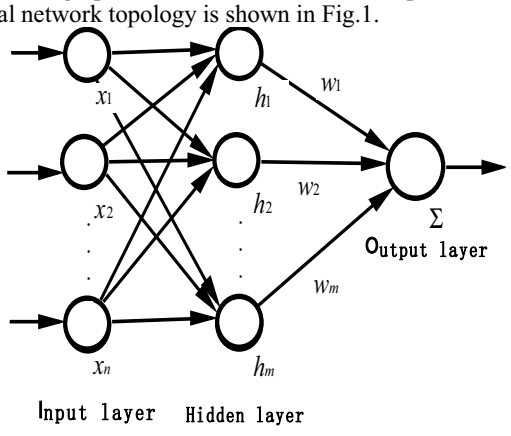

Figure 1. RBF neural network topology

*Corresponding author. hyitzqy@126. Com

978-0-7695-4818-0/12 $26.00 © 2012 IEEE
DOI 10.1109/DCABES.2012.19

III. EXPERIMENTAL ENVIRONMENT

In this paper the experiment is based on RBF neural network. The training function is the *newrbe(P,T,Spread)* and the forecast function is the *sim('MODEL',PARAMETERS)*. The raw data are dozens of different agricultural products from January 2011 to February 2012, a total of 59 weeks of weekly average price. And the first 51 weeks of data is as training samples.

In this experiment, the four weekly average prices are seen as a test sample to forecast the next weekly average price. And a total of eight weeks are forecasted. *Test* is the test sample. Test is given by equation (1). Net is given by equation (2) as net_1. *P* is the training input samples and *T* is the training targets samples. Spreads is given by equation (3).When forecasting the first data, a number of forecast values y_n are gotten by changing different *Spreads* to forecast. y_n is given by equation (4).

$$Test = [t_1, t_2, t_3, t_4] \tag{1}$$

$$net_1 = newrbe(P, T, Spreads) \tag{2}$$

$$Spreads = [spread_1, spread_2, \ldots, spread_{40}] \tag{3}$$

$$y_n = sim(net_1, Test) \quad (n = 1, 2, 3, \ldots, 40) \tag{4}$$

The value is selected from all the forecast value y_n of the minimum error as the final forecast value *Y* and the test sample of the next forecast.

$$(t_1, t_2, t_3) = (t_2, t_3, t_4)$$

$$t_4 = Y_m \quad (m = 1, 2, \ldots, 7)$$

$$Test_k = [t_1, t_2, t_3, t_4] \quad (k = 2, 3, \ldots, 8)$$

Spread is not changing when forecasting after seven data. Bspread is seen as the best *Spread*. *Bspread* is gotten with the $Bspread_1$, $Bspread_2$ and $Bspread_3$ coupled with a custom weight *W*. The $Bspread_1$, $Bspread_2$ and $Bspread_3$ are the *Spreads* of the best three forecast errors when forecasting the first data. *Bspread* is given by equation (6). *W* is given by equation (5) and in this experimental environment *W*=[2,4,2].

$$W = [w_1, w_2, w_3] \tag{5}$$

$$Bspread = \frac{Bspread_1 * w_1 + Bspread_2 * w_2 + Bspread_3 * w_3}{w_1 + w_2 + w_3} \tag{6}$$

$$net = newrbe(P, T, Bspread) \tag{7}$$

$$Y_k = sim(net, Test_k)$$

Following *net* is not repeat trained once being trained. *Net* is given by equation (7). When forecasting, every forecast value will be used as the test sample for the next forecast until the final data is gotten.

IV. EXPERIMENT WITH DIFFERENT DATA

A. Experiment with the Raw Data

The result of experiment with the raw data is shown in Table 1. Ten kinds of agricultural products data analysis is shown in Table 2.

TABLE I. THE BEST AVERAGE ERROR OF THE TEN KINDS OF AGRICULTURAL PRODUCTS

Name	ABE	Name	ABE
Beef	3.15E+04	Pork	5.43E+03
Bean Oil	1.80E-01	Rice	3.45E-03
Egg	1.62E-02	Sugar	4.36E-03
Peanut Oil	2.89E-02	Blend Oil	6.62E-02
Flour	1.08E-03	Mutton	3.25E+03

In Table 1, ABE is the average error of the eight best errors of an agricultural product in the experiment with the raw data.

In Table 1 to Table 6, Name is the names of ten different agricultural products. And in Table 2, Table 4 and Table 6, Max is the maximum of the training sample data. Min is the minimum of the training sample data. Ave is the average of the training sample data. A is the absolute of the difference of the Max and Min. B is the absolute of the difference of the Max and Ave. C is the absolute of the difference of the Min and Ave. D is the absolute of the difference of the B and C.

TABLE II. 10 KINDS OF AGRICULTURAL PRODUCTS DATA ANALYSIS

Name	Max	Min	Ave	A	B	C	D
Beef	3.15E+04	32.09	3.41E+01	4.55	2.53E+00	2.02E+00	5.08E-01
Bean Oil	1.21E+01	11.29	1.17E+01	0.81	3.75E-01	4.35E-01	5.94E-02
Egg	1.62E-02	9.01	9.72E+00	1.46	7.46E-01	7.14E-01	3.25E-02
Peanut Oil	3.27E+01	20.82	2.26E+01	11.84	1.00E+01	1.81E+00	8.22E+00
Flour	5.16E+00	4.73	5.00E+00	0.43	1.61E-01	2.69E-01	1.08E-01
Pork	5.43E+03	18.9	2.30E+01	7.54	3.41E+00	4.13E+00	7.14E-01
Rice	3.45E-03	5.23	5.68E+00	0.72	2.66E-01	4.54E-01	1.88E-01
Sugar	4.36E-03	8.59	9.63E+00	1.75	7.08E-01	1.04E+00	3.34E-01
Blend Oil	1.40E+01	13.17	1.36E+01	0.8	3.85E-01	4.15E-01	3.10E-02
Mutton	4.56E+01	37.2	4.05E+01	8.42	5.11E+00	3.31E+00	1.80E+00

Name: Agricultural product name; ABE: Average of the best errors; Max: The maximum value of the training sample data; Min: The minimum value of the training sample data ; Ave: The average of the training sample data ; A:ABS(Max-Min); B:ABS(Max-Ave); C:ABS(Min-Ave); D:ABS(B-C);

In Table 2, in this experiment, the data is the raw data.

The following conclusions can be drawn after analyzing and comparing experimental results with the actual results. When A is relative to larger, ABE is also very large. And in this case, experimental forecast results are not satisfactory. Certainly, there is also ideal forecast in the results, such as peanut oil. The A of the peanut oil is the largest but its ABE is satisfactory. It is shown that raw data have a larger range when A is relative to larger and D is relative to smaller which leads to a distortion of the RBF neural network in this experimental environment in forecasting. However, A of the peanut oil is the largest and its D is also relative to larger which shows that raw data have a little range and local big fluctuations lead to a large A. In this case, RBF neural network in this experimental environment does not suffer too much in the forecast and the results are satisfactory.

B. *Experiment Data with the Magnitude Enhanced*

The magnitude of the raw data of the flour and rice has changes. The result is shown in Table 3. Ten kinds of agricultural products data analysis is shown in Table 4.

TABLE III. THE BEST AVERAGE ERROR OF THE TEN KINDS OF AGRICULTURAL PRODUCTS

Name	ABE	Name	ABE
Beef	3.15E+04	Pork	5.43E+03
Bean Oil	1.80E-01	Rice	3.45E-03
Egg	1.62E-02	Sugar	4.36E-03
Peanut Oil	2.89E-02	Blend Oil	6.62E-02
Flour	1.21E-03	Mutton	3.25E+03

In Table 3, ABE is the average error of the eight best errors of an agricultural product in the experiment with the data which is enhanced the magnitude.

TABLE IV. 10 KINDS OF AGRICULTURAL PRODUCTS DATA ANALYSIS

Name	Max	Min	Ave	A	B	C	D
Beef	36.64	32.09	3.41E +01	4.55	2.53E +00	2.02 E+00	5.08 E-01
Bean Oil	12.1	11.29	1.17E +01	0.81	3.75E -01	4.35 E-01	5.94 E-02
Egg	10.47	9.01	9.72E +00	1.46	7.46E -01	7.14 E-01	3.25 E-02
Peanut Oil	32.66	20.82	2.26E +01	11.8 4	1.00E +01	1.81 E+00	8.22 E+00
Flour	51.6	47.3	5.00E +01	4.3	1.61E +00	2.69 E+00	1.08 E+00
Pork	26.44	18.9	2.30E +01	7.54	3.41E +00	4.13 E+00	7.14 E-01
Rice	59.5	52.3	5.68E +01	7.2	2.66E +00	4.54 E+00	1.88 E+00
Sugar	10.34	8.59	9.63E +00	1.75	7.08E -01	1.04 E+00	3.34 E-01
Blend Oil	13.97	13.17	1.36E +01	0.8	3.85E -01	4.15 E-01	3.10 E-02
Mutton	45.62	37.2	4.05E +01	8.42	5.11E +00	3.31 E+00	1.80 E+00

In Table 4, in this experiment, the data is the data which is enhanced the magnitude.

After analyzing the experimental results, it can be seen that the results obtained by this method are near the results obtained by the direct use of the raw data. The forecast effect is not improved. Liters of magnitude do not reduce the fluctuation range of the raw data and A of some agricultural products is still relatively large. Therefore, this method is not applicable in this experimental environment.

C. *Experiment Data with the Magnitude Reduced*

The magnitude of the raw data of the beef, peanut oil, pork, blend oil and mutton has changes. The result is shown in Table 5. The analysis for ten kinds of agricultural products data is shown in Table 6. In Table 5, ABE is the average error of the eight best errors of an agricultural product in the experiment with the data which is reduced the magnitude

In Table 6, in this experiment, the data is the data which is reduced the magnitude.

TABLE V. THE BEST AVERAGE ERROR TABLE OF THE TEN KINDS OF AGRICULTURAL PRODUCTS

Name	ABE	Name	ABE
Beef	2.44E-02	Pork	7.35E-02
Bean Oil	1.80E-01	Rice	3.45E-03
Egg	1.62E-02	Sugar	4.36E-03
Peanut Oil	9.10E-03	Blend Oil	1.29E-03
Flour	1.08E-03	Mutton	4.15E-03

As shown in Figure 2, under the three different methods, ten different agriculture products' average forecast errors are different. There are little differences in average forecast errors of some agriculture products under the three methods. And there are large differences in average forecast errors of others. So some agriculture products are selected to be seen as the examples, such as pork, beef, mutton etc. As shown in Fig. 3 to Fig. 5, the best price forecast of three agricultural products under the three methods is given.

In the Fig. 2, *X* label is the three different methods. Method 1 is the experiment with the raw data. Method 2 is the experiment with the data which is enhanced the magnitude. Method 3 is the experiment with the data which is reduced the magnitude. *Y* label is the Mean Absolute Error.

TABLE VI. 10 KINDS OF AGRICULTURAL PRODUCTS DATA ANALYSIS

Name	Max	Min	Ave	A	B	C	D
Beef	3.664	3.209	3.41E +00	0.455	2.53E -01	2.02 E-01	2.44 E-02
Bean Oil	12.1	11.29	1.17E +01	0.81	3.75E -01	4.35 E-01	1.80 E-01
Egg	10.47	9.01	9.72E +00	1.46	7.46E -01	7.14 E-01	1.62 E-02
Peanut Oil	3.266	2.082	2.26E +00	1.184	1.00E +00	1.81 E-01	9.10 E-03
Flour	5.16	4.73	5.00E +00	0.43	1.61E -01	2.69 E-01	1.08 E-03
Pork	2.644	1.89	2.30E +00	0.754	3.41E -01	4.13 E-01	7.35 E-02
Rice	5.95	5.23	5.68E +00	0.72	2.66E -01	4.54 E-01	3.45 E-03
Sugar	10.34	8.59	9.63E +00	1.75	7.08E -01	1.04 E+00	4.36 E-03
Blend Oil	1.397	1.317	1.36E +00	0.08	3.85E -02	4.15 E-02	1.29 E-03
Mutton	4.562	3.72	4.05E +00	0.842	5.11E -01	3.31 E-01	4.15 E-03

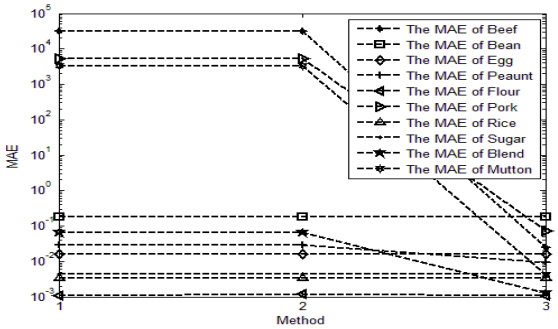

Figure 2. MAE of ten kinds of agricultural products under the three methods

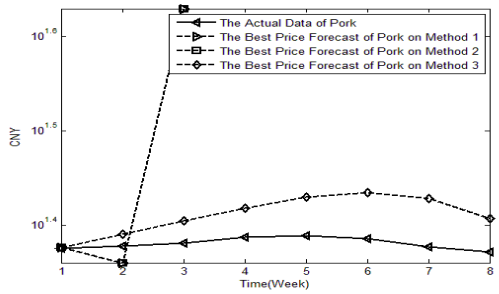

Figure 3. The best price forecast of pork under the three methods

In the Figure 3-Figure 5, *X* label is the eight weeks. *Y* label is the CNY (China Yuan). Method 1 is the experiment with the raw data. Method 2 is the experiment with the data which is enhanced the magnitude. Method 3 is the experiment with the data which is reduced the magnitude.

Analyzed and compared with the experimental results obtained by the other two methods, it can be seen that there is a clear effect on improving the stability on price forecasting with the RBF neural network in this method. After reducing the magnitude of the raw data, A also has been reduced relatively. Fluctuation range of the raw data is reduced to a certain range, so RBF neural network is more stable in the forecast price.

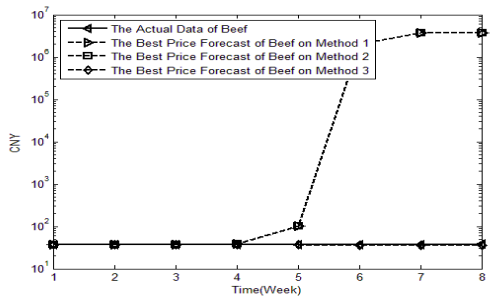

Figure 4. The best price forecast of beef under the three methods

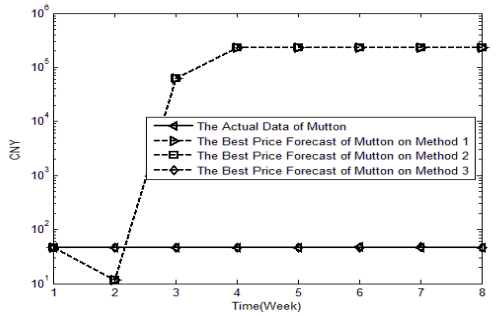

Figure 5. The best price forecast of mutton under the three methods

CONCLUSION

This shows that, in this experimental environment, reducing the magnitude of the raw data can improve the stability on price forecasting with the RBF neural network. Whether this method being applicable to other experimental environment needs further explore and further experimental validation, such as modifying custom weight and modifying the forecast period.

ACKNOWLEDGMENT

This work is supported by the National Sparking Plan Project of China (2011GA690190), the fund of Huaian Industry Science and Technology. China (HAG2011052, HAG2011045，HAG2010066).

REFERENCE

[1] ZENG Lian, MA Dan-di , LIU Zong-xin. Gold Price Forecast Based on Improved BP Neural Network. Computer Simulation,2010

[2] XU Jia-bing, QI Zhi-guo, HANG Wen, HE Jie, LI Xu-hong. Research on Application of Improved BP Algorithms in Price Prediction for Highway Engineering Main Material. Journal of Highway and Transportation Research and Development,2008

[3] MIAO Kai, CHEN Fang, ZHAO Zhi-gang. Stock Price Forecast Based on Bacterial Colony RBF Neural Network. Journal of Qingdao University,2007

[4] Chih-Ming Hsu.Forecasting stock/futures prices by using neural networks with feature selection, 2011 6th IEEE Joint International on Information Technology and Artificial Intelligence Conference (ITAIC) , Publication Year: 2011 , Page(s): 1 – 7

[5] Srinivasan, D.; Zhang Guofan; Khosravi, A.; Nahavandi, S.; Creighton, D.Hybrid neural-evolutionary model for electricity price forecasting, The 2011 International Joint Conference on Neural Networks (IJCNN), Publication Year: 2011 , Page(s): 3164 – 3169

[6] Azadeh, A.; Ghadrei, S.F.; Nokhandan, B.P.One day-ahead price forecasting for electricity market of Iran using combined time series and neural network model, 2009. HIMA '09. IEEE Workshop on Hybrid Intelligent Models and Applications, Publication Year: 2009 , Page(s): 44 – 47

[7] Mori, H.; Awata, A. Normalized RBFN with Hierarchical Deterministic Annealing Clustering for Electricity Price Forecasting. Power Engineering Society General Meeting, 2007. IEEE

[8] Sun Chao; Meng Jun. The Study on Chaotic Identify of Price Index Time Series of Agricultural Products . Second International Conference on Intelligent Computation Technology and Automation, 2009. Publication Year: 2009 , Page(s): 346 - 349

[9] Shouhua Yu; Jingying Ou. Forecasting Model of Agricultural Products Prices in Wholesale Markets Based on Combined BP Neural Network -Time Series Model. 2009 International Conference on Information Management, Innovation Management and Industrial Engineering .Publication Year: 2009 , Page(s): 558 - 561

[10] Chen, X.; Dong, Z. Y.; Meng, K.; Xu, Y.; Wong, K. P.; Ngan, H. W. Electricity Price Forecasting With Extreme Learning Machine and Bootstrapping. IEEE Transactions on Power Systems, Publication Year: 2012 , Page(s): 1 - 1

[11] Mori, H.; Takahashi, A. Hybrid intelligent system for daily maximum temperature forecasting in smart grids . 2011 IEEE International Symposium on Circuits and Systems (ISCAS), Publication Year: 2011 , Page(s): 1852 - 1855

[12] Anbazhagan, S.; Kumarappan, N.; Gnanaprakasam. A temporal input based day-ahead price forecasting in Asia's first liberalized electricity market using GRNN . International Conference on Sustainable Energy and Intelligent Systems (SEISCON 2011), Publication Year: 2011 , Page(s):42

VaR and CVaR Estimate based on Distributed Parallel Algorithm

FU Shu-huan
Business School of Hohai University
Nanjing, China
fushuhuan0314069@yahoo.com.cn

CAO Jia-he
Business School of Hohai University
Nanjing, China
Caojh2011@126.com

***Abstract*—CVaR has more advantages, than the VaR as portfolio risk measurement tool, but with the calculation of VaR, the Monte Carlo simulation method of the CVaR is difficult, and the cost is high. The establishment of the system of distributed parallel algorithm can reduce costs and speed up the calculation, which is conducive to the promotion of the CVaR Monte Carlo algorithm.**

Keywords- VaR; the CVaR; Distributed Parallel Algorithm

I. THE IMPORTANCE AND VARIOUS INDICATORS OF RISK MEASURE

As accelerate of globalization, the financial industry has developed rapidly. It also makes the risks of financial institutions to further aggravate. How to accurately measure the financial risk becomes the importance of financial risk and portfolio management research.

Transaction platform use a variety of Greek values to detect the risks in the transaction, and these Greek values includes Delta (Δ), Gamma (Γ) and the Theta (Θ). But these Greek values can not provide a complete picture of overall risk. VaR and CVaR can precisely reflect the overall risk of financial institutions.

II. VAR AND CVAR

VaR (Value at Risk) is the biggest loss at a certain period of time and a certain level of probability, mathematical expressions can be expressed as:

$$VaR_\alpha \triangleq -\inf\{x|P(R_p \le x) \ge \alpha\} = -F_{R_p}^{-1}(\alpha)$$

CVaR (Credit Value at Risk) is the average loss at a certain probability level α, mathematical expressions can be expressed as:

$$CVaR_\alpha(R_P) \triangleq -E(R_P|R_P \le -VaR_\alpha(R_P))$$

Clearly, CVaR based on the conditional expectation can discuss the income changes of a quartile (VaR) and it's the bottom, so CVaR is superior to the VaR in describing the tail behavior of portfolio return distribution.

III. THE METHOD OF CALCULATION OF VAR AND CVAR

The method of calculation of VaR and CVaR can be divided into two categories: Local-valuation Method and Full-valuation Method.

The Local-valuation Method is a valuation at the initial state of the portfolio, which infers possible changes and calculation risk measure values. Delta-normal distribution law is a typical Local-valuation Assume that portfolio returns follow a normal distribution:

$$VaR(R_P) = z_{1-\alpha}\sigma_P - \mu_P$$

$$CVaR(R_P) = \frac{\varphi(z_{1-\alpha})}{\alpha}\sigma_P - \mu_P$$

The Full-valuation Method measures the risk through re-definition of the portfolio in a variety of contexts. The historical simulation and Monte Carlo simulation is a typical Full-valuation Method.

The core of the historical simulation method is to simulate the distribution of profit and loss of portfolio according to the market factors in the history of the sample changes, and estimates VaR.

The calculation steps are:

(1) Calculate the yield (Ri) of the securities at time t ;

(2) Calculate the return(R) of virtual portfolio;

(3) Order the possible virtual combinations yield from small to large, calculate the VaR at a given confidence level and the CVaR calculated by computing the average blow the confidence rate.

The principle of Monte Carlo simulation is similar to the historical simulation method, the difference is that changes in market prices do not come from historical observations, but obtained by stochastic simulation. The basic idea is the assumptions of asset prices depending random process, and use computer simulation to produce random price and build the distribution of assets return, the VaR is calculated on the basis. The calculation steps are as follows:

(1) Select the appropriate description of the stochastic process of asset price channels.

(2) According to the random process to simulate a virtual asset price approach.

(3)According to simulation results, build the distribution of return on assets, and calculation the VaR and the CVaR of the portfolio.

Compared with the Delta-normal distribution and the historical simulation method, Monte Carlo simulation has many advantages. It does not require the restrict assumptions of normal distribution, and does not need a lot of historical data like the historical simulation method. Monte Carlo simulation can handle the temporal variability of the non-normal distribution of variables, thick tail, asymmetry and extreme conditions.

However, due to a large number of calculations and complicatedly sampling, the requirements of Monte Carlo simulation to computer is very high. So this method is restricted.

978-0-7695-4818-0/12 $26.00 © 2012 IEEE
DOI 10.1109/DCABES.2012.73

IV. DISTRIBUTED PARALLEL ALGORITHM

Distributed parallel algorithm can establish a parallel computing system using more than one processor, to calculate VaR and CVaR. This system can effectively reduce the computational cost, but also be conducive to the popularity of the Monte Carlo simulation.

The achievement of distributed parallel computing need to meet two conditions: First, the system provides completely independent processors; second, the problem can be broken down into many parts independently. So this paper proposes the main – subordinate distributed parallel model to calculate the VaR and CVaR, the main process only achieve the distribution of data and calculation of a small amount of work, a large number of repeat operators are assigned to the subordinative processes. The algorithm has a high degree of parallelism.

V. VAR AND CVAR OF DISTRIBUTED PARALLEL COMPUTING

The distributed parallel algorithm is implemented by the LAN system of multiple computers, which can exchange data with each other.

The core of the algorithm is to select the random process and distribution of changes of market factors, and in order to calculate the changes in the value of the portfolio, and finally calculate the VaR and the CVaR at the specific confidence level by the results of simulation. The detailed steps are as follow:

A. The calculation of the VaR

According to Yuan, the computation of VaR based on distributed parallel algorithm is the following ways.

The main computing node:

1) Select the random process and distribution of the changes of market factors, estimate the corresponding parameters, the parameters are passed to the subordinate compute nodes (*i*);

2) Receive the computation results of the portfolio value from the subordinate;

3) According to the simulation results, calculate the VaR under the specific degree of confidence.

The subordinative compute nodes (i):

1) Received parameters from the main compute node;

2) Simulate the changes of market factor in circumstances, namely, the various possible values of the future market factors;

3) To each possible value of the future market factors, use the asset pricing formula or other method to calculate the value of the portfolio and its changes;

4) Pass the calculated value of the portfolio results to the main computing nodes.

B. The calculation of the CVaR

The calculation of the CVaR is roughly same with VaR. By definition, CVaR is the average loss of an asset or a portfolio under a certain probability level α.

The main computing node:

1) Select the random process and distribution of the changes of market factors, estimate the corresponding parameters, the parameters are passed to the subordinate compute nodes (*i*);

2) Receive the computation results of the portfolio value from the subordinate;

3) According to the simulation results, calculate the average of the loss under a certain probability level, namely, the CVaR.

The subordinative compute nodes (i):

1) Received parameters from the main compute node;

2) Simulate the changes of market factor in circumstances, namely, the various possible values of the future market factors;

3) To each possible value of the future market factors, use the asset pricing formula or other method to calculate the value of the portfolio and its changes;

4) Pass the calculated value of the portfolio results to the main computing nodes.

VI. CONCLUDING REMARKS

By assigning the a large number of repeat operator to subordinative the process, the main process only complete data distribution and calculation a small amount of work, which overcomes the shortcomings(a large amount and time long of computation) of the Monte Carlo simulation method of CVaR, and effectively reduces the computation. This is benefit of the extension of the Monte Carlo simulation of CVaR.

REFERENCES

[1] R.T. Rockafellar, S. Uryasev. “Optimization of conditional value-at-risk,” The Journal of Risk, 2000, 2(3): 21-41.

[2] P. Artzner, F. Delbaen, J. Ebert, D. Heath. “Coherent measures of risk,” Mathematical Finance, 1999,9(3): 203-228.

[3] G. Ananth. “Introduction Parallel Computing,” Beijing: China Machine Press, 2003.

[4] R. Yuan. “Quantitative models of financial risk management and its distributed parallel computing,” the Eighth National Parallel Computing Conference proceedings, Dalian University of Technology Press, 2004, 4-6.

The Analysis of Industrial Power Consumption Structure in Jilin Province

Qiushi Du[1], Xiangyu Lv[1], Huifang Qin[2]

[1] Electric Power Research Institute of Jilin Electric Power Co.Ltd
Changchun, 130061,China
[2] School of Business Administration, North China Electric Power Univ.
Baoding, 071003,China
E-mail: ncepudqs@126.com, caulxy@163.com, whffzw@163.com

Abstract-Power supply and industrial growth are closely related, along with the development of industrial sectors and the diversification of power consumption structure. Effective and rational grasp of current power demand structure is conducive to stable power supply. In this paper, we build the evaluation index system of industrial power consumption structure in allusion to the structural characteristics of it in Jilin Province and combined with the actual situation, then proposed the structure evaluation model of industrial power consumption based on PSO (Particle Swarm Optimization) and support vector machine algorithms. In addition, we collect the industrial power consumption data in recent 60 months of Jilin Province to do empirical analysis, and testify that the method has high accuracy. The results show that the model works well, and the method are practical and feasible.

Keywords-power consumption structure; PSO; SVM (support vector machines)

I. INTRODUCTION

Industry has an important position and role in the national economic development, today, the raise of the electrification level result in great increase of the proportion of our country's electric energy in final energy consumption, and the industrial power consumption of electricity accounted for a significant proportion of the community, which determines the power and economic development are closely related and the industrial economy has an important position in macroeconomic research. The power consumption structure of China's industry develops imbalance, and China's power structure is irrational. Therefore, this paper used the composite method of PSO and support vector machine (SVM) method to analysis the current situation of industrial power consumption structure in Jilin province.

This paper build the industrial power consumption structure index system, and proposed the industrial power consumption structure evaluation model based on PSO and support vector machine regression. Using Particle swarm optimization with support vector machines to make up for deficiencies in the search for information, and the generalization ability of support vector machine is better than PSO. From the results of empirical analysis and application point of view, the model has high evaluate accuracy, and has a good application value.

II. INDUSTRIAL POWER CONSUMPTION STRUCTURE EVALUATION MODEL

Building a scientifically sound evaluation system, it is an important prerequisite to achieve the industrial power consumption structure evaluation, and it is the basis for a comprehensive evaluation.

This article, in view of the industrial structure characteristics of Jilin province, builds the power consumption indicators including mining, manufacturing, electric power industry, gas and other industries (See Table 1).

TABLE I. THE INDEX SYSTEM OF INDUSTRIAL POWER CONSUMPTION STRUCTURE IN JILIN PROVINCE

One class indexes	Secondary indexes
Mining power indexes	Coal mining and washing industry P1 Petroleum and natural gas extraction industryP2 Ferrous metal mining industry P3 Non-ferrous metal mining industry P4 Non-metallic mining industry P5 Other mining industry P6
Manufacturing power indexes	Food, beverage and tobacco manufacturing P7 Textile industry P8 Garments, leather and feather products industry P9 Products and wood processing and furniture industry P10 Paper and paper products industry P11 Printing and reproduction of recorded mediaP12 Petroleum processing, coking and nuclear fuel processing industry P13 Sporting goods manufacturing P14 Chemicals and chemical products manufacturing P15 Pharmaceutical Manufacturing P16 Chemical fiber manufacturing industry P17 Rubber and plastic products industry P18 Non-metallic mineral products P19 Ferrous metal smelting and rolling processing industry P20 Non-ferrous metal smelting and rolling processing industry P21 Fabricated metal products P22 General and special equipment manufacturing industry P23 Transportation, electrical, electronic equipment manufacturing P24 Artwork and Other ManufacturingP25 Recycling and material recovery processing industry P26
Electricity, gas and water production and power supply industry indexes	Electricity, heat production and supply industry P27 Gas production and supply industry P28 Water production and supply industry P29

978-0-7695-4818-0/12 $26.00 © 2012 IEEE
DOI 10.1109/DCABES.2012.70

III. PARTICLE SWARM ALGORITHM

PSO（Particle Swarm Optimization）algorithm was originally put forward by Kennedy and Eberhart inspired by the foraging behavior of birds in 1995. It is based on the algorithm of swarm intelligence optimization theory, and achieves the optimal goal through the process of collective collaboration between the bird groups. PSO algorithm uses speed - location search model. Each possible solution of optimization is called "particles", the pros and cons of the solution were decided by the fitness. The particles adjust themselves by tracking individual optimal solution and the global optimal solution.

In the basic particle swarm algorithm, m particles in a D-dimensional target-space, among them particle i represents a D-dimensional vector $X_i = (x_{i1}, x_{i2}, \cdots, x_{iD})$, $i = 1, 2, \cdots, m$, take X_i into target function and the fitness can be calculated. According to the size of the fitness we can measure the merits of A. The best position experienced by a single particle is recorded as: $P_i = (p_{i1}, p_{i2}, \cdots, p_{iD})$, the corresponding fitness was called as individual optimal solution $P_{best,i}$, the optimal position the whole particle swarm gone through recorded as: $P_{gbest} = (P_{g1}, P_{g2}, \cdots, P_{gD})$, and the fitness is called the global optimal solution g_{best}. The flying speed of part i of particles is a D-dimensional vector $V_i = (v_{i1}, v_{i2}, \cdots, v_{iD})$, so the particles update their velocity and position according to formula (1):

$$\begin{cases} v_{id}^{(k+1)} = w^{(k)} v_{id}^{(k)} + c_1 r_1 \left(p_{id}^{(k)} - x_{id}^{(k)} \right) + c_2 r_2 \left(p_{gd}^{(k)} - x_{id}^{(k)} \right) & (1) \\ x_{id}^{(k+1)} = x_{id}^{(k)} + a v_{id}^{(k)} & (2) \end{cases}$$

Among them, $i = 1, 2, \cdots, n; d = 1, 2, \cdots D$,in the formula, k stands for number of iterations; n stands for the particle size; c_1, c_2 stands for the learning factor; r_1, r_2 stands for the random number on the interval [0，1]；a is the constraint factor to control the speed weight; w is the inertia weight; $v_{id}^{(k)}$, $p_{id}^{(k)}$, $x_{id}^{(k)}$, $p_{gd}^{(k)}$ stands for the no.k iteration value of v_{id} 、p_{id} 、x_{id} 、p_{gd}.

The improved method of this paper is in accordance with formula (3) and (4).

$$R_k = k / G_{\max} \quad (3)$$

$$v_{id}^{(k+1)} = w^{(k)} v_{id}^{(k)} + c_1 r_1 \left(p_{id}^{(k)} - x_{id}^{(k)} \right) + c_2 r_2 \left(p_{rd}^{(k)} - x_{id}^{(k)} \right) \quad (4)$$

In the formula, $G_{\max}$ is the largest evolution algebra, P_{rnd} is selected randomly from other parcel's $P_{best,i}$ and isn't equals to P_{gbest}.

The selection strategy [7]: In the No.k generation of the evolutionary process, randomly generated a uniformly distributed random number r between 0 and 1,and calculate R_k according to the equation (3), if $r \succ R_k$, then randomly select a particle from the PSO, in addition to their own and the best particle, note the best position of this particle as P_{rnd}, Instead of P_{best} in equation (1), this means update the speed of the current particle according to formula (4) ; otherwise, in accordance with (1).

IV. SUPPORT VECTOR MACHINE REGRESSION ALGORITHM

For the training sample set (x_i, y_i), $i = 1, 2 \cdots n$, $x_i \in \boldsymbol{R}^n$ is the value of input variables, $y_i \in \boldsymbol{R}$ is the corresponding output value. During the electricity consumption industrial structure evaluation x_i is the numerical value resulted from particle swarm algorithm, y_i is the overall rating score corresponding to each group of sample. The basic idea of Support vector machine regression theory is to find the nonlinear mapping ϕ from the input space to output space. Through this non-linear mapping, Map data x into a high dimensional feature space $\boldsymbol{F}$, and using the following estimated function to do linear regression in the feature space, form the following:

$$f(x) = [\omega \cdot \phi(x)] + b \quad \phi : \boldsymbol{R}^m \to \boldsymbol{F} \quad (5)$$

Among them, b is the threshold. The function approximation problem is equivalent to the minimum with the following function:

$$\boldsymbol{R}_{reg}[f] = \boldsymbol{R}_{emp}[f] + \lambda \|\omega\|^2 = \sum_{i=1}^{s} \boldsymbol{C}(e_i) + \lambda \|\omega\|^2 \quad (6)$$

Among them, $\boldsymbol{R}_{reg}[f]$ is the target function, s is the sample number, $e(\bullet)$ is the loss function, λ is the adjust constant, $\|\omega\|^2$ reflects the complexity of the flat in the high dimension space. Taking into account that the linear ε insensitive loss function has a good sparse, we can get the following loss function:

$$|y - f(x)|_\varepsilon = \max\{0, |y - f(x) - \varepsilon|\} \quad (7)$$

Empirical risk is:

$$\boldsymbol{R}_{emp}^{\varepsilon}[f] = \frac{1}{n} \sum_{i=1}^{n} |y - f(x)|_\varepsilon \quad (8)$$

According to statistical theory, the Support vector machines can determine the regression function by minimizing the following objective function, means:

$$\min \left\{ \frac{1}{2} \|\omega\|^2 + \boldsymbol{C} \sum_{i=1}^{n} (\xi_i^* + \xi_i) \right\} \quad (9)$$

$$y_i - (\omega \cdot \phi(x) - b \le \varepsilon + \xi_i^* \quad (10)$$

$$(\omega,\phi(x))+b-y_i\le\varepsilon+\xi_i \tag{11}$$

$$\xi_i,\xi_i^*\ge 0 \tag{12}$$

The C used to balance model complexity and training the weight parameters of the error term, ξ_i^* and ξ_i are relaxation factor, ε is the insensitive loss function. The problem can be transformed into the following dual problem:

$$\max[-\frac{1}{2}\sum_{i,j=1}^{n}(a_i^*-a_i)(a_j^*-a_j)K(X_i,X_j)$$

$$\sum_{i}^{l}a_i^*(y_i-\varepsilon)-\sum_{i=1}^{n}a_i(y_i-\varepsilon)] \tag{9}$$

$$\sum_{i=1}^{n}a_i=\sum_{i=1}^{n}a_i^* \tag{13}$$

$$0\le a_i^*\le C \tag{14}$$

$$0\le a_i\le C \tag{15}$$

Solving the above problems, we can receive support vector machine regression function:

$$f(x)=\sum_{i=1}^{n}(a_i-a_i^*)k(X_i,X)+b \tag{16}$$

Using this function to evaluate the test samples, we can get the evaluation value of test samples in each group.

V. APPLICATIONS

This paper selected industrial power consumption data of Jilin Province for empirical analysis, there are 60 groups' data in all. We divided them into two parts, 46groups of them are treated as training samples used to train the model, 6groups are treated as test samples and other 8groups are treated as examination sample, to inspect the accuracy of the model. Finally we use the relative error and mean square error of the evaluation result to evaluate the effect of the model.

A. Data pre-processing

In this paper, we do pre-processing to the collected data, and evaluate the raw data of index system. On account of the input vectors' magnitude vary greatly, prior to network training, we need to normalize the sample data to meet the input requirements of constructing the model, and through pretreatment with the model, we make the input vector be suitable to achieve the purpose of standardization. And we do data correction according to the raw data of industrial consumption. Positive index and reverse index respectively use formula (17) and (18) for processing:

$$y_i=x_i/\max_{1\le i\le n}x_i \tag{17}$$

$$y_i=(\max x_i+\min x_i-x_i)/\max x_i \tag{18}$$

Relative error：

$$E_r=\frac{x_i-y_i}{x_i}\times 100\% \tag{19}$$

Mean square error：

$$MSE=\frac{1}{n}\sum_{i=1}^{n}(x_i-y_i)^2 \tag{20}$$

x_i is the original evaluation value of the No. i sample, y_i is the model evaluation value of the No. i sample, n is the number of test samples.

B. The evaluation process

In this paper, we use Matlab and Libsvm toolboxes to do calculate, and kernel functions uses the Commonly used Gaussian kernel function, and the model training parameters are C =68.6852, ε =0.0018, δ^2 =0.5869.We use the trained model to evaluate the test samples. The evaluation results compared with the original values can be seen in Table 2.

TABLE II. THE COMPARISON BETWEEN INITIAL VALUE AND EXPERIMENTAL VALUE

No.	Initial value	Experimental value	Relative error	Mean square error
1	0.921	0.9236	-0.28%	0.000197434
2	0.862	0.8512	1.25%	
3	0.758	0.7652	-0.95%	
4	0.792	0.7864	0.71%	
5	0.638	0.6537	-2.46%	
6	0.852	0.8379	1.65%	

C. Results analysis

From the evaluation results of Table 2 we can see, the model evaluate value of each test sample has reached a high accuracy. And see from the relative error of each evaluate value, the maximum absolute value of relative error does not exceed 3%, and the minimum relative error is only 0.28%, while the mean square error is only 1.97434E-04.The above indicate that evaluation accuracy is high, and the model has a good adaption to the power grids safety evaluation.

The original evaluation values of the test sample are in the range of 0.6-1.0,if we divided with 0.1 for interval to differentiate interval, we can have four intervals [0.6,0.7]、[0.7,0.8]、[0.8,0.9]、[0.9,1.0].And see from the evaluate effect of each interval, we can get that the model has better evaluate effect to the test sample which sit in the different original evaluate value intervals. In addition, the model needs less test sample, this means the model has good promotion ability, can meet the requirement of actual evaluation.

After repeated training, the model has been relatively stable, can be used as a knowledge base. In this paper, We established the evaluate model based on PSO and SVM, compared with the expert fuzzy evaluation results, we draw a consistency conclusions, but the result is more accuracy, and it shows the effectiveness in the aspects of assessment on industrial electricity consumption structure evaluation. Through the evaluation study, we proposed the corresponding supply response, sequentially to optimize the industrial electricity consumption structure in Jilin province, this promotion can make timely power supply and make sure the business enterprise has stable production. It takes an important role to ensure stable production of electricity enterprises.

VI. CONCLUSION

In this paper, we use PSO optimization algorithm to improve the use of traditional support vector machine regression algorithm, established the evaluation model based on particle swarm optimization for support vector machine and apply it to the industrial power structure evaluation studies of Jilin Province. By taking the electricity consumption of each industry in Jilin Province into test and verification, the results show: Using particle swarm optimization of the support vector machine (SVM) model for the whole social power consumption structure not only has accuracy evaluation calculation, but also the evaluation result has high reliability.

Analysis by PSO and support vector machine, we can grasp the industry power consumption structure of Jilin Province in the macroscopic level, at the same time we can know the position and reasons that various industries electric power development situation in economic development.

REFERENCES

[1] V.Vapnik. The Nature of Statistical Learning Theory [M].New York:Springer-Verlag.2010.12.

[2] Li Jian-Ping, Xu Wei-xuan, Liu Jing-li. The Study of Support Vector Machine in Consumer Credit Assessment. Systems Engineering [M]. 2004.10.

[3] Qiang Wang, Yongping Shen, Yingwu Shen. Multi-attribute decision model and algorithm for support vector machines [J]. Control and Decision, 2006,21(12): 1338-1342.

[4] Kang Chongqing, Li Shunfu. Structure analysis of electricity consumers and its instruction to marketing [J]. Automation of Electric Power Systems, 2003,27(14):27-31.

[5] Yang Junbao, Xia Feng. Efficiency analysis of power consumption of industrial enterprises in Shanghai [J]. Journal of Shanghai University of Electric Power, 2006,22(4): 392-394.

Cell Phones Price Forecast Based on Adaptive Sliding Windows

Yonghua Yin
Faculty of Computer Engineering
Huaiyin Institute of Technology
Huaian, China
1165790450@qq.com

Jiajun Zong and Quanyin Zhu*
Faculty of Computer Engineering
Huaiyin Institute of Technology
Huaian, China
hyitzqy@126.com

***Abstract*—Nowadays, the demand of people on the phones is very large. In order to help consumers have the better reference resources when they buy mobile phones, cell phones price forecasting on adaptive sliding windows is discussed in this paper. One year price for ten type's mobile phone which extracted from www.360buy.com is used as the original data to forecast the price based on the adaptive sliding windows. According to this forecasting method, the experiments are implemented under the different sliding window width for different type's cell phones depend on the accuracy rata. Comparing the experimental results with the original data, the forecast results are very satisfactory. And the forecasting average accuracy obtains 99.4 percent. Experiment results prove that the research is meaningful and useful and it is not only for consumers, but also for businesses in the cell phones market.**

Keywords- price forecast; cell phones; linear backfilling; adaptive sliding windows

I. INTRODUCTION

In recent years, the mobile phone market is developing rapidly. On the one hand, the consumers have a huge demand of the cell phones and the mobile phone has become the essential goods of life. On the other hand, the manufacturer's research and development speed is also very fast. Due to these two reasons, the price fluctuations have the great effect on the cell phones market. However, now most of the price forecasts are concentrated in the electricity prices, agricultural products, gold and the futures etc. According to this, cell phones price forecast is discussed in this paper. The original data used in this paper is the year of price data of ten different models of cell phones from www.360buy.com. And in the price forecast, the adaptive sliding windows of price forecast method is used. The experiments are implemented in this experimental environment and the experimental results show that cell phones price forecast based on adaptive sliding windows are very satisfactory.

II. SLIDING WINDOWS

Definition 1:

Set cycle time series in the time of observation period t is $x_1, x_2,\ldots, x_t, \ldots, f_{t,1}$ is the predictive value of the next time t+1; $f_{t,1}$= the latest forecast average =the average of $x_t, x_{t-1},\ldots,x_{t-N+1}$. N is given the parameters and it is the forecast window. N determines the prediction accuracy. The experimental data are generally based on experience.

*Corresponding author. hyitzqy@126. Com

Definition 2:

x_t is the actual value of the time t and $\hat{x}_t$ is the forecast value of the time t.

Prediction error:

$$e_t = x_t - \hat{x}_t, \quad t = 1,2,\cdots,n \tag{1}$$

Relative prediction error:

$$\tilde{e}_t = \frac{e_t}{x_t} = \frac{x_t - \hat{x}_t}{x_t}, \quad t = 1,2,\cdots,n \tag{2}$$

Mean absolute error:

$$MAE = \frac{1}{n}\sum_{t=1}^{n}|e_t| = \frac{1}{n}\sum_{t=1}^{n}|x_t - \hat{x}_t| \tag{3}$$

The mean absolute percentage error:

$$MAPE = \frac{1}{n}\sum_{t=1}^{n}\frac{|e_t|}{x_t} = \frac{1}{n}\sum_{t=1}^{n}\frac{|x_t - \hat{x}_t|}{x_t} \tag{4}$$

The predicted value of the next time:

$$\hat{x}_{t+1} = f_{t,1} = \frac{x_t + x_{t-1} + x_{t-2} + \cdots + x_{t-(N-1)}}{N} \tag{5}$$

The average absolute error of the observation period t:

$$MSE = \frac{1}{t-N}\sum_{t-N+1}^{t}(x_t - \hat{x}_t)^2 \tag{6}$$

III. EXPERIMENTAL ENVIRONMENT

In this paper, the adaptive sliding windows of price forecast method is used. And the original data is the year of price data of ten different models of cell phones from www.360buy.com.

In this paper, improvements have made on the traditional sliding windows called as the adaptive sliding windows. In this experimental environment, the last seven data of the year of price data of each model of cell phones from www.360buy.com are used as the actual data compared to the forecast price. And the remaining data are used as the forecast samples to forecast prices.

And when forecast the first data, eighteen different sliding windows values are given. *SW* is seen as the sliding windows values. And the *SW* is given by equation (7).

$$SW = (3,4,5,...,20) \tag{7}$$

*Corresponding author. hyitzqy@126. Com

978-0-7695-4818-0/12 $26.00 © 2012 IEEE
DOI 10.1109/DCABES.2012.20

Through the use of different sliding windows values, eighteen forecast values will be gotten. *Yn* is seen as the forecast values.

The value is selected from all the forecast value *Yn* of the minimum error as the final forecast value *Y* and the test sample of the next forecast.

SW is not changing when forecasting after next six data. *Bsw* is seen as the best *SW*. *Bsw* is gotten with the *Bsw1*, *Bsw2* and *Bsw3* coupled with a custom weight *W*. The *Bsw1*, *Bsw2* and *Bsw3* are the *SW* of the best three forecast errors when forecasting the first data. *Bsw* is given by equation (8).

$$Bsw = \frac{Bsw_1 * w_1 + Bsw_2 * w_2 + Bsw_3 * w_3}{w_1 + w_2 + w_3} \quad (8)$$

W is given by equation (9) and in this experiment environment *W*=[2,4,2].

$$W = [w_1, w_2, w_3] \quad (9)$$

When forecasting remaining data, every forecast value will be used as the test sample for the next forecast until the final data is gotten.

IV. EXPERIMENT WITH DATA

The result of experiment with the year of price data of ten different models of cell phones from www.360buy.com is shown in Table 1.

TABLE I. THE BEST AVERAGE ERROR OF THE TEN KINDS OF AGRICULTURAL PRODUCTS

Name	ABE	Name	ABE
Sony Ericsson LT15I	0	Sony Ericsson MT15I	0.014
HTC T9199	0	HTC S710E	0.038
MOTOROLA ME511	0	MOTOROLA ME722	0
NOKIA E66	0	NOKIA E72I	0
SAMSUNG S5670	0.015	SAMSUNG W609	0

In the Table 1, Name is the names of ten different models of cell phones. ABE is the average error of the seven best errors of each model of cell phone in the experiment with the original data.

Original data, forecast data and the best average errors of ten different models of cell phones are shown in Figure 1, Fig. 2 and Figure 3.In the Fig. 1 and Fig.2, *X* lable is the seven days and *Y* label is the CNY (China Yuan). In the Fig. 3, *X* lable is the seven days and *Y* label is the MAE (Mean Absolute Error).

As shown in the Fig. 3, the best average errors of ten different models of cell phones are very satisfactory compared to the original data. Analyzed the results gotten in this experimental environment, it can be seen that forecast price of cell phones with the adaptive sliding windows is useful.

The following figures from Fig. 4 to Fig. 13 show the original data and the best forecast data of the each model of ten type's cell phones.

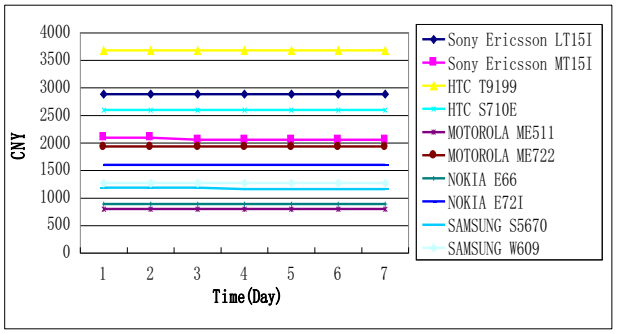

Figure 1. Original data of ten different models of cell phones

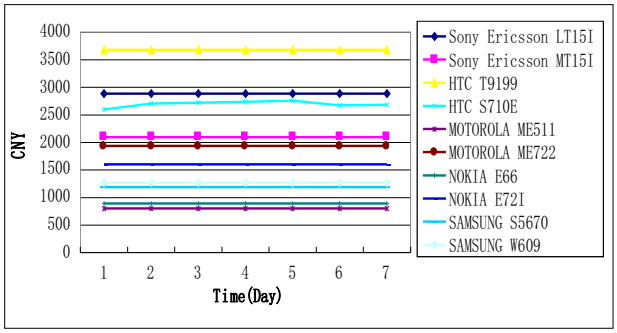

Figure 2. Forecast data of ten different models of cell phones

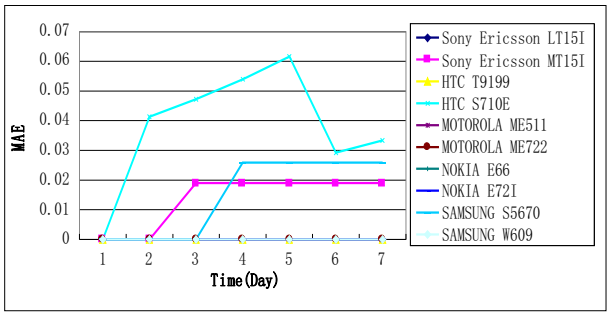

Figure 3. The best average errrors of ten different models of cell phones

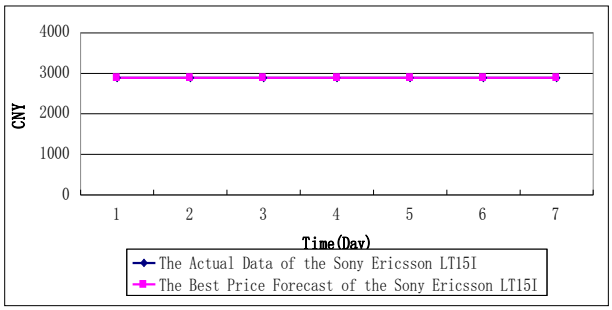

Figure 4. The best price forecast and actual data of the Sony Ericsson LT15I

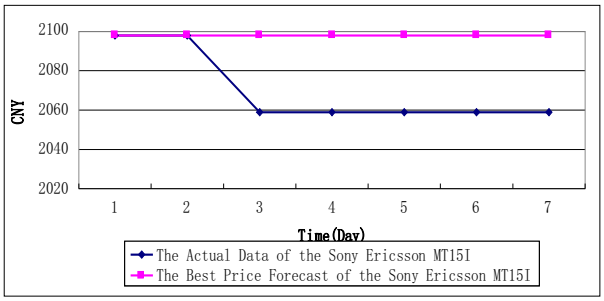

Figure 5. The best price forecast and actual data of the Sony Ericsson MT15I

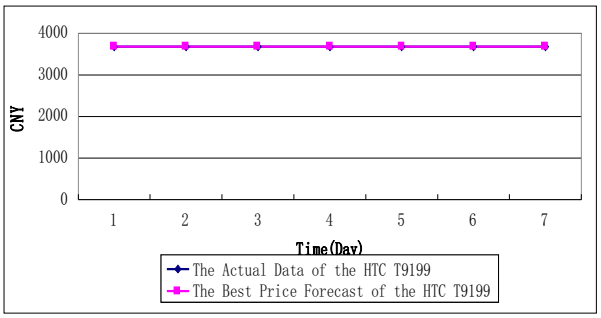

Figure 6. The best price forecast and actual data of the HTC T9199

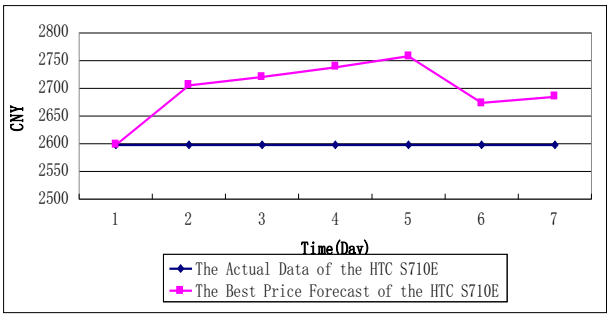

Figure 7. The best price forecast and actual data of the HTC S710E

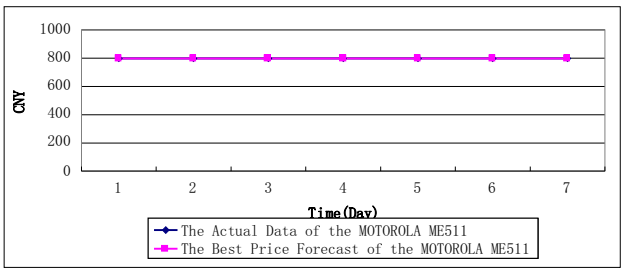

Figure 8. The best price forecast and actual data of the MOTOROLA ME511

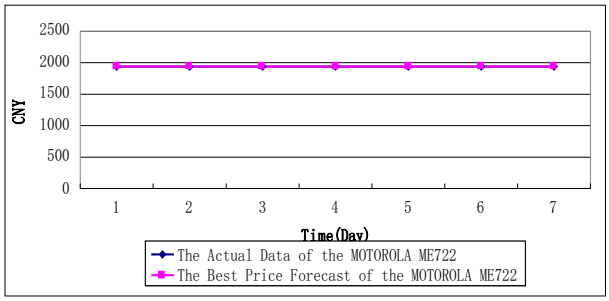

Figure 9. The best price forecast and actual data of the MOTOROLA ME722

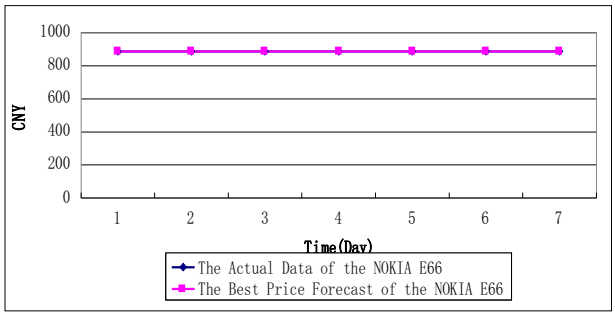

Figure 10. The best price forecast and actual data of the NOKIA E66

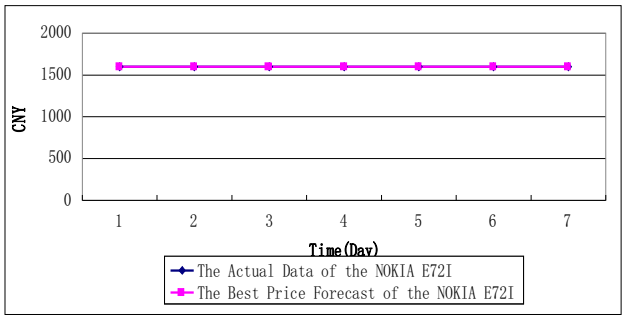

Figure 11. The best price forecast and actual data of the NOKIA E72I

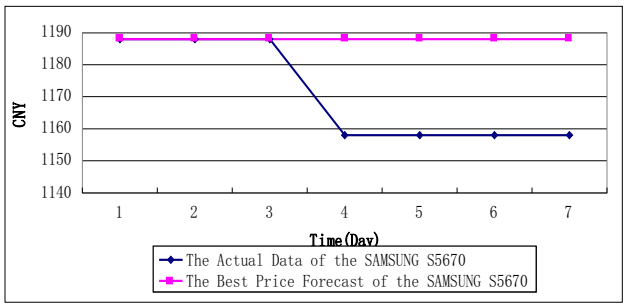

Figure 12. The best price forecast and actual data of the SAMSUNG S5670

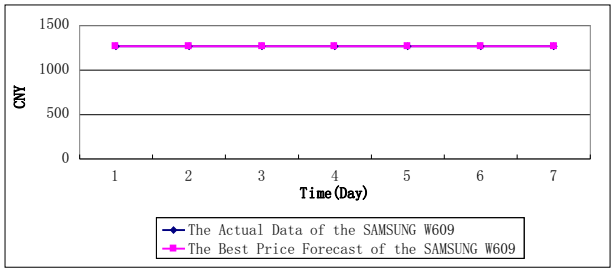

Figure 13. The best price forecast and actual data of the SAMSUNG W609

CONCLUSION

In this paper, seven days prices of ten different models of cell phones are forecasted with the year of price data of each model of cell phones from www.360buy.com based on the adaptive sliding windows. And the results are ideal compared to the original data in this experimental environment. Whether this method being applicable to other experimental environment needs further exploration and further experimental validation, such as modifying custom weight and modify the data processing method.

ACKNOWLEDGMENT

This work is supported by the National Sparking Plan Project of China (2011GA690190), the fund of Huaian Industry Science and Technology. China (HAG2011052, HAG2011045，HAG2010066).

REFERENCE

[1] ZHANG Yu; HE Jia ; YIN Teng-fei. Research on Petroleum Price Prediction Based on SVM. Computer Simulation,2012

[2] ZHU Yancheng; WANG Wenbo; ZHAO Pan. Prediction of steel price based on harmonic wavelet and neural network. Computer Engineering and Applications,2012

[3] Ji Qiang, Zhu Lei; Mo JianLei; Duan Hongbo. International Crude Oil Market Trend Analysis and Price Forecast. Bulletin of Chinese Academy of Sciences,2012

[4] Quanyin Zhu; Sunqun Cao; Jin Ding; Zhengyin Han. Research on the Price Forecast without Complete Data Based on Web Mining, 2011 Tenth International Symposium on Distributed Computing and Applications to Business, Engineering and Science (DCABES), Publication Year: 2011 , Page(s): 120 – 123

[5] Chaang-Yung Kung; Huei-Shr Chen; Chih-Cheng Huang; Using GM(1,1) method to forecast the development of cell phone market in Taiwan. IEEE International Conference on Kun-Li WenFuzzy Systems, 2008. Publication Year: 2008, Page(s): 539 – 543

[6] Hsueh-Fang Chien; Shu-Hua Lee;Lee Wen-chih; Yann-ching.Forecasting Monthly Sales of Cell-phone Companies - the Use of VAR Model. Second International Conference on Tsai Innovative Computing, Information and Control, 2007. Publication Year: 2007 , Page(s): 459

[7] Baoyi Wang; Shaomin Zhang; Qiaoli Xue; Peng Shen. Prediction of power system marginal price based on chaos characteristics. IEEE International Conference on Industrial Technology, 2008.Publication Year: 2008 , Page(s): 1 – 5

[8] Herui Cui; Xiuli Song.Research on Electricity Price Forecasting Based on Chaos Theory International Seminar on Future Information Technology and Management Engineering, 2008. Publication Year: 2008 , Page(s): 398 – 401

[9] Pei-Chann Chang; Chin-Yuan Fan.A Hybrid System Integrating a Wavelet and TSK Fuzzy Rules for Stock Price Forecasting. IEEE Transactions on Systems, Man, and Cybernetics, Publication Year: 2008 ,Volume: 38 ,Issue: 6 Page(s): 802 – 815

[10] Ismail, M.J.; Ibrahim, R.; Ismail, I.Adaptive neural network prediction model for energy consumption. International Conference on Computer Research and Development (ICCRD), 2011 3rd. Publication Year: 2011 , Volume: 4 ,Page(s): 109 – 113

[11] Bo-Tsuen Chen; Mu-Yen Chen; Min-Hsuan Fan; Chia-Chen Chen.Forecasting stock price based on fuzzy time-series with equal-frequency partitioning and fast Fourier transform algorithm. Computing, Communications and Applications Conference (ComComAp), 2012. Publication Year: 2012 , Page(s): 238 – 243

An Empirical Investigation of the Impact of SCM Components on the Logistics Service Performance

Chao Sun[1], Guang-ming Zhang[2]

[1] Department of Economics and Management, Zhixing College of Hubei University, Wuhan, P. R. China
[2] School of Economics and Management, Wuhan University, Wuhan, P. R. China.
10368260@qq.com

Abstract: **The logistics service performance is not only affected by the logistics resources, capability, strategy and external environment, but also by the specific supply chain environment and management components. This paper utilizes the empirical investigation of Chinese manufacturing companies, to verify the relationship of supply chain management (SCM) components and the logistics service performance. The results indicate that, the supply chain partnership and coordination and management have significant impact on the logistics service performance, but the supply chain information does not, and the supply chain integration also has significant impact on logistics service. Enterprises should pay adequate attention to the establishment of supply chain partnership, so as to enhance the integration, coordination and management of supply chain.**

Keywords: **logistics service performance; SCM elements; supply chain partnership; supply chain integration**

I. Introduction

In the environment of supply chain, the logistics service performance is not solely affected by the logistics resources, capability, strategy and external environment, but also by the specific supply chain environment and management components. Therefore, the logistics service performance (LSP) embodies very complicated nonlinear features. The SCM (supply chain management) components comprise the partnership, information sharing, integration, coordination and management. They actually reflect the supply chain management capability cross boundaries of enterprises and also the performance of logistics service. Dyer et al. (1998)[1], Lambert et al. (2004)[2], Panayides et al. (2005)[3], Corsten et al. (2005)[4], Morris et al. (2005)[5] conducted researches on the relationship between the partnership and logistics or supply chain performance from different perspectives. Integration of supply chain logistics indicates that the supplier increases the communications with customers about the logistics, and has bigger coordination of logistics activities and more fuzzy division of organization (Stock et al., 2000)[6]. Daughterty et al. (1996)[7], Stock et al. (2000)[8], Stank et al. (2001)[9], Vickery et al. (2003)[10], Cristina et al. (2005)[11] studied the relationship between the supply chain integration and its performance. Bowersox and Closs (1996) thought that, timely and accurate information was more important to logistics than ever in the history. However, numerous factors also demonstrated that the expansion of information technology might be a waste of company's resources without achieving the intended effects[12]. As pointed out by Porter (2003), many new information technologies were used to improve the operating efficiency and attain the best practice, instead of strengthening the specific positioning; the danger hidden in the new generation IT tools were: too many companies could follow suit and unconsciously result in the homogeneous competition, which were not good for customer to select and might trigger the mutually destructive competitions[13]. Shang Kuo-chung et al (2005), based on a survey of 1200 manufacturing companies in Taiwan, discovered that the information-based logistics capability was the most critical since it could impact upon benchmarking capability, flexibility capability and logistics performance[14]. Wang Zhenzhen and Chen Gongyu (2009) held that the regional brand formed after logistics clustering gathered the logistics companies in the cluster to shape an industrial cluster, so that the companies in the region became more economic in auxiliary services such as information search[15]. A lot of literatures at home and abroad are available for researching the impact of some SCM components, such as IT, cooperation and integration, on the logistics performance or corporate performance. But there is lack of systemic studies, especially systemic and all-around studies on Chinese enterprises. This paper aims to empirically investigate the impact of SCM components on the logistics service components with Chinese manufacturing companies as an example.

II. Relation of SCM Components and LSP

A. Measurement of SCM components

SCM components are mainly reflected in aspects such as supply chain integration, partnership, information sharing, coordination and management etc. The basic feature is crossing the boundaries of enterprises. As an exploratory study, they are used in this paper as the main factors for measuring the SCM components. 16 items are selected to measure these SCM components. These items are selected after referring to and revising the questionnaire and models (Daughterty et al. (1996); Ellinger et al. (2000); Stank et al. (2001); Christopher et

This paper is supported by science research project in Hubei Logistics Development Research Center (2010A05) and (2010Z01)

978-0-7695-4818-0/12 $26.00 © 2012 IEEE
DOI 10.1109/DCABES.2012.120

al. (2004); Kuo-chung et al. (2005). All items apply the 5-point Likert scale, from strongly disagree or very poor to strong agree or very good [16].

B. Measurement of LSP

In this paper, the logistics service performance (LSP) is embodied by the items such as logistics service quality, customer perception, flexibility etc. Because the performance is dynamic and it is difficult to quantitatively describe many performance indicators, the subjective method is used to measure.

C. Hypotheses for the Impact of SCM Components on the LSP

The supply chain partnership is a tailored relationship based on shared information, shared risk and shared reward within some period between companies having mutual relationship in supply chain. The supply chain partnership impacts the LSP by means as follows. Firstly, the relation is favorable for realizing of information sharing, and reduction in the cost of communication, cost of stock and other operating costs. Secondly, the relation is helpful for prompt response to customer demand and improves the logistics service quality, flexibility and differentiation in competition. Thirdly, the relation is good for learning from each other, knowledge sharing and innovation of logistics service among supply chain members and realizes the continual improvements of LSP. The hypothesis is hence proposed in the below:

Hypothesis 1: The supply chain partnership is positively correlated to the logistics service performance.

Due to complexity in the process of logistics activities, the integration of supply chain logistics not just involves the logistics functions, but also the integration of logistics and production, logistics and marketing interfaces, as well as planning, distribution and control of financial and human resources. This is more of integration from the perspective of supply chain than the in-house integration. It is specifically manifested as the integration of organization, process (flow), information and resources etc. The purpose is to have the systemic and coordinated operation of logistics service by all supply chain logistics activities, which may be provided to the customers at the smallest cost. As a result, the overall optimization is achieved.

The supply chain partnership impacts on the LSP by: more effective operation of logistics service, to improve service efficiency; sufficient information sharing, to reduce the stock and cost, lessen the difference in perception and upgrade the customer service level; complementarity and efficacy of resources and capability, to enhance the adaptability to environment. Accordingly, Hypothesis 1 is presented.

Hypothesis 2: The supply chain integration is positively correlated to the logistics service performance.

The cooperation and integration of supply chain are dependent on the information sharing based on advanced information technologies and network technologies. The influences of information technologies on the logistics and company's performance and competitive power attract more and more research attention. In China, the impact of information capability on LSP needs further investigations.

The impacts of use of information technologies and information sharing on LSP are possibly embodied in: to improve the predictability, reduce the uncertainties and bullwhip effect and thus decreasing the stock cost; to promote relationship commitment and reduce the transaction cost and opportunistic behaviors; based on the supply chain learning, to construct the organizational memory and realize the knowledge sharing; improve the operating efficiency. Hence, the Hypothesis 2 is presented.

Hypothesis 3: The information sharing of supply chain is positively correlated to the logistics service performance.

Owing to the complexity of supply chain, the information asymmetry, lack of trust and cooperation, and unfair benefit distribution may lead to the malfunctions of supply chain, such as worse supply chain relationship, increase of production and stock costs, and out of stock, so that the desired competitive advantages can't be achieved. In view of these, the coordination and management of supply chain must be strengthened. Consequently, the Hypothesis 3 is presented.

Hypothesis 4: The coordination and management of supply chain is positively correlated to the logistics service performance.

The coordination and management of supply chain means that the top management has a clear understanding of the SCM concepts, establishes the complete, process-based management system favorable for enhancing supply chain management, and the continuous improvement mechanism based on collaborative relationship, aims at the double-win or multi-win performance evaluation and stimulation system, and owns the logistics talents suitable for supply chain management. As indicated by a lot of researches, the LSP is conductive to increase of market share and enhancement of competitive power and financial performance, through reducing logistics cost and improving customer satisfaction and loyalty. Therefore, the Hypothesis 4 is presented

III. Empirical Analysis

A. Data Collection and Questionnaire Design

Logistics service of manufacturing industry was the subject investigated in this paper. After the questionnaire had been designed, some familiar senior managers were visited, mainly among on-the-job postgraduate students of the Economics and Management School of Wuhan University, MBA students and familiar companies. 200 pieces of questionnaires were distributed and 120 pieces,

60% returned. Among them, 93 pieces are valid response, accounting for 46% of all. The respondents are from state-owned, joint-stock, and private enterprises and joint ventures in industries such as machinery, electronics, automobile, foods and pharmaceutics etc. Most of respondents are working in Wuhan, Shenzhen etc. Generally, they are middle and top managers with more than 4 years' work experience, who are very familiar with their companies' supply chain logistics. The questionnaires are anonymous and perceptive measurement, involving no individual privacy or company's secrets, so the authenticity and trustworthiness can be guaranteed.

B. Data Handling

(1) Reliability

The coefficient of consistency Cronbach α is used as a measure of the reliability of the questionnaire, and the SPSS11.5 software is applied to calculate the reliability of various factors. The ANOVA of 16 supply chain components is F= 14.5849, P≤0.0001; this means a good repeatability of the measure. In the Hotelling T test, F =10.2127, P≤0.0001; this shows a good equality for scores of items, which have the internal relevancy. The Cronbach α value for the reliability test is 0.91, and the standardized Cronbach α value is 0.9092. The reliability test indicates that, 16 supply chain components have very good consistency and stability. The factor analysis is utilized to separate out four main factors, called coordination and management of supply chain, information, partnership and integration. After testing, their Cronbach α values are 0.8723, 0.8611, 0.7928 and 0.7660, respectively. The Cronbach α value for the reliability test of four measuring items of LSP is 0.7370, that for the reliability test of four items of corporate performance is 0.8525, and that of the overall reliability of the whole questionnaire is 0.9236. The reliabilities are high.

(2) Validity — Factor Analysis

The questionnaire has good content validity because it is designed and revised on the basis of related works reported by foreign researchers. The content validity is tested by the factor analysis method. After Bartlett's test, the Bartlett value is 822.717, and P≤0.001. This means the matrix is not a unit matrix, and the factor analysis can be conducted. The principal components analysis (PCA) is utilized to obtain 4 main factors whose eigenvalue is larger than 1, respectively representing the coordination and management of supply chain, information, partnership and integration. See details for the items corresponding to figures in bold in Table I. KMO value in the factor analysis is 0.859, which is larger than 0.5 and approaches to 1. This indicates that the results of factor analysis are acceptable and the validity is good. The accumulated contribution rate of the four factors is 70.347%. This reveals that the four factors can represent all supply chain components, with very good validity. See Table I for the results of factor analysis.

(3) Relevancy of Supply Chain Components and LSP

First of all, the control variables are not considered, and the correlation analysis for main factors of supply chain components and LSP is conducted, as shown in Table II. From Table II it can be seen that at the confidence level 0.01, LSP has no obvious correlation with supply chain information, but with other supply chain components. The supply chain integration is significantly correlated to the LSP. This indicates that the integration impacts on the corporate performance through LSP.

TABLE I
Factor Analysis of Supply Chain Components

Items	Factors			
	1	2	3	4
Information function	.279	.825	.120	.047
Advanced information technologies	.182	.823	.003	.138
Accurate and prompt information	.030	.743	.273	.259
Information method, procedure	.399	.742	.215	-.138
Organizational integration	.382	.325	.629	.007
Orientation of customer demand process	.041	.187	.787	.212
Diversified logistics service	.472	.225	.617	.193
Rapid organization of logistics resources	.138	.000	.740	.245
Mutual trust and commitments	.327	.105	.160	.777
Strengthening of relationship	.132	-.067	.255	.813
Duration of relationship	.131	.287	.126	.697
Implement of SCM	.543	.448	.144	.120
Supply chain logistics system	.692	.425	.247	.074
Continuous improvement of supply chain	.703	.005	.248	.391
Performance and incentive of supply chain	.835	.162	.160	.231
Supply chain logistics talents	.799	.293	.072	.153
Variance contribution rate %	21.289	20.269	21.289	14.054
Accumulated contribution rate %	21.289	41.558	56.292	70.347

TABLE II
Correlation Analysis of Supply Chain Components and LSP

Items		Supply chain coordination	Supply chain information	Supply chain integration	Supply chain partnership
LSP	Pearson correlation coefficient	.489(**)	.206(*)	.285(**)	.327(**)
	Sig.	.000	.048	.006	.001

The analysis discovers that, LSP has no obvious correlation with supply chain information, but with other supply chain components.

TABLE III ANOVA

Model	Sum of square	Degree of freedom	Mean square	F	Sig.
Deviation of regression	15.941	4	3.985	19.082	.000
Residue	18.379	88	.209		
Total deviation	34.320	92			

TABLE IV
Linear Regression Analysis of LSP and Supply Chain Components

Model	Unstandardized coefficient		Standardized coefficient	t	Sig.	Colinearity statistic	
	Coefficient B	Standard error	Beta			Tolerance	Variance inflation factor (VIF)
Constant	3.384	.047		71.418	.000		
CMSC	.299	.048	.490	6.276	.000	1.000	1.000
SCI	.124	.048	.202	2.595	.011	1.000	1.000
ISC	.173	.048	.284	3.635	.000	1.000	1.000
SCP	.196	.048	.322	4.122	.000	1.000	1.000

Notes: ANOVA (Analysis of variance)
CMSC (Coordination and management of supply chain)
SCI (Supply chain information)
ISC (Integration of supply chain)
SCP (Supply chain partnership)
F (Significance value of regression equation)
t (Significance value of regression coefficient)
Sig.(Significance value)

(4) Regression Analysis and ANOVA

LSP is taken as the dependent variable and the four factors of the supply chain components are seen as the independent variables. The ANOVA and regression analysis are conducted. With the Enter (all input) method, the multiple correlation coefficient of the model is $R=0.682$, $R^2=0.464$, $F=19.082$, and $P\leq 0.0001$. This means that the linear relation of the model exists. The Durbin-Watson statistic is 2.316. This tells that the residuals in the regression analysis are independent form each other. Therefore, the multiple linear regression analysis can be further carried out. The results are presented in Table III and Table IV.

Table III and Table IV show that, LSP has obvious correlation with the four supply chain factors at the level 0.05, but at the level 0.01, the "information" has no significant impact on LSP. The tolerance of variables in the colinearity statistic is 1 and the variance inflation factor (VIF) is 1. This indicates that the variables in the regression model do not have multiple colinearity.

IV. Conclusions and Implications

A. Conclusions

The results demonstrate that the Hypotheses 1, 2, 4 are confirmed, but Hypothesis 3 is not true. They are basically consistent with the research results reported by foreign researchers. The supply chain partnership and coordination and management have significant impact on LSP, but the supply chain information has no obvious impact on LSP. It is notable that the supply chain integration has obvious impact on LSP. This is also consistent with the result reported by foreign researchers.

B. Implications

Through the empirical investigation into the impact of supply chain components on LSP and corporate performance, conclusions with theoretical and practical significance are reached and part of hypotheses are supported. Generally, companies implement the supply chain management to different degrees and are fully aware of the importance of strengthening the supply chain partnership, but they are at low level in aspect of coordination and management of supply chain, especially the supply chain performance. This reflects that the companies need enhancing the supply chain performance evaluation and incentive. The supply chain components impact on LSP, but different components have different degrees of significance. Supply chain partnership and coordination and management have direct and obvious impacts, so the companies must give adequate emphasis on the establishment of supply chain partnership and strengthening of supply chain integration and coordination and management. The supply chain integration has direct impacts on LSP, so it is important. In order to better realize the supply chain integration, the companies should use more of third-party or fourth-party logistics services to improve the logistics service performance.

Reference

[1] Dyer Jeffrey H., Harbir Singh, The relation view: cooperative strategy and sources of interorganizational competitive advantage, Academy of Management Review, 23 (4), 1998, pp.660-679.

[2] Lambert D.M., Knemeyer A.M., We're in this together, Harvard Business Review, December, 2004

[3] Panayides, Photis M., Meko So, The impact of integrated logistics relationships on third-party logistics service quality and performance, Maritime Economics & Logistics, 7, 2005, 36-55

[4] Corsten Daniel, Nirmalya Kumar, Do suppliers benefit from collaborative relationships with large

retailers? An empirical investigation of ECR adoption, Journal of Marketing, July, 2005, pp.80-94
[5] Matthew Morris, Craig R Carter, Relationship marketing and supplier logistics performance: an extension the key mediating variables model, Journal of Supply Chain Management, Vol.41, No.4, 2005, pp.32-43.
[6] Stock Gregory N., Noel P. Greis, John D. Kasarda, Enterprise logistics and supply chain structure: the role of fit, Journal of Operations Management, 18, 2000.531–547
[7] Daughterty P.J., A.E.Ellinger, C.M.Gustin, Integrated Logistics: Achieving Logistics Performance Improvements, Supply Chain Management, Vol.1, No.1, 1996, 25~33
[8] Stock Gregory N., Noel P. Greis, John D. Kasarda, Enterprise logistics and supply chain structure: the role of fit, Journal of Operations Management, 18, 2000.531–547
[9] Stank, Theodore P., Scott B.Keller, Daivd J.Closs, Performance Benefits of Supply Chain Logistical Integration, Transportation Journal, Winter/Spring, 2001-2002, pp.32-46
[10] Vickery, Shawnee K. , Jayanth Jayaram, Cornelia Droge, Roger Calantone**,** The effects of an integrative supply chain strategy on customer service and financial performance: an analysis of direct versus indirect relationships, Journal of Operations Management, Dec 2003, Vol.21, Iss.5, pg.523
[11] Cristina Gimenez, Eva Ventura, Logistics-production, logistics-marketing and external integration: their impact on performance, International Journal of Operations and Production Management, Vol.21, No.1, 2005, pp.20-39
[12] David J. Closs, Thomas J. Goldsby and Steven R. Clinton, Information technology influences on world class logistics capability, International Journal of Physical Distribution & Logistics Management, Vol.27, No.1, 1997, pp.4-17.
[13] Michael E. Porter, On Competition, Trans. Gao Dengdi, Li Mingxuan, CITIC PUBLISHING HOUSE, January 2003, pp.20-21.
[14] Shang Kuo-chung; Marlow Peter B. Logistics capability and performance in Taiwan's major manufacturing firms [J].Transportation Research Part E: Logistics and Transportation Review, 2005, 41(3): 217-234.
[15] Wang Zhenzhen, Chen Gongyu: Empirical study of the impact of logistics industrial cluster on industrial added value in china: analysis based on provincial panel data, Journal of Shanghai University of Finance and Economics, Vol. 11, No.6, 2009, pp.52-53.
[16] Wu Zhihui, Liu Weizhan, Li Yahui, Report on Informatization of China Logistics Industry 2005, China Logistics, 2005(5).

A New Model of Describing Mutual Exclusion of Roles And Its Realization

Lou Yuan-sheng, Chen Sheng,Zhang Wen-yuan
College of Computer & Information
Hohai University
Nan Jing, P.R.China, 210098
Wise.lou@163.com, zjsy_cs@163.com

Xu Hong-tao
Data Management Center
Zheng zhou Human Resource & Social Security Bureau.
Zheng Zhou, P.R.China, 450007
xhtl@ hazz.hrss.gov.cn

Abstract—**The mutual exclusion of roles as an effective means of implementing separation of duty, has an important role on access control in RBAC systems. This paper deeply discusses the types that the mutual exclusion of roles come from, and puts forward a model of describing mutual exclusion of roles. The model is similar to the structure of adjacency multiple table, and its basic unit is the role structure which can describe the relations with other roles. The paper also explores the situation after the digestion of the mutual exclusion, and finally gives out a simple application.**

Keywords: RBAC, mutual exclusion of roles, Role distribution, Mutual exclusion digestion

.

I. INTRODUCTION

With the increasing of the network applications' scale, the user manager becomes more and more important. Role based access control (RBAC) introduced the role as the intermediary to set different access rights to different roles, and users in accordance with its responsibilities are assigned to different roles to achieve the logical separation [1].The exclusion relation between roles is the most effective way to achieve separation of duties. Studying the mutually exclusive of roles has a very large significance not only in theory but also in practical application [2].

However, the existing papers of the mutually exclusive roles are generally describing the nature and importance of the mutual exclusive of roles, or about the forms of mutually exclusive roles[3-8]. Refer to the importance of mutually exclusive roles, such as paper [4] and paper [2] which proved the mutually exclusive roles more stringent, the better of the security is. Paper [3] pointed out that the mutually exclusive roles have played a very good effect in the access control management. Paper [8] proposed a descriptive model of the RBAC role with the hierarchy and Exclusion Relations, but the model only describes the two roles that are mutually exclusive, not describes how it comes from.

The mutually exclusive roles are mostly generated from the mutually exclusive between privileges, and this paper focuses on the roles conflict source analysis. Mutually exclusive between privileges [9] is introduced to the role mutually exclusive sources, then reference to a similar multiple adjacency structure model which shows the role hierarchy relations and mutually exclusive relationship[8], and the paper puts forward a model that can describe the sources of mutually exclusive roles , and finally realizes the model.

II. RBAC-RELATED KNOWLEDGE

A *RBAC Model*

The core idea of RBAC is to link the roles and privileges directly ,and roles are assigned to users, allowing users to do some operation.

One famous RBAC model is the RBAC96 [10] model, which can be divided into RBAC0, RBAC1 RBAC2, RBAC3. RBAC0 is the basic model for any RBAC system must have, while RBAC3 adds the concept of the role inheritance and constraints on RBAC0.This paper's research is based on RBAC3 model, and RBAC3 model diagram can be expressed as follows(Figure 1).

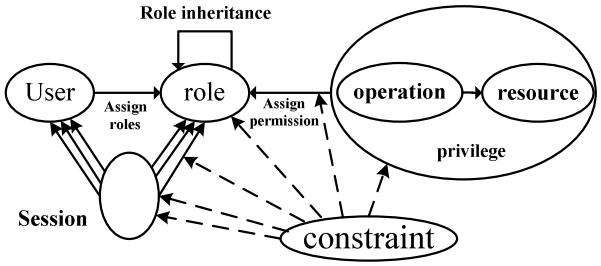

Figure 1: the RBAC3 model

B *RBAC Constraint*

The introduction of constraints in RBAC is whether the current operation can be accepted. There are many constraints, and the separation of role duties is the most important one, as follows:

1. Roles mutually exclusive. The mutual exclusion between roles is to allow user to use only a role in the mutually exclusive roles, then it can support the principle of separation of duties, which make the system safer. A user can only have limited numbers of roles also form the constraints of the role.

2. Prerequisite role. This constraint is if give the user a role B, that you must first assign the role A, and role A is a prerequisite role of role B.

3. Runtime mutually exclusive. This allows a user owns two mutually exclusive roles at the same time, but cannot simultaneously activate these two roles. Dynamic separation of duties can help to switch user's roles.

The role mutual exclusion is used to implement an effective means of separation of duties. We can learn from the RBAC model that roles actually represent a collection privileges set. The user is allocated to a certain role in order to achieve certain types of privileges. In

978-0-7695-4818-0/12 $26.00 © 2012 IEEE
DOI 10.1109/DCABES.2012.78

order to give the description more clearly, first giving the following definitions:

Role: R1, R2, R3, ...,Rn
Privileges: P1, P2, P3, ... ,Pn
Mutually exclusive privileges: (Pi, Pj)
Privilege conflict set: CP
Role conflict set: CR
Privileges set of role i: RiP
The user's role set: RS
The role Ri has privilege Pj: Pj ∈ RiP

The role inheritance: only when all the privileges of role i totally have that of the role j, then role i inherits role j.

III. A NEW MODEL OF DESCRIBING MUTUAL EXCLUSION OF ROLES

A The types of mutually exclusive roles' sources

Before the model is proposed, the paper analyzes the source of mutually exclusive roles. The types can be divided into two categories as follows in Figure 2 according to if internal mutually exclusive between roles exist. The first category is relatively simple, that the numbers of a user's roles reach the upper limit, for an example, when a user has already the allocation of 10 roles, so when the 11th role is assigned to this user and the roles mutually exclusive occur. The second type is caused because of the internal mutually exclusive between roles, and this paper focuses on the second category.

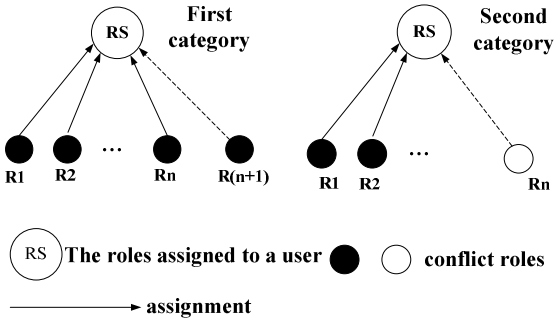

Figure 2: the types of conflict

In the second category, in according to if the role of mutual exclusion is defined by the administrator that also can be divided into two categories:

1. Administrator's own definition of the mutually exclusive roles, such as providing the role A and role B cannot be given the same user. Only when there is no conflict between role A and role B at current it will make the administrators to customize the conflict.

2. The mutually exclusive comes from the privilege conflict. When privilege C and privilege D is mutually exclusive, a role cannot simultaneously contain privilege C and D, and the roles respectively with privilege C and privilege D each other mutually exclusive.

However, the inherit roles may also inherit this mutually exclusive, and the most complex situation is that the conflict roles contain both the role of custom mutually exclusive and the mutually exclusive from the privilege , such as Figure 3.

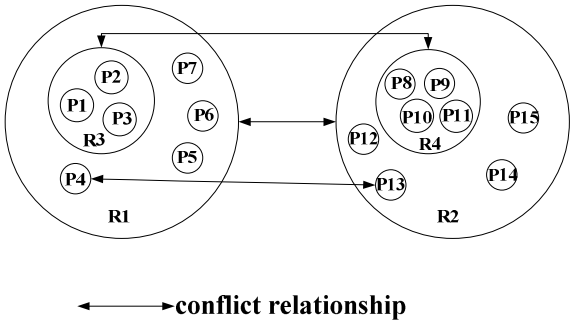

Figure 3: one of the complex conflict

In figure 3, R3 and R4 is a custom role conflict, and R1 and R2 respectively inherited the role of R3 and R4.While there is a conflict between privilege P4 and privileges P13 in R1 and R2, so the role R1 and R2 both have the two types of mutual exclusion. This will be explained in the next part B.

B Graphical representation of the model

To illustrate roles' conflict sources from which conflict privilege, it needs to design a privilege conflict table. The privilege conflict table is mainly composed of three parts: the conflict privilege id, privilege Pi and privilege Pj. All of the (Pi,Pj) in the privilege conflict table constitute the privilege conflict set CP.

Based on the above definition, give the following model as Figure 4:

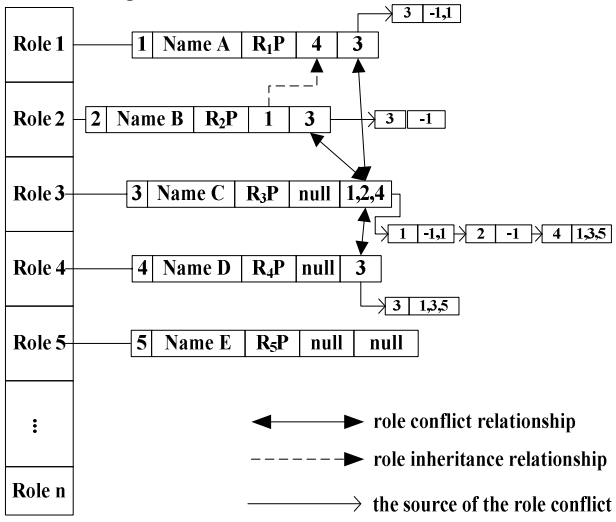

Figure 4: the model of describing roles' exclusion relations

The introduction of this model can make it clear of the source of the role conflict and relationship between roles. The core part of the model --- the role structure [8] is described as follows.

Role structure (role id, role names, privileges set, role hierarchy set, the role conflict set).

If the role hierarchy set in the role structure is not empty, then each element in the role hierarchy set corresponds to a role id to indicate the current role inheriting from.

The key part of this paper is the role conflict set. In

the model, the conflict set is composed of a series of nodes to form a linked list. These nodes have two parts, first part is the conflict role ID, the second part is the collection of the exclusive source, and -1 represents the custom role conflict, and other numbers correspond to the privilege conflict ID.

The interpretation of the model is as follows: the role library stores all the roles, and each role corresponds to a role structure. The last part of the role structure is the role conflict set indicating the conflict role set and their sources of current role.

IV. THE IMPLEMENTATION OF THE MODEL

The model mainly describes the mutually exclusion relationship between roles and its sources. The paper gives the both implementation of the form and digestion of the mutually exclusion.

A The formation of the mutually exclusive relationship

The mutual exclusion roles may be derived from the conflict of privilege and custom role conflict, so here are two cases to consider.

If the conflict is derived from the privilege conflict, then the steps are as follows:

1. For the role Ri and Rj, if there are any privileges Pa ∈ RiP, Pb ∈ RjP making up (Pa,Pb), then perform the following steps.

2. In the Ri's and Rj's role structure, respectively add each other's role number in the role conflict set.

3. Then add the other role's ID and all the IDs of the privilege conflict (Pa,Pb) to the list that the role conflict set points to.

The main part can be expressed as follows:

```
for (Ri belongs to the RS, Rj belongs to
the RS)
        for (Pa belongs to the RiP, Pb belongs
to the RjP)
            {
              If ((Pa, Pb) belong to the CP)
                {
                    (Ri, Rj) belongs to CR
                    Add (Pa, Pb)'ID to the
(Ri,Rj).source
                }
            }
```

The steps of custom roles' conflict are as follows:

1. To customize the mutually exclusive roles Ri and Rj, if they have been mutually exclusive, then cancel the operation.

2. If there is no conflict between Ri and Rj, then add each other's role number to the role conflict set in the roles' role structure.

3. Then add the other role's ID and the number -1 to the list that the role conflict set points to, and prompt whether all the inherited roles of Ri and Rj inherit this conflict.

The main part can be expressed as follows:

```
If (Ri belongs to the RS, and Rj belong to
the RS) {
        If ((Ri, Rj) belong to the CR) return;
        Else
          {
            (Ri, Rj) belongs to CR
            (Ri, Rj). Increase in the souce -1
          }
    }
```

B The digestion of the mutually exclusive relationship

It is similar to the formation of the mutually exclusive relationship that there are also two situations in the digestion of the mutually exclusive relationship.

If you want to eliminate the mutually exclusion between role Ri and the role Rj, first should look for the role structure of Ri and Rj.

1. If the sources of the mutually exclusive between role Ri and Rj only come from the custom role conflict, then cancel the mutually exclusive relationship between Ri and Rj, and prompt whether all the inherited roles of Ri and Rj cancel this conflict.

2. If there are sources of the mutually exclusive between Ri and Rj that come from privilege conflict. Then it depends on the administrator to decide whether to remove all the privilege conflict causing the conflict of Ri and Rj. If the administrator removes some privilege conflicts, then it should automatically digest the role conflicts caused only by these privilege conflicts.

V. THE APPLICATION OF THE MODEL

The model can be applied to design a role assignment controller with the role conflicts detection. When the new role is assigned to the user, the controller can find the user with the roles that have been assigned. Then the controller puts the new assigned roles and the roles already assigned together as the input of the controller. After the disposing of the controller, the role assignment controller can detect the part of role conflict and the other normal part. The role assignment controller structure is shown in Figure 5:

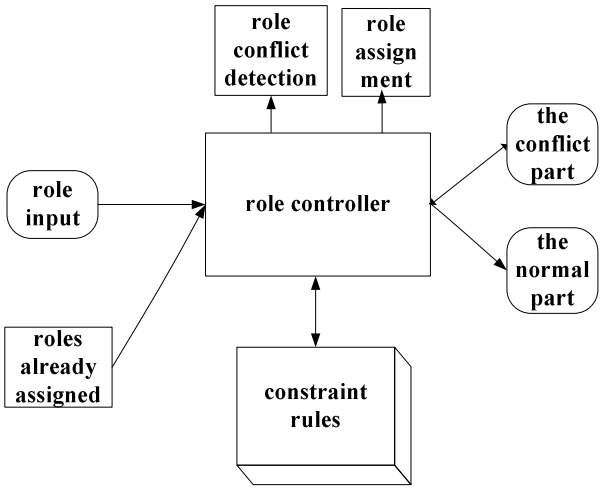

Figure 5: the role controller

The following give the description of the role assignment to the old user.

```
role_new[] =new assigned role;
role_old[] =already assigned role;
i = 0;
Set set;
   // It is a binary group in the set, representing the two mutually exclusive elements.
for (i = 0; i <role_new.length; i++)
      {
      role_confict[] = table(role_new [i]);
         //Find the set of mutually exclusive roles of role_new[i] in the role conflict table
         result[] = compare (role_confict, role_new+role_old);
         //Return part of the mutually exclusive its source
         set.add (result);
         //put the conflicts to the role conflict set.
      }
return the set;
```

VI. CONCLUSIONS

This paper focuses on the mutually exclusive relationship between roles, analyzes the role mutually exclusive sources and mutually exclusive digestion, introduces the privilege conflict to the role conflict sources, and proposes a model with its implementation. Finally, the paper designs a role distributor as an application of the model. The proposed model is able to classify role conflicts and achieves better separation of the roles responsibilities.

REFERENCES

[1]. Fu Zhifeng, Huan-Guo Zhang RBAC system, separation of duties [J]. Computer Engineering, 2003, (06) :61-63.

[2]. Xiao-Jing Yang Zhao Lin RBAC mode in the mutually exclusive nature of the role of its security [J]. Computer Applications, 2003, (S2) :138-140.

[3]. Hu Heping Zou loose roles are mutually exclusive in the role-based access control system [J]. Computer Engineering, 2002, (04) :124-126

[4]. Xiaosheng Feng; Bin Ge; Yang Sun; Zhenwen Wang; Daquan Tang; Broadband Network and Multimedia Technology (IC-BNMT), 2010 3rd IEEE International Conference on Digital Object Identifier: 10.1109/ICBNMT.2010.5705176 Publication Year: 2010, Page (s): 677 - 683

[5]. Habib, MA; Internet Technology and Secured Transactions (ICITST), 2010 International Conference for

The Year of publication: 2010, Page (s): 1 - 6

[6]. Hu Jinzhu; Juan-juan; RBAC model, the role of inheritance and mutual exclusion problem [J]. Computer Science, 2003, (11) :160-163.

[7]. Sun Xiaolin; LU Zheng-ding; Li Ruixuan; Wang Zhigang; Chen Xinhua; role-based access control based on the role of the description logic mutually exclusive [J]. Computer Engineering and Science, 2007, (09) :37-40 +44.

[8]. Section of lung vibration; Wen Feng; yellow water; Feng Yu Hua; a descriptive model of the RBAC role hierarchy and Exclusion Relations [J]. Nanchang University (Natural Science), 2006, (06): 601 -604

[9] Zhang Lei; to macro; Hai-Bo Hu; semantics RBAC model, privileges-based conflict detection method [J]. Computer Engineering and Applications, 2011, (26) :74-78

[10]. Sandhu R, Coyne E, Feinstein H, et al.Role-based Access Control Model [J], the IEEE Computer, 1996,29 (2): 38 –

A New Linear Programming Based Load-shedding Strategy

Ouyang Lin
School of Computer Science and Technology
Wuhan University of Science and Technology
Wuhan, China
e-mail: ouyanglin@wust.edu.cn

Qi Jingjing
School of Computer Science and Technology
Wuhan University of Technology
Wuhan, China
e-mail: ginjiq@126.com

Zhou Qin
Department of Electrical Engineering
Shanghai Dian Ji University
Shanghai, China
e-mail: rainbow.zhou@tom.com

Pu Qiumei
School of Information Engeering
Minzu University of China
Beijing, China
puqm@whut.edu.cn

***Abstract*—There is a large class of applications that high-frequency data produced continuously in 7 days per week and 24 hours per day. The traditional data processing system can not deal with them efficiently because of the active data pushing and the passive queries. With the purpose of dealing with these data, data stream management systems (DSMS) appeared. For the geographical distribution of data streams, distributed data stream processing systems are studied recently. As an important aspect of distributed data stream management system (DDSMS), load management can balance system load incurred by unpredictable incoming data stream and inappropriate query operators' distribution. Load-shedding acts as an important role in load management of distributed data stream system. In this paper, a new linear programming based load-shedding strategy is proposed to degrade system load on a simple query network with network constraint. Compared with previous work which concentrates on one factor only, it takes two factors; include CPU capacity and network constraints. Experiments indicate that it can increase system stability and to decrease the loss of query accuracy with low extra cost.**

Keywords-Load-shedding; Linear Programming; Network Constraint; DDSMS

I. INTRODUCTION

A large class of data-intensive applications that produce high-frequency update data, such as stock markets, network monitoring, online transaction, sensor applications and pervasive environments, have appeared in the past few years. In these typical applications named data stream applications, data are usually unbounded, continuous, and huge in amount, fast arriving, time various and out bursting.

The traditional data processing, which can deal with the snapshot queries perfectly, can not satisfy the requirements of these data stream applications. Till now, a number of Data Stream Management Systems (DSMS), such as Aurora [1], Medusa [2], STREAM [3], TelegraphCQ [4], Borealis [5] and Argus [6], have been developed for the purpose of dealing with these continuous streaming data. In these DSMS, the queries are passive and the data are active. On the contrary, the data are passive and the queries are active in traditional data processing systems. Many applications of DSMS system are under real time constraint on query processing. However, delays in data stream processing are very difficult to control because of the outbursting of data incoming and the unpredictable pattern of resource consumption. Therefore, system overloading is very common in data stream systems, especially in distributed data stream processing systems. In order to implement the load balancing in these systems, many kinds of methods are adopted such as operator distribution or redistribution, operator migration and load-shedding etc.. Usually, the load management system takes advantage of load balancing to degrade the system load.

Including other load management methods, load-shedding is also a very efficient and effective method to implement the real time constraint of these applications by dropping incoming data appropriately especially when the incoming data burst out and can't be processed in time through normal load balancing methods.

II. RELATED WORK

Some work has been done in this area recently. The Aurora system [7] uses Quality of Service (QoS), including a latency graph, a value-based graph and a loss-tolerance graph, to implement load-shedding. In Aurora, three basic questions (when, where and how much data should be dropped) are raised for load-shedding, but it mainly focuses on where instead of when and how much to drop data tuples. In [8], load-shedding strategies for a single continuous query operator on sliding window model are presented. The TelegraphCQ [4] system discusses a load-shedding strategy that takes advantage of a data summary method by using a data classifying algorithm to increase the accuracy of

978-0-7695-4818-0/12 $26.00 © 2012 IEEE
DOI 10.1109/DCABES.2012.31

queries. In [9], load-shedding strategies that minimize the loss of accuracy of aggregation queries in DSMS are discussed. In [10], a data triage approach is proposed to exploit synopses of discarded data to increase query accuracy. The LoadStar [11] project discusses semantic load-shedding in a stream mining environment. In [12], a systematic approach that takes advantage of well-established feedback control techniques is proposed. In [13], a QoS adaptation framework that smartly adjusts application QoS and performs admission control-based on the current and historical system status is proposed. In [14], a different method is used that focuses on the memory resource utilization in order to give the data some buffer and avoid using the operator selectivity to guide load-shedding. In [15], Nesime Tatbul proposed a region-quadtree-based division method of input rate. The answers satisfied a pre-defined error ε. But it will spend a lot of time to calculate the result of all the sub spaces.

As we know, various system resources including CPU, memory, especially the network bandwidth may become the bottleneck in DDSMS query processing. Most of current research mainly concentrates on the management of CPU cycles or memory utilities and assumes that the other resources are sufficient. However, it is not true in the real world. Sometimes almost all the resources, especially the network bandwidth, should be taken into account in order to balance the load and to increase the accuracy of queries. In this paper, a linear programming based load-shedding strategy, in which the network bandwidth and the node capacity are taken into consideration, is proposed.

III. LINEAR PROGRAMMING BASED LOAD-SHEDDING

A. Linear Programming

Linear programming, also named linear optimization, is a mathematical method for determining a way to achieve the best outcome (such as maximum profit or lowest cost) in a given mathematical model for some list of requirements represented as linear relationships. Usually, linear programming is an optimization technique of a linear objective function, subject to linear equality and linear inequality constraints. The objective function is a real-valued affine function defined on its feasible region. A linear programming algorithm can find the best value point in the feasible region if such value point exists. It can be applied to various fields of study, not only to business and economics, but also to some engineering problems.

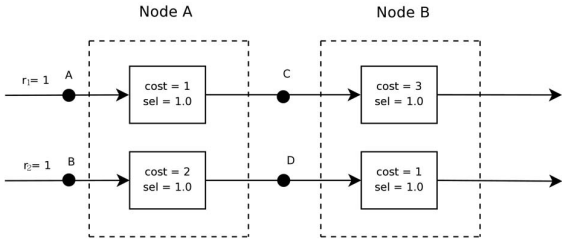

Figure 1. Simple query network without network constraint

Linear programs are problems that can be expressed in canonical form: maximize/minimize $c^T x$, which subjects to some constraints, for example, $Ax \geqslant b$ and $x \leqslant 0$. Where x represents the vector of variables, c and b are vectors of coefficients, A is a matrix of coefficients, and T is the matrix transpose. The c, b, and A are known value and x are to be determined. The expression $c^T x$ to be maximized or minimized is called the objective function.

B. Load-shedding Strategy without Network Constraint

Weighted throughput is adopted to metric the performance. Assumption that there are d output streams in a query network. A weighting factor p_j is given to each output stream. The output rate of stream is ro_j. The weighted throughput WT can be calculated by (1).

$$WT = \sum_{j=1}^{d} ro_j p_j \tag{1}$$

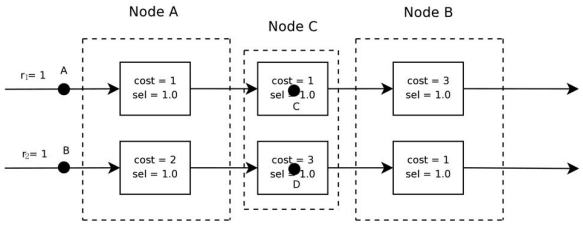

Figure 2. Simple query network with network constraint

TABLE I. PLAN OF LOAD-SHEDDING WITHOUT NETWORK CONSTRAINT

Plan	Input rate after dropping	Load of Node A	Throughput of Node A	Load of Node B	Throughput of Node B	Weighted throughput	Weighted throughput
1	1, 1	3	1/3, 1/3	4/3	1/4, 1/4	1/2	A, B overloaded
2	1/3, 1/3	1	1/3, 1/3	4/3	1/4, 1/4	1/2	B overloaded
3	1, 0	1	1, 0	3	1/3, 0	1/3	A optimal、B overloaded
4	0, 1/2	1	0, 1/2	1/2	0, 1/2	1/2	Not optimal
5	1/5, 2/5	1	1/5, 2/5	1	1/5, 2/5	3/5	Optimal

TABLE II. LOAD-SHEDDING WITH NETWORK CONSTRAINT

Input rate after dropping	Load of Node A	Throughput of Node A	Load of Node C	Throughput of Node C	Load of Node B	Throughput of Node B	Weighted throughput
1/4,1/4	3/4	1/4,1/4	1	1/4,1/4	1	1/4,1/4	1/2
1/5, 2/5	1	1/5, 2/5	7/5	1/7, 2/7	5/7	1/7, 2/7	3/7

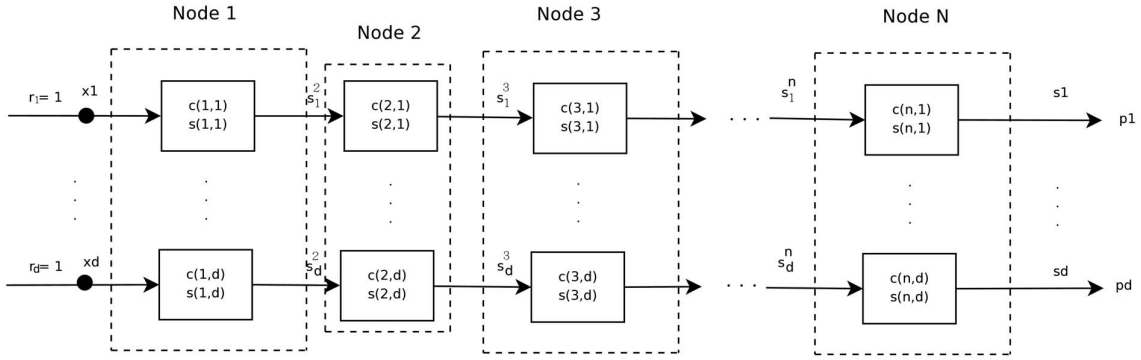

Figure 3. General simple query network with network constraint

Consider a simple query network with two queries distributed on two nodes separately in Fig. 1. Each small box represents a sub query with a certain cost and selectivity. Cost indicates the processing time of one tuple. Selectivity is the select ratio of tuples to be processed by this sub query. Here we choose 1.0 as the value of selectivity. In order to simplify the calculation, all the probabilities of output streams are set to the same value 1.0. Some dropping operator can be settled at A, B, C and D. In [15], Nesime Tatbul has proved that if the dropping operator is settled at A, B only, the query network will lead to the same result.

Table I shows various plans of the simple network shown in Fig. 1. From A's point, plan 2 is the best one. But from the global point, plan 5 is the best one. After dropping (4/5, 3/5) tuples, the load of node A is 1, and the throughput of node A is (1/5, 2/5). All tuples stream to node B leads to the full load of node B and (1/5, 2/5) throughput. So the weighted throughput of the whole simple network is 3/5.

C. Load-shedding Strategy with Network Constraint

Consider another simple query network with network constraint shown in Fig. 2. In this query network, the connection between node A and node B can be abstracted to a node C. Cost of each tuple determined by the length of tuple. Now we get another abstract simple network without network constraint. There are three nodes in this abstract simple network. With network constraint, the optimal plan (1/5, 2/5) for query network in Fig. 1 is not the best one now. For the limitation of the transfer drop some tuples, which will lower the whole weighted throughput to 3/7.

If the input rate is (1/4, 1/4), the node A, B and the network connection will not overloaded, the weighted throughput is 1/2, which is better than 3/7. These two plans are shown in table II.

D. Linear Programming on Query Network

For more nodes in a simple query network with network constraint is shown Fig. 3. Where odd nodes are truly nodes and even nodes are abstracted from network connection between its previous node and next node. Assumption that there are d streams which has a dropping operator d_i located at the beginning of the input of node 1. The selectivity of dropping operator di is xi. $c(i, j)$ is the cost of sub query j on node i. r_j is the input rate of stream j. p_j is the weight of output stream. C_i is the capacity of node i. s^i_j is the total selectivity of stream j from input of node 1 to node i. sj is the total selectivity of stream j from the input to the output. In even nodes, C_i is determined by the bandwidth of network and $c(i, j)$ is determined by the transfer time of one tuple from previous node to next node, and the selectivity is 1.0. Now we should maximize the weighted throughput WT in (2).

$$\text{Maximize} \quad WT = \sum_{j=1}^{d} r_j x_j s_j p_j$$

$$\text{Subjects to} \sum_{j=1}^{d} r_j x_j s^i_j c(i,j) \le C_i \qquad (2)$$

$$0 \le x_j \le 1$$

s_j and s^k_j can be calculated by (3) and (4) separately. s^l_j is set to 1.0 by (5).

$$s_j = \prod_{i=1}^{n} s(i,j), \quad 1 \le i \le n, 1 \le j \le d \tag{3}$$

$$s_j^k = \prod_{i=1}^{k-1} s(i,j), \quad 1 < k \le n, 1 \le j \le d \tag{4}$$

$$s_j^1 = 1.0, \qquad 1 \le j \le d \tag{5}$$

The distributed load-shedding problem can be defined as a linear programming problem. Our goal is to find x_j to make WT maximized according a determined input rate r_j.

E. Space Division

In [15], Nesime Tatbul proposed a region-quadtree-based division method of input rate. The answers satisfied a pre-defined error ε. But it will spend a lot of time to calculate the result of all the sub spaces. The time is increased very rapid with the increasing of the query streams. Experiments indicates that it will spend more than 1000s within error of 5% in a simple two nodes query network with network constraint with 8 input streams. It is not a ideal static load balancing method. We should decrease the items of sub spaces.

According to the importance factor of streams, we can divide the space in a variable method instead of quadtree division. First, find the full load input rate r_j' of stream j, which is the input rate of the maximal output rate without other streams. The importance factor k can be calculated by (6).

$$k_j = p_j / r_j' \tag{6}$$

We can discrete r_j' which is the normalization of k_j. to 2n based on the lowest r_j'. For example, in a simple query network with 4 streams has r_j' series: 0.067, 0.133, 0.266 and 0.534. We can discrete them to 20, 21, 22 and 23. So, the division of the No. 4 dimension is 2 times faster than the No. 3 dimension, 4 times faster than the No. 2 dimension, and 8 times faster than No. 1 dimension. It will decrease the count of sub space efficiently.

Experiments indicate that the static load balancing plan of all the sub space can be calculated very faster than classic region-quadtree-based division.

IV. CONCLUSIONS

Previous work on this area mainly takes only one factor into account, such as CPU or memory utilization etc.. But it does not satisfy the reality in which several coupled factors should be concentrated, especially with the network constraint factor. In this paper, a linear programming based load-shedding in load management of distributed data stream processing system is proposed. We define the simple query network with network constraint problem as linear programming problem. We proposed a input rate space division method to decrease the count of sub spaces. It will save time to calculate the whole static scheduling plan. Future work should be focused on the dynamic load balancing with linear programming to get more efficient and effective, and to decrease the loss of accuracy of queries.

REFERENCES

[1] Aurora Site. http://www.cs.brown.edu/research/aurora/

[2] Medusa. http://nms.csail.mit.edu/projects/medusa/

[3] STREAM Website. http://www-db.stanford.edu/stream/

[4] TelegraphCQ Project. http://telegraph.cs.berkeley.edu/

[5] Borealis. http://www.cs.brown.edu/research/db/borealis/

[6] Argus website. http://www.db.pku.edu.cn/argus/

[7] M. Cherniack, H. Balakrishnan, M. Balazinska, D. Carney, U. Cetintemel, Y. Xing, S. Zdonik. Scalable Distributed Stream Processing [C]. In proceedings of the First Biennial Conference on Innovative Database Systems (CIDR'03), Asilomar, CA, January 2003: 257-268.

[8] Abhinandan Das, Johannes Gehrke, Mirek Riedewald. Approximate Join Processing Over Data Streams [C]. In Proc. of the 2003 ACM SIGMOD Intl. Conf. on Management of Data. 2003: 40-51.

[9] Brian Babcock, Mayur Datar, Rajeev Motwani. Load Shedding for Aggregation Queries over Data Streams [C]. Proceedings. 20th International Conference on Data Engineering, 30 March-2 April 2004: 350-361.

[10] F. Reiss and J. M. Hellerstein. Data Triage: An Adaptive Architecture for Load Shedding in TelegraphCQ [C]. In Pro ceedings of ICDE, pages 155-156, April 2005.

[11] Y. Chi, H. Wang, and P. S. Yu. Load Star: Load Shedding in Data Stream Mining [C]. In Procs. of the 31st VLDB Conf., pages 1302-1305, August 2005.

[12] Yi-Cheng Tu and Sunil Prabhakar. Control-Based Load Shedding in Data Stream Management Systems [C]. In Procs. of DEXA 2005, p 746-755, Aug 22-26 2005.

[13] Yi-Cheng Tu, Yuni Xia, and Sunil Prabhakar. Quality of Service Adaptation in Data Stream Management Systems: A Control-Based Approach [C]. In Proceedings of 30th International Conference on Very Large DataBases (VLDB'04), Toronto, Canada, August 2004.

[14] Hu, Zijing, Li, Hongyan, Qiu, Baojun, et al. Using control theory to guide load shedding in medical data stream management system [C]. Source: Lecture Notes in Computer Science (including subseries Lecture Notes in Artificial Intelligence and Lecture Notes in Bioinformatics), v 3818 LNCS, Advances in Computer Science - ASIAN 2005: 10th Asian Computing Science Conference, Proceedings, 2005, p 236-248, Dec 7-9 2005.

[15] Nesime Tatbul, U Cetintemel, Stan Zdonik. Staying FIT: Efficient Load Shedding Techniques for Distributed Stream Processing[C]. VLDB 2007, Vienna, Austria. Septemble 2007. 232~243.

Numerical Simulation and Experiment Study on Internal Flow Field in Impeller of Torque Converter

Ying Yu,Qingliu Yang,Gang Wang

School of Automobile and Traffic Engineering
Jiangsu University, Zhenjiang,212013,China

Email:yying@ujs.edu.cn;yangqingliu0378@126.com;gangwanglctu@126.com

***Abstract*—The internal flow field in impeller of a torque converter will have great effect on the working characteristics of the torque converter. The numerical model of internal flow field in impeller of the torque converter was established by using the hexahedron grids based on the turbulent model k~ ε and SIMPLE algorithm. To solve the interaction between the various stages with different speeds, the mixing plane theory was used in the calculation. In order to get the distribution of velocity and pressure of the flow passage, the torque converter 280 was modeled in detail and the internal field was analyzed by using the Fluent software. The distribution rules of velocity and pressure at inlet, outlet of the impeller, the flow field pattern were analyzed. The external performance of the impeller was calculated. To verify the accuracy of the numerical simulation, the results were validated experimentally. The computed results showed good agreement with the experimental results, and the characteristics of the torque converter were predicted.**

Key words: Torque converter; Impeller; Internal flow field; Numerical simulation

I. INTRODUCTION

Torque converter is an important component of the vehicle automatic transmission system. It transfers power, changes torque through the conversion of mechanical energy between hydraulic energy, and can make vehicle start and change gear smoothly. The automobile with torque converter could affect fuel economy in large extent, so the study on internal flow field in the impeller will be very important [1]. Based on mixing plane theory, to calculate and analyze the internal flow field in the impeller using CFD, the calculation model of the flow field in the impeller is established.

II. ESTABLISHING MODEL AND GRID PARTITION

A impeller was modeled using the PRO / E software, and a three-dimensional model of the flow passage was made from the impeller model. Considering the symmetry circulation, only one flow passage was analyzed. After the model was completed, the grids of flow passage were partitioned by using GAMBIT. In order to improve the calculation accuracy, hexahedral grid was used. Figure 1 is the ultimate grid model, and the total grid number is 179066.

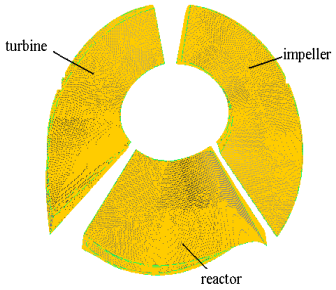

Fig 1 Grids of single flow passage of the converter

III. NUMERICAL CALCULATION METHOD

A. Control Equation

The basic control equation used in analyzing fluid with finite volume method mainly includes the momentum equation and continuity equation [2]. In the relative coordinate system,

Momentum equation is expressed as:

$$\frac{dW}{dt} + 2\omega \times W + \omega \times (\omega \times r) = F - \frac{1}{\rho}\nabla p + \frac{1}{\rho}\mu \nabla^2 W$$

Continuity equation is expressed as: div W = 0

Wherein W is relative velocity, ω is rotation speed, F is volume force, P is pressure, r is fluid particle position vector, u is the kinematic viscosity, ∇ is Hamilton operator, ∇^2 is Laplasse operators.

B. Hypothesis ofAnalysis

1) All the components in torque converter are absolute rigid body.

2) This paper only studies the distribution of velocity and pressure field, regardless of the effect of temperature.

3) Ignore the leakage of no blade area between two blades, working oil from upstream completely equivalently flow to the downstream impeller.

4) Relative to each rotating reference frame, internal flow field is stable.

5) Under the same operating conditions, the same impeller has the same flow field characteristics [3].

C. Boundary Conditions

There are three different kinds of boundary surface in calculation region: the blade surface, core surface and

978-0-7695-4818-0/12 $26.00 © 2012 IEEE
DOI 10.1109/DCABES.2012.33

shell surface, inlet and outlet surface, split surface of the flow passage. Blade surface, core and shell surface are set to no gliding boundary conditions; split surface of the flow passage is set to periodic boundary conditions; to compute each component of different rotational speed together, mixed plane model is adopted at inlet and outlet surface [4]. As shown in Figure 2.

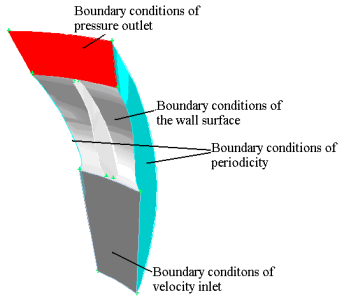

Fig 2 Setting of boundary conditions of the impeller

D. *Mixed Plane Theory*

The inlet boundary conditions of flow passage of the impeller is set to the velocity boundary conditions, and outlet boundary conditions is set to the pressure boundary conditions. Uniform distribution of pressure and velocity are respectively given at inlet and outlet surface. In circular calculation of the three impellers, the average of outlet velocity of the impeller of upstream is served as the inlet velocity boundary conditions of the impeller of downstream, inlet pressure of the impeller of downstream as outlet pressure boundary conditions of the impeller of upstream [5], as shown in Figure 3.

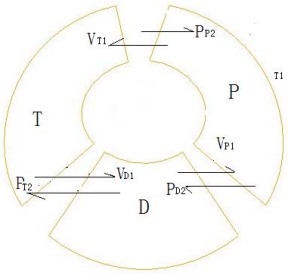

Fig 3 Mixed plane schemes

E. *Selection of Calculation Model and Algorithm*

1) The separated solver is selected according to the flow conditions;

2) Standard model k~ ε is adopted for turbulence model;

3) The SIMPLE algorithm is adopted for velocity pressure coupling algorithm;

4) The discrete format: beginning with the first order upwind scheme, then turn to the second order upwind scheme after initial iteration;

5) When the residual error of control equation is less than 10-3, the results converge.

IV. CALCULATION RESULTS AND ANALYSIS

To get the flow field characteristics in the impeller, the velocity and pressure field of three kinds of typical operating conditions in the inlet and outlet of the impeller are mainly analyzed, according to the calculation results of CFD [6, 7].

A. *Velocity and Pressure Distribution in the Inlet Surface of the impeller*

Figure 4 and Figure 5 are the velocity and pressure distribution in the inlet surface of the impeller.

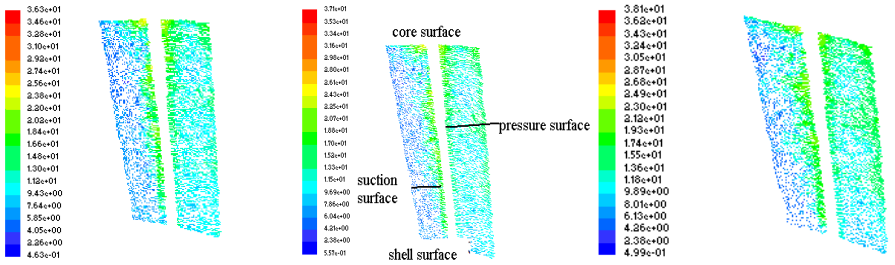

(1) i=0.0 (2) i=0.4 (3) i=0.8

Figure 4 Vector graph of velocity in the inlet of the impeller

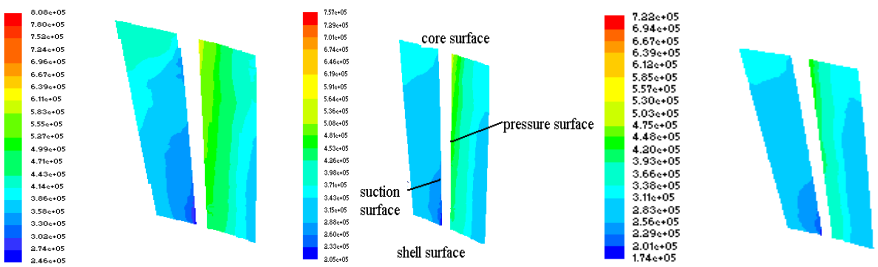

(1) i=0.0 (2) i=0.4 (3) i=0.8

Figure 5 Pressure contour in the inlet of the impeller

As shown in figure 4, due to the reactor static, the flow direction of the impeller at the entrance changes very little under different operating conditions, so the velocity distribution in the inlet surface is basically the same under different operating conditions. The velocity in the pressure surface is low, and high in the suction surface. The velocity decreases gradually from core to shell surface. As the speed ratio increases, the flow of torque converter decreases and the velocity component of vertical flow decreases, so the velocity in the inlet surface under operating conditions of high speed ratio should be less than the operating conditions of low speed ratio; As shown in figure 5, under three kinds of operating conditions, pressure distribution in the inlet surface of the impeller is basically the same, where is proportional distribution along the radial direction from core to shell surface and the pressure gradually increases. Pressure is high in the pressure surface and low in the suction surface; the pressure increases gradually from core to shell surface, the minimum pressure is in the junction of pressure surface and shell surface.

B. Velocity and Pressure Distribution in the Outlet Surface of the impeller.

Figure 6 and Figure 7 are the velocity and pressure distribution in the outlet surface of the impeller.

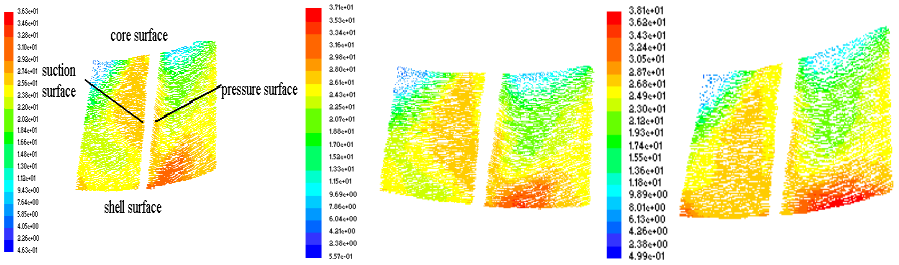

(1) i=0.0 (2) i=0.4 (3) i=0.8

Figure 6 Vector graph of velocity in the outlet of the impeller

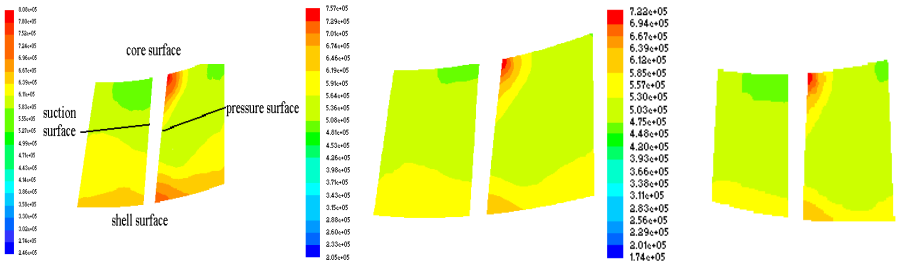

(1) i=0.0 (2) i=0.4 (3) i=0.8

Figure 7 Pressure contour in the outlet of the impeller

As shown in Figure 6, when the speed ratio is at 0, 0.4 and 0.8, the velocity distribution in the outlet surface of the impeller is uneven, high speed region is in the shell surface near the pressure surface and low velocity region in the core surface near the suction surface, reverse flow appears in the core surface. As the speed ratio increases, except for reverse flow region, high speed region moves to the angle region of pressure surface and shell surface, low-speed wake turbulence region appears near the angle region of pressure surface and core surface. Jet flow region closes to the pressure surface, and a clear circulation does not appear in the secondary flow; As shown in figure 7, the pressure distribution of the outlet surface assumes the characteristics of proportional distribution along the radial, this is mainly because the outlet surface is almost perpendicular to the axial, the radius of shell surface is larger than the core surface, static pressure is mainly affected by the influence of the centrifugal force. With the speed ratio rising, static pressure distribution tends to be uniform gradually, the maximum pressure in the outlet surface of the pump decreases gradually.

C. Analysis of Secondary Flow and Reverse Flow

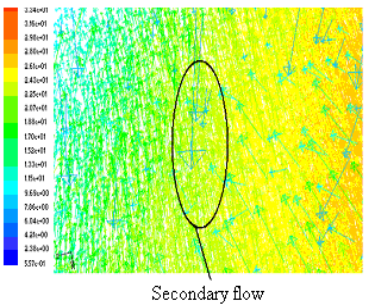

Figure 8 Secondary flow in the center of flow passage

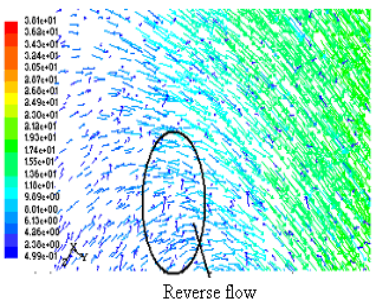

Figure 9 Reverse flow in the junction between core and pressure surface

The secondary flow appears in the impeller in large extent, which will affect mainstream region, increase the flow loss [8,9], this is one of the main causes that affect the efficiency. Besides, the reverse flow phenomenon occurs in the pressure surface from the shell to the core near the entrance, as shown in Figure 9. The main causes of reverse flow are that: after the liquid flow from the reactor outlet, the flow region increases, the flow of this region can be seen as the jet. Low velocity region and even reverse flow will appear at the out boundary of the jet [10], the appearance of reverse flow also increases the energy loss.

D. Performance Prediction and Analysis

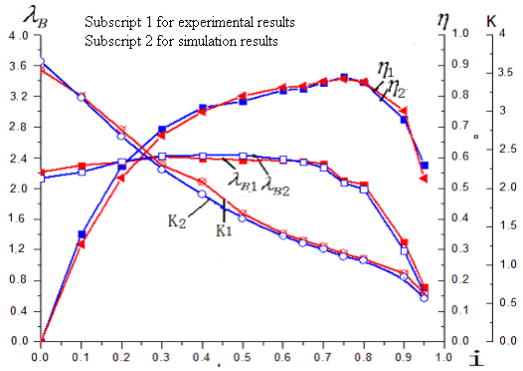

Figure10 the comparison of flow calculation and experimental results

In order to verify the accuracy of numerical calculation, the torque converter 280 is researched, and the simulation results and experimental results are compared, as shown in Figure 10. As we can see, the variation trend of torque ratio K, torque coefficient B and the efficiency η consists with experimental results. The relative error of torque ratio is less than 4%, the error reaches to the minimum when the speed ratio is about 0.6; the relative error of torque coefficient is less than 5%, the relative error of efficiency η is less than 1.4%. The causes of error are mainly because the flow passage is simplified to be some degree in the establishment of flow passage, and there are some differences in the actual flow conditions and the mixing plane theory. Overall, the results of numerical calculation are accurate.

V. CONCLUSION

(1) There is reverse flow phenomenon in the pressure surface at the inlet of the pump, and stalling appears in the intersection of pressure surface and shell surface. Tangential flow phenomenon is clear in the inlet surface.

(2)The velocity distribution in the outlet surface of the pump is uneven, high speed region is in the shell surface near the pressure surface and low speed region in the core surface near the suction surface. Reverse flow appears in the core surface.

(3) The secondary flow appears in the flow passage of the pump in large extent, the maximum intensity of the secondary flow is at the starting time, with the speed ratio increasing, the secondary flow gradually weakens. The velocity gradient between the pressure surface and suction surface is the main reason for secondary flow.

(4) CFD technology is used to the simulation analysis of the flow field of the torque converter, which can reduce the development costs, shorten the research cycle and then improve design and manufacture process. It has high accuracy， reliability and can replace the part of the experimental work of converter.

ACKNOWLEDGEMENT

This work was supported by The General Armaments Department Science & Technology Priority in Advance Research Fund (2209).

REFERENCES

[1] Wenxing Ma. Hydraulic transmission theory and design [M] Beijing: Chemical Industry Press, 2004

[2] Xiaokang Xin. Turbomachine three dimensional flow and quasi-orthogonal surface method [M].Shanghai: Fudan University press,1988

[3] Jinhai Cao & Wenxing Ma. A Finite Element Method for Flow Field Computation in a Torque Converter [J] Automotive Engineering, 1993,(5):291-297

[4] Xuexun Guo. Numerical Calculation of Flow Field in a Hydraulic Torque Converter with Pressure Correction. [J] Automotive Engineering,1996,(2):89-93

[5] SHIN Sehyun, CHANG Hyukjae, ATHAVALE Mahesh.Numerical investigation of the pump flow in an automotive torque converter[C]// SAE Paper 1999-01-1056.

[6] Marco Cigarini, Sreenadh Jonnavithula .Fluid Flow in an Automotive Torque Converter: Comparison of Numerical Results with Measurements.SAE950673, 1995:61~67

[7] Hua TIAN, Anlin Ge, Wenxing Ma. Numerical analysis on internal flow field in pump wheel of a torque converter[J] Journal of Jilin University of Technology(Natural Science Edition), 2004

[8] KLAUS Brun, RONALD D Flack. The flow field inside an automotive torque converter: laser velocimeter measurements[C]// SAE 960721.

[9] BY R R, KUNZ R. LAKSHMINARAYANA B. Navier-stokes analysis of the pump flow field of an automotive torque converter[J]. ASME, 1995,117:116-122.

[10] Peng Yan Guangqiang Wu & Shuo Xie. Numerical Analysis on Pump Flow Field in a Torque Converter. Automotive Engineering, 2004,(2):183-186

AN INTEGRATED HYBRID PETRI NET AND GA BASED APPROACH FOR SCHEDULING OF MIXED BATCH/CONTINUOUS PROCESSES

LIAO WEI-ZHI
College of Computer and Information Engineering
Guangxi Teachers Education University
Nanning, China
e-mail: weizhiliao2002@yahoo.com.cn

LI WEN-JING
Guangxi Experiment Centre of Science and Technology
Guangxi University
Nanning, China
e-mail: liwjgood@126.com

***Abstract*—This paper presents an efficient way to maximize the throughput of mixed batch/continuous process based on integrated hybrid time Petri nets and genetic algorithm. The scheduling problem of process is mapped as the solution of the optimal regional state sequence in HTPNs. The transition firing decision model is developed according to the enabling and firing rules, and a genetic algorithm of scheduling of mixed batch/continuous process is presented. The optimal feasible scheduling policy can be efficiently obtained by the proposed algorithm. In addition, algorithm is illustrated through case study.**

Keywords- batch process;Hybrid Petri nets; genetic algorithm; scheduling

I. INTRODUCTION

Mixed batch/continuous processes are one of the important processing modes in the process industries. The behaviors of this kind of process can no longer be considered as either continuous or discrete, and pose therefore a difficult problem with regards to formulation and solution algorithm. The sugar milling system is a typical system. The smallest milling plant consists of a batch pan system, followed by a communal, limited storage facility before the remainder of the downstream process, which is generally considered to operate continuously. Furthermore, although the batch units have

a fixed quantity to process, each batch may take a variable length of time to process, which is referred to as having variable cycle time. Constraints are specified by the limits on the cycle time of the pans, the capacity of the storage facility, as well as possible flow rate ranges through the continuous units. Variable cycle time and changeable flow rate make the formulation and solution algorithm extremely difficult [1].

Petri nets, as a graphical and mathematical tool, provide a powerful and uniform environment for modeling, analysis, and design of discrete event systems [2]. One of the major advantages of using Petri nets is that the same methodology can be used for the modeling, qualitative and quantitative analysis, supervisory and coordination control, planning and scheduling, and system design in some production system.

Recently, Timed Petri net-based approach have been examined to formulate complicated operations and to solve scheduling problems for multipurpose/multiproduct batch plants [3,4]. This approach has also been extended to deal with the scheduling problems of bath plants with variable batch sizes [5]. With the introduction of continuous places and transitions, continuous Petri net (CPNs) and hybrid Petri nets were defined in [6][7]. The continuous places can contain tokens of a positive real number, and continuous transition can be continuously fired at some speed. Hence, the continuous part can model systems with continuous flows and the discrete part models the logic functions. A similar approach, hybrid flow net, was presented in [8]. This modeling tool presents a continuous flow net interacting with a Petri net according to a control interaction. Unfortunately, timed Petri net, hybrid Petri net and hybrid flow net can not model a mixed batch/continuous process. Gu. have proposed a model called hybrid time Petri nets (HTPNs) to model mixed batch/continuous process in [9]. Through the analysis of HTPNs model, the feasible schedule for mixed batch/continuous process can be found efficiently. However, the behavior analysis algorithm can only find a feasible schedule but an optimization for scheduling.

The aim of this paper is to develop an efficient way to maximize the throughput of mixed batch/continuous process based on hybrid time Petri nets. Firstly, the mathematic model for maximizing throughput is presented. Secondly, transition firing decision model is developed according to the enabling and firing rules. Thirdly, a genetic algorithm of scheduling of mixed batch/continuous process is presented. Finally, the proposed algorithm is illustrated through case studies.

II. HYBRID TIME PETRI NETS[9]

Definition 2.1 A Hybrid Time Petri Nets (HTPNs) is a structure $N=(P, T, F, W, S_t, S_f)$, where

1) The set of places $P= P_d \cup P_c$ is partitioned into a set of discrete places P_d (represented as circles) and a set of continuous places P_d (represented as double circles).

2) The set of transitions $T= T_d \cup T_c$ is partitioned into a set of discrete transitions T_d (represented as black bar)and a set of continuous places T_c (represented as white boxes).

Supported by Guangxi Experiment Centre of Science and Technology(LGZXKF201108)

978-0-7695-4818-0/12 $26.00 © 2012 IEEE
DOI 10.1109/DCABES.2012.49

3) $F \subseteq (P \times T) \cup (T \times P)$ is a relation function that defines arcs between places and transitions.

4) W: $(P \times T_d) \cup (T_d \times P) \rightarrow Z^+$ (positive integer) is a weight function.

5) The function S_t: $T_T \rightarrow (R^+ \cup \{0\}) \times (R^+ \cup \{0\})$ specifies the time stamp to time discrete transitions.

6) The function S_f: $T_c \rightarrow (R^+ \cup \{0\}) \times (R^+ \cup \{0\})$ specifies the flow rate ranges stamp to continuous transitions. For any continuous transition $t_i \in T_c$, we let $S_f(t_i) = (V_i^{min}, V_i^{max})$, with $V_i^{min} \le V_i^{max}$. Here V_i^{min} represents the minimal flow rate and V_i^{max} represents the maximal flow rate.

The enabling of a discrete and continuous transition both depends on the marking of all its places, both discrete and continuous.

*Definition*2.2 Let <*N*, m> be a GHPN system. A discrete transition *t* is enabled at m if all $p_i \in {}^\bullet t$, $m_i \ge W(p_i, t)$.

For any enabled discrete transition *t*, if *t* fires, $\forall p_i \in ({}^\bullet t - t^\bullet)$, $m_i' = m_i - W(p_i, t)$; $\forall p_i \in (t^\bullet - {}^\bullet t)$, $m_i' = m_i + W(p_i, t)$.

*Definition*2.3 Let <*N*, m> be a GHPN system. A continuous transition *t* is enabled at m if all $p_i \in {}^\bullet t \cap P_d$, $m_i \ge W(p_i, t)$, and all $p_i \in {}^\bullet t \cap P_c$, $m_i > 0$.

For any enabled continuous transition *t*, if *t* fires at instantaneous flow rate *v*, $\forall p_i \in ({}^\bullet t - t^\bullet) \cap P_d$, $m_i' = m_i - W(p_i, t)$, $\forall p_i \in (t^\bullet - {}^\bullet t) \cap P_d$, $m_i' = m_i + W(p_i, t)$; $\forall p_i \in ({}^\bullet t - t^\bullet) \cap P_c$, $m_i' = m_i - v \bullet \Delta$, $\forall p_i \in (t^\bullet - {}^\bullet t) \cap P_c$, $m_i' = m_i + v \bullet \Delta$, where Δ is a time difference and $v \in [V^{min}, V^{max}]$.

III. FORMULATION VIA HTPN[9]

A sugar milling system is a mixed batch/continuous process plant. It consists of a batch pan system, followed by a communal, limited storage facility before the remainder of the downstream process, which is generally considered to operate continuously. Furthermore, although the batch units have a fixed quantity to process, each batch may take a variable length of time or a deterministic/exponentially distributed time to process. Constraints of the physical system are specified by bounds on the time of the pans, the limited storage facility as well as possible flow rates through the continuous units. A smaller system having the important characteristics of the sugar milling process is shown in Fig.1, where the storage tank receives discrete inputs from two batch units, and sends continuous flow to the continuous process.

Essentially, the mixed batch/continuous processes consists of three parts: a discrete batch stage, an intermediate storage facility and a continuous stage. The key elements are batch operations with variable cycle time and storage tank with discrete batch and continuous variable flow rate. The global HTPNs model can be developed through formulating each part and integrating them using the constructing algorithm which was proposed in [9].

The HTPN model of a sugar milling system is shown in *Fig.2.*

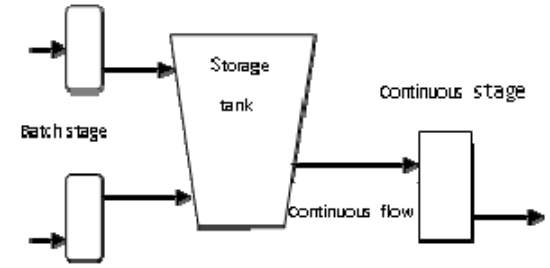

Figure 1 A sugar milling system

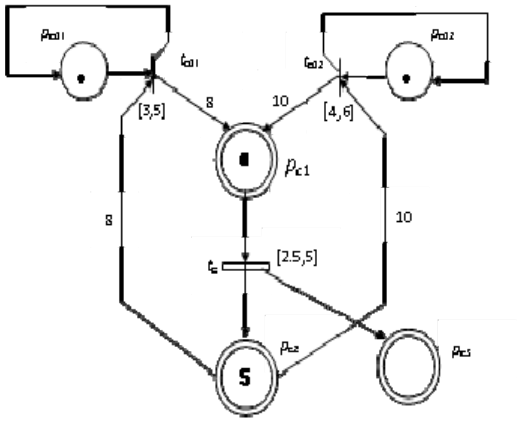

Figure 2. HTPN model for a sugar milling system

IV. SCHEDULING OF MIXED BATCH/CONTINUOUS PROCESSES

A. Mathematic model for maximizing the throughput

Once a mixed batch/continuous process is modeled by HTPNs, its dynamical behavior evolution is totally described by markings and their related parameters of this model. Due to continuous firing flow and time stamp, there are actually infinite reachable makings in a GHPNs. For scheduling purposes, this renders it impossible to use the reachability tree technique as in traditional Petri nets. Therefore, the concept of regional states is introduced. In this framework, the scheduling of mixed batch/continuous processes is proposed by genetic algorithm.

The following notations are used through the paper:

τ_k : the initial time of the regional state k+1;

$m(p_{ci\text{-}j}, \tau_k)$: the marking of the place $p_{ci\text{-}j}$ at time τ_k ;

$EE(t_{cdi\text{-}j}, k+1)$: the earliest enabling time of the transition $t_{cdi\text{-}j}$ in the regional state k+1;

$LE(t_{cdi\text{-}j}, k+1)$: the latest enabling time of the transition $t_{cdi\text{-}j}$ in the regional state $k+1$;

$EF(t_{cdi\text{-}j}, k+1)$: the earliest firing time of the transition $t_{cdi\text{-}j}$ in the regional state $k+1$;

$LF(t_{cdi\text{-}j},k+1)$: the latest firing time of the transition $t_{cdi\text{-}j}$ in the regional state $k+1$;

$[l_{cdi\text{-}j}^{min}, l_{cdi\text{-}j}^{max}]$: the time stamp of the transition $t_{cdi\text{-}j}$;

firing-time$(t_{cdi\text{-}j}, k+1)$: the firing time of the transition $t_{cdi\text{-}j}$ in the regional state $k+1$;

$token_{arr}$ $(p_{cdi\text{-}j})$: the time of the marking arriving at the place $p_{cdi\text{-}j}$, at initial time $token_{arr}(p_{cdi\text{-}j})=0$;

$v(t_{ci},k+1)$: the firing speed of the continuous transition t_{ci} in the regional state $k+1$;

*Definition*4.1 A regional state for HTPNs is defined by $rs=(\boldsymbol{m}^d(\tau_{i-1}), \boldsymbol{m}^c(\tau_{i-1}),v_i,[\tau_{i-1}, \tau_i])$, where $\boldsymbol{m}^d(\tau_{i-1})$ is a partial marking vector of discrete places at time τ_{i-1}, $\boldsymbol{m}^c(\tau_{i-1})$ a partial marking vector of continuous places at time τ_{i-1}, v_i a flow rate of continuous transitions and $[\tau_{i-1}, \tau_i]$ a time interval. They satisfy: during $[\tau_{i-1}, \tau_i]$, the marking of discrete place remains unchanged; and during $[\tau_{i-1}, \tau_i]$, the flow rates of continuous transitions stay constant.

*Definition*4.2 A sequence of regional state $(\boldsymbol{m}^d(\tau_0), \boldsymbol{m}^c(\tau_0),v_1,[\tau_0, \tau_1]) \rightarrow (\boldsymbol{m}^d(\tau_1), \boldsymbol{m}^c(\tau_1),v_2,[\tau_1, \tau_2]) \rightarrow \cdots \rightarrow (\boldsymbol{m}^d(\tau_{k-1}), \boldsymbol{m}^c(\tau_{k-1}), v_{k-1},[\tau_{k-1}, \tau_k])$ is called a regional state sequence if only if for any two regional state $(\boldsymbol{m}^d(\tau_{i-1}), \boldsymbol{m}^c(\tau_{i-1}), v_i,[\tau_{i-1}, \tau_i])$ and $(\boldsymbol{m}^d(\tau_i), \boldsymbol{m}^c(\tau_i), v_{i+1},[\tau_i, \tau_{i+1}])$, the regional state $(\boldsymbol{m}^d(\tau_i), \boldsymbol{m}^c(\tau_i), v_{i+1},[\tau_i, \tau_{i+1}])$ is deduced from the regional state $(\boldsymbol{m}^d(\tau_{i-1}), \boldsymbol{m}^c(\tau_{i-1}), v_i,[\tau_{i-1}, \tau_i])$ since a discrete transition is fired at time τ_i, where $1 \leqslant i \leqslant k-1$.

*Definition*4.3 A regional state $rs=(\boldsymbol{m}^d(\tau_{i-1}), \boldsymbol{m}^c(\tau_{i-1}),v_i,[\tau_{i-1}, \tau_i])$ is called a feasible regional state in process if there does not exits any discrete transition t_{cdj} in process such that *fiingr-time*$(t_{cdj}, i) \in (\tau_{i-1}, \tau_i)$.

*Definition*4.4 A regional state sequence $rsq=(\boldsymbol{m}^d(\tau_0), \boldsymbol{m}^c(\tau_0),v_1,[\tau_0, \tau_1]) \rightarrow (\boldsymbol{m}^d(\tau_1), \boldsymbol{m}^c(\tau_1),v_2,[\tau_1, \tau_2]) \rightarrow \cdots \rightarrow (\boldsymbol{m}^d(\tau_{k-1}), \boldsymbol{m}^c(\tau_{k-1}), v_{k-1},[\tau_{k-1}, \tau_k])$ in process is called a feasible scheduling within time horizon [0,TH] if the following conditions are satisfied:

(1) $\tau_k \geqslant TH$.

(2) Every regional state in *rsq* is a feasible regional state.

Let *RSQT* is the set of feasible scheduling policy for mixed batch/continuous process within a specified time horizon [0,TH], the mathematic model for maximizing the throughput is

$$J = \max_{rsq \in RSQT} \{ \sum_{i=1}^{k-1} v_i \cdot (\tau_i - \tau_{i-1}) + v_i \cdot (TH - \tau_{k-1}) \} \quad (1)$$

Where v_i is the flow rate in the *ith* regional state.

It is difficult to find the solution with conventional optimization and search procedures according to (1). Since genetic algorithm can search a solution from population of points and only use objective function information, it is an efficient way to solve the optimization control of complex system. Thus, we design a genetic algorithm for the optimal average flow of machine. We will discuss the initialization process, evaluation fitness, selection, crossover and mutation operations in turn.

B. GA of mixed batch/continuous processes

In this section, we present the transition firing decision model which is used to determine the feasible regional state firstly. According to the enabling and firing rules, we have the following properties.

*property*4.1 When $m(p_{ci\text{-}2}, \tau_k) \geqslant W(p_{ci\text{-}2}, t_{cdi\text{-}j})$, we have

(a) $$EE(t_{cdi\text{-}j}, k+1)= token_{arr}(p_{cdi\text{-}j})+ l_{cdi-j}^{min} \quad (2)$$

$$LE(t_{cdi\text{-}j}, k+1)= token_{arr}(p_{cdi\text{-}j})+ l_{cdi-j}^{max} \quad (3)$$

(b) If $LE(t_{cdi\text{-}j}, k+1) \leqslant \tau_k$, then the transition $t_{cdi\text{-}j}$ can not fire.

(c) If $\tau_k < LE(t_{cdi\text{-}j}, k+1)$, then

$$EF(t_{cdi\text{-}j}, k+1)= EE(t_{cdi\text{-}j}, k+1) \quad (4)$$

$$LF(t_{cdi\text{-}j}, k+1)= LE(t_{cdi\text{-}j}, k+1) \quad (5)$$

$$v(t_{ci}, k+1) \in [V_i^{min}, V_i^{max}] \quad (6)$$

(d) If $EE(t_{cdi\text{-}j}, k+1) \leqslant \tau_k < LE(t_{cdi\text{-}j}, k+1)$, then

$$EF(t_{cdi\text{-}j}, k+1)= \tau_k + \xi \quad (7)$$

$$LF(t_{cdi\text{-}j}, k+1)= LE(t_{cdi\text{-}j}, k+1) \quad (8)$$

$$v(t_{ci}, k+1) \in [V_i^{min}, V_i^{max}] \quad (9)$$

where $\xi > 0$, $i,j=1,2$.

*Property*4.2 When $m(p_{ci\text{-}2}, \tau_k) < W(p_{ci\text{-}2}, t_{cdi\text{-}j}), V_1 \leqslant V_i^{min}$ or $V_i^{min} < V_1 \leqslant V_i^{max}$, we have

(a) $$EE(t_{cdi\text{-}j}, k+1)= token_{arr}(p_{cdi\text{-}j})+ l_{cdi-j}^{min} \quad (10)$$

$$LE(t_{cdi\text{-}j}, k+1)= token_{arr}(p_{cdi\text{-}j})+ l_{cdi-j}^{max} \quad (11)$$

(b) If $LE(t_{cdi\text{-}j}, k+1) \leqslant \tau_k$, then the transition $t_{cdi\text{-}j}$ can not fire.

(c) If $\tau_k < LE(t_{cdi\text{-}j}, k+1)$, then

$$EF(t_{cdi\text{-}j}, k+1)= EE(t_{cdi\text{-}j}, k+1) \quad (12)$$

$$LF(t_{cdi\text{-}j}, k+1)= LE(t_{cdi\text{-}j}, k+1) \quad (13)$$

$$v(t_{ci}, k+1) \in \begin{cases} [V_i^{\min}, V_i^{\max}] & V_1 \leq V_i^{\min} \\ [V_1, V_i^{\max}] & V_i^{\min} < V_1 \leq V_i^{\max} \end{cases} \quad (14)$$

(d) If $EE(t_{cdi\text{-}j}, k+1) \leqslant \tau_k < LE(t_{cdi\text{-}j}, k+1)$, then

$$EF(t_{cdi\text{-}j}, k+1)= \tau_k + \xi \quad (15)$$

$$LF(t_{cdi\text{-}j}, k+1)= LE(t_{cdi\text{-}j}, k+1) \quad (16)$$

$$v(t_{ci}, k+1) \in \begin{cases} [V_i^{\min}, V_i^{\max}] & V_1 \leq V_i^{\min} \\ [V_1, V_i^{\max}] & V_i^{\min} < V_1 \leq V_i^{\max} \end{cases} \quad (17)$$

where $\xi > 0$, $i,j=1,2$, $V_1 = \dfrac{W(p_{ci-2}, t_{cdi-j}) - m(p_{ci-2}, \tau_k)}{l_{cdi-j}^{min}}$.

*Property*4.3 When $m(p_{ci\text{-}2}, \tau_k) < W(p_{ci\text{-}2}, t_{cdi\text{-}j})$, $V_i^{min} \leqslant V_2$ and $V_1 \leqslant V_i^{max}$, we have

(a) $$EE(t_{cdi\text{-}j}, k+1)= token_{arr}(p_{cdi\text{-}j})+\eta \quad (18)$$

$$LE(t_{cdi\text{-}j}, k+1)= token_{arr}(p_{cdi\text{-}j})+ l_{cdi-j}^{max} \quad (19)$$

Where $\eta=\frac{W(p_{ci-2},t_{cdi}-j)-m(p_{ci-2},\tau_k)}{v(t_{cdi-j},k+1)}$

(b) If $LE(t_{cdi\text{-}j}, k+1)\leqslant \tau_k$, then the transition $t_{cdi\text{-}j}$ can not fire.

(c) If $\tau_k < LE(t_{cdi\text{-}j}, k+1)$, then

$$EF(t_{cdi\text{-}j}, k+1)= EE(t_{cdi\text{-}j}, k+1) \quad (20)$$

$$LF(t_{cdi\text{-}j}, k+1)= LE(t_{cdi\text{-}j}, k+1) \quad (21)$$

$$v(t_{ci}, k+1)\in [V_1 ,V_2] \quad (22)$$

(d) If $EE(t_{cdi\text{-}j}, k+1)\leqslant \tau_k < LE(t_{cdi\text{-}j}, k+1)$, then

$$EF(t_{cdi\text{-}j}, k+1)= \tau_k + \xi \quad (23)$$

$$LF(t_{cdi\text{-}j}, k+1)= LE(t_{cdi\text{-}j}, k+1) \quad (24)$$

$$v(t_{ci}, k+1)\in [V_1 ,V_2] \quad (25)$$

where $\xi >0$, i,j=1,2, $V_1=\frac{W(p_{ci-2},t_{cdi-j})-m(p_{ci-2},\tau_k)}{l^{min}_{cdi-j}}$, $V_2=\frac{W(p_{ci-2},t_{cdi-j})-m(p_{ci-2},\tau_k)}{l^{max}_{cdi-j}}$.

*Property*4.4 If $m(p_{ci\text{-}2}, \tau_k)<W(p_{ci\text{-}2}, t_{cdi\text{-}j})$, $V_2<V_{min}$, then the transition $t_{cdi\text{-}j}$ can not fire, where $V_2=\frac{W(p_{ci-2},t_{cdi-j})-m(p_{ci-2},\tau_k)}{l^{max}_{cdi-j}}$, i,j=1,2.

- Initialization process

We use a regional state sequence $RSS=(\boldsymbol{m}(\tau_0), v_1, [\tau_0, \tau_1]) \rightarrow (\boldsymbol{m}(\tau_1), v_2, [\tau_1, \tau_2]) \rightarrow \cdots \rightarrow (\boldsymbol{m}(\tau_{n-1}), v_k, [\tau_{n-1}, \tau_n])$ as a chromosome to represent a solution to optimize the average flow of machine and define *pop-size* as the number of chromosomes. *Pop-size* chromosomes will be randomly initialized by the following steps:

Step1. Input $m(\tau_0)$, *TH*, $i\leftarrow 1$, $\tau_0=0$.

Step2. 1) According to $\boldsymbol{m}(\tau_{i-1})$, $\tau_{i-1}$and property 4.1~ 4.4 construct the *i*th regional state and insert the regional state into the regional state sequence *RSS*.

2) If $\tau_i \geqslant TH$ then one feasible solution *RSS* is obtained and go to step3, else $i\leftarrow i+1$, go to 1).

Step3. Repeat step2 and produce *pop-size* initial feasible solutions.

- Evaluation fitness

For each individual within the population, a fitness value is calculated based upon the objective function defined as (1).Do not mix complete spellings and abbreviations of units: “Wb/m2” or “webers per square meter”, not “webers/m2”. Spell out units when they appear in text: “. . . a few henries”, not “. . . a few H”.

- Selection operation

The probability of one individual being selected is defined as

$$P_{Si}= f_i \ / \ \sum_{j=1}^{n} f_j \ , \ i=1,2, \ \cdots, n \quad (26)$$

Where n is the number of population, f_i, f_j are the fitness of individual i and j, respectively. By this means, the fitter individual is more frequently selected and produces more copies in the next generation..

- Crossover operation

We define a parameter P_c of a genetic process as the probability of crossover. This probability gives us the expected number $P_c \cdot pop\text{-}size$ of chromosomes which undergo the crossover operation.

Firstly we generate a random real number r in [0,1]; secondly, we select the given chromosome for crossover if $r<P_c$. Repeat this operation *pop-size* times and produce $P_c \cdot pop\text{-}size$ parents, averagely. For each pair of parents (regional state sequence RSS^1 and RSS^2), the crossover operator on RSS^1 and RSS^2 will produce two children C-RSS^1 and C-RSS^2 as the following steps:

Step1. Input $\boldsymbol{m}(\tau_0)$, *TH*, $i\leftarrow 1$, $k\leftarrow 1$.

Step2. $v_i\leftarrow \lambda_1 \cdot v_1^1 +\lambda_2 \cdot v_1^2$.

Step3. If $v_i \in [V_i^{min} ,V_i^{max}]$ then go to step 4, else give up this operation.

Step4. If $i=1$ then go to Step6.

Step5. 1) According to $\boldsymbol{m}(\tau_{i-1})$, $\tau_{i-1}$and property 4.1~ 4.4 Construct the *i*th regional state and insert the regional state into the children regional state sequence C-RSS^k.

2) If $\tau_i \geqslant TH$ then one feasible solution *RSS* is obtained and go to step3, else $i\leftarrow i+1$, go to 1).

Step6. If $\tau_i \geqslant TH$ then output C-RSS^k, $k\leftarrow k+1$ and go to Step7, else $i\leftarrow i+1$, go to Step5.

Step7. If $k<3$ then $i\leftarrow 1$, $v_i\leftarrow \lambda_2 \cdot v_1^1 +\lambda_1 \cdot v_1^2$ and go to Step3, else end.

Where $\lambda_1, \lambda_2>0$ and $\lambda_1+\lambda_2=1$, v_1^1 and v_1^2 is the *IFS* vector of the first regional state in RSS^1 and RSS^2 respectively.

- Mutation operation

We define a parameter P_m of a genetic system as the probability of mutation. The parameter is defined as

$$P_m = min\{1,\exp(-(f_{max}-f_{avg})/f_{max})\} \quad (27)$$

Where f_{max} (f_{avg}) is the maximum fitness value(the average fitness value) between the parent chromosome and the children chromosome.

For each selected parent, denoted by $RSS=(\boldsymbol{m}(\tau_0), v_1, [\tau_0, \tau_1]) \rightarrow (\boldsymbol{m}(\tau_1), v_2, [\tau_1, \tau_2]) \rightarrow \cdots \rightarrow (\boldsymbol{m}(\tau_{n-1}), v_k, [\tau_{n-1}, \tau_n])$, We mutate it by the following way. We choose a mutation regional state $(\boldsymbol{m}(\tau_{k-1}), v_k, [\tau_{k-1}, \tau_k])$ $(1\leqslant k<n)$ in *RSS* randomly and determine a chromosome RSS^1 as the following steps:

Step1. $i \leftarrow k-1$, RSS^1 $(k-1) \leftarrow RSS$ $(k-1)$.

Step2. 1) According to $\boldsymbol{m}(\tau_{i-1})$, $\tau_{i-1}$and property 4.1~ 4.4 Construct the *i*th regional state and insert the regional state into the children regional state sequence RSS^1.

2) If $\tau_i \geqslant TH$ then one feasible solution *RSS* is obtained and go to step3, else $i \leftarrow i+1$, go to 1).

Step3. If $\tau_i \geqslant TH$ then output RSS^1, else $i \leftarrow i+1$, go to Step2.

Where $RSS(k-1)=(\boldsymbol{m}(\tau_0), v_1, [\tau_0, \tau_1]) \rightarrow (\boldsymbol{m}(\tau_1), v_2, [\tau_1, \tau_2]) \rightarrow \cdots \rightarrow (\boldsymbol{m}(\tau_{k-1}), v_k, [\tau_{k-1}, \tau_k])$.

V. CASE STUDY

One case study is presented in this section to show the applicability of the proposed approach in scheduling of mixed batch/continuous processes. The example in Fig.2 is revisited. The related parameters are batch size of unit 1=8, batch size of unit 2=10, cycle time for unit 1=[3,5], cycle time for unit 2=[4,6], storage range=[2,15], initial storage amount=10, flow rate limit =[2.5, 5.0].

(1) Let time horizon=10, through the scheduling algorithm, the maximization of throughput is 42.8, and the optimal feasible scheduling policy (i.e. optimal regional state sequence) is:

$(-,-,2.6,[0,3]) \xrightarrow{t_{cd1}} (-,-,5,[3,4.1]) \xrightarrow{t_{cd2}} (-,-,5,[4.1,6.1]) \xrightarrow{t_{cd1}} (-,-,5,[6.1,8.1]) \xrightarrow{t_{cd2}} (-,-,5,[8.1,10.1])$

(2) Let time horizon=15, through the scheduling algorithm, the maximization of throughput is 65.7, and the optimal feasible scheduling policy is:

$\mathbf{(-,-,2.6,[0,3])} \xrightarrow{t_{cd1}} \mathbf{(-,-,5,[3,4.1])} \xrightarrow{t_{cd2}} \mathbf{(-,-,5,[4.1,6.1])} \xrightarrow{t_{cd1}} \mathbf{(-,-,5,[6.1,8.1])} \xrightarrow{t_{cd2}} \mathbf{(-,-,5,[8.1,9.3])} \xrightarrow{t_{cd1}} \mathbf{(-,-,4.2,[9.3,12.3])} \xrightarrow{t_{cd1}} \mathbf{(-,-,5,[12.3,13.9])} \xrightarrow{t_{cd2}} \mathbf{(-,-,5,[13.9,15.3])}$.

VI. CONCLUSION

Hybrid time Petri nets is a new modeling and analysis tool for systems with both discrete and continuous behaviors. In this paper, the scheduling algorithm for maximizing throughput of mixed batch/continuous process based on hybrid time Petri nets was developed. Through the HTPNs model and the proposed algorithm, the optimal feasible scheduling policy for mixed batch/continuous process can be found efficiently. The HTPNs have great potential for handling complicated operations in mixed batch/continuous processes. It is expected that other related problems of both discrete and continuous characteristics such as supervisory control might be solved easily in the framework of HTPNs. Further work is under way to incorporate different complicated storage polices into the model, addressing the algorithms for optimal scheduling based on Gene Expression Programming (GEP) [10] and implementing the integration of scheduling and control.

REFERENCES

[1] Nott, H.P. Modeling alternatives for scheduling mixed batch/continuous process plants with variable cycle time. Ph D Thesis, Murdoch University, Australia.

[2]Murata,T.Petri nets: properties, analysis and applications. Proceedings of the IEEE, 77, (1987) 541-580.

[3]Gu,T. and P.A.Bahri. Timed petri-net representation for short term scheduling of multiproduct batch plants. In: Proceedings of the 1999 American Control Conference, San Diego, USA, 1999, pp.4092-4096.

[4]P.A.Bahri.andGu,T. Petri-net based modeling and scheduling of batch processing plants----A heuristic algorithm. In: International Symposium on Advanced Control of Chemical Processes, Pisa, Italy, June 14-16, 2000, pp.467-472.

[5]P.A.Bahri.andGu,T. A novel approach for batch processes scheduling with variable batch size. In: CHEMECA 2000, Perth, Australia, June 9-12,2000.

[6] H. Alla, R. David,A Modeling and Analysis Tool for Discrete Event Systems: Continuous Petri Nets, Performance Evaluation, 33, (1998) pp.175-199.

[7]F.Balduzzi, A.Giua and G.Menga, First-Order Hybrid Petri Nets: a Model for Optimization and Control, IEEE transactions on robotics and automation, Vol.16,No.14, (2000) 382-399.

[8]Flaus, J.M. and G.Ollagnon. Hybrid flow nets for hybrid processes modeling and control. In: Proc. Of the Int. Workshop on Hybrid and Real-Time systems, Grenoble, France, March,1997, pp.213-217.

[9]Gu,T. and P.A.Bahri. Development of Hybrid Time Petri Nets for Scheduling and Control of Mixed Batch/Continuous Processes. In: Proceedings of the 15th IFAC World Congress, Barcelona, Spain, 2002.

[10]Yuan Chang-an, Tang Chang-jie, Zuo Jie et al. Function Mining Based on Gene Expression Programming—Convergency Analysis and Remnant-Guided Evolution Algorithm. Journal of SICHUAN University (Engineering Science Edition), 36(6), (2004) 100-105.

Dynamic parallel computing model of the aircraft landing on atrocious sea condition

Wang Dan Shesheng Zhang
Association of Mathematical Modeling, Wuhan University of Technology, Wuhan, 430070
Contact: sheshengz@qq.com

Li Mengyu
Association of Mathematical Modeling, Wuhan University of Technology, Wuhan, 430070
limengyu@qq.com

***Abstract*— In the atrocious sea conditions, the aircraft forced landing on water is a significant research project of the military affairs and aerospace. Considering the impact of waves on aircraft, the dynamic parallel computing model of aircraft forced landing is established, and the impact force's function of the angle between the aircraft and the slant wave surface is established, and the relationship between this angle and impact force at different wind speeds is obtained. The results show that the aircraft's best forced landing status is: aircraft pitch angle parallel to the wave angle.**

Keywords- aircraft, atrocious sea conditions, dynamic model

I. INTRODUCTION

The aircraft forced landing on water is a focused attention event for defense and aviation. Due to the significant fault or the cause of the accident, aircraft may be forced landing on water of the sea. Plane in the sea landing has the potential to cause heavy casualties, especially in storm conditions, where there is greater difficulty and risk. Because the plane in the sea landing is a possible accident, the aircraft ditching has been become a hot research project in many countries.

Based on numerical model of the aircraft ditching, Hug[2] considered the plane ditching numerical models for the plane crash criteria, design approaches and analysis method. He thought that we should consider not only the hard landing, but also consider ditching situations. This was due to a water landing relates to multi fields coupling, is a very complicated problem.

Yang[3] develops a modified smoothed particle hydro-dynamics (SPH) in Lagrange averaged Navier Stokes alpha(LANS-α) model to simulate water entry flow, and simulates water entry of a half buoyant cylinder and a neutrally buoyant cylinder were simulated. Liu[4] establishes the fluid structure interaction finite element analysis model for the dynamic model of airdropping equipment landing water. His results of numerical simulation are approached to the experiment. Article[5-8] discuses American Airlines A320 accident, and shows that the way of control is much more important.

II. PHYSICAL MODEL

As we know, there are three mainly postures for an aircraft forced landing: (1) sideslip; (2) head first landing; (3) tail first landing. However, to make the personnel safe evacuation, considering only the time is not enough. Because only aircraft ditching stable, personnel can safely away. To ensure the success of ditching, these three indicators must be met as much as possible:

(1) To ensure that the aircraft structural integrity, to protect the safety of passengers;

(2) In an aircraft landing process, the passengers will not bear larger impact load;

(3) To provide sufficient time for passengers to escape from the floating.

Because of above indicators (1) and (2) are about impact force, so we attributed them to the aircraft impact study. In addition, we cannot ignore the effect of the waves. In this model, the role of the waves will be considered to solve the impact force (mainly by means of the momentum theorem in physics); In addition, the impact of different floating angle on sink rate is combined to determine forced landing of posture of ditching, namely: the pitch angle range. Aircraft can be taken as a n ×m×k hexahedral as shown in Fig.1-2. θ is the angle between the aircraft axis and horizontal, x-axis parallels to the sea level, y-axis is vertically downward, y=0 is for the sea level, h is the aircraft thickness of aircraft.

Simply, the wave shape is set to be serrated and only the downwind situation is considered.

III. MATHEMATIC MODEL

Consider aircraft is an elastic body, at point (x,y,z) of body, the displacement is (u,v,w). The x and y axis is defineded in Fig.1, axis x is horizontal direction, and axis y is vertical direction. Suppose X,Y,Z is inernal force, according to the elastic mechanics, the motion equations of plane are as follows:

$$\begin{aligned} \rho u_{tt} &= He_x + G\Delta u + X \\ \rho v_{tt} &= He_y + G\Delta v + Y \\ \rho w_{tt} &= He_z + G\Delta w + Z \end{aligned} \tag{1}$$

Here:

$$e = u_x + v_y + w_z$$

$$G = \frac{E}{2+2\mu} \qquad H = \frac{G}{1-2\mu}$$

And operator

978-0-7695-4818-0/12 $26.00 © 2012 IEEE
DOI 10.1109/DCABES.2012.12

$$\Delta = \frac{\partial}{\partial x} + \frac{\partial}{\partial y} + \frac{\partial}{\partial z}$$

In above formula, E is the modulus of elasticity, μ is lateral contraction coefficient.

The boundary condition:

(1) on the wetted surface, the force of wave and water acted on the plane is F(x,y,z);

(2) on the other surface, acted on the plane is F(x,y,z)=0;

The initial condition:

(1) At beginning t=0, the displacement is (u_0,v_0,w_0).

(2) At t=0, the derivation of displacement speed is (u'_0,v'_0,w'_0).

From above boundary and intial condition, the more important job is to find force F(x,y,z).

IV. THE IMPACT FORCE OF WAVES ON THE AIRCRAFT

Let γ is the angle between waves and horizontal plane, v_w is the speed of the waves, α_1 is the angle between aircraft with water and waves slant. The ultimate speed of impacted aircraft is as same as the one of wave. According to the Fig.2, the pitch angle of the aircraft is: $\theta = \alpha_1 + \gamma$.

We can infer from the horizontal and vertical direction of momentum conservation that x-direction momentum F_x is:

$$F_x = \frac{mv_{y0}}{g}(v_{x0}\cot\theta - v_{y0}) \tag{2}$$

Where m is the aircraft quality, v_{x0} and v_{y0}, respectively mean velocity components of x and y directions when the aircraft is making forced landing, respectively, and t is time, as follows:

$$\begin{aligned} t &= \frac{A\sin\alpha_1 + B\sin\alpha_1}{g\sin(\gamma-\alpha)} \\ A &= v_{y0}\cos\gamma + (v_{x0} - v_w)\sin\gamma \\ B &= v_{y0}\sin\gamma - (v_{x0} - v_w)\cos\gamma \end{aligned} \tag{3}$$

The average resultant impact force of the aircraft is:

$$F = \sqrt{1+(\tan\alpha_1)^2}F_x \tag{4}$$

Assume that when the aircraft impacts on the wave surface, the surface wave speed can reach 70% of the wind speed. According to the relationship between wind speed, wave height and wave angle, and taking m = 70000kg, v_{x0} = 2m/s, v_{y0} = 12m/s, the relationship between the aircraft's average resultant force and angle of elevation in level 3 sea state can be calculated. The results show that when the pitch angle increases, the aircraft force increases rapidly, at 68^0 up to the threshold, which generates destructive force.

V. FORCE ANALYSES IN VERTICAL DIRECTION

Now aircraft force in vertical direction will be analyzed. Ignoring air drag and water buoyancy, the aircraft is only impacted by gravity and water resistance. Water resistance is determined by momentum law. Specific method is as follows:

Set the section of aircraft in contact with water is D. For a sufficiently short time Δt, we regard the aircraft as static and water in contact with it in motion, then water speed is actually the superposition of its own speed and aircraft speed. For the speed of the water in contact with the aircraft cross section, we add an average speed u to it, taking into account that u is a random amount of change and the overall change is small; we have differential equation of y(t)

$$\begin{cases} my'' = -k(y'+u)^2 + mg \\ y'(0) = v_{y0}, y(0) = 0 \end{cases} \tag{4}$$

The sink ratio is defined as:

$$\psi(t) = \frac{y(t)}{h\cos\theta} \tag{5}$$

In the case of a given time t and vertical speed v_{y0} during forced landing, we studied the relationship between sinking ratio ψ and θ, and calculated results are shown in Figure 3(We take the overall regional water flow speed of the aircraft fluctuating within ±0.5m/s2 range). The solid line is the static surface of the water situation. Dots are calculated values of different wind speed. With this Figure, we find that the sinking rate basically increases with the pitch angle increases. That is the greater the pitch angle, the sooner the aircraft sank; at the same time, we can also find the slope of this function image is constantly larger, that is the sinking speed increases unceasingly. The front function image is relatively stable, while at a later stage, namely, when the pitch angle is relatively large, small-scale fluctuations in the angle will produce a relatively great impact on the time; if a longer evacuation time is expected, a relatively small pitch angle should be selected.

VI. PARALLEL COMPUTATION

The function v=y' can be solved from above section, and suppose w=z' is much smaller compare with u=x', all varies is only function of (x,y), internal force X=0, then Eq.(1) can be reduce to

$$\rho u_{tt} = Hu_x + G\Delta u + Hv_y \tag{6}$$

The Eq.6 is solved by using parallel computation with 16 CPU. The domain is divided into 16 sub-domains. Every sub-domain is divided into $38\times12\times4$hexahedra, data is exchanged between sub-domains. Let h is space step length, $x_i=x_0+ih$, $y_j=y_0+jh$, $t_k=k\tau$, τ is time step length.According

to the difference method, take second order difference formula as:

$$u_{tt}(x_i, y_j, t_k) = \frac{u_{ij}^{(k+1)} - 2u_{ij}^{(k)} + u_{ij}^{(k-1)}}{\tau^2}$$

$$u_x(x_i, y_j, t_k) = \frac{u_{i+1j}^{(k)} - u_{i-1j}^{(k)}}{2h} \quad (7)$$

$$v_y(x_i, y_j, t_k) = \frac{v_{ij+1}^{(k)} - v_{ij-1}^{(k)}}{2h}$$

$$\Delta u(x_i, y_j, t_k) = \frac{u_{i+1j}^{(k)} + u_{i-1j}^{(k)} - 4u_{ij}^{(k)} + u_{ij-1}^{(k)} + u_{ij+1}^{(k)}}{h^2}$$

We may obtain difference equation:

$$u_{ij}^{(k+1)} = 2u_{ij}^{(k)} - u_{ij}^{(k-1)} + \frac{\tau^2}{\rho}(Hu_x + G\Delta u + Hv_y) \quad (8)$$

Above is two steps difference equation, and k=1,2,3,…. By using initial condition, we have:

$$u_{ij}^{(1)} = u_{ij}^{(0)} + \tau u_t(x_i, y_j, t_1) \quad (9)$$

VII. RESULTS

According to the above analysis, in the case of that the aircraft is not big damage, and passenger can evacuate safely, we should try to select a smaller angle α_1 as

$$\theta = \alpha_1 + \gamma$$

.

Here γ is fixed, γ=0.08(radians), about 4.58°. But according to the above analysis, we take α_1 =0 if it's expected to make an emergency landing as safe as possible. That is, the aircraft pitching angle parallels to the wave angle and takes direction of longitudinal waves. It's also concluded that, except in high wind speed, to make the impact force as small as possible, the landing angle between plane and wave surface should be kept around zero, the aircraft should land parallel to the main surge. In fact, when the wave angle is fixed at γ = 0.08 and the wind speed is high, v_t = 20m/s, 25m/s, and 30m/s respectively are taken to carry out research. The conclusions reach that in the case of wind, if wind speed is extremely high, the aircraft should maintain a small elevation with wave slant when landing. If we want to make an emergency landing as safe as possible, just take of α_1 = 0, that is, the aircraft pitch angle parallels to the wave angle and takes the longitudinal wave direction.

VIII. CONCLUSION

In the atrocious sea conditions with wave and wind, the aircraft force landing on water is difficult researching project. This paper discusses the physic and mathematic models of aircraft force landing on water in the atrocious sea conditions, and gives initial and boundary condition. The pitching angle is calculated according to the different wind velocity. The results show that passenger can evacuate safely if pitching angle is same as wave angle.

ACKNOWLEDGMENT

The paper is financially supported by by China national natural science foundation (No.51139005).

REFERENCES

[1] Zhang Tao, Civil aircraft ditching analytical models and numerical simulation, Nanjing University of Aeronautics and Astronautics, 2010(3), 392-394.

[2] Hu Dayong, The numerical model of a certain aircraft ditching, Journal of Beijing University of Aeronautics and Astronautics, 2008(12), 1369-1383.

[3] Yang Xiufeng, et al, Simulation of Water Entry with Smoothed Particle Hydrodynamics Method[J], Chinese Journal of Computational Physics, 2011(4), 523-528.

[4] Liu Xin et al, Analysis of Dynamic Characteristic Parameters of Airdropping Equipment Landing Water and Optimization[J], Journal of System Simulation, 2011(2), 252-256.

[5] Wang S. Y., The initial analysis American Airlines A320, International Aviation, 2009(2),1-3.

[6] Wang Xianfu, Zhang Shesheng , Super cavitating hydrofoil numerical calculation of flat plate hydrofoil[J], China ship building, 1986(4), 1-9.

[7] DayongYang et al, Numerical model for a commercial aircraft water landing[J], Journal of Beijing University of Aeronautics and Astronautics, 2008(12), 1369-1376.

[8] He Qian et al, Research on the load of aircraft landed on water[J], Structure & Environment Engineering, 2009(4),28-33..

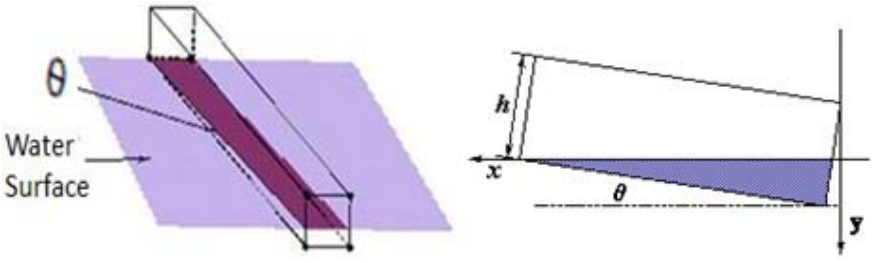

Figure 1. Three-dimensional view of forced sectional view landing and sinking of the aircraft

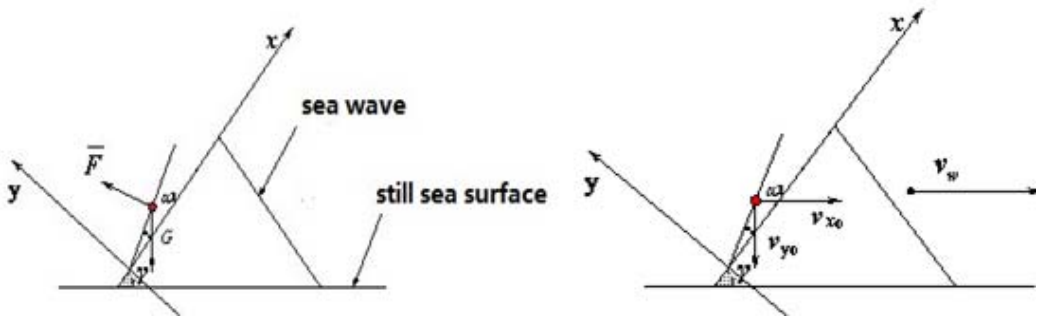

Figure 2. Force schematic when the aircraft contacts water surface

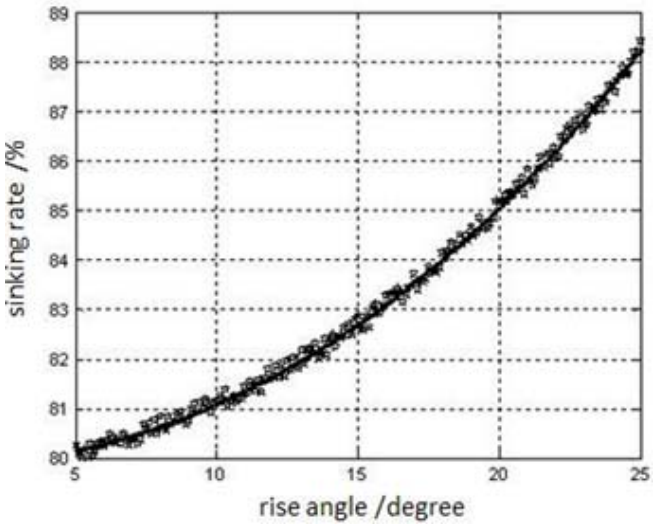

Figure 3. relationship between ψ and θ

Modeling and Assessment of the Xijiang FPSO Turret Mooring System

Yang Jiaxuan, Shi Guoyou
Navigation College
Dalian Maritime University, Dalian, China
ytyjx@163.com

***Abstract*—This paper uses the information of the Xijiang floating production storage and offloading (FPSO) mooring system coupled with dynamic analysis of the system to generate scenarios for the most likely causes of the damage to the wires and predict if this is likely to result in further progressive damage of the mooring system. The modeling reflects the fundamentals of the Xijiang FPSO mooring system and can be used to further investigate potential causes for the mooring leg damage. The mooring dynamic analysis has been used to investigate the indicative behavior of the mooring lines under various conditions when Buoyant Turret Mooring (BTM) is connected. The model has been used to investigate the tensions, bending moments and bending radiuses near the lower socket. Further more the models have been checked to determine that they produce results of the correct order for the mooring system.**

Keywords-FPSO; BTM; modeling; mooring

I. INTRODUCTION

The production facilities at the Xijiang Oil field, which are located around 100 m of water in the Pearl River Mouth Basis approximately 130km offshore from Hong Kong in the South China Sea, consist of two wellhead platforms (PF 24-3 and PF 30-2) with the production fluids transported via two 10 ins flow lines to an Floating Production Storage and Offloading (FPSO) Unit located centrally between the platforms. The FPSO is held on station with by a disconnectable Buoyant Turret Mooring (BTM) consisting of a submerged mooring buoy tethered by eight catenary anchor legs. The mooring system, which is attached to the FPSO via a disconnectable Buoyant Turret Mooring (BTM) consists of 8 legs each comprising:

(1) Drag anchor
(2) 1000m of 124 mm diameter 6x36 strand wire rope
(3) Variable length (approx 25m) of 108 mm diameter chain
(4) 200m of 120 mm diameter chain
(5) 90m of 102 mm diameter spiral strand wire rope
(6) 10.2m of 108 mm diameter chain connected to the chain stopper on the BMT.

The water depth at the BTM is approximately 100 m. The BTM system allows the FPSO to be disconnected from the mooring system when typhoon conditions are expected at the field. When disconnected the BTM is designed to float 31 m below the sea surface. The FPSO remain connected during all other weather conditions.

II. MODELING OF MOORING SYSTE

A. General

OrcaFlex is a non-linear time domain, finite element software program principally used for the static and dynamic modeling of systems used in offshore construction environment, including marine risers of the flexible and rigid types, mooring systems and towed array's. It has the unique capability in its class to be used as a Windows DLL, allowing ready integration into 3rd party software. The mooring system has been modeled using the software OrcaFlex 9.2a. The three Dimensions (3D) representation of the model is shown in Figure 1 below.

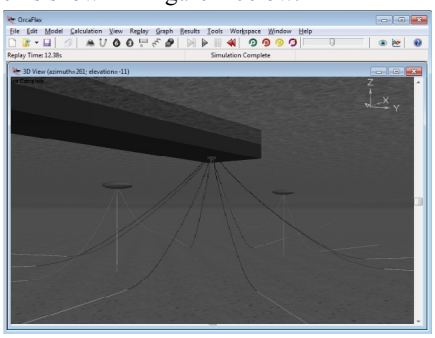

Figure 1. Model of Mooring System.

The orientation of each of the eight mooring legs relative to the BTM is shown in Figure 2 below. Flexible risers in a Lazy S configuration connect the pipeline end manifold (PLEM) at the end of each flow line to the BTM. The risers are located approximately equidistant from mooring legs #1 and #8, and #4 and #5, as shown in Figure 2. Space was provided between mooring legs #6 and #7 for an additional flexible riser. This spare riser slot has not yet been utilized.

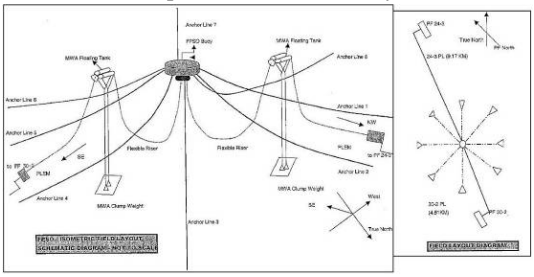

Figure 2. Xijiang Field Layout.

978-0-7695-4818-0/12 $26.00 © 2012 IEEE
DOI 10.1109/DCABES.2012.109

As shown in Figure 3 below, each mooring leg is made up from the following components:

(1) High holding power marine drag anchor

(2) 1000 m of 124 mm (4⅞ ins) diameter galvanized six stranded wire rope

(3) 45 m (approx.) 108 mm (4¼ ins) diameter stud link chain

(4) 200 m of 120 mm (4¾ ins) diameter stud link chain (approx mass: 320 kg/m)

(5) 90 m of 102 mm (4 ins) diameter galvanized spiral strand wire rope (approx mass: 64 kg/m)

(6) 27.5 m of 108 mm (4¼ ins) stud link chain connected to a chain stopper at the BTM (approx mass: 255 kg/m)

The spiral strand wire rope was selected to reduce the suspended weight on the mooring buoy, allowing this to be optimized. The 120 mm (4¾ ins) diameter stud link chain was shown to experience partial lift off at the seabed during the design analysis. As a result the diameter of this chain is oversized compared to that required from the extreme loads to account for possible wear of the chain in this area. In addition the relatively high suspended weight of this segment stiffens up the anchoring system around the mean FPSO excursions, reducing the amplitude of slow drift oscillations and avoiding slack in the pulling cable during the reconnection operations. The 1000 m of 124 mm (4⅞ ins) diameter wire between the chain and the anchor is only partially lifted during extreme FPSO excursions. The low linear weight of the wire was selected to significantly reduce the peak loads in the chain at extreme excursions.

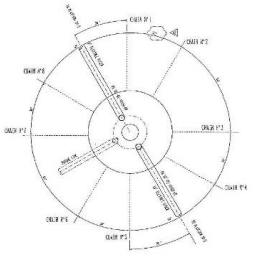

Figure 3. Xijiang FPSO Mooring Leg Orientation.

B. *Mooring Legs*

All the mooring legs have been modeled to represent the various components in each leg. Each wire and chain segment has been modeled separately to have the correct length, weight, and stiffness properties. The sockets have been modeled as cylinders have the appropriate diameter and weight properties. The mooring legs are attached to the BTM at the upper end and given the configuration as shown in Figure 3. Mooring leg #4 and leg #5 has been modeled in more detail than the other legs with smaller elements in the area around the transition to the lower socket. For these two legs the socket/link plate between wire and chain has also been modeled as a 2 m long, 0.35 m diameter stiff cylinder with a weight of 0.8 Tonne/m.

C. *Buoyant Turret Moorin* (*BTM*)

The BTM has been modeled as two 6 degrees of freedom cylinders connected together. The dimensions and weight of the BTM have been estimated from the SBM drawings. The volume and weight of the BTM have been slightly tuned in the model in order to reach the anchor system freely floating equilibrium position of -31 meters in accordance with the design criteria. Each mooring leg has been attached in a radius of 4 m from the centre of the BTM and 2.5 meters above BTM bottom.

D. *Risers*

The 10 inch flexible risers have been modeled, with the assumption that each riser is water filled. Each riser has been modeled as two risers; one from the PLEM to the Mid Water Arch (MWA) tanks, and one from the tanks to the BTM. The MWA buoyant tanks are held down by clump weights so that the tanks do not move in vertical direction. The lengths of the risers have been estimated to be 200 + 130 m.

E. *Floating Production Storage & Offloading* (*FPSO*)

The Response Amplitude Operators (RAOs) for the FPSO were not readily available within the information; as a result data for a similar ship was used to represent the FPSO within the OrcaFlex simulation. The detailed hydrodynamic data for this ship, which was 280 m long, was derived from the program AQWA and transferred to OrcaFlex as part of the input for the simulation model. The basic data of the ship used to represent the FPSO is shown as Table 1.

TABLE I. THE BASIC DATA

***Length* (*m*)**	***CoG vert* (*m*)**	***Draft* (*m*)**	***CoG long* (*m*)**
280.00	18.00	12.20	134.00
***Breath* (*m*)**	***CoG trans* (*m*)**	***Weight* (*T*)**	/
52.00	0	148600	/

The BTM has been connected to the vessel 250 m forward of the aft perpendicular.

F. *Environment*

The water depth in the model was set to 100 m and the seabed friction factor is set to 0.5.

The environmental conditions at the Xijiang Field are primarily driven by monsoon conditions. From October to March the NE monsoon winds prevail and from May to August the SW monsoon winds prevail. April and September are transitional seasons.

III. DYNAMIC ANALYSIS OF MOORING SYSTEM

The model of the complete system with the BTM connected to the FPSO was run for both static and dynamic cases. The results from each are presented in the Sections below.

The static analysis was performed with the FPSO in the equilibrium position as means of checking the basic set up of the model. With the FPSO in this position the mooring line arc length to touch down is in the segments between 145 and 160 meters which mean that the 120 mm diameter stud link chain is in the touchdown zone.

TABLE II. PRE-TENSION IN MOORING LEGS AT EQUILIBRIUM POSITION

Length(m)	*Pre-Tension*	
	Buoy(KN)	*Anchor(KN)*
#1	339	225
#2	339	217
#3	359	235
#4	364	236
#5	371	236
#6	319	200
#7	307	189
#8	316	197

The Load Excursion curve for the mooring system was derived by positioning the FPSO at 2.5 m increments from the equilibrium position in a south westerly direction for a total offset of 30 m. The loads in each of the mooring legs were combined to give the total system restoring force variation with offset, as shown in Figure 4 below.

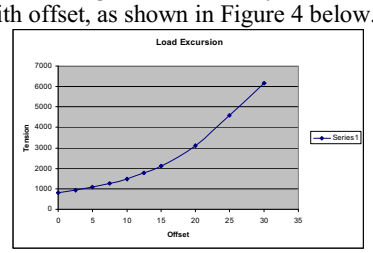

Figure 4. Load Excursion Curve for Mooring System (South West offsets).

A series of dynamic simulations with the FPSO connected to the mooring system were performed with various environmental conditions. The main aim of these simulations was to derive information on the mooring system behavior which could be used to give indications as to the reasons for the damaged wire strands found during the system inspection. The results from these simulations are presented below.

A. Maximum with FPSO Connected

In order to check that the model was producing results of the correct order of magnitude a regular wave simulation was performed using the maximum conditions for the FPSO connected. The following environmental conditions were used for this simulation:

Hmax: 13.7 m
Tz: 10 s
Wind Speed: 32.4 m/s
Current Speed : 1.10 m/s

The waves and wind were applied from the North East and the current applied from the East. The results from the simulation are shown in Figures 5, 6 and 7 below. From the results of BTM offset (Figures 5 and 6) the total offset is around 30 m from the static equilibrium position. As a result of the direction of the environmental conditions, mooring leg #2 is the most heavily loaded line. The maximum tension in this leg is about 330 T, which is some what lower than the extreme value of 450 T derived from the model tests. However the value is considered to be sufficiently close to use the model for investigation purposes as this was not a direct simulation of the model tests only an approximation using a single wave.

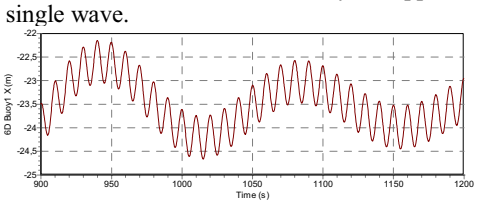

Figure 5. BTM X Motion (Max with FPSO Connected).

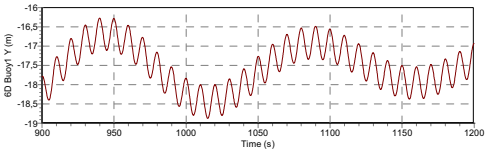

Figure 6. BTM Y Motion (Max with FPSO Connected).

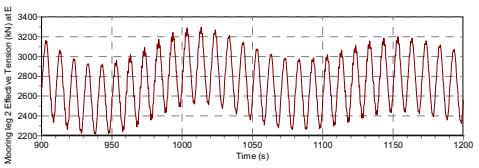

Figure 7. #2 Tension (Max with FPSO Connected).

B. Most Likely Conditions with FPSO Connected (3 hour simulation)

In order to get information which could be of interest for fatigue behavior, a full 3 hour simulation was performed using the most likely weather conditions with the FPSO connected. These conditions were shown below:

Hs : 1.9 m
Tz : 6 s
Wind Speed : 8 m/s
Current Speed : 0.3 m/s

The waves and wind were applied from the North East and the current applied from the East. The results from the simulation are shown in Figures 8 and 9 below. The main purpose of this simulation was to get an appropriate offset for the BTM which could be applied to the model for a series of regular wave runs. It can be seen from the results that this is of the order of 2.1 m.

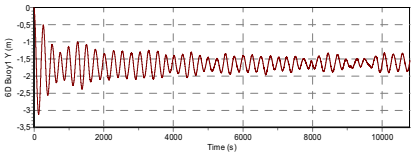

Figure 8. BTM Y Motion (Most Likely with FPSO Connected).

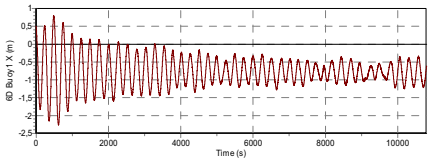

Figure 9. BTM X Motion (Most Likely with FPSO Connected).

C. *2.1m Offset to SouthWest with Regular Waves (H=1-7m)*

One possible cause of damage to the mooring legs is bending of the wire at the connection to the lower socket. In order to investigate this further a series of regular wave simulations were performed with the BTM positioned at a 2.1 m offset to the South West and the waves coming from the North East. This providing a series of simulations in conditions which are most likely with the FPSO connected. The simulations were performed for a range of wave heights (1 - 7m) and each wave height was run with a range of periods (4 - 8 s) to provide a large coverage of conditions. The results for the minimum bending radius of the wire of #4 close to the lower socket are presented in Figures 10 and the dynamic variance presented in Figure 11. The minimum bending radius is in the range of 8.6 - 9.7 m, with a dynamic variance in the rage of 0.1 - 2 m.

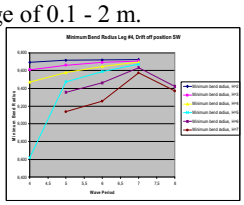

Figure 10. Minimum Bending Radius #4 (FPSO Connected).

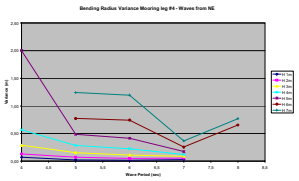

Figure 11. Bending Radius Variance #4 (FPSO Connected).

D. *Most Severe Likely Conditions with FPSO Connected (3 hour simulation)*

In order to investigate further possibilities of dynamic effects at the wire - lower socket interface a full 3 hour simulation was performed with weather conditions which represent the most severe likely conditions with the FPSO connected. These conditions were used as below:

Hs : 3.5 m
Tz : 6.4 s
Wind Speed : 20 m/s
Current Speed : 0.6 m/s

The waves and wind were applied from the North East and the current applied from the East. The results for the mooring leg #4 are presented in Table III below

TABLE III. RESULTS FOR THE MOORING LEG #4

#4	***Tension***			***Bend Moment***			***Bend Radius***		
Hs=3.5	*Min*	*Max*	*Mean*	*Min*	*Max*	*Mean*	*Min*	*Max*	*Mean*
Tz=6.4	*210.4*	*394.7*	*296*	*0.8*	*1.2*	*1.0*	*8.5*	*11.9*	*10.2*

IV. SUMMARY

The results presented above demonstrate that the modeling reflects the fundamentals of the Xijiang FPSO mooring system and can be used to further investigate potential causes for the mooring leg damage. The selected vessel seems to be adequate for the use in this analysis, since the maximum tension in the mooring system gives tensions close to the design limit.

The model has been used to investigate the tensions, bending moments and bending radiuses close to the lower socket. This is a potential cause of damage to the wire rope, particularly on mooring legs, which are not the most highly loaded. Due to the relatively low tension in the mooring leg the appropriate Line Factor is very high and outside the rage of the data. As a result it is reasonable to conclude that bending fatigue under these conditions is not a potential cause of damage to the mooring lines.

ACKNOWLEDGMENT

Authors are grateful for the financial supported by “the fundamental research funds for the central universities”. The project number is “2012QN010”.

REFERENCES

[1] Mooring Integrity Guidance, Oil & Gas UK, November 2008

[2] O. Vennemann, I. Frazer, and R. Törnqvist, “Extending the Use of Conventional Construction Technology for the Installation of Subsea Production Facilities in Deep Water,” Offshore Technology Conference, May 2008

[3] J. W. Yang, J. L. Wang, Y.T. Xu, X. Ma, X. H. Pang, “The FPSO-DML algorithm for 1-DOA estimation of wideband signals”, International Conference on Wireless communication and signal processing 2010, pp.1-4

[4] J. Trienekens, B. Braun, J. Gillham, B. Christ, “Field trials of the rope and rise crawling vehicle”, Oceans 2010, pp.1-6

[5] R. Sangsoo, M. H. Kim, “Coupled dynamic analysis of thruster -assisted turret-moored FPSO”, Oceans 2003, vol. 2, pp. 1613-1620

[6] Q. Gao, M. Han, S. L. Hu, H. J. Dong, “Design of fault diagnosis system of FPSO production process base on MSPCA”, Fifth International Conference on Information Assurance and Security, 2009, vol. 2, pp.729-733

[7] B. Tong, “Study on the Deepwater FPSO Offloading Buoy System”, Naval Architecture and Ocean Engineering, 2012, (1), pp.21-25

[8] Y. D. Liu, J. X. Liu, A. Q. Tan, “The Motion and Mooring Forces of a Turret Moored FPSO with the Wind,Waves and Currents Loads”, Ship and Ocean Engineering, 2011, vol. 40(6), pp. 146-149

[9] S. S. Liu, Y. Wang, "Application of Catenary Function in Relevant Calculation of FPSO Mooring System", Shipbuilding of China, 2011, vol.52(S1), pp.115-122

[10] Z. Q. Hu, J. M. Yang, Y. N. Zhao, "Full scale measurement for FPSO on motions in six-degrees of freedom and environmental loads and deduction of mooring system loads", Science China (Physics, Mechanics and Astronomy), 2011, vol.54(1), pp. 26-34

Tree Crown Reconstruction Model Based on Maximum Lighted Area

Shanshan Chen Shesheng Zhang
Association of Mathematical Modeling, Wuhan University of Technology, Wuhan, 430070
Contact: sheshengz@qq.com

Zefeng Tao
Association of Mathematical Modeling, Wuhan University of Technology, Wuhan, 430070
taozefeng@@qq.com

***Abstract*—This paper provides a tree crown reconstruction method. We calculate the total lighted area a leaf receives in a day and analyze the best included angle between a pair of leaves when their mutual overlap is considered. By using discrete summation and equilibrium condition of forces we conclude that when leaf angle is consistent with light angle, the sunlight a pair of leaves receives is the maximum. We make different types of leaf shapes cover the crown to get different coverage, in which the maximum corresponds to the most appropriate shape. This method follows the law of maximum light area in plant growth and once user set the tree crown, the leaf shape can be fixed. Then the whole tree crown is reconstructed. It can be used in tree model reconstruction in broad scene.**

Keywords- Leaf shape; Tree crown; Reconstruction model; Maximum lighted area

I. INTRODUCTION

Trees in nature generally consist of crown and leaves. There are two types of trees modeling: from local to global and from global to local [1]. In the former method, the user firstly set up a local nature, and then get the global structure, namely the crown shape. In contrast to this method, a crown-leaf method asks users to set the shape of tree crown, and then deduces leaf shape. Such a modeling approach that uses global information to deduce local details first appeared in paper wrote by Reeves and Blan in 1985 [2]. In 2003, Frederic Boudon and Przemyslaw Prusinkiewicz put up with a global to local modeling method [4] for bonsai trees based on Cascatti's work [3]. In this paper, we get the leaf shape satisfying the maximum coverage and finally create a new method of modeling of trees from global to local. The advantages of this method are that it is easier for users to control the process. Besides, tree structures it constructs own natural postures, which is suitable for tree construction in the large-scale scenes.

II. ONE LEAF MODEL

We believe that the leaves always minimize overlapping part to maximize exposure to sunlight. Leaf photosynthetic area is a function of independent variables:s=s(t). The Fig.1 shows that only the top surface accepts the light to carry out photosynthesis. When sunlight angle is less than the leaf angle, leaf top surface can not get light, so there is no effective light area, so when $15(t-6)<\alpha$, $s(t)=0$;When sunlight angle is wider than the leaf angle, leaf top surface can get the sunlight. if

$$15(t-6)>\alpha, s(t)=l\times d\times\sin(15t-\frac{\pi}{2}-\alpha).$$

The overall sunlight area a leaf accepts in a day is $s(\alpha)=\int_6^{18}s(t)dt$. To solve the equation above, we just select an group of orderly moments to stand for the day time during which the effective illumination is got by leaves to calculate overall effective illumination area .

$$s(\alpha)=s(6)+s(7)+s(8)+\cdots\cdots s(17)+s(18) \quad (1)$$

So we can conclude that when $\alpha\approx 45^{\circ}$, then lighted area a leaf gets in a day is the most.

III. TWO LEAFS MODELS

Assume that there are only two leaves in a tree, and their horizontal angle is α and β . if $15(t-6)<\alpha$, we take $S_c=\sin[\alpha-15(t-6)]$, if $\alpha<15(t-6)<\pi-\beta$, we take $S_c=0$, if $16(t-6)>\pi-\beta$, we take

$$. S_c=\sin[\beta+15(t-6)-\pi]$$

.Then we value and get the total sunlight area in a day under different leaf angles. Because the set of value of and is identical, so, the sunlight area two leaves get is twice as much as a single one (we ignore the blocked area between the two leaves): $S_a=2S(\alpha)$ .So coverage ratio is: $\mu=S_c/S_a\times100\%$ .Then we get Fig.3. From the figure 3, we can see that when the two leaf angles are both zero, exposure time is longest. So we can conclude: In the case of two leaves, the more leaf field angle is closer to the range of sunlight angle, the more beneficial it is to extend the exposure time.

978-0-7695-4818-0/12 $26.00 © 2012 IEEE
DOI 10.1109/DCABES.2012.15

IV. TWO LEAFS IN A TREE

We assume that there are two leaves in a tree, the lighted area a leaf got is less due to the block of tree crown. That is to say, the value range of t is changed. But there is no change in the value range of angle. So if we replace the ground line in the last model with tree crown in this model, we can calculate it in the same way. Assume $\theta = 30^\circ$ is the vertex of the tree crown triangle, the range of t is: $(180^\circ - \theta)/30 + 6 < t \le 18$. See Fig.4.

.

V. MODEL DEDUCTIONS

The quality of the leaf is α. We assume that the quality is in leaf centroid. Leaf gravity takes moment about the point of intersection: $M = ag \times 0.5l\cos\alpha$ .So when $\alpha = 90^\circ$, M_1 is least. So this is the best force condition of leaf. We can conclude that the smaller the included angle, the better their force condition. Based on this, we try to decrease included angle without affecting the lighted area. Considering the force factor, we make the include angle least. In a word, when light angle is γ, the included angle is γ, too..

VI. LEAF SHAPE CLASSIFICTIONS

Considering that leaf shapes in nature world are mostly symmetrical shape and limited, we make a rectangle to cover the leaf. Its length and width are respectively along the reference direction and the area of rectangle is smallest. We measure the length and width to be l_2 , l_2 ($l_1 \ge l_2$). According to several normal leaf shapes distributed in nature world, we simplified the leaf shapes as follows: needle-like, oval, round, palm-like. Judgment method is as follows: $l_1 / l_2 \ge 6$ Needle-like; $1.3 \le l_1 / l_2 < 6$ Oval; $1 \le l_1 / l_2 < 1.3$, $l_1 / l_3 \ge 1.2$, palm-like; or it is round

VII. DEDUCE LEAF SHAPE BY TREE CROWN

We assume tree crown is a cone and its profile vertex angle is θ. By using results above, we conclude that when the light angle is γ, the included angle is γ, too. So when the light angle is $\gamma=(\pi+\theta)/2$, the included angle is $\gamma=(\pi+\theta)/2$ .The cone is divided into n layers. Leaves uniformly distributed on each floor so we can think each pair of leaves on each layer is distributed within a rectangular area. Underside diameter of cone is D , so its circumference is πD , the perimeter of each layer decrease $4l_1\pi\sin\frac{\theta}{2}\cos\frac{\pi-\theta}{4}$ up one floor. S_k characterizes the middle value of the perimeter of two layers.

$$S_k = \pi D - (2k-3)4l_1\sin\frac{\theta}{2}\cos\frac{\pi-\theta}{4} \qquad (2)$$

We assume that leaf width distributes in S_n , so the number of leaves in each floor is $N = S_k / l_2$, the total number of leaves is $N_A = \sum_{k=1}^{n} S_k$ .We get the overall covered area: $S_{leaf} = N_A l_1 l_2 \tau$. Finally we can get the leaf coverage ratio of a cone crown:

$$C = 4N_A l_1 l_2 \tau \sin\frac{\theta}{2} / (\pi D^2) \qquad (3)$$

In a word, when crown shape is fixed, different shapes of leaves (leaf shape coefficient is different) will come with different coverage ratios. The leaf shape owing most coverage ratio is the most suited shape to this tree crown, by which we can fix the leaf shape. At last, through computer simulation we can put leaves chosen above on the crown to get the information of whole tree.

VIII. DISCUSSION

Tree crown reconstruction model based on maximum light area is suitable for tree reconstruction in large scene. Users can adjust crown shape according their needs and different kinds of scenes. Following the law of maximum light area in plant growth, the leaf shape is generated by using discrete summation and an optimization method, which corresponds with the ecological characteristics of tree growth and fractal characteristics of the branching patterns of tree.

ACKNOWLEDGMENT

The paper is financially supported by by China national natural science foundation (No.51139005).

REFERENCES

[1] G. Eason, B. Noble, and I. N. Sneddon, “On certain integrals of Lipschitz-Hankel type involving products of Bessel functions,” Phil. Trans. Roy. Soc. London, vol. A247, pp. 529–551, April 1955. *(references)*

[2] J. Clerk Maxwell, A Treatise on Electricity and Magnetism, 3rd ed., vol. 2. Oxford: Clarendon, 1892, pp.68–73.

[3] I. S. Jacobs and C. P. Bean, “Fine particles, thin films and exchange anisotropy,” in Magnetism, vol. III, G. T. Rado and H. Suhl, Eds. New York: Academic, 1963, pp. 271–350.

[4] K. Elissa, “Title of paper if known,” unpublished.

[5] R. Nicole, “Title of paper with only first word capitalized,” J. Name Stand. Abbrev., in press.

[6] Y. Yorozu, M. Hirano, K. Oka, and Y. Tagawa, “Electron spectroscopy studies on magneto-optical media and plastic substrate interface,” IEEE Transl. J. Magn. Japan, vol. 2, pp. 740–741, August 1987 [Digests 9th Annual Conf. Magnetics Japan, p. 301, 1982].

[7] M. Young, The Technical Writer's Handbook. Mill Valley, CA: University Science, 1989.

[8] Electronic Publication: Digital Object Identifiers (DOIs):

Article in a journal:

[9] D. Kornack and P. Rakic, "Cell Proliferation without Neurogenesis in Adult Primate Neocortex," Science, vol. 294, Dec. 2001, pp. 2127-2130, doi:10.1126/science.1065467.

Article in a conference proceedings:

[10] H. Goto, Y. Hasegawa, and M. Tanaka, "Efficient Scheduling Focusing on the Duality of MPL Representatives," Proc. IEEE Symp. Computational Intelligence in Scheduling (SCIS 07), IEEE Press, Dec. 2007, pp. 57-64, doi:10.1109/SCIS.2007.357670.

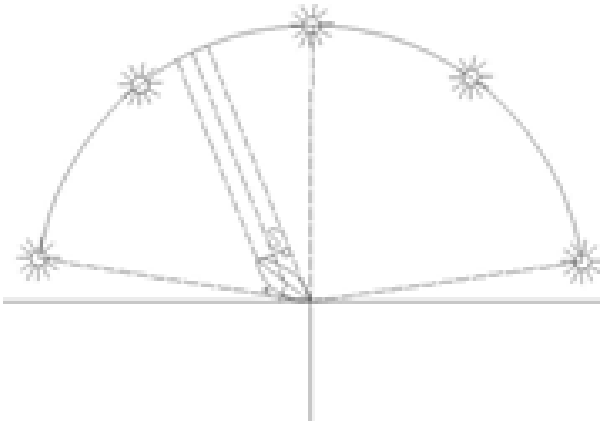

Figure 1. Basic model.

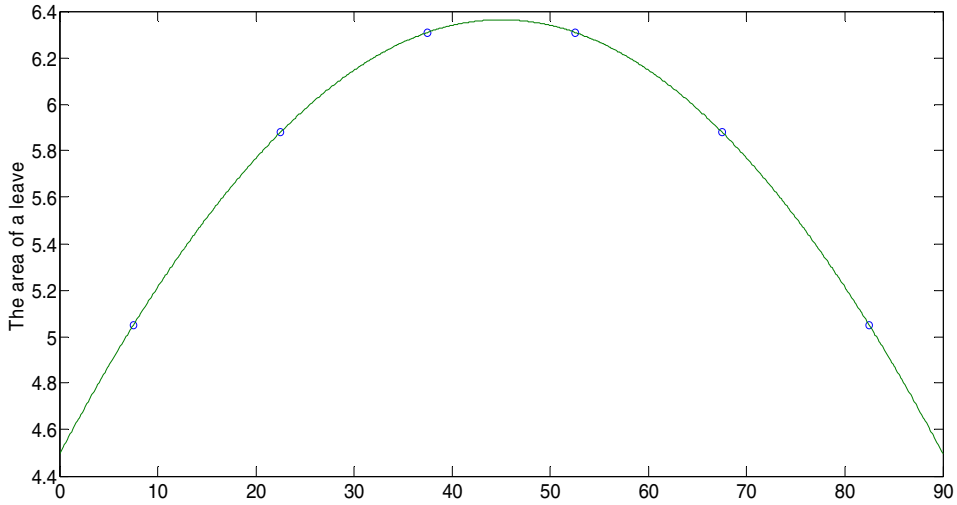

Figure 2. The lighted area a leaf gets in a day is the most

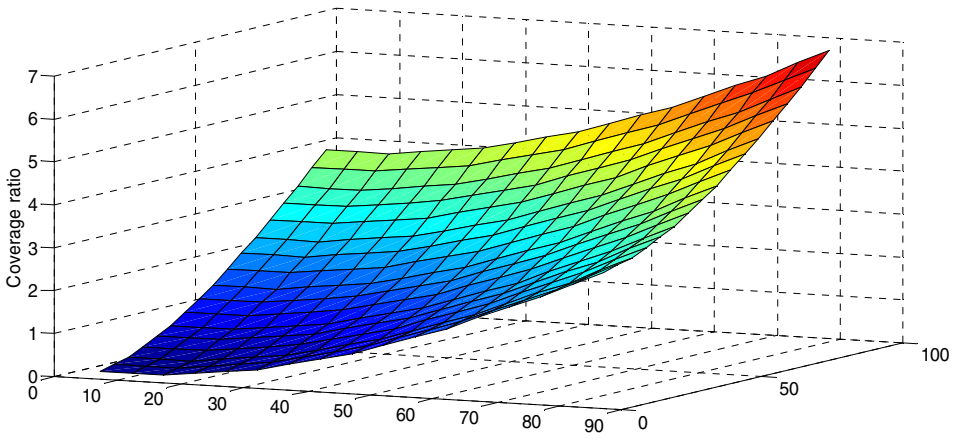

Figure 3. The sunlight coverage ratio of one leaf at different angles

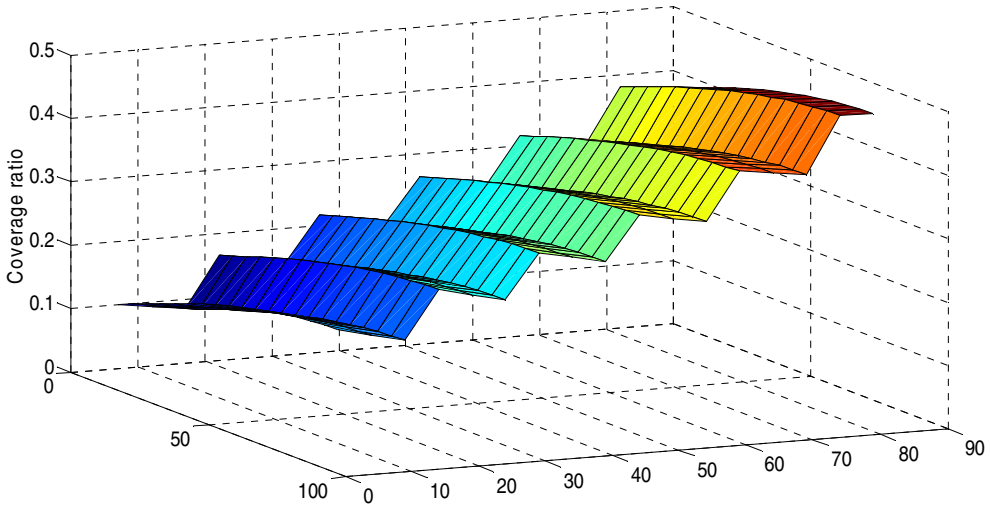

Figure 4. The sunlight coverage ratio in a day at different angles

A Novel Image Encryption Scheme Based on Dynamical Multiple Chaos and Baker Map

XiaoJun Tong , Yang Liu, Miao Zhang
School of Computer Science and Technology, Harbin Institute of Technology, Weihai 264209, China
E-mail: tong_xiaojun@163.com

Zhu Wang
School of Information Science and Technology, Harbin Institute of Technology, Weihai 264209, China

***Abstract*—Chaotic encryption has a series of good characteristics such as sensitivity to initial value, pseudo-random properties and so on. However, the traditional low-dimensional chaotic sequence is truncated because of the limitation of finite precision in computer. Precision degradation has seriously affected the security of encryption. An image encryption scheme based on high-dimensional dynamical multiple chaotic maps is proposed in this paper. In order to produce fast encryption and more avalanche effect, a novel Baker map is utilized to permute the positions of the image pixels in the spatial domain. The experimental results show that it is more efficient than traditional encryption schemes. Compared with simple low-dimensional chaotic system, the proposed scheme does not readily lead to precision degradation and it has passed NIST sp800-22 standards, it provides a secure way for image encryption.**

Keywords- *Image encryption; Dynamical Multiple chaotic; Baker; Bilateral - diffusion*

I. INTRODUCTION

Encryption is to rearrange the message into another form to keep it secret. It is one of core techniques in confidential communication. The requirements to fulfill the security needs of digital images have led to the development of good encryption techniques. In recent years, using chaotic theory to design encryption algorithm is a new research in cryptography, because chaotic systems are characterized by ergodicity, sensitivity depend on initial conditions and random-like behaviors. These properties are of great importance in permutation and substitution process [1]. So encryption algorithms based on chaotic map are widely applied in cryptography frontier. In 1998, Baptista publicly published a paper about chaotic encryption algorithm. Many researches are carried based on this paper, a large number of experiments based on his proposed method started and some improved methods were proposed. At the same time, aimed at finding a safe and efficient image encryption method, many image encryption algorithms based on chaotic map had been extensively studied [2-4]. And chaotic maps are widely used in the algorithms such as Logistic map, Arnold cat map, Baker map, Standard map and Lorenz map [5].

However, the most serious problem in chaotic encryption algorithm is the finite precision effect [6]. Due to the limitation of computer finite precision, the finite precision effect may cause an existing sequence of infinite cycle into a sequence of short period. This will lead to the fact that actual results is very differ to theoretical conclusion; the confidentiality reduced greatly and can not reach adequate security for encryption algorithm. Many scholars put forward their views on the finite precision effect. Tao Yang uses neural network to decrypt low-dimensional chaotic system, some academics have also decrypted simple one-dimensional multiple-chaotic system [7, 8]. So a high-dimensional multiple-chaotic map encryption algorithm is proposed in this paper, which based on Devaney chaotic theory, to improve the security and confidentiality of the chaotic system. [9]

The rest of the paper is organized as follows：Firstly, the proposed image encryption algorithm is described in Section 2, including the production of chaotic sequence by multiple-chaotic maps and the image permutation and substitution. Secondly, experimental results and performance analysis are presented in Section 3. Finally, a conclusion is drawn in the last section.

II. THE PROPOSED ENCRYPTION ALGORITHM

The proposed encryption algorithm includes two parts: firstly, the positions of the original image pixels are permuted by Baker map; secondly, the values of the permuted pixels are encrypted by multiple-chaotic map.

A. Dynamical Multiple Compound chaos algorithm

The dynamical multiple-chaotic sequence that used in this encryption algorithm is generated according to the following rules:

$$\begin{cases} f_0(x_{n-1}) = 2x_{n-1}^2 - 1 \\ f_1(x_{n-1}) = 4x_{n-1}{}^3 - 3x_{n-1} \\ x_n = F(x_{n-1}) = \begin{cases} f_0(x_{n-1}) & , x_{n-1} < 0 \\ f_1(x_{n-1}) & , x_{n-1} \geq 0 \end{cases} \end{cases} \quad (1)$$

where $x \in I = [-1,1]$, mark $f_0(x) = 2x^2 - 1$, $f_1(x) = 4x^3 - 3x$. The system takes $f_0(x) = 2x^2 - 1$ or $f_1(x) = 4x^3 - 3x$ as the generator of the current chaotic random sequence dynamically. whereas the control parameter of $f_0(x)$ is generated by $f_1(x) = 4x^3 - 3x$ .If the result generated by $f(x_{n-1})$ is less than zero, the system takes the output of $f(x_{n-1})$ as the input of $f_0(x)$, while if the result is greater than zero, the system takes the output of $f(x_{n-1})$ as the input of $f_1(x)$.

978-0-7695-4818-0/12 $26.00 © 2012 IEEE
DOI 10.1109/DCABES.2012.94

So this key stream is more random than it just generated by one chaotic map. Formula (1) is passed chaos proof by Devaney's definition of chaos and has good randomness [10, 11].

B. Permutation algorithm of image

Permutation is based on the fact that ordinary image data have strong correlation among adjacent pixels. A large number of image statistical analysis shows that averagely every adjacent 12 pixels are correlative in horizontal, vertical and also diagonal directions. In order to disturb this high correlation, Baker map is used to permute the pixel positions of the original image [12]. Owe to the well property of Baker map, it is widely used in image permutation. A standard definition of Baker map is described by formula (2):

$$\begin{cases} \mathrm{B(x,y)} = (\mathrm{x}/\mathrm{a}, \lambda_{\mathrm{a}}\ \mathrm{y}) & x < \alpha \\ \mathrm{B(x,y)} = ((\mathrm{x}-\mathrm{a})/\beta, (1-\lambda_{\mathrm{b}}) + \lambda_{\mathrm{b}}\ \mathrm{y}) & x \geq \alpha \end{cases} \quad (2)$$

Where $\alpha + \beta = 1$, $\lambda_a + \lambda_b = 1$. (x, y) is the pixel position in the N*N image, and $B(x, y)$ is the transformed position after permutation. The determinate value of the matrix is made to be one, thus the transformation would keep the same area. According to formula (2), Baker map has two typical factors: tension and fold, which bring chaotic movement. The position of pixels is keep changing by repeated Baker map permutation.

To a image , suppose that W is width and L is high . Baker map is described as formula (3):

$$B(x,y) = \begin{cases} (2x, 2y+1) \\ 0 \le x \le \frac{W}{2} - 1, 0 \le y \le \frac{L}{2} - 1 \\ (2x+1, 2y+1-L) \\ 0 \le x \le \frac{W}{2} - 1, \frac{L}{2} - 1 < y \le L - 1 \\ (2W - 2x - 1, 2y) \\ \frac{W}{2} - 1 < x \le W - 1, 0 \le y \le \frac{L}{2} - 1 \\ (2W - 2x - 2, 2y - 1) \\ \frac{W}{2} - 1 < x \le W - 1, \frac{L}{2} - 1 < y \le L - 1 \end{cases} \quad (3)$$

C. Substitution algorithm of image

Chaotic random sequence is generated by multiple-chaotic map given by formula (1), the steps are shown in Fig.1：

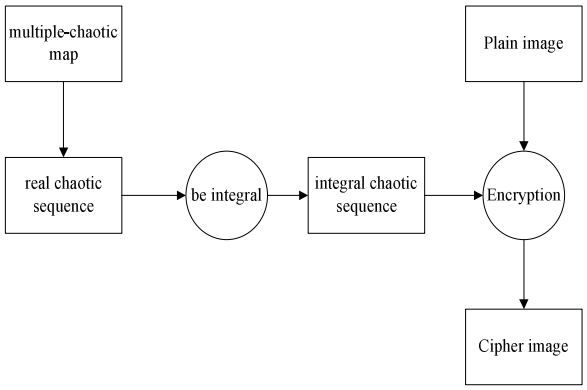

Fig. 1 Multiple-chaotic map encryption

Conduct to be integral is a produce that dividing chaotic domain $[-1,1]$ into N=256 parts sub domain π_i , i=0,1,…,N-1. $\pi_i = [t_i, t_{i+1})(i = 0,1,..., N-2)$, $\pi_{N-1} = [t_{N-1}, t_N]$. Where t_i is described as formula (4):

$$t_i = -\cos(\frac{i}{N}\pi), i = 0,1,..., N-1 \quad (4)$$

Mark the 256 parts sub domain as 0,1,…,255 from left to right and make real chaotic sequence $\{z_k\}_{k=1}^{\infty}$ into integral chaotic sequence $\{S_1(k)\}_{k=1}^{\infty}$ using formula (5), where $S_1(k)$ is described as formula (5):

$$S_1(k) = \begin{cases} \left\lfloor (1 - \arccos(F_k)/\pi) \bullet 256 \right\rfloor, & \text{if } F_k \in [-1,1) \\ 255, & \text{if } F_k = 1 \end{cases} \quad (5)$$

III. EXPERIMENT RESULTS AND SECURITY ANALYSIS

The security analysis of the proposed image encryption is discussed here, such as sensitivity analysis, statistical analysis, sp800-22 testing, and entropy testing and so on to prove that the proposed encryption scheme is secure against the most common attacks [13].

Experimental parameters ： multiple-chaotic map is given by formula (1),Baker map is described as formula (3), the image is "24bit Lena" with size 256×256.

A. Sensitivity analysis

A good encryption algorithm should be sensitive to the secret key and the plaintext [14]. If the algorithm is sensitive to the secret key, and then use another key with only small different for image encryption; the results should be very different. The sensitivity to the secret key can be quantified by correlation coefficient given by formula (6), Where x_j and y_j are the values of two adjacent pixels in the

image and N is total number of image pixels.

$$C_r=\frac{N\sum_{j=1}^{N}(x_j\times y_j)-\sum_{j=1}^{N}x_j\times\sum_{j=1}^{N}y_j}{\sqrt{(N\sum_{j=1}^{N}x_j^2-(\sum_{j=1}^{N}x_j)^2)\times(N\sum_{j=1}^{N}y_j^2-(\sum_{j=1}^{N}y_j)^2)}} \quad (6)$$

Two key pairs KEY1=0.27589136510264, and KEY2=0.27589136510265 which have only 10^{-14} different are chosen. The experimental results in Table 1 show that the proposed scheme is sensitive to the secret key.

Table 1 sensitivity of secret key

Testing Content			Testing Results
Sensitivity of cipher to key（difference level of key is 10^{-14}）			6.478121e-004
Sensitivity of cipher to plaintext testing（plaintext change 1 bit）	NPCR	Blue component	0.99513244
		Green component	0.99501037
		Red component	0.99501037
	UACI	Blue component	0.33441963
		Green component	0.33439768
		Red component	0.33585026
	Avalanche effect		0.49684923

B. Statistical analysis

Many cipher texts have been successfully analyzed with the help of statistical analysis and an ideal cipher text should be robust against any statistical attack. The experimental results that are shown in histograms have proved the robustness of the proposed image encryption scheme.

An image-histogram illustrates how pixels in an image are distributed by graphing the number of pixels at each color intensity level. Using the image “Lena” with size 256×256, the histograms are shown in Fig.2.

(a) Plain text

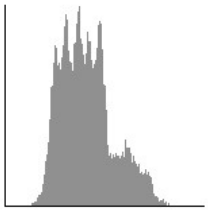

(b) Blue component

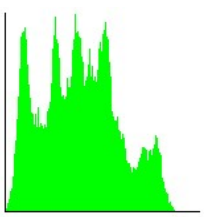

(c) Green component

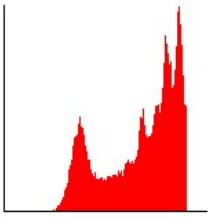

(d) Red component

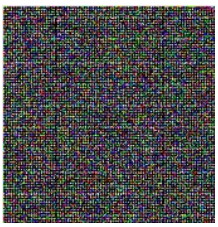

(e) Cipher text

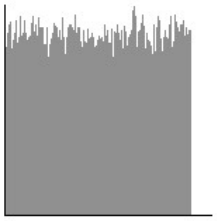

(f) Blue component

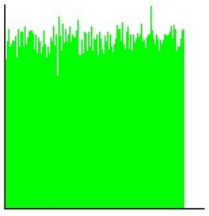

(g) Green component

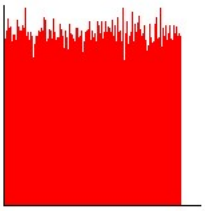

(h) Red component

Fig.2 Statistical analysis tests

Correlation coefficient could be gained via formula (6). For an ordinary image, each pixel is usually highly correlated with its adjacent pixels either in horizontal, vertical. This property can be quantified as the correlation coefficient for comparison. In order to compute correlation coefficient, the following procedure is carried out: randomly select 1000 pairs of two adjacent (in horizontal, vertical) pixels from an image, then calculate the correlation coefficient of each pair via formula (6). Correlation coefficient of two adjacent pixels in original and encrypted images is shown in table 2.

Table 2 Correlation coefficient

Direction	Horizontal	Vertical
Plain text the first dimensional	0.9080049847	0.9483989149
Plain text the second dimensional	0.9472608203	0.9733051021
Plain text the third dimensional	0.9487292891	0.9734415817
Cipher text the first dimensional	0.0076856231	0.0146355078
Cipher text the second dimensional	0.0128994115	0.0038638383
Cipher text the third dimensional	0.0129194833	0.0129927796

Table 2 shows that the two adjacent pixels of an ordinary image are highly correlated, whereas the pixel of cipher image is little correlated with its adjacent pixels.

These correlation analyses prove that the proposed encryption technique satisfied zero co-correlation.

C. Sp800-22 Testing

Key stream and cipher text have successfully passed NIST sp800-22 Testing, show as table 3 and table 4.

Table 3 SP800-22 Testing for key stream

Statistical test		P-value	Result
Frequency		0.714365	Success
Block frequency （m=128）		0.535645	Success
Runs		0.788802	Success
Long runs of ones (M=10000,N=100)		0.779335	Success
Binary Matrix Rank		0.513760	Success
Spectral DFT		0.381032	Success
No overlapping templates （m=9 B=101001100）		0.274010	Success
Overlapping templates （ m=9 ，M=1032，N=968）		0.320457	Success
Universal （ L=7 ， Q=1280 ，K=141577）		0.233111	Success
Lempel ziv complexity		0.712487	Success
Linear complexity （M=1000）		0.063098	Success
Serial	P-value1	0.902226	Success
	P-value2	0.788699	Success
Approximate entropy （m=10）		0.377541	Success
Cumulative sums	Forward	0.986241	Success
	Reverse	0.733656	Success
Random excursions	x = -1	0.473722	Success
Random excursions variant	x = -1	0.255064	Success

Table 4 SP800-22 Testing for cipher text

Statistical test		P-value	Result
Frequency		0.197746	Success
Block frequency （m=128）		0.086322	Success
Runs		0.782286	Success
Long runs of ones (M=10000,N=100)		0.456772	Success
Binary Matrix Rank		0.149383	Success
Spectral DFT		0.881361	Success
No overlapping templates （m=9 B=101001100）		0.914747	Success
Overlapping templates （ m=9 ，M=1032，N=968）		0.799101	Success
Universal （ L=7 ， Q=1280 ，K=141577）		0.910857	Success
Lempel ziv complexity		0.628152	Success
Linear complexity （M=1000）		0.765961	Success
Serial	0.419508	Success	Success
	0.779478	Success	Success
Approximate entropy （m=10）		0.766167	Success
Cumulative sums	0.100695	Success	Success
	0.208323	Success	Success
Random excursions	0.140347	Success	Success
Random excursions variant	0.409574	Success	Success

D. Entropy Testing

Message entropy formula is as follows:

$$H(S) = \sum_{S} P(s_i) \log_2 \frac{1}{P(s_i)} bits \qquad (7)$$

where $P(s_i)$ indicates that the probability of each symbol appearance. A statistical unit is 8 bytes, if the probability of every symbol in accordance with uniform distribution would be 1/8, so the entropy should be 8. But because of actually the probability is not in the same, a good encryption algorithm should make the entropy to 8 as close as possible. The entropy of experimental results is 7.9991079128248206.

E. Compare of encryption speed

The results of each encryption scheme are shown in table 5.

Table 5 encryption speed of each scheme

Image for encryption	DES encryption time (unit: s)	Multiple-chaotic map encryption time
House 8 bits	0.78714529360575158	0.26401996484973417
Lena 24 bits	4.7489820633628019	0.79646979050817512
Lena 8 bits	1.5772688987008125	0.27734989802663523

Compared with DES encryption scheme, dynamical multiple-chaotic encryption scheme has more quickly than traditional encryption methods. Meanwhile, the probability of precision degradation is lower than simple-chaotic map encryption scheme.

IV. CONCLUSIONS

In the paper, a fast image encryption scheme is proposed which utilizes dynamical multiple-chaotic map confuse the relationship between the cipher image and the plain image. Baker map is used to permute the positions of image pixels in the spatial-domain and the mixing of confusion and diffusion can produces more randomness. The experimental results demonstrate that the proposed image encryption technique has advantages of high-level security, such as high robust against statistic attacks and the precision of cipher be sensitive to the secret key approach to 10^{-14}. At the same time, the probability of precision degradation is lower than simple-chaotic map encryption scheme and has high encryption than other famous encryption methods.

ACKNOWLEDGMENT

This work was supported by the National Natural Science Foundation of China (Grant No. 60973162), the Science and technology of Shandong Province (Grant No.2012GGX10110), Science and technology of Shandong Province of China (Grant No.2010GGX10132), the Scientific Research Foundation of Harbin Institute of Technology at Weihai (Grant No. HIT(WH) ZB200909), and the Key Natural Science Foundation of Shandong Province of China (Grant No. Z2006G01).

REFERENCES

[1] L. Zhang, X. Liao and X. Wang. “An image encryption approach based on chaotic maps”. Chaos, Solitons & Fractals. 2005(24):759-765.

[2] Li CQ, Lo KT. Optimal quantitative cryptanalysis of permutation-only multimedia ciphers against plaintext attacks[J], Signal Process, 2011, 91(9):49–54.

[3] Y. Wang, K.-W. Wong, X. Liao, G. Chen, A new chaos-based fast image encryption algorithm[J], Applied Soft Computing. 2011(11):514–522.

[4] Solak E, Yildiz OT, Biyikog_lu T. Cryptanalysis of Fridrich’s chaotic image encryption[J], Bifurcat Chaos, 2010,20(5): 05–13

[5] C. Fu, Z. C. Zhang, and Y. Y. Cao, “An Improved Image Encryption Algorithm Based on Chaotic Maps”, IEEE Proceedings of the third International Conference on Natural Computation (ICNC 2007), Haikou, China, v3:189-193

[6] H. Kwok, W. Tang, “A fast image encryption system based on chaotic map with finite precision representation”. Chaos, Solitons & Fractals, 2007, 32:1518-1529

[7] J. C. Chen, J. I. Guo, “A new chaotic key based design for image encryption and decryption”. Proceedings of the IEEE International Symposium Circuits and Systems, 2000(4):49-52

[8] J. Wei, X. F. Liao, K.W. Wong, X. Tao. “A new Chaotic Cryptosystem”. Chaos, Solutions & Fractals. 2006,30:1143-1152

[9] T. Xiang, X. F. Liao, G. Tang, Y. Chen, K. W. Wong, “A novel block cryptosystem based on iterating a chaotic map”. Phys. Lett. A 2006(349):109-115

[10] X.J. Tong, M. Cui .Image encryption with compound chaotic sequence cipher shifting dynamically. Image and vision computing, 26(6) (2008) 843-850.

[11] X.J. Tong, M. Cui . Image encryption scheme based on 3D baker with dynamical compound chaotic sequence cipher generator, Signal Processing , 2009，89(4) 480-491

[12] D. Xiao, X. F. Liao, P. C. Wei, “Analysis and improvement of a chaos-based image encryption algorithm”. Chaos, Solitons & Fractals, 2009, 40(5):2191-2199

[13] N. K. Pareek, V. Patidar, K. K. Sud. “Image Encryption using Chaotic Logistic Map”. Image and Vision Computing.2006, 24(5):926-934

[14] G. Alvarez, F. Montoya, M. Romera, G. Pastor. “Key stream Cryptanalysis of a Chaotic Cryptographic Method”. Computer Physics communications. 2004,156:205-207

Memory Confidentiality and Integrity Protection Method based on Variable Length Counter

Ma Haifeng [1,2], Yao Nianmin[1], Cai Shaobin[1], Han Qilong[1]

[1]Computer Science and Technology Institute
Harbin Engineering University
Harbin, China
mahaifeng@hrbeu.edu.cn

[2]Computer and Information Engineering Institute
Heilongjiang Institute of Science and Technology
Harbin, China

***Abstract*—Focusing on the problem of high overhead and frequent overflow of counter mode encryption, this paper proposed an efficient scheme to protect data confidentiality and integrity. Based on the locality character of data accessing, the scheme set different counter length for memory area according to different accessing frequency and the counter length can be dynamic adjusted. The analysis and the simulation results indicated that compared with the counter mode encryption, the scheme can decrease memory space overhead and the number of overflow. The proposed scheme can be applied to other schemes of protecting confidentiality and integrity based on counters and can satisfy performance requirement for most applications.**

Keywords-counter mode encryption; confidentiality; integrity

I. INTRODUCTION

Recently, the attack behaviors that aim at computer system emerge frequently. The storage systems become the main target because of its large number of user data. On critical computing platforms, attackers who have enough accessibility to the system can break security measures in any imaginable way such as using customized hardware. Specifically, in order to get the protected information, attackers may dump all the transactions of data on the system buses and then construct the customized spoofing devices or hardware and replay the data got from the bus. Software or even light weight hardware based protection cannot resist this kind of physical attacks.

Realizing these threats, researchers have proposed many secure architectures for uniprocessor [1-7] and multiprocessor [8-12]. These secure architectures rely on the tamper-resistant processors and certain cryptographic hardware (Trust computer base, TCB) for supporting a tamper-resistant and tamper-evident (TE) computing environment [13]. Realizing integrity verification for untrusted storage needs utilizing the un-tampered information stored in TCB. Although many security architectures have been proposed, these schemes either have inadequate security protection or have high performance overheads. The Merkle tree scheme [1] causes severe performance degradation on runtime. The log hash scheme [1] employs lazy authentication in which a program is authenticated only a few times during its execution. The CHTree scheme [2] improves runtime performance at the cost of cache space. The Authenticated Speculative Execution proposed [3] employs timely authentication, but requires extensive modifications to the memory controller and on-chip caches. Reference [14] proposes a prediction ciphertext scheme, which save the data and encrypted data of the most recently used on chip.

Our security model was presented in Section 2. The architecture of our scheme was described in Section 3. The overhead and performance analysis were discussed in section 4. We evaluated the scheme in section 5 and concluded the paper in Section 6.

II. SECURE COMPUTING MODEL

In this paper, the systems were built around a single processor with external memory and peripherals. The multi-processors platform would not be discussed here. Figure 1 illustrates the secure computing model we discussed. The model comprises a tamper-resistant processor (TCB, trusted computing base), external memory and peripherals.

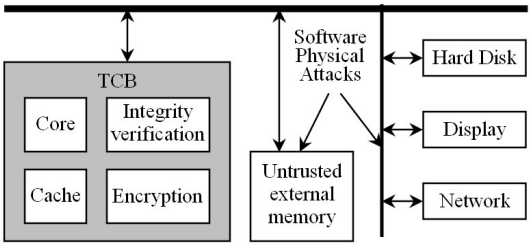

Figure 1. Secure Computing Model

The TCB consists of the processor core, on-chip cache, encryption and integrity verification mechanism. The processor's core is assumed trusted, which means that the processor is invulnerable to physical attacks and its internal state can't be tampered or observed. The processor can contain a secret data that allows it to produce keys to perform cryptographic operations such as signing [15]. The secret data can be a private key from a public key pair, as described in XOM [1]. The processor is used in a multitasking environment, which uses virtual memory and runs mutually mistrusting processes. Once a program executes some special instructions to enter the security executing environment, TCB is responsible for the

978-0-7695-4818-0/12 $26.00 © 2012 IEEE
DOI 10.1109/DCABES.2012.55

protection of the program. The TCB or the processor needs to detect that whether memory operations are normally executed or not.

The off-chip memory, the system bus and peripheral devices are untrusted. Their states can be observed and tampered by an adversary. The target of an adversary is to tamper with the contents of external memory in such a way that the system produces an incorrect result while looks correct to the system user. To make it simple, the untrusted memory in this paper only means the RAM, although in fact, the scheme presented here can be applied to other data storage devices such as hard disks only with a little change.

The adversary can attack off-chip memory and the processor needs to check that whether the content got from memory is right. If the data read from an address in main memory is the same as the value that recently stored, we deem that the memory is safe so far. If the contents of the on-chip memory have been tampered by an adversary, the memory may not behave correctly. If such tampering has occurred, the scheme we proposed allows the processor to detect with high probability. If tampering is detected, the processor will raise an integrity exception.

III. METHOD DESCRIPTION

Focusing on the problem of high counter memory overhead and frequent overflow of counter mode encryption, we propose MCIPIC (memory confidentiality and integrity protection based on inequality counter) scheme.

A. The principle of MCIPIC

The MCIPIC is the improvement of counter mode encryption, which dynamically adjusts counter length base on memory write frequency. To realize MCIPIC through processes: initialization, data block encryption/decryption and data page migration. To facilitate the description, cache block size is the same as memory block size.

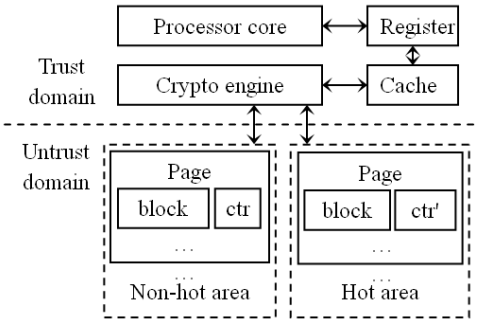

Figure 2. MCIPIC principle

1) Initialization: The principle of MCIPIC is shown in figure 2. The upper part is the processor (Trust domain) that includes crypto engine, cache and registers. The under part is the memory (Untrust domain). In initialization, the memory was divided into two regions: Hot area (hot area) and Non-hot area (non-hot area). The hot area saved the data blocks that write frequency exceed a certain threshold. The hot area is empty in initialization. Both hot area and non-hot area contain many pages and they have different key. We set an local counter for each page. The hot area has shorter counter size and the non-hot area has longer counter size. The corresponding counter value is increased by 1(or proper size) when a block of one page write once. In addition, we add a structure for calculating write back frequent for each page and set an immigration threshold.

2) Data block encryption and decryption: When a new generated cache line writes back to memory, it will be write to non-hot area. When a modified block writes back, it will be write to it's orginal area. Writing back to non-hot area and non-hot area basically has same steps, the different is counter length. The writing process is: at first, counter value is increased by 1, and it concatenates cache address to generate encryption seed. And then the cache line is encrypted with the seed and key. At last, the encrypted cache line and corresponding counter write to corresponding area of memory. The reading process is: at first, the encrypted data block and its counter value are read to on-chip memory. And then counter value concatenates block address and counter value to generate decryption seed. At last the cache line is decrypted with the seed and key to obtain plaintext.

- For an L2 cache write-back
  write-back-block (addr, B)
  (1) Increment Timer.counter = $\text{Timer}_{\text{non-hot}}$
  (2) For each $0 \le i \le 3$
  $\text{OTP}[i]=\text{AES}_{\text{non-hot-key}}(\text{counter}+i,\ \text{addr})$
  $\text{EB}[i]=\text{B}[i] \oplus \text{OTP}[i]$
  3) Write counter and EB to the Non-hot area
- For an L2 cache miss
  read-block (addr, EB)
  1) Read counter from the Non-hot area
  2) For each $0 \le i \le 3$
  $\text{OTP}[i]=\text{AES}_{\text{non-hot-key}}(\text{counter}+i,\ \text{addr})$
  $\text{B}[i]=\text{EB}[i] \oplus \text{OTP}[i]$

Take non-hot area as the example, we gave algorithms of reading and writing block. In description, **addr** is cache address, **non-hot-key** is non-hot area key, $\textbf{Timer}_{\textbf{non-hot}}$ is a counter of hot area, **B** is a plaintext compose of B[0], B[1], B[2] and B[3], **EB** is a ciphertext compose of EB[0], EB[1], EB[2] and EB[3].

3) Data page migration: Data page migration has two processes: immigration and emigration. Immigration will be carried out when the write back frequency of one page in non-hot area reach the threshold. The steps are: at first, the page is read to cache, and data blocks of the page are decrypted with non-hot-key. New longer counters are generated for each block by $\text{Timer}_{\text{hot}}$. The blocks are encrypted with hot-key, new counters and block address. At last, the update page mirrored to the hot-area. If the hot area is full, we choose a page of the lowest write frequent to emigrate and then mirror the page to the hot-area. The emigration steps are similar with immigration.

The algorithms of data page immigration and emigration is followed. In description, Psize is the page size, Bsize is block size, $counter_i$ is the counter of *i*-th block, $addr_i$ is the address of *i*-th block，OTP_i is the pad of *i*-th block，EB_i is the *i*-th ciphertext block，B_i is the *i*-th plaintext block.

- For an page of write-back frequency reach threshold

  Page-immigration (addr, B)

  (1)For each $0 \le i \le$ (Psize/Bsize)

  1) Read $counter_i$ and EB_i from the Non-hot area

  2) For each $0 \le j \le 3$

  $OTP_i[j]=AES_{non\text{-}hot\text{-}key}(counter_i+j，addr_i)$

  $B_i[j]=EB_i[j] \oplus OTP_i[j]$

  3)Increment $Timer.counter=Timer_{hot}$

  4) For each $0 \le j \le 3$

  $OTP_i[j]=AES_{hot\text{-}key}(counter+j，addr_i)$

  $EB_i[j]=B_i[j] \oplus OTP_i[j]$

  (2) Mirror the page to the Hot area

- For an page of the lowest write-back frequency

  Page-emigration (addr, B)

  (1)For each $0 \le i \le$ (Psize/Bsize)

  1) Read $counter_i$ and EB_i from the Hot area

  2) For each $0 \le j \le 3$

  $OTP_i[j]=AES_{hot\text{-}key}(counter_i+j，addr_i)$

  $B_i[j]=EB_i[j] \oplus OTP_i[j]$

  3)Increment $Timer.counter_i=Timer_{non\text{-}hot}$

  4) For each $0 \le j \le 3$

  $OTP_i[j]=AES_{non\text{-}hot\text{-}key}(counter_i+j，addr_i)$

  $EB_i[j]=B_i[j] \oplus OTP_i[j]$

  (2) Mirror the page to the Non-hot area

Compared with counter mode, the MCIPIC has two advantages. First, the MCIPIC decreased storage overhead of saving counters. The reason is the counter length of hot area is longer, but the ratio of hot area is very small. In the meanwhile, the counter length of non-hot area is shorter, but the ratio of hot area is very big. Second, the MCIPIC reduce the number of counter overflow. The motivation is the character of program locality. In run time, most of access requests focus on hot area, so the counter values in hot area increased very quickly. However, the counter is very long, so it is difficult to overflow. For non-hot area, the access number of data block is smaller. Therefore, the counter is difficult to overflow although counter length is short.

B. Storage gain analysis

Next we analyses the storage performance of the MCIPIC, the comparison object is counter mode encryption. The parameters are: total block number is *N*, the hot area ratio is α, the counter length of hot area is L_h, the counter length of non-hot area is L_c. The parameters value are: L_n =16 *bits*， L =512 *bits*， L_c =64 *bits*. The storage overhead of MCIPIC is：

$$Cost = \alpha N \times (L_h + L) + N(1-\alpha) \times (L_n + L) \quad \ldots(1)$$

The storage overhead of the counter mode is:

$$Cost' = N \times (L_c + L) \quad \ldots(2)$$

The storage gain rate of MCIPIC relative to counter mode is:

$$\beta = (Cost' - Cost) / Cost' \quad \ldots(3)$$

(1) and (2) substitute to (3) and simplify, the storage gain is:

$$\beta = \frac{8 - (L_h - 2)\alpha}{72} \quad \ldots(4)$$

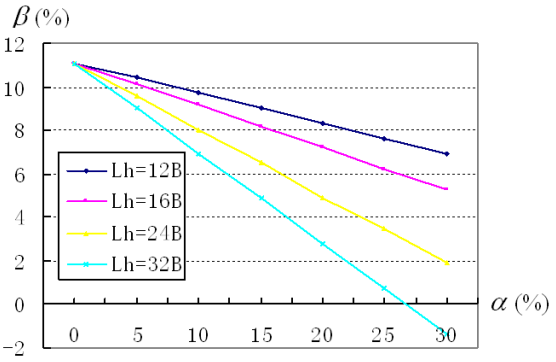

Figure 3. Storage gain of MCIPIC

We set L_h is 12B, 16B, 24B, 32B separately. The storage gain is shown in figure 3, the horizontal coordinate is the ratio of hot area, and the vertical coordinate is the storage gain rate. When L_h is constant, the gain rate is inversely proportional to the hot area ratio. The reason is that the counter length in hot area is longer which led to the storage overhead also increase. When α is constant, the gain rate reach the maximum when L_h is minimum, and the gain rate decreased along with L_h increased. When the counter length exceeds certain degree, the gain rate is negative.

IV. SIMULATIONS

A. Simulation Framework

Our simulation framework is evaluated by using modified SimpleScalar simulator [17] which models speculative out-of-order execution and is configured to execute X86 binaries. The modified simulator supports the counter mode and MCIPIC. The key architectural parameters used in the simulations are shown in Table 1.

Simulation used six SPEC2000 [18] CPU benchmarks as representative applications: vortex, vpr, art, parser, mcf and gzip. To capture the characteristics in the middle of computation, each benchmark is simulated for 100 million instructions after skipping the first 1 billion instructions. Performance parameter base on IPC (Instruction Per Cycle).

TABLE I. ARCHITECTURAL PARAMETERS USED IN SIMULATIONS

Parameters	Values
Clock frequency	2Hz
L1 I-caches	64K,2-way,32B line
L1 D-caches	64K,2-way,32B line
L2 caches	Unified,1MB,2-way,64B line
L1 latency	2 cycles
L2 latency	10 cycles
Memory latency	80 cycles, 10cycles
Memory size	2G
Memory bus	200MHz, 8B wide (1.6G)/s
AES latency	40 cycles
AES throughput	3.2G/s
Hash latency	80 cycles
Hash throughput	3.2G/s
Hash buffer	32
Hash length	128 bits

B. *Encryption mode performance evaluation*

At first, we evaluate the MCIPIC performance in condition no overflow happened. The comparison object is **counter mode** and direct encryption mode (**Direct**). The evaluation benchmark is memory mechanism of no encryption (**Baseline**). The counter length is: 32 *bits* in counter mode, 8 *bits* in non-hot area of MCIPIC, 64 *bits* in hot area of MCIPIC. The ratio of hot area is 10% and of non-hot area is 90%. Both MCIPIC and counter mode have on-chip counter cache (seq cache), both counter size are set for 64K. For convenience of simulation, the hot area and non-hot area of MCIPIC use a global counter separately.

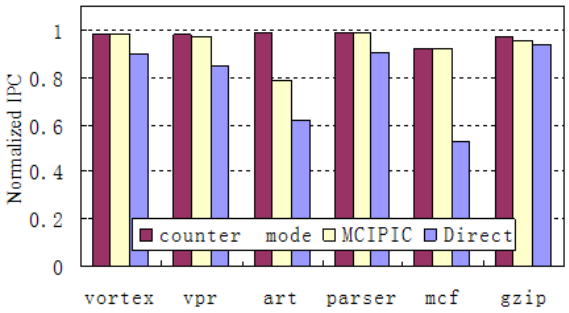

Figure 4. The overhead of counter mode encryption, MCIPIC and direct encryption

Figure 4 compares **MCIPIC**, **counter mode** and **Direct**. The IPC of each benchmark is normalized by the baseline IPC. As shown in figure, all schemes decrease system performance because of access counter will increase bandwidth overhead and encryption latency. However, the performance decrease degree is different. The encryption mode has performance decrease as much as 47% (mcf) in worst case and 20.9% in average. The MCIPIC has performance decrease as much as 21% (art) in worst case and 6.1% in average. The counter mode has performance decrease as much as 8%（mcf）in worst case and 2.8% in average. The reason is direct encrypt delays in critical path which decrease performance. Both counter mode and MCIPIC have seq cache to save part counters. In most cases, needed counter can be found in seq cache. Therefore, read data blocks and AES encryption can be parallel processing [16] which hide the decryption latency.

Compare with counter mode, MCIPIC performance is constant or decreased slightly. The reason is MCIPIC add migration and immigration operations, they all need AES encryption. However, basing on local principle, the number of s migration and immigration decreased obviously after the program running becomes stable.

C. *Overflow Performance evaluation*

In this section we evaluate the performance when counter overflow happened. Benchmark program based on gzip. We assumed that counter has been generated and AES encryption has been finished before cacheline generated. The counter length is: 22 *bits* in counter mode, 24 *bits* in hot area of MCIPIC and 20 *bits* in non-hot area of MCIPIC. The hot area and non-hot area use a global counter separately.

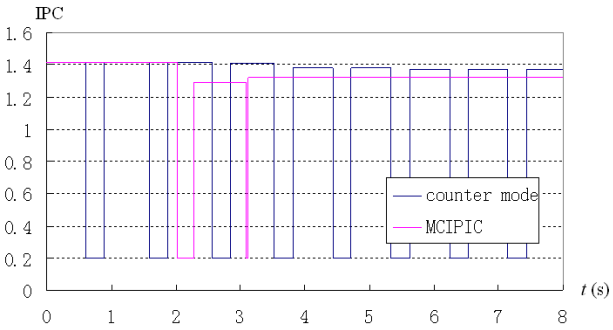

Figure 5. The performance compare of MCIPIC and counter mode

Simulation result is show in figure 5, in a range of time (8s), the counter mode overflow eight times while MCIPIC only overflow two times. The reason is: for the non-hot area, its write frequent is so low that the overflow time is longer than counter mode even though the counter length is shorter. For the hot area, the counter length is so long that the overflow time of hot area is longer than counter mode even though the write frequency of hot area is very high. Furthermore, when overflow happened, the counter mode needs re-encrypt all the memory that needs protecting which led very high space and time overhead. However, the MCIPIC only needs re-encrypt hot area or non-hot area. Therefore, in the case, the MCIPIC has lower computation overhead than counter mode.

From above simulations we know that the performance of MCIPIC and counter mode is very close. The MCIPIC has less overflow times and lower encryption overhead.

V. CONCLUSION

This paper proposed MCIPIC, an improved method of counter mode. Mathematical analysis and simulations indicated that the MCIPIC has lower space overhead and less overflow times than counter mode. Therefore, we can say the MCIPIC is an efficiency integrity and confidentiality protection method. The future of work is research the application of MCIPIC on multi-processor platform.

ACKNOWLEDGMENT

This work is supported by the National Natural Science Foundation of China under Grant No. 61073047; Fundamental Research Funds for the Central Universities: HEUCFT1007, HEUCF100607, HEUCFT1202, Harbin Special funds for Technological Innovation Talents:2012RFLXG023.

REFERENCES

[1] Suh, D. Clarke, B. Gassend, M. van Dijk, and S. Devadas. Efficient memory integrity verification and encryption for secure processors. The 36th International Symposium on Microarchitecture, pp. 339-350, 2003.

[2] B. Gassend, G. Suh, D. Clarke, M. Dijk, and S. Devadas. Caches and Hash Trees for Efficient Memory Integrity Verification. In Proc of the 9th International Symposium on High Performance Computer Architecture (HPCA-9), 2003.

[3] W. Shi, H.-H. Lee, M. Ghosh, and C. Lu. Architectural Support for High Speed Protection of Memory Integrity and Confidentiality in Multiprocessor Systems. In Proceedings of the International Conference on Parallel Architectures and Compilation Techniques, pages 123–134, September 2004.

[4] W. Shi, H.-H. Lee, M. Ghosh, C. Lu, and A. Boldyreva. High Efficiency Counter Mode Security Architecture via Prediction and Precomputation. In Proceedings of the 32nd International Symposium on Computer Architecture, June 2005.

[5] R. B. Lee, P. C. Kwan, J. P. McGregor, J. Dwoskin, and Z. Wang. Architecture for Protecting Critical Secrets in Microporcessors. In Proc.of the International Symposium on Computer Architecture, 2005.

[6] C. Yan, B. Rogers, D. Englender, Y. Solihin, and M. Prvulovic. Improving cost, performance, and security of memory encryption and authentication. In Proc. of the International Symposium on Computer Architecture, 2006.

[7] Elbaz, R., Champagne, D., Lee, R.B., Torres, L., Sassatelli, G., Guillemin, P. TEC-Tree: A Low Cost and Parallelizable Tree for Efficient Defense against Memory Replay Attacks. In: Cryptographic Hardware and embedded systems (CHES), pp. 289–302 (2007)

[8] R. Huang, D. Y. Den, and G. E. Suh. Orthrus: Efficient software integrity protection on multi-cores. In Proceedings of the 15th International Conference on Architectural Support for Programming Languages and Operating Systems, pages 371–383, Pittsburgh, PA, March 2010.

[9] Y. Zhang, L. Gao, J. Yang, X. Zhang, and R. Gupta. SENSS: Security Enhancement to Symmetric Shared Memory Multiprocessors. In International Symposium on High-Performance Computer Architecture, February 2005.

[10] M. Lee, M. Ahn, and E. Kim. I2SEMS: Interconnects-Independent Security Enhanced Shared Memory Multiprocessor Systems. In Proc.of the International Conference on Parallel Architectures and Compilation Techniques, 2007.

[11] B. Rogers, Y. Solihin, and M. Prvulovic. Efficient data protection for distributed shared memory multiprocessors. In International Conference on Parallel Architectures and Compilation Techniques, 2006.

[12] Brian Rogers, Chenyu Yan, Siddhartha Chhabra, Single-Level Integrity and Confidentiality Protection for Distributed Shared Memory Multiprocessors. In Proc.of the International Symposium on Computer Architecture, 2008.

[13] G. E. Suh, D. Clarke, B. Gassend, M. van Dijk, and S. Devadas. aegis: Architecture for tamper-evident and tamper-resistant processing. In Proceedings of the 17th Int'l Conference on Supercomputing, June 2003.

[14] W. Shi and H.-H. Lee. Accelerating memory decryption and authentication with frequent value prediction. In Proceedings of the 4th International Conference on Computing Frontiers (CF), pages 35–45, May 2007.

[15] ROGERS, B., CHHABRA S., SOLIHIN, Y. AND PRVULOVIC. Using address independent seed encryption and bonsai merkle trees to make secure processors os and performance friendly In Proceedings of the 40th International Symposium on Microarchitecture. IEEE Computer Society, Los Alamitos, CA, 183–196. 2007

[16] N. I. of Science and Technology. FIPS PUB 197: Advanced Encryption Standard (AES), November 2001.

[17] Todd Austin, Eric Larson, and Dan Ernst. SimpleScalar: An Infrastructure for Computer System Modeling. Computer, 35(2):59–67, 2002

[18] A. KleinOsowski, J. Flynn, N. Meares, and D. Lilja. Adapting the spec 2000 benchmark suite for simulation-based computer architecture research. In Proceedings of the International Conference on Computer Design, September 2000.

Preventing ARP Spoofing Attacks through Gratuitous Decision Packet

Haider Salim, Zhitang Li, Hao Tu, Zhengbiao Guo
Department of Computer Science and Technology, Network Center
Huazhong University of Science and Technology
430074 Wuhan, China
{hideriraq, leeying, tuhao, zbguo}@mail.hust.edu.cn

***Abstract*—Owing to its great need for mapping an IP address to the corresponding MAC address over an Ethernet topology, Address Resolution Protocol (ARP) has been, and still is, capable of accomplishing this task efficiently. At the same time, it suffers from some security shortcomings; because of the malicious hosts have the possibility of poisoning the ARP cache for another host on the same LAN. In this paper, by gratuitous ARP request packets, we propose a solution to the problem of ARP poisoning. Our suggested mechanism which is named a Gratuitous Decision Packet System (GDPS) seeks to achieve two main goals: (1) Detection of suspicious ARP packets, by implementing a real-time analyzing for received ARP packets. (2) The distinction between a legitimate and malicious host through sending a modified request packet of the gratuitous ARP packets. Furthermore, the experiments show that the presented design has the efficiency and accuracy, as well as it does not require any additional software or hardware.**

Keywords-ARP Cash Poisoning, Man-In-The-Middle attack, Network Security

I. INTRODUCTION

Through Address Resolution Protocol [1] a host or the getaway router must send an ARP request packet, if he wants to discover the physical addresses which well-known a Media Access Control (MAC) of another host on its network. Any ARP request packet contains the sender MAC address and the source-target IP addresses. The request packet is broadcast over the network, and then all hosts on the network should deal with this packet. However, only the intended host can distinguish its IP address and sends back an ARP reply packet. A reply packet contains the IP, MAC of destination host (inquirer host) and his IP, MAC addresses; this packet must be sent directly in unicast mode through a destination MAC address to the inquirer host. Alternatively, the IP address and corresponding MAC will be kept in a table called the ARP cache. Despite the widely applied to the ARP specifications to map IP addresses to the physical addressees in different Ethernet technologies, there is a real hazard threatens information security in these kinds of telecommunications and information transmission systems. That risk cannot be avoided as long as the ARP is still suffering from some kind of insecurity. A malicious host on the network can easily handle ARP cache table. Since there is no authentication to specify the sender host.

On the other hand, any malicious user may modify (poisoning) the ARP caches for alive hosts (overwrites on the existing entry or adds an entry if one does not exist), through mapping the victim IP with attacker MAC (IP_{victim}, $MAC_{attacker}$).

Therefore, an attacker could easily of impersonating another host who leads to launch of a Man-In-The-Middle attack (MITM). The MITM attack can be performed between the attacker and any host. Furthermore, the attacker could organize an attack between the host and a default gateway on its network, other important types of attacks, which occur as a result of ARP cash poisoning are denial of service (DoS) attacks [2].

Motivated by the aforementioned challenges, we propose a solution to the ARP weakness problem. Our design is a practical method to defend against ARP poisoning attacks, by monitoring ARP packets and diagnostic every abnormal ARP packet. Nonetheless, we concentrate on communication mapping of ARP that allows being a technique in order to differentiate between a genuine host and attacker host. In this paper, we develop a rigorous algorithm named Gratuitous Decision Packet System GDPS that can be used to protect any host from attacks of ARP spoofing performed by a malicious host. The GDPS method is a feasible solution because it could be as software installed on the host to being protected. The GDPS must accomplish two processes are as follows:

- The GDPS implements a real-time traffic analysis to ARP packets for the host who we plan to protect it. This mechanism can deal with the suspects of the ARP packets, which are sent from a malicious user on the same LAN.
- If we received abnormal ARP packet, the GDPS considers this ARP packet to be solicited to send GDP packet, which represent a modified ARP packet; the GDP packet headers will be elaborated shortly.

We consider this manner is capable of provide protection against variety ARP poisoning attacks scenarios; moreover, it does not need another software or hardware. On the other hand, the proposed approach is characterized with resilience, since the GDPS algorithm can be applied and work on any host. Therefore, it backward compatible to communicate with the standards of current ARP, as well as, it is not costly and easy to implement. Our contribution is to prove that the gratuitous ARP request packet could be used to distinguish between a victim and attacker MAC address without the need for additional hardware or software, then, submitting an overview on the attacks as a result of the ARP weakness. We have been made the several experiments to evaluate the proposed scheme.

The remainder of the paper is organized as follows: Section II provides the potential types of ARP attacks. In section III, We discuss related works in this area, which have been proposed to manipulate the ARP spoofing attacks. We will describe our GDPS algorithm to solve the problem of ARP poisoning in section IV. Section V illustrates our experimental

978-0-7695-4818-0/12 $26.00 © 2012 IEEE
DOI 10.1109/DCABES.2012.71

results on this topic. Finally, Section VI concludes the paper.

II. THREATS AND PROBLEMS OF ARP

In this section, we show the most important types of attacks, which can be accomplished by exploiting the ARP poisoning; we first describe the reasons. More precisely a Transmission Control Protocol (TCP) depends on a solid base of quality; nonetheless, the *Ethernet* relies not only on TCP/IP to deliver the packets. The TCP/IP inherits the security weakness from ARP protocol. Furthermore, there are wide varieties of software available on the internet like Cain & Abel [3], ettercap [4] and dsniff [5] which make the attacker able to perform the attack easily, on the other hand; it is difficult to detect and prevent active attacks absolutely. We now illuminate on a set of attacks that are achieved as a result of the ARP poisoning:

1. *Man-in-the-middle (MITM) attack:* This is an active eavesdropping attack; it occurs when an attacker manipulates the ARP cache of two devices, MITM means an attacker can establish the connection between a victim host and default gateway or host. In cases like these, a victim believed he sent packets directly to another host. MITM attack enables the attacker to monitoring the communication between devices of the victims, on the other hand; the attacker can not only intercept and access to sensitive information, but also modify the information before retransmit it to a victim host on LAN, or to outside world through the gateway router.

2. *MITM attacks with Public Key Exchanging:* In such scenario, the impact of these attacks on web-based financial transaction services, e.g., payment gateways, credit card servicing, and internet banking. An MITM attacker may intercept the encrypted connections (e.g., SSL, SSH, TLS, PPTP) between the client and the server, If an attacker could change the public keys, to remove any doubt from victims, when the attacker receives encrypted messages and reading or updating it. The attacker must use the correct public keys to decrypt and encrypt the messages, and then resend them to another victim. Although most browsers warn the victim user that, something is wrong, but many users ignore these warnings, furthermore, using the social engineering method makes this kind of attacks easy to occur.

3. *Denial of Service (DoS) attacks:* The attacker could prevent any host from access to any service on the network, through poisoning the ARP table of a victim host; therefore the packets will be sent to the attacker instead of the actual destination. Otherwise, the attacker sends ARP packet with unreal MAC address, which causes the data frames sent to the lost host.

4. *The Bombing Packets Attack:* This attack occurs when a malicious host sends a flood of poisoned ARP map to a victim frequently, which leads to cause filled of a victim cash, therefor many of the system resources will spend to maintain ARP cash, and the data will flood, as a result of the buffer overflow.

5. *MAC, IP Cloning Attacks:* The attacker could assign to himself the IP, MAC of the victim computer, recently IP, MAC can be changed easily without spoofing software, especially in Linux systems. After identify this duplicate in the IP, AMC, the victim computer will disconnect his network interface, since the MAC addresses are designed to be globally unique, and on the other hand each computer must be assigned to a single IP address in the same network.

The attacker can also pretend to be a receiver devise. This means impersonated an important entity like bank and obtain private information about user. In fact, ARP poisoning attacks violate all the security rules: confidentiality, integrity, and availability. Since the attacker can read and modify secret information or prevent a victim host from access to any service on its LAN or WAN [6], [7].

III. RELATED WORK

Several solutions have been proposed for manipulate the ARP poisoning problem. The ARP watch [8], ARP Guard [9] are manual solutions, so these depend on administrator to process the ARP cache, which is achieved by specialized network tools. This solution involves assigning a static IP addresses to all hosts in the LAN, also setting VLAN (Virtual LAN) and so on. This technique laborious for administrators and there is no mechanism to distinguish between a malicious and genuine host, as well as this solution is unsuitable for DHCP environments.

In Hou et al. [10] is a dynamic detection approach, which depends on snort tool founder et al. [11]. A snort is Intrusion Detection System (IDS); it can be used to detect ARP spoofing attacks; it is active and can detect different kinds of attacks through its ability to achieve a real-time packet analyzing on IP networks. But it has a lot of statuses of false-positive warning, which inform unreal reports to a network administrator; moreover, the inability to detect all categories of ARP spoofing attacks. Currently, other prevention techniques produced from some manufacturers to detect ARP spoofing attacks, like routers and switches merged with some functions of a firewall. Carnut et al. [12] proposed switched networks to detect ARP spoofing attacks, it can reduce significantly of false positive, but involves a complex setup; however, these devices cannot distinguish between the legitimate modification and malicious update for ARP mapping, and they are incapable of give us high credibility in additional to the cost.

In addition to the former schemes, a solution of encryption and authentication like [13], [14], [15] that used to prevent ARP attacks. This solution includes upgrade the existing ARP protocol, because, the shared pair keys must be applying to authenticate all ARP request response packets. This method can overcome the ARP spoofing problem effectively, but cryptographic techniques lead to failure point in a network, also performance of address resolution protocol decrease. Moreover, the limitations with DHCP (Dynamic Host Configuration Protocol) which means the auto determination for IP address, the reason that it involves DHCP server upgrade, and requires high computational rate.

Tripunitara et al. [16] proposed approach depends on a middleware technology; it seems capable of prevent ARP cache poisoning attacks, but it requires modifications on all the hosts on the same LAN. Middleware approaches applied streams based networking subsystem, which means adding some modules into the network system kernel. Therefore, in this mechanism, all inflow and outflow packets will be monitored and controlled. This manner is effective to detect and defense

TABLE I. REQUEST-REPLAY OF NORMAL GRATUITOUS ARP PACKET AND PROPOSED GDP PACKET

Opcode	Normal Gratuitous ARP Packet				Proposed GDP Packet			
	SIP	TIP	SMAC	TMAC	SIP	TIP	SMAC	TMAC
Request	10.0.0.1	10.0.0.1	78:2b:cb:f2:5e:01	Broadcast	0.0.0.0	10.0.0.2	78:2b:cb:f2:5e:01	00:21:9b:6a:9d:8a
Replay	10.0.0.1	0.0.0.0	00:21:9b:6a:9d:8a	Broadcast	10.0.0.2	0.0.0.0	00:21:9b:6a:9d:8a	00:10:5c:f0:38:14

This table illustrates the difference between the request-reply of normal gratuitous ARP packet and the proposed GDP packet, the IPs, MACs addresses in this table are obtained through laboratory experiments. The packets have been generated by packETH tool

against ARP attacks. However, the significant disadvantage in this method is the incapability of response for legitimate host when he spoofed by attacker, and using this method include great constraints in the case of DHCP.

Finally, there are basic points that should be taken into account for any ideal solution; any scheme should have backwards compatible and do not change the classic ARP. In addition, the solution does not breach network layer principles. The solution is necessary to be easy to apply, usage and availability, in additional to the low cost. On the other hand; any solution should not spend a lot of resources or cause high traffic in the network. However, a solution needs to be capable of detection and defense against all kinds of attacks, which occur as a result of the vulnerabilities in ARP.

IV. PROPOSED SCHEME

In the present work, we propose a new mechanism to the problem of ARP cache poisoning. Traditional structure of each ARP [1] packet there are fields specified for the Source-Target IP addresses (SIP,TIP) and fields to the corresponding Source-Target MAC Addresses (SMAC, TMAC), and the packet must be described in operation type fields (*Opcode*) through the value (1) for a request and (2) for the reply. A host that works with these specifications has to send his SIP, SMAC and TIP in request packets via broadcast mode; In contrast, the received host must send back his SIP, SMAC and TIP, TMAC in reply packets through unicast mode.

In some circumstances, a host sends broadcast ARP request without solicit any reply, or send a broadcast reply to which no request has been sent, these kinds of request/reply packets called gratuitous ARP packets [17], [18]. The gratuitous ARP packets apply in the following scenarios:

- IP misconfiguration, In case of a host receives an ARP packet includes a SIP that equals to its IP address (SIP =TIP), which implies IP conflict.
- Changing the Network Interface Card (NIC) status from inactive to active, connecting network cable, the host associates with a new station in case of wireless LANs, and so on.

A lot of operating systems send gratuitous ARP in the following cases: startup, wakes from sleep, and any changing in the network connection status. As previously stated, our proposed algorithm GDPS has two modules, the first module is detection module, it is used to perform a real-time traffic analysis of ARP packets. The second module of GDPS relies on a principle of the gratuitous packets structure to distinguish between the genuine and malicious hosts; it begins work during detection any abnormal ARP packet by detection module.

1. *Design Consideration*

We now introduce the packet structure of our suggested system, which is called Gratuitous Decision Packet (GDP). In a normal gratuitous ARP request, addresses of SIP, TIP are the same values and these addresses identical to IP address of a host who broadcasting the gratuitous ARP packet (SIP=TIP=IP address of a source host) [17].

The GDP packet is inspired from a gratuitous ARP packet, the only difference between GDP and normal ARP request packet just in the address of SIP, where in GDP the SIP address is equal to zeros (0.0.0.0), and this packet sent in unicast mode. In this case, because of ARP specifications to answer on any ARP request [1] the target host who has TIP on the same LAN. It must send an ARP reply to tell the sender host about his IP, MAC mapping, regardless of whether the received host owns in his ARP cache entries the IP address of the sender, also no matter if the sender IP address identical to receiver IP address. Table 1, shows the difference between normal gratuitous ARP request packet and the proposed GDP packet, where we assume that there are two hosts A, B with IPs 10.0.0.1, 10.0.0.2 and MACs 78:2b:cb:f2:5e:01, 00:21:9b:6a:9d:8a respectively; also we assume host A sends ARP request to the host B.

Consequently, in the current implementation, we used ARP packet to inquire about IP, MAC addresses of any host; for this, a host will be forced to answer all our questions. However, this paper does not aim to modify the existing ARP protocol and not violate the standards of the Open System Interconnection (OSI) model. In the following paragraphs, we will consider the tables which must be employed by modules of the GDPS:

Legitimate hosts table (LHT): In order to avoid a high traffic in the network, a GDPS depends on LHT table to retain authenticated hosts on its LAN. There are three fields in the table; IP, MAC and host live time (H_LT). The value of H_LT field identifies the host presence period as a legally host, H_LT is necessary to be compatible to the network configuration, for example, in dynamic addressing network (DHCP) H_LT must be less than *Lease Time* (a *lease time* is the total time that the DHCP server grants permission for a machine to use a specific IP address).

Check table, CHT: This table has three fields; IP, MAC to keep IP, MAC of a destination host. Packet time (PAT) used to determine the time of sending and receiving packets. Packet type (P_T) this field to classify the packet nature, it is used to denote and keep the values of flags, where; RP, SP request packet, response packet; which are sent from other hosts on the same LAN, and PO packet out, this packet is sent by GDPS.

2. *Detection Algorithm*

The work of GDPS is based on information in tables mentioned above (LHT, CHT) and the data in those tables will be updated continuously by the same algorithms. The first algorithm (DA) of a GDPS is responsible for reading received ARP packets, which sent from another host on LAN and then determine any attempt from a malicious host to poisoning ARP cash. We assume the IP_a, MAC_a mapping is in a received ARP request packet. The DA will check if the IP_a exists in LHT; in this case, we have to search on MAC_a in LHT, if a match is found that means the IP_a, MAC_a mapping is related to a legitimate host in the same LAN in this state the H_LT value should be extended to a new period, as show in Fig. 1. Nonetheless, in several times the IP_a is existing in LHT, but it is associated with a different MAC (IP_a==IP_i, $MAC_a \neq MAC_i$, where *i* is an entry number in LHT table; *i*=1, 2, 3, .., n), now the DA should send ARP request to existing MAC_i in unicast mode [19], [20]. Sending an ARP request by AD in the last case is to make sure that the received ARP packet which consists of IP_a, MAC_i mapping has been sent from a legitimate host, we can proof that through the number of received ARP replies. Subsequently, the AD algorithm must then wait a specified time period. Upon receiving just one or no response (received packets <=1) this situation forces us to maintain a current MAC_i and disregarded MAC_a (attempting to poison by MAC_a), because this implies that MAC_i is used by another host, also in case we have not received any response, herein means the machine (which owns MAC_i) is inactive or under influence of the *DoS* attack. Whilst, if we receive more than one reply (or if IP_a does basically not exist in LHT), at this time, the GDPS will launch GPA algorithm to investigate who is the genuine MAC. Elaboration for GPA algorithm will be presented in next sub-section. Even though both above cases involve static and dynamic (DHCP) addressing environments, however, in DHCP networks an IP address moves from one host to another at specific times that depends on a *Lease Time* in DHCP configuration. For this reason, we were assumed the H_LT value has to be less than *Lease Time*, owing to that the IP may be replaced at the end of *Lease Time*. Herein, we should note that in case received IP_a==IP_i, $MAC_a \neq MAC_i$, that means the possibility of ARP attack because this condition must occur just if the MAC_i not in a LHT table. The DA processes can be defined as follows.

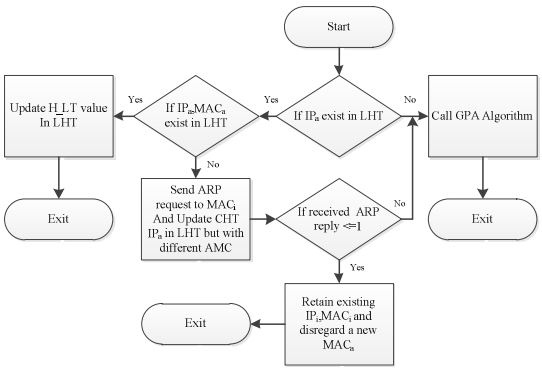

Figure 1. Flow chart for Detection Algorithm

Algorithm 1: Detection Algorithm (DA)

INPUT: (CHT, LHT) Tables
OUTPUT: Update (CHT, LHT) Tables
// Receive ARP packet with (IP_a, MAC_a)
if (IPa exists in LHT) **then**
  if (IP_a, MAC_a exists in LHT) **then**
    Update H_LT in LHT and **exit**
  else
    if (IP_a in LHT but with different AMC_i) **then**
      Send ARP request to existing MAC_i
      Update CHT
      if (ARP reply <=1) **then**
        Retain existing IP_i, MAC_i
        Disregard a new MAC_a **exit**
      else
        if (ARP reply >1)
          Call GPA algorithm
        end if
      end if
    end if
  end if
else
  Call GPA algorithm
end if

3. *Gratuitous Packet Algorithm*

Clearly, there has been a particular duty should be achieved by DA algorithm; a DA is merely used to discover that there are two MACs (MAC_a, MAC_i) correspond just one IP address (IP_a). Then DA will call GPA algorithm to differentiate between legitimate and malicious host. However, we have to process a case of IP_a not exists in a LHT; a GPA will send normal ARP request to IP_a (Broadcast mode), and if we received just one ARP reply, the received IP, MAC will be saved in LHT. Nonetheless, if we received more than one reply such as occurred in DA algorithm, in this case we must send 50 requests of the GDP packets to the received MACs (unicast mode), the GDP packet will contain zeros in source IP address (SIP=0.0.0.0) and target IP address is equal to the same value of received IP address (TIP= IP_a).

For whatever reason, we emphasize sending a GDP packet just in unicast mode to avoid poisoning ARP caches in other hosts on the same LAN. After sending 50 requests of GDP packets to MAC_a, MAC_i we have to wait a limited period to receive the responses, as show in Fig. 2.

Indeed, according to the experimental results, we have observed that the attacker host is unable to respond to GDP packets. In spite of this, we also should not rule out that the attacker capable of sending replies of GDP packets; which means receiving replies from two MACs. In this case, we consider the replies of GDP packets (as shown in table 1) are sent from a genuine host, and any other normal ARP replies are fraudulent packets.

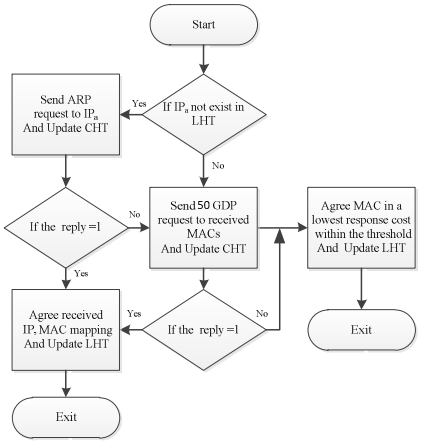

Figure 2. Flow chart for GPA algorithm

In a nutshell, we can depend on the number of replies of GDP packets to agree the IP, MAC in a lowest response cost and within the threshold condition, since this reply unavoidable and disregard another MAC or spoofing alarm in other situations, like the equivalence in response cost between those two MACs. The GPA processes can be defined as follows.

Algorithm 2: Gratuitous Packet Algorithm (GPA)

INPUT: IP_a
OUTPUT: Update (CHT, LHT) Tables
if (IPa not exists in LHT) **then**
  Send ARP request to IP_a
  Update CHT
  if (ARP reply =1) **then**
    Agree received IP, MAC
    Update LHT and **exit**
  end if
end if
Send 50 GDP request to received MACs
Update LHT
if (ARP reply from one MAC) **then**
  Agree received IP, MAC
  Update LHT and **exit**
end if
if (ARP reply from two MACs) **then**
  Agree MAC in a lowest response cost and within the threshold
  Ignore another, Update LHT and **exit**
else
  ARP spoofing alarm
end if

V.EXPERIMENTAL EVALUATION

Our findings in the paper have significant implications in ARP spoofing researchers, because of using different types of operating systems namely Windows7 running on A-B machines, Windows XP and Linux Ubuntu 11.10 running on C-D machines respectively. As important part of our experiments, we have depended on two of the ARP spoofing attack tools. The tools are Cain & Abel were deployed on the machine A, and Ettercap on machine D. Interestingly, we found that the attack machines do not have the ability to reply to the proposed ARP packet (GDP), whilst the victim machines were capable of responding normally, through a GDP reply as shown in table 1. We have run several scenarios of ARP spoofing attacks on those machines mentioned above, nevertheless; the results were identical. However, we must keep in mind that the attacker will try to send reply of GDP packets. Therefore, a GPA algorithm designed to send a set of GDP packets, hence it calculates the response cost for these two MACs to distinguish between legitimated and attacker MAC. Our results show that the attacker sends ARP reply packets equal to double the number of the packets which are sent by the victim. Because of the lack of the possibility of ARP poisoning attack software to respond to proposed GDP packets, we have achieved our experiments to monitoring and analysis the ARP packet by sending normal gratuitous ARP request packets as shown in table 1 to the victim and attacker. On the other hand, we generated the ARP packets by packETH 1.6 tool, which enabled us to create and modified ARP packets flexibly. Another basic tool of our experiments is the monitoring; Wireshark is free software designed to network protocol analysis, and we relied on it to track the ARP packets and collect the results.

Recent work has shown the main characteristics of the ARP behavior between the victim and attacker during sending 50 of normal gratuitous ARP request packets within a specified time (two seconds). Fig. 3 shows the difference between ARP reply packets that have received from victim and attacker, where the victim machine has Core 2 Duo CPU 2.53GHz (two CPUs) and

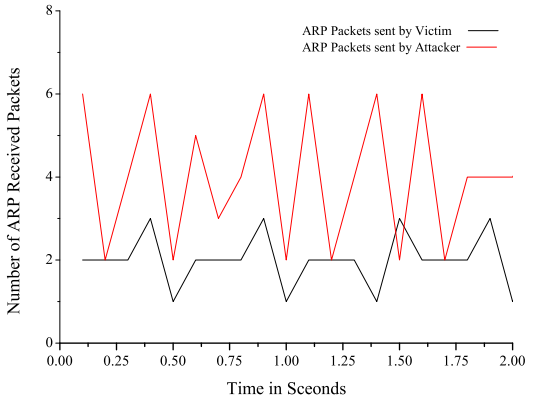

Figure 3. The difference between ARP replies packets which are sent from a victim and attacker.

TABLE II. LEGITIMATE HOST TABLE (LHT)

Hosts	IP	MAC	Host Live Time (H_LT)
Victim	10.0.0.2	00:21:9b:6a:9d:8a	
Attacker	10.0.0.2	78:2b:cb:f2:5e:01	

An ARP poisoning attack by Cain & Abel tool

TABLE III. CHECK TABLE (CHT)

IP (Sender)	MAC (Sender)	Packet Time (PAT)	Packet type (P_T) (RP, SP, PO)

The CHT table is used by GDPS system and it shows all input and output IP's, MAC's for other machines.

the attacker machine specifications are Core i5 CPU 2.67GHz (four CPUs).

We have run extensive experiments to test operating systems behavior and we found the Linux Ubuntu 11.10 system deals with our proposed of ARP packet (GDP) efficiently in addition of the Windows7 and Windows xp system.

As described in Sec. IV, the modules of our proposed system employed two tables as can be seen in table 2 and table 3; working to reduce the traffic in the same LAN. In table 2, there is a real scenario of ARP poisoning attack; this attack triggered by Cain & Abel tool. Finally, we investigate for traffic overhead for the GDPS system, because of sending the broadcast of ARP request packets by GPA algorithm. We consider M represents the total number of active machine in LAN, and we assume the IPs addresses of our LAN are assigned through DHCP addressing with a *lease time* LT. let us assume the broadcast ARP request occurs by GPA algorithm when a machine wakes up with a new assigning of the IP address identical to the same IP address in LHT table (the LHT table is on another machine works with GDPS system in the same LAN). Consequently, we can calculate the overhead incurred during using GPA algorithm by $(M-1) \times 28 \times 8 / LT = 0.224 (M-1) / LT$ Kbps. Hence, if we assume M = 255, considering all machines in LAN are working within the GDPS system, the equation will read like this 0.224 M (M-1) / LT, in case of LT is one day. So the overhead for this situation would be about 0.17 Kbps and this is quite reasonable for any LAN.

VI. CONCLUSION

This paper has presented a new mechanism to detection and prevents ARP spoofing attacks, which it significantly solves a problem of ARP weaknesses. The proposed method named a Gratuitous Decision Packet System GDPS achieves a detection of suspicious ARP packets, by implementing a real-time analyzing for received ARP packets. Hence, the recognition between a legitimate and malicious MAC is made by sending a modified request packet of the gratuitous ARP packets.

Recently, there have been a lot of researches aim to resist ARP poisoning. The technique of manual detection is laborious for administrators, and loses the advantage of DHCP mechanism, since it involves on assigned static IP addresses. The encryption solution upgrades the existing ARP protocol, and it leads to failure point in a network, furthermore; it requires high computational cost. The middleware technologies also include great constraints in approach of automatic network configuration (DHCP). However, those solutions have more drawbacks, and until now, no radical solution of this risk. Our solution backwards compatible with current ARP and it is easy to apply broadly and matched to run with the dynamic environments.

In the end, as a future work, we plan to extend our work through accomplishing several experiments to include wide scenarios of ARP spoofing attacks. As well as, take advantage of presented work in [21] to improve the efficiency of GDPS system.

REFERENCES

[1] D. Plummer. "An Ethernet address resolution protocol", RFC 826, Nov. 1982.

[2] C. L. Abad, R. I. Bonilla, “An Analysis on the Schemes for Detecting and Preventing ARP Cache Poisoning Attacks”, In Proceedings of 27th Distributed Computing Systems Workshops, IEEE Int. Conf., PP. 60, Jun. 2007.

[3] Oxid.it, Cain & Abel, http://www.oxid.it/cain.html/, last accessed Apr. 2012.

[4] A. Ornaghi, http://ettercap.sourceforge.net/, last accessed Apr. 2012.

[5] D. Song, http://monkey.org/~dugsong/dsniff/, last accessed Apr. 2012.

[6] L. Wu, T. Yu, D. Wu, "The Research and Implementation of ARP Monitoring and Protection", In Proceedings of Internet Technology and Applications, IEEE Int. Conf., PP. 1-4, Aug. 2011.

[7] T. Demuth and A. Leitner, "ARP spoofing and poisoning: Traffic tricks", Linux Magazine, 56:26-31, Jul. 2005.

[8] LBNL's Network Research Group, Information and Computing Sciences Division, at Lawrence Berkeley National Laboratory in Berkeley, California, ftp://ftp.ee.lbl.gov/arpwatch.tar.gz, last accessed Apr. 2012.

[9] ISL GmbH, ARP-Guard, http://www.arp-guard.com, last accessed Apr. 2012.

[10] X. Hou, Z. Jiang, X. Tian, "The detection and prevention for ARP Spoofing based on Snort", In Proceedings of Computer Application and System Modeling, IEEE Int. Conf., PP. V5-137-V5-139, Oct. 2010.

[11] S. founder, M. Roesch, "Network Intrusion Detection and Prevention System, (IDS/IPS)", http://www.snort.org, last accessed Apr. 2012.

[12] M. Carnut and J. Gondim, “ARP spoofing detection on switched Ethernet networks: A feasibility study”, in Proceedings of the 5th Simposio Seguranca em Informatica, Nov. 2003.

[13] W. Lootah, W. Enck, P. McDaniel, "Tarp: Ticket-based address resolution Protocol", In Proceedings of 21st Annual Computer Security Applications Conference, IEEE, Dec. 2005.

[14] M. Gouda, C.T. Huang, "A secure address resolution protocol", The International Journal of Computer and Telecommunications Networking, Elsevier North-Holland, Inc. New York, NY, USA,Vol. 41, Issue 1, pp. 57-71, Apr. 2003.

[15] D. Bruschi, A. Ornaghi, E. Rosti, “S-ARP: a secure address resolution protocol,” in Proceedings of 19th Annual Computer Security Applications Conference, IEEE, pp. 66-74, Dec. 2003.

[16] M. V. Tripunitara, P. Dutta, "A middleware approach to asynchronous and backward compatible detection and prevention of ARP cache poisoning", In Proceedings of the 15th Annual Computer Security Applications Conference, IEEE, pp. 303-309, Dec. 1999.

[17] S. Cheshire, "IPv4 Address Conflict Detection", RFC 5227, Jul. 2008

[18] Wireshark Wiki, http://wiki.wireshark.org/Gratuitous_ARP, last accessed Apr. 2012.

[19] F.A. Barbhuiya, N. Hubbali, S. Roopa, R. Ratti, S. Biswas, S. Nandi, A. Sur, and V. Ramachandran, “An active host-based detection mechanism for ARP related attacks”, In Proceedings of Network and Communications Security, Springer Berlin Heidelberg Int. Conf., vol. 132, Part 2, pp. 432-443, Apr. 2011.

[20] I. Teterin, Antidote, SecurityFocus, http://online.securityfocus.com/archive/1/299929, last accessed, Apr. 2012.

[21] H. Salim, Z. Li, H. Tu, Z. Guo, "A Client/Server Based Mechanism to Prevent ARP Spoofing Attacks", In proceedings of 3rd Advances in Swarm Intelligence, Springer Berlin Heidelberg Int. Conf., Lecture Notes in Computer Science Vol. 7332, pp. 254-263, Jun. 2012.

An Approach for Searching on Encrypted Data Based on Bloom Filter

Yao Hanbing, Xiang Dong, Peng Dewei, Huang Jing
School of Computer Science and Technology, Wuhan University of Technology, Wuhan, China
yaohanbing@gmail.com, xianglt@gmail.com, pengdewei@gmail.com, 405366153@qq.com

***Abstract* — It is desirable to store data on data storage servers such as file servers in encrypted form to reduce security risks. But this usually implies that one has to sacrifice functionality for security. For example, if a client wishes to retrieve only documents containing certain words, it was not previously known how to let the data storage server perform the search and answer the query without loss of data confidentiality. In this paper, we describe our schemes for the problem of searching on encrypted data based on Bloom Filter. Our schemes have a number of crucial advantages: The untrusted server cannot learn anything about the plaintext when only given the ciphertext in our solution. Our schemes provide query isolation for searches, meaning that the untrusted server cannot learn anything more about the plaintext than the search result. The algorithms we present are simple, fast, and introduce almost no space and communication overhead.**

Keywords: Bloom Filter; Encrypted Data; Hash Function.

1 INTRODUCTION

Increasingly, organizations and users are storing their data on servers outside their direct control. Backups and remote data storage are commonly outsourced to data warehousing companies. Even when data is stored locally, organizations hire system administrators (sysadmins) to backup on storage servers. In either case, sysadmins typically have full administrator access to storage systems, and can read confidential data. Therefore, sensitive documents should be encrypted before being storing remotely.

With files encrypted on a remote server, it is difficult to retrieve files based on their content. For example, consider a user Alice who stores her work documents on an untrusted file server. Suppose Alice wishes to retrieve all documents containing the word "Alice". Since the document files are encrypted and the server cannot be trusted with the document keys or their contents, Alice has to download all the document files, decrypt them, and then search the decrypted documents on her local machine. This naive solution is inefficient. The ideal solution is to let the server search the encrypted documents and return only relevant ones, while ensuring that it learns nothing about the keyword or document contents. Previous work shows how to build encrypted file systems, but typically one must sacrifice functionality to ensure security. The fundamental problem is that moving the computation to the data storage seems very difficult when the data is encrypted, and many computation problems over encrypted data previously had no practical solutions.

In this paper, we show how to support searching functionality without any loss of data confidentiality. An example is where a mobile user with limited bandwidth wants to retrieve all files containing the word "Alice" from an untrusted file server. This is trivial to do when the server knows the content of the data, but how can we support search queries if we do not wish to reveal all our files to the server?

Our answer is to present cryptographic schemes that enable searching on encrypted data without leaking any information to the untrusted file server. This paper is structured as follows. We first introduce the problem of searching on encrypted data in Section 1 and briefly review some important background in Section 2. Then we describe our solution in Section 3. Finally we conclude in Section 4.

2 RELATED WORKS

2.1 Plaintext Full Text Search

The importance of full text search has received attention in the context of plaintext searching in information retrieval community [1]. They addressed this problem in the traditional information-access paradigm by allowing user to search without using try-and-see approach for finding relevant information based on approximate string matching. The approximate string matching algorithms among them can be classified into two categories: on-line and off-line [2,3]. The on-line techniques, performing search without an index, are unacceptable for their low search efficiency, while the off-line approach, utilizing indexing techniques, makes it dramatically faster. A variety of indexing algorithms, such as suffix trees, metric trees, Inverted Index methods, have been presented [4]. At the first glance, it seems possible for one to directly apply these string matching algorithms to the context of searchable encryption by computing the trapdoors on a character base within an alphabet. However, this trivial construction suffers from the dictionary and statistics attacks and fails to achieve the search privacy.

2.2 Searching on Encrypted Data

Traditional searchable encryption has been widely studied in the context of cryptography. Among those works, most are focused on efficiency improvements and security definition formalizations. The first construction of searchable encryption was proposed by Song et al. [5], in which each word in the document is encrypted independently under a special two-layered encryption

Supported by "the Fundamental Research Funds for the Central Universities"

978-0-7695-4818-0/12 $26.00 © 2012 IEEE
DOI 10.1109/DCABES.2012.40

construction. Boneh et al. [6,7,8] presented a public-key based searchable encryption scheme. In their construction, anyone with the public key can write to the data stored on the server but only authorized users with the private key can search. As an attempt to enrich query predicates, conjunctive keyword search, subset query and range query over encrypted data, have also been proposed in [7]. Note that all these existing schemes support only exact keyword search, and thus are not suitable for Cloud Computing. Private matching [9], as another related notion, has been studied mostly in the context of secure multiparty computation to let different parties compute some function of their own data collaboratively without revealing their data to the others. These functions could be intersection or approximate private matching of two sets, etc. The private information retrieval [10] is an often-used technique to retrieve the matching items secretly, which has been widely applied in information retrieval from database and usually incurs unexpectedly computation complexity. However, their method suffes from:

The searching technique is not practical for large dataset; each query requires the server to search through the whole dataset linearly. That means accessing the entire dataset needs o(n) operations. And a very large number of disk accesses are required.

The limitation of the cryptography system. Their study did not discuss how to send encrypted data to another client and enable him to search it, so it does not present technique for exchanging encryption parameters. Note that we can't send the parameters using public key because the other side can distribute the parameters to a third party , so any one can search and decrypt the data .

The use of static word length, which require padding. Because the system presented encrypt the text word by word so it needs fixed word length. This not the case in natural languages so padding technique is required. The fixed length must be the longest word length, which leads to waste of space.

3 Searching on Encrypted Data Based on Bloom Filter

3.1 Bloom Filter

The structure of Bloom Filter provides a fast set membership test, with possible false positives. A Bloom Filter is stored as an array of bits. Initially, a Bloom Filter's internal array is set to all 0s. When an element is added to the set, a number of hashes are performed. The input to all of these hashes is the element being added, and the output from each is an index into the array (normally different for each hash). After these hashes are calculated, each bit in the filter at the indexes specified by the hash outputs is set to 1. An example Bloom Filter, using three hash algorithms is show in Figure 1. This figure also shows the addition of three different words, x, y and z. As this image shows, it is quite possible for two hash outputs to result in the same bit-index.

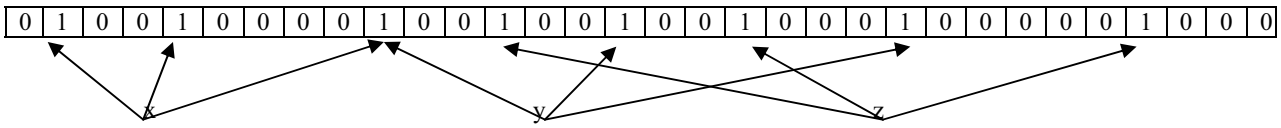

Figure 1: A 32-bit Bloom Filter with the words x, y and z have been added as members.

Mullin's analytical approach [11] has provided the theoretical false drop rate for Bloom Filter, as follows. Given that *t* transformations are used on *w* differrent words, the probabiltity that a particular bit in the b bits of the filters is not set (given that all bits are equally likely to be seleted) is

$$Pset' = (1 - 1/b)^{tw}$$

This is the probability that each of the *tw* transforms set some other of the b bits. The probability that a bit is set is

$$Pset = 1 - (1 - 1/b)^{tw}$$

The probability that all bits are set by a random word and hence of a false drop is

$$Pallset = pset^{ta}$$

Where *a* is the number of words in the query request. In order to keep the analysis tractable, the parameter *a* can be set to 1.

It has been shown that the optimum number of transformations is that where half of the number of bits in the filter are set to 1, i.e. Pset=1/2. Thus, at optimum, the probability of a false drop on a single word query would be

$$Pallset = Pset^{t} = (1/2)^{t}$$

To test an element for membership, it is hashed using the same algorithms and the conjunction of the resultant bits is returned (so only if they are all set to 1 is the element considered a member). Clearly, due to possible overlaps and an increased saturation level as progressive elements are added, false positives can occur when all the bits specified by the hash outputs are set to 1, even when the element wasn't originally added to the filter.

The different hash algorithms can be created in a number of different ways. One option is to use a hand-implemented set of distinct hash functions. This choice can be quite limiting, and quickly makes the Bloom Filter complex to implement. Double and triple hashing trivially triple the number of distinct hashes, but this will still mean developing and implementing at least two unique hash functions, producing six hashes in total. The number of hash algorithms to produce an acceptable false-positive rate will vary dependent on the number of elements and will be

explored more thoroughly later.

3.2 Key Generation and Trapdoors

We use a Bloom Filter as a document index to track words in each document. In our scheme, a word is represented in an index by a codeword derived by applying pseudo-random functions twice, once with the word as input and once with a unique document identifier as input. This non-standard use of pseudo-random functions ensures that the codewords representing a word x are different for each document in the set, and this technique together with blinding indexes with random tokens, ensures that the indexes are secure. Furthermore, the different codewords for a word x can be efficiently reproduced given just a short trapdoor for x. Both efficiently computable codewords and short trapdoors are important for the application of searching on encrypted data.

The key generation algorithm, Keygen(s) takes a security parameter (e.g. a password) and generates a master key, K_{priv} which is, in turn, comprised of a set of r keys.

$K_{priv} = (k1, ..., kr)$

These will be used throughout the scheme. A specific implementation of this might be a 512-bit hash (using SHA-512) of the input password to create the master private key, K_{priv} , which is then split into sixteen 4-byte keys (r = 16).

A trapdoor is a transformation of the term being searched for such that an untrusted file server can find potential matches, without gaining knowledge of the plaintext. In our scheme, a trapdoor is formed of the input word W, the private key K_{priv} and a series of hash functions. Given the master key K_{priv} and word w, Trapdoor(K_{priv},w) outputs the trapdoor T_w for w. This algorithm is described as Trapdoor(K_{priv},w) and given the necessary arguments, the trapdoor T_w is computed (where f is a suitable hash algorithm) as

$T_w = (f_{k1} (w), ..., f_{kr} (w))$

For the trapdoor implementation, the key k was chosen to be 512 bits in length. This is quite easy to produce using an existing 512 bit hash algorithm. SHA-512 was used for this purpose. With the 512 bit key (64 bytes), the individual elements of (k1, . . . , kr) were chosen to be 32 bits in length (4 bytes, meaning r = 16). The output of f is kept to 2 bytes, resulting in a 32 byte trapdoor. The key data is combined with the input word through concatenation.

3.3 Encryption

The encryption process centres on generation of the index. BuildIndex(D, K_{priv}), as it is termed in the literature, takes the private key and a document, D which consists of the plaintext and a unique identifier, D_{id} and returns a Bloom Filter representing the document index. The document identifier D_{id} is used to stop two identical documents from generating the same index (or documents containing a large number of repeated words from generating similar indexes).

The client, given a document and the private key can then create the document's index as follows.

Firstly, the document is split into a set of words. We can actually ignore punctuation (unless we predict the user is likely to want to search for it in our particular application). This is thanks to the fact that the entire, unmodified document will be encrypted and uploaded to the server, whilst the index can merely contain words that the user is likely to search on.

For each word, W_i, the following algorithm is then performed.

1. A trapdoor is constructed from the word w_i and the private key K_{priv} using the Trapdoor(K_{priv},w) algorithm described previously.

$T_w = (f_{k1} (w_i), ..., f_{kr} (w_i))$

2. A codeword is then constructed based on the trapdoor T_w. This simply takes each element of T_w and hashes it with the document ID.

$C_w = (f_{Did} (T_w \downarrow 1), ..., f_{Did} (T_w \downarrow r))$

3. This codeword can now be added to the Bloom Filter that represents the document index. The index created through this step could now be used as the document index. Figure 2 shows the process through which the trapdoor (T_w) and the codeword (C_w) are calculated.

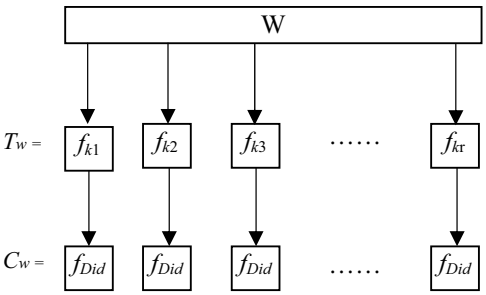

Figure 2: The generation of the trapdoor and codeword from a given input word w, using a key k = (k1...kr), for document with ID D_{id}.

Both of these algorithms use the same underlying hash algorithm f. Since this operation will be performed a large number of times when encrypting a document, performance is important. Attempts to use a cryptographically secure algorithm such as SHA-1 proved to be far too slow. Even algorithms that result in a far smaller output, such as a CRC-32 with a 4 byte output were still too slow. Because of this, it was decided to use a hash algorithm from the Bloom Filter set. If this algorithm proves to not give a normal distribution of output for a random set of input, then this could be used to derive patterns and could potentially be used as an attack vector on the system. Ideally a secure algorithm should be used, but the performance penalties in practice are far too drastic.

3.4 Search on encrypted data

When the user wants to perform a search for word W, the trapdoor T_w for the search term is generated using the

Trapdoor(K_{priv}, w) algorithm. Once this is generated, it can be handed to the untrusted file server which will then iterate over all of its stored documents and perform the following:

1. Generate the codeword from the trapdoor in the same manner as previously.

2. The document's Bloom Filter index is then checked to see if this codeword is a member.

3. If the Bloom Filter replies positively, the document is added to the set of documents to return to the user.

The trapdoor is used to hide the search term from the server, whilst the second-stage codeword is used to cleanly separate indexes of documents with similar content.

3.5 Analysis

Because the Bloom Filter is capable of returning false positives, the document set returned to the client must not be taken for granted – each document returned will need to be decrypted and manually searched client-side. This may sound like a huge pitfall in the scheme, but in reality, the false positive count is small. It's also a nice way of obfuscating the actual result set from the server, which would see more documents than necessary returned by a query, therefore reducing the amount of information available to it for cryptanalysis.

One problem that should be obvious is the possibility of saturating a Bloom Filter. If incorrect parameters are used, such as the size of the bit array being too small, or the number of hashes too large, a large document could potentially result in a Bloom Filter comprised of all 1s. In this situation, the result set of any search query will include this document.

One problem with the usage of plaintext document identifiers is that these themeselves might contain information that should be kept secure – a lot could potentially be derived from the name of a document. A simple solution to this is to use a meaningless identifier (such as an incremented number, or a hash of the document's actual name), which can be mapped by the client application to its meaningful representation after the search results are returned.

4 CONCLUSIONS

With the increasing popularity of data-storage outsourcing, there has been, in recent years, a growing interest in techniques related to searching on encrypted data. Encryption is commonly utilized to protect users' information. However, encryption methods introduce some negative effects such as inefficiency and malfunctioning. The research area of producing searchable ciphertext is currently an immature field. The key problem lies in the fact that patterns are required in order to search, and patterns are exactly what you don't want when producing ciphertext, since they give an adversary a possible method of attack.

In this paper, we have described new techniques for remote searching on encrypted data using an untrusted file server. Our techniques have a number of crucial advantages: they support controlled and hidden search and query isolation; they are simple and fast; and they introduce almost no space and communication overhead. Our scheme is also very flexible, and it can easily be extended to support more advanced search queries.

REFERENCES

[1] Baeza-Yates, R., Ribeiro-Neto, B. Modern Information Retrieval. Chapter 8. ACM Press 1999.

[2] Hao Yan, Shuai Ding, Torsten Suel. Inverted index compression and query processing with optimized document ordering. Proceedings of the 18th Int. World Wide Web Conf. (WWW), 2009, pp. 401-410.

[3] S. Ji, G. Li, C. Li, and J. Feng. Efficient interactive fuzzy keyword search. in Proc. of WWW'09,2009.pp. 371-380.

[4] M.Patil,S.V.Thankachan,R.Shah. Inverted Indexes for Phrases and Strings. Proceedings of the 34th Annual ACM SIGIR (SIGIR'11),2011,pp:555-564.

[5] D. Song, D.Wagner, and A. Perrig. Practical techniques for searches on encrypted data. IEEE Symposium on Security and Privacy (SP), 2000: 44-55.

[6] D.Boneh, G.D.Crescenzo, R.Ostrovsky, and G.Persiano. Public-key encryption with keyword search. In: Proceedings of Eurocrypt 2004, LNCS. 2004: 506-522

[7] D.Boneh, B.Waters. Conjunctive, Subset, and Range Queries on Encrypted Data. In: Vadhan, S.P. TCC 2007. LNCS, vol. 4392, pp. 535‑554.

[8] Eu–Jin Goh. Secure indexes. In the Cryptology ePrint Archive, Report 2003/216, March 2004.

[9] J. Feigenbaum, Y. Ishai, T. Malkin, K. Nissim, M. Strauss, and R. N. Wright. Secure multiparty computation of approximations. in Proc. of ICALP'01.

[10] K. N. A. Beimel, P. Carmi and E. Weinreb. Private approximation of search problems. in Proc. Of 38th Annual ACM Symposium on the Theory of Computing, 2006, pp. 119-128.

[11] J.Mullin, Accessing Textual Documents using Compressed Indexes of small Bloom Filters. The Computer Journal. 1987,30(4),343-348.

A Memory Integrity Protection Method based on Bloom Filter

Yao Nianmin[1], Ma Haifeng[1, 2], Cai Shaobin[1], Han Qilong[1]

[1]Computer Science and Technology Institute
Harbin Engineering University
Harbin, China
yaonianmin@hrbeu.edu.cn

[2]Computer and Information Engineering Institute
Heilongjiang Institute of Science and Technology
Harbin, China

***Abstract*—Today, attackers are capable of using software or hardware methods to intrude computer network system. The phenomena of confidential information being tampered with or disclosed are emerging everywhere. Hardware-based attacks have emerged and caused tremendous losses. Focus on this question, this paper proposed new architectural mechanisms to ensure data integrity which improved previous work in this area without compromising security. The new integrity mechanism offers significant higher performance, space advantages and adjustable level of security over existing ones. This paper evaluated the overhead of the scheme and compared it with the conventional integrity checking scheme CHTree. For most benchmarks, the overhead of the new method is much better.**

Keywords-memory integrity; replay attacks;Bloom filter

I. INTRODUCTION

Recently, phenomena such as business software being cracked, confidential information being tampered or disclosed are emerging everywhere. On critical computing platforms, attackers who have enough accessibility to the system can break security measures in any imaginable way such as using customized hardware [1]. Specifically, in order to get the protected information, attackers may dump all the transactions of data on the system buses and then construct the customized spoofing devices or hardware and replay the data got from the bus. Software or even light weight hardware based protection cannot resist this kind of physical attacks [2].

The research area of data integrity and confidentiality is now very active. Many work presented new schemes for uniprocessor [3-8] and Multi-processors platform [9-11]. In this paper, we only focused on the uniprocessor platform.

Authentication in XOM (eXecute Only Memory) [3] cannot detect replay attacks. The log hash scheme in Suh et al. [4] employs lazy authentication in which a program is authenticated only a few times during its execution. The Merkle tree scheme used in Gassend et al. [5] causes severe performance degradation on runtime. The CHTree scheme [6] improves runtime performance at the cost of cache space. The Authenticated Speculative Execution proposed by Shi et al. [7] employs timely authentication, but requires extensive modifications to the memory controller and on-chip caches. The TEC-Tree [8] reduces computational overhead, the Bonsai Merkle Tree (BMT) [12] is a novel Merkle tree-based memory integrity verification technique, to eliminate these system and performance issues associated with prior counter-mode memory encryption and Merkle tree integrity verification schemes. TEC-Tree and BMT both need to maintain a hash tree. Although many security architectures have been proposed, these schemes either have inadequate security protection or have high performance overheads.

This paper proposes a scheme to efficiently verify all or a part of untrusted external memory using a limited amount of trusted on-chip storage. The scheme is one-level hash structure, and it takes linear time while checking memory operations. In addition, the security strength of the scheme can be adjusted according to the requirements. In the scheme, there is an one-dimensional Bloom filter array where multi-set hashes of all memory are recorded to verify all the chunks of memory while reading at run-time.

The security model was presented in Section 2. The architecture of the scheme was described in Section 3. The overhead and performance analysis were discussed in section 4. The scheme was evaluated on the simulator in section 5 and the paper was concluded in Section 6.

II. ATTACKS AND SECURE COMPUTING MODEL

Broadly, attacks can be classified into software and physical (hardware) attacks, and physical attacks can be classified into two main categories: *passive attacks* and *active attacks* [13]. Passive attacks are the ones that the adversary simply observes the data going to and from the processor chip in a non-intrusive way. Active attacks are the ones where the adversary corrupts the data residing in memory or transiting over the bus.

The common objective of memory authentication techniques is to thwart active attackers. The most common active attacks are discussed below:

1) Spoofing attacks: the attacker tries to change the data value at a memory location and tries to pass it off as valid data.

*2) Splicing attacks:*involve taking valid data values and duplicating them or replacing them with values at other locations.

*3) Replay attacks:*the attacker records old values of data blocks and replays them at a later point of time.

In this paper, the systems were built around a single processor with external memory and peripherals. The multi-processors platform would not be discussed here.

978-0-7695-4818-0/12 $26.00 © 2012 IEEE
DOI 10.1109/DCABES.2012.101

Figure 1 illustrates the secure computing model. It can resist three active attacks. The model comprises a tamper-resistant processor (TCB, trusted computing base), external memory and peripherals. The TCB consists of the processor core, on-chip cache, encryption and integrity verification mechanism. The processor's core is assumed trusted, which means that the processor is invulnerable to physical attacks and its internal state can't be tampered or observed. The processor can contain a secret data that allows it to produce keys to perform cryptographic operations such as signing. The secret data can be a private key from a public key pair, as described in XOM [3]. The processor is used in a multitasking environment, which uses virtual memory and runs mutually mistrusting processes. Once a program executes some special instructions to enter the security executing environment, TCB is responsible for the protection of the program. The TCB or the processor needs to detect that whether memory operations are normally executed or not.

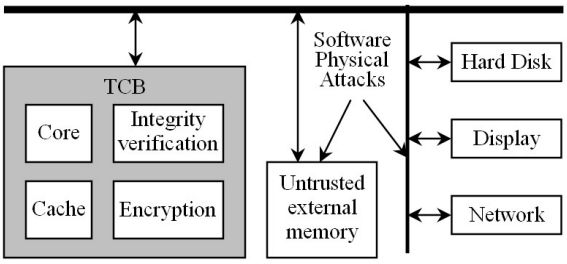

Figure 1. Secure Computing Model

The off-chip memory, the system bus and peripheral devices are untrusted. Their states can be observed and tampered by an adversary. The target of an adversary is to tamper with the contents of external memory in such a way that the system produces an incorrect result while looks correct to the system user. To make it simple, the untrusted memory in this paper only means the RAM, although in fact, the scheme presented here can be applied to other data storage devices such as hard disks only with a little change.

III. INTEGRITY PROTECTION APPROACH

A. The Principle of IV-BF

Bloom filter [14] is a simple space-efficient randomized data structure. It is a set of m elements which form an array and can judge whether y is a member of the set quickly. Bloom filter has the characters of low overhead and parallel computing. Bloom filter may yield false positive, which means that an element x is in the set even though it is not, but the "false positive rate" is very low if the hash function is good.

Applied Bloom filter to the memory integrity protection, a memory integrity protection scheme called IV-BF (Integrity Verification approach based on Bloom Filter) is proposed. Figure 2 illustrates the architecture of the IV-BF. Initially, the memory space is divided into n equal blocks. An array of m entries is maintained on chip and each entry is a counter. Initially all counters are set to 0. L.Fan [15] has proved that 4 bits per counter should be sufficient for most applications. Therefore, we set 4 bits for each counter whose range is 0-15. We also setup k independent hash functions which can mirror any data to [0…m-1].

Because of the character of Bloom filter, the IV-BF has certain "false positive rate" when checking whether a block is tampered. However, as long as the false positive rate is sufficiently low (for instance lower than 0.01%), it will satisfy the requirement of integrity verification. The factors of false positive rate including the memory space of protecting, the bits of array and the number of hash function. When memory space of protecting is fixed, the false positive rate is inversely proportional to bits of the array, that is, lower false positive rate (fewer collisions) leads to longer array length. On the other hand, when false positive rate is fixed, the array length is proportional to the memory space being protected, that is, more space leads to longer array length. When the memory space and the bits of array are fixed, increase the number of hash function will decrease the false positive rate.

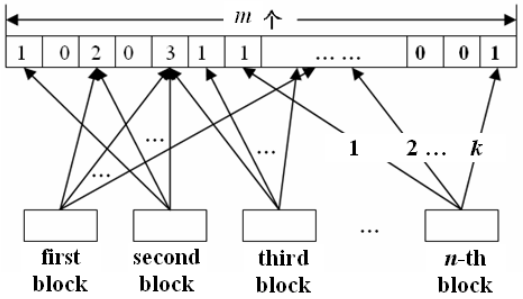

Figure 2. IV-BF architecture

There are three advantages of IV-BF compared with hash tree scheme. First, it has lower computation overhead. When checking or updating a block in the hash tree scheme, it can only do the computing level by level from down up to the root, while in IV-BF, it can compute the multi-hash functions in pipeline or parallel mode. The second advantage is lower space overhead. The hash tree needs a lot of memory space to save internal nodes, while the IV-BF only needs a little on-chip memory space to maintain an array and don't needs extra memory space. So the IV-BF can save lots of space at the cost of extremely low false positive rate. Third, the security strength of the IV-BF is adjustable. When data integrity requirement of application is extremely high, the lower false positive rate can be set, and accordingly, the computing overhead will be higher. When the requirement is not too high, it means certain of false positive rate are permitted.

The conventional hash tree scheme is proven to be secure [4]. The proposed IV-BF scheme is an extension of hash tree, and both hash and IV-BF mirror the whole memory to a small security area. The difference is that the hash tree has

multilayer while the IV-BF has only one layer. Therefore, IV-BF has the same security as hash tree if the hash function is the same.

B. Rules and Arithmetic of IV-BF

In order to make IV-BF work efficiently, some regulations and algorithms are given. The term "chunk" is used as the minimum memory block that is read from and written to memory for integrity checking.

1) Regulations:

a) The memory space protected was divided into multiple same size chunks.

b) An array of m counters is set.

c) k independent and perfectly random hash functions are set.

2) The Process:

Initial Operation

a) All counters of the array are set to 0.

b) k hash computations are done on each data chunk combined with its address.

c) Hash results are mapped to the array and the mapping position $h_i(x)$ of i-th hash is increment by 1.

d) Cache all the counters of array $[h_1(x), h_2(x), ...]$ in trusted memory.

Integrity Checking Operation

To check the integrity of a chunk, the processor:

a) Read the chunk's data.

b) Do a hash computation with the chunk's data and its address.

c) Check whether the mapped counter $h_i(x)$ is 0 (i from 0 to $k-1$).

d) If $h_i(x)$ equal to 0, raise an integrity exception.

e) Check whether current hash function is the last one.

f) If it's not, do the next hash function and go to *c).*

Update Operation

To update a chunk, the processor:

a) Read the chunk's data.

b) Do k hash computations in sequence.

c) All mapped counters $h_i(x)$ are decrement by 1.

d) If $h_i(x)$ less than 0, raise an integrity exception.

e) Update the data chunk.

f) Do k hash computations to the data in sequence.

g) All $h_i(x)$ are increment by 1.

IV. Overhead and Performance Analysis of IV-BF

In this part the overhead and performance of IV-BF is analyzed. The binary hash tree is compared with IV-BF.

A. The IV-BF Operation Overhead

The IV-BF's operations include setup protection, reading (checking) data and modifying data. The former two both do k hash computations for each data block, therefore, they have equivalent overhead. The last process does $2k$ hash computations for each data block, therefore, the last one is twice the overhead of the former two. The overhead of each of the former two are:

$$E = T[(\alpha \times s + k \times \bar{t} \times s)] \quad (1)$$

Among (1), α is the byte access time, s is the memory block size, k is the number of hash functions, $\bar{t}$ is the average time of each byte of hash computation and T is the overhead function. Simplifying (1) we can get: $E = T[s(\alpha + k\bar{t})]$, or shown as:

$$Cost = s(\alpha + k\bar{t}) \quad (2)$$

From (2) we know that the operation overhead of data is proportional to block size when k, α and $\bar{t}$ are fixed.

B. Hash Tree Operation Overhead

For hash tree, the overhead of operating a data block is $E' = E_l + E_i \times d$. In the formula, E_l is the leaf node overhead, E_i is the internal node overhead, and d is the depth of hash tree. We have known $E_l = T[s'(\alpha + t)]$, $E_i = T[i(2\alpha + t)]$, and $d = \log_2(A/s')$. In the formulas, s' is the memory block size, t is the time of hash computation of each byte, i is the internal node length and A is the whole memory space needs to be protected. Therefore, the whole operation overhead is: $E' = T[s'(\alpha + t)] + T[i(2\alpha + t)] \times d$, or shown as:

$$Cost' = s'(\alpha + t) + i(2\alpha + t) \times d \quad (3)$$

C. The IV-BF Performance Gain Compared with Hash Tree

In general condition, hash tree uses one hash function, e.g. MD5 or SHA-1, while IV-BF uses k different functions. For computation convenience, we set $\bar{t} = t$ which means each byte's average computing time of IV-BF is equal to hash tree, then using (6) and (7) we got the speed gain is:

$$\beta = \frac{E' - E}{E} = \frac{Cost' - Cost}{Cost} = \frac{[s'(a+t) + (2a+t) \times i \times d]}{s(a + kt)} - 1 \quad (4)$$

Set $\alpha = p \times t$. p is a ratio of a and t, simplifying (4), we got:

$$\beta = \frac{[s'(p+1) + (2p+1) \times i \times d]}{s(p+k)} - 1 \quad (5)$$

We assume that the space being protected is 4GB. The parameters of the two schemes for comparison are stated below. The IV-BF's block size is 1024 bytes, hash tree's block size is 64KB, hash tree's internal node size is 16

bytes, p is set 1/4, 1/2, 1, 5, 10 separately and k is set 2, 4, 6, 8, 10. Then we obtained performance gain of IV-BF compared with hash tree and the results are shown in Figure 3. The horizontal coordinate is the number of hash function, and vertical coordinate is the speed gain.

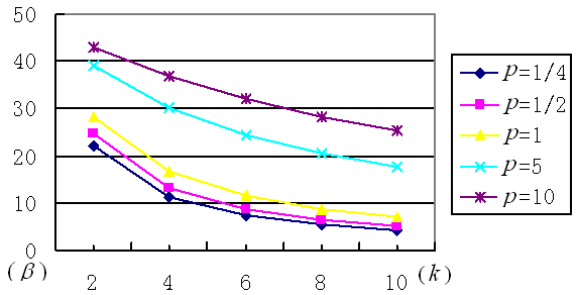

Figure 3. IV-BF gain rate compared with hash tree

As shown in Figure 3, when p is fixed the gain rate is inversely proportional to the number of hash functions, because the more hash functions, the more each operation overhead of IV-BF and the less gain rate. When k is fixed, increasing p means longer byte access time and leads to the more gain rate, because when p is larger, there is higher operation overhead of each data block while verifying Hash Tree. In addition, the gain rate will increase when the data block size of IV-BF is decreased.

V. SIMULATION

A. Simulation Framework

The simulation framework is evaluated by using modified SimpleScalar [16]. Considering significant performance degradation of the standard hash tree, we use the improved hash tree, CHTree for compare. The modified simulator supports the IV-BF and CHTree. The term "baseline" is used to refer to a standard processor without integrity verification or encryption. The overhead of memory authentication mechanisms are evaluated against baseline system.

The main architectural parameters are: L1 cache is 64KB (2-way, 32B line), L2 cache is 1MB (4-way, 64B line), memory latency is 80 cycles, memory bus is 200Mhz and 8B wide(1.6GB/s), memory space protected is 1GB, hash latency is 160 cycles, hash length is 128bits and hash throughput is 3.2GB/s.

For all the simulations in this section, eight SPEC2000 CPU benchmarks [17] are used as representative applications: vortex, vpr, art, parser, mcf, gzip, mesa and equake. These benchmarks show varied characteristics such IPC (instructions per cycle), cache miss rates. To capture the characteristics in the middle of computation, each benchmark is simulated for 100 million instructions after skipping the first 1.5 billion instructions. The major logic component to implement the IV-BF and CHTree is a hash (MAC) computation unit. To evaluate the cost of computing hashes, we choose the MD5 [18] hashing algorithms.

B. IPC impact

We first investigate the IPC of IV-BF and CHTree. For the convenience of comparison, both IV-BF and CHTree use the MD5 hashing algorithms and occupy 64KB L2 cache. CHTree cached part of inner node of hash tree and IV-BF cached the Bloom filter array. And then CHTree sets block size for 64B and IV-BF sets the block size for 16K.

Figure 4 illustrates the impact of memory authentication on the run-time program performance. The normalized IPC of IV-BF and CHTree are shown. It means that the IPC are normalized to the baseline performance with the same configuration. The results clearly show the advantage of the IV-BF scheme over the CHTree scheme. For all cases we simulated, the IV-BF outperforms the CHTree. The performance overhead of the IV-BF scheme is mostly less than 15% and less than 50% even for the worst case (mcf and equake). On the other hand, the CHTree has as much as 80% overhead in the worst case and 20-30% in general. The reason is: first, the IV-BF has fewer hash computations than the CHTree when L2 cache occupation is same; second, the IV-BF can compute hashes in parallel, while the CHTree can only serially compute hashes from leaf to root.

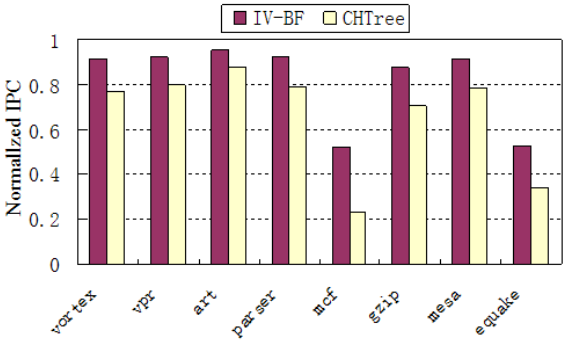

Figure 4. IPC comparison of CHTree and IV-BF

C. Cache Pollution

In IV-BF, we cached an array sharing the same L2 cache with a program executing on a processor, and both the array and application data contend for L2 cache. This can increase the L2 miss-rate for a program and degrade performance.

Figure 5 depicts the L2 miss-rate of the baseline (Base) and IV-BF scheme. For a 256KB L2 cache, the miss-rate of both scheme are very high. Compared with Base scheme, for all benchmarks, the L2 miss-rate of IV-BF can be noticeably increased (35%-150%). The reason is the Bloom filter array contends for L2 cache. In fact, cache contention is the major source of performance degradation for most applications.

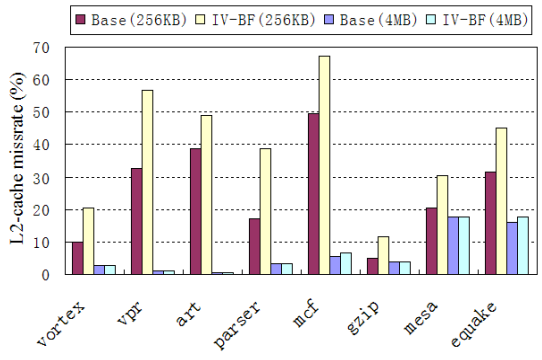

Figure 5. L2 miss-rate comparison of Base and IV-BF

Moreover, the performance degradation decreases rapidly as the L2 cache size increases. For a 4MB L2 cache, the miss-rate of both Base and IV-BF schemes are fairly low (0.5%-18%). Compared with Base scheme, for all benchmarks, the IV-BF didn't show noticeable L2 miss-rate degradation (less 10%). The reason is that the array size is determined, then as L2 cache size increase, the proportion of array size is decreased which alleviated the cache contention by reducing the number of hashes.

VI. CONCLUSION

We have presented a memory integrity protection scheme with low run-time and low memory space overhead. By integrating an array of Bloom filter with an on-chip cache, we arrived at a memory authentication scheme with high reliability. The performance analysis and simulation results have showed that the scheme we proposed has high efficiency and low overhead. Ongoing work includes investigation of memory verification schemes of lower overhead, combining the Bloom filter authentication with encryption and the generalization of authentication schemes to SMP and DSM systems.

ACKNOWLEDGMENT

This work is supported by the National Natural Science Foundation of China under Grant No. 61073047; Fundamental Research Funds for the Central Universities: HEUCFT1007, HEUCF100607, HEUCFT1202, Harbin Special funds for Technological Innovation Talents:2012RFLXG023.

REFERENCES

[1] Siddhartha Chhabra, Brian Rogers , Yan Solihin. SecureME: A Hardware-Software Approach to Full System Security. Proceedings of the international conference on Supercomputing. New York, NY, USA. 2011.

[2] D. Champagne and R. Lee. Scalable Architectural Support for Trusted Software. In HPCA, 2010.

[3] David Lie, Speciftying and Verifying hardware D. Lie, J. Mitchell, C. Thekkath, and M. Horowitz. Specifying and Verifying Hardware for Tamper-Resistant Software. In IEEE Symp. on Security and Privacy, 2003.

[4] Suh, D. Clarke, B. Gassend, M. van Dijk, and S. Devadas. Efficient memory integrity verification and encryption for secure processors. The 36th International Symposium on Microarchitecture, pp. 339-350, 2003.

[5] B. Gassend, G. Suh, D. Clarke, M. Dijk, and S. Devadas. Caches and Hash Trees for Efficient Memory Integrity Verification. In Proc of the 9th International Symposium on High Performance Computer Architecture (HPCA-9), 2003.

[6] G. E. Suh, D. Clarke, B. Gassend, M. van Dijk, and S. Devadas. Hardware mechanisms for memory integrity checking. In Technical Report MIT-LCS-TR-872, November 2002.

[7] W. Shi, H.-H. Lee, M. Ghosh, and C. Lu. Architectural Support for High Speed Protection of Memory Integrity and Confidentiality in Multiprocessor Systems. In Proceedings of the International Conference on Parallel Architectures and Compilation Techniques, pages 123–134, September 2004.

[8] Elbaz, R., Champagne, D., Lee, R.B., Torres, L., Sassatelli, G., Guillemin, P. TEC-Tree: A Low Cost and Parallelizable Tree for Efficient Defense against Memory Replay Attacks. In: Cryptographic Hardware and embedded systems (CHES), pages. 289–302,2007.

[9] Yang, L. and Peng, L. 2006. SecCMP: a secure chip-multiprocessor architecture.In Proceedings of the 1st Workshop on Architectural and System Support For Improving Software Dependability. ASID '06. ACM, New York, NY, 72-76, 2006.

[10] Brian Rogers, Chenyu Yan, Siddhartha Chhabra, Single-Level Integrity and Confidentiality Protection for Distributed Shared Memory Multiprocessors. In Proc.of the International Symposium on Computer Architecture, 2008.

[11] M. Lee, M. Ahn, and E. Kim. I2SEMS: Interconnects-Independent Security Enhanced Shared Memory Multiprocessor Systems. In Proc.of the International Conference on Parallel Architectures and Compilation Techniques, 2007.

[12] Siddhartha Chhabra, Brian Rogers, Yan Solihin,Milos Prvulovic. Making secure processors OS- and performance-friendly. ACM Transactions on Architecture and Code Optimization, Volume 5, Issue 4, March 2009.

[13] Austin Rogers, Aleksandar Milenković. Security extensions for integrity and confidentiality in embedded processors. Microprocessors & Microsystems. Volume 33, Issue 5-6, August 2009. Pages: 398-414.

[14] A. Broder and M. Mitzenmacher. Network applications of Bloom filters: A survey. Internet Mathematics, 1(4):485-509, 2004.

[15] L. Fan, P. Cao, J. Almeida, and A. Z. Broder. Summary Cache: A Scalable Wide-Area Web Cache Sharing Protocol. IEEE/ACM Transactions on Networking 8:3 (2000), 281-293

[16] Waseem Ahmad, Enrico Ng. A Quantitative/Qualitative Study for Optimal Parameter Selection of a Superscalar Processor using SimpleScalar. Computer Sciences Technical Report, 2004.

[17] A. KleinOsowski, J. Flynn, N. Meares, and D. Lilja. Adapting the spec 2000 benchmark suite for simulation-based computer architecture research. In Proceedings of the International Conference on Computer Design, 2000.

[18] D. Eastlake and P. Jones. RFC 3174: US secure hashing algorithm 1 (SHA1), Sept. 2001.

SIS: Secure Incentive Scheme for Delay Tolerant Networks

Cheng Gong, Wang Bo, Zhao Faru
(CNCERT/CC, Beijing, China, 100029)
E-Mail: wbxyz@163.com

***Abstract*: Due to the lack of end-to-end connectivity between mobile nodes, delay tolerant networks (DTNs) exploit the opportunistic forwarding mechanism. This mechanism requires nodes to forward messages in a cooperative way. Nevertheless, nodes may exhibit selfish behavior, in particular when they are constrained with respect to the battery energy, computational power, and/or storage space. In this paper, we propose a new secure incentive scheme (called SIS) enhance the cooperation among nodes and thwart the selfish behaviors by rewarding the intermediate nodes for their actively forwarding behavior. Moreover, we implement the scheme by ONE, and we conduct a complete set of simulations to compare its performance in terms of message delivery ratio and average delivery delay metrics. Our analysis provides a comparison of the proposed scheme's performance with Epidemic Routing and SprayAndWait Routing. The Extensive simulation results demonstrate that our SIS scheme can improve the cooperation level among the nodes.**

Keywords: ***Delay Tolerant Networks; selfish; incentive scheme; security; ONE***

I. INTRODUCTION

Delay Tolerant Networks (DTNs) are wireless networks in which nodes are intermittently connected and there is no guarantee that a path exists from source to destination at any time instance. Today, there are many examples of such networks including wildlife tracking networks [1], military networks [2] and vehicular networks [3]. In such networks, routing is largely based on nodal contact probabilities (or more sophisticated parameters based on nodal contact probabilities). The new working mechanism for routing is called store-carry-and-forward [3], which exploits the opportunistic contacts between nodes and mobility to relay and carry messages respectively. Consequently, it requires the nodes to forward messages in a cooperative and altruistic way. However, nodes may exhibit selfish behavior, that is, a selfish DTN node may be reluctant in the cooperation that is not directly beneficial to it, in particular when they are constrained with respect to energy, computational power, and/or storage space. Therefore, how to efficiently and effectively resolve the selfishness problem in DTNs has become a very challenging issue to achieve better packet delivery performance of DTNs.

In this paper, we focus on evaluating the impact of node selfishness on the performance of DTN, so as to enhance the cooperation among nodes and thwart the selfish behaviors by rewarding the intermediate node for its forwarding message. We use a reward calculation model based on each node's receiving, forwarding and copying behaviors to assign the corresponding reward. Then, we propose the SIS scheme to enhance the cooperation among nodes and thwart the selfish behaviors. At last, we also compare its performance with Epidemic Routing and SprayAndWait Routing schemes by simulation.

The rest of this paper is organized as follows: After presenting the related work in Section II, we describe the system model, give the rewarding calculation model in Section III. In Section IV, we give the framework of the SIS scheme. We validate the accuracy of our system model by simulation. Then, we describe the settings for performance evaluation and present numerical results in Section V. Finally, we conclude this paper in Section VI.

II. RELATED WORK

In this section, we discuss cooperation stimulation in wireless networks and DTN data transmission protocols, which are highly related to this work..

In terms of node selfishness, Panagakis et al. [8] evaluate the DTN routing performance under different levels of cooperation through simulation. Resta and Santi [9] present a theoretical framework to study the effects of different degrees of node cooperation. However, the proposed framework only allows performance evaluation in terms of message transmission delay but does not allow the study of the tradeoff between transmission delay and cost caused by non-cooperative behaviors. Zhu et al. [20] proposes a secure credit based incentive scheme for DTNs. However, the emphasis of [7] is on generation and verification of secure bundle and does not deal with pricing. Shevade et al. [6] consider the individually selfish behaviors of users and propose a robust and practical incentive mechanism to stimulate selfish nodes to forward messages in the system. Li et al. [5] consider the social selfishness and propose a social selfishness aware routing algorithm to allow user selfishness behaviors and provide better routing performance in an efficient way. Karaliopoulos [10] evaluates the impact of individual selfishness on DTN unicast routing by only considering the message transmission delay, and Li et al. [11] evaluate the impact of social selfishness on DTN unicast routing by considering the delay and cost. From these related works, we can see that they study the problem of DTN unicast routing, and most of them either neglect the node selfishness or only consider the individual selfishness [5], [6], [16].In this paper, we does not distinguish the two cases and give a generalize solution to study the incentive problem.

III. SYSTEM MODEL

In this section, we firstly give the some basic network model and assumptions. Then, we present a rewarding calculation model for message forwarding in DTNs.

A. Network Model and Assumptions

DTNs are typically characterized by the unguaranteed connectivity and the low frequency of encounters between a given pair of nodes within the network [4]. In our model, we

978-0-7695-4818-0/12 $26.00 © 2012 IEEE
DOI 10.1109/DCABES.2012.56

consider a DTN as a directed graph $G = (V, E)$, where V and E represent the set of DTN nodes and opportunistic contact edges, respectively. In the DTN, a source S can deliver packets to a destination D via the movement of DTN nodes with proper data forwarding algorithm. Currently, contingent upon whether they allow multiple copies of a message relaying within the network, the existing data forwarding algorithms may be categorized into single-copy and multi-copy algorithms.

We assume that each node has an effectively unlimited buffer for messages that they originate, but a fixed-size buffer for carrying messages originated by others. We assume that forwarding opportunities are limited both in duration and bandwidth. We assume each node has no a priori knowledge of network connectivity, no control over their movement, no knowledge of geographic location, and there are no always-on stationary nodes in the environment.

In the case of node selfishness, we characterize it by 1) the probability that a node holding a message does not forward the message and 2) the probability that a node not holding the message does not copy the message from other nodes.

B. Rewarding Calculation Model

In the DTNs, if all nodes store a message longer and propagate the message to more nodes, the probability that the destination will get the message increases. Therefore, an intermediate node's contribution of relaying a message contains the following aspects: the number of times that the intermediate node i receives one copy of the message from some other nodes, $m_r(i)$, the number of times that i successfully forwards one copy of the message to another node, $m_f(i)$, the number of times that i copies the message which it has successfully received, $m_c(i)$, and the number of meeting records submitted by i, $n_{rec}(i)$. The measurement of rewarding, $C(i)$, for an intermediate node i can be calculated as:

$$C(i) = \alpha \cdot m_r(i) + \beta \cdot m_f(i) + \gamma \cdot m_c(i) + u \cdot n_{rec}(i)$$

Where: α, β and γ are the rewards for the receiving, forwarding and copying behaviors, respectively, u is the unit amount of reward for reporting a meeting record between nodes. $u \cdot n_{rec}(i)$ is the amount of reward to node i for reporting the meeting records. Note that the destination node can be viewed as an intermediate node, which only receives copies without further forwarding behavior, the source node can also be viewed as an intermediate node, which only forwards and copies the message without the receiving behavior.

IV. THE PROPOSED SIS SCHEME

Under the unique setting of a DTN with selfish nodes, we propose a novel incentive scheme (called SIS) that incorporates rewarding stimulation mechanism to enhance cooperation.

A. Overview of SIS Scheme

We propose the core of the SIS scheme in this section. We assume that there is a PKI in the DTNs. Each node i has a public/private key pair K_{p_i}, K_{s_i} and a certificate that is digitally signed by a trusted certificate authority. Denote $(sign_{K_p}(), verify_{K_s}())$ as the digital signature scheme in DTNs.

The complete incentive scheme consists of the programs installed at each node in the DTNs and the algorithm running at the TTP. The programs at each node can further be divided into three groups of functions:1) the source node sending phase;2) the intermediate node forwarding phase;3) the destination node receiving phase, respectively. The detailed architecture of this incentive scheme is shown in Fig.1.

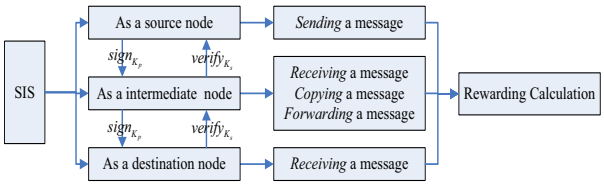

Fig.1. SIS scheme implementation architecture

B. The sending phase of source node

Suppose that the source node (*src*) wants to send a message M to the destination node (*dest*). *The src* node computes a digital signature $sign_{K_{src}}(md(M))$ based on the message it will send. In addition, the *src* node will send the message (or copies) together with the message-specific digital signature $sign_{K_{src}}(md(M))$ to the adjacent intermediate nodes, where $md()$ is a message digest function.

C. The forwarding phase of intermediate node

When a node carrying M meets a subsequent node, the two nodes first verify each other's identity using authentication certificates. Each node keeps a brief record of their meeting information (ts, id, R_{info}), where ts denotes the time when they meet. id is the identity of the other node, and R_{info} is the routing information available (which may need to be exchanged with the other node in many forwarding protocols). In this paper, R_{info} can be the expected probabilities of encounter with other nodes in the DTNs (such as the encounter-based routing in [15]).

If the node carrying M decides to forward according to some forwarding protocol, then it sends the message M together with $sign_{K_{src}}(md(M))$ to the subsequent node. After receiving M, the intermediate node saves the $sign_{K_{src}}(md(M))$ as secure evidence. Nodes submit their meeting reports and message evidence to TTP whenever they can connect to it.

D. The receiving phase of destination node

If the *dest* node receives M or its copies, then it verify the signature from the *src* node. Then, it runs the normal communication process. Moreover, when the *dest* node connects to TTP, it submits its secure evidence.

V. PERFORMANCE EVALUATIONS

In this section, we would like to evaluate our SIS algorithm, and contrast its performance against the simple

multi-copy routing algorithm (SprayAndWait) [13] and Epidemic Routing [12] with custom simulations and real trace analysis.

A. Experiment Setup

We conduct simulations under a map-driven DTN with pedestrians and transportation systems in the opportunistic network environment (ONE) simulator [14].In the map-driven DTN model (as shown in Fig.2), the nodes move along the streets on an imported map of downtown Wuhan, China. The size of the map is 8300×7300 m^2, and the nodes' transmission range is 250m. About 15% of the nodes are configured to follow the predefined routes with speed uniformly distributed in the range of [0,10] m/s, and other settings are default in the ONE simulator for tram vehicle. The remaining nodes are divided into three groups. For each group, there are points of interest (POIs), and we assign a different probability for picking the next node from a particular group of POIs to simulate the phenomenon that people visit certain areas of a place more frequently than other areas based on feature, such as age and profession. The default parameters used in the simulation are given in Table 1.

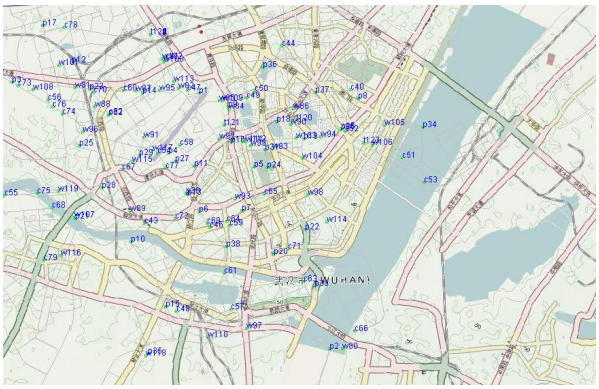

Fig.2. The imported map of downtown Wuhan, China

Table 1 Simulation parameters

Parameter	*Value*
Number of nodes	200
Rectangular	8300 m×7300m
Simulation time	500s
Transmission radius of each node	250m
Maximum mobile speed	10m/s
Storage space of each node	5Mbytes
Data payload size	512 bytes
Traffic model	Random pairs
The sending rate of each packet	4 packets/s
The number of selfish nodes	0~30
α	0.5
β	0.8
γ	0.8
u	0.5

B. Performance Metrics

To evaluate the impact of our incentive scheme on system performance, we measure both the message delivery ratio and average delivery delay with Epidemic Routing and SprayAndWait Routing copy=20 protocols.

(1) The message delivery ratio is the fraction of generated messages that are successfully delivered to the final destination within a given time period;

(2) The average delivery delay is defined as the average time between when a message is generated at some source and when it is successfully delivered to its destination.

C. Simulation Results

Fig.3 and Fig.4 show message delivery ratio and average delivery delay versus the number of selfish nodes in the network, respectively.

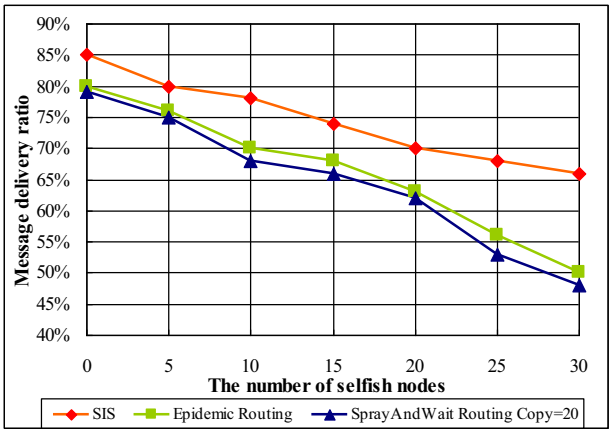

Fig.3. Message delivery ratio VS. the number of selfish nodes

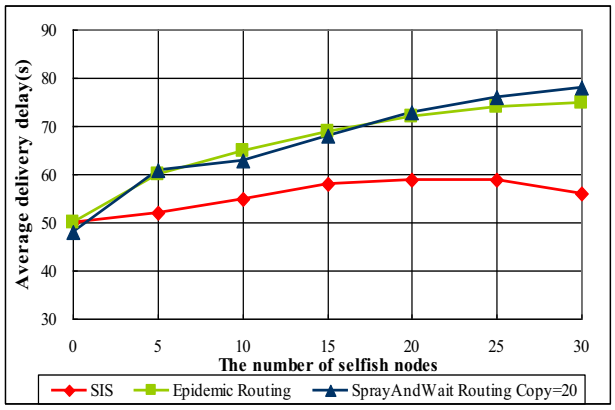

Fig.4. Average delivery delay VS. the number of selfish nodes

Fig.3 presents the message delivery ratio comparison of the three schemes under the different number of selfish nodes. As the number of selfish nodes increases from 0% to 30%, the message delivery ratio of three schemes reduces gradually. However, the proposed SIS shows better performance than the other schemes. The reason is that the proposed SIS scheme improves the cooperation of the whole network by distributing the rewards for each forwarding node and alleviates the selfish behaviors. Hence, the other two schemes haves the weaker ability against on the selfish attacks than the SIS scheme.

Fig.4 shows that message delivery delay changes with the number of selfish nodes: as the amount of selfish nodes increases, the message delivery delay of the three protocols decreases correspondingly. From the curve of each protocol,

they manifest the same variety and almost have the same delay. However, Epidemic Routing and SprayAndWait routing protocols behave a little worse than SIS, as the metric of SIS contain rewarding calculation model to resist the attack of selfish nodes, and maintain the normal communication so as to prolong the lifetime of the whole network, so this scheme can reduce the delay overhead.

VI. CONCLUSION AND FUTURE WORK

In this paper, we have proposed a novel incentive scheme that rewards the intermediate nodes to thwart the selfish behaviors in DTNs. The incentive scheme mainly adopts the rewarding calculation model according to each node's forwarding behaviors. The effectiveness of SIS is validated by using ONE，simulation results show that SIS has better performance than Epidemic Routing and SprayAndWait Routing in several metrics, especially in message delivery ratio and message delivery delay. In our future work, we hope to incorporate the QoS assurance into the SIS scheme to enhance the network performance. Meanwhile, we extend this scheme to multicast settings in DTNs.

Acknowledgment

The work is supported by National Natural Science Foundation of China (Project No. 60633020，60970117). The authors wish to thank many referees for their suggestions on this paper.

REFERENCES

[1] K. Fall, "A delay-tolerant network architecture for challenged Internets,"in Proc. ACM SIGCOMM, 2003, pp. 27–34.

[2] K. Fall and S. Farrell, "DTN: An architectural retrospective," IEEE J. Sel.Areas Commun., vol. 26, no. 5, pp. 828–836, Jun. 2008.

[3] S. Burleigh, A. Hooke, L. Torgerson, K. Fall, V. Cerf, B. Durst, K. Scott, and H. Weiss, "Delay-tolerant networking: An approach to interplanetary Internet," IEEE Commun. Mag., vol. 41, no. 6, pp. 128–136, Jun. 2003.

[4] S. Jain, K. Fall, and R. Patra, "Routing in a delay tolerant network," in Proc. ACM SIGCOMM, 2004, pp. 145–158.

[5] Q. Li, S. Zhu, and G. Cao, "Routing in socially selfish delay tolerant networks," in Proc. IEEE INFOCOM, 2010, pp. 1–9.

[6] U. Shevade, H. Song, L. Qiu, and Y. Zhang, "Incentive-aware routing in DTNs," in Proc. IEEE ICNP, 2008, pp. 238–247.

[7] H. Zhu, X. Lin, R. Lu, Y. Fan, and X. Shen, "SMART: A secure multiplayer credit-based incentive scheme for delay-tolerant networks," IEEE Trans.Veh. Technol., vol. 58, no. 8, pp. 4628–4639, Oct. 2009.

[8] A. Panagakis, A. Vaios, and I. Stavrakakis, "On the effects of cooperation in DTNs," in Proc. COMSWARE, 2007, pp. 1–6.

[9] G. Resta and P. Santi, "The effects of node cooperation level on routing performance in delay tolerant networks," in Proc. IEEE SECON, 2009,pp. 1–9.

[10]M. Karaliopoulos, "Assessing the vulnerability of DTN data relaying schemes to node selfishness," IEEE Commun. Lett., vol. 13, no. 12, pp. 923–925, Dec. 2009.

[11]Y. Li, P. Hui, D. Jin, L. Su, and L. Zeng, "Evaluating the impact of social selfishness on the epidemic routing in delay tolerant networks," IEEE Commun. Lett., vol. 14, no. 11, pp. 1026–1028, Nov. 2010.

[12]A. Vahdat and D. Becker, "Epidemic routing for partially connected ad hoc networks," Duke Univ., Durham, NC, Tech. Rep. CS-200006,2000.

[13]T. Spyropoulos, K. Psounis, and C. Raghavendra, "Efficient routing in intermittently connected mobile networks: The multiple-copy case,"IEEE/ACM Trans. Netw., vol. 16, no. 1, pp. 77–90, Feb. 2008.

[14]A. Kernen, J. Ott, and T. Karkkainen, "The ONE simulator for DTN protocol evaluation," in Proc. Int. Conf. Simul. Tools Tech., 2009, p. 55.

[15] S. Nelson, M. Bakht, and R. Kravets, "Encounter-based routing in DTNs,"in Proc. IEEE INFOCOM, 2009, pp. 846–854.

Research On Cloud Computing And Security

Ting-ting Yu
Internet Of Things Department
Wuxi Institute Of Technology
Wuxi, China
e-mail: yutt@wxit.edu.cn

Ying-Guo Zhu
Internet Of Things Department
Wuxi Institute Of Technology
Wuxi, China
e-mail: zhuyg@wxit.edu.cn

***Abstract*—Cloud computing is the hottest technology discussed on the internet recent years, which is considered as the trend in the development of the Internet. With the further application of cloud computing , security issues became one of the focuses concerned by people . From a practical point of view, this article combined with cloud computing framework, focus on the threats to cloud computing environments, as well as appropriate countermeasures**

Keywords- Cloud computing; Architecture; Threat Countermeasures

I. INTRODUCTION

Cloud computing is a flexible, cost- effective and proven delivery platform for providing business or consumer IT services over the Internet. NIST describes cloud computing as "a model for enabling convenient, on-demand network access to a shared pool of configurable computing resources (e.g., networks, servers, storage, applications, and services) that can be rapidly provisioned and released with minimal management effort or service provider interaction".

In march 2006, Amazon release Elastic Compute Cloud (EC2) service. In the same year, Eric Schmidt (Google CEO) first proposed Cloud Computing in SES San Jose 2006. February 1, 2008, IBM announced the establishment of the world's first Cloud Computing Center (Cloud Computing Center) for Chinese software companies in China Wuxi Taihu New Town Science and Education Industrial Park. March 5, 2010, Novell and Cloud Security Alliance (CSA) announced a vendor-neutral program, called "TTrusted Cloud Initiative".

From a practical point of view, this article combined with cloud computing framework, focus on the threats to cloud computing environments, as well as appropriate countermeasures.

II. CLOUD ENVIRONMENT ARCHITECTURE

The cloud computing model consists of five characteristics, three delivery models, and four deployment models. The five key characteristics of cloud computing are: location-independent resource pooling, on-demand self-service, rapid elasticity, broad network access, and measured service. These five characteristics represent the first layer in the cloud environment architecture (see Figure1).

The three key cloud delivery models are infrastructure as a service (IaaS), platform as a service(PaaS), and software as a service (SaaS).

<table>
<tr><th>Layer</th><th colspan="3">Cloud Computing Components</th></tr>
<tr><td rowspan="4">Five Characte -ristics</td><td colspan="3">On-demand self-service</td></tr>
<tr><td colspan="3">Broad network access</td></tr>
<tr><td>Resource</td><td colspan="2">Rapid elasticity</td></tr>
<tr><td colspan="3">Measured Service</td></tr>
<tr><td>ThreeDelivery model</td><td>IaaS</td><td>PaaS</td><td>SaaS</td></tr>
<tr><td rowspan="2">Four Deployment</td><td colspan="2">Public</td><td>Private</td></tr>
<tr><td colspan="2">Community</td><td>Hybrid</td></tr>
</table>

Figure 1: Cloud Environment Architecture.

- Infrastructure (storage, computation and network capabilities) as a Service (IaaS), basically consisting on the deliverance of virtual machines (VMs) to an IaaS provider, who can rise or shrink the number of VMs so as to offer fast and easy scalability according to variable workloads.
- Platform (development, service lifecycle, etc. support tools) as a Service (PaaS), offering facilities to develop software products and host them in third-party infrastructures.
- Software as a Service (SaaS),where the user buys a subscription to some on-line software.

Among these three, IaaS is, arguably, the most established cloud service model, already offering a wide variety of products and advanced capabilities: automated scalability, pay-per-use, and on-demand provisioning are some of the most relevant.This model represents the second layer in the cloud environment architecture.

Cloud deployment models include public, private, community, and hybrid clouds. A cloud environment that is accessible for multi-tenants and is available to the public is called a public cloud. A private cloud is available for a

978-0-7695-4818-0/12 $26.00 © 2012 IEEE
DOI 10.1109/DCABES.2012.28

particular group, while a community cloud is modified for a specific group of customers. Hybrid cloud infrastructure is a composition of two or more clouds (private, community, or public cloud). This model represents the third layer in the cloud environment architecture.

Kamara and Lauter present two types of cloud infrastructure only, namely private and public clouds. The infrastructure that is owned and managed by users is in the private cloud. Data that is accessed and controlled by trusted users is in a safe and secure private cloud, whereas the infrastructure that is managed and controlled by the cloud service provider is in a public cloud. In particular, this data is out of the user's control, and is managed and shared with unsafe and untrusted servers.

III. THE STATUS OF CLOUD COMPUTING

At present, ICT giants ,such as Google, Amazon, Microsoft, IBM, are actively promoting research and deployment of cloud computing services and applications, including Google App Engine, Amazon's Elastic Compute Cloud EC2 and Simple Storage Service S3Microsoft's Azure cloud platform, IBM's "Blue cloud".

Although cloud service providers can offer benefits to users, security risks play a major role in the cloud computing environment. According to the IDC report released at the end of 2009,the three market challenges faced by cloud computing services are security, stability, and performance. Ranking of the three challenges faced by cloud computing service is the same as that of IDC in 2008 findings . In November 2009, the survey of the ForresterResearch company indicates that 51% of small and medium enterprises believe that security and privacy issues is the main reason why they haven't used cloud services.

This shows that safety is the first consideration when customers choose the cloud. because of its high concentration of users, information resources, security consequences and risks associated with Cloud computing have more than raditional application. In 2009, Google, Microsoft, Amazon, the company's cloud computing services have a major fault, resulting in thousands of customer information services affected, which further increased the industry's concerns about application security in the cloud.

IV. CLOUD COMPUTING SECURITY RISKS AND COUNTERMEASURES

In this section, we have analyzed the security threats present in the cloud and their mitigation based on our experience of implementing the cloud.

A. VM-Level attacks

The cloud computing is based on VM technology. For implementation of cloud, a hypervisor such as VMWare vSphere, Microsoft Virtual PC, Xen etc. are used. This threat arises because of the vulnerabilities appearing in these hypervisors due to some facts being overlooked by developers during the coding of these hypervisors.

The threat arising due to VM-Level vulnerabilities can be mitigated by monitoring through IDS (Instruction Detection System)/IPS (Intrusion Prevention System) and by implementing firewall.

B. Abuse and Nefarious use of cloud computing

This threat arises due to relatively weak registration systems present in the cloud computing environment. In cloud computing registration process, anyone having a valid credit card can register and use the service. This facilitates anonymity, due to which spammer, malicious code authors and criminals can attack the system.

This type of threat can be mitigated in following ways:

- By implementing stricter registration process and validation process.
- By credit card fraud monitoring and coordination.
- Detailed introspection of user's network traffic.
- Network blocks through monitoring public black lists.

C. Insecure Interfaces and APIs

Customers use a set of software Interfaces or APIs to interact with cloud services. The provisioning, management, orchestration and monitoring of the cloud service are generally done using these interfaces .If the weak set of interfaces and APIs are used, this may expose organizations to various security threats, such as anonymous access, reusable tokens or password, clear-text authentication or transmission of content, inflexible access controls or improper authorizations, limited monitoring, and logging capabilities.

To mitigate the above threats, the security model of cloud provider interfaces should be analyzed. Strong authentication and access controls should be implemented. Encryption should be used for transmission of content and, dependency chain associated with the API should be clearly understood.

D. Malicious Insides

When the lack of knowledge about cloud vendor programs and processes the risk of malicious insiders will increase. Enterprises should know about information security of vendors and management policies, forcing them to use strict supply chain management as well as to strengthen close cooperation with suppliers. At the same time, should also have clearly specifies instructions in legal contracts to regulate carriers deal with these hidden processes such as user data in the cloud.

E. Sharing Technology

IaaS vendors in infrastructure is not safe to provide the strong isolation in a user schema. Cloud computing provider uses virtualization technology to narrow this gap, but due to the possibility of security vulnerabilities , companies should supervise the unauthorized changes and behavior, and promote the implementation of patch management and strong user authentication.

F. Data loss or leakage

Data loss or leakages have an adverse effect on the business. The brand or reputation is completely lost and the customers' morale and trust are eroded. This data loss or

leakage may be due to insufficient authentication, authorization and audit controls, inconsistent use of encryption and software keys, disposal challenges, a data center reliability, and disaster recovery.

The threats arising due to data loss or leakage can be mitigated by encrypting and protecting integrity of data in transit, analyzing data protection at both design and runtime, implementing strong key generation, storage and management. Contractually demanding provider to wipe persistent media before it is released in to pool and contractually specifying provider backup and retention strategies.

G. Account or service Hijacking

Phishing, fraud, and exploitation are wellknown issues in IT. The cloud adds a new dimension to this threat: "if an attacker gains access to your credentials, they can eavesdrop on your activities and transactions, manipulate data, return falsified information, and redirect your clients to illegitimate sites.Your account or service instances may become a new base forthe attacker".

To mitigate the above threats, sharing of account credentials between users and services should not be allowed, multi-factor authentication techniques should be used wherever possible, strict monitoring should be done to detect unauthorized activity, and security policies, as well as SLAs of the cloud provider, should be clearly understood.

H. Unknown risks

Knowing the security configuration used by users, including versions of the software, code updates, security practices, vulnerability profiles, intrusion attempt or security design.Find out who is sharing the user's infrastructure, to get network intrusion logs as soon as possible and related information in an attempt to redirect.

V. CONCLUSION

With the rapid development and wider application of cloud computing technology, cloud computing will face more security risks. Although there are several standards organizations in the study of cloud computing security industry on cloud computing security solution and there is no uniform standards and solutions. Many companies have introduced cloud computing security products, but innovation is obvious enough, but usually only address one small aspect of the problem. In order to cope with the ever-changing security threats, we need to constantly explore new cloud security solutions, and gradually establish an effective cloud security system, the maximum extent possible to reduce the security threats of the cloud computing system, to improve the continuity of the cloud services to protect the cloud computing applications for health and sustainable development.

REFERENCES

[1] (NIST), http://www.nist.gov/itl/cloud/

[2] H. Takabi, J.B.D. Joshi and G.-J. Ahn, "Security and Privacy Challenges in Cloud Computing Environments", IEEE Security & Privacy, 8(6),2010, pp. 24-31

[3] S. Kamara and K. Lauter, "Cryptographic cloud storage", FC'10: Proc. 14thIntl.Conf. on Financial cryptograpy and data security,2010, pp. 136-149

[4] S. Subashini and V. Kavitha, "A survey on security issues in service delivery models of cloud computing", Journal of Network and Computer Applications, 34(1), 2011, pp 1-11

[5] J. Viega, "Cloud computing and the common man",Computer, 42, 2009, pp. 106-108

[6] Meiko Jensen ,Jorg Sehwenk et al., "On Technical Security,Issues in cloud Computing "IEEE International conference on cloud Computing, 2009

[7] M.Jensen ,N.Gruschka et al., "The impact of flooding Attacks on network based services "Proceedings of the IEEE International conference on Availiabilty,Reliability and Security (ARES) 2008

[8] Armbrust ,M. ,Fox, A., Griffth, R., et al "Above the clouds: A Berkeley View of Cloud Computing" , UCB/EECS-2009-28,EECS Department University of California Berkeley, 2009

Encryption System Design Based On DES And SHA-1

Jian Zhang, Xuling Jin
School Of Science,Beijing University Of Civil Engineering And Architecture,Beijing, China
zhangjian@bucea.edu.cn, sahjxl@sina.com

***Abstract*—For modern society, The concealment and completeness of data is particularly important. To solve this problem, developed a mixed DES and SHA-1 encryption system based on VC + + environment. The system on the one hand by Triple DES and RSA algorithms for data encryption to hide, on the other hand, by the SHA-1 algorithm to validate the integrity of data, it has a wide range of practicality.**

***Keywords*—data encryption standard; public key cryptography; secure hash algorithm; data encryption system**

I. INTRODUCTION

The rapid development of information network creates favorable conditions for the rapid flow of data, the shadow of the figures can be found everywhere in people's lives, the relationship between people and the data becomes closer, and its position is gradually rising. For modern society, the concealment and integrity of data is extremely important. Therefore, important data files, usually require the encryption algorithm for processing to turn it into obscure "garbled", in order to achieve its secretive, calculation and check of the authentication algorithm to verify whether the data was falsified. This system uses DES (Data Encryption Standard) algorithm and SHA-1 hash function as a combination of methods to achieve this objective.

II. THE DESIGN OF THE DATA ENCRYPTION SYSTEM

A. Design Scheme

In order to achieve the concealment and security of data, we must increase the complexity and irreversibility of the algorithm. Data encryption system uses the Triple DES algorithm based on CBC mode to encrypt important data files and then get the encrypted file. Next, we can sign on the files by the hash function SHA-1 to get the corresponding hash sequence, and the bulk of the original file column hash value add to the end of the encrypted files; then decrypt the encrypted data file, remove the hash value attached to the end of the corresponding to get the decrypted file; and calculate the hash value of the declassified documents, compared with the original hash value, in order to verify whether The file has been falsified. Using Triple DES and RSA encryption algorithm in the system design, increase the key length to ensure the security; The authentication algorithm using SHA-1, as the irreversible algorithm, so that its safety can be guaranteed. The specific design shown in Figure 1:

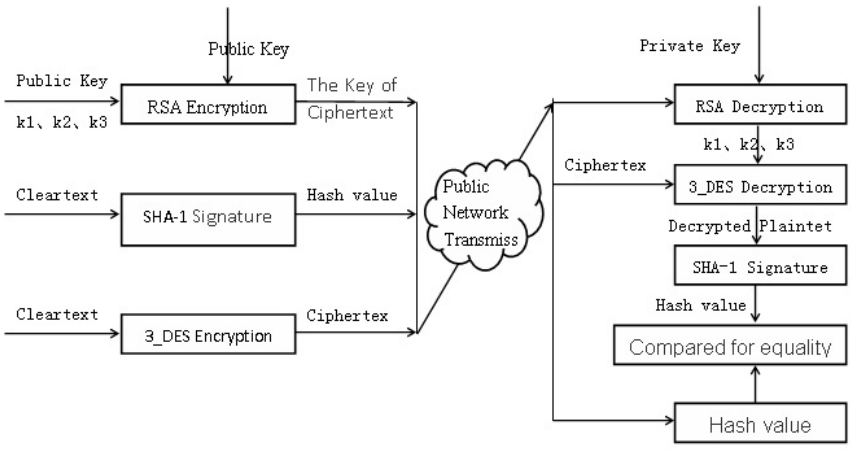

Figure 1. data encryption system design

B. Program analysis

1). Analysis of CBC mode

In CBC mode, before encryption, each plaintext group Pi should be added with the prior one ciphertext by bit mode 2, and then sent to the DES encryption, CBC mode overcomes the packet reorganizing disadvantage of ECB mode. This mode has a limited (two steps) error propagation characteristics, self-synchronization, and can not easily be attacked, etc.

978-0-7695-4818-0/12 $26.00 © 2012 IEEE
DOI 10.1109/DCABES.2012.42

2). Analysis of encryption algorithm

With the development of cryptanalysis techniques and computing capability, the security of DES is threatened. Short key is one of a main shortcoming of DES. The actual DES key length is 56 bits, the key quantity is only 256 ≈1017. As the computing capability of contemporary computers, DES can not resist exhaustive key search attack. In January 1999, the Electronic Frontier Foundation (EFF) successfully deciphered the DES in just 22 hours, 15 minutes.

However, triple DES can resist the half-way encounter attack:

$$y = DES_{k3}(DES_{k2}{}^{-1}(DES_{k1}(x)))$$

Where x represents the plaintext, y on behalf of the ciphertext, which is equivalent to the key length is extended from the original 56 bits to 168 bits, and these three keys have different arrangements, greatly improving the resistance to exhaustive key search attack. Although now a new Advanced Encryption Standard AES is announced, Triple DES is still widely in various fields of practical, such as encrypted the transmission of cardholder PIN, IC card and two-way authentication in POS, financial transactions, data packet MAC calibration, etc., all of them adopt the triple DES algorithm.

3). Analysis of key management algorithm

Its biggest flaw for DES is the shortage of key. For the purpose of enhancing the anti-attack capability of encryption algorithm, although it can not increase the length of the key, it can be processed to enhance the difficulty of exhaustive key search attack on DES key. The system uses the RSA asymmetric encryption algorithm to manage the keys for the following reasons:

a) The RSA encryption algorithm is based on the puzzle of large prime integer decomposition, in order to decipher the RSA, they must decompose a large prime integer, but there is not a confirmed algorithm yet to achieve this factorization. It can only be tested by quotient test method, so that the difficulty of deciphering greatly increased;

b) RSA as a asymmetric encryption algorithm, is in line with the encrypted during transmission very well. Public key is open to the public as a key transport user; private key is kept secret by the individual, only the recipient know the encryption key used in the algorithm; thus it can avoid the DES symmetric key of falsified and intercepted during the process of recipient and transmission, and greatly improving the safety performance of the key;

c) Although the RSA algorithm is complex, has large consumption of computer memory and time, while applied to the 64-bit DES key, it can just reduce its disadvantage in the encryption process. On one hand, it could save time and memory space for the system. On the other hand, it greatly improved the security of the encryption algorithm, the encryption algorithm of the anti-attack capability.

4). Analysis of authentication algorithm

SHA-1 is the national standards promulgated by the American Standards and Technology (NIST), it is the most widely used hash function algorithm. The password community, which has been published, is a strict inspection and has not been found unsafe, it is now considered security.

SHA-1 is similar to the MD-5 algorithm and is based on the same principle with MD4 same in the design, and imitate the MD4 algorithm. The algorithm is designed to used in conjunction with the Digital Signature Standard (DSS). Therefore, the anti-exhaustive is better. It is currently the most advanced encryption technology, used by government departments and private owners to deal with sensitive information, to prevent information from being maliciously falsified.

C. Functional design

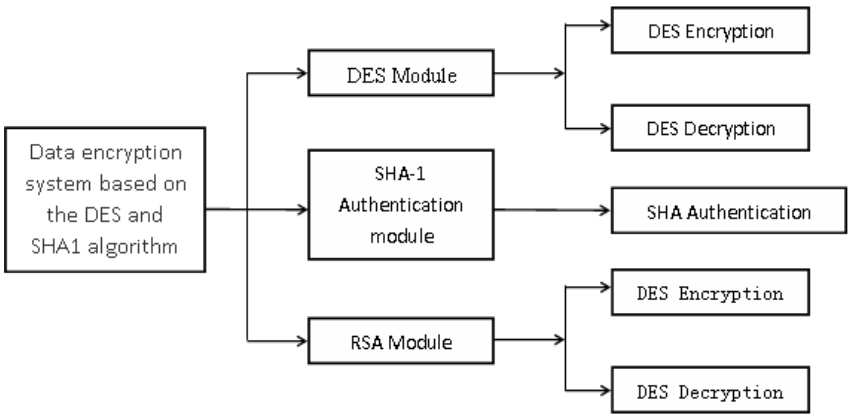

Figure 2. Functional block diagram

III. THE KEY TECHNOLOGIES OF MIXED ENCRYPTION SYSTEM

A. Processing of Word documents

Visual C + + Class Wizard mechanisms, from the Office type library to generate a wrapper class, and then call the appropriate library functions of word reading and writing. Required to read and write word documents Application class, Document class, the Selection class. Documents class and Selection class in accordance with the steps to add Application class, is added to the application.

B. System integration

1). Analysis on the interface

Three algorithms 3-DES、RSA、SHA-1 Input, output and actions. Such as table1

TABLE 1. INFORMATION OF THREE ALGORITHMS

Algorithm	Function	Input	Output	Actions
3-DES	Plaintext encryption、Ciphertext decryption	Plainte、Ciphertext、k1、k2、k3	Ciphertext 、Decrypted plaintext	Encrypt、Decrypt
RSA	Key encryption Key decryption	Prime number Status P 、Q	P 、Q 、M 、N 、Public key 、Private key	Prime number generate、Key generate、Encrypt、Decrypt
SHA-1	Plaintext signature 、Authentication	Binary plaintext	Hexadecimal Hash value	Sign、Authenticate

The link between the relevant functional modules, as well as the interface between the module and the module can be seen through the table. for example, the interface between the 3-DES and RSA module three key DES module.

2). Module integration

Through the analysis of the above interfaces, has been associated with the interface between the related modules, Figure 3 shows the module inputs and outputs and the behavioral characteristics of the interface design:

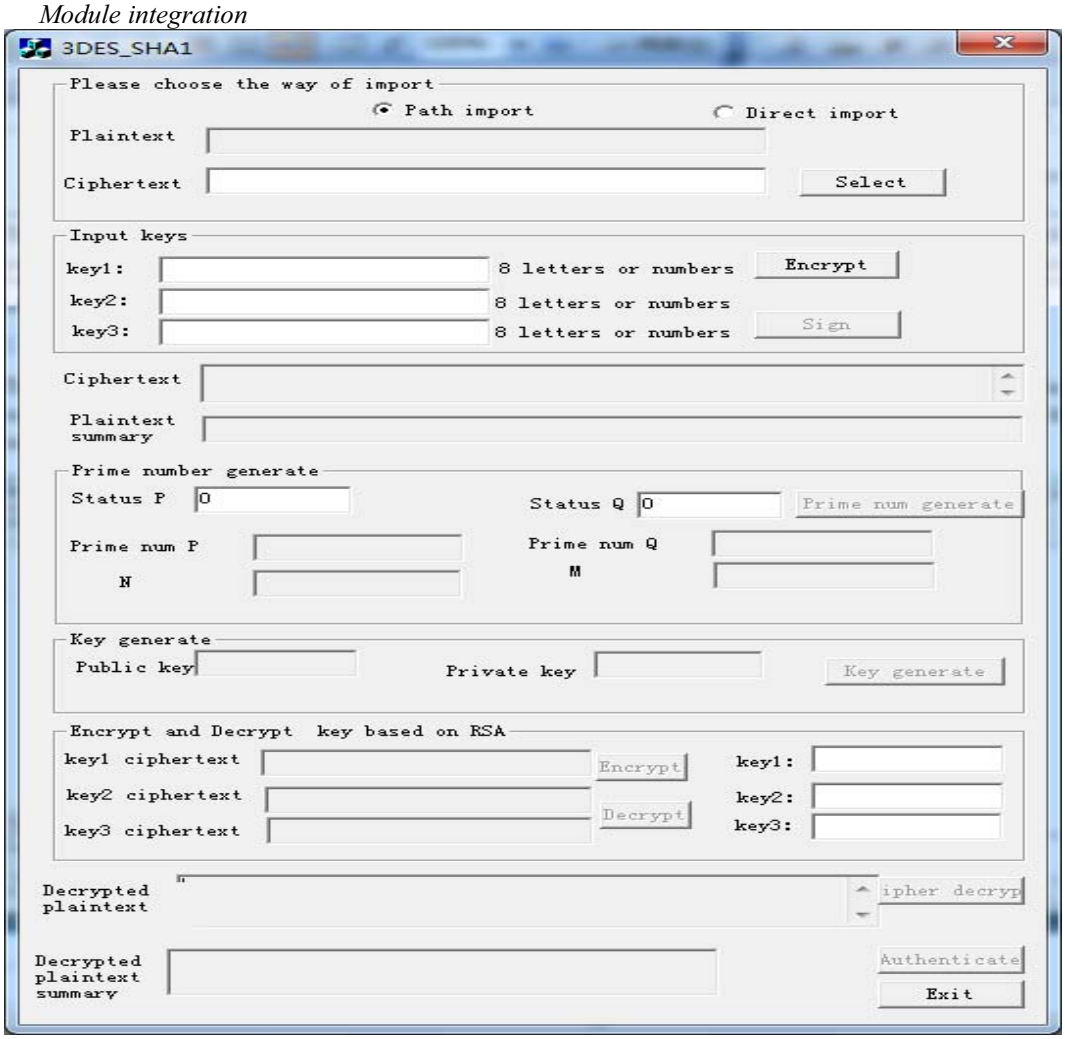

Figure 3. Interface design

IV. SOFTWARE FUNCTIONAL VERIFICATION

A. The operating environment test

Test environment: Windows XP operating system, VC6.0 development environment

Test method: according to the workflow of the software system, each module to be tested.

Test Conclusion: friendly software interface, the various functions operating normally. The overall operating condition is fine.

B. The encryption and decryption functional test

Test environment: Windows XP operating system, VC6.0 development environment

Test method: the traditional encryption of files on local computer. Test the decryption functions under the mode local storage system.

Test results: the files under operation can be selected correctly and encrypted. When the keys are error or changed, it can be reported immediately. So the encryption to the files could fulfil the requirements of system.

C. The software efficiency test

Test environment: Windows XP operating system, VC6.0 development environment

Test method: test the speed of encryption and decryption of the files in different size while under the same environment. Then, record the time of encryption and decryption.

In the same environment, the use of three encryption methods to encrypt different document, collecting some of the encryption/decryption time, can demonstrate the superiority of mixed algorithm in the encryption and decryption speed.

V. CONCLUSION

The system is suitable for the transmission of important data between companies. When company A needs to transfer data to company B, company A can use the system for data encryption package, and then transmit over the Internet to company B, company B authenticate via the same system to decrypt the file, and get the corresponding data. At the same time, they could identify whether the data has been tampered during the transmission, thus the security and integrity of the data transfer process can be ensured.

REFERENCES

[1] Aqi Zheng、Youhe Ding VC++ Tutorial 1st Edition Beijing, Tsinghua University Press, 2005: 49-132

[2] Haoqiang Tan C Programming 3rd Edition Beijing, Science Press, 2008: 49-175

[3] Hong Yan Data Encryption Technology And Its Development Trend Computer and Modernization, 2005, Total 115: 1-3

[4] Tuhao Shen WORD Documents Created With VC + + Language Computer Engineering and Design, 2004, 6 of 25: 1-3

Remark--The paper is supported by BMEC(KM201010016003)

Research and Development of Intelligent Transportation Systems

Yan, Xinping; Zhang, Hui; Wu, Chaozhong
Intelligent Transportation Systems Research Center Wuhan University of Technology
ITSC of WHUT, Wuhan, China
Engineering Research Center for Transportation Safety, Ministry of Education
ERCTS, MoE, Wuhan, China
xpyan@whut.edu.cn, kakanicolas@yahoo.com.cn, wucz@whut.edu.cn

***Abstract*—Intelligent Transportation Systems (ITS) have been developed for more than ten years in China. Furthermore, a new generation Intelligent Transportation Systems should be launched to meet the requirement of rapid development of transportation in China. Firstly, the development history of Intelligent Transport Systems is summarized in this paper. Secondly, as one of the earliest ITS research center in China, the Intelligent Transportation Systems Center, Wuhan University of Technology is also introduced. It was established in September, 2000, and aims to improve traffic safety, reduce vehicle emission, and save transportation energy in roadway and waterway transportation fields. Its research fields include: driving behavior & safety, traffic safety management and control, assistant driving and intelligent vehicles in roadway, information collection technologies, accident simulation systems, safety warning and emergency systems in water transportation. Several major research projects or fields mentioned above will be introduced in details. Finally, the key areas of ITS during next five years are described, and the development and cooperation in the future are also discussed.**

Keywords-intelligent transportation systems; automotive driving; traffic safety; atrfical intelligence

I. INTRODUCTION

Intelligent Transportation Systems (ITS) are advanced technologies which aim to provide innovative services relating to different modes of transport and traffic management. It enables various users to be better informed and make safer, more coordinated, and 'smarter' use of transport networks. Compared with the traditional transportation system, the most significantly characteristic of ITS is the combination of artificial intelligence and transportation system. ITS encompass a broad range of wireless and wire line communications based information and information processing, control algorithm, electronics and other technologies. When integrated into the transportation system's infrastructure, and in vehicles themselves, these technologies relieve congestion, improve safety and enhance productivity.

The development of ITS in different countries can be divided into two stages. The typical characteristic of the first stage is mainly on transportation information acquisition and processing intelligentialize.

Transportation telematics was probably origin from the beginning of the 1970s in Japan, where several technological programs were conducted to deal with the large number of traffic deaths and injuries as well as the structural ineffective traffic process. In Europe, the first formalized transportation telematics program PROMETHEUS (PROgraM for European Traffic with Highest Efficiency and Unprecedented Safety) (PROMETHEUS, 1989) was initiated by European automotive companies in 1986, while in 1988 the DRIVE program (Dedicated Road Infrastructure and Vehicle Environment) was set up by the European authorities (DRIVE, 1990). The USA followed in 1990 by forming Mobility 2000 in 1989 and in 1990 by establishing the IVHS program (Intelligent Vehicle Highway Systems) (IVHS, 1992), that has been renamed into ITS (Intelligent Transportation System) in 1994.

National ITS Architectures for several countries were designed and planned in this stage, including the research area and transportation service. The American national ITS Architectures[1] is shown in Fig.1

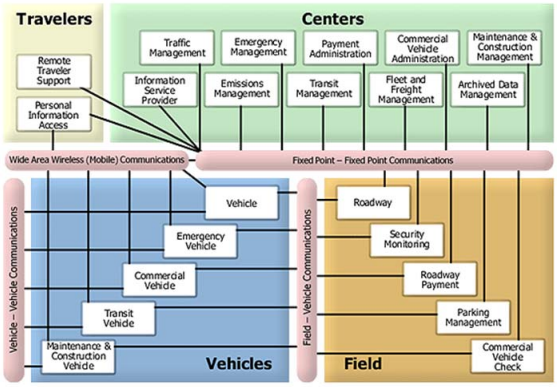

Figure 1. National ITS Architectures of America

The technologies for Vehicle active safety, collision avoidance and intelligent vehicle were rapidly developed in stage2.

The DEMO' (demonstration) 97 and PATH 1986 (Partners for Advanced Transportation TecHnology) were most influential project in automated highway system in America, In European Union, the European Road Transport Telematics Implementation Organization, ERTICO take advantage of the information and communication to develop the active safety and autonomous driving, the project eSafety was initiated in 2003. In 2010 VisLab launched VIAC, the

978-0-7695-4818-0/12 $26.00 © 2012 IEEE
DOI 10.1109/DCABES.2012.107

VisLab Intercontinental Autonomous Challenge, a 13,000 km test run for autonomous vehicles, from Italy to China, shown in Fig.2 .

Figure 2. The VisLab autonomous vehicle and reseaerch staff

Benefit from the rapid development of ITS technologies and innovated equipment, the transportation system can be more efficient, smart and green, the application of ITS is mainly in following aspects.

- Traffic surveillance and management
- Dynamic traffic optimization
- Autonomous driving
- Driver statues identification and active safety
- Driver behavior mechanism
- Collision avoidance systems
- Accident analysis and prevention

II. THE DEVELOPMENT OF ITS IN CHINA

Over the past decade, ITS technologies have greatly improved traditional transportation conditions, and improved the traffic capacity of the road network and transport security in China. In 1999, the National Engineering Technology Research Center of Intelligent Transportation System (ITS) was established. Many universities and research institutions also set up ITS Research Center to research ITS theories and technologies.

A. Research on ITS

Many universities and institutes of scientific research have carried out ITS research from the following three aspects.

For driver, studies on driving behavior were conducted. These included driver's behavior acquisition, recognition, and criterion given. More representatives of them were from Jilin University, Shanghai Jiao Tong University, Wuhan University of Technology, and Chang'an University.

For vehicle, studies on intelligent vehicles were conducted. These included vehicle system composition, vehicle state information acquisition, and vehicle control strategy design. More representative of intelligent vehicles were CITAVT series from National University of Defense Technology, JLUIV series from Jilin University, THMR series from Tsinghua University, and CyberC3 from Shanghai Jiao Tong University, shown in Fig.3.

Figure 3. Intelligent vehicles in universities

For road, experimental fields were constructed to test driver's behavior and comprehensive features of vehicles. More representative of them were Beijing proving ground and Xi'an proving ground, shown in Fig.4.

Figure 4. proving grounds for ITS in China

B. Application of ITS

The Tenth Five-Year period (2001-2005) first took the fields of intelligent transportation systems as content of the national planning. In 2001, China had selected ten cities as "model cities" for ITS field testing and evaluation. Those cities included Beijing, Shanghai, Guangzhou and so on [1]. During this period, many important aspects and key issues in ITS research and development were addressed on a high scientific and engineering level: agent-based and vision-based technologies; traffic modeling, control, and simulation; communication and location-based services; and driving safety and assistance, etc. For instance, the digital bus station systems has come into use in many cities, such as Beijing, Guangzhou, Chongqing, Shanghai, Hangzhou, Shenzhen, Nanjing, Shenyang, etc. Many information technologies of this system, such as computer control technology, wireless network communication technology and LED display control had been completely developed.

During the Eleventh Five-Year period (2006-2010), ITS had more opportunity to develop, especially in transport services for major international events. Olympic traffic management command and control system was established in Beijing in 2008 as shown in Fig.5. Which include bus operations management system, floating vehicle dynamic traffic information collection processing and publishing systems. These systems have four major functions: command, signal control, integrated monitoring and regional traffic optimization. The systems comprehensively support Beijing public security traffic management work in 2008 Olympic,

and achieved unified, efficient command and management of road traffic.

Figure 5. 2008 Olympic Traffic Management Command and Control Systems

Electronic Toll Collection System (ETC) and demonstration projects of Beijing, Tianjin and Hebei Region were established. Until June 2011, 22 provinces and cities had opened more than 2100 ETC lane, shown in Fig.6. Ocean shipping and cargo transportation online monitoring system were built during this period. It completed global coverage.

Figure 6. ETC lane

III. RESEARCH STATUS IN ITSC OF WHUT

A. Experiment Platform and Conditions

ITSC of WHUT was founded in Sept., 2000. It focuses both on waterway and roadway transportation, including fundamental research and application. In terms of road transportation, it is especially interested in three fields, namely analysis of driving behavior mechanisms and accident causes, operation management and control for road transportation safety, driver assistance system and autonomous driving system. Concerned with waterway transportation, waterway information detecting technologies and equipment, simulation system for waterway transportation accidents and early warning & emergency system are the three mainly research directions. All these research work have been supported with adequate experimental equipment or platforms. And the achievements of them, in turn, further improve the overall scientific research conditions. Particularly, we feel proud in the following four experimental systems.

The simulation platform for automotive driving is shown in Fig.7. It is consisted of three systems, i.e. the integrated driver operation data collection system, the 5-channel 180 deg view virtual graphical system and the physiological, psychological and graphical information collection system. It can simulate various traffic scenarios in different weather conditions with high reality. Figure 7 also shows some of the devices in information collection system.

A series of driving simulator products based on this have been applied to the assessment of road transportation safety and driver assistance systems, detection of driver fatigue and behavior characteristics as well as the training of new driver. All of the applications have been successful.

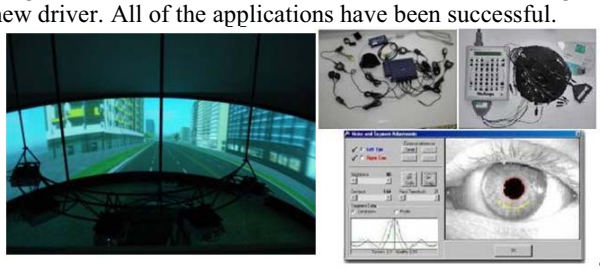

Figure 7. Driving simulation platform and the physiological information collection devices

As shown in Fig.8, the experimental vehicle for transportation safety is an integration of several subsystems, including an on board computer, the image acquisition system, eye view monitoring system, vehicle-infrastructure integration system, physiology measurement system, dynamic GPS etc. With them, the vehicle is able to detect various kinds of information about the driving environment and the driver whose psychological, physiological and behavioral data can be recorded for later research and safety analysis.

Virtual simulation platform for road transportation system, as shown in Fig.9, is a 1:10 scaled model based on the road network of urban Wuhan. It consists of three parts, i.e., the road sand table subsystem, simulation platoon subsystem and the road-side information gathering and monitoring subsystem. It can be used for traffic monitoring, collection and publishing of the traffic information, vehicle-infrastructure communication and autonomous driving.

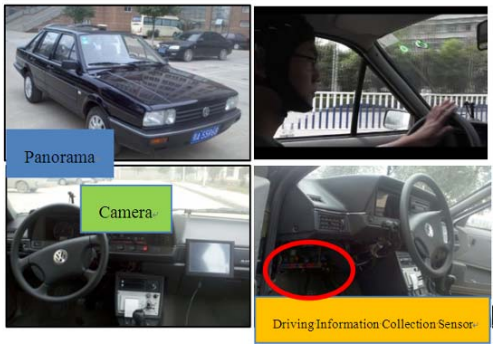

Figure 8. The experimental vehicle for transportation safety in ITSC

Figure 9. Virtual simulation platform for road transportation system in ITSC

B. Driving Behavior

Driving behavior is the foundation of intelligent transportation systems. Studies on driving behavior in Wuhan University of Technology are mainly embodied in the following aspects: driving fatigue, driving intention, driving emotion, etc.

There are some obvious characters in driver's physiology and behavior, vehicle states when driver is fatigue. After compared the different mental state of driver physiology signals (heart rate, skin conductance, electromyogram, skin temperature, and depth / frequency of breath), the physiology characteristics of fatigued driver were extracted, and driver fatigue was recognized by fuzzy clustering. The driving fatigue simulation real-time monitoring software was developed, which replayed the experimental process of video and experimental data, could use playback data for real-time monitoring the mental state of driver[2]. The characteristics of driving behavior were also extracted, and driver fatigue was identified using these features. When fatigue driving, the velocity is higher, the driver is easy to speeding. Along with the increase of the driver fatigue, the main frequency component of acceleration become more and more high, spectrum amplitude and energy decreases significantly[3] . The mean standard deviation and energy of steering angle become big when fatigue deepening and these tendencies would diminish the differences causing by different road alignment[4] . In order to improve the precision of the driving fatigue recognition, both physiological signals and driving behavior characteristics were considered, the relationship between them was explored[5]. Using these studies of the theory of the driving fatigue, fatigue analysis experiment system based on driving simulator and motorist fatigue real-time monitoring system were developed.

Study on driving intention is useful to improve the risk assessment accuracy of vehicle driving safety precaution system. The correlation between driver's behavior and intentions was dissected on mechanism level. The hidden Markov recognition model was established to recognize the intention of lane-change and car-follow. The model was verified through actual driving experiment on straight sections and intersections, and it is effectual[6]. The experiments based on driving simulator were done. Three driving intentions (free driving, car following, lane change) were recognition based on genetic algorithm and ant colony optimization [7]. Acceleration intention of car drivers was also recognized based on fuzzy clustering[8].

Driver's emotion is a psychological state which influences driver's cognition. Research on driving anger was summarized by studying a large number of domestic and foreign literatures on driving anger[9] . According to research on driving anger at present and Chinese actual traffic circumstance, China driving anger expression scale (CDAES) was designed, and the impact of angry driving on traffic safety was explored. the driver most easily generates distraction, followed by lapse of vehicle control when anger[10]. The operation of the vehicle control is more frequent, the operation amplitude become large and uneven, and steering wheel angle varied more obvious while angry driving[11].

Numerous researches indicate that the psychology of driver and traffic accidents have a certain relationship. Traffic accidents are prone to occurrence in drivers who lack awareness of safe driving. The methods and technologies were explored to improve safe driving awareness such as multimedia technology and simulated driving, etc[12]. A dual-tasks experiment based on driving simulator was used to study driving distraction. The results demonstrated that when approaching risky situations the Mean Lateral Deviation of increased and the lateral distance decreased while the dual-tasks group compared with the control group [13].

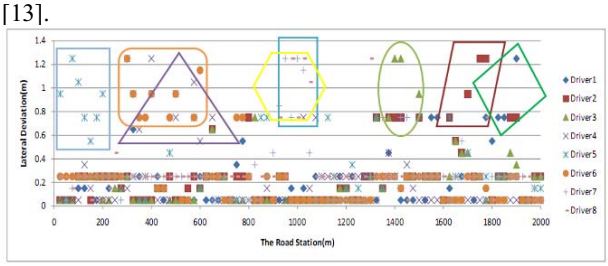

Figure 10. Distribution of lateral deviation under dual task

Motorist's personality test questionnaire was designed to classify automobile student pilot compatibility. The relationship between driver personality and traffic safety was discussed. Five kinds of personality (discrete, dedicated, the risks, resourceful, stability) have high correlation with road traffic accidents and violations [14].

C. Advanced Driver Assistance Systems

Research results of the driving behavior have laying a solid foundation for driver assistant system, and ITSC take advantage of these achievements and have focused on two aspect of advanced driver assistance system: vehicle statues warning and driver hazardous pre-warning.

The image information of road marking was recorded by camera, and sent to the processing computer, and by computing the camera position, lane edge, vehicle width and other lane parameters, the result of lane position was for Lane Departure Warning, LDW. The pedestrian collision warning system adopted similar methods.

Millimeter wave radar was installed in the front and two sides of experiment vehicle, therefore, the distance from the

front vehicle or lateral vehicle can be calculate by the feedback of radar, when the distance was approaching the safety threshold, the Forward Collision and Lateral Collision was informed to drivers.

The lane position and steering parameters, combined with the GPS information are the source information for vehicle and operation stability analysis, and the impaired driver status which may be caused by fatigue, distraction or angry driving could be used for warning drivers.

With the development of vehicle2vehicle and vehicle2infrastructure communication technology, ITSC was exploring an innovated driver assistance system based on driving intention. When the vehicle steering or speed can be acquired, predicted and send to the neighbor vehicle, the potential danger could be predicted for warning.

D. Collaborative Vehicle Infrastructure systems

The cooperative vehicle-infrastructure system is a cooperative human-vehicle-infrastructure system for real-time Vehicle to Infrastructure (V2I) and Vehicle to Vehicle (V2V) information interaction using advanced wireless communication and network technology.

1) 1:10 Mechatronic testbed system: ITS center of Wuhan University of technology takes cooperative vehicle-infrastructure experiment on Mechatronic testbed. The intelligent vehicle platoon driving simulation experiment is a process that simulates intelligent vehicle platoon driving and completes V2V and V2I information exchange by the established wireless communication networks. Process of information interaction between road and vehicles has shown in Fig.11. The road-side Infrastructure gather vehicle velocity, acceleration, vehicle spacing information and receive information from the regional console, including platoon velocity, acceleration information, etc. The center console receive information came from road-side infrastructure in order to get vehicle located information and send control commands to vehicle based on a variety of information received of vehicle platoon. ZigBee technology is used for V2V communication and V2I communication. WiFi technology is used to build a wireless local area network to achieve communication between regional console and center console. .

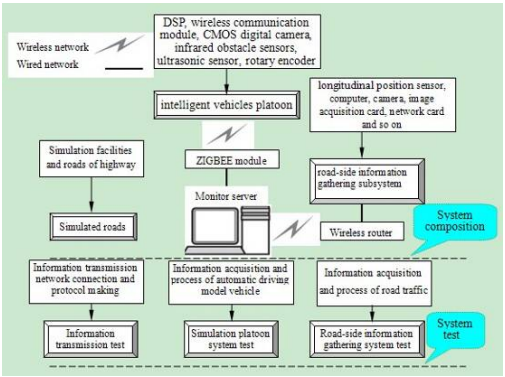

Figure 11. Process of information interaction between road and vehicles

2) The vehicle-to-infrastructure driving safety system: The system including the vehicle-to-infrastructure driving safety system, vehicle-to-vehicle cooperative control system and the traffic coordination control system is used to subsystem integration, testing and validation, shown in Fig.12.

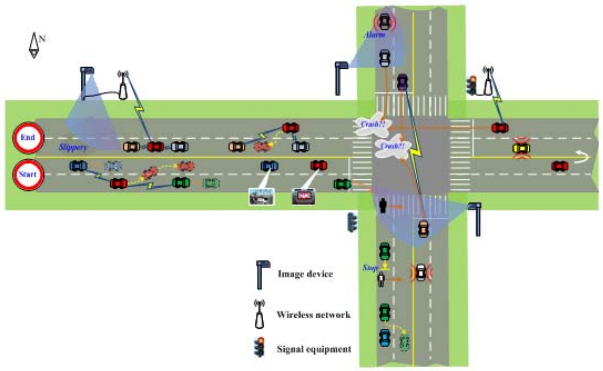

Figure 12. Integrated playing of Cooperative Vehicle-Infrastructure System

Adaptive cruise control (ACC) based on road condition is a part of the vehicle-to-infrastructure driving safety system, shown in Fig.13. It adds V2I communication, providing the previous systems with more and better information about the oncoming road conditions. The communication devices on vehicle, including Dedicated Short Range Communication (DSRC), Global Positioning System (GPS), can be used with the digital road map to obtain the position of the car and road condition in the case of real implementation.

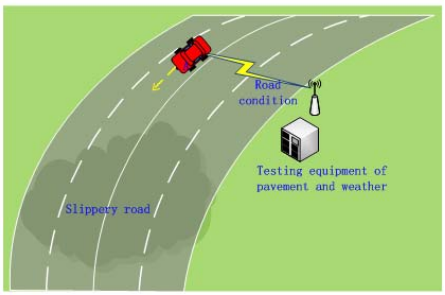

Figure 13. Adaptive Cruise Control based on road condition

E. Shipping Intelligent Transportation Systems

In the field of maritime transportation, the ITSC exploited several products and platforms, which are introduced below.

- Automatic Identification System(AIS)

The Ship-borne AIS system can display both static and dynamic information of own ship and ships nearby. The information includes position, speed and course, drought, ship type and so on, which are very important for the prevention of accident such as collision and grounding. The AIS has been certificated by the CCS register of shipping.

Figure 14. Automatic Identification System(AIS)

Based on the AIS system, the ITSC further developed some derivative products, such as fishing-net tracker, Class A and Class B chart machine. The devices are shown in the following Fig.15.

Figure 15. Derivative products of AIS exploited by ITSC

The shore-based AIS devices can receive message sent by ships near the base station. It can help the maritime administrations obtain ship traffic flow situation in real-time. The SAAB R40 AIS base-station is shown in the following Fig.16.

Figure 16. SAAB R40 AIS base-station

- Inland waterway electronic chart platform

The system is composed of three parts, which are information center management system, shipping company management system and ship-borne AIS application system.

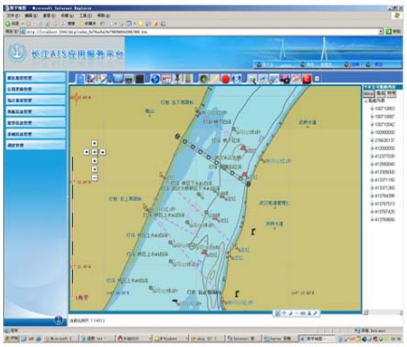

Figure 17. Electronic chart application platform

- Multi-function buoy

The buoy not only have the ordinary buoy's function, but also can send the information of the sensors installed on the buoy to the management center in real-time. The information includes hydro meteorological information, such as water level, current speed, visibility and so on. It can also give an alarm when oil spill accident happens in the water area.

IV. THE PROSPECT OF ITS

The cooperative driving platoons and intelligent transportation management were considered as two major prospect of ITS development, and they comprehensive integrate the emerged innovated technology for established safer, greener and smarted transportation systems.

A. Cooprative Driving for Platoons

Nowadays, advanced vehicle control and assistance technology has been wide used in intelligent vehicles, such as ACC, Forward Collision Warning (FCW), Lane Departure Warning (LDW) and other intelligent driver information system. With the development of cooperative vehicle-infrastructure systems, it organizes intelligent vehicles into multi-lanes, flexible platoons by cooperative maneuvers including following, merging and/or splitting, and lane-changing. For one lane, platoons can increase safety and vehicle density resulting from small relative velocity and small relative spacing between each other. For different lanes, platoons can plan their routes by means of vehicle to road communication and vehicle to vehicle communication, thus to increase the whole traffic capacity.

B. Intelligent Transportation Management

In the field of transportation management, Intelligent Transportation Management System (ITMS), already serving millions of vehicles and company, is a new generation management tool for bus and commercial coach transportation.

The GPS and 3G video servers should be installed in each vehicle, ITMS surveillance center could tracking their position and speed, when the speed was beyond the limit, the center would shown the vehicle, the manager could sent the information to warning them to speed down. The 3G video servers could sent back the picture of driving and the panorama of bus, when fatigue driving or emergency happened, the situation could be recorded, this ITMS could guarantee the safety driving. The taxi and other ITMS have also been developed in several counties.

Electronic Toll Collection systems would not only be applied in highway or expressway, in near future, you would also see them in city, and the toll system can be used in the congestion area or road. And the promotion of Electronic License Plate (ELP) application could make ETC easier and it could also be for traffic violation surveillance.

ACKNOWLEDGMENTS

This study is supported by the National Nature Science Foundation of China (60974094). The authors also

appreciate Zhang Rui, Lei Hu, Zheng Huarong and Zhang Jinfeng for their hard work in collecting data and documents.

REFERENCES

[1] National ITS Architecture Version 7.0, http://www.its.dot.gov/arch/index.htm

[2] S. Tang, F. Wang,G. Wang, X. Jia, and F. Liu, "Development and Research of Intelligent Transportation Systems in China's Tenth Five-Year Plan," Proc. of the IEEE ITSC 2006, Canada, pp. 377–382, September 2006.

[3] Zhe Mao. Research on the Recognizing Arithmetic of Fatigue Driving Based on the Physiologic Factor Analysis [D]. Wuhan: Wuhan University of Technology, 2006.

[4] Mao Zhe, Yan Xin-ping, Wu Chao-zhong, Zhang Hui, Huang De-qi. Analysis of Velocity Changing Rules Under Driving Fatigue [J]. Journal of Beijing University of Technology,2011,37(8):1175-1183.

[5] Zhe Mao, Deqi. Huang. Analysis of Steering Angle under Driving Fatigue. etcs, vol. 3, pp.650-653, 2010 Second International Workshop on Education Technology and Computer Science, 2010

[6] Wu Chao-zhong, Zhang Hui, Mao Zhe, Chu Xiu-min, Yan Xin-ping. A Model for Identifying Fatigue Status of Vehicle Drivers Based on Driving Operation [J]. China Safety Science Journal. 2007, 17(4):162-165.

[7] Liangli Zhang.Research on Motorist's Intention Recognition for Traffic Safety Precaution [D]. Wuhan: Wuhan University of Technology, 2011.

[8] Shenpei Zhou, Chaozhong Wu. A Recognition Method for Driver's Intention Based on Genetic Algorithm and Ant Colony Optimization[A]. 2011 Seventh International Conference on Natural Computation (ICNC). Donghua University Shanghai, China: IEEE, 2011: 1033-1037.

[9] Rui Zhang, Xinping Yan, Chaozhong Wu. A Recognition Model for Acceleration Intention of Automobile Drivers Based on Fuzzy Clustering[A]. Proceedings of the 1st Int. Conf. on Transportation Information and Safety. Wuhan, China: ASCE, 2011: 1938-1947.

[10] Wu Chao-zhong, Lei Hu. Review on the Study of Motorists' Driving Anger [J]. China Safety Science Journal. 2010,20(7):3-8.

[11] Hu Lei. The Characteristics of Angry Driving Behaviors and Its Effects on Traffic Safety [D]. Wuhan: Wuhan University of Technology, 2011.

[12] Lei Hu, Yan Xin-ping, WuChao-zhong, Zhang Hui. A Study on Chinese Motorists' Operational Behavior in Angry Driving.[C]. The 1st International Conference on Transportation Information and Safety (ICTIS 2011). American Society of Civil Engineers (ASCE), 2011:1905-1911.

[13] Zhang, H. and X. Yan, et al. (2010). Research on the Technology for Improving Safe Awareness Based on Driving Simulator. 2010 International Conference on Logistics Engineering and Intelligent Transportation Systems (LEITS). Wuhan, IEEE computer society: 63-66.

[14] Hui Zhang, Xin-ping Yan, Chao-zhong Wu. The Impact of Dual-Task on Lateral Performance: A Simulation-Based Study of Driving Distraction when Approaching Risky Situations. 11th International Conference of Chinese Transportation Professionals (ICCTP) Nanjing, ChinaAugust 14-17, 2011: 2326-2335

[15] Hongding Fan. Automobile Student Pilot Compatibility Examination Echnology and Taxonomic Approach Research [D]. Wuhan: Wuhan University of Technology, 2010.

[16] Y. L. Ma, X. P. Yan, Q. Wu and R. Zhang, "Research on Intelligent Vehicle Platoon Driving Simulation Experiment System under the Coordination between Vehicle and Highway" Journal of Computers, vol. 5, 2010, pp. 1767–1774.

An In-Vehicle System for Pedestrian Detection

Gang Liu
[1]Intelligent Transportation System Research Center
[2]College of Computer Science & Technology
Wuhan University of Technology
Wuhan, China
liu_gang@whut.edu.cn

Yufen Sun
College of Computer Science & Technology
Wuhan University of Technology
Wuhan, China
yufen@whut.edu.cn

***Abstract*—Pedestrian detection is a significant task in driver assistance systems. This paper presents an in-vehicle system for pedestrian detection. To speed up computation, we parallel implemented the state of the art detection algorithm on a NVIDIA GPU. The experiments demonstrate that our implementation can achieve accurate and real time detection.**

Keywords-pedestrian detection; in-vehicle; GPU; parallel processing; CENTRIST descriptor

I. INTRODUCTION

Currently, pedestrian collisions [1] become a serious traffic problem in our society. Because accurately detecting people in front of vehicles is an efficient way to enhance road safety, vision based pedestrian detection has been widely researched in driver assistance systems.

However, pedestrian detection in cars still remains a challenging problem. First of all, it is impossible to use simple method to find pedestrian in an image. Because there exist huge differences among pedestrians such as clothes, articulations, and background, the detection algorithm needs to deal with all these complex situations. Furthermore, the detection system is required to work in complex vehicle environments.

As detecting pedestrian in images is a classic application of object detection, many recognition methods have been introduced to solve this problem. Early methods [2] often applied template matching algorithms. Now more methods adopt features to detect pedestrian. The features commonly used are Haar-like feature [3], Histogram of Oriented Gradient (HOG) feature [4], and CENsus Transform hISTogram (CENTRIST) feature [5]. The C4 algorithm that uses CENTRIST feature is the state of art algorithm that shows good performance. At the same time, this algorithm is suited for processing in parallelism. Thus we choose the C4 algorithm as our method for pedestrian detection, and attempt to accelerate it by parallel computation.

Because new-generation general purpose GPUs (GPGPUs) consist of hundreds of small cores and support massively parallel processing, we use a GPGPU as the platform for implementing the C4 algorithm. By utilizing NVIDIA CUDA C [6], developers can easily code multi-thread program, and implement parallel processing.

In this paper, we design an in-vehicle system for pedestrian detection, and introduce a parallel implementation of the C4 algorithm via CUDA programming model. The experiment results demonstrate that our implementation can achieve accurate and real time pedestrian detection.

The reminder of the paper is organized as follows: the related works are briefly reviewed in section 2. In section 3, the in-vehicle system for pedestrian detection is introduced. In section 4, the parallel implementation of C4 algorithm is discussed in details. In section 5, the experiment results are provided. In section 6, the conclusion is given.

II. RELATED WORK

Pedestrian detection is an active research topic in vision applications such as video surveillance and intelligent vehicle. Numerous methods have been proposed in recent years.

Gavrila et al. [2] proposed a shape-based pedestrian detection method based on Distance Transforms. To solve the problem of human articulations, they have built a database of about 1000 pedestrian shapes.

Viola [3] introduced their Haar wavelet-based cascade framework to detect walking person. Based on cascade adaboost method, Cerri [7] developed a specific night-time classifier for poorly illuminated environments and designed an all-day-long pedestrian classification system.

Dalal et al. [4] first described HOG features for the problem of pedestrian detection in static images. Using HOG features, pedestrian's appearance and shape can be described by the distribution of intensity gradients or edge directions. Prisacariu [8] used the GPU and the NVIDIA CUDA framework to implement HOG.

Wu et al. [5], [9] believe that contour is the most important information for pedestrian detection. Therefore they designed the CENTRIST descriptor to detect human contour. Using the CENTRIST descriptor, they proposed the C4 algorithm that can accurately detect pedestrians. The steps of the algorithm are suitable for parallel processing to further improve the performance. Thus, it is beneficial to exploit a parallel implementation for C4 algorithm by using GPGPU.

III. PEDESTRIAN DETECTION SYSTEM DESIGN

The device of our pedestrian detection system is illustrated in Fig. 1. An in-vehicle industrial computer is chosen to process images. The industrial computer is designed to be compact, low power consumption, anti-vibration, and operating in a wide range of temperature from -20℃ to 60℃.

978-0-7695-4818-0/12 $26.00 © 2012 IEEE
DOI 10.1109/DCABES.2012.80

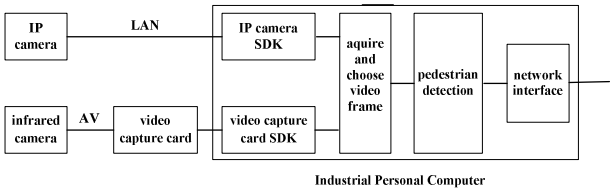

Figure 1. Design of pedestrian detection system.

The system is designed to work all 24 hours. There are two vision sensors, an IP camera and an infrared camera. A video capture card is responsible for acquiring video image from infrared camera.

A video card is installed in a PCI-E slot in order to accelerate image processing. After an image is written to the memory of industrial computer, it is then transferred to the memory of video card. The GPU in video card detects pedestrians in the image. The results of detection are returned to CPU and sent to another computer.

IV. GPU IMPLEMENTATION FOR THE C^4 ALGORITHM

Since the C4 algorithm is an efficient method for pedestrian detection, we present a GPU implementation using the NVIDIA CUDA framework.

A. The C^4 Algorithm

The execution process of our method is shown in Fig. 2. The detection program is divided into 2 parts: host and GPU processing. The host part runs on CPU. It converts a color image to grey image, copies the grey image into GPU memory, and fuses multiple overlapping results. The GPU part executes on the GPU, and it implements the C4 algorithm in parallel.

The basic idea of C4 algorithm is to detect human based on their contour information using a cascade classifier and CENTRIST. In the algorithm, a 36×108 sliding window is moved across at all locations in an image. In a window, the CENTRIST descriptors are extracted and a feature vector is calculated. Then the feature vector is multiplied with a trained linear classifier. The window is considered containing a human when the product is larger than a threshold.

The CENTRIST descriptor is obtained based on Census transform (CT) images, which is computed using Sobel images.

After an image has been scanned by at one scale, it is resized to a smaller scale. The algorithm is end after all scales have been processed.

An important advantage of C4 algorithm is that it makes use of an integral image substituting for the multiplication between classifier and feature vector.

Therefore, the main steps of GPU part contain computing Sobel image, CT image, integral image, and detecting human.

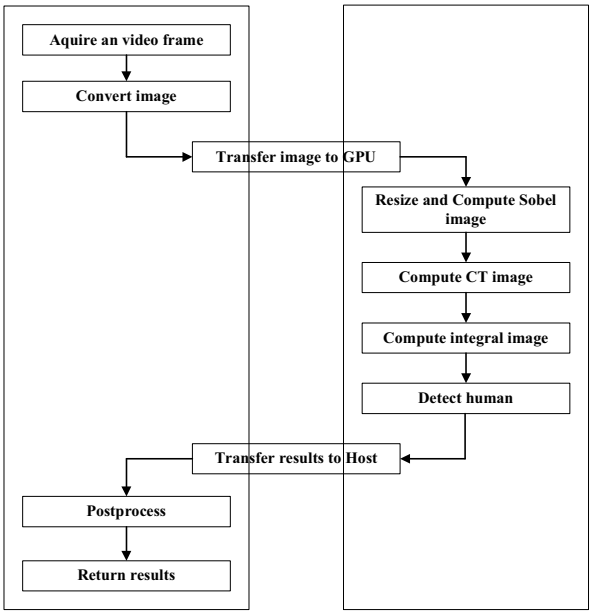

Figure 2. Execution process of GPU implementation.

B. Resizing Image and Computing Sobel Image

Traditionally, Sobel images are calculated based on two 3×3 Sobel operators. Before computing the value at a pixel in a Sobel image, it is needed to read the intensities of eight neighbouring pixels in the original image. If the original image is stored in global memory, the GPU should spend much time to access memory. Moreover, the borders of image require different processing, which decreases the parallelism of algorithm.

Instead of Sobel operators, we use texture memory to compute Sobel images. Texture memory is a type of read-only memory that is designed for classical graphics applications. It is also useful for image processing. Because texture memory is cached on chip, it can provide higher effective bandwidth by reducing memory requests to off-chip DRAM.

The resizing process is also implemented by texture. Thus computing Sobel image and resizing image are combined. After a grey image is transferred to GPU memory, it is then copied inside a texture. The intensity of each pixel in a resized image can be obtained by texture. To reduce memory traffic, resized images are not needed. The intensities of pixels are directly used to compute Sobel images, and not stored in memory.

C. Computing CT Image

Census transform compares the value of a pixel in a Sobel image with its eight neighbouring pixels. The result is a CT image. If the central pixel is larger than one of its neighbouring pixel, the corresponding bit of an 8 bits number is set to 1. The number is stored in the same location in CT image, so each value in CT image is between 0 and 255. The CENTRIST descriptor is a histogram of these CT

values. As there is no collision when computing the CT values, we use a thread for each pixel.

D. Computing CT Image

Although integral image is useful for speeding up such computation, it is still time-consuming when it is sequentially executed in GPU.

It is necessary to utilize the parallel processors of a GPU to speed up computation of integral image. An efficient parallel method is parallel prefix sum (scan) algorithm [10], the idea of which is to build a balanced binary tree on the input data and sweep it to and from the root to compute the prefix sum. Parallel prefix sum algorithm consists of two phases: the reduce phase (or the up-sweep phase) and the down-sweep phase.

In the reduce phase, the tree is traversed from leaves to root, computing partial sums at internal nodes of the tree, as shown in Fig. 3. At the end of this phase, the root node holds the sum of all data.

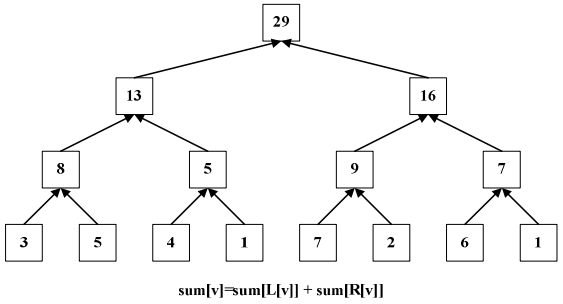

Figure 3. Reduce phase of parallel prefix sum.

In the down-sweep phase, the tree is traversed back down from the root, using the partial sums form the reduce phase, as shown in fig. 4. At the beginning, the value of root is set to zero. Then at each step, a node at the current level passes its value to its left child, and the value of its right child is equal to the sum of its value and the previous value of its left child.

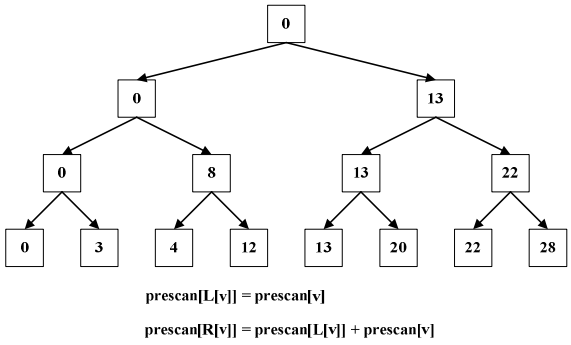

Figure 4. Down-sweep phase of parallel prefix sum.

When the input data is a two dimensional image, parallel prefix sum algorithm is first executed in every row, and then in every column. The result is the integral image that we want.

For a program running in the GPU, it is much faster to access data in shared memory than in global memory. So the parallel prefix sum algorithm is performed on an array in shared memory. The shared memory is made up of multiple banks. If a bank is accessed by multiple threads in a same warp simultaneously, a bank conflict occurs. The way to avoid bank conflicts is to add a variable amount of padding to each shared memory index. The added amount is equal to the value of the index divided by the number of memory banks.

E. Detecting Human

As described above, the C4 algorithm detects human by the product of a feature vector and the classifier. When calculating a feature vector, a sliding window is divided into 4×9 blocks. Adjacent 2×2 blocks are treated as a super-block. A CENTRIST descriptor is the histogram of a super block in the CT image. The feature vector of a sliding window is 24 CENTRIST descriptors.

Histogram computations are also processed by parallelism [11]. There are 256 different numbers of a CT value, so a histogram contains 256 bins. The size of a super-block is 18×24. 16×22 pixels are included in a histogram computation. We launch 11 thread blocks and every block consists of 32 threads. Each execution thread deals with a pixel and stores the result into a certain number of sub-histogram. Finally, all the sub-histograms are merged into a single histogram.

The sub-histogram is stored in shared memory, saving the time of writing off-chip. But it also brings the problem of bank conflicts if multiple threads in a same warp access their sub-histogram. The solution is as same as what we have done for integral image.

V. EXPERIMENTS

We have implemented the C4 algorithm using NVIDIA CUDA C. The program has run on a PC with Intel Core i7-2600 CPU, 8G memory, and NVIDIA GeForce GTX560 Ti video card. Fig. 5 shows a result of detecting pedestrian in a 400×300 image.

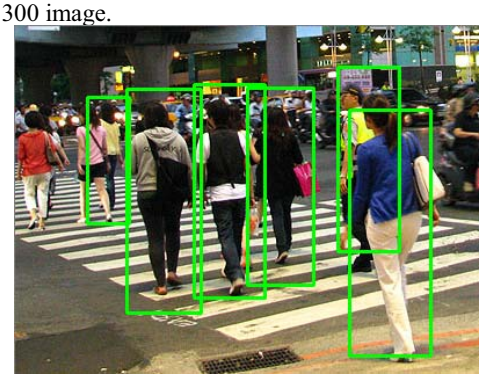

Figure 5. Result of pedestrian detection.

We use 30 images to test the correct rate of our implementation, and it can detect 80% pedestrian per image. An important reason is that people is occluded by obstacles, as shown in Fig. 6. Another reason is that the people's height

in an image is smaller than 108, for example the left people in Fig. 5.

Figure 6. Example that people is occluded.

The processing time of Fig.5 is 164 ms, so the program can run in real time.

VI. CONCLUSIONS

In this paper, an in-vehicle system has been designed for detecting pedestrian, and a GPU implementation of the C4 algorithm is introduced. The main steps, such as computing Sobel image, CT image, integral image, histogram, are processed in parallel. The experiment results show the performance of the system is good.

ACKNOWLEDGMENT

This work is supported by the National Natural Science Foundation of China (51179146) and the Fundamental Research Funds for the Central Universities (2012-IV-041).

REFERENCES

[1] M. Enzweiler and D. M. Gavrila, "Monocular Pedestrian Detection: Survey and Experiments," *IEEE Transactions on Pattern Analysis and Machine Intelligence*, vol. 31, pp. 2179-2195, Dec. 2009.

[2] D. M. Gavrila, "Pedestrian Detection from a Moving Vehicle," in *Proc. ECCV'00,* 2000, pp. 37-49

[3] P. Viola, M. J. Jones, and D. Snow, "Detecting Pedestrian Using Patterns of Motion and Appearance," in *Proc. ICCV'03*, 2003, pp. 734-741.

[4] N. Dalal, and B. Triggs, "Hisograms of oriented gradients for human detection," in *Proc. CVPR'05*, 2005, pp. 886-893.

[5] J. Wu, C Geyer, and J. M. Rehg, "Real-Time Human Detection Using Contour Cues," in *Proc. ICRA*, 2011, pp. 860-867.

[6] NVIDIA. NVIDIA CUDA C Programming Guide. [Online]. Available: http://developer.download.nvidia.com/compute/DevZone/docs/html/C/doc/CUDA_C_Programming.pdf

[7] P. Cerri, L. Gatti, L. Mazzei, F. Pigoni, H. G. Jung, "Day and Night Pedestrian Detection Using Cascade Adaboost System," in *Proc. ITS*, 2010, pp. 1843-1848.

[8] V. A. Prisacariu, and I. Reid. fastHOG – a real-time GPU implementation of HOG. [Online]. Available: http://www.robots.ox.ac.uk/~victor/papers/pdf/prisacariu_reid_tr2310_09.pdf.

[9] J. Wu and J. M. Rehg, "CENTRIST: A visual descriptor for scene categorization," *IEEE Transaction on Pattern Analysis and Machine Intelligence*, vol. 33, pp. 1489-1501, Aug. 2011.

[10] B. Bilgic, B. K. P. Horn, and I. Masaki, "Efficient Integral Image Computation on GPU," in *proc. Intelligent Vehicles Symposium*, 2010, pp. 528-533.

[11] T. Scheuermann, J. Hensley, "Efficient Histogram Generation Using Scattering on GPU," in *proc. Interactive 3D graphics and games*, 2007, pp. 33-37.

Evaluation of Traffic Control in Virtual Environment

Wang Xiaojing [a,b], Ye Wei[a], Wu Haowei[a,*], Ding Linjie[a], Zhang Chi[c]
[a]School of Computer Science and Technology, Huazhong University of Science and Technology, Wuhan, 430074, China
[b]Wuhan National Laboratory for Optoelectronics, Wuhan, 430074, China
[c]College of Optoelectronic Science and Engineering, Huazhong University of Science and Technology, Wuhan, 430074, China
*E-mail: richardkszero@gmail.com

***Abstract*—Due to the development of hardware technology, virtualization has been drawing more attention recently. Virtualization brings the benefits of ease management to users but also poses challenges to researchers. As multiple virtual machines run on a single hardware platform, the problem of resource allocation and scheduling, and performance of the system should be taken into consideration. In network environment, performance decreased significantly as more and more virtual machines sharing hardware resources. Since each user may have different demands, to improve the network QoS, we bring traffic control into Xen virtual platform to manage the network traffic and satisfy several desirable properties. Users are incentivized to share the network resources by ensuring that resources are weighted partitioned among them. And performance is improved by the optimized scheduler scheme. By classifying the requests into different priorities, scheduling the network request could improve the performance by decreasing 60% of latency and an adjustable throughput control.**

Keywords-Evaluation; Traffic Control; Quality of Service; Xen; Virtual machine

I. INTRODUCTION

Due to the development of hardware technology, virtualization has been drawing more attention recently. A physical machine can simulate various virtual machines via virtualization. The capability of sharing physical resources with multiple virtual machines increases resource utilization, saves energy, reduces cost and integrates resources [1]. Virtualization brings the benefits and convenience to users and also challenges to researchers. Multiple virtual machines are deployed on one physical machine, and then quality of service (QoS) is observably affected by the sharing, allocation and scheduling scheme [2].

Various network QoS requirements are demanded owing to the variety of applications and services. Video hosting service, such as YouTube, requires guaranteed bandwidth and low latency. As for file sharing, bandwidth is a bottleneck of network. Social networking, such as Twitter and Facebook, puts forward higher requirements of parallel processing and response delay [3]. Since multiple virtual machines run on a single hardware platform, resource allocation and scheduling should be taken into consideration. If the requirement is not satisfied, it will result in poor resource utilization and lower performance.

We have simulated and observed a simple scenario as services running in a virtual environment. In Xen virtual platform [4], multiple domains were delivering services at a same time. As Figure 1 shows, virtual machine 1 (VM1) had occupied all the network resources while the other domains were suspended. When VM2 started up, throughput was divided into two parts, and the latency of VM1 increased from a few micro-second to six hundred. The network became unacceptable for latency sensitive applications such as VoIP services and online game servers. As more VMs were added in, throughput of VM1 has dropped to 1/n and latency has multiplied accordingly, and the service is breaking down.

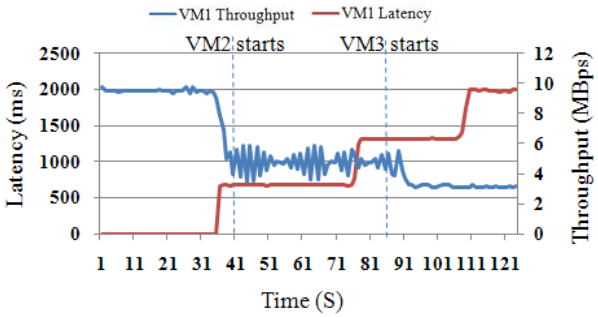

Fig. 1. Throughput and latency affected by other domains

Despite the vast works of work on resource allocations, the focus so far has been primarily on fair allocation. To ease the problem above, we classify the requests from virtual machines into several priorities. We use traffic control [5] implemented in Linux kernel to sort the requests by priority in Domain 0 in order to guarantee network QoS and satisfy users' requirement. Preliminary results indicate that while using traffic control to manage network data, latency of network applications with high priority is obviously shorter, furthermore, performance of the system is shown to be improved.

The rest of this paper is organized as follows: In Section 2, we present the management strategy used in current systems, and our solutions on scheduling packages to improve the performance of network applications via traffic control. Section 3 describes the test bed and experimental results of kinds of applications on servers. Section 4 concludes this paper and discusses avenues for future work.

978-0-7695-4818-0/12 $26.00 © 2012 IEEE
DOI 10.1109/DCABES.2012.53

II. TRAFFIC CONTROL STRATEGY

A. Network Virtualization in Xen

Before we explore where to undertake traffic control in a virtualization platform, we must first introduce the Xen networking model. In this section, we briefly introduce the para-virtualization in Xen, and the data path of network packages. In Xen, there is a Virtual Machine Monitor (VMM, or Hypervisor), providing virtual hardware resources for guest VMs, managing the resources and ensuring the performance isolation between virtual machines. Para-virtualization minimizes virtualization overhead between a guest OS and VMM. Dom0 is a privileged domain running on VMM in charge of managing other guests VMs (DomU). The architecture is shown as Fig 1.

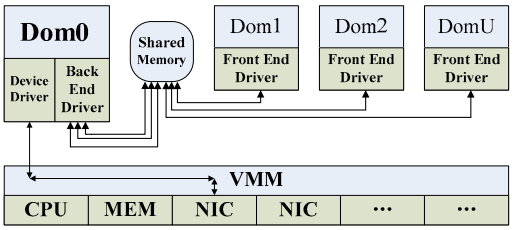

Fig. 1. Network virtualization in Xen

For guest OS in unprivileged domains, DomU uses a shared memory and event channel to convey a network I/O request from front-end driver to back-end driver. After receiving the request, the back-end driver maps it to the physical NIC and delivers the request to the corresponding device driver in Dom0. Commonly, Xen shares a physical network interface among multiple guest domains. Each virtual NIC in a guest domain can be connected to Xen in three primary modes-bridging, routing, or network address translation.

B. Traffic Control

To improve the network QoS in virtual environment, we introduce traffic control [6] in Xen, a bandwidth management system offered by Linux since the 2.2 series. The name traffic control represents the sets of queuing systems and mechanisms used for receiving and transmitting packets on a router. On the input of an interface, traffic control decides whether and which packets to accept and the rate of acceptance; on the output, it determines which packets to transmit and the order. Queues, which compose traffic control, collect entering packets and dequeue them as quickly as the underlying device can accept them. Traffic control in Linux is based on packet scheduling, adopting different queuing disciplines for different purposes.

There are two kinds of queuing disciplines, one is classless, the other classful. Classless ones, for example, FIFO, SFQ, ESFQ and TBF, are simple and usually used as the primary queuing disciplines on an interface, or inside a leaf class of a classful one. Classful ones, for example, CBQ, HTB, HFSC and PRIO, are complex and can attach filters, by which packets are classified into classes and subqueues.

Figure 2 shows how packages processed by Linux kernel to be transferred. When packets arrive, de-multiplexing module figures out the destination address. If it is local, packets will be transferred to upper layers in the protocol stack for further processing. If not, “Forwarding” will take them. Selection of the output interface, the next hop, encapsulation and other things will be decided in this module. After all of this manipulation, packets are queued on the separate output interface, where “Traffic Control” works. Using queuing discipline, “Traffic Control” may queue, drop, transmit or delay the packages by strategy. Once a packet is released, it is picked up by the device driver and emitted on the network.

Figure 2 shows approximately how data received from the network is processed by Linux kernel and how new data are created and sent on the network. When packets arrive at the input interface, it will be handled by “Input de-multiplexing”, which figures out the destination address from the header of datagram. If the destination address is local, packets will be transferred to upper layers in the protocol stack for further processing. If it is not, “Forwarding” will take them. Selection of the output interface, the next hop, encapsulation and other things will be decided in this module. After all of this manipulation, packets are queued on the separate output interface, which is under the control of “Traffic Control”. By means of queuing discipline, “Traffic Control” may queue them, drop them, transmit some of them, or delay the sending of them. Once a packet is released, it is picked up by the device driver and emitted on the network.

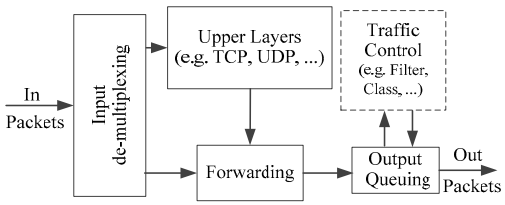

Fig.2. Workflow of Processing Network Data

C. Management strategy

The FIFO algorithm forms the basis for the default scheduler on all Linux network interfaces. It performs no shaping or rearranging of packets. To improve the performance of network applications, we used traffic control to rearrange the packets. “Traffic Control” consists of three main control elements: queuing discipline works as scheduler, class offers shaping capabilities, filter performs the classification. Each network device has an associated queuing discipline that controls how packets are queued on it. Briefly, a queuing discipline is a scheduler that manages the incoming and outgoing queues of a device in conformity

with the rules. Classless queuing disciplines contain no class. No filters can be attached to them, thus they don't have any utility for classifying. Classless ones have a handle to attach filters that contains further queuing discipline. Figure 3 shows an example of this queuing discipline.

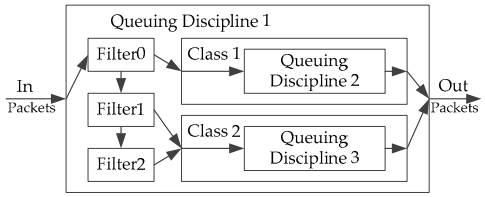

Fig. 3. An Example of Classful Queuing Discipline

The following properties we list should be followed in order to build traffic control framework efficiently.

a) Only the traffic transmitted can be shaped.
b) Every interface has a queuing discipline, when none is explicitly attached, the default one is pfifo_fast.
c) Classful queuing discipline without children classes can do nothing but consumes processor in vain.
d) When the bandwidth of a link is known, HTB is an ideal choice.
e) If the bandwidth varies, choose PRIO.
f) Use SFQ or ESFQ to split bandwidth with application.
g) To fairly share bandwidth with N IP addresses, N classes should be set.

In our experiment, in order to set priorities in different services, we use the classful queue discipline HTB as root queuing discipline 1:0, and set up the root class 1:1, which contains three subclasses: subclass 1:11 with high priority for VoIP, subclass 1:12 with second-high priority for HTTP service, subclass 1:13 with low priority for ftp service. Three SFQ queues are created to normalize every TCP connection which will treat each TCP connection equally. Eight filters are added to classify packets.

III. EXPERIMENT

A. Test bed

In this section, we evaluated the strategy of traffic control in Xen. We have a test bed on physical sever with Intel E5500, 8GB memory, 1G Ethernet. All the guest domains are built on Cent OS 5.4 with Xen 3.4. Each VM has one virtual CPU and 128MB memory. All VMs are connected to the network by virtual bridge in Xen. We used the following benchmarks to measure the latency of applications and throughput they use [7].

httping [8]: a ping-like tool for HTTP requests to measure how long the system takes to connect, send a request and retrieve the reply.

hping: Like the httping, this benchmark is used to create IP packets containing TCP, UDP payloads.

Iperf: Producing network requests to measure maximum TCP and UDP bandwidth.

B. Result

First, we present the effect on request latency by network-intensive workload. We experimented with two applications on two guest domains, HTTP server and httping. HTTP server is a heavy workload simulating file downloading in the network. We used httping to measure the variation of request delay while HTTP server is maintaining a download services.

As Figure 4 shows, the network latency increases significantly while one of the VMs running a network-intensive workload. To decrease the latency, we add a SFQ queue discipline and attach it to the class which manages the HTTP flow. The SFQ queuing discipline can provide equal chances for connections in the same class, which means a heavy load on a single TCP connection won't starve other machines in the same network. As results shown in Figure 4, by applying network QoS, the latency of the network decreases considerably from the previous 150ms to 50ms.

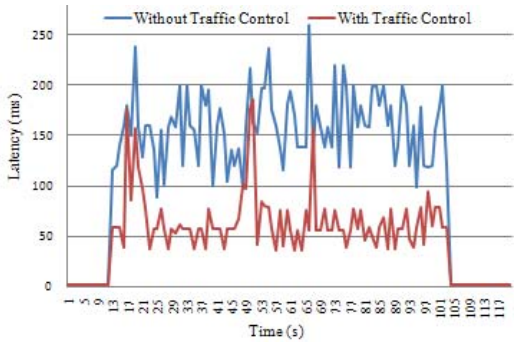

Fig.4. Latency with HTTP workload

Then, we demonstrate the effect on request latency of multiple network-intensive workloads. We used two guest domains, a HTTP server and a FTP server, on a single host. Another computer in the same subnet measures HTTP respond time instead of ICMP ping latency of the HTTP server. While FTP server is serving file downloads, figure 5 indicates that the HTTP response time arises significantly. This means that, the user is encountering a low QoS in web browsing.

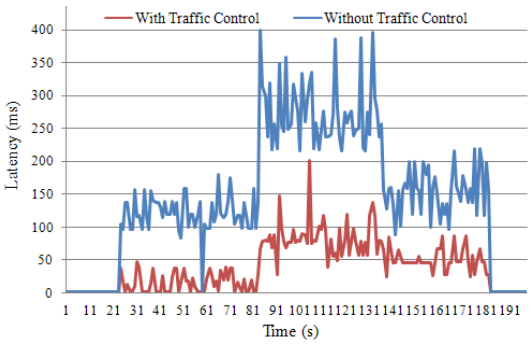

Fig.5. Latency with HTTP and FTP workloads

To ensure the quality of web service, we made two HTB Traffic Control classes for the HTTP Server and FTP Server to ensure the web service. As HTTP is always used for web browsing, we set its priority to 3, which is higher than the FTP Server's measurement. In Figure 5, the HTTP response time was about 60% lower than the one without the QoS.

In the third experiment, we test the latency of VoIP service under the circumstance of heavy network workload. Two VMs are respectively deployed with HTTP server and FTP server, whereas the VoIP service is installed on the third VM listening to the port 8080. The latency of VoIP connection is measured from a guest computer. In this experiment, both HTTP and FTP services are adjusted to the full speed. As Figure 6 shows, the latency of VoIP service without traffic control is significantly increased.

Packets of VoIP are marked using iptable. A prio 0 (the highest priority) filter was set up to classify these marked packets into the prio 0 Traffic Control class. As a result, the VoIP packets gain the highest priority when compete with other services.

The traffic control produced satisfying result.. As is shown in the Figure 6, VoIP service maintained comparatively low latency under the condition of saturated bandwidth, which demonstrates the significant effect of QoS.

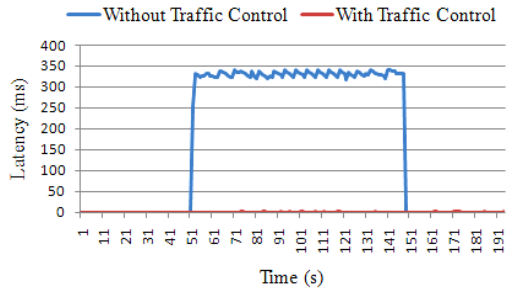

Fig. 6. Latency with VoIP workload

In experiment 4, we made a test about the effect of bandwidth control using QoS. At this time, HTTP and FTP services run on two separate VMs. As HTTP that is commonly used for web browsing produces bandwidth bursts while FTP that is used for bulk download produces long-lasting bandwidth.In order to optimize the network, we expect the FTP service to make a concession when HTTP requests burst. In our test without QoS, both HTTP and FTP shared a balanced proportion of bandwidth. Two filters are used to divide the flow into two TC classes where HTTP has higher priority. When QoS strategy is applied, there is a significant change. As the number of HTTP requests increased in Figure 7, the FTP service, whose bandwidth dropped down to a low level, yield to the demand of HTTP. When the HTTP responses are completed, the bandwidth of FTP returned normal. The strategy used here are beneficial to the QoS.

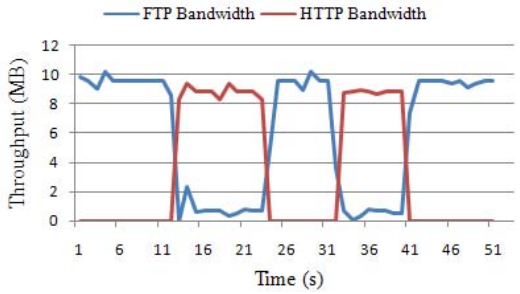

Fig. 7. Throughput with HTTP and FTP workload

IV. CONCLUSION

In this paper, we present the traffic control strategy for network QoS and compare different approaches in Xen virtual machine environment to achieve higher performance. We evaluated both latencies and throughput utilization with variety workloads using httping, hping, iperf benchmark. Tests show that latencies of virtual machine are significantly affected by heavy workload. Through traffic control, latency of HTTP request decreases by 60% that improved the quality of HTTP services. And throughput of every virtual domain could be allocated by this QoS strategy according to the system administrator. The module of traffic control has little CPU cost in the experiment which increases the CPU utilization by 2~3%.

ACKNOWLEDGEMENTS

This work is supported by the National Basic Research 973 Program of China under Grant No. 2011CB302301, 863 project 2009AA01A402, NSFC No.61025008, 60933002, 60873028, Changjiang innovative group of Education of China No. IRT0725.

REFERENCES

[1] Bratanov, S., R. Belenov and N. Manovich, Virtual machines: a whole new world for performance analysis. SIGOPS Oper. Syst. Rev., 2009. 43 (2): p. 46-55.

[2] Wiegert, J., G. Regnier and J. Jackson. Challenges for Scalable Networking in a Virtualized Server. in Computer Communications and Networks, 2007. ICCCN 2007. Proceedings of 16th International Conference on. 2007.

[3] Le, M., et al. Maintaining Network QoS Across NIC Device Driver Failures Using Virtualization. Proceedings in Network Computing and Applications, 2009. NCA 2009.

[4] Barham, P., et al., Xen and the art of virtualization, in 19th ACM Symposium on Operating Systems Principles (SOSP'03). 2003, ACM: USA. p. 164-177.

[5] Clark, David D.; Shenker, Scott; Zhang, Lixia.Supporting Real-Time Applications in an Inte-grated Services Packet Network: Architecture and Mechanism, Proceedings of SigComm'92, Baltimore, MD, August 1992.

[6] Werner Almesberger. Linux traffic control - implementation overview. Technical report, EPFL, Nov 1998. http://tcng.sourceforge.net.

[7] F. Heusden. httping. http://www.vanheusden.com/httping/X.

[8] X. Luo and R. Chang. Novel approaches to end-to-end packet reordering measurement. In Proceding of ACM/USENIX IMC, Oct.2005. Berkeley, CA. 2005.

Restoring Method of Vessel Track Based on AIS Information

Sang Ling-zhi[1,2] *Yan Xin-ping*[1,2] *Mao Zhe*[1,2] *Ma Feng* [1,2]
1 Intelligent Transportation System of research Center, Wuhan University of technology;
2 Engineering Research Center of Transportation Safety (Ministry of Education)
Wuhan, China
sanglz@126.com; xpyan@whut.edu.cn; yaner@whut.edu.cn; martin7wind@163.com

***Abstract*—Based on Automatic Identification System (AIS) information, the existing vessel track is combined by linking the two adjacent points. The linked track is very different from the real track of the vessel. So a fitting method is needed for restoring the real track vividly. AIS information is processed when the vessel is stand-on and turning by Piecewise Linear Interpolation, Piecewise Cubic Interpolation and Piecewise Cubic Spline Interpolation. The results show that the three tracks are nearly the same when the vessel is stand-on, the track presents by Piecewise Cubic Spline Interpolation is best, which proves that Piecewise Cubic Spline Interpolation is a good method to restore the vessel track in utilizing AIS information.**

Keywords- vessel；track；restore；AIS

I. INTRODUCTION

Automatic Identification System (AIS) is a digital navigation equipment used by vessels, which integrated network technology, modern communication technology, computer technology and electronic information display technology. Information provided by AIS equipment, such as unique identification, position, speed, course, change course rate and the other static information, voyage information, can be broadcasted in the band of Very High Frequency (VHF) to other nearby vessels and AIS Base stations for identifying and locating vessels.

With the development of AIS, AIS plays a more and more important role in protecting the maritime safety[1-3].AIS information can be used to statistic and forecast the vessel traffic[4], analysis the characteristics of the vessel traffic flow[5,6], manage the traffic and process maritime accident[7-10].

Vessel track is the key to research the characteristics of the vessel traffic flow and process the maritime accident. According to the vessel track, nearby vessels' intention can be determined, and effective measures can be taken to avoid accidents in advance. The distribution of traffic flow, the situation and measures before the accident which are very important can all get by the track. Currently, the existing vessel track is combined by linking the two adjacent points according time series [11], as a result, this track is different from the real track. For restoring the real track vividly, a fitting method needs to be designed.

II. MATHEMATICAL MODELS

The transmit frequency of AIS messages is determined by the speed of vessels, and Global Positioning System information is included in the messages. So the received ship position values are a time series of discontinuous points. There are $n+1$ discontinuous points, and the abscissa values in the interval $[a,b]$ meet the condition: $a \le x_1 < x_2 < \cdots < x_{n+1} \le b$, correspondingly, the ordinate vales are y_1, y_2,$\cdots$, y_{n+1}.

A. Piecewise Linear Interpolation

Currently Piecewise Linear Interpolation is generally adopted in restoring vessel track, every two adjacent points in time series get one piece, the track of one piece can be drawn by linear interpolation, and then get the whole vessel track. The formulas of the vessel track $f(x)$ adopted in Piecewise Linear Interpolation are:

$$f(x)=\sum_{i+1}^{n} f(x_i,y_i)$$

$$f(x_i,y_i)=y_i+(x-x_i)\frac{y_{i+1}-y_i}{x_{i+1}-x_i}$$

B. Piecewise Cubic Interpolation

Piecewise Cubic Interpolation can make a continuous and smooth curve based on the vessel positions, and the vessel track $g(x)$ would have a continuous tangent.

The vessel track can be constructed by this method: there are a cubic polynomial and a continuous first derivation between x_i, x_{i+1}. The formulas are:

$$g(x)=ax^3+bx^2+cx+d$$

$$g'(x)=ax^2+bx+c$$

For every one piece, there are:

$$\begin{cases} g_i(x)=ax_i^3+bx_i^2+cx_i+d \\ g_i(x)=ax_{i+1}^3+bx_{i+1}^2+cx_{i+1}+d \\ g_i'(x)=ax_i^2+bx_i+c \\ g_i'(x)=ax_{i+1}^2+bx_{i+1}+c \end{cases} \qquad i=1,2,\cdots,n$$

978-0-7695-4818-0/12 $26.00 © 2012 IEEE
DOI 10.1109/DCABES.2012.84

C. *Piecewise Cubic spline Interpolation*

Piecewise Cubic Spline Interpolation can make a continuous and smooth curve which not only has a continuous tangent, but also has a continuous curvature. The restored track by this method is more consistent with the real track.

The vessel track can be constructed by this method:

The track $s(x)$ meets the conditions:

$$\begin{cases} s(x) \in C^2[a,b] \\ s(x) \text{ is a cubic polynomial in interval } [x_i, x_{i+1}] \\ s(x) = f(i = 1,2,\cdots,n+1) \end{cases}$$

Add the corresponding boundary conditions:

$$s'(x_1) = f_1', \quad s'(x_{n+1}) = f_{n+1}'$$

By solving three bending moment equations:

$$\begin{bmatrix} 2 & 1 & & & \\ \mu_2 & 2 & \lambda_2 & & \\ & \ddots & \ddots & \ddots & \\ & & \mu_n & 2 & \lambda_n \\ & & & 1 & 2 \end{bmatrix} \begin{bmatrix} M_1 \\ M_2 \\ \vdots \\ M_n \\ M_{n+1} \end{bmatrix} = \begin{bmatrix} d_1 \\ d_2 \\ \vdots \\ d_n \\ d_{n+1} \end{bmatrix}$$

$$M_i' = s''(x_i) \quad i = 1,2,\cdots,n+1$$

$$\mu_i = \frac{x_i - x_{i-1}}{x_{i+1} - x_{i-1}}$$

$$\lambda_i = 1 - \mu_i$$

$$d_i = 6f[x_{i-1}, x_i, x_{i+1}] \quad i = 2,3,\cdots,n$$

$$d_1 = \frac{6}{x_1 - x_2}(f[x_1, x_2] - f_1)$$

$$d_{n+1} = \frac{6}{x_{n+1} - x_n}(f_{n+1} - f[x_n, x_{n+1}])$$

The cubic spline interpolation function in interval $[x_i, x_{i+1}]$ can get by the formula:

$$s_i(x) = \frac{(x_{i+1} - x)^3}{6h_i} M_i + \frac{(x - x_i)^3}{6h_i} M_{i+1} + \frac{x_{i+1} - x}{h_i}\left(f_i - \frac{h_i^2}{6} M_i\right) + \frac{x - x_i}{h_i}\left(f_{i+1} - \frac{h_i^2}{6} M_{i+1}\right)$$

So the three bending moment equations must be solved to get M_i , and then get $s(x)$.

III. TRACK RESTORING AND ANALYSIS

When the vessel is on voyage, the track can be divided into two classes: stand-on and turning, so the vessel should be either stand-on or turning. The two situations could be restored to analysis the whole track.

After parsing the AIS message collected in 10th Jan 2012, a couple of information when the vessel is stand-on and another couple of information when the vessel is turning are selected to analysis the tracks restored by the three methods above in MATLAB.

A. *Stand-On Track Restoring*

The stand-on vessel's information of time and vessel positions are showed in table.1 in time series.

Table.1 Information of Stand-On Ship

Time	East Longitude	North Latitude
2012-01-10 01:28:11	114.473155	30.685823
2012-01-10 01:28:41	114.472363	30.685588
2012-01-10 01:29:11	114.471595	30.685362
2012-01-10 01:29:41	114.470845	30.685123
2012-01-10 01:30:11	114.470158	30.684925
2012-01-10 01:30:41	114.469443	30.684737
2012-01-10 01:31:11	114.468797	30.684598
2012-01-10 01:33:43	114.465807	30.683693
2012-01-10 01:34:13	114.465252	30.683502
2012-01-10 01:34:43	114.464685	30.683315
2012-01-10 01:36:12	114.463013	30.682747
2012-01-10 01:36:42	114.462463	30.682568
2012-01-10 01:37:12	114.461938	30.682410
2012-01-10 01:37:42	114.461347	30.682245
2012-01-10 01:38:12	114.460817	30.682085
2012-01-10 01:38:42	114.460257	30.681897

In MATLAB, the tracks restored by the three methods are showed in fig.1-fig.4.

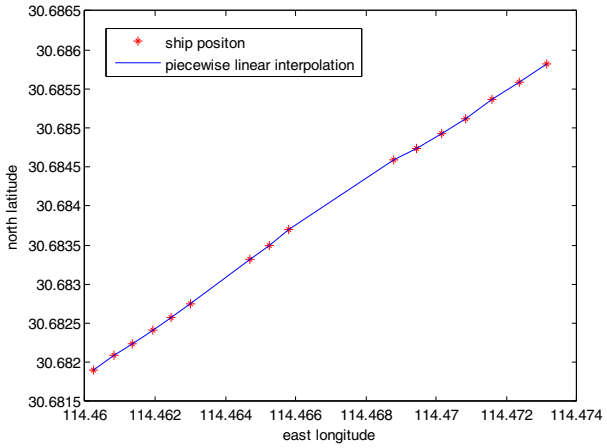

Fig.1 Track Restored by Piecewise Linear Interpolation

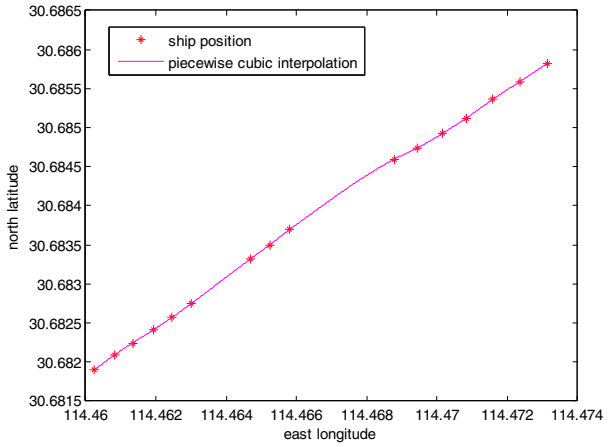

Fig.2 Track Restored by Piecewise Cubic Interpolation

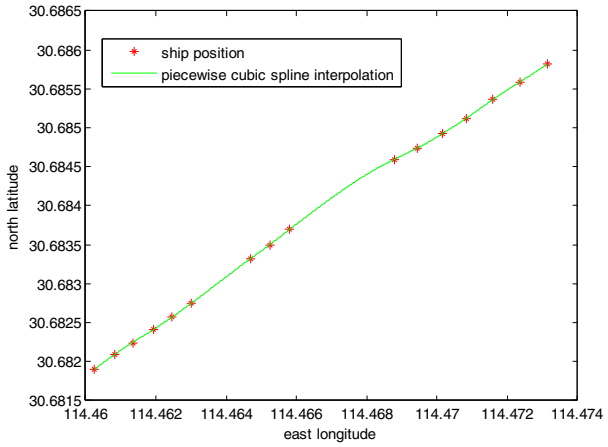

Fig.3 Track Restored by Piecewise Cubic Spline Interpolation

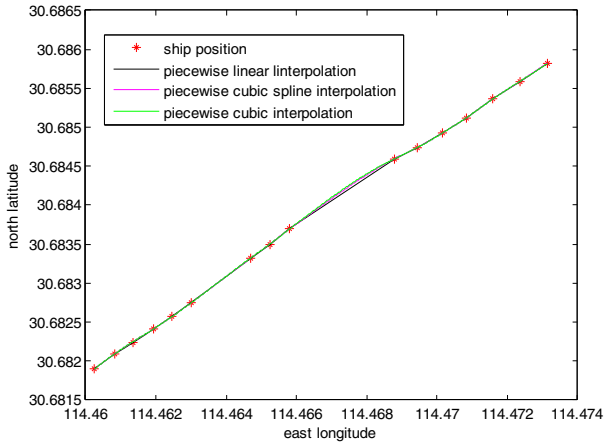

Fig.4 Comparison of Three Tracks

It can be showed from the four figures that these four tracks are nearly the same when the vessel is stand-on.

B. Turning Track Restoring

The turning vessel's information of time and vessel positions are showed in table.2 in time series.

Table.2 Information of Turning Ship

Time	East Longitude	North Latitude
2012-01-10 14:50:33	114.374320	30.643837
2012-01-10 14:52:57	114.374280	30.643917
2012-01-10 14:53:28	114.374053	30.644327
2012-01-10 14:54:28	114.373240	30.645190
2012-01-10 14:54:29	114.373227	30.645203
2012-01-10 14:54:56	114.372747	30.645463
2012-01-10 14:54:58	114.372707	30.645473
2012-01-10 14:54:59	114.372693	30.645477
2012-01-10 14:55:29	114.372240	30.645463
2012-01-10 14:56:00	114.371853	30.645297
2012-01-10 14:57:00	114.371093	30.644727
2012-01-10 14:57:31	114.370680	30.644377
2012-01-10 14:57:56	114.370280	30.644093
2012-01-10 14:58:00	114.370227	30.644057
2012-01-10 14:58:01	114.370213	30.644047
2012-01-10 14:59:02	114.369200	30.643327

In MATLAB, the tracks restored by the three methods are showed in fig.5-fig.9.

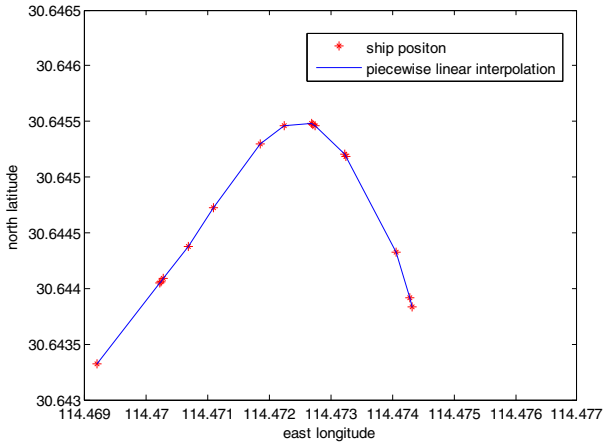

Fig.5 Track Restored by Piecewise Linear Interpolation

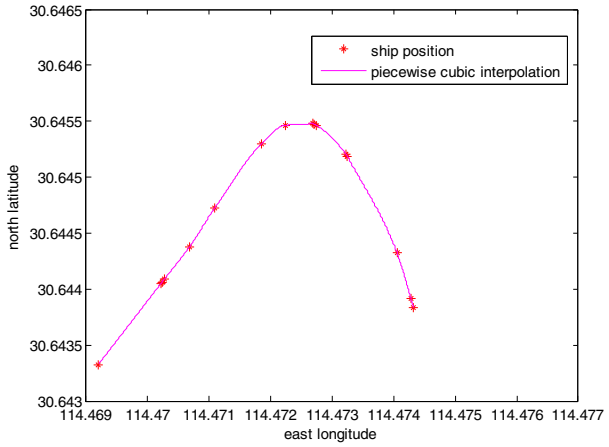

Fig.6 Track Restored by Piecewise Cubic Interpolation

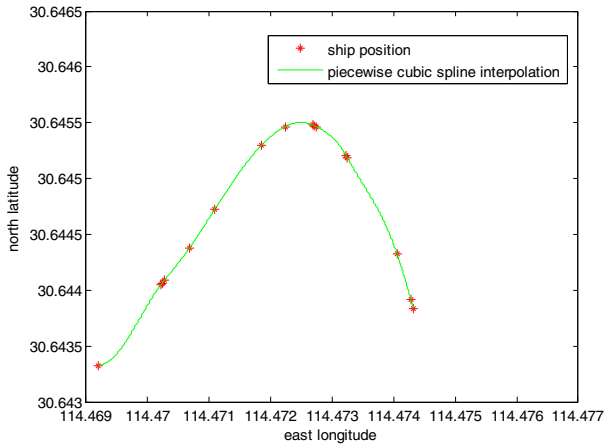

Fig.7 Track Restored by Piecewise Cubic Spline Interpolation

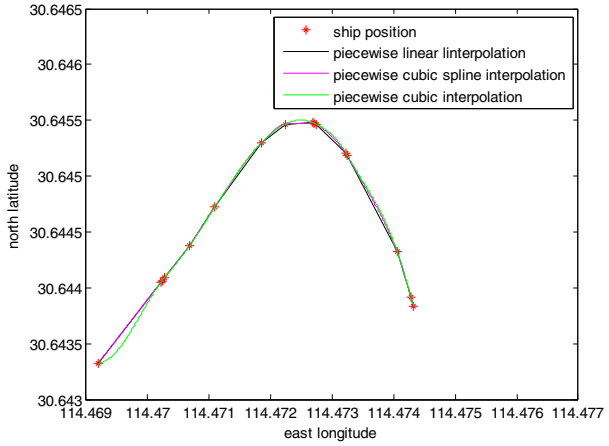

Fig.8 Comparison of Three Tracks

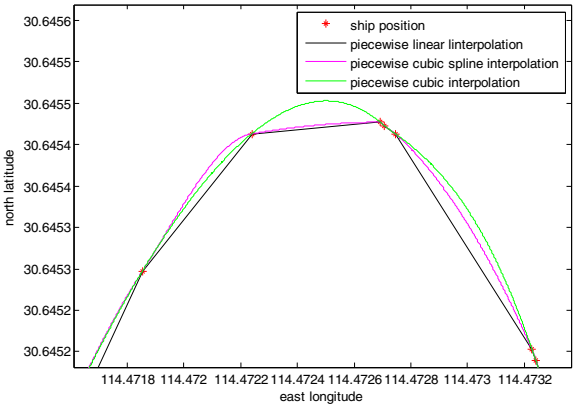

Fig.9 Comparison of Three Tracks by Larger Scale

When the vessel is turning, the tracks restored by these three methods are very different, which is obviously in Fig.9. The track restored by Piecewise Cubic Spline Interpolation has the best smooth effect.

C. Analysis

Piecewise Linear Interpolation, Piecewise Cubic Interpolation and Piecewise Cubic Spline Interpolation are all useful to restore the vessel track. And the first method is adopted to get the track now. When the vessel is stand-on, the tracks restored by these three methods are nearly the same, but when it turning, the track restored by the third method has the best smooth effect.

IV. CONCLUSION

Divide the vessels' tracks into two classes: stand-on track and turning track. AIS massages are parsed and then the two classes are selected to restore tracks with Piecewise Linear Interpolation, Piecewise Cubic Interpolation and Piecewise Cubic Spline Interpolation. The three tracks are nearly the same when the vessel is stand-on, but when the vessel is turning, the third method has the best smooth effect.

ACKNOWLEDGMENT

This paper is supported by Western Communications Construction Scientific and Technological Project of Ministry of Transportation of the People's Republic of China (Grant No. 201132820190), National High Technology Research and Development Program of China (Grant No. SS2012AA112303).

REFERENCES

[1] Elhillali Y; Tatkeu C; Deloof P; etc. Enhanced high data rate communication system using embedded cooperative radar for intelligent transports systems[J]. Transportation Research Part C-Emerging Technologies, 2009,(03): 429-439.

[2] Kawaguchi A ; Inaishi M ; Kondo H ; etc. Towards the development of intelligent navigation support systems for group shipping and global marine traffic control[C]. 10th Applications of Advanced

Technologies in Transportation Conference, Athens, 2008.
[3] Zhao Haibo, Zhang Yingjun. Study on applications of AIS in the northern sea region of China[J]. Journal of Dalian Maritime University, 2007,(s2): 81-86. (in Chinese)
[4] Li Hongxiang, Fang Xun. Statistical Method Research of Vessel Traffic Flow Based on AIS[J]. Journal of Wuhan University of Technology(Transportation Science & Engineering),2011,(04): 853-857. (in Chinese)
[5] Jin Xingfu; Fu Yuhui; Zhang Liandong. Research on vessel traffic flow at Chengshantou water area based on AIS Data[J]. Journal of Dalian Maritime University, 2012,(01): 33-36. (in Chinese)
[6] Chang SJ, Hsu GY, Yang JA, etc. Vessel Traffic Analysis for Maritime Intelligent Transportation System[C]. 2010 IEEE 71st Vehicular Technology Conference, Taipei, 2010.
[7] Li Xudong; Hu Shenping. Application of AIS information analysis in ship collision cases[J]. Journal of Shanghai Maritime University, 2007,(01): 132-136. (in Chinese)
[8] Bai Yuming; Dai Ran; Sun Licheng; etc. Application of AIS in Marine Traffic Investigation[J]. Navigation of China, 2006,(01): 82-85. (in Chinese)
[9] Qu XB; Meng Q; Li SY. Ship collision risk assessment for the Singapore Strait[J]. Accident Analysis And Prevention, 2011,(06): 2030-2036.
[10] Cervera MA; Ginesi A; Eckstein K. Satellite-based vessel Automatic Identification System: A feasibility and performance analysis[J]. International Journal of Satellite Communications and Networks, 2011,(2): 117-142.
[11] Tang CB, Shao ZP, Tang QR, etc. Vessel Track Distribution Algorithm Based on AIS[J]. Journal of Jimei University(Natural Science), 2011,(03): 109-112. (in Chinese)

An Algorithm for Trip Planning with Constraint of Transfer Connection in Urban Mass Transit Network

Jianyuan Guo
School of traffic and transportation
Beijing Jiaotong University
Beijing, China
e-mail: jyguo@ bjtu.edu.cn

Limin Jia*, Jie Xu,Yong Qin
State Key Laboratory of Rail TrafficControl and Safety
Beijing Jiaotong University
Beijing, China
e-mail: guojy116@126.com

***Abstract*—In large scale urban mass transit (UMT) network, different lines in a transfer station always stop at different time. Thus, in the time span of last trains running, passengers are easy to face a problem when transferring: the next line already stopped. This brings big inconvenience to passengers. A survey from 276 passengers in Beijing shows that 51 percent passengers have ever missed the last trains when transferring. As to solve this problem, we analyzed the factors which affect the transfer such as: the topology of UMT network, schedule, distribution of passengers' transfer time. Then we introduced an algorithm with the constraint of transfer connection. Experiments were conducted to validate this algorithm based on the real UMT network in Beijing China. The result shows that the algorithm is efficient to tackle this problem. With the development of the trip planning system based on this algorithm, it will make the late trip more convenient for passengers.**

Keywords- trip planning; transfer connection; last train; urban mass transit

I. INTRODUCTION

With the development of the large scale urban mass transit (UMT) network, it is common that passengers transfer between different lines to reach their destinations. For example, in London, about 70% of Underground trips and 30% of bus trips involve at least one transfer [1]. Because of transfer, more routes are provided and more uncertainty is brought in. Especially in the span of last trains running (SLTR), passengers are easy to face a problem when transfer that the next line stopped and no train is available.

It is very inconvenient for passengers missing last train. In some developed city, UMT always stop at midnight (such as Tokyo), or runs over night (such as NewYork), or there are supplementary public transit mode running all day along (such as in London). So few passengers will miss the last trains and the trip planning in SLTR hasn't been paid attention to by researchers.

However, in the city developing UMT, such as Beijing, Shanghai, Guangzhou, Shenzhen, new lines joined the network continuously and the stopping time of UMT networks are more early considering the maintenance of new lines. The number of passengers is large in SLTR, and there are quite a lot of passengers have ever missed the last trains. According to the survey in Beijing, 74 percent passengers have experienced missing last trains. In these 74 percent passengers, 51 percent of them missed last trains after transfer. So, it is necessary to look into the trip planning problem in SLTR.

The trip planning problem focuses on path searching and path cost computing. Multi-costs are considered in path finding process. In-vehicle time, waiting time, walking time and a time penalty were taken into account for each line change by Tong [2,3] and Cepeda [4]. Huang[5,6] concerned schedule coordination for trip planning, and used forward or backward search algorithm to the optimal path for an expected arrival time at the destination with departure time or arrival time. Tan[7] computed the reasonable paths for passengers concerning trip time, transfer times, walking time, waiting time and trip fare.

For all the researches stated in above, no one concerns about the factors which affects transfer connections. Aiming to tackle the problem, the factors affecting transfer connections are analyzed in section 2. An algorithm is presented in section3. Experiments based on the real UMT network in Beijing China are shown in section 4.

II. FACTORS AFFECTING TRANSFER CONNECTIONS.

1) The topology of UMT network

It is the pre-condition to guarantee transferring successfully that the origin and destination are connected in a topology of UMT network. Meanwhile passengers' transfer cost are influenced by the conditions such as transfer space , transfer distance .

2）Schedule

It is the general condition to guarantee transferring successfully that the scheduling departure time and arriving time in a transfer station must satisfy formula 1. It means that passengers must be ready for a train before its departure time in the scheduling.

$$D=TD-TA-TR \geq 0 \quad (1)$$

Where TR means passengers' transfer time. TA means the time when passengers getting off from a train in previous line.TD means the departure time of a train that passengers want to get on after transfer.

3）Distribution of passengers' transfer speed

According to[8], the distribution of passengers' transfer time is described as follows:：

$$f(TR)=\frac{1}{\sigma\sqrt{2\pi}}e-\frac{(x-u)^2}{2\sigma^2} \quad \textbf{(2)}$$

Where u means average transfer time, σ means the fluctuations of the transfer time.

978-0-7695-4818-0/12 $26.00 © 2012 IEEE
DOI 10.1109/DCABES.2012.79

If TR≤ TD-TA , the condition of transfer connection will be satisfied. The formula is shown as follows:

$$F(TR)=f(TR \le TD\text{-}TA)=\int_{-\infty}^{TD-TA}\frac{1}{\sigma\sqrt{2\pi}}e-\frac{(x-u)^2}{2\sigma^2}dx \quad (3)$$

III. ALGORITHM OF SLTR

A. Definitions

G a schedule-based UMT network

R a set of potential-routes connecting all possible OD in G

R_{o-d} a set of potential-routes connecting OD pair o-d in G (SPPR)

$\overline{R}_{o-d}$ the total number of the SPPR

$r_i \in R_{o-d}, i=1,2,...,\overline{R}_{o-d}$ a route in SPPR

P_i the trip connecting r_i ,

$L(r_i)$ a set of lines in r_i

$\overline{L}(r_i)$ total number of the lines in r_i

$l_j \in L(r_i)$, $j=1,...,\overline{L}(r_i)$ a line in $L(r_i)$

$S(r_i)$ the set of stations on r_i

$\overline{S}(r_i)$ total number of the stations in r_i

$S_k \in S(r_i)$, $k=1,2...,\overline{S}(r_i)$ a station in $S(r_i)$

$TR^s_{l_f-l_w}$ the transfer time from line l_f to l_w at s

v a train run on G

$\overline{SV}$ the total number of the train departing from or arriving at s

Dir(v) the direction of v

$Dir_{S_{k-1}-S_k}$ the direction from S_{k-1} to S_k

$ta^{s_k,v}_{l_j}$ the arrival time of v at s_k on l_j

$td^{s_k,v}_{l_j}$ the departure time of v at s_k on l_j

TD_{p_i} the departure time of P_i

TA_{p_i} the arrival time of P_i

$VL^{s_k}_{l_j}$ the last train arriving s_k on l_j

SO_v the origin of v

SD_v the destination of v

$VN(S_k,v)$ the first train departing from S_k after v arriving S_k ,

$VP(S_k,v)$ the first train arriving S_k before v departing from S_k ,,

$VA(l_j,S_k,t)$ the train arriving S_k before t,,and there is no other train arriving S_k after $ta^{s_k,v}_{l_j}$ and before t

$VD(l_j,S_k,t)$ the train departing S_k after t , and there is no other train departing S_k before $td^{s_k,v}_{l_j}$ and after t

$BTR(S_k)$ if it equals to 1, passenger must transfer at s_k

$ATP^s_{l_f-l_w}$ the probability of transferring successfully from l_f to l_w at station s, which can be obtained according to formula 3

AP_{p_i} the reliabilityof P_i, it means the probability of reaching destination through P_i

$\underline{AP}$ Minimum reliability accepted by passengers

T_{p_i} trip time of P_i

$\overline{TR}_{p_i}$ the number of transfer in P_i

TA_s the time of walking to s

LT_{p_i} if it equals to 1, P_i is the latest trip though r_i ,if it equals to -1 , it means the station is closed. If it equals to 0, it means the other situation left.

B. Framework of the algorithm

The purpose of the algorithm is to compute T_{p_i} , $\overline{TR}_{p_i}$ and AP_{p_i} , It consists of three main steps as following:

Step1: Compute all potential routes for the possible origin and destination in the transit network. The physical topology of transit network are constant in a time slot, but the scheduling of trains is always different in weekend, holiday, or changing for other reasons. This step is done as a preparation for next steps. It is implemented by a branch and bound algorithm[9], and the bound is constrained by the number of transfer and the distance difference between a route to the shortest distance in R_{o-d} .

Step2: For a specified origin and destination, find the latest trip P_i (LT_{p_i} =1)connecting every potential route .If the start time passengers chosen is later than latest trip, return.

Step3: According to the start time, compute T_{p_i} , $\overline{TR}_{p_i}$, AP_{p_i} .

C. Procedure of ccomputing the latest trip for r_i

AP_{p_i} :=1;

j= $\overline{L}(r_i)$;

for k:= $\overline{S}(r_i)$ downto 1

{if (k= $\overline{S}(r_i)$)

$\widetilde{V} := VL_{l_j}^{s_k}$, $\widetilde{t} := ta_{l_j}^{s_k,\widetilde{v}}$;

else

{ if($BTR(S_k)$ =1)

{ j=j-1,

if (Dir($\widetilde{V}$)≠Dir(S_{k-1}, S_k))

{

$\widetilde{V}$:=VA($l_j, S_k, ta_{l_{j+1}}^{s_k,\widetilde{v}} - TR_{l_j-l_{j+1}}^{s_k}$);

while （ $AP_{p_i} * ATP_{l_f-l_w}^{s_k} < \underline{AP}$ ）

$\widetilde{V} := VP(S_k, \widetilde{V})$;

$AP_{p_i} := AP_{p_i} * ATP_{l_f-l_w}^{s_k}$;

}

}

else if ($S_k = SO_{\widetilde{v}}$) $\widetilde{V} := VP(S_k, \widetilde{V})$;

}

}

k=k-1;

}

$TD_{p_i} = td_{l_j}^{s_k,\widetilde{v}}$;

D. Procedure of computing T_{p_i} , $\overline{TR}_{p_i}$ *the and* AP_{p_i} ,

if （TD> TD_{p_i} ）

return;

j=1;

for k:=1 to $\overline{S}(r_i)$

{ if k=1

$\widetilde{V} := VL_{l_j}^{s_k}$, $\widetilde{t} := TD_{p_i}$, $TA_s := TA_{s_k}$;

else

{ if $BTR(S_k)$ =1

{ j=j+1;

if (Dir($\widetilde{V}$)≠Dir(S_{k-1}, S_k))

{

$\overline{TR}(r_i) := \overline{TR}(r_i) + 1$;

$\widetilde{V}$:=VD($l_j, S_k, ta_{l_{j-1}}^{s_k,\widetilde{v}} + TR_{l_j-1-l_j}^{s_k}$);

while （ $AP_{p_i} * ATP_{l_f-l_w}^{s_k} < \underline{AP} \cap LT_{p_i}$ =1）

$\widetilde{V} := VN(S_k, \widetilde{V})$;

$AP_{p_i} := AP_{p_i} * ATP_{l_f-l_w}^{s_k}$

}

}

else

{if($S_k = SD_{\widetilde{v}}$) $\overline{TR}(r_i) := \overline{TR}(r_i) + 1$, $\widetilde{V} := VN(S_k, \widetilde{V})$; }

}

k=k+1;

}

$T_{p_i} = ta_{l_j}^{s_k,\widetilde{v}} + TA_s$;

IV. EXPERIMENT

A. Efficiency of the algorithms

The procedure developed in this paper was tested on urban mass transit network in Beijing, China. There are 163 stations and 12 lines in Beijing urban mass transit network (2011) (shown in figure 1). The real schedule of the transit network is used as well.

Figure 1. The map of urban mass transit network in Beijing, China(2011)

The algorithm was coded in C#. The computational experiment was performed on a personal computer with an Intel Core(TM)2 Duo 2.26GHz computer processor and 2GB of RAM. The time of computing 3000 OD ($\overline{TR}(r_i)$ >1) is less than 1s. The time used to compute all OD in experimental network is less than 10 minutes. It proved that the algorithm is efficient.

B. Samples

Several samples of these experiments are shown in table 1-3. The transfer times are obtained by survey. In these samples, the Origin is Haidianhuangzhuang, and destination is Sihui.

The information of the potential routes is shown in table 1.

The departure time of the trip is 22:20 in table 2 and 22:39 in table 3. Seven routes are chosen from table 1, on which the times of transfer is less than two. Here $\underline{AP}$ =0.5.

In table2, the smaller the value of AP_{p_i} is, the higher the probability of not missing the nearest train in the connecting station is. The trip though route 1, 3,7 is the latest trip. So the AP_{p_i} of the three route indicate the reliability of last train availability.

In table 3, passengers will be failed to reach destinations through route 1, 3, 7. Passengers miss last train through Route1 and 7 because of late start time. Passengers miss last

train through Route 3 because of failure of transfer at Xizhimen .

TABLE I. THE INFOEMATION OF THE ROUTES

No.	The station where changing lines	Distance of the trip/km	Average transfer time
1	Guomao	22	2
2	Xizhimen, Fuxinemen	22.3	3’17,1’35
3	Xizhimen(A), Jianguomen	23.5	3’17, 1’41
4	Xidan	22	5’4
5	Xizhimen(B)、Jianguomen	23.5	3’17, 1’41
6	Xuanwumen, Jianguomen	23.5	2’20,1’41
7	Huixinxijienankou, Dongdan	22.7	1’ ,3’50
8	Xuanwumen, Fuxingmen	26.6	2’20,2’48
9	Xizhime,Yonghegong, Dongdan	23.4	3’17,2’03,3’50
10	Xizhimen,Chongwenmen, Dongdan	23.5	3’17,3’51,3’50
11	Xizhime, Xuanwumen,Xidan	23.6	3’17,2’23,5’44
12	Huixinxijienankou,Yonghegong,Jianguomen	22.8	1’,2’23

TABLE II. CASE 1

序号	T_{p_i} (minutes)	TD-TA	AP_{p_i}	LT_{p_i}
1	47’43	3’47	0.96	1
2	53	5’03,5’51	0.96	0
3	53.4	7’05,2’50	0.95	1
4	53.4	9’29	1	0
5	53.4	5’03,2’25	0.72	0
6	53.4	2’20,4’15	0.5	0
7	57’4	6’30,5’01	0.86	1

TABLE III. CASE 2

序号	T_{p_i} (minutes)	TD-TA	AP_{p_i}	LT_{p_i}
1	+∞	-∞	0	-1
2	55’47	7’41,6’21	1	1
3	+∞	<0	0	-1
4	51.2	7’34	0.99	0
5	56.47	7’41,2’45	0.84	1
6	53.4	6’54,2’40	0.82	1
7	+∞	-∞	0	-1

From the sample in the tables, the change of the cost and the reliability of the trip are shown clearly. Also, it shows this algorithm is adaptive for the trip planning in SLTR.

V. CONCLUSION

In this paper, an algorithm is introduced to compute the cost and reliability of transfer connection of the trip in the time span of last trains running. The experiments based on a real urban mass transit network show that the algorithm is efficient and adaptive.

According to the survey, 43 percent passengers are willing to use a trip planning system frequently in a span of last trains running. And 91 percent passengers are willing to adjust trip according to the trip planning system. Thus, with the development of the trip planning system based on the algorithm introduced, it will make the trip more convenient for a large number of passengers.

This algorithm can be applied into bus transit network or multimodal schedule-based transit network as well.

ACKNOWLEDGMENT

Research is sponsored by National Key Technology Research and Development Program (2011BAG01B02), Research Found of State Key Laboratory of Rail Traffic Control and Safety (RCS2009ZT002, RCS2011ZZ004).

REFERENCES

[1] Zhan Guo a, Nigel H.M. Wilson , Assessing the cost of transfer inconvenience in public transport systems: A case study of the London Underground Transportation Research Part A 45 (2011) 91−104

[2] Tong C.O. and Richardson A.J. A computer model for finding the time-dependent minimum path in a transit system with fixed schedules, Journal of Advanced Transportation, vol.18,1984 , pp.145–161.

[3] Tong CO, Wong SC. A stochastic transit assignment model using a dynamic schedule-based network. Transportation Research Part-B vol.33,1998,107–21.

[4] Cepeda M., Cominetti R. and Florian M, A frequency-based assignment model for congested transit networks with strict capacity constraints: characterization and computation of equilibria, Transportation Research Part B,2006, 40, pp.437–459.

[5] Huang, Ruihong and Zhong-Ren Peng, 2002. An Object-Oriented GIS Data Model for Transit Trip Planning System. Transportation Research Record. No.1804.

[6] Huang R, Peng Z. Schedule-based path finding algorithms for transit trip planning systems, Journal of Transportation Research Board: Transportation Research Record vol.1783,2002, pp. 142–148.

[7] Tan MC, Tong CO, Wong SC, Xu J. An algorithm for finding reasonable paths in transit networks. Journal of Advanced Transportation; vol 41(3) ,2007,285–305.

[8] Knoppers, P., Muller, T., Optimized transfer opportunities in public transport. Transportation Science 29 (1995), 101–105.

[9] Markus Friedrich, Ingmar Hofsäß, Steffen Wekeck, Timetable-based Transit Assignment Using Branch & Bound Transportation Research Record 2001 p. 100-107

Influence and Countermeasures on the Ship-borne Communication Equipment of Naval Field Complex Electromagnetic Environment

RONG Hua
Department of Operational Commands
Dalian Naval Academy
Dalian.116018 China
Email: ming19850216@163.com

CHEN Ming-rong
Department of Graduate Management
Dalian Naval Academy
Dalian.116018 China
Email: chenmr1985@yahoo.cn

***Abstract*—In modern naval combat missions, the ability of warships communication to complete all distance communication is required, and warships communication provide adequate, stable and reliable performance communication lines for all the shore, sea, air and underwater environment, and possess the communication ways and means to resist all the harsh environment, and also requires the use of advanced communication technology, to withstand the strong electromagnetic interference and destruction in the sea battlefield environment. But in the naval battlefield environment, the influence of the wireless communication during the field environment is not only natural weather conditions; the more important influence is the complex electromagnetic environment of the naval battles. On the basis of analysis of the concept and connotation of complex electromagnetic environment, the influence and countermeasures on the ship-borne communication equipment of naval field complex electromagnetic environment are all discussed in this paper.**

Keywords- sea battlefield; complex electromagnetic environment; communications equipment)

I. INTRODUCTION

The modern warship communication system can cover the range of war zone and provides a flexible, general-purpose public operating environment information transmission platform and information processing platform, and it is also the information network, which links to the command center and sensors, weapons systems for efficient functioning. It must have to complete all far away, close communications capabilities for all the shore, sea, air and underwater to provide adequate, stable and reliable performance communication lines, and possess the communication ways and means to resist all the harsh environment, and also requires the use of advanced communication technology, to withstand the strong electromagnetic interference and destruction in the sea battlefield environment. In order to ensure the coordinated operations with the military, arms meanwhile, it requires that all ships communication system have a very strong compatibility and interoperability capabilities. But in the naval battlefield environment, the influence of the wireless communication during the field environment is not only natural weather conditions; the more important influence is the complex electromagnetic environment of the naval battles. Because the communication equipment is influenced by complex electromagnetic environment, their normal operational effectiveness and the timeliness of operations are all affected seriously.

II. THE CONCEPT AND CONNOTATION OF COMPLEX ELECTROMAGNETIC ENVIRONMENT

The complex electromagnetic environment of the sea battlefield can be defined as: in the naval battle field of certain airspace, time domain and frequency domain, a variety of electromagnetic (acoustic) signal are concentrated and overlapping, and impede the normal work of information systems and electronic equipment. The significant adverse effects of electromagnetic environmental conditions for weapon use and operations are produced. The definition of complex electromagnetic environment of the sea battlefield can be understood from the following four aspects:

(1) The place to produce a complex electromagnetic environment is the place of the sea battlefield;

(2) The quantity of the radiation source is large and the power of the radiation source is great;

(3) The naval battle field electromagnetic has strong confrontation;

(4) There are significant impacts on maritime operations.

III. THE ANALYSIS OF THE INFLUENCE ON THE SHIP-BORNE COMMUNICATION EQUIPMENT OF NAVAL FIELD COMPLEX ELECTROMAGNETIC ENVIRONMENT

A. The spectrum conflicts

In the sea operations, especially in the absence of strict spectrum management measures, the spectrum conflicts are prone to happen in the formation and the ship radar, communications, navigation and other equipment, and it makes the ships communication system difficult to avoid the strong self-interference even in the absence of enemy active interference, and the efficiency of the system reduced seriously.

B. The appropriate command

In addition to the spectrum of conflict caused by the lack of the technical and management, Different operational modes or command methods can lead to different communication needs and communication organization, so the appropriate command is an important factor for causing self-interference and mutual interference, and the complex electromagnetic environment affects the communication more seriously.

978-0-7695-4818-0/12 $26.00 © 2012 IEEE
DOI 10.1109/DCABES.2012.89

C. The environment noise

Besides the impacts of ship electromagnetic environment on the shipboard communications and other electronic information systems, the naval shore-based radio communication stations and shore-based command post is also facing the problem of self-interference and mutual interference in the complex electromagnetic environments.

IV. The Representations of the Influence on the Ship-borne Communication Equipment of Naval Field Complex Electromagnetic Environment

A. The interrupts of data transferring

The traditional HF and VHF communication, which are the basic radio communication application forms and widely used in a variety of weapons platforms and combat troops, are influenced by the battlefield electromagnetic environment and this effects are self-evident.

The relay communication, also known as radio relay communications, usually work in UHF or microwave band. The distance between each relay stations are not more than 50kilometers for the propagation distance limit, and it cannot exist other electromagnetic radiation sources with the same frequency, otherwise it will causes serious interference and interrupts the microwave radio relay.

The working quality of satellite communications in a certain time period is influenced largely by the solar daily variation. In addition, if it happens to have one party encounters the satellite transit phenomenon in the shore-ship communication process, the satellite communications will also be forced to be interrupted.

B. The increase of error rate

In most cases the communications link is not completely interrupted by the radio communications activities, which suffers the effects of battlefield electromagnetic environment. But the increase of error rate will definitely leads to the distortion of the transmission information, which affects the stability of command and control seriously. If higher probability of error in a battle command appeared in the message, it will cause serious consequences.

C. The influence of data link

The data link can realize data information exchange between airborne, land-based and carrier-based tactical data system, using the wireless network communication and application protocols, and thereby the tactical system effectiveness are maximized.

V. The Countermeasures of the Ship-borne Communication Equipment for the Influence on of Naval Field Complex Electromagnetic Environment

A. Tactical Measures

1) The pre-war COMINT

Electronic surveillance has been the main force of battlefield information acquisition. The COMINT is the foundation and an important part of communication confrontation. It cannot carry out the effective communication jamming and communication electronic defense without accurate and thorough communications countermeasure reconnaissance. So it's hard to grasp the opportunity, seize the initiative and win in the communications confrontation. Know the enemy and know yourself, and you can fight a hundred battles with no danger of defeat. It will be possible to carry out anti-interferences and even the firepower to destroy and other operations even when the leading role of communication countermeasure reconnaissance was played fully and identify the weaknesses of enemy communications systems.

2) Set the radio communication barrier, protecting our own communication

In order to basically cover the frequency range of our own communication and form an interference shielding, a kind of wideband noise was launched to a certain area (the enemy-occupied areas) and a certain direction (our radio communications direction of enemy reconnaissance) using the directional antenna. Therefore the enemy reconnaissance stations will only receive the noise in our communication frequency range, while our communication signal is completely submerged in the noise and forms an obstacle for the enemy's communications reconnaissance, and this will confirm our own communication security.

3) The broadcast communications to the enemy

It is necessary to carry out the broadcast communication during the war. Because it will not only occupy the war frequency of enemy using and disturb enemy communications, but also undermine the morale of an army in spiritual and disrupt the enemy's combat effectiveness by broadcasting. This means has not been given up in the modern high-tech war; however, it is a meaningful application in communicate confrontation in fact.

4) Measures against the aerial detection of submarine

The specific measure is that the submarines release a number of communication confrontation buoys to the interest water. These buoys are specially using for the reconnaissance of the data communication lines of sonobuoys, and they will immediately cast the interference for suppression once sonobuoys began to send messages. Then the enemy aircrafts for detecting submarines cannot get the exact information and we will achieve the purpose of protecting ourselves.

B. Technical Measures

In order to achieve the purpose of anti-jamming and low probability of intercept under the complex environment, communications technology has made rapid development, and the representations are mainly lying in the following aspects from the perspective of communication countermeasure:

1) The technology of spread spectrum

Spread spectrum is the technology of transmission through expanding information spectrum. It has several notable features, such as: a wider signal spectrum, complex waveform, safety hidden, etc. The technology increases the

difficulty of interception, monitoring, location and interference for enemy.

2) The technology of source and channel coding

The anti-interception performance will be improved for using the technology of source coding if the rate of the baseband signal is reduced, and the possibility of signal intercepted can also be reduced for using the technology of source coding if the transmission time is shorten. They are all under the condition of certain RF signal bandwidth and transmission quality. The anti-jamming performance of communication systems will be improved for using the technology of channel coding.

3) The technology of antenna beam forming and control

The technology of antenna beam forming and control contains the directional narrow beam in the microwave communication, the fan-beam in the mobile communications of CDMA, spot beam in the satellite communications, the technology of adaptive nulling antenna, etc.

4) The technology of multiple using of the transmission channel and adaptive routing network

The application of this kind of technology will increase the difficulty of jamming our communication under the enemy's interference of a single routing.

VI. CONCLUSION

The operational effectiveness of communications equipments is greatly limited under the complex electromagnetic environment. The complex electromagnetic environment has several main effects for communication equipments, such as: electromagnetic compatibility, the interrupts of data transferring, increasing the error rate and influencing the data link, reducing the combat effectiveness of the communications equipments, etc.

In order to improve the reconnaissance performance, the following measures could be adopted, such as: improving the key technology of signal sorting, the use of the technology of fingerprint feature analysis, good counter measures for low intercept probability and pulse loss. In order to improve the interference effect, the jamming style and technology system should be improved and enhanced. The interference signals in the environment can also be eliminated by the use of dynamic shielding technology.

REFERENCES

[1] LIU Li-ming, HUANG Wen-liang, SUN Lu-lu, "Construction method of complex electromagnetic environment in sea battlefield",. *Shipboard Electronic Countermeasure*, vol. 33, pp. 15-17, 2010.

[2] DING Lan, "Impact analysis of complex electromagnetic environment on ship borne combat system", *Ship Science and Technology*, vol. 33, pp. 100-102, 2010.

[3] ZHAO Zhi-gang, "ZHANG Feng. Research on fault diagnosis expert system in shipborne communication equipments", *Shipboard Electronic Countermeasure*, vol. 30, pp. 97-101, 2007.

[4] LIU Cui-hai; WANG Wen-qing, "Key technology and developing trend of foreign navies' submarine communications", *Telecommunication Engineering*, vol. 51, pp. 187-192, 2011.

[5] Cheng Lan; Zhou Xue-jun; Lü Zhi-jun, "Efficiency evaluation of basic communication services in surface ship", *Marine Electric & Electronic Engineering*, vol. 31, pp. 61-63, 2011.

[6] ZHANG Zhi-gang; XIE Hui; DING Lei, "Analysis and calculation of HF ground-wave marine communication link between warships",. *Telecommunication Engineering*, vol. 50, pp. 53-56, 2010.

[7] WANG Qing-sheng; XUAN Xiao-ying; LU Lei, "EMC analysis of shipborne communication countermeasure system", *Communication Countermeasures*, vol. 1, pp. 14-17, 2009.

Capability Evaluation of Maritime Emergency Management System

Hao Yong, Jiang Changyun, Tan Qinwen

Navigation School
Wuhan University of Technology
Wuhan, China
marinehao@126.com, jiangcy571@163.com, 82216223@qq.com

Abstract—: **The maritime emergency management system was analyzed and evaluated to identify the contingency factors and defective factors and provide a selection criterion for assessing the capacity of maritime emergency management system. Combined with the system running processes, a four-level indicator system of maritime emergency management was designed and then the Analytic Hierarchy Process and Fuzzy Comprehensive Evaluation Method were used to evaluate the capability of maritime emergency management system by taking one Maritime Safety Agency as an example. The evaluation result was basically consistent with fact, thus the measures to improve emergency capabilities were proposed.**

Keywords-Maritime Emergency Management System; Capability Evaluation; Analytic Hierarchy Process; Fuzzy Comprehensive Evaluation

I. INTRODUCTION

With the rapid development of water transportation, maritime emergency occurrence probability has also increased. Within the jurisdiction of Yangtze River Maritime Safety Administration (MSA), for example, 315 accidents and danger occurred in 2009, leading to great losses of life and property with 43 deaths (missing), 28 shipwrecks and 37.799 million Yuan direct economic loss.

Thus, it has been the particular concern of MSA and even the whole society that we must improve maritime emergency management system and enhance the response capability for maritime emergency.

Although there are oceans of capability evaluation researches on different objects with various methods [1-3], the maritime emergency capability evaluation has been rarely studied yet. In this paper, taking one MSA for example, by analyzing its maritime emergency management system and constructing indicator system which is suitable for its emergency capacity assessment, we established a comprehensive capability evaluation model of maritime emergency management system which could provide an alternative criterion for MSA to assess maritime emergency response capability.

II. ESTABLISHMENT OF EVALUATION INDICATOR SYSTEM

Maritime emergency management system is a huge and complex system [4], the impact factors of which are diverse, ambiguous and uncertain. Therefore, Analytic Hierarchy Process - Fuzzy Comprehensive Evaluation method [5-7] was chosen to assess its emergency response capability, which could model and quantify the emergency response capability evaluation process.

In order to fully reflect every influencing factor of maritime emergency management system, based on field surveying and expert interviewing, also with the reference to *Emergency Response Law of the People's Republic of China*, *the National Maritime Search and Rescue Emergency Plan* and other laws, regulations and rules, combined with the practical operation process of water emergency management system, we designed a four-level indicator system of water emergency management system, including 6 second-level indicators of organization structure, emergency prevention and preparation, emergency support, monitoring and early warning, emergency response and rescue, post-processing and recovery, which were further refined into 22 third-level indicators and 29 fourth-level indicators, showed in Table 1 in detail.

III. DETERMINATION OF INDICATOR WEIGHT

According to expert judgment matrix, the weights of evaluation indicators at all levels were calculated by using paired comparison method.

We interviewed and distributed questionnaires to 20 experts from MSA, emergency workers, maritime rescue professional personnel, advisory specialists, social rescue force etc., of which 3/4 were post-evaluation-meeting expert, and the rest 1/4 were professor or associate professor of related major in college and university.

First of all, taking indicator weight judgment matrix from one expert for instance, we checked the consistency of the judgment matrix and calculated its maximum eigenvalue $\lambda_{\max}=2,\ CI=0,\ CR=0<0.1$, so the matrix met the demands of consistency checking. Then, square-root method of AHP was used to calculated single factor indicator weight, shown in Table 2.

Namely the weight is

$W=(0.0825, 0.2519, 0.2519, 0.1273, 0.2313, 0.0552)$

Just as the method above, we got consistency checking results of the other 19 experts' weight judgment matrix. Then we synthesized all of the experts' judgment results and supposed that every expert's judgment result was of equal importance. We obtained the weight of each indicator of the system, shown as Fig.1.

978-0-7695-4818-0/12 $26.00 © 2012 IEEE
DOI 10.1109/DCABES.2012.95

Table 1 Indicator System of Emergency Response Capability Evaluation

Emergency response capability of Maritime emergency management system U	Organization Structure U1 U1	Completeness of the Organizational Structure U11	
		Definition of Staffs' Responsibilities in different positions at all levels U12	
	Emergency Prevention and Preparation U2	Water Emergency Plan System U21	Completeness of the Plan System U211
			Basis of Plan Preparation U212
			Normalization of the Overall Plan U213
		Updating of Emergency Plan U22	
		Management of Hazards and hazardous areas U23	
		Training and Exercise U24	Formulation of the Training and Exercise Plan U241
			Implementation Frequency of Training and Exercise U242
			Completeness of the Content and Form of Training and Exercise U243
		Propaganda and Education U25	Timely Release of Water Emergency Plan System U251
			Comprehensive Publicity of Safety Knowledge U252
	Emergency Support U3	Guarantee of Emergency Response Rules U31	
		Security of Emergency Personnel U32	Emergency Commander U321
			Emergency Operational Staff U322
			Emergency Expert Group U323
			Social Assistance Forces U324
		Logistical Support U33	Financing Safeguards U331
			Material Support U332
			Medical Security U333
		Technical Support U34	Communication and Information Technology Support U341
			Other Related Department Technology Support U342
	Monitoring and Early Warning U4	Formulation of Watch System U41	
		Receiving of a Distress Alarm U42	Completeness of Alarm Mode U421
			Standardization of Alarm Process U422
			Verification of Danger Information U423
		Reception and Dissemination of Early Warning Information U43	Promptness of Early Warning Information Reception and Dissemination U431
			Accuracy of Early Warning Information Reception and Dissemination U432
			Real-Time of Early Warning Information Reception and Dissemination U433
	Emergency Response and Rescue U5	Danger Information Report U51	
		Emergency Plan Activation U52	
		Emergency Response Capability U53	Standardization of Response Process U531
			Accuracy and Effectiveness of Response Decision-Making U532
			Response Speed of Emergency Team at all levels U533
		Emergency Rescue Capability U54	Definition of Staffs' Responsibilities in different positions U541
			Emergency Rescue Capability of Professional Team U542
			Organizational Coordination of Linkage Department U543
	Post-Processing and Recovery U6	Dissemination of Information Afterwards U61	
		Recovery of Accident Scene U62	
		Investigation and Analysis of Accident U63	
		Summary and Improvement of Emergency Decision-Making U64	

Table 2 Emergency Capability Indicator Weight Table

	U1	U2	U3	U4	U5	U6	W
U1	1	1/3	1/3	1/2	1/3	2	0.0825
U2	3	1	1	2	1	5	0.2519
U3	3	1	1	2	1	5	0.2519
U4	2	1/2	1/2	1	1/2	2	0.1273
U5	3	1	1	2	1	3	0.2313
U6	1/2	1/5	1/5	1/2	1/3	1	0.0552
λ_{max}=6.0556			CI=0.0111		CR = 0.0088 < 0.1		

IV. Determination of Membership Degree of Evaluation Indicator

The order of evaluation was divided to 5 grades, expressed as set V={V1, V2, V3, V4, V5}={very poor, poor, moderate, good, very good}, and the corresponding value set was $F = \{1, 2, 3, 4, 5\}$, shown as Table 3.

Table 3 Emergency Capability Evaluation Grades

Evaluation Grades	Corresponding Value
Emergency Capability is Very Poor	1
Emergency Capability is Poor	2
Emergency Capability is Moderate	3
Emergency Capability is Good	4
Emergency Capability is Very Good	5

By summarizing the evaluation forms of 20 experts, the number of marking times m of each indicator was obtained, and the value of m/20 was defined as membership degree of corresponding indicator. Statistical results of experts' evaluation were summarized in Table 4.

V. Fuzzy Comprehensive Evaluation (FCE)

Each of the evaluation results was analyzed with the method of normalization, and taking maritime emergency plan system U21 for example, the single factor judgment matrix was:

$$R21 = \begin{bmatrix} 0 & 0.1 & 0.7 & 0.2 & 0 \\ 0 & 0 & 0.35 & 0.5 & 0.15 \\ 0 & 0 & 0.6 & 0.3 & 0.1 \end{bmatrix}$$

Its corresponding single factor weight was

$W21 = (0.5609, 0.1433, 0.2958)$

Thus we could obtained the first-level comprehensive judgment

$B21 = W21 \cdot R21 = (0, 0.0561, 0.6203, 0.2726, 0.0511)$.

In the same way, the second-level comprehensive judgment results could be worked out and based on these results, the third-level comprehensive judgment matrix R was as the following:

$$R = \begin{bmatrix} 0 & 0 & 0.5100 & 0.2800 & 0.2100 \\ 0.0625 & 0.3573 & 0.4469 & 0.1150 & 0.0183 \\ 0.1255 & 0.3323 & 0.2910 & 0.2430 & 0.0081 \\ 0 & 0.0368 & 0.3536 & 0.4336 & 0.1760 \\ 0.0653 & 0.1196 & 0.3819 & 0.3482 & 0.0850 \\ 0 & 0.1615 & 0.3791 & 0.3261 & 0.1333 \end{bmatrix}$$

While the weight of R was

$W = (0.0802, 0.2497, 0.2487, 0.1273, 0.2402, 0.0539)$

The third-comprehensive judgment result was

$B = W \cdot R = (0.0626, 0.2140, 0.3819, 0.2681, 0.0734)$

VI. Defuzzification Calculation

According to the classification of emergency capability grades, set Cj as parameter of grades, namely the parameter column vector of evaluation result B corresponding to every evaluation grade was

$C = (c1, c2, c3, c4, c5)^T = (1, 2, 3, 4, 5)^T$

The final result was 3.0756 with the method of level parameters

$$P = BC = (b1, b2, \cdots, b5)(c1, c2, \cdots, c5)^T = \sum_{j=1}^{5} b_j c_j = 3.0756$$

Ⅶ Analysis of the Evaluation Result

According to the result，the conclusion showed that the emergency capability of maritime emergency management system of one MSA in case-studying, was between Moderate and Good, and just only a bit higher than the moderate evaluation standard, which was basically consistent with the experts' qualitative evaluation conclusions of several accidents within jurisdiction of the MSA, such as the 6.8 Accident and 6.14 Accident. It showed that the emergency capability of maritime emergency management system of the MSA met the requirements of current emergency response, but needed to be further improved. From the results of the second-level indicator, the marks of U2, U3, U5, U6 were on the low side, leading to the final mark of emergency capability comprehensive evaluation. Thus, the MSA should improve its emergency prevention and preparation, emergency support, emergency response and rescue, post-processing and recovery, specifically including enhancing the training and exercise of emergency personnel, keeping the refinements and updating of emergency plan, implementing the supporting measure and so on.

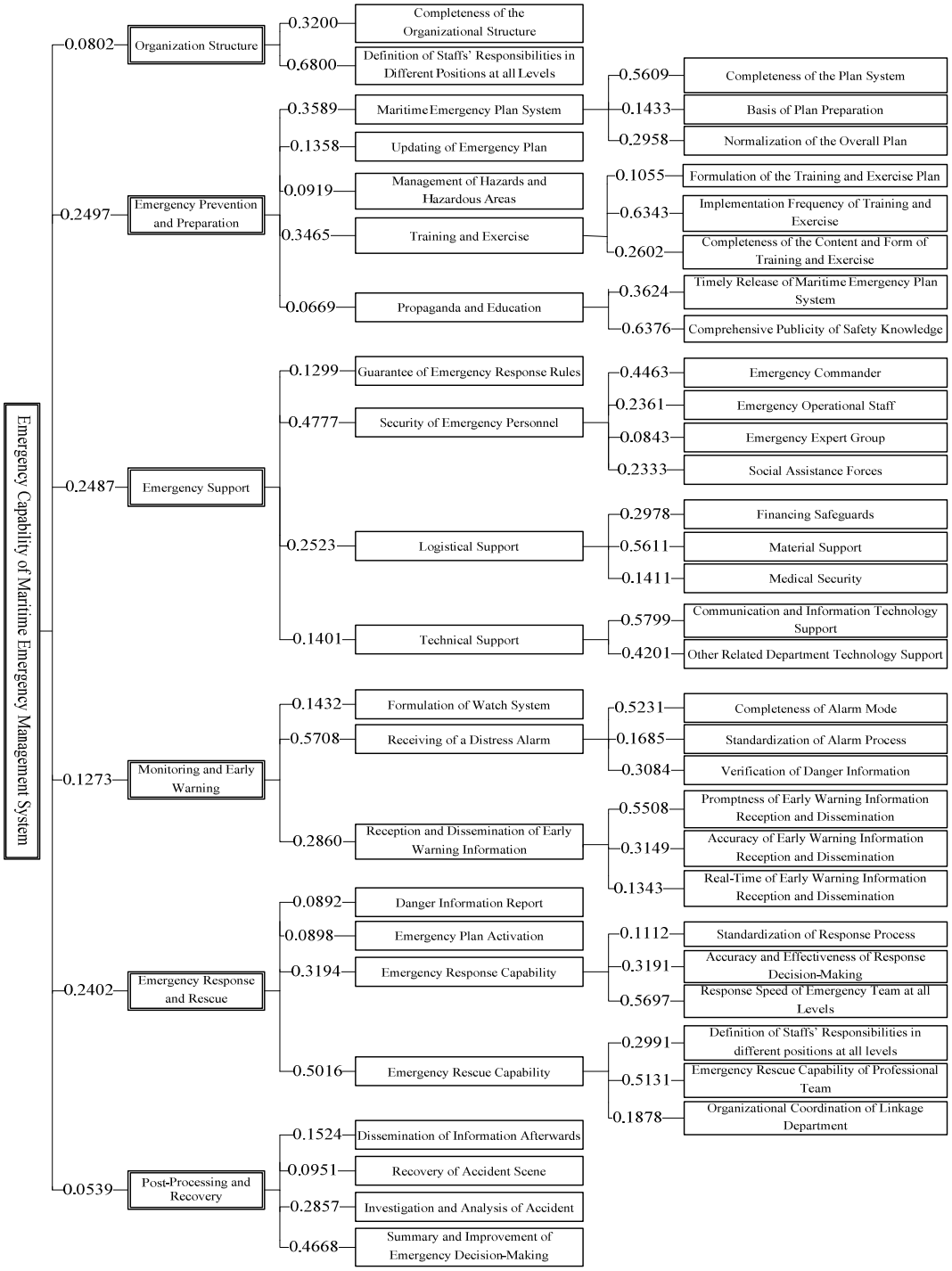

Fig.1 Evaluation Indicator System Weight of Water Emergency Management System

Table 4 Fuzzy Comprehensive Evaluation Statistical Table of Expert's Evaluation

Indicator Grade	Very Poor	Poor	Moderate	Good	Very Good
U11	0	0	0	0.45	0.55
U12	0	0	0.75	0.2	0.05
U211	0	0.1	0.7	0.2	0
U212	0	0	0.35	0.5	0.15
U213	0	0	0.6	0.3	0.1
U22	0.15	0.55	0.3	0	0
U23	0.1	0.65	0.25	0	0
U241	0	0.25	0.65	0.1	0
U242	0.1	0.6	0.3	0	0
U243	0	0.3	0.55	0.15	0
U251	0.1	0.55	0.35	0	0
U252	0.2	0.5	0.3	0	0
U31	0.4	0.45	0.15	0	0
U321	0	0	0.4	0.6	0
U322	0	0	0.65	0.35	0
U323	0	0.55	0.45	0	0
U324	0.1	0.75	0.15	0	0
U331	0.5	0.4	0.1	0	0
U332	0.1	0.7	0.2	0	0
U333	0.3	0.6	0.1	0	0
U341	0	0	0.15	0.75	0.1
U342	0	0.3	0.45	0.25	0
U41	0	0	0	0.25	0.75
U421	0	0	0.45	0.55	0
U422	0	0.1	0.4	0.5	0
U423	0	0.1	0.6	0.3	0
U431	0	0	0.2	0.45	0.35
U432	0	0	0.25	0.6	0.15
U433	0	0.25	0.55	0.2	0
U51	0	0	0.2	0.35	0.45
U52	0	0	0.35	0.55	0.1
U531	0	0	0.2	0.65	0.15
U532	0	0	0.1	0.6	0.3
U533	0.1	0.45	0.45	0	0
U541	0	0	0.55	0.45	0
U542	0	0	0.55	0.45	0
U543	0.5	0.4	0.1	0	0
U61	0	0.6	0.4	0	0
U62	0	0	0.4	0.55	0.05
U63	0	0	0	0.55	0.45
U64	0	0.15	0.6	0.25	0

REFERENCES

[1] Yu Zhu, Huai-ying Lei, "Fuzzy AHP analysis on enterprises' independent innovation capability evaluation," Proc. 2010 International Colloquium on Computing, Communication, and Management (CCCM2010). Yangzhou, pp.287-290. 2010.

[2] J.Sutherland, D.J.R Walstra, T.J.Chesher, et al, Evaluation of coastal area modeling systems at an estuary mouth, Coastal Engineering, vol.51(2), 2004, pp. 119-142.

[3] N. Dahl-Tacconi, Investigating information requirements for evaluating effectiveness of marine protected areas- Indonesian case studies, Coastal Management, vol.33 (3), pp. 225-246, 2005, doi: 10.1080/08920750590951956.

[4] Qingdong Li, Study on evaluation index system and method of technological innovation, Modern Information, vol.9, pp.174-176, 2005.

[5] Baoan Yang, Kejing Zhang, Multi-objective decision analysis theory, methods and applied research, Donghua University Press, pp.47-68, 2008. (in Chinese)

[6] Hai Li, Qiang Mei, AHP and Fuzzy Comprehensive Evaluation Method Analysis and Study, China Safety Science Journal, vol.07, pp. 86-89, 2004. (in Chinese)

[7] Denghua Zhong, Jianshe Zhang, Guangjing Cao, Project risk analysis method based on AHP, Journal of Tianjin University, vol.02, pp. 162-165, 2002. (in Chinese)

Study on Large Crude Oil Wharf Mooring Condition Simulation

Shuzhe Chen
School of Navigation
Wuhan University of Technology
Wuhan, China
cszcsz79@163.com

Kezhong Liu
School of Navigation
Wuhan University of Technology
Wuhan, China
63327026 @qq.com

***Abstract*—Analysis of open type wharf berthing condition is a complex process. It is hardly to simulate the environment and test results, which are consistent with the actual situation with physical model. In this paper, ship-mooring test during mooring is conducted applying the Large Ship Maneuvering Simulation Platform on the basis of the hydrological, meteorological and underwater terrain data. Combined with actual situation and the experience since the dock put into operation, the safety ship mooring conditions and safety berthing measures during mooring are determined.**

Keywords- Mooring;Simulation;Large oil terminal

I. INTRODUCTION

In this paper the large crude oil terminal is mainly responsible for crude oil loading and unloading and transit shipment for crude oil terminal for the VLCC (very large crude carrier) oil tankers from the Middle East, of which the designed throughput is 15 million tons / year. Two broken cables events occurred when the ship berthing and offloading in the four years since the dock put into operation (see Table 1-1). Though serious accidents such as oil spills have not yet caused by the events, but the normal unloading operation has been seriously interfered. And it may become accident potential in the future. Due to the high level of wharf and big tonnage and large scale of vessel, safety-mooring condition of crude oil wharf is an urgent realistic problem which has been paid high attention by the parties concerned and need to be solved imminently.

TABLE 1-1 BROKEN ROPE EVENTS

Time	Events
SEPTEMBER 31, 2007, 15:30 P.M.	SAUDI ARABIA "JINYANG" OIL TANKER WITH LOAD OF 30 TONS CRUDE OIL WAS OFF CABLE DURING BERTHING AND OFFLOADING
August 18,2011 17: 20 p.m.	Greek "ASTIPALAIA" Oil tanker with Load of 27 tons of crude oil was off cable during berthing and offloading

In order to ensure the mooring safety of crude oil tanker and avoid similar accidents, mooring condition analysis study must be done aiming at 300,000 DWT (Dead Weight Tonnage) crude oil wharf. The crude oil wharf is an open wharf, and the mooring condition analysis is a very complex process. It is related to wharf structure, scale, layout, wind, water wave, water current, tide and other natural conditions as well as ship tonnage, loading condition, mooring equipment strength, number and arrangement of the actual situation on the wharf. To this wharf, it is almost at full load during the unloading, current condition plays a decisive role. The oil terminal is under the combined action of islets, underwater topography, tide and etc. The macro and the local flow field environment are very complicated.

In this case, the study is based on the existing hydrological, meteorological observation data and chart, project area under-water terrain data. The mooring test is conducted with the application of Large Ship Maneuvering Simulation Platform for ship mooring. Safety mooring condition is determined combined with the condition and experience since the wharf is put into operation. Finally the corresponding measures and suggestions to mooring safety equipment during mooring are proposed.

II. SIMULATION MATHEMATICAL MODEL OF MOORING CONDITIONS

A. Ship motion equation

Ship motion equations are based on mathematical model of hydrostatic steering motion, and the interfere force of wind, wave and current are added to the right of equation.

$$(m+m_x)\dot{u}-(m+m_y)vr=X_H+X_P+X_R+\mathrm{X_{Wind}}+\mathrm{X_{Wave}}+X_{Curren} \quad (1)$$

$$(m+m_y)\dot{u}+(m+m_x)ur=Y_H+Y_R+\mathrm{Y_{Wind}}+\mathrm{Y_{Wave}}+Y_{Current} \quad (2)$$

$$(I_z+J_{zz})\dot{r}=N_H+N_R+\mathrm{N_{Wind}}+\mathrm{N_{Wave}}+N_{Current} \quad (3)$$

In above equations, the subscript H, P, R, Wind, Wave, Current, represent the hull, propeller, rudder, wind, wave and flow forces respectively, m represents quality of ship, u, v represent the x-Velocity component and y-Velocity component, r represents turned angular velocity, Iz and Jzz represent the moment of inertia of center of gravity, all the subscript x, y represent along the x axis or y axis, X,Y represent longitudinal and transverse force of fluid, N represent moment of fluid of z axis.

B. Ship maneuverability in the wind

The wind force can be expressed as:

$$\left.\begin{aligned} X_{wind}&=0.5\rho_a A_f U_R^2 C_{wx}(\alpha_R)\\ Y_{wind}&=0.5\rho_a A_s U_R^2 C_{wy}(\alpha_R)\\ N_{wind}&=0.5\rho_a A_s L_{OA} U_R^2 C_{wn}(\alpha_R)\end{aligned}\right\} \quad (4)$$

Among them ρ_a is the air density, U_R and α_R are relative wind speed and angle, A_f and A_s are projected area and lateral projection area for the ship above the waterline. L_{OA} is the ship length.

978-0-7695-4818-0/12 $26.00 © 2012 IEEE
DOI 10.1109/DCABES.2012.113

$C_{wx}(\alpha_R)$, $C_{wy}(\alpha_R)$ and $C_{wn}(\alpha_R)$ are the wind pressure coefficient for x, y direction and wind pressure moment coefficient around the z-axis respectively, X,Y represent longitudinal and transverse force of fluid, N represent moment of fluid of z axis.

C. Ship maneuverability in the wave

Considering the influence on the performance of the ship maneuvering caused by waves, the formula to calculate wave drift force and moment are as the following:

$$X_{wave} = 0.5\rho g L \zeta_D^2 C_{XD}(\lambda)\cos\chi \quad (5)$$

$$Y_{wave} = 0.5\rho g L \zeta_D^2 C_{YD}(\lambda)\sin\chi \quad (6)$$

$$N_{wave} = 0.5\rho g L^2 \zeta_D^2 C_{ND}(\lambda)\sin\chi \quad (7)$$

Among them, ζ_D is the average wave amplitude, $C_{XD}(\lambda)$, $C_{YD}(\lambda)$ and $C_{ND}(\lambda)$ are the wave drift force coefficients for x, y direction and wave drift force moment coefficient around the z-axis respectively. λ is wavelength, χ is wave encounter Angle. According to the experimental results of ship model of England, waves drift coefficient for the force and moment obtained via regression are as follow：

$$\left.\begin{aligned} C_{XD}(\lambda) &= 0.05 - 0.2(\frac{\lambda}{L}) + 0.75(\frac{\lambda}{L})^2 - 0.51(\frac{\lambda}{L})^3 \\ C_{YD}(\lambda) &= 0.46 - 6.83(\frac{\lambda}{L}) - 15.65(\frac{\lambda}{L})^2 + 8.44(\frac{\lambda}{L})^3 \\ C_{ND}(\lambda) &= -0.11 + 0.68(\frac{\lambda}{L}) - 0.79(\frac{\lambda}{L})^2 + 0.21(\frac{\lambda}{L})^3 \end{aligned}\right\} \quad (8)$$

D. Ship maneuverability in the flow

Set the flow velocity value in the fixed coordinate system as V_c , its direction as ψ_C , so the components in the coordinate system on board of the ship are:

$$\left.\begin{aligned} u_C &= V_C\cos(\psi_C - \psi) \\ v_C &= V_C\sin(\psi_C - \psi) \end{aligned}\right\} \quad (9)$$

In ship coordinate system, u, v are the ship's speed components. Set the relative flow speed of the ship motion as u_r, v_r . There are:

$$\left.\begin{aligned} u_r &= u - u_C \\ v_r &= v - v_C \end{aligned}\right\} \quad (10)$$

It can also be written as:

$$\left.\begin{aligned} \dot{u}_r &= \dot{u} - rv_C \\ \dot{v}_r &= \dot{v} + ru_C \end{aligned}\right\} \quad (11)$$

In above equations, r represents turned angular velocity. In uniform flow, the angular velocity of the first roll of the ship, whether it is ground, or relative to water is consistent, using r to represent. Through time derivative, we can get the relationship about the component of acceleration:

$$\left.\begin{aligned} \dot{u} &= \dot{u}_r + \dot{u}_C = \dot{u}_r + V_C r\sin(\psi_C - \psi) \\ \dot{v} &= \dot{v}_r + \dot{v}_C = \dot{v}_r - V_C r\cos(\psi_C - \psi) \end{aligned}\right\} \quad (12)$$

Can also write for:

$$\left.\begin{aligned} \dot{u}_r &= \dot{u} - rv_C \\ \dot{v}_r &= \dot{v} + ru_C \end{aligned}\right\} \quad (13)$$

So we get the relative velocity and relative acceleration of the ship on the water. Ship maneuvering in the hydrostatic equation of motion of the hull motion parameters converted to the relative motion parameters of the hull and the water flow. That means considering the influence of currents.

III. ENVIRONMENTAL SIMULATION OF THE TEST WATERS

A. Simulation platform

Navi-Trainer Professional 4000(NTPRO 4000) is chosen for the simulation platform of this case, and the multi-purpose oil/product 700,000 m3 terminal, capable of processing VLCC and LCC tankers, was chosen as the prototype.

The configuration of simulation platform can be shown as figure 3-1.

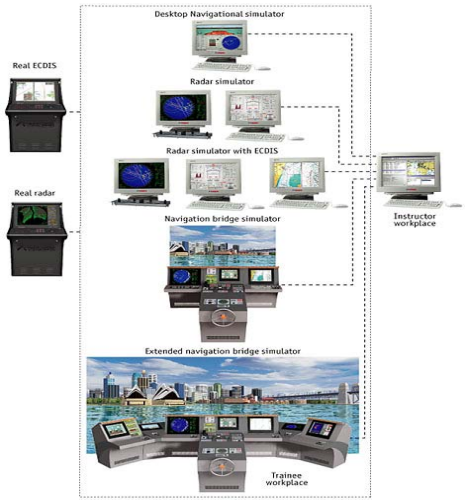

Figure 3-1 The configuration of NTPRO 4000

The real tanker loading/unloading exercises at the terminal can be united in one technological cycle, or applied as separate items. This enables training in strictly appointed operations of separate systems or their individual elements. The simulator provides the downloading of the exercise, which describes the initial condition and approximate training scenario. Instructors can change the course of exercises and bring in different scenarios and limitations. The exercise will stop only in the event of significant equipment failure or ecocatastrophe input.

B. *Electronic charts and three-dimensional topography of the Test waters*

Based on the latest available actual topographic map of crude oil terminal, make data recording, data conversion, coordinate transformation, data entry processes to the test waters and then build the relative electronic charts and the three-dimensional scene around the test water[1]. As shown in figure 3-2.

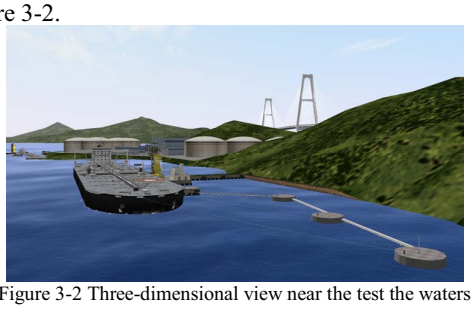

Figure 3-2 Three-dimensional view near the test the waters

C. *Ship model parameters for Simulation*

According to the designed ship of the terminal, select the 30-ton oil tankers as the main ship of the simulation test. See table 3-1.

Table 3-1 Test Ship Type of Oil Tanker

Tonnage	Total length (m)	width (m)	depth (m)	Loaded draft (m)	remarks
300000tons	334	60.0	31.2	22.5	

D. *Simulation conditions setting*

According to the statistics of the anemometers for wind data, often wind is N (including NNW and NNE). The wind statistical frequency is about 34.8%. Secondary often wind is SE(including ESE and SSE). The wind statistical frequency is about 34.4%. The strong wind is N, and the maximum wind speed is 26.0m/s. In addition, according to the analysis of short-term wind measurement station, often wind of this area in summer and autumn is SE~SSE. The statistical frequency is about 24.6%. Secondary often wind is WNW~NW. The statistical frequency is about 15.2%. Strong wind direction is SSE. In the simulation process, the conditions of the wind set as the most adverse directions and waves consistent with the wind. The current data used in the test conditions during the simulations is the actual measured flow data of Wharf forefront in September 2011.

IV. SIMULATION TEST FOR SHIP MOORING CONDITIONS

A. *Mooring arrangement*

Ship mooring adopt the pattern of 4-2-2-2, four Head Line(HL), two Fore Breast Line 1(FB1), two Fore Breast Line 2(FB2), two Fore Spring Line(FS), four Stern Line(SL),two Stern Breast Line 1(SB1), two Stern Breast Line 2(SB2), two Stern Spring Line(FS).

B. *Simulation technology route*

Simulation technology route can be shown as figure 4-1.

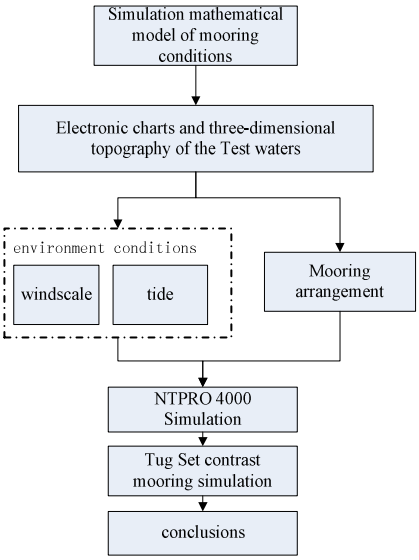

Figure 4-1 Simulation technology route

C. *Cable force simulation in different working conditions*

Since the complexity of the test conditions, and the simulation run last long, tanker simulations using current data as the test conditions during the spring tide. Simulation progress[2] is under the conditions of no wind, 4 and 6 wind conditions. Spring tide、N wind 6、Loaded and each cable (elongation 5%) simulation test data[3,4] see figure 4-2 to 4-3.

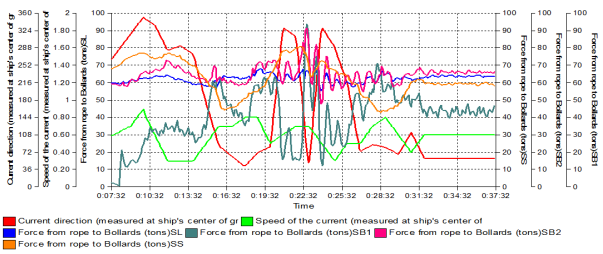

Figure 4-2 Timing diagram stress

Ship Diagram

TIME	Current direction (measured at ship's center of gr	Speed of the current (measured at ship's center of	Force from rope to Bollards (tons)SL	Force from rope to Bollards (tons)SB1	Force from rope to Bollards (tons)SB2	Force from rope to Bollards (tons)SS
	deg	m / sec	tons	tons	tons	tons
0:00:00	0.000	0.000	0.000	0.000	0.000	0.000
0:01:00	34.800	0.080	0.000	0.000	0.000	15.745
0:02:00	69.900	0.150	64.724	21.642	95.562	10.004
0:03:00	105.000	0.230	69.984	33.852	80.990	54.048
0:04:00	140.100	0.310	73.064	50.228	91.026	55.875
0:05:00	175.200	0.390	74.905	53.345	77.861	58.940
0:06:00	210.300	0.470	55.932	30.653	54.256	58.644
0:07:00	245.400	0.540	59.348	12.539	59.519	64.775
0:08:00	280.500	0.620	59.562	1.221	58.536	69.626
0:09:00	315.600	0.700	61.179	14.476	61.115	74.778
0:10:00	351.200	0.900	62.545	24.134	65.795	77.025
0:11:00	335.600	0.600	63.517	31.674	66.460	73.946
0:12:00	283.200	0.300	64.236	33.243	71.906	76.466
0:13:00	292.400	0.300	61.777	34.556	68.662	74.317
0:14:00	274.700	0.300	58.937	27.786	62.450	69.463
0:15:00	173.600	0.500	57.652	40.142	60.647	61.142
0:16:00	86.300	0.700	60.044	63.163	62.899	50.148
0:17:00	63.800	0.700	62.775	47.513	59.864	45.525
0:18:00	42.600	0.800	62.556	41.180	59.376	50.245
0:19:00	69.900	0.800	66.807	59.935	70.851	55.153
0:20:00	83.300	0.510	65.952	59.826	72.221	63.794
0:21:00	326.000	0.600	60.513	15.922	59.616	77.985
0:22:00	311.300	0.700	61.764	19.041	64.491	79.699
0:23:00	44.200	0.700	67.005	87.358	85.044	70.185
0:24:00	327.200	0.500	55.439	11.444	47.381	72.821
0:25:00	290.300	0.300	59.942	28.156	61.126	67.303
0:26:00	216.200	0.500	60.586	26.737	64.590	64.146
0:27:00	75.400	0.500	59.414	50.698	61.293	54.658

Figure 4-3 Stress numerical

D. Tug Set contrast mooring simulation with VLCC draft of 18m

The test conditions selected ship draft of 18 meters, north wind of six, wave height of one meter, tide measure the tidal current field. At the beginning of the test, tightening the cable, the same direction and location of the same force, single cable breaking force is 70t, the elongation rate is 5%.

1. Simulation under the conditions without tug(See figure 4-4 and 4-5).

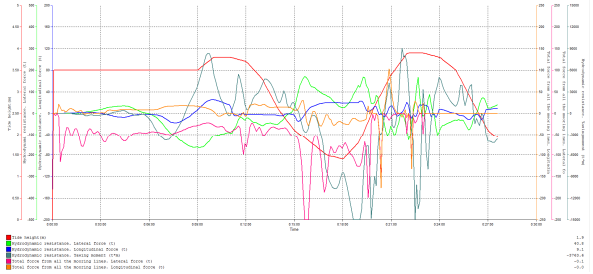

Figure 4-4 Timing diagram (no tugboat)

2.Simulation with tug (since simulation conditions is numerous[5]，choosing typical tug simulation results, See figure 4-6 and 4-7).

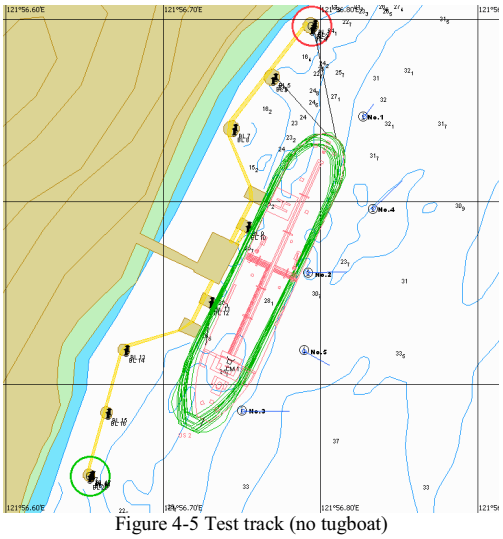

Figure 4-5 Test track (no tugboat)

results： Stern cable break (SS1-SS2 break first, SL break)

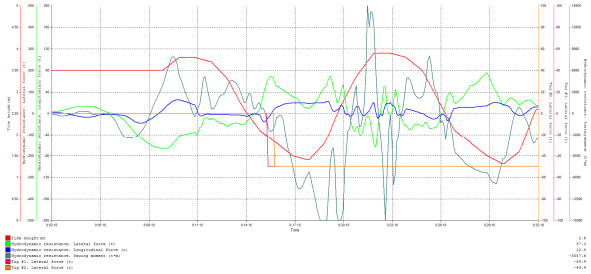

Figure 4-6 Timing diagram (Tug pushing force 49.9t)

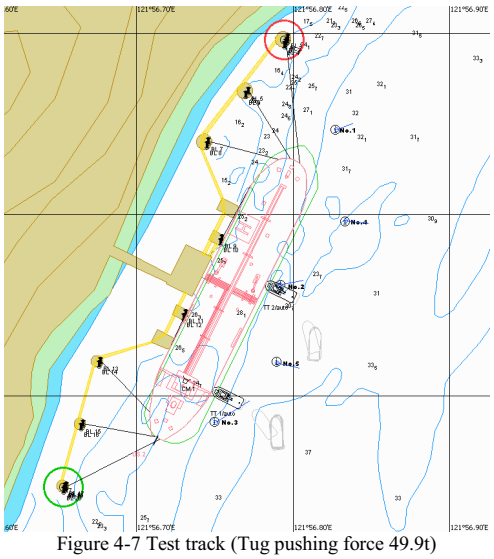

Figure 4-7 Test track (Tug pushing force 49.9t)

results： mooring stable

V. THE MAIN CONCLUSIONS AND RECOMMENDATIONS OF THE SIMULATION TEST

According to most adverse directions and other simulation conditions, simulation test analysis conclusions[6] as follows:

1. In the case of the current mooring configuration, when the oil tank is under effect of wind and current, the fore breast cable and stern Breast cable is strongly stressed. The main reason is about the complexity of flow in mooring water and the influence of wind, secondary reason is that the fore breast cable and the stern breast cable is relatively short. Because of the combined effect of wind, flow, waves, the cables may be broken under the most unfavorable joint force[7].

Advise: 300,000 tons VLCC Wharf shall ensure that the length of single point mooring is almost same, oil tank's length of the fore spring line and stern line should be as long as possible.

2. If instantaneous gust of wind suddenly increased, and the flow field changes significantly due to the small elongation of the wire rope, instantly excessive force result in the cable breaking[8].

3. The total number of VLCC mooring cables are 20, ship mooring pattern is 4-2-2-2, basically meet the requirements of the ship mooring stability. Reason for the cable broken is:

(1)The flow field changes significantly and the impact of the waves, complex Wharf waters flow. The force of the wind, flow, waves produce torque, causing ship stirs. The ship mooring force rapid change stirs in magnitude exceeding the cable elongation, resulting in cable broken;

(2)Tidal changes and vessel offloading lead hull up and down, causing change of ship mooring cable force, leading to the increasing of ship stirs rate and mooring unstable;

(3) Length of Breast Line and Spring Line is insufficient, the type of cable elongation is difficult to overcome the ship stirs Dayton;

(4)Mooring management does not reach the designated position, resulting in uneven force of the cable in the same direction and location;

(5)In low tide periods, the trend of tide change is significant. Cable force change significantly and cable is easily broken.

4. Through adjusting the force of each cable and strength the management during the berthing mooring, the accident of the cable broken can be effectively reduced[9].

5. Under the conditions of VLCC draft down to 18m, north wind 6, spring tide, cable broken can still happens. Two maneuver tugs should be configured to assist. The data shows single tugboats jacking force is less than 50 tons, the control of mooring stability is still of difficult. So the configuration of a single tugboats pushing force shall not be less than 50 tons.

VI. CONCLUSION

Simulation studies for large crude oil Wharf mooring conditions have shown that the factors which influence the Wharf ship mooring safety are various [4]. But to this Wharf, the decisive factors are the current, the reliability of the mooring equipment and the management of the cable stress state in ship mooring. Wharf owners should guide the application of the actual mooring equipment and mooring force management based on the simulation result and built a set of fast and effective communication mechanisms with the oil tanker. Wharf tensile testing equipment and practical work experience shall be made full use of to enhance the management of the ship mooring system, maintaining the balance of the mooring forces of the same parts of the ship and rationally allocate the forces between different parts of the mooring.

REFERENCES

[1] Tahar A, RAN Z, KIM M H. Hull/mooring/riser coupled Spar.motions analysis with buoyancy-can effect[C]. Proceedings of the 12th International offshore and polar engineering conference,Kitakyushu, Japan, 2002.

[2] Li B B, OU J P, Teng B. Fully coupled effects of hull, mooring and risers model in time domain based on an innovative deep draft multi-Spar[J]. China Ocean Engineering, 2010, 24(2):219-233. (in Chiness)

[3] Liu Z, Teng B. Wave-current interactions with three-dimensional,floating bodies[J]. Journal of Hydrodynamics, 2010, 22(2):229-240. (in Chiness)

[4] Xu G, Duan W Y. Time domain simulation of irregular wave,diffraction[C]. 8th International Conference on Hydrodynamics,September 30-October 3, 2008, Cité des Congrès Nantes. (in Chiness)

[5] H. Ormberg, K. Larsen. Coupled analysis of floater motion and mooring dynamics for a turret-moored ship, Applied Ocean Research, 20 (1998), pp. 55−67

[6] K. Nishimoto, C.H. Fucatu, I.Q. Masetti, Dynasim − a time domain simulator of anchored FPSO, Journal of Offshore Mechanics and Arctic Engineering, 124 (2002), pp. 203−211

[7] Y.M. Low, R.S. Langley, A hybrid time/frequency domain approach for efficient coupled analysis of vessel/mooring/riser dynamics, Ocean Engineering, 35 (2008), pp. 433−446

[8] A. Naess, O. Gaidai, P.S. Teigen, Extreme response prediction for nonlinear floating offshore structures by Monte Carlo simulation, Applied Ocean Research, 29 (2007), pp. 221−230

[9] A.O. V á zquez-Hern á ndez, G.B. Ellwanger, L.V.S. Sagrilo, Reliability-based comparative study for mooring lines design criteria, Applied Ocean Research, 28 (2006), pp. 398−406

Denoising Method of Inland AIS Information Based on Vessel Track

Zhang Wen-juan[1] *Wu Qing*[1] *Sang Ling-zhi*[2,3] *Mao Zhe*[2,3]
1 School of Logistics Engineering, Wuhan University of technology;
2 Intelligent Transportation System Research Center, Wuhan University of technology;
3 Engineering Research Center of Transportation Safety (MOE)
Wuhan, China
Zhang_wj123@126.com; wq@whut.edu.cn; sanglz@126.com; yaner@whut.edu.cn

***Abstract*—Through the analysis of vessel track, the characteristics of traffic flow can be well obtained, and waterway traffic safety can be ensured. In order to restore inland water vessel track which is more consistent with real one, noise in the AIS information is supposed to be removed. This paper presents a denoising method of inland vessel track which consists of three basic steps. Firstly, the points outside the valid range of latitude and longitude are roughly removed. Secondly, the points significantly deviating from the normal course are removed according to vessel's speed. Lastly, the points show non-smooth turn in the track are removed according to course over ground(COG) .And the effectiveness of the method have been verified on the VC++6.0 platform.**

Keywords-inland river; vessel track; Automatic Identification System; denoising

I. INTRODUCTION

Automatic Identification System（AIS）is a ship and shore-based radio navigational aids system, which broadcasts own ship information to other ships and shore stations automatically and continuously and receives broadcast information of other ships and shore stations at the same time. AIS information includes vessel position, course, speed and other dynamic information as well as the vessel's name, type of vessel and other static information[1]. Due to the widely use of AIS, crew and maritime management authorities can quickly access to real-time information of waterway traffic situation[1-3]. A growing number of scholars use the AIS information to implement their research.

Through the use of the vessel position information in the AIS message, vessel track can be restored, which can be used to identify the waterway traffic trend[4], analyze accidents[5] and study traffic flow distribution[6-7]. For most inland water vessels, AIS class-B are equipped, the performance of which is relatively low compared with class-A. As a result, the data is mixed with a small amount of erroneous data. The existence of the error data will lead to unpredictable deviation of the restored vessel track, which thereby mislead the nearby vessels and regulatory authorities and endanger the security of waterway transportation. Therefore, when restoring vessel track, an effective denoising method is needed to remove the error data.

II. DENOISING ALGORITHM

A. Difference Method of First Order

Difference Method of First Order is a simple and effective method to remove individual data which significantly deviate from the normal value. The process[8] of implementation of the method is as follows. Set an error limitation value W and x_t is the sampled value at time point t. Get the predicted value $x_t^{'}$ at time point t according to equation (1).

$$x_t^{'} = x_{t-1} + (x_{t-1} - x_{t-2}) \tag{1}$$

$$\left| x_t - x_t^{'} \right| > W \tag{2}$$

If formulae (2) is met, x_t will be considered as noise point and removed from the data sequence. Then replace x_t with $x_t^{'}$.

There is a possible situation that the starting point is noise point. So three consecutive points should be found and set as starting points. These three points should meet the following relationship formulae.

$$\left| x_t - x_{t-1} - x_{t-1} + x_{t-2} \right| \le W \tag{3}$$

Another possible situation is that several consecutive points are all noise points. When two consecutive noise points is found then following relationship formulae should be checked.

$$\begin{cases} W_2 > \left| x_t - x_t^{'} \right| > W \\ W_2 = KW \end{cases} \tag{4}$$

$$\left| x_t - x_t^{'} \right| > W_2 \tag{5}$$

978-0-7695-4818-0/12 $26.00 © 2012 IEEE
DOI 10.1109/DCABES.2012.99

$$\left|x_t - x_t^{'}\right| \le W \tag{6}$$

According to practical experience, coefficient K =5. If the next point of the noise points meets formulae (4), then this point will be considered as normal point. If relationship formulae (5) is met, then this point will be removed as noise point.

Consecutive noise points will lead significant deviation from the normal data sequence. New starting points should be selected when one of the following situations happens.

- A point is found within 6 points after the consecutive noise points which meet formulae (6).
- Continuously process 6 points meet formulae (4), but no points meet formulae (6).

The key of the Difference Method of First Order is to set a proper error limitation value *W*. Consider the specific situation of inland vessel track restoration, corresponding identification parameters and the value of *W* are discussed below.

B. Characteristic Analysis of Noise

Noise points present different characteristics in the track without denoising. According to the characteristics, the noise points can be divided into three categories: (1)the latitude and longitude are not in the normal range, such as latitude is 91° and longitude is 181° ,(2) the latitude and longitude are within the normal range, but the values significantly deviate from the normal course and show a thorn-like bulge on the vessel track, and (3) the values are not significantly deviate from the normal course, but show a non-smooth turn of course on the track.

The first category noise points can be removed from the data sequence by detecting whether the latitude and longitude are in the valid range. As the acceleration of inland vessel is relatively small, the speed and course of vessel at two adjacent positions will not change dramatically. The existence of second category and third category noise points will respectively change average speed and course dramatically. So average speed and course are used as determine indicators when remove the second category and third category noise points.

C. Determination of The Second Category Noise Points

In order to remove the second category noise points, determinant criterion based on speed is constructed. Latitude and longitude of certain point is given in AIS messages, so average speed between two adjacent points can be calculated. The determinant criterion of the second category noise points is as follows.

$$\left|v_t - v_t^{'}\right| > W \tag{7}$$

v_t is the average speed between two adjacent points P_{t-1} and P_t.

$v_t^{'}$ is the corresponding predicted value. Set $W = v_{t-1}$.

If the criterion above is met, then point P_t will be considered as noise point and be removed from the data sequence.

D. Determination of The Third Category Noise Points

In order to remove the third category noise points, determinant criterion on COG is constructed. When vessel sail at speed v, rotate the rudder to some rudder angle. Then the vessel makes curvilinear motion to complete the steering. From the steering process, at the stage of steady rotation, vessel do constant circular motion around a fixed point at a certain lateral speed and rotation angular.

$$V_G = R_0 \cdot r_0 \tag{8}$$

V_G is the linear velocity of the center of gravity G . In the simplified linear case, use the speed v as an approximate.

R_0 is the curvature radius of the track of the center of gravity, namely steady radius of gyration.

On this basis, the threshold of the steering angle of inland vessel is discussed as follows.

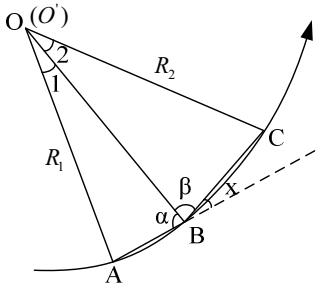

Figure 1. Diagram of ship steering

As show in Figure 1, take three consecutive point A, B, C from the vessel track. The corresponding circle center of arc AB is point O, and the radius is R_1.The corresponding circle center of arc BC is point $O^{'}$, and the radius is R_2.

$$\begin{cases} \dfrac{\Delta t_1}{T_1} = \dfrac{\angle 1}{2\pi} \\ \dfrac{\Delta t_2}{T_2} = \dfrac{\angle 2}{2\pi} \end{cases} \tag{9}$$

$$\begin{cases} \angle\alpha = \dfrac{\pi}{2} - \dfrac{\Delta t_1}{T_1}\pi \\ \angle\beta = \dfrac{\pi}{2} - \dfrac{\Delta t_2}{T_2}\pi \end{cases} \tag{10}$$

T_1 is the time period of the vessel do circular motion at speed v_1.

T_2 is the time period of the vessel do circular motion at speed v_2.

Δt_1 is the time interval of the vessel move from A to B.

Δt_2 is the time interval of the vessel move from B to C.

$$\angle x = \pi - \angle\alpha - \angle\beta \tag{11}$$

For inland vessel, tactical diameter is at least once as much as the ship length l [9].

$$\begin{aligned} \angle x &\le \frac{\Delta t_1 v_1 + \Delta t_2 v_2}{l} \\ &= \frac{l_1 + l_2}{l} \end{aligned} \tag{12}$$

v_1 is the average speed of the vessel from A to B.

v_2 is the average speed of the vessel from B to C.

l_1 is the distance between A and B.

l_2 is the distance between B and C.

$$W = \frac{l_1 + l_2}{l} \tag{13}$$

Get the course over ground r_t and corresponding predicted value r_t' .The determinant criterion of the third category noise points is as follows.

$$\left| r_t - r_t' \right| > \frac{l_1 + l_2}{l} \tag{14}$$

If the criterion above is met, then point P_t will be considered as noise point and be removed from the data sequence.

E. Steps of Denoising

In order to remove all of the three categories of noise points, three determinant criterions must be used comprehensively. So the denosing method of the inland water vessel track consists of three basic steps. Firstly, the points outside the valid range of latitude and longitude are roughly removed. Secondly, the points significantly deviating from the normal course are removed according to vessel's speed. Lastly, the points show non-smooth turn in the track are removed according to course over ground(COG) .

III. IMPLEMENTATION AND VERIFICATION

Implement the method on the VC++6.0 platform and display the restored vessel track after denoising on the Inland-waterway Electronic Chart.

Select two typical vessel tracks as experimental subjects. The MMSI of these two vessels are respectively 600008437 (1#) and 413806453(2#). The data ware collected on January 10, 2012 at TianXingzhou of Yangtze River. The track of vessel 1# is shown on Figure 2. The track without denoising is presented in Figure 2(a), and the denoised track is shown in Figure 2(b).There are two noise points in this track. Point C significantly deviates from the normal track, and show a thorn-like protrusion, so it is the second category noise point. Point D is the third category noise point. Comparing track in Figure 2 (a) with track in Figure 2 (b), these two noise points are removed in Figure.2 (b) and the other points in the track are not changed. This indicates that the denoising method removes the noise points and keeps the normal points at the same time. The track of vessel 2# is shown on Figure 3. Point E slightly derivate from the normal track while point F derivate from the normal track farther. So point E is the third category of noise point and point F is the second category of noise point. As shown in Figure 3(b), both of them are removed and other normal points are retained. It can be concluded that the denoising method can effectively remove the noise points in the inland vessel track.

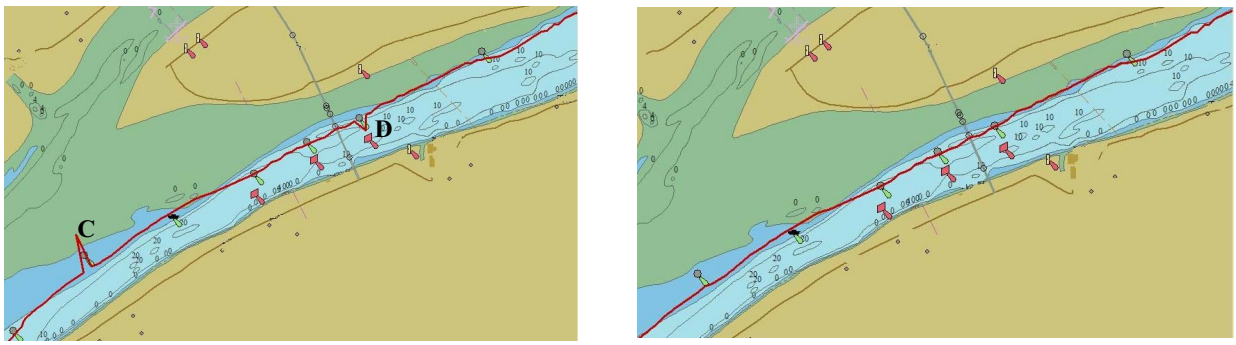

(a) (b)

Figure 2. Restored track of vessel 1#: (a)The track without denoising. (b) The denoised track

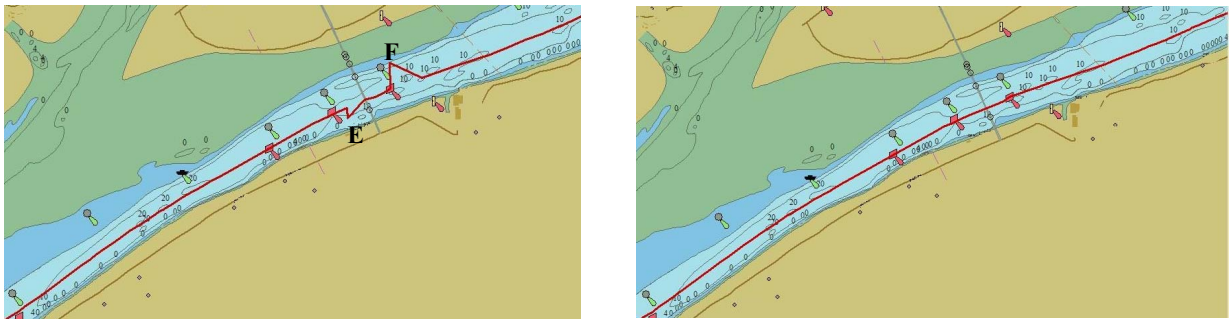

(a) (b)

Figure 3. Restored track of vessel 2#: (a)The track without denoising. (b) The denoised track

IV. CONCLUSIONS

The noise in the AIS information will make the restored track deviating from the real track, which endangers the waterway traffic safety. So an effective denoising method is needed. In this paper, according to the characteristics of the noise in the inland water vessel track restored from the AIS information, three denoising criteria have been constructed based on Difference Method of First Order. And a denoising method of inland AIS information based on vessel track is constructed. The method consists of three basic steps. In each step, one determinant criterion is suggested. And the feasibility and effectiveness of the method has been verified.

ACKNOWLEDGMENT

This paper is supported by Western Communications Construction Scientific and Technological Project of Ministry of Transportation of the People's Republic of China (grant No.201132820190), National High Technology Research and Development Program of China (Grant No.2012AA112303).

REFERENCES

[1] Xie Li Zhi,Pan Qi Hao. Application of AIS in Real-time Multi-ship Collision Detection[J]. Ship & Ocean Engineering,2009,(05):177-180 (in Chinese).

[2] Yan Zhongzhen, Yan Xinping, Ma Feng, Chu Xiumin. Green Yangtze River Intelligent Shipping Information System and Its Key Technologies[J]. Journal of Transport Information and Safety,2010,29(06):76-81 (in Chinese).

[3] Ingo Harre. AIS Adding New Quality to VTS Systems[J]. The Journal of Navigation,2000,53(03):527-539.

[4] Yan Xinping, Ma Feng, Chu Xiumin, Chen Chen. Key Technology of Collecting Traffic Flow on the Yangtze River in Real-Time[J]. N avigation of China,2010,33(02): 40-45 (in Chinese).

[5] Li Xudong, Hu Shenping. Application of AIS information analysis in ship collision cases[J]. Journal of Shanghai Maritime University, 2007,(01): 132-136 (in Chinese).

[6] Jin Xingfu, Fu Yuhui, Zhang Liandong. Research on vessel traffic flow at Chengshantou water area based on AIS Data[J]. Journal of Dalian Maritime University, 2012,(01): 33-36 (in Chinese).

[7] Chang SJ, Hsu GY, Yang JA, etc. Vessel Traffic Analysis for Maritime Intelligent Transportation System[C]. 2010 IEEE 71st Vehicular Technology Conference, Taipei, 2010.

[8] Sun Tao,Zhang Hongjian. A Method of Outlier Detection and Correction Based on First Order Diffetential[J]. Chinese Journal of Scientific Instrument,2002,(02):197-199 (in Chinese).

[9] Wu Xiuheng.Operability and Seakeeping of Vessel(2th Edition)[M]. Beijing: China Conmmunication Press,1999 (in Chinese).

Research on Service Platform of Three Gorges Lockage Maritime Security

Zhang Jian[1] *Cheng Yan-fen*[1] *Yin Qi-zhi*[2,3] *Chu Xiu-min*[2,3] Zhou Chen[2,3] Huang Gang[2,3]
1 School of computer science and technology, Wuhan University of technology;
2 Intelligent Transportation System Research Center, Wuhan University of technology;
3 Engineering Research Center of Transportation Safety (MOE)
Wuhan, China
whzj2050@126.com

***Abstract*-The security inspection service platform of the Three Gorges shiplock is very important for the navigation safety of the Three Gorges Reservoir and it will improve the efficiency of Three Gorges shiplock. The current model and demand of the Three Gorges Reservoir security inspection is analyzed in this paper. The security inspection service platform of the Three Gorges shiplock is constructed according to the demand. In this platform, the ships, which need to be inspected, are selected by the Analsis Hierarchy Process(AHP), the security inspection service route optimization is realized by the Shortest Seek Time First, and the real time monitoring to ships is realized by Web GIS. The Three Gorges Reservoir is more safeguuard and the ship security inspection is more and more scientific and pertineced by this platform.**

Keywords- security inspection; ships selection;Web GIS

I. INTRODUCTION

As the jugular region of yangtze river, the Three-Gorge Section includes two dams: the Three Gorges Dam and Gezhouba. And the ships on round trip are limited between the two dams. So improving shiplock capacity the Three Gorges palys an important role in full playing the strategic effect of yangtze river and promoting the economy of the basin[1]. The ships on round trip of the Three Gorges are huge, and there are much difference in the quality, tonnage, type of ships. The efficiency of shiplock and the safety of people near the lower yangtze river have been affected if the accidents happened in the lock chamber or the gorges. So it is necessary to inspect the ships on round trip of the Three Gorges.

The current security inspection of the three gorges is mostly completed by manual operation, the automation level and information degree are low. So the security inspection of maritime process will be complex, the maritime people and ship managers will have plenty of work and the real time monitoring of ships could not be realized. Through the study on the security inspection service platform, diversified declaration modes for lockage, simplified ship declaration procedures, shortened waiting time and real time monitoring during lockage could be achieved. Meanwhile, the handheld devices can be used to take photo of the unqualified indexes of ships during security inspection, which enhances the reliability of the law enforcement.

II. THE THREE GORGES SECURITY INSPECTION MODEL AND PROCESS ANALYSIS

At present, if there is a ship which needs pass the three gorges, it should propose request to maritime affairs center at first. There are different declare means according to whether the ship with a GPS device. If the ship equipped with GPS device, it can send declaration information to center data by GPS device directly. But if the ship was not installed GPS device, it is needed to go to maritime affairs center to fill manual declaration form; or the ship proposes request to maritime affairs center through the internet, fax and other way. Then maritime affairs center would assign security personnel to inspect and verify the ship which needs to inspect in anchorage. If the ship passed security inspection, it can go into the scheduling system. Security inspection flowchart of ship is shown in figure 1. At present, there are some problems which exist in the security inspection process: (1) the declaration process is very complicated for the ship which is not installed GPS device; (2) it costs a lot of time for the security personnel to search for the ships waiting for security inspection when they arrive in anchorage. In this case, it also may cause ship undetected; (3) when the ship is from the anchorage to the lock chamber, it lacks the necessary monitoring and it may be loaded dangerous goods in this process.

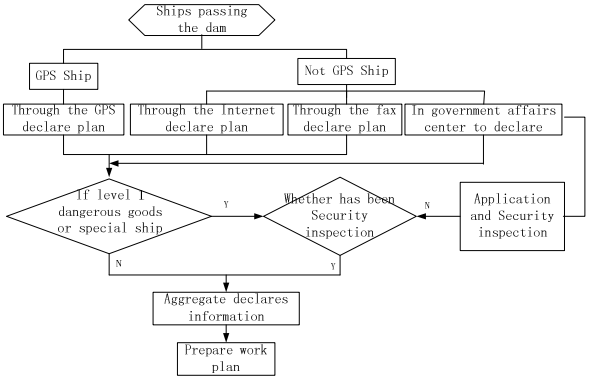

Figure 1. security inspection flowchart of ship

978-0-7695-4818-0/12 $26.00 © 2012 IEEE
DOI 10.1109/DCABES.2012.91

III. THE GENERAL FRAMEWORK OF PASSING THREE GORGES SECURITY SERVICE PLATFORM

For the above problems, the Three Gorges service platform shiplock is studied in the paper. This platform mainly includes three parts: ship information collection, ship monitor and ship security inspection. The general framework is designed as shown in figure 2.

The first part is information collection, which is the ship with GPS equipment which sends AIS, GPS[2] information to PC by the wireless. The data is classified and analyzed by PC, and then the data will be saved to the data center. While the ship is not installed GPS, the data could be stored to the data center by manual way.

The second part is ship monitor. Firstly ,the basic information of the ship is read out from data center, such as longitude and latitude of the ship, ship speed, heading, etc. Secondly with the electronic chart display and information system (ECDIS), the ship dynamic monitor is realized .

The final part is ship security inspection which is selected ship through screening algorithm firstly. And then the order of ship security inspection is determined through the resource scheduling algorithm in order to shorten the time of security personnel searching for ship.

IV. KEY TECHNOLOGY OF PASSING THREE GORGES SECURITY SERVICE PLATFORM

A. Screened ship of security inspection

In the process of ship selection[3], it should be followed as the following principles. (1) Scientific principle. Based on the risk to ship for screening, the assessment of risk and the ship security elements are closely connected. The history of the ship security information is also one of the factors should be considered[4]. (2) Systematic principle. Related factors of ship security inspection should be considered as far as possible. (3) Operability principles. Try to Choose evaluation index which meaning clear, data accessible and easy to calculate.

The analytic hierarchy process[5] is used in the process of ships selection [2]. We can determine the security indexes which affect the safe navigation according to the above principles. These indexes contain ship basic attribute, ship management attribute and ship inspection history. Ship basic attribute mainly contains three factors: ship type, ship age and tonnage of ship. Ship management attribute mainly contains two factors: ship inspection organization and the ship management company. Ship inspection history mainly contains five factors: average number of defects, the number of detained in recent three years, from the last detained time, whether there is not correct defects and the last time from inspection. The hierarchical structure model is constructed according to these indexes, as shown in figure 3.

According to the comparing of the importance of every layer elements and the former layer elements in the ship selection evaluation system, establish the judgment matrix.Judgment matrix M = (a_{ij})n has the following properties:

$$a_{ij} > 0, a_{ij} = \frac{1}{a_{ji}}, a_{ii} = 1 \qquad (i, j = 1, 2...n)$$

Where a_{ij} $(i, j = 1, 2...n)$ means the elements U_i and U_j ' ratio relative to the former layer. Values are usually in between 1 to 9.

According to the Hierarchical Structure Model shown in the figure 3, the expert investigation method is chosen to determine the weight of the indexes. The each index shown in the chart 1 is compared by thirty experts. The weight calculation of the "ship basic attribute" is list out, the calculation method of other indexes is similar to the "ship basic attribute".

The matrix A is constucted to calculate the weight ratio of the ship basic attribute according to the expert questionnaire:

$$A = \begin{Bmatrix} 1 & 8 & 4 \\ 1/8 & 1 & 1/4 \\ 1/4 & 4 & 1 \end{Bmatrix}$$

The maximum eigenvalue of the matrix A λ_{max}=3.0343;

The consistency index $CI = \frac{\lambda_{max} - n}{n-1}$ =0.017,(n is the order of the matrix)

$CR = \frac{CI}{RI}$ =0.033. Because CR value is less than 0.1,so this through the consistency check. (CR is the consistency ratio,RI is the consistency constant corresponding to the n order matrix);

the weight W =(0.71，0.07，0.22).

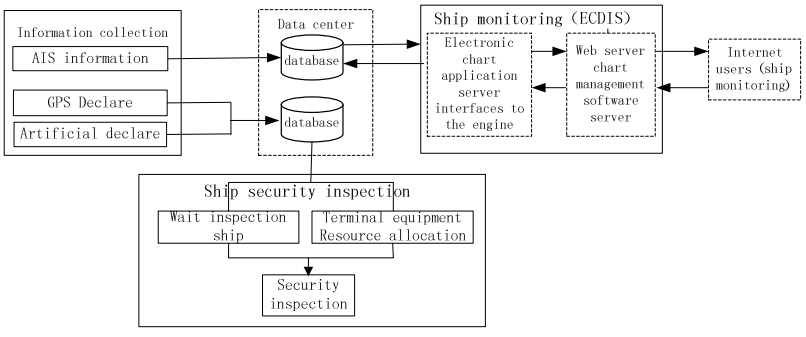

Figure 2. General framework

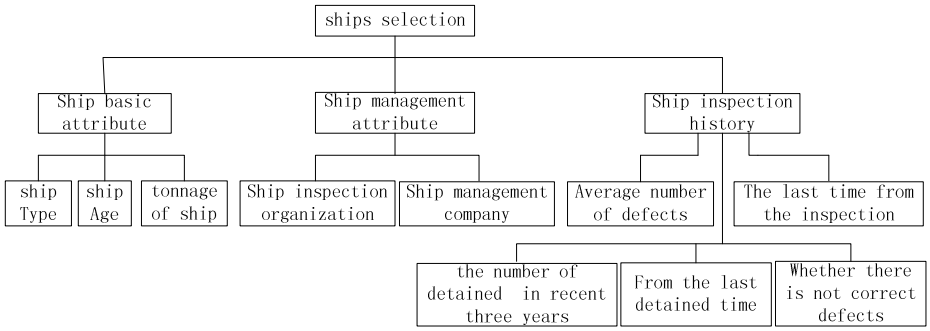

Figure 3. Hierarchical Structure Model

Thirty series of the weight value of the indexes of the "ship basic attribute" are obtained according to the data from above mentioned questionnaires of experts. Then the ultimate weight of the indexes of the "ship basic attribute" is obtained after calculating the average of the thirty weight values. The weight of other indexes should be obtained by using the similar method. As is shown in table Ⅰ:

TABLE I. SELECT SHIP INDEX WEIGHT LIST

	first grade indexes		second index	
	name	**weight** ω	**name**	**weight** β
Select ship index	Ship basic attribute	0.35	ship Type	0.45
			ship Age	0.22
			tonnage of ship	0.33
	Ship management attribute	0.3	Ship inspection organization	0.5
			Ship management company	0.5
	Ship inspection history	0.35	Average number of defects	0.20
			the number of detained in recent three years	0.25
			From the last detained time	0.05
			Whether there is not correct defects	0.05
			The last time from the inspection	0.45

Evaluation set is established. Hypothesis the risk rank of ship use a set representation,such as $V=\{v_1, v_2, \cdots v_n\}$, according to the weight of the indexes shown in chart 1, the score of target ship which can be calculated by follow formula:

$$B = \sum_{i=1}^{n} \omega_i \sum_{j} \beta_j v_j$$

In the above formulae: B is the total score of the target ship; ω_i is the weight of the item i index; β_j is the weight of the item i index of the item j ; v_j is the score of the item i of the item j.

$\overline{B}$, which is the threshold of B, is set. When B is greater than $\overline{B}$, the ship is considered as the critical one and should be carried out for security inspection. Otherwise the ship is considered as the good one and does not need security inspection.

B. Security resource allocation and scheduling

There is a contradiction that ships are more and more but the security personnel are little relatively during the security inspection of the Three Gorges shiplock. The contradiction will become more and more outstanding because of the security personnel could not to be infinitely increasing. So improving the efficiency of the ship security is very important. Usually the distance between the two anchorages that the ships anchored is too long. It costs a lot of time for the security personnel to search for the ships waiting for security inspection when they arrive in anchorage. In this case, it also may cause ship undetected. In order to solving the problem, the position of maritime affairs center could be viewed as a point of origin, and the ships which are waiting in anchorage as nodes. The ship is inspected which is the shortest distance from the current position, until all the ships are inspected. A scheduling algorithm of the ship security inspection can be designed which is similar to the algorithm of the Shortest Seek Time First according to the above requirements.

Firstly, the distance from ship to the maritime affairs center should be calculated according to the coordinates of the ships which wait in anchorage. And the distance between two ships also should be calculated. Then to sorting ships which are waiting in anchorage by the algorithm of Shortest Seek Time First[6]. The ship is inspected which is the shortest distance from the security personnel. Until all the ships are inspected. The ship is inspected which is the shortest distance from the security personnel, until all ships are inspected. A lot of time can be saved for security personnel and the efficiency can be improved by using this algorithm[7].

C. Base on Web GIS technology of ship monitoring

Ships can go to the chamber for lockage dispatching if their security inspection are finished to be qualified. It is impossible to track each ship during the process from anchorage to chamber. On the other hand, it has to prevent the illegal loading goods (such as explosives and other

dangerous goods). So it can be effective to regulate the ship through the electronic chart and Electronic Chart Display and Information System (ECDIS).

Inland-river Electronic Chart refers to the display platform of the inland-river Electronic Chart, the main principle is: the System Electronic Navigational Chart[8] (SENC) is transferred from the data of S-57 which is measured to the IMO standard and completed according to S-52 Presentation Library, then the Inland-river Electronic Chart is showed in the computer display[9][10]. With the development of web technology, the traditional mode of C/S is transferred to the mode of B/S, the real time monitoring could be easy realized by the users whose computer only need to be installed the Web browser. The operation and maintenance of the system has been reduced and the work efficiency is improved by this way.

V. CONCLUSIONS

Three functions are realized by the security inspection service platform of the Three Gorges shiplock. They are the automatic censoring of the ships which need to be inspected, the optimal assignment and scheduling of the security inspection reasource, and the overall monitoring to the ships. The platform plays positive roll in improving the efficiency of security inspection of the Three Gorges and ensuring the safety of the ships and Three Gorge shiplock.

ACKNOWLEDGMENT

The research has been supported by the projects from traffic science and technology, Ministry of Transport of the People's Republic of China, "Research on enhance technology of carrying capacity of three gorge ship lock in complicated conditions"(No. 201132820190).

REFERENCES

[1] WANG Haijiang. Strategy of Improving Integrated Throughput in Three Gorges Project[J]. Journal of Transport Information and Safety,2010,28(06):11-13.(in Chinses)

[2] Yan Xinping, Ma Feng, Chu Xiumin, Chen Chen. Key Technology of Collecting Traffic Flow on the Yangtze River in Real-Time[J]. N avigation of China,2010,33(02): 40-45. (in Chinses)

[3] Gan Zheng. Research on the Seagoing Ship-selecting System of FSC Inspection[D]. Dalian maritime university 2009. (in Chinses)

[4] Gao Deyi. Port state supervision and examination questions and answers[M]. Dalian:Dalian maritime university press,2002. (in Chinses)

[5] Saaty.T.L. the Analytical Hierarchy Process. MeGraw Hill,N.Y. 1980 .

[6] Qiu Decheng.Research on Cache Replacement and Disk Scheduling Algorithms in Network Storage[D].Lanzhou university 2007. (in Chinses)

[7] Xie Kai. Analysis of Lock Construction in China[J]. Journal of Transport Information and Safety. 2010,28(12):69-71. (in Chinses)

[8] Wei Guirong. The use of electronic chart prospect and countermeasures[J]. Journal of Qingdao Ocean Shipping Mariners College,1998,19(04):46-48. (in Chinses)

[9] IHO S57 IHO TRANSER STANDARD for DIGITAL HYDROGRAPHIC DATAEDITION 3.1.1[S]. The International Hydrographic Bureau MONCAO.2007.

[10] IHO ECDIS PRESENTATION LIBRARY Edition Users' Manual, Edition 3.4[S]. International Hydrographic Bureau, 2008.

Research on Inland Ship Navigation Status Monitoring System

Li Kun[1,2,3], Yan Xinping[1,2,3], Mao Zhe[1,2,3], Sang Lingzhi[1,2,3]

1 Intelligent Transportation System of Research Center, Wuhan University of technology
2 School of Energy and Power Engineering, Wuhan University of technology
3 Engineering Research Center for Transportation Safety (MOE), Wuhan University of technology
Wuhan, China
likun1720@126.com;xpyan@whut.edu.cn

***Abstract*-Inland ship navigation status monitoring system plays an important role in the prevention and reduction of inland ship accident as well as navigation security. The system has functions of ship status data collection and recording, status monitoring and alarming. The hardware and software of the system are designed and the feasibility of the system is discussed. The hardware part of the system achieves the function of data collection, including the collection of ship status information, operation information, speech information, radar information, AIS information and so on. The software part of the system realizes the function of data processing and monitoring.**

Key words-inland ship; navigation; status; monitoring; early-warning

I. INTRODUCTION

The accidents of inland ships will cause the human life and property loss and social influence[1]. However, the reduction and the prevention of the accidents mainly depend on instantaneity and the effectiveness of various insurance measures which are based on the collection and the monitoring of the information about the vessels' navigation status, the inland ship navigation status monitoring system plays an important role in the reduction and the prevention of the vessels' accidents as well as the accident investigation and analysis.

The monitoring system of the inland ships' navigation status uses the facilities and transformers installed on the vessels to collect all kinds of the parameters about the vessels' navigation status and then display the parameters collected and stored in the memory. In addition, because of the specialty of the navigation environment of the inland river, the system plays well in stability, validity and the anti-interference[2].

II. WHOLE SYSTEM DESIGN

a. System Composition

The structure diagram of the inland ship navigation status monitoring system is shown as Figure 1.The system is composed of main controller, power, collection module of ship navigation status, speech 1, speech 2, radar image, AIS, etc[3][4].

1. Main controller

The main controller is the core of the monitoring system, and composed of industrial computer, alarming circuit, etc. It is responsible for the coordination and management of the entire system, communicating among the modules, alarming, storing data, etc.

2. Collection module of ship navigation status

It is mainly used to collect the information of ship status and operating.

3. Speech module 1

Speech module 1 is mainly used to collect the speech information of VHF wireless phone.

4. Speech module 2

Speech module 2 is mainly used to collect the speech information of microphones in the bridge.

5. Collection module of radar image

It is mainly used to collect radar image information in the bridge.

6. Automatic Identification System[5][6] (AIS)

AIS can realize ship's automatic identification and avoid ship collision through information exchanging between ships as well as ship and shore, which can improve the intelligent management of the ship.

7. Power

The main power can convert 220V alternating current to direct current 24V, standby power is the battery which has the automatic charging devices.

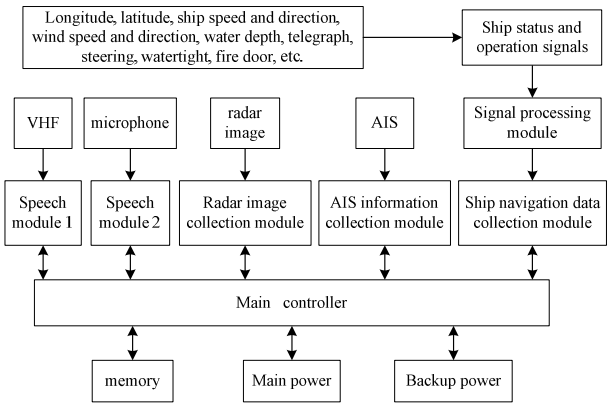

Figure 1 The structure diagram of the inland ship navigation status monitoring system

b. Main Functions of the System

1. Data collection

The information which collected by inland ship navigation status monitoring system includes static

978-0-7695-4818-0/12 $26.00 © 2012 IEEE
DOI 10.1109/DCABES.2012.86

information, operation information, radar image information, speech information, etc[7][8][9].

① Static information includes the fixed data, such as the name, coding, and call sign of the ship. This information is inputted into system while system is installed and is saved in the collecting system permanently.

②Status information includes ship's longitude and latitude, ship speed, course, automatic operation information, wind speed and direction, water depth, the status of watertight door and fire door.

③Operation information includes telegraph instruction and the replied information, steering instruction and the replied information, and main alarming.

④Speech information includes bridge telephone speech, VHF wireless phone speech, the speech of microphone in the bridge, chart room, central control room[10].

⑤Radar image includes the image information on the radar display, such as ship's position, course, etc.

There are three ways to obtain data of the ship navigation status monitoring system.

①The serial transmission is realized by I/O directly in which the data meets the international standard protocol, such as GPS.

②It could be collected by the microphone, such as the talking, telephone of the ship operator and the VHF speech.

③It could be transmitted by the interface conversion, by which the data is not met the international standard protocol. The data format can be obtained by conversion circuit, and then it is transmitted by I/O. For example, the velocimeter, echosounder, telegraph and steering instruction and replied information, main alarming, etc.

2. Status monitoring and alarming

An audible and visual alarm will be sent out when ship navigation status operation error (such as the steering inconsistent with instruction) and the data is more than the setting value range (such as ultra draft), meanwhile the system can realize ship yawing, collision, grounding early-warning and display the reason about alarming on the screen so that the driver can take the corresponding measures.

3. Equipment self-checking

During the data collection of the inland ship navigation status monitoring system, the equipment will have self-checked regularly to ensure it is in good operation. The process of self-checking is shown as Figure2.

4. Switched automatically when power is lost

①Switched automatically to ship's emergency power when main power is lost, and supply power for ship navigation status collecting and monitoring system. During the switching process, the continuity of system operation is guaranteed.

②Special and backup power could keep power supply for more than 2 hours when the emergency power is lost.

③System stops working when power is lost. System starts automatically and works normally when power is supplied again, and the working status is monitored through the self-checking device.

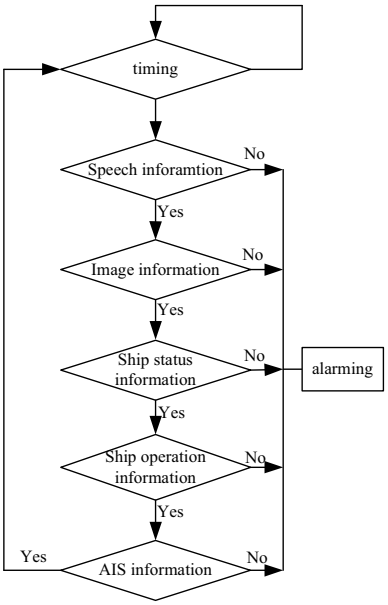

Figure 2 The process of equipment self-checking

III. THE REALIZATION OF HARDWARE AND SOFTWARE SYSTEM

a. The realization of hardware system

1. Switch and analog signals collection

The information collected by the ship navigation status monitoring system includes a large number of switch and analog information, and this information collection can be completed by 8051 single chip microcomputer which is the main intelligence module. The circuit module is allowed to install in the vicinity of the sensor to complete the information collection and conversion.

The circuit principle is shown as Figure 3. If the operation action or equipment operation status changes (such as telegraph instruction), then the single chip microcomputer will transfer information to the host controller, it will collect and monitor the data in time, the switch signal interface will do photoelectric isolation and level matching for switch information, the analog signal information will do information conditioning and resistance proceeding for analog information, then complete A/D conversion[11][12]. A/D conversion principle is shown as Figure 4.

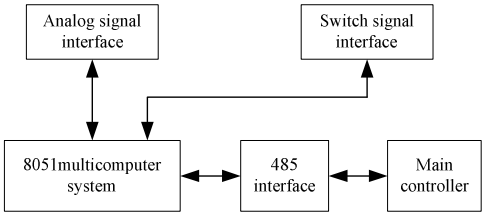

Figure 3 Switch and analog signal structure

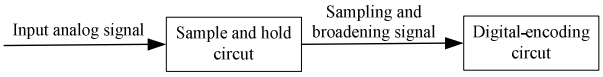

Figure 4 A/D conversion principle

2. Speech information collection

The digital processing of speech information is realized by digital signal processor (DSP). The principle is shown as Figure 5.

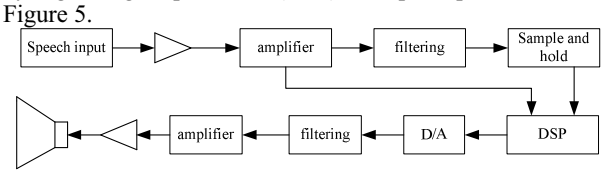

Figure 5 DSP circuit

3. Memory

The ship navigation status monitoring system uses the new high-capacity memory CF+Ⅱ card as memory bank[13]. The characteristics of emi-free (electromagnetic interference free), shock resistance and impact resistance make it adapting to the harsh environment of inland navigation environment.

b. The realization of software system

Configuring the interface and initializing of the device at the entrance of the program, once successfully, the system will start to collect information when received the order from the main controller, then processing the data and storing it in memory. The software process of inland ship navigation status monitoring system is shown as Figure 6.

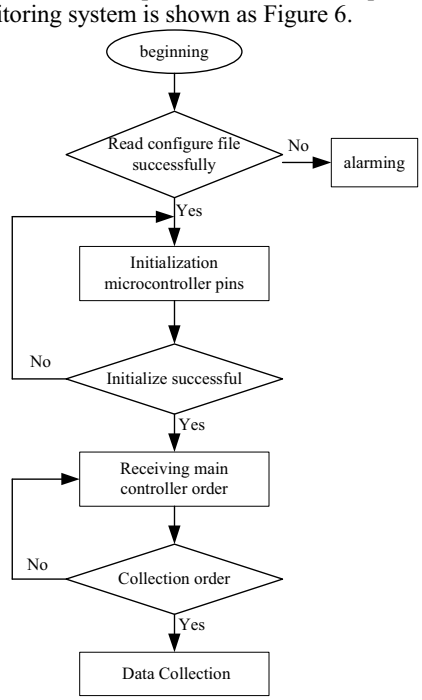

Figure 6 The software process of data collection

1. Data collection of the ship navigation status monitoring system can be divided into the following two situations:

① Data collection under normal conditions

When the ship is under normal navigation status, there is no telegraph or steering instruction, i.e there is no ship navigation statue changing, the data collection and monitoring system will collect and store the data in memory in accordance with the setting time cycle. The data collection process under normal status is shown as Figure 7.

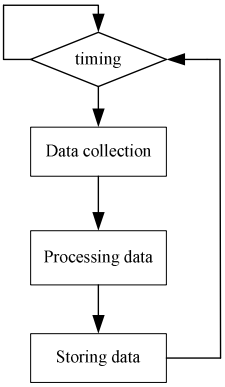

Figure 7 Data collection under normal status

② Data collection when ship navigation status changes

When ship navigation status changes, i.e., as soon as the telegraph instruction or steering instruction are sent out, the system will immediately start data collection, record the telegraph replied information or the steering replied information and compare them, if the orders are inconsistent, an audible and visual alarm will be sent out and the data will be stored in real-time. The data collection process is shown as Figure8.

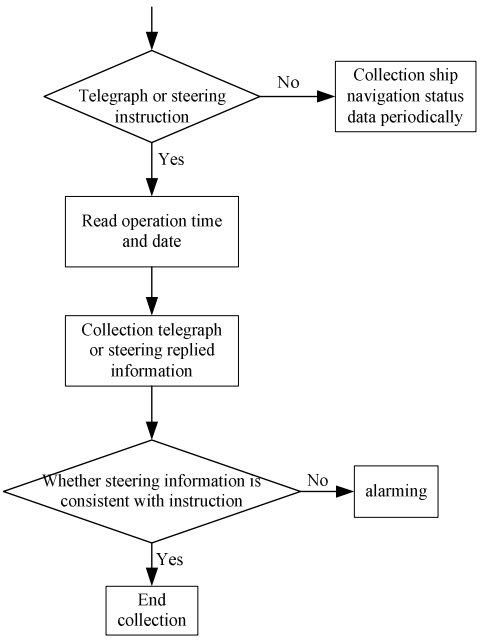

Figure 8 Data collection when the ship navigation status changes

2. The inland ship navigation status monitoring system realized the function of early-warning of yawing, collision and grounding.

①Ship yawing warning

When the ship sails in the inland river, an audible and visual alarm will be sent out so that the driver can take the corresponding measures if the distance between ship and channel boundary is less than the setting value. The early-warning process of yawing is shown as Figure 9.

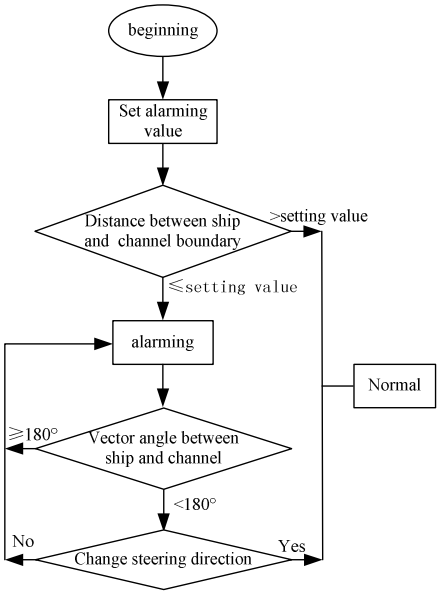

Figure 9 The early-warning process of yawing

②Ship grounding warning

The environment of inland navigation is complex and waterway depth is changing with the seasons, once water depth is less than the setting value on navigation, an audible and visual alarm will be sent out. The early-warning process of grounding is shown as Figure 10.

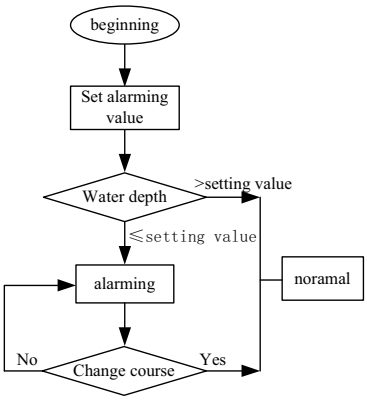

Figure 10 The early-warning process of collision

③Ship collision warning

When the ship meets other ships during navigation, the calculation on the time to closest point of approach （TCPA） and the distance to closest point of approach(DCPA) will be established according to the relative position between them, the formula are shown as formula (1),(2).The schematic diagram of the relative position of the own ship and other ship is shown as Figure 11.

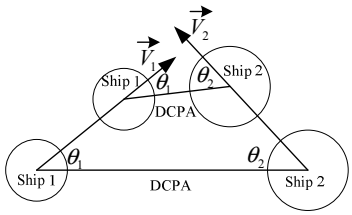

Figure 11 The schematic diagram of the relative position of the own ship and other ship.

$$① \quad V_1\cos\theta_1 + V_2\cos\theta_2 \le 0 \qquad TCPA = \infty \qquad (1)$$

$$② \quad V_1\cos\theta_1 + V_2\cos\theta_2 > 0 \qquad TCPA = \frac{DCPA}{V_1\cos\theta_1 + V_2\cos\theta_2} \qquad (2)$$

Where V_1, V_2 are the ship's speed; θ_1, θ_2 are the angle between $\vec{V}$ and the connection of the own ship and other ship.

An audible and visual alarm will be sent out when the $TCPA$ is less than the setting value. The early-warning process of collision is shown as Figure 12.

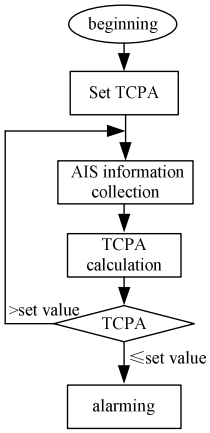

Figure 12 The early-warning process of grounding

CONCLUSION

The environment of inland navigation is complex which leads to many accidents, thus it is of great significance for inland traffic safety to develop the inland ship navigation status monitoring system. The system realized monitoring and alarming on the status data of ship navigation with high efficiency, so the ship failure and accident risk data can be

provided to the ship crew timely, who can then clearly know about the navigation status. This has a positive effect in reducing and preventing inland traffic accidents and guaranteeing the safe ship operation.

ACKNOWLEDGMENT

This paper is supported by Western Communications Construction Scientific and Technological Project of Ministry of Transportation of the People's Republic of China (grant No.201132820190), National High Technology Research and Development Program of China (Grant No.SS2012AA112303).

REFERENCES

[1] Mao Zhe,Yan Xinping,Chen Hui.Overview on Maritime Accident Analysis and Its Research Trends[J].China Ssfety Science Journal. 2010,Vol.20No.12.86-92.

[2] Morsi,M.S.Zaghloul,N.Essam.Future Voyage Data Recorder Based on Multi-Sensors and Human Machine Interface for Marine Accident[J].International Conference on Control,Automation and System2010.1635-1638.

[3] CHEN Shuzhe,LI Heming,YU Ruifeng.Design of the main program of the voyage data recorder[J].Ship&Ocean Engineering.2006, No.6(Serial No.175).100-102.

[4] Chen Jianjia,Chou Shouyao,Huang Mingho.System design and implementation for the management of voyage data of vessels[J]. Oceans Conference Record(IEEE).2007.

[5] YAN Zhongzhen,YAN Xinping,Ma Feng.Green Yangtze River Intelligent Shipping Information System and Its Key Technologies[J]. Jouranl of Transport Information and Safety.2010,Vol.29 No.6.76-81..

[6] SU Qiaoli. The design and realization of Marine Information Gathering System[D].Shanghai Maritime University.

[7] Nie Keping. Study on the data acquisition system of voyage data recorder of ship[J].Ship&Ocean Engineering.2004,No.5(Serial No.162). 49-51.

[8] TONG Yanyan, ZENG Qian, YUAN Gannan. The design and realization of data collection system in VDR[J].2005, Vol.26 No..5. 583-585.

[9] LIU Ming.Technical Research of the Voyage Recorder[D].Shanghai Maritime University.

[10] Zhou Wen, Hao Yanling. Disquisition of speech recognition in VDR[J]. Proceeding of the 6th world Congress on intelligent control and Automation, 2006,9562-9564.

[11] YU Fangping.The Design of Voyage Data Recorder(VDR)[J]. Navigatin of China. 2002, No.2(Serial No.51).5-8.

[12] CHANG Yong.The System of Voyage Data Recorder and some Key Technology Research[D].Wuhan University of Technology.

[13] YAN Wei.Design on Voyage Data Recorder[D].Tianjin University.

Portable Ship Information Querying System Based on Android

Liu Xinglong[1,2], Chu Xiumin[1,2], Wang Enjun[3], Yu Yuhuan[1,2], Chen Zhenyi[1,2], Liu Tong[1,2]
1 Intelligent Transportation System Research Center, Wuhan University of Technology;
2 Engineering Research Center for Transportation Safety (MOE), Wuhan University of Technology;
3 Transportation Research Center, Wuhan Institute of Technology.
Wuhan, China
liuxinglong_its@163.com, chuxm@whut.edu.cn

Abstract—At present, Ship IC Cards were adopted by all of the ships sailing on the Yangtze River, this greatly promotes the development of informatization of shipping system in Yangtze River. This paper proposed a Ship IC Card remote reading technical framework based on Android Hand-held Terminal. By utilizing Bluetooth, 3G, Wi-Fi wireless communication technology and android software programming technology, Ship IC Card information can be read and displayed on Android Hand-held Terminals. It is useful for improving the efficiency of maritime security inspection. Meanwhile, this technical scheme can play a significant role in the visa of ships turnover the port and ship lockage security inspection.

Keywords-IC card identification; android platform; remote database access

I. INTRODUCTION

With the development of computer technology and communication technology, ship identification made long-term development. At present, ship identification technology including Automatic Identification System (AIS), Radio Frequency Identification (RFID), video surveillance technology, etc[1]. Ship IC Card, as an application of RFID technology, is widely used in the visa of ships turnover the port in the Yangtze River due to its large amount of information storage, data confidentiality, anti-interference ability, ability to work offline and low-cost advantage[2][3]. However, the Ship IC Card did not play its proper role in the inland maritime security and ship lockage security inspection because of the lack of mobile Ship IC Card reading device.

Android, pushed out by the Google Corporation in 2008, is an open source operating system based on Linux. Due to the good operation experience and opening source, Android quickly occupied the mobile communication market. So, by using wireless communication technology and computer network technology to build up a Network Office System, which is based on Android platform, should be very simple and easy to spread out.

In this paper, the Android Hand-held Terminal, Ship IC Card reader and ship information database are integrated to build a portable Ship IC Card information querying system, which can be used in ships security inspection and the visa of ships turnover the port in the Yangtze River.

II. SYSTEM DESIGN

Mobile Ship IC Card reading system is composed of Ship IC Card, card reader, Android Hand-held Terminal, Bluetooth device, 3G and Wi-Fi wireless communication network, the server and backend database. System composition is shown in figure 1 below.

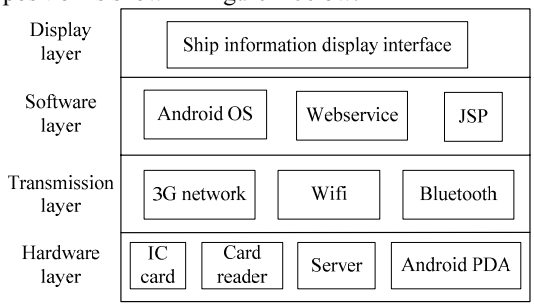

Figure 1. System Composition

A. Ship IC Card

Ship IC Card is the certificate of a ship. By reading the Ship IC Card, ship information such as ship ID identification, ship basic information, certificate information, record of ship safety inspection, ship entering or departing ports information and visa information etc, can be viewed. Among the information above, the ship ID identification, ship basic information and certificate information are static. Safety inspection input information, entering or departing ports record and visa information are dynamic. In this paper, Ship IC Card only stores Ship ID Numbers. Ship ID Number can be obtained when a ship registers in maritime department and it is unique. Therefore, Ship IC Card and ship ID have one-to-one relationship.

B. Card Reader

The card reader can read the ship's IC card information. The electromagnetic effect of IC card is aroused by the electromagnetic wave with specific frequency emitted out by card reader[4]. By this way, the data in IC card is broadcast to the air and received by the card reader. In order to communicate with Android Hand-held Terminal, the portable card reader should possess Bluetooth function and owns high capacity battery.

978-0-7695-4818-0/12 $26.00 © 2012 IEEE
DOI 10.1109/DCABES.2012.103

C. Android Hand-held Terminal

Any portable hardware platform using android operating system can be called Android Hand-held Terminal. Android Hand-held Terminal is around us in our daily life, such as mobile phones, tablet computer, PDA with android. Android Hand-held Terminal connected with card reader by Bluetooth can receive the Ship IC Card information read by Card Reader. After obtained the IC card information, the Android Hand-held Terminal accesses the remote database of ship information via 3G and Wi-Fi wireless network, and then displays the ship information which is got from database, on screen.

D. Server

The Server is a computer which stores the database of ship information and provides web service for client. Android Hand-held Terminal can not directly access a remote database through the network, therefore, in order to access the remote database by android, web service should be applied[5]. The Server must connect with Android Hand-held devices through the network. the Android Hand-held devices access web service published by the server by using the SOAP protocol.

E. Ship Information Database

The Ship Information Database, which is the core of the Ship IC Card reading system, records all the information of ships. Ship information includes the ship name, the ship ID number, ship types, ship tonnage etc. , the ship ID number is set as the primary key in database.

The schematic diagram of the whole system is shown in Figure 2 below.

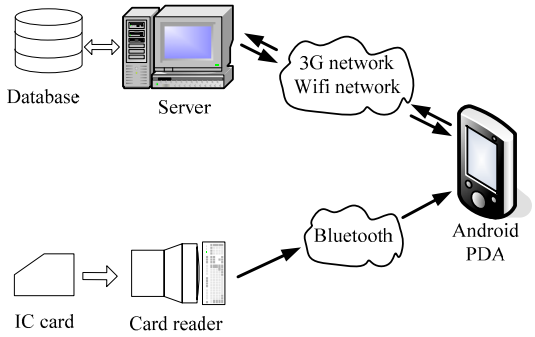

Figure 2. Schematic Diagram of The Whole System

III. SYSTEM REALIZATION

A. Ship IC Card reader

IC card reader emits out electromagnetic wave with specified frequency. It triggers the resonance of LC association vibration circuitry inside the IC card. As the electric charges gathered in capacitance in IC card, it is possible to launch out the data in IC Card.

The security should be concerned when data transfer from Ship IC Card to Reader. The security mainly includes the data's confidentiality, integrity, availability and authenticity. The data's confidentiality, integrity and availability are fulfilled by data encryption and decryption, and the data's authenticity is fulfilled by mutual authentication technology. At present, there are many password algorithms that are widely used. Such as symmetric key algorithm DES (Data Encryption Standard), IDEA (International Data Encryption Algorithm), public key algorithm RSA (put forward by Rivest, Shamir, Adleman in 1978), DSA (Digital Signature Algorithm), etc[6]. DES algorithm is the representative of traditional grouping cipher code study, it has been widely used because of its fast operating speed. But the key of DES algorithm is so short (56 bit) that it can be broken down by exhaustive method. So there is an improved DES algorithm, named 3DES algorithm[7]. There are three times' DES treatment when primitive plaintext is encrypted through 3DES algorithm, which use three different keys K1, K2, K3 (length is 8B), as shown in figure 3 below. The ciphertext is declassified in reverse order to back to the primitive plaintext when ciphertext is decrypted. In order to reduce the occupation rate of the system while generating and managing the key, the K1, K3 are set to the same value generally. But K1, K2 can never be same, or it will lose the significance of 3DES. Although 3DES reduces the operating speed of system, the key length is doubled, so its security has been greatly improved. Until now, 3DES has not yet been breached, and it becomes an international recognized encryption standard.

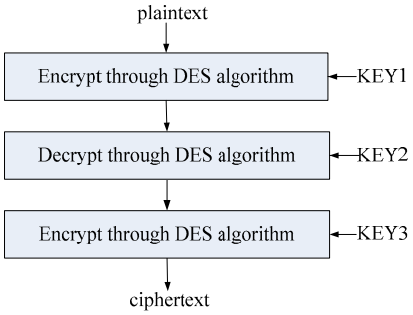

Figure 3. The Progress of Encryption through 3DES

B. Communication between Card reader and Android Hand-held Terminal.

Communication between Card Reader and Android Hand-held Terminal is accomplished through Bluetooth. Bluetooth is a wireless communication technology standard, it can connect mobile devices and fixed devices by wireless link over a short range[8].

Every Bluetooth device has a unique 48-bit BD_ADDR (Bluetooth Device Address). All the system control parameters of Bluetooth, such as frequency modulation sequence, channel access code, encryption keys are calculated by 48 BD_ADDR.

During data transmission between Bluetooth devices, the one which actively sends connection request is called master device, other devices which passively accept the connection request are called slave devices. In Ship IC Card Reading System, the Card Reader is master device and the Android

Hand-held Terminal is slave device. As Card Reader and Android Hand-held Terminal were connected, a physical channel will be established in Bluetooth's baseband layer.

The figure 4 shows the process of communication between Card Reader and Android Hand-held Terminal. Both the Card Reader and Android Hand-held Terminal are set to query status, then Android Hand-held Terminal will receive a query signal, an ID package that contains General Inquiry Access Code(GIAC) or Dedicated Inquiry Access Code(DIAC), from the Card Reader. After received a query signal, Android Hand-held Terminal returns the Frequency Hopping Synchronization(FHS) package to inform Card Reader about its BD_ADDR address, internal timing, device types and data which indicate how long to access the calling scanning status. Card Reader enters the calling scanning status and connects to the Android Hand-held Terminal after it gets the Android Hand-held Terminal's address data from the FHS packet. At this time, Android Hand-held Terminal is in calling scanning status and constantly receives the Device Access Code (DAC). Android Hand-held Terminal enters into calling responsing status when it received the calling signal, and then it will return an ID package as acknowledgement. Card Reader also enters the calling responsing status after receiving the ID package, and then it will send a FHS package to the Android Hand-held Terminal. The FHS package contains Card Reader timing order, BD-ADDR address, BCH Parity Bit, connection member address and so on. Then Android Hand-held Terminal returns a package as response after it received the FHS package. Then the Card reader and Android Hand-held Terminal were connected.

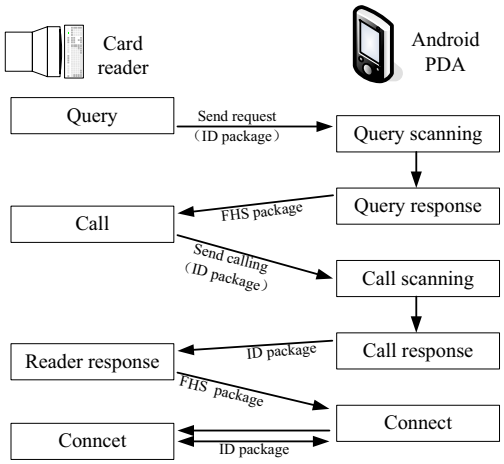

Figure 4. Progress of Card Reader Connected to Android PDA

C. Access to Remote Database by Android

Because it's not secure and reliable to access remote database by android directly, the web service will help us to realize it.

Web service provides a way to visit the business functions by web deployment, with the specific of multi-platform, simple, and high integration ability. Web service is an application component, provides data and service for other application programs logically. Every application program visits the web service through network protocol and standard data format(such as HTTP, XML, SOAP), and obtains the result by executing web service inwardly. Ship Information Query System is installed in the server to provide ship query function through web service. The Android Hand-held Terminal is connected with the server by 3G or Wi-Fi wireless communication network. As shown in figure 5.

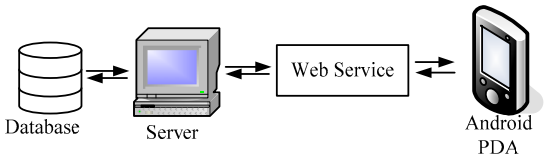

Figure 5. Schematic Diagram of Android Access to Remote Database

IV. REALIZATION OF SOFTWARE

A. Bluetooth Connection

Android platform provides a technical assistant package for developers to develop Bluetooth application. As shown in table 1.

TABLE I. THE EXPLANATION OF THE MAIN CLASS/INTERFACE OF ANDROID.BLUETOOTH PACKAGE

Class/Interface	Explanation
BluetoothAdapter	represents the adapter of a local bluetooth device
BluetoothDevice	indicates a bluetooth device
BluetoothServerSocket	the bluetooth socket which is used in interception
BluetoothSocket	already connected or being connected bluetooth socket
BluetoothClass	describes the general characteristics and performance of a bluetooth device

To transfer data between the Card Reader and Android Hand-held Terminal, the Bluetooth services should be started firstly. And in order to start and access the Bluetooth, the Bluetooth license must be added to the AndroidManifest file. After start of the Bluetooth service, the local Bluetooth device adapter begins to find the remote device. The Bluetooth service controls the communicate process by getting the input and output stream of socket connection.

B. Display of The Ship Information

To display the ship information on Android Hand-held Terminal, an user interface (UI) should be created. The user interface is composed of various controls such as button, textview, editview, radiogroup etc.

There are two methods to develop displaying UI on android, one is programming code and the other is compiling the XML layout file. It is better to use the former method to design UI when the controls' attribute changes as the program running. And it may be easier to design UI by the latter method when the controls' attribute unchanged as the program running. After the user interface layout file is

compiled, the interface can be displayed on Android Virtual Device (AVD).

V. CONCLUSIONS

Android is an embedded operating system, and it is the most popular operating system in nowadays. Due to its open-sourcing, android is very suitable to be used as a platform to develop extending functions. In this study, IC Card Reader is an extensional device connected to android platform by Bluetooth, and a mobile Ship IC Card Reading System was established combined with web service, which can be applied in ship security inspection and shipping visa.

The technical scheme proposed in this paper, indicates how to read information stored in IC card through wireless communication network at anytime and anywhere. Other remote database access systems, such as campus IC card identification system and electronic credentials identification system, can refer to this paper.

ACKNOWLEDGMENT

The research has been supported by the projects from traffic science and technology, Ministry of Transport of the People's Republic of China, "Research on enhance technology of carrying capacity of three gorge ship lock in complicated conditions"(No. 201132820190).

REFERENCES

[1] Yan Xinping, Ma Feng, Chu Xiumin, Chen Chen. Key Technology of Collecting Traffic Flow on the Yangtze River in Real-Time[J]. NAVIGATION OF CHINA.2010,33(2).

[2] Wang Wenqiang. Present and Development of Ship IC Card[J]. JOURNAL OF WUHAN INSTITUTE OF SHIPBUILDING TECHNOLOGY.2006,5(5).

[3] Sun Xing, Wu Yong, Chu Xiumin. Intelligent Yangtze River Shipping and Its Prospects Based on Coordination of Ship-mark-bank[J]. COMPUTER AND COMMUNICATIONS. 2010,28(6).

[4] Zhang Liangli, Yan Xinping, Zhang Cunbao. Development of Experimental Equipment for Autonomous Vehicle Based on RFID[J]. JOURNAL OF WUHAN UNIVERSITY OF TECHNOLOGY (TRANSPORTATION SCIENCE & ENGINEERING).2009,33(5).

[5] Paul Pocatilu. Developing Mobile Learning Applications for Android Using Web Services[J]. INFORMATION ECONOMIC.2010.

[6] Badra, M. Urien, P. Introducing smartcards to remote authenticate passwords using public key encryption[C]. Advances in Wired and Wireless Communication.2004.

[7] Liang Ya, Liu Lan. Implementation of DES and 3DES Cryptography Algorithm Based on Java Cards[J]. JOURNAL OF WUHAN UNIVERSITY OF TECHNOLOGY(INFORMATION & MANAGEMENT ENGINEERTING). 2006,28(11).

[8] C. Bisdikian. An Overview of the Bluetooth Wireless Technology[C]. IEEE Communication Magazine. 2001, 39 (12) p86-94.

Research on the Recognition of the Inland Ship Motion Status under the Stopping and Low-speed Sailing Condition

Liu Chen-guang[1,23] *Ma Feng*[1,2,3] *Mao Zhe*[1,2,3]
1 Intelligent Transportation System Research Center, Wuhan University of technology;
2 Engineering Research Center of Transportation Safety (MOE)
3 School of Energy and Power Engineering, Wuhan University of technology
Wuhan, China
liu_chenguang@qq.com; martin7wind@163.com; yaner@whut.edu.cn

Abstract- Due to interferences and some other reasons, the GNSS(global navigation satellite system) module in AIS would provide fault information, it is difficult to distinguish whether is the vessels are stopping or low-speed sailing without the help of Kalman filter algorithm. This paper has proposed a method to handle the error in GNSS information in AIS messages, which turns out to be effective in the experiment.

Key words: AIS; GPS Error; Recognition

I. INTRODUCTION

As an significant supplement to Radar and some other navigation equipments, The AIS (automatic identify system) of the VHF digital communication system is able to supply abundant useful navigation information, such as ship name, length, width, draft, course state, etc, under the range of 30 km, which would be a great help for maritime safety[1]. According to the IMO (international maritime organization) safety convention, AIS equipment must be installed in any new-built vessel which is 300 gross tonnage or above after 2002. The Chinese government has paid a lot of attention on the construction of the maritime networks. It is believed that all the Chinese coastal water areas have been covered by AIS basestations. Along with the rapid development of economy, AIS will play a more and more important role in inland shipping[2].

The GNSS module in AIS provides location information. In fact, most of the AIS terminals adopt the GPS system. Due to the fault of the GPS module or some other reasons, it is difficult to distinguish the moving state of the ship under the condition of low speed sailing and anchoring. For example, when ship is in the state of anchoring, the AIS terminal would transmit a bunch of messages which shows the ship is moving continuously in a small area; when ship is in the state of low speed moving (Under 2 knots), the messages would show the ship is moving like random beating point with uncertain course, this is difficult to distinguish from the state of stopping.

The phenomenon above is caused by non-sufficient positioning accuracy of GPS. Factors which affect the positioning accuracy can be divided into 4 categories [3].

a) Related to GPS satellites. It mainly includes satellite ephemeris error, satellite clock error, phase center offsets of satellite signal transmitting antenna.

b) Related to propagation path. It mainly includes ionosphere delay, troposphere delay and multipath effect.

c) Related to receiver. It mainly includes receiver clock error, phase center offsets of receiver signal transmitting antenna, and error caused by software and hardware of the receiver. In practical operation, GPS antenna is commonly installed on the top of the ship. Only under the condition of good sea state, GPS antenna and the movement of ship are basically identical. If the sea state is bad, GPS antenna can be affected by the pitching and rolling of the ship, the recorded positioning data jumps greatly, whose error is high. At this time, the path and course of the ship also change greatly, which can not show the real path and course[4].

d) Other factors. It mainly includes relativistic effect, noise error, artificial error, etc.

Aiming at solving the problem that GPS accuracy is not high, the solution is divided into two categories: one is to improve the positioning accuracy of the GPS receiver, such as using the carrier phase measurement to replace the pseudo-range measurement, using the relative positioning to replace the absolute positioning, using the precise ephemeris to replace or partly replace the broadcast ephemeris, selecting the station position, etc[5]. The other is removing the noise signals through the filtering algorithm to improve the accuracy of the target motion status recognition without changing the positioning accuracy of the GPS receiver. The most common of filtering methods is Kalman filtering.

The research focuses on how to improve the GPS accuracy by using the combination of GPS and other auxiliary navigation, and the main fusion systems are inertial navigation system, GPS navigation system, Doppler navigation system, hyperbolic navigation system, etc[6]. The most common fusion system are inertial and GPS navigation system, mainly used in military field such as submarine, missile, long range aircraft and in civil field such as car navigation, train positioning, robot localization.

In the inland environment, the density of the ship is large and the requirement of ship's motion status

978-0-7695-4818-0/12 $26.00 © 2012 IEEE
DOI 10.1109/DCABES.2012.105

recognition is high, the maritime administration apartment needs the every ship's motion status in real-time. Due to the economics and complexity of Inland river, inland ships wouldn't choose the fusion mode of inertial navigation system and GPS navigation system, and is unlikely to change the positioning accuracy of the GPS receiver. Therefore, it is more suitable by using the filtering algorithm to improve the motion status recognition in the low-speed status, it can be realized by designing the filtering algorithm in the software layer to avoid the complexity of the ship positioning equipment and reduce the work of the maritime administration apartment. The Kalman filtering is chosen since it is a representative of the temporal filtering, the engineering application is wide, and it is easy to perform on the computer.

II. DISCRETE KALMAN FILTER BASIC EQUATIONS

Kalman filtering algorithm is a linear minimum variance filtering algorithm. It not only considers the statistical property of signal and measured value, but also describes the system by state equations. Therefore, Kalman filtering algorithm can estimate stable random signal as well as non-stable random signal. It is not necessary to store the previous measured value for Kalman filter, it can estimate the real-time signal by carrying out recursive calculation in computer according to current measured value and previous estimated value[7].

Suppose that estimating state X_k is driven by system noise sequence W_{k-1} at time t_k, the driving mechanism is represented by state equation as shown below.

$$X_k = \Phi_{k,k-1} X_{k-1} + \Gamma_{k-1} W_{k-1} \tag{1}$$

The measurement to X_k fulfills the linear relationship, measurement equation as shown like this.

$$Z_k = H_k X_k + V_k \tag{2}$$

$\Phi_{k,k-1}$ is the one-step transfer matrix from moment t_{k-1} to moment t_k, Γ_{k-1} is the driving matrix of system noises, H_k is the measurement matrix, V_k is the measured noises sequence, W_k is the system driving noise sequence.

Meanwhile, W_k and V_k fulfill the following equations.

$$\left.\begin{aligned} E[W_k] = 0, Cov[W_k, W_j] = E[W_k W_j^T] = Q_k \delta_{kj} \\ E[V_k] = 0, Cov[V_k, V_j] = E[V_k V_j^T] = R_k \delta_{kj} \\ Cov[W_k, V_j] = E[W_k V_j^T] = 0 \end{aligned}\right\} \tag{3}$$

Q_k is the variance matrix of system noise sequence, and assuming it is nonnegative definite matrix, R_k is the variance matrix of measured noise sequence, and assuming it is positive definite matrix.

The equation of status predict is shown in format(4).

$$\hat{X}_{k/k-1} = \Phi_{k,k-1} \hat{X}_{k-1} \tag{4}$$

The equation of state estimation is shown in format(5).

$$\hat{X}_k = \hat{X}_{k/k-1} + K_k (Z_k - H_k \hat{X}_{k/k-1}) \tag{5}$$

The equation of filter gain is shown in format (6).

$$K_k = P_k H_k^T R_k^{-1} \tag{6}$$

The equation of one step prediction mean-square error is shown in format(7).

$$P_{k/k-1} = \Phi_{k,k-1} P_{k-1} \Phi_{k,k-1}^T + \Gamma_{k-1} Q_{k-1} \Gamma_{k-1}^T \tag{7}$$

The equation of estimate mean-square error is shown in format(8).

$$P_k = (I - K_k H_k) P_{k/k-1} (I - K_k H_k)^T + K_k R_k K_k^T \tag{8}$$

Formula (4)-(8) are the basic equations of discrete Kalman Filter. The state estimation $\hat{X}_{k\,(k=1,2,\ldots)}$ of moment k can be recursively calculated according to the measurement value Z_k at time k, as long as the initial value $\hat{X}_0$ and P_0 were given. In one filtering period, taking from the precedence of system information and measurement information used by filtration, Kalman filter represents two data updating procedures that are time updating process (relative to formula (4), (7)) and measurement updating process (relative to formula (5), (6), and (8))[5].

III. Establish the discrete Kalman filter model

The location information and speed information the AIS device received are taken as the state variables of the model, namely $X=[x_h, x_v]^T$, among which x_h, x_v are the position components of the X, Y directions, and the X direction is defined as east direction, and Y direction is defined as west direction[8]. The influence of the GPS error is the noise of the equation of state, assuming that the noise is white noise. Then it comes out the state equation of the system:

$$X_k = A_{k,k-1} X_{k-1} + B_{k-1} u_{k-1} + W_{k-1} \tag{9}$$

$$A = A_{k,k-1} = \begin{pmatrix} 1 & 0 \\ 0 & 1 \end{pmatrix}$$

There is no control inputs in the system, $u=u_{k-1}=0$, so equation (9) can be simplified as

$$X_k = A X_{k-1} + W_{k-1} \tag{10}$$

The measurement equation is shown as

$$Z_k = H_k X_k + Y_k + V_k \tag{11}$$

The observed value of the noise is a direct

manifestation of the state value, the systematic measurement error is negligible, namely Y_k=0, so

$$H = H_k = \begin{pmatrix} 1 & 0 \\ 0 & 1 \end{pmatrix}$$

Equation (11) can be simplified as

$$Z_k = HX_k + V_k \tag{12}$$

The time-update equation is

$$P_{k/k-1} = P_{k-1} + Q_{k-1} \tag{13}$$

$$\hat{X}_{k/k-1} = \hat{X}_{k-1} \tag{14}$$

The measurement-update equation is shown as

$$\hat{X}_k = \hat{X}_{k/k-1} + K_k(Z_k - H_k \hat{X}_{k/k-1}) \tag{16}$$

$$K_k = P_k(P_k + R_k)^{-1} \tag{15}$$

$$P_k = (I - K_k)P_{k,k-1} \tag{17}$$

IV. THE DISCRETE KALMAN FILTER EXPERIMENT

Almost any initial value of the mean square error is not equal to 0, and the ultimate convergence of the filter could be realized. In the actual system, state noise variance matrix Q_k and observational variance matrix R_k will be changed by each time of iterative calculation of the filter model. The Q_k and R_k are assumed constant.

The Kalman filter experiment has been completed by selecting 50 points, which is collected by the AIS equipments of laboratory. These points are GPS data of a vessel near in some port of the inland river, the original GPS data before Kalman filter is shown in Figure 1, and the result after calculated by the above Kalman filter model is shown in figure 2.

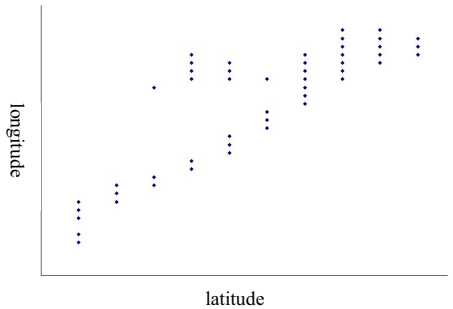

Figure 1 The original GPS data before Kalman filter

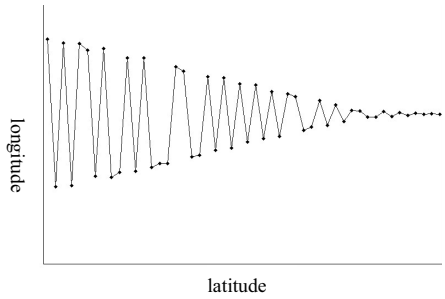

Figure 2 The GPS data after Kalman filter

As you can see from figure 2, GPS data have tended to converge with this filter method. GPS data could be stabilized within a smaller error range. If GPS error is less than 2 m after filtering, under the assumption that transferring period of AIS messages is not more than 10 s, a ship's speed of AIS message in the stopping state would not be greater than 0.2 m/s (approximately 0.4 knots). If a ship's speed is between 0.4 and 2.0 knots while sailing, the status of this ship should be thought as low speed navigation.

V. CONCLUSIONS

When a certain ship is at the state of stopping or low-speed, the recognition of its motion state is often not accurate enough. In this paper, the reasons of this phenomenon are discussed. Meanwhile, Kalman filter is applied to reduce the GPS errors. Experiment has shown that the motion state recognition of stop or low-speed ship can meet the demand to a certain extent with Kalman filter processing. Since GPS errors always exist, the application scope of Kalman filter is not confined to the recognition of stop or low-speed ship. When the ship is in a state of normal navigation, Kalman Filter can also be tried to improve the accuracy of GPS positioning, which will improve the security of inland water transportation.

In this paper, the data used for verification is from a certain ship. So the conclusion could not apply universally. This study is aimed at proposing a possible solution of the problem and further study is still needed to improve the universality of data and the optimization of the algorithm.

ACKNOWLEDGMENT

This paper is supported by National High Technology Research and Development Program of China (Grant No.2012AA112303).

REFERENCE

[1] Ma F. The Research on the Development and Application of AIS Equipment in In-Land Rivers[D]. Wuhan: Wuhan University of Technology, 2010. (in Chinese)

[2] Sun X, Wu Y, Chu X M. Intelligent Yangtze River Shipping and Its Prospects Based on Coordination of Ship-mark-bank[J]. Journal of Transport Information and Safety,2010: 48-52. (in Chinese)

[3] He L. The study and Design of the Hand-held GPS Equipment[D]. Wuhan: Wuhan University of Technology, 2007. (in Chinese)

[4] He W Y. The Impacts and Measures of Ships' Position for GPS Error[J]. China Water Transport,2009,9(4): 16-17,33. (in Chinese)

[5] Wang Y D. GPS Error Analysis and Precision Control[J]. Geomatics & Spatial Information Technology,2011,34(6): 235-236. (in Chinese)

[6] Qin Y Y, Zhang H Y,Wang S H. Kalman Filter & the Schedule of Combination Navigation[M]. Xi'an: the Press of Northwestern Polytechnical University,1998: 238. (in Chinese)

[7] Ma Y F. Research on MSINS/GPS Integrated Navigation System and Its Data Fusion Technology[D]. Nanjing: Southeast University,2006. (in Chinese)

[8] Chang H Z. The Study on the Accuracy of Shipborne AIS Information and the Establishment of Information Correction and Error Prewarning System[D]. Dalian: Dalian Maritime University, 2011. (in Chinese)

Marching Cube Based Marker-controlled Watershed Segmentation for CryoEM Density Map

Guihua Shan, Jun Liu, Dong Tian, Maojin xie, Xuebin Chi
Supercomputing Center
Computer Network Information Center, Chinese Academy of Sciences
Beijing, China
e-mail: {sgh,liujun,tiandong,xiemaojin,chi}@sccas.cn

***Abstract*—Cryo-electron microscopy (CryoEM) is a very important method for studying the structures of macromolecules. Segmentation is one of the key problems in CryoEM technique. We propose a new 3D watershed, where marching cube is employed as a marker method to control the segmentation. It can transform the domain knowledge into watershed by an interactive interface with isosurface, by which we avoid over-segmentation and obtain the correct segmentation results. Lastly we illustrate the efficiency of the algorithm by testing it on two typical CryoEM density maps.**

Keywords-CryoEM density map; image processing; watershed; marker; segmentation

I. INTRODUCTION

CryoEM is one of the three most important methods for studying the structures of macromolecular machines. The macromolecular is made up of multiple components. For understanding the underlying structure of the complex macromolecular, the segmentation of the macromolecular density map into more manageable substructures is indispensable. However, segmentation is considered as one of the hardest open problems in CryoEM [1].

Currently, such segmentation is typically carried out by hand. The popular visualization tools for analyzing density map only support manual segmentation, such as Chimera and Spider. This results in inconveniency that the users have to decompose the density map by tracing the elements of interest with a graphical interface. It is tedious and time-consuming. Moreover, it segments the mesh of a specific iso-surface, not 3D volumetric data. When iso-value changed, user has to restart a new segmentation.

To resolve this issue, we propose a 3d watershed method where marching cube actors as a marker. It makes use of the topology characteristics and the knowledge of domain scientists to realize an automatic segmentation.

The rest of this paper is organized as follows. In Section 2, we summarize the related work on segmentation of CryoEM density map. Then we propose the marching cube based marker to control the watershed algorithm in section 3. Section 4 describes experimental results on the two typical data. Finally we conclude this paper in Section 5.

II. RELATED WORK

Segmentation is one of the hardest fields in image processing, especially 3D volumetric map. Many people have contributed to this topic and obtained a lot of advances. But there are no general methods that are effective in all application fields. Most of the segmentation methods are related with specific application areas. Currently the segmentation works on density map of CryoEM are very few. Several papers involve in this kind of automatic segmentation. Volkmann [2] proposed a 3d watershed immersive method, where a step length is employed to control the granularity of segmentation, but it's hard to get a suitable value for this parameter. Frangakis and Forster [3] proposed a normalized graph and eigenvector analysis. Both of them attempt an automatic segmentation at cell and molecule level. Yu et al. [4] describe an automatic segmentation at virus level, in which critical points are obtained by gradient vector filter.

The watershed is likely to cause over-segmentation. The most effective way to eliminate over-segmentation is the notation. Lezoray and Cardot proposed the check marker from the results of the Bayesian classifiers [6]. Neves morphological operation automatically select the maximum value of the wavelet coefficients using the marker [7]. Frucci builds the image pyramid to select the markers at low resolution [8].

Based on the characteristics of the CryoEM data, we employ marching cube method as marker which can intuitively and directly make good use of domain scientists' to avoid over segmentation, and realize semi-automatic segmentation f.or CryoEM density maps.

III. MARCHING CUBE BASED MARKER-CONTROLLED WATERSHED

In the two-dimensional image segmentation, usually the gradient data of image is used as the input for watershed. While for CryoEM 3D density map, the ideal boundary is the minimum area of the density. Therefore, we directly use the density data as the input for the segmentation and regard the density as the fourth dimension. Considering the topography of the four-dimensional space, we inject water from high-density maximum area, which rise up the minimum of the density.

In order to prevent over-segmentation, we employ marching cube method as marker to control the segmentation. With interactive graphical interface, iso-value and the number of sub-areas that the density map need to divided into are easily set. Then the largest n sub-areas are automatically counted out, all the area whose density value are higher than the current iso-value are filling with water.

There are two key steps in this watershed algorithm. The first one is to get the largest n areas by the marching

978-0-7695-4818-0/12 $26.00 © 2012 IEEE
DOI 10.1109/DCABES.2012.98

cube isosurface; the second one is to get the coordination of all the grid points in each closed surface .

Now we discuss how to get the largest n areas by the marching cube isosurface. With marching cube algorithm, we get all the triangles and the connectivity relationship, the number of triangles in each connective surface. The triangles connected together form a closed surface. The density values of the grid points in these close surfaces are no less than the current threshold of the isosurface. we denote these closed surfaces by $Q_i, i = 1,2,...,m$, then the top n closed surfaces are the initial areas which we are looking for.

With the principle of marching cube algorithm, we know that each closed surface is composed by triangles, whose vertexes must lie on one of the twelve edges of the voxel. And the two vertexes of these edges must have different density values, where one must be greater or equal to the isosurface threshold, the other must be less than the threshold. ie.one vertex is at status1, the other is status 0, respectively. All other grid points, connected with vertex at status1and themselves also at status 1, are the whole grid points that inside the same closed surface.

By these two steps, we can obtain the whole coordinates of the grid points in the closed surfaces $Q_i, i = 1,2,...,m$. We sort these surfaces by the number of the grid points. Suppose $Q_i, i = 1,2,...,n$ is the top n surfaces. We fill water from these top n close surfaces, and denote the subset of grid points in Q_i by $J(Q_i)$, which is the set of point in the basin related with a maximum.

Let min and max be minimum and maximum of the density map $I(x, y, z)$ respectively. In traditional 2D image segmentation, the images usually are grayscale map or gradient map, whose range is 0-255. In CryoEM density map, the density value is float. To control the step size of the water immersion, the density value is quantized into 0-MAX_STEP. Usually MAX_STEP is equal to 1023, i.e.

$$I'(x, y, z) = 1023 \times \frac{I(x, y, z) - \min}{\max - \min} \qquad (1)$$

Because the points with higher density are surrounded by points with lower density, the water is rise up from high density to low density in the watershed algorithm, i.e. the point with high density is the low point in watershed algorithm, while the point with low density is the high point in watershed algorithm. For simplification, we define the height of image as following

$$H(x, y, z) = 1023 - I'(x, y, z) \qquad (2)$$

$G[h] = \{(i, j, k) \mid H(i, j, k) \le h\}$, $G[h]$ means the height of quantized image, $H(x, y, z)$ is the set that is not greater than h.

Quantizing the current *iso _ value* by formulation (1), we get the image height threshold $H_{th} = 1023 - iso\_value$. As the water rise up from $H_{th}+1$ to $H_{\max}+1 = 1024$ gradually, the topology in the image will be immersed. Let $J_h(Q_i)$ be the set of points which are in the immersive basin, which means if $(i, j, k) \in J(Q_i)$ and $(i, j, k) \in G(h)$, $J_h(Q_i) = 1$ for point (i, j, k), else $J_h(Q_i) = 0$.

Let $J(h)$ be the set of immersed basin at height h:

$$J(h) = \bigcup_{i=1}^{n} J_h(Q_i)$$

In the following immersive process, we suppose intially $J[\min+1] = G[\min+1]$. Let the water rise up gradually from $H_{th}+1$. The deduction of $J(h+1)$ from $J(h)$ go as follows. For each connective member p in $G(h)$, there are three different cases:

(1) $p \cap J(h) = NULL$;

(2) $p \cap J(h)$ includes one connective member of $J(h)$;

(3) $p \cap J(h)$ includes several connective member of $J(h)$;

According the principle of deducing $J(h+1)$ from $J(h)$: when meet a new minimum, which is the case 1,then combine p and $J(h)$ to construct $J(h+1)$; when p is already in a basin, which is case2, then combine p and $J(h)$ to construct $J(h+1)$; if p is the ridge, which is case 3, a dam is needed to prevent overflow of basin.

Each step comply the above principle as h is gradually added up to $H_{\max}+1$. At last $J(H_{\max}+1)$ are the final segmentation results.

Now we conclude the above procedure into the following algorithm:

Marching cube based marker-controlled watershed algorithm

Initialize:

a) Compute the closed surfaces Q_i ($i = 1, \cdots, m$), by marching cube, select top n surfaces Q_i ($i = 1, \cdots, n$) which have the largest n number of points.

b) compute the coordinates of all the points in each Q_i ($i = 1, \cdots, n$)

c) obtain the initial basins by filling water of all the points in Q_i ($i = 1, \cdots, n$),

d) to control the step size, quantize the density into 0-1023.

Loop step

For h from $H_{th}+1$ to $H_{\max}+1$

For each connective member p, judge cross set of p and $J(h)$

If $p \cap J(h) = NULL$, then combine p and $J(h)$ to construct $J(h+1)$;

If $p \cap J(h)$ includes one connective member of $J(h)$, then combine p and $J(h)$ to construct $J(h+1)$;

If $p \bigcap J(h)$ includes several connective member of $J(h)$, construct a ban to prevent overflow.

If $h = H_{\max} + 1$, exit loop, $J(H_{\max} + 1)$ is the final segmentation results.

$h = h + d$.

IV. EXAMPLES

In this section, we apply the marching cube based marker-controlled watershed to two typical data sets. One is a symmetry chaperone density map from CryoEM, the other is an asymmetry ribosome density map from CryoEM.

We evaluate the segmentation results by visual comparison and cross relation score. Fig.1 and Fig2 show the segmentation results in visualization, from which we can see clearly the segmentation subunit by visual sense. For more quantity evaluation the cross-correlation score is also provided, which is calculated between the segmented subunit of density map and simulated density map from the corresponding atomic model after transformation with the score function described in [8]:

$$score_{f,g} = 1 - \frac{\sum_{i,j,k} |f(i,j,k) - g(i,j,k)|}{\sum_{i,j,k} \max(f(i,j,k), g(i,j,k))} \quad (3)$$

where f, g are two scalar maps. The highest score 1.0 means they are identical, 0 indicates there are no similarity. We also give the score of segmentation by hand and simulated density map from its corresponding atomic model. The validation results are summarized in table 1.

The first example is the CryoEM density map of the ribosome with a resolution 12 $\mathring{A}$, which is asymmetry and composed of two different subunits. Segmentation results are shown in Fig.1. Fig1.a is original isosurface view. Fig1.b is the traditional watershed, which segments the density map into 9801 blocks. Fig1.c is the segmentation from our improved watershed. With this algorithm, the number of segmentation objects and initial immersive areas are automatically set, which makes good use of domain knowledge, avoid over-segmentation, and divide the density map into two subunits. From table 1, the scores of the subunits by automatic segmentation and the simulated density maps of its corresponding crystal structures are 0.96 and 0.95, respectively. The scores of the segmented subunits by hand and the simulated density maps of its corresponding crystal structures is 0.98and 0.94, respectively, which show the automatic segmentation is as good as manual segmentation. But manual segmentation is time-consuming and its results highly depend on the users' subjectivity.

The second example is the CryoEM density map of the chaperone beta with a resolution 10 $\mathring{A}$, which is 9-fold symmetry. Segmentation results are shown in Fig.2. Fig2.a is original isosurface view. Fig2.b is the traditional watershed, which segments the density map into 3377blocks. Fig2.c is the segmentation from our improved watershed, by which the density map is divided into 9 symmetry subunits. From table 1, the score of the subunit by automatic segmentation and the simulated density map of its corresponding crystal structure is 0.71, and the score of the subunit by manual segmentation and the simulated density map of its corresponding crystal structure is 0.72. All the scores in this example are not as good as the ones in the first example because the structure of protein has changed in different environment which cause the structure in density map is not exactly the same with the original crystal structure. And, the segmentations themselves are correct.

V. CONCLUSION

Segmentation is an important method of analyzing Cryo-EM density map. Based on CryoEM data characteristics, we proposed a semi-automatic segmentation method named marching cube based marked-controlled watershed algorithm which can transform the domain knowledge to watershed by an interactive interface with isosurface. So we avoid over-segmentation and obtain the correct segmentation results. The segmentation of reconstruction 3D density map from CryoEM is one of the key problems of CryoEM technique. Compared with the pure manual methods of traditional software, Our work is expected to offer biologists a new data analysis tools, which is friendly and effectively. The future, we will further the study of the segmentation of the CryoEM density data to carry out further study of the algorithm, such as using the GPU to accelerate the marching cube speed.

ACKNOWLEDGMENT

This work are supported by The work was supported by Chinese National Science Fund grant No.60673064 and Knowledge Innovation Project of The Chinese Academy of Sciences (No.KGCX1-YW-13). The authors would like to thanks professor Fei Sun from Institure of Biophysics of Chinese Academy of Sciences for the data and his constructive suggestions.

REFERENCES

[1] M. L. Baker, T. Ju, W. Chiu, Identification of Secondary Structure Elements in Intermediate Resolution Density Maps, Structure, 15(1):7-19, 2007.

[2] Pruggnaller S, Mayr M, Frangakis AS.Computational Approaches for Automatic Structural Analysis of Large Bio-molecular Complexes, J Struct Biol. 2008,Volume164(1):161-165,

[3] Zeyun Yu, Chandrajit Bajaj,Computational Approaches for Automatic Structural Analysis of Large Biomolecular Complexes, IEEE/ACM Transactions on Computational Biology and Bioinformatics, Volume 5 , Issue 4 (October 2008): 568-582

[4] Niels Volkmann, A novel three-dimensional variant of the watershed transform for segmentation of electron density maps, Journal of structural Biology 2002, 138,123-129

[5] A. Frangakis and R. Hegerl, Segmentation of two and three dimensional data from electron microscopy using eigenvector analysis Journal of Structural Biology, 2002, 138(2), 105–113.

[6] V. Grau, A. U. J. Mewes, M. Alcaniz, R. Kikinis and S. K. Warfield. Improved watershed transform for medical image segmentation using prior information, IEEE Trans. Medical Image, 2004, 23(4):447-469

[7] Olivier Lezoray, Hubert Cardot: Bayesian Marker Extraction for Color Watershed in Segmenting Microscopic Images. ICPR 2002:739-742

[8] S. R. Neves, E. A. B. Silva and G. V. Mendonca. Wavelet-watershed automatic infrared image segmentation method. Electronics letters,2003,39(12):903-904

[9] M. Frucci, G. Ramella and G. S. D. Baja, Using resolution pyramids for watershed image segmentation. Image and Vision Computing, 2007, 25:1021-1031

TABLE1. THE SCORE REPRESENTS THE CROSS CORRELATION VALUE (0-1)BETWEEN THE DENSITY MAP AND ATOMIC MODEL AFTER TRANSFORMATION

Segmentation mode	CryoEM density map	Simulated density map from	scores
Automatic segmentation	The large subunit of ribosome	Its corresponding crystal structure	0.96
Manual segmentation	The large subunit of ribosome	Its corresponding crystal structure	0.98
Automatic segmentation	The small subunit of ribosome	Its corresponding crystal structure	0.95
Manual segmentation	The small subunit of ribosome	Its corresponding crystal structure	0.94
Automatic segmentation	One subunit of the chaperone	Its corresponding crystal structure	0.71
Manual segmentation	One subunit of the chaperone	Its corresponding crystal structure	0.72

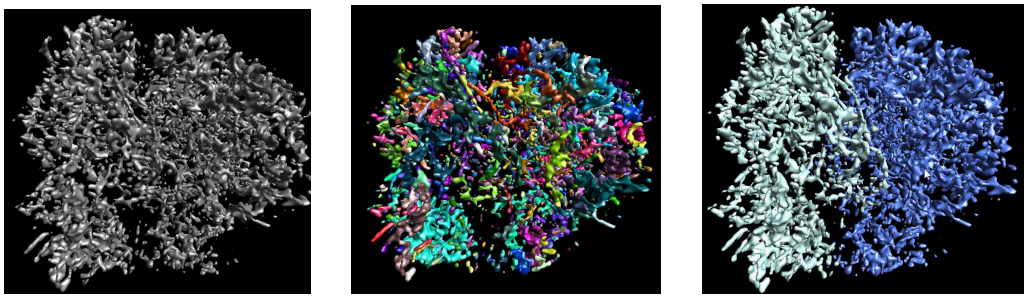

(a) (b) (c)

Figure 1. the segmentation of ribosome. a)the original isosurface view;b) the over-segmented results by the traditional watershed, where the density is divided into 9801blocks; c)the segmentation results by the marching cube based marker-controlled watershed, where the density is divided into a large unit and a small unit.

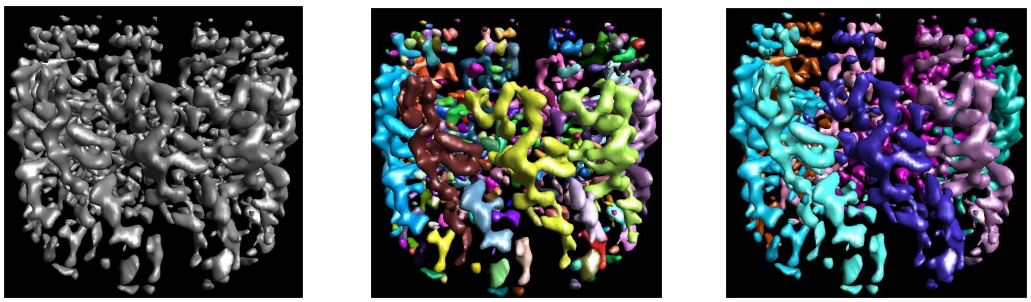

(a) (b) (c)

Figure 2. Segmentation of chaperone Beta.a) the original isosurface view; b) the over-segmented results by the traditional watershed, where the density is divided into 9801blocks;c) the segmentation results by the marching cube based marker-controlled watershed, where the density is divided into 9 symmetry subunits.

Image Retrieval Using ESNs and Relevance Feedback

Yuan-feng Yang[1,2]
1.JiangSu Province Support Software Engineering R&D Center for Modern Information Technology Application in Enterprise
Suzhou, China, 215104
2.The Institute of Intelligent Information Processing and Application, Soochow University
Suzhou 215006, China
e-mail: jianwu@suda.edu.cn

Jian Wu[1,2], Jing Fang[2], Zhi-ming Cui[1,2]
1.JiangSu Province Support Software Engineering R&D Center for Modern Information Technology Application in Enterprise
Suzhou, China, 215104
2.The Institute of Intelligent Information Processing and Application, Soochow University
Suzhou 215006, China

***Abstract*—In order to overcome "semantic gap" between bottom features and high-level semantic in the image retrieval, this paper introduces the echo state network to strengthen the mapping between the high-level vision content and the bottom visual feature and designs a feedback category screening strategy. We extract the feature of the queried image and get the characteristic vector of the image; through introducing the echo state network for image and constructing sample testing model for each kind of image data, we can calculate the category probability of the queried image, so as to achieve similarity discrimination of the queried image and library image. After users make feedbacks to the retrieval results and systems use related feedback algorithm to amend image feature, we retrieve and screen the category of the returned image. Experiments show that our retrieval architecture can achieve very good retrieval results.**

Keywords-image retrieval; feature extraction; ESNs; relevance feedback

I. INTRODUCTION

In order to quickly find images interested from the mass images， people intend to use a variety of methods of representing images' features in the content-based image retrieval[1] to achieve the best description of the image. The characteristics specified by the user and related weight combined into a "best" representation and the image retrieval system queries the most similar image. Performance of this kind of system is not high and it's retrieval efficiency is not satisfactory because of the high-level semantics of the things is hard to corresponding to their underlying characteristics.

In order to overcome "semantic gap"[2] between bottom features and high-level semantic in the image retrieval, this paper introduces the echo state network to strengthen the mapping between the high-level vision content and the bottom visual feature and designs a feedback category screening strategy. Figure 1 is the specific retrieval process of this chapter. We extract the feature of the queried image and get the characteristic vector of the image; through introducing the echo state network for image and constructing sample testing model for each kind of image data, we can calculate the category probability of the queried image, so as to achieve similarity discrimination of the queried image and library image. After users make feedbacks to the retrieval results and systems use related feedback algorithm to amend image feature, we retrieve and screen the category of the returned image.

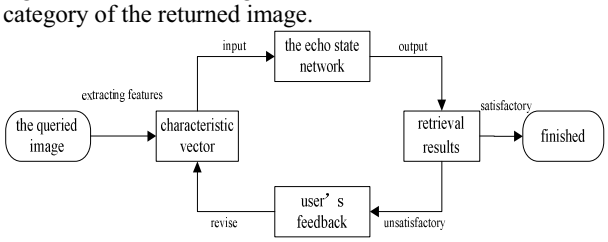

Figure 1. Retrieval process

II. IMAGE FEATURE EXTRACTION

Considering the actual requirements, this paper selects scalable color descriptors and edge histogram descriptors of the MPEG-7[3] as the input features of echo state network.

Scalable color descriptor(SCD)[4] uses the HSV color space and the space's three channels are quantified into sixteen plus four plus four equal portions. Make haar transformation for the initial 256 histogram to achieve the "scalable" and one transformation changes coefficient number into half of numbers of the original histogram. Figure 2 represents the haar transformation process. Firstly, make nonuniform quantization for the 256 histogram, then make haar transformation. Following is the linear quantization and we get 256 coefficients from it. Coefficients decrease from the first. Scalable color descriptor can describe the image color features better while it's size are smaller. The size is also mutable for different needs.

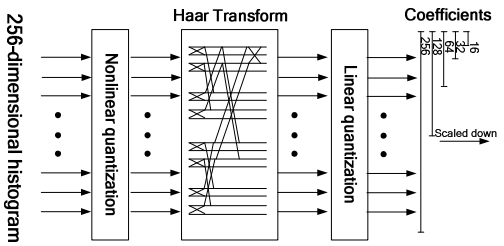

Figure 2. The haar transformation process

978-0-7695-4818-0/12 $26.00 © 2012 IEEE
DOI 10.1109/DCABES.2012.34

The edge histogram descriptor[5] is the most commonly used texture features in the airspace, which can be used in the routinely inquiries and press painted inquiries, and the retrieval results of irregular images are better.

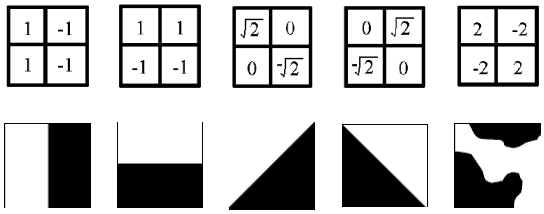

Figure 3. Edge detection operators of edge histogram

The edge histogram descriptor for the expression of the image edge is divided into five types: vertical、horizontal、45°、135° and directionless. Figure 3 descript five Canny edge operators for the edge histogram descriptor. First, the image is divided into 4 × 4 sub-region, using the Canny operator to determine the edge type for each sub-region, and count the histograms of the edge direction. Finally, the edge of the histogram of the 16 sub-regional are merged into 80 (16 × 5)-dimensional texture features.

III. ECHO STATE NETWORK MODEL CONSTRUCTION

Echo State Network[6] is a new type of recurrent neural networks proposed by H.Jaeger in 2001 and has been improved in nonlinear system identification. Echo state network ensure the stability of the network by setting the spectral radius of the weight matrix. It has a good generalization ability and the training process is simple and has no the problem of local minimum[7].

A. Echo State Network Model and Training Methods

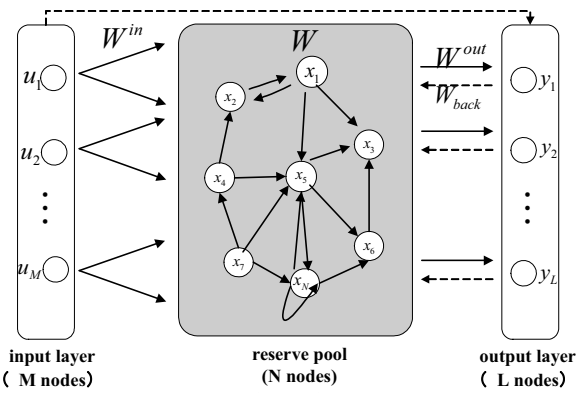

Figure 4 The topology of ESNs

The topology of ESNs[8] is shown in Figure 4. The system has M input nodes; N internal processing units; L output nodes. Input variables, state variables, output variables of echo state network are as follows:

$$u(n) = [u_1(n), u_2(n), \cdots, u_M(n)]^T \quad (1)$$

$$x(n) = [x_1(n), x_2(n), \cdots, x_N(n)]^T \quad (2)$$

$$y(n) = [y_1(n), y_2(n), \cdots, y_L(n)]^T \quad (3)$$

The state equation and output equation as follows:

$$x(n+1) = f(W^{in}u(t) + Wx(t) + W^{back}y(t)) \quad (4)$$

$$y(t+1) = f_{out}(W^{out}[u(t+1), x(t+1), y(t)] + W^{out}_{bias}) \quad (5)$$

$W^{in} = (w^{in}_{ij}) \in R^{N\times M}$ 、 $W = (w_{ij}) \in R^{N\times N}$ and $W^{back} = (w^{back}_{ij}) \in R^{N\times L}$ are respectively connection weight matrix of input to the state variables 、connection weight matrix 、connection weight matrix of output to the state variables. $W^{out} = (w^{out}_{ij}) \in R^{L\times(M+N+L)}$ represent connection weight matrix of preserve pool. $f = [f_1, f_2, \cdots, f_N]$ and $f_{out} = [f^1_{out}, f^2_{out}, \cdots, f^L_{out}]$ are respectively the internal neuron activation and output functions. W^{in} 、 W and W^{back} are randomly generated and remain unchanged. W^{out} is obtained by the systematic input and output data. The training process is to solve a linear regression problem.

The training process can be expressed like this: generate state variables randomly, input and output the connection weight matrix W , W^{in} and W^{back} , input and output training data，motivate processing units of reserve pool to generate the state variables by W^{in} and W^{back} ,collect state variables and the target output variable, get W^{out} by using the linear regression training method to minimize the mean square error.

The training process of echo state network involves two steps: sampling stage and weight calculation[9].

a) sampling stage

Given the sample data $(u(n), y(n), n = 1, 2, \cdots, M)$, among which u is the input sequence, M represents dimension, y is the output sequence and its dimension is L; we get a corresponding mapping from $U = (u(1), u(2), \cdots, u(M))$ to $Y = (y(1), y(2), \cdots, y(M))$. Select the network initial state $x(0) = 0$, training samples $(u(n), n = 1, 2, \cdots, M)$ and sample output data $(y(n), n = 1, 2, \cdots, M)$ are respectively transmitted into the reserve pool through W^{in} and W^{back} , neurons of the reserve pool shock. Complete the operation of the network status according to the following formula while one pair of $(u(n), y(n))$ is output.

$$x(n+1) = f(W^{out}[u(n+1), x(n+1), y(n)] + W^{out}_{bias}) \quad (6)$$

Accordingly, computing network output:

$$\hat{y}(n+1) = f_{out}(W^{out}[u(n+1), x(n+1), y(n)] + W^{out}_{bias}) \quad (7)$$

In order to calculate the output connection matrix, and to eliminate the impact of the initial state, get sample data of the internal state variable from the moment m to M . Vector $(x_1(i), x_2(i), \cdots, x_N(i))$ $(i = m, m+1, \cdots, M)$ constitutes the matrix $B(M-m+1, N)$ and collect the sample data $\hat{y}(n)$ to constitute the matrix $T(M-m+1, 1)$.

b) weight calculation

The system state matrix and sample data of the sampling phase can be used to calculate the output connection weights matrix W^{out}. In order to make the network actual output $\hat{y}(n)$ approaching the desired output $y(n)$, that is,

$$y(n) \approx \hat{y}(n) = \sum_{i=1}^{L} w_i^{out} x_i(n) \tag{8}$$

Hope that the values of the weights w_i^{out} can minimum mean square error of the system, namely,

$$\min_{w_i^{out}} \frac{1}{M-m+1} \sum_{n=m}^{M} (d(n) - \sum_{i=1}^{L} w_i^{out} x_i(n))^2 \tag{9}$$

Mathematically, this problem can be seen as a linear regression problem, that is to calculate the inverse matrix of matrix B. In practice, B may be an ill-conditioned matrix, and can be treated as pseudo-inverse problem of matrix B, scilicet,

$$(W^{out})^T = B^{-1}T \tag{10}$$

B. Construction of Image Retrieval ESNs

The key of echo state networks lies in the establishment of the reserve pool, and its purpose is to generate the complex dynamics space constantly changing with the input. Then through this complex dynamic space, corresponding output is returned by linear combination. The establishment process of echo state network for image retrieval is shown in Figure 5.

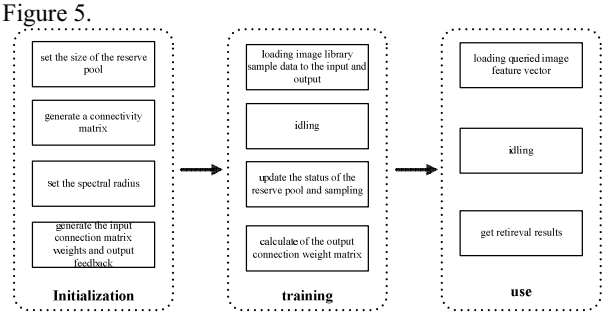

Figure 5 The establishment process of ESNs reserve pool

The initialization key of reserve pool is to determine the various parameters in the network, including the size of the reserve pool, the input and output dimension, sparsity and spectral radius. Firstly, according to the problem of image retrieval set the input and output dimension. The input dimension is determined by the characteristic dimension and output dimension is determined by an image library built. In this paper, the experimental data uses eight classes of images, so the output is 8-dimensional. Secondly, we should determine the size of the reserve pool. Considering input and output dimension and repeated experiments and comparison, we finally set the number of nodes is 200.Identifying size of reserve pool and dimension of input and output, we set the sparsity of the reserve pool is 5%. Randomly generate a reserve pool connection matrix with N being 200 and sparse being 5%. The matrix with 32 inputs and 8 outputs constitute a recurrent neural network. In order to make sure that the echo state network has echo state features, set the weight matrix spectral radius of reserve pool less than 1. Finally, generate the connection weight matrix W^{in} and W^{back} whose absolute value of the spectral radius is less than 1.

Establish one to one relationship between the input、output signal and the input network, and use the hyperbolic tangent function $\tanh$ as activation function to stimulate the internal state of the reserve pool. Calculate the sample and record state variables $(x_1(i), x_2(i), \cdots, x_N(i))$ of the reserve pool，while recording the actual output value $\hat{y}(n)$ of the corresponding output. Considering the system state variables, the corresponding actual output value and the expectation output value of corresponding sample, calculate reserve pool and output connection weights matrix W^{out} according to its linear regression relationship. At this point, training of the echo state networks for image retrieval has been finished and we get the echo state network which can provide the use of image retrieval. Image retrieval of echo state network regards image retrieval problem as the problem of pattern recognition, constructing the detection model of sample data of all kinds of images to judge similarity of the queried image and library image. In the testing phase of the image retrieval, calculate feature vector of queried image which is used as input of trained network and return output value by calculating the input. Compare output value of network with that of initial network to get the probability of queried image assigned to each category. Each category returns the image with the least D-value of actual output value and output value of user's query image. For every category the number of images returned is proportional to the probability values assigned to the category.

Definition: Assume that q is the query image and p_{ij} is the j-th image of the i-th class in the image library; the similarity of the user's query image and image of the library is $S(q, p_{ij})$;we can calculate $S(q, p_{ij})$ by the following formula.

$$S(q, p_{ij}) = \alpha_i d(y_q, y_{p_{ij}}) \tag{11}$$

Among them, α_i is the probability of queried image q assigned to the i-th class; y_q and $y_{p_{ij}}$ are respectively the output vector of the query image q and the library image p_{ij}. $d(y_q, y_{p_{ij}})$ is the distance of output vector of q and p_{ij}; Euclidean distance is the computing method.

The retrieval process using echo state network is very simple in computation, avoiding the complex processing in conventional retrieval process, and completely unrelated images in the library are filtered in the retrieve results returned.

IV. LEARNING BASED ON USER'S FEEDBACK

In order to improve the retrieval accuracy, this paper introduces relevance feedback strategy in the retrieval process. After a significant region detection and feature extraction about user's query image, we get the output value by echo state network and the system returns number of

images whose output difference are most similar. Users make feedbacks to the images by flags.

This paper selects the relevance feedback algorithm based on the query vector point's moving to learn users' feedback[10] and class screening strategy is designed to optimize the retrieve results of the feedback. The basic idea of the algorithm can be described like this: for the retrieval needs of the user, there must be an ideal point representing the intent of the user's query in the feature space because the image features are based on the vector form; in order to improve the estimates of the ideal query point, the query point move towards the positive point and away from the point of counter-examples. Move vector-point using the following iterative formula[11].

$$Q_{i+1} = \alpha Q_i + \beta(\frac{1}{N_{R'}}\sum_{i\in D_R'} D_i) - \gamma(\frac{1}{N_{N'}}\sum_{i\in D_N'} D_i) \qquad (12)$$

Among them, Q_{i+1} and Q_i are respectively querying points' location of the first i+1 times and the first i times; D_R' and D_N' are respectively positive feedback collection and negative feedback collection submitted by users; N_R' and N_N' are respectively number of images in D_R' and D_N'; α 、 β and γ are constant parameters. The formula strengthens the features of related images and weakens that of unrelated ones. Move the location of the sample image in the feature space based on user feedback to be close to the location of ideal query point.

In this paper, the similarity's computation method of the image between the user's query image and image library is based on the formula (11); whether or not to return the image is related to not only output difference but also the probability values assigned to the category. The classes of images returned may be just a few of all categories and other categories of images will not appear.

We get an idea: delete or select feedback category based on user feedback. In this content we set three related scales: related 、 meaningless and unrelated. Users mark similar retrieve results with relevance. In the case of clear query intent, the related image signed by users should be the same category. The opposite should be returned from other categories. System uses iterative algorithm based on query vector point's moving to calculate the new query vector. According to the user feedback on the categories, don't return those who have been marked as irrelevant images.

Due to limited classes of images, retrieve results will quickly locate a particular category consistent with the user's intention within less several feedback queries. The accuracy of the retrieved results is also very high.

V. EXPERIMENTAL RESULT AND ANALYSIS

Experiments in this paper are based on Visual Studio2008 and OpenCV2.1. In order to verify the performance of the algorithm this paper builds a database of natural things to test. The image library contains about 6000 images, including African elephants, horses, dinosaurs, flowers, butterflies, motorcycles, aircraft and coins.

Based on our algorithm, figure 6 is an example of getting a retrieve result of motorcycles and figure 7 shows an example of getting a retrieve result of the African elephant. From the experimental results we can know that the selected features in this article for image rotation, translation and scale transformation are robust. And our echo state network architecture can be better to retrieve the results of customer's satisfaction.

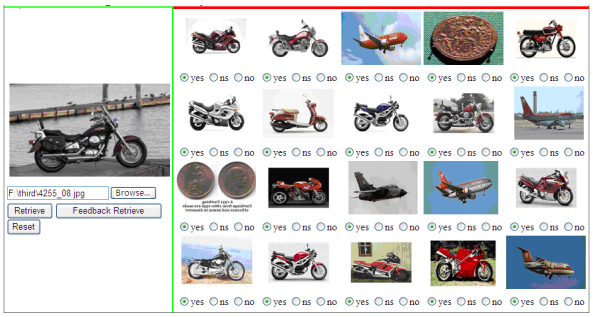

Figure 6 Retrieval results of motorcycles

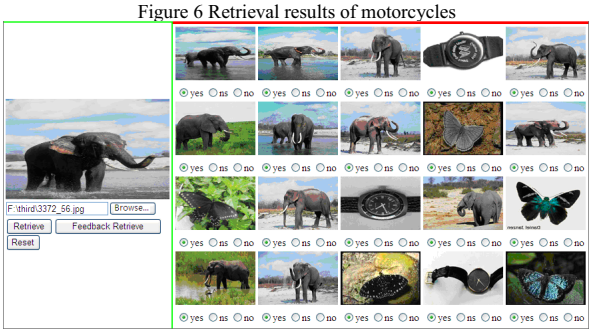

Figure 7 Retrieval results of African elephants

Figure 8 shows the retrieval results for the first time feedback of figure 6. Figure 9 shows the retrieval results for the second time feedback of figure 6. It can be seen from the experimental results that the application of relevance feedback improves the retrieval accuracy.

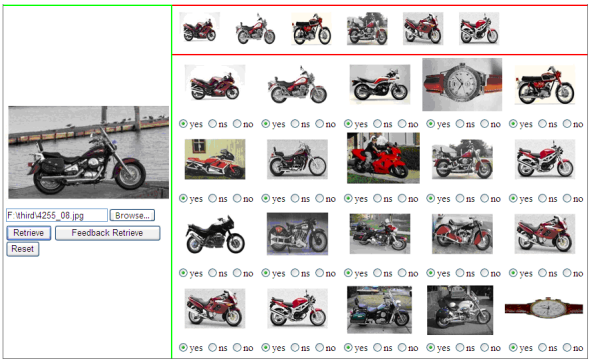

Figure 8 Feedback retrieval results for the first time

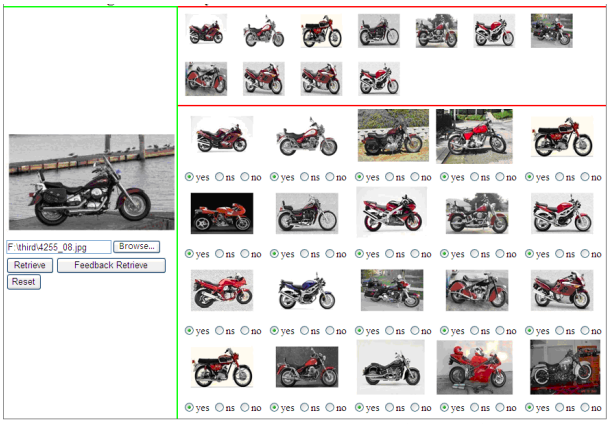

Figure 9 Feedback retrieval results for the second time

Figure 10 is the average retrieval precision curve of initial query precision changing with feedback times. The experimental data shows that the architecture designed in this paper trains all the data in the database using the trained network to retrieve the user image. And similarity calculation is related to the category, so the accuracy of the initial retrieval higher. Relevance feedback strategy gets rid of irrelevant categories in the initial query so that retrieval precision has a faster improvement and retrieval needs of users are better met.

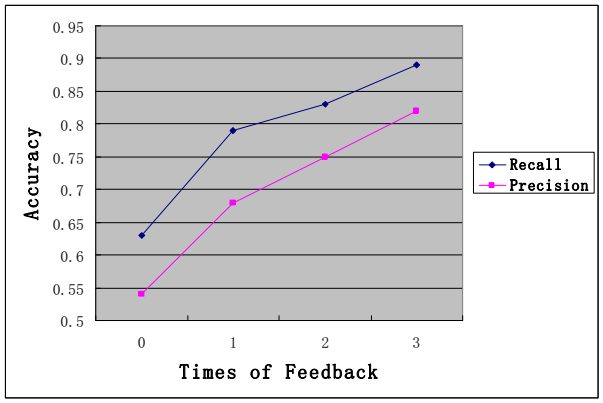

Figure 10 The curve of the retrieval accuracy changing with feedback times

VI. CONCLUSION

In order to overcome "semantic gap" between bottom features and high-level semantic in the image retrieval, this paper introduces the echo state network to strengthen the mapping between the high-level vision content and the bottom visual feature and designs a feedback category screening strategy. We extract the feature of the queried image and get the characteristic vector of the image; through introducing the echo state network for image and constructing sample testing model for each kind of image data, we can calculate the category probability of the queried image, so as to achieve similarity discrimination of the queried image and library image. After users make feedbacks to the retrieval results and systems use related feedback algorithm to amend image feature, we retrieve and screen the category of the returned image. Experiments show that our retrieval architecture can achieve very good retrieval results.

ACKNOWLEDGMENT

This research was partially supported by the Natural Science Foundation of China under grant No. 60970015, 61003054 and 61170020, the opening project of Jiangsu Province Support Software Engineering R&D Center for Modern Information Technology Application in Enterprise under grant No. SX201102 and SX201202, the Program for Postgraduates Research Innovation in University of Jiangsu Province in 2011 under grant No. CXLX11_0072, and the Beforehand Research Foundation of Soochow University.

REFERENCES

[1] A. Smeulders, M. Worring, S Santinis. Content-Based Image Retireval at the end of the Early Years[J]. IEEE Trans. On PAMI, 2000, 22(12):1349-1379.

[2] WEN Chao, Geng Guo-hua. Review and research on "semantic gap" problem in the content based image retrieval[J]. Journal of Northwest University, 2005, 35(5): 536-540.

[3] Shi-Fu Chang, T. Sikora, A. Puri. Overview of the MPEG-7 Standard[J]. IEEE Trans. On Circuits and Systems for video technology. 2001, 6(11):688-695.

[4] JI Min. MPEG-7Color ,Texture and Shape Descriptors[J]. Computer Engineering and Applications, 2004, 40(26):44-48.

[5] Manjunath B S, Ohm J R, Vasudevan V V, et al. Color and texture descriptors[J]. IEEE Trans. on Circuits and Systems for Video Technology, 2001, 11(6):703-715.

[6] H. Jaeer. Tutorial on Training Recurrent Neural Networks, Covering BPTT, RTRL, EKF and the "echo state network" approach[R]. GMD Report 159, German National Research Center for Information Technology, 2002.

[7] Jager H, W. Maass, C. Pricipe. Special Issue On Echo State Networks and Liquid State Machine-Editorial[J]. Neural Networks, 2007, 20(3):287-289.

[8] PENG Yu, WANG Jian-min, PENG Xi-yuan. Survey on Reservoir Computing[J]. Acta Electronica Sinica, 2011, 39(10):2387-2396.

[9] LUO Xiong, LI Jiang, SUN Zeng-qi. Review on echo state networks[J]. Journal of University of Science and Technology Beijing, 2012, 32(2):217-222.

[10] R. B. Yates, B. R.Neto. Modern Information Retrieval[M]. ACM Press, New York,1999.

[11] Rocchio, Jr., J.J. Relevance Feedback in Information Retrieval In the SMART Retrieval System. Experiments in Automatic Document Processing,2007:313-323.

The NiosII Dual-Core Processor Realizing the Digital Image Watermark

Xinliang He, Yuhui Li, Bo Li, Bowen Zhu
Kunming University of Science and Technology
Kunming, China
he516805542@126.com, dearyuhuili@sina.com, lbly9177@163.com, zhubowen117@163.com

***Abstract*—Digital watermark is the effective way to realize the copyright protection, the digital watermark application with the multi-core technology is being more and more widely in embedded systems today. This paper proposes a way that NiosII dual-core realizes the digital images embedding watermarking, including the DCT algorithm, NiosII dual-core parallel processing, barrier synchronization mechanism, realizing digital images embedding watermarking. The experiment results shows that dual-core is more efficient than single-core, images embedded with watermark comparing with the original one have no change in vision.**

Keywords-NiosII dual-core; DCT; parallel processing; barrier synchronization.

I. INTRODUCTION

PC field has entered the era of multi-core processor, multi-core research is being also more and more widely in embedded system [1]. NiosII processor is a characteristic soft-core CPU, it is programmable based on general FPGA architecture [2]. There are a lot of methods that NiosII single-core processor realizes the digital images watermark. However, these methods mostly consume a lot of time, inefficiency. This paper puts forward the method that NiosII dual-core processor realizes digital image watermark, the method includes double discrete cosine transform (DCT) algorithm [3], communication technology between two cores, barrier synchronization mechanism, compared with the single-core processor, this method not only ensures the embedded watermark invisible but also increases the system speed significantly[4].

II. DCT/ IDCT HARDWARE MODULE

For an image $f(x,y)$ with N×N resolution, if an entire image is done by DCT, the computation were very huge. Therefore in this paper, an image is divided into several blocks with 8×8 resolution, then we do DCT for those blocks [5]. The double DCT is defined as the equation:

$$F(u,v)=\frac{2}{N}c(u)c(v)\sum_{x=0}^{N-1}\sum_{y=0}^{N-1}f(x,y)\cos\left(\frac{(2x+1)\pi u}{2N}\right)\cos\left(\frac{(2y+1)\pi v}{2N}\right)$$

$$c(u)=\begin{cases}\frac{1}{\sqrt{2}}, u=0\\ 1, u=1,2,\ldots,N-1\end{cases}\qquad c(v)=\begin{cases}\frac{1}{\sqrt{2}}, v=0\\ 1, v=1,2,\ldots,N-1\end{cases}$$

Getting a DCT coefficient needs N×N multiplications and N×N-1additions from above equation. If we use the software programming to achieve DCT, this would be a serial processing way. But this approach can not meet the real-time requirements, and drag on the speed of the system [6].

FPGA is a programmable logic device, supporting parallel processing. It embeds high-speed adders, multipliers and large-capacity cache. We can make use of this FPGA features, using the hardware description language Verilog to program the DCT to be a hardware module on FPGA. Compared with the software programming, the DCT hardware module is faster [7].

The IDCT is the DCT inverse transformation, The IDCT hardware module is similar with DCT, only the transmission parameter is different, the paper will not go into it.

III. NIOSII DUAL-CORE

There are two main problems in the realization of the NiosII dual-core, one is communication between two cores, the other is synchronization in two cores parallel running.

A. Communication between two cores

When one core is reading/writing an area of the memory, the other is also doing this at that time, two cores have terrible conflicts.

Qsys is a powerful system integration tools for SOPC design, it integrates in the QuartusII 11.0 development software, there is an IP-core named Mutex in the Qsys component library. Mutex can control over the sharing of peripheral resources [8]. Each NiosII core must obtain the ownership of Mutex before access to the peripheral resources. Therefore Mutex is a key for the communication between two cores. Its working process is follows:

1) The NiosII core tests the Mutex real-time to determine whether it is available.

2) If the Mutex is available, this NiosII core would obtain ownership in one operation cycle.

3) This core could access to the peripheral resources by Mutex.

978-0-7695-4818-0/12 $26.00 © 2012 IEEE
DOI 10.1109/DCABES.2012.36

4) After the core's work finished, it unlocks on the Mutex. The other cores can access to the peripheral resources using the same way.

B. Barrier synchronization mechanism

Because of the data sharing, when two cores are parallel running, the previous stage task must be all completed before the next stage's parallel processing start. In the previous stage, if each core has different processing rate, there should be a wait mechanism for the next stage starting. This paper uses the barrier synchronization to achieve this mechanism [9]. See Figure 1. If one core arrives at a barrier firstly, it would wait the other cores in the same stage, then they might enter the next stage simultaneously. In this paper, NiosII dual-core processor realizing the digital image watermark, two cores can not guarantee to synchronize all the time, thus it is necessary to use the barrier synchronization mechanism.

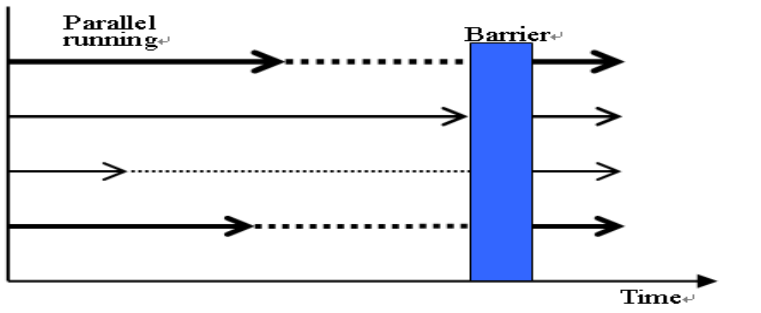

Figure 1. Schematic of barrier synchronization.

IV. NIOSII DUAL-CORE REALIZING THE DIGITAL IMAGE WATERMARK

NiosII is a 32-bit soft core processor, it is compiled by the hardware description language, realized with the logical resource in the FPGA. Accurately, the NiosII architecture is a set of instruction set [10]. So it is custom-made according to the demand.

A. System building

Firstly, the necessary components are added to the system by Qsys, and then we manually make the components interconnected following the logical relationship, the system assigns the base address and interrupt number automatically [11]. The system structure is complex, parts of them are shown in figure 2.

Figure 2. SOPC configuration diagram

B. NiosII dual-core embedding the Watermark

After SOPC system building completed, the system function is realized in the NiosII IDE [2]. The process diagram is shown in figure 3. The NiosII processor contains a couple of core, one is master core (represented by M), the other is slave core (represented by S). Two core work according to the Mutex technology and the barrier synchronized mechanism.

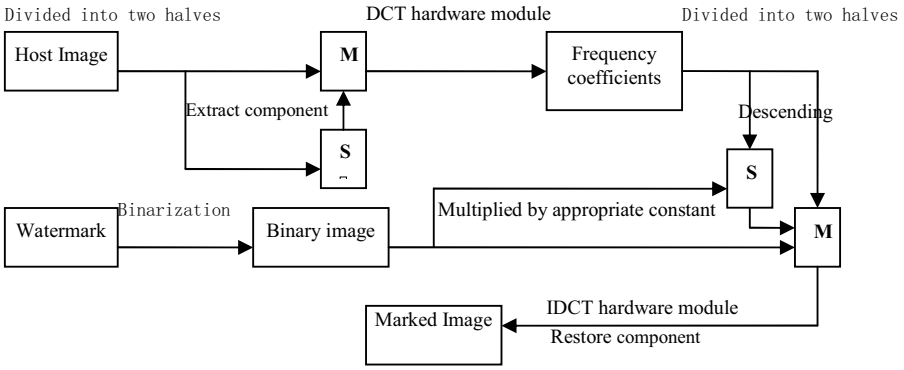

Figure 3. watermark embedding flow chart

There is a BMP image with 640×480 resolution and a 8-bit watermark image with 100×100 resolution, for example with them, NiosII Due-core realizing the digital image watermark as follows.

1) M reads the watermark image from the SD card, turns it into a binary image. S is waiting.

2) M reads the original image from SD card. M divides it into two parts according to the column, M processes the image data from 0 to 239 columns, S is from 240 to 479.

3) M and S's data are respectively sent to the DCT hardware module to get their frequency coefficients.

4) The watermark data are added to the low frequency coefficients multiplied by appropriate constant.

5) Two parts of new frequency coefficients are respectively sent to the IDCT hardware module to form new image date.

6) The new image date in S are sent to M to merge together.

7) The new BMP image embedded watermark is written back to the SD card by M.

V. EXPERIMENTAL

The program is downloaded to Altera's DE2-70 FPGA development board, inserting the SD card saving the original image and the watermark image in the slot. Turn on the power, system is going to run, the image embedded watermark is also stored in the SD card. Compared with the original watermark, the extracted watermark is implemented by Matlab.

A. Watermark embedding and extracting

Figure 4 is an original image, figure 5 is an embedded watermark image, figure 6 is an original watermark, figure 7 is an extracted watermark.

Figure 4. original image

Figure 5. embedded watermark image

Figure 6. original watermark

Figure 7. extracted watermark

B. *NiosII dual-core increase the system speed*

To be compared with the NiosII dual-core system, we designed a NiosII single-core system, it has the same algorithms and processes as dual-core systems, so this paper no longer gives the more detail realization about the NiosII single-core system.

Analyzing by the development software simulation, the dual-core system uses the logic gate number is 20219, but the FPGA chip has the logic gate number is 68416 on the DE2-70 board, the utilization rate is 29.55%. The single-core system use the logic gate number is 15756 , the utilization rate is 23.02% .See Figure 8 and Figure 9.

Total logic elements	20,219
Total combinational functions	13,872
Dedicated logic registers	16,392
Total registers	16392
Total pins	45
Total virtual pins	0
Total memory bits	247,712
Embedded Multiplier 9-bit elements	264
Total PLLs	1

Figure 8. embedded watermark image

Total logic elements	15,756
Total combinational functions	10,533
Dedicated logic registers	13,091
Total registers	13091
Total pins	49
Total virtual pins	0
Total memory bits	187,264
Embedded Multiplier 9-bit elements	260
Total PLLs	1

Figure 9. embedded watermark image

Single-core system and dual-core system embed the same watermark to a BMP image with 640×480 resolution respectively, the time consuming shows in Figure 10 and Figure 11. Single-core system lasts about 31 seconds, however dual-core system consumes 14 seconds approximately. Compared with their logic gate utilization rate, the dual-core system is more efficient than single-core system.

```
MASTER_CPU: read - 6008ms (149 KB/s)
MASTER_CPU: write - 6638ms (134 KB/s)

MASTER_CPU: Watermark_V11 Test Finished
Global processing time=31548ms
```

Figure 10. dual-core spends time

```
MASTER_CPU: read - 4966ms (180 KB/s)
MASTER_CPU: write - 5639ms (159 KB/s)

MASTER_CPU: Watermark_V1_Multi_proc Test Finished
Global processing time=14083ms
```

Figure 11. single-core spends time

VI. CONCLUSIONS

In this paper ,we present a new scheme that NiosII dual-core processes image watermark based on DCT .The experiment shows that: the scheme does not affect the use value of the original image , the extracted watermark is clear. More importantly, Compared with the single-core system, the dual-core system using hardware resource probably was single-core system 's 1.3 times, but the processing speed approximately is 2.2 times; obviously ,the NiosII Dual-Core processing digital image watermark can increase speed significantly.

ACKNOWLEDGMENT

This work is partially supported by Yunnan Science and Technology Plan Projects (2008CA012-4), Science and Technological Personnel Service Enterprise Action Items (2009GJF30050) and Kunming Science and Technology Innovation Fund (CJ2011096).

REFERENCES

[1] Xiangwei Kong, Yu Liu, Huajian Liu, Deli Yang. Object watermarks for digital images and video. Image and Vision Computing 22 (2004) 583-595.

[2] Mentor Graphics.Designing Digital Signal Processing with FPGAs.2003.

[3] Yuhui Li, Wei Gou and Bo Li. A New Digital Watermark Algorithm Based on the DWT and SVD. 2011 10th International Symposium on Distributed Computing and Application to Business, Engineering and Science. IEEE computer society.207-210.

[4] Liwei Chen,Mingfu Li,CAD Eng.An effective blind watermark algorithm based on DCT[J].WCICA 7th World Congress ,2008.25(27):6822.

[5] C.I.Podilchuk.Digital watermarking:algorithms and applications[J].IEEE Signal Processing Magazine,2001.18(4):33-46.

[6] M.Barni, F.Bartoiini, V.Cappeiiini and A. Piva. A DCT- domain system for robust image watermarking. Signal Processing, 1999, 66(3): 357~ 372.

[7] Hien T D, Nakao Z,Chen Y W,Robust multi—logo watermarking by RDWT and ICA[J].Signal Processing,2006,86:2981—2993.

[8] Altera Corp.Qsys Sytem Design Tutorial[M].Altera,2011:5-10.

[9] Mentor Graphics.Designing Digital Signal Processing with FPGAs.2003.

[10] Altera Corp.Nios II System Architect Design Tutorial[M].Altera,2009:13-21.

[11] Quartus II Handbook Version 11.0:Design and Synthesis[M].Altera,2011:167-171

The solution to background segmentation and extraction in traffic video detection

Zewei Xu
School of Computer Science and Technology
Wuhan University of Technology
Peace Avenue 1004, Wuhan, Hubei Province, China
569602418@qq.com

Qizhi Qiu[1,a],Lu Wang[2,b]
1. School of Computer Science and Technology
2.School of Economic
Wuhan University of Technology
Peace Avenue 1004, Wuhan, Hubei Province, China
a:qqz@whut.edu.cn b: 295276730@qq.com

***Abstract* -This paper proposes a solution to the background segmentation and extraction in traffic video detection system. Weighted average method, Bimodal method and Median filter are employed to preprocess the video in the proposed solution. The preprocessing provides the satisfied precondition for the backgroud extraction .Furthermore, Gaussian Mixture Model is applied to extract the background from the grayscale image. The experiment results show the validity and the practicality of the solution. Its achievement will lay the foundation for the further work, such as extracting moving vehicle.**

Keywords: video;* grayscale image*; Gaussian Mixture Model; background segmentation

Introduction

Tradition monitoring system in manual way depends on the subjective analysis and judge by human beings, which is heavy-workload and low-accuracy. While, intelligent video monitoring emerges as the times demand. It integrates several subjects and applies related technologies, such as image processing and analysis, artificial intelligence, pattern recognition and machine vision etc. It improves production efficiency. Intelligent traffic monitoring system [1] applies intelligent video monitoring technology to traffic engineering, which can figure out the appearance and action of the moving targets. The system collects and analyzes data, performs actions such as alarming, recording and analyzing according to preconditions.

In traffic monitoring system, Coterminous Frame differencing is usually used to model the background. This method has high sensitivity, and is simple and flexible. However, it can't detect whole objective. So this paper makes full use of Gaussian Mixture Model and puts forward a solution to the background processing in traffic video analysis, as figure 1 shows. According to the requirements of the traffic video detection, the solution integrates the appropriate algorithms during the background segmentation and extraction

The preprocessing of color images in video files is presented in Section I. The process of background segment and extraction is described in Section II. Conclusion and further work is discussed in Section III.

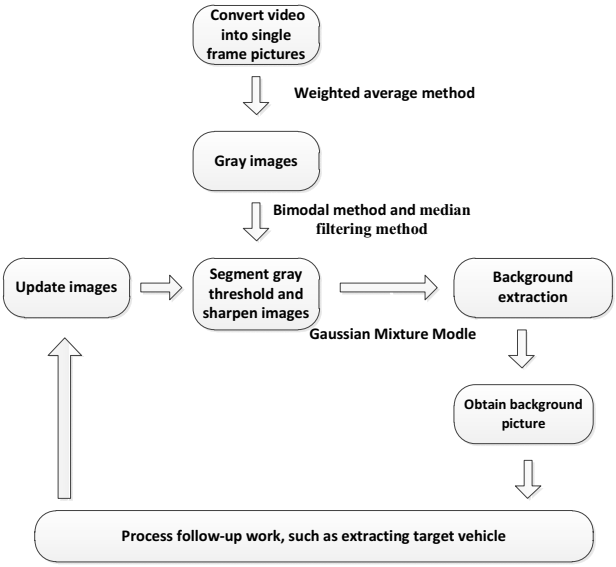

Figure 1. The solution to the background of video files

I. THE PREPROCESSING OF VIDEO COLOR IMAGES

Generally the video information obtained by the camera can't be used directly. At first, original images need preprocessing, such as gray correction and noise filtering ,to highlight the characters required.

A. Images graying

The images obtained from video are 24-bit true color images (bmp format), which have variable colors and make the calculation more time-consuming. This will greatly effect the processing speed of images, so image graying is needed firstly. Currently there are lots of methods to gray images, such as component method, maximum value method and so on. This paper selects weighted average method[2] and can get gray value much more suitable for human visual experience. The relationship between the gray-scale conversion and GRB color of gray value is as follows:

$$Gray = 0.299R + 0.587G + 0.114B \quad (1)$$

$$R = G = B = Gray \quad (2)$$

Where:
Gray represents the gray value of image pixels,

978-0-7695-4818-0/12 $26.00 © 2012 IEEE
DOI 10.1109/DCABES.2012.85

R represents red component of the pixels,
G represents green component,
B represents blue component.
Figure 2 shows the grayscale obtained by using the weighted average method which is implemented in Matlab.

(a) The original image (b) image after the gray-scale processing

Figure 2. The gray-scale processing of the image

B. Gray threshold segmentation

To isolate meaningful regional, we need to do gray threshold segmentation with gray images [3]. Gray threshold segmentation namely means to determine a gray threshold in the range of the image grayscale, and compare the gray value of all image pixels with the threshold, and then divide the corresponding pixels into two categories according to the comparison. As a result, the pixels of the image are divided into two different regions so as to achieve the aim of segmentation.

Currently there are lots of segmentation methods, such as maximum between-class variance method[4], one-dimensional cross-entropy method etc. Unlike high-accuracy detection system, such as Medical diagnosis system, Face Recognition System, the accuracy rating in the traffic video detection is relatively low. According to this requirement the paper applies Bimodal method to segment threshold. When gray histogram shows a clear bimodal shape, the corresponding gray level of the trough between the two peaks is defined as threshold for segmentation. Bimodal Method is a simple and easy to implement threshold segmentation method. More importantly, it satisfies the accuracy requirements and maintain the overhead in a lower range.

The Figure 3 is gray histogram and threshold segmentation by bimodal method.

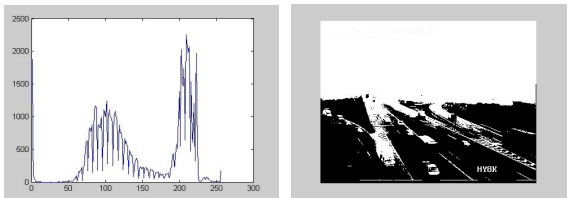

(a). Gray histogram (b).threshold segmentation by bimodal method

Figure 3. Gray histogram and threshold segmentation by

C. Image filtering

In order to improve image recognition, we use image filtering to remove noise. At present, the commonly used filtering methods are mean filtering method, Wiener filtering method and so on. Because of the salt and pepper noise randomly occurring in gray image, the paper adopts median filtering method, which is a classic method to smoothening noise. It keeps both the low frequency components of the image and the details, and it's very effective to remove salt and pepper noise.

Median filtering method [5] is a kind of nonlinear filtering methods. It can be implemented as follows: Firstly, sort the odd data extracted from a certain sampling window. Then replace the data to be processed with the median value after sorting.

The relationship between the corresponding location in the template center and the corresponding pixels is as follows:

$$g_{\min}(x_0) = Mid(x_0), x_i \in N[x_0] \quad (3)$$

Figure 4 shows the result by using Median Filter which is implemented in Mat lab

(a) The original image (b) Image after median filtering

Figure 4. Figures by median filtering method

D. Image sharpening

In intelligent traffic monitoring system, vehicle outline is immensely significant. To make it easy to extract vehicle outline, images need to be sharpened to enhance gray-scale contrast and edge information [6]. The paper selects edge detection operator to sharpen images, such as *Sobel* operator, *Canny* operator, *Robert* operator, *Prewitt* operator and *Log* operator.

Table 1. The effects of different operators

Operator type	Effect of sharpening
Sobel operator	Edge information is relatively vague
Canny operator	The actual result is not satisfactory , vague
Robert operator	Edge effect is common, edge is lost
Prewitt operator	Edge information is relatively vague
Log operator	Edge information is relatively vague

By analyzing the sharpening effects of operators in Table 1, the paper selects *Sobel* operator to detect the edge information of images. The experiment results show the

Sobel operator meets the accuracy requirements of the vehicles detection.

II. SEGMENTATION AND EXTRACTION OF THE IMAGES' BACKGROUND AND FOREGROUND

In order to analyze traffic flow parameters (such as vehicle flow, vehicle speed etc.), we need to segment the foreground and background of real-time video image sequence so as to extract target vehicle. Currently the popular segmentation method of foreground and background mainly is coterminous frame differencing method, background subtraction method and optical flow method etc.

Coterminous frame differencing method[7] cannot figure out the change of light condition in time. Background subtraction method[8] has the advantage of high speed, simple to calculate and high-accuracy detection, but it's very sensitive to the change of dynamic scenes such as light and noise. Optical flow method[9] uses the physical characteristics of the optical flow field varying with time to recognize the moving target effectively. But because it has the disadvantage of complicated calculation, it is hard to satisfy real-time requirements.

Comparison shows that the Gaussian Mixture Model can provide the desired results. So our solution integrates Gaussian Mixture Model.

A. Gaussian Mixture Model

Gaussian Mixture Model (GMM for short) builds each pixel's color distribution model according to the distribution of each pixel in time domain, thus achieves the goal of modeling background. Shiwen Chen etc, offers the formula of GMM in [10].

Each pixel of background image is modeled by co-Gaussian model of K Gaussian distributions, namely:

$$P(X_t) = \sum_{i=1}^{K} \omega_{i,t} * \eta(X_t, \mu_{i,t}, \sum_{i,t}) \tag{6}$$

Where:

K is the number of Gaussian distributions in co-Gaussian model, usually value in the 3 to 5 ;

X_t represents the value of pixel at time t , which is composed of red, green and blue components;

$\omega_{I,t}$ represents the estimate of weigh coefficient of i Gaussian distribution in co-Gaussian model at time t;

$\mu_{i,t}$, $\Sigma_{i,t}$ respectively represent mean vector and covariance matrix of i Gaussian distribution in co-Gaussian model at time t (we assume that the red, green and blue components are independent here);

η represents Gaussian distribution probability density function.

$$X_t = (x_t^r, x_t^g, x_t^b) \tag{7}$$

$$\mu_{i,t} = (\mu_{i,t}^r, \mu_{i,t}^g, \mu_{i,t}^b) \tag{8}$$

$$\sum_{i,t} = \begin{pmatrix} \sigma_t^2 & 0 & 0 \\ 0 & \sigma_g^2 & 0 \\ 0 & 0 & \sigma_b^2 \end{pmatrix} \tag{9}$$

$$\eta(X_t, \mu_{i,t}, \sum_{i,t}) = \frac{1}{(2\pi)^{n/2} \left|\sum\right|^{1/2}} e^{-\frac{1}{2}(X_t-\mu_t)^T \Sigma_j^{-1}(X_t-\mu_t)} \tag{10}$$

Figure5 is about the results of by applying the background subtraction and GMM to the same frame in a video file

(a). Original image

(b).background subtraction image (c). background image processed by Gaussian mixture model

Figure 5. Background subtraction and Gaussian mixture model renderings comparison

Figure 5 shows the distinguished results by two methods, Gaussian mixture model provides the better cleans.

III. CONCLUSIONS AND FUTURE WORK

This paper studies the methods to extracting and segmenting the background of traffic video files, achieves the aim of extracting a single video image ,and does a series of work on the single-frame picture such as graying, gray threshold segmentation, filtering, image sharpening, and other pretreatments, then uses the Gaussian Mixture Model to extract the background and foreground. The integration solution achieves the goal of segmenting the background.

The proposed solution provides an appropriate treatment on the video image, and will lay the perfect foundation for the subsequent processing, such as detecting moving vehicles. From the overall effect, it meets the accuracy requirements. However the main aspects of the further work are as follows:

1) In this paper there is less study on vehicle occlusion. And it may have bad impact on the follow-up vehicle detection.
2) Video is susceptible to the influence of light, occlusion, shadows and other factors. Therefore，

we will consider combining other moving target detection algorithm for traffic detection.

REFERENCES

[1] Dihua Sun,Weining,Liu,Wei Song.a suitable for intelligent transportation systems, traffic information collection and monitoring system Chongqing University School of Automation, 2002. (in Chinese)

[2] Jinhe Zhou.A Method of Selective Image Graying.Beijing Information Technology Institute of Information and Communication Engineering, 2006，32（20）：198-200. (in Chinese).

[3] Beibei Wang, Yuliang Li, Hao Hu.Single-threshold segmentation method based on MATLAB .2010.05, Chinese scientific and technological papers online. (in Chinese).

[4] Siqi Han, Lei Wang. A Survey of Thresholding Methods for Image Segmentation. Beijing Institute of Technology Department of Electronic Engineering,2002，24(6)：91-95. (in Chinese).

[5] Xin Wen. Research on Vehicle Detection Algorithm based on Video Image Processing[D]. Guangxi : Control Theory and Control Engineering，2010 (in Chinese).

[6] Yuanyuan Zhu. The Study of Vehicle Detection Based on Video.Chang an: Chang'an University.2008.. (in Chinese)

[7] Jiayi Lin,Zhezhou Yu,Jian Zhang,Anna Ma,Yefeng Chu. A New Moving Detection Method Based on Background Differencing and Coterminous FramesDifferencing. Computer Science and Technology of Jilin University.2008，29(4),111-114. (in Chinese)

[8] Qiang Li,Yigong Zhao,Yongjing Gao. Moving Object Detection Algorithm Based on Background Difference. Xi'an University of Electronic Science and Technology Pattern Recognition and IntelligentControl.2007,28(6),68-72: (in Chinese)

[9] Chengzhi Sun,Tianzhong Xiong,Shunping Ji,Jiahai Zhang. Applicationg of Optincal Flow Algorithms Based on Difference in Target Detection and Tracking.2010,38(24),59-62. (in Chinese)

[10] Shiwen Chen,Nian Cai,Xiaoyan Tang. ImproVed MoVing Object Detection Algorithm Based on Gaussian Mixture Model. Information Engineering, Guangdong University of Technology 2010.2, 125-130.

[11] Jiangli Nan,Qiuguang Wang. Research of Video Moving Object Detection and Tracking Alorithm and OpenCV Implementation. Harbin University of Science and Technology of Electrical and Electronics Engineering.2009,14(1),160-164(in Chinese)

[12] Jun Yang,Runsheng Run. Video Image Analysis Technologies for Smart Traffic Surveillance. National University of Defense Technology.2006,9(24),74-76. (in Chinese)

Research on the algorithm of pedestrian recognition in front of the vehicle based on SVM

Ying Yang[1], Weiguo Liu[2] , Youcai Wang[1] , Yuanjun Cai[1]

1: School of Mechanical Engineering and Automation
Northeastern University,
Shenyang, China
E-mail: yangyingsy@163.com

2: Safety Technology Development Division
Geely Automobile Research Institute CO.,
LTD Hangzhou, China
E-mail: lwg@rd.geely.com

***Abstract*—After extracting the candidate region from an image, it is necessary to take a kind of technology to determine whether the split target is a pedestrian. By analysis and feature extraction to segmentations of pedestrian candidate region, the classification of pedestrians has been studied. The pedestrian classifier of the SVM (Support Vector Machines) has been trained with pedestrian's typical characteristics. This paper mainly studies the efficient algorithms of splitting pedestrian target from other non-pedestrians. As the pedestrians in the image will show different shapes, postures and sizes, and they are usually in different light conditions, it is complicate to describe the pedestrians. This paper proposes a pedestrian segmentation method, which effectively solves the problems, making the classifier be able to deal with the complicate problems. Secondly, the paper uses the pedestrian image texture and shape features to describe the pedestrian. The extracted features are taken as the input of SVM. In order to solve the impact of lighting and other factors to pedestrian recognition, some characteristics have been considered, such as the pedestrian's grayscale images have certain gray symmetry and texture features, and the pedestrians successive edge makes outline of the image features clear. By using lots of events to train the SVM algorithm the recognized pedestrian classification can be obtained. The test results show that the proposed algorithm can effectively recognize different pedestrians in front of the vehicle and get a good real-time effect.**

Keywords- *feature extraction; pedestrian segmentation; image texture features; support vector machines; SVM classifier.*

I. INTRODUCTION

Computer vision-based pedestrian detection, because of its important application value in driver assistance systems, is becoming one of the hottest topics on computer vision and intelligent vehicles now [1-3]. It detects pedestrians by the frame grabber installed on the moving vehicle in order to estimate the potential risk to adopt strategies to protect pedestrians.

Pedestrian detection is a major difficult area of target detection. There is no a universal, robust, precise, high-performance, real-time detection and tracking algorithm till now. Pattern recognition methods in Image processing include statistical classification, data clustering, neural networks and structural pattern recognition [4]. These methods use different pattern classification methods in different applications [5]. It is a typical second-class pattern classification problem whether the divided area is a pedestrian, because the SVM have a better adaptability to classification and recognition of second-class images, in this paper, the method based on SVM is used for the pedestrian recognition.

II. PEDESTRIAN GRAY IMAGE TEXTURE FEATURE EXTRACTION

SVM, are areas of statistical learning theory, it has many unique advantages in dealing with the small sample, nonlinear and high dimensional pattern recognition problems [6]. SVM for nonlinear problems can be transformed into linear problem of high-dimensional space, then transform the space to find out the optimal classification surface.

In this paper, the extraction of pedestrian image texture features and shape characteristics are regarded as the input of SVM classifier training [7]. Before training for target classification, the target characterization is required. Characteristic is the key to determine the classification. When the target of the classification is established, how to find the proper characteristics become the key issues of awareness and recognition, get characteristics from the original information inputted need complex non-linear operations, it is often difficult to find this algorithm directly [8].

In image processing, texture is an important feature. In the pedestrian detection, the external environment is complex, in order to confirm the real pedestrian area, some pedestrian image texture features can be used for classification.

Pedestrian areas have obvious texture features such as pedestrian foot contact with the ground, pedestrian head and shoulders with the boundary between the backgrounds where texture features are very strong. For a single human body, its jacket and pants color is certain, the textures in the image are more consistent, and the area they occupy in the image is relatively large [9]. But to some noise, the gray distribution is generally messy, texture features are not obvious. Therefore, the image texture features can be used for judging whether the candidate region is for pedestrians.

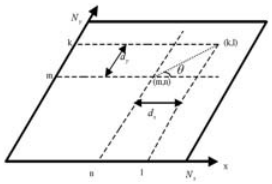

Fig. 1 Calculation diagram of Gray co-occurrence matrix

978-0-7695-4818-0/12 $26.00 © 2012 IEEE
DOI 10.1109/DCABES.2012.108

Statistical analysis methods of texture play a dominant position in texture analysis, it is the common method to describe the texture which by the research to the gray space-related features. The GLCM-based texture analysis methods are used to describe the image texture features. Assume, starting from the pixel of (m, n) which the grayscale is i, shown in figure 1, distance (dx, dy) pixel at the same time, the grayscale is j. Define the two grayscale probability of occurrence in the whole image with a mathematical expression (1), expressed as:

$$p(g_a, g_b, \delta, \theta) = \{(x, y) \left| f(x, y) = i, f(x + d_x, y + d_y) = j \right.\} \quad (1)$$

Where i, j=0,1,2, ..., L-1, x = 0,1,2,..., Nx-1, y=0,1, 2,..., Ny-1, x, y is image pixel coordinates, L is the number of gray level, δ is the interval between two pixels, θ is the direction of the selected pixels.

Thus, the two pixels gray level probability of simultaneous can transform the space coordinates (x, y) into a pair of gray (i, j) for description, they form the matrix called the GLCM. The texture features extracted based on the GLCM mainly reflects the energy characteristics which represent the thickness of texture, the entropy characteristics which represent the complexity of the texture, the contrast characteristics which represent the image resolution, the local uniform characteristics which represent the uniformity of local gray image. Based on the calculation of the characterization of the pedestrian samples, we use the four statistical parameters above as the main parameters for GLCM texture analysis; they can be combined to become the characteristic parameters of texture analysis.

In order to avoid uneven illumination effects on the texture feature extraction, first make the collected training sample images histogram equalization processing, and normalize the sample size into an image of size 64×128 pixel [10]. According to several texture analysis to make sure the two-pixel interval δ=5, the size of texture block region is 16×16 pixel, usually the image is divided into several texture blocks when calculating, and take the average as the image feature. Calculate the GLCM of image in 0°, 45°, 90°, and 135° four directions respectively. Each feature has four different values of four different directions respectively [10]. Finally, take the average value of the four values as the Sample texture.

III. PEDESTRIAN GRAY IMAGE SHAPE FEATURE EXTRACTION

The methods of shape feature extraction, whether based on region, edge information, or the threshold method, are aiming to get the accurate closed profile of the object. As the pedestrians showing a certain edge features in the image, pedestrian profiles have a clear edge, and the quantity of the most vertical edge is bigger than horizontal edge, especially the edge of the pedestrian's legs. The edge characteristics of the image can be extracted to describe the characteristics of some typical features of the pedestrian.

A. Adaptive edge extraction algorithm adaptive threshold method

Because many shapes of people are vague, and the resolution of the candidate region image is limited, it will cause great difficulty in the edge detection. In addition to this limitation of the classical algorithm, pedestrian body is close to the background gray value, and other adverse factors, make the edge that the Canny operator detected will be a lot of "fracture" phenomenon, so that the shape outline will be fragmentary [11]. As shown in figure 2.

Fig. 2 The "incomplete outline" of using Canny detection

Previous edge extraction method, mainly use the edge detection operator to calculate the gray gradient for each pixel point, then take the gray gradient map for the threshold processing to get the edge image. This method does not fully reflect the image gray gradient. In this paper, we use a four-direction gradient integrated approach [12]. Using gradient operator to calculate the gray gradient of each pixel in four directions: horizontal, vertical, northeast diagonal, on the northwest corner respectively, then select the maximum of the four values as the current pixel grayscale gradient. Improved results shown in figure 3(b), It can be seen that when the pedestrian's clothing close to the background brightness, gray gradient do not change significantly. However, since the horizontal symmetry of the pedestrian, the distribution of its gray gradient also has this feature.

Figure 3 selects a more typical pedestrian case diagram; the body clothing areas are darker and the gray gradient contrast is not obvious. Upper and lower body regions two single-pixel were selected to analysis the gray gradient distribution characteristics, from figure 3(c), Shown on the right the lower body regional gray gradient distribution have distinctive edge characteristics, With four significant peaks; Shown on the left The upper body regional gray gradient distribution is flat, But there are still smaller extremes in the border. The border points have local extremes in the single local area. The gray gradient diagram makes the equalization process in horizontal single-line, it can be achieved more clear gradient information, shown in Figure 4 (c).

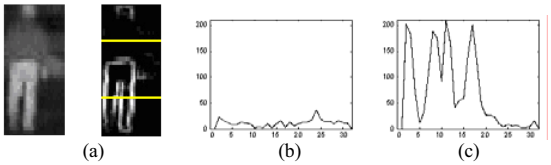

(a) (b) (c)

Fig. 3 Single pixel gradient distribution contrast

(a) original grayscale (b) gray gradient map(c) the results of the upper and lower two single-pixel grayscale gradient contrast line equalization

(a) (b) (c)

(a) Original image, (b) gray gradient map, (c) gray gradient

Fig. 4 Gray gradient map

Therefore, in order to extract more complete boundary information, a more targeted and adaptive threshold method is used to get binary boundary map.

In local dynamic threshold processing, Threshold of pixel points are selected as a reference neighborhood in single line pixel, selecting the local maximum in the 1×L neighborhood scope. The reason for this avoid valid losing the valid border point's information, that is the gradient change local extreme point, and striving to minimize the impact of uneven distribution of pedestrian region gray. Canny operator is essentially the application of the gradient operator to detect unit function maximum value and to detect and connect the edges with dual-threshold. Specific procedures are as follows:

- Filter de-noising: First of all, one-dimensional Gaussian function is used respectively for convolving the rows and columns of the image, in order to reduce noise interference, the Gaussian function is selected:

$$G(x) = \frac{1}{2\pi\sigma^2} e^{\frac{-x^2}{2\sigma^2}} \quad (2)$$

- Calculating gray gradient map G in candidate region.
- Select the threshold: In order to extract the edge of the image, one must set the appropriate threshold. In this paper, progressive scan gray G is used, calculating current line minimum threshold T(y):

$$T(y) = k \cdot \frac{\sum_{x=0}^{W} G(x, y)}{W} \quad (3)$$

- Where W is the image width, k is the experience factor.

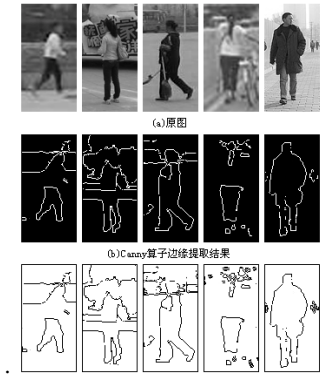

Fig. 5 Comparison of Adaptive and Canny edge detection

Making thresholds treatment for all the pixels on the current line to determine whether it is the maximum in1×L neighborhood (L value of 5), and making a comparison with the minimum threshold value T (y)

- The threshold value is the one as boundary points.

It can be seen in Figure 5, improved adaptive edge detection algorithm is better than the Canny algorithm to retain effective border points. The more obvious improvements are especially in pedestrian areas and the situation of gray similar neighboring areas.

B. Characteristic analysis of gray gradient orientation

Image gradient direction is received in the use of Canny operator extracting the edge, Gradient direction is in the range of (0, π), In order to use the image displaying, the gradient direction is representing with 0 to 255 grayscale images, The greater of the brightness means the greater of the gradient direction. Usually the maximum of the direction gradient appears in the more obvious edge. Due to the complex background, the upper body of pedestrians, especially the pedestrian's head region where the gradient direction changes is more significant, and the gradient range is relatively large; In the area where the lower body of pedestrian, usually the background is a road picture, As the leg occupied the most of the image, the edge is more obvious, and in some gradient direction will show a certain peak.

(a) (b) (c)

Fig. 6 Sample images of the gradient, the gradient direction and region

The amount of calculate will increase. If the gradient direction of the whole image as a feature vector trains the classifier, based on the above analysis, mainly making the gradient direction's statistical analysis at the lower half of the image, figure 6 (c) shown the lower half of the sample image is divided into a, b regions.

As the gradient direction is continuous change quantity from 0 to π, reducing the amount of computation, this paper will use histogram to indicate the gradient direction; the gradient direction is divided into eight intervals, respectively counting the probability of the each point's gradient direction falling in the eight intervals. Figure 6 is the gradient directions comparison chart of a region. Calculate a, b two regional the gradient distribution histograms

Calculate a, b two regional gradient distribution histograms, each region received a total of eight gradient directions probability value, so to obtain 16 features.

IV. ALGORITHM AND EXPERIMENT OF PEDESTRIAN RECOGNITION BASED ON SVM

Getting a small error from the finite training samples can still guarantee having a small error form an independent test set, which is the SVM's characteristic. In addition, because SVM is a convex optimization problem, the local optimal solution must be global optimal solution, preventing over-learns problems. And all these advantages are the traditional neural network algorithms no having.

Pedestrian recognition uses support vector machines, first need training to get training samples of SVM, Then according to selected characteristics describe the image with the corresponding eigenvectors, inputting to SVM and training to get supported the vectors and the weight; Finally, test samples can be input to the trained SVM to make classify performance tests and to output results. In this article, through experimental comparison, to make respectively SVM training under the premise of setting the same of penalty function, in table 1. Through the data in the table can be seen that the obtained detection rate is very similar in the polynomial kernel and radial basis function, but the radial basis function training is used to get a larger number of support vector, therefore, the polynomial kernel function is selected for inner product operation.

TABLE I. SVM TEST PERFORMANCE DIFFERENT FUNCTION (C=1000)

Kernel function	Parameter settings	Number of support vectors	Detection rate (%)	False alarm (%)
Polynomial $K(x,x_i)=[(x\cdot x_i)+1]^q$	q=0.5	77	87.97	16.0
	q=1	77	87.97	16.0
	q=2	64	84.21	22.48
	q=3	64	84.21	23.66
Radial basis function $K(x,x_i)=\exp\{-\frac{\lvert x-x_i\rvert^2}{\sigma^2}\}$	σ=0.5	181	78.11	26.97
	σ=1	112	87.97	20.45
	σ=2	85	81.20	24.38
	σ=3	91	82.71	17.65
	σ=10	91	91.73	17.91

While training in application of polynomial kernel function, the penalty factors C and the order of polynomial q is the main two parameters selected. Through calculating Penalty factor C and the order of polynomial q is greater, the number of support vectors are fewer, while the classifier's performance of the detection is worse. This choice of SVM training pedestrian recognition parameters are q=2, C=100, at this time the supported vector has 70 form training, which pedestrians sample accounts for 33, the other accounts for 37. Using test samples to test the classifier, the detection rate can reach at 78.54% and the false alarm rate is 21.82%.

In this paper, the support vector machine training is implemented by Matlab, to get the SVM support vector through training, Lagrange multipliers αi* and classification threshold b, Then import this data into the software of Visual C++, through VC programming realist the pedestrian identification on line. Use of the system to test pedestrian on campus for online, the test results as shown in Figure 7, the system achieves good results for the larger pedestrian in the pictures, if the pedestrians are nearer to the car, the detecting results are more accurately, which is a good support for the vehicle warning system. Especially in the case of fewer pedestrians, the pedestrian detection results are much better, as shown in Figure 7 (a) (b).

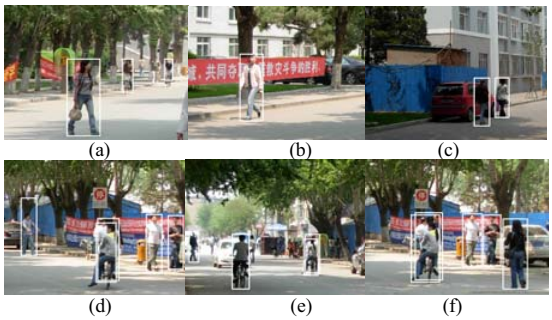

Fig. 7 Pedestrian-detection image

But there are some problems in this system, there will be some leakage of pedestrian recognition or identification error in complex environments. In the figure some of the smaller pedestrian recognition are easy missed, as shown in Figure 7 (d); the identification prone missed which the pedestrians and background colors are similar, as shown in Figure 7 (c). In addition to missed identification, because the colors are similar background and pedestrians, there will be not accurate segmentation, as shown in Figure 7 (e). In addition, pedestrians are blocked; it will also appear the recognition of phenomenon is not accurate, as shown in Figure 7 (f).

In summary, this system can meet the general pedestrian recognition, and playing a supporting role in vehicle warning. By testing samples to test the classifier, the detection rate can reach at 81.23%; false alarm rate is 22.41%.

V. CONCLUSIONS

In this paper, the principles for how the pedestrian's texture and edge features are extracted from the images through analyzing the shape characteristics of the pedestrian have been discussed. The SVM based pedestrian recognition classifier training procedures have been described. The pedestrian recognition algorithm has been implemented with Matlab and Visual C++, which can recognize pedestrians online. Using training samples to test the pedestrian classifier, the detection rate can reach at 81.23% and false alarm rate is 22.41%.

REFERENCES

[1] Wohler C, Kressler U, Anlauf J K. Pedestrian recognition by classification of image sequences: global approaches vs. local spatio-temporal processing. In: Proceedings of 15th International Conference on Pattern Recognition. Barcelona, Spain. IEEE, 2000.2: 540-544.

[2] Curio C, Edelbrunner J, Kalinke T, Tzomakas C, Werner von Seelen. Walking pedestrian recognition. IEEE Transactions on Intelligent Transportation Systems, 2000, 1(3): 155-163.

[3] Bertozzi M, Broggi A, Fascioli A, Graf T. Meinecke M M Pedestrian detection for driver assistance using multiresolution infrared vision. IEEE Transactions on Vehicular Technology, 2004, 53(6): 1666-1678.

[4] Lowe DG. Distinctive image features from scale-invariant key points. International Journal of Computer Vision, 2004, 60(2): 91-110.R. Nicole, "Title of paper with only first word capitalized," J. Name Stand. Abbrev., in press.

[5] Fanzhi Kong, Xingzhou Zhang, Yaoju Xie. "Based on Adaboost face detection technology" [J], Application Technology. 2005, 32(6): 7-9.

[6] Xuegong Zhang. "On statistical learning theory and support vector machines" [J]. Automation Academic Journal, 2000.01, 26(1): 32-42.

[7] Jianmin Li, Ba Zhang, Fuzong Lin. "Training algorithm of support vector machine[J]", Academic Journal of Tsinghua University, 2003, 43(1): 120-124.

[8] Yinkuo Meng, Zhensu Lv, Jianrong Liu. "Support Vector Machine and its application in pattern classification [J]", Academic Journal of Gansu science, 2003, 15(2): 66-70.

[9] Honglei Jin, Zhenhua Zhang, Liyuan Li. "Surface roughness level identification based on texture analysis [J]", China Graph Academic Journal, 2000, 5(7): 612-615.

[10] Huichun Liu, Shuyuan Ma. "Research current situation on Support Vector Machines [J]", China Graph Academic Journal, 002, 7(6): 618-623.

[11] Yuanjian Feng, Pengfei Shi. "Color image face detection method based on support vector machines [J]", Academic Journal of Shanghai Jiaotong University, 2003, 37(6): 947-955.

[12] V.Vapnik, Xuegong Zhang(Translate). "Essence of statistical learning theory [M]", Beijing, Tsinghua University Press, 2000, 96-101.

A Video Front Collection Method of Watermarking Embedding and Blind-extraction

Chengxu Luo , Yuhui Li , Bo Li , Ji Huang
Kunming University of Science and Technology
Kunming, China
forten2010@163.com, lbly9177@163.com, dearyuhuili@sina.com, a2748832@163.com

***Abstract*—In this paper, we put forward a video front collection method of watermark embedding and blind extraction. Under the premise of not affecting the video quality and the use value, this method uses the relationship of DCT coefficients to realize embedding watermark and takes the proper treatment in the corresponding position of the coefficients. We achieve the simulation which can satisfy the needs of real-time video and realize the blind extraction of the watermark. The experiment results show that it is robust against MJPEG compression.**

Keywords-Video Watermark;Discrete Cosine Transform (DCT); Blind-Extraction; MJPEG compression

I. INTRODUCTION

With the development of information technology, the digital multimedia plays an important role in people life. While it provides people convenience, its copyright protection has become increasing prominent[1]. As an important branch of the information hiding technology, the watermarking technology, bases on its special superiority in digital content protection, has attracted more and more attention on the issue of copyright protection[2].

At present, the digital watermarking technique has achieved great development. However, most of the research and paper are in the image. In recent years, watermarking research about video watermark and audio presents rising trend[3]. Video watermark, because of its distinctive characteristics, such as real-time processing, random testing, blind extraction, etc. And combines with the video coding standard together, meets video rate constant and against attack, faces many challenges[4]. In view of this, this paper proposed a video front collection method of watermark embedding and blind extraction. Each frame will be embedded the watermark in the acquisition of the original video; use the binary image as watermark which is scrambled to improve the security; choose DCT transform domain and use the relationship of DCT transform intermediate frequency coefficients to realize embedding watermark, and takes the proper treatment to enhance the robustness of watermark in the corresponding position of the coefficients. This method realizes real-time simulation in Simulink and realizes the blind extraction of the watermark. It is robust against MJPEG compression.

The rest of the paper is organized as follow. Section II provides a video watermark algorithm. Section III covers the simulation aspect of the algorithm using Matlab/Simulink. Section IV analyses some simulation results. Finally section V gives the conclusion of the present work.

II. VIDEO WATERMARKING ALOGORITHM

1.Watermarking Image Preprocessing

As a kind of the image encryption technology, the scrambling technology is used for digital watermarking techniques to increase the concealment and security of the watermark. It makes the watermark more random and weaker among the relevance of the watermarking signal to enhance the offensive of watermarking signal[2]. The transformation matrix used for Arnold transform must be a square and Arnold transform owns the periodic characteristics, the cycle of image of the different sizes is different, the relationship is shown in Table 1. N is the length of the image matrix, T is its scrambling cycle.

TABLE 1. Arnold Transform Cycle of Different Image Sizes

N	10	20	30	40	60	128	256	512
T	30	30	60	30	60	96	192	384

Therefore, we employ Arnold transform. The original watermark image is binary image which is 40×40, the effect of Arnold scrambling as shown in Figure 1.

(a) (b) (c)

Figure 1. Scrambling Process of the 40×40 Watermarking Image: (a)Original Image; (b)Arnold times=12 Image; (c)Arnold times=30 Image.

2.Watermarking Embedding Position

Firstly, in order to be convenient for transmission and storage, video generally has to be encoded and compressed, so video watermarking also has to be link with video compression coding standard that it is robust against video encoding and compression[3]. The current international standard of video compression contains MPEG-x, MJPEG, H.26x, and so on. These adopt hybrid encoding which includes the DCT transformation, so we choose DCT domain

978-0-7695-4818-0/12 $26.00 © 2012 IEEE
DOI 10.1109/DCABES.2012.13

to embed watermark. Secondly, most of the energy of a image are in the DC components and the low frequency components of AC in DCT transform coefficients. If modified, they will may affect the quality of the image, and high frequency components easily are lost in the video compression[5], so the watermark is embedded into the Intermediate frequency. Finally, it's considered effectively resist against special attacks of video watermark, watermark is embedded into each frame.

3.Video Watermarking Embedding Algorithm

In this paper, the watermark algorithm is partly mentioned in [9], it is mainly used in image watermarking. According to the characteristics of the video watermarking requirements, we improved the algorithm, so that it can adapt to the video watermarking requirements. And we use the camera to capture the original video frame that is 640×480 and the binary watermark image is 40×40, the embedding process is followed.

(1) First of all, according to the stated above Arnold scrambling algorithm scrambles the watermark, and get the key K, and transform the watermark scrambling information into a 1-D matrix.

(2) The quantification, compression and encoding of the video are generally in YCbCr space, so switch the color space of the original video frame from RGB space to YCbCr space.

(3) Get the Y brightness component in YCbCr space, divide into 8×8 block, the number is (640/8)×(480/8), and do 2-D DCT transform respectively, get DCT transform coefficient matrix dct_block of Y component.

(4) According to the value of elements in the matrix dct_block, adjust intermediate frequency coefficients of DCT transform to realize embedding watermark. Among the simulation experiments, considering the visual effect of the collected video, k takes 0.024.

The adjustment process as follows:

A. When $W=0$, if $dct\_block(3,2) \le dct\_block(2,3)$, the $dct\_block(3,2)$ and $dct\_block(2,3)$ are exchanged , and if $dct\_block(3,2) - dct\_block(2,3) < k$, then $dct\_block(3,2) = dct\_block(3,2) + (k/2)$, $dct\_block(2,3) = dct\_block(2,3) - (k/2)$, others aren't changed.

B. When $W=1$, if $dct\_block(3,2) > dct\_block(2,3)$, the $dct\_block(3,2)$ and $dct\_block(2,3)$ are exchanged , and if $dct\_block(3,2) - dct\_block(2,3) < k$, then $dct\_block(3,2) = dct\_block(3,2) - (k/2)$, $dct\_block(2,3) = dct\_block(2,3) + (k/2)$, others aren't changed.

(5) Do 2-D IDCT transform in changed matrix of DCT coefficients to get new Y brightness component, and combine with color component Cb and Cr, convert to RGB space and form a new video frame which contains watermark. According to the different compression and encoding standard, form marked video files. The embedding process is shown in Figure2.

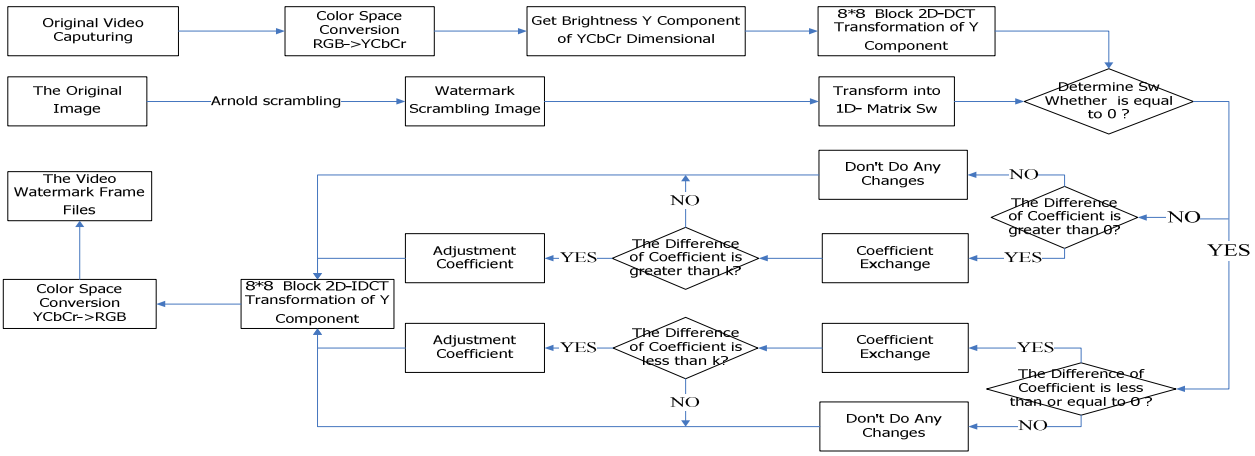

Figure 2. Watermarking Embedding Flow Chart

4.Video Watermark Extraction Algorithm

The video watermark's extraction is the inverse of the embedding process, and the process is as follows:

(1) Extract arbitrary a frame of the marked video, and convert to YCbCr space, do 8×8 block 2-D DCT transform in Y brightness component, get coefficient matrix dct_block.

(2) if $dct\_block(3,2) > dct\_block(2,3)$, get $W'=0$; Otherwise, $dct\_block(3,2) \le dct\_block(2,3)$,make $W'=1$. Get a new 1-D matrix W' , and then transform it into the image W' whose resolution is the same with the original image.

(3) Finally, according to the key K, get the watermark image by Arnold scrambling algorithm. Use the NC value measure the correct rate of the extracted watermark image:

$$NC = \frac{\sum_{i=1}^{m}\sum_{j=1}^{n} W'(i,j)W(i,j)}{\sum_{i=1}^{m}\sum_{j=1}^{n} W^2(i,j)}$$

$W(i,j)$ is the pixels of the original image, $W'(i,j)$ is the pixels of the extracted watermark.

As we know, in the process of extracting, use no information of the original video, so it is a blind extraction algorithm. The extracted process as shown in Figure 3.

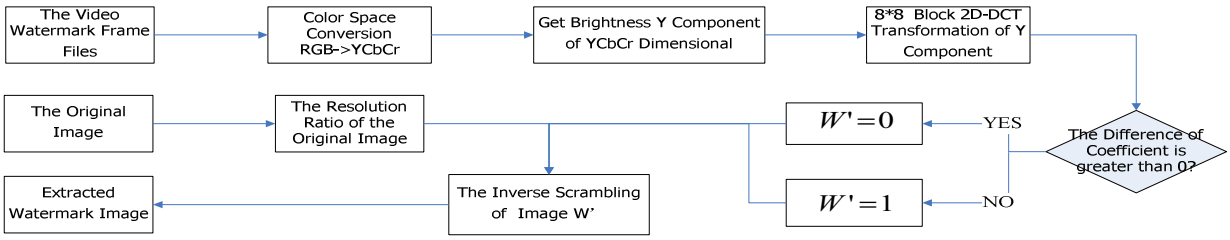

Figure 3. Watermark Extraction Flow Chart

III. SIMULINK IN MATLAB/SIMULINK

Simulink is graphic simulation design environment in the Matlab, and the video and image processing module kit provides all kinds of subsystem model used in video and image processing. In Simulink, we build the real-time simulation model of the video watermark algorithm proposed in this paper, the model as shown in Figure 4.

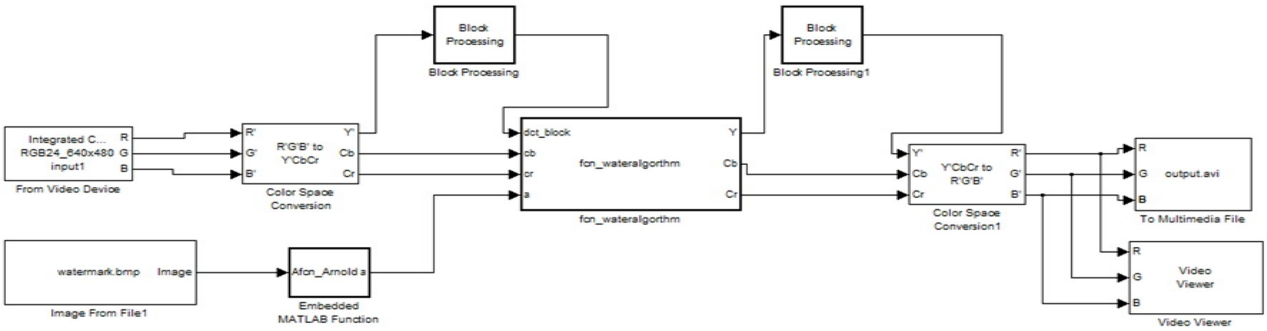

Figure 4. Real Time Simulation Model in Matlab/Simulink

Briefly introduce these function modules:

1. Form Video Device: real-time Video acquisition module;
2. Image From File1: watermark Image module;
3. Color Space Conversion: Color Space Conversion module, realize the RGB->YCbCr;
4. Block Processing: 8×8 block of 2-D DCT transform module;
5. Embedded Matlab Function: watermarking scrambling module;
6. Fcn_wateralgorthm: watermarking embedded algorithm module;
7. Block Processing1:8×8 block of 2-D IDCT transform module;
8. Color Space Conversion1: Color Space conversion module, realize YCbCr->RGB;
9. To Multimedia File: form marked video File module;
10. Video Viewer: Video browsing module.

IV. RESULTS ANALYSIS

The simulation experiments in Matlab R2009b, this video collection is in the local computer integrated camera, format is RGB24 640 × 480, frame rate is 30 fps, original watermark image is 40×40 binary. The marked video file is uncompressed avi video format file, named output.avi.

Experiment simulation time is 10s, We extract watermark of any frame in the marked uncompressed video files, as shown in Figure5. Then we simulated video processing by combining changing frame rate and MJPEG compressed. We extract 30 times, use the NC value to measure the correct rate of the watermark extracted, these corresponding relation as shown in Figure 6. Table 2 shows the averaged NC value over test videos.

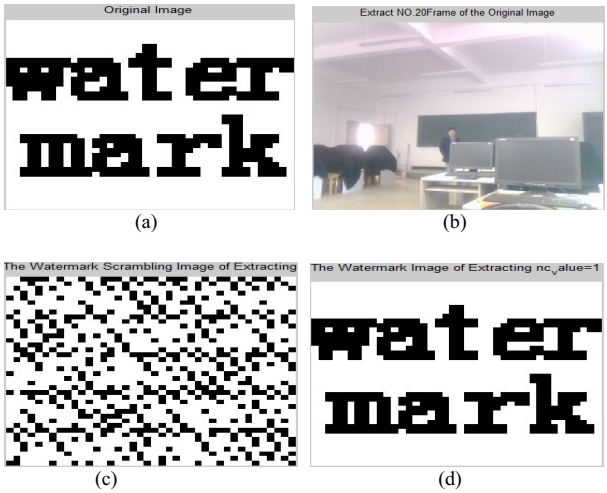

Figure 5. Extract watermark of NO.20 frame in the marked video files, uncompressed, frame rate=30 fps: (a)Original Watermark Image; (b)Extract NO.20 Frame of the Original Video; (c)The Watermark

Scrambling Image of Extracting ; (d)The Watermark Image of Extracting, nc_value=1.00000.

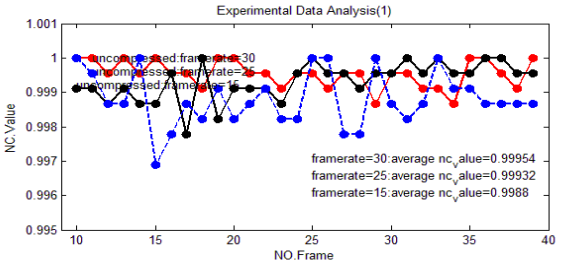

(a)Uncompressed Marked Video

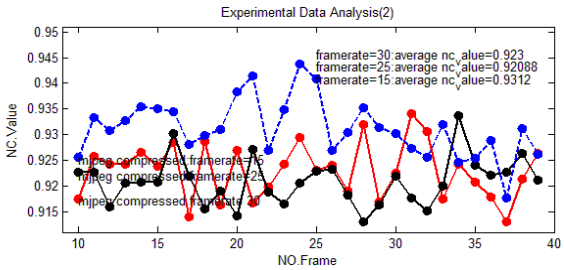

(b) MJPEG Compressed Marked Video

Figure 6. NC Value of the 30 Frames Over Test Videos

TABLE 2. Averaged NC Value Over Test Videos

Marked Video	Resizing	Uncompressed	MJPEG compressed
Frame rate 30 fps	640×480	0.99954	0.92300
Frame rate 25 fps	640×480	0.99932	0.92088
Frame rate 15 fps	640×480	0.99880	0.93120

Experiments show that our simulation system can embed watermark into the collected real-time video to generate marked video, and the watermark is good invisibility. The algorithm has good feasibility and good resistance to MJPEG compression.

V. CONCLUSION

Our major contribution is that we have proposed a video watermarking method for video front collection that is robust against the MJPEG compression. Our video watermarking algorithm is blind watermarking not using original videos and it is simple and effective that can satisfy the real-time video. The drawback is the system's weakness against other compression and geometric attack which will be solved we will use the algorithm in video encoder in our further work. However, it is a great practical significance that the authentication of video in special occasions (such as public security, Banks, etc) video surveillance.

ACKNOWLEDGMENT

This work is partially supported by Yunnan Science and Technology Plan Projects (2008CA012-4), Scientific and Technological Personnel Service Enterprise Action Items (2009GJF30050) and Kunming Science and Technology Innovation Fund (CJ2011096).

REFERENCES

[1] Min-Jeong Lee, Dong-Hyuck Im, Hae-Yeoun Lee, Kyung-Su Kim, Heung-Kyu Lee. Real-time Video Watermarking System on the Compressed Domain for High-definition Video Contents: Practical issues. Digital Signal Processing. 22(2012) 190-198.

[2] Yuhui Li, Wei Gou and Bo Li. A New Digital Watermark Algorithm Based on the DWT and SVD. 2011 10th International Symposium on Distributed Computing and Application to Business, Engineering and Science. IEEE computer society.207-210.

[3] Di Wu, Wenhai Kong, Bian Yang, Xiamu Niu. A fast SVD based video watermarking algorithm compatible with MPEG2 Standard. Soft Compute (2009) 13:375-382.

[4] Xiangwei Kong, Yu Liu, Huajian Liu, Deli Yang. Object watermarks for digital images and video. Image and Vision Computing 22 (2004) 583-595.

[5] M.Barni, F.Bartoiini, V.Cappeiiini and A. Piva. A DCT-domain system for robust image watermarking. Signal Processing, 1999,66(3): 357~ 372.

[6] J.Sun, J.Liu. A novel blind video water- marking scheme based on independent dynamic component. Springer Science Business Media, Inc.2006. Multidim Syst Sig Process (2006) 17:59-74.

[7] Wenhai Kong, Bian Yang, Di Wu, and Xiamu Niu. SVD Based Blind Video Watermarking Algorthm. 2006 IEEE. Proceedings of the First International Conference on Innovative Computing, Information and Control(ICICIC'06).

[8] Soumik Das, Pradosh Bandyopadhyay, Dr.Monalisa Banerjee, Prof.Atal Chaudhuri. Uncompressed Video Authentication Through A Chip Based Watermarking Scheme. 2011 Second International Conference on Emerging Applications of Information Technology. Page NO:395-398.

[9] KONG Xue-li and GAO Bao-jian. A Novel Robust Watermarking Algorithm Based on Swapping DCT Coeffcients. Microcomputer Information. Control and Automation Publication Group, Vol 12-3, No.24, 2008.

[10] Yoonki Choi and Kiyoharu Aizawa. Wat- ermark Detection Based on Error Probability and Its Applications to Video Watermarking. Electronics and Communications in Japan, Part 3, Vol.87, No.6,2004.

[11] M.Luong, Q.B.Do, A.Beghdadi. A blind image watermarking using multiresolution visibility map. J Glob Optim (2011) 49: 435- 448.

An Adapting to Light Change Pixel Layer Based Background Model for Moving Objects Detection in a Dynamic Scene

LIU Chen-guang
Software Engineering
School of Computer (software), Sichuan University
Chengdu, China
772561140@qq.com

WANG Shang
Software Engineering
School of Computer (software), Sichuan University
Chengdu, China
nevery07@hotmail.com

Abstract — **A novel background model based on pixel layer for moving objects detection in a dynamic scene is one of the common methods in motion detection. This paper proposes an adapting to light change pixel layer based background model for moving objects detection and this improved model can deal with the problem of illumination change and complexity of background updating. First, a new model parameter was selected, a fixed learning rate was used and the adaptive factor to update the variance was added which are helpful to adapt to illumination change rapidly. Second, a statistical decision is used to solve the complexity of background updating. Experimental results show that the improved method can adapt to illumination change, and improve the precision and robustness of motion detection.**

Keywords-pixel layer for moving objects detection; adapting to light changes; complexity of background updating

I. INTRODUCTION

Moving objects detection of video images is an important content of the applications of computer vision and video surveillance. In real life, a large number of meaningful visual information is included in moving objects and extracting moving objects from constantly changing background rapidly and accurately is a critical step. Consecutive frames subtraction and background subtraction are common image object detection algorithms [1]. Consecutive frames subtraction has a strong adaptability for moving objects in dynamic scene, but it cannot extract all relevant feature pixels completely, easy to produce cavitation in the internal of moving entity which results in the inaccuracy of the experimental results[2]. Background subtraction method is easy to put into practice. When the background is known, it could provide the complete attribute data and fully detect moving objects [3]. However, due to the error in the image sampling process, background light change and other confounding factors in the environment, background subtraction method is easy to be affected [4].

In recent years, scholars at home and abroad do profound research of moving object detection and present a based on pixel layer background model which takes advantage of locality and temporal and spatial variation characteristics, which detects moving objects accurately and robustly in complex background. Fast mean shift approach is used to cluster domain into layers where pixels share similar statistics and then the background is modeled as a group of pixel layers [5]. Moving foreground pixels detection is realized through matching adjacent layers. When nonstationary change appears in the background, it still could detect moving objects rapidly and robustly, however, this algorithm cannot exclude the impact of illumination change [6]. This paper analyzes the problem that based on pixel layer background model cannot deal with the light mutation through the way which includes choosing a new model parameter, using fixed learning rate and adding an adaptive factor to update the variance. The improved method could adapt to the illumination change and enhance the versatility, accuracy and robustness.

II. P IXEL LAYER BASED ON BACKGROUND MODEL FOR MOVING OBJECTS DETECTION

Pixel layer based on background model could detect and abstract moving objects in complex background, this algorithm uses fast mean shift approach to cluster domain into layers where pixels share similar statistics and then the background is modeled as a group of pixel layers [5]. Moving foreground pixels detection is realized through matching adjacent layers. This method could detect moving target accurately in due time, especially when the camera pulsates or other causes bring about background domain irregular change, which is more efficient than classical method based on Gaussian mixture background model. But it has following drawbacks: With the influence of light, the algorithm does not show great detection results, it is likely to cause false positives and undetected error [6].

III. ADAPTING TO ILLUMINATION CHANGES MOVING OBJECT DETECTION METHOD

An improved background model is proposed which aims at Gaussian mixture background model which cannot deal with light rapid change [7]. First, choosing a new model parameter, using fixed learning rate and adding an adaptive factor to update the variance, therefore, the method could adapt to local rapid illumination change. Second, inter-frame processing is added to adapt to global rapid change. The improved method could adjust to light change under various conditions, improve the accuracy of moving objects detection.

978-0-7695-4818-0/12 $26.00 © 2012 IEEE
DOI 10.1109/DCABES.2012.90

IV. Adapting to Light Changes Pixel Layer Based Background Model for Moving Objects Detection

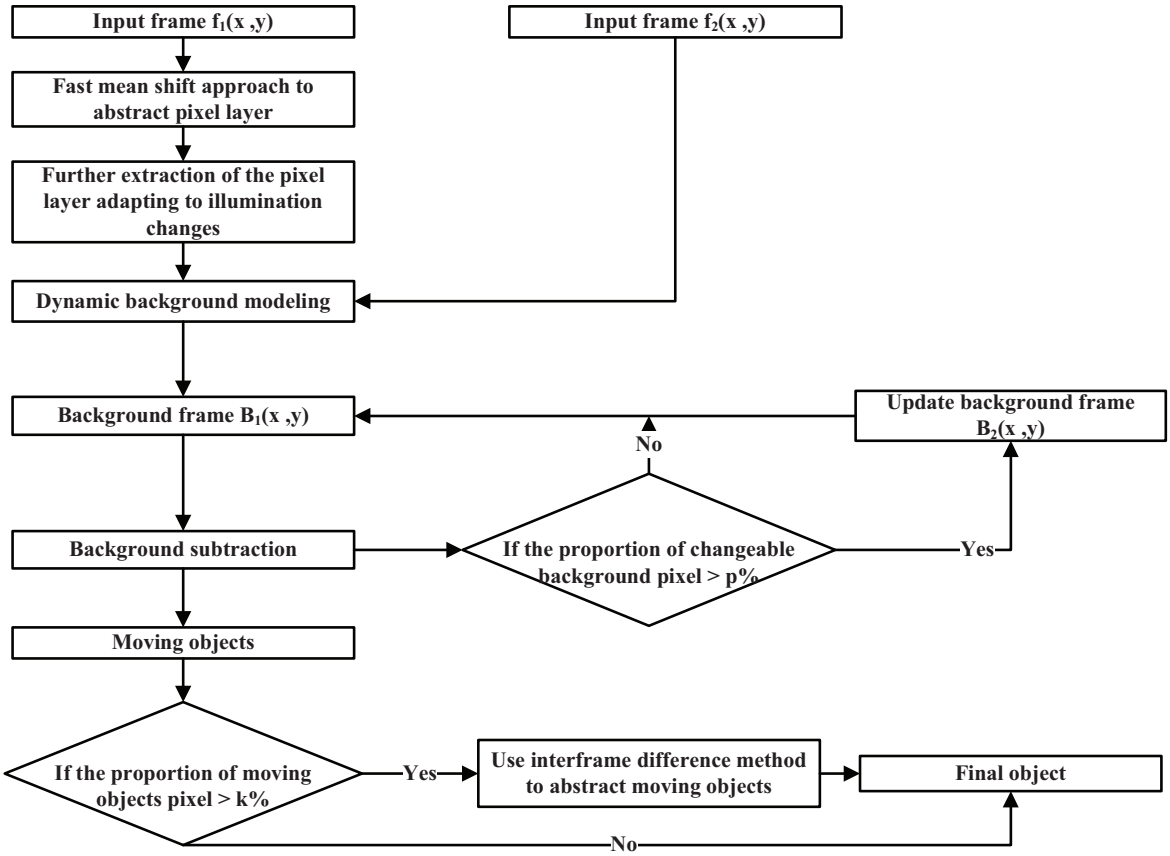

Figure 1 Process of adapting to light change pixel layer based background model

A. Fast mean shift approach to abstract background pixel layer

Let $A=\{x_i|i= 1,\ldots,N\}$ be a collection of pixels of the background frame, xi be the RGB vector of pixel i, fast mean shift approach is used to cluster the background frames in RGB color space, the background frames are divided into a group layer $L_k(\mu_k,\sum_k)_k=1,\ldots,M$, and estimate the parameters of the layer, μ_k, $\sum_k$ are the mean vector and covariance matrix of the k-th layer respectively, M represents the number of layer. To begin with, divide A into several subsets $S=\{s_j(n_j,c_j)|j=1,\ldots,m\}$,$n_j$,$c_j$ respectively represent number of elements and the mean vector included by subset s_j.

Procedure is as follows:

1) Initialize S as $\{s1(x_1, 1)\}$

2) k = 2, 3,…, N, if j, make normal number$\|x_k - c_j\|_\infty$ less than threshold r, arrange x_k in s_j; Otherwise, generate a new subset s_{new} $(x_k, 1)$

3)Update mean vector of each subset $c_j=[\sum x_i \in s_j]\backslash n_j$ in $\{s_j(n_j,c_j)|j = 1,\ldots,m\}$, from $c_j^{(0)} = c_j$, initiate the mean shift approach using the equation[8] :

$$c_j^{(k+1)} = \frac{\sum_{i=1}^{m} n_i c_i g\left[\left\|\frac{c_j^{(k)}-c_i}{h}\right\|^2\right]}{\sum_{i=1}^{m} n_i g\left[\left\|\frac{c_j^{(k)}-c_i}{h}\right\|^2\right]} \quad (1)$$

$g[\|y\|^2]$ is a non-negative function whose center is at zero and integral equals to 1 in field, Gaussian kernel function is used in this paper, h represents smoothing bandwidth, set h 18.

Through the mean shift iterative process, we get a set of cluster centers μ_i(i= 1,…,Q). For arbitrary two cluster centers μ_a and μ_b, if $\|\mu_a - \mu_b\|<\varepsilon$, and then merge them. Set $\{ c_{k1}, c_{k2},\ldots,c= \}$ as subset centers converge to μ_k, all of the pixels correspond to c_{k1}, $c_{k2},\ldots,c_{kt}$ consist of a pixel layer, μ_k is the mean vector of this layer. $\sum_k$ is a diagonal matrix.

B. *Further extraction of the pixel layer adapting to illumination change*

Use 5 Gaussian distributions to count similar pixel of each frame in adjacent t frames $\{x_1, x_2,\ldots,x_t\}$, and get probability density function of RGB vector[9]:

$$P(x) = \sum_{i=1}^{k} \frac{\omega_{i,t}}{(2\pi)^{\frac{-n}{2}}|\sum_{i,t}|^{\frac{-1}{2}}} \exp[-\frac{1}{2}(x_i - \mu_{i,t})^T(\sum_{i,t})^{-1}(x_i - u_{i,t})] \quad (2)$$

$$\sum_{i,t} = \sigma_{i,t}^2 * I \quad (3)$$

K is the number of Gaussian distribution, n represents dimensionality of x. $\omega_{i,t}$ is the weights of Gaussian components at time t, $\mu_i$and $\sum_{i,t}$ are respectively mean and variance of the i-th Gaussian components, $\sigma_{i,t}$ is standard deviation, I is unit matrix. According with the size of $\frac{\omega_{i,t}}{\sigma_{i,t}}$ from high to low sort the K Gaussian components, take the first B Gaussian components to establish background model.

$$B = \text{argm in}_b (\sum_{i=1}^{b} \omega_i > T) \quad (4)$$

Threshold T measures the smallest proportion of the background Gaussian components in the entire probability distribution of the RGB vector. The new observation x_i, t match with sorted k Gaussian distributions and matching condition is: $|x_{i,t} - \mu_i| < 25\sigma_i$, set weights of learning factor α= 0. 005, mean update rate $\rho_\mu = 0.0015$

When it comes to the situation that new pixels are judged the background, the formula of adapting to illumination change is

$$\omega_{i,t} = (1-\alpha)\omega_{i,t} + \alpha(M_{i,t}) \quad (5)$$

$$\mu_{i,t} = (1-\rho)\mu_{i,t-1} + \rho_{x_{i,t}} \quad (6)$$

$$\sigma_{i,t}{}^2 = (1 - k*\rho)\sigma_{i,t-1}^2 + k*\rho(x_{i,t} - \mu_{i,t})^T(x_{i,t} - \mu_{i,t}) \quad (7)$$

$$k = X_t - \mu_{i,t} \quad (8)$$

C. *Dynamic background modeling*

Input frame f2(x, y), dynamic modeling due to the results of step A and B.

D. *Background updating*

Dynamic background updating will bring a huge computational burden, add the statistical decision: only if the background pixels change to the extent which has an effect on the detection. It is an on-demand trade-offs.

E. *Adapt to illumination change*

Light mutations (such as open and turn off the lights) will cause the brightness of most pixel change greatly in the scene. In this case, most of the background pixels were mistaken to be foreground because the majority of background pixels deviate from the original model. To avoid this case, make a statistic of the results of the Gaussian mixture model, if the number of foreground pixels exceeds the 50% of the entire image, there must be a light mutation and Gaussian mixture model is ineffective. Then Gaussian mixture model should be initialized. When an abnormal object moves in the monitored scene, there will be obvious differences between frames. Subtract two frames and get the absolute value of the difference of image brightness. Through judging whether it is greater than the threshold to analyze the motivation characteristics of the video or image sequences, whether the objects are moving or not will be known. The differential of the image sequence frame by frame is equal to high-pass filtering in time domain.

$$d=|IL(x, y, i)-IL(x, y, i-1)| \quad (9)$$

$$IDL (x, y, i) = d, \quad \text{if} \quad d \geqslant T_0 \quad \text{if} \quad d < T_0 \quad (10)$$

IDL is adjacent frame difference, IL(x,y,i)and IL(x,y,i-1)are respectively luminance component of the i-th frame and the i-1-th frame, i represents the number of frame (i = 1 ,⋯,N)

Figure 1 shows the process of the adapting to light change pixel layer based background model.

V. EXPERIMENTAL RESULTS AND ANALYSIS

According this method, result is given on the VC++6.0 platform. In order to verify the effectiveness and applicability of the improved algorithm, two video sequences are selected. One is about indoor environment, local illumination change is controlled by the manual switch lamp. Another one is tested in outdoor environment,

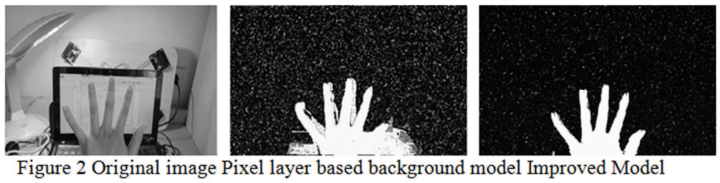

Figure 2 Original image Pixel layer based background model Improved Model

global illumination change occurs in a frame.

Figure 2 is the experimental contrastive results between based on pixel layer background model detection and the improved method. Because of the local illumination changes caused by a table lamp in the scene, pixel layer background model cannot deal with local light mutation and lead to the mistake that treat background pixels as foreground pixels, the method proposed in this

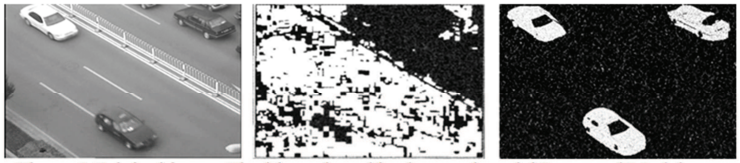

Figure 3 Original image Pixel layer based background model Improved Model

paper solve this problem.

Figure3 is about a group of outdoor traffic video. Although extraneous light change a lot, the improved method achieve satisfactory results. Experimental results substantiate that the improved method could deal with the false positives due to illumination change and improve the accuracy and robustness of original pixel layer based background model for moving objects detection in dynamic scene.

VI. CONCLUSION

Based on pixel layer background detection, we propose an improved method for the problem of illumination change. We take advantage of locality and temporal and spatial variation characteristics. A new model parameter was selected, a fixed learning rate was used and the adaptive factor to update the variance was added which are helpful to adapt to illumination change rapidly. For that matter, a statistical decision is used to solve the problem of background updating. The experiment also shows that although the rate of false alarm decreases the rate of true alarm decreases. Increasing the rate of true alarm will be needed for further study.

REFERENCES

[1] Sun J, Zhang W, Tang X, Proceedings of IEEE Europe Conference on Computer V is ion. Washington DC, USA: IEEE Computer Society, 2006: 628-641.

[2] Jodi P M, Menotti M, Conrad J Statistical background subtraction using spatial cues [J]. IEEE Transactions on Circuits and System s for Video Technology, 2007, 17(12): 1758-1763.

[3] H an J, Zhang M, Pan Z. Accurate foreground segmentation unaffected by cast shadows based on graph cut [J]. Journal of Computation al in formation System s, 2008, 4 (4): 1607-1612.

[4] Zhang K, Tang M, James T K. Applying neighborhood consistency for fast clustering and kernel density estimation[C]//Proceedings of Computer Vision and Pattern Recognition. Washington DC, USA: IEEE Computer Society, 2007: 1001-1007.

[5] Toyama K, Krum J, Burritt B, Wallflower: principles and practice of background maintenance [C] / /Proceedings of IEEE International Conference on Compute Vision. Washington DC, U SA: IEEE Computer Society, 1999: 255-261.

[6] Stauffer C, Grison W. Learning Patterns of Activity Using Real-Time Tracking [J]. IEEE Transactions on Pattern Analysis and Machine Intelligence, 2000, 22(8): 747- 757.

[7] Stauffer C, Grison W. Adaptive background mixture models for real- time tracking[C] / /Proceedings of IEEE Conference on Computer Vision and Pattern Recognition. [s. .l]: [s.n.], 1999: 246-252.

[8] Bouwmans T, Baf FEI, Vachon B. Background Modeling using Mixture of Gaussians for Foreground Detection - A Survey[P]. Recent Patents on Computer Science, 2008: 219- 237..

[9] Schindler K, Wang Han Smooth Foreground- Background Segmentation for Video Processing [J]. Lecture Notes in Computer Science, 2006, 3852: 581- 590.

Recognition of Off-line Arabic Handwriting using Hidden Markov Model Toolkit

Dong Xiang, Hu Liu, Xianqiao Chen, Yanfen Cheng, Hanbing Yao
School of Computer Science and Technology, Wuhan University of Technology
Wuhan 430063, PR China
E-mail: xiangdong@whut.edu.cn

***Abstract*—This paper presents an off-line Arabic handwriting recognition system using the Hidden Markov Model Toolkit (HTK). HTK is a portable toolkit for speech recognition system. The recognition system extracts a set of features on binary handwritten images using sliding widow, builds character HMM models and learns word HMM models using embedded training without character pre-segmentation. Moreover this paper studies the relationship between frame overlap and number of stats. Experiments that have been implemented on the benchmark IFN/ENIT database show the average recognition rate of this system is 85.43%.**

Keywords-optical character recognition; Arabic handwriting recognition; hidden markov model, sliding window

I. INTRODUCTION

The recognition of cursive handwriting is still an open problem due to the existence of many difficulties such as the variability of the handwritten styles and shapes, writing skew or slant and the size of the lexicon. Unconstrained Arabic handwriting is naturally cursive and makes it difficult to pre-segment, and result in a challenging automatic off-line recognition. Moreover the Arabic alphabet contains 28 letters. Each has between two and four shapes and the choice of which shape to use depends on the position of the letter within its word or subword. Ligatures between consecutive letters are of variable lengths as well as inter and intra word spaces. Arabic words include diacritical points and marks that can change their meaning. Sometimes one letter appears above or below the previous letter. Also difficult is the rare situation when a preceding letter appears to the left of a succeeding letter. In addition to the existence of horizontal ligatures between letters within words or sub- words, vertical ligatures can occur between two or three Arabic characters. Many of the above aspects render the Arabic recognition task more difficult than other script[1].

Considering the cursive and connected nature of Arabic printed and handwritten script, many recognition systems are based on the hidden markov models (HMM) framework [2~7]. HMM-based methods provide the advantage of joint segmentation and recognition. Thus, even in the case where words are modeled as the concatenation of compound characters, HMMs avoid pre-segmentation of words into characters in both training and classification stages. This can eliminate error introduced by pre-segmentation. Furthermore, the stochastic modeling offered by HMMs, is able to cope with sequences of observations of variable lengths and nonlinear distortions.

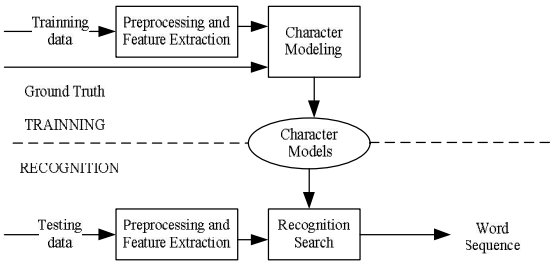

Figure 1. Block diagram of the recognition system

An off-line Arabic cursive handwritten word recognition system was presented in this paper as shown in figure 1. The recognition system can be divided into two basic functional components: training and recognition. Both training and recognition share a common pre-processing and feature extraction. The feature extraction program computes a feature vector as a function of the horizontal position within each sliding window. For each sliding window we compute foreground pixel density, concavity and arc length features, which results in a total of 36-features vector per sliding window.

The recognition system models each character with a multi-state, left-to right HMM. Training is performed using the Baum-Welch or Forward-Backward algorithm, which aligns the feature vectors with the character models to obtain maximum likelihood estimates of HMM parameters. For our system the HMM parameters are the means and variances of the component Gaussians in the Gaussian mixture model of the state output probabilities, the mixture component weights, and the state transition probabilities. During recognition we search for the sequence of characters that is most likely given the feature-vector sequence and the trained character-models,

This paper is organized as follows. Section 2 presents the preprocessing and feature extraction. The feature vectors are extracted using sliding window technique. Section 3 details the HMM classifier as used in our system. The performance of the recognition system has been experimented on the benchmark database IFN/ENIT [8] which includes Tunisian city names. The obtained experimental results are shown and analyzed in Section 4. Finally, Section 5 draws the conclusion.

II. PREPROCESSING AND FEATURE EXTRACTION

Some of the basic pre-processing steps like image binarization, word segmentation, and noise reduction have already been performed during the development of the

This work was supported by "the Fundamental Research Funds for the Central Universities"

978-0-7695-4818-0/12 $26.00 © 2012 IEEE
DOI 10.1109/DCABES.2012.66

IFN/ENIT database. So we skip these procedures and directly extract features on the binary image.

A. *Sliding Window*

Windowing is a common localization technique in signal processing domain. Since the character string runs in certain direction, a movable window called sliding window following the same order can be used to draw an interested zone and then extract features within it.

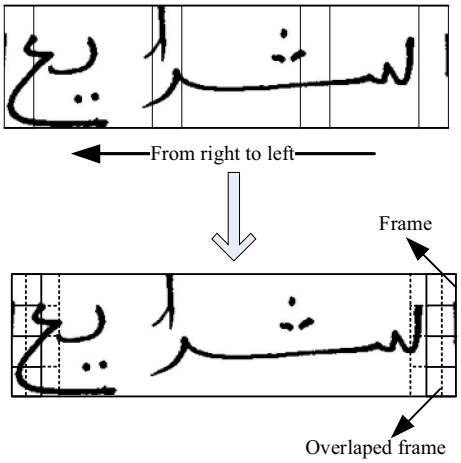

Figure 2. Word image divided into vertical frames

Generally the window width is fixed and in our system is 8 pixels, while window height depends on each word image. In our system we didn't scale the image height and width to same value. The sliding window is divided equally into four cells as shown in figure 2 and shifted along the word image from right to left and a feature vector is calculated for each frame. And the succeeding widows can be overlap or not. The overlap is also a system parameter which varies from 0 to 1. The overlap and number of stats may interact on each other and influence the recognition performance.

In order to study the relation between the overlap and number of stats, we test the recognition performance on different overlap and number of stats and the result is shown in figure 3 . From the figure and figure 2 we can see that with the increment of overlap, the number of divided frames increase too. So the recognition system need more stats to achieve better performance. When the overlap is 0.25, the recognition system with 7 stats achieves best performance but degrades greatly with 9 stats; When the overlap is 0.5, the recognition system with 9 stats achieves best performance but degrade with stat increment; When the overlap is 0.75, the recognition system with 13 stats achieves best performance then the achievement saturates. with stat increases. Considering the computation complexity and performance we select the overlap is 0.5 and number of stat is 9.

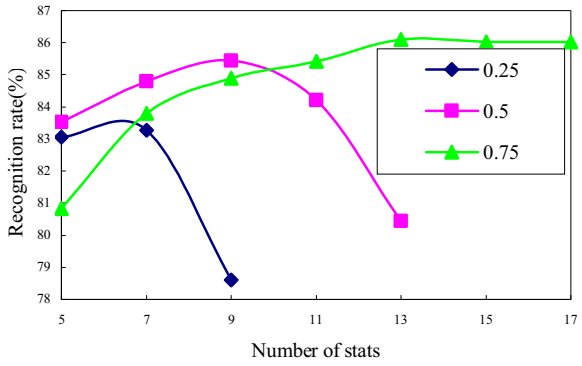

Figure 3. The recognition rate varies with overlap and number of stats

B. *Feature Extraction*

There are three types of features: distribution features based on foreground (black) pixel densities, concavity features which provide local concavity information and stroke direction, and arc length to calculate the stroke length in each frame

Let H be the height of the frame in an Arabic word image, h_i be the height of the i_{th} cell, w the width of a frame, $f_i(j)$ be the number of foreground pixels in the j_{th} row of the i_{th} cell. The first feature F_1 is calculated as following:

$$F_1 = \sum_{j=1}^{h_i} f_i(j) \Big/ h_i \times w \qquad (1)$$

The concavity features in this paper are used to calculate the average distance scanning pixel by pixel from the cell border to the first met stroke. So there are four concavity features to respectively calculate the average distance from the top, bottom, left and right cell border to the first met stroke along down, up, right and left.

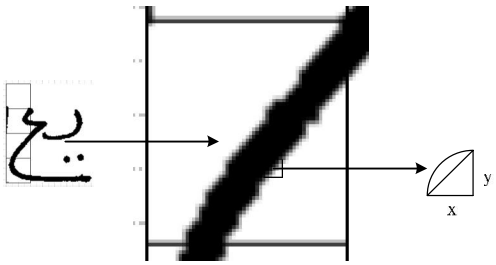

Figure 4. One type of arc length features

The arc length features are used to calculate the arc length of stroke from the top, bottom, left and right direction. We only calculate the maximal arc length of stroke even if the stroke was break into small pieces, so it is reasonable to use the square root of sum of squares of x and y as show in figure 4 to calculate arc lengths.

During the feature extraction phase, we extract one foreground pixel density, four concavity and four arc length features . Because we divide the each frame into four cells, this results in a total of 36-features vector per frame.

III. HTK INFERENCE ENGINE

The hidden Markov model toolkit (HTK) [9] is a portable toolkit for building and manipulating hidden Markov models. It is primarily designed for building HMM-based speech recognition systems. HTK was originally developed at the Speech Vision and Robotics Group of the Cambridge University Engineering Department.

HTK allows HMMs to be built with any desired topology using simple text files. The training tools adjust HMM parameters using the prepared training data coupled with the data transcription. These tools apply the Baum–Welch re-estimation procedure to maximize the likelihood probabilities of the training data given the model.

HTK provides a recognition tool to decode the sequence of observations and output the associated state sequence. The recognition tool requires a network to describe the transition probabilities from one model to another. The dictionary and language model can be input to the tool to help the recognizer to output the correct state sequence.

The result analysis tool evaluates the performance of the recognition system by matching the recognizer output data with the original reference transcription. This comparison is performed using dynamic programming to align the two transcriptions, the output and the ground truth, and then count the number of: substitution (S), deletion (D) and insertion (I).

A. HMM Theoretical Framework

Supposing the sequence of feature vectors corresponding to handwritten image is $O = o_1, \ldots, o_m$, The transitions between states represent the shifts of character segments and each state of the chain associates a probability density spanned on a *d*-dimensional feature space. A continuous-density HMM (CDHMM) can be notated as follows:

$$\lambda = (\pi, A, B) \tag{2}$$

where π is the initial parameter set concerning the HMM topography, mean vector and covariance matrix in each state, mixture coefficients etc, $A=(a_{ij})$ is the state transition probability. $B=\{b_j(o)\}$ is the observation probability. Further, the probability of observation o for state j, $b_j(o)$ can be approximated by finite mixture of Gaussian density of the form:

$$b_j(o) = \sum c_{jk} \Omega(o, \mu_{jk}, \sum_{jk}), \quad j=1,\cdots,N \tag{3}$$

where N is the total states, c_{jk} the mixture coefficient and μ_{jk}, $\sum_{jk}$ the mean vector and covariance matrix for Gaussian distribution Ω, respectively.

B. Character and word modeling

As discussed above our system models each character with 9 states, left-to-right topology, and 3 transitions for each state: a self transition, a transition to the next state, and a transition that permits the skipping of a single state as shown in Fig. 5. The model parameters need to be estimated include the means and variances of the component Gaussians in the Gaussian mixture model of the state output probabilities, the mixture component weights, and the state transition probabilities.

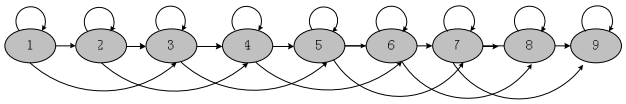

Figure 5. Left to right character HMM

During models training procedure we need initialize the state transition probability matrix $A=(a_{ij})$. Through experiments we initialize the matrix as follows:

$$\begin{bmatrix} 1 & 0 & 0 & \ldots & 0 & 0 & 0 \\ 0 & 0.6 & 0.2 & \ldots & 0 & 0 & 0 \\ 0 & 0 & 0.6 & \ldots & 0 & 0 & 0 \\ \vdots & \vdots & \vdots & \ldots & \vdots & \vdots & \vdots \\ 0 & 0 & 0 & \ldots & 0..6 & 0.2 & 0.2 \\ 0 & 0 & 0 & \ldots & 0 & 0.6 & 0.4 \\ 0 & 0 & 0 & \ldots & 0 & 0 & 0 \end{bmatrix}$$

Although the Arabic alphabet contains 28 letters, each has between two and four shapes and the choice of which shape to use depends on the position of the letter within its word or subword. Moreover some ligatures between consecutive letters are very common. We built up to 158 character models. Then, each word in the diction is built by concatenating the appropriate character models.

C. Training and Recognition

The HMM-based classifier contains a training module and a recognition module. The training module estimates the parameters (transition probabilities and feature probability distributions) of each of the character HMMs–uses what has been known, alternately, as the Baum-Welch or Forward-Backward algorithm. The training is not performed on a character per character basis; rather whole words are used for this training while the character models are shared between the words' models. It iteratively aligns the feature vectors with the character models to obtain maximum likelihood estimates of HMM parameters. The algorithm guarantees a convergence of a local maximum of the likelihood function. The feature probability distributions in our system are characterized by the means, variances, and weights of the Gaussian mixtures.

In the recognition phase, feature vectors extracted from an image are passed to a network of word lexicon entries formed of character models. The character sequence providing the maximum likelihood identifies the recognized entry. If required, the recognition can generate N best output hypotheses rather than just the single best one. To determine the best output hypotheses, the Viterbi algorithm is used.

IV. EXPERIMENTS AND RESULTS

A. IFN/ENIT Database

To evaluate the performance of our recognition system, experiments are implemented on the benchmark database IFN/ENIT. The IFN/ENIT contains a total of 26459 handwritten words of 946 Tunisian town/villages names written by different writers and divided into four subsets a, b, c, and d. The occurrence of examples in the IFN/ENIT database is different from one town/village name to another: they vary from 3 to 381[10]. So the data for each character models vary too.

B. *Mixture Component Selection*

Our recognition system is a tied-mixture system in which all Gaussian components are stored in a pool and all state output distributions share this pool. Each state output distribution is defined by *M* mixture component weights and since all states share the same components, all of the state-specific discrimination is encapsulated within these weights. The *M* value not only impacts the system performance but also the codebook training time. To select best *M* values we test several *M* values and the result is shown in figure 6. From the figure we can see that with the increment of *M* values, the training time increase, especially at value 256, the time increase 110 minutes, while the system performance achieve best at 192 and then degrade. Considering the system performance and training time, we select the 192 as the best *M* value.

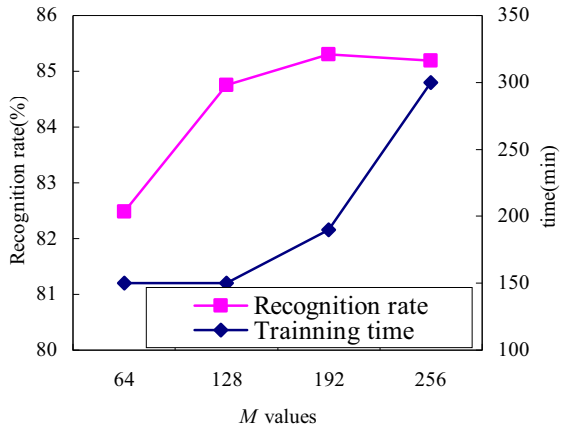

Figure 6. The recognition rate and training time at different *M* values

C. *Experiments and Results*

In our experiment we use sliding widow to extract feature. Four experiments are implemented by taking alternatively one subset of the database for testing and the remaining three ones for training. This leads to a non-parametric estimation of the error rate.

Table I shows the experimental results of the performance evaluation of our recognition system. This system achieves almost same performance on 4 training and recognition settings and leads to an average recognition rate of 85.43%.

A preliminary error analysis shows different causes for wrong classifications according to the nature of the Arabic cursive handwritten words. Diacritical marks and extensions are often not at the exact position on top or under the main part of the letter, and character ligatures are of variable lengths. The frequencies of occurrences of word in IFN/ENIT database vary leading the data for each character model is different. In addition the ratio of width to height is found widely different for some word image. All these may reduce the character recognition accuracy

TABLE I. RECOGNITION RESULTS

Test	Training data set	Testing data set	Recognition rate
1	b, c, d	a	85.83
2	a, c, d	b	84.94
3	a, b, d	c	85.26
4	a, b, c	d	85.68

V. CONCLUSION

This paper presents a new HMM based system for offline handwritten recognition. The extracted features are based on the densities of foreground pixels, concavity and arc length in a sliding window. The presented system has been experimented and the results are provided on a subset of the benchmark database IFN/ENIT. The results show our system achieve advance performance.

REFERENCES

[1] A. Amin, "Off-line Arabic character recognition: the state of the art," Pattern Recognition, 1998, Vol. 31, pp: 517-530.

[2] R. Al-Hajj, C. Mokbel, L. Likforman-Sulem," Combination of HMM-Based Classifiers for the Recognition of Arabic Handwritten Words," International Conference on Document Analysis and Recognition, 2007, pp: 959 – 963.

[3] Al-Muhtaseb A. Husni, Mahmouda A. Sabri, Qahwaji S. Rami, "Recognition of off-line printed Arabic text using Hidden Markov Models," Signal Processing, 2008, Vol. 88(12), pp: 2902-2912.

[4] M. Dehghan, K. Faez, M. Ahmadi, M. Shridhar, "Handwritten Farsi (Arabic) word recognition: a holistic approach using discrete HMM," Pattern Recognition, 2001,Vol. 34, pp: 1057-1065.

[5] M. Decerbo, E. MacRostie, P. Natarajan, "The BBN Byblos Pashto OCR System," Proceedings of the 1st ACM workshop on Hardcopy document processing, 2004, pp:29-32.

[6] N. Amara Ben Essoukri, F. Bouslama, "Classification of Arabic script using multiple sources of information: State of the art and perspectives," IJDAR, 2003, Vol. 5 (4): 195-212.

[7] S. M. Khorsheed, "Recognizing Arabic manuscripts using a single hidden Markov model," Pattern Recognition Letters, 2003, Vol. 24, pp: 2235-2242.

[8] H. El Abed, V. Margner, "The IFN/ENIT database-a tool to develop Arabic handwriting recognition systems," ISSP, 2007, pp: 1-4.

[9] S. Young, G. Evermann, D. Kershaw, "The HTK Book," Http://htk.eng.cam.ac.uk/

[10] R. Al-Hajj, L. Likforman-Sulem, and C. Mokbel, "Arabic handwriting recognition using baseline dependant features and hidden markov modeling," Proc. of ICDAR 05, 2005, pp. 893-897.

A Survey for Region-based Level Set Image Segmentation

Yuting Jiang, Meiqing Wang*, Haiping Xu
College of Mathematics and Computer Science, Fuzhou University
Fuzhou, Fujian, China
jiangyuting11@126.com, mqwang@fzu.edu.cn, 676323843@qq.com

***Abstract*—Partial differential equations are widely used in image segmentation. Meanwhile, topological change of Curve evolution, which is very difficult to solve previously, was effectively handled by level set method proposed by Osher and Sethian. In this paper, several region-based level set image segmentation models in recent years are described in details. By experimenting some of the models, the main limitations and development potential of this field are discussed.**

Keywords- image segmentation; level set method; partial differential equations

I. INTRODUCTION

Image segmentation is a fundamental problem in the image processing and computer vision. The stand or fall of partition results have a direct influence on the subsequent processing of the high-level image analysis and understanding. Up to now, a variety of algorithms have been proposed to solve the image segmentation problems. Among them, the partial differential equations (PDE) based image processing method with its high accuracy and keeping edge continuity get a wide range of use.

Partial differential equations in image segmentation applications began in snake active contour model [1] proposed by Kass et al in 1987. The snake model consists basically of anelastic curve which can dynamically conform to object shapes in response to minimize the energy function and stop in the edge of the object finally. However, parametric snake models have their drawbacks. For examples, they are too sensitive to initial conditions due to the non-convexity of the energy functional. Meanwhile, they can hardly to deal with topological changes like merging and splitting of the evolving curve. Moreover, these methods only detect boundaries defined by gradient. Many researchers have done great efforts to improve these shortcomings. The region-based level set [2] image segmentation with its better capacity to handle the shortcomings stands out from numerous of methods.

In this paper, some of typical global region based models and local region based models are reviewed in Section II and Section III. Contrast experiments and analyses are given in Section IV. This paper is summarized in Section V.

II. GLOBAL REGION BASED LEVEL SET ACTIVE CONTOUR MODEL

Region-based image segmentation model was first put forward by Mumford and Shah in the 1980s. Since it is difficult to find optimal solution in practical application, Chan and Vese [3] proposed a simplify M-S model, namely C-V model.

A. C-V model

For a given image $I(x)$ on the image domain Ω, let C represents a closed curve and c_1 and c_2 denote the average intensities inside and outside the curve, respectively. The C-V model implements segmentation by minimizing the following energy functional:

$$F(c_1,c_2,C)=\mu\cdot Length(C)+\nu\cdot Area(insideC) + \lambda_1\int_{inside(C)}|I-c_1|^2\,dxdy+\lambda_2\int_{outside(C)}|I-c_2|^2\,dxdy \quad (1)$$

where $\mu>0,\ \nu\geq 0,\ \lambda_1,\lambda_2>0$ are fixed parameters. Using variational level set method, the PDE evolution equation corresponding to the C-V model is stated as follows:

$$\frac{\partial\phi}{\partial t}=\delta(\phi)\left[\mu div\left(\frac{\nabla\phi}{|\nabla\phi|}\right)-\nu-\lambda_1(I-c_1)^2+\lambda_2(I-c_2)^2\right] \quad (2)$$

$$c_1=\frac{\int_\Omega I(x,y)H(\phi(x,y))\,dxdy}{\int_\Omega H(\phi(x,y))\,dxdy} \quad (3)$$

$$c_2=\frac{\int_\Omega I(x,y)(1-H(\phi(x,y)))\,dxdy}{\int_\Omega (1-H(\phi(x,y)))\,dxdy} \quad (4)$$

where $\delta(x)=\frac{d}{dx}H(x)$ is the one-dimensional Dirac measure, $H(x)$ is the Heaviside function $H(x)=\begin{cases}1, if\ x\geq 0\\ 0, if\ x<0\end{cases}$.

Although the C-V model greatly facilitates the development of the region-based active contour model, it still has some intrinsic limitations. The model assumes that the intensities in each region always maintain constant, which doesn't work for the images with intensity inhomogeneity. Furthermore, in order to maintain stable curve evolution, the re-initialization step is adopted which makes the computational cost more expensive.

B. ICV model

Zhang et al analyzed the C-V model in details and proposed a novel model that is Improved C-V (ICV) model

* Corresponding author

978-0-7695-4818-0/12 $26.00 © 2012 IEEE
DOI 10.1109/DCABES.2012.44

[4]. They considered that the evolution of the level set function mainly relied on the term $-\lambda_1(I-c_1)^2+\lambda_2(I-c_2)^2$. Meanwhile, employing $|\nabla\phi|$ instead of $\delta_\varepsilon(\phi)$ would enlarge the capture range. As a result, the energy functional of the ICV model is simplified as:

$$\frac{\partial\phi}{\partial t}=|\nabla\phi|\left(I-\frac{c_1+c_2}{2}\right) \tag{5}$$

where c_1 and c_2 as shown in (3), (4) and $\delta_\varepsilon(\phi)$ is one-dimensional regularized Dirac function. In [5], Zhang further modified the model in the following way:

$$\frac{\partial\phi}{\partial t}=\alpha|\nabla\phi|(I-\frac{c_1+c_2}{2})/\max|(I-\frac{c_1+c_2}{2})| \tag{6}$$

C. GCV model

Zhang et al [6] considered that using intensity information to describe an image was too simple. Therefore, by introducing gradient information, the GCV model is proposed. The model abided by the following energy functional:

$$\begin{aligned}E(\phi,c_1,c_2,d_1,d_2)&=\mu\int_\Omega\frac{1}{2}\left(|\nabla\phi|-1\right)^2dxdy\\&+\lambda_1\int_{inside(C)}|I-c_1|^2dxdy+\lambda_2\int_{outside(C)}|I-c_2|^2dxdy\\&+\eta_1\int_{inside(C)}|I_g-d_1|^2dxdy+\eta_2\int_{outside(C)}|I_g-d_2|^2dxdy\end{aligned} \tag{7}$$

where I_g represents gradient modulus matrix of image, d_1 and d_2 denote the average density in the region ω_1 and ω_2.

At the same time, many other methods are put forward to overcome the limitations of the C-V model. In [7], Sobolev gradient was utilized to calculate the internal energy because it was more effective than the gradient descent method when minimizing the curve length. In [8], because the gradient of the image can reflect the characteristic of interior contour, the intensity $I(x)$ in C-V model was replaced by $K(x,y)=|\nabla G_\delta * I(x,y)|^2$. Correspondingly, the constant c_1 and c_2 became the average values of $K(x,y)$ inside and outside the curve, respectively.

III. Local Region Based Level Set Active Contour Model

For the sake of solving the limitations of C-V model, many efficient implementation schemes have been proposed. To efficiently perform the segmentation of images with intensity inhomogeneity and reduce the cost of computation, a new class of models which incorporate with the local statistic information have been proposed. The typical representatives include the local binary fitting (LBF) model [9, 10] and local image fitting (LIF) model [11].

A. LBF model

LBF model proposed by Li et al introduced a local binary fitting energy with a kernel function. For arbitrary x in the image domain, the fitting energy is defined by

$$\begin{aligned}E_x&=\lambda_1\int_{inside(C)}K(x-y)|I(y)-f_1(x)|^2\,dy\\&+\lambda_2\int_{outside(C)}K(x-y)|I(y)-f_2(x)|^2\,dy\end{aligned} \tag{8}$$

where λ_1 and λ_2 are two positive constant, f_1 and f_2 are two values that approximate local image intensities inside and outside of the curve C, and $K(u)$ is a Gaussian kernel function. Then the entire fitting energy in image domain is given by:

$$E(C,f_1,f_2)=\int_\Omega E_x^{LBF}(C,f_1(x),f_2(x))dx \tag{9}$$

Taking advantage of level set function ϕ, and inserting a penalizing term to avoid re-initialization and a regularized length term to keep the contour smooth, we have

$$\begin{aligned}F(\phi,f_1,f_2)&=E^{LBF}(C,f_1,f_2)+\beta\int_\Omega\frac{1}{2}(|\nabla\phi(x)|-1)^2dx\\&+\nu\int_\Omega\delta(\phi(x))|\nabla\phi(x)|dx\end{aligned} \tag{10}$$

B. LIF model

The LIF model is proposed by Zhang et al. At first, LIF model defined a local fitted image formulation in the following way:

$$I^{LIF}=m_1H_\varepsilon(\phi)+m_2\left(1-H_\varepsilon(\phi)\right) \tag{11}$$

where $\begin{cases}m_1=mean\left(I\in\left(\{x\in\Omega\,|\,\phi(x)<0\}\cap W_k(x)\right)\right)\\m_2=mean\left(I\in\left(\{x\in\Omega\,|\,\phi(x)>0\}\cap W_k(x)\right)\right)\end{cases}$ and $W_k(x)$ is a regularized window function. By minimizing the difference between the fitted image and original image, the energy functional can be described as:

$$E^{LIF}=\frac{1}{2}\int_\Omega|I(x)-I^{LIF}(x)|^2\,dx,\quad x\in\Omega \tag{12}$$

Meanwhile, the model made use of Gaussian filtering to smooth level set function in each iteration which avoided re-initialization in numerical implementation.

In the meantime, many scholars modified the C-V model directly to handle image with intensity inhomogeneity. In [12], two spatially shifty functions were delimited as follows to replace two constant c_1 and c_2 :

$$c_1(x)=\frac{\int_\Omega g_k(x-y)\left(I(y)H(\phi(y))\right)dy}{\int_\Omega g_k(x-y)H(\phi(y))dxdy} \tag{13}$$

$$c_2(x)=\frac{\int_\Omega g_k(x-y)\left(I(y)\left(1-H(\phi(y))\right)\right)dy}{\int_\Omega g_k(x-y)\left(1-H(\phi(y))\right)dy} \tag{14}$$

In [13], Wang et al proposed an efficient local Chan-Vese (LCV) model. This model consists of three term: global term E^G, local term E^L and regularization term E^R. Thus the overall energy functional is given by:

$$
\begin{aligned}
E^{LCV} &= \alpha \cdot E^{G} + \beta \cdot E^{L} + E^{R} \\
&= \alpha \int_{inside(C)} |I - c_1|^2 \, dxdy + \alpha \int_{outside(C)} |I - c_2|^2 \, dxdy \\
&+ \beta \int_{inside(C)} |g_k * I - I - d_1|^2 \, dxdy \\
&+ \beta \int_{outside(C)} |g_k * I - I - d_2|^2 \, dxdy + \oint_C dp
\end{aligned} \tag{15}
$$

where g_k is a averaging convolution operator with $k \times k$ size window, d_1 and d_2 are the intensity averages of difference image $(g_k * I - I)$ inside and outside C, respectively.

IV. Experimental Results and Analysis

After the text edit has been completed, the paper is ready for the template. Duplicate the template file by using the Save As command, and use the naming convention prescribed by your conference for the name of your paper. In this newly created file, highlight all of the contents and import your prepared text file. You are now ready to style your paper.

In this section, part of the above mentioned models are experimented on synthetic and real images. All the experiments are implemented in matlab 7.0 on Windows XP system.

Fig. 1 shows the comparisons between C-V and LBF model as the representative of global and local based model, respectively. The C-V gets a good performance for the single goal of homogeneous regions with different intensities. While the LBF model only considers local statistic information which makes it get stuck in local minima and get wrong edge. As to test on an image with intensity homogeneity, C-V model fails due to its intrinsic limitation. On the contrast, the LBF model deals with it very well.

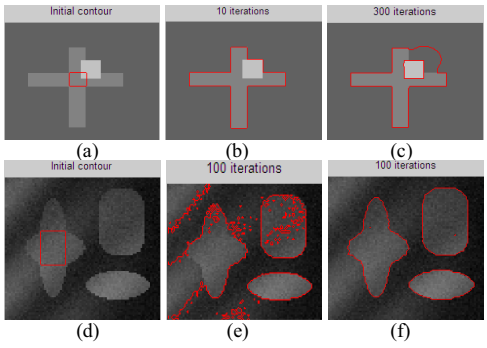

Figure 1. comparisons between C-V and LBF model (column 1: initial contour; column 2: results of C-V model; column 3: results of LBF model)

Fig. 2 demonstrates the comparisons between LBF and LIF model. As the representatives of local based models, both of them have their own advantages. When applied in multiple objects segmentation, especially the intensity of background is neither highest nor lowest, the LIF model works very well compared to the LBF. Nevertheless, may due to the set of initial parameters, the LIF model is defeated by the LBF in vessel image segmentation.

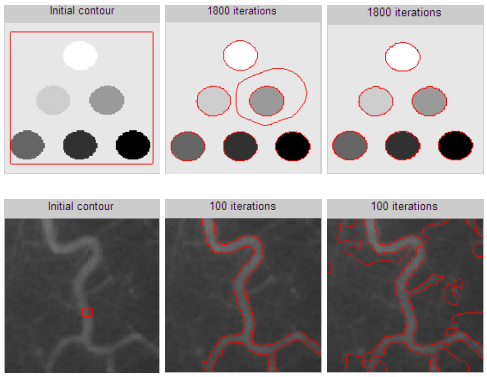

Figure 2. comparisons between LBF and LIF model (column 1: initial contour; column 2: results of LBF model; column 3: results of LIF model)

Fig. 3 shows the segmentation result on structural damage of pavement images. To compare with others, GCV model obtains better results than others. Meanwhile, GCV just iterates 20 times to achieve the real edge. Thus the GCV model is more efficient in computation.

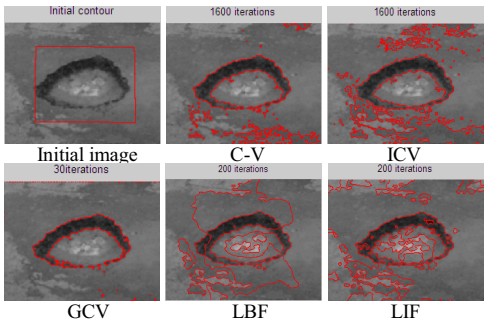

Figure 3. applications in detecting structural damage of pavement

At the same time, the ICV model and GCV model are applied in the picture (a) and (d) as shown in Fig. 1. And table I indicates that the ICV model is more efficient in region based active contour models. Because the evolution equation of ICV model is an ordinary differential equation, it is no necessary to meet specific differential rules and to adjust the various parameters in numerical implementation.

TABLE I. Implement time of C-V, ICV and GCV model with 10 iterations and 30 iterations, respectively

	C-V	ICV	GCV
Pic (a)	0.2500	0.1563	0.3133
Pic (d)	0.6875	0.3594	0.821

The experimental results show that specific model mentioned above can be used for some particular class of images. But, in general, there are still some problems for region based level set image segmentation models. For examples, the models can't really convergence to borders of objects. In usual, it gradually converges to zero after a great deal of iterations. And the segmentation result always depends on the initial contour placement and the choice of

initial parameters. Especially, the set of parameters in the LIF model plays an import role in evolution process.

V. CONCLUSION

The active contour model has obvious advantages when compared with other traditional segmentation methods. The level set method for its excellent handling topology also has been widely used. This paper summarized the region based level set image segmentation methods in the past few years. Some experimental results are given for comparative analysis. It seems that some specific models can be used for some particular class of images, but no model is suitable for all image segmentation.

ACKNOWLEDGMENT

This work was partially supported by NSFC under Grant No. 11071270 and Natural Science Foundation of Fujian Province under Grant No. 2010J01328.

REFERENCES

[1] M. Kass, Witkin, D.Terzopoulos, Snakes: active contour models, International Journal of Computer Vision 1 (1988) 321-331

[2] S.Osher, J.A.Sethian, Fronts propagating with curvature dependent speed: algorithms based on Hamilton-Jacobi formulations, Journal of Computational Physics 79(1988) 12-49

[3] T.Chan, L.Vase, Active Contour without edges, IEEE Transaction on Image Processing 10(2)(2001)266-277

[4] K.H.Zhang, W.G.Zhou, Z.Zhang and X.J.Zheng, Improved C-V active contour model,OPTO-ELECTRONIC ENGINEERING, vol.35, no.12, 2008.

[5] K.H.Zhang, Lei Zhang, H.H.Song and W.Zhou, Active contours with selective local or global segmentation: a new formulation and level set method. Image and Vision Computing, vol.28, issue 4, pp.668-676, April 2010.

[6] Yunping Zhang, Yan Huang, Meiqing Wang, An improved C-V Model Without Reinitialization 2009

[7] Ye Yuan, Chuanjiang He, Variational level set methods for image segmentation based on both L2 and Sobolev gradients, Nonlinear Analysis: Real World Applications 13 (2012) 959-966

[8] Na Zhang, Jianxun Zhang and Ruizhi Shi, An Improved Chan-Vese Model for Medical Image Segmentation in: IEEE Conference on International Conference on Computer Science and Software Engineering, 2008

[9] C.M Li, C. Gao, J. Gore, Z. Ding, Implicit active contours driven by local binary fitting energy, in: IEEE Conference on Computer Vision and Pattern Recognition, 2007

[10] C. Li, C. Kao, J. C. Gore, and Z. Ding, "Minimization of Region-Scalable Fitting Energy for Image Segmentation", IEEE Trans. Image Processing, vol. 17 (10), pp. 1940-1949, 2008

[11] Kaihua Zhang, Huihui Song, Lei Zhang, Active contours driven by local image fitting energy, Pattern recognition, 43(4), pp.1199-1206, 2010.

[12] Shigang Liu, Yali Peng, A local region-based Chan-Vase model for image segmentation, Pattern Recognition, 2012

[13] Xiaofeng Wang, Deshuang Huang, Huan Xu, An efficient local Chan-Vase model for image segmentation, Pattern Recognition 43(2010) 603-61

Extraction of Answer Image of Choice Questions in examination paper

Xu Zhipeng
School of Physics Science and Information Engineering, Liaocheng University
Liaocheng, China
xuzhipeng@lcu.edu.cn

***Abstract*—firstly, the skewed image of examination paper is corrected by Hough transform, and then mathematical morphology methods are used to locate the frame lines in table. Then connected component analysis is utilized to locate the form region based on maximum area feature. Finally the form frame line is removed according to the vertical gradient, and the answer image is achieved by analyzing the coordinates of objects.**

Keywords- document image processing, form recognition, mathematical morphology

I. INTRODUCTION

Examination paper is the main method of modern education; it plays an important role from primary school to high school and college. Marking examination papers is not a light work. In college entrance examination several million papers should be marked in about two weeks. The work is burdensome. The teachers can not avoid making mistakes in marking examination papers. Other necessary procedures are used to check the examination papers. If the computer can mark the examination paper automatically, then the efficiency will be improved greatly.

Answer sheet in Standardized Test is the earlier method of recording the answer of objective items. The answer is marked with a special kind if pencil. The answer sheet is processed by the Optical Mark Reader (OMR). According to the voltage level of photo sensor, the mark can be distinguished. The answer sheet should be marked by special pencil and processed by special device. These characteristics will increase the cost of school and restricted the application. In fact a usual form of examination paper is shown in figure 1. The single choice question of part II in figure 1 is grouped in a form. If the answers can be processed automatically by computer, then the teachers can be relieved of heavy task. The complete analysis of figure 1 should include the processing of part I. This will involve the OCR of handwriting, which is a future research. In this paper the extraction of answer image of single choice questions is discussed.

II. PREPROCESSING

Slant Correction is the necessary step of image preprocessing. Several methods can be used, including projection method, Hough transform, Fourier transform etc.

The Hough transform is accurate method with strong robust [1][2]. But the calculation of Hough transform is time-consuming. In this paper the Hough transform is performed in two steps, firstly the oblique angle α is roughly calculated in degrees. Then more accurate angle is calculated in 0.1X degree in neighborhood of α.

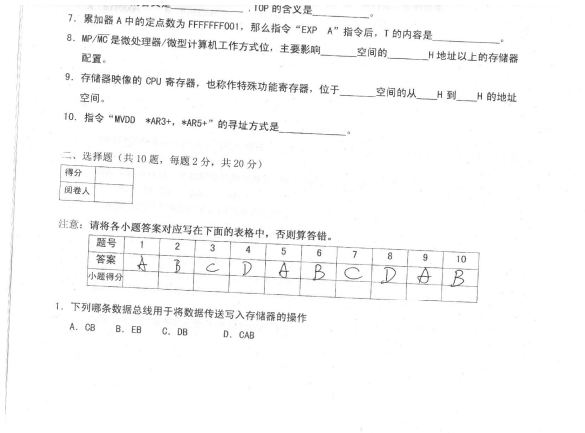

Figure 1 image of examination paper

Image binaryzation is the previous process of Hough transform. Edge detection is the usual algorithm of image binaryzation. But the edge detection can produce many details, as shown in figure 2. The form line is the useful information while the other edges of character have no effect. And the other edges could be regarded as form line. So in this paper the mathematical morphology methods are used to detect the form lines [3]. Firstly closed operation with horizontal mode is performed on the image; the approximate horizontal lines can be detected. Then image is converted to binary image and is corrected with previous methods with Hough transform, as shown in figure 3. Figure 4 is the corrected image.

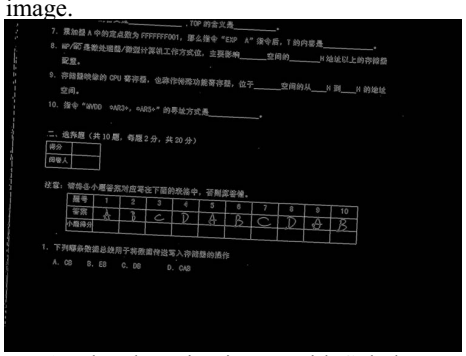

Figure 2 edge detection image with Sobel operator

978-0-7695-4818-0/12 $26.00 © 2012 IEEE
DOI 10.1109/DCABES.2012.69

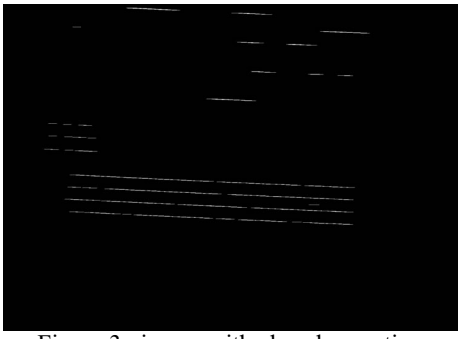

Figure 3 image with closed operation

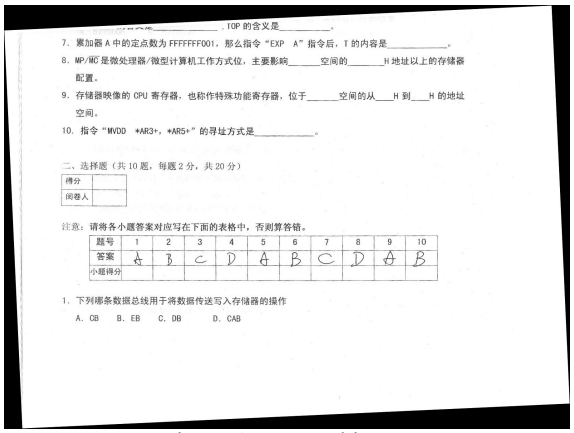

Figure 4 corrected image

III. LOCATION OF FORM

Usually the form region occupies fairly large size in the examination paper. The analysis based on connected domain can be used and the part with maximum area should be form. Of cause other big elements maybe produce large area, such as figures. So the length and number of horizontal lines should be considered as a factor to identify the form.

Firstly the horizontal lines and vertical lines are detected with mathematical morphology methods, and then dilation operation is performed to remove the effect of frame line breaks because of printing. The image is shown in figure 5. The form region is located with maximum and horizontal lines, and then the original image is cropped as shown in figure 6.

IV. ELIMINATION OF FRAME LINES

Elimination of frame line becomes difficult because of overlapping the character. In this paper the method proposed by Zhang is used to determine whether to reserve the frame line [4]. When character and frame line intersect, then the vertical gradient changes at the intersection. If the gradient of a point on frame line exceeds the normal threshold, then the point should be kept. Closing operation can be used to remove little objects. The image is shown in figure 7.

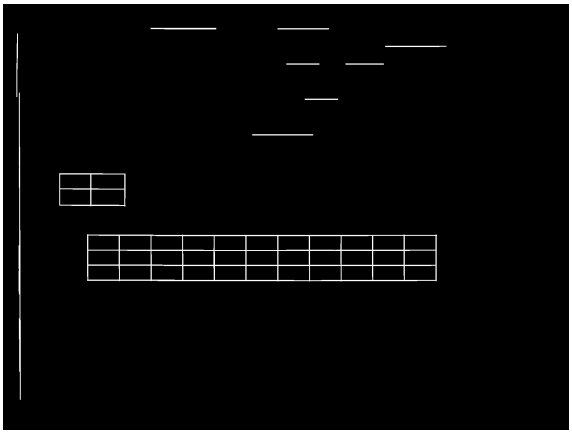

Figure 5 regions computed with morphology methods

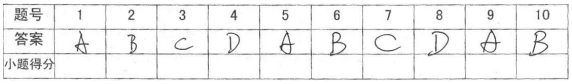

题号	1	2	3	4	5	6	7	8	9	10
答案	A	B	C	D	A	B	C	D	A	B
小题得分										

Figure 6 the form region

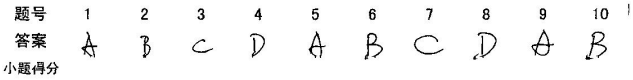

Figure 7 image after removal of frame lines

The connected component analysis is then used to determine the coordinate of each object, and then priori knowledge of answer position will locate the answers. The extracted images are shown in figure 8.

Figure 8 the final extracted images

V. CONCLUSION

In this paper, the answer image is extracted with several procedures, including slant correction, position of form, removal of frame lines, connected component analysis. The algorithm is tested with Matlab. The result shows the algorithm is functional and effective. The future research will be the recognition of the answers.

[1] Chandan Singh, Nitin Bhatia, Amandeep Kaur, "Hough transform based fast skew detection and accurate skew correction methods," Pattern Recognition, vol. 41, pp. 3528-3546, 2008.

[2] Huijie Fan, Linlin Zhu, Yandong Tang, "Skew detection in document images based on rectangular active contour," International Journal on Document Analysis and Recognition, vol. 13, pp. 261-269, 2010.

[3] Xiangyun Ye , Mohamed Cheriet , Ching Y. Suen , Ke Liu, "Extraction of bank check items by mathematical morphology," International journal on document analysis and recognation, vol.2,pp 53-66,1999.

[4] ZHANG Chong-yang, LOU Zhen, XU Yong, YANG Jing-yu, "Detection and removal of form lines from bill images," Computer Engineering and Design,Vol 26,pp 1778-1780,July 2005.

An Image Recognition Method Using Multi- features

Junjun Shang
Tianjin Polytechnic University
TJPU
Tianjin City, China
junjunyeti@yahoo.com.cn

Yongzhen Ke
Tianjin Polytechnic University
TJPU
Tianjin City, China
keyongzhen@tjpu.edu.cn

Abstract—For recognizing the objects in the image, the existing image recognition methods only can identify certain kinds of objects in the image recognition field and the recognition rate is also not high. This paper proposes an image recognition method which is based on shape feature and texture feature. This method divides the objects images into two types, foreground images and background images. Then extract shape features to foreground images and extracted texture features to background images. Finally match the extracted features with corresponding established feature library. This method uses Mahalanobis distance to match the objects in the images. Experiment results have proved that this method not only can identify several different kinds of objects but also has a good recognition rate.

Keywords: image recognition; feature extraction; texture feature; shape feature; moment invariants

I. INTRODUCTION

On the base of image processing and analysis, image recognition combines with artificial intelligence and pattern recognition theory to analysis the image. The existing image recognition methods mainly have three categories: statistical pattern recognition, structure pattern recognition, and the fuzzy pattern recognition [5].

With the development of image recognition technology, there have been many researches on the image recognition based on image characteristics so far. Based on the HU invariant moments, Wang Yan [7] proposed a method for recognizing blade pictures. This method's mean recognition rate has reached 87%. Based on color features and texture features, Zhang Tong used SVM (Support Vector Machine) to train outdoor scene pictures, and recognize them. Experiment result shows that Zhang Tong [13] improved recognition rate of the outdoor scene pictures. Based on the package features (Bag of Features), histogram and Gabor filter, Yanai [14] improved the image recognition rate of food pictures.

From above description, firstly researchers extract features of the objects in pictures. Then train image features and store the training results in a dataset. In order to achieve the purpose of image recognition, researchers finally match results with the data in the dataset [1] [3] [7]. But generally these recognition methods only can recognize a specific certain type objects, such as leaves, outdoor scene, foods, etc. This is because that the training dataset generally is limited to one certain kind of objects. If we want to recognize meanwhile several kinds of objects, we have to repeat the identification process many times with different objects' datasets. Apparently this is a tedious process.

To solve the above problems, this paper proposes an image recognition method which is based on the shape features and texture features. After segmenting the target image, we extract different features data from different regions according to the different attributes' important degree in different regions. Finally match these data with data in corresponding dataset. Thus we can obtain the recognition results. This method can identify different kinds of objects meanwhile, not a single kind of object. In addition, on the choice of texture attributes, we don't choose the frequently-used energy, entropy and the correlation attributes. But, through the experiment we choose the contrast, coarseness, linearity and directionality attributes. These four texture attributes can effectively separate different objects apart.

II. RELATED WORK

At present, there are a lot of researches on image features, such as SIFT (the Scale Invariant Feature Transform), color, texture etc. we can use these features to recognize image. Bayramoğlu[2] etc. put forward to a new matching method about range images. It uses local feature attributes and the geometry description of the local area. And combines SIFT feature and SI (shape index) together to match the object information in different sizes and directions. And further confirm objects in images.

Wang [3] etc. present a method which can identify and extract the tree image. The method combines color features and texture features. Firstly it takes use of filters to reduce noise. Then transform the Lab color space into three separated color channels. Based on 'a channel', they take a two-dimensional OTSU segmentation. Then, based on the texture information they extract the tree image. Finally, they use the mathematical morphology correction method to get the accurate tree images.

Yang [4] etc. present a method to extract texture features from different areas in binary images, with the combination of texture structure analysis method and the statistical method. Texture feature mentioned in paper [4] is gray level co-occurrence matrix (GLCM). GLCM includes fourteen attributes. Yang etc. extracted four attributes including energy, entropy, contrast, correlation. Theoretical analysis and experimental results showed that the texture feature extraction method has accuracy.

And Shi Jian-fang [6] etc. analyse and compares HU invariant moments, Zernike invariant moments and wavelet invariant moments. They took the research using BP neural network and the SVM for these moment invariants. And the experimental results proved that invariant moment had great superiority in recognition of the small sample. And the identification accuracy is high. Wang Yan [7] etc. use HU invariant moments to recognize the blade images. Firstly they took a preprocessing on the

978-0-7695-4818-0/12 $26.00 © 2012 IEEE
DOI 10.1109/DCABES.2012.54

blade images. Then they extracted geometric features, HU invariant moments. Lastly match different blade images using the correlation coefficient method. The method's average rate is 87%.

As above description, we can know that most researches for image recognition are based on the features' extraction on certain type objects. After training the features, match the target image to achieve image recognition [1] [3] [7]. But these methods only can recognize certain type objects from the image, not various objects. This paper do some research to this problem, and make an improvement on the choice of texture features.

III. RELATED THEORY

This paper mainly selects the texture features and shape features to describe objects in images.

The texture features are described by mathematical statistical methods. It reflects the spatial distribution on pixel level. This property generally includes the position of texture basic elements, correlation between pixels, regularity, linearity etc. If the object's surface has the same gray level or similar between the pixels, we assume the object has no texture. In order to describe the texture better, we firstly take quantification operation on the gray level.

We use shape features to describe object's outline. It is mainly realized through HU invariant moments. HU invariant moments are put forward by M.K.Hu. It is an invariant moment algorithm, and has the stability characteristics in condition of translation, rotation and zoom. At present, the invariant moments have become important characteristics and are widely used in image recognition [1]. It mainly represents geometrical characteristics of the object's shape. The first order moment is relevant to shape. The second order moment shows the expansion degree of the average, and the average comes from the curve which is around linear. The third order moment is about the measurement of average's symmetry.

For digital images, we assume the image's gray distribution is f (x, y), after discrete, the (p + q) order ordinary moments and center moments' formulas as follows:

$$m_{pq} = \sum_{x=1}^{M} \sum_{y=1}^{N} x^p y^q f(x,y) \quad \text{——————} (1)$$

Where, p,q=0,1,2,...

$$\mu_{pq} = \sum_{x=1}^{M} \sum_{y=1}^{N} (x - x_0)^p (y - y_0)^q f(x,y) \quad \text{———} (2)$$

Where, p,q=0,1,2,...

The normalized center moment:

$$y_{pq} = \frac{\mu_{pq}}{\mu_{00}^{r}} \quad \text{————————————} (3)$$

Where, $r = \frac{p+q+2}{2}$ p+q=2,3,...

Formula (1) and Formula (2) directly use ordinary moments or center moments to represent shape feature. This makes the features have not stability in the condition of translation, rotation and zoom at the same time. If we use the normalized center moment, the shape feature not only has stability in translation, but also has in zoom.

HU invariant moments use the second order moment and the third order to construct seven invariant moments. They keep translation, zoom and rotation invariant in continuous image [1], the formulas as follows:

$$HU_1 = y_{20} + y_{02} \quad \text{————————————} (4)$$

$$HU_2 = (y_{20} + y_{02})^2 + 4y_{11}^2 \quad \text{————————————} (5)$$

$$HU_3 = (y_{30} + 3y)^2 + (3y_{21} - y_{03})^2 \quad \text{————————————} (6)$$

$$HU_4 = (y_{30} + y_{12})^2 + (y_{21} + y_{03})^2 \quad \text{————————————} (7)$$

$$HU_5 = (y_{30} - y_{12})(y_{30} + y_{12})[(y_{30} + y_{12})^2 - 3(y_{21} + y_{03})^2] + (3y_{21} - y_{03})(y_{21} + y_{30})[3(y_{30} + y_{12})^2 - (y_{21} + y_{03})^2] \quad \text{————————————} (8)$$

$$HU_6 = (y_{20} - y_{02})[(y_{30} + y_{12})^2 - (y_{21} + y_{03})^2] + 4y_{11}(y_{30} + y_{12})(y_{21} + y_{03})] \quad \text{————————————} (9)$$

$$HU_7 = (3y_{21} + y_{03})(y_{30} + y_{12})[(y_{30} + y_{12})^2 - 3(y_{21} + y_{03})^2] + (y_{30} - 3y_{12})(y_{21} + y_{30})[3(y_{30} + y_{12})^2 - (y_{21} + y_{03})^2] \quad \text{————————————} (10)$$

IV. PROPOSED METHOD

Before recognizing objects in complex images, we need to choose the appropriate texture information and shape information's description method. And the texture information and shape information's description method also influence objects' recognition rate. So firstly we select appropriate methods to describe texture information and image information. In this paper, through experiments we select four texture features as the texture descriptors. These four features can divide different objects better as the texture descriptors [4] [8] [10] [11]. For shape information, we select HU invariant moments as the shape descriptors [1] [9].

After selecting the appropriate texture descriptors and shape descriptors, the following work is to establish the texture matching library and shape matching library. At this phase, we train the shape features which are extracted from MPEG library. Then take the trained shape features as shape matching library. For the texture matching library, we train texture features which are extracted from texture images (texture image includes BRODATZ library and other image from Internet). Then take the trained texture features as texture matching library.

After establishing the shape matching library and the texture matching library, the next work is to recognize test image. In recognizing phase, firstly we segment the test image. The purpose of segmenting is to divide the test image into several meaningful regions. We call these meaningful regions as ROI (regions of interest). Then we divide the ROI into foreground regions and background regions two categories. For the foreground regions, we extract shape features; for the background regions we extract texture features. Finally, match the extracted features to corresponding matching library. To be specific, match the features which are extracted from the foreground regions with shape matching library; match the features which are extracted from background regions with texture matching library. Take the matching result as the recognition result. The design method is shown in Figure 1.

Figure 1 is the overall design method. The following describes the concrete processing steps how to recognize the objects in image.

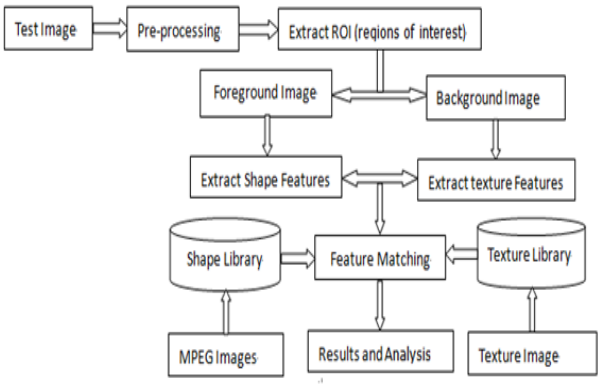

Figure1. Designed method

A. *Pre-processing*

The pre-processing mainly is segmenting the target image. Then we can obtain several meaningful regions, called ROI. The ROI can be divided into the background regions and foreground regions. The following work, extracting feature, are based on the two types of regions.

In this paragraph we'll describe how to obtain the ROI. We get ROI through image segmentation. In order to correctly segment image, this paper manually annotated the pixels. Based on these annotated pixels, procedure automatically divide target image into several different regions. These different regions are ROI. The specific steps are manually annotated pixels on boundary of different regions. According to the marked pixels, procedure can return several polygon regions, and these polygon regions are ROI. Finally we do normalized operation on ROI. Then we divide ROI into foreground regions and background regions.

B. *Feature Extraction*

We extract different features to foreground regions and background regions. These two kinds of regions are from ROI. For background regions, we extract image texture features. For foreground regions, we extract shape features. We use HU invariant moments to present shape features.

Before extracting texture features form background regions, transform the background regions' image into gray image. Due to the image gray level generally is 256, the image data is big and the mass data increase the computation. Therefore, we compress the gray level to 16 and then extract texture features. We use the contrast, coarseness, linearity, directionality degrees to describe texture attributes. These four attributes belong to GLCM [8] [10] [11].

Before extracting the shape features, transform the foreground regions' image into the image which is same to the image in MPEG library. The transform is realized through pixel conversion. We then extract seven HU invariant moments [9].

C. *Classification and Recognition*

Mahalanobis distance can effectively calculate the similarity of two unknown samples. It considers the correlation between data and various characteristics in computational process. It is proposed by Indian statistician p. c. Mahalanobis. Mahalanobis distance can present the covariance distance. Therefore, we use Mahalanobis distance to recognize image [12].

We use the formula (11) to calculate the Mahalanobis distance between sample i and sample j. Formula (11) is Mahalanobis distance's formula:

$$D_{ij} = \sqrt[2]{(x_i - x_j)^T S^{-1} (x_i - x_j)} \quad \text{——————} (11)$$

Where, x_i and x_j is a vector which is consist of m attribute data. The m attribute data are from sample i and sample j. S is sample's covariance matrix.

V. EXPERIMENT AND RESULTS ANALYSIS

The experiment is operated on MATLAB environment. And the texture matching library and the shape matching library is extracted separately from the BRODATZ library and the MPEG library. The test image is got from the Internet.

To recognize the test image, Figure 2, we need to extract corresponding texture features and corresponding shape features. The corresponding texture feature data in the texture matching library is showed in Table I and the corresponding invariant moment data in shape matching library is showed in Table II. And the results of the test image's features are showed in Table III.

Figure2.Test image

A. *Texture Features*

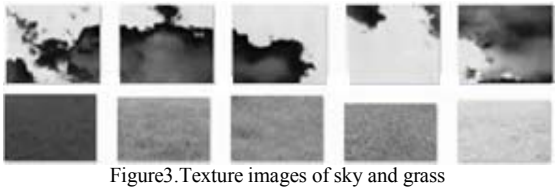

Figure3.Texture images of sky and grass

Figure 3 is texture images in the BRODATZ library (top five) and texture images which are got from the Internet (back five). According to methods in [3] and [4], we extract energy, entropy, the correlation from four different angles on images in Figure 3. The four angles respectively are 0^0、45^0、90^0、135^0. And the extracted energy, entropy, the correlation data are shown in Table I. According to Table I, we draw the corresponding texture distribution which is shown in Figure 4. Then extract contrast, roughness, linearity, directionality based on images in Figure 3. The contrast, roughness, linearity, directionality data is shown in Table II. According to Table II, we draw the corresponding texture distribution that is shown in Figure 5.

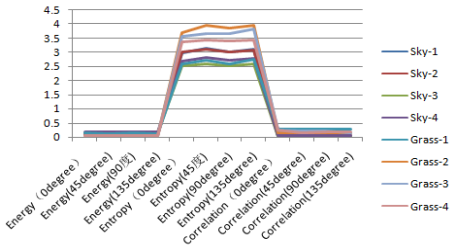

Figure4.Texture features（energy, entropy and the correlation）

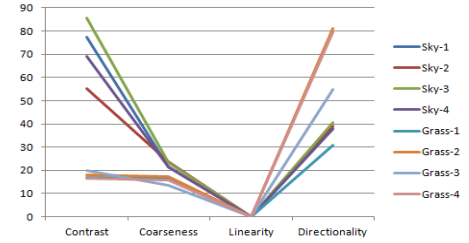

Figure5. Texture features（contrast, coarseness, linearity and directionality

From the above two figures, we can observe that, energy, entropy, and the correlation, cannot obviously distinguish objects in Figure 4. In Figure 5, the contrast, roughness, linearity, the directionality can distinguish different objects [8] [10] [11]. Therefore, this paper selects the texture features in Figure 5 to describe texture.

B. Shape Features

Figure 6 is the template images of horse and people in MPEG library. We extract invariant moments. The invariant moments' data are shown in Table III.

According to the data in Table III, we can draw the invariant moment distribution as shown in figure 7. From Figure 7, we can observe that different objects have different nvariant moment distribution. So we can recognize objects based on invariant moments.

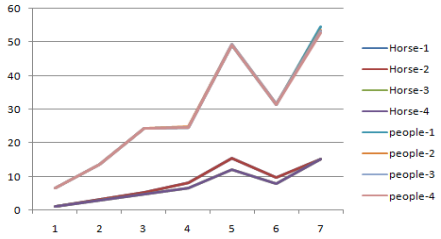

Figure7. Invariant moment distribution

C. Recognition and Testings

In this phase, we mainly use the texture matching library and the shape matching library to recognize images. Experiment environment is MATLAB. To the test image, that is Figure 2, we obtain the ROI. The ROI are show on Figure 8 and Figure 9. Where, Figure 8 is foreground regions and Figure 9 is the background regions of Figure 2. We take pixels conversion on Figure 8 and the result is show as Figure 10.We convert Figure 9 to gray- level image and the result is show as Figure 11.

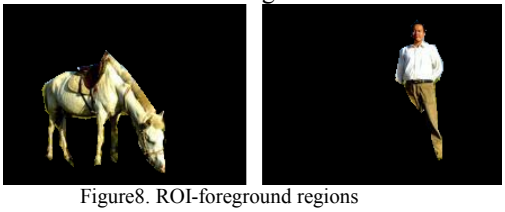

Figure8. ROI-foreground regions

Figure9. ROI-background regions

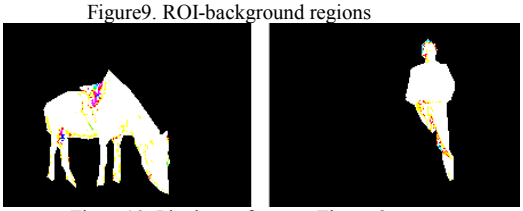

Figure10. Pixel transform on Figure 8

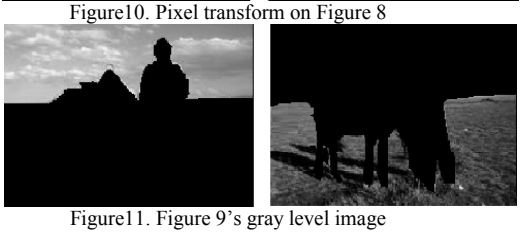

Figure11. Figure 9's gray level image

For the Figures 8~ Figures 11, we extract invariant moments information on Figure 10 and get Table IV. Extract texture features on Figure 11 and get Table V.

Lastly, we classify the data in Table IV and Table V. The classification results are the results of the image recognition.

Figure 6.Template images of horse and people

TABLE II. TEXTURE FEATURE DATA (CONTRAST, COARSENESS, LINEARITY AND DIRECTIONALITY) OF SKY AND GRASS

Sample	Contrast	Coarseness	Linearity	Directionality
Sky-1	77.18906	21.47708	0.023588	38.10612
Sky-2	55.3765	23.7228	0.028568	39.0259
Sky-3	85.65026	23.17529	0.037517	40.45605
Sky-4	69.17744	21.60277	0.042927	37.86732
Grass-1	17.08617	16.37895	0.043644	30.85968
Grass-2	17.9223	17.22926	0.079098	81.17303
Grass-3	20.04628	13.49141	0.035175	54.86959
Grass-4	16.48188	15.80318	0.042843	79.44685

TABLE V. TEXTURE DATA (CONTRAST, COARSENESS, LINEARITY AND DIRECTIONALITY) ON TEST IMAGES

Texture Features	Contrast	Coarseness	Linearity	Directionality
The first image in Figure.11（sky）	22.03486	10.07434	0.076399	15.28941
The second image in Figure.11（grass）	18.39103	10.09522	0.141094	59.18242

Table I. TEXTURE FEATURE DATA (ENERGY, ENTROPY AND THE CORRELATION) OF SKY AND GRASS

Sample	Energy				Entropy				Correlation			
	0^0	45^0	90^0	135^0	0^0	45^0	90^0	135^0	0^0	45^0	90^0	135^0
Sky-1	0.110967	0.104167	0.11021	0.105944	3.009893	3.158134	3.023252	3.121529	0.035794	0.035525	0.035782	0.035572
Sky-2	0.076878	0.072158	0.076412	0.072997	3.004517	3.117929	3.033072	3.089519	0.051851	0.051519	0.051699	0.051647
Sky-3	0.151357	0.147128	0.150574	0.147334	2.522679	2.602038	2.545337	2.587173	0.029769	0.029662	0.029756	0.029705
Sky-4	0.166795	0.16112	0.167669	0.162254	2.694255	2.829065	2.731755	2.784815	0.038495	0.038178	0.038462	0.038293
Grass-1	0.124171	0.111455	0.127041	0.107453	2.60164	2.720566	2.579505	2.757326	0.278186	0.274656	0.283773	0.27217
Grass-2	0.044059	0.033486	0.036062	0.033144	3.703893	3.945188	3.864066	3.951272	0.125555	0.115046	0.119898	0.115057
Grass-3	0.044056	0.040924	0.04022	0.033842	3.568111	3.661034	3.671569	3.826371	0.221672	0.192184	0.193119	0.126435
Grass-4	0.052126	0.047887	0.048858	0.047874	3.356188	3.425569	3.404441	3.418225	0.231783	0.155724	0.1868	0.168666

Table III. INVARIANT MOMENTS DATA ON MPEG TEMPLATE IMAGES

Sample	HU1	HU2	HU3	HU4	HU5	HU6	HU7
Horse-1	1.124366	3.289528	5.263642	8.128252	15.35925	9.773036	15.03422
Horse-2	1.124345	3.289351	5.263602	8.130277	15.3625	9.774973	15.03711
Horse-3	1.069157	2.788709	4.878987	6.496839	12.18668	7.959953	15.29078
Horse-4	1.068872	2.788166	4.877985	6.498011	12.18801	7.961402	15.27435
People-1	6.648094	13.59431	24.34377	24.70289	49.22623	31.50184	54.57988
People-2	6.653955	13.609	24.42692	24.77374	49.3742	31.57829	53.47498
People-3	6.662685	13.63207	24.33685	24.70283	49.22283	31.52008	53.24401
People-4	6.667318	13.64488	24.28398	24.69487	49.18465	31.52511	52.80203

TABLE IV. INVARIANT MOMENTS DATA ON TEST IMAGES

Invariant Moments	HU1	HU2	HU3	HU4	HU5	HU6	HU7
The first image in Figure. 10 （horse）	1.221386	3.998284	5.559063	10.3727	23.0161	13.1064	18.33864
The first image in Figure. 10 （people）	6.638446	13.59809	23.87502	24.63586	48.89222	31.60974	52.13744

After training 680 template images in the MPEG library (20 images for each object, a total of 34 objects) and 110 of texture images (these texture images contains 90 images in BRODATZ library, and 20 images on the Internet, a total of 15 objects), recognize complex images on the Internet. The final results show that the method achieves the highest recognition rate to 94.87%, the lowest rate of 83.97%. Though this method's recognition rate is almost the same as other methods, but the highest recognition rate is high. And it can recognize several types of objects meanwhile.

VI. CONCLUSION

Because of invariant moments have the stability characteristics in condition of translation, zoom and rotation, this paper combines with invariant moments and texture features to recognize image. The proposed method not only can recognize multiple kinds of objects, but also improves the recognition rate. However, when we transform background images into gray image, a number information will be lost and this will have an influence on the result of the recognition. So how to minimize the influence will be the following major work.

REFERENCES

[1] Han Jian-ning, W.M., Research on Digital Image Recognition System Based on Multiple Invariant Moments Theory and BP Neural Network, International Asia Conference on Informatics in Control , Automation and Robotics. IEEE. 2010. p. 399-403.

[2] Bayramoğlu, N.A.A.A., Shape Index SIFT: Range Image Recognition Using Local Features, in Pattern Recognition (ICPR), 2010 20th International Conference. 2010: Istanbul. p. 352 – 355..

[3] Wang, X., X. Huang and H. Fu, A Color-Texture Segmentation Method to Extract Tree Image in Complex Scene, in Machine Vision and Human-Machine Interface (MVHI), 2010 International Conference. 2010. p. 621 – 625.

[4] Yang, J. and J. Guo, Image Texture Feature Extraction Method Based on Regional Average Binary Gray Level Difference Co-occurrence Matrix, in Virtual Reality and Visualization (ICVRV), 2011 International Conference. 2011: Beijing. p. 239 - 242.

[5] Haralick, R.M. and L.G. Shapiro, Image segmentation techniques. in Elsevier, 1985. 29(1): p. 100–132.

[6] Shi Jian-fang, S.B., Research on Image Recognition Based on Invariant Moment and SVM, in Pervasive Computing Signal Processing and Applications (PCSPA), 2010 First International Conference. 17: Harbin. p. 598 - 602

[7] Wang Yan, Z.X., Leaf Image Recognition Technology Research Based on HU Invariant Moments. in Intelligent Control System and Its Application, 2011(6): p. 70-72.

[8] Zhao Hai-ying, X.G.M.,P.H., Performance Evaluation for the Algorithms to Measure Texture Coarseness. in Computer Science, 2011. 38(6): p. 288-292

[9] Rai, H.G.N., et al., Hybrid Feature to Encode Shape and Texture for Content Based Image Retrieval, in Image Information Processing (ICIIP), 2011 International Conference. 3: Himachal Pradesh. p. 1 – 6

[10] Gupta, A.G.M. and A. Mittal, A Comparative Performance Evaluation of Segmented Image with Obstacle for Textural Coarseness, in Computational Intelligence and Computing Research (ICCIC), 2010 IEEE International Conference. 28: Coimbatore. p. 1 - 6

[11] Hao. C., An Efficient Image Editing Method Based on Texture Regularity and Synthesis. in Institute of Computing Technology, 2012. 24(2): p.183-190.s

[12] Zhang, X., Mahalanobis Distance Metric Based Laplacian Mapping for Image Recognition, in Internet Computing for Science and Engineering (ICICSE), 2010 Fifth International Conference. 1: Heilongjiang. p. 1 – 5.

[13] Zheng Meng-xing, X.J.,Z.T., Recognition of Outdoor Scene Image Features Based on SVM. in Computer Simulation, 2011. 28(4): p. 250-253 339.

[14] Yanai, H.H.T.J., Image Recognition of 85 Food Categories by Feature Fusion, in IEEE International Symposium on Multimedia. 2010. p. 296-301..

Parallel Hierarchical K-means Clustering-based Image Index Construction Method

Yuan-feng Yang[1,2], Jian Wu[1,2], Jing Fang[2], Zhi-ming Cui[1,2]
1.JiangSu Province Support Software Engineering R&D Center for Modern Information Technology Application in Enterprise, Suzhou, China, 215104
2.The Institute of Intelligent Information Processing and Application, Soochow University, Suzhou, China, 215006
e-mail: jianwu@suda.edu.cn

***Abstract*—Content-based image retrieval often uses the integration of various features. The characteristic dimensions are up to hundreds of dimensions. The capabilities for image representation、storage、 management far exceed that of the database. Retrieval and matching of large-scale image are the urgent problems which need to be solved. To solve the construction of image indexing of large-scale image retrieval, this paper introduces a parallel level K-means clustering method. Firstly, image clustering based on the level K-means reduces the size of matching data in retrieval; secondly, considering the inherent defects in the cluster, we put forward optimization program and calculate cluster rapidly with parallel computing algorithms. The experimental results show that this method can quickly build a massive image index for fast image retrieval.**

Keywords-image feature; index constructing; K-means; parallel computing

I. INTRODUCTION

Image retrieval system based on the content applies computer vision、machine learning and pattern recognition techniques in the retrieval of large-scale image data. During the retrieval process, the size of the image library is often millions; the image and its characteristics, storage and matching will have a huge impact on system performance.

Clustering methods and parallel processing technology have played a more significant role in many aspects, such as text retrieval, calculation of large-scale data. Its theories and methods of research have made great progress in recent years, and dozens of clustering algorithms have been proposed and continue to be improved. They are based on different theories and methods for different issues and areas and application system for specialized image cluster analysis have been raised. Main cluster analysis methods are outlined below.

(1) Level approach: the given data object collection is divided into multiple levels; partitioning clustering for collections of different levels; outputs are the hierarchical classification trees. According to the formation of hierarchical decomposition, two types can be divided: cohesion classes and split classes. The shortcomings of the hierarchical method are that: once a step (merge or split) is completed, the operation can't be undone, that is, the operation is not reversible. Common methods are BIRCH[1] and CURE, etc.

(2) Split method: also known as partitioning clustering. Build multiple partitions for given data collection; using the method of iterative positioning, divide an object from a class to another to optimize the quality of segmentation. Common methods are K-means、K-medoids[2] and CLARANS, etc.

(3) Density-based approach: this density can generate clustering based on the density function or the unique density of object in the field. Common algorithms are DBSCAN、OPTICS、DENCLUE, etc.

(4) Grid-based methods: quantify spaces of object data into a limited number of units with multi-resolution mesh data. All cluster operations are carried out in the quantization unit. Usually processing speed of this method is only related to the quantification spatial unit. Common algorithms are STING、STING+ and CLIQUE, etc.

This paper presents a parallel level K-means clustering method to solve the problem of excessively high cost of data and time-consuming of back-office processing and user feedback. Firstly, we introduces image clustering method based on the level K-means; generate a search query tree; retrieve domain is divided into multi-layer and multi-subdomain in order to reduce the scale of retrieval and matching. Secondly, calculate optimal solution of cluster by parallel algorithm of K-means clustering. The experiments show that the proposed method can improve the efficiency of large-scale data retrieval.

II. IMAGE CLUSTERING METHOD BASED ON HIERARCHICAL K-MEANS

K-means is first proposed by MacQuen[3] and has been widely used for its simple and rapid calculation. Assume that time complexity of calculation is $O(tKmn)$, where t is the number of iterations, K is the number of clusters, m is the characteristic dimension, n is the amount of data to be classified, under normal circumstances $K, m, t << n$. There are huge amount of data in the practical application systems. Hierarchical clustering and partitioning clustering are combined with multi-layer K-means clustering method to cluster large-scale image database index. Firstly, extract feature vectors of all the images n in the image library as the data type of the clustering. Randomly select data $c_1, c_2, \ldots, c_k$ as the first layer of the cluster center. Make clustering for all data and steps are :

978-0-7695-4818-0/12 $26.00 © 2012 IEEE
DOI 10.1109/DCABES.2012.35

(1) Initialize the cluster centers. Randomly select data $c_1, c_2, \ldots, c_k$ as the cluster center.

(2) Classify the remaining data x_i . For each of the remaining data x_i , calculate the distance to each cluster center and choose the closest cluster center c_v .The category c_v of is assigned to that of x_i ; update cluster center c_v ; c_v is updated into a new central location.

(3) Calculate the variance D , $D = \sum_{i=1}^{n} [\min_{r=1,\ldots,K} d(x_i, c_r)^2]$. Determine the convergence of the variance. If is convergent, return classification results $c_1, c_2, \ldots, c_k$; perform step(4); otherwise perform step (2).

(4) Perform the underlying clustering. If the number of class members of $c_1, c_2, \ldots, c_k$ is greater than the threshold Thd ; perform step(1); otherwise perform step (5).

(5) Return number of sub-class and upper class; generate the search query tree and save vector $\boldsymbol{T}_j$ (cluster center of that layer) of each bifurcation.

Ideally, multi-class, multi-level search query tree from hierarchical K-means clustering image library has formed nodes of automatic clustering with semantic. When a user submits a query image, system extracts image features. Firstly, classify images of sparse representation into each category; calculate distance of image feature and center vector of the query tree for each layer by Euclidean distance to the nearest cluster until the leaf subclass; match feature for image of leaf subclass to get similarity sorting and return the result.

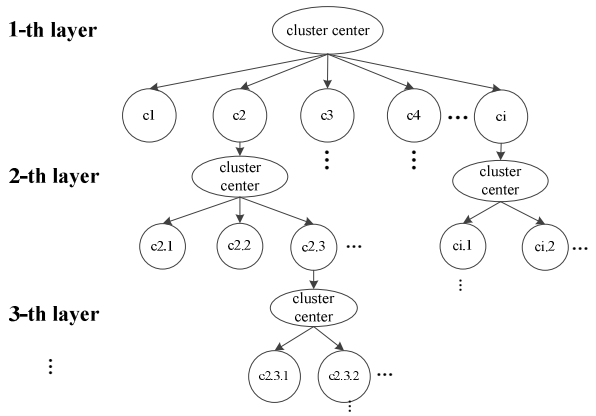

Figure 1 Retrieval query tree generated by hierarchical K-means

III. PARALLEL COMPUTING OF IMAGE CLUSTERING

A. Hierarchical K-means Problem

Although in the previous section we used K-means in processing large-scale data, there are a variety of shortcomings itself. Mainly in the following areas:

(1) In initialization, the initial cluster centers randomly selected、the number of clusters and the input sequence of data will affect the clustering results;

(2) The algorithm can't guarantee to find the best solution to locate the cluster centers, but can guarantee convergence to a solution;

(3) The algorithm assumes that the spatial covariance matrix has been normalized, therefore we are unable to determine importance of data's attribute.

(4) Variance may cause the jitter of the cluster center and the results are only circular distribution.

Despite a lot of the improvement on K-means clustering algorithm[4], such as variants of two points and K-means clustering algorithm, most of them belong to the based on the "interpreting variance of the data" and better clustering optimal solution can't be proposed. Each cluster center has its data members; calculate the variance of the class; the optimal solution minimizes variance with smaller complexity. Therefore, solving the problem can be improved as follows:

(1) Calculate the K-means several times and each initial cluster centers take a different random value.

(2) The first category is set to 1, then we increase the number of categories (up to a limit) and each cluster uses the method in (1). Under normal circumstances, the total variance declines very rapidly until reaching the inflection point; save the number of categories.

(3) Normalize data by multiplied by the inverse covariance matrix.

B. Image Clustering Method Using Parallel Computing

Parallel computing is a process using a variety of computing resources to solve the problem of computing and other non-computing. Parallel computing can be divided into two types of technologies: one is time parallel based on pipeline technique; one is spatial parallel based on concurrent execution of multi-processing resources. From the point of view of algorithm designers, parallel computing can be divided into two categories - data parallelism and task parallelism. Data parallelism is to split the large amount of data into small amount of data; task parallelism is to resolve a big task into a number of the same sub-task processing. Physical environment of parallel computation do not have a unified computational model. Several valuable models are: PRAM、the BSP and C^3,etc[5].

Optimization algorithm proposed in the previous section shows that time-consuming of clustering is bottleneck of the overall system. The paper considers this as a focus of parallel computing to achieve the enhancement of retrieval performance of system clustering. In the clustering process, we use computing cluster consisted by multiple hosts to process clustering to improve the efficiency of clustering. Computing in parallel environments, supporting parallel computing algorithm need to match the above problems. Considering above problems, we study parallel computing algorithms of the hierarchical k-means clustering and design an effective solution. Compared with existing methods[6,7], our method uses a task parallel mode to ensure the optimality

of the results, not dividing all data, and it has a simple calculation steps with high efficiency.

The algorithm uses the master-slave mode, and it is divided into two parts -the master and slave. Assume that the number of slave is K ; the initial data set is S_0 ; i is the level of cluster; initialization time-consuming of nodes of clusters is T_{startup} ; transmission time-consuming of unit data unit (such as 4-byte) is T_{data} ;clustering time-consuming of data is T_{kmeans} ;the specific process is as follows:

The parallel K-means clustering	Time complexity
Host：（$i=0$， $j \in N$）	
1.select K samples of N classes as initial cluster centers from S_i;	$T_{\text{startup}}+$
2.send data set S_i and initial cluster centers of the j-th class to the j-th slave machine;	$S_i \cdot T_{data}$
3.accept D_i from N slave machines;	T_{startup}
4.get D_i returned by slave and save the classification results;	$T_{\text{startup}}+$
5.$i=i+1$;	$S_i \cdot T_{data}$
6.Judge end conditions; if satisfied, perform step (7), or re-perform step (1);	
7. Save the final result, and the process is over.	
Slave j：	$T_{\text{startup}}+$
1.accept data set S_i and initial cluster centers of the j-th class;	$S_i \cdot T_{data}$
2.calculate K-means clustering according available parameters；	$S_i \cdot T_{kmeans}$ / S_0
3.return D_i to host machine and wait for the results；	T_{startup}
4.discard the result if D_i is not least, or perform step(5) ;	
5.return the results of S_i to host machine and wait for the next task.	$T_{\text{startup}}+$ $S_i \cdot T_{data}$

IV. EXPERIMENTAL RESULT AND ANALYSIS

The study content of this paper is combined with practical application projects. The experimental data from the Internet site by crawling reptiles tool, mainly about various types of men and women shoes. These pictures cover almost all type of shoes in the market. The amount of data is about 50000 images.

In parallel computing, parallel platform can be divided into: based on shared address space platforms and based on message interlink[8]. The former generally needs support from the SPMD programming, with multiple processors, shared address space, higher cost and strong performance, such as massively parallel processor (MPP). The parallel platform based on message interlink generally consists of multi-processing nodes, each has its own independent address space, with lower cost and easy structures, such as a network of workstations clusters (NOW). This experimental project uses the latter platform to apply for the use of Suzhou University High Performance Computing and Applications [9] The Twilight of high-performance cluster as the experimental environment. The experimental tools include Matlab R2010b, Linux, Gcc, OpenMPI v1.4.5[10], and OpenCV 2.0. The process for the parallel algorithm shown in Figure 2.

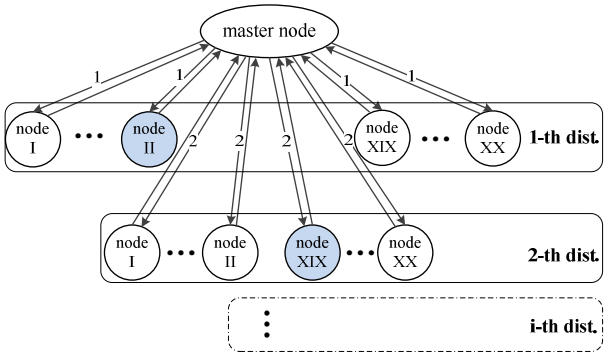

Figure 2 The parallel algorithm process diagram

Depending on the cluster experimental environment, the design of implementation process of the parallel clustering algorithm system shown in Figure 2. Firstly, determine the number of slave-nodes which need to apply for parallel computing (this time we excerpt with 20 sub-nodes).If the apply is successful, the host node will initialize the cluster centers, distribute data sets and different initial cluster centers to different slave nodes. Then the slave nodes do the k-means clustering calculation, return the clustering result to the host, thus far as the first distribution and calculation. Secondly, the host receives the results for screening, and does the same operation as a second distribution and calculation. As above, the i-th times distribution and calculation will be done in turn. The host node is mainly responsible for data distribution, receiving and screening. The slave nodes are mainly responsible for the calculation of the data.

Set the time complexity of serial k-means clustering is $O(x)$. Ideally, the time complexity of the above improved algorithm as the same scale will be $O(x/N)$. N is the number of slave nodes.

Table 1 Serial and parallel clustering speedup using five nodes with different amount of data

Cluster scale(K)	Serial cluster time(K)	parallel cluster time (M)	speedup
1	0.6	0.2	3.00
2	1.3	0.4	3.25
5	3.1	0.9	3.44
10	6.9	1.9	3.63
20	15.1	4.0	3.78
50	42.0	10.7	3.92
100	91.0	20.6	4.41

(Note: unit K is 1000, M represent minute)

Consider the fact that the comparison of serial and parallel speedup has the significance of evaluation only when the computer's hardware configuration should be the same. So in this section the serial clustering will be running on the master node of the cluster. The following data is experiment of serial, parallel clustering speedup with different data size,

and different number of nodes. Table 1 shows serial and parallel clustering speedup using five nodes with different amount of data.

Table 2 shows the speedup of serial and parallel clustering when faced with different amount of data, using 20 nodes.

size of the cluster(K)	time-consuming of serial clustering(K)	time-consuming of parallel clustering(M)	speedup
2	1.3	0.1	10.0
5	3.1	0.2	12.5
10	6.9	0.5	13.9
20	15.1	1.0	14.9
50	42.0	2.6	15.8
100	91.0	5.5	16.5
200	213.0	12.2	17.5
400	460.0	24.0	19.1

(Note: unit K is 1000, M represent minute)

From table 1 and table 2, we can know that the speedup is located between 3.0 to 4.4 when using five nodes and located in the 10.0 to 19.1 when using 20 nodes. Regardless of the number of nodes, the speedup is always higher values in the large amount of data due to large communication overhead between the nodes. The proportion of node communication overhead by the total time-consuming is lower with large amount of data and the speedup is higher. It is worth noting that when dealing with small amount of data (such as 2000), the number of nodes increases 4 times but the speedup has not been a corresponding increase. Parallel clustering methods with 20 nodes to deal with massive amount of data can still get higher speedup.

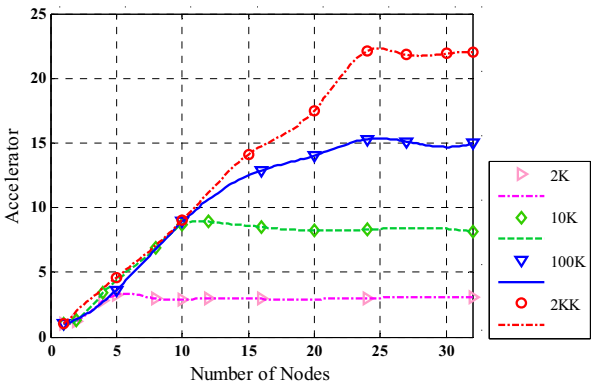

Figure 3 the speedup of different data size with different nodes

Figure 3 shows the speedup of different data size with different nodes. It can be seen from the figure speedup is not increasing with the node's increase. There are certain obstacles values. Increasing the number of nodes is useless to improve the speed of parallel clustering. Obstacles values can be different with different data size.

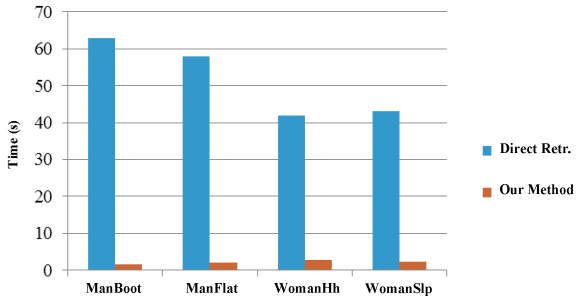

Figure 4 comparison of retrieval time before and after optimization

Figure 4 shows the comparison of retrieval time before and after optimization. Direct retrieval uses the primary index constructed by Lucene. The figure shows the retrieval time has greatly improved in the large-scale data processing.

V. CONCLUSION

This paper describes the efficiency of the image retrieval system in the face of large-scale data retrieval, and proposes k-means image clustering method based on level to generate the search query tree, to retrieve the domain which is divided into multi-layer, multi-subclass and to reduce retrieval match scale. Secondly, to solve the problem that k-means clustering used in excessive dependence on initial conditions and cannot obtain the optimal clustering, we complete the parallel algorithm of means clustering on the parallel computer and achieve the optimal clustering. Finally, we combine the project of building a experimental environment of large-scale image data with an image retrieval system for footwear dataset. The experimental results show that the proposed method can improve the efficiency of large-scale data retrieval.

ACKNOWLEDGMENT

This research was partially supported by the Natural Science Foundation of China under grant No. 60970015, 61003054 and 61170020, the opening project of Jiangsu Province Support Software Engineering R&D Center for Modern Information Technology Application in Enterprise under grant No. SX201102 and SX201202, the Program for Postgraduates Research Innovation in University of Jiangsu Province in 2011 under grant No. CXLX11_0072, and the Beforehand Research Foundation of Soochow University.

REFERENCES

[1] Zhang T, Ramakrishnan R, Livny M. BIRCH: An efficient data clustering method for very large databases[C], ACM Special Interest Group on Management of Data, 1996, 25(2):103-114.

[2] Chu S C, Roddick J F, Chen T Y, et al. Efficient search approaches for K-medoids based algorithms[C], IEEE Region 10 Annual International Conference, 2002:712-715.

[3] MacQueen J B. Some methods for classification and analysis of multi-variant observations[C]. The 5th Berkeley Symposium on Mathematical Statistics and Probability, 1967: 281-297.

[4] Savaresi S M, Boley D. On the Performance of Bisecting K-Means and PDDP[C]. Proc. of the 1st SIAM International Conference on Data Mining, 2001:1-14.

[5] JI Yong Chang, DING Wei Qun, CHEN Guo Liang, AN Hong. A Realistic Parallel Computational Model[J]. Chinese Journal of Computers, 2001, 24(4):437-441.

[6] Ni Weiwei, Lu Jieping, Sun Zhihui. An Effective Distributed k-Means Clustering Algorithm Based on the Pretreatment of Vectors Inner-Product[J]. Journal of Computer Research and Development, 2005, 42(9):1493-1497.

[7] Kantabutra S, Couch A L. Parallel K-means clustering algorithm on NOWs[J]. NEC-TEC Technical journal, 2000:1(6):243-247.

[8] Ananth G, George K, Vipin K, et al. Introduction to Parallel Computing (2nd Edition) [M]. USA: Addison Wesley, 2003.

[9] http://hpc.suda.edu.cn.

[10] http://www.open-mpi.org.

A Research on Foam-Detection Based on Image Analysis in the Process of Sewage Treatment

Liang Zhu
Computer Department, Chongqing Industry Polytechnic College,
Computer College, Chongqing University,
Chongqing ,China
e-mail: Kcsj_2005@126.com

***Abstract*—At present, suspended solids and temperature detected by sludge concentration meter in sewage are commonly used as operational status data of oxidation pond in Chinese sewage treatment works. But there are some problems in this method such as the inaccuracy of detection and difficulty of maintenance. Therefore, the method of foam-detection based on image analysis in the process of sewage treatment analysis is introduced in this article and by which we can get the operational status of oxidation pond. It turned out that the Rate of Foam was better calculated with this method and the accuracy met the operational requirements.**

Keywords-sewage treatment; image analysis; foam-detection

I. INTRODUCTION

With the strengthening of environmental protection awareness, the technology of sewage treatment has become a hot spot in recent years. At present, the improved biochemical process of oxidation ditch is popularly adopted by sewage treatment works in China. And sewage treated in this way can reach the emission standard of first national level, B class. Committed steps of sewage treatment thereinto is to degrade organics and to take off phlegm when sewage circulates around oxidation ditch and repeatedly flows through aerobic zone and anoxic zone. Meanwhile, the proper control over dose of medicine means a lot. Either deficiency in dose or overdose will make trouble. Traditionally, the dose of medicine relies on data status such as the suspended solids and temperature detected by sludge concentration meter. But this method is unreliable. First of all, sludge concentration meter is fixed on the wall of oxidation pond, besides, sewage in the pond is not homogenous. Accordingly, the data detected by sludge concentration meter can hardly stand for the whole status of oxidation pond. Second, the measuring section of sludge concentration meter is easily encased by contaminants, causing deviation. So, it needs washing frequently. Third, the foul smell will do harm to field personnel if they stay there for times to read the meters and to wash them. For reasons above, the new detection technology is needed to improve the accuracy of operational status and to effectively reduce damage to field personnel caused by foul smell .

We promote a new kind of detection technology. Pictures of oxidation pond are regularly taken by high-resolution digital camera and these pictures are sent back to data processing center. By image analysis and the data of foam floated on surface, we can get the operational status of oxidation pond and report it to worker as a reminder of controlling dose of medicine. After practising in sewage treatment works, it proved accurate in detection of operational status and effective in reduction of contaminant damage to field personnel. In summary, this method shows a great engineering value.

II. SYSTEM ARCHITECTURE

The structure of this system is made up of 3 parts, as shown in figure 1.

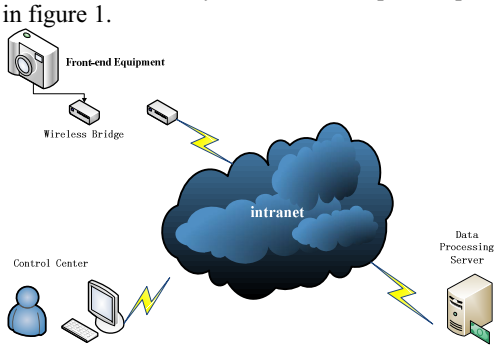

Figure 1. The system architecture

The first part is front-end equipment, composed of high-resolution digital camera and wireless bridge. Digital cameras are responsible for photographing oxidation pond regularly and connected to intranet through wireless bridge. In most cases, it is inconvenient to connect cable with intranet , so wireless bridge is preferred.

The second part is the data processing server located in the office center. This is the place where pictures taken in the first part are analysed and thus we can get the result.

The third part is control center. Workers can access the data processing server from their working terminal to get results and to operate accordingly.

III. MODEL OF FOAM IN OXIDATION POND

A. The Analysis of the foam and water conditions

There are many foams floated on the surface of oxidation pond, as shown in figure 2. Some of them are connected into

978-0-7695-4818-0/12 $26.00 © 2012 IEEE
DOI 10.1109/DCABES.2012.21

a sheet; Others are scattered on the surface into small pieces. The shapes of foam change quickly because of quick flow velocity and big wave.

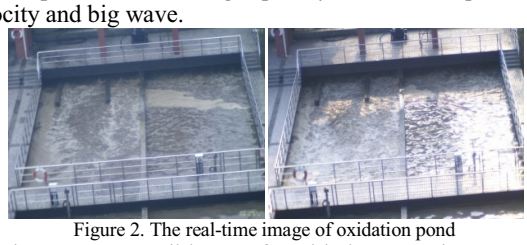

Figure 2. The real-time image of oxidation pond

The water conditions of oxidation pond are easily affected by weather factors such as sunlight, wind, cloud and fog since it is in the open.

B. The Process of Image Color Balance

Since the oxidation pond is in the open, the brightness and chroma of pictures vary with light source and thus it will influence the detection of foam on the surface. So the process of color balance is necessary to eliminate the effects caused by changes in light source.

In this article we adopt the color balance of Gray World [2] to achieve the purpose. The basic idea of this computing method is to get the average of Gray by R_{avg}(average of R), G_{avg}(average of G), B_{avg}(average of B). The original value of R, G, B is read from the image. After that, we will recalculate Pixels of R, G, B, and try to make new R_{avg}, G_{avg}, B_{avg} close to $Gray_{avg}$.

Step1, Calculate R_{avg}、G_{avg}、B_{avg} and $Gray_{avg}$.

And,

$$Gray_{avg} = (R_{avg}+G_{avg}+B_{avg}) / 3 \quad (1)$$

Step2, Calculate the correction factor of R, G, B.

And ,

$$F_r=Gray_{avg} / R_{avg} \quad (2)$$

$$F_b=Gray_{avg} / B_{avg} \quad (3)$$

$$F_g=Gray_{avg} / G_{avg} \quad (4)$$

Step3, Adjust the value of R,G,B by correction factor and replace those values of R,G,B whose values are over 255 with 255. Formula is as follows,

$$R=((R*F_r)>255)?255:(R*F_r) \quad (5)$$

$$B=((B*F_b)>255)?255:(B*F_b) \quad (6)$$

$$G=((G*F_g)>255)?255:(G*F_g) \quad (7)$$

C. The Features of Foam in Oxidation Pond

To describe foam more clearly, we finally decide to adopt the BGR color space to describe the feature values of foam after comparing values of BGR with values of HSV, YCrCb and Lab.

Since the absolute values of foam point of R, G, B in BGR color space are greatly affacted by environment, it may not be used to describe features of foam, for example, $Value_{bgr}$（186,189,182）and $Value_{bgr}$（146,147,138） are both foam points.

Besides, influenced by flow, the shape of foam changes quickly, so it could not be used to describe features.

After due consideration, We use following formulas to describe features of foam in the article,

$$V_g>V_b \quad (8)$$

$$V_g-V_{avg}<7 \quad (9)$$

$$V_r-V_{avg}<7 \quad (10)$$

$$V_{avg}-V_b>V_{bluefactor} \quad (11)$$

And $V_{avg}=(V_b+V_g+V_r)/3$, $V_{bluefactor}$ is correction factor, limited from10 to 20.

The formula of ROF(Rate of Foam) is as follow,

$$ROF = \sum P_{foam} / \sum P_{pool} \quad (12)$$

And $\sum P_{foam}$ means the total amount of foam, and $\sum P_{pool}$ means the total amount of oxidation pond.

IV. THE ANALYSIS OF INDUSTRIAL EXPERIMENT DATA

Digital cameras with technical grade are poled on both sides to photograph oxidation pond every 10 minutes—the same as the required interval of industrial technology. Pictures are sent back to the server of office center through wireless bridge. Here are some experiment results,

(a) (b) (c)

Figure 3. The result of foam in a sunny day

In pictures above, Picture (a) was the original one sent back to office; since it was sunny, influenced by sunlight, the color of picture was out of balance and too bright. After processed by Gray World of color balance method, here was Picture (b). And picture (c) was the analysis result of the foam in the right oxidation pond. The foam was processed white for convenience by system and the ROF is 20.11%.

(a) (b) (c)

Figure 4. The result of foam in a cloudy day

In pictures above, Picture(a) was the original one sent back to office; since it was cloudy, the color of picture was out of balance and too dark. After processed by Gray World of color balance method, here was Picture (b). And picture (c) was the analysis result of the foam in the right oxidation pond. The foam was processed white for convenience by system and the ROF is 19%.

Data showed that the accuracy of analysis results would be affected by complex environmental factors, such as the reflective surface and reflection. However, ROF can still be calculated relatively accurately, at the same time, the accuracy is able to meet the operation requirements.

V. CONCLUSION

Traditional equipment detection can hardly obtain the specific operational status of oxidation pond. However, with the method of foam-detection mentioned in this article, we can.

So it gives scope to remote management of oxidation pond's operational status. Meanwhile, the industrial experiment result showed that the accuracy of ROF calculated by the method of foam-detection was reliable enough to be used as the indication of oxidation pond's operational status. Therefore, the foam-detection based on image analysis in the process of sewage treatment can not only improve the management standard in industrial operation but also reduce the damage of contaminant to field personnel effectively. In a word, it shows great practical industrial value.

ACKNOWLEDGMENT

I would like to express my sincere appreciation to Chongqing Educational Committee and Yubei District Science and Technology Committee of Chongqing for sponsor this project.

REFERENCES

[1] GaoHaibo, Hong Wenxue, Cui Jianxin, Xu Yonghong, et al. Optimization of PrinciPal Component Analysis in Feature Extraction. Mechatronic and Automation, 2007: 3128~3132

[2] CAI J, GOSHTASBY A. Detection human faces in color images [J]. Image and Vision Computing, 1999, 18(1):63-75.

[3] Xiangyoujun and Xieshengli, Overview of Image Retrieval Technology, (Natural Science) 2006, Vol.8(03)

[4] R. Datta, J. Dhiraj, J. Li, J. Z. Wang. Image Retrieval: Ideas, Influences, and Trends of the New Age. ACM Computing Surveys, 2008(40): 1-60.

[5] S. Deb, Y. C. Zhang. An Overview of Content-based Image Retrieval Techniques. AINA 2004

[6] Xuqing, Yangweiwei, Chengshengtan. Content-based Image Retrieval Technology, Computer Technology and Development, 2008(01)

[7] R. Zhao, W. I. Grosky. Bridging the Semantic Gap in Image Retrieval. Distributed multimedia databases: Techniques and applications, 2001: 14-36.

[8] F. Jurie and B. Triggs. Creating efficient codebooks for visual recognition. ICCV, 2005: 604-610.

[9] F. F. Li, P. Perona. A Bayesian Hierarchical Model for Learning Natural Scene Categories. CVPR, 2005: 524--531.

An Early Termination Criterion for Fast Video Coding

Dong Xiang, Hu Liu, Hanbing Yao
School of Computer Science and Technology, Wuhan University of Technology
Wuhan 430063, China
E-mail: xianglt@gmail.com , xiangdong@whut.edu.cn

***Abstract*—In this paper, we propose an early termination criterion for fast video coding. This criterion is based on the modified successive elimination algorithm and a model of transform coefficients distribution. This method can speed up not only the motion estimation procedure, but also other functions, such as the quarter-pixel interpolations, transform, quantization, inverse quantization and inverse transform. Simulation results show that our method can decrease the computation complexity significantly with negligible rate distortion performance loss.**

Keywords- video coding, motion estimation, early termination, computational complexity

I. INTRODUCTION

Modern video compression techniques offer the possibility to store or transmit the vast amount of data necessary to represent digital video in an efficient and robust way. Almost all of today's MPEG and ITU video coding algorithms are based on the hybrid block-based motion compensation/discrete cosine transformation systems (MC/DCT) [1]. For example, in the state-of-art H.264 video coding standard [2, 3], each input video frame is divided into 16×16 pixels macroblocks. The motion-compensated prediction (MCP) is done for every macroblock and motion estimation (ME) is used to find the best match within a search region in the multiple reference frames for allowable block sizes, such as 16×16, 16×8, 8×16, 8×8 etc. The most common matching criterion used is the sum of absolute difference (SAD) because its simplicity and similar performance to mean square error (MSE). When get the best block size and its associate motion vectors (MV), the MCP error is transformed by a 4×4 integer transform (IT). The transformed coefficients then are quantized (Q), zigzag scan and entropy coding. In order to get the same reconstructed frames for MCP, the encoder must do the inverse quantization (IQ) and inverse integer transform (IIT) as do in the decoder.

Motion estimation plays a key role in the hybrid block-based motion compensation/DCT systems. Although the exhaustive search algorithm (ESA) can obtain the optimal result by searching exhaustively for the best matching block within a search window, its high computational cost limits its practical applications. To reduce the computational complexity of the ESA, many fast algorithms, such as the 2-D log search[4], one-at-a-time search (OTS)[5], three step search (TSS) [6] and cross search [7] have been developed. All of these algorithms rely on a monotonically increasing matching criterion around the location of the optimal motion vector to iteratively determine that location[8]. The computational burden is reduced by considering a limited number of positions within the search window for a motion vector. As the motion-estimation algorithm becomes optimized, to speed up the video encoders further we also need to optimize other functions, such as IT and IIT. For example, the ME using ESA and IT in H.264 would consume about 80% and 5% of computation resource [9], respectively. As the time spent on motion estimation declines, the time spent on other functions will become relatively more significant. To further speed up the computations in the video encoders, it is important to reduce the computations of IT/IIT and Q/IQ.

In this paper, we propose an early termination criterion for fast video coding. This criterion is based on the modified successive elimination algorithm (SEA) [10] and a model of the transform coefficients distribution [11]. We divide the MC block into 4×4 sub blocks whose size equals to the transform matrix. This division can not only improve the efficiency of eliminating in-viable search points, but also get the DC coefficients of each sub block. Based on the gotten DC coefficients and the model of transformed coefficients, we can get a criterion to detect whether all the quantized transformed coefficients of current MV difference block are zeros. When the criterion is matched, we can terminate the ME procedure early, skip computations of quarter-pixel interpolations and IT/IIT/Q/IQ. Simulation results show that our method can speed up the encoder processing speed with negligible video quality degradation.

II. THE MODIFIED SEA

The aim of motion estimation is to find the best matching block in the reference frames. The most common matching criterion used is SAD. SAD is defined as follows:

$$\mathrm{SAD}(i,j) = \sum_{k=0}^{M-1}\sum_{l=0}^{N-1}\left|C(x+k,y+l)-R(x+i+k,y+j+l)\right| \quad (1)$$

where $C(x+k,y+l)$ and $R(x+i+k,y+j+l)$ are the pixels in the current and reference frame respectively, $-p \le i \le p$ and $-p \le j \le p$ ([-p, p] is the search range), M and N are the MC block dimensions. For each search point, SAD computation needs MN subtractions, MN absolute operations and MN-1 additions. Applying the mathematical inequation $\|a|-|b\| \le |a-b|$, we can get the inequation used in SEA:

This work was supported by "the Fundamental Research Funds for the Central Universities"

978-0-7695-4818-0/12 $26.00 © 2012 IEEE
DOI 10.1109/DCABES.2012.65

$$\mathrm{ADBS}(i,j)=\left|\sum_{k=0}^{M-1}\sum_{l=0}^{N-1}C(x+k,y+l)-\sum_{k=0}^{M-1}\sum_{l=0}^{N-1}R(x+i+k,y+j+l)\right|\le \mathrm{SAD}(i,j) \quad (2)$$

ADBS (Absolute Difference of Block Sum) symbol is used for simple expression. In inequation (2) the first and second sum are calculated in the block of current frame and reference frame. Because ADBS(i,j) is not larger than SAD(i,j), If it is larger than current minimum SAD, the SAD computation can be skipped. For each MC block, the first sum needs to be computed once and the second item can reuse the already computed value [10]. So the computational saving can be achieved.

In inequation (2), ADBS is much less than SAD because the sums are calculated in the total block area. In the new fast successive elimination algorithm (NFSEA) [12], the MC block is partitioned into sub blocks. A reasonable compromise is dividing the MC block into 8×8 sub blocks. For a 16×16 macroblock, the inequation used in NFSEA can be expressed as:

$$\begin{aligned}&\mathrm{ADBS}(i,j)=\left|\sum_{a=0}^{1}\sum_{b=0}^{1}\left\{\sum_{k=0}^{8}\sum_{l=0}^{8}C(x+8a+k,y+8b+l)-\sum_{k=0}^{8}\sum_{l=0}^{8}R(x+8a+i+k,y+8b+j+l)\right\}\right|\\&\le\sum_{a=0}^{1}\sum_{b=0}^{1}\left|\sum_{k=0}^{8}\sum_{l=0}^{8}C(x+8a+k,y+8b+l)-\sum_{k=0}^{8}\sum_{l=0}^{8}R(x+8a+i+k,y+8b+j+l)\right|\\&=\mathrm{SADSB4}(i,j)\le\sum_{a=0}^{1}\sum_{b=0}^{1}\left|\sum_{k=0}^{8}\sum_{l=0}^{8}C(x+8a+k,y+8b+l)-\sum_{k=0}^{8}\sum_{l=0}^{8}R(x+8a+i+k,y+8b+j+l)\right|\\&=\mathrm{SAD}(i,j)\end{aligned} \quad (3)$$

where a, b are the horizontal and vertical coordinate of sub block in the MC block, SADSB4 (Sum of Absolute Difference of 4 Sub Blocks Sum) symbol is used for simple expression. As in SEA, inequation (3) can be used for eliminating in-viable candidate motion vectors. As SADSB4 is not less than ADBS, the possibility of elimination becomes higher. So SADSB4 can eliminate in-viable candidate motion vectors more effectively than ADBS.

In our method we divide the MC block into 4×4 sub blocks whose dimension equals to that of transform matrix. Although this division increases extra computation [12], its efficiency to eliminate in-viable search points is higher than 8×8 division because SADSB8 is not less than SADSB4 according to SADSB4 is not less than ADBSB, which will contribute to reduce the extra computation. In addition, when computing the difference of the corresponding sub block sum in reference and current frame, the DC transformed coefficients can be got at the same time (In H.264, the scale operation is integrated into quantization):

$$\begin{aligned}&\sum_{k=0}^{4}\sum_{l=0}^{4}C(x+k,y+l)-\sum_{k=0}^{4}\sum_{l=0}^{4}R(x+i+k,y+j+l)\\&=\sum_{k=0}^{4}\sum_{l=0}^{4}\left(C(x+k,y+l)-R(x+i+k,y+j+l)\right)\\&=DC\end{aligned} \quad (4)$$

III. The Early Termination Criterion for Fast Video Coding

In video coding, the distribution of the residual values after MCP can be modeled by a Laplacian distribution with zero mean and a separable covariance $r(m,n)=\sigma_f\rho^{|m|}\rho^{|n|}$, where m and n are the horizontal and vertical distances between two residual values respectively, σ_f is the variance of the residual values, and $\rho\le 1$ is the correlation coefficient. The transform can be expressed in matrix form as $\boldsymbol{F}=\boldsymbol{HfH}^T$, where $\boldsymbol{H}^T$ is the transpose matrix of $\boldsymbol{H}$. The variance of the (u, v)th transformed coefficient σ_F can be written as[11]:

$$\sigma_F^2(u,v)=\sigma_f^2\left[\boldsymbol{HRH}^T\right]_{u,u}\left[\boldsymbol{HRH}^T\right]_{v,v} \quad (5)$$

where

$$\boldsymbol{R}=\begin{bmatrix}1&\rho&\rho^2&\rho^3\\\rho&1&\rho&\rho^2\\\rho^2&\rho&1&\rho\\\rho^3&\rho^2&\rho&1\end{bmatrix}$$

The correlation coefficient ρ commonly ranges from 0.4 to 0.75[11], we choose ρ equal to the average value 0.6. Using the integer transform adopted in H.264, the variance of the transform coefficients will be:

$$\begin{aligned}&\sigma_F^2(u,v)=\sigma_f^2M[u,v]\\&=\sigma_f^2\begin{bmatrix}5.6074&2.1293&1.0609&0.6744\\2.1293&0.8086&0.4028&0.2561\\1.0609&0.4028&0.2007&0.1276\\0.6744&0.2561&0.1276&0.0811\end{bmatrix}\end{aligned} \quad (6)$$

The above equation shows that the variances of the transformed coefficients can be estimated by the variances of the residual values at the input. It also shows that the variance of the DC coefficient is larger than that of other AC coefficients. This means, after quantization (if the same quantization parameter (QP) is used for both DC and AC coefficients), the probability of AC coefficients' being quantized into zeros is greater than that of DC coefficients. In other words, it makes sense to treat the DC coefficients separately from other AC coefficients (e.g., under some situations, if DC coefficient is zero, all AC coefficients can be set to zeros).

To not spend extra computations calculating the variance of residual values at the input of transform, the variance can be estimated from the SAD. The expected mean absolute value of a signal with Laplacian distribution

and zero mean is $\sigma_f / \sqrt{2}$, For a 16×16 MC block, σ_f can be calculated as follows:

$$\sigma_f = \sqrt{2} * SAD / 256 \quad (7)$$

The SAD value is readily available after searching each candidate blocks in the search window. For a zero-mean Laplacian distribution, the probability that a value will fall within (-3σ, 3σ) is about 99%. When adopting the quantization method in H.264 standard, we can get the inequation for determining whether the transformed coefficient of inter coding will be quantized into zero:

$$5/6q > 3\sigma_F[u,v] \quad (8)$$

where q is the quantization step size. If 5/6q is larger than 3σF[u, v], then 99% of the time this transformed coefficient will be zero after quantization.

From the above discussion, given the SAD, quantization step size and model of transformed coefficients distribution, we can get the criterion to detect whether all quantized AC coefficient are zeros:

$$5q/6 > 3\sqrt{2M[0,1]} * SAD / 256 \quad (9)$$

The above inequation can also be express as:

$$SAD < 34.47 \times q \quad (10)$$

In [11], the similar inequation was deduced to determine whether all quantized coefficient are zero after ME procedure, which can reduce the computations in DCT, IDCT, quantization, and IQ stages. In the modified SEA the DC transformed coefficient can be gotten as byproduct. If all quantized DC coefficients are zeros and SAD is less than 34.47q, we can think all quantized coefficients are zeros. Comparison with method in [11], this method can decrease the probability of misjudgment. This is because that DC coefficient are more important than AC coefficients for reconstructed image quality, when all quantized DC coefficients are zeros, setting nonzero AC coefficients to zeros will not cause large PSNR loss.

In modern video coding standards the ME first checks the integer-pixels. After the integer-pixel search, a fraction-pixel refinement will be done around the best integer MV. The half-pixel interpolation in H.264 standard is a 6-tape filter and the quarter-pixel interpolation is only an average operation. As the tradeoff between memory requirement and computational complexity, the better method is to store the pre-compute half-pixel interpolation values and interpolate the quarter-pixel values on demand. After getting the final MV for one reference, the same procedure will be repeated on other allowable reference frames.

During the ME procedure, we can use

$$\forall DC_{a,b} < 5/6q \;\&\; SAD < 34.47q \quad (11)$$

as the early termination criterion. If all quantized DC coefficients are zeros and SAD is less than 34.47q, all quantized transformed coefficients of current MV can be thought to be zeros, then we can terminate ME procedure, so the computational saving of search points, quarter-pixel interpolations and IT/IIT/Q/IQ can be achieved. This may lead to PSNR performance loss because the early termination may miss the best search points. Owing to all quantized transformed coefficients of current MV are zeros, So the PSNR performance improvement by searching more points may be limited, and this improvement may be lagged by the increased bit rates because the farther the MV leave away from the search center, the more the bit rates need to code it.

IV. Simulation Results and Discussion

We implement our method on an open source project T264, which is fast software implementation of H.264 standard. The ME method adopted in T264 is a simple predictive motion vector field adaptive search technique (SPMVFAST) and the early termination criterion is integrated in it [13].

TABLE I. Simulation results

Sequence	QP	Saving (%)			Average PSNR gain(dB)	Average bit rate saving (%)
		Search points	*1/4 interpolation*	*IT/IIT, Q/IQ*		
News	28	44.92	47.34	46.34	-0.026	-0.4
	34	57.23	59.97	58.36		
Akiyo	28	63.94	65.99	45.61	-0.004	-0.07
	34	75.92	78.25	74.05		
Foreman	28	14.57	8.67	7.62	-0.031	-0.67
	34	31.61	29.35	26.68		
Flower	28	31.84	31.64	30.69	-0.031	-0.46
	34	35.4	36.01	34.8		
Paris	28	15.45	14.67	14.06	-0.01	-0.16
	34	29.65	29.71	28.64		
Container	28	15.03	14.75	14.33	-0.008	-0.2
	34	45.17	46.33	45.61		
Average					-0.018	-0.33

Several common intermediate format (CIF) sequences are processed with QP fixed on 28, 30, 32 and 34 to eliminate the impaction of rate control algorithm to RD performance. These sequences are encoded in an IPPP structure at 30Hz using two reference frames and a search range of 16 pixels.

Tab. I shows the simulation results at different QP. The complexity reduction of our method are mainly dependent on the saving of search points, 1/4 interpolations, IT/IIT/Q/IQ. These computational reductions are listed in the columns of the Tab. 1. Their computational complexity are fixed and easily to be analyzed for different hardware platform. For example each 16×16 SAD calculation needs 256 subtractions, 255 additions and 256 absolutions for a pc based software implementation wherever in original method or ours. So we can use the saving of these functions to evaluate the complexity reduction. The last two columns are the average PSNR gain and bit rate saving. Fig. 1 shows the RD curve comparison and complexity reduction varied on different QP.

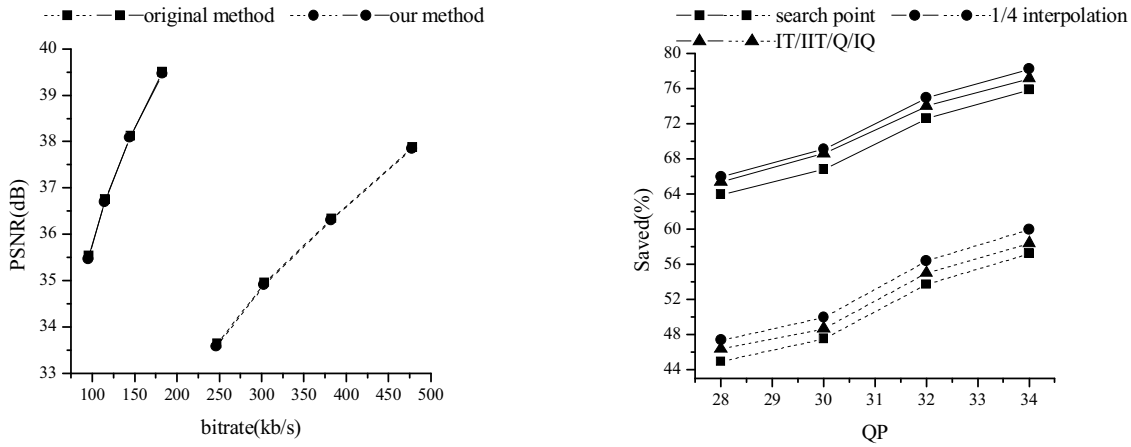

(a) RD curve comparison (b) complexity reduction

Figure 1. Performance comparison, Where the solid lines and dash lines represent Akiyo and News sequences, respectively.

As shown in Tab. I and Fig. 1 the RD performance of our method is very close to that of the original method. The average PSNR gain is -0.018dB, the average bit rate saving is -0.33%. For low bit-rate or low motion active situations our method can decrease the complexity reduction significantly, but for high bit-rate and high motion active situations the reduction is comparatively small. This is because that the SAD at low motion active situation is generally smaller than that at high motion active situation, and with the increase of QP the possibility of DC transformed coefficients' being quantized into zeros increases.

V. CONCLUSION

In this paper an early termination criterion for fast video coding was presented, which is based on the modified SEA algorithm and a model of transformed coefficients distribution. We divide the MC block into 4×4 sub blocks whose size equals to the transform matrix. This division can not only improve the efficiency of eliminating in-viable search points, but also get the DC coefficients of each sub block. Based on the gotten DC coefficients and a model of transformed coefficients, we get a criterion to determine whether terminate ME procedure early, and skip the computation of quarter-pixel interpolations and other functions. Simulation results show that our method can decrease the computational complexity significantly with slight RD performance loss.

REFERENCES

[1] Thmoas Sikora, "Trends and perspectives in image and video coding," IEEE Proc., VOL. 93, NO. 1, Jan. 2005, pp. 6-17.

[2] T. Wiegand and G. Sullivan, Draft ITU-T Recommendation and Final Draft International Standard of Joint Video Specification (ITU-T Rec. H.264 | ISO/IEC 14496-10 AVC), Document JVT-G050, March, 2003.

[3] T. Wiegand, G. J. Sullivan, G. Bjontegaard and Ajay Luthra, "Overview of the H.264 / AVC video coding standard," IEEE Transactions on Circuits and Systems for Video Technology, VOL. 13, NO.7, 2003, pp. 1-19.

[4] J. Jain and A. Jain, "Displacement measurement and its application in interframe image coding," IEEE Trans. on Communications, VOL. 29, NO.12, Dec. 1981, pp. 1799-1808.

[5] R. Srinivasan and K. Rao, "Predictive coding based on efficient motion estimation," IEEE Transactions on Communications, VOL. 33, NO. 8, Aug. 1985, pp:888 – 896.

[6] T. Koga, K. Iinuma, A. Hirano, Y. Iijima, and T. Ishiguro, "Motion compensated interframe coding for video conferencing," in Proc. NTC 81, Nov. /Dec. 1981, pp. C9.6.1-9.6.5.

[7] M. Ghanbari, "The cross-search algorithm for motion estimation," IEEE Trans. Commun., VOL. 38, NO. 7, July 1990, pp. 950-953.

[8] B. Liu and A. Zaccarin, "New fast algorithms for the estimation of block motion vectors," IEEE Trans. Circuits Syst. Video Technol., VOL. 3, NO. 2, Apr. 1993, pp. 148-157.

[9] Jianning Zhang, Yuwen He, Shiqiang Yang, Yuzhuo Zhong, "Performance and Complexity Joint Optimization for H.264 Video Coding," Proceedings of the 2003 International Symposium on Circuits and Systems, Volume 2, May, 2003 PP:II-888-II-891.

[10] W. Li and E. Salari, "Successive Elimination Algorithm for Motion Estimation," IEEE TRANSACTIONS ON IMAGE PROCESSING, VOL. 4, NO. 1, JANUARY 1995, pp.105-107.

[11] I-Ming Pao and Ming-Ting Sun,"Modeling DCT Coefficients for Fast Video Encoding", IEEE TRANSACTIONS ON CIRCUITS AND SYSTEMS FOR VIDEO TECHNOLOGY, VOL. 9, NO. 4, JUNE 1999, pp.608-616.

[12] Soo-Mok Jung, Sung-Chul Shin, Hyunki Baik, Myong-Soon Park, "New Fast Successive Elimination Algorithm", Proc. 43rd IEEE Midwest Symp. on Circuits and Systems. Lansing MI, Aug. 2000,pp.616-619.

[13] Alexis M. Tourapis, Oscar C. Au, and Ming L. Liou, "Highly Efficient Predictive Zonal Algorithms for Fast Block-Matching Motion Estimation", IEEE TRANSACTIONS ON CIRCUITS AND SYSTEMS FOR VIDEO TECHNOLOGY, VOL. 12, NO. 10, 2002 pp.934-947.

Residue Signed-Digit Arithmetic and the Conversions between Residue and Binary Numbers for a Four-Moduli Set

Shugang Wei and Changjun Jiang
Department of Production Science and Technology, Gunma University, Japan
{wei}@gunma-u.ac.jp

***Abstract*—By introducing a signed-digit (SD) number arithmetic into a residue number system (RNS), arithmetic operations can be performed efficiently. In this paper, a high-speed modulo m SD addition algorithm is proposed, where $m \in \{2^n - 1, 2^n + 1, 2^{2n} + 1, 2^n\}$. By using the modulo m SD adders, a modulo m SD multiplier can be implemented with a binary adder tree structure. We also present an algorithm for the conversion from residue SD numbers to SD numbers for the four-moduli set $\{2^n - 1, 2^n + 1, 2^{2n} + 1, 2^n\}$ which can be designed using a two-level binary tree structure of the residue SD number additions. The comparison of the new converter using SD number arithmetic with the converter using binary arithmetic yields reductions in delays of 44%, 60% and 75% for $n = 4$, $n = 8$ and $n = 16$, respectively.**

I. Introduction

A well-known advantage of the residue number system (RNS) is that provides the ability to add, subtract or multiply without the need to wait for the carry propagation in arithmetic operations as required by conventional binary number system [1]. Digital signal processing hardware based on RNS is currently considered important for high-speed and low-cost hardware realization [2].

Since the RNS does not have weights in the residue digits, it needs to be interfaced efficiently with a weighted number system by converting it to weighted number. Therefore, the research of an efficient residue to binary conversion algorithm is an important task in realizing the RNS-based applications and signal processors. There are a number of conversion algorithms available. These can be categorized into two groups, Chinese Remainder Theorem (CRT) and the Mixed Radix Conversion (MRC)[2]. The MRC approaches are strictly sequential with $O(k)$ time complexity, where k is the number of moduli. The CRT method is faster than the MRC method because the conversion processes can be done in parallel. However, the direct implementation of CRT is not efficient since modulo a complicated M operation is necessary, where M is the dynamic range of the RNS.

Many three-moduli sets have been suggested for residue-to-binary conversion. In recent years, large dynamic range is required for high-performance computation system. Hence, several residue-binary converters for four-moduli sets have been proposed [6]- [9]. However, the residue arithmetic operations of these converters run with the binary arithmetic. The operation speed of the RNS using binary is bounded by the carry propagation within binary-based residue arithmetic. Another major mask in popularizing the RNS-based application is to speed up the residue arithmetic.

The redundant binary number representation was first introduced by Avižienis in 1961 [3]. A radix-two signed-digit (SD) number system, which has a set of {-1, 0 1} and no need for a separate sign digit, is well known to offer advantages in arithmetic circuit implementation without the carry propagation [4]. Residue arithmetic hardware algorithms using SD number representation have been proposed [5].

This paper proposes a high-speed modulo m SD addition algorithm where $m \in \{2^n - 1, 2^n + 1, 2^{2n} + 1, 2^n\}$. By using the modulo m SD adders, a modulo m SD multiplier can be implemented with a binary adder tree structure. We also present an algorithm for the conversion from SD residue numbers to SD binary numbers for the four-moduli set $\{2^n-1, 2^n+1, 2^{2n}+1, 2^n\}$ which can be designed using a two-level binary tree structure of the SD number residue additions. Therefore, it can be used directly after the SD number residue arithmetic without converting the residue number represented by SD number to binary residue number beforehand. Another feature of this conversion method is it possesses both the advantages of CRT and MRC.

II. Residue Number System

A Residue Number System (RNS) is defined in terms of a set of pairwise relatively prime moduli $\{m_1, m_2, \cdots, m_k\}$, that is $GCD(m_i, m_j) = 1$, for $i \neq j$. Let $M = \prod_{i=1}^{k} m_i$ be a dynamic range of the RNS. Any arbitrary integer A in the range $[0, M-1]$ can be uniquely represented in the defined residue number system as a set of k integers $\{a_1, a_2, \cdots, a_k\}$, where

$$a_i = A \bmod m_i = |A|_{m_i}, 0 \leq a_i < m_i.$$

Arithmetic operation between integers $A = \{a_1, a_2, \cdots, a_k\}$ and $B = \{b_1, b_2, \cdots, b_k\}$ in an RNS can run as

$$C = A \otimes B = \{c_1, c_2, \cdots, c_k\},$$

where, $c_i = |a_i \otimes b_i|_{m_i}$, $i = 0, 1, \cdots, k$. $\otimes$ means addition, subtraction or multiplication.

978-0-7695-4818-0/12 $26.00 © 2012 IEEE
DOI 10.1109/DCABES.2012.100

The RNS to binary conversion is based on CRT or MRC normally. The Chinese Remainder Theorem is formulated as

$$X = \left| \sum_{i=1}^{k} P_i \cdot \left| P_i^{-1} \cdot r_i \right|_{m_i} \right|_M , \quad (1)$$

where $M = \prod_{i=1}^{k} m_i$, $P_i = M/m_i$, P_i^{-1} is the multiplicative inverse of $|P_i|_{m_i}$, namely $|P_i^{-1} P_i|_{m_i} = 1$, and $r_i = |X|_{m_i}$.

The Mixed Radix Conversion is fairly simple in principle. A number X is represented by mixed radices and their coefficients as

$$X = a_k \prod_{i=1}^{k-1} m_i + \cdots + a_3 m_2 m_1 + a_2 m_1 + a_1, \quad (2)$$

where m_i is the *i*th mixed radix. a_i is the *i*th coefficient, that is, $a_1 = |X|_{m_1}$ and $a_i = \left| \left[\frac{X}{m_1 m_2 \cdots m_{i-1}} \right] \right|_{m_i}$ for $i > 1$.

In the case of $k = 2$, we have

$$X = a_2 m_1 + a_1, \quad (3)$$

the coefficients can be obtained as

$$\begin{aligned} a_1 &= |X|_{m_1} = r_1 \\ a_2 &= \left| \frac{(r_2 - a_1)}{m_1} \right|_{m_2} = \left| \left| \frac{1}{m_1} \right|_{m_2} (r_2 - r_1) \right|_{m_2} . \end{aligned}$$

where $r_1 = |X|_{m_1}$ and $r_2 = |X|_{m_2}$.

III. Signed-Digit Number System for RNS

In the radix-two SD number representation, an n-digit radix-two SD integer $X = [x_{n-1} \cdots x_0]_{SD}$ has the value

$$X = x_{n-1} 2^{n-1} + x_{n-2} 2^{n-2} + \cdots + x_1 2^1 + x_0, \quad (4)$$

where, $x_i \in \{\bar{1}, 0, 1\}$ and $\bar{1}$ denotes -1. This representation permits several ways to represent an integer, thus making it a redundant number system. For example, $[0101]_{SD}$, $[1\bar{1}1\bar{1}]_{SD}$, $[10\bar{1}\bar{1}]_{SD}$ all represent "5". However, "0" is uniquely represented.

A. Residue Signed-Digit Number

In the SD number representation, integer X has a value in the range as

$$L_{sd} = \{-(2^n - 1), \cdots, 0, \cdots, (2^n - 1)\}.$$

Definition 1: Let X be an integer and m be a modulus. Then $x = \langle X \rangle_m$ is defined as an integer in L_{sd}. When $\langle X \rangle_m \neq 0$, x has one of two possible values:

$$x = \langle X \rangle_m = |X|_m, \text{ and } x = \langle X \rangle_m = |X|_m - m. \quad (5)$$

For example, the value of $\langle 29 \rangle_{17}$ is $\langle 29 \rangle_{17} = |29|_{17} = 12$, or $\langle 29 \rangle_{17} = |29|_{17} - 17 = -5$.

When $|X|_m = 0$ for $m = 2^n - 1$, x has three possible values, that is, $-m$, 0 and m.

Obviously, the following properties exist in the residue SD number representation.

Property 1: Let a and b be SD integers. Then

1) $\langle a + b \rangle_m \equiv \langle \langle a \rangle_m + \langle b \rangle_m \rangle_m$,
2) $\langle a \times b \rangle_m \equiv \langle \langle a \rangle_m \times \langle b \rangle_m \rangle_m$,
3) $\langle -a \rangle_m \equiv -\langle a \rangle_m$,

where $\equiv$ indicates congruent modulo m.

B. Residue Addition with SD Number Representation

Residue additions for the moduli in the form of $2^n \pm 1$ and 2^n are widely used, because they offer the ability to generate remainders without any memory. However, when a binary number system is used to perform the residue addition, the carry propagation will arise inside the residue digit and the speed of arithmetic operation will be limited.

A common addition $Z = X + Y$ in SD number system, X and Y are *n*-digit SD numbers, can be performed in parallel as follows: Let c_i and s_i be the carry and the intermediate sum of *i*th digit position, respectively. Their values are determined by a particular rule with respect to the values of x_i, y_i, x_{i-1}, y_{i-1}, as shown in Table I, then compute the final sum by $z_i = s_i + c_{i-1}$, where $i = 0, 1, \cdots, n-1$, $x_{-1} = 0$, $y_{-1} = 0$ and $c_{-1} = 0$.

Residue generation for such popular moduli can be done easily by the additional end-around-carry operation, as follows.

1) Modulo $2^n - 1$:

Step1: Use Table I to determine c_i and s_i, where $x_{-1} = x_{n-1}$, $y_{-1} = y_{n-1}$.

Step2: Compute the final sum by $z_i = s_i + c_{i-1}$, where $c_{-1} = c_{n-1}$.

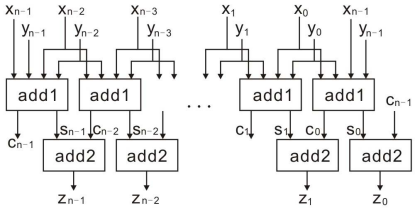

Fig. 1. Modulo m adder using SD number($m \in \{2^n - 1, 2^n, 2^n + 1\}$)

2) Modulo 2^n:

Step1: Use Table I to determine c_i and s_i, where $x_{-1} = 0$, $y_{-1} = 0$.

Step2: Compute the final sum by $z_i = s_i + c_{i-1}$, where $c_{-1} = 0$.

3) Modulo $2^n + 1$:

Step1: Use Table I to determine c_i and s_i, where $x_{-1} = -x_{n-1}$, $y_{-1} = -y_{n-1}$. And use Table II to determine c_{-1}.

Step2: Compute the final sum by $z_i = s_i + c_{i-1}$.

Figure 1 illustrates the circuit diagram of a modulo m SD number adder consisting of n add1s and n add2s, where $m \in \{2^n - 1, 2^n, 2^n + 1\}$. The add1 generates the c_i and the s_i, and the add2 sums the c_{i-1} and s_i. The residue addition can be performed in parallel without the carry propagation.

According to the Table I and II, $c_i \in \{\bar{1}, 0\}$ and $s_i \in \{0, 1\}$, where $\bar{1} = -1$. That means, the carry and the intermediate sum have only two possible values, respectively. Therefore,

TABLE I
RULES FOR ADDING SD NUMBERS

	$abs(x_i) = abs(y_i)$				$abs(x_i) \neq abs(y_i)$	
	$x_i = \bar{1}$ or $y_i = \bar{1}$		$x_i \geq 0$ and $y_i \geq 0$		—	—
	$x_{i-1} \leq 0$ and $y_{i-1} \leq 0$	$x_{i-1} = 1$ or $y_{i-1} = 1$	$x_{i-1} \leq 0$ and $y_{i-1} \leq 0$	$x_{i-1} = 1$ or $y_{i-1} = 1$	$x_{i-1} \leq 0$ and $y_{i-1} \leq 0$	$x_{i-1} = 1$ or $y_{i-1} = 1$
c_i	$\bar{1}$	$\bar{1}$	0	0	$\bar{1}$	0
s_i	0	1	0	1	1	0

Note: $abs(x_i)$ and $abs(y_i)$ are the absolute values of x_i and y_i.

TABLE II
RULES FOR CALCULATING c_{-1}

	$abs(x_{n-1}) = abs(y_{n-1})$		$abs(x_{n-1}) \neq abs(y_{n-1})$	
	$x_{n-1} = 1$ or $y_{n-1} = 1$	$x_{n-1} \leq 0$ and $y_{n-1} \leq 0$	$x_{n-2} \leq 0$ and $y_{n-2} \leq 0$	$x_{n-2} = 1$ or $y_{n-2} = 1$
c_{-1}	$\bar{1}$	0	0	$\bar{1}$

the operation of $s_i + c_{i-1}$ in the add2 can be simplified than that using the addition rules shown in [5] obviously. Moreover, the carry and the intermediate sum can be represented with one binary digit, though they actually are signed digits.

Example 1: Let $n = 6$, $X = 21 = 1\bar{1}011\bar{1}$ and $Y = 57 = 11101\bar{1}$. We compute the residue addition $\langle 21 + 57 \rangle_{2^6-1} = 15$, $\langle 21 + 57 \rangle_{2^6} = 14$, $\langle 21 + 57 \rangle_{2^6+1} = 13$ as follows.

x	$1\bar{1}011\bar{1}$		x	$1\bar{1}011\bar{1}$	0	x	$1\bar{1}011\bar{1}$	$\bar{1}$
y	$11101\bar{1}$	1	y	$11101\bar{1}$	0	y	$11101\bar{1}$	$\bar{1}$
s	110001		s	110000		s	110000	
c	$0\bar{1}000\bar{1}$	0	c	$0\bar{1}000\bar{1}$	0	c	$0\bar{1}000\bar{1}$	$\bar{1}$
	$0100\bar{1}1$	15		$0100\bar{1}0$	14		$0100\bar{1}\bar{1}$	13

C. Residue Multiplication with SD Number Representation

To calculate $\langle x \times y \rangle_m$, where x and y are integers in the p-digit radix-2 SD number representation, $x \times y$ is expanded as follows:

$$\begin{aligned} x \times y &= (x_{p-1}2^{p-1} + x_{p-2}2^{p-2} + \cdots + x_0) \\ &\quad \times (y_{p-1}2^{p-1} + y_{p-2}2^{p-2} + \cdots + y_0) \\ &= \sum_{i=0}^{p-1} y_i 2^i \times (x_{p-1}2^{p-1} + x_{p-2}2^{p-2} \\ &\quad + \cdots + x_0). \end{aligned}$$

Thus, by using Property 1 we have

$$\begin{aligned} \langle x \times y \rangle_m &= \langle \sum_{i=0}^{p-1} \langle y_i 2^i \times (x_{p-1}2^{p-1} + x_{p-2}2^{p-2} \\ &\quad + \cdots + x_0) \rangle_m \rangle_m \\ &= \langle \sum_{i=0}^{p-1} pp_i \rangle_m, \end{aligned}$$

where

$$pp_i = \langle y_i 2^i \times (x_{p-1}2^{p-1} + x_{p-2}2^{p-2} + \cdots + x_0) \rangle_m \quad (6)$$

denotes as a partial product. Since $y_i \in \{-1, 0, 1\}$,

$$pp_i = y_i \langle 2^i \times (x_{p-1}2^{p-1} + x_{p-2}2^{p-2} + \cdots + x_0) \rangle_m. \quad (7)$$

Thus, a parallel algorithm for the modulo m multiplication can be implemented with the following three steps.

Let x and y be two p-digit radix-two SD numbers.

1) Calculate the residue of i-digit shifted numbers in parallel for $i = 0, 1, \cdots, p-1$,
$$sx_i = \langle 2^i \times x \rangle_m. \quad (8)$$
2) Multiply sx_i by y_i to obtain the partial product, pp_i $(i = 0, 1, \cdots, p-1)$, shown in Eq.(7).
$$pp_i = y_i \times sx_i$$
3) Calculate the modulo m sum of these partial products by performing the residue additions repeatedly.
$$\langle x \times y \rangle_m = \langle pp_0 + pp_1 + \cdots + pp_{p-1} \rangle_m$$

The algorithm can be implemented by using a binary tree of modulo m SD adders(MSDAs) for the modulo m sum of the partial products. The modulo m multiplication is performed in a time proportional to $\log_2 p$.

IV. BINARY-RESIDUE AND RESIDUE-BINARY NUMBER CONVERSIONS

In this study, we choose four moduli set $S = \{m_1, m_2, m_3, m_4\} = \{2^n - 1, 2^n + 1, 2^{2n} + 1, 2^n\}$. For the moduli set S, an integer X can be represented as $X = \{r_1, r_2, r_3, r_4\}$ in the RNS, where $r_i = \langle X \rangle_{m_i}$ and $i = 1, 2, 3, 4$. The dynamic range is $M = m_1 \cdot m_2 \cdot m_3 \cdot m_4 = 2^{5n} - 2^n$.

A. Weighted-Residue Number Conversion

Let X be a $5n$-digit SD number and represented as

$$\begin{aligned} X[5n-1:0] &= X_{5n-1}2^{5n-1} + X_{5n-2}2^{5n-2} \\ &\quad + \cdots + X_1 2^1 + X_0, \end{aligned}$$

where $0 \le X < 2^{5n} - 2^n$ and $X_i \in \{-1, 0, 1\}$. Then we have

$$\begin{aligned} r_1 &= \langle X \rangle_{m_1} \\ &= \langle X[n-1:0] + X[2n-1:n] + X[3n-1:2n] \\ &\quad + X[4n-1:3n] + X[5n-1:4n] \rangle_{2^n-1} \end{aligned}$$

$$\begin{aligned} r_2 &= \langle X \rangle_{m_2} \\ &= \langle X[n-1:0] - X[2n-1:n] + X[3n-1:2n] \\ &\quad - X[4n-1:3n] + X[5n-1:4n] \rangle_{2^n+1} \end{aligned}$$

$$\begin{aligned} r_3 &= \langle X \rangle_{m_3} \\ &= \langle X[2n-1:0] - X[4n-1:2n] \\ &\quad + X[5n-1:4n] \rangle_{2^{2n}+1} \end{aligned}$$

and

$$r_4 = X[n-1:0].$$

Consequently, several modulo m SD additions are performed for the conversion.

B. Residue-Weighted Nunber Conversion

In order to simplify the modulo operation we decompose S into two subsets, $S1 = \{2^n - 1, 2^n + 1, 2^{2n} + 1\}$ and $S2 = \{2^n, (2^n - 1) \cdot (2^n + 1) \cdot (2^{2n} + 1)\} = \{2^n, 2^{4n} - 1\}$. Therefore, the modulo $M_{S1} = 2^{4n} - 1$ addition can be implemented efficiently using the SD modulo adder. Hence, we can calculate integer $X_{S1} = \{r_1, r_2, r_3\}$ for the subset $S1$ by CRT, and the equation $X_{S1} = \langle X \rangle_{2^{4n}-1}$ exists.

Next, by using the MRC in the case of $k = 2$, we can calculate the integer X_{S2} from residue representation $\{r_4, X_{S1}\}$ for the subset $S2 = \{2^n, 2^{4n} - 1\}$. And it is obvious that X_{S2} is identical with the integer X.

Three multiplicative inverses for moduli set $S1$ can be obtained as follows:

$$\begin{aligned} \left| P_1^{-1}(2^n + 1)(2^{2n} + 1) \right|_{2^n-1} = 1 &\Rightarrow P_1^{-1} = 2^{n-2}, \\ \left| P_2^{-1}(2^n - 1)(2^{2n} + 1) \right|_{2^n+1} = 1 &\Rightarrow P_2^{-1} = 2^{n-2}, \\ \left| P_3^{-1}(2^n - 1)(2^n + 1) \right|_{2^{2n}+1} = 1 &\Rightarrow P_3^{-1} = 2^{2n-1}. \end{aligned}$$

By substituting $m_1 = 2^n - 1$, $m_2 = 2^n + 1$, $m_3 = 2^{2n} + 1$ and the values of P_1^{-1}, P_2^{-1} and P_3^{-1} into (1), we have

$$\begin{aligned} X_{S1} &= \Big\langle (2^n + 1)(2^{2n} + 1) \left\langle 2^{n-2} \cdot r_1 \right\rangle_{2^n-1} \\ &\quad + (2^n - 1)(2^{2n} + 1) \left\langle 2^{n-2} \cdot r_2 \right\rangle_{2^n+1} \\ &\quad + (2^n - 1)(2^n + 1) \left\langle 2^{2n-1} \cdot r_3 \right\rangle_{2^{2n}+1} \Big\rangle_{2^{4n}-1} \end{aligned} \quad (9)$$

Next, the coefficients of MRC for set $S2$ are calculated as follows:

$$\begin{aligned} a_1 &= r_4, \\ a_2 &= \left\langle \left\langle \frac{1}{2^n} \right\rangle_{2^{4n}-1} (X_{S1} - r_4) \right\rangle_{2^{4n}-1} \\ &= \left\langle 2^{3n}(X_{S1} - r_4) \right\rangle_{2^{4n}-1}. \end{aligned}$$

Then, using (3) we have

$$X = X_{S2} = r_4 + 2^n \langle 2^{3n}(X_{S1} - r_4) \rangle_{2^{4n}-1}. \quad (10)$$

Finally, by substituting X_{S1} into (10), the weighted integer X can be calculated from residue representation $\{r_1, r_2, r_3, r_4\}$ as follows:

$$X = 2^n \langle A + B + C + D \rangle_{2^{4n}-1} + r_4, \quad (11)$$

where,

$$\begin{aligned} A &= \left\langle 2^{3n}(2^n + 1)(2^{2n} + 1) \left\langle 2^{n-2} \cdot r_1 \right\rangle_{2^n-1} \right\rangle_{2^{4n}-1}, \\ B &= \left\langle 2^{3n}(2^n - 1)(2^{2n} + 1) \left\langle 2^{n-2} \cdot r_2 \right\rangle_{2^n+1} \right\rangle_{2^{4n}-1}, \\ C &= \left\langle 2^{3n}(2^n - 1)(2^n + 1) \left\langle 2^{2n-1} \cdot r_3 \right\rangle_{2^{2n}+1} \right\rangle_{2^{4n}-1}, \\ D &= \left\langle 2^{3n}(-r_4) \right\rangle_{2^{4n}-1}. \end{aligned} \quad (12)$$

Multiplication of a p-digit SD number A by 2^r modulo $2^p - 1$, 2^p and $2^p + 1$ can be accomplished by using the following equations:

$$\begin{aligned} \left\langle 2^r \cdot A \right\rangle_{2^p-1} &= A_{p-r-1} \cdots A_0 A_{p-1} A_{p-2} \cdots A_{p-r}, \\ \left\langle 2^r \cdot A \right\rangle_{2^p} &= A_{p-r-1} \cdots A_0 \underbrace{0 \cdots 0}_{r}, \\ \left\langle 2^r \cdot A \right\rangle_{2^p+1} &= A_{p-r-1} \cdots A_0 \overline{A_{p-1}}\ \overline{A_{p-2}} \cdots \overline{A_{p-r}}, \end{aligned}$$

where $r \le p$.Therefore, we apply above rules recursively to represent the addends in (12) in $4n$-digit SD numbers by shifting, connection and negation operations of the residue number strings, respectively.

$$\begin{aligned} A &= r_{1,1} r_{1,0} r_{1,n-1} \cdots r_{1,2} r_{1,1} r_{1,0} r_{1,n-1} \cdots r_{1,2} \\ &\quad r_{1,1} r_{1,0} r_{1,n-1} \cdots r_{1,2} r_{1,1} r_{1,0} r_{1,n-1} \cdots r_{1,2} \\ B &= \overline{r_{2,1}}\ \overline{r_{2,0}} r_{2,n-1} \cdots r_{2,2} r_{2,1} r_{2,0} \overline{r_{2,n-1}} \cdots \overline{r_{2,2}} \\ &\quad \overline{r_{2,1}}\ \overline{r_{2,0}} r_{2,n-1} \cdots r_{2,2} r_{2,1} r_{2,0} \overline{r_{2,n-1}} \cdots \overline{r_{2,2}} \\ C &= r_{3,n} \cdots r_{3,0} \overline{r_{3,2n-1}} \cdots \overline{r_{3,0}} r_{3,2n-1} \cdots r_{3,n+1} \\ D &= \overline{r_{4,n-1}} \cdots \overline{r_{4,0}} \underbrace{0 \cdots 0}_{3n}. \end{aligned} \quad (13)$$

The result of modulo m SD number addition will be in the range of $(-m, m)$ according to (5). If it is necessary that the result to be in the range $[0, m)$, we must add m to the result if it is negative.

V. Hardware Implementation

In hardware realization, an 1-digit SD number a requires two bits. In this paper, we define the 2-bit binary coding as $a = [a_1, a_0]$, such as $0 = [00]$, $1 = [01]$ and $\bar{1} = [10]$. All of these circuits have been coded in VHDL language and have been synthesized and optimized using the 0.18μm CMOS gate array technology in Synopsys Design Compiler. Table III shows the area and delay of modulo $2^n + 1$ adders and multipliers using SD number and the modulo $2^n + 1$ parallel-prefix adder which is widely used in the design of efficiency residue adder based on binary [10] with Sklansky structure. By comparison with these adders' performances in Table III,

TABLE III
PERFORMANCE OF RESIDUE ADDERS AND MULTIPLIERS USING SD NUMBER

Circuit		Area(μm^2)			Delay(ns)		
		$n=4$	$n=8$	$n=16$	$n=4$	$n=8$	$n=16$
Parallel prefix Residue adder	modulo 2^n+1	597.23	1397.92	3205.99	1.26	1.79	2.60
Proposed Residue Adder	modulo 2^n+1	913.64	1856.35	3741.76	0.82	0.82	0.82
Proposed Residue Multiplier	modulo 2^n+1	3774.55	16921.22	71463.08	2.33	3.54	4.76

TABLE IV
PERFORMANCE OF REDIDUE-WEIGHTED NUMBER CONVERTERS

Converter	Area(μm^2)			Delay(ns)		
	$n=4$	$n=8$	$n=16$	$n=4$	$n=8$	$n=16$
Residue$_{binary}$ $\longrightarrow$Binary[6]	9111.46	18251.78	36567.73	5.04	8.29	14.62
Residue$_{SD}$ $\longrightarrow$SD number(Fig.2)	14315.39	28624.39	57242.06	3.59	4.04	4.49

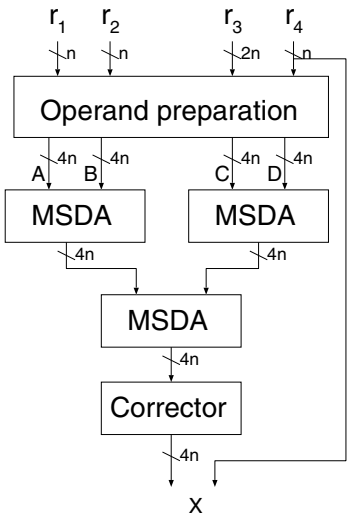

Fig. 2. Residue-binary SD number converter architecture

our proposed residue SD number adders have more efficiency using area$\times$time metric.

A residue multiplier includes a partial product generator which generates partial products by end-around shifting; a residue adder tree which add all partial products together by using the presented SD number residue adder.

For the proposed covertor, Three modulo $2^{4n}-1$ adders using SD number are applied to implement the addition $\langle A+B+C+D\rangle_{2^{4n}-1}$ in (11), as shown in Fig.2. At the first level, $\langle A+B\rangle_{2^{4n}-1}$ and $\langle C+D\rangle_{2^{4n}-1}$ are accomplished.

We evaluate the performance of the proposed residue arithmetic circuits using SD number and residue to binary conversions. We also compare our proposed converters with a current binary-based residue to binary converter reported in [6].

Table IV compares the performance of the proposed converts to that of the converter in [6]. In the case of input and output are both SD number representation as Fig.2, the delay time is reduced by approximately 44% when $n=4$, 60% when $n=8$, and 75% when $n=16$.

VI. CONCLUSION

In this paper, we have proposed the efficient residue SD addition and conversion algorithms between residue and binary numbers for moduli set $\{2^n-1, 2^n+1, 2^{2n}+1, 2^n\}$. The residue-binery converter using our algorithm requires only 2-level modulo $2^{4n}-1$ SD number adders. Then, the SD integer result can be easily converted to binary representation if necessary. Comparing with the existing binary-based converter for the same moduli set [6], our residue to binary converters offer a better time efficiency. Thus, by using our residue to binary converters and residue arithmetics will achieve greater efficiency in RNS-based applications.

REFERENCES

[1] N.S.Szabo and R.I.Tanaka, Residue Arithmetic and Its Applications to Computer Technology, New York: McGrawHill, 1967.

[2] Amos Omondi and Benjamin Premkumar, Residue Number Systems: Theory and Implementation, Imperial College Press, Sept. 2007.

[3] A.Avižienis, "Signed-digit number representations for fast parallel arithmetic," IRE Trans. Elect. Comput., EC10,pp.389-400, Sept. 1961.

[4] Mitch Thornton, "A signed binary addition circuit based on an alternative class of addition tables," Computers and Electrical Engineering, 29 pp.303-315, 2003.

[5] S.Wei and K.Shimizu, "A Novel Residue Arithmetic Hardware Algorithm Using a Signed-Digit Number Representation," IEICE TRANS.INF. & SYST., Vol.E83-D, No.12, pp.2056-2064, Dec. 2000.

[6] Bin Cao, Chip-Hong Chang, Thambipillai Srikanthan, "An Efficient Reverse converter for the 4-Moduli Set $\{2^n-1, 2^n, 2^n+1, 2^{2n}+1\}$ Based on the New Chinese Remainder Theorem," IEEE Trans. Circuits and Systems, Vol. 50, NO.10. pp.1296-1303, 2003.

[7] A.P. Vinod and A.B. Premkumar, "A residue to Binary converter for the 4-moduli superset $\{2^n-1, 2^n, 2^n+1, 2^{n+1}-1\}$," JCSC, Vol.10, pp.85-99, 2000.

[8] B. Cao, T. Srikanthan and C. H. Chang, "Efficient reverse converters for the four-moduli sets $\{2^n-1, 2^n, 2^n+1, 2^{n+1}-1\}$ and $\{2^n-1, 2^n, 2^n+1, 2^{n-1}-1\}$" IEE Proc. Computers & Digital Techniques, Vol. 152, no. 5, pp.687-696, Sept. 2005.

[9] W. Zhang, P. Siy, "An efficient design of residue to binary converter for four moduli set $(2^n-1, 2^n+1, 2^{2n}-2, 2^{2n+1}-3)$ based on new CRT II," Information Sciences 178 pp. 264-279, 2008.

[10] R. Zimmerman, "Efficient VLSI Implementation of Modulo $(2^n \pm 1)$ Addition and Multiplication," Proc. 14th IEEE Symp. Computer Arithmetic, pp. 158-167, Apr. 1999.

An Improved Pattern Matching Algorithm Based on BMHS

Jingbo Yuan , Jinsong Yang
Institute of Information Management Technology and Application
Northeastern university at Qinhuangdao
Qinhuangdao, China
jingboyuan@hotmail.com

Shunli Ding
Dept. of Information Engineering
Environmental Management College of China
Qinhuangdao, China
dingsl@163.com

***Abstract*—Pattern matching plays an important role in intrusion detection system. Based on analysis and discussions for BM, BMH and BMHS algorithms, an improved algorithm is proposed. The improved algorithm takes advantage of position information of the last character and its adjacent character in current attempt window to get bigger jump distance in each jump so to make the algorithm more efficient. Experimental results show that the number of character comparisons and windows shifts of improved algorithms is clearly reduced comparing with the BM and BMH and BMHS algorithms.**

Keywords- Pattern matching; BM algorithms; BMH algorithms; BMHS algorithms

I. INTRODUCTION

Pattern matching is an important algorithm and plays an important role in various applications. For example, it is used in data compression to compress web traffic [1], used in security applications to detect certain suspicious keywords [2] and so on.

Pattern matching can be defined as finding the occurrences of a particular string from an input string. If required to find all occurrences of the pattern in the given input text, it is known as single pattern matching, which is widely used in network security environments. In network security the pattern is a string indicating a network intrusion, attack, virus, and snort, spam or dirty network information [3], etc. In this paper, we present an improved pattern matching algorithm designed for and applied to network intrusion detection system. The rest of the paper is organized as follows. Section 2 analyses the related pattern matching algorithms. Section 3 deals with proposed improved algorithm based on BMH. Section 4 presents test and discussion. Section 5 gives the conclusions and further work.

II. ANALYSIS ON CORRELATION ALGORITHMS

Let the text, $T=T_0T_1T_2...T_{n-1}$ is a string with n characters in an alphabet. The pattern, $P=P_0P_1P_2...P_{m-1}$ is a string with m characters in the same alphabet, here, $m \leq n$. A substring of *T* corresponded with *P* in matching process is called a window. A window length is m. A comparing in some window is called an attempt.

A) BM algorithm

Among the algorithm for finding substrings, BM (Boyer-Moore) algorithm a widely known search algorithm for a single pattern and is easy to understand. It was developed by Bob Boyer and J Strother Moore in 1977[4].

BM algorithm is an exact string matching algorithms. It uses the information gained from that attempt to rule out as many positions of the text as possible where the string could not match. Its basic idea is: First P and T align left in an attempt window. From right to left characters in P compare with corresponding characters in T. If all characters are matched, then the algorithm successfully exits. If mismatching, then the algorithm calculates the distance of P to right shift. Pattern string P right shifts and starts a new round of match attempt.

At the time of pattern matching, BM algorithm focused on using information in completed matching process for calculation of the right shift distance in order to achieve fast matching purposes. The algorithm uses two heuristic rules, bad character rule and good suffix rule, to calculate the distance, and takes the largest value of two methods to shift *P* as much as possible to the right when needed.

1) bad character rule

Let function Skip(x) is the distance of P right shift, Skip(x) is defined as follows formula (1).

$$Skip(x) = \begin{cases} m & \text{If character x does not appear in the P} \\ m - Max(x) & \text{If character x does appear in the P} \end{cases} \quad (1)$$

Here m is the length of pattern string P, and max(x) is the nearest right location character x appears in P.

In the process of scanning from right to left, if finding a mismatching character x, then shifts P according to the following two situations.

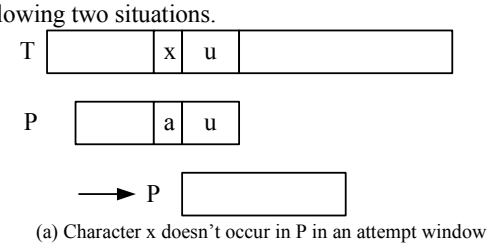

(a) Character x doesn't occur in P in an attempt window

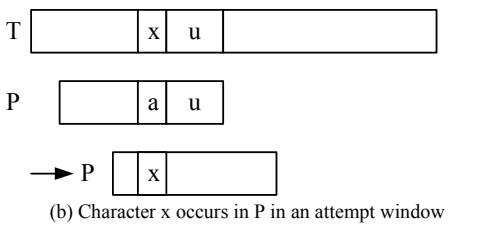

(b) Character x occurs in P in an attempt window

Figure 1. Bad character rule

978-0-7695-4818-0/12 $26.00 © 2012 IEEE
DOI 10.1109/DCABES.2012.115

If a character *x* of text T in an attempt window doesn't appear in P, apparently m characters starting from character x in T are also impossible to match with P, so can skip directly the m characters as shown in Fig. 1(a).

If a character x of text T in an attempt window doesn't appear in P, then aligns T and P by the characters x in next attempt window as shown in Fig. 1(b).

2) good suffix rule

In the process of scanning from right to left, assuming substring u (u= $P_{j..m}$, that is u is suffix of P) of P has successfully matched, that is, u=$T_{s..s+m-j-1}$= $P_{j..m}$ but $T_{s-1}\neq P_{j-1}$, then shifts P according to the following two situations.

If u occurs somewhere else in the pattern, set starting at position t, that is, u= $P_{t..t+m-j-1}=P_{j..m}$, then shift right P to align Ts and Pt to get a new attempt window as shown in Fig. 2(a). If suffix u occurs in P more than twice, then take the minimum of t.

Only a part of u occurs at the beginning of the pattern, aligns T and P according to the same longest suffix v of u to get a new attempt window as shown in Fig. 2(b).

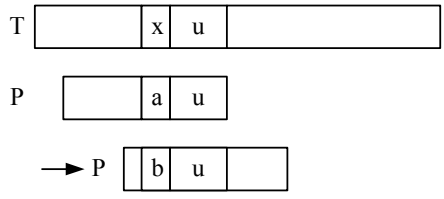

(a) Suffix u repeated occurrence in P

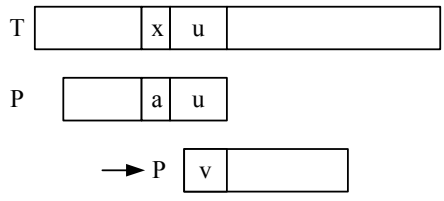

(b) Suffix u only a occurrence in P

Figure 2. Good suffix rule

In searching the algorithm compares the characters of the pattern from right to left with the text. Once finding mismatch the pattern is shifted to the right by the maximum of the values given by the good suffix and the bad-character rule. The best case is attained if at each attempt the first compared text symbol does not occur in the pattern. This moment the time complexity of BM algorithm, for a text of length n and a fixed pattern of length m, is only $O(n/m)$. The worst case is attained if the text string consists of repetitions of a single character, and the pattern string consists of m-1 repetitions of that character preceded by a single instance of a different character. In this scenario, the time complexity of BM algorithm is O(mn).

B) BMH algorithm

BM algorithm uses two kinds of heuristic steps to determine the greatest shift distance in mismatch. For two kinds of heuristic steps the greatest shift distance all can reach m. As in "good suffix" rule preprocessing and calculation procedures are more complicated, an improved and simplified BM algorithm, that is, Boyer-Moore-Horspoo (BMH) algorithm, was published by Horspol in 1980[5].

BMH algorithm considers only the "bad character" policy for skipping comparisons rather than both the Bad Character and Good Suffix Heuristics. First the last character in the attempt window is compared with the last character of the pattern. If they match the whole window is compared against the pattern to check for a match. Regardless of which character in the text to cause mismatch, it will right move window according to the last a character of the window. The shift distance calculation formula is as follows formula (2).

$$Skip(x) = \min\{h \mid P_{m-h} = x, h > 0\} \qquad (2)$$

Where x is the last character of the window, that is, is the last character of the pattern P. If the character x does not appear in the pattern Skip(x) = m. It is defined as the distance from the end of the pattern $P_1P_2\ldots P_m$ to the last occurrence of the character x.

In preprocessing phase, time complexity of the BMH Algorithm is O(m+s) and space complexity is o(s). In searching phase time complexity is in O(mn). Under best case time complexity is O(n/m). Under the worst case time complexity is O (mn). In general, the BMH algorithm has better performance than the BM algorithm.

C) BMHS algorithm

Based on BMH algorithm, Sunday proposed BMHS algorithm (Boyer-Moore-Horspool-Sunday) [6]. When calculating the bad character function, the BMHS algorithm considers the next character, that is, uses next a character to determine the shift distance. Its core idea is, first of all, left align strings T and pattern string P and match corresponding character of T and P from right to left. As mismatching judge if the next character x= T_{i+m} of the current attempt window appear in the pattern P. If don't appear, P shift right m+1 characters, or else right align the character x. So the shift distance function is defined as follows formula (3).

$$Skip(x) = \begin{cases} m+1 & \text{next character x does not appear in the pattern} \\ m - j + 1 \;\; j = \text{Max}\{j \mid P[j] = x, 0 \le j < m\} & \text{next character x appears in the pattern} \end{cases} \qquad (3)$$

When next character T_{i+m} isn't in pattern P, its shift right distance is more larger than that of BMH algorithm, where BMHS algorithm m is shift right m+1 characters but BMH algorithm is shift right bad-char[j+m-1] characters. However, when the character T_{j+m-1} don't occur and but the character T_{j+m} occur in pattern P, that is, when Badchar[j+m-1]>Badchar[j+m], the BMHS algorithm is not as good as the BMH algorithm[8]. But in typically case the BMHS algorithm is much fast than BMH algorithm. Under best case the time complexity of BMHS algorithm is O(n/m+1).

By analysis and comparison on above several single pattern matching algorithms, it can be found that the purpose of these algorithms is to right shift distance as

large as possible when a mismatch occurs between the pattern string and text strings in order to reduce the number of character comparisons and windows shifts. BM algorithm considers more comprehensive and BMH algorithm and BMHS algorithm effectively simplify and improve on the basis of BM. After comprehensive consideration the paper presents an improved algorithm, called IBMHS, based on BMHS algorithm. In general, the improved algorithm is able to make the pattern string to the maximum right distance, thereby effectively improve the efficiency of pattern matching.

III. IMPROVED BMHS ALGORITHM

By analysis and comparison on above several algorithms, it can be found that the purpose of these algorithms is to right shift distance as large as possible when a mismatch occurs between the pattern string and text strings in order to reduce the number of character comparisons and windows shifts. Based on comprehensive consideration the paper presents an improved algorithm, called IBMHS.

IBMHS algorithm considers the comparison results of characters T_{i+m-1}, Ti+m and T_{i+m+1} and P. In order to implement the algorithm, defines the following two functions.

Single character function Bchar1(x) is defined as below formula (4).

Double character function Bchar2(x,y) is defined as below formula (5).

$$\text{Bchar1}(x)=\begin{cases} m+1 & \text{character } x \text{ don't occur in the pattern string } P \\ m-1 & \text{the rightmost occurrence of character } x \text{ in the pattern } P \end{cases} \tag{4}$$

$$\text{Bchar2}(x,y)=\begin{cases} 0 & \text{string } xy \text{ don't occur in a pattern string } P \\ m\text{-}i\text{-}1 & \text{the rightmost occurrence of string } xy \text{ in the pattern } P \end{cases} \tag{5}$$

The proposed Improved BMHS (IBMHS) algorithm compares pattern P with text string T from right to left. If there is a mismatch, it need determine the rightmost shift distance of the pattern P and shift accordingly. Key processes of the algorithm are as follows.

(1) When the strings P and strings T do not match, firstly to determine whether character T_{i+m} appear in the P. If character T_{i+m} doesn't appear at all, then the algorithm can safely shift P by m+1 characters and begins next attempt as shown in the Fig. 3.

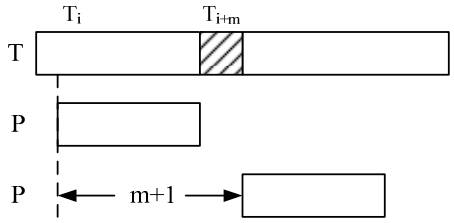

Figure 3. Character T_{i+m} does not appear in the pattern P.

(2) When the string P contains Ti+m, the algorithm determines whether string $T_{i+m}T_{i+m+1}$ appear in the P. If doesn't appear, then the algorithm can safely shift P by m+2 characters and begins next attempt as shown in the Fig. 4 (a).

(3) When the string P contains $T_{i+m}T_{i+m+1}$, the algorithm determines whether string $T_{i+m-1}T_{i+m}$ appear in the P. If doesn't appear, then the algorithm can safely shift P by m+1 characters and begins next attempt as shown in the Fig. 4 (b) ,else shift P by MAX(Bchar2[$T_{i+m-1}T_{i+m}$], Bchar2[$T_{i+m-1}T_{i+m}$]) characters and begins next attempt as shown in the Fig. 4 (c).

The IBMHS algorithm consists mainly of the preprocessing and the pattern matching. The first stage is a preprocessing of the set of patterns. The preprocessing calculates the value of functions bchar1(x) and bchar2(x,y) and uses two-dimensional array to save skip distances described briefly as following Fig. 5.

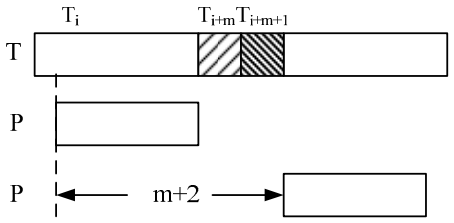

(a) String $T_{i+m}T_{i+m+1}$ does not appear in the pattern P

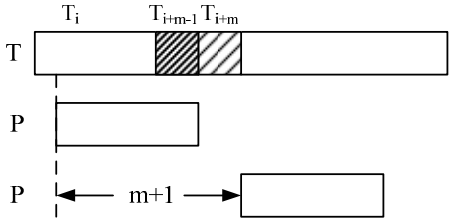

(b) String $T_{i+m-1}T_{i+m}$ does not appear in the pattern P

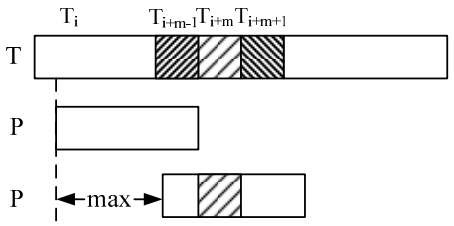

(c) String $T_{i+m-1}T_{i+m}$ and $T_{i+m}T_{i+m+1}$ all appear in the pattern P

Figure 4. Character T_{i+m} appears in the pattern P

```
// calculates the value of functions bchar1(x)
for(i=0,i<maxchar;i++)
      Bchar1[i]=m+1;
for(i=0,i<maxchar;i++)
      Bchar1[P[i]]=m-i;
// calculates the value of function bchar2(x,y)
for(i=0,i<maxchar;i++)
   For(j=0,j<maxchar,j++)
       Bchar2[i][j]=0;
for(i=0;1<maxchar;i++)
      Bchar2[i][P[0]]=m;
for(k=0;k<m-1;k++)
      Bchar2[P[k]][P[k+1]]=m-k-1;
```

Figure 5. The preprocessing process

The pattern matching process mainly performs to match given pattern and text using the results of the preprocessing process described briefly as following Fig.

```
while(i<n-m)
{for(k=1;(k<=m)&&(P[m-k]= =T[i+m-k]);k++);
 if(k>m) //match
      {S[count++]    =i;
       skip_distence=m;   }
 else
 {//mismatch
  if(T[i+m] does not appear in the pattern P)
  { skip_distence = m+1; }
 else
    { if (T[i+m]T[i+m+1] don't appear in the
pattern P)
      {if(T[i+m] is the last character of the P)
          skip_distence =1;
       else i+= m+2; }
    else
       if(T[i+m-1]T[i+m] don't appear in the
pattern P)
          { skip_distence =m+1;}
       else
       skip_distence=
       max(Bchar2(T[i+m],T[i+m+1]),Bchar2(T[i
                                  +m-1],T[i+m]));}}
    i=i+ skip_distence;
}
```

Figure 6. The pattern matching process

IV. PERFORMANCE ANALYSIS AND TEST ON IMPROVED ALGORITHM

The maximum shift size of IBMHS algorithm can reach m+2. Therefore, the occurring probability of the maximum shift distance in IBMHS algorithm is larger than BM, BMHS and BMH algorithm. In the best case the time complexity of IBMHS algorithm is O(n/m+2), which is superior to other three algorithms.

To further test the performance of the IBMHS algorithm, we ran tests on English text to compare the IBMHS algorithm with the BM and BMH and BMHS algorithm. Four algorithms were implemented using C language. We obtained these evaluation parameters with some function in program executing. The different length pattern string matching was performed respectively.

In test, 50 text strings are chosen randomly from kjv.txt and each text string contains 10000 characters. Each text string is matched with 50 pattern strings that also randomly chosen by random function from kjv.txt. The number of characters in pattern strings is 3 to 30.

Each algorithm is evaluated with the number of compared characters and the number of attempt windows, that is, the number of skips. The contrast of test results show in Fig. 7 and Fig. 8.

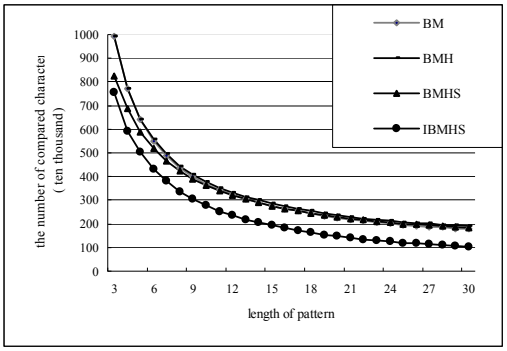

Figure 7. The number of compared characters

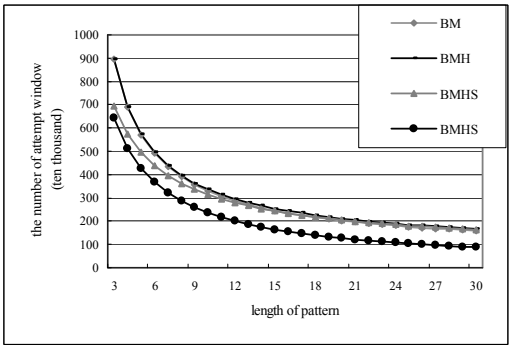

Figure 8. The number of attempt windows

Fig. 7 compares the total number of compared character for four algorithms in different length pattern. Fig. 8 compares the total number of attempt windows for four algorithms in different length pattern.

The testing results have shown that the IBMH algorithm has less number of comparisons and less number of attempt windows in comparison with the BMH and BMHS algorithms. On average the number of comparisons and the number of attempt windows of the IBMH algorithm decrease about 30% and 32% respectively comparisons with BMHS algorithms. The longer the pattern string, the more the number of reduction. It is thus clear that the IBMH algorithm has

efficiently performance improvement and has great practical value.

V. CONCLUSION AND FURTHER WORK

The paper analyses BM, BMH and BMHS pattern matching algorithms, and proposes an improved algorithm IBMHS. IBMHS takes two successive characters in the text string to calculate skip distance in order to increase the probability of pattern string right shift by largest movement distance. Experimental results show that the performance of IBMHS algorithm is better than the other three algorithms in terms of number of comparisons and shifts. Further work is to study the application of IBMHS in intrusion detection system to improve the performance of intrusion detection.

REFERENCES

[1] Bremler-Barr, A.; Koral, Y.; Zigdon, V.H. Shift-based pattern matching for compressed web traffic. IEEE 12th International Conference on high Performance Switching and Routing (HPSR), Page(s): 222 – 229, 2011.

[2] Yang Wang and Hidetsune Kobayashi. High Performance Pattern Matching Algorithm for Network Security. IJCSNS International Journal of Computer Science and Network Security, VOL.6 No.10. pp. 83-87, 2006.

[3] Raju Bhukya, DVLN Somayajulu. AN EVEN ODD MULTIPLE PATTERN MATCHING ALGORITHM. International Journal of Engineering Science and Technology (IJEST), Vol. 3 No. 3,pp. 2118-2126, 2011.

[4] S Boyer, J S Moore. A Fast String Searching Algorithm[J]. Communications of the ACM, 1977, 20(10): 762- 772.

[5] Horspool R N. Practical Fast Searching in Strings[J]. Software practics & Experience, 1990(10) : 501- 506.

[6] Daniel M S. A very fast substring search algorithm [J].Communications of the ACM, 1990, 33 (8):132-142.

The Research and Analysis of Hungarian Algorithm in the Structure Index Reduction for DAE

Yan Zeng[1,2], Xuesong Wu[1], Jianwen Cao[1]

1. Laboratory of Parallel Software and Computational Science of Software, Institute of Software Chinese Academy of Sciences, Beijing, 100190, China;
2. Graduate University of Chinese Academy of Sciences, Beijing, 100049, China.

Email: zengyan_616@yahoo.cn ; xuesongwu@msn.cn; caojianwen@gmail.com

***Abstract*—Modeling of complex physical systems with Modelica usually leads to the high-index differential algebraic equation system (DAE), index reduction is an important part of solving the high-index DAE. The structure index reduction algorithm is one of the popular methods, but in special cases, it fails. Combinatorial relaxation algorithm can detect and correct the breakdown situation. And the maximum weight matching of bipartite graph is an important part of the combinatorial relaxation algorithm. In order to choose the proper method for the large-scale, dense bipartite graph, this paper provides three implementations of the Hungarian algorithm. The experiment results and the theory show that the BFS single-augmented method is better than others.**

Keywords—Modelica; Bipartite Graph; DAE; Hungarian Algorithm; Augmenting Path

I. INTRODUCTION

With development of complex products, they are often related to many different domains, such as mechanical, control, electronic, hydraulic, pneumatic, etc. One of the areas of research on complex products is multi-domain modeling and simulation. Modelica[1] is a object-oriented physical modeling language for physical modeling of complex physical system modeling and simulation. Modeling of complex physical systems with Modelica usually leads to high-index differential algebraic equation system (DAE), which consists of large-scale equations. The structure index reduction algorithm is a popular method for the large-scale, high-index DAE, such as Pentelides algorithm [3] transforming the high-index DAE to the low-index DAE. But in some special cases, the structure index algorithm fails. Based on combinatorial optimization theory, Kazuo Murota[4] corrected the breakdown situation through such mathematical theories as polynomial matrix and standard form, so that the robustness of the structure index reduction algorithm can be enhanced in the algorithm library.

The combinatorial relaxation algorithm includes three phases: The first phase—using available combined algorithm (such as Hungarian algorithm [5], KM algorithm [5, 6]) to solve the maximum weight matching of bipartite graph. The second phase—tight testing, checking whether the maximum weight matching $\hat{\delta}_k(A)$ of the structure matrix of A(x) with cardinal number k is equal to the maximum degree $\delta_k(A)$ of k-order sub-matrix of the real matrix A. The third phase—correcting fails, if $\hat{\delta}_k(A) \neq \delta_k(A)$, transforming the matrix A to matrix A' by biproper transform[7], to reduce the difference between $\hat{\delta}_k(A)$ and $\delta_k(A)$. Repeat these three phases until$\hat{\delta}_k(A) = \delta_k(A)$.

The maximum weight matching of bipartite graph is a key part of the combinatorial relaxation algorithm. In order to choose a good method for the large-dense bipartite graph, this paper presents and analyses the three implementations of the Hungarian algorithm through theory analysis and experiments. The three implementations include BFS single-augmented method, DFS single-augmented method, and multi-augmented method. Compared with the theory analysis, the experiment results are consistent with it. According to the experiment results,

978-0-7695-4818-0/12 $26.00 © 2012 IEEE
DOI 10.1109/DCABES.2012.110

it can take advantage of different implementations for different DAE system to complement the structure index reduction of the high-index DAE.

This paper is organized as follows. Section 2 presents the Hungarian algorithm. Section 3 introduces and analyses three implementations of the Hungarian algorithm. Comparing and analyzing the three implementations by experiment results in section 4. Section 5 gives a conclusion.

II. THE HUNGARIAN ALGORITHM

The Hungarian method is a combinatorial optimization algorithm which solves the assignment problem in polynomial time and which anticipated later primal-dual methods. It was developed and published by Harold Kuhn in 1955, and the algorithm was largely based on the earlier works of two Hungarian mathematicians: Dénes König and Jenö Egervávy [5]. Later, based on the Berge theorem and Hall theorem, it was improved by Edmonds in 1965[8].

The Hungarian algorithm is a classical algorithm for solving the maximum matching of bipartite graph, it not only detects the existing of the maximum matching, but also gives out the maximum matching.

The idea of Hungarian algorithm for solving the maximum matching of bipartite graph is: Given a bipartite graph G=(X, Y, E) and a match M, firstly, select a vertex *x* unsaturated for M from the set X. Then, search for augmenting path, if there is no any augmenting path with starting point *x*, it shows that there is no saturated match for X according to Hall theory [9]. If there is an augmenting path P with starting point *x*, then M is not the maximum matching of G, and there is a matching $M'(M' = M \oplus E(P))$ being greater than M. Use M' to replace M, and continue searching for augmenting path related M. Repeat above operations, until there is no augmenting paths in G, so the last matching M is the maximum matching of G. The process of searching for augmenting shows in Figure 2.1:

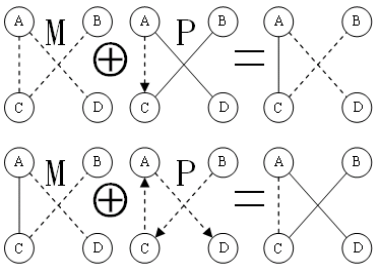

Figure 2.1 Searching for Augmenting Path

For any problem which can be modeled as the maximum matching of bipartite graph, we can consider to use the Hungarian algorithm to solve it. And, there are many algorithms about bipartite graph are based on it, such as KM algorithm which solves the maximum weight matching of bipartite graph.

III. THREE IMPLEMENTATIONS FOR THE HUNGARIAN ALGORITHM

From the section 2, we can see that searching for augmenting path is a key part of the Hungarian algorithm. Breadth-first search and depth-first search are two classical algorithms for finding augmenting path. They just find one augmenting path when using the Hungarian algorithm to solve the maximum matching of bipartite graph. Hopcroft and Karp[10] put an idea of finding multi-augmented path in 1972. That is, concurrently search for more than one shortest augmenting path without same vertex at every step, and all the shortest augmenting paths form into maximal augmented path set S. Then, augment the paths in S at the same time. Based on these ideas, this paper provides three implementations of the Hungarian algorithm: BFS single-augmented method, DFS single-augmented method, and multi-augmented method, for the large-scale bipartite graph. In this paper, we use the adjacent matrix to storage the large-scale bipartite graph G(X, Y, E), and hypothesize $|X| = |Y| = n$.

A. BFS single- augmented method

BFS (Bread-first search) is a common kind of graph search algorithm, and its idea is: Given a graph G(V, E) and the origin vertex s, search all the edges in G to find all vertices u which can be arrived from the origin vertex s, and compute the distances between s and the vertices u. That is, it will find the vertices with distance k starting from s at first, and then find the

vertices with distance k+1 starting from s. BFS always extends the border which is between discovered and undiscovered vertices along the span direction.

The process of searching for single-augmented path by BFS is as follows:

Input: bipartite graph G=(X, Y, E)

Output: the maximum matching M

Step 1: Initialize $M = \emptyset$.

Step 2: select an unmatched vertex x from set X, and search for all vertices y ($y \in Y$), which are not matched by x, and can be arrived from vertex x with distance k. If there is a vertex y_i satisfying the conditions, mark the match vertex of the vertex y_i as x, and modify the match M. Then it obtains a shortest augmenting path with distance k. Continue searching for the vertices until there is no vertex y satisfying the conditions.

Step 3: According to Step 2, search for the vertices y ($y \in Y$), which are not matched by vertex x, and can be arrived from vertex x with distance k+1. Repeat this step, and continue searching for all other vertices with distance k+2, k+3 … until there are no vertex satisfying the conditions.

Step 4: If there is no augmenting path in G, stop, and output the maximum matching M. Otherwise go to Step 2.

The Hungarian algorithm is polynomial time. It updates the matching when it finds an augmenting path, and the edges of matching M is increased by one, so there is at most n times searching for augmenting path. For the adjacent matrix, the time complexity of searching for one augmenting path by BFS is $O(n^2)$ [11]. So that, the time complexity of the Hungarian algorithm, searching for single-augmented path by BFS, is $O(n^3)$.

B. DFA single- augmented method

Depth-first search is a graph algorithm, and it obeys the search strategy searching a graph deeply as possible. During the search of the DFS, for the current vertex u, if there is an un-searched edge with the starting point u, continue searching along this edge until all edges with the starting point u are searched. Back to the parent vertex of u, and continue to search the other edges until all vertices which can be arrived form origin vertex are found. If there are un-found vertices, select one as an origin vertex, and repeat above steps until all vertices are found.

The process of searching for single-augmented path by DFS is as follows:

Input: bipartite graph G=(X, Y, E)

Output: the maximum matching M

Step 1: Initialize $M = \emptyset$.

Step 2: Select an un-matched vertex x from the set X, and search for all vertices y in the set Y($y \in Y$), which are abject to vertex x, and are not matched by x. If it finds out such a vertex y_i, it finds out an augmenting path. Then mark the vertex y_i being matched, and modify the matching M, the recursion ends.

Step 3: If there is no augmenting path in graph G, stop, and output the maximum matching M. Otherwise go to Step 2.

This method needs to search augmenting path for n times, and the time complexity of searching for an augmenting path by DFS is $O(n^2)$. So the time complexity of the Hungarian algorithm, searching for single-augmented path by DFS, is $O(n^3)$.

C. Multi-augmented method

Hopcroft and Karp put up an idea of finding multi-augmented path in 1972. That is, at the step of searching for augmenting path, it searches for more than one shortest augmenting path concurrently, rather than one shortest augmenting path. All the shortest augmenting paths form into a maximal augmenting path set S, and then augment the paths in S at the same time.

The process of searching for multi-augmented path is as follows:

Input: bipartite graph G=(X, Y, E)

Output: the maximum matching M

Step 1: Initialize $M = \emptyset$.

Step 2: Select all un-matched vertices from set X, and all these vertices form into a set S. Then for the vertex x_i in the set S, respectively, search for un-matched vertex y_j in set Y($y_j \in Y$), which can be arrived from vertex x_i with distance k, and these vertices are different with each other , and form into a maximum augmenting path set P.

Step 3: Along with all augmenting paths p in the set P, augment all paths p by DFS. For every path p_i, hypothesizing that the vertex x_i is the origin vertex, if there is an un-matched vertex y_k in the set Y, satisfying the conditions that it can be arrived from x_i, and is on the augmenting path p_i, then it finds out an augmenting path p_i'.

Step 4: If there is no augmenting path in graph G, stop, and output the maximum matching M. Otherwise go to Step 2.

All the shortest augmenting paths searched by the BFS in every time have same length. With the executing of the algorithm, the length of the shortest augmenting paths increases gradually. At last, it needs $n^{0.5}$ times to gain the maximum matching [10]. And augmenting the path in set P by DFS, its time complexity is $O(n^2)$. Therefore, the time complexity of the Hungarian algorithm, searching for multi-augmented paths, is $O(n^{2.5})$.

D. Analysis of the three methods

The bread-first search technology has no backtracking operation, but the depth-first search technology has, so for the Hungarian algorithm, BFS single-augmented method is faster than DFS single-augmented method. As it needs to storage all vertices produced during the bread-first search, but the depth-first search does not, the memory needed by BFS single-augmented method is more than DFS single-augmented method. Multi-augmented method combines DFS technology and BFS technology, so it is faster than DFS single-augmented method, but slower than BFS single-augmented method. And the memory needed by multi-augmented method is more than DFS single-augmented method, but less than BFS single-augmented method.

IV. EXPERIMENTAL RESULTS AND ANALYSIS

Modeling of complex physical systems with Modelica usually gets high-index DAE system. Before using the combinatorial relaxation algorithm to reduce the index, construct a bipartite graph G(X, Y, E) for the DAE system. The vertex x_i in the set X stands for the i-th equation, and the vertex y_j in the set Y stands for the j-th variable. In these examples, we use adjacent matrix G[n][n] to storage the relationship between differential algebraic equations and variables. The rows stand for the differential algebraic equations X, and the clowns stand for variables. Hypothesizing $|X| = |Y| = n$, $|E| = m$, the edge e_{ij} stands for the relationship between the i-th differential algebraic equation and the j-th variable.

In the three examples, the data scales respectively are: (1) n=500, m=500*500; (2) n=5000, m=5000*5000; (3) n=10000, m=10000*10000. Experiment environment is: Linux platform(Debian 4.4.5-8), Intel(R) Xeon(R) CPU X5472 @3.00GHz, Memory 16 GB, Compiler Gcc version 4.4.5. The experiment results show in "Table I".

Table I. The experiment results of the three implementations

Examples / Run time(s)	**Case 1** n=500 m=500*500	**Case 2** n=5000 m=5000*5000	**Case 3** n=10000 m=10000*10000
DFS single-augmented method	0.11s	72.12s	549.87s
BFS single-augmented method	0.04s	6.9s	28.32s
Multi-augmented method	0.05s	7.96s	34.61s

The "Table I" shows, for the dense bipartite graph, BFS single-augmented method is the fastest, multi-augmented method is later, and DFS single-augmented method is the slowest. In the examples, the runtime ratio of BFS single-augmented method and multi-augmented method is stable, and it keeps up about 83%. The runtime ratio of BFS single-augmented method and DFS single-augmented method is about 33%—5%. The runtime ratio of multi-augmented method and DFS single-augmented method is about 50%—6%. With the scale increasing, the difference of runtime between BFS single-augmented method, multi-augmented method and DFS single-augmented method are more and more large respectively. The experiment results are consistent with the theory analysis. According to the experiment results, for the large-scale, dense bipartite graph, BFS single-augmented method and multi-augmented method are better than DFS single-augmented method.

V. CONCLUSION

Modeling of complex physical systems with Modelica usually gets high-index DAE system. The structure index reduction algorithm is a popular method to reduce the high-index DAE to low-index DAE, but it fails in some special cases. The combinatorial relaxation algorithm can detect and correct the breakdown phenomenon, and the maximum weight matching of bipartite graph is a key part of it. For the large-scale dense bipartite graph, this paper gives three different implementations of the Hungarian algorithm. The experiment results are consistent with the theory analysis: BFS single-augmented method is the fastest, multi-augmented method is later, and DFS single-augmented method is the slowest. With the scale increasing, the runtime of the three methods are very long. Searching for augmenting path is important for the three methods, so in the future, we will consider parallelizing the three methods to solve the large-scale or super large-scale bipartite graph fast and efficiently. So it is more efficient for solving DAE system.

ACKNOWLEGEMENTS

This research has been supported by National Natural Science Foundation (61170325).

REFERENCE

[1] Fritzson P. Principles of Object-Oriented Modeling and Simulation with Modelica 2.1. New York: IEEE Press, 2003.

[2] Mikael Zebbelin Poulsen. Structural Analysis of DAEs. Denmark: Informatics and Mathematical Modeling Technical University of Denmark, 2001.

[3] Constantino C.Pantelides. The Consistent Initialization of Differential-Algebraic Systems. SIAM Journal on scientific and statistical computing,1988, 9(2): 213-231.

[4] Kazuo Murota .http://www.misojiro.t.u-tokyo.ac.jp/~murota/index.en.html.

[5] Hungary algorithm. http://en.wikipedia.org/wiki/Hungarian_algorithm.

[6] J. Munkres. Algorithms for the Assignment and Transportation Problems. Journal of the Society for Industrial and Applied Mathematics, 5(1):32–38, 1957.

[7] Wei Zhang. The Research and Analysis of Structural Index Reduction Algorithm via Combinatorial Relaxation. Beijing, ISCAS, 2009.

[8] J.Edmonds. Path, tree and flowers, Canad. J. Math., 17(1965)449-467.

[9] Sui xiang Gao. Graph Theory and Network Flow Theory. Higher Education Press, p-83,2009.

[10] Hopcroft-Karp algorithm. http://en.wikipedia.org/wiki/Hopcroft%E2%80%93Karp_algorithm .

[11] Thomas H.Cormen Charles E.Leiserson, Ronald L.Rivest Cliford Stein. Introduction to Algorithms, Second Edition . China Machine Press, 2007.

Improved Particle Swarm Optimization Algorithm of Inverse Heat Conduction

Qi Jingjing, Guo Yucheng*, Zhou Ming
School of Computer Science and Technology
Wuhan University of Technology
Wuhan 430063,China;
E-mail: ginjiq@126.com; 15972111920@139.com

Zhang Shesheng
Department of Statistics
Wuhan University of Technology
Wuhan.430070 China
zhangshesheng@sohu.com

***Abstract*—Inverse Heat Conduction Problem (IHCP) has the characteristics of non-linearity, ill-posedness and heavy computation, because of which, there haven't been any theories or algorithms with broad application scope to solve it yet. In this paper, we use standard Particle Swarm Optimization (PSO) algorithm to solve fine-mesh 2 Dimensions (2D) IHCP. The experimental data shows that the standard PSO algorithm is not suitable for solving fine-mesh 2D IHCP. Considering the particular application fine-mesh 2D IHCP, the paper gives an improved strategy for the standard PSO algorithm. Results show that the improved PSO algorithm has a great improve in global search capability and solution precision.**

Keywords-2D IHCP, Fine-mesh, PSO Algorithm, Improved PSO Algorithm

I. INTRODUCTION

Inverse Heat Conduction Problem [1][2][3](IHCP) is a classical Mathematical Physics inverse problem ,and is applied in many engineering fields.

IHCP can be divided into four types:

1) Known initial temperature (initial value), the boundary temperature functions and the additional conditions, find heat conduction coefficients (parameters of heat conduction equation), heat source term etc.
2) Known part of the boundary temperature functions, heat conduction coefficients, heat source term, find another boundary temperature function.
3) Known temperature distribution inside the boundary, heat conduction coefficients, find the boundary temperature functions.
4) Known part of the boundary temperature functions, heat conduction coefficients, temperature function somewhere within the boundaries, find another boundary temperature function.

This paper researches the fourth types. Inverse Heat Conduction Problem (IHCP) has the characteristics of non-linearity, ill-posedness and heavy computation, because of which, there haven't been any theories or algorithms with broad application scope to solve it yet. Commonly used heuristic algorithms: conjugate gradient method, steepest descent method, regularization method, Newton method, variable-metric method, relaxation method etc are flawed. Such as the regularization method, it is relatively perfect in theory, but in specific application, it is difficult to determine its stability of function, function's normed spaces, and regularization parameters. And the accuracy of those methods is not too high. In addition, most current researches are focused on one-dimensional IHCP and a single case volume of IHCP, compared with the multi-dimensional IHCP and many volumes of IHCP, which greatly limits IHCP's application in engineering field. Therefore, the introduction of the new algorithm has become the only way to solve the problem.

II. 2-DIMENSIONS IHCP

Numerical computation method is adopted to resolve IHCP usually. With the engineering background of predicting the inner wall's temperature of ceramic or the cylinder of internal combustion engine with metal gradient thermal barrier coatings, we have done some researches on IHCP and its value is that we can judge the thermal properties of composite materials when we know the temperature of the outer wall and the internal measuring points. In this paper the boundary conditions is a two-dimensional, nonlinear time-varying function.

The mathematical model of IHCP is described as equation(1):

$$\frac{\partial u}{\partial t}=\frac{\partial}{\partial x}(k1\frac{\partial u}{\partial x})+\frac{\partial}{\partial y}(k2\frac{\partial u}{\partial y})+g \quad 0\le x,y\le 1, t\ge 0 \quad (1)$$

In the equation above, k1 is the thermal conductivity on the x direction and k2 is the thermal conductivity on the y direction, g is the term of heat source. Since the heat source is on the boundary in this paper, the problem is transformed into solving the problem of boundary temperature function and the simplified mathematical model is described as below:

$$\frac{\partial u}{\partial t}=\frac{\partial}{\partial x}(k1\frac{\partial u}{\partial x})+\frac{\partial}{\partial y}(k2\frac{\partial u}{\partial y}) \quad 0\le x,y\le 1, t\ge 0 \quad (2)$$

In this paper, the model of research is the ceramic / metallic internal combustion engine. In this model the height of the internal combustion engine is much greater than the thickness (Namely: $h >> l$), so we can regard that the thermal conductivity changes only on the direction of thickness (the x direction). According this k1 is equal to k2

* Corresponding author.E-mail: 15972111920@139.com

978-0-7695-4818-0/12 $26.00 © 2012 IEEE
DOI 10.1109/DCABES.2012.29

in equation (1), we named them as k. Adding to the boundary conditions, we can get the Two-dimensional mathematical model of heat conduction:

$$\begin{cases} \frac{\partial u}{\partial t}=\frac{\partial}{\partial x}(k\frac{\partial u}{\partial x})+\frac{\partial}{\partial y}(k\frac{\partial u}{\partial y}) & 0<x,y<1,t>0 \\ u(x,y,0)=0 & 0\le x,y\le 1 \\ u(1,y,t)=0 & 0\le y\le 1,t>0 \\ u(x,0,t)=0 & 0\le x\le 1,t>0 \\ u(x,1,t)=0 & 0\le x\le 1,t>0 \\ u(x',y',t)=u^*(x',y',t) \end{cases} \quad (3)$$

The mathematical model above describes the temperature of a new type of composite materials changing over time in the two-dimensional space ($x\in[0,1],y\in[0,1]$). In the equation(3), u*(x',y',t) stand for the temperature of point (x',y') at time t and k is the thermal conductivity .

This paper needs solving the left boundary conditions, Ideas for the solution : According to certain conditions for boundary conditions are given for the left, add the known three conditions can use heat conduction problem is a method to solve the temperature within the boundary field of all internal points, This can get somewhere in the known condition of the temperature u^0(x',y',t) ; There is an error between u^0(x',y',t) and u*(x',y',t) for the temperature on the boundary is not the correct value, but given by some conditions. So we can get the error by extracting the square root of the sum of the two temperatures:

$$E=\frac{1}{n}\cdot\sum_{i=1}^{n}\left(u^0-u^*\right)^2 \qquad (4)$$

And we can adjust the boundary conditions until the error E meets the expected precision. Thus, the heat conduction problem is the basis for solving the inverse problem. In this paper we use multigrid method and the virtual boundary prediction method proposed by Professor Guo Qingping to solve the heat conduction problem [4], which greatly reduces the computation and improves the speed and accuracy of computation.

Here we divide the space into different grids according to the different space steps and solve it using PSO algorithm when we do researches on the two-dimensional IHCP.

III. THE INTRODUCTION OF PSO ALGORITHM

The PSO (Particle Swarm Optimization) algorithm was first proposed by James Kennedy which is a social psychologist of and Russell Eberhart which is an electrical engineer in America. It is an evolutionary algorithm similar to the genetic algorithm which simulates the natural laws.

Searching for the optimal solutions in solution space is the essence of PSO, so the individual mentioned above is also called particles and each particle is a feasible solution. PSO is the iteration of a group of particles, here we assume the number of particles is N, the dimension of solution space is M, and then each particle can be mapped to a vector of the M-dimensional solution space.

Suppose the current vector of particle is as below:

$$p_i=(p_{i1},\quad p_{i2},\quad \cdots\quad p_{iM})$$

The current velocity vector of particle:

$$v_i=(v_{i1},\quad v_{i2},\quad \cdots\quad v_{iM})$$

The fitness function of particle which determines whether the location of particle is good:

$$f(p_i)=f(p_{i1},\quad p_{i2},\quad \cdots\quad p_{iM})$$

Local optimum vector is the best location for particle pi currently.

$$pbest_i=(pbest_{i1},\quad pbest_{i2},\quad \cdots\quad pbest_{iM})$$

Global optimum vector is the best location in the N local optimum vector:

$$gbest=(gbest_1,\quad gbest_2,\quad \cdots\quad gbest_M)$$

The formula of updating the velocity and position:

$$v_i^{k+1}=v_i^k+r_1*c_1\left(pbest_i-p_i^k\right)+r_2*c_2\left(gbest-p_i^k\right)$$

$$p_i^{k+1}=p_i^k+v_i^{k+1}$$

In the formula above, i range from 1 to N, k is the current number of iterations and k+1 is the current number of iterations. c1, c2, r1, r2 are the random numbers. r1 and r2 range from 0 to 1 which keep the diversity. c1 and c2 range from 0 to 2 which are called the learning factors. c1 indicates the self-learning ability of particles and c2 indicates the learning ability from the best particle. The particles can keep close to the group through continuous learning from the best particle.

IV. USING PSO FOR IHCP

The research of IHCP in this paper is the left boundary conditions (u(0,y,t)) in the two-dimensional space($x\in[0,1],y\in[0,1]$), thus it is related to the division of two-dimensional problem when we solve the specific problems. We use PSO to solve the IHCP under three different meshes here.

1): The coarse mesh inverse problem when space step h=0.1

In this mesh each particle has 11-dimensional, that is each left boundary is simulated by 11 points range from 0 to 1.0. The result is as Figure1.

In the Figure1, the blue points are the values by computing and the red points are the actual values. As seen the PSO can solve the two-dimensional IHCP precisely under the coarse mesh.

2): The fine mesh inverse problem when space step h=0.05

In this mesh each particle has 21-dimensional, and it is belong to the fine mesh inverse problem. The result is as Figure2.

In the Figure2, the blue curve is the value by computing and the red curve are the actual value. This result shows that the accuracy is not high when solving the two-dimensional IHCP using PSO under the fine mesh.

3): The fine mesh inverse problem when space step h=0.02

Through further refinement of the space, there are 51-dimensional under this fine mesh inverse problem. The result is as Figure3.

In the Figure3, the blue curve is the value by computing and the red curve are the actual value. This result shows that

we can not solve the two-dimensional IHCP using PSO under this fine mesh.

V. ERROR ANALYSIS

By analyzing the experimental data, we can get the primary reasons which affect the accuracy when we use PSO to solve the IHCP under the fine mesh.

The first reason: one-dimensional degenerate

In essence, the PSO algorithm is the evolutionary algorithm using group iterative and searches for the best solution following the best particle. Although seen from the whole, the fitness is decreasing and evolving continually, there is no mechanism to ensure the particles constantly to evolve close to the true value in each dimension.

When the space step is much small, maybe the fitness of a particle is not very good but some of its dimensions meet the accuracy during a particular iteration, then the next iteration happens, the fitness of this particle become better but the dimensions meet the accuracy last have been updated, so their accuracy become pool, which is called one-dimensional particle degradation.

The second reason: premature

Each particle is actually a feasible solution in PSO, which is the left boundary we need to solve. If the space step was too small, the solution space would be too large and the phenomenon of premature would happen for falling into local optimum.

VI. THE IMPROVED PSO

From the analysis of the previous section, we can see that the capability of searching is week when the num of particle dimensions is too large. This is the defect of PSO because there is no mechanism to prevent the phenomenon of one-dimensional particle degradation happening.

Combined with the practical application of this paper is solving the two-dimensional IHCP using PSO. The fitness function of PSO algorithm is:

$$f(p_i) = E = \frac{1}{n} \cdot \sum_{i=1}^{n} \left(u_i - u_i^0 \right)^2 \quad (5)$$

This is the source of the error：according to the position of the particles, that is the value of each dimension particles, as a left boundary conditions, with the known condition: the right boundary, the lower boundary, the boundary, the initial value (t = 0 time value), 2 D heat conduction problem is the mathematical model of solving the measuring point out the actual temperature measuring and calculating the error between the temperature.

When solving two-dimensional heat conduction problem we use a 5-point implicit iterative method:

$$u_{i,j}^{k} = \frac{1}{A}\left[u_{i,j}^{k-1} + \lambda \left(a_{i+\frac{1}{2},j}^{k-1} \times u_{i+1,j}^{k} - a_{i-\frac{1}{2},j}^{k-1} \times u_{i-1,j}^{k} + a_{i,j+\frac{1}{2}}^{k-1} \times u_{i,j+1}^{k} - a_{i,j-\frac{1}{2}}^{k-1} \times u_{i,j-1}^{k} \right) \right] \quad (6)$$

In the formula above, $u_{i,j}^{k}$ is the temperature of point (i,j) at time k. The meaning of 5-point implicit iterative method is that if we want to get the value of $u_{i,j}^{k}$, we need to know the temperature of five points: $u_{i,j}^{k-1}$ is the temperature of point (i,j) at time k-1, which is a known condition, $u_{i+1,j}^{k}$ is the temperature of point (i+1,j) at time k, $u_{i-1,j}^{k}$ is the temperature of point (i-1,j) at time k, $u_{i,j+1}^{k}$ is the temperature of point (i,j+1) at time k, $u_{i,j-1}^{k}$ is the temperature of point (i,j-1) at time k.

Seen from the formula, the computing error of a point comes from the four points around it, so we can know that a point on the boundary would bring error to some of the measuring points, but not all. Similarly ,can be launched on the edge of a point, y_j , $j \in [0,1]$， Only may affect two point value: $u(x, y_{j+1}, t)$ and $u(x, y_{j-1}, t)$， the error of this two point should be made by the boundary point yi,but the other point error should be make by the other corresponding the boundary point 。So for every boundary point yi，Can find a concrete plan to measure the accuracy: the calculated value of practical value and the error between the point $u(x, y_{j+1}, t)$ and $u(x, y_{j-1}, t)$,here the error can also take two points of the mean error. In the PSO, the point y_j , $j \in [0,1]$ which is on the boundary is the j-dimensional of the particle, so we can translate checking the accuracy of the boundary into checking the accuracy of the j-dimensional of particle. When using this method in the PSO, we can make sure that each dimension of the particle is evolving toward the true solution. And we can add new particles to enrich the diversity of population to prevent the occurrence happening.

The strategy adopted in this paper is:

In the standard PSO algorithm, add a step: when getting the fitness of a particle, we use the method above to check the accuracy of each dimension of the particle and then generate a new particle which will inherit the dimension with high accuracy, improve the dimension with low accuracy, So the improved particle can keep the dimension with high accuracy in the group. After getting the fitness of the new particle which is better than the fitness of local optima, we replace the local optimum location with this particle, which can prevent the population from expansion infinitely.

This strategy can ensure that the particles evolve as a unit in each dimension, rather than the entire particle and there are new particles joining to the group each iteration.

At last we compare the PSO with the improved PSO under the fine mesh when space step h=0.02. The result is as Figure4.

VII. CONCLUSIONS

The PSO algorithm can do well in IHCP under the coarse mesh but can not do well under the fine mesh because the one-dimensional degenerate and premature will happen when the dimension is many. In this paper we analysis the two problems which are one-dimensional degenerate and premature and propose the improved PSO. The results show

that the improved PSO is much better than PSO when the dimension is many.

ACKNOWLEDGMENT

This work is supported by National Key Open Computer Laboratory Fund of China Academy of Science (NO. SYSKF1009).

REFERENCES

[1] Lin jiansheng.Particle swarm algorithm and neural network algorithm in the application of heat conduction problem solving[D].wuhan: Computer college of wuhan university of technology,2010.

[2] Qi Jingjing, Zhang Shesheng, Lin Jiansheng. Half Analytic Half Numeric Multigrid Virtual Boundary Parallel Numerical Model of Inverse Heat Conduction Problems. DCABES 2008 PROCEEDINGS [C], Wuhan,2009:32-34.

[3] Qi Jingjing, Lin Jiansheng ,Zhang Shesheng. Parallel PSO algorithm of invert heat conduction problem. DCABES 2010 PROCEEDINGS [C], HongKong,2010:5-9.

[4] Guo qingping,Zhang shesheng.In a multi-layered grid area in parallel computing division virtual boundary conditions prediction algorithms. Numerical calculation and computer applications[J].2000(4):287-293.

[5] Guo Qingping, Shen Dingcai, GuoYucheng, C.-H. Lai, Parallel Genetic Algorithms for the solution of Inverse Heat Conduction Problems [J]. International Journal of Computer Mathematics (IJCM), March 2007：1-9.

[6] Guo Qing-ping, at el. Parallel Computing using Domain Decomposition for Cyclical Temperatures in Geramic/Metal Composite. DD12 Internal Conference[C]. London, UK, Dec, 1998.

[7] Guo Qingping , Y. Paker , Parallel Multi-grid Algorithm with Virtual Boundary Forecast Domain Decomposition Method for Solving Non-linear Heat Transfer Equation[J]. Lecture Notes in Computer Science, High Performance Computing and Networking. Spreinge Press May 2000, 1823:568-571.

[8] Guo Qingping,Y. Paker. Optimum Tactics of Parallel Multi-grid Algorithm with Virtual Boundary Forecast Method Running on a Local Network with the PVM Platform [J]. Journal of Computer Science and Technology, July 2000, 15(4): 355-359.

[9] Lin Jiansheng, Guo Qingping, Qi Jingjing. A Back Propagation Neural Network Parallel Algorithm for Inverse Heat Conduction Problems. DCABES 2009 PROCEEDINGS [C], Wuhan, 2009: 38-42.

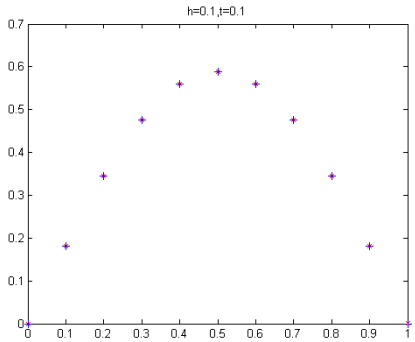

Figure1. The accuracy of coarse mesh inverse problem using PSO

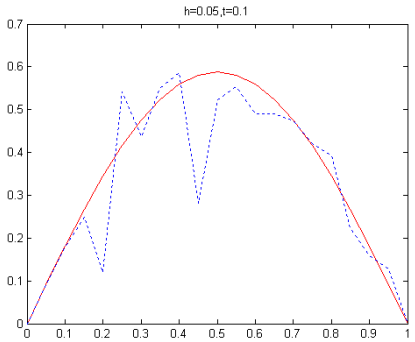

Figure2. The accuracy of fine mesh inverse problem using PSO

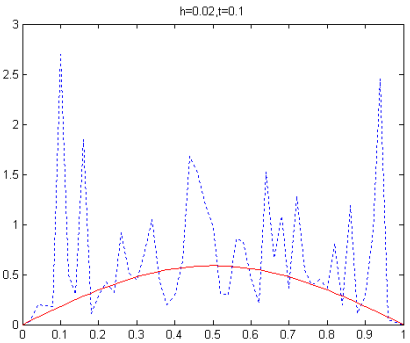

Figure3. The accuracy of fine mesh inverse problem using PSO

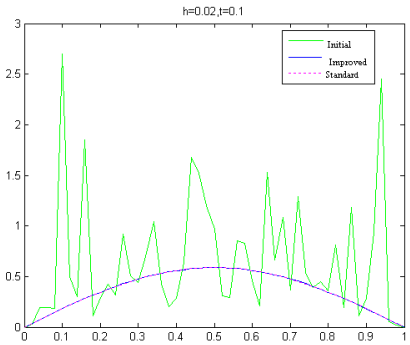

Figure4. Accuracy Comparison

Clustering Gene Expression Data Based on Harmony Search and K-harmonic Means

Anping Song[1, a], Jianjiao Chen [2, b], Tran Thi Anh Tuyet[1, c], Xuebin Bai[1, d], Jiang Xie[1, e], Wu Zhang[1, f,*]
[1]*School of Computer Engineering and Science, Shanghai University, Shanghai 200072, China*
[2] *School of Information Science and Engineering, Xinjiang University, Xinjiang 830046, China*
Email: a. apsong@shu.edu.cn b;cjj83@126.com c; yingxue@shu.edu.cn; d. bxbxbai@shu.edu.cn; e. jiangx@shu.edu.cn; f.wzhang@shu.edu.cn*.

***Abstract*—Clustering is one of the most commonly data explorer techniques in Data Mining. K-harmonic means clustering (KHM) is an extension of K-means (KM) and solves the problem of KM initialization using a built-in boosting function. However, it is also suffering from running into local optima. As a stochastic global optimization technique, harmony search (HS) can solve this problem. HS-based KHM, HSKHM not only helps KHM clustering escaping from local optima but also overcomes the shortcoming of slow convergence speed of HS. In this paper, we proposed a hybrid data-clustering algorithm, HSKHM. The experimental results on four real gene expression datasets indicate that HSKHM is superior KHM and HS in most cases. The HSKHM algorithm not only improves the convergence speed of HS but also helps KHM escaping from local optima.**

Keywords-KHM; HS; Clustering; Gene expression data Introduction

I. INTRODUCTION

Gene expression profiles can discriminate different cancer types or subtypes. Nowadays, the importance of gene expression data in cancer diagnosis and treatments has attracted more and more attentions from the researchers [1-3]. High throughput technology makes large volumes of high-dimensional gene expression data and it is easy for data mining community and cancer researchers to be available and accessible. A typical microarray gene expression dataset contains the expression values of tens of thousands of genes in different samples and commonly, only several tens of genes have unique expression patterns to each cluster of samples [4], which are called the relevant genes.

Microarray data sets have the characteristics of high dimension and small samples. In this context, it is often infeasible for using traditional clustering algorithms to detect the clusters in high-dimensional data. Therefore, high-dimensional data put demands on the efficiency and effectiveness of the learning algorithm. One of the major challenges of microarray data analysis is the overwhelming number of measures of gene expression levels compared with the small number of cancer samples, specifically, the samples displaying different behaviors in only a few of the genes. On the other hand, the behaviors of most of the genes in different classes are roughly the same. Many methods have been proposed to address this problem [5-6]. In these methods, dimensional reduction methods such as feature selection or extraction is the simplest approach and are carried out as a preprocessing step, that include principal component analysis (PCA) and random projection (RP).

Additionally, most of existing methods work by a supervised way, at the same time; the lack of training data intensifies the problem. In recent years, various unsupervised methods have also been developed to detect bi-clusters [7-8]. Here, we consider PCA and RP for the dimensionality reduction.

Cluster analysis is one of the major data analysis methods widely used for many practical applications in emerging fields. The goal of data clustering or cluster analysis is to discover the natural groupings of a set of patterns, points, or objects. Clustering is the process of grouping a set of objects in high dimensional space, which is an unsupervised learning technique. A good clustering approach will produce high quality clusters with low intra-cluster dissimilarity and high inter-cluster dissimilarity. The quality of a clustering result is decided by both the dissimilarity measure used by the method and its implementation and also by its ability to discover some or all of the hidden patterns.

K-harmonic Means (KHM) is the extension of the standard k-means (KM) algorithm [5, 8], which is developed for low dimensional data, and often does not work well for high dimensional data. Compared to KM algorithm, KHM is more stable for being less sensible to the initialization. However, it is easily converging to a local minimum rather than the global minimum solution and needs predefining the number of clusters. To settle local optimal problem it might be a good idea to run the algorithm several times with different initializations. If the results converge to the same partition then it is likely that a global minimum has been reached. This, however, has the weakness of being very time consuming and computationally expensive.

In this work, to address the high-dimensionality, local optima and the number of clusters predefined, we proposed that a new clustering method, harmony search automatic KHM (HSAKHM), which makes full use of the advantages of two algorithms and avoid their disadvantages. The working process is as following: First, to remove the noise, redundant and irrelevant features from data and obtained the reduced data, gene expression data are preprocessed by the two step feature selection algorithm, ReliefF-FCBF, which is designed in our previous work [9]. Then, using the HSKHM algorithm clustering the processed gene expression data, where harmony search (HS) technology can help KHM escape the local optima. HSKHM algorithm can

978-0-7695-4818-0/12 $26.00 © 2012 IEEE
DOI 10.1109/DCABES.2012.77

automatically find the number of inherent clusters in data sets. We compared the performance of the proposed method on the four open gene expression data. Experimental results demonstrated the efficiency and effectiveness of HSKHM approach in addressing high dimensional gene expression data and ultimately identifying corresponding cancer types.

The remainder of this paper is organized as follows. Section II describes the algorithms of KHM and HS, respectively. Section III presents the proposed method. The experimental results are presented and discussed in section IV, and section V concludes the paper.

II. KHM CLUSTERING ALGROITHM

K-harmonic means algorithm is a center-based, iterative algorithm that refines the clusters defined by k centers, which is similar to KM, yet it addresses the intrinsic problem, the dependency of the KM performance on the initialization of the centers, by replacing the minimum distance from a data point to the centers, used in KM. The following notations are used to formulate the KHM algorithm [10-12]:

X = $\{x_1, \ldots, x_n\}$: the data objects to be clustered.

C = $\{c_1, \ldots, c_k\}$: the set of cluster centers, k is the number of clusters.

$U(c_j|x_i)$: the membership function defining the proportion data point x_i belongs to center c_j.

P: an input parameter, typically $p \geqslant 2$.

$w(x_i)$: the weight function defining that to what degree data point x_i influences the re-computing of the center parameters in the next iteration.

KHM clustering algorithm is shown as follows:

Step1: Initialize the algorithm with guessed centers C, i.e., randomly choose the initial centers.

Step2: Calculate objective function value according to

$$KHM(X,C) = \sum_{i=1}^{n} \frac{k}{\sum_{j=1}^{k} \frac{1}{\| x_i - c_i \|^p}} \tag{1}$$

Step3: For each data point x_i, compute its membership $U(c_j|x_i)$ in each center c_j according to

$$U(c_j, x_i) = \frac{\| x_i - c_j \|^{-p-2}}{\sum_{j=1}^{k} \| x_i - c_j \|^{-p-2}} \tag{2}$$

Step4: For each data point x_i, compute its weight $w(x_i)$ according to

$$w(x_i) = \frac{\sum_{j=1}^{k} \| x_i - c_j \|^{-p-2}}{(\sum_{j=1}^{k} \| x_i - c_j \|^{-p})^2} \tag{3}$$

Step5: For each center c_j, re-compute its location from all data points x_i according to their memberships and weights:

$$c_j = \frac{\sum_{i=1}^{n} U(c_j \mid x_i) w(x_i) x_i}{\sum_{i=1}^{n} U(c_j \mid x_i) w(x_i)} \tag{4}$$

Step6: Repeat steps 2-5 predefined number of iterations or until $KHM(X, C)$ does not change significantly.

Step7: Assign data point x_i to cluster j with the biggest $U(c_j|x_i)$.

Many experimental results showed that KHM has the following many advantages. It is essentially insensitive to the initialization. Even when the initialization is really very bad, it can also converge nicely, including the converge speed and clustering results. And it is also suitable for the large-scale data sets. Because of the above strengths, we use KHM to develop our new clustering algorithm.

III. PBMF INDEX

The results of clustering are often evaluated by clustering validity index (CVI). Pakhira et al. [13] proposed a new validity function, PBMF-index, which achieved more satisfying results by comparison with the extended Xie-Beni index [14]. In the paper, the PBMF-index is used for choosing the optimal number of clusters, which is defined as follows:

$$PBMF(k) = (\frac{1}{k} \times \frac{E_1}{J_m} \times D_k)^2 \tag{5}$$

where k is the number of clusters, $E_1 = \sum_{j=1}^{N} \mu_{1,j} \left\| x_j - w_1 \right\|$, w_1 is the center of the unique cluster for the whole data set, and $D_k = \max_{i,j=1}^{k} \left\| c_i - c_j \right\|$ .Moreover, $J_m = \sum_{i=1}^{N} \sum_{i=1}^{n_c} \mu_{i,j=1}^{m} \left\| x_j - c_i \right\|$ .The optimal number of clusters should maximize the value of the PBMF-index which can ensure the formation of a small number of compact clusters with large separation between at least two.

IV. HARMONY SEARCH ALGORITHM

The nature of clustering is a combinational optimal problem. Metaheuristics are general heuristic methods, which are used to deal with a wide range of different optimization problems. The main goal of metaheuristic algorithms is to avoid the weakness of iterative improvement and especially, the local optima problem. These features such as its simplicity, robustness and flexibility make them very attractive research area [15]. Many of them are inspired by natural phenomena.

The harmony search algorithm [16] mimics the improvisation process of music players and is one of the most recently developed population-based meta-heuristic optimization algorithm. Moreover, it is also one of the most efficient algorithms in the field of combinatorial optimization [17]. Harmony search algorithm had been very successful in a widely various optimization problems [18-19]. It presents several advantages such as the Following [19]:

1) HS algorithm has fewer mathematical requirements and does not require setting the initial value for decision variables;

2) Derivative information is also unnecessary for HS algorithm using stochastic random search;

3) The HS algorithm generates a new vector considering all of the existing vectors, whereas the methods like genetic algorithm (GA) only considers the two parent vectors;

4) HS does not have to encode and decode the decision variables into binary strings;

5) HS deals with continuous variables without any loss of precision.

The above features increase the flexibility of the HS algorithm and produce better solutions. In fact, in term of optimization problems, HS method searches the solution space more efficiently.

HS include the following five steps [20] and it is sketched in Fig. 1.

1) The initialization of the optimization problem and HS parameters. The optimization problem is formulated as follows:

$$\text{Minimize/maximum } f(x),\quad \text{Subject to } \begin{matrix} x_i \in X_i = \{x_i(1),\mathrm{K}\ ,x_i(k),\mathrm{K}\ ,x_i(K)\} \\ or\ x_i^L \le x_i \le x_i^U \end{matrix} \tag{6}$$

The function $f(x)$ is optimized objective function by HS. The HS algorithm finds the optimal solution vector $x=\{x_1,x_2,\mathrm{K}\ ,x_N\}$ through searching entire solution space. If the decision variable is discrete values, the set of its candidate values is $x_i \in X_i = \{x_i(1),\mathrm{K}\ ,x_i(k),\mathrm{K}\ ,x_i(K)\}$; and if the decision variable is continuous values, the set of its candidate values is $x_i^L \le x_i \le x_i^U$. Then, the three parameters of the HS are initialized. They are as follows:

a). Harmony memory size (HMS) (i.e., number of solution vectors in harmony memory);

b). Harmony memory considering rate (HMCR), where $HMCR \in [0,1]$;

c). Pitch adjusting rate (PAR), where $PAR \in [0,1]$;

d). Stopping criteria, i.e., number of improvisations (NI).

2) Initialize harmony memory

The harmony memory (HM) is a matrix of solutions with a size of HMS, where each harmony memory vector in (7) represents one solution. The solutions are randomly constructed and rearranged in a reversed order based on their objective function values such as $f(x^1) \le f(x^2) \le \mathrm{L}\ \le f(x^{HMS})$

$$HM = \left[\begin{array}{cccc|c} x_1^1 & x_2^1 & \mathrm{K} & x_n^1 & f(x^1) \\ x_1^2 & x_2^2 & \mathrm{K} & x_n^2 & f(x^2) \\ \mathrm{M} & \mathrm{K} & \mathrm{K} & \mathrm{K} & \mathrm{M} \\ x_1^{HMS} & x_2^{HMS} & \mathrm{K} & x_n^{HMS} & f(x^{HMS}) \end{array}\right] \tag{7}$$

3) Improvise new harmony

This step is the HS generates (improvises), a new harmony vector, $x' = (x_1', x_2', x_3', \mathrm{K}\ , x_N')$ and it is the cornerstone and the essence of the HS algorithm. It includes three operators: memory consideration, pitch adjustment and random consideration. In the memory consideration, the values of the new harmony vector are randomly inherited from the historical values stored in ***HM*** with a probability of *HMCR*. The value of decision variable x_1' is chosen from $x' = (x_1^1, x_1^2, x_1^3, \mathrm{K}\ , x_1^{HMS})$ that is stored in ***HM***. The next decision variable x_2' is chosen from $x' = (x_2^1, x_2^2, x_2^3, \mathrm{K}\ , x_2^{HMS})$ and the other decision variables $(x_3', x_4', \mathrm{K}\ , x_N')$ are chosen consecutively in the same manner with the probability of $HMCR \in [0,1]$. This cumulative step ensures that good harmonies are considered as the elements of new harmony vectors. Beyond that, the other decision variable values are not chosen from ***HM***, and they are randomly chosen according to their possible range, $x_i' \in X_i\ or\ x_i^L \le x_i \le x_i^U$. The case is referred to as random consideration with a probability of (1-HMCR),which increases the diversity of the solutions and makes the system obtain the global optimality by the further to explore various solutions.

The following equation summarized the two steps i.e., memory consideration and random consideration.

$$x_i' \leftarrow \begin{cases} x_i' \in \{x_i^1, x_i^2, x_i^3, \mathrm{K}\ , x_i^{HMS}\}\ w.p.\ HMCR \\ x_i' \in X_i\ \ w.p.\ (1-HMCR) \end{cases} \tag{8}$$

Moreover, the additional good solutions in the search space is attained using PAR operator, which tunes each decision variable in the new harmony vector, $x_i' = (x_1', x_2', x_3', \mathrm{K}\ , x_N')$ inherited from ***HM***. These decision variables x_i' are adjusted with the probability of $PAR \in [0,1]$ as in (9).

$$x_i' \leftarrow \begin{cases} \text{Adjusting P int ch} & w.p.\ PAR \\ \text{Do nothing} & w.p.\ (1-PAR) \end{cases} \tag{9}$$

If a generated random number $rand \in [0,1]$ within the probability of PAR, the new decision variable $x_i^{'}$ will be adjusted based on the following equation:

$$x_i^{'} = x_i^{'} \pm rand() \ \ bw \qquad (10)$$

Where *bw* is an arbitrary distance bandwidth that is used to improve the performance of HS and rand ( ) is a function generating a random number $\in [0,1]$ .Actually, *bw* determines the amount of movement or changes that may have occurred to the components of the new vector. The value of *bw* is based on the optimization problem itself i.e., continuous or discrete. In general, the way that the parameter (*PAR*) modifies the components of the new harmony vector is an analogy to the musicians' behavior when they slightly change their tone frequencies in order to get better harmonies. Consequently, it explores more solutions in the search space and improves the searching abilities.

4) Updating the new harmony

In order to update ***HM*** with the newly generated vector $x_i^{'} = (x_1^{'}, x_2^{'}, x_3^{'}, \mathrm{K}\ , x_N^{'})$, the objective function $f(x^{'})$is calculated for each new harmony vector. If the objective function value for the new vector is better than the worst harmony vector stored in ***HM***, then the worst harmony vector is replaced by the new vector. Otherwise, this new vector is ignored. However, for the diversity of harmonies in ***HM***, other harmonies (in terms of least-similarity) can be considered. Also, the maximum number of identical harmonies in ***HM*** can be considered in order to prevent premature ***HM***.

5) Checking the stopping criterion

The iteration process in steps 3 and 4 is terminated when the maximum number of improvisations (*NI*) is reached. Finally, the best harmony memory vector is selected and is considered to be the best solution to the problem.

V. THE PROPOSED HYBRID CLUSTEIRNG ALGORITHM HSKHM

Since stochastic optimization approaches are good at avoiding convergence to a locally optimal solution, these approaches could be used to find a globally optimal solution. However, the stochastic approaches take a large amount of time to converge to a globally optimal partition. The KHM algorithm tends to converge faster than the HS algorithm because it requires fewer function evaluations, but it usually gets stuck in local optima. In this paper, we propose a hybrid clustering algorithm based on HS and KHM (HSKHM), which maintains the merits of KHM and HS. A harmony vector is a vector of real numbers of dimension k* d, where k is the number of clusters and d is the dimension of data to be clustered. The fitness function of the HSKHM algorithm is the PBMF index. To demonstrate the effectiveness of HSKHM, we have applied HSKHM algorithm on standard gene expression and got very good results compared to the KHM. The evaluation of the experimental results shows considerable improvements and robustness of HSKHM. Fig.2 summarizes the hybrid HSKHM algorithm.

HS Algorithm

```
Begin
Define fitness function f(x), x=(x1, x2... xN)T
Define (HMCR), (PAR), (HMS)
Define Maximum number of iterations (NI)
HM←Generation InitialPopulation()
min=minimum visible value
max=maximum visible value
While (Iter≤NI) do
    While (xi≤number of variable) do
        If (rand∈(0,1)≤HMCR) then
            Choose a value from HM for i
               If (rand∈(0,1) ≤PAR) then
                  adjust the value of i by
                     xi^New = xi^New + rand ∈(0,1)× bw
        end if
    end while
    If((f(x^New)≤f(x^Worst)) then
        accept the new harmony and replace the worst in HM with it
    end if
end while
Best=find the current solution
End
```

Figure 1. Pseudo-code of the HS algorithm

HSKHM algorithm

Step 1: Define the fitness function $PBMF(k)=(\frac{1}{k}\times\frac{E_1}{J_m}\times D_k)^2$, where *k* is the number of clusters.

Step 2: Initialize the harmony search memory by generating *HMS* vectors; *HMS*= *sqrt* (instance num), each vector is established by randomly choose k instance from the dataset as *k* cluster centroids in one solution. This way, each vector in the ***HM*** will have the length of *N*= *k*d*, here d is the number of attributes in each instance.

Step 3: Calculate the objective function *PBMF* of each vector in ***HM***, find out the best and worst solution among them.

Step 4: Generate a new vector X^{new} considering the *HMCR* and *PAR* arguments.

The values of X^{new} are randomly inherited from the historical values stored in ***HM*** with a probability of *HMCR*. Out of that, values of X^{new} are randomly chosen from min to max value:

$$x_i^{'} \leftarrow \begin{cases} x_i^{'} \in (x_i^1, x_i^2, x_i^3, \ldots, x_i^{HMS}) & w.p.\ HMCR \\ x_i^{'} \in X_i & w.p.\ (1-HMCR) \end{cases}$$

Then these values will be tuned with the probability of *PAR*:

$$x_i^{'} \leftarrow \begin{cases} \text{Adjusting Pitch} & w.p.\ PAR \\ \text{Do nothing} & w.p.\ (1-PAR) \end{cases}$$

Step 5: Calculate the objective function PBMF of new vector X^{new}. If the objective function value for the new vector is better than the worst harmony vector stored in ***HM***, then the worst harmony vector is replaced by the new vector.

Step 6: If the maximum number of iterations *NI* is reached. Then output the best solution as the initial cluster centroids. Otherwise add 1 to the iteration number and go to step 3.

Step 7: Executive KHM algorithm.

Step 8: Assign each instance to the cluster with maximum membership value.

Figure 2. The hybrid clustering algorithm HSKHM

VI. EXPERIMENT RESULTS

Four data sets are employed to validate our method. These data sets, named Leukemia, Lung, Lymphoma and small round blue cell tumor (SRBCT). Table 1 summarizes the characteristics of these data sets. Table 2 shows the parameters set in our algorithm.

Table 1. Characteristics of data sets considered

Name of data set	No. of classes	No. of features	Size of data set (size of classes in parentheses)
Leukemia	2	7129	72(47,25)
Lung	2	5000	181(150,31)
Lymphoma	3	4026	62 (42,9,11)
SRBCT	4	2308	63(23,20,12,8)

Table 2. The HSKHM algorithm parameters setup

Parameters	Value
HMCR	0.9
PAR	0.3
NI	1000
p	2 ,2.5

A. Datasets

The Leukemia dataset [1] consists of 72 microarray experiments (samples) with 7129 gene expression levels. The problem is to distinguish between two types of Leukemia, Acute Myeloid Leukemia (AML) and Acute Lymphoblastic Leukemia (ALL).

The Lung cancer data [21] consists of gene expression profiles of 5000 genes for 181 tissue samples (31 MPM and 150 ADCA). The problem is to distinguish between malignant pleural mesothelioma (MPM) and adenocarcinoma (ADCA) of the lung.

The Lymphoma dataset[2] is a dataset of the three most prevalent adult lymphoid malignancies and it contains gene expression profiles of 4026 genes for 62 patients.

The SRBCT dataset [22] has 2308 genes and 63 experimental conditions. The 63 training samples included both tumor biopsy material (13 EWS and 10 RMS) and cell lines (10 EWS, 10 RMS, 12 NB and 8 Burkitt lymphomas (BL; a subset of NHL)).

B. Experimental results

a). The sum over all data points of the harmonic average of the distance from a data point to all the centers, as defined in (1). Clearly, the smaller the sum is, the higher the quality of clustering is.

b). The F-Measure uses the ideas of precision and recall from information retrieval [22]. Each class i (as given by the class labels of the used benchmark dataset) is regarded as the set of n_i items desired for a query; each cluster j (generated by the algorithm) is regarded as the set of nj items retrieved for a query; n_{ij} gives the number of elements of class i within cluster j. For each class i and cluster j precision and recall are then defined as: $r(i,j)=n_{ij}/n_i$, $p(i,j)=n_{ij}/n_j$ .And the corresponding value under the F-Measure is $F(i,j) = (b^2+1)\cdot p(i,j)\cdot r(i,j)/b^2\cdot p(i,j)\ r(i,j)$ where we chose b = 1 to obtain equal weighting for $p(i, j)$ and $r(i, j)$. The overall F-Measure for the dataset of size n is given by

$$F = \sum_i \frac{n_i}{n} \max_j \{F(i,j)\} \qquad (11)$$

c). The experimental results showed are the best results selected from the results of 10 independent runs. The HSKHM algorithms are implemented with preprocessed data by ReliefF-FCBF in weka 3.5.8 platform on a Pentium (IV) D CPU 2.66 GHz with 4.00 GB RAM. Tables 3-4 give the best results over 10 independent runs when p is 2, 2.5.Additionally; they show the runtimes of the algorithms.

d). In terms of F-Measure, compared to KHM and HS, HSKHM all obtained the best F-Measure on the four gene expression data sets and it achieved the lowest function value of KHM(X, C) on datasets with the exception of SRBCT when p=2. The F-measure of HSKHM is equal or better than that of HS, and that of KHM is relatively bad when p=2.HSKHM obtained the best F-Measure on the three gene expression data sets except lymphoma and it had the lower function value of KHM(X, C) on datasets with the exception of SRBCT when p=2.5.

Table 3. Results of KHM, HS, and HSKHM clustering on four real data sets when p = 2.

Datasets	KHM	HS	HSKHM
Leukemia			
KHM(X,C)	***2819.421***	5990.603	**2477.58**
F-Measure	0.883	***0.907***	**0.986**
Runtime(ms)	**15**	5047	***4579***
Lung			
KHM(X,C)	4917.056	***4878.071***	**4057.36**
F-Measure	0.666	***0.915***	**0.984**
Runtime(ms)	**16**	***10391***	15047
Lymphoma			
KHM(X,C)	2231.138	***1427.057***	**1406.742**
F-Measure	***0.805***	**0.906**	**0.906**
Runtime(ms)	**15**	2781	***2547***
SRBCT			
KHM(X,C)	**3424.6**	***3588.472***	3655.322
F-Measure	0.555	***0.694***	**0.765**
Runtime(ms)	**16**	***2890***	*4703*

Note: The quality of clustering is evaluated using KHM(X,C) and the F-Measure. Runtimes (s) are additionally provided. The table shows the best results for 10 independent runs. Bold face indicates the best and italic face indicates the second best result out of the three algorithms.

[1] http://www.broad.mit.edu/cgibin/cancer/publications/

[2] http://genome~www.stanford.edu/lymphoma

Table 4. Results of KHM, HS, and HSKHM clustering on four real data sets when p = 2.5.

Datasets	KHM	HS	HSKHM
Leukemia			
KHM(X,C)	**7319.923**	16418.49	***7762.378***
F-Measure	***0.883***	0.8	**1**
Runtime(ms)	**0**	3578	***3328***
Lung			
KHM(X,C)	15167.17	***10668.8***	**10512.2**
F-Measure	0.672	***0.954***	**0.968**
Runtime(ms)	**15**	***17578***	23922
Lymphoma			
KHM(X,C)	5527.499	**2878.653**	***3326.614***
F-Measure	0.826	**0.906**	***0.886***
Runtime(ms)	**0**	7031	***3812***
SRBCT			
KHM(X,C)	**9429.11**	14277	***11809.57***
F-Measure	***0.555***	0.536	**0.788**
Runtime(ms)	**15**	3063	***2688***

Note: The quality of clustering is evaluated using KHM(*X*, *C*) and the F-Measure. Runtimes (s) are additionally provided. The table shows the best results for 10 independent runs. Bold face indicates the best and italic face indicates the second best result out of the three algorithms

VII. CONCLUSION

This paper investigates a hybrid clustering algorithm (HSKHM) based on the KHM algorithm and the HS algorithm. The experiment is done on four gene expression data sets. The HSKHM algorithm searches robustly the data cluster centers based on the sum over all data points of the harmonic average of the distance from a data point to all the centers. Using the same metric, HS is shown to need more runtime to achieve the global optima, while KHM may run into local optima. The HSKHM algorithm not only improves the convergence speed of HS but also helps KHM escaping from local optima. Experimental results also show that HSKHM is better than KHM and HS in terms of F-Measure in most cases. One drawback of HSKHM is that it requires more runtime than KHM.

ACKNOWLEDGMENT

This work is partially supported by Key Project of Science and Technology Commission of Shanghai Municipality [No.10510500600], Shanghai Leading Academic Discipline Project [No.J50103], Innovation Program of Shanghai Municipal Education Commission [No.11YZ03].

REFERENCES

[1] T. Golub, D. Slonim, P. Tamayo, C. Huard, M.Gaasenbeek, J. Mesirov, H. Coller, et al., "Molecular classification of cancer: class discovery and class prediction by gene expression monitoring,"Science, Vol.286, no.5439,pp. 531-537,1999.

[2] R. Shyamsundar, Y. Kim, J. Higgins, K. Montgomery, M.Jorden, A. Sethuraman,et al., "A DNA microarray survey of gene expression in normal human tissues," Genome Biology, Vol.6, R22, 2005.

[3] J. Khan, J. Wei, M. Ringnér, L. Saal, M. Ladanyi, F.Westermann, et al., "Classification and diagnostic prediction of cancers using gene expression profiling and artificial neural networks," Nature Medicine, Vol.7, no.6,pp. 673-679, 2001

[4] S. L. Pomeroy, P. Tamayo, M. Gaasenbeek, L. M. Sturla, M. Angelo, M. E. McLaughlin, et al., "Prediction of centralnervous system embryonal tumour outcome based on gene expression，"Nature, Vol.415,no.6870,pp.436–442, 2002.

[5] A. Ben-Dor, L. Bruhn, N. Friedman, I. Nachman, M.Schummer, and Z. Yakhini, "Tissue classification with gene expression profiles," J Comput Biol. Vol.7,no.3-4,pp.559-583,2000.

[6] G. Cawley and N. Talbot, "Gene selection in cancer classification using sparse logistic regression with Bayesianregularization," Bioinformatics, Vol. 22, no. 19, pp. 2348-2355, 2006.

[7] A. Tanay, R. Sharan, and R. Shamir, "Biclustering algorithms, a survey", Handbook of Computational Molecular Biology, Edited by S. Aluru, Chapman, 2004.

[8] R. Xu, S. Damelin, and D. Wunsch II, "Clustering of high-dimensional gene expression data with feature filtering methods and diffusion maps", Artif Intell Med.,Vol.48,no.2-3,pp.91-98, 2010.

[9] Jianjiao Chen, Anping Song, Wu Zhang. A novel hybrid gene selection approach based on ReliefF and FCBF, International Journal of Digital Content Technology and its Applications[J], 2011, 5(10):404-411.

[10] Hammerly, G. and Elkan, C., "Alternatives to the k-means algorithm that find better clusterings,"In:Proceedings of the 11th international conference on information and knowledge management, pp. 600-607, 2002.

[11] Onler A. and Güngör Z. "Applying K-harmonic means clustering to the part machine classification problem," Expert Systems with Applications. doi:10.1016/j.eswa.2007.11.048.

[12] Fengqin Yang, Tieli Sun and Changhai Zhang, "An efficient hybrid data clustering method based on K-harmonic means and Particle Swarm Optimization," Expert Systems with Applications, doi:10.1016/j.eswa,2009.

[13] [13]Hammerly, G. and Elkan, C., "Alternatives to the k-means algorithm that find better clusterings,"In:Proceedings of the 11th international conference on information and knowledge management, pp. 600-607, 2002.

[14] [14]Onler A. and Güngör Z. "Applying K-harmonic means clustering to the part machine classification problem," Expert Systems with Applications. doi:10.1016/j.eswa.2007.11.048.

[15] YagiuraM, Ibaraki T. On metaheuristic algorithms for combinatorial optimization problems. Syst ComputJpn,2001,32(3):33–55.

[16] Geem ZW, Kim JH and Loganathan G (2001).A new heuristic optimization algorithm: harmony search. Simulation,2001, 76(2):60–68

[17] Geem ZW, Music-inspired Harmony search algorithm theory and applications. Springer, Berlin,2009c.

[18] Lee KS and Geem ZW.A new meta-heuristic algorithm for continues engineering optimization: harmony search theory and practice. Comput Method Appl Mech Eng ,2004,194:3902–3933. doi:10.1016/j.cma.2004.09.007

[19] Geem ZW, Tseng C, Park Y.Harmony search for generalized orienteering problem: best touring in China, Springer. Lect Notes Comput Sci ,2005,3412: 741–750

[20] Geem ZW, Tseng C-L, Park Y.Harmony search for generalized orienteering problem: Best touring in china. In: Wang L,Chen K, Ong Y (eds) Advances in natural computation[M]. Springer,Berlin, pp 741–750,2005.

[21] G. J. Gordon, R. V. Jensen, and L. Hsiaoand. "Translation of microarray data into clinically relevant cancer diagnostic tests using gene expression ratios in lung cancer and mesothelioma," Cancer Research, Vol.62, no.17, pp.4963-4967, 2002.

[22] J. Khan, J. Wei, M. Ringnér, L. Saal, M. Ladanyi, F.Westermann, et al., "Classification and diagnostic prediction of cancers using gene expression profiling and artificial neural networks," Nature Medicine, Vol.7, no.6,pp.673-679, 2001.

The Algorithm of Color Petri Nets Transform into the Place/ Transition Nets and its Implementation

LI Wen-jing , YANG Wen, LI Shuang, LIAO Wei-zhi
College of Computer and Information Engineering
Guangxi Teachers Education University
Nanning, China
e-mail:liwjgood@126.com

***Abstract*— With the aim of solving the problems of the Petri nets to the place/transition nets automatic conversion and realization of Petri nets parallel control and running, the algorithm is proposed to transform Color Petri net systems transform into P/T nets. The algebraic model of colored Petri nets and P/T nets, and its intrinsic mechanism is analyzed, the process and theory verification of the colored Petri nets into P/T nets are given. The colored Petri nets into P/T network algorithm is proposed, through the network model of formal, colored Petri nets correlation matrix pretreatment. Experimental results show that it is an effective method to solve Color Petri Net systems transform into P/T nets, lay the foundation for various senior Petri nets system transformation into P/T nets and achieve the parallelism and simulation of running.**

Keywords- Color Petri nest; P/T net; Algebraic Model; Relating Matrix; Algorithm and Implementation

I. INTRODUCTION

Petri nets of parallelism process including three steps, the first is extraction P/T nets structure model, the second is solving About P/T nets Place Don't variables, the thread is Nets' subnet (processes) classified. But as considering the problem of different applications or to solve different problems, People use different Petri nets model to describe the system structure and behavior. Petri nets model of various kinds, Including Color Petri Net, time Petri nets, hybrid Petri nets, fuzzy Petri nets and all kinds of other senior Petri nets system. Although all kinds of model in the simulation of the practical system operation process simulation ability to almost, and can switch between them. But the question of which kind of Petri nets model to Parallelization or function division of the system is the most convenient and the most ideal is must be consider[1]. Because Petri basic nets too simple, it Can't effectively simulation the behavior of the system and the symbol of the state library when the transition occur In the actual system operation process; but under the P/T nets basis of Color Petri Net, extended time Petri nets and so on in the complex net-work system are not Petri nets parallelization ideal model, because they are included variables, the color and so on functional division process redundant information. P/T nets model increase the capacity of the library and the function of the set weight function based on the prototype Petri nets, It can aptly described system structure, behavior, and the change Signs of state library[2] [3]. It is an ideal choice that the P/T nets model as the research object of parallelism. So We put forward the algorithm about Color Petri Net systems transform into P/T nets, it is laid a foundation For various senior Petri nets system parallelism and operation simulation, also has an important practical significance.

* Supported by the National Natural Science Foundation of China (61163012), Guangxi Natural Science Foundation (0991105, 2012GXNSFAA053218)

II. COLOR PETRI NET AND P/T NETS INTERNAL RELATIONS

A. Petri nets related definitions

Petri net is a model which is used to describe complex distributed system, not only can it describe the structure of the system, but also simulates the operation of the system. This paper introduced the following with the definition of Color Petri Net and P/T nets [4] [5].

Definition 1 A seven-tuple $N=(P,T;F,K,W,M)$ as a P/T net system, such that:

$W:F \rightarrow \{1,2,3,\ldots\}$, which is called weight function

(1) $K:P \rightarrow \{1,2,3,\ldots\}$, which is called capacity function

$M:P \rightarrow \{0,1,2,3,\ldots\}$,which Is a mark of the N , meeting the conditions$\forall p \in P$: $M(p) \leqslant K(p)$.

(2) About the transition$t \in T$, t is enabled , remark it as $M[t>$ have condition is :

$\forall p \in \cdot t$: $M(p) \geqslant W(p,t)$

$\forall p \in t\text{-}t$: $M(p)+W(t,p) \leqslant K(p)$

$\forall p \in t \cdot \cap \cdot t$: $M(p)+W(t,p)- W(p,t) \leqslant K(p)$

(3) If we get a new mark M' from M to t, then $\forall p \in P$:

$$M'(p)=\begin{cases} M(p)- W(p,t), & if\ p \in \cdot t- t \cdot \\ M(p)+ W(t,p), & if\ p \in t\text{-}\cdot t \\ M(p)+W(t,p)- W(p,t), & if\ p \in t \cdot \cap \cdot t \\ M(p), & else \end{cases}$$

978-0-7695-4818-0/12 $26.00 © 2012 IEEE
DOI 10.1109/DCABES.2012.25

We note it M[t> M′ .

Definition 2 A seven-tuple $N=(P,T;F,C,K,W,M)$ as a color Petri net, where $(P,T;F)$ is a network, C is a finite color set $\{c_1,c_2,c_3,\ldots,c_n\}$

(1) $W:F\rightarrow C$, $K:P\rightarrow C$, $M:P\rightarrow\{0, C\}$, is an identity of N, to meet the conditions of $\forall p\in P$: $M(p)\leqslant K(p)$.

(2) About the transition $t\in T$, t is enabled, remark it as M[t> have condition is :

$\forall p\in\cdot t$: $M(p)\geqslant W(p,t)$

(3) If from M into t get a new mark M' , then $\forall p\in P$:

$$M'(p)=\begin{cases} M(p)-W(p,t), & if\ p\in\cdot t-t\cdot \\ M(p)+W(t,p), & if\ p\in t\cdot-\cdot t \\ M(p)+W(t,p)-W(p,t), & if\ p\in t\cdot\cap\cdot t \\ M(p), & else \end{cases}$$

We note it $M[t>M'$.

B. Formal and its incidence matrix preprocessing

P/T nets is in Petri nets of prototype based on the increase the capacity of the place collection on the edge of the set of function and weight function get. The main difference is the prototype nets have 3 points, (1) increase the capacity and the right two functions; (2) change t in marking the M is there happen right, and change before and after about the place, and prototype nets only with former about place; (3) change occurs, place asked before and after token (token) change the volume is equal or greater than 1, and change the volume of the prototype nets for 1.

Color Petri Net are to P/T nets of abstract and folding, Is mainly to the nets model "of the sort or token analytical, reduce nets model the basic elements, reduce the size of the network model. The relative to the P/T nets of features: (1) the P/T nets model will only a "type, with an integer said, and senior nets, will have a variety of types (color), here in the place's token K-dimensional vector with said; (2) P/T nets side the weight function of the set value is a nonnegative integer, and Color Petri Net of weight function value is a nonnegative K-dimensional vector; (3) When modeling complex problems, P/T nets model is more complex, but easy to parallelism and function division; And Color Petri Net model is simple-if given enough opportunities-and clear, but the implied color, transition, and many other information, go against the system function decomposition and parallelism, and against the automatic computer simulation of the practical operation of the system.

C. Nets Model Internal Mechanism

Between P/T nets and Color Petri Net have difference, but there is also the close inner link. In the algebra model, P/T nets is composed in Petri nets of prototype based on increase capacity function and weight function;(1) Color Petri Net is in the P/T nets basis, classification the token of the library, every kind of token said a color, so called colored (color) Petri net; Its capacity function and weight function by original P/T in the net one-dimensional function into a K-dimensional nonnegative mapping function. So P/T nets through further after folding can convert equivalent Color Petri Net.(2) Through the modification of the Petri nets' colored library collection and edge sets, the K-dimensional nonnegative mapping function decomposition into K one-dimensional mapping function, Color Petri Net can be converted into P/T nets model. So between P/T nets and nonferrous Petri nets can transformation. (3) For a distributed concurrent systems, can use the prototype Petri nets, P/T nets or Color Petri Net system to describe, the complexity of the model though different, but the simulation of the practical system capability of implementation are not significant, Namely stronger ability of the simulation that colored nets is not better than P/T nets. So, the application of the P/T nets that equivalent to the Color Petri Net to simulate the real the operation of the system with the same effect [5] [6].

III. TRANSFORMATION ALGORITHMS OF COLOR PETRI NETS INTO P/T NETS MODEL

According to the definition 2 and definition 1 we can know that Color Petri nets and P/T nets place with P, side set F, color sets are not the same, weights function and capacity function is not the same, put the Color Petri nets to be automatic into P/T nets, including three steps. First, transformation and validation the set of place, edge set, color set, right value function and capacity function; second, transition Color Petri nets , P/T nets formalized and its incidence matrix; Third, automatic conversion algorithm and implementation.

A. Transformation process and verification

By definition 2 know, Color Petri nets transit to P/T nets, the place will need the K-dimensional vector converted into each place that contains only one color (token), edge of the set of K-dimensional vector also converted into each weights for only on the side of the form of an integer, Concrete conversion as follows:

The first step: Put the Color Petri nets place collection transformation into P/T nets place collection. Check all the k-dimensional vector of Color Petri nets place, Statistics of each place' k-dimensional vector is not zero value the number of components, and get a P/T nets place with P contains the number of the place. Namely in the original Color Petri nets place, after each place generated by its k-dimensional vector of the component is not zero new place, delete the original place, and the color network place transformation into P/T nets place collect.

The second step: The edge set of Color Petri nets transformation into edge sets of P/T nets. Check all the k-dimensional vector of color Petri nets, Statistics of each edge' k-dimensional vector is not zero value the number of components, and get the number of the article of P/T nets

edge sets F. Namely in the original Color Petri nets edge, after each edge generated by its k-dimensional vector of the component is not zero new place, delete the original edge, and the color network edge collect transformation into P/T nets edge collect.

The third step: Keep the original Color Petri nets transformation of the same set, delete the color set of color nets, the three mapping of color nets respectively transformation into three mapping of definition 1.

The following give theorem 1 and theorem 2, and through the theoretical proof and examples, Verify the correct of the first step that place conversion and the second step that edge set conversion.

Theorem 1 Hypothesis colored Petri nets' any one repository contains of *K* color, m token, then transformation into P/T nets, of the place can be decomposed into h ($h \leqslant k$) a monochrome place, *H* monochrome place token number is still m sum.

Proof: For any color Petri net place of the p contains K color, then $p = (c_1, c_2, ..., c_k)$, and $c_1 + c_2 + ... + c_k = m$;

According to the definition 2 of *K*-dimensional mapping $K:P \rightarrow C,(c_1, c_2, ..., c_k) = (\{c_1\},\{c_2\},\ldots,\{c_k\})$, The k-dimensional vector down into $p_1=\{c_1\},p_2=\{c_2\},\ldots,p_k=\{c_k\}$, then p_1, p_2, ... p_k meet the capacity of the function definition 1 $k:p\rightarrow\{1,2,3,\ldots\}$, namely: $p_1\rightarrow c_1,p_2\rightarrow c_2,\ldots, p_k\rightarrow c_k$, and $c_1 + c_2 + ... + c_k = m$ unchanged. Then $h=K$. $c_1, c_2, ..., c_k$, If the number of K at least one number is 0, According to the definition 1of the capacity function, we can know that does not exist the place and its corresponding, So the decomposition of the number of the place h<K. But c1 + c2 +... + ck = m unchanged.

Proof end.

Theorem 2 Hypothesis color Petri nets of any a side of the weights are k-dimensional, then transformation into P/T nets, the edge can be decomposed into s side ($s\leqslant k$).

Proof: For color Petri nets' any an edge, the right value $f=(c_{11},c_{12},\ldots,c_{1k})$ is a k-dimensional vector;

According to the definition 2, k-dimensional mapping $K:F\rightarrow C,(c_{11},c_{12},\ldots,c_{1k})=(\{c_{11}\},\{c_{12}\},\ldots,\{c_{1k}\})$, the k-dimensional vector down into $f_1=\{c_{11}\}$, $f_2=\{c_{12}\},\ldots, f_k=\{c_{1k}\}$,then $f_1,f_2,\ldots f_k$ Meet the right value function of definition 1 $K:F\rightarrow\{1,2,3,\ldots\}$,namely: $f_1\rightarrow c_{11},f_2\rightarrow c_{12},\ldots, f_k\rightarrow c_{1k}$.

If $c_{11},c_{12},\ldots,c_{1k}$ *K* number at least 1 number is 0, according to the definition 1 of the rights value function we can know that don't exist its corresponding edge, so the decomposition of the article on the edge of the number $s < K$.

If $c_{11},c_{12},\ldots,c_{1k}$ all the k number is not zero, according to the definition 1 of the rights value function we can know that exist its corresponding edge, so the decomposition of the article on the edge of the number s = *K*. Prove end.

Example 1: Colored Petri nets model *N*1 are given, as shown in figure 1 show, translate into P/T nets model.

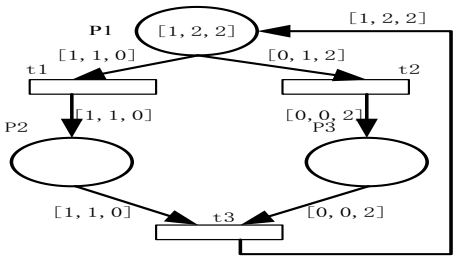

Figure 1 Three kinds of color Petri nets N_1

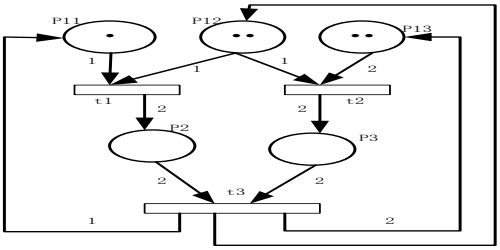

Figure 2 N1 transformation into P/T nets $N_1^{'}$

Figure 2 is Color Petri nets *N*1 translate into P/T nets results. Among them, place of p_1 has three kinds of color token, respectively into P/T nets of p_{11},p_{12}, p_{13}, three place, token number respectively is: 1, 2, 2. The place p_2, p_3 have no color's token, remain unchanged. If the library of k-dimensional vector column subscript the same, for the same kind of color said the place. Transition t_1, t_2 and t_3 corresponding into P/T nets three transition, remain unchanged. The place p_1 to transition t_1 have one side, now p_{11} to t_1, p_{12} to t_1 total of two side, on the edge of the right value is 1, 1 respectively; The place p_1 to transition t_2 haven't side, but now the place p_{12} to transition t_2 have one side, on the edge of the right value is 1; the place p_{13} to transition t_2 have one side, on the edge of the right value is 2, respectively.

B. Formal and its incidence matrix preprocessing

Color Petri nets system formal, with two-dimensional incidence matrix, output matrix and input matrix [5][7] to said, among them, Relating matrix: $G= G^+- G^-$, output matrix: $G^+=[g_{ij}^+]$, input matrix: $G^-=[g_{ij}^-]$,the relationship between elements: $g_{ij}=g_{ij}^+-g_{ij}^-$.

Exist as follows mapping:

f:P∪T→G It's the color of the domain mapping, G is color set.

$c_{ij}^+:f(t)\rightarrow bag(f(p))$ and $c_{ij}^-f(t)\rightarrow bag(f(p))$

P/T network system's formal, each with *n* line *m* column relating matrix: $E=E^+ -E^-$, output matrix: $E^+=[e_{ij}^+]$ and input matrix: $E^-=[e_{ij}^-]$ to say, among them $e_{ij}=e_{ij}^+- e_{ij}^-$.

According to the definition 1:

$$e_{ij}^+=\begin{cases} W(t_i,p_j), & if\ (t_i,p_j)\in T\times P \\ 0, & else \end{cases}$$

$$e_{ij}^{-}=\begin{cases} W(p_j, t_i)\ ,\ if\ (p_j,t_i)\in P\times T \\ 0, \quad else \end{cases}$$

$i\in\{1,2,\ldots,n\}, j\in\{1,2,\ldots,m\}$

Among them, $W(p_j, t_i)$ 、 $W(t_i, p_j)$ respectively, mean $p_j \rightarrow t_i$ 、 $t_i \rightarrow p_j$ right on the edge of value. Color Petri nets system formal, with two-dimensional incidence matrix, output matrix and input matrix [5][7] to said, among them, Relating matrix: $G= G^{+}- G^{-}$, output matrix: $G^{+}=[g_{ij}^{+}]$, input matrix: $G^{-}=[g_{ij}^{-}]$,the relationship between elements: $g_{ij}=g_{ij}^{+}-g_{ij}^{-}$. Their definition formal will be see reference [4] [5].

Two Petri nets with relating matrix said, but matrix elements are not the same meaning. Color Petri nets association matrix element is transition K-dimensional vector, P/T nets association matrix element is an integer; to realize the automatic computer conversion, the color Petri nets relating matrix into P/T nets association matrix is the key.

The color Petri nets relating matrix preprocessing. Color Petri nets' input matrix elements $g_{ij}^{-}$is to point to when transition t_j occurs with color β_i , the increase of the number of token in the *i* output place *pi* .

（1）Place kind of K color with structure to present:

Structure Pnet {

Datatype1 g_1; Datatype2 g_2; …; Datatype*k* g_k;}; among them, data type *k* means data types about Class k color of g_k

(2) Statement input and output matrix elements $g_{ij}^{-}$and g_{ij}^{+} for structures Pnet' 2-dimensional array element, set Structure Pnet $G^{-}[m][n]$,$G^{+}[m][n]$.

（3）Input and output matrix element is a *K*-dimensional vector, their line *i* and *j* column elements can be expressed as value respectively （$G^{-}[i][j].g_1$, $G^{-}[i][j].g_2$,…, $G^{-}[i][j].g_k$）and（$G^{+}[i][j].g_1$, $G^{+}[i][j].g_2$,…, $G^{+}[i][j].g_k$）.

C. Transformation algorithm

Put the non-ferrous Petri nets of input and output matrix transformed into P/T nets of input and output matrix, next to solve the P/T nets association matrix, In order to achieve the color Petri nets to P/T nets automatic conversion. Algorithm as follows:

Begin:

Input: color Petri nets of input and output matrix;

Output: association matrix of P/T nets.

Step1: Input color Petri nets' input matrix array and output matrix array;

Step2: for (i=1;i<=m,i++) { for (j=1;j<=n,j++) {

step21: Statistical input matrix line i column j g_{ij} elements of K-dimensional vector Not 0 component *r*;

step22: if(Not 0 component≥2) { Put this line of the corresponding to the place set up a "real" value sign, make pi=true. And all the K-dimensional elements of the line i vector adding together, calculating the place pi contains every kind of color' token number;

Exit for; } }

Step23: if($0\leqslant r_i\leqslant 1$) { Then this line of the corresponding place set by a "false" signs, make pi=false;} }

Step3: for (i=1;i<=m;i++) {

If (p_i=true) { In P/T nets which place p_i generate K new places ($p_{i1}, p_{i2},\ldots, p_{ik}$);

Else { In P/T nets which place p_i not generate new places, p_i keeping it status ;}}

Step4: Dynamically generated two matrix array $PT^{-}[mk+v][n]$ and $PT^{+}[mk+v][n]$, which for storage P / T net input and output.

Step5: while (i<=m) { // A cycle with colored nets input, output matrix element into the P / T nets input and output matrix elements

If (p_i=true) { for (*j*=1; *j*<=*mk*+*v*; *j*++) { for (*k*=1;*k*<=*n*;*k*++) { $PT^{-}[j][k]= p_i^{-}[i][k]$;$PT^{+}[j][k]= p_i^{+}[i][k]$; }

Else { For (s=1;s<=n;s++) { $PT^{-}[i][s]$ += g_{ij}^{-}; $PT^{+}[j][s]= g_{ij}^{+}$; } }}}

Step6: for (*i*=1; *i*<=*mk*+*v*;*i*++)

for (*j*=1;*j*<=*n*;*j*++) { $PT[i][j]= PT^{+}[i][j] - PT^{-}[i][j]$;//Solving the P / T nets incidence matrix printf("%d", $PT[i][j]$);// Output P / T nets incidence matrix elements }

End.

IV. EXPERIMENTS AND RESULTS ANALYSIS

The algorithm is programmed in Visual Stadio.Net 2005 environments, and takes color Petri net model of Figure 1 as an example. The input of the three lines three columns for output matrix: {{(0,0,0),(0,0,0),(1,2,2)}, {(1,1,0),(0,0,1),(0,0,0)}, (0,1,0),(0,0,2),(0,0,0)}}; the input matrix: {{(1,1,0),(0,1,2),(0,0,0)}, {(0,0,0),(0,0,0),(1,1,0)}, (0,0,0),(0,0,0),(0,0,2)}}.The experimental results is a five lines three columns of incidence matrix of P/T nets, in particular: {{-1,0,0},{-1,-1,2},{0,-2,0},{2,0,-2},{0,2,-2}}.

Correlation matrix from the experiment can be expressed as the P / T net model in figure 2, the experimental results coincide with the structure model transformation method of section 3.1.So, the approach which transforms color Petri nets into P/T nets through the algorithm is feasible and effective. It will provide an effective method for various senior Petri nets systems transform into P/T nets, after achieve the parallelization and simulation execution of Petri nets that provides an effective method.

V. CONCLUSIONS

Application of colored Petri net model to describe the complex distributed concurrent systems; described model is simple, clear. But to the system parallel or simulated running, use P/T nets is more close to the actual running of the system. Through the analysis of colored Petri nets and P/T nets internal mechanism, research the colored Petri nets into P/T network algorithm. In accordance with the theoretical proof, an instance of verification and programming, Validation of the colored Petri net system is transformed into a P/T network algorithm is feasible and effective. As will other senior Petri nets parallelization and simulation running provide an effective method when senior Petri nets transform into P/T nets.

REFERENCES

[1] LI Wen-jing, WANG Ru-liang, LIAO Wei-zhi. Research on Petri nets parallelization method based on P-invariants[J]. Computer Engineering and Design.2009,30(16),pp.3758-3762.

[2] W.El Kaim and F.Kordon. An integrated framework for rapid system prototyping and automatic code distribution[C]. Proc.In 5thIEEE International Workshop on Rapid System Prototyping,Grenoble,IEEE Comp.Soc.Press. 1994,pp.52-61.

[3] M.Paludetto. Sur la commande de procedes industriels:unemethodologie basee objets et reseaux de Petri[D].France These de doctorat, Universite Paul Sabatier,Toulouse.1991, pp.34-47.

[4] Girault C and Valk R.Petri Nets for Systems Engineering: A Guide to Modeling, Verification, and Applications [M].Springer-Verlag Berlin Heidelberg. 2003,pp.159-235.

[5] WU Z H.Petri Nets Introduction[M]. Beijing: Mechanical industry publishing house.2006, pp.144-155.

[6] ZENG Q T. A Construction Method for the Process Expression of a Petri Net Based on Synchronization Composition [J]. Chinese Journal of Computers. 2008, 31(3),pp .283-583.

[7] LI W J,WANG R L and LAN Z X .Research on Petri net systems parallelization method[J].Journal of Guangxi University :Nat Sci Ed. 2009,34(3),pp.400-404.

FCM-Based QPSO for Evolutionary Fuzzy-System Design

Wenqing Guan
School of IOT Engineering
Jiangnan University
Wuxi， China
123guanwen@163.com

Jun Sun
School of IOT Engineering
Jiangnan University
Wuxi, China
sunjun@jiangnan.edu.cn

Jian Xu
Chongqing Medical and
Pharmaceutical College
Chongqing, China

Wenbo Xu
School of IOT Engineering
Jiangnan University
Wuxi, China
xwb@jiangnan.edu.cn

***Abstract*—This paper proposes a FCM-based QPSO algorithm for evolutionary fuzzy-system design. The objective of this paper is to learn TSK type fuzzy rules with high accuracy. In the designed fuzzy system ,data is firstly clustered into classes by fuzzy c-means algotithm so that each rule defines its own fuzzy sets, the number of fuzzy rules is also determined by the number of clusters..Then Quantum-behaved particle swarm optimization learning algotithm then used for optimising the parameters of the fuzzy system. We illustrates the algorithm in details with computer simulation to solve nonlinear problems and compare the rusults between basic PSO and our algorithm.**

Keywords-FCM; QPSO; Fuzzy System; TSK; design

I. INTRODUCTION

Fuzzy system is becoming an increasingly popular field of research. Because with the development of technology, we recognized the real world is complex that often can not be accurately described. Therefore, in order to get a reasonable and traceable model must introduce the concept of fuzzy. At the same time, we need a theory to describe the system of human knowledge and together with other information to embedded systems. The fuzzy system is the perfect realization of these two functions.

Starting from the 1960s, with the continuous development of fuzzy theory, fuzzy system design method is also varied. Though the training process and then generate the adaptive fuzzy system which called evolutionary fuzzy system is research focus in recent years. ANFIS is one of the representatives[1]. As the design of FSs can be regarded as an optimization problem, genetic algorithms (GAs) [2], and particle swarm optimization (PSO)[3],[4] are applied for fuzzy system design by researches. But because of basic PSO algorithm can not make sure the convergence is global , Sun et al. proposed the Quantum-behaved particle swarm optimization to overcome the shortcomings[5]. This article is on this basis, through the FCM clustering method to find the cluster centers of training samples, then use QPSO algorithm the powerful optimization capabilities, iterate to find the best parameter values.

This paper is organized as follows. Section II describes the FS applied in this article. Section III introduces the QPSO concepts. Section IV illustrates the details of the algorithm. Section V presents FS-optimization results of simulations and compare with PSO method while Section VI provides a discussion of the results..

II. FUZZY SYSTEMS STRUCTURE

Almost all practical systems are nonlinear systems. Thus identification of nonlinear systems is essential in a variety of non-linear system identification methods. TSK fuzzy model [6] can be defined on arbitrary-precision approximation of nonlinear function on a compact set. And is the most important one in fuzzy models because of its successful application in complex system identification.

In TSK fuzzy system , the following "If-Then" rules are used to define the fuzzy system rules:

R : IF $x_1(k)$ is A_{I1} and ..... $x_n(k)$ is A_{in} THEN y(k)= $p_0 + p_1 x_1 + ... + p_n x_n$ (1)

Where A is the fuzzy sets, p is the parameter with real value , y is the output from the system according to the rules. In other words, then if part of TSK fuzzy systems is ambiguous, but then part is determined by the output of the linear combination of input variables. For an input vector x in terms of true value, TSK fuzzy system output y is equal to the weighted average of x. The fuzzy set A_{ij} uses a Gaussian membership function given by:

$$M_{IJ}(x_j) = \exp\{-\frac{x_j - m_{ij}}{\sigma_{ij}}\}^2 \quad (2)$$

978-0-7695-4818-0/12 $26.00 © 2012 IEEE
DOI 10.1109/DCABES.2012.83

Where m_{ij} and σ_{ij} represent the center and width respectively of the fuzzy set A_{ij} . Thus , given an input dataset x the output y can be caculated by:

$$y = \frac{\sum_{i=1}^{\tau} y(k) u_i(x)}{\sum_{i=1}^{\tau} u_i(x)} \tag{3}$$

Where $u_i(x)$ is the product of membership function.and y(k)= $p_0 + p_1 x_1 + ... + p_n x_n$. The proposed algorithm determines the number of rules τ and optimizes all free parameters $m_{ij} \sigma_{ij} p_n$ in each rule.

III. QUANTUM-BEHAVED SWARM OPTIMIZATION

The QPSO algorithm based on quantum behavior is improved from classical particle swarm optimization (PSO algorithm)[7]. It is mainly a combination of quantum theory to improve global optimization performance. The evolution equation is caculated by：

$$mbest = \frac{1}{M}\sum_{i=1}^{M} p_i = \left[\frac{1}{M}\sum_{i=1}^{M} p_{i1}, \cdots \frac{1}{M}\sum_{i=1}^{M} p_{iD} \right] \tag{4}$$

$$p_{id} = \theta \times p_i + (1-\theta) \times p_{gd} \quad \theta = rand(0,1) \tag{5}$$

$$x_{id} = p_{id} \pm a \times |mbest - x_{id}| \times \ln\left(\frac{1}{u}\right) \tag{6}$$

Among them, M is the total number of particles, D is the particle dimension, p_i is current best position of particle i and p_{gd} is best position of the swarm , the mbest represents the middle best particle position, p_{id} as a random point between (pbest) and (gbest) , a is the contraction expansion coefficient, which is an important for QPSO convergence parameter. It can be fixed, and also can also dynamic changes in a certain way.

DO

For i = 1 to M

If $f(x_i) < f(p_i)$

then $p_i = x_i$

$p_{gd} = \min(p_i)$

We can use function（4）get $mbest$

For i = 1 to M

$p_{id} = \theta \times p_i + (1-\theta) \times p_{gd}$, $\theta = rand(0,1)$

$u = rand(0,1)$

if $rand(0,1) > 0.5$

$x_{id} = p_{id} - a \times |mbest - x_{id}| \times \ln\left(\frac{1}{u}\right)$

else

$x_{id} = p_{id} + a \times |mbest - x_{id}| \times \ln\left(\frac{1}{u}\right)$

until termination criterion is satisfied

IV. USING QPSO ALGOTITHM FOR FUZZY RULE SYSTEM

STEP1: In general, the QPSO algorithm is an evolutional computing technology when solving complex and global problems. However, the necessary training time is unsuitable for large population sizes and many adjustable parameters. To quickly approximate the actual output of nonlinear functions, the input-output training data is initially clustered by FCM algorithm. We can use the data centers calculated by cluster algorithm to our model. Since each rule defines its own fuzzy sets , the rule number is also determined by the number of clusters.

STEP2: The intial data of QPSO is important , so then we should find the proper initial values. The velocity evolutionary parameter c1 and c2 , popsize of every swarm , dimention of each particle and max generation times.

STEP3: Calculate each individual‘s fitness value, and then compare each individual’s evaluation value with best global particle value (Gbestx) and the personal best value (Gbestx). Finally, select the new best value (Pbest and Gbest).The fitness is calculated by the mean square error between actual output and desired output , which can be described by :

$$RMSE = \sqrt{\frac{\sum_{i=1}^{n} (y(i) - y_0(i))^2}{n}} \tag{7}$$

STEP4: For every particle, update its own velocity and position value according to Eq.(4) ~Eq.(6).g=g+1.

STEP5: If g matches the default values , go to exit , otherwise go to STEP 3.

Then the best value will be chosen to form the desired fuzzy system to get best accuracy.

.

V. SIMULATIONS

A. *Non-linear SISO System Identification*

A first-order TSK-type FS is applied to model the following non-nlinear plant:

$$y = (2 + x_1^{1.5} - 1.5\sin(3x_2))^2$$

The 100 input data is randomly generated between 0 and 3.We use Fuzzy c-means clustering to separate the input data into 5 cluster. The initial parameter is seted as c1=c2=1.2 .Since x1 and x2 both random number , only choose x1 as input. We use PSO and QPSO to generate fuzzy system for 50 runs seperatedly and get the best result shown in Table. The output is shown in Figure1. We can see the two methods both coincide with the desired output. But QPSO is far more better.

Table 1 The comparion of two algorithms

	PSO	QPSO
Best-RMSE	0.0233	0.0142
Aver-RMSE	0.0715	0.0563

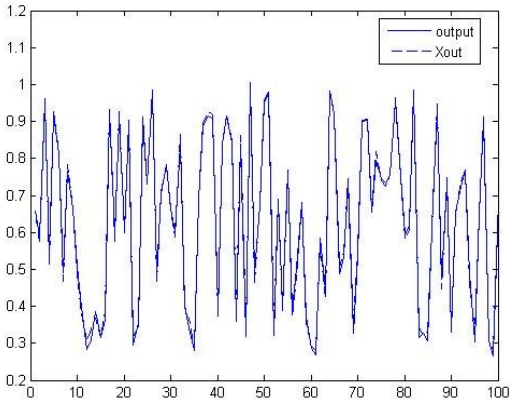

Figure 1 Comparison of output and Xout

B. A Non-linear MISO Dynamic System Identification

$$y(t+1)=\frac{y(t)y(t-1)(y(t)+2.5)}{1+y(t)^2+y^2(t-1)}+u(t)$$

The parameter u(t) is applied as $u(t)=\sin(0.04\pi t)$ and 100 training data are generated by t varying from 1 to 100.The system is started from zero state.We choose y(t) and u(t) as input parameters and y(t+1) as output. The simulation result is in Figure2. We can see the algorithm Smooths the edge. The average RMSE 0.0753 is better than PSO's 0.0982.

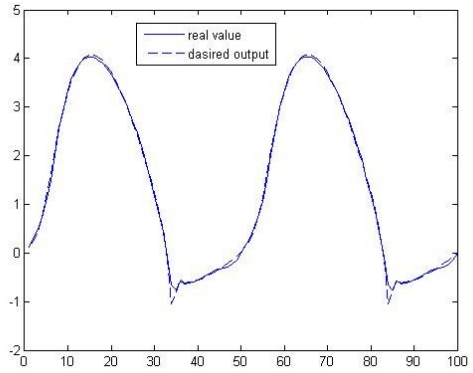

Figure 2 Comparison between real value and desired output

C. *Chaotic Series Prediction*

In this problem ,we use chaotic Mackey–Glass time series, which is generated from the following differential equation for time-series prediction problem:

$$\frac{dx(t)}{dt}=\frac{0.2x(t-\tau)}{1+x^{10}(t-\tau)}-0.1x(t)$$

As in previous studies [8], the parameter τ = 30, and x(0) = 1.2.We use four past data for this pridiction.And the fuzzy system is generated as

$$[x(t-24), x(t-18), x(t-12), x(t-6); x(t)]$$

When t varying from 124 to 1123,We choose the generated 1000 datas for our datas. And apply the first 500 datas for training , the last 500 datas for prediction.The best training RMSE of QPSO can reach 0.0391 as well as the PSO gets 0.0601. And to the test RMSE , QPSO is 0.0521 ,PSO can only do 0.0763. The output trace the desired value well can be seen from Figure3.

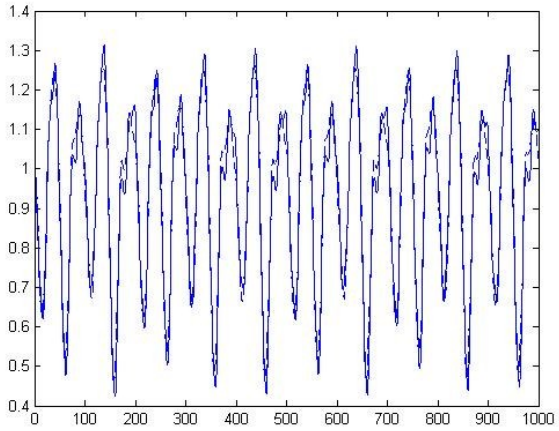

Figure 3 Comparison between output and Xout

VI. CONCLUSION

This paper proposed an algotithm based on FCM and

then use QPSO for fuzzy system optimization. The two major considerations in FS design are accuracy and interpretability[9]. The simulation results show that the this method can design fuzzy system with high accuracy and better than basic PSO method. The shortcomings are the fuzzy sets may be overlapped lead to less interpretability. And the iteration process to find a best-performed FS is also not suitable for changing environment. The hybridization of other optimization algorithms and QPSO will be explored in the future.

REFERENCES

[1] Jang, J.-S.R., "ANFIS : Adaptive-Network-Based Fuzzy Inference System," *IEEE Systems, Man, and Cybernetics Society*, vol. 23, no. 3, pp. 665-685, May/Jun 1993.

[2] C. F. Juang, "A TSK-type recurrent fuzzy network for dynamic systems processing by neural network and genetic algorithms," *IEEE Trans. Fuzzy Syst.*, vol. 10, no. 2, pp. 155–170, Apr. 2002.

[3] J. Kennedy and R. Eberhart, "Particle swarm optimization," in *Proc. IEEE Int. Conf. Neural Netw.*, Dec. 1995, pp. 1942–1948.

[4] K. D. Sharma, A. Chatterjee, and A. Rakshit, "A hybrid approach for design of stable adaptive fuzzy controllers employing Lyapunov theory and particle swarm optimization," *IEEE Trans. Fuzzy Syst.*, vol. 17, no. 2, pp. 329–342, Apr. 2009.

[5] Sun J, XuW.B. "A Global Search Strategy of Quantum behaved Particle Swarm Optimization[C]," Proceedings of IEEE Conference on Cybernetics and Intelligent Systems, 2004:111-116

[6] C. T. Lin and C. S. G. Lee, "*Neural Fuzzy Systems: A Neural-Fuzzy Synergism to Intelligent Systems*," Englewood Cliffs, NJ: Prentice-Hall, May.1996.

[7] Gao.H.A, "Quantum-behaved Particle Swarm Optimization With Learning Approach," Journal of Computational Information Systems,2008,10.

[8] K. B. Cho and B. H. Wang, "Radial basis function based adaptive fuzzy systems and their applications to system identification," *Fuzzy Sets Syst.*, vol. 83, pp. 325–339, 1996.

[9] Chia-Feng Juang, Che-Meng Hsiao, Chia-Hung Hsu, "Hierarchical Cluster-Based Multispecies Particle-Swarm Optimization for Fuzzy-System Optimization," IEEE Trans on FuzzySystems,vol. 18, no. 1, February.2010.

Hypothesis Test of Parameter in Exponential Distribution

Shuping Ruan[1] Tao Jiang[2]
[1]Wuhan Institute of Shipbuilding Technology, Wuhan 430050 , China, Email: 77096248@qq.com
[2]School of Science, Wuhan University of Technology, Wuhan, 430070, China, Email: 303345228@qq.com

Cheng Wenfang[3]
[3]Polar research institute of China, ShangHai, 200136, China
Contact: chengwenfang@pric.gov.cn

***Abstract*—In this paper, the hypothesis testing is investigated in the case of exponential distribution, and the corresponding rejection region is discussed. At last, an application is demonstrated, it is shown that the hypothesis test is feasibility..**

Keywords- Parametric hypothesis test, Exponential distribution, Gamma distribution, Rejection region

I. INTRODUCTION

With the development of science and technology and production, mathematical statistics is applied more and more extensively. And the hypothesis testing plays an important role in statistical inference. How to garreteer the correctness of the conclusion on the basis of sub-sample is that the statistical hypothesis testing problem. Many practical problems can be used as statistical hypothesis testing problem to solve. Research for various assumptions of normal distribution, the overall test is relatively complete, while the overall exponential distribution is also frequently encountered in practice (Such as the radio component of life, animal life, the talk time the phone problem, stochastic service system service time, etc.). Although more research on the exponential distribution (see [1-6]), as I know, its hypothetical test problem was less (see [7-8]). In this paper, the hypothesis testing is investigated in the case of exponential distribution for the unknown parameters, and an application is demonstrated, it is shown that the hypothesis test is feasibility.

Definition 1 If the density function of random variable ξ is

$$p(x)=\begin{cases}\lambda e^{-\lambda x}, if & x\geq 0\\ 0 \quad , if & x<0\end{cases} \tag{1}$$

Then the random variable ξ is called an exponential distribution, and its distribution function is

$$F(x)=\begin{cases}1-e^{-\lambda x}, if & x\geq 0\\ 0 \quad , if & x<0\end{cases} \tag{2}$$

Note: λ is a constant and $\lambda>0$.

Lemma 1. Set the density function of the random variable ξ is a parameter for the exponential distribution, then $E\xi=\frac{1}{\lambda}$.

Proof: By the definition of the expectations we can see

$$E\xi=\int_0^{+\infty}x\lambda e^{-\lambda x}dx=-\int_0^{+\infty}xde^{-\lambda x}$$
$$=\int_0^{+\infty}e^{-\lambda x}dx=\frac{1}{\lambda} \tag{3}$$

Note1. Proved above, A component of the lifetime distribution parameters for the exponential distribution of λ , the average life expectancy is λ^{-1} . If some components of the average life span of $10^k(k=1,2,\cdots)$ hours, then the corresponding n=2. In the electronics industry, people called it "k -class" products .Therefore, k is larger, then the product of the average life is longer, and the use is more reliable. K is usually interpreted that the average occurrence of the incident rate per unit time.

Definition 2 Let n and λ be two constants with $n>0,\lambda>0$. If the random variable ξ has density function

$$p(x)=\begin{cases}\frac{\lambda^n}{\Gamma(n)}x^{n-1}e^{-\lambda x}, if & x\geq 0\\ 0 \quad , if & x<0\end{cases}, \tag{4}$$

then ξ is a random variable, which to obey the parameters（λ,n）distribution Γ, and the corresponding distribution is called the parameters （λ,n）of the distribution of Γ.

II. IMAIN RESULTS AND THEIR PROOFS

Theorem 1. If the random variable $\xi_i, i=1,2,\cdots,n$ are independent and identically distributed and subject to the same exponential distribution $\exp(\lambda)$, then

$$\sum_{i=1}^{n}\xi_i\sim\Gamma(\lambda,n) \quad .$$

Proof : mathematical induction. Let n=2,assume ξ_1 and ξ_2 were independent and identically distributed and obey $\exp(\lambda)$,then

978-0-7695-4818-0/12 $26.00 © 2012 IEEE
DOI 10.1109/DCABES.2012.102

$$P(\xi_1+\xi_2<x)=\int_0^x P(\xi_1+\xi_2<x\,|\,\xi_1=x_1)f(x_1)dx_1$$

$$=\int_0^x P(\xi_2<x-x_1)f(x_1)dx_1$$

$$=\int_0^x\int_0^{x-x_1}\lambda e^{-\lambda\xi_2}d\xi_2\lambda e^{-\lambda x_1}dx_1$$

(5)

$$=\int_0^x(1-e^{-\lambda(x-x_1)})\lambda e^{-\lambda x_1}dx_1=1-e^{-\lambda x}-\lambda x e^{-\lambda x}$$

by the total expectation formula.

So the density function for $\xi_1+\xi_2$ is

$$f(x)=\frac{dP(\xi_1+\xi_2<x)}{dx}=\lambda^2 x e^{-\lambda x}=\Gamma(2,\lambda)$$

Suppose the conclusion was established for n , and $\xi_1,\xi_2,\cdots\xi_n$ was independent and identically distributed and obey $\exp(\lambda)$ .When n+1, , $\xi_1,\xi_2,\cdots\xi_{n+1}$ independent and identically distributed and obey $\exp(\lambda)$,so

$$P(\xi_1+\xi_2+\cdots+\xi_n+\xi_{n+1}<x)$$

$$=\int_0^x P(\xi_1+\xi_2+\cdots+\xi_{n+1}<x\,|\,\xi_1+\xi_2+\cdots+\xi_n=x_1)f(x_1)dx_1$$

$$=\int_0^x P(\xi_{n+1}<x-x_1)f(x_1)dx_1$$

$$=\int_0^x\frac{\lambda^n}{\Gamma(n)}x_1^{n-1}e^{-\lambda x_1}dx_1\int_0^{x-x_1}\lambda e^{-\lambda\xi_{n+1}}d\xi_{n+1}$$

$$=\int_0^x\frac{\lambda^n}{\Gamma(n)}x_1^{n-1}e^{-\lambda x_1}\left(1-e^{-\lambda(x-x_1)}\right)dx_1 \qquad (6)$$

by the total expectation formula.

Then the density function for $\xi_1+\xi_2+\cdots+\xi_n+\xi_{n+1}$ is

$$f(x)=\frac{dP(\xi_1+\cdots+\xi_{n+1}<x)}{dx}$$

$$=\frac{\lambda^{n+1}}{\Gamma(n+1)}x^n e^{-\lambda x}=\Gamma(\lambda,n) \qquad (7)$$

So, to n+1 the conclusion is established . The theorem is proved.

Note 2. Suppose $\xi_i\sim\exp(\lambda)=\Gamma(1,\lambda)$, according to Γ distribution function can add properties ,this conclusion can prove.

Theorem 2. Set overall ξ obey the exponential distribution with the parameter for $\lambda(\lambda>0)$, $\xi_1,\xi_2,\cdots\xi_n$ is one random sample of ξ with the capacity for n ,whose sample mean is $\overline{\xi}$ .Let statistics $G_n=n\overline{\xi}$,then G_n obey Γ distribution with the parameters for（λ,n）,and its density function is

$$p(x;n)=\begin{cases}\dfrac{\lambda^n}{\Gamma(n)}x^{n-1}e^{-\lambda x}, if\ \ x\ge 0\\ 0\qquad ,if\ \ x<0\end{cases} \qquad (8)$$

Proof: For $\xi_1+\xi_2+\cdots+\xi_n=n\overline{\xi}=G_n$,Using Theorem 1,we see that G_n obey Γ distribution with the parameters for（λ,n）.

Inference can be obtained by the theorem 2.

Inference. In the conditions of theorem 2, the statistic $\gamma_n=\lambda G_n=\lambda n\overline{\xi}$ obey Γ distribution of parameter $(1,n)$ .That is, distribution density function of γ_n is

$$f(x;n)=\begin{cases}\dfrac{1}{\Gamma(n)}x^{n-1}e^{-x}, if\ \ x\ge 0\\ 0\qquad ,if\ \ x<0\end{cases} \qquad (9)$$

Theorem 3. Assume overall is subject to the exponential distribution parameters $\lambda(\lambda>0)$, one of the samples is $\xi_1,\xi_2,\cdots\xi_n$, then test the original hypothesis: $H_0:\lambda=\lambda_0$, the denial region of the alternative hypothesis $H_1:\lambda\ne\lambda_0$ is

$$C=\left\{0<\gamma_n<\gamma_{\alpha/2}\quad or\quad \gamma_n>\gamma_{1-\alpha/2}\right\},$$

which $\gamma_n=\lambda_0 n\overline{X}$, $\alpha(\alpha\in(0,1))$ is given significance level.

Proof: Select statistics $\gamma_n=\lambda_0 n\overline{X}$, when the original hypothesis H_0 was established, Γ distribution of $\gamma_n(1,n)$. The given significance level $\alpha(\alpha\in(0,1))$, for

$$\int_0^{\gamma_{\alpha/2}}f(x,n)dx=\frac{\alpha}{2},\quad \int_0^{\gamma_{1-\alpha/2}}f(x,n)dx=1-\frac{\alpha}{2},$$

According to the density function $f(x;n)$ of γ_n distribution, then only critical value is $\gamma_{\alpha/2}$ and $\gamma_{1-\alpha/2}$,having

$$P\left\{0\le\gamma\le\gamma_{\alpha/2}\right\}=P\left\{\gamma\ge\gamma_{1-\alpha/2}\right\}=\frac{\alpha}{2}.$$

Hence the rejection region is $\left[0,\gamma_{\alpha/2}\right]\bigcup\left[\gamma_{1-\alpha/2},+\infty\right)$.

Note 3: We calculate statistic γ_n 's value by the sample, and reject the null hypothesis H_0 if the γ_n 's value fall into the rejection region; otherwise accept H_0 . In addition, similar to Theorem3, we can discuss the case of one-side test.

III. APPLICATIOON

Below is actual example of application of exponential distribution parameter hypothesis testing in production. It's known that the service life of some electronic elements is subject to the exponential distribution parameters λ , now extract 20 components from the sample for life test, data as follows (unit: hour)

1050 1100 1080 1200 1300 1060
1090 1080 1180 1320 1250 1340
1060 1150 1150 1250 1310 1090
1140 1160

Whether the average life expectancy of this kind of electronic components can be thought as 1170 hours（ $\alpha = 0.05$ ）?

Test original hypothesis H_0 : $\frac{1}{\lambda} = 1170$ That is, $\lambda = \frac{1}{1170}$.

As $n = 20$, when the establishment of H_0 , statistics $\gamma = \frac{20}{1170}\bar{\xi}$ is subject to the Γ distribution parameters(1,20).

As $\alpha = 0.05$,

$$\int_0^{\gamma_{\alpha/2}} f(x,n)dx = \frac{\alpha}{2}$$

And

$$\int_0^{\gamma_{1-\alpha/2}} f(x,n)dx = 1 - \frac{\alpha}{2}, \qquad (10)$$

the calculated critical value

$\gamma_{0.025(20)} = 12.22, \gamma_{0.975(20)} = 29.67$,

So the denial region is $C : [0,12.22] \cup [29.67,+\infty)$.

According to sample observation value, $\overline{X} = 1168$, then $\gamma = \frac{20}{1170}\bar{\xi}\ \frac{23360}{1170} = 19.97 \notin C$, hence accept the original hypothesis H_0 , that the average life expectancy of such electronic components is 1170 hours .

Note 4. Similar to the normal distribution, we make the critical value of the form of different sample size and significant level for later reference, but for space limitations, this is omitted here.

REFERENCES

[1] TaoWan, Cailian Yao, Minghui Jia, Zhigao Zhang.Parameter estimation of exponential distribution [J].Journal of Inner Mongolia University for Nationalities, Vol. 14,Mar. 2008,pp.8-10.

[2] Wentao Huang, Chingjui Shi. Testing in two parameter exponential distributions via empirical Bayes method . Journal of Applied Mathematics and Computing, 2009, 30(1): 409-426

[3] R. Heuts. Parameter estimation in the exponential distribution, confidence intervals and a monte carlo study for a goodness of fit test. Statistical Papers, 1972, 13(3): 225-246

[4] Yineng Wu, Jingbo Lu. Exponential distribution of random sequence and the application in inventory model[J]. Statistics and Decision, 2009, Vol.15,pp.146-147.

[5] Guoping Tang, Cihua Liu. Exponential distribution parameters of the sequential probability ratio test. Statistics and Decision, 2007 , Vol.10,pp.30-32

[6] Dongyuan Xu, CinanYe, Meichen Wang. Estimations of Parameters for a class of multivariate exponential distribution. Journal of System Science and Mathematical Science , 2006 ,Vol. 26,pp. 619-628

[7] Yijing Wang. Index of the overall hypothesis test .Gansu Science and Technology, Vol. 25, Feb 2009, pp.72-73

[8] Fukun Jiang , Zhengchun Liu. Interval estimation and hypothesis testing of exponential distribution parameter. Journal of Jiaxing College ,Vol. 16, Mar 2004,pp.12-14.

.

A Glimpse on Environmental Probes

Craig C. Douglas
School of Energy Resources and
Department of Mathematics
University of Wyoming
Laramie, WY, USA
e-mail: cdouglas6@uwyo.edu

Mauricio Vieira Kritz
Dept. of Computational and Applied Mathematics
LNCC – National Laboratory for Scientific Computation
Petrópolis, RJ, Brasil
e-mail: kritz@lncc.br

***Abstract*— Environmental systems and landscapes are extremely complex systems whose observation is difficult, resulting in incomplete observations scattered in time and space with respect to relevant factors. They are ever changing systems far from thermo-dynamical equilibrium. Moreover, the nature of these observations typically varies from one environmental sphere to all others. We address the problem of obtaining systematic and extensive enough observations about these systems to build reliable dynamical models of them, focusing on long term behavior, adaptation, and sustainability.**

Keywords*— *environmental modeling, data driven simulations, real-time smart sensing, adaptive behavior, sustainability

I. INTRODUCTION

Tradition establishes that the environment of an object, system, or phenomenon is everything surrounding it. Regarding environmental investigations, this creates a tendency to prioritize the impact of climate, water systems, and soil changes over biotic systems. However, if we look for a basic unit of study for the environmental sciences, it is less obvious what should be regarded as an environmental system.

All environmental phenomena take place in a thin spheroid slab lying between the lithosphere and outer space. In this slab thermodynamic turmoil is driven by the difference in temperature between terrestrial magma and outer space and by differences in the quantity of solar radiation reaching each of its portions. Granted that we can trace a meaningful boundary in this slab, what should be considered as the environmental system: the "interior" of the boundary or what is in the slab outside it?

Otherwise, the long run observation of environmental systems in the wild is difficult due to accessibility constrains, environmental conditions, and the number of relevant factors and their interdependence. Furthermore, not all intervening factors and interactions of an environmental system are known in advance since they may change in consequence of its dynamics [1]. Therefore, provision must be made for finding new things to observe and new perspectives to do it.

Observing the environment is difficult not just because of the above issues but also as a consequence of intrinsic characteristics of environmental systems that stem from complex interaction networks and variegated superimposed dynamical regimes. Moreover, organizational and dynamical aspects determine the behavior and evolution of their biological and ecological components. Also, environmental studies frequently neglect possible impacts of biotic processes upon non-biotic environmental processes. Nevertheless, studies in tropical regions "indicate" that biosphere components do affect the behavior of geophysical, geochemical and climatic systems of a landscape, although their ranges in time and space may be quite distinct. Extensive, systematic, and integrated observation of landscapes is needed to improve our understanding of environmental systems.

Our work addresses the problems of: specifying environmental systems, how to select them for observation, and how to assemble probes capable of observing landscapes in a sustained and adaptive manner. Part of its content result from three workshops held at LNCC in July, 2006, August, 2008, and August 2011, the latter two organized by us and Prof. Pedro L. da Silva Dias. The discussions then held revealed that there is knowledge and technology available that allow for facing the above problems and to develop innovative ways to systematically observe untouched environmental systems. The workshop talks are archived at http://www.dddas.org in the Virtual Proceedings area [2].

This paper is organized as follows:

- Introduction
- Environmental systems
- Environmental data
- Systematic observation of environmental systems
- Conclusions

II. ENVIRONMENTAL SYSTEMS

The environment of an object (system or phenomena) surrounds and/or directs it. To give a meaning to this statement we need to consider the existence of something dividing the universe, that is, clearly stating what is "inside" it, what is "outside" it, as well as what may interact with the object. Although this consideration looks rather simple or naïve, it is often not, as will be soon apparent.

While referring to environmental systems, we focus on something that surrounds us. However, to construct an environmental science, it is necessary to have a less anthropocentric manner of recognizing and delineating environmental systems. A good concept of environmental system should allow for a systematic delimitation and identification of them and their interacting components, and

978-0-7695-4818-0/12 $26.00 © 2012 IEEE
DOI 10.1109/DCABES.2012.68

be directed to processes supporting life. Moreover, both the interacting components of environmental systems as well as the strength and quality of interactions among them may change as a consequence of the environmental dynamics and a good concept should allow for tracking these changes.

We live on Earth. Life on Earth is confined to a thin spheroid slab 16 km thick, squeezed between the hot and dense *lithosphere* and the void, virtually unbounded, *outer space*. This region is flooded by solar energy and usually subdivided into: a *pedosphere* **P** (mostly solid or grained soil), a *hydrosphere* **H** (that may be saline of fresh), a *cryosphere* **C** (either solid or powdered), and an *atmosphere* **A** (mostly gaseous, sometimes liquid). The pedosphere (soil) is indeed the interface of the lithosphere with the atmosphere, the cryosphere, and the hydrosphere. Humans live and interact in this relatively thin layer between the hot and dense and the freezing void.

In this highly inhomogeneous and ever changing layer, states of matter powered by sun radiation continuously vary from the mostly solid at its bottom (closer to the Earth's center) to liquid and gaseous forms in higher altitudes. However, this variation is not random. Although much of the present aspects of our landscapes are a consequence of geo-physical and geo-chemical stresses as well as of thermo-dynamical forces, the composition and the constitution of these phases, from the lower pedosphere to highest atmosphere, is organized to an extent that cannot be explained in terms of out–of–equilibrium thermodynamics and self-organization. These four spheres relate each to a thermodynamic phase and their associated states of matter. Nevertheless, these spheres do not encompass all states of matter enduring in Earth's spheroid slab.

Driven by solar energy, inheriting from the natural tendency of systems to self-organize when far from equilibrium, there is a phenomenon on Earth giving rise to organized matter—here considered as a fifth state of matter. It is called life. Life processes and behavior have a propensity to qualify and organize their surroundings. It is important to recall that not just the soil and atmosphere's present composition and aspect are a large consequence of organisms' activities. Also, ecosystems are said to adapt the biochemical milieu of its surroundings to their needs [3]. Hence, there is another sphere in the slab.

The *biosphere* **B** is formed by living biological material—organized matter and organized biological processes—which can be found anywhere. The biosphere, thus, permeates the slab and is intertwined with all other spheres. Organisms group themselves into populations and communities that organize into ecosystems, which are smallest stand-alone unities from the biological perspective. Biomes, large collections of ecosystems and organisms [4], surely affect the amount of sunlight reaching the soil, the soil composition itself, the time water is retained in the upper layers of the soil, and how water flows on the soil surface. It is also well accepted that our atmosphere would not have its present day composition were it not for oxygen producing bacteria and that the structure and composition of the pedosphere is largely a consequence of roots, worms, and vegetation.

Due to differences in time scales and characteristic times of interactions among subsystems of different spheres, handling reciprocal influences simultaneously and in the same model is uncommon. The many facts about environmental interactions that are known relate mostly to which effects the preponderant physico-chemical spheres (**H**,**P**,**C**,**A**) have on biomes. Nonetheless, the intervention of components of the biosphere in the other spheres is also relevant. To get a better picture of biomes and the role of the biosphere in the thin slab of our environment, we also need to investigate each Earthly sphere as molded by biotic processes.

Hence, an *environmental system* is any portion of Earth landscapes that takes into account interactions between components of the biosphere (organisms, biomes) and elements of the other spheres, highlighting the effects the biosphere may have on phenomena of the other spheres. Of course, this implies considering the effects induced by the (less-organized) phases in the other spheres upon biosphere components of the system. However, the exact delimitation of ecosystems or environmental systems is a difficult task. The sound establishment of environmental systems can only be achieved gradually [5].

III. Environmental Data

Delineating a system requires that its boundary is traced, their interacting components enrolled, and their possible and potential interactions identified. It should be clear from previous arguments that the delimitation of environmental systems is a delicate matter. Besides being ever-changing, the borders of environmental systems are fuzzy since they depend on existing knowledge about spatial behavior of populations, interdependencies of the variegated factors during large time intervals, and the relative strength of interactions. Populations may be highly mobile and the strength and nature of interaction may vary in time [6]. This imposes a strong burden in establishing boundaries. Boundaries are necessary if we want to understand the whole environment slab in its extreme complexity and variability altogether.

Therefore, data are needed to identify environmental components, describe their actual and possible localization in time and space, and register possible and potential interactions. Key components of environmental systems may be physical-chemical, biological, ecological, or human. Nevertheless, ecosystems, that contain a collection of interacting populations, are central in environmental descriptions. Ecosystems may interpenetrate spatially even when not interacting. To characterize ecosystems, data about populations are needed. Their localization in space and time is a long standing subject. Artifacts and methods for this kind of observations have been developed and observations and modeling seamlessly merged [6], although the artifacts may be dependent on each population.

Components of environmental systems are characterized by a set of aspects and their variation in space and time. Often, aspects are quantifiable, even measurable, while some are not (phenotypical traits characterizing a species and preferences prioritizing interactions, for instance). In

principle, the collection of all observed aspects and their variations should univocally identify all components of a system. Quantifiable aspects may be measurable, like flows of mass and energy, intensities, concentrations and velocities, or result from population counts and proportions, expressed as densities, growth rates and the like.

However, identifying new components of environmental systems may be utterly difficult. The aspects identifying them and the interactions in which they take part are usually unknown. Worse, a new component can be characterized by aspects already being observed, but only under a different pattern or organization. Their presence and influence in a monitored system are recognized through mismatches or "stresses" between what is being observed and our inferred expectations about the environment's behavior. If formal descriptions of the system are available, these "stresses" take the form of observations not being explained or accounted for by a model representing what is known about the environmental system's behavior. The identification of which mismatches derive from the approximation inherent in the model and which are derive from yet unknown factors is at the core of this difficulty.

Contrary to physical phenomena, where components interact freely with each other, there are interaction restrictions in chemical, biological and higher systems, as well as any system having them as elements. That is, any component of an environmental system may interact with just some of its collection of components, while having their interaction with certain others totally forbidden. Therefore, recording interactions, their properties and features is important in systems containing complex objects as components [5]. Interactions are grounded on exchanges and in channels that allow for exchanges to take place. Any aspect may be exchanged. In environmental systems exchanges are in a way or another attached to transfer of mass, energy, or information. Observing interactions in environments may then be performed by identifying possible and potential exchange-channels and tracking flows of mass, energy or information in these channels.

It is clear that obtaining data about interactions is critically dependent on identifying the objects that interact, as well as on knowing whatever constraints on interactions exist. This information is of a relational type. Interactions among clearly identifiable objects are traditionally observed afterwards, while analyzing quantitative data collected about events and aspects associated to the objects under observation. For environmental systems, however, being able to observe interactions and their intensities simultaneously with the observation of events and aspects associated with its components may help identifying yet unknown though relevant environmental players and thus improve the delimitation and identification of the environmental systems proper.

IV. Systematic Observation of Environmental Systems

The previous discussion points to some uncommon features of the process of observation of environmental systems, like the direct observation of interaction channels and exchanges composing interactions. New sensor technologies and data-driven modeling can be used to solve many of these challenges as described below.

Dynamic data-driven application systems (DDDAS) assumes that application components, resource requirements, application mapping, interfaces and control of the measurement system can be modified during the course of the application simulation. Many DDDAS applications are multiscale in nature. As the scale changes, models change, which in turn, changes which numerical algorithms must be used and possibly the discretization methods. DDDAS applications involve a complicated time dependent, nonlinear set of coupled partial differential equations, stochastic or agent-based simulation methods, which add to the complexity of dynamically changing models and numeric algorithms. It also causes computational requirements to change, particularly if dynamic adaptive grid refinement or coarsening methods are used, in response to the dynamically streamed data into the executing model.

In a simplified software framework of a DDDAS system, the data used to drive a DDDAS system are retrieved periodically by a data retrieval service, extracted, converted, quality controlled, and then staged as dynamic inputs to simulation models. The extraction process reads the retrieved data based on the metadata associated with them and feeds the extracted values to the conversion model whose major purpose is unit conversion, e.g., from inches to millimeters. The converted data are then analyzed for potential errors and missing values by the quality control model. This control process ensures the correctness and quality of the data, which is of great importance for the model simulation accuracy. The quality controlled data are then fed to the data storage model, which either saves the data to a central file system or loads them to a central database (this depends on project requirements). The data store model may also need to register the data in a metadata database so that other models can query it later.

DDDAS environments require new software capabilities for application modeling and composition, dynamic runtime, resource management, data management, and measurement control aspects, as well software architecture drilling across all layers and end-to-end software infrastructure. DDDAS applications must effectively inject continuous streams of data from disparate sensor networks into running simulations. These data streams most often will be noisy, from a variety of sources and sensor types, incomplete, arriving at unexpected times, and limited in scale based on the sensor specifications. We need better scheduling of computational and network resources so that multiple models, possibly running at different locations, can be coordinated and data can be exchanged in a timely manner. We need to understand when warm restarting of simulations is needed as a result of incorporating new data into parallel or distributed computations, which are sensitive to both communication speeds and data quality. We need to differentiate between tracking and steering of remote simulations to efficiently interact with the computations and to collaborate with other researchers. We need adequate tools for interpretation and analysis of results.

DDDAS provides a natural programming and modeling paradigm for environmental probes, which are strictly dynamic by definition.

- A DDDAS must have flexibility in order to run for a very long period of time.
- Understanding errors or omissions in either the data or the model is essential.
- A DDDAS must also be able to change its basic model as new features are discovered and added, which can require a restart if the DDDAS code has to be modified during a simulation.
- Using different scales in different parts of domains at different times is essential to a DDDAS.
- Finally, a symbiotic relationship between sensors and the running models so that intelligent data collection and modeling are both achieved simultaneously is considered the true measure of a successful DDDAS.

All of these points are essential for environmental probes.

V. CONCLUSIONS

The observation of environmental systems poses significant challenges, like the direct observation of interaction channels and exchanges, as well as the identification of novel interacting components. The systematic observation of environmental systems, particularly of those in the wild, requires that these steps are made as automatic as possible and implemented in autonomous observation equipment.

However, new modeling methodologies and sensor technologies that allow for a symbiotic merging of modeling and data acquisition can be efficiently employed while addressing these challenges and blueprints for environmental probes may be soon available.

ACKNOWLEDGMENT

We would like to thank all participants of all three workshops on "modeling and sensing environmental systems," the GEOMA network, CNPq, FINEP, FAPERJ, and the National Science Foundation for financial and operational support.

REFERENCES

[1] Rowntree, J K, D M Shuker, and R F Preziosi. "Forward From the Crossroads of Ecology and Evolution." *Philosophical Transactions of the Royal Society of London Series B, Biological Sciences* 366, no. 1569 (March 28, 2011): 1322–1328.

[2] C. C. Douglas and M. V. Kritz, Proceedings of the DDDAS, Modeling and Environmental Systems Workshops I, II, and III, http://www.dddas.org/virtual_proceedings.html, 2006, 2008, and 2011.

[3] R. E. Ulanowicz, Growth and Development: Ecosystems Phenomenology. New York:Springer-Verlag, 1986.

[4] A. M. Jones, Environmental Biology. Routledge Introductions to Environment, London:Rutledge 1997

[5] M. V. Kritz, Boundaries, interactions, and environmental systems. Mecánica Computational, vol. XXIX, pp: 2673–2687, 2010 (http://www.amcaonline.org.ar).

[6] A. Okubo and S. A. Levin. Diffusion and Ecological Problems: Modern Perspectives, 2nd ed. Interdisciplinary Applied Mathematics, v.14. New York:Springer-Verlag, 2001.

Enquiring Semantic Relations among RDF Triples

Wenping Zhang [1, 2]
[2]School of Management
Wuhan University of Science and Technology
Wuhan, China, 430081
wp_zhang2002@sina.com

Zhonghua Deng[1]
[1]School of Information Management
Wuhan University
Wuhan, China, 430072
sim.dzh@gmail.com

***Abstract*—This paper presents the research work of extending the semantic web retrieval language SPARQL and the ARQ engine in Jena to searching semantic relations among RDF triples by introducing a new query pattern which retrieves semantic relation paths between a pair of RDF nodes or radiating from a single node. It would promote ability of disclosing latent correlation between or around the semantic nodes and provide feasible mechanism for the Semantic Web-based applications.**

Keywords- semantic relation retrieval; SPARQL; RDF triples

I. INTRODUCTION

The Resource Description Framework (RDF) enables data to be decentralized and distributed. The RDF models can be merged together easily, and the serialized RDF data can be simply exchanged over HTTP. Applications can be loosely coupled to multiple RDF data sources over the Web [1]. But how can you find and manipulate the data you need within RDF graphs? Nowadays the query language widely used to retrieve RDF data in the Semantic Web is SPARQL. SPARQL does retrievals by matching the basic RDF graph data model to the query which does not support the query of semantic relations between RDF data nodes or related relations around a specific node. That makes SPARQL insufficient in fully disclosing the useful relations between the networked semantic nodes, and exploiting the distinctive features of RDF data, which are definitely important for applications based on the Semantic Web.

In order to support retrieving possible direct or indirect relations between two specific nodes and adjacent relations around a given node within the Semantic Web, some extensions should be made against W3C SPARQL syntax. An extension of SPARQL syntax is designed to achieve enhanced functionality of SPARQL query. Then part of the open-source ARQ component in Jena is redesigned which is concrete software realizing SPARQL query. With the new SPARQL extended search functionality, the value of the RDF data model could be mined and utilized more comprehensively.

II. RDF AND SPARQL

A. RDF Graph Data and RDF Triples

RDF is a unified standard defined by the W3C for describing network resources forming the basis of the Semantic Web [2]. The network resources described by RDF specification constitute the basis of the data structure of the Semantic Web.

RDF identifies resources using Web identifiers (URIs), and describes resources with properties and property values [3]. A *Resource* is a *Subject* described by RDF and has a URI. A *Property* is used to describe the characteristics (such as: author, date, language of a book) which is also called *Predicate*. A *Property Value* is the value of a property, which is also called *Object*. The combination of a Resource, a Property, and a Property value forms a Statement known as a *Triple* <subject, predicate, object >.

The RDF specification of resources can be depicted as a directed graph of nodes and arcs representing the resources, their properties and values. For example, a web page was described as shown in Figure 1. The page, i.e. subject, is represented in ellipse node and the property, also predicate, expressed by arc with arrow, which connect subject with property value (object) of a given property. A property value can be literal value, expressed by rectangle, or a subject in another RDF statement. Typically, the description of a subject may contain multiple properties and property values. Here, three properties of the page are presented in the figure.

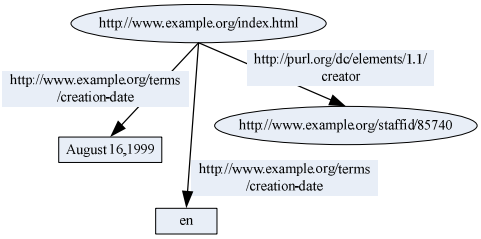

Figure 1. RDF graph data

In addition to the above graphical representation, RDF statements can also be presented in the form of triples. In this way, each description of certain property of a resource can be written into a <subject, predicate, object> triple, thus the aforementioned example in Figure 1 can be directly expressed as follows:

<http://www.example.org/index.html> <http://purl.org/dc/elements/1.1/creator> <http://www.example.org/staffid/85740>.

<http://www.example.org/index.html> <http://www.example.org/terms/creation-date> "August 16, 1999".

<http://www.example.org/index.html> <http://purl.org/dc/elements/1.1/language> “en".

978-0-7695-4818-0/12 $26.00 © 2012 IEEE
DOI 10.1109/DCABES.2012.48

B. SPARQL Syntax and Implementation

SPARQL is a W3C proposed standard on the operation of the RDF data. The role of SPARQL for the Semantic Web is similar to the SQL query language for relational databases [4] [5].

The SPARQL language specifies four different query variations for different purposes, namely SELECT, CONSTRUCT, ASK and DESCRIBE. Each of these query forms takes a WHERE block to restrict the query although in the case of the DESCRIBE query the WHERE is optional [6]. The SPARQL query processor will search for sets of triples that match these four triple patterns, binding the variables in the query to the corresponding parts of each triple.

Jena is an open source Semantic Web framework in Java. It provides APIs to extract data from and write to RDF graphs. The graphs are represented as an abstract "model" that can be queried through SPARQL and updated through SPARUL [7]. ARQ is a SPARQL query engine in Jena for RDF database retrieval. In order to achieve the power of retrieval of relation paths between nodes and adjacent relations around a given node in RDF data source on the basis of the original ARQ function, we need to know the workflow of ARQ query engine, including the query string parsing, the establishment of abstract syntax tree, query optimization, the calculation of the mathematical expression, etc.

C. SPARQL Query Process in ARQ

In order to do SPARQL extensions in ARQ component, we first need to understand the work process in which ARQ performs the SPARQL retrieve, shown in Figure 2.

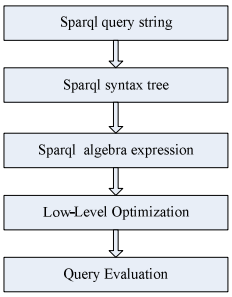

Figure 2. SPARQL query process in ARQ

The first step is SPARQL parsing. This step turns a SPARQL query string into a Query object. The class Query represents the Abstract Syntax Tree (AST) for the query and provides methods to create the AST, primarily for the use by the parser. The query object also provides methods to serialize the query to a string. Because this is the AST, the string produced is very close to the original query with the same syntactic elements, but without comments, and formatted with a whitespace for readability. It is not usually the best way to build a query programmatically and the AST is not normally an extension point.

The second step is algebra generation. ARQ generates the SPARQL algebra expression for the query. After this a number of transformations can be applied, but the first thing is the application of the algorithm in the SPARQL specification for translating a SPARQL query string, as held in a Query object into a SPARQL algebra expression. This includes the process of removing joins involving the identity pattern.

The third step is high-level optimization and transformations. There is a collection of transformations that can be applied to the algebra, such as replacing equality filters with a more efficient graph pattern and an assignment. When extending ARQ, a query processor for a custom storage layout can choose which optimizations are appropriate and can also provide its own algebra transformations.

The last step is low-level optimization and evaluation. Low-level optimizations include choosing the order in which to evaluate basic graph patterns. These are the responsibility of the custom storage layer. Evaluating a query is the process of executing the algebra expression, as modified by any transformations applied, to yield a stream of pattern solutions. Low-level optimization can be carried out dynamically as part of evaluation.

III. SPARQL QUERY EXTENSION

This part presents the extending SPARQL syntax to support the retrieval of relational path. The basic principle of extension is not affect the original SPARQL query syntax and features. In this study the method to achieve the function extension of SPARQL is to introduce a new query pattern and new keywords to SPARQL standard to support the query of relations between RDF data nodes or related relations around a specific node. The realization of the function is by adapting the open source of ARQ in Jena to meet the objective of SPARQL query function extension.

A. Query Variations Extension

In the RDF data based semantic Web there are many relation paths between a pair of nodes or many related relation paths radiating from a node. It is not easy to find out one or multiple valuable such paths [8] [9].

To achieve these objectives, a new query pattern and several keywords are added to the SPARQL standard. The first key word is SEEK, which used to indicate the relation path query type and its usage is similar to the keywords such as SELECT, ASK, DESCRIBE, and CONSTRUCT. SEEK needs aid of some other restrictive keywords to restrict query conditions, thus the keywords START and END are introduced to refer to start node and end node that we want to get relation paths between them. The fourth keyword NODE is used to describe the graph patterns of the nodes in the relation path, as well as their connection modes to the start and end nodes. The fifth keyword CONSTRAINT, which is similar to FILTER, describes the constraints of the relation paths, mainly used to limit the shortest and the longest length of relation paths between the start node and end node, and the variable prefix of start node, end node, and relation path.

B. Retrieving Relation between RDF Nodes

In the semantic Web environment, two nodes without direct link between them usually indirectly linked to each other via

other nodes and there must be one or multiple relation paths. This relationship model can be abstracted as "find the possible relation paths between any two semantic nodes". Of course, these associations can also be constrained to more accurately find such kind of relation path [10].

With the aid of the extended SPARQL we can do some complex retrieval on the semantic Web to find some valuable relation paths between nodes and around a specific node. By specify the start node set by START and the end node set by END, all the relation paths among them can be found. If any constrictive factor needed to assign on nodes, we can use NODE and CONSTRAINT to describe a variety of additional constraints on the query.

The following example is to query possible relations between China and the United States based on pre-existing RDF database for testing. Due to complex relations between two nations, there must be multiple relation paths linking two nodes in RDF database. In order to find the valuable relation paths that may exist in the semantic network and users really care about, certain restrictions should be assigned in NODE and CONSTRAINT blocks. It is not difficult to find that here in the extended SPARQL query statement we used the NODE and CONSTRAINT to set constraints on query. In NODE block, the *power* factor is required to set the weight of node in the relation path. As for weight of nodes, it is not in the range of this study and in latter test, we just take it for granted that the weights of nodes in testing dataset are calculated in advance. In CONSTRAINT block, the depth of relation path is set to specify the length from the start node to the end node. Here the maximum length is 6 and the minimum length is 3. Usually the depth of the path is determined according to the actual need.

```
SEEK  ?node, ?power, ?link
WHERE {
        START{ ?s1 <http://jena.test/element/type> "country".
               ?s1 <http://jena.test/element/type> "China".
             }
        END{ ?s2 <http://jena.test/element/type> "country".
             ?s2 <http://jena.test/element/type> "America".
           }
      NODE{ ?s1 ?link ?node.
            ?node ?link ?s2.
            ?node <http://jena.test/elements/type> "keypoint".
             ?node <http://jena.test/elements/power> ?power.
             Filter(?power>1)
           }
       CONSTRAINT{ LinkName("link")
                   NodeName("node")
                   MinDepth(3)
                   MaxDepth(6)
                  }
       }
```

Figure 3. SPARQL query for relation paths between two nodes

C. Searching Relations around a Single Node

In a network of relationships, it is of great significance and value to get related nodes around a certain node. That reveals latent valuable truth hided in the ocean of information for users to find true knowledge. Back to the semantic network environment, this problem can be abstracted into "find any related node directly or indirectly connect to a specific node." Of course, this kind of query can also be constrained by NODE and CONSTRAINT in order to find more accurately this kind of relation paths [11].

When this kind of query is performed, the query statement uses the START to describe the start node from which one or multiple relation paths are expected to be found. Here no END is need to specify the end node.

The example shown in Figure 4 is to find any possible relation paths linking to the specific node "NPC AND CPPCC". Since there must be many complex relation paths around the node, certain limitations should be assigned in NODE and CONSTRAINT blocks to make the retrieval results meet the requirement of users.

```
SEEK  ?node, ?power, ?link
WHERE{
        START{?s1<http://jena.test/element/type> "conference".
              ?s1<http://jena.test/element/type>"NPC and CPPCC".
              }
        NODE{ ?s1 ?link ?node.
              ?node ?link ?s2.
              ?node <http://jena.test/elements/type> "keypoint".
              ?node <http://jena.test/elements/power> ?power.
               Filter(?power>1)
              }
        CONSTRAINT{ LinkName("link")
                    NodeName("node")
                    MinDepth(3)
                    MaxDepth(6)
                   }
     }
```

Figure 4. SPARQL query for relation paths around a node

IV. IMPLEMENTING THE SPARQL EXTENTION

To realize the extended functions of SPARQL, certain modifications should be made on the open source of ARQ in Jena. The extension part is added to the original code of ARQ, and re-packages the ARQ engine data model.

A. Constructing Abstract Syntax Tree

The SPARQL syntax extensions require corresponding functionality extensions of the ARQ query engine, i.e. adding the implementation of SEEK into ARQ. This makes SPARQL query types to five, namely SELECT, ASK, DESCIRBE, CONSTRUCT, and SEEK. According to different query type, *ParserSPARQL* will call one of the five private methods *SelectQuery*, *ConstructQuery*, *DescribeQuery*, *AskQuery*, and *SeekQuery* respectively to conduct its further syntactical checking.

The parsing rule for SEEK query statement checks there should be the START block in the WHERE clause to describe the start node of the relation path. The END block is optional in WHERE, which depends on what kind of retrieval the query statement makes. It is necessary to appoint the end node when querying relation paths between two specific nodes and not required in querying related paths around the start node. The NODE block is optional to determine the mode of nodes in relation path and the CONSTRAINT block is optional too,

which sets additional restraint on the query. If the SEEK statement cannot meet these basic syntactical rules, the query syntax tree will be failed its creation, then a message would be sent to the client to report syntax error. Figure 5 shows the abstract syntax tree derived from the example shown in Figure 3.

```
(project ( ?node, ?link, power)
   (path (
         START(bgp( triple(?s1<http://jena.test/element/type> "country")
                    triple(?s1 <http://jena.test/element/name> "China")
                   )
               )
         END( bgp( triple( ?s2 <http://jena.test/element/type> "country")
                   triple( ?s2 <http://jena.test/element/name> "America")
                   )
              )
         NODE( bgp(triple(?s1 ?link ?node)
                   triple(?node ?link ?s2)
                   triple(?node <http://jena.test/elements/type>
                          "keypoint")
                   triple(?node <http://jena.test/elements/power> ?power)
                    )
               )
    )    )
 )
```

Figure 5. AST for SEEK query statement

B. Establishing Query Context

In the original iterator model, the abstract syntax tree and algebra expression are used to support the query execution of the iterators. The query of relation paths is different from the traditional SPARQL retrieval pattern that only match against the connections between nodes, so *SeekQueryContext* object is introduced into the implementation of SEEK query to record the contextual information, which includes those of the start node and end node, the node key factor filter, the nodes relation key factor filter, and the minimum and maximum depth of the relation path.

Variable *nodeName*, *linkName, powerName* correspond to three query objects in the SEEK statement, i.e. node, relation between two nodes and weight of node or relation between two nodes. In the SEEK query statement shown in Figure 3, *nodeName* corresponds to *?node*, *linkName* to *?link, powerName* to *?power*. *?node*, *?link*, and *?power* are used to obtain IRI of nodes, the relation between nodes, and the weight of the relation respectively.

Variable *startNode* is used to store the constraints that the start node should meet. This makes setting additional demands on the start node by user possible when it is needed, rather than simply specifying the IRI of the start node. So does the variable *endNode* on the end node. It contains constraints that the end node must comply with, rather than IRI of the end node.

The following variables are used to set auxiliary parameters. *nodeFilter* is used to store the constraints for intermediate nodes in relation path, and it is optional to filter out unwanted intermediate nodes. *powerFilter* is used to store the threshold of the weight of relation, to ensure the retrieval to get the nodes and relations of weights above this threshold, and is an optional setting as well. *minDepth* is used to record the minimum length of relation path; and those not reaching the minimum path length will be filtered out. The default value of *minDepth* is 3. *maxDepth* is used to limit the maximum length of the path that can be search out, to prevent the retrieval of unlimited depth. The default value of *maxDepth* is 6.

The variable *startNodeInfo* and *endNodeInfo* in the contextual object *SeekQueryContext* are used to store IRI of start node and end node. IRI of start node is necessary in a query; otherwise the query is illegal in syntax. *endNodeInfo* is optional, if it exists, the query will search the relation paths in between two nodes; otherwise the query will search the meaningful relation paths around the start node if any.

C. Generating Algebra Expression

The abstract syntax tree generated from query statement will be translated into algebra expression that can be executed by ARQ. In ARQ every kind of algebra expression has a corresponding component object to store and package related information for executing algebra expression. That makes query executed successfully.

After adding SEEK query to SPARQL standard, there is no corresponding component object to execute the algebra expression generated from SEEK query statement, so a new component object *PathOp* has to be built into ARQ engine. This algebra operator needs combining the two basic graph pattern operators for the start node and end node, as well as its own relation path concatenation operator. *PathOp* is designed to reuse the existing operators, and build a new one for relation path concatenation in such a way that it ensures the original structure and method of the engine could work correctly.

D. Testing and Results

Table 1 lists some main part of the test scenarios triples used to test the semantic nodes and the relations between nodes.

TABLE I. A SECTION OF TESTING DATA

subject	predicate,	object
China	launch	space weapons
space weapons	destroy	satellite
America	launch	satellite
China	purchase	national debt
America	issue	national debt
China	invite	Kim Jong
Kim Jong	president of	North Korea
America	threaten	North Korea
China	raise	interest
interest	dominate	inflation
China	cancel	car subsidy
car subsidy	encourage	consumption
China	dominate	rare earth materials quota
rare earth materials quota	exchange for	business priority
China	territory	DiaoYu Islands
Japan	covet	DiaoYu Islands
China	premier	Wen Jiabao
Wen Jiabao	steady	house price

The first experiment is designed to search possible relation paths between two nodes by setting the start node as "China",

the end "United States", and the key factor threshold 0, without any other constraints putted on the start node and end node. The retrieval outcome gives three relation paths between the start node and end node. Figure 6 shows the basic information of the three paths, including the relations with their key factor values between two nodes, as well as the individual nodes and the node key factor values.

China(1.0) → invite(0.8)→ Kim Jong (0.9)→ president of(0.8)→ North Korea(1.0)← threaten(0.8)← America(1.0)

China(1.0) → purchase(0.8)→ national debt(0.7)← issue(0.8)← America(1.0)

China(1.0) → launch(0.8)→ space weapons(0.9)→ destroy(0.8)→satellite(0.8)← launch(0.8) ← America(1.0)

Figure 6. Smantic relation paths between two nodes

The second experiment tests finding the relation paths radiating from a given node without the limitation on the end node of the path. In this case, the node "China" is chosen as the start node without setting other constraints, and the key factor threshold is set to 0. The retrieval result gives seven relation paths from the testing data set. Figure 7 shows the basic information of the seven relation paths.

China(1.0) → invite(0.8)→ Kim Jong (0.9)→ president of(0.8)→ North Korea(1.0)

China(1.0) → purchase(0.8)→ national debt(0.7)← issue(0.8)← America(1.0)

China(1.0) → launch(0.8)→ space weapons(0.9)→ destroy(0.8)→satellite(0.8)← launch(0.8) ← America(1.0)

China(1.0) → raise (0.8)→ interest (0.8)→ dominate (0.8)→ inflation (0.8)

China(1.0) → dominate (0.8)→ rare earth materials quota (0.9)→ exchange for(0.8)→ business priority(0.8)

China(1.0) → cancel (0.8)→ car subsidy (0.8)

China(1.0) → premier (0.8)→ Wen Jiabao(0.8) → steady (0.8)→ house price (0.8)

Figure 7. Smantic relation paths radiating from a node

The experiments show that the extension work has achieved the desired objectives. However, in more complex semantic environments, the relations between the nodes are more complicated, to find meaningful relation paths from so many relations remains as a challenge. Using a power factor to describe the individual importance of the relations, to some extent, can alleviate this problem, but there are still large inadequacies.

V. CONCLUSION

In order to retrieve the semantic relations among RDF triples, firstly two relation searching patterns are identified. One is finding the relations between two RDF nodes, which tells us how many relations existing between the two given nodes. The other is finding the relations radiating from a single RDF node, which tells us how many relations involving the given node. Secondly, a new SPARQL query is introduced based on the two relation searching patterns by adding new keywords and structures to SPARQL syntax. Thirdly, new functionality is built upon the ARQ engine in Jena to realize the new SPARQL query SEEK. In order to be consistent with original logical architecture of ARQ, the code is added to the phrase of constructing abstract syntax tree and generating algebra expression. Finally, the experiments show the SPARQL based extension approach for semantic relation paths retrieval is effective and successful.

Further researches need to be carried out to improve the semantic relation paths searching efficiency. One possible way is to find a more efficient searching algorithm to replace the original iterator model used by ARQ as described in [12].

ACKNOWLEDGMENT

This work is supported by the National Natural Science Foundation of China under Grant 71173163. The authors would like to thank the colleagues for their inspiring discussions and the anonymous reviewers for their valuable comments and suggestions for the better presentation of this paper.

REFERENCES

[1] Philip McCarthy, Search RDF data with SPARQL, http://www.ibm.com/developerworks/xml/library/j-sparql/.

[2] RDF Working Group, Resource Description Framework, http://www.w3.org/standards/techs/rdf, 2004-02-10.

[3] RDF and SPARQL, http://www.bearcave.com/misl/misl_tech/rdf_query_languages.html, 2005-12-8.

[4] F. Manola and E. Miller, RDF Primer, http://www.w3.org/ TR/2004/REC- rdf- primer-20040210, 2007-03-02.

[5] E. Prud'hommeaux and A. Seaborne, SPARQL Query Language for RDF, http://www.w3.org/TR/rdf- sparql- query, 2007-03-02.

[6] SPARQL, http://en.wikipedia.org/wiki/SPARQL, 2012-4-27.

[7] Jena framework, http://en.wikipedia.org/wiki/Jena_(framework), 2012-5-4.

[8] G. Tummarello, R. Delbru, and E. Oren, "Sindice.com: Weaving the open linked data," Proc. the 6th Int. and 2nd Asian Semantic Web Conference (ISWC2007 + ASWC2007), Berlin:Springer, 2007, pp. 552-565.

[9] Li Ding, et al. "Finding and ranking knowledge on the semantic Web," Proc. the 4th Int. Semantic Web Conference, Berlin: Springer, 2005, pp. 156-170.

[10] G. Klyne and J.J. Carroll, Resource Description Framework (RDF): Concepts and Abst ract Syntax, http://www.w3.org/TR/2004/REC-rdf-concepts-20040210/.

[11] C. Mannino and A. Sassano, "Solving hard set covering problems," Operations Research Letters, vol. 18, no. 1, 1995, pp. 1-5.

[12] W. Zhang and Z. Deng, "Searching semantic relation paths using an RDF digraph retrieval model," in press.

Discussion on Usability and Optimization Issues in Overseas University Websites: A British University as an Example

Ai Xu
International Business Faculty
Beijing Normal University Zhuhai
Zhuhai, China
e-mail: gdxuai@163.com

Shufeng Gao
College of Computer Science & Technology
Beijing Institute of Technology Zhuhai
Zhuhai, China
e-mail: gsfdl@163.com

Abstract--According to the reality that visitor's expectations for search quality are far beyond what today's overseas university websites actually deliver, the paper discusses some usability and optimization issues in the overseas university websites. Taking a British university--Bournemouth University as an example, the paper makes a detailed analysis by identifying the usability issues, evaluating the language used and the effect of the email system, and analyzing problems about a degree scheme "landing page" with regard to Search Engine Optimization. Then some website optimization suggestions are proposed in order to further improve the presentation effectiveness of the university website.

Keywords-Usability; optimization; web design; university websites; search engine optimization

I. INTRODUCTION

Nowadays, more and more people choose to go abroad for further study. How to apply for a satisfactory university is not an easy thing. Acquiring enough and high-quality information plays a very important role for a successful admission. University website is a critical and powerful channel, both for the applicants to gain more valuable information about their application, and for the universities to gain more qualified applicants. Of course, a well-designed website can also provide adequate information for their current students and staffs. However, it can be found that there are many usability and other problems about the design of many university websites, which has already become an obstacle for effective information media. Taking the Website of Bournemouth University as an example, some common usability and website optimization issues are discussed. The paper begins with identifying the usability issues, and then evaluates the language used and the effect of the email system. The problems about a degree scheme "landing page" with regard to Search Engine Optimization are also analyzed. At last the paper puts forward some website optimization suggestions, which would be helpful for the oversea universities to further improve their presentation effectiveness.

II. WEBSITE TRAFFIC OF BOURNEMOUTH UNIVERSITY WEBSITE

Before starting to our analysis, we'd better know the current website traffic of Bournemouth University. While logging on Alexa website to see the traffic rank of Bournemouth University website, it can be found from the Statistics Summary that the three-month global Alexa traffic rank is 813363 and Rank in GB is 4241. Relative to the overall population of internet users, the site appeals more to users who have postgraduate educations; its visitors also tend to consist of childless women browsing from school and work. From Alexa website, we can further know that there are estimated 21 reach per million global internet users and about 4 pageviews per user for bournemouth.ac.uk during the past three months. Estimated daily time on site for bournemouth.ac.uk is only 4:04. Roughly 37% of visits to the site consist of only one pageview (i.e., are bounces), and approximately 24% of visits to Bournemouth.ac.uk are referred by search engines. Although the traffic rank doesn't reveal the actual traffic of one website definitely, but it can really show that the current traffic of Bournemouth University website is not ideal.

III. USABILITY ISSUES IN BOURNEMOUTH UNIVERSITY WEBSITE

Usability is a concept that can be applied to the analysis and design for a range of products which defines how easy they are to use [1]. Here usability refers to the ease with which visitors are able to use a website. Usability is essential for an effective website experience. Web visitors often have defined goals. For a university website, the goals of most visitors are to find out enough information they need. After a comprehensive analysis of Bournemouth University website, it can be found that there are many usability issues exist.

A. Legibility problems

According to Jakob Nielson's investigation, about two-thirds of the voters complained about small font sizes or frozen font sizes, and about one-third complained about low contrast between text and background [2]. Here we can identify legibility problems from the small font sizes and low contrast issues on the Bournemouth University website. The font size of some words on the website is too small to read. And the color would get lighter after the link is clicked,

978-0-7695-4818-0/12 $26.00 © 2012 IEEE
DOI 10.1109/DCABES.2012.17

resulting low contrast between text and background, which makes it harder to identify.

B. Not changing the color of visited links

A good web design should differentiate visited and unvisited links. By doing so, the visitors can know which pages they've already visited [3]. Currently, more than 70% of websites use different colors for visited and unvisited links, making this design approach a strong convention that people have come to expect [4]. But on some pages of Bournemouth University website, we can see that they do not obey this convention. There is no color change for the visited links, and even more curious that there are underlines on the link after the moment we come back from the linked page and then the underlines disappear after a few seconds.

C. Violation of the design conventions

Consistency is one of the most powerful usability principles: when things always behave the same, users don't have to worry about what will happen [5]. The oldest usability guideline for any type of navigational design is to help users understand where they've been, where they are, and where they can go. So there is often a current path on a web page. Usually the current path is on the top of the page, which can not only indicate the current path, but also become an important element for SEO, but on BU website, the current path is on the bottom. It is obviously not easy to find for a newer visitor.

Also, the page style changes in BU website, especially the home page and the inside pages. It can be found that the Home Page, Student Portal and Information for Staff are in different styles. Maybe this is a result of their redesign of some pages, but these changes would make the visitors feel inconsistency and get lost.

In general, the website of Bournemouth University is not easy to navigate and clearly organized because of the above usability issues, so that visitors cannot easy to find the information they're looking for.

IV. LANGUAGE AND ITS EFFECT OF BOURNEMOUTH UNIVERSITY WEBSITE

Language and expression are very important for the visitors to understand the context of the website and even motivate them to make some decisions. As for the language used, the analysis is mainly from the following two perspectives.

A. The role of language itself

If some important content of a university website, such as prospectus, can be provided in different languages, e.g. Chinese, it will be definitely helpful for international students. Anyway they would understand well by reading something in their own mother languages.

B. The effectiveness of language expressions

How to express is somewhat hard but really important for the web design. Clear, concise, interesting copywriting or expressions would have good effect, which would be helpful to establish a 'buying' environment. According to AIDA (Attention, Interest, Desire and Action) and FAB (Features Advantages and Benefits) theories, here we have tried to find one page and to change the expression to make it more attractive to the visitors, by focusing on B-word rather than the F-word, which suggest to use Benefit word rather than Feature word.

Here is the copy on the BU website about "IT support for students".

"The IT group is a key enabler to the efficient operation of the University, by providing central services such as Open Access computing, email and audio visual facilities. In addition, the group offers support via workshops, 1-1 training and e-learning support.

We are currently building some new pages for IT support and hope to have this information live here shortly. In the meantime, please visit the current web pages for the IT group. "

And the linkage of "IT group" is one page titled by "IT service".

We can changed the second paragraph into a new copy, focusing on the benefits to students and also changed the link name to 'IT services' so that it would be consistent with the page linked.

"In our pages you can find everything you need to know to make the best use of our services and your time at Bournemouth. Welcome to IT services. "

It is obvious that the revised copywriting is better than the former one, because of the focus on B-word.

V. EMAIL RESPONSES OF BOURNEMOUTH UNIVERSITY WEBSITE

Email system is often used as a communication and interactive tool by a website. In order to make clear about the using effects of the email system, we have made some experiments during our stay in the UK. Here we will illustrate the responses of Bournemouth University Email System from two aspects:

A. Reponses of the request for a prospectus

Concerning about the fact that most visitors are potential students of a university, prospectus is usually with much demand and appeal. Normally, there is a function of requesting for a prospectus at most university websites. How about the effect? Can it work? Followed the linkage of "request a prospectus", we had made a request for a prospectus of Information Technology Course, but we received nothing in the following week. And then we had received the printed prospectus in the next week, which shows this system is effective in deed. However, we also think Bournemouth University should improve their Email system, and make it reply an email to the subscriber automatically, to indicate that they have already received the request from the subscriber and at approximately what time the subscriber would receive the prospectus. This would be a better way.

B. Responses of some previous emails

We had sent some emails respectively to Bournemouth University email address at askBUhome@bournemouth.ac.

uk and askbustudents@bournemouth.ac.uk while we were considering about out visit in the UK on Nov. 2010. We have received reply from askbustudents@bournemouth.ac.uk on the following day, but there is no reply from askBUhome@bournemouth.ac.uk. That indicates that some of the email system of Bournemouth University can work promptly, and some of them can not. So improvements should be undertaken.

VI. WEBPAGE OPTIMIZATION STATUS OF BOURNEMOUTH UNIVERSITY WEBSITE

We have mentioned in the above part that approximately 24% of visits to Bournemouth.ac.uk are referred by search engines. This is often a universal phenomenon for most universities. Thus the search effect is worthy to be paid close attention to. Here the analysis of Bournemouth University website is conducted about the landing page of a very popular degree scheme--Accounting and Finance, with regard to Search Engine Optimization (SEO).

A. Search results (by Google Engine)

We choose Google Engine to make some search and observe the corresponding results. We can find that:

- With the most common keyword "Accounting and Finance", no result found in the first TEN pages.
- With the keyword "Accounting and Finance BA", we can find the landing page result at the 9th page.
- With the keyword "Courses in Accounting and Finance", we can find the landing page result at 2nd page.

The results indicate that there are some problems of the webpage design with regards to SEO, so that the desired result does not appear in the front pages.

B. Some shortages with regards to SEO

*1) Bad prominence:*On the landing page, the most common keyword "Accounting and Finance" is not at the beginning of the heading, both in the left navigation and in the page text. This will obviously affect the search result while using the "Accounting and Finance" as a keyword.

*2) Low keyword density:*The keyword "Accounting and Finance" appears only three times in this page, the first one is in the heading of the left navigation, the second one is in the navigation linkage, and the third one is in the page text on the right. There is also a familiar one "Accounting & Finance" in the current path at the bottom of the page. So the density is too low, which will not get the optimum.

*3) Not clear Meta description:*From the Google Engine search result, the description of the landing page of "Accounting and Finance" is:

"Courses in Accounting and Finance. » Accounting and Business BA (Hons); » Accounting and ... Why Study an Undergraduate Course in Accounting and Finance? ..."

We can see that the description is not simple, clear, concise and characteristic, which could decrease Search Engine friendliness.

VII. WEB PAGE OPTIMIZATION SUGGESTIONS

The above-mentioned usability and other relevant issues should be solved as soon as possible. More efforts should be spent in improving the design, structure and especially the content of the current website of the oversea universities so as to provide as adequate as possible information to the visitors. The following suggestions are with good value.

- Ensure the pages easy to read by choosing suitable font size, breaking up blocks of text and creating short paragraphs.
- Make the colour changed for those visited links and keep the colour consistent for the same items, e.g. the headings.
- Add clear click paths to indicate the current position and provide link to the homepage.
- Ensure the pages load as quickly as possible. Eliminate unnecessary graphics, especially flash graphics they can be time hogs.
- Pay attention to prominence, proximity and density, which are the three basic rules of keyword deployment. Try to improve the prominence and density of the page.
- Highlight some important headlines by using different colour or signals to attract attention from the visitors.
- Try to add a few magical "meta tags" (including TITLE tag, META DESCRIPTION tag, and META KEYWORDS tag) to the web pages to gain a top ranking on some search engines.
- Integrate breadcrumbs into the web design to help with usability and SEO.
- Try to deploy video to increase interest & time on the page, because the longer you keep a searcher on your site the better a page will rank on search engines.
- Try to offer free, original, and high-quality content on the website and keep it up to date and relevant.

VIII. CONCLUSIONS

In a word, it is very important to have a well-designed website for overseas universities in order to improve the effectiveness of the website, which would be helpful not only for the new visitors to gain more information about the university and thus make final decision about the application, but also for the university to provide adequate information for their current students and staffs. It should be pointed out that the above-mentioned usability and optimization issues are somewhat universal both for the overseas universities and for our domestic university websites. Therefore the suggestions are also valuable for the design of our domestic universities.

REFERENCES

[1] D. Chaffey, F. Ellis Chadwick, K. Johnston, R. Mayer, Internet Marketing - Strategy, Implementation and Practice, 3rd Ed., England: Pearson Education Limited, 2006, pp. 312.

[2] J. Nielsen, “Top Ten Mistakes in Web Design of 2005,” Jakob Nielsen’s Alertbox, http://www.useit.com/alertbox/designmistakes. html, 2005

[3] J. Nielson, H. Loranger, Website Optimization: Construct User-satisfied Website by Improving Web Usability, L. Zhang Transl. Beijing: Electronic Industry Press, 2007.

[4] J. Nielsen, “Change the Color of Visited Links,” Jakob Nielsen’s Alertbox, http://www.useit.com/alertbox/20040503.html, 2004.

[5] J. Nielsen, “Top Ten Mistakes in Web Design,” Jakob Nielsen’s Alertbox, http://www.useit.com/alertbox/9605.html, 2011.

[6] John Doe, “Twenty Network Tools with Very High Usability,” http://home.ebrun.com/space.php?uid=4986&do=blog &id=6720

[7] John Doe, “Ten Ways to Improve the Usability of Your Ecommerce Site,” http://www.webcredible.co.uk/user-friendly-resources/web-usability/ecommerce-usability.shtml, 2005.

[8] John Doe, “How to Optimize Keywords Quality,” http://e.baidu.com/pro/cjwt/2009-04-14/120046220346. html, 2009 (in Chinese)

[9] N. Turner, “Ten Ways to Improve the Usability of Your Ecommerce Site,” http://www.webcredible.co.uk/user-friendly-resources/web-usability/ecommerce-usability.shtml, 2005.

[10] T. Zhang, “Optimization Strategy of Searching Engine for Enterprise Website,” Journal of Hubei University of Technology, vol.24, Oco. 2009, pp.61-63.

[11] J. Kyrnin, “Searching Your Site: Adding Search Functionality to Your Web Site,” http://webdesign.about.com/od/administration/a/aa091399. htm.

Searching Semantic Relation Paths using an RDF Digraph Retrieval Model

Wenping Zhang[1, 2]
[2] School of Management
Wuhan University of Science and Technology
Wuhan, P. R. China, 430081
wp_zhang2002@sina.com

Zhonghua Deng[1]
[1] School of Information Management
Wuhan University
Wuhan, P. R. China, 430072
sim.dzh@gmail.com

***Abstract*—In order to retrieve the semantic relations among RDF data, a new query pattern is introduced to SPARQL [1]. This paper presents the research work of extending the ARQ engine to realize the new SPARQL query in a more efficient way by using a digraph retrieval model for searching RDF data instead of the iterator model adopted by the original ARQ engine. The design and implementation of the digraph retrieval model and its application to the semantic relation retrieval are discussed in detail. With the new query pattern, many interesting semantic relations among the RDF data can be explicitly and easily enquired.**

Keywords-RDF triples; semantic relation retrieval; SPARQL extension; ARQ extension ; RDF digraph retrieval model

I. INTRODUCTION

SPARQL is the de facto standard query language used to query the Resource Description Framework (RDF) data. SPARQL currently specifies four kinds of queries, namely SELECT, CONSTRUCT, ASK, and DESCRIBE. As discussed in [1], there are some important and interesting semantic relations existing among the RDF data that are difficult or impossible to be found out by only using the current four SPARQL queries.

In order to facilitate retrieving semantic relations among RDF triples, a new query pattern SEEK is introduced into SPARQL with the intention of searching the semantic relation paths in between two RDF nodes or radiating from a single node [1]. To realize the extension of SPARQL, the extension of the ARQ engine in Jena is carried out. For the purpose of improving the semantic relation retrieval efficiency, a digraph retrieval model for operating RDF triples is designed and implemented. Using the new SEEK query, many interesting semantic relations among the RDF data can be explicitly and easily enquired.

II. DEFINITIONS

A. Semantic Relation Paths in RDF Data

The RDF data are intrinsically linked graph data, which can be naturally depicted as digraphs. Intuitively, a semantic relation path between two RDF nodes is the arcs linked from one node to the other.

An RDF statement is usually presented as a triple of subject, predicate, and object, denoted as <*Subject*, *Predicate*, *Object*>, or simply <*S*, *P*, *O*>. *P* is also called a semantic relation or relation between *S* and *O*. For a collection of RDF triples T, a finite sequence of triples from T is called a semantic relation path if for any two consecutive triples in the sequence, the object of the former is the same as the subject of the latter.

For a semantic relation path $<S_1, P_1, O_1><S_2, P_2, O_2>\ldots<S_n, P_n, O_n>$, where $O_i = S_{i+1}$ for i = 1, 2,…,n-1, will also be denoted as $<S_1, P_1, P_2,\ldots P_n, O_n>$ for the purpose of simplicity.

B. SPARQL Query Pattern for Semantic Relation Paths

As aforementioned, a new query pattern SEEK is introduced into SPARQL in [1]. The SEEK query pattern is shown in Figure 1.

```
SEEK  ?node, ?power, ?link
WHERE {
        START{ ?s1 <http://jena.test/element/type> "country".
               ?s1 <http://jena.test/element/type> "China".
             }
        END{ ?s2 <http://jena.test/element/type> "country".
             ?s2 <http://jena.test/element/type> "America".
             }
      NODE{ ?s1 ?link ?node.
            ?node ?link ?s2.
            ?node <http://jena.test/elements/type> “keypoint”.
             ?node <http://jena.test/elements/power> ?power.
             Filter(?power>1)
            }
       CONSTRAINT{ LinkName(“link”)
                   NodeName(“node”)
                   MinDepth(3)
                   MaxDepth(6)
                  }
      }
```

Figure 1. SEEK query for relation paths between two nodes

The query presented in Figure 1 can be described intuitively as finding those possible relation paths starting from the node specified by the START block and ending with the node specified by the END block while the nodes and their relations in between the given start and end nodes satisfying the conditions specified by the NODE block as well as the conditions specified by the CONSTRAINT block.

978-0-7695-4818-0/12 $26.00 © 2012 IEEE
DOI 10.1109/DCABES.2012.41

SEEK, START, END, NODE, and CONSTRAINT are new keywords added to SPARQL [1].

III. DIGRAPH RETRIEVAL MODEL

The current processing of a SPARQL query in the ARQ engine uses the iterator model, which adopts the basic idea of flow iteration so each time when executing an algebra operator in the query algebra expression, it will match against the triples in the RDF data record table one by one. This process is mainly based on the relational database cursor technology. The operational performance of an algebra operator is still acceptable, but when the SPARQL query itself is more complex, involving several algebra operators and their combinations, the matching time of the query increases in exponential growth curve. If the semantic RDF database is relatively large, the performance bottleneck of the retrieval model is even more apparent.

Inspired by the works presented in [2-6], in response to these performance issues, a digraph retrieval model for operating RDF triples is introduced to deal with the efficient problem in searching semantic relation paths caused by the iteration. The rest of the section will discuss in which way the digraph retrieval model for operating RDF triples can do this and how to do it.

A. Dijkstra's Algorithm

Since the RDF data are intrinsically linked graph data, which form semantic node networks, finding the semantic relation paths between two RDF nodes is finding all the possible arcs linked from one node to the other. This is basically similar to the idea of finding shortest paths in a digraph, so the introduction of the digraph retrieval model for operating RDF triples is entirely reasonable and the logical and physical structure is basically the same.

Why the digraph retrieval model for operating RDF triples surpasses the performance of the iterator model. From the aforementioned analysis, we can know that using the iterative model to execute the query of the semantic relation paths, the time complexity is $O(n_1 * n_2 * ... * n_m)$, where n_i is the number of RDF triple records extracted from the semantic node record table for the execution of the i-th algebra operator in the query algebra expression; m is the number of the algebra operators in the query algebra expression in the final executable form. If m or n is large, the time complexity will rather high. In practical applications, these two values are often relatively large, so there is a priori bottleneck in the performance of the iterative model. The directed graph theories and techniques in graph theory and their applications have been in-depthly studied and extensively practiced, especially the shortest path problem has been had very efficient and sophisticated algorithms.

Dijkstra's algorithm to the shortest path problem is one of the most widely used algorithms in the field. Here the same algorithm is adopted in the introduction of the digraph retrieval model for operating RDF triples. The basic idea of the algorithm is as follows: store the shortest path found so far for each vertex *v* from the start vertex *s* to *v* to work. Initially, the path length of *s* is assigned to 0, that is, d[*s*] = 0, at the same time the path lengths of the other vertexes are set to infinity, which indicates whether there is any path leading to these vertices is unknown at the moment. At the end of the calculation the value stored in d[*v*] is the shortest path from *s* to *v*; when the path does not exist, this value is infinite. Its basic operation is the edge expansion: If there is an edge from *u* to *v*, the shortest path from *s* to *v* through the edge *(u*, *v*) will be added to the tail of the path *s* to *u* to expand. The length of the path is d[*u*] + w(*u*, *v*), where w(*u*, *v*) is the weight of the edge *(u*, *v*). If the value is less than the current d[*v*], it will be used to replace the current value of d[*v*]. The edge expansion will go on until d[*v*] represents the shortest path from *s* to *v* for all vertices *v* in the digraph. This algorithm can be appropriately modified so that when d[*u*] reaches its final value, each edge (*u*, *v*) only be extended once. From the above algorithm description, it can be known that the time complexity of Dijkstra's algorithm is O(VlgV + E), where V and E is the number of vertices and edges respectively. This time complexity is significantly better than the iterative model whose time complexity is of O(nm).

B. Key Factors as Weights

In order to apply Dijkstra's shortest path algorithm in the digraph retrieval model for operating RDF triples, the weights of edges must be decided. Weights play an important role in the shortest path problem, and directly determine which paths will be preserved in the calculation process or thrown away eventually.

Then using what to play the role of weights in digraph-based semantic nodes networks? By careful consideration and practice, we propose to add a key factor, which represents the importance of the object, to each semantic node, as well as to each relation in between two nodes. If a relation is not assigned a key factor, the default value will be the average of the key factors of the two nodes' connected by the relation. Having key factors to act as the role of the weights, Dijkstra's algorithm could be used to choose the relation paths. However, Dijkstra's algorithm itself is only for the shortest path, which means the one with the minimum sum of key factors, so it does not meet the needs of retrieving semantic relation paths. Here the path selection strategy in Dijkstra's algorithm needs to be changed so that a path is eliminated is not dependent on whether it is of the shortest length, but for any single relation in the obtained path, its key factor is not less than a specified threshold, and the average of all the threshold for each relation in the path is not less than the overall threshold. In such a way, the eliminated relation paths are those semantic relation paths which satisfy the query conditions.

How to determine the value of the key factor of a node or a relation between two nodes? The following principles are proposed:

- The importance of the semantic content represented by the node itself or its hot extent;
- the node degree of concern in the search;
- the indegree of the node;
- the distribution of the key factors of the related nodes with the node;

- the significance of the relation itself;
- the degree of concern of the relation;
- the key factors of the two nodes connected to the relation in between.

Based on the above principles of reference, during the creation of a semantic nodes network, a base value will be assigned to a node or a relation to reflect the importance of the node or relation itself. This process requires manual intervention in the current testing phase. After this, the key factors of nodes and relations can be calculated according to other principles, which can basically reflect the importance of the current node and its connected relations.

C. Relation Paths Sorting on Key Factors

Using the digraph retrieval model earlier discussed can retrieve the semantic relation paths between semantic nodes, but the result is only a rough path collection, which only shows a path array of records in the order of the searching results. It appears that the misplaced priorities cannot directly give users the most valuable path information.

In order to solve this problem, sorting the rough result path collection to reflect the importance between the relation paths are taken according to the following principles:

- The key factor in the value of any node in the relation path should be greater than a certain threshold;
- the key factor in the value of any relation in the relation path should be greater than a certain threshold;
- the average of the key factors of all nodes in the relation path;
- the average of the key factors of all relations in the relation path;
- the key factor of each node is close to the average node key factor in the relation path to maintain the importance in a smooth transition between the nodes;
- the key factor of each relation is close to the average relation key factor in the relation path to maintain the importance in a smooth transition between the relation s.

Formally, for an independent relation path, let the set of the key factors of the semantic nodes be V, $V = \{v_1, v_2, ..., v_n\}$, $v_i \in V$ ($1 \leqq i \leqq n$); let the key factor set of relations between nodes be L, $L = \{l_1, l_2, ... l_{n-1}\}$, $l_j \in L$ ($1 \leqq j \leqq n-1$). By definition, v_i is the key factor of the i-th node in the relation path, and l_j is the key factor of the j-th relation in the relation path.

Based on the average node key factor strategy, the average value of node key factors in the relation path is as in Formula 1:

$$PVE = \frac{\sum_{i=1}^{n} vi}{n} \tag{1}$$

According to the average relation key factor strategy, the average value of relation key factors in the relation path is as in Formula 2:

$$PLE = \frac{\sum_{j=1}^{n-1} lj}{n-1} \tag{2}$$

Considering the node key factor similarity strategy, get the node key factor average correction formula:

$$PV = \frac{\sum_{i=1}^{n} (vi - |vi - PVE|)}{n} \tag{3}$$

Consider the inter-node connection relation key factor similarity strategy, get the relation key factor average correction formula:

$$PL = \frac{\sum_{j=1}^{n-1} (lj - |lj - PLE|)}{n-1} \tag{4}$$

Considering the node key factor strategy and the relation key factor strategy, get the integrated relation path key factor formula:

$$P = A * PV + B * PL \tag{5}$$

In Formula 5, the parameter A is the weight taken by the node key factors in the integrated key factor, and the parameter B is the weight taken by the relation key factors in the integrated key factor, and A + B = 100%. Since the role of relations is more important than that of nodes in relation path retrieval, here A can be set to 40%, while B 60%. Sorting the relation paths can be carried out in accordance with the integrated relation path key factor formula.

IV. Design of Algorithms

This section discusses the design of the data structure for digraphs and the conversion of the RDF triples from the database structure into digraph storage structure, and the implementation of the searching and sorting algorithms using Java.

A. Digraph Class Structure

Since in a digraph representing RDF data there are often several relations in between two nodes with the same direction and each of such relation may have different meaning or key factor, so it is impossible to use the two-dimensional matrix structure to describe the connections between the nodes like in the traditional use of Dijkstra's shortest path algorithm. If the multi-dimensional array is chosen, it would make the logic of the data structure and algorithm too complicate. In this design,

adjacency list is taken to store all the connections around a single node, so that node objects and adjacency list objects constitute the most typical key-to-value form, which can not only effectively manage the basic information of digraph, but facilitate understanding and maintenance.

The class Vertex represents the nodes in a digraph mainly describing the node name and key factor. The class VertexLink represents the connection between two nodes and the description information includes the start node, end node, relation name, and relation key factor. The collection ArrayList <VertexLink> is used to store the adjacency list information for fixed nodes and the HashMap <the Vertex, the ArrayList <VertexLink>> to store the association information between the nodes and their adjacency lists. The class diagram is shown in Figure 2.

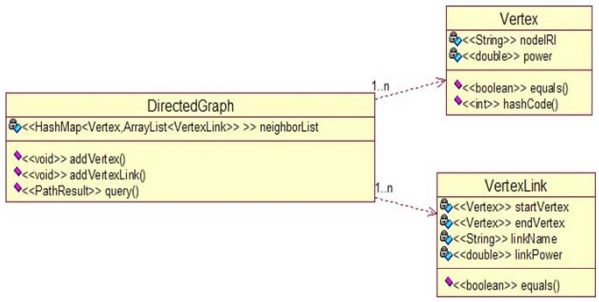

Figure 2. Class structure for digraph data model.

B. Algorithm Implementation

Based on the data representation for the digraph retrieval model, here we will discuss the search algorithm, and we will see the benefits such a clear and concise model brings to us.

Before a query is carried out, we will get a query context object, which records the start node, end node, minimum depth, maximum depth, and key factor threshold of the relation path [1]. Only the end node is optional. If the end node is there, it means to find the relation paths between two specified nodes; otherwise, to find the relation paths radiating from the start node. With the complete query context information, it can start the query process. The basic idea of the algorithm is as follows:

Check if there are the specified start node and end node in the digraph. If not exist, exit; otherwise, find the adjacency list of the start node, traverse the adjacency list and for each link in it check whether the target node is the end node of the relation path in search. If it is and the current search depth satisfies the requirement specified by the query context, a valid relation path is found, and put it into the result set. If it is not and the current search depth is less than the maximum depth, use the target node restart this step, repeat the above search process until a valid relation path is found or exceeds the maximum depth. Go back and continue to traverse the adjacency list on the step until the traversal is complete. When the whole recursive procedure is finished, all the relation paths added to the result set will be the relation paths to be found. The core of the algorithm code is as follows:

```
public PathResult query(QueryContext context) {
    PathResult rs = new PathResult(context.getStartVertex(),
        context.getEndVertex());
    if(this.getNeighborList().containsKey(context.getStartVertex())){
    if(context.getEndVertex()!=null
    && !this.getNeighborList().containsKey(context.getEndVertex())){
                return rs;
                }
    Path path =
    new Path(context.getStartVertex(), context.getEndVertex());
    query(context.getStartVertex(),path,1,context,rs);
    }
    return rs;
}
```

```
private void query(Vertex lastNode, Path currentPath,
                int currentDepth, QueryContext context,
                PathResult rs){
    if(currentDepth>context.getMaxDepth()){      return;    }
    ArrayList<VertexLink> neighborLinkList
        = neighborList.get(lastNode);
    if(neighborLinkList!=null && neighborLinkList.size()>0){
    for(VertexLink vl:neighborLinkList){
        if(vl.getEndVertex().equals(context.getEndVertex())) {
            Path newPath = currentPath.copy();
            newPath.addNode(vl);
            rs.addPath(newPath);
        }else{
            if(currentPath.contains(vl.getEndVertex())
            || vl.getLinkPower()<context.getPower()
            || vl.getEndVertex().getPower()<context.getPower()) {
                continue;}
            else{
                Path temp = currentPath.copy();
                temp.addNode(vl);
                query(vl.getEndVertex(),temp,currentDepth+1,
                        context,rs);
            }}}else{
            if(context.getEndVertex()==null
            &&currentDepth>=context.getMinDepth()){
                Path newPath = currentPath.copy();
                rs.addPath(newPath);
            }        }        }
```

C. Sorting the Results

Using the search algorithm, the valid relation paths can be obtained and put into the PathResult object. The information of each valid relation path is stored in a Path object, which contains the following information:

```
public class Path {
    // Path's start vertex
    private Vertex startVertex;
    // Path's end vertex
    private Vertex endVertex;
    // The sum of the vertex key factors in the path
    private double vertexPower = 0;
    // The sum of the vertex relation key factors in the path
    private double linkPower = 0;
    // The average of the vertex key factors in the path
    private double averageVertexPower = 0;
    // The average of the vertex relation key factors in the path
    private double averageLinkPower = 0;
    // List of vertex connections
    private ArrayList<VertexLink> nodeList;
    ……
}
```

The properties of Path object has all necessary information needed to calculate the integrated relation path key factor given

in Formulas 5, so the function to calculate this key factor is designed as a member of Path directly, called power(). The core code segment is as follows:

```
public double power(){
    if(power!=-11111) return power;
    double averageVertexPower = averageVertexPower();
    double averageLinkPower = averageLinkPower();
     double vertexPowerTemp
       = Math.abs(startVertex.getPower()-averageVertexPower);
    double linkPowerTemp = 0;
    for(VertexLink vl:nodeList){
        vertexPowerTemp
          += Math.abs(vl.getEndVertex().getPower()
                                - averageVertexPower);
        linkPower += Math.abs(vl.getLinkPower()
                                        - averageLinkPower);
    }
    power = 0.4*(averageVertexPower
                    - vertexPowerTemp/(nodeList.size()+1))
              + 0.6*(averageLinkPower
                                - linkPowerTemp/nodeList.size());
    return power;
}
```

PathResult uses variable array ArrayList to store all the result Path objects. In Java, java.util.colletions provides a very good sorting function for ArrayList, so here only need to implement the interface Comparable. The code segment of the sorting function realized in PathResult is as follows:

```
public void sort(){
    class PathSort implements Comparator{
        public int compare(Object obj1,Object obj2){
            Path path1=(Path)obj1;
            Path path2=(Path)obj2;
            if(path1.power()>path2.power())
                return 0;
            else
                return 1;
        }
    }
    Collections.sort(pathList, new PathSort());
}
```

All the valid relation paths are stored in pathList in a descending order on the key factor value by default. This arrangement is in accordance with the idea that the more important relation path, the more the first feedback to the user. This completes the sorting of the query results.

V. TESTING AND ANALYSIS

In the case of retrieving semantic relation paths, the recall rate refers to in the specified semantic node network database to find out all the semantic relation paths satisfying the user query conditions; the accuracy rate refers to all the valid relation paths retrieved must meet the needs of users. The system functional testing is carried out in three directions, namely, the recall rate test, the accuracy rate test, and the comprehensive test. The test data used are the same as in [1].

In the recall rate test, by removing the pattern matching conditions for the start node and end node and setting the key factor threshold to 0, all the nodes and relations are connected to the relation paths and appear in the result set, so as long as all the nodes and relations are in accordance with the desired design in a relation path can pass through basic recall rate test.

The accuracy rate test is the opposite to the recall rate test. In the query, add the appropriate matching pattern to the start node and end node, and specify the thresholds of the key factors. As long as those nodes and relations that meet the requirements appear in the relation path, while those that do not are excluded from the result set of the relation paths can complete the accuracy test.

In the comprehensive test, the goal is to consider a compromise between these two test parameters, making the returned result set can basically meet the recall and accuracy rate, which is also the principle taken by most of the current information retrieval systems. After several comparative analyses, when the value range of key factor is set to between 0.6 and 0.7, the result is more reasonable. If the user requires a high level of correlation, can increase the key factor threshold, and vice versa reduce it.

VI. CONCLUSION

The introduction of the digraph retrieval model to realize the search of semantic relation paths effectively solves the performance bottleneck of the iterator model used by ARQ in Jena. The introduction of semantic node network key factors to represent the importance of semantic nodes and relations provides a simple and feasible means to eliminate unwanted relation paths, and to sort the result relation paths.

This work successfully extends the SPARQL query for directly retrieving the semantic relation paths among RDF graph data so that many interesting semantic relations among the RDF data can be explicitly and easily enquired.

ACKNOWLEDGMENT

This work is supported by the National Natural Science Foundation of China under Grant 71173163. The authors would like to thank the colleagues for their inspiring discussions and the anonymous reviewers for their valuable comments and suggestions for the better presentation of this paper.

REFERENCES

[1] W. Zhang and Z. Deng, “Enquerying semantic relations among RDF triples,” in press.

[2] G. Wu, J. Tang, J. Li, and K. Wang, “Fine-grained semantic web retrieval,” J. of Tsinghua University:Sci & Tech, vol. 45, no. S1, 2005, pp. 1865-1872.

[3] C.-C. Jennifer, P. John, C. Krzysztof, F. David, and D. Pablo, “Semantic search via XML fragments: A high-precision approach to IR,” Proc. the 29th Annual Int. ACM SIGIR Conf. on Research and Development in Information Retrieval, ACM, 2006, pp. 445-452.

[4] L. Guo, S. Feng, B. Chavdar, and S. Jayavel, “XRANK: Ranked keyword search over XML documents,” Proc. ACM SIGMOD Int. Conf. on Management of Data, ACM, 2003, pp. 16-27.

[5] Kacholia Varun, et al. “Bidirectional expansion for keyword search on graph databases,” Proc. the 31th Int. Conf. on Very Large Data Bases, ACM, 2005, pp. 505-516.

[6] H. He, H. Wang, J. Yang, and P.S. Yu, “BLINKS: Ranked keyword searches on graphs,” Proc. ACM SIGMOD Int. Conf. on Management of Data, ACM, 2007, pp. 305-316.

Author Index

Author Index

Author Index

Author Index

IEEE Computer Society Technical & Conference Activities Board

IEEE Computer Society Publications

The world-renowned IEEE Computer Society publishes, promotes, and distributes a wide variety of authoritative computer science and engineering texts. These books are available from most retail outlets. Visit the CS Store at *http://www.computer.org/portal/site/store/index.jsp* for a list of products.

IEEE Computer Society *Conference Publishing Services* (CPS)

The IEEE Computer Society produces conference publications for more than 300 acclaimed international conferences each year in a variety of formats, including books, CD-ROMs, USB Drives, and on-line publications. For information about the IEEE Computer Society's *Conference Publishing Services* (CPS), please e-mail: cps@computer.org or telephone +1-714-821-8380. Fax +1-714-761-1784. Additional information about *Conference Publishing Services* (CPS) can be accessed from our web site at: *http://www.computer.org/cps*

Revised: 18 January 2012

CPS Conference Publishing Services — CPS Online™ IEEE Online Collaborative Publishing Environment

CPS Online is our innovative online collaborative conference publishing system designed to speed the delivery of price quotations and provide conferences with real-time access to all of a project's publication materials during production, including the final papers. The ***CPS Online*** workspace gives a conference the opportunity to upload files through any Web browser, check status and scheduling on their project, make changes to the Table of Contents and Front Matter, approve editorial changes and proofs, and communicate with their CPS editor through discussion forums, chat tools, commenting tools and e-mail.

The following is the URL link to the ***CPS Online*** Publishing Inquiry Form:
http://www.computer.org/portal/web/cscps/quote